



**Orano TN**

7160 Riverwood Drive  
Suite 200  
Columbia, MD 21046  
USA  
Tel: 410-910-6900  
Fax: 434-260-8480

August 19, 2021  
E-58750

U. S. Nuclear Regulatory Commission  
Attn: Document Control Desk  
One White Flint North  
11555 Rockville Pike  
Rockville, MD 20852

Subject: TN Americas LLC Application for Approval of the TN-32  
Transportation Package (Docket No. 71-9377)

In accordance with the provisions of Title 10, Part 71 of the Code of Federal Regulations, TN Americas LLC (TN) hereby applies for package approval for a Type B(U)F-96 spent fuel transportation package developed by TN for the TN-32 design and initially designated as Model No. TN-32B.

Please find enclosed a TN-32 transportation safety analysis report (SAR) for the Model TN-32B transportation package. TN has an NRC approved quality assurance program (Docket Number 71-0250), which satisfies the requirements of 10 CFR 71 Subpart H.

This submittal includes TN proprietary information which may not be used for any purpose other than to support the NRC staff's review of the application. In accordance with 10 CFR 2.390, we are providing an affidavit specifically requesting that you withhold this proprietary information from public disclosure. This submittal also contains appropriately labeled security-related sensitive information, which should be withheld under 10 CFR 2.390.

The affidavit pursuant to 10 CFR 2.390 is provided herein as Enclosure 1. The SAR is provided herein as Enclosures 2 and 3, for the proprietary and public SAR versions, respectively. Enclosure 4 provides a listing of the computer files contained in Enclosure 5. Enclosure 5 is a portable hard drive containing computer files associated with this initial application. These files exceed the file size accepted by the NRC EIE application and Enclosure 5 is therefore being provided separately. Since Enclosure 5 contains entirely proprietary information, no public version is provided.

For this CoC 9377 Revision 0 application, TN is applying for a one-time transportation of the DOE-EPRI High Burnup (HBU) Demonstration Project Cask. The HBU Demonstration Project Cask is part of the DOE/EPRI High Burnup Dry Storage Research Project (HDRP) to collect confirmatory data on the conditions of HBU fuel in dry storage. This project supports data on the initial conditions of the

fuel rods (before storage), data from the loading and initial storage period, and data on the fuel rods after storage.

To obtain the data after storage, the TN-32B cask needs to be transported to an examination facility with a large hot cell to open the cask and extract the fuel rods to be examined. To support the goals of this important industry project, it is desired to ship the cask as early as October 2023.

Should the NRC staff require additional information to support review of this application, please contact Peter Vescovi at 336-420-8325 or by email at [peter.vescovi@orano.group](mailto:peter.vescovi@orano.group).

Sincerely,

A handwritten signature in black ink that reads "A. Prakash". Below the signature, the letters "P.O." are printed in a small font.

Prakash Narayanan  
Chief Technical Officer

cc: Pierre Saverot (NRC), Storage and Transportation Licensing Branch, Division of Spent Fuel Management

Enclosures:

1. Affidavit Pursuant to 10 CFR 2.390
2. TN-32 Transportation Cask Safety Analysis Report, Revision 0a (Proprietary version)
3. TN-32 Transportation Cask Safety Analysis Report, Revision 0a (Public version)
4. List of Computer Files Contained in Enclosure 5
5. Computer Files Associated with CoC 9377 Initial Application (Proprietary)

**AFFIDAVIT PURSUANT**  
**TO 10 CFR 2.390**

TN Americas LLC                     )  
 State of Maryland                 )     SS.  
 County of Prince George's         )

I, Prakash Narayanan, depose and say that I am Chief Technical Officer of TN Americas LLC, duly authorized to execute this affidavit, and have reviewed or caused to have reviewed the information which is identified as proprietary and referenced in the paragraph immediately below. I am submitting this affidavit in conformance with the provisions of 10 CFR 2.390 of the Commission's regulations for withholding this information.

The information for which proprietary treatment is sought is contained in Enclosures 2 and 5, and are listed below:

- Enclosure 2 - Portions of certain chapters and appendices of the Safety Analysis Report (SAR) for Certificate of Compliance No. 9377, Revision 0, Docket 71-9377 (Proprietary Version)
- Enclosure 5 - Certain computer files associated with CoC 9377 (Proprietary)

This document has been appropriately designated as proprietary.

I have personal knowledge of the criteria and procedures utilized by TN Americas LLC in designating information as a trade secret, privileged, or as confidential commercial or financial information.

Pursuant to the provisions of paragraph (b) (4) of Section 2.390 of the Commission's regulations, the following is furnished for consideration by the Commission in determining whether the information sought to be withheld from public disclosure, included in the above referenced document, should be withheld.

- 1) The information sought to be withheld from public disclosure involves certain design details associated with the SAR analyses, SAR drawings, and analysis computer files for the TN-32 System, which are owned and have been held in confidence by TN Americas LLC.
- 2) The information is of a type customarily held in confidence by TN Americas LLC and not customarily disclosed to the public. TN Americas LLC has a rational basis for determining the types of information customarily held in confidence by it.
- 3) Public disclosure of the information is likely to cause substantial harm to the competitive position of TN Americas LLC because the information consists of descriptions of the design and analysis of a radioactive material transportation system, the application of which provide a competitive economic advantage. The availability of such information to competitors would enable them to modify their product to better compete with TN Americas LLC, take marketing or other actions to improve their product's position or impair the position of TN America LLC's product, and avoid developing similar data and analyses in support of their processes, methods or apparatus.

Further the deponent sayeth not.

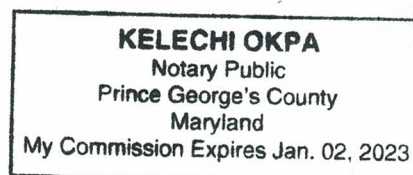
*A. Prakash*

Prakash Narayanan  
 Chief Technical Officer, TN Americas LLC

Subscribed and sworn before me this 18<sup>th</sup> day of August, 2021.

*[Signature]*  
 Notary Public

My Commission Expires 01/02/2023



**Enclosure 2 to E-58750**

**TN-32 Transportation Cask Safety Analysis Report,  
Revision 0a  
Withheld Pursuant to 10 CFR 2.390**



**Enclosure 3 to E-58750**

**TN-32 Transportation Cask Safety Analysis Report, Revision 0a  
(Public version)**



**TN Americas LLC**

**TN-32 Transportation Cask Safety Analysis  
Report**

**Docket Number 71-9377**

**Revision 0a**

**August 2021**

## TABLE OF CONTENTS

### **Chapter 1 General Information**

1.1	Introduction .....	1-1
1.2	Package Description.....	1-2
1.2.1	Packaging .....	1-2
1.2.2	Contents.....	1-8
1.2.3	Special Requirements for Plutonium .....	1-12
1.2.4	Operational Features.....	1-12
1.3	References.....	1-13
1.4	Appendices .....	1-18
1.4.1	General Arrangement Drawings .....	1-18

**Chapter 2 Structural Evaluation**

2.1	Description of Structural Design .....	2-1
2.1.1	Discussion.....	2-1
2.1.2	Design Criteria .....	2-3
2.1.3	Weights and Centers of Gravity.....	2-7
2.1.4	Identification of Codes and Standards for Package Design .....	2-7
2.2	Materials.....	2-8
2.2.1	Material Properties and Specifications.....	2-8
2.2.2	Chemical, Galvanic, or Other Reactions.....	2-8
2.2.3	Effects of Radiation on Materials .....	2-9
2.2.4	Fracture Toughness Requirements .....	2-9
2.3	Fabrication and Examination .....	2-10
2.3.1	Fabrication .....	2-10
2.3.2	Examination .....	2-10
2.4	General Standards for All Packages .....	2-11
2.4.1	Minimum Package Size .....	2-11
2.4.2	Tamper-Indicating Feature .....	2-11
2.4.3	Positive Closure .....	2-11
2.4.4	Chemical and Galvanic Reactions.....	2-11
2.5	Lifting and Tie-Down Standards for All Packages .....	2-14
2.5.1	Lifting Devices.....	2-14
2.5.2	Tie-Down Devices .....	2-19
2.6	Normal Conditions of Transport.....	2-20
2.6.1	Heat .....	2-21
2.6.2	Cold .....	2-22
2.6.3	Reduced External Pressure (N5).....	2-23
2.6.4	Increased External Pressure (N4) .....	2-23
2.6.5	Vibration.....	2-23
2.6.6	Water Spray .....	2-24
2.6.7	Free Drop.....	2-25
2.6.8	Corner Drop .....	2-25
2.6.9	Compression .....	2-25
2.6.10	Penetration.....	2-25
2.6.11	Lid Bolt Analysis.....	2-25
2.6.12	Fatigue Analysis of the Containment Boundary .....	2-26

2.6.13	Structural Evaluation of the Basket under Normal Condition Loads .....	2-29
2.6.14	Summary of NCT Cask Body Structural Analysis .....	2-30
2.7	Hypothetical Accident Conditions .....	2-31
2.7.1	30 Foot Free Drop .....	2-32
2.7.2	Crush .....	2-36
2.7.3	Puncture .....	2-36
2.7.4	Thermal .....	2-40
2.7.5	Immersion – Fissile material .....	2-41
2.7.6	Immersion – All Packages .....	2-41
2.7.7	Deep Water Immersion Test (for Type B Packages Containing More than 105 A2) .....	2-41
2.7.8	Summary of Damage .....	2-43
2.8	Accident Conditions for Air Transport of Plutonium .....	2-44
2.9	Accident Conditions for Fissile Material Packages for Air Transport .....	2-44
2.10	Special Form .....	2-44
2.11	Fuel Rods .....	2-44
2.12	Appendices .....	2-23
2.12.1	References .....	2.12.1-1
2.12.2	Structural Analysis of Cask Body .....	2.12.2-1
2.12.2.1	Introduction .....	2.12.2-1
2.12.2.2	ANSYS® Analysis .....	2.12.2-2
2.12.2.3	Pressure Distribution over Contact Area for Impact Load .....	2.12.2-22
2.12.2.4	Analysis Results .....	2.12.2-24
2.12.2.5	References .....	2.12.2-25
2.12.3	Closure Lid Bolt Analysis .....	2.12.3-1
2.12.3.1	Introduction .....	2.12.3-1
2.12.3.2	Closure Lid Bolt Load Calculations .....	2.12.3-2
2.12.3.3	Summary of Closure Lid Bolt Loads .....	2.12.3-7
2.12.3.4	Closure Lid Bolt Load Combinations .....	2.12.3-7
2.12.3.5	Closure Lid Bolt Stress Calculations .....	2.12.3-10
2.12.3.6	Analysis Results .....	2.12.3-12
2.12.3.7	Closure Lid Bolt Fatigue Analysis .....	2.12.3-12
2.12.3.8	Lid Seal Contact Evaluation .....	2.12.3-16
2.12.3.9	Engagement Length for Bolt and Flange .....	2.12.3-17

2.12.3.10	Conclusions.....	2.12.3-18
2.12.3.11	References.....	2.12.3-19
2.12.4	Structural Analysis of the Outer Shell .....	2.12.4-1
2.12.4.1	Introduction .....	2.12.4-1
2.12.4.2	Description .....	2.12.4-1
2.12.4.3	Materials Input Data .....	2.12.4-1
2.12.4.4	Applied Loads .....	2.12.4-2
2.12.4.5	Partial Groove/Fillet Weld Calculations.....	2.12.4-2
2.12.4.6	Method of Analysis .....	2.12.4-2
2.12.4.7	Analysis Results.....	2.12.4-8
2.12.4.8	References.....	2.12.4-8
2.12.5	Fracture Toughness Evaluation of the TN-32B HBU Cask.....	2.12.5-1
2.12.5.1	Introduction .....	2.12.5-1
2.12.5.2	Fracture Toughness Requirements of the Cask .....	2.12.5-1
2.12.5.3	Fracture Toughness Evaluation of Cask Components and Welds .....	2.12.5-2
2.12.5.4	Methodology.....	2.12.5-2
2.12.5.5	Locations of Maximum Stresses.....	2.12.5-2
2.12.5.6	Material Fracture Toughness.....	2.12.5-3
2.12.5.7	Fracture Toughness Criteria.....	2.12.5-4
2.12.5.8	Stress Intensity Factor Calculations .....	2.12.5-4
2.12.5.9	Conclusions.....	2.12.5-4
2.12.5.10	NDE Inspection Plan .....	2.12.5-5
2.12.5.11	References.....	2.12.5-6
2.12.6	Structural Analysis of the TN-32B HBU Cask Basket.....	2.12.6-1
2.12.6.1	Introduction .....	2.12.6-1
2.12.6.2	Fuel Basket Stress Analysis .....	2.12.6-2
2.12.6.3	Fuel Basket Buckling Analysis.....	2.12.6-9
2.12.6.4	Fusion Welds .....	2.12.6-10
2.12.6.5	Conclusions.....	2.12.6-12
2.12.6.6	References.....	2.12.6-12
2.12.7	Dynamic Load Factor for Basket Drop Analysis.....	2.12.7-1
2.12.7.1	Introduction .....	2.12.7-1
2.12.7.2	Modal Analysis of Basket Side Drop Loading Condition .....	2.12.7-1
2.12.7.3	Dynamic Load Factor Calculations .....	2.12.7-3



2.12.7.4	References.....	2.12.7-4
2.12.8	Structural Evaluation of the Fuel Rod Cladding under Accident Impact .....	2.12.8-1
2.12.8.1	Side Drop Analysis .....	2.12.8-1
2.12.8.2	End Drop Analysis.....	2.12.8-4
2.12.8.3	Material Properties of Fuel .....	2.12.8-12
2.12.8.4	Determination of Side Drop g-Loading with Dynamic Load Factor.....	2.12.8-13
2.12.8.5	Conclusions.....	2.12.8-14
2.12.8.6	References.....	2.12.8-15
2.12.9	Structural Evaluation of the Impact Limiters.....	2.12.9-1
2.12.9.1	Introduction .....	2.12.9-1
2.12.9.2	Methodology.....	2.12.9-1
2.12.9.3	Assumptions.....	2.12.9-13
2.12.9.4	Computation.....	2.12.9-13
2.12.9.5	Normal Conditions of Transport Results .....	2.12.9-15
2.12.9.6	Hypothetical Accident Conditions Results .....	2.12.9-16
2.12.9.7	Conclusions.....	2.12.9-24
2.12.9.8	References.....	2.12.9-25
2.12.10	TN-40 Package Impact Limiter Testing.....	2.12.10-1
2.12.10.1	Introduction .....	2.12.10-1
2.12.10.2	Scaling Relationships .....	2.12.10-1
2.12.10.3	Test Article Description .....	2.12.10-2
2.12.10.4	Test Description .....	2.12.10-2
2.12.10.5	Data Measurement.....	2.12.10-7
2.12.10.6	Test Data and Results.....	2.12.10-8
2.12.10.7	Conclusions.....	2.12.10-15
2.12.10.8	References.....	2.12.10-17
2.12.11	Deep Water Immersion.....	2.12.11-1
2.12.11.1	Hoop and Axial Compressive Stresses.....	2.12.11-1
2.12.11.2	Axial Compressive Stress and Buckling Stresses.....	2.12.11-4
2.12.11.3	Amplified Axial Stress.....	2.12.11-5
2.12.11.4	Interaction Equations for Local Buckling.....	2.12.11-6
2.12.11.5	References.....	2.12.11-7
2.12.12	Structural Analysis of Thermocouple Lance Assembly .....	2.12.12-1
2.12.12.1	Introduction .....	2.12.12-1

2.12.12.2 Lance Closure Calculations.....	2.12.12-2
2.12.12.3 Thermocouple Lance Oversheath .....	2.12.12-11
2.12.12.4 Lance Seal Lateral Displacement Test .....	2.12.12-14
2.12.12.5 Conclusions.....	2.12.12-16
2.12.12.6 References.....	2.12.12-17
2.12.13 ASME B&PV Code Alternatives.....	2.12.13-1

**Chapter 3 Thermal Evaluation**

3.1	Description of Thermal Design .....	3-2
3.1.1	Design Features .....	3-2
3.1.2	Content's Decay Heat .....	3-2
3.1.3	Summary Tables of Temperatures .....	3-4
3.1.4	Summary Tables of Maximum Pressures .....	3-4
3.2	Material Properties and Component Specifications.....	3-5
3.2.1	Material Properties .....	3-5
3.2.2	Component Specifications.....	3-6
3.3	Thermal Evaluation under Normal Conditions of Transport.....	3-18
3.3.1	Heat and Cold .....	3-18
3.3.2	Maximum Normal Operating Pressure.....	3-30
3.4	Thermal Evaluation under Hypothetical Accident Conditions .....	3-31
3.4.1	Initial Conditions .....	3-31
3.4.2	Fire Test Conditions .....	3-31
3.4.3	Maximum Temperatures and Pressure.....	3-32
3.4.4	Maximum Thermal Stresses .....	3-33
3.4.5	Accident Conditions for Fissile Material Packages for Air Transport.....	3-33
3.5	References.....	3-34
3.6	Appendix .....	3-61

**Chapter 4    Containment**

4.1	Description of the Containment System.....	4-1
4.1.1	Containment Vessel .....	4-1
4.1.2	Containment Penetrations .....	4-2
4.1.3	Seals and Welds .....	4-2
4.1.4	Closure.....	4-4
4.2	Containment under Normal Conditions of Transport.....	4-4
4.2.1	Containment of Radioactive Material .....	4-5
4.2.2	Pressurization of Containment Vessel .....	4-5
4.2.3	Containment Criterion .....	4-5
4.3	Containment under Hypothetical Accident Conditions .....	4-5
4.3.1	Fission Gas Products .....	4-5
4.3.2	Containment of Radioactive Material .....	4-5
4.3.3	Containment Criterion .....	4-6
4.4	Leakage Rate Tests for Type B Packages.....	4-6
4.5	References.....	4-7

## Chapter 5 Shielding Evaluation

5.1	Description of Shielding Design .....	5-1
5.1.1	Design Features .....	5-1
5.1.2	Summary of Maximum Radiation Levels .....	5-2
5.2	Source Specification .....	5-2
5.2.1	Gamma Source .....	5-4
5.2.2	Neutron Source .....	5-4
5.3	Shielding Model .....	5-5
5.3.1	Configuration of Source and Shielding .....	5-5
5.3.2	Material Properties .....	5-7
5.4	Shielding Evaluation .....	5-7
5.4.1	Methods .....	5-7
5.4.2	Input and Output Data .....	5-8
5.4.3	Flux-to-Dose-Rate Conversion .....	5-9
5.4.4	External Radiation Levels .....	5-9
5.5	References .....	5-13
5.6	Input File Listing .....	5-14
5.6.1	ORIGEN-ARP Input File .....	5-14
5.6.2	NCT Primary Gamma MCNP Model Input File .....	5-16
5.6.3	NCT Side Neutron MCNP Model Input File .....	5-49

**Chapter 6 Criticality Evaluation**

6.1	Description of Criticality Design .....	6-1
6.1.1	Design Features .....	6-1
6.1.2	Summary Table of Criticality Evaluations .....	6-2
6.1.3	Criticality Safety Index .....	6-3
6.2	Fissile Material Contents .....	6-3
6.2.1	Burnup Credit Methodology .....	6-4
6.3	General Considerations .....	6-5
6.3.1	Model Configuration .....	6-5
6.3.2	Material Properties .....	6-16
6.3.3	Analysis Methods and Nuclear Data .....	6-17
6.3.4	Demonstration of Maximum Reactivity .....	6-22
6.4	Single Package Evaluation .....	6-26
6.4.1	Configuration .....	6-26
6.4.2	Results .....	6-26
6.5	Evaluation of Package Arrays under Normal Conditions of Transport .....	6-26
6.5.1	Configuration .....	6-26
6.5.2	Results .....	6-26
6.6	Package Arrays under Hypothetical Accident Conditions .....	6-27
6.6.1	Configuration .....	6-27
6.6.2	Results .....	6-27
6.7	Fissile Material Packages for Air Transport .....	6-27
6.8	Benchmark Evaluations .....	6-27
6.8.1	Applicability of Benchmark Experiments .....	6-28
6.8.2	Bias Determination .....	6-32
6.9	Burnup Credit .....	6-38
6.9.1	Limits for the Licensing Basis .....	6-38
6.9.2	Code Validation .....	6-39
6.9.3	Licensing Basis Model Assumptions .....	6-44
6.9.4	Loading Curve and Burnup Verification .....	6-45
6.9.5	Assigned Burnup Loading Value .....	6-46
6.9.6	Estimate of Additional Reactivity Margin .....	6-46
6.10	Appendix .....	6-48
6.10.1	References .....	6-48
6.10.2	Sample Input Files .....	6-50



**Chapter 7 Operating Procedures**

7.1	Package Loading.....	7-1
7.1.1	Preparation for Loading.....	7-1
7.1.2	Loading of Contents .....	7-1
7.1.3	Preparation for Transport .....	7-1
7.2	Package Unloading .....	7-4
7.2.1	Receipt of Package from Carrier .....	7-4
7.2.2	Removal of Contents.....	7-5
7.3	Preparation of Empty Package for Transport.....	7-6
7.4	Other Operations.....	7-7
7.5	References.....	7-7

**Chapter 8 Acceptance Tests and Maintenance Program**

8.1	Acceptance Tests .....	8-1
8.1.1	Visual Inspections and Measurements .....	8-1
8.1.2	Weld Examinations.....	8-2
8.1.3	Structural and Pressure Tests .....	8-2
8.1.4	Leakage Tests.....	8-3
8.1.5	Component and Material Tests .....	8-6
8.1.6	Shielding Tests.....	8-8
8.1.7	Thermal Tests .....	8-10
8.1.8	Miscellaneous Tests.....	8-11
8.2	Maintenance Program .....	8-12
8.2.1	Structural and Pressure Tests .....	8-12
8.2.2	Leakage Rate Tests .....	8-12
8.2.3	Component and Material Tests .....	8-12
8.2.4	Thermal.....	8-13
8.2.5	Miscellaneous Tests.....	8-13
8.3	References.....	8-14

## **Chapter 1**

### **General Information**

#### TABLE OF CONTENTS

1.1	Introduction .....	1-1
1.2	Package Description.....	1-2
1.2.1	Packaging .....	1-2
1.2.2	Contents .....	1-8
1.2.3	Special Requirements for Plutonium .....	1-12
1.2.4	Operational Features .....	1-12
1.3	References.....	1-13
1.4	Appendices .....	1-18
1.4.1	General Arrangement Drawings.....	1-18

#### LIST OF TABLES

Table 1-1	Dimensions and Weights of the TN-32B HBU Demonstration Cask .....	1-14
Table 1-2	TN-32B HBU Demonstration Cask Fuel Data.....	1-15

#### LIST OF FIGURES

Figure 1-1	General Arrangement, TN-32B HBU Demonstration Cask .....	1-16
------------	--	------

## **Chapter 1**

### **General Information**

#### **1.1 Introduction**

For the CoC 9377 Revision 0 application, TN is applying for a one-time transportation of the DOE-EPRI High Burnup (HBU) Demonstration Project Cask. The HBU Demonstration Project Cask is part of the DOE/EPRI High Burnup Dry Storage Research Project (HDRP) to collect confirmatory data on the conditions of HBU fuel in dry storage.

TN's application is for a transportation package developed by TN for the TN-32 design and initially designated as Model No. TN-32B, which is the HBU Project Cask. Accordingly, this initial revision of the TN-32 transportation cask safety analysis report (SAR) is for the Model TN-32B transportation package.

This chapter of the SAR presents a general introduction and description of the TN-32B HBU demonstration cask, Serial Number TN-32B-81, as a Type B(U)-96 spent fuel transport packaging developed by TN Americas, LLC. This SAR describes the design features, and presents the safety analyses that demonstrates the TN-32B HBU demonstration cask complies with applicable requirements of 10 CFR Part 71 [1]. The format and content of this SAR follow the guidelines of Regulatory Guide 7.9 [2].

The TN-32B HBU demonstration cask is a unique, dual purpose cask intended for both storage and transport. This cask was specifically selected for the High Burn-up Dry Storage Cask Research and Development Project, sponsored by the Department of Energy (DOE) and the Electric Power Research Institute (EPRI). The TN-32B HBU demonstration cask is currently licensed for storage only at the North Anna Power Station (NAPS) Independent Spent Fuel Storage Installation (ISFSI) [SNM-2507, Docket No. 72-16]. A separate License Amendment Request (LAR) was submitted by Dominion Generation in support of the site-specific storage license application. That amendment addresses the safety related aspects of storing HBU spent fuel in TN-32B HBU demonstration cask in accordance with 10 CFR 72 [3].

The TN-32B HBU demonstration cask is a standard TN-32B storage cask that was modified to insert seven thermocouple lance assemblies (TLAs) through the closure lid into seven specific spent fuel assemblies. The thermocouple lances measure the fuel temperatures in real time during the 5.87-year storage period. The TN-32B HBU demonstration cask is to be licensed for a single, specific HBU payload, and one-time use for transportation. That is, for shipment of the HBU spent fuel that was selected and stored for the storage period. This one-time use is defined to include any sequence of shipments as long as the HBU spent fuel originally loaded has not been removed. The cask is intended to be shipped as an exclusive use package. The Criticality Safety Index (CSI) for nuclear criticality control for the TN-32B HBU demonstration cask is determined to be zero in accordance with 10 CFR 71.59. Refer to Chapter 6 for details of this determination.

TN Americas has an NRC approved quality assurance program (Docket Number 71-0250), which satisfies the requirements of 10 CFR Part 71 Subpart H.

## 1.2 Package Description

### 1.2.1 Packaging

The TN-32B HBU demonstration cask will be used to transport 32 intact pressurized water reactor (PWR) HBU spent fuel assemblies with six poison rod assemblies (PRAs) inserted into specific assemblies. In its transport configuration, the TN-32B HBU demonstration cask consists of the following components:

- A basket assembly that locates and supports the fuel assemblies, transfers heat to the cask inner shell, and provides sufficient neutron absorption to satisfy nuclear criticality requirements.
- A containment vessel, including a closure lid, vent and drain covers, metallic O-ring seals, and the thermocouple lance assemblies, which provide containment of the radioactive materials, and maintains an inert gas atmosphere.
- A thick-walled, forged steel gamma shield shell, a bottom shield, and closure lid shield plate provide shielding that surrounds the containment vessel.
- A radial neutron shield surrounding the gamma shield shell that provides additional radiation shielding. The neutron shielding is enclosed within a welded steel outer shell.
- A set of impact limiters consisting of redwood and balsa wood, encased in stainless steel shells, which are attached to each end of the cask body during transport. A puncture resistant plate over the closure lid, and lance cover plates that cover the lance assemblies are also present to prevent a postulated puncture bar impact from contacting the thermocouple lance assemblies. The puncture resistant plate also provides a smooth contact surface between the upper impact limiter and the closure lid. The impact limiters are secured to the cask with tie-rods and attachment bolts.
- Sets of upper and lower trunnions that provide lifting and rotational capability, respectively, for the cask.

A personnel barrier is mounted to the transport skid to prevent unauthorized access to the surface of the cask body. The overall dimensions of the TN-32B HBU demonstration cask are 263.2 inches long and a diameter of 144 inches with the impact limiters installed. The cask body is 184.3 inches long (with the closure lid installed), and 87.75 inches in diameter. The closure lid is 79.50 inches in diameter. The cask outside diameter including the radial neutron shield is 98.14 inches. The cask cavity is 163.38 inches long and 68.80 inches in diameter. The general arrangement of the TN-32B HBU demonstration cask is illustrated in Figure 1-1. Detailed design drawings for the TN-32B HBU demonstration cask are provided in Appendix 1.4.1. The materials utilized to fabricate the cask are provided in the Parts List on Drawings 19885-71-1 through 19885-71-7, and the materials utilized to fabricate the impact limiters are presented in the Parts List on Drawings 19885-71-8 through 19885-71-10. Where more than one material has been specified for a component, the most limiting properties are used in the analyses in the subsequent chapters of this SAR.

The gross weight of the loaded package is 269.0 kips, including a payload weight of 49.6 kips. Table 1-1 summarizes the dimensions and weights of the TN-32B HBU demonstration cask. Trunnions welded to the cask body are provided for lifting and handling operations, including rotation of the packaging between the horizontal and vertical orientations. The TN-32B HBU demonstration cask is loaded in the vertical configuration, and transported in the horizontal orientation on a specially designed transport skid.

The maximum normal operating pressure (MNOP) of the TN-32B HBU demonstration cask is 30.5 psig. However, a cask cavity pressure of 100 psig is conservatively utilized for the purposes of structural analyses. The HBU spent fuel payload is shipped dry in a helium gas atmosphere. The heat generated by the HBU spent fuel assemblies is rejected to the surrounding air by convection and radiation. No forced cooling or cooling fins are required.

The following sections provide a physical and functional description of each major component. Engineering drawings delineate dimensions of significance to the safety analyses, welding, and NDE information, and a complete materials list are provided in Appendix 1.4.1. Reference to these drawings is made in the following physical description sections and in general, throughout this SAR. Fabrication of the TN-32B HBU demonstration cask was performed in accordance with these drawings.

#### 1.2.1.1 Containment Vessel

The containment boundary components consist of the inner shell and bottom inner plate, shell flange, closure lid outer plate, closure lid bolts, penetration cover plates and bolts (vent and drain), the TLAs, and the inner metallic seals of the lid seal, the vent and drain seals, and the thermocouple lance seals (refer to Figure 1-1). The containment vessel prevents potential leakage of radioactive material from the cask cavity. It also maintains an inert atmosphere (helium) in the cask cavity. Helium gas assists in removal of decay heat, and provides a non-reactive environment to protect fuel assemblies against fuel cladding degradation that might otherwise lead to gross cladding rupture.

The overall containment vessel length is 171 inches with a wall thickness of 1.5 inch. The cylindrical cask cavity has an inner diameter of 68.8 inches and a length of 163.38 inches. The closure lid outer plate is 4.5 inches thick, and is secured to the body by 48 high-strength closure lid bolts and hardened washers. Double metallic O-ring seals are provided for the lid closure. To preclude air in-leakage, the cask cavity was pressurized with helium gas above atmospheric pressure at the time of payload loading in November 2017.

The cask cavity can be accessed using two penetrations through the lid. These penetrations are for draining and venting the cavity. Double metallic O-ring seals are also utilized to seal these two lid penetrations.

The over-pressure (OP) port provides access to the volumes between the double seals in the closure lid, cover plates, and the thermocouple lances for leakage rate testing purposes. The OP port cover is not part of the containment boundary.



The material for the inner shell, bottom inner plate, and the closure lid outer plate is SA-203 Grade D. The material for the inner shell flange and thermocouple penetration sleeve forgings is SA-350 Grade LF3. The TLA structural materials are dual-certified Type 304/304L austenitic stainless steel and annealed Inconel (UNS N06600). The design of the thermocouple lance is essentially the same as that for in-core instrumentation utilized in a PWR, which typically has a design pressure of 2,250 psig.

The cask cavity surfaces have a sprayed metallic coating of aluminum for corrosion protection. Additionally, a stainless steel overlay was applied to the O-ring seating surfaces on the cask body, vent, drain, and TLAs for corrosion protection.

The TN-32B HBU demonstration cask containment vessel is designed, fabricated, examined, and tested in accordance with the requirements of Subsection NB [4] of the ASME Boiler and Pressure Vessel (B&PV) Code to the maximum practical extent. In addition, the design meets the requirements and Regulatory Guides 7.6 [5] and 7.8 [6]. Alternatives to the ASME B&PV Code are discussed in Section 2.11. The construction of the containment boundary is shown on Drawings 19885-71-2, -3, -5, and -7 provided in Appendix 1.4.1. The design of the containment boundary is further discussed in Chapter 2, and the fabrication requirements (including examination and testing) of the containment boundary are discussed in Chapter 4.

#### 1.2.1.2 Gamma and Radial Neutron Shielding

A gamma shield is provided around the inner shell and the bottom inner plate of the containment vessel, by an independent shell and bottom plate of carbon steel (Drawing 19885-71-3). The gamma shield shell completely surrounds the containment vessel inner shell and bottom inner plate. The 8.0-inch thick gamma shield shell and the 8.75-inch thick bottom plate are SA-266 Gr 2 and SA-516, Grade 70 material, respectively.

In order to obtain a close fit between the inner shell and the gamma shield shell for heat transfer, the gamma shield shell was heated prior to assembly with the inner shell. As the gamma shield shell cools, an axial gap may form between the shell upper flange and the top of the gamma shield shell. This gap is filled with shims. The shims are machined to fill the gap, and act as a backing plate for the weld between the shell upper flange and the gamma shield shell.

A 6.0-inch thick shield plate (SA-516, Grade 70) is also welded to the inside of the closure lid outer plate (Drawing 19885-71-3). Lance cover plates (SA-240, Type 304), which are 2.13 inches thick, are placed over the thermocouple lances and welded to the closure lid outer plate (Drawing 19885-71-2).

Radial neutron shielding is provided by a borated polyester resin compound surrounding the gamma shield shell. The resin compound is cast into long, slender aluminum alloy boxes. The total radial thickness of the resin and aluminum is 4.52 inches. The array of resin-filled boxes is enclosed within a 1/2-inch thick outer steel shell (SA-516, Grade 70) constructed of two half cylinders. In addition to serving as resin containers, the aluminum containers provide a conduction path for heat transfer from the gamma shield shell to the outer shell surface. A pressure relief valve is mounted on top of the resin enclosure to limit the internal pressure increase that may result from heating of the resin enclosure during the hypothetical accident conditions.

The resin material is an unsaturated polyester cross-linked with styrene, with approximately 50 weight % (wt%) mineral and fiberglass reinforcement. The components are polyester resin, styrene monomer, alpha methyl styrene, aluminum oxide, zinc borate, and chopped fiberglass, which produce the nominal elemental resin composition shown below.

Element	wt%
H	5.05
B	1.05
C	35.13
Al	14.93
O + Zn (balance)	43.84

The resin utilized for the radial neutron shield is a proprietary formulation that has been utilized for the TN-32/TN-32B, TN-40, and TN-68 casks, which have been licensed for storage. The TN-40 and TN-68 cask designs are also licensed for transport. Information on this proprietary resin has been provided to the NRC in support of those licensing applications. The average measured hydrogen weight percent in the resin for TN-32B HBU demonstration cask is 5.21. Appendix 9A of the TN-32 storage UFSAR (NRC Docket No. 72-1021) provides information on the resin, which is provided below.

### Thermal Stability

Thermal aging tests on a material with the same components in slightly different proportions have been performed by Transnucleaire, Paris (TNP). The tests by TNP evaluate weight loss and off-gassing at 260 °F (125 °C) and 311 °F (155 °C). An exponential weight loss occurs that rapidly approaches a maximum value. After 106 hours, the weight loss is about 1.0%, and extrapolation of the results indicates maximum weight loss of about 1.3%. This effect diminishes rapidly with decreasing temperature. An analysis of the gas released from a sample heated from 77 °F (25 °C) to 257 °F (125 °C) over one hour demonstrated the resin consisted to be 99.9% styrene.

These results obtained with small samples (2-inch thick × 2-inch diameter [50 mm thick × 50 mm diameter]) are conservative with respect to the material in a larger enclosed form, such as the TN-32B HBU demonstration cask radial neutron shield, where volatile constituents must diffuse through a much greater distance to be released.

## **Radiation Stability**

The European Organization for Nuclear Research (CERN) has published a compilation of its own testing and of prior published data on the radiation resistance of various materials. The data demonstrate that while unfilled polyester has poor radiation resistance, both mineral- and glass-filled polyester, such as used in the TN-32B HBU demonstration cask radial neutron shield, are among the most radiation-resistant of thermosetting resins.

In addition, the maximum bulk and peak temperatures in the radial neutron shield are 256 °F (124 °C) and 299 °F (148 °C), respectively, at the beginning of storage period (November 2017) per Chapter 3 of the TN-32B HBU demonstration cask DLBD [7]. For NCT, the bulk average and maximum resin temperatures are 250 °F (121 °C) and 298 °F (148 °C), respectively. These temperatures are bounded by the temperatures in the thermal aging tests. Therefore, the resin degradation and weight loss are expected to be bounded by the test results.

There are over (100) TN-32, TN-40, and TN-68 casks currently in storage at various ISFSI sites in the United States. Periodic inspections and dose rate measurements of the casks in storage have not indicated any evidence of deterioration of the radial neutron shielding.

Furthermore, prior to transport of the TN-32B HBU demonstration cask, dose rate measurements shall be performed to demonstrate that they comply with the 10 CFR 71.47 criteria. This process ensures that the resin material has retained adequate properties to satisfy transportation requirements.

The structural analysis of the TN-32B HBU demonstration cask shielding is presented in Chapter 2.

Noncontainment welds were inspected in accordance with the NDE acceptance criteria of ASME B&PV Code, Section III, Subsection NF [8].

### **1.2.1.3 Impact Limiters**

Upper (front) and lower (rear) impact limiters, illustrated on Drawings 19885-71-8, 19885-71-9, and 19885-71-10, form a part of the TN-32B HBU demonstration cask. The impact limiters are attached to each other utilizing 13 tie-rods, and to the cask body by attachment bolt brackets that are welded to the outer shell in eight locations. The impact limiters consist of redwood and balsa wood blocks, encased in sealed stainless steel shells (ASTM A240, Type 304) that maintain a dry atmosphere for the wood, and confine the wood when crushed during a potential free drop. The impact limiters also include internal radial gussets for added strength and confinement.

The impact limiters have an outside diameter of 144 inches, and an inside diameter of 89 inches to accommodate the cask ends. The bottom limiter is notched to fit over the lower trunnions. The impact limiters extend axially 38 inches from either end of the cask, and overlap the sides of the cask by 12 inches.

There are 13, 1½-inch diameter tie-rods utilized to secure the impact limiters to the cask. The tie-rods span the length of the cask and connect to both impact limiters via mounting brackets. The impact limiters are also attached to the outer shell of the cask with eight 1½-inch diameter bolts. The bolts are inserted through brackets that are secured to bars that are welded to the cask outer shell, and threaded into each impact limiter. There are a total of eight bracket sets, four per impact limiter. Refer to Drawings 19885-71-8, -9, and -10 in Appendix 1.4.1.

Each impact limiter is provided with 16 fusible plugs that are designed to melt during a hypothetical fire accident, thereby relieving excessive internal pressure due to any combustion of the wood. Each impact limiter has two lifting lugs for handling, and two support angles for supporting the impact limiter in a vertical position during storage. The lifting lugs and the support angles are welded to the stainless steel outer shells.

A 1.75-inch thick puncture resistant steel plate is placed on the closure lid, and bolted to the cask body prior to installing the upper impact limiter. The purpose of this plate is to provide a smooth contact surface between the closure lid and the upper impact limiter, and to preclude the puncture bar free drop per 10 CFR 71.73(b)(3) from impacting any of the thermocouple lance assemblies. The lip of the puncture resistant plate is designed to make up the difference between the closure lid and cask outer diameters so that the upper impact limiter cavity mates with a surface of constant diameter. The plate also incorporates two elastomer O-ring seals to provide an additional boundary to prevent any postulated releases of radioactive material from the vent, drain, and/or TLAs (refer to Drawing 19885-71-4).

The functional description, as well as the performance analysis of the impact limiters, is provided in Appendix 2.12.9.

#### 1.2.1.4 Tie-Down and Lifting Devices

Threaded holes are provided in the closure lid to attach component lifting devices, and are utilized as attachment points for sling systems or other lifting tools. These threaded holes are equally spaced 90-degrees apart, as shown on Drawing 19885-71-3. Prior to transport, any attachments will be removed. Access to these threaded holes is prevented by the presence of the puncture resistant plate.

Four trunnions, which form part of the cask body, are attached for lifting and rotating the cask. Two of the trunnions are located near the top of the body, and two near the bottom. The upper trunnions are welded to the 8-inch thick gamma shield shell and are designed to meet the requirements of 10 CFR 71.45(a). This compliance is accomplished by evaluating the trunnions to the stress design factors of 6 and 10 when compared with yield and ultimate stress limits, respectively. These design loads exceed the 10 CFR §71.45(a) requirements. The lower trunnions are also welded to the 8-inch thick gamma shield shell and bottom shield, and are utilized for only rotating the cask between the vertical and the horizontal positions.

The tie-down devices are described in Section 2.5.2 of Chapter 2.

### 1.2.1.5 Fuel Basket

The basket structure is designed, fabricated, and inspected in accordance with ASME B&PV Code, Section III, Subsection NB/NF. Section 2.1.2.2 of Chapter 2 discusses use of Subsection NB/NF rather than Subsection NG. Alternatives to the Subsection NB code are provided in Appendix 2.12.13. The basket structure consists of an assembly of stainless steel cells joined by a proprietary fusion welding process and separated by aluminum and poison plates, which form a sandwich panel. The panel consists of 1/2-inch thick aluminum plate and a 0.040-inch thick poison plate. The aluminum plates provide the heat conduction paths from the fuel assemblies to the cask cavity wall. The poison material provides the necessary criticality control. This method of construction forms a very strong honeycomb-like structure of cell liners that provide compartments for 32 fuel assemblies. The open dimension of each cell is 8.70 inch × 8.70 inch, which provides a minimum of 1/8 inch clearance around the irradiated HBU fuel assemblies. The overall basket length (160.0 inch) is less than the cask cavity length to allow for thermal expansion and fuel assembly handling.

### 1.2.2 Contents

The characteristics for the specific 32 HBU fuel assemblies in the TN-32B HBU demonstration cask are as follows:

- a) Fuel is unconsolidated;
- b) The HBU PWR fuel assemblies were limited to three fuel types and four cladding materials:
  - i. Westinghouse LOPAR 17×17 with Zirc-4 cladding,
  - ii. Westinghouse NAIF 17 × 17 with ZIRLO™ and Low SN Zr-4 cladding, and
  - iii. AREVA Advanced MK-BW (AMBW) 17×17 with M5™ cladding
- c) Fuel includes six PRAs installed in specific fuel assemblies;
- d) The maximum combined weight of a fuel assembly and a PRA is 1,551 lb;
- e) The combined weight of the HBU fuel assemblies and the PRAs in the cask is less than 50,000 lb;
- f) The initial enrichment is less than or equal to 4.55 weight percent U-235;
- g) The burnup for each assembly is greater than 50,000 MWd/MTU;
- h) The HBU fuel payload shall not be transported earlier than October 1, 2023;
- i) The minimum cooling time prior to transport for any of the HBU fuel assemblies is 11.56 years;
- j) The maximum total heat load is 25.84 kW with a maximum of 0.878 kW for any HBU fuel assembly;
- k) The characteristics of the specific fuel types authorized for shipment in the TN-32B HBU demonstration cask are provided in Table 1-2. The table presents the pre-irradiated nominal design dimensions and specifications for the HBU fuel assemblies.

- l) The fuel burnup data for all 32 HBU fuel assemblies in the TN-32B HBU demonstration cask are provided in the following table.



Cell #	Fuel Assembly ID	Fuel & Cladding Type	Cooling Time as of 10/1/23 (years)	Burnup (MWd/MTU)	Decay Heat as of 10/1/23 (Watts)
1	6T0	NAIF, ZIRLO™	18.00	54,223	816
2	3K7	AMBW, M5™	14.57	53,414	846
3	3T6	NAIF, ZIRLO™	18.00	54,298	817
4	6F2	NAIF, ZIRLO™	19.41	51,904	738
5	3F6	NAIF, ZIRLO™	19.41	52,138	742
6	30A	AMBW, M5™	13.05	52,020	851
7	22B	AMBW, M5™	11.56	51,155	875
8	20B	AMBW, M5™	11.56	50,477	859
9	5K6	AMBW, M5™	14.57	53,268	843
10	5D5	NAIF, ZIRLO™	23.55	55,496	748
11	5D9	NAIF, ZIRLO™	23.55	54,579	732
12	28B	AMBW, M5™	11.56	50,966	871
13	F40	LOPAR, Zirc-4	36.45	50,646	525
14	57A	AMBW, M5™	13.05	52,154	854
15	30B	AMBW, M5™	11.56	50,623	863
16	3K4	AMBW, M5™	14.57	51,841	807
17	5K7	AMBW, M5™	14.57	53,335	845
18	50B	AMBW, M5™	11.56	50,870	868
19	3U9	NAIF, ZIRLO™	16.54	53,074	810
20	0A4	NAIF, Low SN Zr-4	29.06	50,047	593
21	15B	AMBW, M5™	11.56	50,972	871
22	6K4	AMBW, M5™	14.57	51,868	815
23	3T2	NAIF, ZIRLO™	18.00	55,087	833
24	3U4	NAIF, ZIRLO™	16.54	52,850	805
25	56B	AMBW, M5™	11.56	50,952	870
26	54B	AMBW, M5™	11.56	51,340	878
27	6V0	AMBW, M5™	14.57	53,506	855
28	3U6	NAIF, ZIRLO™	16.54	52,968	808
29	4V4	AMBW, M5™	15.04	51,183	794

Cell #	Fuel Assembly ID	Fuel & Cladding Type		Cooling Time as of 10/1/23 (years)	Burnup (MWd/MTU)	Decay Heat as of 10/1/23 (Watts)
30	5K1	AMBW, M5™		14.57	53,012	838
31	5T9	NAIF, ZIRLO™		18.00	54,890	829
32	4F1	NAIF, ZIRLO™		19.41	52,285	745

### 1.2.3 Special Requirements for Plutonium

Per the requirements of 10 CFR 71.63 [2], "Shipments containing plutonium must be made with the contents in solid form, if the contents contain greater than 0.74 TBq (20 Ci) of plutonium." The TN-32B HBU demonstration cask contains plutonium in solid form in the fuel rods of the HBU spent fuel assemblies and therefore, satisfies this requirement.

### 1.2.4 Operational Features

There are no complex operational features associated with the TN-32B HBU demonstration cask. The cask and basket are designed to be compatible with typical spent fuel pool loading/unloading methods. The sequential steps to be followed for cask loading, testing, and unloading operations are provided in Chapter 7. The loading operations for this unique cask are summarized below.

Upon arrival at the NAPS in October 2017, the empty cask was inspected. Preparation of the packaging for loading required the cask to be rotated to the vertical orientation, and removed from the shipping frame. A heavy haul transporter was then utilized to move the cask into the spent fuel building of the plant. Access to the cask cavity and fuel basket was obtained by removing the protective cover, loosening and removing the 48 closure lid bolts, and removing the closure lid using standard hoist rings threaded into the lid. The cask was lowered into the cask pit/spent fuel pool. The HBU fuel assemblies were then loaded into specific fuel cell compartments that were selected for positioning each fuel assembly. The six 6 PRAs were installed in the specified fuel assemblies in the array, as well as the funnel guides to assist the installation of the seven thermocouple lance assemblies.

The closure lid was then installed and the cavity vented. The cask was lifted so that the lid was above the surface of the water, and the closure lid bolts/washers were installed hand tight. The cask was then moved from the cask pit/spent fuel pool to the decontamination area. The closure lid bolts and washers were tightened to the specified torque. At this point, the thermocouple lance assemblies were installed, secured to the closure lid, and sealed. The cask cavity was dried utilizing a vacuum system, and then back-filled with helium gas. The closure lid seals, the penetration cover seals, and the thermocouple lance assembly seals were leakage rate tested. Following a thermal soaking period, the TN-32B HBU demonstration cask was transported to the NAPS ISFSI site for the planned 5.87-year storage period, which commenced in November 2017. When transported off site, the external surface radiation and contamination levels will be verified to ensure that the levels are within regulatory transportation limits.

### 1.3 References

1. Title 10, Code of Federal Regulations - Energy, Part 71 (10 CFR 71), "Packaging and Transportation of Radioactive Material," 1-1-2021 Edition, U.S. Nuclear Regulatory Commission, Washington, D.C.
2. U.S. NRC Regulatory Guide 7.9, "Standard Format and Content of Part 71 Applications for Approval of Packages for Radioactive Material," Revision 2, March 2005.
3. Title 10, Code of Federal Regulations - Energy, Part 72 (10 CFR 72), "Licensing Requirements for the Independent Storage of Spent Nuclear Fuel and High-Level Radioactive Waste," 1-1-2021 Edition, U.S. Nuclear Regulatory Commission, Washington, D.C.
4. American Society of Mechanical Engineers, ASME Boiler and Pressure Vessel Code, Section III, "Rules for Construction of Nuclear Facility Components," 1992 Edition.
5. U.S. NRC Regulatory Guide 7.6, "Design Criteria for the Structural Analysis of Shipping Cask Containment Vessel," Revision 1, March 1978.
6. U.S. NRC Regulatory Guide 7.8, "Load Combinations for the Structural Analysis of Shipping Cask," Revision 1, March 1989.
7. TN Americas, LLC, "TN-32B HBU Demonstration Cask Design/Licensing Basis Document," Revision 8, Document No. E-42038, dated March 2017.
8. American Society of Mechanical Engineers, ASME Boiler and Pressure Vessel Code, Section III, "Rules for Construction of Nuclear Facility Components," Subsection NF, 1992 Edition.

**Table 1-1**  
**Dimensions and Weights of the TN-32B HBU Demonstration Cask**

Overall nominal length (with impact limiters, inch)	263.2
Overall length (w/o impact limiters, puncture resistant and lance cover plates, inch)	184.3 (184.0)
Impact limiter outside nominal diameter (inch)	144.0
Outside diameter (without impact limiters, inch)	98.14 (97.75)
Cavity diameter (inch)	68.80 (68.75)
Cavity length (inch)	163.38 (163.25)
Containment shell side thickness (inch)	1.53 (1.50)
Containment shell bottom thickness (inch)	1.63 (1.50)
Body wall thickness (inch)	9.58 (9.50)
Containment lid nominal plate thickness (inch)	4.50
Overall closure lid nominal thickness (inch)	10.50
Bottom thickness (inch)	10.38 (10.25)
Resin and aluminum box nominal thickness (inch)	4.50
Neutron shield outer shell plate nominal thickness (inch)	0.50
Overall basket nominal length (inch)	160.00
Weight of fuel assemblies (with PRAs) (kips)	49.64
Loaded weight of TN-32B HBU demonstration cask (w/o impact limiters, puncture resistant plate, brackets, tie-rods/hardware) (kips)	229.72
Weight of impact limiters, puncture resistant plate, brackets, and tie-rods (kips)	39.28
Total loaded weight of TN-32B HBU demonstration cask (w/o shipping skid) (kips)	269.00

Note: Listed dimensions are as-built dimensions for this cask with the corresponding nominal dimensions presented in parentheses.

**Table 1-2**  
**TN-32B HBU Demonstration Cask Fuel Data**

Description	Value		
	AMBW	LOPAR	NAIF
Top nozzle inside height to corner post, inch	2.842	2.842 – 3.000	
Length between top of inner flat part of top nozzle to top of bottom end plug, inch	152.5 – 153.8		
Fuel assembly max length, inch	159.85	159.765	159.975
Fuel assembly max width, inch	8.425	8.426	
Fuel density, % theoretical	96.0%	95.0%	≤ 96.0%
Fuel rod pitch, inch	0.496		
Number of fuel rods	264		
Maximum uranium weight per fuel assembly, kg	469	467	467
Fuel assembly max growth, end of life, inch	0.611		
Guide tube outside diameter, inch	0.482	0.482	0.474
Guide tube wall thickness, inch	0.016		
Guide tube radial centerline spacing, inch	1.488		
Number of guide tubes	24		
Instrumentation tube outside diameter, inch	≤ 0.482		
Instrumentation tube wall thickness, inch	0.016	≤ 0.016	
Number of instrumentation tubes	1		
Fuel rod cladding thickness, inch	0.0225	≤ 0.0225	≤ 0.0225
Active fuel column length, inch	144		
Fuel rod diameter, inch	0.374	≤ 0.374	≤ 0.374
Maximum fuel assembly dry weight, lb	1,488		
Cladding material	M5™ (Zircaloy)	Zirc-4 (similar to Zr alloy)	Low-tin Zirc-4, Zirc-4, or Zirlo™ (similar to Zr alloy)
Top nozzle material	Type 304 SS	Similar to 300 series SS	
Fuel assembly overall length including non-compressed hold down springs, inch	161.62	161.50 – 162.00	

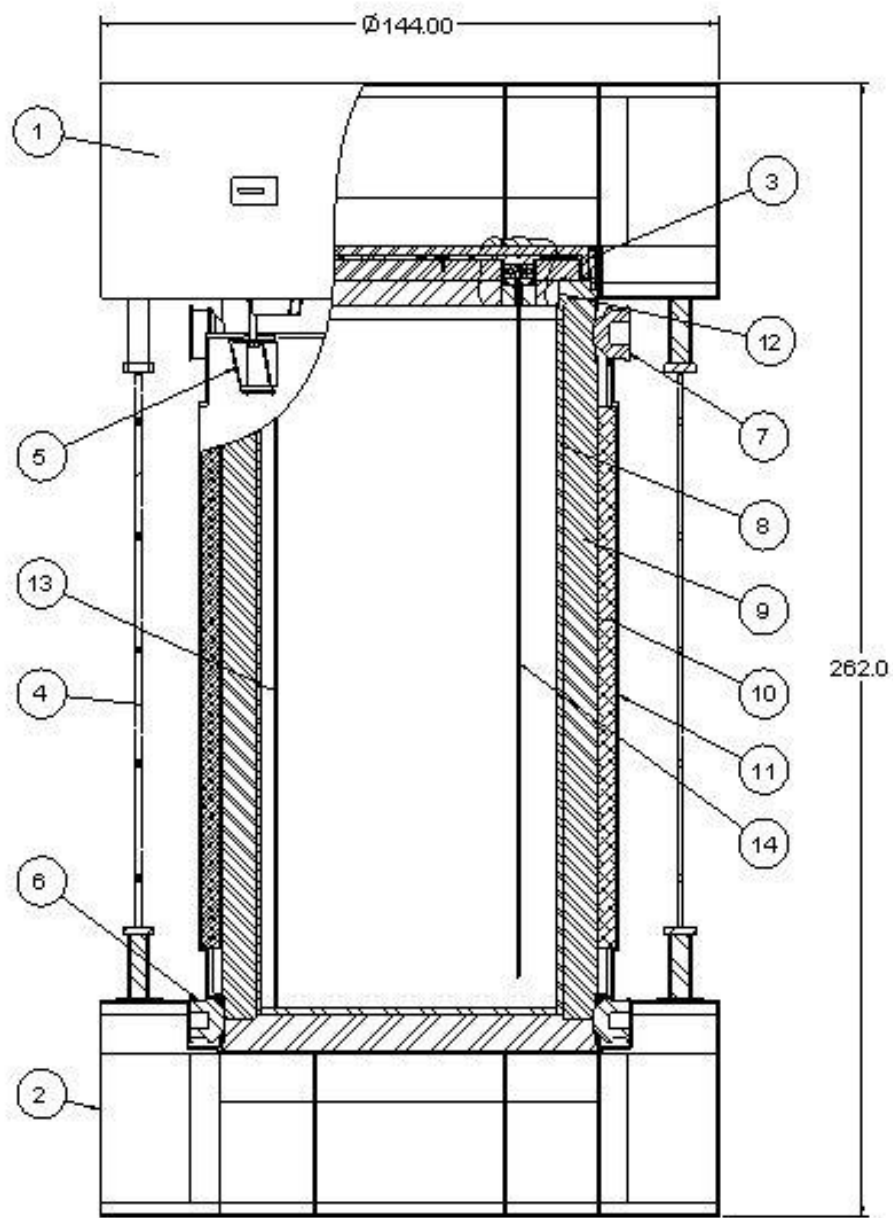


**Figure 1-1**  
**General Arrangement, TN-32B HBU Demonstration Cask**

## Notes to Figure 1-1

- A. Some details exaggerated for clarity.
- B. Components are listed below:
  - 1 Upper (front) Impact Limiter
  - 2 Lower (rear) Impact Limiter
  - 3 Puncture Resistant Plate
  - 4 Tie-Rod
  - 5 Impact Limiter Bolting & Bracket
  - 6 Lower Trunnions
  - 7 Upper Trunnions
  - 8 Containment Shell (Inner Shell & Bottom Inner Plate)
  - 9 Cask Body (Gamma Shield Shell & Bottom Shield)
  - 10 Radial Neutron Shielding
  - 11 Outer Shell
  - 12 Closure Lid Assembly
  - 13 Drain Tube
  - 14 Thermocouple Lance Assembly



## 1.4 Appendices

### 1.4.1 General Arrangement Drawings

The following TN Americas drawings are enclosed:

<b>Drawing No</b>	<b>Title</b>
19885-71-1	TN-32B HBU Demonstration Cask, General Arrangement Assembly
19885-71-2	TN-32B HBU Demonstration Cask, General Assembly
19885-71-3	TN-32B HBU Demonstration Cask, Lid Assembly and Parts List
19885-71-4	TN-32B HBU Demonstration Cask, Puncture Resistant Plate Assembly
19885-71-5	TN-32B HBU Demonstration Cask, Trunnion Details
19885-71-6	TN-32B HBU Demonstration Cask, Basket Assembly and Parts List
19885-71-7	TN-32B HBU Demonstration Cask, Thermocouple Lance Assembly, Lance Cover Plate
19885-71-8	TN-32B HBU Demonstration Cask, General Assembly, Impact Limiters
19885-71-9	TN-32B HBU Demonstration Cask, Bottom Impact Limiter Assembly
19885-71-10	TN-32B HBU Demonstration Cask, Top Impact Limiter Assembly

**Proprietary and Security Related Information  
for Drawing 19885-71-1, Rev. 0A  
Withheld Pursuant to 10 CFR 2.390**

**Proprietary and Security Related Information  
for Drawing 19885-71-2, Rev. 0A  
Withheld Pursuant to 10 CFR 2.390**

**Proprietary and Security Related Information  
for Drawing 19885-71-3, Rev. 0A  
Withheld Pursuant to 10 CFR 2.390**

**Proprietary and Security Related Information  
for Drawing 19885-71-4, Rev. 0A  
Withheld Pursuant to 10 CFR 2.390**

**Proprietary and Security Related Information  
for Drawing 19885-71-5, Rev. 0A  
Withheld Pursuant to 10 CFR 2.390**

**Proprietary and Security Related Information  
for Drawing 19885-71-6, Rev. 0A  
Withheld Pursuant to 10 CFR 2.390**

**Proprietary and Security Related Information  
for Drawing 19885-71-7, Rev. 0A  
Withheld Pursuant to 10 CFR 2.390**



**Proprietary and Security Related Information  
for Drawing 19885-71-8, Rev. 0A  
Withheld Pursuant to 10 CFR 2.390**

**Proprietary and Security Related Information  
for Drawing 19885-71-9, Rev. 0A  
Withheld Pursuant to 10 CFR 2.390**

**Proprietary and Security Related Information  
for Drawing 19885-71-10, Rev. 0A  
Withheld Pursuant to 10 CFR 2.390**

## Chapter 2 Structural Evaluation

### TABLE OF CONTENTS

2.1	Description of Structural Design .....	2-1
2.1.1	Discussion .....	2-1
2.1.2	Design Criteria .....	2-3
2.1.3	Weights and Centers of Gravity .....	2-7
2.1.4	Identification of Codes and Standards for Package Design .....	2-7
2.2	Materials.....	2-8
2.2.1	Material Properties and Specifications .....	2-8
2.2.2	Chemical, Galvanic, or Other Reactions .....	2-8
2.2.3	Effects of Radiation on Materials.....	2-9
2.2.4	Fracture Toughness Requirements .....	2-9
2.3	Fabrication and Examination .....	2-10
2.3.1	Fabrication .....	2-10
2.3.2	Examination .....	2-10
2.4	General Standards for All Packages .....	2-11
2.4.1	Minimum Package Size.....	2-11
2.4.2	Tamper-Indicating Feature.....	2-11
2.4.3	Positive Closure .....	2-11
2.4.4	Chemical and Galvanic Reactions .....	2-11
2.5	Lifting and Tie-Down Standards for All Packages .....	2-14
2.5.1	Lifting Devices .....	2-14
2.5.2	Tie-Down Devices.....	2-19
2.6	Normal Conditions of Transport.....	2-20
2.6.1	Heat.....	2-21
2.6.2	Cold .....	2-22
2.6.3	Reduced External Pressure (N5) .....	2-23
2.6.4	Increased External Pressure (N4) .....	2-23
2.6.5	Vibration .....	2-23
2.6.6	Water Spray.....	2-24
2.6.7	Free Drop .....	2-25
2.6.8	Corner Drop.....	2-25
2.6.9	Compression.....	2-25

2.6.10	Penetration .....	2-25
2.6.11	Lid Bolt Analysis .....	2-25
2.6.12	Fatigue Analysis of the Containment Boundary.....	2-26
2.6.13	Structural Evaluation of the Basket under Normal Condition Loads .....	2-29
2.6.14	Summary of NCT Cask Body Structural Analysis .....	2-30
2.7	Hypothetical Accident Conditions .....	2-31
2.7.1	30 Foot Free Drop.....	2-32
2.7.2	Crush .....	2-36
2.7.3	Puncture .....	2-36
2.7.4	Thermal .....	2-40
2.7.5	Immersion – Fissile material .....	2-41
2.7.6	Immersion – All Packages.....	2-41
2.7.7	Deep Water Immersion Test (for Type B Packages Containing More than 105 A2).....	2-41
2.7.8	Summary of Damage .....	2-43
2.8	Accident Conditions for Air Transport of Plutonium.....	2-44
2.9	Accident Conditions for Fissile Material Packages for Air Transport .....	2-44
2.10	Special Form .....	2-44
2.11	Fuel Rods.....	2-44
2.12	Appendices .....	2-23

LIST OF TABLES

Table 2-1	Evaluation Method Employed to Demonstrate Compliance with Specific Regulatory Requirements .....	2-45
Table 2-2	Containment Vessel Stress Limits.....	2-46
Table 2-3	Containment Bolt Stress Limits .....	2-46
Table 2-4	Non Containment Structure Stress Limits .....	2-47
Table 2-5	Basket Stress Limits .....	2-48
Table 2-6	Cask Material Properties <sup>(1)</sup> .....	2-49
Table 2-7	Cask Weight and Center of Gravity .....	2-52
Table 2-8	Trunnion Section Properties and Applied Loads .....	2-53
Table 2-9	Trunnion Stresses when Loaded by Factors 6 and 10 of Cask Weight (Lifting).....	2-54
Table 2-10	TN-32B HBU Cask Performance Evaluation Overview (Normal Conditions of Transport).....	2-55
Table 2-11	Individual Load Cases for Normal Conditions of Transport TN-32B HBU Demonstration Cask Body Analysis.....	2-56
Table 2-12	Summary of Load Combinations for Normal Conditions of Transport .....	2-57
Table 2-13	Reference Temperatures for Stress Analysis Acceptance Criteria .....	2-59
Table 2-14	NCT Load Combinations – Lid Stress Intensity Results .....	2-60
Table 2-15	NCT Load Combinations – Penetration Sleeves Stress Intensity Results.....	2-62
Table 2-16	NCT Load Combinations – Gamma Shield Shell Stress Intensity Results.....	2-63
Table 2-17	NCT Load Combinations – Closure Lid Shield Plate Stress Intensity Results.....	2-64
Table 2-18	NCT Load Combinations – Shell Flange Stress Intensity Results .....	2-65
Table 2-19	TN-32B HBU Performance Evaluation Overview (Hypothetical Accident Conditions of Transport) .....	2-66
Table 2-20	Summary of Individual Loads for Hypothetical Accident Conditions of Transport .....	2-67
Table 2-21	Summary of Load Combinations for Hypothetical Accident Conditions of Transport .....	2-68
Table 2-22	HAC Load Combinations – Lid Stress Intensity Results .....	2-69
Table 2-23	HAC Load Combinations – Penetration Sleeves Stress Intensity Results.....	2-71
Table 2-24	HAC Load Combinations – Gamma Shield Shell Stress Intensity Results.....	2-72
Table 2-25	HAC Load Combinations – Bottom Shield Plate Stress Intensity Results.....	2-73

Table 2-26	HAC Load Combinations – Bottom Inner Plate Stress Intensity Results.....	2-74
Table 2-27	HAC Load Combinations – Inner Shell Stress Intensity Results .....	2-75
Table 2-28	HAC Load Combinations – Top Shield Plate Stress Intensity Results .....	2-76
Table 2-29	HAC Load Combinations – Shell Flange Stress Intensity Results .....	2-77

#### LIST OF FIGURES

Figure 2-1	Geometry of Upper (front) and Lower (rear) Trunnions .....	2-78
Figure 2-2	Nonlinear Buckling Finite Element Model for Immersion Analysis .....	2-79
Figure 2-3	290 psig Immersion Analysis Finite Element Model Loads and Boundary Conditions.....	2-80

## **Chapter 2 Structural Evaluation**

### **2.1 Description of Structural Design**

This chapter, including its appendices, presents the structural evaluations that demonstrate the TN-32B HBU demonstration cask meets all of the applicable structural criteria. Normal conditions of transport (NCT) and hypothetical accident condition (HAC) evaluations, utilizing analytical and empirical techniques that comply with the methodology presented in NRC Regulatory Guides 7.6 [1] and 7.8 [2]. These evaluations also consist of bench-marking to impact limiter testing that demonstrate that the TN-32B HBU demonstration cask satisfies applicable requirements for a Type B(U) packaging.

#### **2.1.1 Discussion**

The structural integrity of the packaging under NCT and HAC specified in 10 CFR Part 71 [3] is demonstrated to meet the design criteria described in Section 2.1.2. The TN-32B HBU demonstration cask consists of three major structural components: the cask body, the fuel basket, and the impact limiters (top and bottom). These components are described in Chapter 1, and are shown on drawings provided in Appendix 1.4.1.

The cask body is described in Section 1.2. Drawing 19885-71-1 illustrates the general arrangement for transport. Drawing 19885-71-2 illustrates the overall assembly of the TN-32B HBU demonstration cask package. Drawing 19885-71-3 present the closure lid assembly and details. Drawing 19885-71-4 illustrates the puncture resistant plate assembly, and Drawing 19885-71-5 illustrates the trunnion/basket rails/neutron shield details. Drawing 19885-71-6 illustrates the basket assembly and parts list. Drawing 19885-71-7 provide the details for the thermocouple lance assemblies, the lance cover plate, and parts list. Drawings 19885-71-8 through 19885-71-10 provide details of the impact limiter design. The regulatory plate is specified on Drawing 19885-71-2.

The inner containment shell, the bottom inner containment plate, and the closure lid outer plate are constructed from SA-203, Grade D material. The material for the inner shell flange and thermocouple penetration sleeve forgings is SA-350 Grade LF3. The thermocouple lance assembly materials are Type 304/304L austenitic stainless steel and Inconel (UNS N06600). The closure lid shield plate and the bottom shield are constructed from SA-516, Grade 70 carbon steel plate. The gamma shield is SA-266 Grade 2 carbon steel material.

In order to obtain a close fit between the inner shell and the gamma shield shell, for better heat transfer, the gamma shield shell was heated prior to assembling it with the inner shell. The inner shell flange was then circumferentially welded to the gamma shield shell with a 1/2-inch groove weld.



The four upper and lower trunnions are cylindrical, SA-105 forgings that are welded to the gamma shield shell of the cask body. The two upper trunnions are designed to lift the loaded TN-32B HBU demonstration cask. The lower trunnions provide the capability to rotate the cask on the upending/downending frame. The trunnions are shown in Drawing 19885-71-5.

The outer shell around the neutron shield consists of a cylindrical shell section, with closure plates at each end of the neutron shield. The closure plates are welded to the outer surface of the gamma shield shell. The outer shell provides an enclosure for the resin-filled aluminum containers, and maintains the resin in the proper location with respect to the active length of the fuel assemblies in the cask cavity.

The basket is a welded assembly of stainless steel fuel compartment boxes, and is designed to accommodate 32 fuel assemblies. The fuel compartment stainless steel box sections are attached together locally by cylindrical stainless steel plugs (that pass through the aluminum and borated plates) that are fusion welded to the adjacent box sections. The basket contains 32 compartments for proper spacing and support of the fuel assemblies. Neutron poison plates, constructed from borated aluminum, are sandwiched between the sections of the stainless steel walls of the adjacent box and the adjacent stainless steel plates. Drawing 19885-71-6 provide details of the basket assembly.

Structural rails oriented parallel to the axis of the cask are attached to the inner surface of the inner shell to establish and maintain basket orientation, to prevent twisting of the basket assembly, and to support the edges of those plates adjacent to the rails, which would otherwise be free to slide tangentially around the cask cavity wall under lateral inertial loadings.

The cask body and the fuel basket together with the two impact limiters, form the packaging which is designed to meet all of the applicable 10 CFR Part 71 requirements for a Type B(U) packaging. The maximum normal operating pressure (MNOP) is 30.5 psig.

The wall thickness of the cask body (excluding the outer shell and outer shell closure plates) enables the packaging to withstand the hypothetical puncture accident. The top and bottom impact limiters absorb the kinetic energy for the 1-foot NCT and the 30-foot HAC free drops.

Table 2-1 summarizes the specific evaluation methods that are used to demonstrate compliance with the regulations. Numerical analyses have been performed for the NCT and HAC event, as well as for the lifting and tie-down loads. In general, numerical analyses have been performed for all of the regulatory events. These analyses are summarized in the main body of this section, and are described in detail in Appendices 2.12.2 through 2.12.12. Testing of one-third scale impact limiters has been performed to benchmark the design basis impact loads utilized in the structural analyses of the TN-32B HBU demonstration cask. The results of the testing are provided for reference in Appendix 2.12.10.

The detailed structural analyses of the TN-32B HBU demonstration cask are included in the following appendices:

- Appendix 2.12.2 Structural Analysis of Cask Body
- Appendix 2.12.3 Closure Lid Bolt Analysis
- Appendix 2.12.4 Structural Analysis of the Outer Shell
- Appendix 2.12.5 Fracture Toughness Evaluation of the TN-32B HBU Cask
- Appendix 2.12.6 Structural Analysis of the TN-32B HBU Cask Basket
- Appendix 2.12.7 Dynamic Load Factor for Basket Drop Analysis
- Appendix 2.12.8 Structural Evaluation of the Fuel Rod Cladding under Accident Impact
- Appendix 2.12.9 Structural Analysis of the Impact Limiters
- Appendix 2.12.10 TN-40 Package Impact Limiter Testing
- Appendix 2.12.11 Deep Water Immersion
- Appendix 2.12.12 Structural Analysis of Thermocouple Lance Assembly
- Appendix 2.12.13 ASME B&PV Code Alternatives

## 2.1.2 Design Criteria

The packaging consists of three major components:

- Cask Body
- Fuel Basket
- Impact Limiters

The structural design criteria for these components are described below.

### 2.1.2.1 Cask Body

#### 2.1.2.1.1 Containment Vessel

The containment vessel consists of the inner shell with the shell flange out to the seal seating surface, the bottom inner plate, and the closure lid. The closure lid bolts and seals are also part of the containment vessel as are the drain and vent port cover plates, bolts and seals, and the thermocouple lance assemblies and seals. The containment vessel was designed to the maximum practical extent as an ASME Class I component in accordance with the rules of the ASME Boiler and Pressure Vessel Code, Section III, Subsection NB [3]. The Subsection NB rules for materials, design, fabrication, and examination are applied to all of the above components to the maximum practical extent. In addition, the design meets the requirements of Regulatory Guides 7.6 and 7.8. Alternatives to the ASME Code are discussed in Appendix 2.12.13.

The acceptability of the containment vessel under the applied loads is based on the following criteria:

- Title 10, Energy, Code of Federal Regulations, Chapter I, Part 71
- Regulatory Guide 7.6, Design Criteria
- ASME B&PV Code Design Stress Intensity Limits
- Preclusion of Fatigue Failure
- Preclusion of Brittle Fracture

The stresses due to each load are categorized as to the type of stress induced (e.g., membrane, bending) and the classification of stress (e.g., primary, secondary). Stress limits for containment vessel components, other than bolts, for NCT and HAC loads are provided in Table 2-2. The stress limits used for HAC conditions, determined on an elastic basis, are based on the entire structure (containment vessel and gamma shielding material) resisting the accident load. Local yielding is permitted at the point of contact where the load is applied.

The primary membrane stresses and primary membrane-plus-bending stresses in the cask are limited under NCT to  $S_m$  ( $S_m$  is the code allowable stress intensity) and  $1.5 S_m$ , respectively.

The HAC impact events are evaluated as short duration, Level D conditions. The stress criteria are extracted from Section III, Appendix F of the ASME B&PV Code [3]. As a nonlinear elastic-plastic analysis of the basket is utilized for HAC, the primary membrane stress intensity  $P_m$  is limited to the greater of  $0.7 S_u$  and  $S_y + 1/2(S_u - S_y)$ . The membrane plus bending stress intensity  $P_m + P_b$  is limited to  $0.9 S_u$ . For the containment vessel components, the HAC stress limits are specified in Table 2-2.

The allowable stress limits for the containment bolts are listed in Table 2-3. The allowable stress limits for the closure lid bolts are listed separately in Appendix 2.12.3, Tables 2.12.3-3 and 2.12.3-4.

The allowable stress intensity values  $S_m$  or  $S_u$  as defined by the ASME B&PV Code, are selected at the maximum component temperature calculated for each service load condition.

The welding procedures, welders and weld operators were qualified in accordance with Section IX of the ASME B&PV Code [5].

#### 2.1.2.1.2 Non-Containment Structure

Certain components of the cask body such as the gamma shield shell, the neutron shield outer shell and the trunnions, do not provide containment, but do have structural functions. These components (referred to as non-containment structures) are required to withstand the environmental loads, and in some cases, share the loads with the containment vessel. The stress limits for these non-containment structures are provided in Table 2-4. The gamma shield shell and neutron shield outer shell were designed, fabricated, and inspected in accordance with the ASME B&PV Code, Subsection NF [6], to the maximum practical extent. Structural and structural attachment welds were examined by the liquid penetrant or the magnetic particle method, in accordance with Section V, Article 6 of the ASME B&PV Code [7]. The magnetic particle and liquid penetrant examination acceptance standards are in accordance with Section III, Subsection NF, Paragraphs NF-5340 and NF-5350 [6].

The welding procedures, welders and weld operators were qualified in accordance with Section IX of the ASME B&PV Code [5].

The radial neutron shield, including the carbon steel outer shell, has not been designed to withstand all of the HAC loads.

#### 2.1.2.2 Basket

The basket is designed in accordance with the ASME B&PV Code, Section III, Subsections NB [4] and NF [6], to the maximum practical extent. The TN-32B HBU demonstration cask was developed as a storage cask, and as such, the basket and containment were designed utilizing the stress limits from ASME B&PV Code, Section III, Subsection NB. NCT stress limits specified in Subsection NB are the same as Subsection NG, which is currently used for transportation packages. For HAC, both Subsections NB and NG require utilization of Appendix F for the stress limits. Therefore, the basket design meets the NG stress limits, as specified in the Standard Review Plan [8]. The alternatives to ASME B&PV Code requirements are listed in Appendix 2.12.13.

The neutron poison sheets are not included in the structural analysis. Therefore, the materials are not required to be ASME B&PV Code materials. The aluminum plates between the fuel compartments and aluminum basket rails are not ASME Class 1 material. Aluminum was selected for its excellent thermal conductivity and a high strength-to-weight ratio. Reference [8] and Reference [9] allow materials other than ASME Code materials to be used in the cask fabrication. The ASME B&PV Code does provide the material properties for the aluminum alloy, and also permits the material to be utilized for Section III applications (Class 2 or 3).

The stress limits for the basket are summarized in Table 2-5. The wall thickness of the basket fuel compartment is designed to satisfy the heat transfer, nuclear criticality, and the structural requirements. The basket structure provides sufficient rigidity to maintain a subcritical configuration under the applied loads.

The basis for the allowable stresses for the compartment box and the fusion welds is Section III, Division I, Subsection NB of the ASME B&PV Code [3]. The primary membrane stresses and primary membrane-plus-bending stresses in the basket are limited to  $S_m$  ( $S_m$  is the code allowable stress intensity) and  $1.5 S_m$ , respectively, for NCT loads.

The HAC events are evaluated as short duration, Level D condition. The stress criteria are extracted from Section III, Appendix F of the ASME B&PV Code [3]. The membrane and membrane plus bending stresses were compared against greater of  $0.7 S_u$  and  $S_y + 1/3(S_u - S_y)$  and  $0.9 S_u$  elastic-plastic analysis stress criteria values for the HAC drop events.

The fuel compartment walls under compressive loads are also evaluated to ensure that buckling will not occur. ANSYS® nonlinear buckling analysis is used to calculate the buckling load. Refer to Appendix 2.12.6 for complete details of criteria for these conditions.

The fusion welds in the basket are not code welds (alternative to codes are listed in Appendix 2.12.13). The fusion welds are qualified by testing. The testing program ensures that the fusion welds are stronger than the base metal. Additionally, it is shown that the maximum stress in the base metal is lower than the ASME Subsection NB (identical to NG) allowable stress thus, basket integrity is maintained, and the welds are qualified. The testing program is described in Section 2.12.6.4 of Appendix 2.12.6.

#### 2.1.2.3 Impact Limiters (Top and Bottom)

The TN-32B HBU demonstration cask includes impact limiters at each end of the cask body. The limiters are nearly identical. The inside diameter of the limiter is determined by the diameter of the gamma shield shell. The length and outside diameter of the limiter are sized to limit the cask inertial loads during the 1-foot NCT and 30-foot HAC free drop events so that the containment vessel (and the non-containment structures) satisfies the design criteria.

The impact limiter stainless steel shells, gussets, and end plates are designed to position and confine the redwood and balsa wood blocks so that the impact energy is properly absorbed. The stainless steel shell is also designed to support and protect the wood blocks under NCT environmental conditions (moisture, pressure, temperature, etc.).

The impact limiters and attachments are designed to withstand the applied loads and to prevent separation of the limiters from the cask during any NCT or HAC impact event. The design criteria for the impact limiters and attachments are specified in Appendix 2.12.9.

#### 2.1.2.4 Trunnions

The evaluation and design criteria for the lifting trunnions are based on the requirements of 10 CFR 71.45 [3]. The details of the evaluation are presented in Section 2.5. The evaluation demonstrates that the upper trunnions, used for lifting, have a minimum factor of safety of six against yield or ten against ultimate, whichever is most restrictive. These design loads exceed the 10 CFR 71.45(a) requirements.

#### 2.1.3 Weights and Centers of Gravity

The gross weight of the TN-32B HBU demonstration cask is 269 kips. The weights of the major individual subassemblies are listed in Table 2-7. The center of gravity of the cask is located approximately 93.7 inches from the base of the cask body along the axial centerline.

The calculations that follow typically use conservative weights that are slightly higher than those listed in Table 2-7. These are:

1. Lifting (w/o impact limiters), 240 kips
2. Tie-down analyses, 270 kips
3. Cask body analysis 271 kips

#### 2.1.4 Identification of Codes and Standards for Package Design

The cask containment boundary was designed, fabricated, and inspected in accordance with Subsection NB of the ASME B&PV Code to the maximum practical extent. The basket was designed, fabricated, and inspected in accordance with Subsection NB/NF of the ASME B&PV Code to the maximum practical extent. The ASME code alternatives for the cask, basket, and thermocouple lance assemblies are specified in Appendix 2.12.13.

## 2.2 Materials

### 2.2.1 Material Properties and Specifications

This section provides the mechanical properties of materials utilized in the structural evaluation of the TN-32B HBU demonstration cask. Drawings 19885-71-2 through 19885-71-7 (refer to Appendix 1.4.1) list the materials selected for each component of the transport cask. Table 2-6 lists the minimum yield, ultimate, and design stress values specified by the ASME B&PV Code, Section II, Part D [10] [11].

Mechanical properties of the energy absorbing redwood and balsa wood used in the impact limiters are specified in Table 2.12.9-3 of Appendix 2.12.9.

### 2.2.2 Chemical, Galvanic, or Other Reactions

The materials of the TN-32B HBU demonstration cask have been reviewed to determine whether chemical, galvanic or other reactions between the materials, contents and environment might occur during any phase of loading, unloading, handling or transport.

The TN-32B HBU demonstration cask components are exposed to the following environments:

- During loading, the cask was submerged in pool water, which is borated. The cask was only maintained in the spent fuel pool for approximately 12 hours to load the HBU fuel assemblies. After removing the cask from the pool, water or water vapor was present during installation of the thermocouple lance assemblies, and the draining and drying process. This process required approximately 36 hours to install the seven thermocouple lance assemblies, drain the cask cavity, and completely dry, evacuate, and backfill the cavity with helium.
- During handling and transport to/storage on the independent spent fuel storage installation (ISFSI) pad, the exterior of the cask was exposed to normal environmental conditions of temperature, rain, snow, etc.
- During transportation, the cask cavity is exposed to an inert helium environment. The helium environment does not support chemical or galvanic reactions because both moisture and oxygen must be present for a reaction to occur. The cask was thoroughly dried by a vacuum drying process, sealed, and backfilled with helium gas during loading in November 2017.
- The radial neutron shielding materials and the aluminum resin boxes are sealed inside the outer shell for normal operations. The resin material is inert after it has cured and does not affect the aluminum boxes or the carbon steel housing.

The material properties of the Type 304/304L stainless steel plates are extracted from the ASME B&PV Code, Section II, Part D. The material properties of the aluminum alloy (6061-T6) are also extracted from the ASME B&PV Code [10] [11], and aluminum standards and data [12].

### 2.2.3 Effects of Radiation on Materials

Gamma radiation has no significant effect on metals. The effect of fast neutron irradiation of metals is a function of the integrated fast neutron flux. Studies on fast neutron damage in aluminum, stainless steel, and low alloy steels rarely evaluate damage below  $10^{17}$  n/cm<sup>2</sup> because it is not significant. Extrapolation of the data available down to the  $10^{14}$  n/cm<sup>2</sup> range confirms that there will be virtually no neutron damage to any of the cask metallic components.

The neutron absorbers consist of aluminum with boron added in the form of boron carbide. The durability of this material in the radiation environment is similar to aluminum, which has been demonstrated over many years in service for spent nuclear fuel storage systems and transportation casks.

Radiation levels and temperature on the cask exterior surface are not sufficiently high to damage the paint. This fact is confirmed by dry cask experience. Paint is also subject to routine maintenance and touch-up during the cask storage period and prior to being transported from the ISFSI site.

#### **Seals**

There is no significant degradation of the metallic O-ring seals resulting from the effects of long-term exposure to neutron or gamma radiation.

#### **Neutron Shielding**

The radial neutron shield material is a proprietary resin that has been developed and tested for applications, such as the TN-32B HBU demonstration cask. The neutron and gamma fluence expected for this application are below those levels that could degrade the effectiveness of the resin material.

### 2.2.4 Fracture Toughness Requirements

The cask body and closure lid materials are ferritic steels and are, therefore, subject to fracture toughness requirements in order to ensure ductile behavior at the lowest service temperature (LST) of  $-20$  °F. Refer to Appendix 2.12.5 for fracture toughness evaluation. The fracture toughness evaluations in this appendix demonstrate that the TN-32B HBU demonstration cask materials satisfy the fracture toughness criteria of NUREG/CR-3826 [13] and NUREG/CR-1815 [14].



## **2.3 Fabrication and Examination**

### **2.3.1 Fabrication**

Fabrication of the TN-32B HBU demonstration cask was conducted per the requirements of the ASME B&PV Code to the maximum extent possible. Refer to Section 2.1.2 and Section 2.1.4.

### **2.3.2 Examination**

Examination of the TN-32B HBU demonstration cask was conducted per the requirements of the ASME B&PV Code to the maximum extent possible. Refer to Section 2.1.2 and Section 2.1.4.

## 2.4 General Standards for All Packages

The TN-32B HBU demonstration cask is designed to comply with the general standards for all packages specified by 10 CFR 71.43 [3].

### 2.4.1 Minimum Package Size

The overall package dimensions of 263.2 inches long and 144 inches in diameter exceed the minimum dimension requirement of 10 cm (4 inches).

### 2.4.2 Tamper-Indicating Feature

The only access path into the package is through the closure lid and associated lid closure bolts. During transport, the puncture resistant plate and the top (front) impact limiter entirely covers and prevents access to the cask closure lid, and the vent, drain, and access port penetrations in the lid. A wire security seal is installed in the top (front) impact limiter attachment tie-rod prior to shipment. The presence of this seal demonstrates that unauthorized opening of the package has not occurred during transit.

### 2.4.3 Positive Closure

Positive fastening of all access openings through the containment vessel is accomplished by bolted closures which preclude unintentional opening. In addition, the presence of the impact limiters and security seal described in Section 2.4.2 provide further protection against unintentional opening.

### 2.4.4 Chemical and Galvanic Reactions

#### 2.4.4.1 Cask Interior

The TN-32B HBU demonstration cask materials are identified in the Parts List on Drawings 19885-71-2 through 19885-71-7 (refer to Appendix 1.4.1).

The containment vessel is constructed from SA-203 Grade D steel plate, SA-350 Grade LF3 forging, Inconel (UNS N06600), and Type 304/304L stainless steel materials. The vessel interior cavity surfaces were grit blasted, and then coated with an aluminum metal-spray.

The aluminum metal-spray coating is subject to the following service environments:

- After fabrication, the cask was closed and shipped with helium gas in the cask cavity during the extended non-use storage period.
- At fuel loading, borated spent fuel pool water was present in the cavity for 12 hours.
- The cask was vacuum-dried and backfilled with helium gas for the minimum storage period of 5.87 years, and/or off-site transport.

The coating is not subject to abrasion except for the one-time insertion of the basket into the containment vessel.

All sealing surfaces are stainless steel clad by weld overlay. The metallic O-ring seals have a stainless steel liner and a silver jacket.

Within the cask cavity, there are six basket rails constructed from 6061-T6 or -T651 aluminum. The rails are illustrated on the drawings provided in Appendix 1.4.1. These rails are not coated.

The cask basket was assembled from SA-240, Type 304 stainless steel boxes that are joined together by a fusion welding process, and are separated by borated aluminum poison plates, which form a sandwich panel. The aluminum plates are 6061 -T651 aluminum. The aluminum plates are held in place by the stainless steel plugs to which the boxes are welded. The aluminum is not welded or bolted to the stainless steel.

The borated aluminum sheets are also held in place by the stainless steel plugs and are captured between the stainless steel boxes. The borated aluminum is not welded or bolted to the stainless steel.

#### 2.4.4.2 Cask Exterior

The exterior of the cask is carbon steel. The exterior of the cask, with the exception of the trunnion bearing surfaces, was blasted clean, and then painted using an epoxy polysiloxane, or equivalent coating. The paint was selected to be compatible with the pool water, and to be easily decontaminated.

The paint was visually inspected prior to immersion of the cask in the spent fuel pool and prior to transport. Prior to shipping off-site, touch up painting or re-coating is performed if the paint has deteriorated.

#### 2.4.4.3 Lubricants and Cleaning Agents

Loctite N-5000 was utilized to coat the threads of the TN-32B HBU demonstration cask closure lid bolts. Never-Seez or equivalent is used to coat the contact areas of the top and bottom trunnions prior to lifting operations to prevent impregnation of contamination into the trunnion surface. The lubricant was selected for compatibility with the North Anna Power Station spent fuel pool water and the cask materials.

The cask body was cleaned in accordance with approved procedures to remove cleaning residues prior to shipment to the loading site. The basket is also cleaned prior to installation in the cask. The cleaning agents and lubricants have no significant effect on the cask materials and their safety related functions.

#### 2.4.4.4 Hydrogen Generation

Prairie Island's report to the NRC [15] [16] in response to NRC Bulletin 96-04 demonstrates that galvanic reactions in hydrogen generation are insignificant for the TN-40 cask, which is similar to TN-32B HBU demonstration cask. Unlike welded canisters, the TN-32B HBU demonstration cask has a bolted closure. Therefore, there is no source of ignition to result in an explosion or fire.

#### 2.4.4.5 Effect of Galvanic Reactions on the Performance of the Cask

There are no significant reactions that could reduce the overall integrity of the cask or its contents during storage. The cask and fuel cladding thermal properties are provided in Chapter 3. The emissivity of the basket fuel compartment is 0.3, which is typical for non-polished stainless steel surfaces. If the stainless steel is oxidized, this value would increase, improving heat transfer. The fuel rod emissivity value used is 0.8, which is a typical value for oxidized the M5™ (Zircaloy), Zirloy™, Low-Sn Zr-4, and Zirc-4 fuel cladding of the HBU assemblies. Therefore, the passivation reactions would not reduce the thermal properties of the component cask materials or the fuel cladding.

There are no reactions that would cause binding of the mechanical surfaces or the fuel to basket compartment boxes due to galvanic or chemical reactions.

The stainless steel, borated aluminum, and thermal aluminum spray are negligibly affected by the short-term exposure to borated water during loading. While formation of blisters in Boral® during vacuum drying and heating has been reported, this condition has not been associated with displacement of the borated core aluminum material containing the boron carbide and, therefore, has no effect on the boron criticality safety design function. Furthermore, in the TN-32B HBU demonstration cask, the borated aluminum is captured between the structural basket components to provide it with added mechanical support and durability. The outer closure lid seal with a silver jacket will also not experience any combination of crevice and galvanic corrosion when exposed to water for an extended period of storage prior to transport.

There is no significant degradation of any safety components caused directly by the effects of the reactions or by the effects of the reactions combined with the effects of long-term exposure of the materials to neutron or gamma radiation, high temperatures, or other possible ambient or operating conditions.

## 2.5 Lifting and Tie-Down Standards for All Packages

### 2.5.1 Lifting Devices

10 CFR 71.45(a) [3] requires that a minimum factor of safety of three against yield is required for all lifting attachments which are structural parts of the package. In addition, the package must be designed such that failure of any lifting device under excessive load would not impair the ability of the package to meet the requirements of 10 CFR Part 71. The stress analyses of the trunnions are provided in the following section.

#### 2.5.1.1 Trunnion Analysis

The trunnion geometry is shown in Figure 2-1. The front (upper) and rear (lower) trunnions are constructed from SA-105 forging material, and are welded to the cask body with a groove and fillet cover weld. A flat surface is machined on the cask body outer surface at each trunnion location for this purpose.

The following calculation is provided to demonstrate the acceptability of the trunnion design. Additionally, it is shown that the trunnions can be overloaded to failure without compromising the safety of the TN-32B HBU demonstration cask.

The upper trunnions are utilized for vertical lifting of the cask. The total weight of the cask is conservatively assumed to be 240,000 lb<sub>m</sub>. The trunnions are designed to a safety factor of 6 when compared to yield stress and a factor of 10 when compared to ultimate stress. These design loads are very conservative, and exceed the 10 CFR 71.45(a) requirements. The load applied to each upper trunnion is then:

$$F_{Y(UPPER)} = 1/2(6)(240,000) = 720,000 \text{ lb}_f/\text{trunnion}$$

$$F_{U(UPPER)} = 1/2(10)(240,000) = 1,200,000 \text{ lb}_f/\text{trunnion}$$

The two lower trunnions are not used for lifting, but only to support the cask as it is upended or downended. Thus, they are assumed to support 1/2 of the cask weight since the upper trunnions share the load. Therefore, the load of each of the lower trunnions is:

$$F_{Y(LOWER)} = 1/4(6)(240,000) = 360,000 \text{ lb}_f/\text{trunnion}$$

$$F_{U(LOWER)} = 1/4(10)(240,000) = 600,000 \text{ lb}_f/\text{trunnion}$$

#### Upper Trunnions

Using the dimensions shown in Figure 2-1, the cross sectional areas and moments of inertia are:

Section A-A:

$$A_{A-A} = \frac{\pi}{4}(12.0^2 - 5.0^2) = 93.415 \text{ in}^2$$

$$I_{A-A} = \frac{\pi}{64}(12.0^4 - 5.0^4) = 987.20 \text{ in}^4$$

Shoulder Section B-B:

$$A_{B-B} = \frac{\pi}{4} (11.25^2 - 5.0^2) = 79.77 \text{ in}^2$$

$$I_{B-B} = \frac{\pi}{64} (11.25^4 - 5.0^4) = 755.6 \text{ in}^4$$

The lifting force applied to the upper trunnion results in a shear load and a bending moment at Sections A-A and B-B.

For Section A-A, the moment arm,  $L_{A-A}$ , is 5.58 inch. For Section B-B, the moment arm,  $L_{B-B}$ , is 1.75 inch.

For the 6 times lift evaluation, the loads at the respective cross-sections are:

$$F_{6x} = 720,000 \text{ lb}_f$$

$$M_{6x \text{ A-A}} = 720,000(5.58) = 4,017,600 \text{ lb}_f\text{-in}$$

$$M_{6x \text{ B-B}} = 720,000(1.75) = 1,260,000 \text{ lb}_f\text{-in}$$

For the 10 times lift evaluation, the loads at the respective cross-sections are:

$$F_{10x} = 1,200,000 \text{ lb}_f$$

$$M_{10x \text{ A-A}} = 1,200,000(5.58) = 6,696,000 \text{ lb}_f\text{-in}$$

$$M_{10x \text{ B-B}} = 1,200,000(1.75) = 2,100,000 \text{ lb}_f\text{-in}$$

### Lower Trunnions

Cross-sectional areas and moments of inertia of the lower trunnions can be calculated using the dimensions provided in Figure 2-1:

Section A-A:

$$A_{A-A} = \frac{\pi}{4} (10.0^2 - 5.0^2) = 58.91 \text{ in}^2$$

$$I_{A-A} = \frac{\pi}{64} (10.0^4 - 5.0^4) = 460.19 \text{ in}^4$$

Shoulder Section B-B:

$$A_{B-B} = \frac{\pi}{4} (8.67^2 - 4.0^2) = 46.47 \text{ in}^2$$

$$I_{B-B} = \frac{\pi}{64} (8.67^4 - 4.0^4) = 264.80 \text{ in}^4$$

The supporting force applied to the lower trunnion results in a shear load and a bending moment at Sections A-A and B-B.

For Section A-A, the moment arm,  $L_{A-A}$ , is 5.58 inches. For Section B-B, the moment arm,  $L_{BB}$ , is 1.75 inches.

For the 6 times lift evaluation, the applied loads at the respective cross sections are:

$$\begin{aligned} F_{6x} &= 360,000 \text{ lb}_f \\ M_{6x \text{ A-A}} &= 360,000(5.58) = 2,008,800 \text{ lb}_f\text{-in} \\ M_{6x \text{ B-B}} &= 360,000(1.75) = 630,000 \text{ lb}_f\text{-in} \end{aligned}$$

For the 10 times lift evaluation, the loads at the respective cross sections are:

$$\begin{aligned} F_{10x} &= 600,000 \text{ lb}_f \\ M_{10x \text{ A-A}} &= 600,000(5.58) = 3,348,000 \text{ lb}_f\text{-in} \\ M_{10x \text{ B-B}} &= 600,000(1.75) = 1,050,000 \text{ lb}_f\text{-in} \end{aligned}$$

The section properties and applied loads calculated above are summarized in Table 2-8.

### Stress evaluation

#### Upper Trunnions

For the factor of 6 lifting load at Section A-A, the shear ( $\tau_{A-A}$ ) and bending ( $\sigma_{B,A-A}$ ) stresses, and the stress intensity ( $S_{A-A}$ ) are:

$$\begin{aligned} \tau_{A-A} &= \frac{720,000}{93.415} = 7,708 \text{ psi} \\ \sigma_{B,A-A} &= \frac{4,017,600(6.0)}{987.2} = 24,418 \text{ psi} \\ S_{A-A} &= \left[ (24,418)^2 + 4(7,708)^2 \right]^{1/2} = 28,877 \text{ psi} \end{aligned}$$

For the factor of 6 lifting load at Section B-B, the stresses are:

$$\begin{aligned} \tau_{B-B} &= \frac{720,000}{79.77} = 9,026 \text{ psi} \\ \sigma_{B,B-B} &= \frac{1,260,000(5.625)}{755.6} = 9,380 \text{ psi} \\ S_{B-B} &= \left[ (9,026)^2 + 4(9,380)^2 \right]^{1/2} = 20,818 \text{ psi} \end{aligned}$$

For the factor of 10 support load at Section A-A, the stresses are:

$$\begin{aligned} \tau_{A-A} &= \frac{1,200,000}{93.415} = 12,846 \text{ psi} \\ \sigma_{B,A-A} &= \frac{6,696,000(6.0)}{987.2} = 40,697 \text{ psi} \\ S_{A-A} &= \left[ (40,697)^2 + 4(12,846)^2 \right]^{1/2} = 48,128 \text{ psi} \end{aligned}$$

For the factor 10 support load at Section B-B, the stresses are:

$$\begin{aligned}\tau_{B-B} &= \frac{1,200,000}{79.77} = 15,043 \text{ psi} \\ \sigma_{B-B} &= \frac{2,100,000 (5.625)}{755.6} = 15,633 \text{ psi} \\ S_{B-B} &= \left[ (15,043)^2 + 4(15,633)^2 \right]^{1/2} = 34,697 \text{ psi}\end{aligned}$$

### Lower Trunnions

For the factor of 6 lifting load at Section A-A, the stresses are:

$$\begin{aligned}\tau_{A-A} &= \frac{360,000}{58.91} = 6,111 \text{ psi} \\ \sigma_{B,A-A} &= \frac{2,008,800 (5.0)}{460.19} = 21,826 \text{ psi} \\ S_{A-A} &= \left[ (21,826)^2 + 4(6,111)^2 \right]^{1/2} = 25,015 \text{ psi}\end{aligned}$$

For the factor of 6 lifting load at Section B-B, the stresses are:

$$\begin{aligned}\tau_{B-B} &= \frac{360,000}{46.47} = 7,747 \text{ psi} \\ \sigma_{B,B-B} &= \frac{630,000 (4.34)}{264.80} = 10,326 \text{ psi} \\ S_{B-B} &= \left[ (10,326)^2 + 4(7,747)^2 \right]^{1/2} = 18,620 \text{ psi}\end{aligned}$$

For the factor of 10 support load at Section A-A, the stresses are:

$$\begin{aligned}\tau_{A-A} &= \frac{600,000}{58.91} = 10,185 \text{ psi} \\ \sigma_{B,A-A} &= \frac{3,348,000 (5.0)}{460.19} = 36,376 \text{ psi} \\ S_{A-A} &= \left[ (36,376)^2 + 4(10,185)^2 \right]^{1/2} = 41,691 \text{ psi}\end{aligned}$$

For the factor of 10 support load at Section B-B, the stresses are:

$$\begin{aligned}\tau_{B-B} &= \frac{600,000}{46.47} = 12,912 \text{ psi} \\ \sigma_{B,B-B} &= \frac{1,050,000 (4.34)}{264.80} = 17,209 \text{ psi} \\ S_{B-B} &= \left[ (17,209)^2 + 4(12,912)^2 \right]^{1/2} = 31,033 \text{ psi}\end{aligned}$$

Table 2-8 presents the section properties and applied loads for the trunnions, and Table 2-9 presents a summary of the stresses at the same locations to compare against the trunnion yield and ultimate strengths. Also listed are the allowable stresses (yield and ultimate strengths).



Conservatively assuming a material temperature of 400 °F, the minimum margin of safety (M.S.) for the factor 6g lift of the upper trunnion is at Section A-A:

$$\text{M.S.} = 30,800/28,877 - 1.0 = +0.07$$

For the lower trunnion, the minimum margin is also at Section A-A:

$$\text{M.S.} = 30,800/25,462 - 1.0 = +0.21$$

For the factor 10g lift of the upper trunnion, the minimum M.S., again at Section A-A is:

$$\text{M.S.} = 70,000/48,128 - 1.0 = +0.45$$

For the lower trunnion, the minimum M.S. is:

$$\text{M.S.} = 70,000/41,691 - 1.0 = +0.68$$

The results presented above demonstrate that all of the calculated stresses in both the upper and lower trunnions are acceptable, and that the minimum M.S. is +0.21 for the yield condition in the lower trunnion, and +0.46 for the ultimate condition for the upper trunnion. Therefore, the requirements of 10 CFR 71.45(a) are met.

10 CFR 71.45(a) requires that any lifting attachment that is a structural part of the package must not fail in such a manner that the ability of the packaging to meet other requirements is impaired. The trunnions are welded to the 8-inch thick gamma shield. The gamma shield is a thick walled cylinder that transmits the lifting load to the balance of the cask. The Bijlaard analysis provided in Section 2.6 yields a maximum stress in the gamma shell of 17.32 ksi due to the trunnion moment, internal pressure, and thermal stress. The outer surface of the gamma shield can be considered the same temperature as the trunnions and thus, the allowable stress is identical. Therefore, the margin when compared to yield strength for the shell is much greater than either the trunnion shoulder or weld margin. This ensures the trunnion failure due to excessive load will not affect the performance of the cask because the trunnion will separate from the cask before the cask gamma shield wall fails. Note also that the containment vessel is inside the gamma shield, and is unaffected by a postulated trunnion failure.

## 2.5.2 Tie-Down Devices

The longitudinal forces experienced by the transport package, per 10 CFR 71.45(b), are resisted by steel end restraints that react against the impact limiters. The vertical and lateral forces that act on the transport package, according to 10 CFR 71.45(b) and NUREG-1815 [14], are restrained by a dual saddle/strap tie-down system. Specifically, the tie-down straps resist uplifting and lateral overturning forces whereas the saddles react downward and strap reaction forces. This restraint system is also designed to preclude yielding in the load bearing material of the transport package during normal transport conditions. The premise for both of these tie-down systems is to add extra safety margin by utilizing the large load-bearing surface areas available to distribute transport loads, instead of creating the relatively large localized stresses associated with utilizing the trunnions as tie-down points for transportation. This loading condition, Load Step IL-9, is analyzed in Appendix 2.12.2. The stress results from the tie-down load are presented in Table 2.12.2-2. All the calculated stresses are less than the lowest yield strength of 30.0 ksi (gamma shield shell).

## 2.6 Normal Conditions of Transport

### Overview

This section describes the response of the TN-32B HBU demonstration cask to the loading conditions specified by 10 CFR 71.71 [3]. The design criteria established for the TN-32B HBU demonstration cask for the NCT are described in Section 2.1.2. These criteria are selected to ensure that the package performance standards specified by 10 CFR 71.43 and 71.51 are satisfied. Under NCT, there will be no loss or dispersal of radioactive contents, no significant increase in external radiation levels, and no substantial reduction in the effectiveness of the packaging.

Detailed structural analyses of various TN-32B HBU demonstration cask components subjected to individual loads are provided in the Appendices to this chapter. The limiting results from these analyses are used in this section to quantify package performance in response to the NCT load combinations, specified in 10 CFR 71.71 and Regulatory Guide 7.8 [2]. Table 2-10 provides an overview of the performance evaluations reported in each load combination subsection. Each subsection provides the limiting structural analysis result for the affected cask component(s) in comparison to the established design criteria. This comparison permits the minimum M.S. for a given component subjected to a given loading condition to be readily identified. In all cases, the acceptability of the TN-32B HBU demonstration cask design with respect to established criteria, and consequently with respect to 10 CFR Part 71 performance standards is demonstrated.

The structural analysis of the cask body is presented in Appendix 2.12.2 and covers a wide range of individual loading conditions. The stress results from the various individual loads must be combined in order to represent the stress condition in the cask body under the specified condition evaluated in this section. An explanation of the reporting format used for the results, and the stress combination technique used in applying the results from Appendix 2.12.2 is provided here.

### Reporting Method for Cask Body Stresses

Appendix 2.12.2 provides the detailed description of the structural analyses of the TN-32B HBU demonstration cask body. The appendix describes the detailed ANSYS® [17] model used to analyze various applied loads. Table 2-11 identifies the individual loads (IL) analyzed which are applicable to NCT.

Detailed stresses are available at as many locations as there are nodes in the finite element model. However, for practical considerations, only the maximum stresses in the lid, penetration sleeves, closure lid shield plate, flange, inner shell, gamma shield shell, and bottom shield are reported for each load case. These components were selected to be representative of the stress distribution in the cask body. The maximum stress may occur in different components for each individual load.

The stress results for the individual load case (tables reported in Appendix 2.12.2) are for one individual load only. Two or more individual load cases must be combined to determine the total stresses at any stress reporting locations for the various load combinations. This is accomplished using the ANSYS® post-processor.

For those load combinations that include trunnion reactions, the local stresses at the trunnion locations found by the Bijlaard method [18] are superimposed on the ANSYS® combined stresses.

Table 2-12 provides a matrix of the individual loads, and the various combinations, to determine the cask body stresses for the specified NCT load combination. An “x” in Table 2-12 indicates that the stress results for the individual load case are used in the load combinations.

For the increased external pressure load combination, it is assumed that the TN-32B HBU demonstration cask cavity is at 0 psia. For conservatism, a 25 psig external pressure is used for load combinations.

## 2.6.1 Heat

Chapter 3 describes the thermal analyses of the TN-32B HBU demonstration cask, subjected to high and low temperature environmental conditions. The analyses results are utilized to support various aspects of the structural evaluations as described in the following subsections.

### 2.6.1.1 Summary of Pressures and Temperatures

Allowable stresses for the packaging components are a function of the component temperatures, which are based on actual maximum calculated temperatures or conservatively selected higher temperatures. Chapter 3 summarizes the significant temperatures calculated for the TN-32B HBU demonstration cask subjected to high temperature environmental conditions. These temperatures are used in establishing the allowable stress values for every NCT load combination, evaluated in this Safety Analysis Report.

Table 2-13 summarizes the thermal analysis results from Chapter 3. The table also lists the selection of cask and basket component design temperatures for structural analysis purposes.

The thermal analysis presented in Chapter 3 also provides the average cavity gas temperature under high temperature environmental conditions. This value is used in Chapter 4 to determine the MNOP. For purposes of the structural analysis of containment, a value of 100 psig (much higher than the Chapter 4 value, 30.5 psig) is conservatively assumed for the cask body stress calculation. This pressure loading is analyzed using the ANSYS® model of the cask body described in Appendix 2.12.2 and the results are reported in Table 2.12.2-2. This load case and corresponding results are designated as individual load IL-3, which is utilized to support evaluations of the load combinations listed in Table 2-12.

### 2.6.1.2 Differential Thermal Expansion

The thermal analysis of the TN-32B HBU demonstration cask is performed as described in Chapter 3. The temperature distribution from that analysis is utilized to perform an ANSYS® thermal stress analysis of the cask body. The stress results for this load case are reported on Table 2.12.2-2. This load case is designated as IL-6 (thermal stresses at 100 °F ambient) and is used to support various load combinations.

### 2.6.1.3 Stress Calculations

Cask body stresses for the high temperature environment for NCT, are obtained by a combination of individual loads as summarized in Table 2-12. For this condition, it is assumed that the cask is in its transport configuration, mounted horizontally on the transport cradle, and supported by the front and rear saddles. Pre-load effects on the lid bolts, fabrication stress, 100 psig internal pressure, thermal stresses, and the local stresses at the tie-down straps are combined to give the maximum nodal stress intensity in each component for this load combination. The results are given in Table 2-14 through Table 2-18.

### 2.6.1.4 Comparison with Allowable Stresses

Section 2.1.2 presents the design criteria for structural evaluation of the TN-32B HBU demonstration cask. From the analysis results in Table 2-14 through Table 2-18, it can be observed that the NCT loads will not result in any structural damage to the cask, and that the containment function of the cask will be maintained.

## 2.6.2 Cold

### 2.6.2.1 Thermal Stresses for Cold Environment at -20 °F Ambient Temperature (N2)

The Regulatory Guide 7.8 [2] requires that the stresses due to the normal load condition be combined with the thermal stresses for cold environment conditions at -20 °F (-29 °C) ambient temperature. The thermal stresses are determined in Load Case IL-7 with results tabulated in Table 2.12.2-2. Again, closure lid bolt preload, fabrication stress, external pressure, and gravity loads are also included in this combination. The maximum nodal stress intensity in each component for this load combination is listed in Table 2-14 through Table 2-18.

### 2.6.2.2 Cold Environment Load Combinations at -40 °F Ambient Temperature (N3)

The Regulatory Guide 7.8 [2] cold environment load combination results in all cask components in thermal equilibrium at -40 °F (-40 °C). Containment vessel thermal stresses do occur in this case due to the differential thermal expansion between the steels. The thermal stresses are determined in load case IL-8 with results tabulated in Table 2.12.2-2. The cask cavity pressure at the cold environment condition is conservatively assumed to be 0 psia. This results in a net external pressure loading of 14.7 psig (25 psig is conservatively used). The stresses due to 25 psig external pressure are determined in load case IL-4 with results also given in Table 2.12.2-2. Again, lid bolt preload, fabrication stress, and gravity loads are included. The maximum nodal stress intensity in each component for this load combination is listed in Table 2-14 through Table 2-18.

### 2.6.3 Reduced External Pressure (N5)

Cask body stresses for the 3.5 psia ambient NCT external pressure decrease are obtained by a combination of individual loads as summarized in Table 2-12. The net internal pressure is calculated as  $(30.5 + 14.7 - 3.5) = 41.7$  psig (cask stresses are conservatively calculated based on 100 psig pressure). For this condition, the cask is in the horizontal orientation supported on the transport cradle by front and rear saddles. Closure lid bolt pre-load, fabrication stress, gravity, and the local tie-down strap effects are included. The thermal stresses for the hot thermal condition are included in the load combination. The maximum nodal stress intensity in each component for this load combination is listed in Table 2-14 through Table 2-18.

### 2.6.4 Increased External Pressure (N4)

Cask body stresses for the NCT increased external pressure, 20 psia, are obtained by a combination of individual loads as summarized in Table 2-12. The conservatively assumed minimum cask cavity pressure of 0 psia results in a net external pressure loading of 20 psig (25 psig is conservatively used). For this condition, the cask is assumed to be in the horizontal orientation, supported on the transport cradle front and rear saddles. Lid bolt pre-load, fabrication stress, gravity, and the local tie-down strap effects are included. In addition, the thermal stresses for the -20 °F minimum temperature are also included in the combination. The maximum nodal stress intensity in each component for this load combination is listed in Table 2-14 through Table 2-18.

### 2.6.5 Vibration

#### 2.6.5.1 Transport Shock Loading (N14 & N15)

The transport rail shock loadings used to evaluate the TN-32B HBU transport cask are based on NUREG-766510 [19], which specifies a maximum inertia loading of 4.7g in each of the three x-y-z coordinate directions:

- Vertical 4.7g
- Longitudinal 4.7g
- Lateral 4.7g

The resultant transverse load is  $(4.7^2 + 4.7^2)^{1/2} = 6.65 \text{ g}$

The stresses due to the transport rail shock individual load case are presented in Table 2.12.2-2. Table 2-14 through Table 2-18 list the combined stresses (N14) under hot thermal conditions where the load combination is performed for the maximum temperature thermal stresses. Lid bolt pre-load, fabrication stress, internal pressure, and the local tie-down strap effects are included.

In addition, Table 2-14 through Table 2-18 list the combined stresses (N15) under -20 °F thermal conditions where the load combination is performed for the -20 °F thermal stresses. Lid bolt pre-load, fabrication stress, external pressure, and the local tie-down strap effects are included.

#### 2.6.5.2 Transport Vibration Loading (N12 & N13)

The input loading conditions used to evaluate the TN-32B HBU demonstration cask for transport rail vibration are obtained from NUREG-766510 [19]. The peak inertia values used are:

- Vertical 0.37g
- Longitudinal 0.19g
- Lateral 0.19g

The resultant transverse load is  $(0.37^2 + 0.19^2)^{1/2} = 0.42 \text{ g}$

The stresses due to the transport rail car vibration individual load case are presented in Table 2.12.2-2. Table 2-14 through Table 2-18 list the combined stresses (N12) under hot thermal conditions where the load combination is performed for the maximum temperature thermal stresses. Lid bolt pre-load, fabrication stress, internal pressure, and the local tie-down strap effects are included.

In addition, Table 2-14 through Table 2-18 also list the combined stresses (N13) under -20 °F thermal conditions where the load combination is performed for the -20 °F thermal stresses. Closure lid bolt pre-load, fabrication stress, external pressure, and the local tie-down strap effects are included.

#### 2.6.6 Water Spray

All exterior surfaces of the TN-32B HBU demonstration cask body are metal and, therefore, are not subject to soaking or structural degradation from water absorption. The water spray test identified in 10 CFR 71.71(c)(6) is, therefore, of no consequence to the TN-32B HBU demonstration cask.

### 2.6.7 Free Drop

Two drop orientations are considered credible for the one-foot NCT free drop (see Section 2.12.9.5 of Appendix 2.12.9 for detail descriptions). The structural response of the TN-32B HBU demonstration cask body is evaluated for a one-foot end drop of the package, representing both the bottom end and closure lid end drops; and a one-foot side drop. The assessment of cask body stresses follows the same logic as that established in the previous sections. For these drop cases, the evaluations are performed for both the hot temperature environment and at the -20 °F minimum transport ambient temperature.

The load combinations performed to evaluate these drop events are indicated in Table 2-12. In all cases, bolt pre-load effects and fabrication stress are included. For the hot environment condition, thermal stress load, 100 psig internal pressure, and impact load cases are combined. For the cold environment evaluation, -20 °F thermal stress, 25 psig external pressure, and impact load cases are combined.

Table 2-14 through Table 2-18 list the combined stress intensities for the bottom end, lid end and side drop under hot and cold environment conditions.

### 2.6.8 Corner Drop

This test does not apply to the TN-32B HBU demonstration cask since the package weight is in excess of 100 kg (220 lb<sub>m</sub>), as identified in 10 CFR 71.71(c)(8).

### 2.6.9 Compression

This test does not apply to the TN-32B HBU demonstration cask since the package weight is in excess of 5,000 kg (11,000 lb<sub>m</sub>), as identified in 10 CFR 71.71(c)(9).

### 2.6.10 Penetration

Due to lack of external protuberances, the one meter (40 inch) drop of a 13-pound steel bar of 1¼ inch diameter, with a hemispherical head, as delineated in 10 CFR 71.71(c)(10), is of negligible consequence to the TN-32B HBU demonstration cask.

### 2.6.11 Lid Bolt Analysis

The closure lid bolts are analyzed for both NCT and HAC loadings in Appendix 2.12.3. The analysis is based on NUREG/CR-6007 [20]. The bolts are analyzed for the following NCT loadings: operating pre-load, gasket seating load, internal pressure, temperature changes, and impact loads.

The bolt preload is calculated to withstand the worst-case load combination and to maintain a clamping (compressive) force on the closure joint, during NCT and HAC events.



A summary of the calculated stresses is listed Section 2.12.3.6 of Appendix 2.12.3. The calculations result in a maximum NCT average tensile stress of 56.9 ksi, which is below the allowable tensile stress of 93.5 ksi. The average NCT shear stress in the bolts is due to torsion during pre-loading. This stress is 14.5 ksi, which is well below the allowable shear stress of 56.1 ksi. The maximum combined stress intensity due to NCT tension-plus-shear-plus-bending is 65.8 ksi, which is also less than the allowable maximum stress intensity of 126.2 ksi.

Because the TN-32B HBU demonstration cask will only be transported once, fatigue of the closure lid bolts will not occur. However, a fatigue analysis for a conservative 50 round trips for the closure lid bolts is provided in Section 2.12.3.7 of Appendix 2.12.3. The resultant cumulative damage factor for all of the NCT events is less than 1.0 (unity).

## 2.6.12 Fatigue Analysis of the Containment Boundary

The purpose of the fatigue analysis is to demonstrate that the containment vessel stresses are within acceptable NCT fatigue limits. This demonstration is performed by determining the fatigue damage factor for each NCT event at locations on the containment vessel with the highest stresses. The cumulative fatigue damage or usage factor for all of the events is conservatively determined by adding the fatigue usage factors for the individual events, assuming these maximum stress intensities occur at the same location.

The fatigue analysis is based on the procedure described in Regulatory Guide 7.6 [1] and Section III of the ASME B&PV Code Appendices [3]. When determining the stress cycles, consideration is given to the superposition of individual loads which can occur together and produce a total stress intensity range greater than the stress intensity range of individual loads. Also, the maximum stress intensities for all individual loads are conservatively combined simultaneously. The sequence of events assumed for the fatigue evaluation is given below. For this analysis, even though the cask will only be transported once, the fatigue evaluation assumes 50 round trip shipments.

1. Bolt Preload
2. Lifting
3. Test pressure
4. Road shock/vibration
5. Pressure and temperature fluctuations
6. 1 foot normal condition drop

### Preload

The specified bolt preload is to ensure a leaktight seal, which produces significant stresses in the closure lid. Therefore, this loading is conservatively included in the fatigue evaluation. The maximum stress calculated in Table 2.12.2-2 for the penetration sleeves due to the preload is 12,320 psi. It is assumed that the lid is installed twice per trip, resulting in 100 cycles.

### Lifting

The stresses due to the 6g lifting load are listed in Section 2.12.2.4 of Appendix 2.12.2. The maximum stress intensity, which occurs in the gamma shield shell, is 11,440 psi. However, when the maximum stress intensity calculated in Table 2.12.2-3 is combined with the pressure and thermal stress calculated in Table 2.12.2-2 the stress intensity increases to 20,990 psi. This value is conservatively used in the fatigue evaluation. This loading is assumed to occur twice per round trip, so the total number of cycles is 100.

### Test Pressure

The proof test is  $1.25 \times (\text{maximum design pressure}) = 125 \text{ psi}$ , and will only be performed once. The test pressure stresses are obtained by ratioing the 100 psig internal pressure stresses given in Table 2.12.2-2 (Load Case IL-3).

The maximum stress due to a 100 psi internal pressure of 5,550 psi is in the penetration sleeves. Therefore, the stress due to the test pressure is  $1.25 \times 5,550 = 6,938 \text{ psi}$ . This pressure test only occurs once per trip.

### Shock

Since the TN-32B HBU demonstration cask will be transported by railcar, the shock and vibration loadings are extracted from Reference [19].

### Rail Car Shock

Rail car shock values were obtained from Reference [19]. This reference states that the rail car can be expected to experience a 4.7g load in each direction nine times every 100 miles. Since the TN-32B HBU demonstration cask will only be transported once with the HBU spent fuel payload, the rail car shock will assume an average of a 3,000 mile one-way trip. Therefore, the total number of cycles is  $3,000 \text{ (miles)} \times 1 \text{ trip} \times 1 \text{ shipment} \times 0.09 \text{ (Shocks per mile)} = 270 \text{ cycles per trip}$ .

The stress intensities due to the rail shock load are listed in Tables 2-12.2-2 (Load Case IL-11). The maximum stress intensity in the gamma shield shell is 2,230 psi.

### Vibration

According to Reference [19], the peak vibration loads at the bed of a railcar are 0.19g longitudinal, 0.19g lateral, and 0.37g vertical. The maximum stress intensity resulting from these loads in any of the containment components is 140 psi, which is negligible.

### Pressure and Temperature Fluctuations

There are four environmental conditions identified for NCT. These are hot environment, cold environment, reduced external pressure, and increased external pressure. The containment vessel stresses in response to these environmental load combinations were reported in Table 2-14 through Table 2-18. The highest total stress intensity from these four cases, 44,000 psi, was calculated to occur in the inner shell during the hot environment condition.

The temperature and pressure fluctuations are assumed to occur once per round trip, since there is no payload during the return trip, and therefore no pressurization or heat generation. So, the total number of cycles of pressure and temperature fluctuation is 1 per trip.

### 1 Foot NCT Drop

The stress intensities due to the 1-foot end drop, with an acceleration of 26g, on bottom end are listed in Table 2.12.2-2 (Load Case IL-13). The maximum stress intensity occurs in the penetration sleeves portion of the containment vessel and is 6,380 psi.

The stress intensities due to the 1-foot end drop, with an acceleration of 26g, on the closure lid end are listed in Table 2.12.2-2 (Load Case IL-12). The maximum stress intensity is in the top shield plate portion of the containment vessel and is 2,860 psi.

The stress intensities due to the 1-foot side drop, with an acceleration of 20g, are listed in Table 2.12.2-2 (IL-14). The maximum stress intensity in the gamma shield is 9,890 psi.

This fatigue evaluation conservatively assumes that the cask is dropped once per shipment, resulting in one normal condition drop, and using the maximum side stress intensity of 9,890 psi for the damage factor calculation.

### Damage Factor Calculation

The following table is a summary of the fatigue evaluation. Although the maximum stress intensities for the different loading conditions do not occur at the same location, it is conservatively assumed that they do for the purpose of the fatigue evaluation. The value of the alternating stress,  $S_a$ , is determined as follows:

If one cycle goes from 0 to stress intensity(S.I.):

$$S_a = (S.I.)(K_F(K_E/2))$$

If one cycle goes from -S.I. to S.I:

$$S_a = (S.I.)(K_F \times K_E)$$

where:

$K_F$  = fatigue strength reduction factor, 4

$K_E$  = correction factor for modulus of elasticity,  $(30 \times 10^6)/(27.8 \times 10^6) = 1.08$

The fatigue curve shown in Table I-9.1 of ASME B&PV Code, Section III, Appendices [3] is used for this evaluation.

#### Summary of Fatigue Evaluation

Event	Stress Intensity (psi)	S.I. $\times K_F \times K_E$ (psi)	$S_a$ (psi)	Cycles		Damage Factor n / N
				n	N	
Lid Stress due to Bolt Preload	12,320	53,222	26,611	100	$3.2 \times 10^4$	0.003
Lifting	20,990	90,679	45,340	100	$5.9 \times 10^3$	0.017
Test Pressure	6,938	29,972	14,986	50	$3.1 \times 10^4$	0.002
Rail Car Shock	2,230	9,634	9,634	13,500	$1.7 \times 10^8$	0.000
Pressure and Temperature	44,000	190,080	95,040	50	671	0.075
1 Foot Normal Condition Drop	9,890	42,725	21,363	50	$7.2 \times 10^5$	0.000
					$\Sigma$	0.097

The above table shows that the total damage factor is less than one. Therefore, the fatigue effects on the TN-32B HBU demonstration cask containment vessel are acceptable.

A separate fatigue analysis of the closure lid bolts is presented in Appendix 2.12.3.

#### 2.6.13 Structural Evaluation of the Basket under Normal Condition Loads

The loading conditions considered in the evaluation of the fuel basket consist of inertial loads resulting from NCT drop loading (1 foot drop), HAC drop loading (30 foot drop) and thermal loads. The inertial loads of significance for the basket analysis are those transverse to the cask and basket structural longitudinal axes, so that the loading from the fuel assemblies is applied normal to the basket plates and transferred to the cask wall by the basket.

To determine the structural adequacy of the basket plate in the TN-32B HBU demonstration cask fuel assembly basket under a NCT free drop, the basket is evaluated for 13g for both the end and side drops. The g-loads and drop orientations used for structural analysis of the basket are described in Appendix 2.12.. The stress analysis of the basket due to inertial loading is described in detail in Appendix 2.12.6. The results of the analyses are summarized in Tables 2.12.6-4 through 2.12.6-5 of this appendix. Based on the results of these analyses, the basket is structurally adequate, and it will properly support and position the fuel assemblies under NCT loading conditions.

#### 2.6.14 Summary of NCT Cask Body Structural Analysis

Table 2-14 through Table 2-18 lists the highest NCT stress intensities in each of the TN-32B HBU demonstration cask components for all NCT load combinations based on the Section 2.1.2. From the analysis results presented in Table 2-14 through Table 2-18, it can be seen that the NCT loads will not result in any structural damage to the cask and that the containment function of the cask will be maintained.

## 2.7 Hypothetical Accident Conditions

### Overview

This section describes the response of the TN-32B HBU demonstration cask to the HAC loading conditions specified by 10 CFR 71.73 [3]. The design criteria established for the TN-32B HBU demonstration cask for these conditions are described in Section 2.1.2. These criteria are selected to ensure that the packaging performance standards specified by 10 CFR 71.51 are satisfied.

The presentation of the HAC analyses and results is accomplished in the same manner as that used above for the NCT. The detailed analyses of the various packaging components under different loading conditions are presented in the Appendices to this chapter. The limiting results for the specified HAC loadings are extracted from the Appendices, summarized here, and compared to the design criteria. In all cases, the acceptability of the TN-32B HBU demonstration cask design with respect to HAC loads is demonstrated.

Table 2-19 provides an overview of the performance evaluations presented in this section. The stress results for the cask body are obtained by combining the stresses from appropriate individual load cases reported in Appendix 2.12.2 to represent the stress condition under the specified HAC. This combination method is essentially the same as that presented in Section 2.6. Stress analysis results for the closure lid bolts are obtained directly from Appendix 2.12.3. The impact limiter attachment evaluations are described in Appendix 2.12.9.

### Reporting Method for Cask Body Stresses

The structural analysis of the cask body was performed using an ANSYS® finite element model. Stress results are reported at selected representative locations as described in Section 2.6.

Appendix 2.12.2 provides the detailed description of the ANSYS® structural analyses of the TN-32B HBU demonstration cask body under various applied loads. Table 2-20 identifies the individual HAC load cases (IL) analyzed using the ANSYS® model.

Detailed stresses are available at each node in the finite element model. However, for practical considerations, only the maximum stresses in the lid, shell flange, inner shell, shield shell cylinder, and bottom plates are reported for each load case. These components were selected to be representative of the stress distribution in the cask body. The maximum stress may occur in different components for each individual load.

The stress results for the individual load case (table reported in Appendix 2.12.2) are for one individual load only. Two or more individual load cases must be combined to determine the total stresses at any stress reporting locations for the various load combinations. This combination is accomplished utilizing the ANSYS® post-processor.

Table 2-21 provides a matrix of the individual loads, and the various combinations, to determine the cask body stresses for the specified HAC load combinations. An “x” in Table 2-21 indicates that the stress results for the individual load case are used in the load combination.

### 2.7.1 30 Foot Free Drop

In Appendix 2.12.9, LS-DYNA®, an explicit finite element code program, is used to estimate the deformation of the impact limiters, the forces on the cask, and the cask deceleration due to impact of the packaging on an unyielding surface. The full size impact limiter geometry and wood orientation are designed based on these results.

A one-third scale test impact limiter was fabricated to match the full-size impact limiter geometry and wood properties requirements. Four drop orientations were performed to determine the deformations and decelerations of the impact limiters. The test results are used to establish the baseline g loads for the component structural evaluations.

The four drop tests on the one-third scale models of the TN-40 package impact limiters, which are essentially the same as the TN-32B HBU demonstration cask impact limiters, are documented in Appendix 2.12.10. For the slapdown drop case, the secondary impact (combined transverse g-load and rotational g-load) is a more severe impact to the components than the primary impact. Therefore, the reported g-load for the slapdown is based on the second impact. The maximum g-loads for the 90° end drop, 0° side drop, CG-over-corner drop, and 20° slapdown are as follows:

<b>30-Foot Drop Orientation</b>	<b>Loads Measured by Testing (g)</b> (See Table 2.12.10-1 of Appendix 2.12.10)
90° end drop	54 axial
0° side drop	51 transverse
CG-over-corner drop	34 axial
20° slapdown (second impact)	58 <sup>(1)</sup> , 62 <sup>(2)</sup>

(1) The g-load measured at this location represents the maximum combined transverse and rotational g-load for the basket structural analysis due to the slapdown drop case.

(2) Maximum combined g-load at the top end of the cask body (at the outer surface of the cask lid).

### A. Cask Body G-Loads

Based on the LS-DYNA® results from Appendix 2.12.9, the following table summarizes the baseline g-loads that were utilized for the cask body structural evaluations.

**Baseline G-Loads for Cask Body Structural Analyses**

<b>30 Foot Drop Orientation</b>	<b>Appendix 2.12.9 Loads (g)</b>	<b>Bounding Baseline Loads Utilized for Cask Body Structural Analyses (g)</b>
90° end drop	74 axial	80 (axial)
CG-over-corner drop	29 axial	31 (axial), 15 radial
0° side drop	45 transverse	70 side drop analysis bounds both side drop and slapdown drop
20° slapdown (second impact)	34 transverse	

**B. Basket Inertial Loads**

The worst-case g-load load from Appendix 2.12.9, is amplified by the dynamic load factor (DLF) from Appendix 2.12.7. The resultant impact load is then compared to the bounding g-load of 51g and 90g for the side/slapdown and end drop orientations, respectively. As summarized in the following table, the applied g-loads bound the amplified g-loads.

**Applied G-Loads for Basket Structural Analysis**

<b>30-Foot Drop Orientation</b>	<b>Basket Cross Section Location</b>	<b>Appendix 2.12.9 Load (g)</b>	<b>DLF Factor<sup>(1)</sup></b>	<b>Amplified Load (g)</b>	<b>Applied Load (g)</b>
0° side drop	Mid	45	1.13	51	51
20° slapdown (second impact)	Top/Bot	34	1.13	38	51
90° end drop	Uniform	74	1.11	82	90

**C. Fuel Drop G-Loads**

For the fuel drop analyses, the side drop and slapdown orientation, the baseline g-loads are established by first multiplying the g-loads from the scale model impact limiter tests by the appropriate dynamic load factors and factors due to low temperature effect. Dynamic analysis utilizing the testing time history is used in the end drop analysis. The bounding baseline g-loads for the fuel drop analyses are listed in the following table.

**Baseline G-Loads for Fuel Rod Structural Analysis**

<b>Drop Orientation</b>	<b>Bounding Test Loads (g)</b>	<b>Load Factor (g)</b>	<b>Bounding Baseline Load Used in the Fuel Rod Analysis (g)</b>
90° end drop	57	$57(1.11)^{(1)}(1.15)^{(2)} = 73$	75g side drop analysis bounds both side and slapdown drops
0° side drop	45	$45(1.13)^{(1)}(1.15)^{(2)} = 58$	
20° slapdown (second impact)	34	$58(1.13)^{(2)}(1.15)^{(3)} = 44$	

<sup>(1)</sup> Refer to Appendix 2.12.7

<sup>(2)</sup> Wood property low temperature effect



#### D. Cask Body Structural Analysis

The cask body stress evaluations are described in Appendix 2.12.2. The g-loads used in Appendix 2.12.2 stress analyses are based on the LS-DYNA® estimation. The results from the TN-40 1/3-scale impact limiter testing are also presented for reference;

Elastic analyses are used for all the cask body drop analyses in Appendix 2.12.2. Therefore, in order to calculate the stresses due to the bounding baseline g-loads resulted from the testing, the load combinations as described in Table 2-21 are performed as follows:

- calculated load combination stresses based on the individual load stresses calculated in Appendix 2.12.2
- calculated the new load combination stresses by increasing the g values vs. g values used in the earlier calculations
- results of these new load combination stresses are listed in Table 2-22 through Table 2-29

##### 2.7.1.2 End Drop

The TN-32B HBU demonstration cask body end drop stress analysis performed in Appendix 2.12.2 is based on worst-case NCT 1-foot drop load, and then ratioed for the HAC impact.

These increased stress values are used in the end drop load combinations as indicated in Table 2-21 (combination numbers A1 to A4). In all cases, bolt pre-load effects and fabrication stresses are included. For the hot environment condition, 100 psig internal pressure, and impact load cases are combined. For the cold environment evaluation, 25 psig external pressure, and impact load cases are combined.

Table 2-22 through Table 2-29 lists the maximum nodal combined stress intensities ( $P_L + P_B + Q$ ) for the bottom and lid end drop under hot environment conditions and cold environment conditions based on the baseline g values.

From Table 2-22 through Table 2-29, the maximum stress intensity ( $P_L + P_B + Q$ ) is 46.19 ksi. This stress occurs in the closure lid outer plate due to the 30-foot end free drop combination. For this load combination, the allowable stress is 65.0 ksi.

##### 2.7.1.3 Side Drop

The TN-32B HBU demonstration cask body side drop stress analysis performed in Appendix 2.12.2 is based on worst-case NCT 1-foot drop load, and then ratioed for the HAC impact. An envelope of side drop load and slapdown drop conditions is utilized as the side drop g-load.

These stress values are used in the side drop load/slapdown combinations as indicated in Table 2-21 (combination numbers A5 and A6). In all cases, bolt pre-load effects and fabrication stresses are included. For the hot environment condition, 100 psig internal pressure, and impact load cases are combined. For the cold environment evaluation, 25 psig external pressure, and impact load cases are combined.

From Table 2-22, the maximum stress intensity ( $P_L + P_B + Q$ ) is 42.75 ksi. This stress occurs at the closure lid outer plate due to the side drop load combination. The membrane allowable is 65.0 ksi ( $P_m$ ); therefore, the minimum factor of safety is 1.52.

#### 2.7.1.4 Corner Drop

The TN-32B HBU demonstration cask body CG-over-corner drop stress analysis performed in Appendix 2.12.2 is based on the 30.6 g axial and 14.9 g transverse. This is based on a rounded-up value of 34g that is higher than 29.3g base g-load from LS-DYNA® drop analyses.

These stress values are used in the CG-over-corner drop load combinations as indicated in Table 2-21 (combination numbers A7 to A10). In all cases, bolt pre-load effects and fabrication stresses are included. For the hot environment condition, 100 psig internal pressure, and impact load cases are combined. For the cold environment evaluation, 25 psig external pressure, and impact load cases are combined.

Table 2-22 through Table 2-29 list the maximum linearized combined stress intensities for the CG-over-corner drop under hot environment conditions and cold environment conditions, based on the bounding baseline impact values.

From Table 2-22, the maximum stress intensity ( $P_L + P_B + Q$ ) is 43.84 ksi. This stress occurs in the closure lid outer plate due to the corner drop combination. For this load combination, the allowable stress is 65.0 ksi. Therefore, the minimum factor of safety is 1.48.

From the analysis results it can be seen that the HAC loads will not result in any structural damage to the cask, and that the containment function of the cask will be maintained.

#### 2.7.1.5 Closure Lid Bolts

The closure lid bolts are analyzed for normal and accident condition loadings in Appendix 2.12.3. The analysis is based on NUREG/CR-6007 [20]. The bolts are analyzed for the following normal and accident conditions: operating pre-load, gasket seating load, internal pressure, temperature changes, impact loads, and puncture loads.

The calculations result in a maximum HAC average tensile stress of 44.9 ksi, which is below the allowable tensile stress of 115.5 ksi. The average HAC shear stress in the bolts is due to torsion during pre-loading. This stress is 14.5 ksi, which is well below the allowable shear stress of 69.3 ksi.

#### 2.7.1.6 Impact Limiter Attachments

The impact limiters must remain attached to the cask body before, during, and after each HAC drop condition.

The limiting loading condition for the impact limiter attachments is the secondary impact (slap-down) associated with the 20° slap down under a 30 foot drop. This loading condition applies the greatest overturning moment to the impact limiter at the cask body interface. Although this loading condition is not limiting with respect to any other cask components, an evaluation of the attachments is performed to demonstrate that the affected impact limiter remains in place to insulate the cask during the subsequent HAC thermal event.

The analysis and results are provided in detail in Section 2.12.9.6 of Appendix 2.12.9.

The analysis concludes that, while a few of the attachment tie-rods and/or attachment bolts are predicted to fail, the impact limiters will remain secured to the cask body by the undamaged tie-rods and attachment bolts. This post-test resultant is confirmed by the test results in Appendix 2.12.10. The impact limiter attachment design is sufficiently strong to ensure that the impact limiters remain attached to the cask body during and following all HAC drop events.

#### 2.7.2 Crush

This test does not apply to the TN-32B HBU demonstration cask since the package weight is in excess of 500 kg (1,100 lb<sub>m</sub>).

#### 2.7.3 Puncture

The impact limiters will protect the ends of the cask body from a 40-inch drop onto a 6-inch diameter bar. In addition to the impact limiter, the puncture resistant plate and lance cover plates will provide additional protection of the closure lid and the thermocouple lance assemblies from a postulated puncture bar impact. However, an evaluation of the postulated puncture bar impact on the closure lid end is performed.

The most severe damage to the body resulting from the puncture drop will occur on the side walls of the gamma shield shell, between the impact limiters. This portion of the package is not the containment vessel, so that a release of the contents cannot occur unless both the gamma shield shell and the inner containment vessel are punctured.

An evaluation of the puncture drop event includes the local effects on the gamma shield shell at the impact point as well as the overall inertia loading on the packaging components.

For this load condition it is assumed that the gamma shield shell surface impacts the puncture bar directly. No credit is taken for the outer neutron shell or the radial neutron shield.

The puncture bar as specified in 10 CFR 71.73(c)(3) [3], is a vertical, cylindrical, mild steel bar 6 inches in diameter.

The impact force exerted by the bar on the gamma shield surface is calculated assuming the bar behaves as an elastic, perfectly plastic material with a yield stress of 50 ksi, which is the typical yield strength of mild carbon steel. The gamma shield shell is SA-266 Gr 2 carbon steel material, as described in Section 2.1.1.

The weight of the TN-32B HBU demonstration cask is 269,000 lb<sub>m</sub>. For puncture analysis, a conservatively higher weight of 275,000 lb<sub>m</sub> is utilized in this analysis.

Two independent methods are used to compute the stresses in the TN-32B HBU demonstration cask shell due to a puncture event.

#### Puncture Analysis Method 1

The maximum force,  $F_p$ , acting on the cask body due to impact on the puncture bar is:

$$F_p = \sigma_y A_b$$

Where  $\sigma_y$  is the yield strength of the bar, 50 ksi, and  $A_b$  is the cross-sectional area of the 6-inch diameter bar, 28.27 in<sup>2</sup>

Therefore,

$$F_p = 1.414 \times 10^6 \text{ lb}_f$$

This force produces a cask deceleration and induces a bending moment at the midsection of the cask. If the cask is considered a beam uniformly loaded (downward) by its inertial load only (conservatively ignoring the 1g gravity force), and supported by the puncture bar at the center, the deceleration  $g$  caused by the puncture bar force,  $F_p$ , is then the following:

$$g = \frac{F_p}{W_{\text{package}}} = \frac{1.414 \times 10^6}{275,000} = 5.14g$$

If the cask body is considered to be uniformly loaded and supported as described above, then the maximum moment,  $M$ , in the cask shell is:

$$M = \frac{F_p L}{8} = \frac{(1.414 \times 10^6)(179.77)}{8} = 3.177 \times 10^7 \text{ lb}_f \text{--in}$$

where  $L$  is the length of the TN-32B HBU demonstration cask. Conservatively neglecting the inner containment shell, outer shell and neutron shield, the moment of inertia of the cask gamma shell is:

$$I = \frac{\pi}{64} (r_o^4 - r_i^4) = \frac{\pi}{64} (43.90^4 - 35.90^4) = 1.008 \times 10^5 \text{ in}^4$$

where:

$r_o$  = nominal outer radius of gamma shield = 43.90 inches

$r_i$  = nominal inner radius of gamma shield = 35.90 inches

Utilizing the average gamma shell radius, the gamma shield shell bending stress is then:

$$\sigma_b = \frac{Mr_0}{I} = \frac{(3.177 \times 10^7)(39.90)}{1.008 \times 10^5} = 12,576 \text{ psi}$$

Since the stress is nearly constant through the wall thickness, it should be treated as a membrane stress,  $P_m$ . The allowable stress for this accident condition is taken at 300 °F as the smaller of 0.7  $S_u$  ( $0.7(70,000) = 49,000$  psi) or 2.4  $S_m$  ( $2.4(21,300) = 51,120$  psi) per Appendix F-1331.1 [3], where SA-266 is the bounding material. The allowable membrane stress of 49,000 psi is significantly above  $\sigma_b$ .

The thickness of the gamma shield shell that surrounds the containment vessel is 8.00 inches, and provides the following shear area.

$$A = \pi(6)(8.00) = 151 \text{ in}^2$$

The resulting maximum shear stress is the following.

$$\tau = F_p/A = (1.414 \times 10^6)/151 = 9,364 \text{ psi.}$$

The corresponding stress intensity is  $2\tau$  or 18,750 psi. The allowable stress intensity for the gamma shield (ASME SA-266) is 0.7  $S_u$  or  $0.7(70,000) = 49,000$  psi, which is well above the calculated stress intensity.

The deceleration of 5.14g is small compared to the g-loads that will occur during the 30 foot free drop. Therefore, the global stresses that result from the inertial forces will be neglected during the load combination analysis. The bending stress of 12,576 psi at the center of the cask is also negligible compared to stresses due to other loads considered.

### Puncture Analysis Method 2

An additional cask wall puncture analysis is performed utilizing the equations presented in Bechtel BC-TOP-9A [21]. This method provides a conservative estimate for the puncture threshold thickness of a steel element subjected to non-deformable missile perforation. The following equation is a problem specific reproduction of the analysis carried out in Reference [21].

$$T_p = \frac{\left(\frac{MV_s^2}{2}\right)^{2/3}}{672D}$$

Where  $T_p$  is the cask wall thickness required to prevent puncture (inch),  $D$  is the puncture bar outer diameter (inch),  $M$  is the mass of the missile (lb-sec<sup>2</sup>/ft), and  $V_s$  striking velocity of the missile normal to the target surface (ft/sec) absorbed by the puncture event. The velocity of the puncture bar relative to the package and the mass of the missile is calculated using the acceleration due to gravity,  $g = 32.2$  ft/sec<sup>2</sup>, the total drop height,  $h = 40$  inch (3.33 ft), and weight of the package  $W = 275,000$  lb<sub>m</sub>. Therefore,  $V_s = (2gh)^{1/2} = 14.65$  ft/sec, and  $M = W/g = 8540.4$  lb<sub>m</sub>-sec<sup>2</sup>/ft. Substituting  $V_s$ ,  $M$ , and  $D = 6$  inch into the above equation yields a threshold steel thickness of:

$$T_p = \frac{(9.167 \times 10^5)^{2/3}}{(672)(6)} = 2.34 \text{ inch}$$

Since the cask wall is 8.00 inches thick (>2.34 inches), the cask wall will not fail or be breached due to a puncture bar drop event.

### Lid Puncture

The effects of a puncture bar on the bolted lid of the cask are evaluated in this section. For conservatism, the closure lid will be evaluated as a simply supported circular plate to the outer diameter of the lid (79.50 inch), noting that the cask cavity is 68.75 inch nominally. The impact acceleration,  $\eta$ , is calculated above as 5.14g. The TN-32B lid upper assembly includes the closure lid (10.50-inch thick), puncture plate (1.75-inch thick), and the lance cover plates between the closure lid and the puncture plate with a nominal gap of 0.18 inch between the lance cover plates and the puncture resistant plate. It is important to note that the impact limiters will protect the ends of the cask from the puncture bar during transportation. However, the impact limiters are ignored as part of this evaluation for additional conservatism. As a worst-case scenario, it is assumed that the puncture bar impacts the puncture resistant plate and the closure lid at the top center of the cask, and the lid assembly acts as a simply supported plate.

The lance cover plates (seven total) are welded at the top surface of the closure lid, as shown on Drawings 19885-71-2 and 19885-71-7. Any impact to the puncture resistant plate will distribute the impact load from the puncture plate to the lance cover plates, and to then onto the closure lid, thus avoiding damaging the thermocouple lance assemblies. Therefore, the closure lid thickness includes the 1.75-inch thick puncture resistant plate, and ignores the lance cover plate thickness. For this analysis, Table 11.2, Case 16 of Reference [22] will be utilized. In addition, the bolted connection of the puncture resistant plate is not evaluated since failure of the bolted connection will not prevent the puncture resistant plate from performing its design function in a HAC puncture drop condition.

Maximum radial bending moment,  $M_{max}$ , will be:

$$M_{max} = \frac{W_i}{4\pi} \left[ (1 + \mu) \ln \left( \frac{a}{r_0} \right) \right] = 429.26 \text{ kip-in/in}$$

where:

$$\text{impact weight, } W_i = 5.14(275 \text{ kip}) = 1,414 \text{ kips}$$

lid thickness,  $t_1 = 10.5 + 1.75 = 12.25$  inches

Poisson's ratio,  $\mu = 0.3$

lid diameter,  $D_{lid} = 79.50$  inches

lid radius,  $a = 1/2(D_{lid}) = 39.75$  inches

radius,  $r'_0$ , of puncture bar load,

$$r'_0 = (1.6r_0^2 + t_1^2)^{0.5} - 0.675t_1 = 4.56 \text{ inch} \rightarrow \text{if } r_0 < 0.5t_1$$

The maximum bending stress,  $\sigma_b$ , in the closure lid from a puncture bar impact is:

$$\sigma_b = \frac{6M_{MAX}}{t_1^2} = \frac{6(429.26)}{(12.25)^2} = 17.16 \text{ ksi}$$

Zero internal pressure is assumed since any internal pressure would relieve stress on the closure lid. Therefore, this assumption is conservative. The lid yield strength at 300 °F for SA-203 Gr D material is 32.7 ksi. The M.S. for puncture impact resistance on the cask lid is:

$$MS = \frac{(32.7)}{(17.16)} - 1 = +0.91$$

For a postulated skewed angle impact on the closure lid end by the bar, and ignoring the protection from the impact limiter steel and wood, the edge of a puncture bar would initially contact the puncture resistant plate, resulting in a lower impact force than an impact with the bar normal to the plate surface. Since the ultimate strength of the 1.75-inch thick puncture resistance plate is greater than a mild carbon steel bar, the bar is unable to deform or "dig" into the higher strength material, which will cause the edge of the bar to deform and slide across the puncture resistant plate, resulting in no damage to the plate or the containment boundary.

Based on the above evaluations, the containment boundary of the TN-32B HBU demonstration cask will not be breached or significantly damaged by the puncture drop per 10 CFR 71.73(c)(3).

## 2.7.4 Thermal

### 2.7.4.1 Summary of Pressures and Temperatures

The analysis of the thermal accident is presented in Chapter 3. The maximum internal pressure during the HAC thermal accident is calculated in Section 3.4.3.2 of this chapter. The calculated pressure is 31.3 psig. However, the structural analysis is performed conservatively assuming 100 psig internal pressure for the pressure stress calculations.

An ANSYS® transient thermal analysis of the cask for the 30-minute thermal fire accident is reported in Chapter 3. The initial condition is steady state, at an ambient temperature of 100 °F and maximum decay heat. The initial steady state condition is followed by a 0.5-hour fire at 1,475 °F (800 °C), which is then followed by a cool-down period. The temperatures from the thermal analysis are reported in Chapter 3.

#### 2.7.4.2 Differential Thermal Expansion

Differential thermal expansion from exposure to the transient fire event is not of concern for the TN-32B HBU demonstration cask. All of the structural materials for the cask body assembly are carbon steel that have essentially the same thermal expansion coefficients, as shown in Table 2-6. Since both the closure lid bolts and the closure lid plate have the same thermal expansion coefficients, there is no effect on the closure due to differential thermal expansion. Additionally, the temperature differential between the interfacing cask components, e.g., containment shell/gamma shell, for the transient fire event are not significant, as noted in Chapter 3, and will not develop any significant stresses. Therefore, differential thermal expansion is not a concern for the TN-32B HBU demonstration cask.

#### 2.7.4.3 Stress Calculations

Table 2-22 through Table 2-29 presents the combined stress intensities in the closure lid, penetration sleeves, gamma shield shell, bottom shield plate, bottom inner plate, inner shell, top shield plate and flange.

#### 2.7.5 Immersion – Fissile material

The criticality evaluation presented in Chapter 6 considers the effect of water in-leakage. Thus, the requirements of 10 CFR 71.73(c)(5) [3] are satisfied. The cask body stresses for this immersion condition (1.3 psi external pressure) is enveloped by the deep immersion condition for all packages (water pressure of 290 psi) described in Section 2.7.7.

#### 2.7.6 Immersion – All Packages

The immersion loading condition results in an external pressure applied to the cask body corresponding to a 50 foot head of water. Conservatively assuming a 0 psia cask cavity pressure, this results in a maximum external pressure of 36.4 psig (21.7 + 14.7). The cask body stresses resulting from this immersion pressure are enveloped by the deep immersion condition for all packages (water pressure of 290 psig) described in the following section.

#### 2.7.7 Deep Water Immersion Test (for Type B Packages Containing More than 105 A2)

10 CFR 71.61 [3] requires that the containment vessel be subjected to an external water pressure of 290 psig for a period of not less than one hour without collapse, buckling, or in-leakage of water. The containment boundary consists of the inner shell, bottom inner plate shell flange out to the seating surface, the closure lid assembly outer plate, and the thermocouple lance assemblies (Figure 2-2). This analysis evaluates the containment vessel stresses when the 290 psig external pressure is directly applied to the outer surface of the containment vessel. A helpful feature of the packaging design is that the inner shell and bottom inner plate of the containment vessel are completely enclosed by the thick gamma shield shell and bottom shield. Therefore, the containment vessel will never be exposed to an external pressure due to immersion.



The ANSYS® finite element model of the cask described in detail in Appendix 2.12.2 is modified to analyze the immersion accident event. The gamma shield structure, bottom shield plate and trunnion elements are deleted from the original model. Bilinear material properties were defined for the existing material models to account for plasticity and simulate correct material behavior. The material properties are obtained from the ASME B&PV Code [10]. All properties are taken at 400 °F.

All existing loads are removed and replaced by 290 psig pressure load over the outer surface of the model. The maximum normal operating pressure is conservatively ignored and not applied on the inside cavity of the cask. The finite element model load and boundary conditions are shown in Figure 2-3. A large displacement static analysis with nonlinear material properties is conducted using ANSYS® [17]. The results for membrane and bending stresses were compared to ASME B&PV Code allowables.

The critical linearized membrane and membrane-plus-bending stress intensities for each of the cask components are summarized in the table below. The ultimate strengths of the component materials are obtained from Reference [10].

Containment Vessel Component	Stress Category	Computed Stress Intensity (ksi)	Allowable Stress Intensity (ksi)
Bottom Inner Plate	$P_m$	25.56	44.64
	$P_m + P_b$	58.83	65.00
Inner Shell	$P_m$	31.38	44.64
	$P_m + P_b$	51.86	65.00
Top Shield Plate	$P_m$	2.71	49.00
	$P_m + P_b$	7.45	70.00
Shell Flange	$P_m$	6.15	49.00
	$P_m + P_b$	10.93	70.00
Penetration Sleeves	$P_m$	9.96	49.00
	$P_m + P_b$	11.91	70.00
Closure Lid	$P_m$	5.04	44.64
	$P_m + P_b$	8.20	65.00

The theoretical buckling strength of the FEM model is also calculated using an Eigenvalue buckling analysis. A static solution with prestress effects (290 psig pressure loads) included is first performed to calculate the stress stiffness matrix internally in ANSYS®. It is followed by an Eigenvalue buckling solution to calculate the first 10 buckling modes and the critical load factors. The critical buckling factor is calculated as 1.245. Therefore, the critical buckling pressure is  $1.245(290 \text{ psi}) = 361 \text{ psi}$ .

A large displacement static non-linear analysis is also performed to increase the external pressure of 450 psig in a number of sub-steps. The containment cylinder and bottom are perfectly symmetric, so the ANSYS® analysis might fail numerically as non-symmetric buckling responses cannot be triggered. To overcome this problem, small geometric imperfections are artificially introduced into the model to trigger buckling responses. The imperfections in the buckling mode shapes are obtained by adding displacements of the mode shapes reduced by a scaling factor. The imperfections are added as a sum of the first 10 mode shapes extracted in the Eigenvalue analysis to avoid introducing bias to the finite element model.

The containment vessel is assumed to buckle at the load sub-step where the solution begins to diverge. A converged solution was obtained for the last sub-step of the analysis corresponding to a 450 psig external pressure, and thus, there is no potential of buckling of the containment vessel structure. Therefore, it is concluded that cask will not buckle under 290 psig external pressure.

In addition to the finite element analysis described above, a buckling evaluation following the methods of ASME Code Case N-284 was performed and is documented in Appendix 2.12.11. This evaluation included the combination of fabrication induced compressive stresses with those due to the 290 psi that result from immersion pressure. The minimum stress margin is for the combined hoop stress where the amplified plastic stress of 35,100 psi is well below the theoretical buckling stress of 48,152 psi. In addition the interaction check results in a ratio below the limit of 1.0. These results demonstrate that the design has significant margins of safety when both fabrication and immersion compressive loads are considered.

For the thermocouple lance assembly (TLA), an evaluation of the containment boundaries that would be exposed to the deep immersion external pressure of 290 psig was performed and documented in Appendix 2.12.12. [

]

## 2.7.8 Summary of Damage

### Summary of HAC Basket Structural Analysis

To determine the structural adequacy of the basket plates in the TN-32B HBU demonstration cask fuel assembly basket under HAC free drops, the basket is conservatively evaluated for a 90g end drop and a 51g side drop. The baseline g-loads and drop orientations used for structural analysis of the basket are described in Section 2.7.1. The dynamic load factor used in the basket structural analysis is described in Appendix 2.12.7. The stress analysis of the basket due to inertial loading is described in detail in Appendix 2.12.6. A summary of the accident analyses performed is presented in Sections 2.12.6.2 and 2.12.6.3. The analyses demonstrate that the basket is structurally adequate, and will properly support and position the fuel assemblies during HAC loading conditions.

To demonstrate the structural adequacy of the HBU fuel assemblies under the HAC side impact, the fuel cladding is conservatively evaluated for a 75g side drop as documented in Appendix 2.12.8. For the HAC end drop, an explicit dynamic analysis of a single fuel rod is performed using LS-DYNA®. The analysis is based on the work conducted by the Pacific Northwest National Laboratory and the Nuclear Regulatory Commission, as documented in Section 2.12.8.2 of the appendix. The analyses demonstrate that the HBU fuel cladding strains remain below the yield strain at the corresponding temperature for the HAC side and end impact loadings.

#### Summary of HAC Cask Body Structural Analysis

Table 2-22 through Table 2-29 lists the highest stress intensities in each of the TN-32B HBU demonstration cask components for all HAC load combinations described above. Also listed in the tables are the stress limits for the service condition based on the Section 2.1.2.

From the analysis results presented in Table 2-22 through Table 2-29, it can be seen that the HAC loads will not result in any structural damage to the cask body and closure lid, and that the containment functions of the cask will be maintained.

As described above, the integrity of the TN-32B HBU demonstration cask is not compromised by the accident test sequence set forth in 10 CFR 71.73 [3], since it meets the design criteria of Regulatory Guide 7.6 [1] for the Load Combinations identified in Regulatory Guide 7.8 [2].

### **2.8 Accident Conditions for Air Transport of Plutonium**

This section does not apply to the TN-32B HBU demonstration cask.

### **2.9 Accident Conditions for Fissile Material Packages for Air Transport**

This section does not apply to the TN-32B HBU demonstration cask.

### **2.10 Special Form**

This section does not apply to the TN-32B HBU demonstration cask.

### **2.11 Fuel Rods**

As discussed in Chapter 4, containment of the radioactive material is provided by the cask containment boundary. Analyses of the cask boundary for NCT and HAC defined by the 10 CFR Part 71 [3] demonstrate that the boundary remains leaktight.

In addition, Appendix 2.12.7 assesses the response of a typical PWR fuel assembly to a 30-foot HAC end drop and a 30-foot HAC side drop. Results from these analyses demonstrate that the fuel rods will not be breached during the NCT and HAC.

**Table 2-1**  
**Evaluation Method Employed to Demonstrate Compliance with**  
**Specific Regulatory Requirements**

<b>10 CFR Part 71</b>		<b>Numerical Analysis</b>	<b>Material Test**</b>	<b>Model Tests</b>
<b>Normal Condition of Transport</b>	Heat	X		
	Cold	X		
	Reduced External Pressure	X		
	Increased External Pressure	X		
	Shock and Vibration	X		
	One Foot Free drop	X		
<b>Hypothetical Accident Condition</b>	30 foot Free Drop - Cask and Basket	X	X	
	30 foot Free Drop- Impact Limiters	X	X	X
	Puncture	X		
	Thermal Event	X		
	Water Immersion	X		
<b>Others</b>	Lifting	X		
	Tie-Down	X		

\*\* Material tests include compression tests of the wood, and Charpy and tensile tests of the containment boundary materials.

**Table 2-2  
Containment Vessel Stress Limits**

Classification	Stress Intensity Limit
<b>Normal (Level A) Conditions<sup>(1)</sup></b>	
$P_m$	$S_m$
$P_l$	$1.5 S_m$
$(P_m \text{ or } P_l) + P_b$	$1.5 S_m$
Shear Stress	$0.6 S_m$
Bearing Stress	$S_y$
$(P_m \text{ or } P_l) + P_b + Q$	$3.0 S_m$
<b>Hypothetical Accident (Level D)<sup>(2)</sup></b>	
$P_m$	Lessor of $2.4 S_m$ or $0.7 S_u$
$P_l$	Lessor of $3.6 S_m$ or $S_u$
$(P_m \text{ or } P_l) + P_b$	Lessor of $3.6 S_m$ or $S_u$
Shear Stress	$0.42 S_u$

Notes:

1. Classifications and Stress Intensity Limits are as defined in ASME B&PV Code, Section III, Subsection NB [4].
2. Stress intensity limits are in accordance with ASME B&PV Code, Section III, Appendix F [4].

**Table 2-3  
Containment Bolt Stress Limits**

Classification	Stress Intensity Limit <sup>(1)(5)</sup>
<b>Normal (Level A) Conditions <sup>(2)</sup></b>	
Average Tensile Stress	$S_m = 2/3 S_y$
Average Shear Stress	$0.6 S_m$
Maximum Combined Stress	$1.35 S_m = 0.9 S_y$
Bearing Stress	$S_y$
<b>Hypothetical Accident (Level D)<sup>(3)</sup></b>	
Average Tensile Stress	Smaller of $S_y$ or $0.7 S_u$
Average Shear Stress	Smaller of $0.42 S_u$ or $0.6 S_y$
Maximum Combined Stress	$S_u$
Combined Shear & Tension <sup>(4)</sup>	$R_t^2 + R_s^2 \leq 1$

Notes:

1. The stress analysis of the closure lid bolts is performed in accordance with NUREG/CR-6007 [20], and described in Appendix 2.12.3. The stress limits for the closure lid bolts are listed separately in Appendix 2.12.3, Tables 2.12.3-3 and 2.12.3-4.  
The stress limits for the impact limiter tie rods and attachment bolts are described in Appendix 2.12.9.
2. Classification and stress limits are as defined in ASME B&PV Code, Section III, Subsection NB [10] and NUREG/CR-6007, as applicable.
3. Stress limits are in accordance with ASME B&PV Code, Section III, Appendix F [4].
4.  $R_t$ : Ratio of average tensile stress to allowable average tensile stress  
 $R_s$ : Ratio of average shear stress to allowable average shear stress
5. All stresses include the effect of tensile and torsional loads due to bolt preloading.

**Table 2-4**  
**Non Containment Structure Stress Limits**

Classification	Stress Intensity Limit
<b>Normal (Level A) Conditions <sup>(1)</sup></b>	
$P_m$	$S_m$
$P_l$	$1.5 S_m$
$(P_m \text{ or } P_l) + P_b$	$1.5 S_m$
$(P_m \text{ or } P_l) + P_b + Q$	$3.0 S_m$
Shear Stress	$0.6 S_m$
Bearing Stress	$S_y$
<b>Hypothetical Accident (Level D) <sup>(2)</sup></b>	
$P_m$	Smaller of $2.4 S_m$ or $0.7 S_u$
$P_l$	Smaller of $3.6 S_m$ or $S_u$
$(P_m \text{ or } P_l) + P_b$	Smaller of $3.6 S_m$ or $S_u$
Shear Stress	$0.42 S_u$

<b>Weld Allowable Stress<sup>(1)</sup></b>		
<b>Normal Load Condition</b>	Full Penetration	Same as base metal
	Partial Groove/Fillet	Tension - $0.3 S_u$ Shear - $0.4 S_y$
<b>Accident Load Condition</b>	Full Penetration	Same as base metal
	Partial Groove/Fillet	Normal Condition allowables are increased by a factor: Smaller of 2 or $1.67 S_u / S_y$ if $S_u > 1.2 S_y$

## Notes:

- Classifications and stress intensity limits are as defined in ASME B&PV Code, Section III, Subsection NF [6].
- Stress intensity limits are in accordance with ASME B&PV Code, Section III, Appendix F [4].

**Table 2-5  
Basket Stress Limits**

<b>Classification</b>	<b>Stress Intensity Limit</b>
<b>Normal (Level A) Conditions <sup>(1)</sup></b>	
$P_m$	$S_m$
$P_l$	$1.5 S_m$
$(P_m \text{ or } P_l) + P_b$	$1.5 S_m$
$(P_m \text{ or } P_l) + P_b + Q$	$3.0 S_m$
Shear Stress	$0.6 S_m$
<b>Hypothetical Accident (Level D) <sup>(2)</sup></b>	
$P_m$	Smaller of $2.4 S_m$ or $0.7 S_u$
$P_l$	Smaller of $3.6 S_m$ or $S_u^{(3)}$
$(P_m \text{ or } P_l) + P_b$	Smaller of $3.6 S_m$ or $S_u^{(3)}$
Shear Stress	$0.42 S_u$

Notes:

1. Classifications and stress intensity limits are as defined in ASME B&PV Code, Section III, Subsection NB [4].
2. Limits are in accordance with ASME B&PV Code, Section III, Appendix F [4].
3. When evaluating the results from the nonlinear elastic plastic analysis for the accident conditions, the general primary membrane stress intensity,  $P_m$ , shall not exceed the greater of  $0.7 S_u$  and  $S_y + 1/3(S_u - S_y)$ . The maximum primary stress intensity at any location ( $P_l$  or  $P_l + P_b$ ) shall not exceed  $0.9 S_u$  [4].
4. Fusion welds are qualified by testing. The testing program is provided in Section 2.12.6.4.

**Table 2-6**  
**Cask Material Properties <sup>(1)</sup>**  
 (3 Pages)

Material	Class	Temp. (°F)	Ultimate Strength S <sub>u</sub> (ksi)	Yield Strength S <sub>y</sub> (ksi)	Allowable S/S <sub>m</sub> (ksi)	E (10 <sup>6</sup> psi)	$\alpha \times 10^{-6}$ (in/in/°F) <sup>(5)</sup>
SA-203 Gr. D	Sec. III Class 1	70	65.0	37.0	18.6 <sup>(4)</sup> /... <sup>(3)</sup>	27.8	6.4
		100	65.0 <sup>(2)</sup>	37.0	18.6 <sup>(4)</sup> /... <sup>(3)</sup>	...	6.6
		200	65.0 <sup>(2)</sup>	33.9 <sup>(2)</sup>	18.6 <sup>(4)</sup> /... <sup>(3)</sup>	27.1	7.0
		300	65.0 <sup>(2)</sup>	32.7 <sup>(2)</sup>	18.6 <sup>(4)</sup> /... <sup>(3)</sup>	26.7	7.3
		400	65.0 <sup>(2)</sup>	31.6 <sup>(2)</sup>	18.6 <sup>(4)</sup> /... <sup>(3)</sup>	26.1	7.7
		500	65.0 <sup>(2)</sup>	30.0 <sup>(2)</sup>	18.6 <sup>(4)</sup> /... <sup>(3)</sup>	25.7	8.0
		600	65.0 <sup>(2)</sup>	27.8 <sup>(2)</sup>	18.5 <sup>(4)</sup> /... <sup>(3)</sup>	25.2	8.3
SA-350 Gr LF3	Sec. III Class 1	70	70.0	37.5	20.0/23.3	27.8	6.4
		100	70.0 <sup>(2)</sup>	37.5	20.0/23.3	...	6.6
		200	70.0 <sup>(2)</sup>	34.2	20.0/22.9	27.1	7.0
		300	70.0 <sup>(2)</sup>	33.2	20.0/22.1	26.7	7.3
		400	70.0 <sup>(2)</sup>	32.0 <sup>(2)</sup>	20.0/21.4	26.1	7.7
		500	70.0 <sup>(2)</sup>	30.4 <sup>(2)</sup>	20.0/20.3	25.7	8.0
		600	70.0 <sup>(2)</sup>	28.2 <sup>(2)</sup>	18.8/18.8	25.2	8.3
SA-516 Gr. 70	Sec. III Class 1	70	70.0	38.0	17.5/23.3	29.3	6.4
		100	70.0	38.0	17.5/23.3	...	6.6
		200	70.0	34.6	17.5/23.1	28.6	7.0
		300	70.0	33.7	17.5/22.5	28.1	7.3
		400	70.0	32.6	17.5/21.7	27.5	7.7
		500	70.0	30.7	17.5/20.5	27.1	8.0
		600	70.0	28.1	17.5/18.7	26.5	8.3
SA-266 Cl. 2	Sec. III Class 1	70	70.0	35.0	17.5/23.3	29.3	...
		100	70.0	35.0	17.5/23.3	...	5.73
		200	70.0	31.9	17.5/21.9	28.6	6.09
		300	70.0	31.0	17.5/21.3	28.1	6.43
		400	70.0	30.0	17.5/20.6	27.5	6.74
		500	70.0	28.3	17.5/19.4	27.1	7.06
		600	70.0	25.9	17.5/17.8	26.5	7.28
SA-105 (Trunnions)	Sec. III Class 1	70	70.0	36.0	17.5/23.3	29.5	...
		100	70.0	36.0	17.5/23.3	...	5.73
		200	70.0	32.8	17.5/21.9	28.8	6.09
		300	70.0	31.9	17.5/21.3	28.3	6.43
		400	70.0	30.8	17.5/20.6	27.7	6.74
		500	70.0	29.1	17.5/19.4	27.3	7.06
		600	70.0	26.6	17.5/17.8	26.7	7.28



**Table 2-6**  
**Cask Material Properties <sup>(1)</sup>**  
 (3 Pages)

Material	Class	Temp. (°F)	Ultimate Strength S <sub>u</sub> (ksi)	Yield Strength S <sub>y</sub> (ksi)	Allowable S/S <sub>m</sub> (ksi)	E (10 <sup>6</sup> psi)	$\alpha \times 10^{-6}$ (in/in/°F) <sup>(5)</sup>
SA-540 Gr. B23 Cl. 1 (Bolt)	Sec. III Class 1	70	165.0	150.0	33.0/50.0	27.8	6.4
		100	165.0 <sup>(2)</sup>	150.0	33.0/50.0	...	6.6
		200	165.0 <sup>(2)</sup>	140.1	33.0/47.8	27.1	7.0
		300	165.0 <sup>(2)</sup>	135.3	33.0/46.2	26.7	7.3
		400	165.0 <sup>(2)</sup>	131.7	33.0/44.8	26.1	7.7
		500	165.0 <sup>(2)</sup>	127.7	33.0/43.4	25.7	8.0
		600	165.0 <sup>(2)</sup>	122.6	33.0/41.4	25.2	8.3
SA-193 Gr. B7 ( $\varnothing \leq 2 \frac{1}{2}$ -in) <sup>(4)</sup>	Sec. III Class 1	-100	...	...	...	30.4	...
		70	125.0	105.0	25.0/70.0 <sup>(6)</sup>	29.7	6.4
		100	125.0 <sup>(2)</sup>	105.0	25.0/70.0 <sup>(6)</sup>	...	6.6
		200	125.0 <sup>(2)</sup>	98.0	25.0/65.3 <sup>(6)</sup>	29.0	7.0
		300	125.0 <sup>(2)</sup>	94.1	25.0/62.7 <sup>(6)</sup>	28.5	7.3
		400	125.0 <sup>(2)</sup>	91.5	25.0/61.0 <sup>(6)</sup>	27.9	7.7
		500	125.0 <sup>(2)</sup>	88.5	25.0/59.0 <sup>(6)</sup>	27.5	8.0
SA-193 Gr. B8	Sec. III Subsection NF	70	75.0	30.0	18.8/10.0	28.3	6.4
		100	75.0 <sup>(2)</sup>	30.0	18.8/10.0	...	6.6
		200	71.0 <sup>(2)</sup>	25.0	16.7/8.3	27.6	7.0
		300	66.2 <sup>(2)</sup>	22.5	15.0/7.5	27.0	7.3
		400	64.0 <sup>(2)</sup>	20.7	13.8/6.9	26.5	7.7
		500	63.4 <sup>(2)</sup>	19.4	12.9/6.5	25.8	8.0
		600	63.4 <sup>(2)</sup>	18.2	12.1/6.1	25.3	6.4
A-240 SA-240 SA-479 Type 304/304L <sup>(4)</sup>	ASTM, ASME Sec. III Class 1	70	75.0	30.0	20.0/20.0	28.3	8.5
		100	75.0	30.0	20.0/20.0	...	8.7
		200	71.0	25.0	16.7/20.0	27.5	9.4
		300	66.2	22.4	15.0/20.0	27.0	9.9
		400	64.0	20.7	13.8/18.6	26.4	10.2
		500	63.4	19.4	12.9/17.5	25.9	10.5
		600	63.4	18.4	12.3/16.6	25.3	10.6
SA-387 Gr. 91, Cl 2 <sup>(3)</sup>	Sec. III Class 1	70	85.0	60.0	24.3/28.3	31.0	5.8
		100	85.0	60.0	24.3/28.3	...	5.9
		200	85.0	55.9	24.3/28.3	30.3	6.2
		300	85.0	54.8	24.3/28.3	29.7	6.5
		400	84.7	54.7	24.2/28.2	29.2	6.7
		500	84.4	54.7	24.1/28.1	28.6	6.9

**Table 2-6**  
**Cask Material Properties <sup>(1)</sup>**  
 (3 Pages)

Material	Class	Temp. (°F)	Ultimate Strength S <sub>u</sub> (ksi)	Yield Strength S <sub>y</sub> (ksi)	Allowable S/S <sub>m</sub> (ksi)	E (10 <sup>6</sup> psi)	$\alpha \times 10^{-6}$ (in/in/°F) <sup>(5)</sup>
SB-163 UNS N06600 Annealed <sup>(4)</sup> 1/4 < O.D. ≤ 7/8	Sec. III Class 1	70	80.0	35.0	22.9/26.7	31.0	6.8
		100	80.0	35.0	22.9/26.7	...	7.0
		200	80.0	32.0	21.3/26.7	30.3	7.4
		300	80.0	31.2	20.8/26.7	29.9	7.7
		400	80.0	30.7	20.5/26.7	29.4	8.0
		500	80.0	30.3	20.2/26.7	29.0	8.3
SB-166 UNS N06600 Annealed <sup>(4)</sup>	Sec. III Class 1	70	80.0	35.0	22.9/23.3	31.0	6.8
		100	80.0	35.0	22.9/23.3	...	7.0
		200	80.0	32.0	22.9/23.3	30.3	7.4
		300	80.0	31.2	22.9/23.3	29.9	7.7
		400	80.0	30.7	22.9/23.3	29.4	8.0
		500	80.0	30.3	22.9/23.3	29.0	8.3

## Notes:

1. All material properties are provided from Reference [10], unless otherwise specified.
2. Elevated temperature material properties are not provided in Reference [10].  
Values provided from Reference [11] for analysis.
3. Reference [10] does not provide applicable S<sub>m</sub> data.
4. Material properties extracted from ASME Section II, Part D, 2013 [11].
5. Instantaneous coefficient, as noted, otherwise mean coefficient.
6. S<sub>m</sub> defined as 2/3 S<sub>y</sub> per Reference [20].

**Table 2-7  
Cask Weight and Center of Gravity**

<b>Component</b>	<b>Weight (kips)</b>
<b>Cask</b>	<b>221.00</b>
Body	111.86
Closure Lid w/ Bolts, Washers, TLAs	12.90
Bottom	17.54
Aluminum Boxes	1.96
Resin	10.23
Outer Shell	7.24
Trunnions	0.75
Aluminum Rails at Periphery	1.27
Aluminum Plates at Periphery	2.26
Miscellaneous (rail mounting hardware, drain tube, nameplate, shell backing ring, etc.)	0.38
Lance Cover Plates	0.27
Puncture Resistant Plate	4.70
Fuel Assemblies/PRAs/Guide Funnels	49.64
<b>Basket</b>	<b>13.42</b>
Stainless Steel Boxes	5.49
Aluminum Plates of the Basket	6.67
Borated Aluminum Plates	0.24
Steel Plates at Periphery	1.02
<b>Top Impact Limiter</b>	<b>16.60</b>
<b>Bottom Impact Limiter</b>	<b>16.60</b>
<b>Tie-Rods (13)</b>	<b>1.13</b>
<b>Impact Limiter Bolting Brackets (8)</b>	<b>0.25</b>
<b>Total w/ Cask, Fuel, Impact Limiters and Tie-Rods</b>	<b>269.00</b>

\* Center of gravity of the package is approximately 93.7 inches, measured along the axial centerline from the rear (bottom) of the cask.

**Summary of Weights Utilized for Analysis:**

- |   |              |
|---|--------------|
| 1. Upper Trunnion Lifting (w/o impact limiters) | 240,000 lbs. |
| 2. Tie-Down Analyses                            | 270,000 lbs. |
| 3. Cask Body Analysis                           | 271,000 lbs. |

**Table 2-8**  
**Trunnion Section Properties and Applied Loads**

Item	Upper Trunnions		Lower Trunnions	
	Section A-A (Weld)	Section B-B (Shoulder)	Section A-A (Weld)	Section B-B (Shoulder)
Cross Sectional Area (in <sup>2</sup> )	93.415	79.77	58.91	46.47
Area Moment of Inertia (in <sup>4</sup> )	987.20	755.60	460.19	264.80
Yield Condition Shear Force (lbf)	720,000*		360,000*	
Yield Condition Bending Moment (lbf-in)	4,017,600	1,260,000	2,008,800	630,000
Ultimate Condition Shear Force (lbf)	1,200,000**		600,000**	
Ultimate Condition Bending Moment (lbf-in)	6,696,000	2,100,000	3,348,000	1,050,000

Notes:

Trunnion geometry (Sections A-A and B-B) is in Figure 2-1.

\* Trunnion Loads to Support 6 times Cask Weight

\*\* Trunnion Loads to Support 10 times Cask Weight

**Table 2-9**  
**Trunnion Stresses when Loaded by Factors 6 and 10 of Cask Weight (Lifting)**

Location/Stress	Yield Limit		Ultimate Limit	
	Section A-A (Weld)	Section B-B (Shoulder)	Section A-A (Weld)	Section B-B (Shoulder)
<b>Upper Trunnions</b>				
Shear Stress (psi)	7,708	9,026	12,846	15,043
Bending Stress (psi)	24,418	9,380	40,697	15,633
Stress Intensity (psi)	28,877	20,818	48,128	34,697
<b>Lower Trunnions</b>				
Shear Stress (psi)	6,111	7,747	10,185	12,912
Bending Stress (psi)	21,826	10,326	36,376	17,209
Stress Intensity (psi)	25,015	18,620	41,691	31,033
Allowable Stress (psi)	$S_y = 30,800$		$S_u = 70,000$	

## Notes:

1. Trunnion geometry (Sections A-A and B-B) is shown in Figure 2-1.
2. Minimum M.S. is +0.21 for yield limit (lower trunnion) and +0.07 for yield limit (upper trunnion).

**Table 2-10**  
**TN-32B HBU Cask Performance Evaluation Overview (Normal Conditions of Transport)**

Loading Condition	SAR Section	Scope of Evaluation
Heat 10 CFR 71.71(c)(1)	2.6.1.1	Maximum component temperatures for material allowables and maximum cavity pressure (100 psig)
	2.6.1.2	Cask body thermal gradients
	2.6.1.3	Cask body stresses due to hot environment load combinations
	2.6.1.4	Comparison with allowable stresses
Cold 10 CFR 71.71(c)(2)	2.6.2	Cask body stresses due to cold environment load combinations
Reduced External Pressure 10 CFR 71.71(c)(3)	2.6.3	Cask body stresses due to -3.5 psia external pressure load combinations
Increase External Pressure 10 CFR 71.71(c)(4)	2.6.4	Cask body stresses due to 20 psia external pressure load combinations
Shock Loads 10 CFR 71.71(c)(5)	2.6.5	Cask body stresses due to rail shock loads
Vibration Loads 10 CFR 71.71(c)(5)	2.6.5	Cask body stresses due to rail vibration loads
Water Spray 10 CFR 71.71(c)(6)	2.6.6	Negligible for TN-32B HBU cask
Free Drop 10 CFR 71.71(c)(7)	2.6.7	Cask body stresses due to 1 foot bottom end drop
		Cask body stresses due to 1 foot lid end drop
		Cask body stresses due to 1 foot side drop
Corner Drop 10 CFR 71.71(c)(8)	2.6.8	Not applicable
Compression 10 CFR 71.71(c)(9)	2.6.9	Not applicable
Penetration 10 CFR 71.71(c)(10)	2.6.10	Not applicable
Lid Bolt Analysis	2.6.11	Bolt stresses due to preload, pressure loads, temperature, impact and puncture loads
Fatigue Analysis of Containment Boundary	2.6.12	Fatigue evaluation of containment vessel due to lifting, pressure, temperature, shock/vibration, and 1 foot drop loads
Basket Evaluation	2.6.13	Structural analysis of the basket due to 1 foot end drop and 1 foot side drop loads
Summary of Normal Condition Structural Analysis	2.6.14	Lists the highest stress intensities in the containment vessel and gamma shield and compares results with the allowables

**Table 2-11**  
**Individual Load Cases for Normal Conditions of Transport**  
**TN-32B HBU Demonstration Cask Body Analysis**

Run No.	Individual Load Type	Load Utilized in Analysis
IL-1	Closure lid bolt preload and lid seating pressure	-
IL-2	Fabrication stresses	-
IL-3	Internal pressure	100 psig
IL-4	External pressure	25 psig
IL-5	Reduced external pressure	3.5 psia
IL-6	Thermal stresses at 100 °F hot environment	-
IL-7	Thermal stresses at –20 °F cold environment	-
IL-8	Thermal stresses at –40 °F cold environment	-
IL-9	Cask Horizontal – 1g Down (Gravity)	1g
IL-10	Horizontal cask, Rail Vibrations, Rail car shock	0.19g, 0.19g, 0.37g
IL-11	Horizontal cask, Rail Shock tie-down	4.7g all direction
IL-12	End drop on top (closure lid) end	26g
IL-13	End drop on bottom end	26g
IL-14	Side/Slapdown drop	20g
IL-15	Corner drop on top (closure lid) end	
IL-16	Corner Drop on bottom end	
IL-17	Fire accident	
IL-18	Deep immersion (290 psig)	290 psig

**Table 2-12**  
**Summary of Load Combinations for Normal Conditions of Transport**  
(2 Pages)

Load Combination	Applicable Individual Loads												
	IL-1	IL-2	IL-9	IL-3	IL-4	IL-5	IL-6	IL-7	IL-8	IL-12	IL-13	IL-14	Comb. Abbr.
	Bolt Pre-load	Fabrication	Gravity 1g	Internal Pressure	External Pressure	Reduced Ext Press	Thermal 100 °F	Thermal -20 °F	Thermal -40 °F	Top Drop	Bottom Drop	Side Drop	
Hot Environment (100 °F amb)	X	X	X	X			X						N1
Cold Environment (-20 °F amb)	X	X	X		X			X					N2
Cold Environment (-40 °F amb)	X	X	X		X				X				N3
Increased External Pressure	X	X	X		X			X					N4
Reduced External Pressure	X	X	X	X		X	X						N5
1 Ft End Bottom Drop	X	X			X			X			X		N6
	X	X		X			X				X		N7
1 Ft End Top Drop	X	X			X			X		X			N8
	X	X		X			X			X			N9
1 Ft Side Drop	X	X			X			X				X	N10
	X	X		X			X					X	N11



**Table 2-12**  
**Summary of Load Combinations for Normal Conditions of Transport**  
 (2 Pages)

Load Combination	Applicable Individual Loads								Combination Abbreviation
	IL-1	IL-2	IL-3	IL-4	IL-6	IL-7	IL-10	IL-11	
	Bolt Preload	Fabrication	Internal Pressure	External Pressure	Thermal (100 °F)	Thermal (-20 °F)	Rail Vibration	Rail Shock	
Rail Vibration	X	X	X		X		X		N12
	X	X		X		X	X		N13
Rail Shock	X	X	X		X			X	N14
	X	X		X		X		X	N15

**Table 2-13**  
**Reference Temperatures for Stress Analysis Acceptance Criteria**

<b>Component</b>	<b>Normal Transport*</b>	
	<b>Maximum from Chapter 3.0 (°F)</b>	<b>Selected Design** Temperature (°F)</b>
Outer Shell	295	300
Inner Shell	368	400
Basket Rail	320	***
Basket Plate	468	***
Gamma Shell	347	400
Fuel Cladding	510	500
Lid Bolt	<250	300

\* For normal loading condition.

\*\* Temperatures specified are used to determine allowable stresses.  
They are not a maximum use temperature for material.

\*\*\* Allowable stresses for the basket are taken at the temperatures.

**Table 2-14**  
**NCT Load Combinations – Lid Stress Intensity Results**  
 (2 Pages)

Component	Load Case	Service Level	Stress Category	Stress Intensity (ksi)	Allowable Stress (ksi)	Factor of Safety
Closure Lid Outer Plate	N1	A	$P_m$	6.70	18.60	2.78
			$(P_m \text{ or } P_L)$	18.95	27.90	1.47
			$P_m + P_b$	13.08	27.90	2.13
			$P_m + P_b + Q$	43.99	55.80	1.27
	N2	A	$P_m$	7.26	18.60	2.56
			$(P_m \text{ or } P_L)$	17.79	27.90	1.57
			$P_m + P_b$	13.30	27.90	2.10
			$P_m + P_b + Q$	40.63	55.80	1.37
	N3	A	$P_m$	7.25	18.60	2.57
			$(P_m \text{ or } P_L)$	17.77	27.90	1.57
			$P_m + P_b$	13.30	27.90	2.10
			$P_m + P_b + Q$	40.58	55.80	1.38
	N4	A	$P_m$	7.26	18.60	2.56
			$(P_m \text{ or } P_L)$	17.79	27.90	1.57
			$P_m + P_b$	13.30	27.90	2.10
			$P_m + P_b + Q$	40.63	55.80	1.37
	N5	A	$P_m$	6.70	18.60	2.78
			$(P_m \text{ or } P_L)$	18.96	27.90	1.47
			$P_m + P_b$	13.06	27.90	2.14
			$P_m + P_b + Q$	44.00	55.80	1.27
	N6	A	$P_m$	8.57	18.60	2.17
			$(P_m \text{ or } P_L)$	18.12	27.90	1.54
			$P_m + P_b$	16.48	27.90	1.69
			$P_m + P_b + Q$	41.60	55.80	1.34
	N7	A	$P_m$	6.95	18.60	2.68
			$(P_m \text{ or } P_L)$	19.29	27.90	1.45
			$P_m + P_b$	12.78	27.90	2.18
			$P_m + P_b + Q$	44.96	55.80	1.24
	N8	A	$P_m$	7.20	18.60	2.58
			$(P_m \text{ or } P_L)$	18.96	27.90	1.47
			$P_m + P_b$	13.35	27.90	2.09
			$P_m + P_b + Q$	42.03	55.80	1.33
	N9	A	$P_m$	6.60	18.60	2.82
			$(P_m \text{ or } P_L)$	20.12	27.90	1.39

**Table 2-14**  
**NCT Load Combinations – Lid Stress Intensity Results**  
 (2 Pages)

Component	Load Case	Service Level	Stress Category	Stress Intensity (ksi)	Allowable Stress (ksi)	Factor of Safety
Closure Lid Outer Plate	N9	A	$P_m + P_b$	13.98	27.90	2.00
			$P_m + P_b + Q$	45.39	55.80	1.23
	N10	A	$P_m$	7.77	18.60	2.39
			$(P_m \text{ or } P_L)$	17.54	27.90	1.59
			$P_m + P_b$	14.85	27.90	1.88
			$P_m + P_b + Q$	40.56	55.80	1.38
	N11	A	$P_m$	6.92	18.60	2.69
			$(P_m \text{ or } P_L)$	18.71	27.90	1.49
			$P_m + P_b$	13.11	27.90	2.13
			$P_m + P_b + Q$	43.91	55.80	1.27
	N12	A	$P_m$	6.68	18.60	2.78
			$(P_m \text{ or } P_L)$	18.95	27.90	1.47
			$P_m + P_b$	13.08	27.90	2.13
			$P_m + P_b + Q$	43.98	55.80	1.27
	N13	A	$P_m$	7.28	18.60	2.55
			$(P_m \text{ or } P_L)$	17.78	27.90	1.57
			$P_m + P_b$	13.36	27.90	2.09
			$P_m + P_b + Q$	40.62	55.80	1.37
	N14	A	$P_m$	6.77	18.60	2.75
			$(P_m \text{ or } P_L)$	19.02	27.90	1.47
			$P_m + P_b$	12.94	27.90	2.16
			$P_m + P_b + Q$	44.12	55.80	1.26
	N15	A	$P_m$	7.57	18.60	2.46
			$(P_m \text{ or } P_L)$	17.85	27.90	1.56
			$P_m + P_b$	14.06	27.90	1.98
			$P_m + P_b + Q$	40.76	55.80	1.37
	Max N1 to N15	A	$P_m$	8.57	18.60	2.17
			$(P_m \text{ or } P_L)$	20.12	27.90	1.39
			$P_m + P_b$	16.48	27.90	1.69
			$P_m + P_b + Q$	45.39	55.80	1.23

## Notes:

1. Allowable limits are based on temperature of 400 °F.
2. Bending stresses at the lid flange (bolt holes circle region) are secondary stress.  $P_m$  and  $P_m + P_b$  stresses above do not account for local effects of geometric or material discontinuities and stress concentrations in region around bolt holes.

**Table 2-15**  
**NCT Load Combinations – Penetration Sleeves Stress Intensity Results**

Component	Load Case	Service Level	Stress Category	Stress Intensity (ksi)	Allowable Stress (ksi)	Factor of Safety
Penetration Sleeves	N1	A	$P_m$	10.03	21.40	2.13
			$P_m + P_b$	14.95	32.10	2.15
	N2	A	$P_m$	8.24	21.40	2.60
			$P_m + P_b$	15.39	32.10	2.09
	N3	A	$P_m$	8.22	21.40	2.60
			$P_m + P_b$	15.38	32.10	2.09
	N4	A	$P_m$	8.24	21.40	2.60
			$P_m + P_b$	15.39	32.10	2.09
	N5	A	$P_m$	10.01	21.40	2.14
			$P_m + P_b$	14.92	32.10	2.15
	N6	A	$P_m$	8.61	21.40	2.49
			$P_m + P_b$	18.52	32.10	1.73
	N7	A	$P_m$	8.73	21.40	2.45
			$P_m + P_b$	15.30	32.10	2.10
	N8	A	$P_m$	8.66	21.40	2.47
			$P_m + P_b$	15.52	32.10	2.07
	N9	A	$P_m$	10.50	21.40	2.04
			$P_m + P_b$	14.95	32.10	2.15
	N10	A	$P_m$	8.88	21.40	2.41
			$P_m + P_b$	16.99	32.10	1.89
	N11	A	$P_m$	10.92	21.40	1.96
			$P_m + P_b$	15.35	32.10	2.09
	N12	A	$P_m$	10.06	21.40	2.13
			$P_m + P_b$	14.89	32.10	2.16
	N13	A	$P_m$	8.26	21.40	2.59
			$P_m + P_b$	15.45	32.10	2.08
	N14	A	$P_m$	9.42	21.40	2.27
			$P_m + P_b$	15.06	32.10	2.13
	N15	A	$P_m$	7.92	21.40	2.70
			$P_m + P_b$	16.12	32.10	1.99
	Max N1 to N15	A	$P_m$	10.92		1.96
			$P_m + P_b$	18.52		1.73

**Table 2-16**  
**NCT Load Combinations – Gamma Shield Shell Stress Intensity Results**

Component	Load Case	Service Level	Stress Category	Stress Intensity (ksi)	Allowable Stress (ksi)	Factor of Safety
Gamma Shield Shell	N1	A	$P_m$	6.13	20.60	3.36
			$P_m + P_b$	16.73	30.90	1.85
	N2	A	$P_m$	6.15	20.60	3.35
			$P_m + P_b$	15.70	30.90	1.97
	N3	A	$P_m$	6.17	20.60	3.34
			$P_m + P_b$	15.71	30.90	1.97
	N4	A	$P_m$	6.15	20.60	3.35
			$P_m + P_b$	15.70	30.90	1.97
	N5	A	$P_m$	6.12	20.60	3.37
			$P_m + P_b$	16.73	30.90	1.85
	N6	A	$P_m$	6.74	20.60	3.06
			$P_m + P_b$	15.97	30.90	1.93
	N7	A	$P_m$	6.49	20.60	3.17
			$P_m + P_b$	17.01	30.90	1.82
	N8	A	$P_m$	6.42	20.60	3.21
			$P_m + P_b$	12.93	30.90	2.39
	N9	A	$P_m$	6.24	20.60	3.30
			$P_m + P_b$	13.97	30.90	2.21
	N10	A	$P_m$	7.81	20.60	2.64
			$P_m + P_b$	16.45	30.90	1.88
	N11	A	$P_m$	7.92	20.60	2.60
			$P_m + P_b$	17.32	30.90	1.78
	N12	A	$P_m$	6.12	20.60	3.37
			$P_m + P_b$	16.72	30.90	1.85
	N13	A	$P_m$	6.12	20.60	3.37
			$P_m + P_b$	15.68	30.90	1.97
	N14	A	$P_m$	6.22	20.60	3.31
			$P_m + P_b$	16.96	30.90	1.82
	N15	A	$P_m$	6.40	20.60	3.22
			$P_m + P_b$	15.94	30.90	1.94
	Max N1 to N15	A	$P_m$	7.92		2.60
			$P_m + P_b$	17.32		1.78

**Table 2-17**  
**NCT Load Combinations – Closure Lid Shield Plate Stress Intensity Results**

Component	Load Case	Service Level	Stress Category	Stress Intensity (ksi)	Allowable Stress (ksi)	Factor of Safety
Closure Lid Shield Plate	N1	A	$P_m$	7.23	21.70	3.00
			$P_m + P_b$	16.00	32.55	2.03
	N2	A	$P_m$	6.17	21.70	3.52
			$P_m + P_b$	14.95	32.55	2.18
	N3	A	$P_m$	6.15	21.70	3.53
			$P_m + P_b$	14.92	32.55	2.18
	N4	A	$P_m$	6.17	21.70	3.52
			$P_m + P_b$	14.95	32.55	2.18
	N5	A	$P_m$	7.19	21.70	3.02
			$P_m + P_b$	16.00	32.55	2.03
	N6	A	$P_m$	6.25	21.70	3.47
			$P_m + P_b$	15.14	32.55	2.15
	N7	A	$P_m$	6.78	21.70	3.20
			$P_m + P_b$	16.19	32.55	2.01
	N8	A	$P_m$	5.14	21.70	4.22
			$P_m + P_b$	12.07	32.55	2.70
	N9	A	$P_m$	6.47	21.70	3.35
			$P_m + P_b$	13.19	32.55	2.47
	N10	A	$P_m$	9.34	21.70	2.32
			$P_m + P_b$	18.72	32.55	1.74
	N11	A	$P_m$	9.46	21.70	2.29
			$P_m + P_b$	19.24	32.55	1.69
	N12	A	$P_m$	7.21	21.70	3.01
			$P_m + P_b$	15.97	32.55	2.04
	N13	A	$P_m$	6.16	21.70	3.52
			$P_m + P_b$	14.93	32.55	2.18
	N14	A	$P_m$	6.92	21.70	3.14
			$P_m + P_b$	16.24	32.55	2.00
	N15	A	$P_m$	6.27	21.70	3.46
			$P_m + P_b$	15.20	32.55	2.14
	Max N1 to N15	A	$P_m$	9.46		2.29
			$P_m + P_b$	19.24		1.69

**Table 2-18**  
**NCT Load Combinations – Shell Flange Stress Intensity Results**

Component	Load Case	Service Level	Stress Category	Stress Intensity (ksi)	Allowable Stress (ksi)	Factor of Safety
Shell Flange	N1	A	$P_m$	7.66	21.40	2.79
			$P_m + P_b$	9.35	32.10	3.43
	N2	A	$P_m$	8.33	21.40	2.57
			$P_m + P_b$	9.40	32.10	3.41
	N3	A	$P_m$	8.29	21.40	2.58
			$P_m + P_b$	9.34	32.10	3.44
	N4	A	$P_m$	8.33	21.40	2.57
			$P_m + P_b$	9.40	32.10	3.41
	N5	A	$P_m$	7.67	21.40	2.79
			$P_m + P_b$	9.35	32.10	3.43
	N6	A	$P_m$	8.38	21.40	2.55
			$P_m + P_b$	8.96	32.10	3.58
	N7	A	$P_m$	7.69	21.40	2.78
			$P_m + P_b$	8.59	32.10	3.74
	N8	A	$P_m$	8.36	21.40	2.56
			$P_m + P_b$	8.99	32.10	3.57
	N9	A	$P_m$	7.67	21.40	2.79
			$P_m + P_b$	8.26	32.10	3.89
	N10	A	$P_m$	11.00	21.40	1.95
			$P_m + P_b$	13.56	32.10	2.37
	N11	A	$P_m$	11.04	21.40	1.94
			$P_m + P_b$	13.56	32.10	2.37
	N12	A	$P_m$	7.61	21.40	2.81
			$P_m + P_b$	9.30	32.10	3.45
	N13	A	$P_m$	8.28	21.40	2.58
			$P_m + P_b$	9.35	32.10	3.43
	N14	A	$P_m$	7.84	21.40	2.73
			$P_m + P_b$	9.38	32.10	3.42
	N15	A	$P_m$	8.52	21.40	2.51
			$P_m + P_b$	9.42	32.10	3.41
	Max N1 to N15	A	$P_m$	11.04		1.94
			$P_m + P_b$	13.56		2.37



**Table 2-19**  
**TN-32B HBU Performance Evaluation Overview**  
**(Hypothetical Accident Conditions of Transport)**

Loading Conditions	SAR Section	Scope of Evaluation
30 foot Free Drop 10 CFR 71.73(c)(1)	2.7.1.1	Cask body stresses due to bottom end drop
		Cask body stresses due to lid end drop
	2.7.1.2	Cask body stresses due to side drop
	2.7.1.3	Cask body stresses due to corner drop
	2.7.1.4	Lid bolt analysis
	2.7.1.5	Impact limiter attachment analysis
Crush 10 CFR 71.73(2)	2.7.2	Not applicable
Puncture 10 CFR 71.73(c)(2)	2.7.3	Cask body evaluation for 40-inch drop onto the puncture bar
Thermal 10 CFR 71.73(c)(3)	2.7.4.1	Maximum component pressures and temperatures
	2.7.4.2	Cask body thermal stresses due to fire accident
	2.7.4.3	Maximum combined stresses
Immersion 10 CFR 71.73(c)(5) 10 CFR 71.73(c)(6) 10 CFR 71.61	2.7.5	Cask body stresses due to 3-foot water head (1.3 psi)
	2.7.6	Cask body stresses due to 50-foot water head (21.7 psi)
	2.7.7	Containment vessel stresses due to 290 psi external pressure (pressure directly applies to the containment vessel) Buckling analysis of the containment vessel due to 290 psi external pressure
Summary of Damage	2.7.8	Summarizes the structural analysis results for the basket and cask body

**Table 2-20**  
**Summary of Individual Loads for Hypothetical Accident Conditions of Transport**

Run No.	Individual Load Type	Load Used in Analysis
IL-1	Closure lid bolt preload and lid seating pressure	-
IL-2	Fabrication Stresses	-
IL-3	Internal pressure	100 psig
IL-4	External pressure	25 psig
IL-6	Thermal stress to 100 °F (hot) environment	-
IL-7	Thermal stress to -20 °F (cold) environment	-
IL-12	End drop on closure lid	80g
IL-13	End drop on bottom	80g
IL-14	Side drop/slapdown	70g
IL-15	CG-Over-Corner Drop on Front (Lid) Impact Limiter	30.6g axial, 14.9g radial <sup>(1)</sup>
IL-16	CG-Over-Corner Drop on Rear (Bottom) Impact Limiter	30.6g axial, 14.9g radial <sup>(1)</sup>

Notes:

1. Extracted from Section 2.7.1.3

**Table 2-21**  
**Summary of Load Combinations for Hypothetical Accident Conditions of Transport**

Load Combination	Applicable Individual Load										Combination Number
	IL-1	IL-2	IL-3	IL-4	IL-12	IL-13	IL-14	IL-15	IL-16	IL-17	
	Bolt Preload	Fabrication	Internal Pressure	External Pressure	Top End Drop	Bottom End Drop	Side Drop	Corner Lid Drop	Corner Drop Bottom	Fire	
30 Ft. End Drop on Bottom End	X	X	X			X					A1
	X	X		X		X					A2
30 Ft. End Drop on Lid End	X	X	X		X						A3
	X	X		X	X						A4
30 Ft. Side Drop/Slapdown	X	X	X				X				A5
	X	X		X			X				A6
30 Ft. CG Over Corner Drop on Bottom End	X	X	X						X		A7
	X	X		X					X		A8
30 Ft. CG Over Corner Drop on Lid End	X	X	X					X			A9
	X	X		X				X			A10
Fire Accident	X	X	X							X	A11

**Table 2-22**  
**HAC Load Combinations – Lid Stress Intensity Results**  
 (2 Pages)

Component	Load Case	Service Level	Stress Category	Stress Intensity (ksi)	Allowable Stress (ksi)	Factor of Safety
Closure Lid Outer Plate	A1	D	$P_m$	8.11	44.64	5.50
			$(P_m \text{ or } P_L)$	19.24	65.00	3.38
			$P_m + P_b$	16.20	65.00	4.01
			$P_m + P_b + Q$	44.83	65.00	1.45
	A2	D	$P_m$	9.91	44.64	4.50
			$(P_m \text{ or } P_L)$	18.00	65.00	3.61
			$P_m + P_b$	20.44	65.00	3.18
			$P_m + P_b + Q$	41.29	65.00	1.57
	A3	D	$P_m$	7.08	44.64	6.31
			$(P_m \text{ or } P_L)$	21.83	65.00	2.98
			$P_m + P_b$	15.15	65.00	4.29
			$P_m + P_b + Q$	46.19	65.00	1.41
	A4	D	$P_m$	5.85	44.64	7.63
			$(P_m \text{ or } P_L)$	20.61	65.00	3.15
			$P_m + P_b$	13.33	65.00	4.88
			$P_m + P_b + Q$	42.66	65.00	1.52
	A5	D	$P_m$	14.44	44.64	3.09
			$(P_m \text{ or } P_L)$	22.99	65.00	2.83
			$P_m + P_b$	19.92	65.00	3.26
			$P_m + P_b + Q$	42.75	65.00	1.52
	A6	D	$P_m$	16.00	44.64	2.79
			$(P_m \text{ or } P_L)$	23.78	65.00	2.73
			$P_m + P_b$	20.48	65.00	3.17
			$P_m + P_b + Q$	39.29	65.00	1.65
	A7	D	$P_m$	6.35	44.64	7.03
			$(P_m \text{ or } P_L)$	18.59	65.00	3.50
			$P_m + P_b$	11.82	65.00	5.50
			$P_m + P_b + Q$	43.11	65.00	1.51
	A8	D	$P_m$	7.52	44.64	5.94
			$(P_m \text{ or } P_L)$	17.36	65.00	3.74
			$P_m + P_b$	14.45	65.00	4.50
			$P_m + P_b + Q$	39.57	65.00	1.64
	A9	D	$P_m$	8.58	44.64	5.20
			$(P_m \text{ or } P_L)$	20.10	65.00	3.23

**Table 2-22**  
**HAC Load Combinations – Lid Stress Intensity Results**  
 (2 Pages)

Component	Load Case	Service Level	Stress Category	Stress Intensity (ksi)	Allowable Stress (ksi)	Factor of Safety
Closure Lid Outer Plate	A9	D	$P_m + P_b$	15.04	65.00	4.32
			$P_m + P_b + Q$	43.84	65.00	1.48
	A10	D	$P_m$	7.76	44.64	5.75
			$(P_m \text{ or } P_L)$	18.74	65.00	3.47
			$P_m + P_b$	15.81	65.00	4.11
			$P_m + P_b + Q$	40.39	65.00	1.61
	Max A1 to A11	D	$P_m$	16.00	44.64	2.79
			$(P_m \text{ or } P_L)$	23.78	65.00	2.73
			$P_m + P_b$	20.48	65.00	3.17
			$P_m + P_b + Q$	46.19	65.00	1.41

## Notes:

1. Allowable limits are based on temperature of 400 °F.
2. Bending stresses at the closure lid bolt holes circle region are secondary stress.  $P_m$  and  $P_m + P_b$  stresses above do not account for local effects of geometric or material discontinuities and stress concentrations in region around the bolt holes.
3. Range of Primary + Secondary Stress or  $(P_m \text{ or } P_L) + P_b + Q$  are not applicable for HAC.  $(P_m \text{ or } P_L) + P_b$  allowables are utilized above. These values are presented only for completeness.

**Table 2-23**  
**HAC Load Combinations – Penetration Sleeves Stress Intensity Results**

Component	Load Case	Service Level	Stress Category	Stress Intensity (ksi)	Allowable Stress (ksi)	Factor of Safety
Penetration Sleeves	A1	D	$P_m$	11.77	49.00	4.16
			$P_m + P_b$	19.67	70.00	3.56
	A2	D	$P_m$	16.73	49.00	2.93
			$P_m + P_b$	26.41	70.00	2.65
	A3	D	$P_m$	10.84	49.00	4.52
			$P_m + P_b$	13.50	70.00	5.19
	A4	D	$P_m$	9.00	49.00	5.44
			$P_m + P_b$	12.81	70.00	5.46
	A5	D	$P_m$	12.99	49.00	3.77
			$P_m + P_b$	21.14	70.00	3.31
	A6	D	$P_m$	15.48	49.00	3.17
			$P_m + P_b$	24.96	70.00	2.80
	A7	D	$P_m$	7.53	49.00	6.51
			$P_m + P_b$	14.08	70.00	4.97
	A8	D	$P_m$	8.27	49.00	5.93
			$P_m + P_b$	16.37	70.00	4.28
	A9	D	$P_m$	12.92	49.00	3.79
			$P_m + P_b$	14.02	70.00	4.99
	A10	D	$P_m$	10.13	49.00	4.84
			$P_m + P_b$	13.35	70.00	5.24
	Max A1 to A11	D	$P_m$	16.73		2.93
			$P_m + P_b$	26.41		2.65

**Table 2-24**  
**HAC Load Combinations – Gamma Shield Shell Stress Intensity Results**

Component	Load Case	Service Level	Stress Category	Stress Intensity (ksi)	Allowable Stress (ksi)	Factor of Safety
Gamma Shield Shell Cylinder	A1	D	$P_m$	7.56	49.00	6.48
			$P_m + P_b$	15.54	70.00	4.50
	A2	D	$P_m$	7.37	49.00	6.65
			$P_m + P_b$	14.43	70.00	4.85
	A3	D	$P_m$	7.79	49.00	6.29
			$P_m + P_b$	9.39	70.00	7.45
	A4	D	$P_m$	7.51	49.00	6.52
			$P_m + P_b$	8.97	70.00	7.80
	A5	D	$P_m$	17.97	49.00	2.73
			$P_m + P_b$	34.94	70.00	2.00
	A6	D	$P_m$	18.02	49.00	2.72
			$P_m + P_b$	34.95	70.00	2.00
	A7	D	$P_m$	5.19	49.00	9.44
			$P_m + P_b$	14.94	70.00	4.69
	A8	D	$P_m$	4.95	49.00	9.90
			$P_m + P_b$	13.84	70.00	5.06
	A9	D	$P_m$	7.49	49.00	6.54
			$P_m + P_b$	12.47	70.00	5.61
	A10	D	$P_m$	7.42	49.00	6.60
			$P_m + P_b$	11.40	70.00	6.14
	Max A1 to A11	D	$P_m$	18.02		2.72
			$P_m + P_b$	34.95		2.00

**Table 2-25**  
**HAC Load Combinations – Bottom Shield Plate Stress Intensity Results**

Component	Load Case	Service Level	Stress Category	Stress Intensity (ksi)	Allowable Stress (ksi)	Factor of Safety
Bottom Shield Plate	A1	D	$P_m$	7.22	49.00	6.79
			$P_m + P_b$	7.85	70.00	8.92
	A2	D	$P_m$	6.85	49.00	7.15
			$P_m + P_b$	7.06	70.00	9.92
	A3	D	$P_m$	1.61	49.00	30.43
			$P_m + P_b$	4.42	70.00	15.84
	A4	D	$P_m$	1.75	49.00	28.00
			$P_m + P_b$	4.20	70.00	16.67
	A5	D	$P_m$	12.64	49.00	3.88
			$P_m + P_b$	21.16	70.00	3.31
	A6	D	$P_m$	12.67	49.00	3.87
			$P_m + P_b$	20.97	70.00	3.34
	A7	D	$P_m$	3.61	49.00	13.57
			$P_m + P_b$	5.36	70.00	13.06
	A8	D	$P_m$	3.55	49.00	13.80
			$P_m + P_b$	4.55	70.00	15.38
	A9	D	$P_m$	22.22	49.00	2.21
			$P_m + P_b$	61.50	70.00	1.14
	A10	D	$P_m$	21.86	49.00	2.24
			$P_m + P_b$	61.39	70.00	1.14
	Max A1 to A11	D	$P_m$	22.22		2.21
			$P_m + P_b$	61.50		1.14



**Table 2-26**  
**HAC Load Combinations – Bottom Inner Plate Stress Intensity Results**

Component	Load Case	Service Level	Stress Category	Stress Intensity (ksi)	Allowable Stress (ksi)	Factor of Safety
Bottom Inner Plate	A1	D	$P_m$	5.27	44.64	8.47
			$P_m + P_b$	8.20	65.00	7.93
	A2	D	$P_m$	5.25	44.64	8.50
			$P_m + P_b$	8.37	65.00	7.77
	A3	D	$P_m$	5.69	44.64	7.85
			$P_m + P_b$	9.44	65.00	6.89
	A4	D	$P_m$	6.11	44.64	7.31
			$P_m + P_b$	10.24	65.00	6.35
	A5	D	$P_m$	9.31	44.64	4.79
			$P_m + P_b$	13.69	65.00	4.75
	A6	D	$P_m$	9.22	44.64	4.84
			$P_m + P_b$	14.32	65.00	4.54
	A7	D	$P_m$	5.39	44.64	8.28
			$P_m + P_b$	8.80	65.00	7.39
	A8	D	$P_m$	5.76	44.64	7.75
			$P_m + P_b$	9.51	65.00	6.83
	A9	D	$P_m$	4.48	44.64	9.96
			$P_m + P_b$	5.32	65.00	12.22
	A10	D	$P_m$	3.77	44.64	11.84
			$P_m + P_b$	5.68	65.00	11.44
	Max A1 to A11	D	$P_m$	9.31		4.80
			$P_m + P_b$	14.32		4.54

**Table 2-27**  
**HAC Load Combinations – Inner Shell Stress Intensity Results**

Component	Load Case	Service Level	Stress Category	Stress Intensity (ksi)	Allowable Stress (ksi)	Factor of Safety
Inner Shell	A1	D	$P_m$	14.05	44.64	3.18
			$P_m + P_b$	14.74	65.00	4.41
	A2	D	$P_m$	14.56	44.64	3.07
			$P_m + P_b$	15.29	65.00	4.25
	A3	D	$P_m$	13.99	44.64	3.19
			$P_m + P_b$	14.67	65.00	4.43
	A4	D	$P_m$	14.67	44.64	3.04
			$P_m + P_b$	15.39	65.00	4.22
	A5	D	$P_m$	22.44	44.64	1.99
			$P_m + P_b$	26.32	65.00	2.47
	A6	D	$P_m$	22.30	44.64	2.00
			$P_m + P_b$	26.19	65.00	2.48
	A7	D	$P_m$	14.99	44.64	2.98
			$P_m + P_b$	15.70	65.00	4.14
	A8	D	$P_m$	15.49	44.64	2.88
			$P_m + P_b$	16.25	65.00	4.00
	A9	D	$P_m$	15.83	44.64	2.82
			$P_m + P_b$	17.18	65.00	3.78
	A10	D	$P_m$	16.50	44.64	2.71
			$P_m + P_b$	17.06	65.00	3.81
	Max A1 to A11	D	$P_m$	22.44		1.99
			$P_m + P_b$	26.32		2.47

**Table 2-28**  
**HAC Load Combinations – Top Shield Plate Stress Intensity Results**

Component	Load Case	Service Level	Stress Category	Stress Intensity (ksi)	Allowable Stress (ksi)	Factor of Safety
Top Shield Plate	A1	D	$P_m$	6.07	49.00	8.07
			$P_m + P_b$	13.56	70.00	5.16
	A2	D	$P_m$	5.60	49.00	8.75
			$P_m + P_b$	12.34	70.00	5.67
	A3	D	$P_m$	4.07	49.00	12.04
			$P_m + P_b$	9.27	70.00	7.55
	A4	D	$P_m$	3.33	49.00	14.71
			$P_m + P_b$	9.11	70.00	7.68
	A5	D	$P_m$	20.42	49.00	2.40
			$P_m + P_b$	32.62	70.00	2.15
	A6	D	$P_m$	20.16	49.00	2.43
			$P_m + P_b$	31.73	70.00	2.21
	A7	D	$P_m$	5.43	49.00	9.02
			$P_m + P_b$	13.11	70.00	5.34
	A8	D	$P_m$	4.82	49.00	10.17
			$P_m + P_b$	11.89	70.00	5.89
	A9	D	$P_m$	9.31	49.00	5.26
			$P_m + P_b$	19.80	70.00	3.54
	A10	D	$P_m$	7.57	49.00	6.47
			$P_m + P_b$	15.25	70.00	4.59
	Max A1 to A11	D	$P_m$	20.42		2.40
			$P_m + P_b$	32.62		2.15

**Table 2-29**  
**HAC Load Combinations – Shell Flange Stress Intensity Results**

Component	Load Case	Service Level	Stress Category	Stress Intensity (ksi)	Allowable Stress (ksi)	Factor of Safety
Shell Flange	A1	D	$P_m$	7.82	49.00	6.27
			$P_m + P_b$	12.35	70.00	5.67
	A2	D	$P_m$	8.80	49.00	5.57
			$P_m + P_b$	13.97	70.00	5.01
	A3	D	$P_m$	8.70	49.00	5.63
			$P_m + P_b$	12.72	70.00	5.50
	A4	D	$P_m$	9.74	49.00	5.03
			$P_m + P_b$	14.32	70.00	4.89
	A5	D	$P_m$	21.52	49.00	2.28
			$P_m + P_b$	23.09	70.00	3.03
	A6	D	$P_m$	21.20	49.00	2.31
			$P_m + P_b$	22.94	70.00	3.05
	A7	D	$P_m$	6.42	49.00	7.63
			$P_m + P_b$	9.25	70.00	7.57
	A8	D	$P_m$	6.98	49.00	7.02
			$P_m + P_b$	10.89	70.00	6.43
	A9	D	$P_m$	11.54	49.00	4.25
			$P_m + P_b$	13.01	70.00	5.38
	A10	D	$P_m$	11.24	49.00	4.36
			$P_m + P_b$	12.87	70.00	5.44
	Max A1 to A11	D	$P_m$	21.52		2.28
			$P_m + P_b$	23.09		3.03

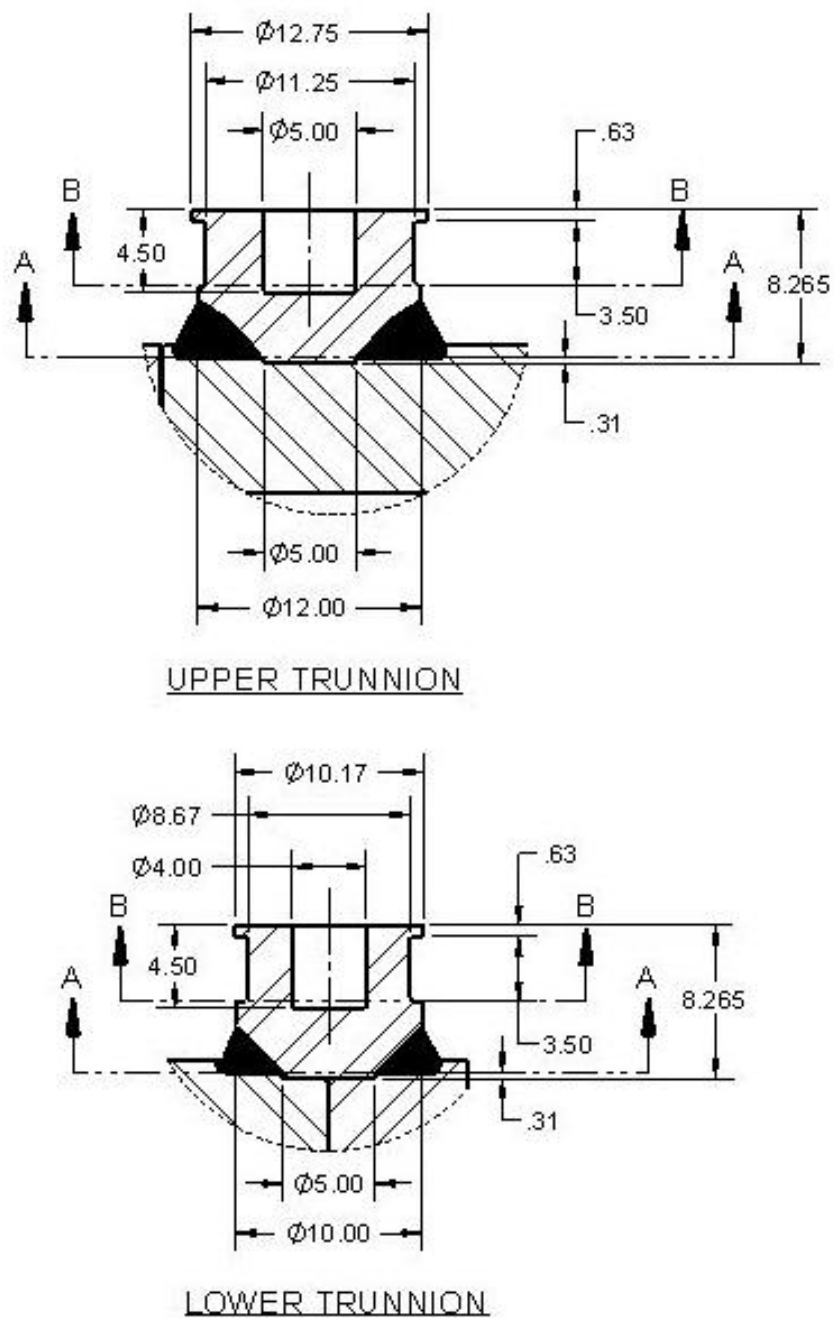
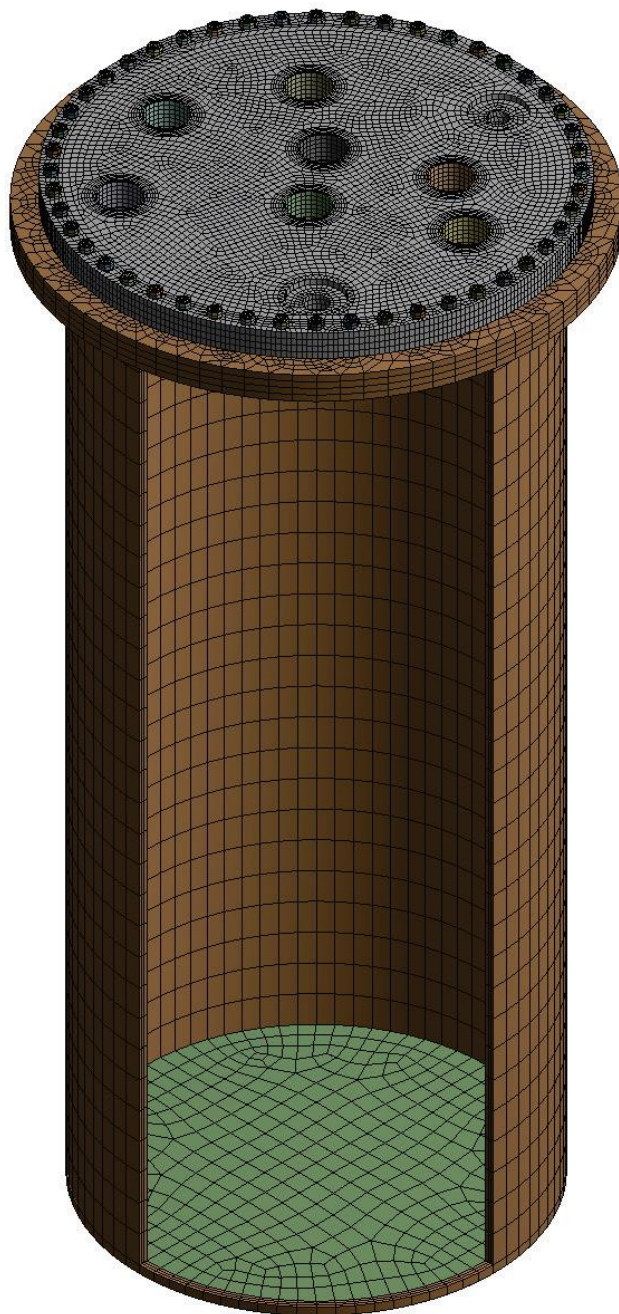


**Figure 2-1**  
**Geometry of Upper (front) and Lower (rear) Trunnions**



Note: Some elements were unselected (hidden) to illustrate the mesh through the thickness of cask.

**Figure 2-2**  
**Nonlinear Buckling Finite Element Model for Immersion Analysis**

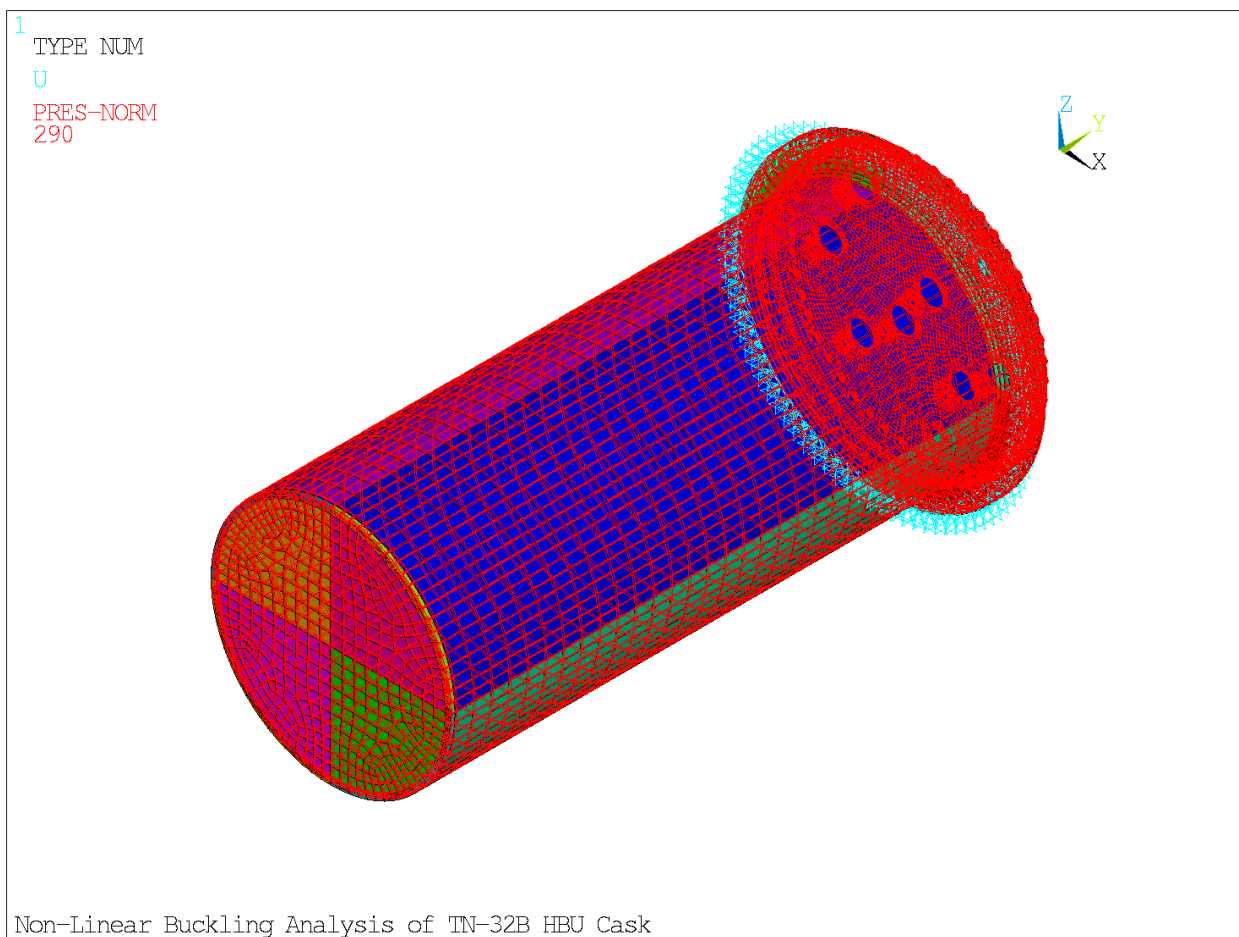


**Figure 2-3**  
**290 psig Immersion Analysis Finite Element Model Loads and Boundary Conditions**

## 2.12 Appendices

The detailed structural analyses of the TN-32B HBU demonstration cask are included in the following appendices:

- Appendix 2.12.1 References
- Appendix 2.12.2 Structural Analysis of Cask Body
- Appendix 2.12.3 Closure Lid Bolt Analysis
- Appendix 2.12.4 Structural Analysis of the Outer Shell
- Appendix 2.12.5 Fracture Toughness Evaluation of the TN-32B HBU Cask
- Appendix 2.12.6 Structural Analysis of the TN-32B HBU Cask Basket
- Appendix 2.12.7 Dynamic Load Factor for Basket Drop Analysis
- Appendix 2.12.8 Structural Evaluation of the Fuel Rod Cladding Under Accident Impact
- Appendix 2.12.9 Structural Evaluation of the Impact Limiters
- Appendix 2.12.10 TN-40 Cask Impact Limiter Testing
- Appendix 2.12.11 Deep Water Immersion
- Appendix 2.12.12 Structural Analysis of the Thermocouple Lance Assembly
- Appendix 2.12.13 ASME B&PV Code Alternatives



## Appendix 2.12.1 References

1. Design Criteria for the Structural Analysis of Shipping Cask Containment Vessels, U. S. Nuclear Regulatory Commission, Regulatory Guide 7.6, Revision 1, March 1978.
2. Regulatory Guide 7.8, "Load Combinations for the Structural Analysis of Shipping Cask", U.S. Nuclear Regulatory Commission, Rev. 1, March 1989.
3. Title 10, Code of Federal Regulations - Energy, Part 71 (10 CFR 71), "Packaging and Transportation of Radioactive Material", 1-1-2021 Edition, U.S. Nuclear Regulatory Commission, Washington, D.C.
4. American Society of Mechanical Engineers, ASME Boiler and Pressure Vessel Code, Section III, Division 1, Subsection NB, Appendices, and Appendix F, 1992 Edition with 1992 Addenda.
5. American Society of Mechanical Engineers, ASME Boiler and Pressure Vessel Code, Section IX, 1992 Edition with 1992 Addenda.
6. American Society of Mechanical Engineers, ASME Boiler and Pressure Vessel Code, Section III, Division 1, Subsection NF, and Appendix F, 2013 Edition.
7. American Society of Mechanical Engineers, ASME Boiler and Pressure Vessel Code, Section V, 1992 Edition with 1992 Addenda.
8. *Standard Review Plan for Transportation Packages for Spent Nuclear Fuel*, NUREG-1617, U.S. Nuclear Regulatory Commission, March 2000.
9. L. E. Fischer, W. Lai, *Fabrication Criteria for Shipping Container*, NUREG/CR-3854, U.S. Nuclear Regulatory Commission, March 1985.
10. American Society of Mechanical Engineers, ASME Boiler and Pressure Vessel Code, Section II, Part D, 1992 Edition with 1992 Addenda.
11. American Society of Mechanical Engineers, ASME Boiler and Pressure Vessel Code, Section II, Part D, 2013 Edition.
12. Aluminum Standards and Data-1, 1976, published by the Aluminum Association.
13. M. W. Schwartz, *Recommendations for Protecting Against Failure by Brittle Fracture in Ferritic Steel Shipping Containers Greater than Four Inches Thick*, NUREG/CR-3826, U.S. Nuclear Regulatory Commission, April 1984.
14. W. R. Holman, R.T. Langland, *Recommendations for Protecting Against Failure by Brittle Fracture in Ferritic Steel Shipping Containers up to Four Inches Thick*, NUREG/CR-1815, U.S. Nuclear Regulatory Commission, June 1981.

15. Northern States Power Company, Response to Bulletin 96-04, August 19, 1996, Docket No. 72-10, Materials License No. SNM-2506.
16. Hydrogen Generation Analysis Report for TN-32B HBU Cask Materials, Test Report No. 61123-99N, Rev 0, Oct 23, 1998, National Technical Systems.
17. ANSYS® Engineering Analysis System, User's Manual for ANSYS® Release 8.0.
18. WRC Bulletin 107, March 1979, "Local Stresses in Spherical and Cylindrical Shells Due to External Loadings".
19. C. F. Magnuson, L.T. Wilson, *Shock and Vibration Environments for Large Shipping Containers on Rail Cars and Trucks*, NUREG-766510, U.S. Nuclear Regulatory Commission, June 1977.
20. G. C Mok, L.E. Fisher, *Stress Analysis of Closure Bolts for Shipping Cask*, NUREG/CR-6007, UCRL-ID-110637, U.S. Nuclear Regulatory Commission, January 1993.
21. Bechtel Power Corporation, "Design of Structures for Missile Impact," BC-TOP-9-A, Rev. 2, September 1974.
22. Roark, Raymond J. and Young, Warren C., "Formulas for Stress and Strain," Seventh Edition, 2002.
23. American Society of Mechanical Engineers, ASME Boiler and Pressure Vessel Code, Section VIII, Divisions 1 and 2, 1992 Edition.

## **Appendix 2.12.2**

### **Structural Analysis of Cask Body**

#### TABLE OF CONTENTS

2.12.2	Structural Analysis of Cask Body .....	2.12.2-1
2.12.2.1	Introduction .....	2.12.2-1
2.12.2.2	ANSYS® Analysis .....	2.12.2-2
2.12.2.3	Pressure Distribution over Contact Area for Impact Load .....	2.12.2-22
2.12.2.4	Analysis Results .....	2.12.2-24
2.12.2.5	References .....	2.12.2-25

#### LIST OF TABLES

Table 2.12.2-1	Major Dimensions .....	2.12.2-26
Table 2.12.2-2	Summary Maximum Nodal Stress Intensities in Cask Components for Individual Load Runs .....	2.12.2-27
Table 2.12.2-3	6g Lifting Load .....	2.12.2-28

LIST OF FIGURES

Figure 2.12.2-1	TN-32B HBU Demonstration Cask Finite Element Model .....	2.12.2-28
Figure 2.12.2-2	TN-32B HBU Demonstration Cask Finite Element Model – Lid and Shield .....	2.12.2-29
Figure 2.12.2-3	Thermal Stresses 100 °F Environment (IL-6) – 270° Cut View of Mapped Thermal Data.....	2.12.2-30
Figure 2.12.2-4	Thermal Stresses -20 °F Environment (IL-7) – 270° Cut View of Mapped Thermal Data.....	2.12.2-31
Figure 2.12.2-5	Thermal Stresses -40 °F Environment (IL-8) – 270° Cut View of Mapped Thermal Data.....	2.12.2-32
Figure 2.12.2-6	Radial Pressure Due to Internals (IL-9) – Loading.....	2.12.2-33
Figure 2.12.2-7	1g Cask Horizontal (IL-9) – Loading and Displacement Boundary Conditions .....	2.12.2-34
Figure 2.12.2-8	Radial Pressure Due to Internals (IL-10) – Loading.....	2.12.2-35
Figure 2.12.2-9	Rail Shock Cask Horizontal (IL-10) – Loading and Displacement Boundary Conditions .....	2.12.2-36
Figure 2.12.2-10	End Drop on Closure Lid (IL-12) – Axial Pressure Due to Weight of Internals .....	2.12.2-37
Figure 2.12.2-11	End Drop on Closure Lid (IL-12) – Loading and Displacement Boundary Conditions .....	2.12.2-38
Figure 2.12.2-12	End Drop on Bottom (IL-13) – Loading and Displacement Boundary Conditions .....	2.12.2-39
Figure 2.12.2-13	Radial Pressure Due to Internals (IL-14) – Loading.....	2.12.2-40
Figure 2.12.2-14	Side Drop (IL-14) – Loading and Displacement Boundary Conditions .....	2.12.2-41
Figure 2.12.2-15	CG-Over-Corner Drop on Top (IL-15) – Radial Pressure Due to Internals Loading.....	2.12.2-42
Figure 2.12.2-16	CG-Over-Corner Drop – Crush Area Pressures (IL-15) .....	2.12.2-43
Figure 2.12.2-17	CG-Over-Corner Drop on Top (IL-15) – Loading and Displacement Boundary Conditions .....	2.12.2-44
Figure 2.12.2-18	CG-Over-Corner Drop on Bottom (IL-16) – Radial Pressure Due to Internals Loading.....	2.12.2-45
Figure 2.12.2-19	CG-Over-Corner Drop – Crush Area Pressures (IL-16) .....	2.12.2-46
Figure 2.12.2-20	CG-Over-Corner Drop on Bottom (IL-16) – Loading and Displacement Boundary Conditions.....	2.12.2-47

## 2.12.2 Structural Analysis of Cask Body

### 2.12.2.1 Introduction

This appendix presents the structural analyses of the TN-32B HBU demonstration cask body, and the local stresses at the trunnion/cask body interface. The cask body includes the inner shell, bottom inner plate, gamma shield shell cylinder, bottom shield plate, shell flange, and the modified closure lid assembly (lid outer plate, lid shield plate, and penetration sleeves). The methods, models, and assumptions utilized in analyzing the cask body under various individual loading conditions as specified in 10 CFR 71.71 and 10 CFR 71.73 [1] are described. These conditions include both the normal conditions of transport (NCT) and the hypothetical accident conditions (HAC). Stress results are reported at selected locations for each load case. Maximum stresses from this appendix are evaluated in Sections 2.6 and 2.7, where the load combinations are performed as outlined in Regulatory Guide 7.8 [2], and the results are evaluated against the American Society of Mechanical Engineers (ASME) Boiler & Pressure Vessel (B&PV) Code [3] and Regulatory Guide 7.6 [4] design criteria, which are described in Section 2.1.2.

Static, nonlinear elastic methods are utilized for the TN-32B HBU demonstration cask body structural analyses. The nonlinear behavior is due to the presence of status-dependent contact elements that are determined by the loading cases. The stresses and deformations resulting from the applied loads are generally determined utilizing the ANSYS® [5] computer program.

The detailed calculations for the closure lid bolts are presented in Appendix 2.12.3. Stress evaluations of the lifting devices and tie-down system are described in Section 2.5.

The two analysis methods described in this appendix, and utilized to evaluate the cask body for the specified loading conditions are:

- ANSYS® Analysis – Static nonlinear elastic analysis using a (three-dimensional) 3-D model
- Bijlaard trunnion local stress analysis [6]

The Bijlaard analyses are performed to determine the local cask body stresses at trunnion locations where general stresses are also reported from the ANSYS® analyses. This permits the localized shell stresses induced by the trunnion loadings to be easily combined with stresses obtained from appropriate ANSYS® load cases. The method of combining stress results from individual load cases and their evaluations are discussed in Section 2.6 and Section 2.7 for NCT and HAC loads, respectively.

### 2.12.2.2 ANSYS® Analysis

#### Cask Geometry Description

The inner shell, bottom inner plate, the shell flange, the closure lid outer plate, and the thermocouple lance assemblies (TLAs) form the primary containment boundary of the packaging. Key dimensions of the cask body are shown in Table 2.12.2-1. The inner shell is 1.5-inch thick cylinder welded to the shell flange and bottom inner plate. The inner shell is shrunk-fit into the 8.0-inch thick gamma shield shell. The 4.5-inch thick closure lid plate is secured to the shell flange by 48, 1.5-inch diameter, high strength bolts with hardened steel washers and a 1.375-inch reduced diameter shank, and sealed with a double metallic O-ring seal. The modified lid assembly, inner shell, bottom inner plate, and gamma shield shell components are fabricated from low alloy steel forgings and plates. The cask is fitted with an impact limiter (IL) at either end. The ILs are attached to each other by 13 tie-rods and to the cask body by attachment bolt brackets that are welded to the outer neutron shield shell in eight locations. Two sets of trunnions are welded to the side of the gamma shield shell upper and lower ends for handling and supporting the cask during lifting and handling operations. A basket assembly inside the cask cavity is utilized to position and support the HBU spent fuel assemblies. A detailed physical description of the containment components is provided in Chapter 1. Appendix 1.4.1, contains reference drawings of the TN-32B HBU demonstration cask package that the analysis models are based.

#### ANSYS® Cask Model

The objective of the analysis is to qualify the cask and the modified lid assembly. There are seven penetrations in the closure lid that accommodate the TLA instrumentation that are modeled. In addition, two existing penetrations (vent and drain) are also modeled. Since the pattern of the penetrations is not in a symmetric configuration, a 3-D finite element model (FEM) of the cask with a modified closure lid is necessary.

The model is created utilizing the ANSYS® program. ANSYS® 8-noded brick elements are utilized to define the solid bodies of the cask assembly. Contact between components is represented by contact pairs. Contact is modeled between surfaces of the closure lid outer plate and shield plate, and between the closure lid plate and shell flange. Contact is also defined between the inner shell and the gamma shield shell cylinder. ANSYS® standard contact allows separation and sliding for all surfaces in contact. The change in contact status facilitates the nonlinear behavior of the model. A coefficient of friction,  $\mu$ , of 0.42 (sliding between hard steel on hard steel) is assumed for all contact elements per Table 3.2.4 of Reference [7]. Bonded contact is defined for the vessel bottom to the shield bottom interface. Note that no contact is modeled between the penetration sleeves and the closure lid/shield plates. This assumption is a very conservative approach especially for the prediction of weld stresses.

Closure lid bolts are modeled utilizing SOLID185 elements. Geometry of the lid bolts is simplified; threaded engagement is modeled through bonded contact (surfaces bonded), as well as the bottom surface of the lid bolt head and washer are fixed to the closure lid outer plate. Bolts also feature pre-tension elements (PRETS179) that enable accurate modeling of the bolt preload. Welded connections are represented by nodal couplings.

Nodal temperatures representing thermal loads are derived from the thermal models discussed in Chapter 3, and interpolated to nodes of this model to obtain thermal stresses.

Figure 2.12.2-1 and Figure 2.12.2-2 depict the geometry of the ANSYS® model and mesh, and Table 2.12.2-1 lists the major bounding dimensions of the model.

### Material Properties

The materials used for TN-32B HBU demonstration cask and their properties are modeled as a function of temperature. For all NCT and HAC load combinations, temperature-dependent linear isotropic material properties are utilized. Immersion buckling analysis (IL-18) utilizes a bilinear kinematic material model as explained in Appendix 2.12.11. The following tables list the material designations and properties of each modeled component.

<b>Cask Component</b>	<b>Material</b>
Lid Outer Plate, Inner Shell & Bottom Inner Plate	SA-203 Gr. D
Inner Shell Flange & Penetration Sleeve Forgings	SA-350 LF3
Lid Shield Plate & Bottom Shield Plate	SA-516, Gr.70
Gamma Shield Cylindrical Forging	SA-266, CL 2
Closure Lid Bolts <sup>(1)</sup>	SA-540 Gr B23, CI 1
Trunnions <sup>(2)</sup>	SA-105

#### Notes:

1. Material properties for the closure lid bolts are provided in Appendix 2.12.3.
2. The density for the upper trunnions is adjusted to 0.342 lb<sub>m</sub>/in<sup>3</sup> in Number 9 in Section 2.12.2.2.

**Material Properties for SA-203 Gr D**

Temp (°F)	E (10 <sup>3</sup> ksi)	S/S <sub>m</sub> (ksi)	S <sub>y</sub> (ksi)	S <sub>u</sub> (ksi)	Coefficient of Thermal Expansion, $\alpha$ (10 <sup>-6</sup> in/in-°F)
70	27.8	18.6/...	37.0	65.0	6.4
200	27.1	18.6/...	33.9	65.0	7.0
300	26.7	18.6/...	32.7	65.0	7.3
400	26.1	18.6/...	31.6	65.0	7.7
500	25.7	18.6/...	30.0	65.0	8.0

## Notes:

1. Density,  $\rho$ , for the lid outer plate is adjusted to 0.521 lb<sub>m</sub>/in<sup>3</sup> in Number 9 in Section 2.12.2.2. Density assumed to be 0.283 lb<sub>m</sub>/in<sup>3</sup>, at all temperatures for the other components. Poisson's ratio,  $\nu$ , is assumed to be 0.3 for all temperatures.
2. No S<sub>m</sub> data is available in the ASME B&PV Code.

**Material Properties for SA-350 LF3**

Temp (°F)	E (10 <sup>3</sup> ksi)	S/S <sub>m</sub> (ksi)	S <sub>y</sub> (ksi)	S <sub>u</sub> (ksi)	Coefficient of Thermal Expansion, $\alpha$ (10 <sup>-6</sup> in/in-°F)
70	27.8	20.0/23.3	37.5	70.0	6.4
200	27.1	20.0/22.9	34.2	70.0	7.0
300	26.7	20.0/22.1	33.2	70.0	7.3
400	26.1	20.0/21.4	32.0	70.0	7.7
500	25.7	20.0/20.3	30.4	70.0	8.0

**Material Properties for SA-516 Gr 70**

Temp (°F)	E (10 <sup>3</sup> ksi)	S/S <sub>m</sub> (ksi)	S <sub>y</sub> (ksi)	S <sub>u</sub> (ksi)	Coefficient of Thermal Expansion, $\alpha$ (10 <sup>-6</sup> in/in-°F)
70	29.3	17.5/23.3	38.0	70.0	6.4
200	28.6	17.5/23.1	34.6	70.0	7.0
300	28.1	17.5/22.5	33.7	70.0	7.3
400	27.5	17.5/21.7	32.6	70.0	7.7
500	27.1	17.5/20.5	30.7	70.0	8.0



**Material Properties for SA-266 Cl 2**

Temp (°F)	E (10 <sup>3</sup> ksi)	S/S <sub>m</sub> (ksi)	S <sub>y</sub> (ksi)	S <sub>u</sub> (ksi)	Coefficient of Thermal Expansion, $\alpha$ (10 <sup>-6</sup> in/in-°F)
70	29.3	17.5/23.3	35.0	70.0	5.62 <sup>2</sup>
200	28.6	17.5/21.9	31.9	70.0	6.09
300	28.1	17.5/21.3	31.0	70.0	6.43
400	27.5	17.5/20.6	30.0	70.0	6.74
500	27.1	17.5/19.4	28.3	70.0	7.06

Notes:

1. Density for the gamma shield cylindrical shell is adjusted to 0.342 lb<sub>m</sub>/in<sup>3</sup> in Number 9 in Section 2.12.2.2.
2. Extrapolated

**Weight Summary**

The weights of different cask components are shown in the table below. These weights are used for different loading conditions of the cask.

No (#)	Component	Weight (lb <sub>m</sub> )
1	Fuel Assembly	49,632
2	Basket Assembly	13,421
3	Guide Funnel	14
4	Thermocouple Lance Assemblies (TLAs)	210
5	Misc. Transportation Hardware	1,263
6	Radial N-Shield Resin	10,233
7	Outer Shell	7,233
8	Lower Trunnion	291
9	Radial N-Shield Aluminum Boxes	1,961
10	Puncture Resistant Plate Assembly	4,676
11	Cask Assembly	235,675
12	Top IL	16,585
13	Bottom IL	16,596
14	Total Weight (#11 to #13)	268,856

Weight of the cask internals ( $W_{int}$ ) is the sum of the weight of the fuel assemblies (#1), the basket assembly (#2), the funnel guides (#3), and the TLAs (#4).

$$W_{int} = 49,632 \text{ lb}_m + 13,421 \text{ lb}_m + 14 \text{ lb}_m + 210 \text{ lb}_m$$

$$W_{int} = 63,277 \text{ lb}_m \approx 63,300 \text{ lb}_m \text{ (rounded-up)}$$

Weight of cask body only:

$$W_{cask} = 235,675 \text{ lb}_m - 63,277 \text{ lb}_m - 1,263 \text{ lb}_m = 171,135 \text{ lb}_m \approx 172,000 \text{ lb}_m \text{ (rounded-up)}$$

Weight of cask body and internals (without ILs and transportation hardware):

$$\text{Total cask weight, } W = (235,675 - 1,263) \text{ lb}_m = 234,412 \text{ lb}_m \approx 236,000 \text{ lb}_m$$

Conservative values of 18,200 lb<sub>m</sub> and 18,400 lb<sub>m</sub> are utilized as weights for the top and bottom ILs, respectively, in this appendix.

### Applied Loadings

The analysis evaluates NCT and HAC applied loadings, as specified in 10 CFR Part 71. Each load case analysis utilizes the FEM of the cask that is defined with pertinent loads and boundary conditions. The 18 individual load cases and load combinations considered in this evaluation are described below.

TN-32B HBU Demonstration Cask Individual Load Cases	
IL-1	Closure Lid Bolt Preload and Lid Seating Pressure
IL-2	Fabrication Stresses
IL-3	Internal Pressure (100 psig)
IL-4	External Pressure (25 psig)
IL-5	Reduced External Pressure (3.5 psig)
IL-6	Thermal Stress Due to Hot Environment (100 °F ambient)
IL-7	Thermal Stress Due to Cold Environment (–20 °F ambient)
IL-8	Thermal Stress Due to Cold Environment (–40 °F ambient)
IL-9	Cask Horizontal – 1g Down (Gravity)
IL-10	Horizontal Cask, Rail Vibrations, Rail Car Shock (0.19g lateral, 0.19g longitudinal, 0.37g vertical)
IL-11	Horizontal Cask, Rail Shock Tie-Down (4.7g all directions)
IL-12	End Drop on Top (Closure Lid) End
IL-13	End Drop on Bottom End
IL-14	Side Drop/Slapdown
IL-15	Corner Drop on Top (Closure Lid) End
IL-16	Corner Drop on Bottom End
IL-17	Fire Accident
IL-18	Deep Immersion (290 psig)

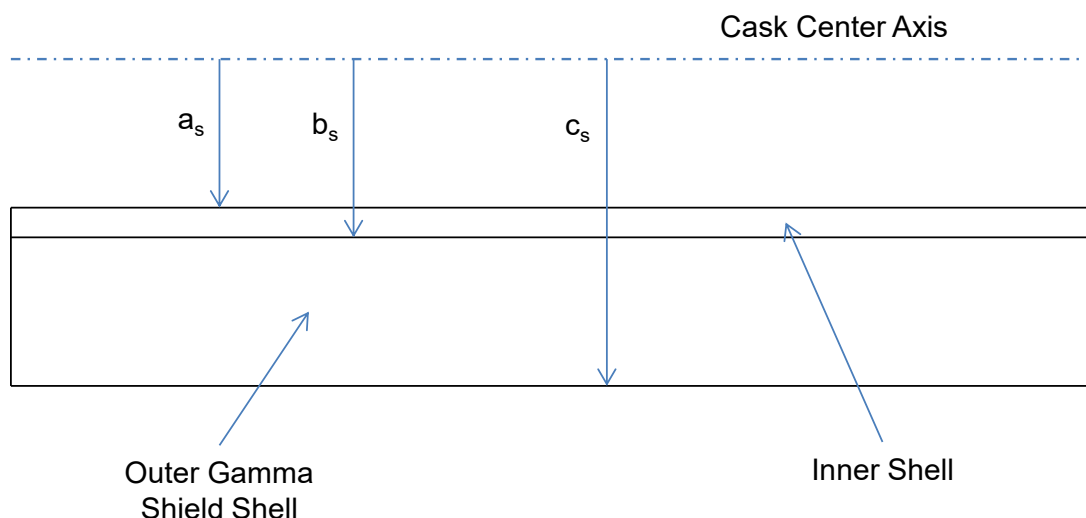
The magnitudes of the applied loads and pressures utilized in each individual load case analysis are computed, as described in the following paragraphs, based on the TN-32B HBU demonstration cask weights discussed in Chapter 2.

#### 1. Closure Lid Bolt Preload and Lid Seating Pressure (IL-1)

The first load case applies the bolt preload. Bolts are modeled using SOLID185 elements, and feature pre-tension elements (PRETS179) that enable accurate modeling of the bolt preload. A bolt preload of 78.5 kips is defined on each bolt utilizing pre-stress elements defined within the bolt shanks.

## 2. Fabrication Stress (IL-2)

The fabrication stresses in the cask are due to the 0.040-inch nominal diametric interference between the inner shell and the gamma shield shell cylinder (Appendix 1.4.1). The fabrication/shrink fit stresses are calculated based on a radial interference of 0.020 inch based on a maximum interference of 0.050 inch, and a maximum gap of 0.020 inch.



The interface pressure at the mating surface,  $p_s$ , can be determined from the following expression from Reference [7]:

$$p_s = \left[ \frac{E_s \delta_s}{b_s} \right] \frac{(b_s^2 - a_s^2)(c_s^2 - b_s^2)}{2b_s^2(c_s^2 - a_s^2)} = 0.578 \text{ ksi} \Rightarrow \text{use } 580 \text{ psi}$$

where:

$$\begin{aligned} \delta_s &= 0.020 \text{ inch} & E_s &= 29.5 \times 10^6 \text{ psi} & a_s &= 34.375 \text{ inch} \\ b_s &= 35.875 \text{ inch} & c_s &= 43.875 \text{ inch} \end{aligned}$$

The interface pressure of 580 psi is applied to the two cylinders, the inner containment shell and the outer shield shell.

## 3. Internal Pressure Loading (100 psig) (IL-3)

An internal pressure of 100 psig is applied to the cavity surface. The pressure is applied up to the metallic seal inner radius. The pressure at modified closure lid penetration sleeves is adjusted (increased by appropriate factor) to compensate for the area of modeled holes. The pressure adjustment factor is calculated below.

Calculation of pressure adjustment factor (AF) for the penetration sleeves is as follows:

$$AF = \frac{\frac{\pi}{4} OD^2}{\frac{\pi}{4} (OD^2 - ID^2)} = \frac{OD^2}{OD^2 - ID^2} = \frac{8^2}{8^2 - 1.5^2} = 1.04$$

where:

OD is the outside diameter of the penetration sleeve, 8.0 in<sup>2</sup>

ID is the inside diameter of the penetration sleeve, 1.5 in<sup>2</sup>

Internal pressure at the penetration sleeves (maximum value) = 1.04(100) = 104 psig.

#### 4. External Pressure Loading (IL-4)

An external pressure of 25 psig is applied to the outer surface of the cask body. The pressure is applied up to the external surfaces of the closure lid, the containment vessel, and the neutron shield shell.

Calculation of the pressure AF for existing drain and vent openings is as follows:

$$AF = \frac{\frac{\pi}{4}OD^2}{\frac{\pi}{4}(OD^2 - ID^2)} = \frac{OD^2}{OD^2 - ID^2} = \frac{9.12^2}{9.12^2 - 4.12^2} = 1.26$$

where:

OD = the outside diameter of the existing opening, 9.12 in<sup>2</sup>

ID = inside diameter of the vent/drain openings (conservative value), 4.12 in<sup>2</sup>

External Pressure at opening (maximum value) = 1.26(25) = 31.5 psig.

#### 5. Reduced External Pressure 3.5 psig (IL-5)

An external pressure of 3.5 psig is applied to the outer surface of the cask body. The pressure is applied similar to the IL-4 load case.

#### 6. Thermal Stress for Hot Environment Condition at 100 °F Ambient Temperature (IL-6)

The thermal analysis of the cask body is described in Chapter 3. The thermal model is utilized to obtain the steady-state metal temperatures in the cask body for the normal condition, which includes 100 °F daily averaged ambient air temperature, HBU payload decay heat, and maximum insolation input. The thermal ANSYS® model is a 180° symmetrical model. The cask nodal temperatures from thermal results file are used to interpolate nodal temperatures in 360° structural model. The resulting temperature distribution is shown in Figure 2.12.2-3. These temperatures are then used as ANSYS® input for the thermal stress analysis. Temperature dependent material properties are used in this run.

#### 7. Thermal Stress for Cold Environment Condition at -20 °F Ambient Temperature (IL-7)

The thermal analysis of the cask body is described in Chapter 3. The cask nodal temperatures from the thermal results file are used to interpolate nodal temperatures in the structural model. The resulting temperature distribution is shown in Figure 2.12.2-4. These temperatures are then utilized as ANSYS® input for the thermal stress analysis. Temperature dependent material properties are used in this run.

## 8. Thermal Stress for Cold Environment Condition at -40 °F Ambient Temperature (IL-8)

The thermal analysis of the cask body is described in Chapter 3. The cask nodal temperatures from thermal results file are utilized to interpolate nodal temperatures in structural model. The resulting temperature distribution is shown in Figure 2.12.2-5. These temperatures are then used as ANSYS® input for the thermal stress analysis. Temperature dependent material properties are used in this run.

## 9. Cask Supported Horizontally by Skid, 1g down Gravity Load (IL-9)

For the gravity loading, the weight of the internals previously calculated ( $W_{int} = 63,300 \text{ lb}_m$ ) is utilized. For the 1g loading, the cask is oriented horizontally and cask front is secured axially and radially on a transport skid. For the inertial loading, a vertical acceleration of 1g is applied in the global Z direction. In addition, the following loads are applied:

Radial pressure ( $P_r$ ) acting on the lower half of the inner cask surface due to the weight of internals is represented as a cosine varying pressure applied around the lower radial portion (0 to 75 degree range) of the cavity. The formula below for cosine distribution is reproduced in Section 2.12.2.3:

$$Pr = [G_{\text{vertical}}] \left( \frac{W}{LR} \right) \left[ \frac{\sin\left(\frac{\pi}{2} + \theta\right)}{\left[\left(\frac{\pi}{2\theta}\right) + 1\right]} + \frac{\sin\left(\frac{\pi}{2} - \theta\right)}{\left[\left(\frac{\pi}{2\theta}\right) - 1\right]} \right]^{-1} \cos\left(\frac{\pi\theta_i}{2\theta}\right)$$

where:

$\theta = 1/2$  angle of contact

$\theta_i =$  circumferential angle at which pressure is applied

$W =$  weight of internals

$L =$  length pressure is applied

A pressure applied at an angle of 7.5° would be calculated as follows:

$$Pr = [1.0] \left[ \frac{63,300}{160.00(34.375)} \right] \left[ \frac{\sin\left(90 + 75\right)}{\left[\frac{180}{2(75)} + 1\right]} + \frac{\sin\left(90 - 75\right)}{\left[\frac{180}{2(75)} - 1\right]} \right]^{-1} \cos\left(\frac{180(7.5)}{2(75)}\right) = 11.280(0.7083)(0.9877) = 8.05 \text{ psi}$$

The maximum pressure at 0 degrees is  $Pr = 8.15 \text{ psi}$ .

The model loading is illustrated in Figure 2.12.2-6.

In addition, radial pressure ( $P_{fr}$ ) due to the front IL weight is applied along the contacting surfaces of the limiter and the closure lid/cask flange. Conservatively ignoring the puncture resistant plate interface, the 12-inch engagement is applied to the 4.5-inch thick lid and 7.5 inches of the flange. The pressure follows a cosine distribution and is applied from the vertical ( $Y=180^\circ$  to  $Y=105^\circ$ ).

It should be noted that because of FEM mesh limitations, some elements lie partially inside and partially outside of the IL footprint. For those elements, average pressure values are applied based on near zero pressure values for nodes lying outside the IL zone.

A radial pressure due to the rear IL weight ( $P_{rr}$ ) is also applied along the contacting surfaces of the limiter and the cask wall. Similar to the front IL, the pressure follows a cosine distribution, and is applied from the vertical ( $Y=180^\circ$  to  $Y=105^\circ$ ).

The values for neutron shield resin (10,233 lb<sub>m</sub>) + outer shell (7,235 lb<sub>m</sub>) + lower trunnions (290.5 lb<sub>m</sub>) + aluminum boxes (1,961 lb<sub>m</sub>) weights are not included in the ANSYS® model, but are incorporated in the outer gamma shield cylinder by increasing its actual density (0.283 lb<sub>m</sub>/in<sup>3</sup>) to an equivalent density of  $1.208(0.283) = 0.342$  lb<sub>m</sub>/in<sup>3</sup>.

Note that the density of the closure lid plate material was adjusted to account for masses that are not physically modeled, but act on the plate. Those items are: the puncture resistant plate, the lance cover plates, and the TLA cables/connections. The density adjustment is calculated below.

The total weight of non-modeled items (puncture resistant plate assembly and thermocouple lances) is 4,746 lb<sub>m</sub> = 4,676 lb<sub>m</sub> + (7×10) lb<sub>m</sub>.

The modeled volume of the top lid plate is 20,064 in<sup>3</sup>, retrieved from the ANSYS® model. The top lid plate modeled weight is 5,678 lb<sub>m</sub> (20,064 in<sup>3</sup> × 0.283 lb<sub>m</sub>/in<sup>3</sup>) extracted from the ANSYS® model.

Therefore, the adjusted density is  $0.521$  lb<sub>m</sub>/in<sup>3</sup> =  $(5,678 \text{ lb}_m + 4,746 \text{ lb}_m \approx 10,450 \text{ lb}_m)/20,064 \text{ in}^3$ .

The cask is supported in the ANSYS® model as shown in Figure 2.12.2-7.

#### 10. Horizontal Cask, Rail Vibration, Rail Car Shock Loading (0.19g lateral, 0.19g longitudinal, 0.37g vertical) (IL-10)

For the rail vibration, rail car shock down loading, the cask is oriented horizontally and cask front is secured axially and radially on a transport skid. The input loading conditions used to evaluate the cask for this loading are obtained from Reference [4]. The peak inertia (acceleration) values utilized are:

Vertical	0.37 g
Longitudinal	0.19 g
Lateral	0.19 g

Two Inertial loads are applied in the model:

- A longitudinal 0.19g acceleration (applied in the axial direction)
- The vector resultant of the vertical & lateral accelerations (applied in the radial direction) is calculated as  $(0.37^2 + 0.19^2)^{1/2} = 0.416g$

A pressure due to the weight of the front IL ( $P_{fa}$ ) is applied axially on the closure lid end, and calculated as:

$$P_{fa} = \frac{0.19(18,200)}{(\pi(43.875)^2)} = 0.57 \text{ psi}$$

It should be noted that actual area of load application in the ANSYS® model for the closure lid portion (with penetrations and bolt heads) is 5,020 in<sup>2</sup> compared to an area of  $\pi(39.75)^2 = 4,964$  in<sup>2</sup>. Hence, the above value for  $P_{fa}$  is conservative.

In addition, pressure loads due to the weight of the internals are applied at the cask inner surface in the axial and radial directions. Axial pressure acting on the inside surface of the rear bottom plate ( $P_{ia}$ ), calculated by:

$$P_{ia} = \frac{0.19(63,300)}{(\pi(34.375)^2)} = 3.24 \text{ psi}$$

Radial pressure ( $P_r$ ) acting on the lower half of the inner cask surface due to the weight of internals is represented as a cosine varying pressure around the lower radial portion (0° to 75° range) of the cavity.

$$Pr = [G_{\text{vertical}}] \left( \frac{W}{LR} \right) \left[ \frac{\sin\left(\frac{\pi}{2} + \theta\right)}{\left[\left(\frac{\pi}{2\theta}\right) + 1\right]} + \frac{\sin\left(\frac{\pi}{2} - \theta\right)}{\left[\left(\frac{\pi}{2\theta}\right) - 1\right]} \right]^{-1} \cos\left(\frac{\pi\theta_i}{2\theta}\right)$$

As an example, pressure applied at an angle of 7.5° would be calculated as follows:

$$Pr = [0.416] \left( \frac{63,300}{160.0(34.375)} \right) \left[ \frac{\sin(90 + 75)}{\left[\left(\frac{180}{2(75)}\right) + 1\right]} + \frac{\sin(90 - 75)}{\left[\left(\frac{180}{2(75)}\right) - 1\right]} \right]^{-1} \cos\left(\frac{180(7.5)}{2(75)}\right)$$

$$Pr = 0.416(11.509)(0.7083)(0.9877) = 3.35 \text{ psi}$$

The model loading is shown in Figure 2.12.2-8.

In addition, radial pressure ( $P_{fr}$ ) due to the front IL weight is applied along the contacting surfaces of the limiter and the lid/cask wall. The pressure follows a cosine distribution and is applied from the vertical ( $Y=180^\circ$  to  $Y=105^\circ$ ).

A radial pressure due to the rear IL weight ( $P_{rr}$ ) is also applied along the contacting surfaces of the limiter and the cask wall. Similar to the front IL, the pressure follows a cosine distribution and is applied from the vertical ( $Y=180^\circ$  to  $Y=105^\circ$ ).

All loads are applied through an ANSYS® macro. The above calculated pressures are “ball park” compared to the maximum pressures calculated by macro, and illustrated in Figure 2.12.2-9. Hand calculated pressures are not at the same location where the macro has computed the first pressure.

Axial support at ILs is applied as displacement boundary condition on cask bottom nodes.

#### 11. Horizontal Cask, Rail Shock Tie-Down (4.7g all directions) (IL-11)

For the tie-down rail car vibration and shock loadings, the exact methodology and displacement boundary conditions utilized for the horizontal cask, rail vibration, and rail car shock loading (IL-10) are applied, with the exception that the inertial loads are based on the following accelerations:

##### Rail Car Shock Accelerations:

Vertical	4.7g
Longitudinal	4.7g
Lateral	4.7g

#### 12. End Drop on Top (Closure Lid) End (IL-12)

The dynamic analysis described in Appendix 2.12.9 determines the inertial load on the cask packaging for a 1-foot (26g) and 30-foot (80g) end drop onto an unyielding surface. This stress evaluation is conducted for a 1-ft drop load. For the drop load cases (IL-12 to IL-16), the CONTA174 elements are set to multipoint constraint (MPC) bonding capability.

The following calculations are for 1-foot end drop with maximum acceleration of 26g, and are applied to the model. The vertical acceleration to the FEM simulates the inertial loading.

An axial pressure due to internals ( $P_i$ ) is applied at the inner lid surface based on:

$$P_i = \frac{26.0(63,300)}{(\pi(34.375)^2)} = 443.35 \text{ psi}$$

A correction factor of 1.04 is applied to compensate for areas around penetrations as shown in IL-3.



The dynamic analysis determines the inertial load on the cask packaging for a 1-foot and 30-foot end drop onto an unyielding surface. This stress evaluation is conducted for a unit load (1g). However, since this analysis is a static (non-transient) analysis without material nonlinearities and ignoring large-deflection effects (small-strain), stresses may be ratioed for the actual g-loads in load combinations. Since the payload and the ILs are not included in the model, their loading effects are simulated as distributed pressures applied on the cask at the appropriate locations.

The model loading is illustrated in Figure 2.12.2-10.

An axial pressure due to the rear IL ( $P_{ri}$ ) is applied at the cask bottom area:

$$P_{ri} = \frac{26.0(18,400)}{(\pi(43.875)^2)} = 79.11 \text{ psi}$$

Loading and displacement boundary conditions are applied through an ANSYS® macro. During the model run, the cask is supported as shown in Figure 2.12.2-11.

### 13. End Drop on Bottom End (IL-13)

An analysis similar to that of top end drop described above is performed for the 26g vertical load. A similar methodology used for the top end drop is applied for this case. The following inertia load (pressure) magnitudes are applied to the model.

A 26g vertical acceleration to the FEM simulates the inertial loading.

An axial pressure due to internals,  $P_i = 443.35$  psi, is applied at the inner bottom surface as noted for the top end in IL-12.

An axial pressure due to the front IL ( $P_{fi}$ ) is applied at the outer lid surfaces based on the projected area:

$$P_{fi} = \frac{26.0(18,200)}{(\pi(43.875)^2)} = 78.25 \text{ psi}$$

The bottom nodes of the cask are supported in vertical direction. Loading and displacement boundary conditions are illustrated in Figure 2.12.2-12.

### 14. Side Drop/Slapdown (IL-14)

The dynamic analyses described in Appendix 2.12.9 determine the inertial loads on the TN-32B HBU demonstration cask for both the 1-foot (20g) and 30-foot (70g) side/slapdown drops onto an unyielding surface. This stress evaluation is conducted for a 20g load. Since the payload and the ILs are not included in the model, their loading effects are simulated as distributed pressures applied on the cask at the appropriate locations.

The contacting IL forces on the cask and closure lid are applied as reaction pressures required to balance the inertial forces of the system. Thus, the cask is in equilibrium under the applied forces. During the side drop or slapdown, the pressure on the inner surface due to the payload/basket, and the reaction pressure on the outer cask surface due to the ILs are assumed to vary as a cosine function over a defined arc length.

The loads acting in this case are:

#### A. Cask Body Inertia

The inertial loading is simulated by applying a 20g vertical acceleration to the FEM in the global Z.

#### B. Pressure Due to Internals

The radial pressure ( $P_i$ ) acting on the lower half of the inner cask surface due to the weight of internals is represented as a cosine varying pressure applied around the lower radial portion ( $0^\circ$  to  $75^\circ$  range) of the cavity:

$$Pr = [G_{\text{vertical}}] \left( \frac{W}{LR} \right) \left[ \frac{\sin\left(\frac{\pi}{2} + \theta\right)}{\left[\left(\frac{\pi}{2\theta}\right) + 1\right]} + \frac{\sin\left(\frac{\pi}{2} - \theta\right)}{\left[\left(\frac{\pi}{2\theta}\right) - 1\right]} \right]^{-1} \cos\left(\frac{\pi\theta_i}{2\theta}\right)$$

where:

$\theta$  = 1/2 angle of contact

$\theta_i$  = circumferential angle where pressure is applied

$W$  = weight of internals

$L$  = length pressure is applied

For example, a pressure applied at an angle of  $7.5^\circ$  would be calculated as follows:

$$Pr = [20.0] \left[ \frac{63,300}{160.0(34.375)} \right] \left[ \frac{\sin(90 + 75)}{\left[\frac{180}{2(75)} + 1\right]} + \frac{\sin(90 - 75)}{\left[\frac{180}{2(75)} - 1\right]} \right]^{-1} \cos\left(\frac{180(7.5)}{2(75)}\right)$$

$$Pr = 20.0(1.509)(0.7083)(0.9877) = 161.03 \text{ psi}$$

The maximum pressure at 0 degrees is  $Pr = 163.04$  psi. The model loading is illustrated in Figure 2.12.2-13.

### C. Impact Reaction Pressures:

Pressures applied by the rear and front IL reactions on the lower longitudinal half of the outer cask body during impact are computed. These pressures are assumed to vary in a cosine distribution around the bottom half of the outer surfaces ( $0^\circ$  to  $89.5^\circ$  range), and are calculated the same as the pressure from the internals above. The total forces on the front and rear ILs are based on the tributary length of the cask. As the two ILs are essentially the same in dimensions and length, the total force (F) applied in the equation is based on the following reactions:

Total cask weight,  $W = 234,420 \text{ lb}_m$ . Use  $236,000 \text{ lb}_m$  (cask + payload/basket)

Reaction force, front (lid) =  $1/2(236,000) = 118,000 \text{ lb}_m$ .

Reaction force, rear (bottom) =  $1/2(236,000) = 118,000 \text{ lb}_m$ .

The total front (lid/cask side) reaction force is divided in the ratio of two lengths:

- Closure lid plate portion with contact length of 4.50 inches and outer radius = 39.75 inch
- Flange portion with contact length of 7.50 inch and outer radius = 43.875 inches

For the rear, reaction pressure,  $P_r$ , is similarly calculated for the 12-inch interface. Loading and displacement boundary conditions are shown in Figure 2.12.2-14.

#### 15. CG-over-Corner Drop on Top (Closure Lid) End (IL-15)

For CG-over-corner, the cask is inclined at approximately  $64^\circ$  from the horizontal, as described in Appendix 2.12.9. All the applied loads and reaction forces are transformed into axial and normal components. The axial pressure components due to the internals, bottom IL and impact reaction are assumed uniformly distributed. All radial pressure components (i.e., pressure due to internals, rear IL, and impact reactions) are assumed to have cosine variation over a determined arc length.

##### a) Cask Body Inertia

The acceleration of 29.3g for the cold corner drop is rounded up to 34g, and then resolved into component accelerations. The component accelerations (30.56g axial and 14.91g radial) are applied as inertial loads in the axial and radial directions. The impact angle of the corner drop is derived from the magnitudes of deceleration components of inertia load experienced at an impact area.

In addition, a rotational acceleration is also applied at the cask CG to counteract the out-of-balance caused by the component's acceleration resultant. Since the component translational accelerations applied have been conservatively rounded, these result in a slight resultant moment (out-of-balance) when the solution is executed. This moment is counteracted by the applied angular acceleration (torque), and the model returned to static equilibrium. The magnitude of applied rotational acceleration (ANSYS DCGOMG value) is obtained by ANSYS® 'trial and error' to obtain zero (or near zero) resultant reactions.

## b) Pressure Due to Internals:

Radial pressure ( $P_{ir}$ ) acting on the lower half of the inner cask wall due to the weight of internals is represented as a cosine varying pressure around the lower radial portion ( $180^\circ$  to  $105^\circ$ ) of the cavity.

In addition, an axial pressure ( $P_{ia}$ ) is applied, due to the weight of the internals, to the closure lid inner surface:

$$P_{ia} = \frac{30.56(63,300)}{(\pi(34.375)^2)} = 521.10 \text{ psi}$$

The model loading is illustrated in Figure 2.12.2-15.

## c) Pressure Due to Rear Impact Limiter:

The inertia load of the non-striking IL is also applied to the cask in two mutually perpendicular directions. The axial component ( $P_{ra}$ ) is applied as a uniform pressure over the outside surface at the interface with the IL on the bottom end. The pressure applied is calculated as:

$$P_{ia} = \frac{30.56(18,400)}{(\pi(43.875)^2)} = 92.98 \text{ psi}$$

The other component ( $P_{rr}$ ) follows a cosine distribution around the lower half of the outside surface ( $0^\circ$  to  $75^\circ$  range) of the cask.

## d) Reaction Pressures Due to Front Impact Limiter

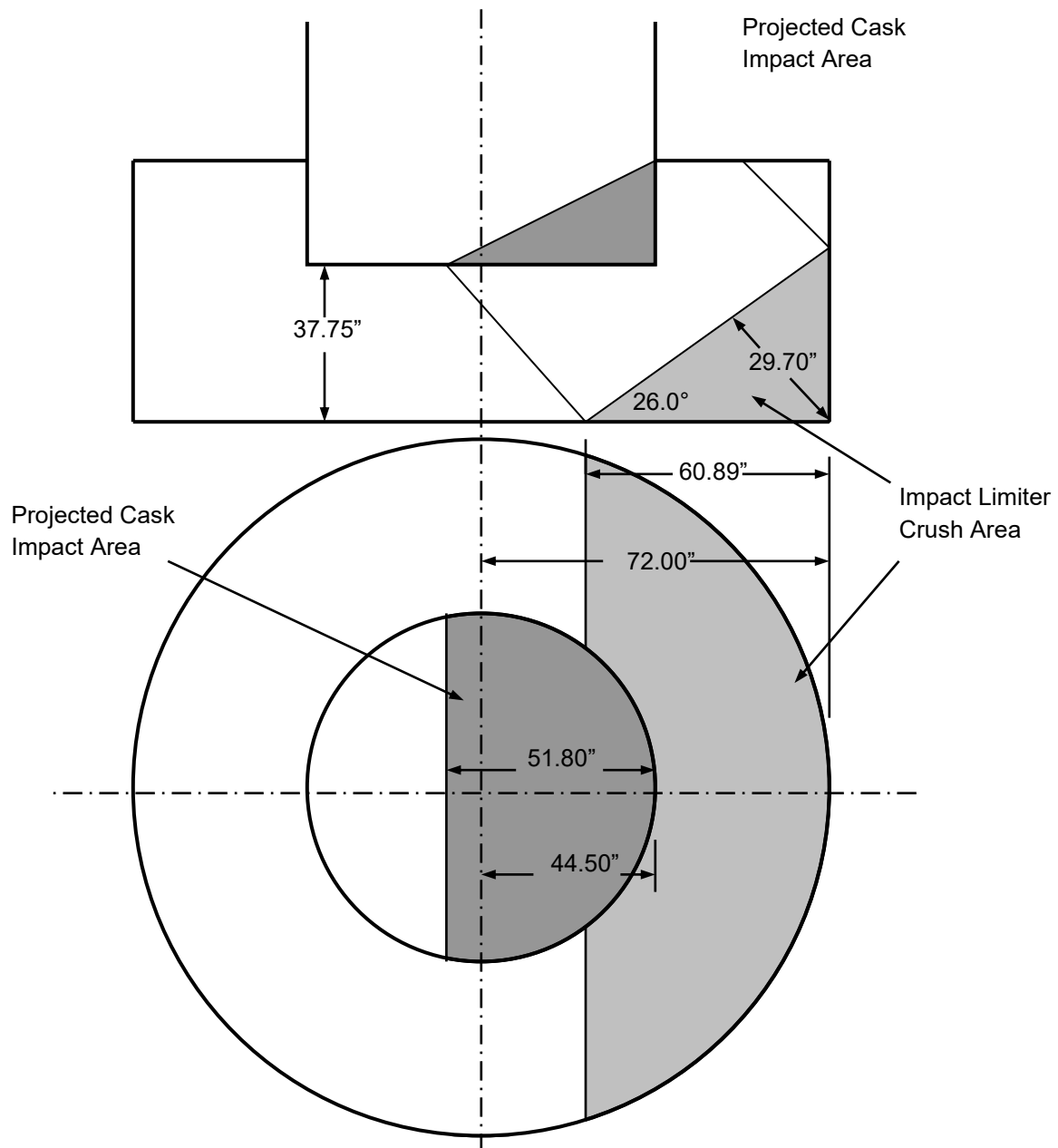
The reaction pressure from the striking IL is applied to the cask in two mutually perpendicular directions. The axial component ( $P_{fa}$ ) is applied as two-step uniform pressure over a portion of the cask interface with the IL on the lid end. The crush footprint of the front IL was projected onto the containment surface based on results obtained from Appendix 2.12.9 and engineering judgment.

Vertical crush depth = 29.70 inches

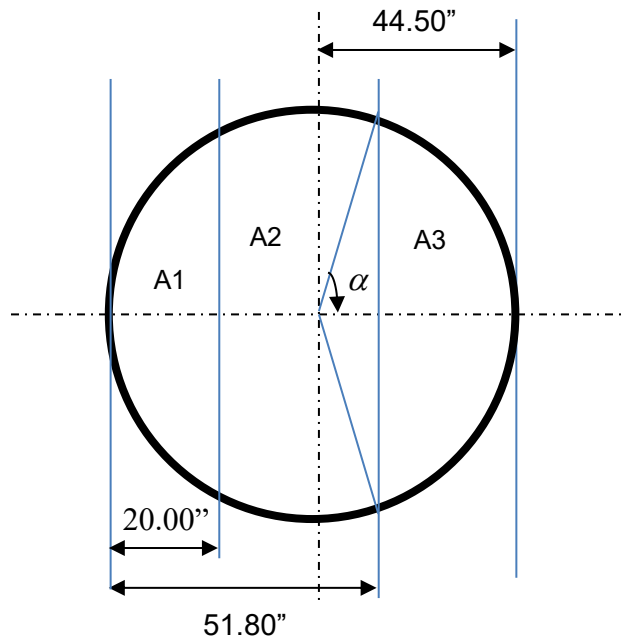
Crush angle =  $26.0^\circ$

Horizontal crush depth =  $(29.70)/\tan(26.0^\circ) = 60.89$  inches

Horizontal projection onto cask =  $60.89 \text{ in.} + (37.75)\tan(26.0^\circ) - (72.00 \text{ in.} - 44.50 \text{ in.}) = 51.80$  inches



For the axial reaction pressure applied, a total crushing area ( $A = 3,757 \text{ in}^2$ ), for a  $360^\circ$  arc, is calculated as follows:



$$\cos(\alpha) = \frac{(51.80 - 44.5)}{44.5} = 0.164, \quad \alpha = 80.558^\circ = 1.406 \text{ rad}$$

$$\text{Area, } A3 = \frac{R^2}{2} [2\alpha - \sin 2\alpha] = \left[ \frac{44.5^2}{2} \right] [2(1.406) - \sin (2(80.558^\circ))] = 2,463.78 \text{ in}^2$$

Total crushing area, A, is calculated as:

$$A = \pi R^2 - A3 = \pi(44.5)^2 - 2,463.78 = 3,757.4 \text{ in}^2$$

The majority of the weight consisting of the cask and the rear end IL is assumed to be reacted by an area bounded by 20 inches from the edge of the cask, and the weight of the internals is to be reacted by the remainder of the crushed area. The axial reaction pressure to the cask is, therefore, applied in two steps - p1 on corner area A1 and p2 on inside area A2, as shown by following formulas.

$$\cos(\alpha) = \frac{44.5 - 20}{44.5} = 0.551 \Rightarrow \alpha = 56.594^\circ = 0.988 \text{ rad}$$

$$A1 = \frac{R^2}{2} [2\alpha - \sin 2\alpha] = \left( \frac{44.5^2}{2} \right) [2(0.98776) - \sin(2(56.594^\circ))] = 1,045.87 \text{ in}^2$$

$$A2 = 3,757.36 - 1,045.88 = 2,711.48 \text{ in}^2$$

Pressure on corner area A1:

The weight of the cask body without the internals,  $W_{\text{cask}} = 172,000 \text{ lb}_m$ .

$$p1 (\text{coner}) = 30.56(172,000 + 18,400)/1,045.88 = 5,563.38 \text{ psi}$$

Pressure on inside area A2:

$$p2 (\text{inside}) = 30.56(63,300)/2.711.48 = 713.43 \text{ psi}$$

Due to element shapes at areas A1 and A2 boundary and the model mesh discretization, the above calculated areas are approximate, and pressures  $p1$  and  $p2$  are therefore, adjusted to balance the applied axial loads. The pressure adjustment is performed by multiplying the above calculated pressures by a factor reflected in macros to obtain zero resultant reaction forces. Note that in the pressure plots, adjusted values applied to the ANSYS® model are illustrated and are in range with the values above. The model loading is shown in Figure 2.12.2-16.

The radial component pressures follow a cosine distribution around the radial crush foot print from  $90.5^\circ$  to  $180^\circ$  of the cask. The radial reaction pressures are calculated using a modified version of cosine formula. Since the crush footprint is a circular segment, and the pressures are being applied to two separate side surfaces (i.e., closure lid and upper flange wall). The total force (F) applied in the equation is based on the percentage of the total length where the specific pressure is applied. For example, the reaction pressure applied to the closure lid at an angle of  $172.5^\circ$  would be calculated as follows:

The calculated reaction axial and radial pressures due to the crushed IL had to be adjusted and a rotational acceleration is applied to balance the applied loads. Loading and displacement boundary conditions are shown in Figure 2.12.2-17.

#### 16. CG-over-Corner Drop on Bottom End (IL-16)

For CG-over-corner, the cask is inclined at approximately  $64^\circ$  from the horizontal as discussed in the dynamic analysis of Appendix 2.12.9. All the applied loads and reaction forces are transformed into axial and normal components, and are applied using the same methodology adopted for the CG-over-corner closure lid drop. All radial pressure components (i.e., pressure due to internals, front IL and impact reactions) are assumed to have a cosine variation over a defined arc length.

The forces acting in this case are:

##### A. Cask Body Inertia

The component accelerations (30.56g axial and 14.91g radial) are applied as translational inertial loads in the axial and radial directions, respectively. In addition, a rotational acceleration is applied at the vessel CG to counteract the out-of-balance mass and return the model to equilibrium.

## B. Pressure Due to Internals

Radial pressure ( $P_{ir}$ ) acting on the lower half of the inner cask wall due to the weight of internals is represented as a cosine varying pressure around the lower radial portion ( $0^\circ$  to  $75^\circ$  range) of the cavity.

In addition, an axial pressure is applied, due to the weight of the internals, to the cask inner lid surface:

$$P_{ia} = [30.56(63,300)]/[\pi(34.375^2)] = 521.10 \text{ psi}$$

The model loading is shown in Figure 2.12.2-18.

## C. Pressure Due to Front Impact Limiter

The inertia load of the non-striking IL is also applied to the cask in two mutually perpendicular directions. The axial component ( $P_{fa}$ ) is applied as a uniform pressure over the outside surface at the interface with the IL on the bottom end. The pressure applied is calculated as:

$$P_{fa} = [30.56(18,200)]/[\pi(43.875^2)] = 91.97 \text{ psi}$$

In addition, radial pressure ( $P_{fr}$ ) due to the front IL weight is applied along the contacting surfaces of the limiter and the lid/cask wall. The pressure follows a cosine distribution and is applied from the vertical ( $Y=180^\circ$  to  $Y=105^\circ$ ).

$$P_{fr} = [G_{\text{Gravial}}] \left( \frac{W}{LR} \right) \left[ \frac{\sin\left(\frac{\pi}{2} + \theta\right)}{\left[\left(\frac{\pi}{2\theta}\right) + 1\right]} + \frac{\sin\left(\frac{\pi}{2} - \theta\right)}{\left[\left(\frac{\pi}{2\theta}\right) - 1\right]} \right]^{-1} \cos\left(\frac{\pi(\theta_i)}{2\theta}\right)$$

## D. Reaction Pressures Due to Rear Impact Limiter:

The reaction pressure from the striking IL is applied to the cask in two mutually perpendicular directions (axial at the cask base and radial at the cask outer wall) as described in the previous loading case, IL-15.

For the axial reaction pressure applied, a total area ( $4,114 \text{ in}^2$ ) and areas A1 and A2 are the same as were calculated for corner drop on closure lid (Case IL-15).

Pressure on corner area A1:

$$p1 (\text{coner}) = 30.56(172,000 + 18,200)/1,045.88 = 5,557.53 \text{ psi}$$

Pressure on inside area A2:

$$p2 (\text{inside}) = 30.56(63,300)/2.711.48 = 713.43 \text{ psi}$$



Due to element shapes at areas A1 and A2 boundary and model mesh discretization, the above calculated areas are approximate and pressures  $p_1$  and  $p_2$  are therefore, adjusted to balance the applied axial loads. It should be noted that A1 and A2 values are slightly different from the lid side due to differences in mesh and absence of penetrations. The pressure adjustment is done by multiplying the above calculated pressures by a factor reflected in macros to obtain zero resultant reaction forces.

The model loading is shown in Figure 2.12.2-19.

The radial component pressure ( $P_r$ ) is assumed to follow a cosine distribution around the radial crush foot print from  $0^\circ$  to  $89.5^\circ$  of the cask. The radial reaction pressures are calculated using a modified version of the cosine distribution, based on the calculated angle of application.

The calculated reaction axial and radial pressures due to the crushed IL had to be adjusted and a rotational acceleration is applied to balance the applied loads. Loading and displacement boundary conditions are shown in Figure 2.12.2-20.

#### 17. Fire Accident (IL-17)

The thermal stresses due to the fire accident are secondary in nature, and therefore, the evaluation for accident fire conditions is not applicable.

#### 18. Deep Immersion (290 psig) (IL-18)

Deep immersion, IL-18, is analyzed in Appendix 2.12.11.

### 2.12.2.3 Pressure Distribution over Contact Area for Impact Load

The impact load acting in the transverse direction is applied as a load over the contact area between the IL and the outer surface of the cask. The pressure distribution is assumed to be in the longitudinal direction over the 12.0-inch IL contact depth, and vary with a cosine distribution around the circumference of the cask. For the impact conditions, the angle of contact is dependent upon the amount of crush occurring in the IL. The most severe loads result from impacts on the side of the IL. For these conditions, the contact angle between the IL and the cask outer surface will be approximately  $180^\circ$ . For non-crushing surfaces, a contact angle of  $150^\circ$  ( $75^\circ$  half angle of contact) is conservatively utilized for the cask impact analysis. The circumferential cosine pressure distribution over a half angle,  $\theta$ , is calculated as follows:

$$P_i = P_{\max} \cos(\pi\theta_i/2\theta)$$

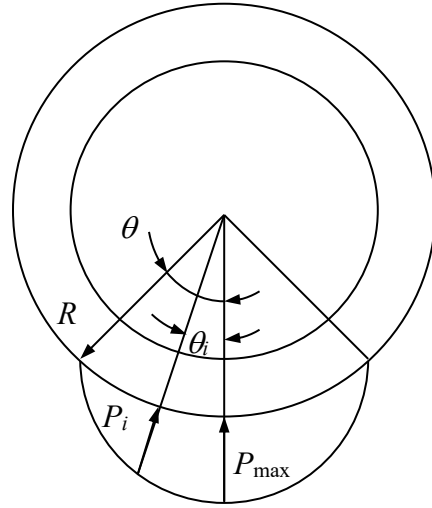
where:

$P_i$  = Pressure load at angle  $\theta_i$ .

$P_{\max}$  = Peak pressure load, at point of impact, and

$\theta_i$  = Angle corresponding to point of interest.

The circumferential pressure distribution is illustrated in the following figure.



The peak pressure load,  $P_{\max}$ , is determined by setting the integral of the vertical pressure components,  $Q_i$ , equal to the total transverse impact load,  $F_t$ , as follows:

$$F_t = \int_{-\theta}^{\theta} Q_i LR d\theta_i = \int_{-\theta}^{\theta} P_i \cos(\theta_i) LR d\theta_i = \int_{-\theta}^{\theta} P_{\max} \cos\left(\frac{\pi\theta_i}{2\theta}\right) \cos(\theta_i) LR d\theta_i$$

$$F_t = \frac{P_{\max} LR}{2} \int_{-\theta}^{\theta} \left[ \cos\left(\frac{\pi\theta_i}{2\theta} + \theta_i\right) + \cos\left(\frac{\pi\theta_i}{2\theta} - \theta_i\right) \right] d\theta_i = P_{\max} LR \left[ \frac{\sin\left(\frac{\pi}{2} + \theta\right)}{\left(\frac{\pi}{2\theta}\right) + 1} + \frac{\sin\left(\frac{\pi}{2} - \theta\right)}{\left(\frac{\pi}{2\theta}\right) - 1} \right]$$

Rearranging terms gives the peak pressure,  $P_{\max}$ :

$$P_{\max} = \frac{F_t}{LR} \left[ \frac{\sin\left(\frac{\pi}{2} + \theta\right)}{\left(\frac{\pi}{2\theta}\right) + 1} + \frac{\sin\left(\frac{\pi}{2} - \theta\right)}{\left(\frac{\pi}{2\theta}\right) - 1} \right]^{-1}$$

Therefore, the pressure at any circumferential location is given by:

$$P_i = \frac{F_t}{LR} \left[ \frac{\sin\left(\frac{\pi}{2} + \theta\right)}{\left(\frac{\pi}{2\theta}\right) + 1} + \frac{\sin\left(\frac{\pi}{2} - \theta\right)}{\left(\frac{\pi}{2\theta}\right) - 1} \right]^{-1} \cos\left(\frac{\pi\theta_i}{2\theta}\right)$$

$$F_t = G_{\text{transverse}}(W)$$

where:

$W$  = weight of internals or IL

$G_{\text{transverse}}$  = acceleration in the transverse direction

Therefore,

$$P_i = G_{\text{transverse}} \frac{W}{LR} \left[ \frac{\sin\left(\frac{\pi}{2} + \theta\right)}{\left(\frac{\pi}{2\theta}\right) + 1} + \frac{\sin\left(\frac{\pi}{2} - \theta\right)}{\left(\frac{\pi}{2\theta}\right) - 1} \right]^{-1} \cos\left(\frac{\pi\theta_i}{2\theta}\right)$$

#### 2.12.2.4 Analysis Results

ANSYS® non-linear elastic analyses are performed for the above individual load cases. These individual loads are to be combined and evaluated for normal operating and accident conditions, as described in Section 2.12.2.1. A summary of maximum nodal stress intensities in each major cask component under each individual load is presented in Table 2.12.2-2.

#### Trunnion Local Stress Analysis Due To Lifting Load

##### Method of Analysis

10 CFR 71.45(a) requires that any lifting attachment (trunnions) that is a structural part of a package must be designed with a minimum safety factor of three against yielding when used to lift the package in the intended manner. The TN-32B HBU demonstration cask trunnion design satisfies the 10 CFR 71.45(a) requirements. The ASME B&PV Code allowable is utilized to evaluate the stresses at the trunnion/gamma shell interface. The maximum local membrane ( $P_i$ ) and local membrane plus secondary ( $P_i + Q$ ) stress intensities are limited to  $1.5S_m$  and  $3.0S_m$  per Reference [4], respectively.

The local stress induced in the gamma shield shell by the trunnions is calculated utilizing "Bijlaard's" method conservatively utilizing 6g. The stresses are calculated by performing the indicated multiplication in the column entitled "Compute Absolute Values of Stress and Enter Result." The resulting stress is inserted into the stress table at the eight stress locations, i.e., AU, AL, BU, BL, etc. The stresses are calculated by completing Table 5 of Reference [7]. Table 2.12.2-3 presents the computation results for the 6g lifting load.

##### Results/Conclusions

The maximum stress intensities on the outside and inside of the gamma shield shell for the lifting loads are calculated in Table 2.12.2-3. The maximum stress intensity calculated in Table 2.12.2-3 is combined with the pressure stress and thermal stress tabulated in Table 2.12.2-2. The maximum  $P_m + P_b$  ( $P_i$ ) and  $P_i + Q$  (thermal) stress intensities are then listed in the following table and compared with the allowables.

Location	Stress Intensity $P_I$ (ksi)	Allowable $1.5S_m$ (ksi)	Stress Intensity $P_I + Q$	Allowable $3.0S_m$ (ksi)
Outside Edge of Gamma Shield Shell	11.44 <sup>(1)</sup>	30.9	20.99 <sup>(2)</sup>	61.8
Inside Edge of Gamma Shield Shell	11.44 <sup>(1)</sup>	30.9	20.43 <sup>(3)</sup>	61.8

Notes:

1. Calculated as follows:  $10.33 + 1.11 = 11.44$  ksi
2. Calculated as follows:  $14.61 + 1.11 + 5.27 = 20.99$  ksi
3. Calculated as follows:  $14.05 + 1.11 + 5.27 = 20.43$  ksi

#### 2.12.2.5 References

1. Title 10, Code of Federal Regulations - Energy, Part 71 (10 CFR 71), "Packaging and Transportation of Radioactive Material," 1-1-2021 Edition, U.S. Nuclear Regulatory Commission, Washington, D.C.
2. Regulatory Guide 7.8, "Load Combinations for the Structural Analysis of Shipping Cask," U.S. Nuclear Regulatory Commission, Revision 1, March 1989.
3. American Society of Mechanical Engineers, ASME Boiler and Pressure Vessel Code, Section III, Division I, Subsection NB and Subsection NF, 1992 Edition with 1992 Addenda.
4. Regulatory Guide 7.6, "Design Criteria for the Structural Analysis of Shipping Cask Containment Vessels," U.S. Nuclear Regulatory Commission, Revision 1, March 1978.
5. ANSYS® Mechanical APDL and Workbench, Version 19.2, ANSYS Inc., Canonsburg, PA.
6. WRC Bulletin 107, March 1979, "Local Stresses in Spherical and Cylindrical Shells Due to External Loadings."
7. John Harvey, "Theory and Design of Modern Pressure Vessels," Second Edition.

**Table 2.12.2-1  
Major Dimensions**

<b>Component</b>	<b>Nominal/Design Dimension (inch), as Modeled</b>
Containment Vessel Flange OD	87.75
Containment Vessel Flange Thickness	4.60
Containment Vessel Thickness	1.50
Containment Vessel ID	68.75
Containment Vessel Length	170.75
Basket Length	160.00
IL Engagement Depth	12.00
Gamma Shield OD	87.75
Gamma Shield Thickness	8.00
Gamma Shield Shell Length	167.4
Gamma Shield Bottom Plate Thickness	8.75 and 7.50
Gamma Shield Bottom Plate OD	87.75
Closure Lid Outer Plate OD	79.50
Closure Lid Outer Plate Thickness	4.50
Closure Lid Shield Plate OD	69.50
Lid Shield Plate Thickness	6.00
TLA Penetration Sleeve OD	8.000
TLA Penetration Sleeve ID	7.00 and 1.50
Vent/Drain Lid Penetration OD	9.12
Vent/Drain Lid Penetration ID	3.38 and 4.12
Bolt Hex Head OD	2.25 across flats
Bolt Shank OD	1.375

**Table 2.12.2-2**  
**Summary Maximum Nodal Stress Intensities in Cask Components**  
**for Individual Load Runs**

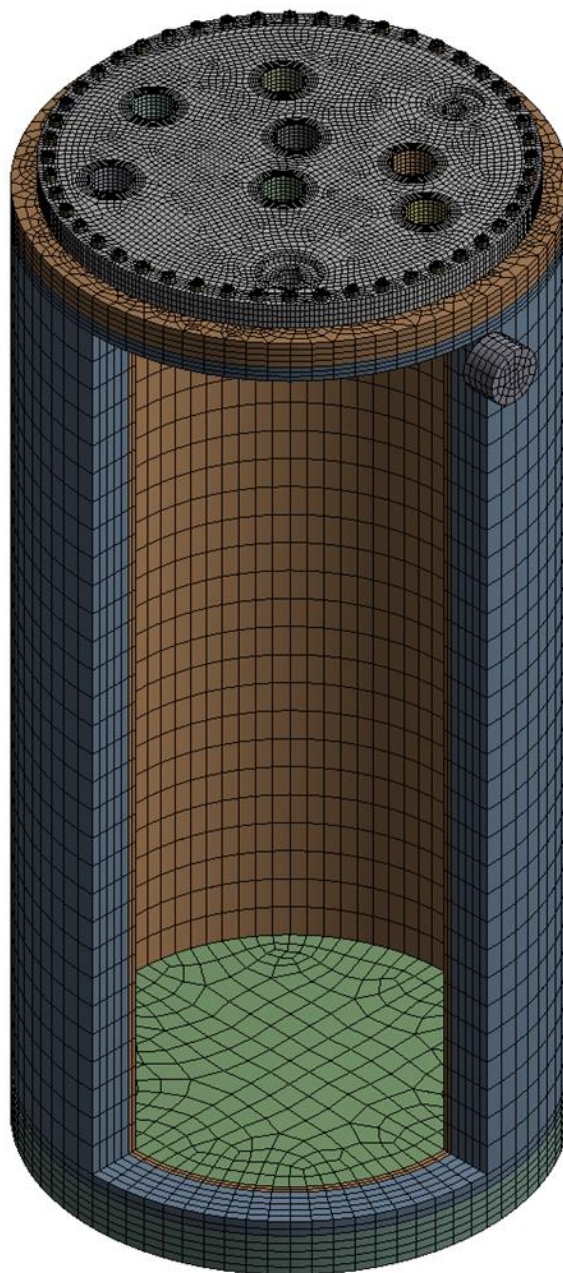
Load Case Number	Maximum Nodal Stress Intensity (ksi)								
	Stress Category	Gamma Shield Shell	Bot. Shield Plate	Bot. Inner Plate	Inner Shell	Top Shield Plate	Shell Flange	Lid <sup>2</sup>	Penetration Sleeves
IL-1	P <sub>m</sub>	1.22	0.02	0.01	0.27	5.00	2.23	5.74	6.03
	P <sub>m</sub> + P <sub>b</sub>	3.55	0.03	0.02	0.42	8.46	3.99	10.31	12.32
IL-2	P <sub>m</sub>	3.74	0.87	2.17	14.31	2.52	6.58	1.41	2.12
	P <sub>m</sub> + P <sub>b</sub>	9.99	2.08	5.14	15.44	7.00	6.97	2.24	2.33
IL-3	P <sub>m</sub>	0.42	0.61	0.62	0.84	1.63	0.96	1.63	4.32
	P <sub>m</sub> + P <sub>b</sub>	1.11	1.90	0.88	1.05	4.19	1.47	3.73	5.55
IL-4	P <sub>m</sub>	0.10	0.09	0.11	0.13	0.35	0.19	0.43	0.99
	P <sub>m</sub> + P <sub>b</sub>	0.22	0.29	0.18	0.13	0.88	0.26	1.00	1.34
IL-5	P <sub>m</sub>	0.01	0.01	0.02	0.02	0.05	0.03	0.06	0.14
	P <sub>m</sub> + P <sub>b</sub>	0.03	0.04	0.03	0.02	0.12	0.04	0.14	0.19
IL-6	P <sub>m</sub>	4.82	3.98	9.63	3.86	1.41	2.00	1.29	1.58
	P <sub>m</sub> + P <sub>b</sub>	5.17	5.48	11.71	4.63	3.13	4.94	2.50	2.83
IL-7	P <sub>m</sub>	5.06	3.99	9.89	4.09	1.46	1.98	1.36	1.60
	P <sub>m</sub> + P <sub>b</sub>	5.48	5.53	12.07	4.78	3.30	5.19	2.63	2.96
IL-8	P <sub>m</sub>	5.07	3.99	9.94	4.06	1.44	1.95	1.36	1.60
	P <sub>m</sub> + P <sub>b</sub>	5.49	5.53	12.14	4.77	3.27	5.09	2.62	2.95
IL-9	P <sub>m</sub>	0.19	0.07	0.04	0.18	0.16	0.12	0.11	0.12
	P <sub>m</sub> + P <sub>b</sub>	0.33	0.09	0.04	0.22	0.37	0.24	0.15	0.15
IL-10	P <sub>m</sub>	0.08	0.03	0.02	0.07	0.06	0.05	0.06	0.08
	P <sub>m</sub> + P <sub>b</sub>	0.14	0.04	0.02	0.09	0.14	0.09	0.07	0.11
IL-11	P <sub>m</sub>	1.20	0.61	0.28	1.15	0.94	0.74	1.05	1.55
	P <sub>m</sub> + P <sub>b</sub>	2.23	0.77	0.31	1.37	2.16	1.43	1.55	2.22
IL-12	P <sub>m</sub>	2.00	0.54	1.29	1.61	2.47	2.13	1.10	0.51
	P <sub>m</sub> + P <sub>b</sub>	2.75	1.44	1.83	1.68	2.86	2.80	1.35	0.73
IL-13	P <sub>m</sub>	2.01	2.08	1.95	2.35	1.81	1.39	2.72	5.45
	P <sub>m</sub> + P <sub>b</sub>	2.27	2.32	2.31	3.07	4.35	1.76	4.58	6.38
IL-14	P <sub>m</sub>	5.10	3.63	2.53	4.81	5.46	5.29	5.01	4.36
	P <sub>m</sub> + P <sub>b</sub>	9.89	5.97	3.04	5.00	7.86	6.15	6.02	5.39
IL-15	P <sub>m</sub>	5.25	8.83 <sup>1</sup>	3.29	6.83	6.01	8.63	8.75	7.59
	P <sub>m</sub> + P <sub>b</sub>	7.43	23.50 <sup>1</sup>	3.82	7.06	13.19	10.08	13.06	10.22
IL-16	P <sub>m</sub>	3.81	3.53	4.21	4.61	2.27	1.73	3.55	6.83
	P <sub>m</sub> + P <sub>b</sub>	4.99	4.21	5.88	4.95	5.15	2.11	5.81	8.00

Table Notes:

- For IL-15, the node at the center of bottom shield plate (Figure 2.12.2-17) is constrained laterally for stability, and has a higher allowable because of local stresses. The stress intensities for this node are not included in the P<sub>m</sub> and P<sub>m</sub> + P<sub>b</sub> values in the table listing.
- Bending stresses at the closure lid flange (bolt holes circular region) are secondary stress. P<sub>m</sub> and P<sub>m</sub> + P<sub>b</sub> stresses above do not account for local effects of geometry or material discontinuities, and stress concentrations in the region around bolt holes.

**Table 2.12.2-3  
6g Lifting Load**

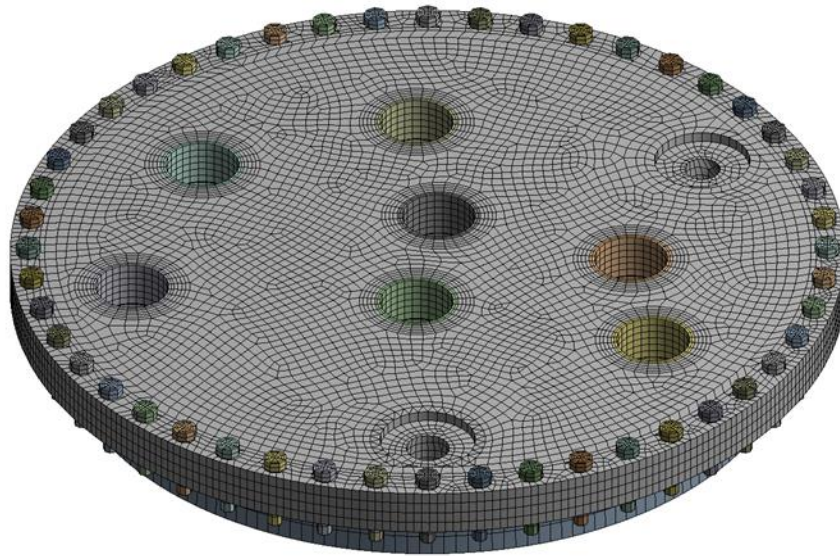
6g Lifting Load											
<b>Trunnion Loading</b>			<b>Geometry</b>			<b>Cask Loading</b>					
Cask Weight lb	240000		Gamma Shield Thickness (in)	7.394		Longitudinal	6				
			Mean Radius (in)	39.572		Vertical g	0				
Moment Arm (in)	9.522		Trunnion Outer Radius (in)	6.000		Lateral g	0				
Circumferential Trunnion Moment Mc (in lb)	0		Geometry Factor Gamma	5.352							
Longitudinal Trunnion Moment ML (in lb)	-6855840		Geometry Factor Beta	0.133							
Torsional Trunnion Moment Mt (in lb)	0										
P (lb)	0										
Circumferential Loading Vc (lb)	0										
Longitudinal Loading VL (lb)	-720000										
<b>Reference Figure</b>	<b>Reference Curve from Fig</b>	<b>Multiplier</b>	<b>Absolute Stress (psi)</b>	<b>Au</b>	<b>Al</b>	<b>Bu</b>	<b>Bl</b>	<b>Cu</b>	<b>Cl</b>	<b>Du</b>	<b>DI</b>
3c or 4c	1.05	0.000	0.0	0.0	0.0	0.0	0.0	0.0	0.0	0.0	0.0
1c or 2c-1	0.19	0.000	0.0	0.0	0.0	0.0	0.0	0.0	0.0	0.0	0.0
3a	0.07	0.000	0.0					0.0	0.0	0.0	0.0
1a	0.105	0.000	0.0					0.0	0.0	0.0	0.0
3b	0.27	-4463.072	-1205.0	1205.0	1205.0	-1205.0	-1205.0				
1b or 1b-1	0.064	-143315.686	-9172.2	9172.2	-9172.2	-9172.2	9172.2				
<b>Summation of Phi Stress</b>				10377.2	-7967.2	-10377.2	7967.2	0.0	0.0	0.0	0.0
3c or 4c	1.05	0.000	0.0	0.0	0.0	0.0	0.0	0.0	0.0	0.0	0.0
1c-1 or 2c	0.18	0.000	0.0	0.0	0.0	0.0	0.0	0.0	0.0	0.0	0.0
4a	0.092	0.000	0.0					0.0	0.0	0.0	0.0
2a	0.064	0.000	0.0					0.0	0.0	0.0	0.0
4b	0.063	-4463.072	-281.2	281.2	281.2	-281.2	-281.2				
2b or 2b-1	0.1	-143315.686	-14331.6	14331.6	-14331.6	-14331.6	14331.6				
<b>Summation of Chi Stress</b>				14612.7	-14050.4	-14612.7	14050.4	0.0	0.0	0.0	0.0
	Torsional Shear Stress	0.0		0.0	0.0	0.0	0.0	0.0	0.0	0.0	0.0
	Circumferential Shear Stress	0.0		0.0	0.0	0.0	0.0				
	Longitudinal Shear Stress	-5166.0						5166.0	5166.0	-5166.0	-5166.0
<b>Summation of Tau Stress</b>				0.0	0.0	0.0	0.0	5166.0	5166.0	-5166.0	-5166.0
<b>Stress Intensity Root 1</b>				14612.7	7967.2	10377.2	14050.4	5166.0	5166.0	5166.0	5166.0
<b>Stress Intensity Root 2</b>				10377.2	14050.4	14612.7	7967.2	5166.0	5166.0	5166.0	5166.0
<b>Stress Intensity Root 3</b>				4235.5	6083.2	4235.5	6083.2	10331.9	10331.9	10331.9	10331.9
<b>Max Stress Intensity</b>	14612.7										
<b>Membrane Stress Intensity Root 1</b>				1205.0	1205.0	281.2	281.2	5166.0	5166.0	5166.0	5166.0
<b>Membrane Stress Intensity Root 2</b>				140.6	140.6	1345.6	1345.6	5166.0	5166.0	5166.0	5166.0
<b>Membrane Stress Intensity Root 3</b>				923.9	923.9	923.9	923.9	10331.9	10331.9	10331.9	10331.9
<b>Max Membrane Stress Intensity</b>	10331.9										



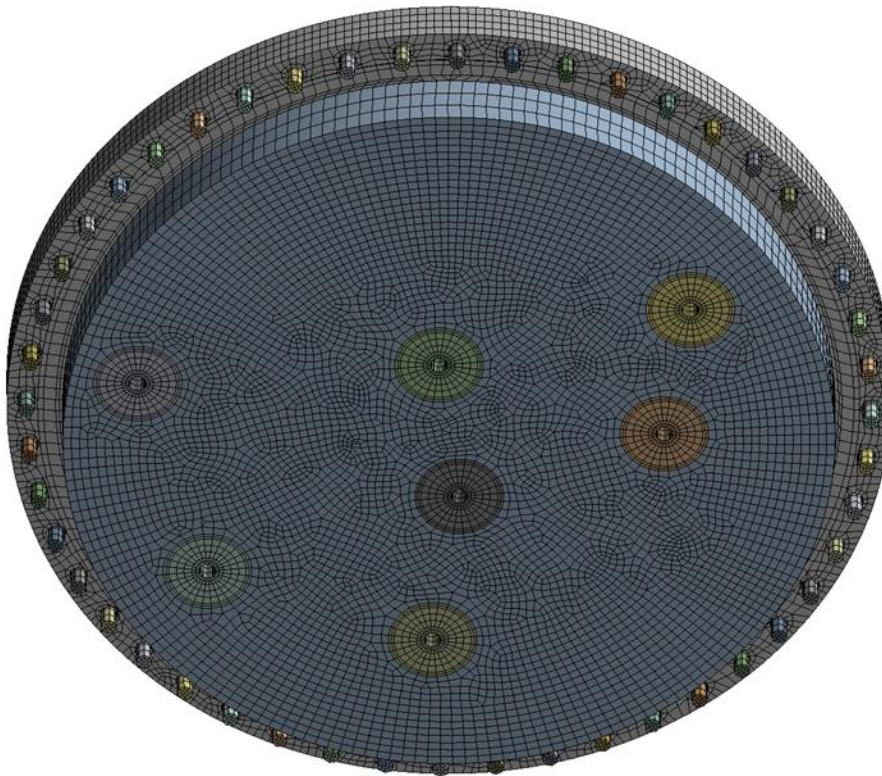
Note: Some elements were unselected (hidden) to illustrate the mesh through the thickness of the cask.

**Figure 2.12.2-1**  
**TN-32B HBU Demonstration Cask Finite Element Model**





Top Isometric View



Bottom Isometric View

**Figure 2.12.2-2**  
**TN-32B HBU Demonstration Cask Finite Element Model – Lid and Shield**

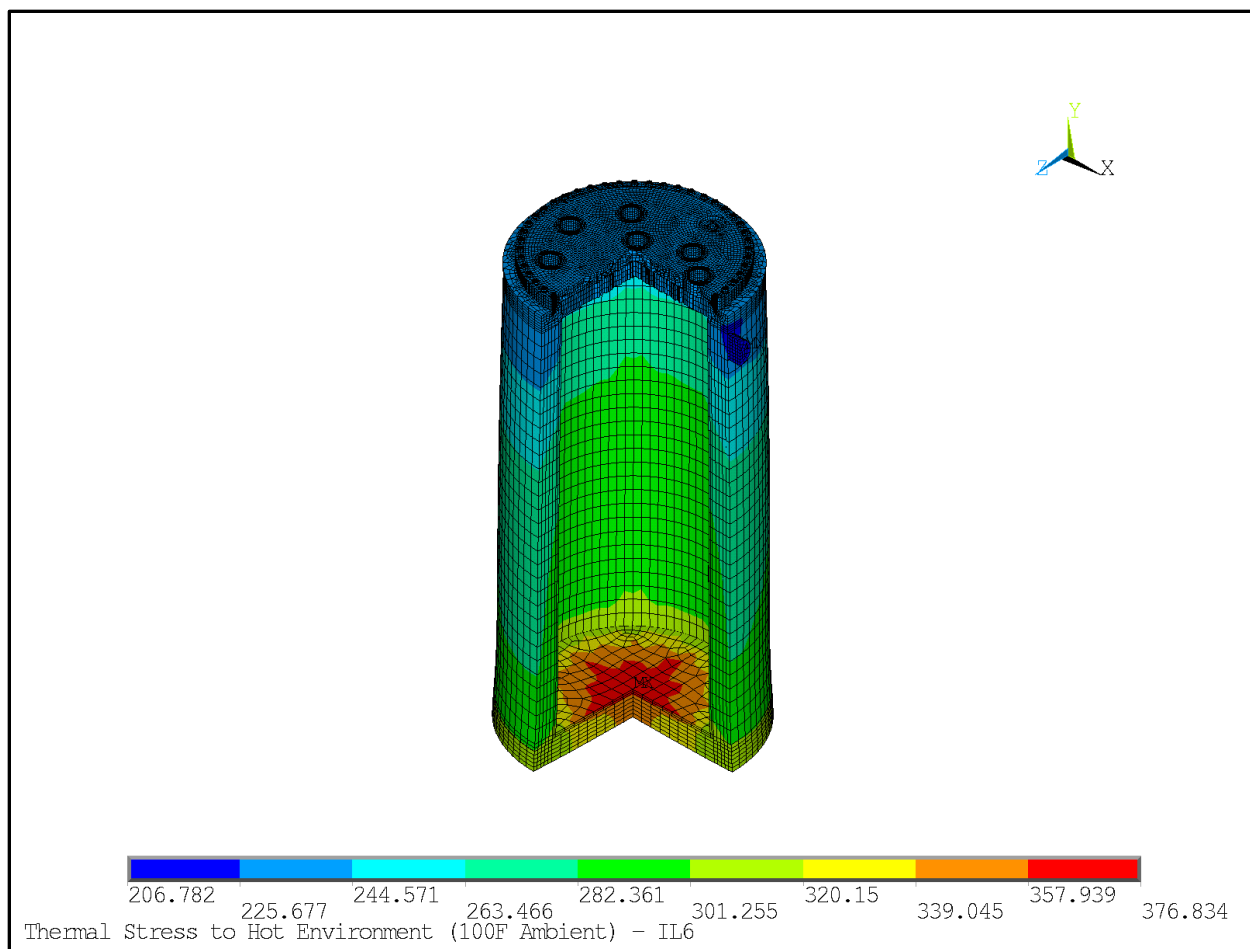


**Figure 2.12.2-3**  
**Thermal Stresses 100 °F Environment (IL-6) – 270° Cut View of Mapped Thermal Data**

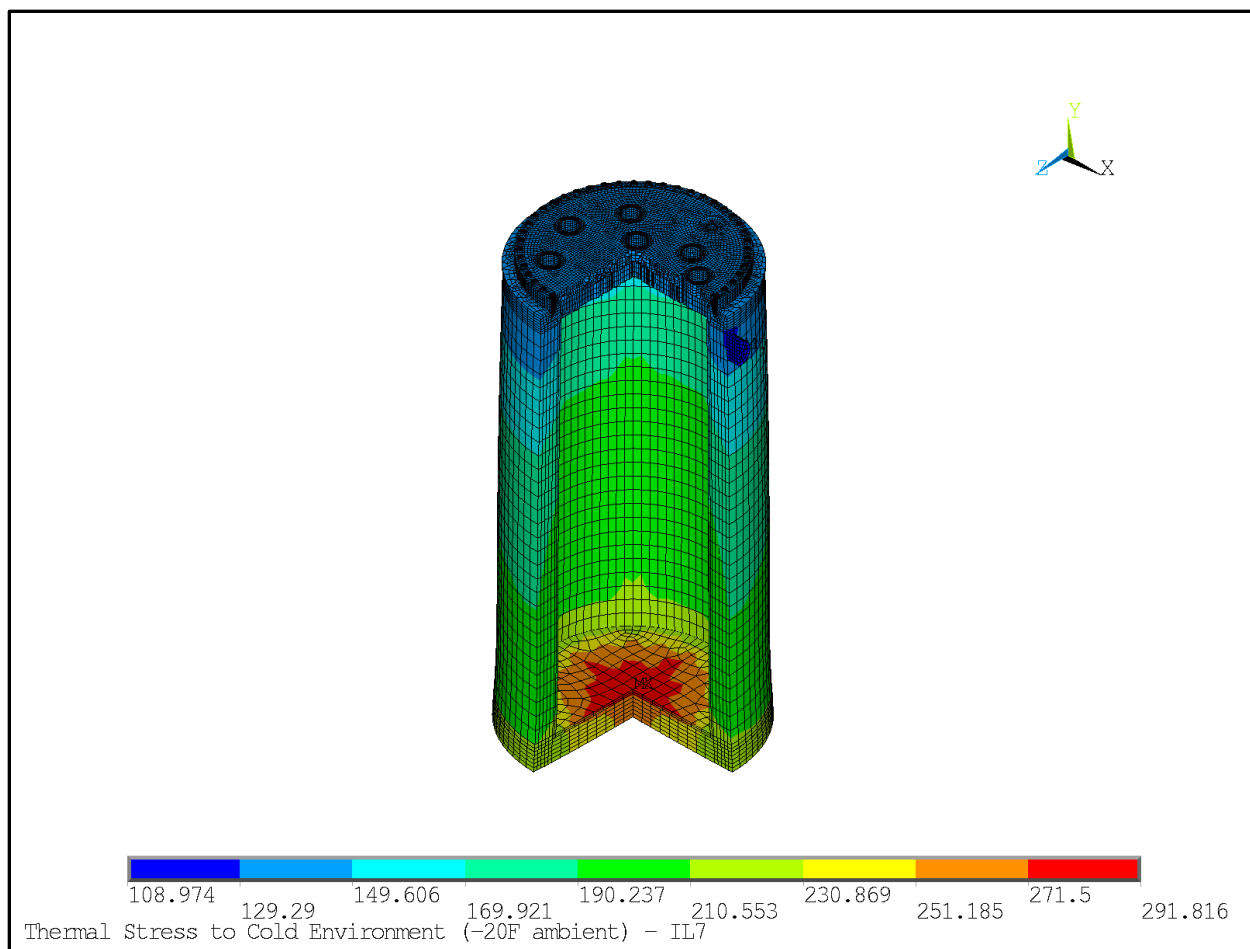


**Figure 2.12.2-4**  
**Thermal Stresses -20 °F Environment (IL-7) – 270° Cut View of Mapped Thermal Data**

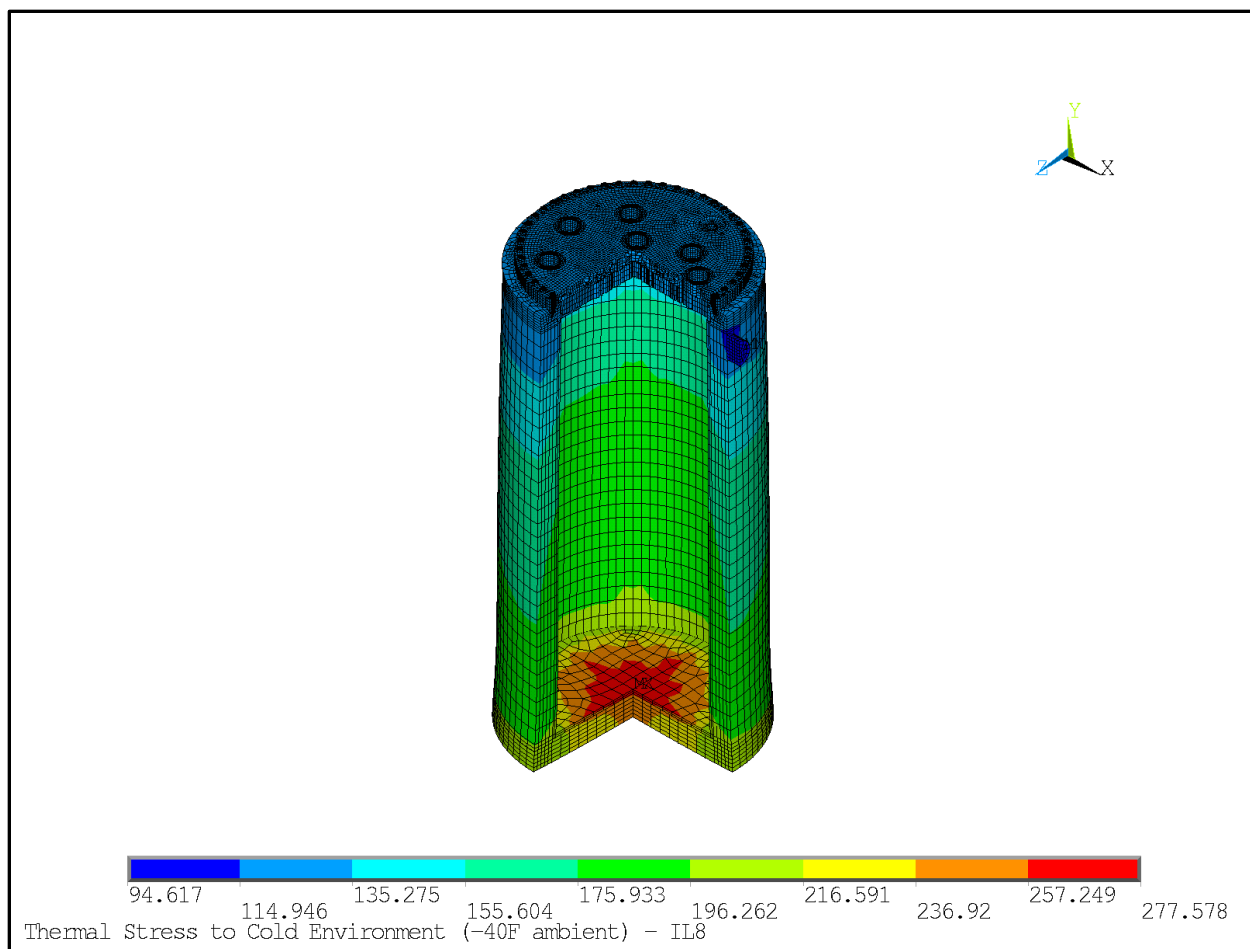


**Figure 2.12.2-5**  
**Thermal Stresses -40 °F Environment (IL-8) – 270° Cut View of Mapped Thermal Data**

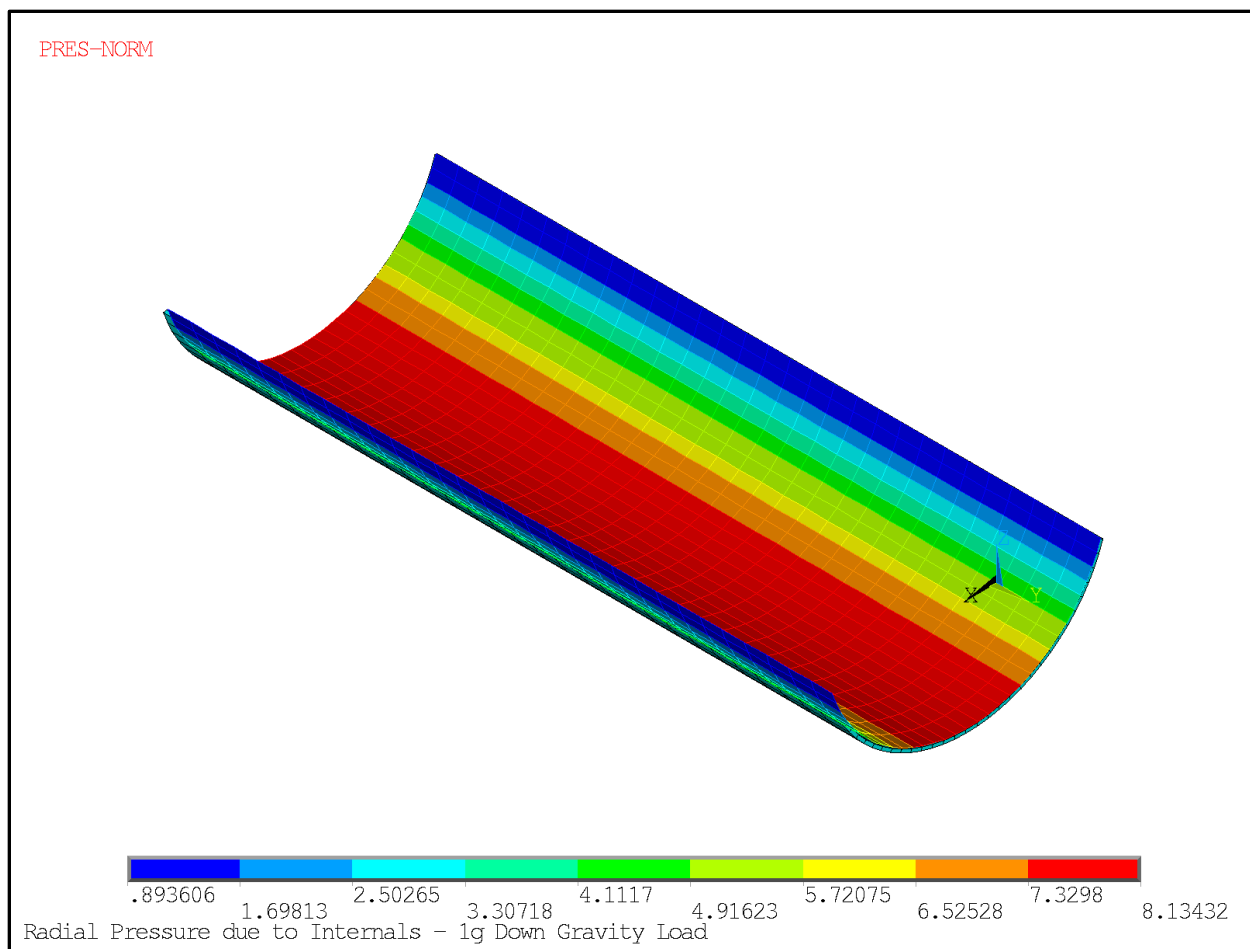


**Figure 2.12.2-6**  
**Radial Pressure Due to Internals (IL-9) – Loading**

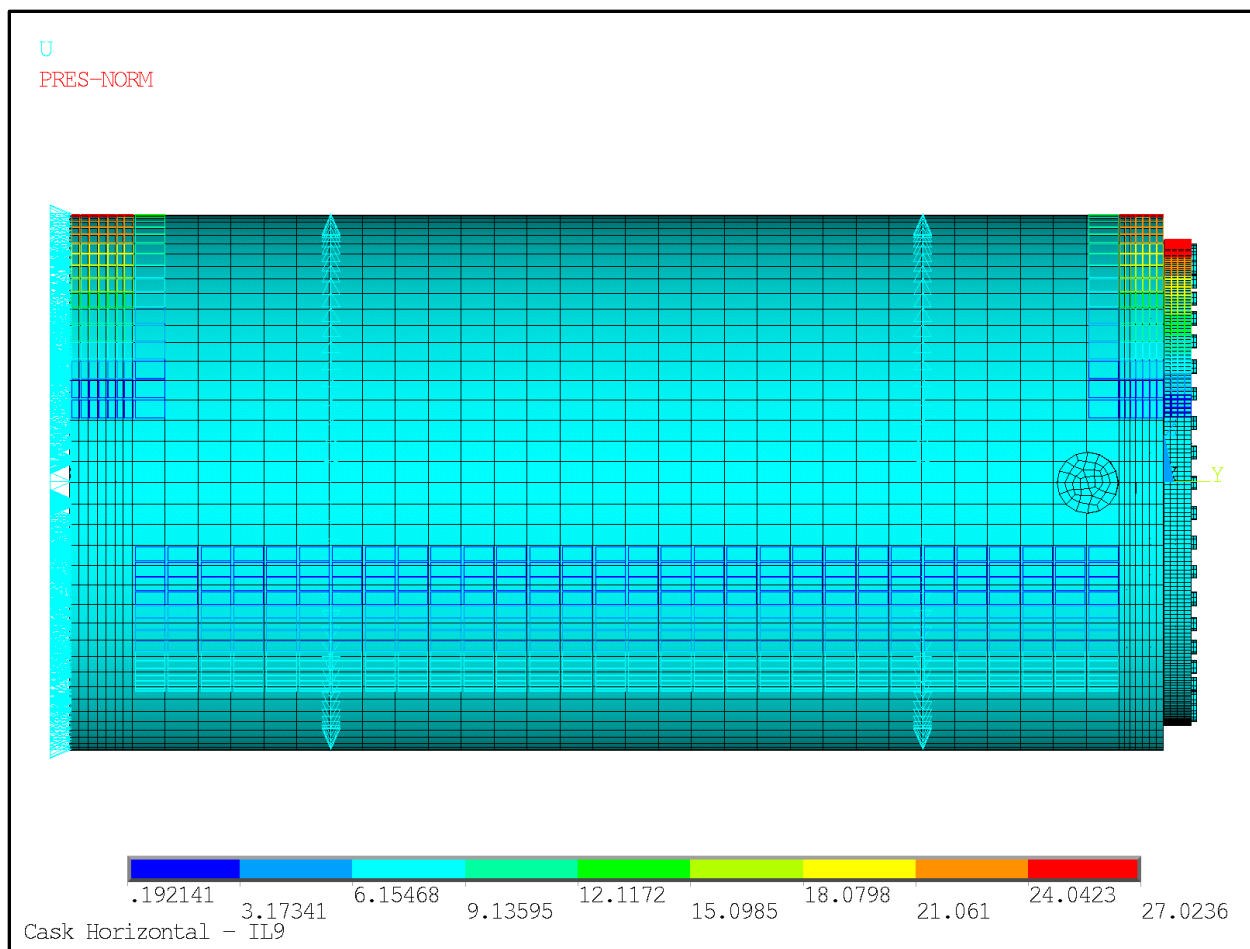


**Figure 2.12.2-7**  
**1g Cask Horizontal (IL-9) – Loading and Displacement Boundary Conditions**

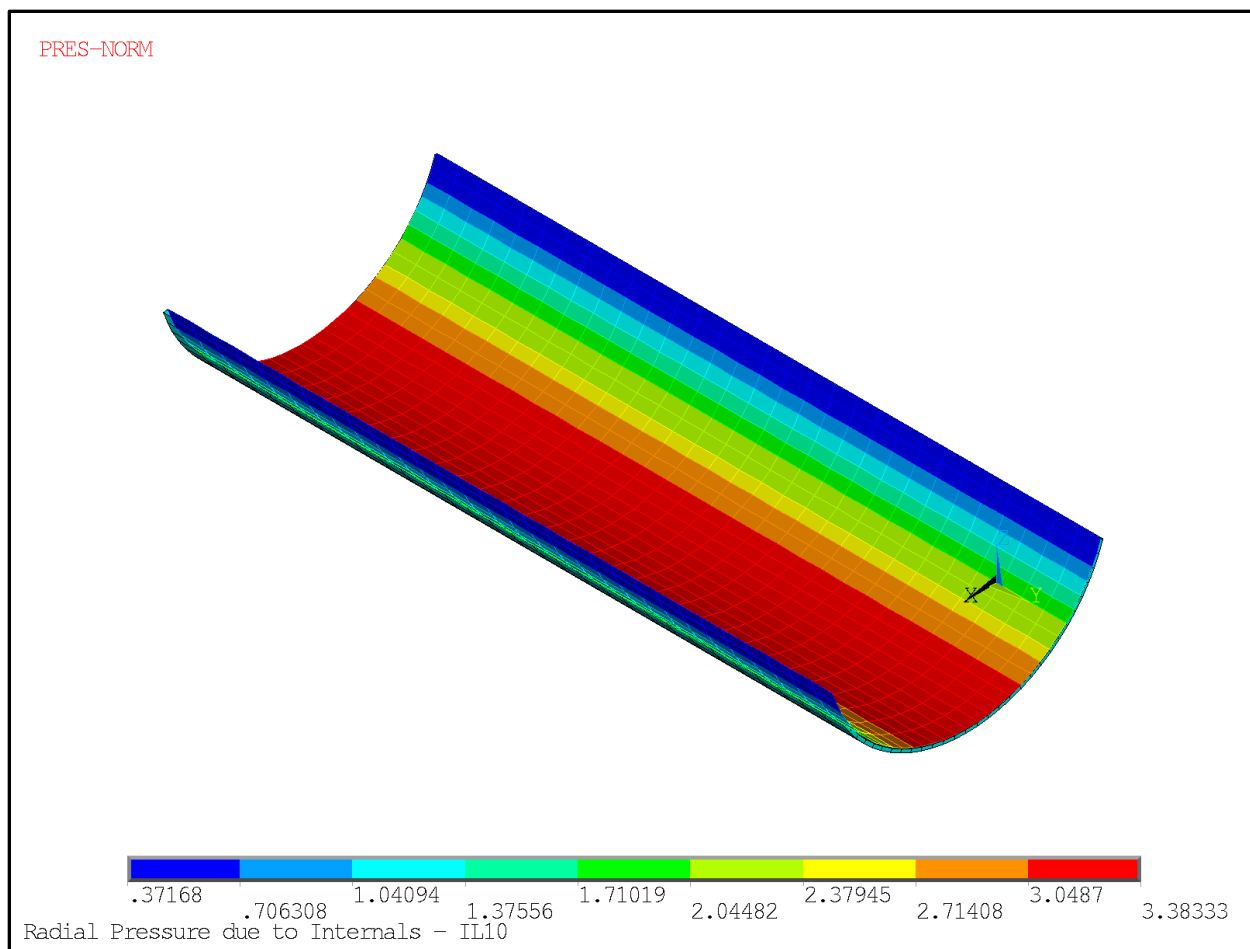


**Figure 2.12.2-8**  
**Radial Pressure Due to Internals (IL-10) – Loading**

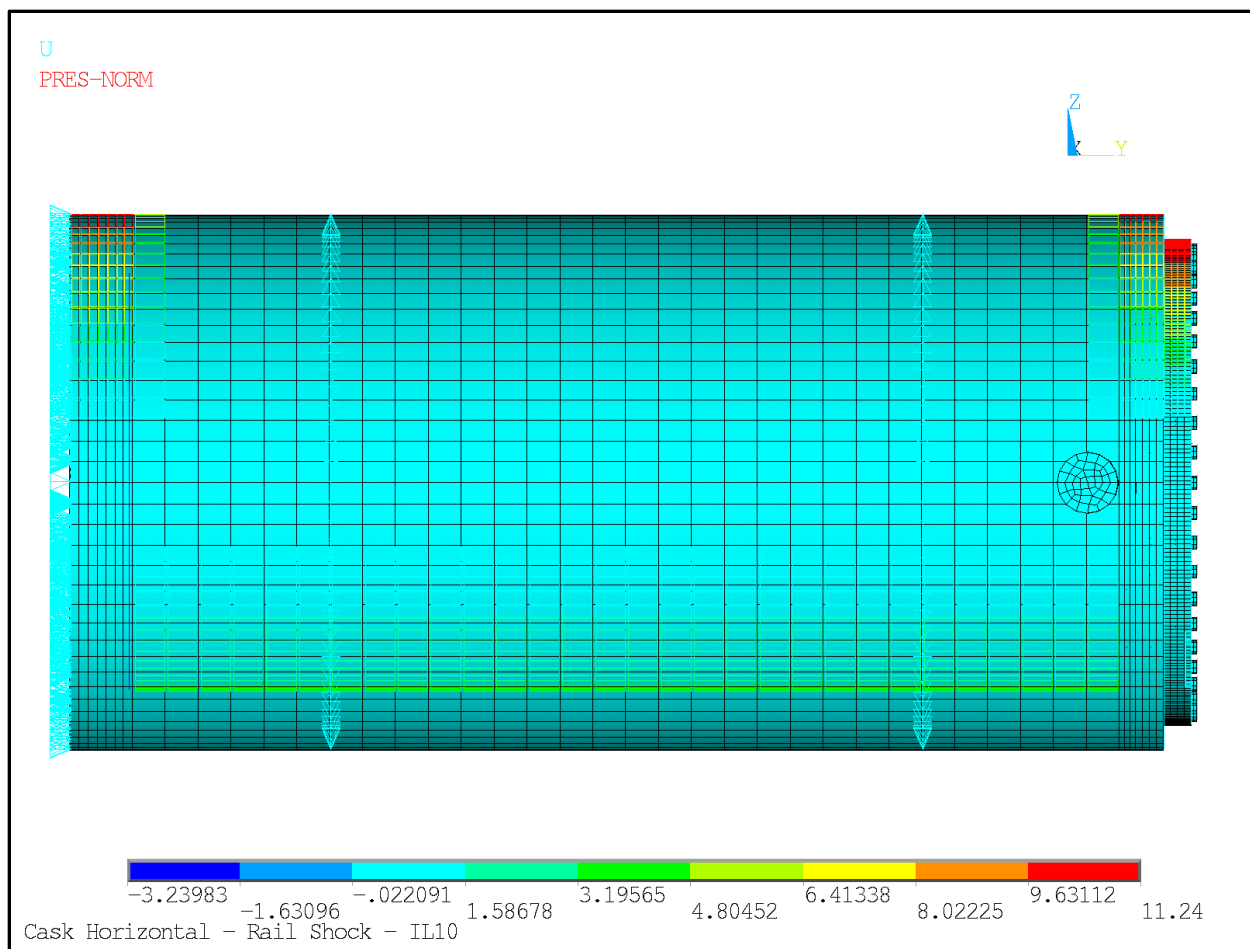


**Figure 2.12.2-9**  
**Rail Shock Cask Horizontal (IL-10) – Loading and Displacement Boundary Conditions**



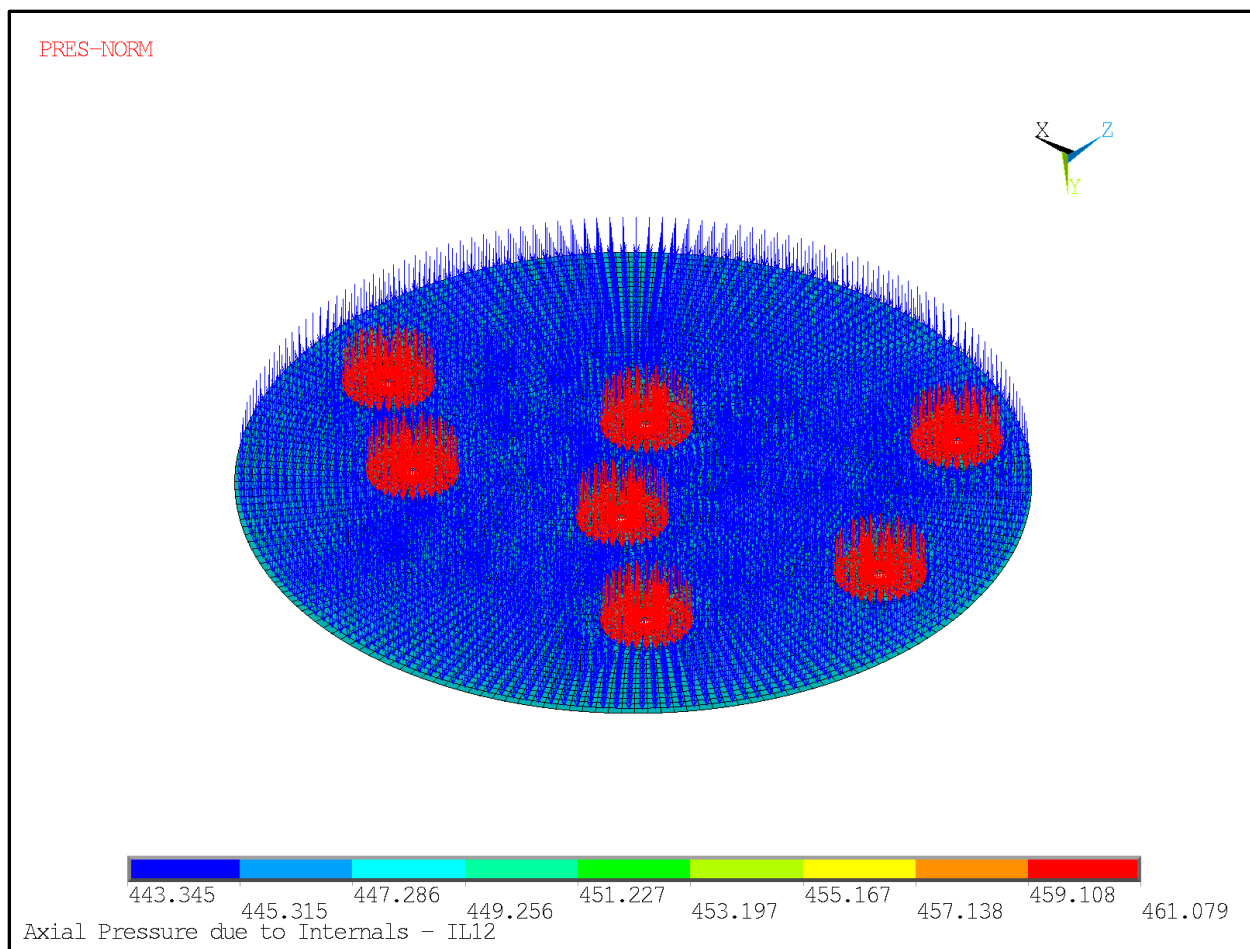


**Figure 2.12.2-10**  
**End Drop on Closure Lid (IL-12) – Axial Pressure Due to Weight of Internals**

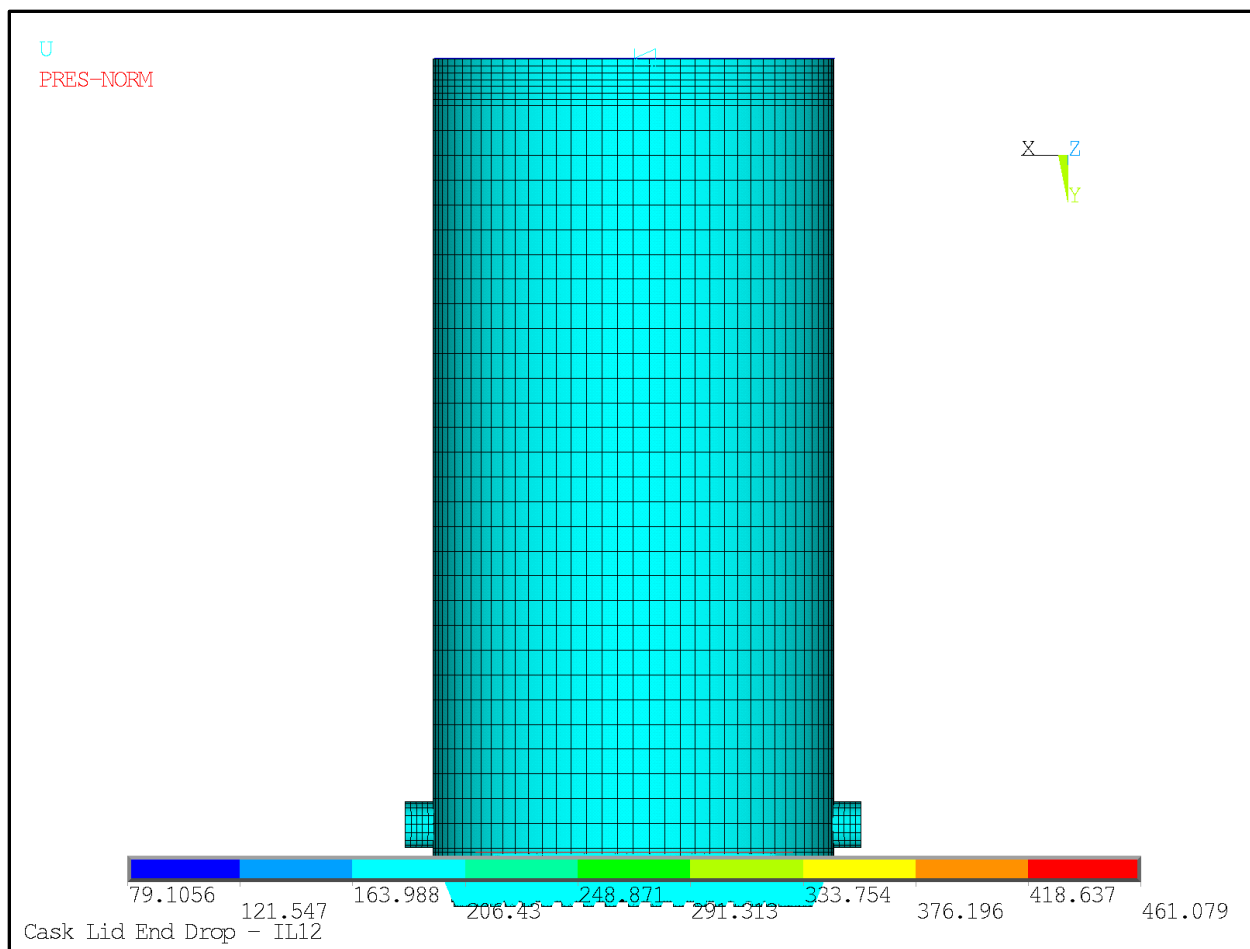


**Figure 2.12.2-11**  
**End Drop on Closure Lid (IL-12) – Loading and Displacement Boundary Conditions**

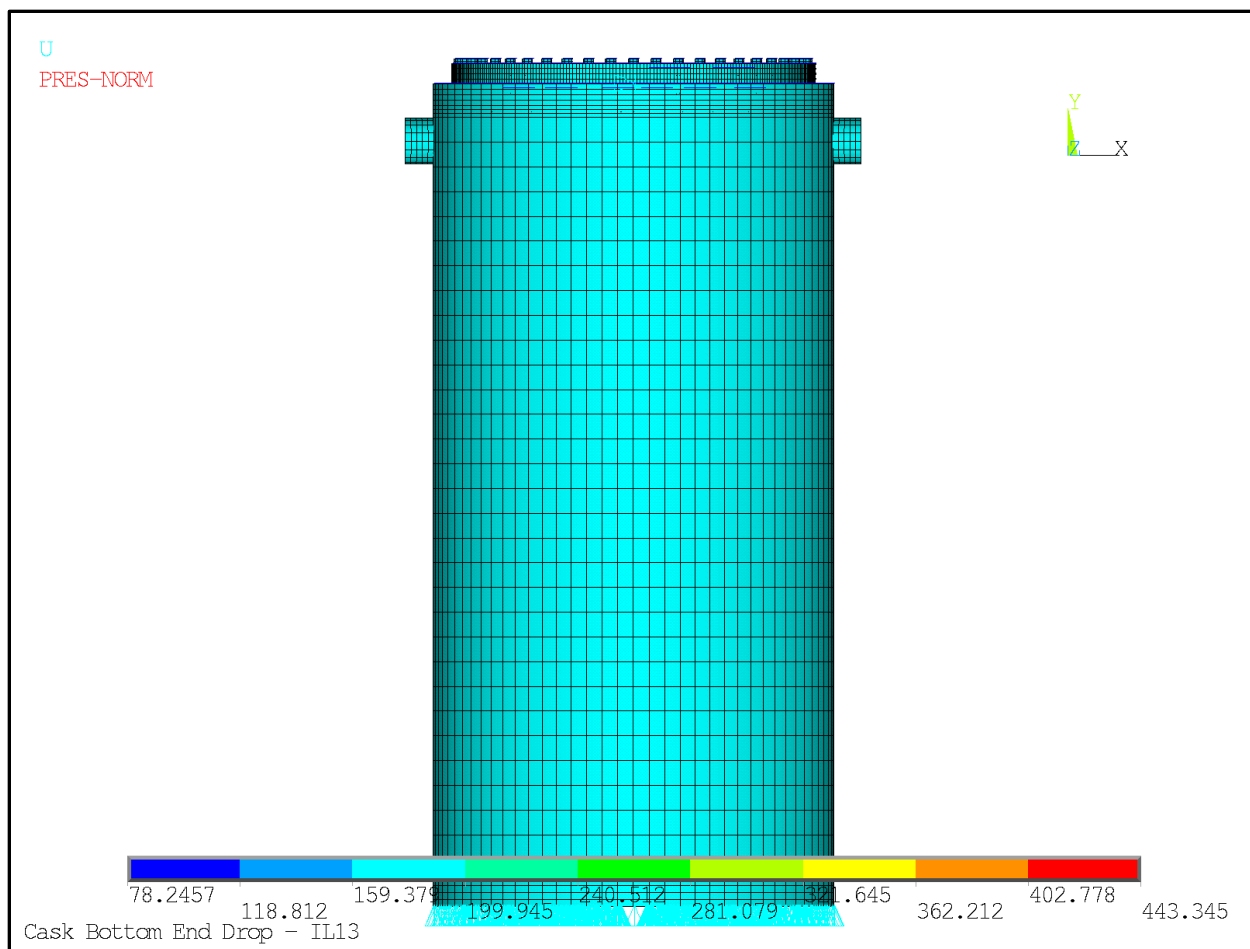


**Figure 2.12.2-12**  
**End Drop on Bottom (IL-13) – Loading and Displacement Boundary Conditions**

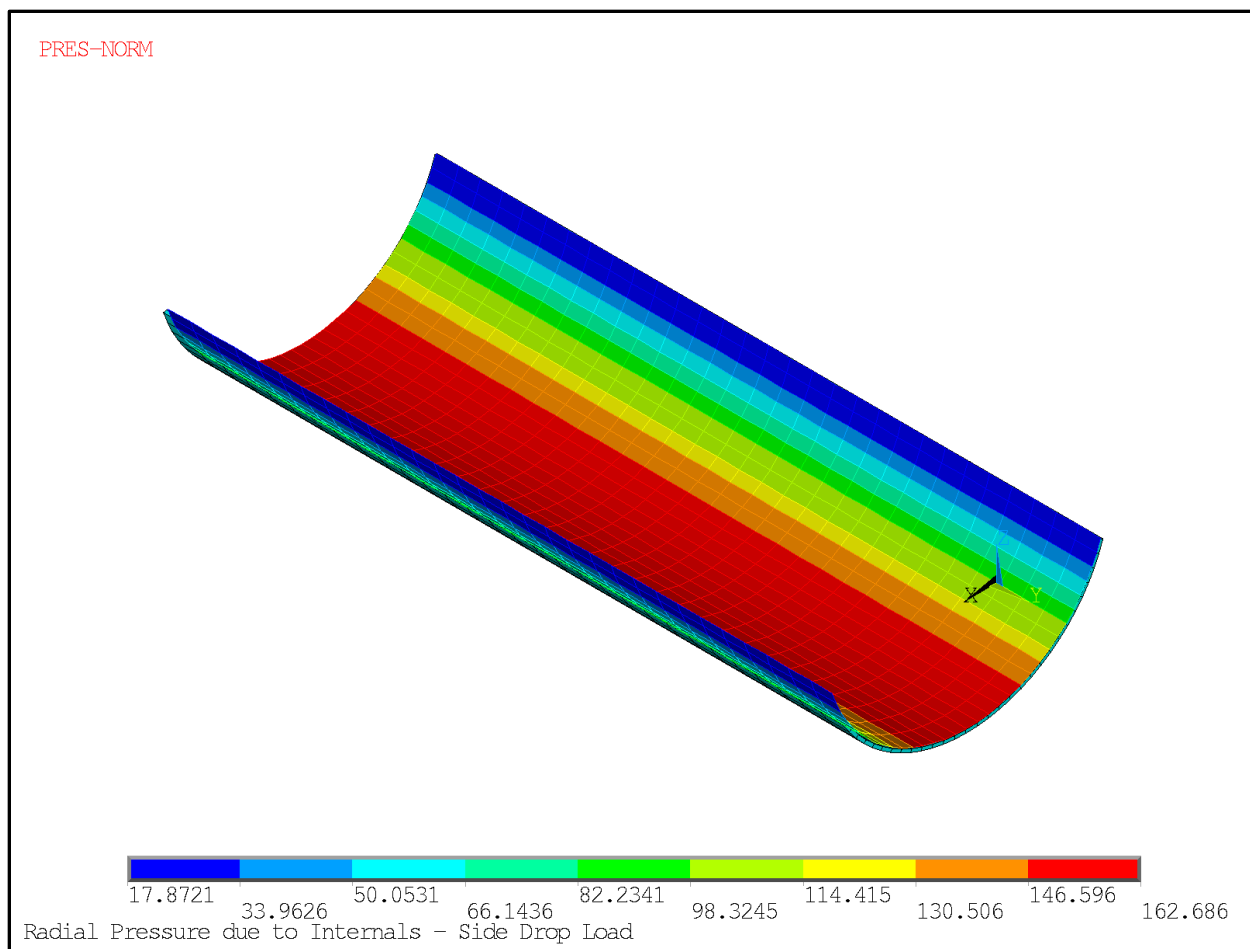


**Figure 2.12.2-13**  
**Radial Pressure Due to Internals (IL-14) – Loading**

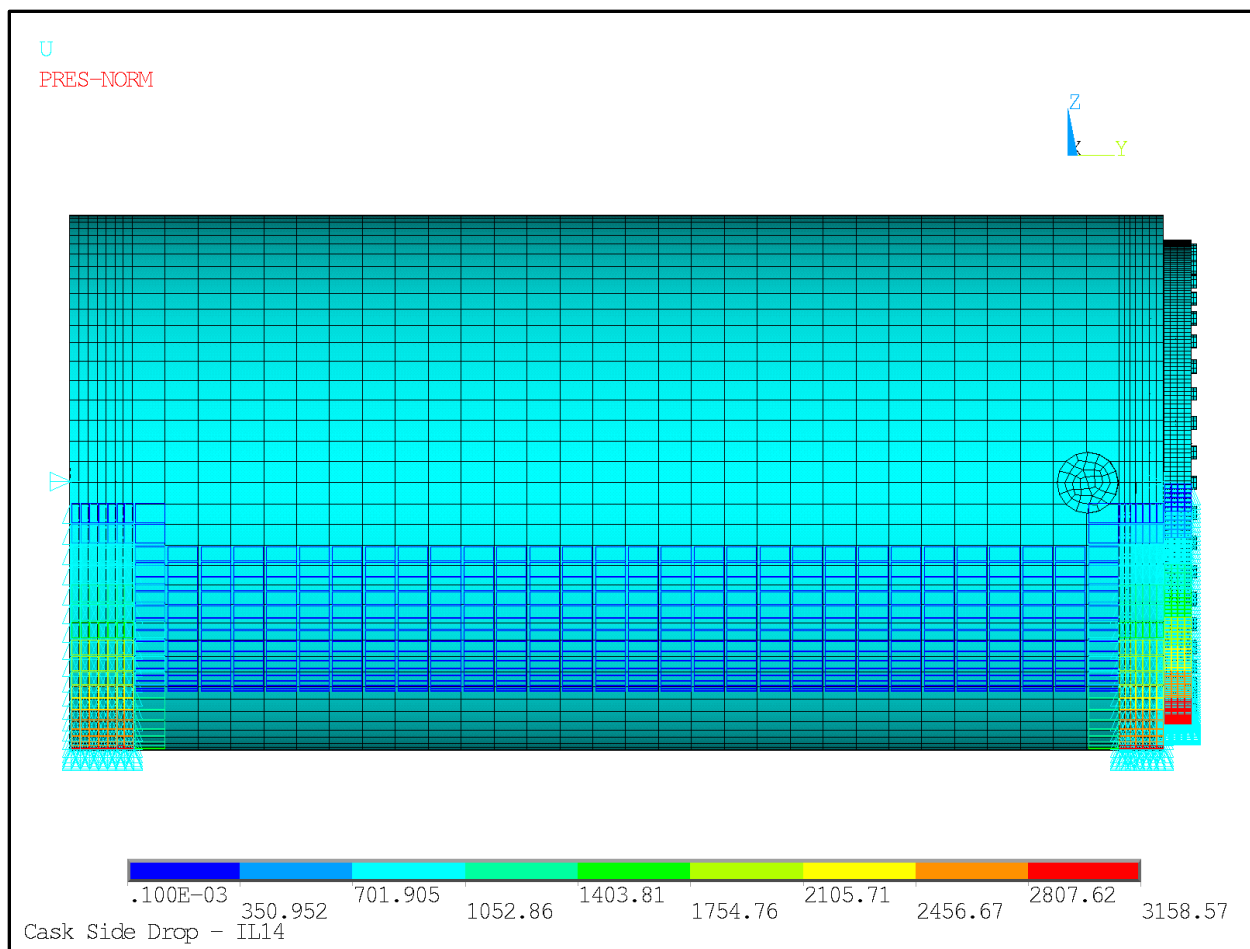


**Figure 2.12.2-14**  
**Side Drop (IL-14) – Loading and Displacement Boundary Conditions**

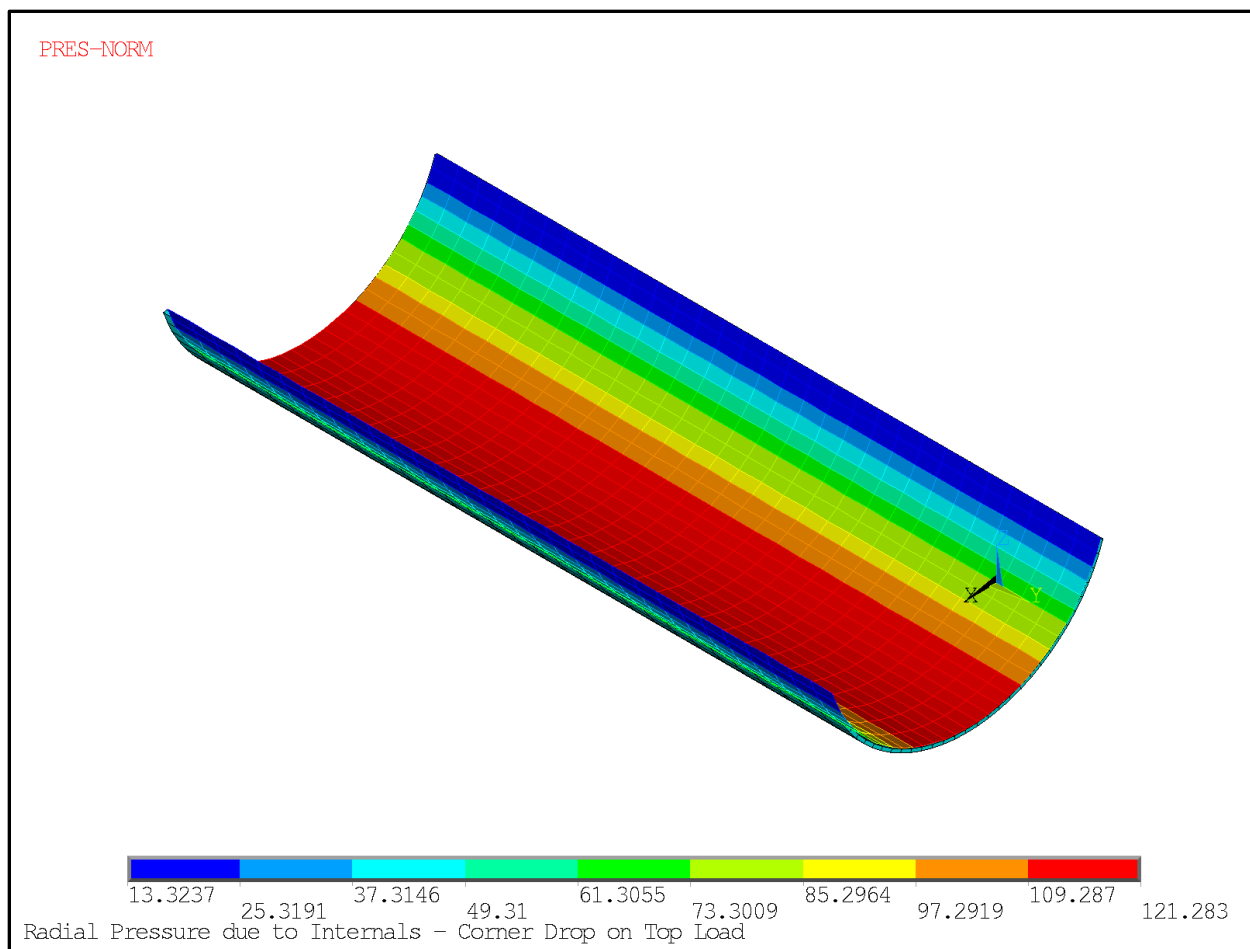


**Figure 2.12.2-15**  
**CG-Over-Corner Drop on Top (IL-15) – Radial Pressure Due to Internals Loading**

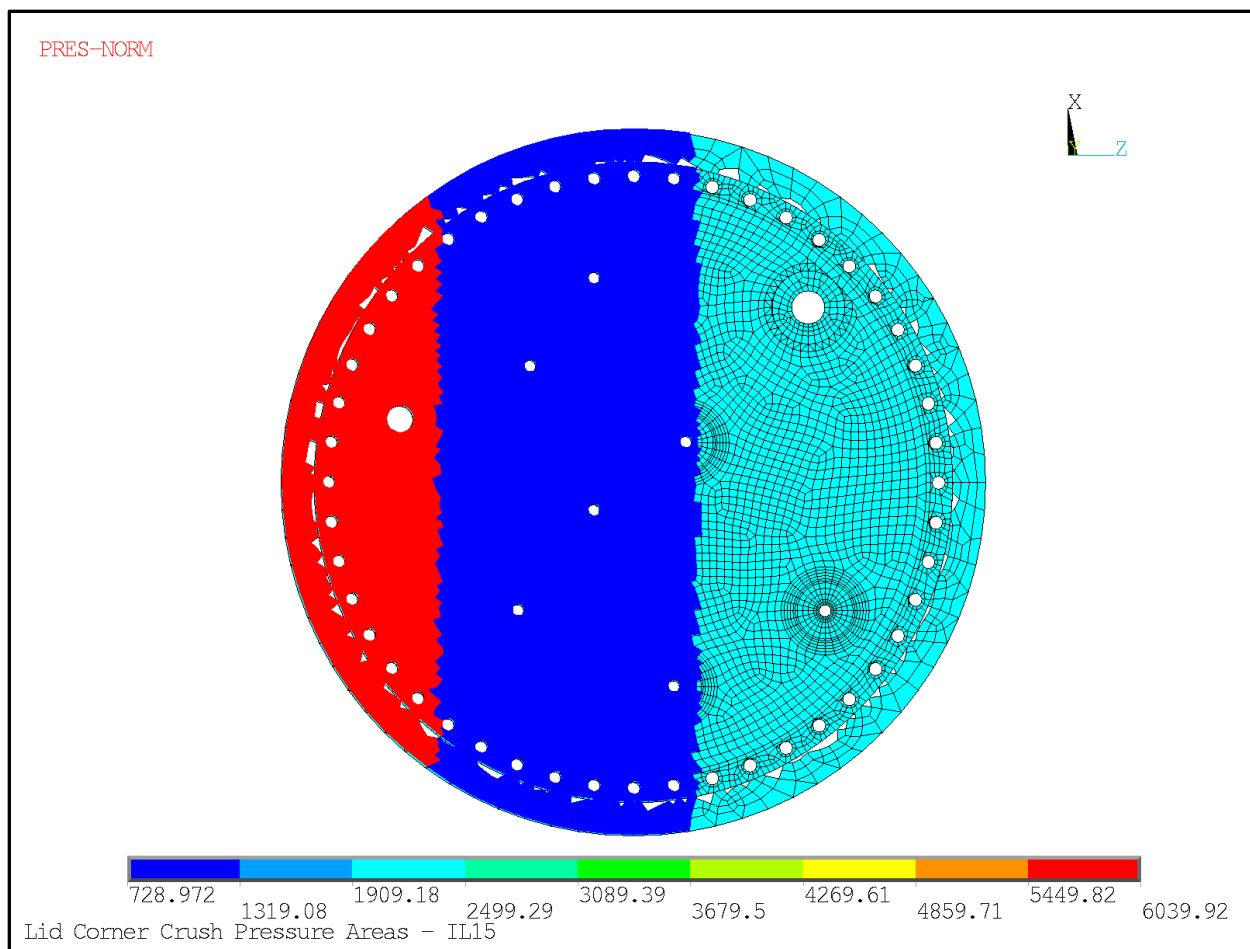


**Figure 2.12.2-16**  
**CG-Over-Corner Drop – Crush Area Pressures (IL-15)**

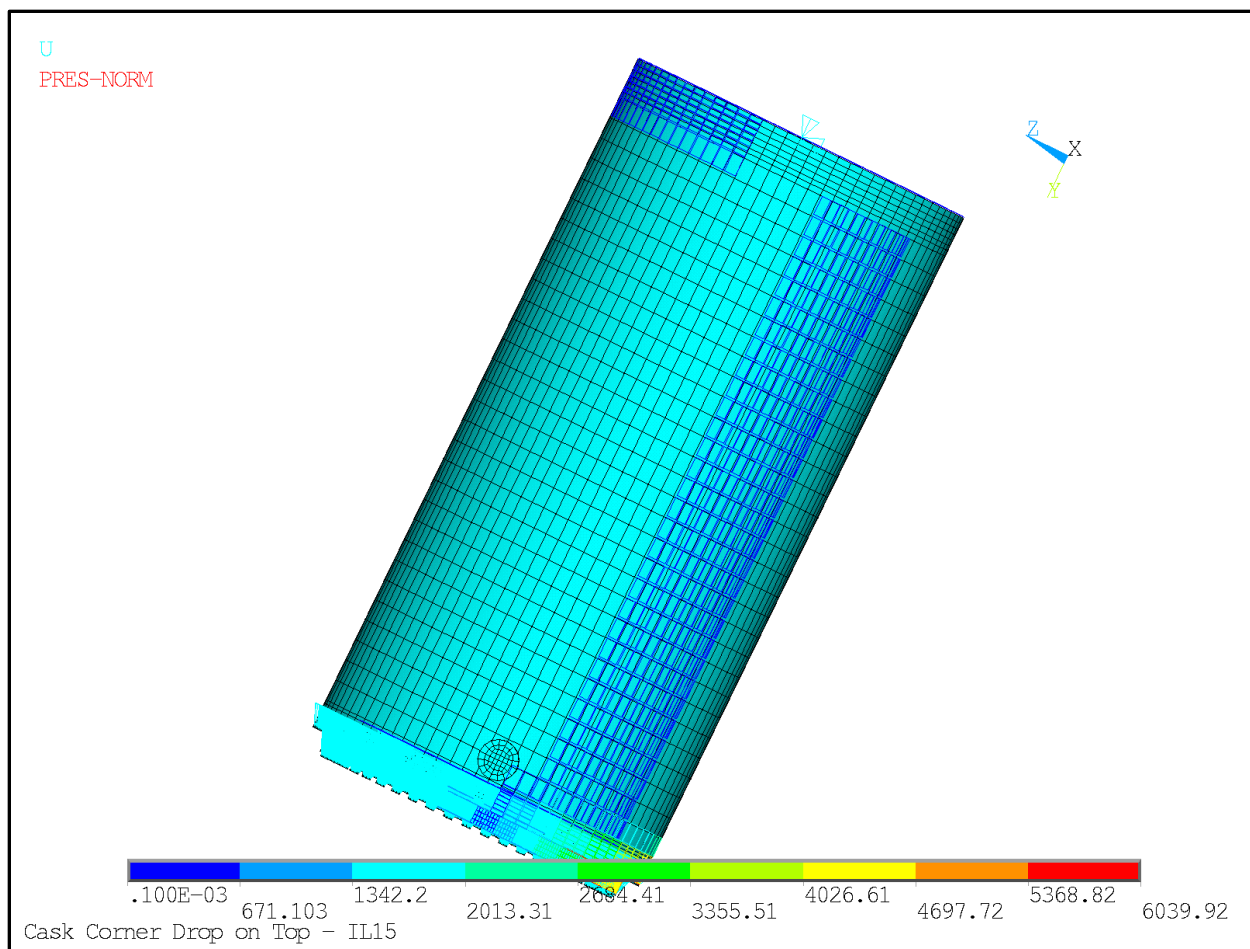


**Figure 2.12.2-17**  
**CG-Over-Corner Drop on Top (IL-15) – Loading and Displacement Boundary Conditions**



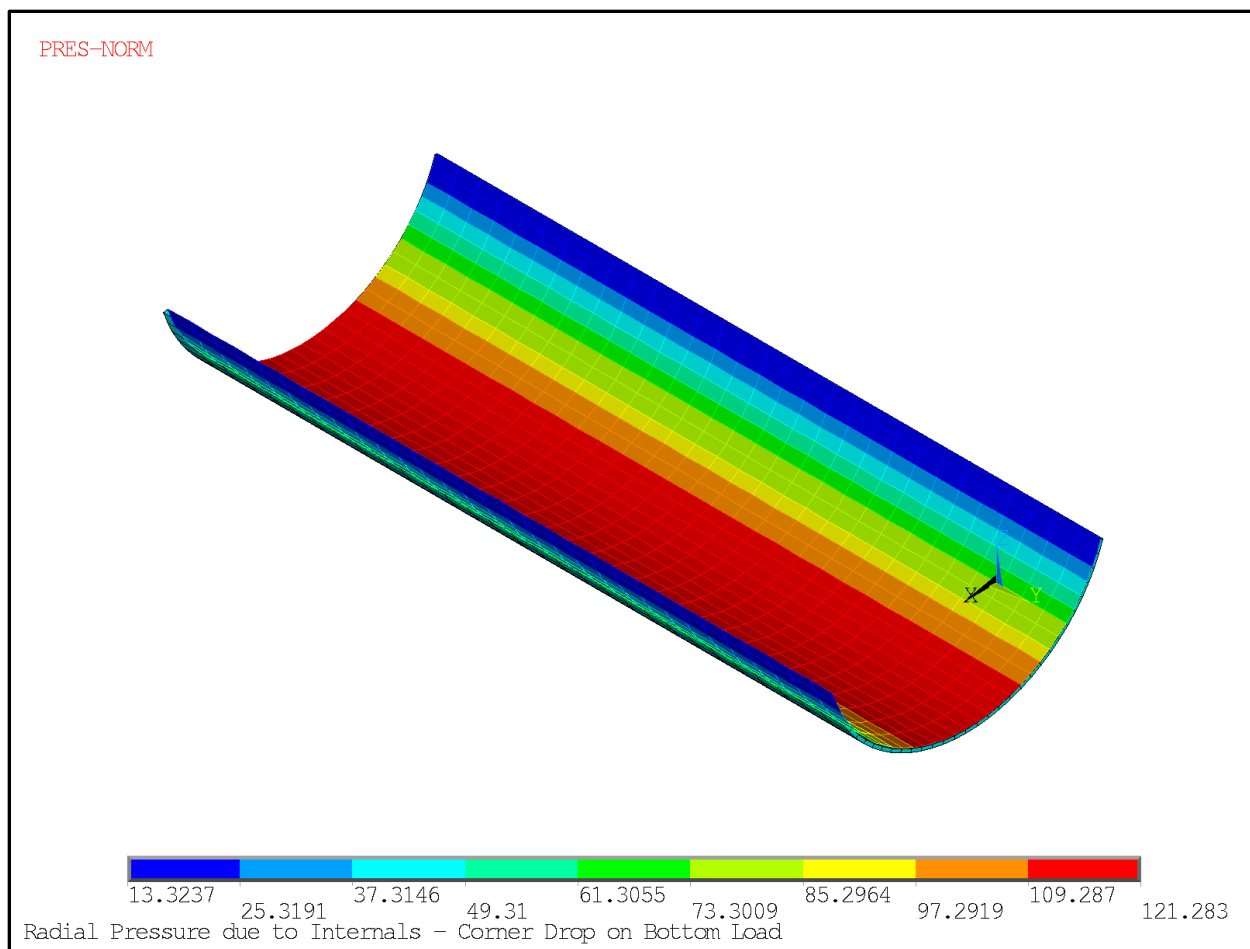


**Figure 2.12.2-18**  
**CG-Over-Corner Drop on Bottom (IL-16) – Radial Pressure Due to Internals Loading**

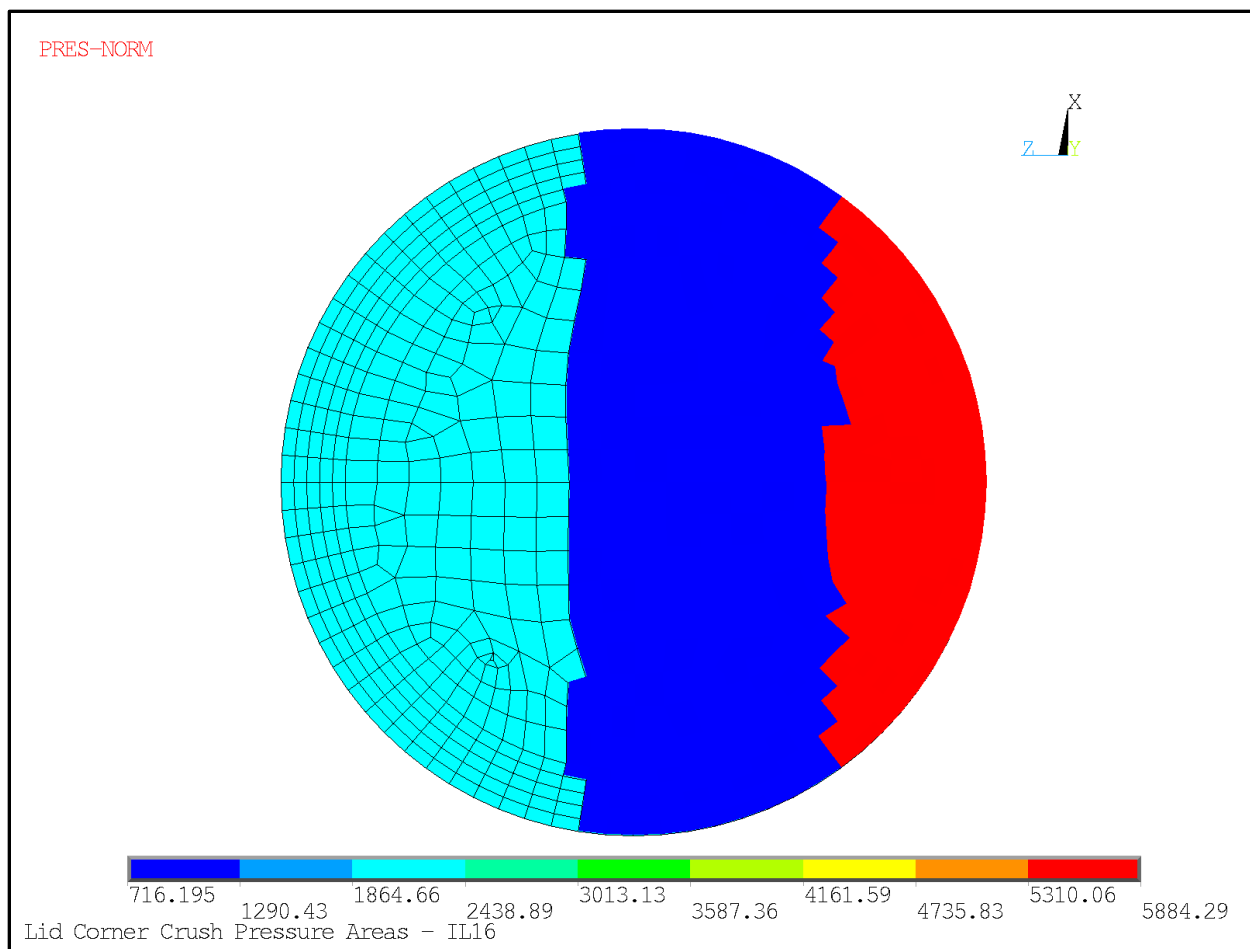


**Figure 2.12.2-19**  
**CG-Over-Corner Drop – Crush Area Pressures (IL-16)**

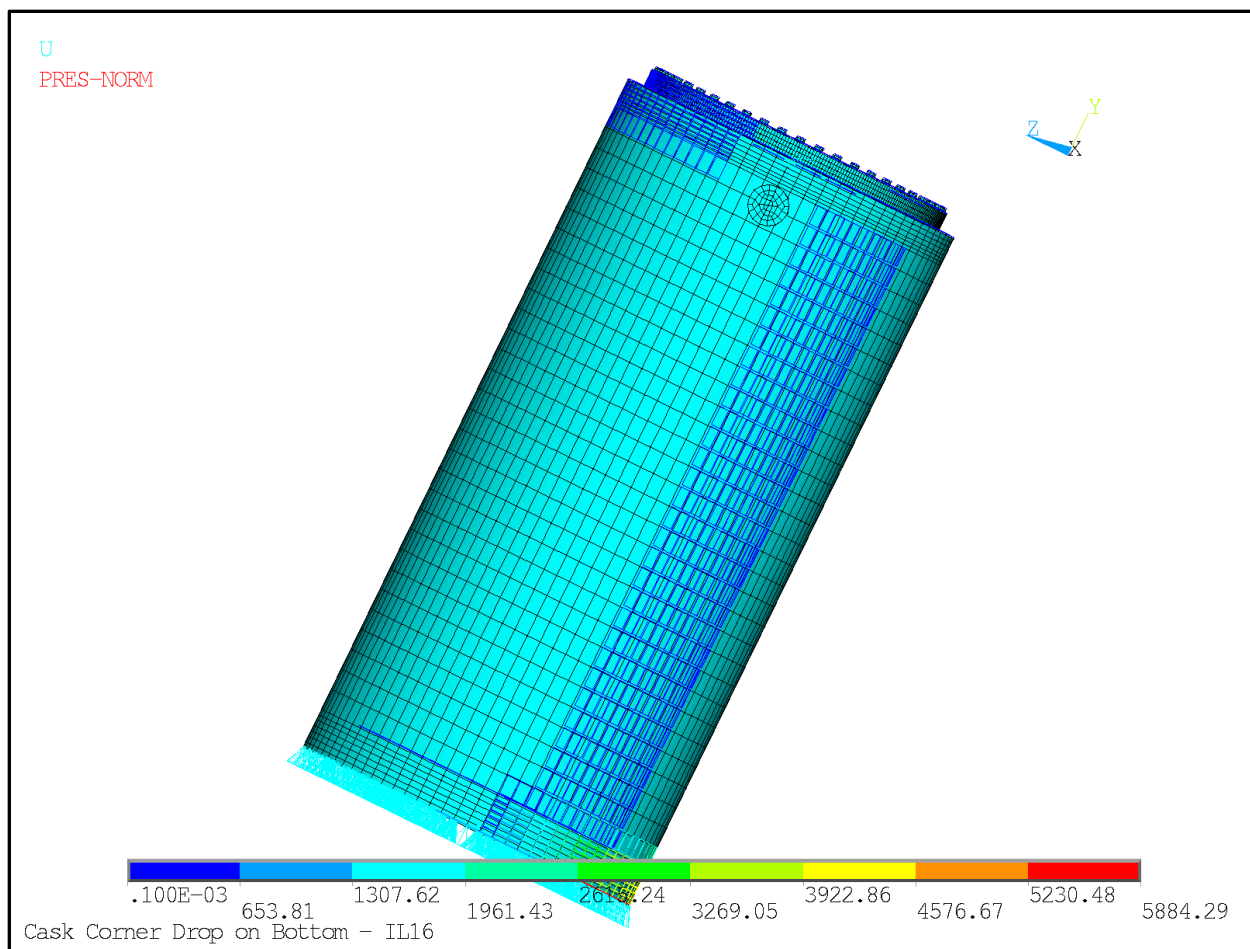


**Figure 2.12.2-20**  
**CG-Over-Corner Drop on Bottom (IL-16) – Loading and Displacement Boundary Conditions**

## **Appendix 2.12.3 Closure Lid Bolt Analysis**

### **TABLE OF CONTENTS**

2.12.3	Closure Lid Bolt Analysis .....	2.12.3-1
2.12.3.1	Introduction .....	2.12.3-1
2.12.3.2	Closure Lid Bolt Load Calculations .....	2.12.3-2
2.12.3.3	Summary of Closure Lid Bolt Loads .....	2.12.3-7
2.12.3.4	Closure Lid Bolt Load Combinations .....	2.12.3-7
2.12.3.5	Closure Lid Bolt Stress Calculations.....	2.12.3-10
2.12.3.6	Analysis Results .....	2.12.3-12
2.12.3.7	Closure Lid Bolt Fatigue Analysis .....	2.12.3-12
2.12.3.8	Lid Seal Contact Evaluation .....	2.12.3-16
2.12.3.9	Engagement Length for Bolt and Flange .....	2.12.3-17
2.12.3.10	Conclusions.....	2.12.3-18
2.12.3.11	References.....	2.12.3-19

LIST OF TABLES

Table 2.12.3-1	Design Parameters for Closure Lid Bolt Analysis .....	2.12.3-20
Table 2.12.3-2	Closure Lid Bolt Data .....	2.12.3-21
Table 2.12.3-3	Normal Condition Allowable Stresses in Closure Lid Bolts .....	2.12.3-22
Table 2.12.3-4	Accident Condition Allowable Stresses in Closure Lid Bolts .....	2.12.3-22

## 2.12.3 Closure Lid Bolt Analysis

### 2.12.3.1 Introduction

This appendix evaluates the ability of the cask closure bolt to maintain a leaktight seal under events defined by normal conditions transport (NCT) and the hypothetical accident conditions (HAC). Also evaluated in this appendix are the bolt thread and internal thread stresses, and lid bolt fatigue. The stress analysis is performed in accordance with NUREG/CR-6007 [1].

The TN-32B HBU demonstration cask closure lid arrangement is a 4.5-inch thick lid with a welded 6.0-inch thick radiation shield. The closure lid is bolted directly to the shell flange by 48 high-strength alloy steel [ ] diameter bolts (with 1½ - 8UN threaded portion) and a hardened flat washer. Close-fitting alignment pins ensure that the closure lid was centered in the vessel during loading. The closure lid bolt material is SA-540 Gr B23 CL1, and the flat washer material is ASTM A564, Type 630, H1075.

The lid bolt analysis presented in this appendix is performed in accordance with NUREG/CR-6007. The closure lid bolt material has yield and tensile strengths of 150 ksi and 165 ksi at 70 °F, respectively.

The following ways to minimize bolt forces and bolt failures for shipping casks are extracted directly from Page xiii of Reference [1]. All of the following design methods are employed in the TN-32B HBU demonstration cask closure system.

- Protect closure lid from direct impact to minimize bolt forces generated by free drops (use impact limiters).
- Use materials with similar thermal properties for the closure bolts, the closure lid, and the cask wall to minimize the bolt forces generated by fire accident.
- Apply sufficiently large bolt preload to minimize fatigue and loosening of the bolts by vibrations.
- Lubricate bolt threads to reduce required preload tightening torque, and to increase the predictability of the achieved preload.
- Utilize a closure lid and bolt design that minimizes the prying actions of applied loads.
- Pay special attention to the interactions between the preload and thermal load, and between the preload and the prying action in selecting bolt preload.

The following closure lid bolt evaluations are presented in this appendix:

- Closure lid bolt tightening torque
- Bolt preload
- O-ring seal seating load
- Pressure load
- Temperature load

- Impact load
- Puncture load
- Bearing stress
- Load combinations for NCT and HAC
- Bolt stresses and allowable stresses
- Closure lid bolt fatigue
- Closure lid/cask seal evaluation
- External thread engagement evaluation

The design parameters of the closure lid, selected from Reference [1] are summarized in Table 2.12.3-1. The closure lid bolt data and material allowables are presented in Table 2.12.3-2 through Table 2.12.3-4. A maximum temperature of 300 °F is utilized in the closure lid bolt region during NCT and HAC based on results of thermal analyses documented in Chapter 3. The following load cases are considered in the analysis.

1. Preload + Temperature Load (NCT)
2. Pressure Load + 1 Foot Drop (NCT)
3. Pressure Load + 30 Foot Corner Drop (HAC)
4. Pressure Load + Puncture Load (HAC)

#### 2.12.3.2 Closure Lid Bolt Load Calculations

##### 2.12.3.2.1 Bolt Preload

The method utilized for the following calculation is extracted from Table 4.1 of Reference [1].

A bolt tightening range of 940 to 1,230 lb<sub>r</sub>-ft torque is utilized for the closure lid bolts. For the minimum tightening torque of 940 lb<sub>r</sub>-ft, the non-prying axial force per bolt,  $F_a$ , is:

$$F_a = \frac{Q_{\min}}{K D_{ba}} \quad \text{where:}$$

$Q_{\min}$  = applied tightening torque = 940(12) = 1,128 lb<sub>r</sub>-in

$K$  = nut factor = [ ] (determined experimentally for TN-32 casks)

$D_{ba}$  = bolt shank diameter = [ ]

For the maximum tightening torque,  $Q_{\max}$ , of 1,230 lb<sub>r</sub>-ft, the non-prying axial force per bolt is:

$$F_a = \frac{Q_{\max}}{K D_{ba}}$$

The residual torsional moment,  $M_{tr}$ , is:

$$M_{tr-max} = 0.5(Q_{max}) = 0.5(1,230 \times 12) = 7,380 \text{ in-lb}_f$$

$$M_{tr-min} = 0.5(Q_{min}) = 0.5(940 \times 12) = 5,640 \text{ in-lb}_f$$

The maximum residual non-prying tensile bolt force,  $F_{ar}$ , will be:

$$F_{ar} = F_a = 84,524 \text{ lb}_f$$

The bolt tensile stress area,  $A_t$ , is [ ] (see Table 2.12.3-2). Therefore, the lid bolt tensile stress,  $\sigma_b$ , for the maximum tightening torque is:

#### 2.12.3.2.2 O-ring Seal Seating Load

O-ring seal characteristics for the Helicoflex® HND 229 seals with a silver jacket, and a 0.276 seal cross section are extracted from Reference [2]. The diameter of the inner seal,  $D_{is}$ , is 70.79 in, and the diameter of the outer seal,  $D_{os}$ , is 72.91 in. The force to seat the seals is approximately 2,512 lb<sub>f</sub>/in for a silver jacket [2]. Therefore, the total force required to seat the seals is:

$$\text{Inner Seal Seat Load: } \pi(70.79)(2,512) = 558,652 \text{ lb}_f$$

$$\text{Outer Seal Seat Load: } \pi(72.91)(2,512) = 575,382 \text{ lb}_f$$

$$\text{Total load to seat the seals, } F_a, = 558,652 + 575,382 = 1,134,034 \text{ lb}_f$$

Therefore, the seal seating load per bolt is:

$$F_a/48 = 1,134,034/48 = 23,626 \text{ lb}_f/\text{bolt}$$

Since the non-prying minimum tensile load in each bolt is 64,596 lb<sub>f</sub>, the specified preload has the required force to seat the seals.

#### 2.12.3.2.3 Pressure Loads

The method used for the following calculation is extracted from Table 4.3 of Reference [1].

Axial force per bolt due to internal pressure is:

$$F_a = \frac{\pi D_{ig}^2 (P_{li} - P_{lo})}{4 N_b}$$

Utilizing the outer seal diameter for  $D_{ig}$  (conservative) = 72.92 in, then,



$$F_a = \frac{\pi(72.92^2)(100-0)}{4(48)} = 8,700 \text{ lb}_f/\text{bolt}$$

The fixed edge closure lid force is:

$$F_f = \frac{D_{lb}(P_{li}-P_{lo})}{4} = \frac{76.06(100-0)}{4} = 1,902 \text{ lb}_f/\text{inch}$$

The fixed edge closure lid moment is:

$$M_f = \frac{(P_{li}-P_{lo})D_{lb}^2}{32} = \frac{(100-0)(76.06^2)}{32} = 18,079 \text{ in-lb}_f/\text{inch}$$

Bolt shear can only occur when the reduced diameter bolt shank contacts the side of the hole in the closure lid. The shield plate, which is welded to the closure lid, has a smaller clearance to the inner diameter of the cask cavity than the clearance between the bolt shank and the hole in the lid. Therefore, the shield plate will contact the cask inner wall prior to the bolt shank contacting the edge of the hole, and no bolt shear will result, i.e.,  $F_s = 0$ .

#### 2.12.3.2.4 Temperature Loads

The closure lid bolt material is SA-540 Grade B23 Class 1 (2Ni - ¾Cr - ¼Mo). This material is Group 1 in the thermal coefficients of expansion tables in Reference [6]. The closure lid is SA-203 Gr D (3½Ni), and the flange is SA-350 Gr. LF3 (3½Ni), which are also in Group 1. Consequently, the closure lid bolts, closure lid, and flange have the same coefficient of thermal expansion, i.e.,  $7.3 \times 10^{-6}$  in/in-°F at 300 °F. Therefore, heating to the maximum isothermal temperature will not generate any additional bolt stress.

#### 2.12.3.2.5 Impact Loads

The method used for the following calculation is extracted from Table 4.5 of Reference [1]. The non-prying tensile bolt force per bolt,  $F_a$ , is:

$$F_a = \frac{1.34 \sin(\alpha)(DLF)(a_i)(W_l + W_c)}{N_b} = \frac{1.34 \sin(\alpha)(1.0)(a_i)(77,000)}{48} = 2,150 (a_i) \sin(\alpha) \text{ lb}_f/\text{bolt}$$

Note:  $W_l + W_c$  is conservatively assumed to be 77,000 lb<sub>m</sub> [actual weights from Table 2-7 are 12,900 lb<sub>m</sub> for closure lid, lid bolts, and TLAs, 13,420 lb<sub>m</sub> for basket, rails, and shims, and 49,650 lb<sub>m</sub> for fuel assemblies resulting in a total weight of 75,970 lb<sub>m</sub>].

The fixed-edge closure lid force,  $F_f$ , is:

$$F_f = \frac{1.34 \sin(\alpha)(DLF)(a_i)(W_l + W_c)}{\pi D_{lb}} = \frac{1.34 \sin(\alpha)(1.0)(a_i)(77,000)}{\pi(76.06)} = 431.8 \sin(\alpha)(a_i) \text{ lb}_f/\text{bolt}$$

The fixed-edge closure lid moment,  $M_f$ , is,

$$M_f = \frac{1.34 \sin(\xi)(DLF)(a_i)(W_l + W_c)}{8\pi} = \frac{1.34 \sin(\xi)(1.0)(a_i)(77,000)}{8\pi} = 4,105 \sin(\xi)(a_i) \text{ lb-in/bolt}$$

### NCT Impact Loads

The TN-32B HBU demonstration cask is lifted vertically and is transported horizontally. Therefore, end and side drop orientations are considered to be credible NCT free drop events. Any other drop orientation will cause the cask to tip over onto its side, which is considered an accident. The analysis of the bolts for the HAC impact loads bound any possible tipping accident.

Since the closure lid bolts are protected by the impact limiter and the puncture resistant plate/lance cover plates during an end drop, the worst-case scenario is assumed to be a 64° CG-over-corner free drop, which is the same orientation for an HAC impact load. From the impact limiter 1 foot normal condition analysis of the very similar TN-40 cask (Appendix 2.10.8 of Reference [3]), the maximum g-load for a 1 foot 64° CG-over-corner drop was calculated to be 5g vertical and 3g horizontal. For the difference in the mass impacting the closure lid, i.e., 82,000 lb<sub>m</sub> (TN-40) versus 77,000 lb<sub>m</sub> (TN-32B HBU cask), the maximum g-loads will be increased by the ratio of the masses, i.e., (82/77) = 1.065. With this ratio, the maximum calculated g-loads would become 5.3g vertical and 3.2g horizontal. However, for the closure lid bolt analysis, the following normal condition g-loading is conservatively utilized:

$$a_i = 10 \text{ gs, and } \xi = 64^\circ$$

Therefore,

$$F_a = (2,150)(10)\sin(64^\circ) = 19,324 \text{ lb}_f/\text{bolt}$$

$$F_s = 0 \text{ lb}_f/\text{bolt}$$

$$F_f = (431.8)(10)\sin(64^\circ) = 3,881 \text{ lb}_f/\text{inch}$$

$$M_f = (4,105)(10)\sin(64^\circ) = 36,895 \text{ lb}_f/\text{inch}$$

### HAC Impact Loads

The impact load resulting from a 30 foot, 64° corner drop are conservatively assumed to be the following (actual impact is 29.3g, Appendix 2.12.9).

$$a_i = 30\text{g, and } \xi = 64^\circ$$

Therefore,

$$F_a = (2,150)(30)\sin(64^\circ) = 57,972 \text{ lb}_f/\text{bolt}$$

$$F_s = 0 \text{ lb}_f/\text{bolt}$$

$$F_f = (438.1)(30)\sin(64^\circ) = 11,643 \text{ lb}_f/\text{inch}$$

$$M_f = (4,105)(30)\sin(64^\circ) = 110,686 \text{ in-lb}_f/\text{inch}$$

## 2.12.3.2.6 Puncture Drop Loads

Omitting the structural protection provided by the impact limiter and the puncture resistant plate, it is conservatively assumed that the puncture bar strikes the center of the closure lid. For this assumption, the method utilized for the following calculation is extracted from Table 4.7 of Reference [1].

The non-prying tensile bolt force,  $F_a$ , per bolt is:

$$F_a = \frac{-\sin(xi)P_{un}}{N_b}$$

where:

$$P_{un} = \text{smaller of } \begin{cases} 0.75\pi D_{pb}^2 S_{yl} = 0.75\pi(6)^2(32,700) = 2.774 \times 10^6 \\ 0.6\pi D_{pb} t_l S_{ul} = 0.6\pi(6)^2(10.5)(65,000) = 7.72 \times 10^6 \end{cases}$$

$$P_{un} = 2.774 \times 10^6 \text{ lb}_f$$

The puncture force is greatest when  $xi = 90^\circ$ . Therefore,

$$F_a = \frac{-\sin(90)2.774 \times 10^6}{48} = -57,792 \text{ lb}_f/\text{bolt}$$

Since the force is negative (inward acting), the actual resulting bolt force,  $F_a = 0$ , because the applied load is supported by the cask wall and not the closure lid bolts. The shield plate, which is welded to the closure lid plate, will react to any shear force from the puncture drop. Therefore,  $F_s = 0$ .

The fixed-edge closure lid force,  $F_f$ , is:

$$F_f = \frac{-\sin(xi)P_{un}}{\pi D_{lb}} = \frac{-\sin(90^\circ)2.774 \times 10^6}{\pi(76.06)} = -11,609 \text{ lb}_f/\text{inch}$$

The fixed-edge closure lid moment,  $M_f$ , is,

$$M_f = \frac{-\sin(xi)P_{un}}{4\pi} = \frac{-\sin(90^\circ)2.774 \times 10^6}{4\pi} = -220,748 \text{ in-lb}_f/\text{inch}$$

## 2.12.3.2.7 External Pressure Load of 290 psig

An external pressure load of 290 psig is evaluated as shown in Table 4.3 of Reference [1]. The axial force per bolt due to internal pressure is,

$$F_a = \frac{\pi D_{lg}^2 (P_{li} - P_{lo})}{4N_b}$$

where the outer seal diameter,  $D_{lg}$ , = 72.92 inches

Then,

$$F_a = \frac{\pi(72.92^2)(0-290)}{4(48)} = -25,231 \text{ lb}_f/\text{bolt}$$

Since this force is negative (inward acting), the actual resulting bolt force,  $F_a = 0$ , because the applied load is supported by the cask wall and not the lid bolts.

The fixed edge closure lid force  $F_f$  is,

$$F_f = \frac{D_{ls}(P_{li} - P_{lo})}{4} = \frac{72.92(-290)}{4} = -5,287 \text{ lb}_f/\text{inch}$$

The fixed edge closure lid moment,  $M_f$ , is,

$$M_f = \frac{(P_{li} - P_{lo})D_{lb}^2}{32} = \frac{-290(76.06^2)}{32} = -52,428 \text{ in-lb}_f/\text{inch}$$

The shield plate, which is welded to the closure lid plate, will react to any shear force during external pressure condition. Therefore,  $F_s = 0$

### 2.12.3.3 Summary of Closure Lid Bolt Loads

The loads calculated in the previous sections are summarized in the following table.

**Closure Lid Bolt Individual Load Summary**

Load Case	Applied Load	Non-Prying Tensile Force, $F_a$ (lb <sub>f</sub> )	Torsional Moment, $M_t$ (in-lb <sub>f</sub> )	Prying Force, $F_r$ (lb <sub>f</sub> /in)	Prying Moment, $M_r$ (in-lb <sub>f</sub> /in)
Preload	Residual	Maximum Torque	84,524	7,380	0
		Minimum Torque	64,596	5,640	0
Seals	Seating Load	23,626	0	0	0
Pressure	100 psig Internal	8,700	0	1,902	18,079
Thermal	300 °F	0	0	0	0
Impact	1 Foot Normal Condition Free Drop	19,324	0	3,881	36,895
	30 foot Accident Condition Free Drop	57,972	0	11,643	110,686
Puncture	Free drop onto a 6-inch diameter bar	0	0	-11,609	-220,748
External Pressure	290 psig External	0	0	-5,287	-52,428

### 2.12.3.4 Closure Lid Bolt Load Combinations

A summary of normal and accident condition load combinations is presented in the following table. The method utilized for the following combinations is extracted from Table 4.9 of Reference [1].

**Closure Lid Bolt Normal and Accident Load Combinations**

Load Case	Combination Description		Non-Prying Tensile Force, $F_a$ (lb <sub>f</sub> )	Torsional Moment, $M_t$ (in-lb <sub>f</sub> )	Prying Force, $F_f$ (lb <sub>f</sub> /in)	Prying Moment, $M_f$ (in-lb <sub>f</sub> /in)
1	Preload + Temperature (Normal Condition)	Maximum Torque	84,524	7,380	0	0
		Minimum Torque	64,596	5,640	0	0
2	Pressure + Normal Impact (Normal Condition)		29,956	0	6,171	58,669
3	Pressure + Accident Impact (Accident Condition)		66,672	0	13,545	128,765
4	Pressure + Puncture (Accident Condition)		8,700	0	-9,707	-202,669
5	Internal & External Pressure		8,700	0	-3,385	-34,349

**Additional Prying Bolt Force**

Since the prying forces applied in Load Cases 4 and 5 acts inward, normal to the closure lid, an additional prying bolt force,  $F_{ap}$ , is generated (Reference [1], Table 2.1). No additional force is generated for the outward loadings; however, (Load Cases 1, 2, and 3), because of the gap between the closure lid and flange at the outer edge. Only Load Case 4 is considered because it bounds Load Case 5.  $F_{ap}$  is calculated utilizing the following method:

$$F_{ap} = -\left(\frac{\pi D_{lb}}{N_b}\right) \left[ \frac{\frac{2M_f}{(D_{li} - D_{lb})} - C_1(B - F_f) - C_2(B - P)}{C_1 + C_2} \right]$$

where:

$$C_1 = 1, C_2 = \left( \frac{8}{3(D_{li} - D_{lb})^2} \right) \left[ \frac{E_f t_{lf}^3}{1 - N_{ul}} + \frac{(D_{lo} - D_{li}) E_{lf} t_{lf}^3}{D_{lb}} \right] \left( \frac{L_b}{N_b D_b^2 E_b} \right)$$

$$C_2 = \left( \frac{8}{3(79.50 - 76.06)^2} \right) \left[ \frac{26.7 \times 10^6 (10.5)^3}{1 - 0.3} + \frac{(79.50 - 69.50)(26.7 \times 10^6)(4.5)^3}{76.06} \right] \left( \frac{4.5}{(48)(1.375^2)(26.7 \times 10^6)} \right) = 18.612$$

$B$  is the non-prying tensile bolt force, and  $P$  is the bolt preload. Since  $F_f = 0$ ,  $F_f < P$ , and therefore  $B = P$ . Parameters  $B$ ,  $P$ ,  $F_f$ , and  $M_f$  are quantities per unit length of bolt circle. In addition, the pressure load is not included because it decreases the magnitude of the applied prying moment, which is less conservative. For the applied inward force,

$$P = B = \frac{F_a N_b}{\pi D_{lb}} = \frac{(84,524)(48)}{\pi(76.06)} = 16,979 \text{ lb}_f/\text{in}$$

$$M_f = -220,448 \text{ in} \cdot \text{lb}_f/\text{inch}, \text{ and } F_f = 0 \text{ lb}_f/\text{in}$$

Therefore,

$$F_{ap} = -\left(\frac{\pi(76.06)}{48}\right) \left[ \frac{\frac{2(-220,448)}{(79.50 - 76.06)} - 1(16,979 - 0) - 18.612(16,979 - 16,979)}{1 + 18.612} \right] = -36,843 \text{ lb}_f/\text{bolt}$$

It is noted that the additional tensile bolt force due to prying for the puncture is less than the accident impact force. Therefore, the puncture drop is not critical for bolt stress evaluation.

### Bolt Bending Moment

The method utilized for the following calculation is extracted from Reference [1], Table 2.2. The maximum bolt bending moment,  $M_{bb}$ , generated by the applied load is evaluated as follows:

$$M_{bb} = \left( \frac{\pi D_{lb}}{N_b} \right) \left[ \frac{K_b}{K_b + K_l} \right] M_f$$

The terms  $K_b$  and  $K_l$  are based on geometry and material properties, and are defined in Table 2.2 of Reference [1]. By substituting the values given above,

$$K_l = \frac{E_l t_l^3}{3 \left[ (1 - N_{ul}^2) + (1 - N_{ul})^2 \left( \frac{D_{lb}}{D_{lo}} \right)^2 \right] D_{lb}} = \frac{26.7 \times 10^6 (10.5^3)}{3 \left[ (1 - 0.3^2) + (1 - 0.3)^2 \left( \frac{76.06}{79.50} \right)^2 \right] 76.06} = 9.971 \times 10^7$$

Therefore:

$$M_{bb} = \left( \frac{\pi 76.06}{48} \right) \left[ \frac{2.091 \times 10^5}{2.091 \times 10^5 + 9.971 \times 10^7} \right] M_f = 0.0100 M_f$$

For Load Case 2,  $M_f = 54,974 \text{ in-lb}_f$ . Substituting this value into the above equation yields:

$$M_{bb} = 549.7 \text{ in-lb}_f/\text{bolt}$$

### 2.12.3.5 Closure Lid Bolt Stress Calculations

The method used for the following calculation is taken from Reference [1], Table 5.1.

#### 2.12.3.5.1 Average Tensile Stress

The bolt preload is calculated to withstand the worst-case load combination, and to maintain a clamping (compressive) force on the closure joint under both normal and accident conditions. Based on the load combinations, it is demonstrated that a positive (compressive) load is maintained on the clamped joint for all load combinations except for the accident condition impact plus pressure load for the minimum tightening torque load case. A more detailed analysis is performed in Section 2.12.3.8 of this appendix to evaluate closure of the closure lid during this event. The maximum non-prying tensile force for normal conditions is 84,524 lb<sub>f</sub> from Load Case 1A. (maximum preload + temperature load), and the maximum non-prying tensile force for accident conditions is 66,672 lb<sub>f</sub> from Load Case 3 (accident impact + pressure load). These loads are utilized to compute bolt stresses below.

Normal Condition (NCT):

[ ]

Accident Condition (HAC):

[ ]

#### 2.12.3.5.2 Bending Stress

Normal Condition:

[ ]

#### 2.12.3.5.3 Shear Stress

For both normal and accident conditions, the average shear stress caused by shear bolt force  $F_s$  is:

$$S_{bs} = 0$$

For normal and accident conditions the maximum shear stress caused by the torsional moment  $M_t$  is:

[ ]

## 2.12.3.5.4 Maximum Combined Stress Intensity

The maximum combined stress intensity is calculated in the following way (Reference [1], Table 5.1).

$$S_{bi} = [(S_{ba} + S_{bb})^2 + 4(S_{bs} + S_{bt})^2]^{0.5}$$

For normal conditions, the combined tension, shear, bending, and residual torsion results in a maximum stress intensity of:

$$S_{bi} = [(56,921 + 2,154)^2 + 4(0 + 14,458)^2]^{0.5} = 65,772 \text{ psi} = 65.8 \text{ ksi}$$

## 2.12.3.5.5 Stress Ratios

In order to satisfy the stress ratio requirement, the following relationship must hold for both normal and accident conditions.

$$R_t^2 + R_s^2 < 1$$

Where  $R_t$  is the ratio of average tensile stress to allowable average tensile stress, and  $R_s$  is the ratio of average shear stress to allowable average shear stress.

For NCT:

$$R_t = 56,921/93,400 = 0.609$$

$$R_s = 14,458/56,100 = 0.258$$

$$R_t^2 + R_s^2 = (0.609)^2 + (0.258)^2 = 0.44 < 1.0$$

For HAC:

$$R_t = 44,899/115,500 = 0.389$$

$$R_s = 14,458/69,300 = 0.209$$

$$R_t^2 + R_s^2 = (0.389)^2 + (0.209)^2 = 0.20 < 1.0$$

## 2.12.3.5.6 Bearing Stress under Lid Bolt/Washer

The maximum NCT axial force is 84,524 lbf. The bolt hole diameter in the closure lid is [ ] The hardened flat washer has outer and inner diameters of [ ] respectively (Appendix 1.4.1). The bearing area,  $A_{\text{Bear}}$ , under the flat washer over the bolt hole in the closure lid is:

The bearing stress for normal conditions is:

$$\text{Bearing Stress} = 84,524/5.0 = 16,904 \text{ psi} = 16.9 \text{ ksi}$$



The allowable normal condition bearing stress on the closure lid is assumed to be the yield stress of the closure lid material at 300 °F. The closure lid is manufactured from SA-203 Gr D material, which has a minimum yield strength of 32.7 ksi at 300 °F (Table 2.12.3-1). Therefore, the margin of safety (M.S.) for bearing stress is:

$$M.S. = \frac{32,700}{16,900} - 1 = +0.94$$

#### 2.12.3.6 Analysis Results

A summary of the lid bolt stresses calculated above is presented in the following table:

**Summary of Stresses and Allowables**

Stress Type	NCT		HAC	
	Stress	Allowable	Stress	Allowable
Average Tensile (ksi)	56.9	93.5	44.9	115.5
Shear (ksi)	14.5	56.1	14.5	69.3
Combined (ksi)	65.8	126.2	Not Required Reference [1]	
Interaction E.Q. $R_t^2 + R_s^2 < 1$	0.44	1.0	0.14	1.0
Bearing Allowable (ksi) ( $S_y$ of lid material)	16.9	32.7	Not Required Reference [1]	

The calculated bolt stresses are all less than the specified allowable stresses.

#### 2.12.3.7 Closure Lid Bolt Fatigue Analysis

The purpose of the fatigue analysis is to demonstrate quantitatively that the fatigue damage to the bolts during NCT is acceptable. This demonstration is accomplished by determining the fatigue damage factor for each NCT event. For this analysis, it is conservatively assumed that the bolts are replaced after 50 round trip shipments, even though the cask will only be transported a single trip. The total cumulative damage or fatigue usage for all events was conservatively determined by adding the usage factors for the individual events. The sum of the individual usage factors was verified to ensure that for the 50 round trip shipments of the TN-32B HBU demonstration cask, the total usage factor was less than one. The following sequence of events was assumed for the fatigue evaluation:

1. Operating Preload (Bolt Tensile stress,  $S_{ba} = 56,921$  psi, and bolt torsional shear stress,  $S_{bt} = 14,458$  psi, corresponding to a bolt tightening torque of 1,230 lb-ft), with 50 round trip shipments considered.
2. Test pressure
3. Rail vibration/shock
4. Pressure and temperature fluctuations
5. 1 foot normal condition free drop

Since the bolt preload stress applied to the TN-32B HBU demonstration cask closure lid bolts is higher than all of the other NCT condition loads, the stress in the bolt will never exceed the bolt preload stress. Consequently, the application and removal of preload is the only real cyclic loading that occurs in the closure lid bolts. The following analysis is therefore, very conservative since it assumes that the damage factor is the sum of all of the individual event damage factors, and not simply the damage factor for bolt preload.

#### 2.12.3.7.1 Operating Preload

Since the TN-32B HBU demonstration cask will only be transported once, the number of preload cycles is two times the single trip or 2 cycles.

The maximum normal condition bolt stress intensity is 65.8 ksi (Section 2.12.3.5.4).

#### 2.12.3.7.2 Test Pressure

Subsection NB-6220 of the ASME B&PV Code-mandated proof test [4] is  $1.25 \times$  (Design Pressure) = 125 psi, and would only be performed once.

From Section 2.12.3.2, the 100 psi internal pressure load analysis can be used by scaling the results upward by a factor of 1.25.

$$F_a = 8,700 \times 1.25 = 10,875 \text{ lb}_f/\text{bolt}$$

$$F_s = 0 \times 1.25 = 0 \text{ lb}_f/\text{bolt}$$

$$F_f = 1,902 \times 1.25 = 2,378 \text{ lb}_f/\text{in}$$

$$M_f = 18,079 \times 1.25 = 22,599 \text{ in-lb}_f/\text{in}$$

$$M_{bb} = 0.0100M_f = 226.0 \text{ in-lb}_f/\text{bolt}$$

With a lid bolt shank diameter of [ ] the following from Reference [1] are determined:

Since internal pressure causes no bolt torsion, and all shear loads are reacted by the closure lid shield plate shoulder,

$$\text{Shear stress: } S_{bs} = 0, \text{ and } S_{bt} = 0.$$

Stress Intensity, S.I.:

$$S.I. = S_{bi} = [(S_{ba} + S_{bb})^2 + 4(S_{bs} + S_{bt})^2]^{0.5} = [(7,324 + 886)^2 + 4(0)^2]^{0.5} = 8,210 \text{ psi}$$

### 2.12.3.7.3 Vibration/Shock

Since the TN-32B HBU demonstration cask will be shipped by rail car, the shock and vibration loadings for rail configurations only will be considered.

#### Rail Car Shock:

Since the TN-32B HBU demonstration cask will only be transported once with the HBU spent fuel payload, the rail car shock will assume an average of a 3,000 mile one-way trip. Reference [5] reports that there are roughly nine shock cycles per 100 miles of rail car transport. Therefore, the total number of cycles is: 3,000 miles  $\times$  1 round trip  $\times$  1 shipment  $\times$  0.09 shocks per mile = 270 cycles. This very low number of cycles due to rail transport will have no fatigue effect on the closure lid bolts.

Reference [5] also specifies a peak shock loading of 4.7g in the longitudinal direction for rail car transport. Consequently, the bolt force due to rail car shock is

#### Vibration:

According to Reference [5], the peak vibration load on the deck of a rail car in the longitudinal direction is 0.19g. This vibration results in a stress of 205 psi, which is negligible for a high strength bolt.

### 2.12.3.7.4 Pressure and Temperature Fluctuations

The lid bolt material is SA-540 Gr 23, Cl 1 (2Ni – 3/4Cr – 1/4Mo), which is in Group 1 in the coefficients of thermal expansion tables in Reference [6]. The closure lid is SA-203 Gr D (3½Ni), and the flange is SA-350 Gr. LF3 (3½Ni), which are also in Group 1. Therefore, the closure lid bolts and all of the materials it contacts have the same coefficient of thermal expansion. Consequently, thermal load will result in no stress in the closure lid bolts.

The pressure fluctuation is conservatively assumed to be the maximum design pressure, 100 psi, which is far greater than the actual maximum normal operating pressure (MNOP). Since the stress intensity in the closure lid bolts is linearly proportional to the internal/external pressure difference, the stress intensity due to 100 psi internal load is:

$$8,210 \text{ psi} \times \frac{100 \text{ psi}}{125 \text{ psi}} = 6,568 \text{ psi}$$

The pressure fluctuation is assumed to occur once per round trip, since there is no payload during the return trip, and therefore no pressurization. Therefore, the total number of cycles of pressure fluctuation is 50.

## 2.12.3.7.5 1 Foot Normal Condition Drop

The normal condition drop consists of a 1-foot drop in an orientation that results in the most damage. For the side drop the resulting shear load is taken entirely by the lid/flange interface. For the end drop, the load is transferred to the cask body via the impact limiters, protecting the bolts. Therefore, the worst case scenario is taken to be roughly a 64° CG-over-corner drop.

The lid bolt analysis above conservatively uses a 64° corner drop axial acceleration of 10g to calculate the following bolt loads:

$$F_a = 19,324 \text{ lb}_f/\text{bolt}$$

$$F_s = 0 \text{ lb}_f/\text{bolt}$$

$$F_f = 3,881 \text{ lb}_f/\text{bolt and}$$

$$M_f = 36,895 \text{ lb}_f/\text{bolt}$$

$$M_{bb} = 0.0100M_f = 369 \text{ in-lb}_f/\text{bolt}$$

The lid bolt diameter is [ ] Therefore, from Reference [1], the following is obtained:

Since internal pressure causes no bolt torsion, and all shear loads are reacted by the shield plate,

Shear stress,  $S_{bs}$ :

$$S_{bs} = 0, \text{ and } S_{bt} = 0.$$

Stress intensity S.I.:

$$\begin{aligned} \text{S.I.} = S_{bi} &= [(S_{ba} + S_{bb})^2 + 4(S_{bs} + S_{bt})^2]^{0.5} \\ &= [(13,013 + 1,446)^2 + 4(0)^2]^{0.5} = 14,459 \text{ psi} \end{aligned}$$

Conservatively assume that the cask is dropped twice during a shipment, resulting in two normal condition drops prior to unloading the cask.

## 2.12.3.7.6 Damage Factor Calculation

The following damage factors are computed based on the stresses and cyclic histories described above, a fatigue strength reduction factor,  $K_F$ , of 4 (Reference [4]), and the fatigue curve shown in Table I-9.4 of Reference [4].

Event	Stress Intensity (psi)	(S.I.)(K <sub>F</sub> ) (psi)	S <sub>a</sub> (psi)	Cycles		Damage Factor n/N
				n	N	
Operating Preload	65,772	263,088	147,329	100	471	0.212
Test Pressure	8,210	32,840	18,390	1	$1.3 \times 10^5$	0.00
Rail Car Shock	5,060	20,240	22,669	270	$4.6 \times 10^4$	0.006
Pressure and Temperature	6,568	26,272	14,712	50	$6.0 \times 10^5$	0.00
1 Foot Normal Condition Drop	14,459	57,836	32,388	100	$1.2 \times 10^4$	0.009
				$\Sigma$		0.227

Here, n is the number of cycles, N is obtained from Figure I-9.4 of Reference [4], and S<sub>a</sub> is defined by the following method:

If one cycle goes from 0 to +S.I., then  $S_a = (1/2)(S.I.)(K_F)(K_E)$

If one cycle goes from -S.I. to + S.I., then  $S_a = (S.I.)(K_F)(K_E)$

where

K<sub>E</sub> is the correction factor for modulus of elasticity,  $30 \times 10^6 / 26.7 \times 10^6 = 1.12$  (Reference [4]).

Since the total damage factor is less than one, the TN-32B HBU demonstration cask closure lid bolts will not fail due to fatigue.

#### 2.12.3.8 Lid Seal Contact Evaluation

The closure lid seal design is analyzed in order to determine the lid/cask seal status when subject to a CG-over-lid corner impact 30 foot free drop.

As noted in Section 2.12.3.4 above, the bolt preload for the minimum specified tighten torque during an accident condition is slightly exceeded by the impact force. To demonstrate that the compression on the O-ring seal is maintained during the accident case, the bolt stretch will be determined and compared to the total initial seal compression.

##### 2.12.3.8.1 Assumptions

- CG-over-corner lid impact with internal pressure is the worst-case condition (Load Case 3).
- The minimum preload for a closure lid bolt is 64,596 lb<sub>f</sub>/bolt.
- The minimum compression of the seal is 0.034 inch.

## 2.12.3.8.2 Analysis

The axial stiffness of a closure lid bolt,  $K_{\text{bolt}}$ , is:

where:

$A$  = cross-section area of bolt shank = [ ] (Table 2.12.3-2)

$E$  = Young's modulus =  $26.7 \times 10^6$  psi at 300 °F (Table 2.12.3-1)

$L$  = bolt shank length = [ ] [drawing 19885-71-2]

The maximum load on each bolt is 66,672  $\text{lb}_f$  for Load Case 3 (Pressure + Accident). For this load case, the amount of additional bolt stretch is due to the difference between the applied load and the minimum preload, or  $66,672 - 64,596 = 2,076 \text{ lb}_f$ . For added conservatism, this excess load will be increased by a factor of 1.5 or 3,114  $\text{lb}_f$  to account for any dynamic effects. The bolt stretch for this additional tensile load,  $\Delta_{\text{acc}}$ , will be:

Since the minimum seal compression is [ ] the additional bolt stretch of [ ] during the C.G.-over-corner free drop impact loading with internal pressure will not result in the loss of compression on the O-ring seal. Therefore, containment of the HBU payload is maintained during a worst-case loading condition.

## 2.12.3.9 Engagement Length for Bolt and Flange

The net engagement length,  $L_e$ , for the closure lid bolts in the body flange is:

From Table 2.12.3-2, the shear area per unit length for a [ ] internal thread is [ ] Therefore, the total shear area ( $A_{\text{intt-}\tau}$ ) for the body flange engagement is:

The shear stress ( $\tau_{\text{int}}$ ) in the internal threads for the 84,524  $\text{lb}_f$  maximum axial non-prying tensile load (Case 1A) is:

The shear allowable stress for the SA-350 Grade LF3 forging is  $0.6S_m$ . From the Certified Material Test Report (CMTR) for the inner shell flange [7], the room temperature yield and tensile strengths are 59.76 ksi and 76.73 ksi, respectively. These actual strengths compare to the minimum material strengths of 37.5 ksi and 70 ksi, respectively, from Table 2-6. Since the actual yield material strength is significantly higher than the minimum yield strength, the allowable stress intensity  $S_m$  for the internal threads may be increased by the ratio of the yield strengths, i.e.,  $59.76/37.5 = 1.594$ . From Table 2-6, the minimum allowable stress intensity ( $S_m$ ) at 300 °F is 22.1 ksi. Based on the actual material strength, the allowable stress intensity is increased to  $(22.1)(1.59) = 35.2$  ksi. Note that this method of computing an increased stress intensity is conservative compared to the method specified in Mandatory Appendix 2 of the American Society of Mechanical Engineers (ASME) Boiler and Pressure Vessel (B&PV) Code [6], which allows  $S_m = 2/3S_y$ . Therefore, the margin of safety (M.S.) for shearing of the internal threads for the maximum tensile load is:

$$M.S. = \frac{0.6S_m}{\tau_{int}} - 1 = \frac{0.6(35.2)}{13.72} - 1 = +0.54$$

For the closure lid bolt, the shear area per unit length for a [ ] from Table 2.12.3-2. Therefore, the total shear area ( $A_{int-\tau}$ ) for the body flange engagement is:

The shear stress ( $\tau_{ext}$ ) in the external threads for the 84,524 lb<sub>f</sub> maximum axial non-prying tensile load (Case 1A) is:

From Table 2.12.3-3, the normal condition shear allowable stress for the SA-540 Grade B23 CL1 material at 300 °F is 56.1 ksi. The margin of safety (M.S.) for shearing of the external threads of the closure lid bolt for the maximum tensile load is:

$$M.S. = \frac{56.1}{18.70} - 1 = +2.00$$

#### 2.12.3.10 Conclusions

- A closure lid bolt torque range of 940 to 1,230 lb<sub>r</sub>-ft is utilized to achieve the desired preload.
- Lid bolt stresses meet the acceptance criteria of NUREG/CR-6007 [1].
- For the recommended preloads, a positive (compressive) load is maintained on the O-ring containment seal during all load combinations.
- Closure of the TN-32B HBU demonstration cask closure lid/body flange interface is evaluated in Section 2.12.3.8 above, and the O-ring seal remains closed during a worst-case impact.
- The bolt and flange thread engagement length is acceptable.

### 2.12.3.11 References

1. G. C Mok, L.E. Fisher, "Stress Analysis of Closure Bolts for Shipping Cask," NUREG/CR-6007, U.S. Nuclear Regulatory Commission, January 1993.
2. HELICOFLEX® Spring Energized Seal Catalog, Technetics Group, EnPro Industries Companies.
3. Document No. E-31030 (NRC Docket No. 71-9313), "TN-40 Transportation Packaging Safety Analysis Report," Revision 16, June 2011.
4. American Society of Mechanical Engineers, ASME Boiler and Pressure Vessel Code, Section III, Division 1, Subsection NB and Appendices, 1992.
5. C. F. Magnuson, L.T. Wilson, "Shock and Vibration Environments for Large Shipping Containers on Rail Cars and Trucks," NUREG766510, U.S. Nuclear Regulatory Commission, June 1977.
6. American Society of Mechanical Engineers, ASME Boiler and Pressure Vessel Code, Section II Part D, 2013.
7. Forgit S.p.A, "Certified Material Test Report, No. 1747/98/CMTR," March 1999.
8. Baumeister, T., Marks, L. S., Standard Handbook for Mechanical Engineers, 7th Edition, McGraw-Hill, 1967.
9. American Society of Mechanical Engineers, Unified Inch Screw Threads, UN and UNR thread Form, ASME B1.1-2003.



**Table 2.12.3-1**  
**Design Parameters for Closure Lid Bolt Analysis**

K	Nut factor for empirical relation between the applied torque and achieved preload is [        ] for N-5000
Q	Applied torque for the preload (lbf-in)
D <sub>lb</sub>	Closure lid diameter at bolt circle, 76.06 inch
D <sub>lg</sub>	Closure lid diameter at the seal (outer), 72.92 inch
E <sub>c</sub>	Young's modulus of cask flange material (SA-350, LF3, 300 °F), $26.7 \times 10^6$ psi
E <sub>l</sub>	Young's modulus of closure lid material (SA-203 Gr D, 300 °F), $26.7 \times 10^6$ psi
N <sub>b</sub>	Total number of closure bolts, 48
N <sub>ul</sub>	Poisson's ratio of closure lid, 0.3, (Reference [8], p. 5-6 use nominal value).
P <sub>ei</sub>	Inside pressure of cask, 100 psig
D <sub>li</sub>	Closure lid diameter at inner edge, 69.50 inch
D <sub>lo</sub>	Closure lid diameter at outer edge, 79.50 inch
P <sub>li</sub>	Pressure inside the closure lid, 100 psig
t <sub>c</sub>	Thickness of cask wall, 9.065 inch (at flange = $[68.75 + 2(1.50+8.00) - 69.62]/2$ )
t <sub>l</sub>	Thickness of lid center, 10.5 inch
t <sub>lf</sub>	Thickness of lid flange, 4.5 inch
l <sub>b</sub>	Thermal coefficient of expansion, lid bolt (SA-540, Gr B23, Cl 1), $6.4 \times 10^{-6}$ R.T., $7.3 \times 10^{-6}$ in/in °F at 300 °F
l <sub>c</sub>	Thermal coefficient of expansion, cask (SA-350, LF3), $6.4 \times 10^{-6}$ at R.T., $7.3 \times 10^{-6}$ in/in °F at 300 °F
l <sub>l</sub>	Thermal coefficient of expansion, closure lid (SA-203 Gr D), $6.4 \times 10^{-6}$ R.T., $7.3 \times 10^{-6}$ in/in °F at 300 °F
E <sub>b</sub>	Young's modulus of bolt material (SA-540, Gr B23, Cl 1, 300 °F), $26.7 \times 10^6$ psi
a <sub>i</sub>	Maximum rigid-body impact acceleration (g) of the cask
W <sub>c</sub>	Weight of contents = 49,650 (fuel) + 13,500 (basket)** = 63,150 lb <sub>m</sub>
W <sub>l</sub>	Weight of lid = 12,900 lb <sub>m</sub>
W <sub>c</sub> +W <sub>l</sub>	63,150 + 12,900 = 76,050 lb <sub>m</sub> , assume 77,000 lb <sub>m</sub>
xi	Impact angle between the cask axis and target surface
S <sub>yl</sub>	Yield strength of closure lid material (SA-203 Gr D, 300 °F), 32.7 ksi
S <sub>ul</sub>	Ultimate strength of closure lid material (SA-203 Gr D, 300 °F), 65.0 ksi
S <sub>yb</sub>	Yield strength of bolt material (SA-540, Gr B23, Cl 1, 300 °F), 140.3 ksi

**Table 2.12.3-2**  
**Closure Lid Bolt Data**

Parameters necessary to use formulas of Reference [1], Table 5.1.

Bolt = 1½ – UN8 – 2A
N = No. of threads per inch = 8
p = Pitch = 1/8" = .125 inch
D <sub>b</sub> = Nominal Diameter = 1.5 inch
D <sub>ba</sub> = Bolt diameter for stress calculations in reduced shank area = [                      ]
Bolt Thread Stress Area = $\pi/4(1.377)^2 = 1.490 \text{ in}^2$
Bolt Shank Stress Area = [                      ]
External thread shear stress area for a 1.50-8UN-2A thread = 2.57 in <sup>2</sup> /inch [9]
Internal thread shear stress area for a 1.50-8UNC-2B thread = 3.50 in <sup>2</sup> /inch [9]

**Table 2.12.3-3**  
**Normal Condition Allowable Stresses in Closure Lid Bolts**

Temperature (°F)	Yield Stress <sup>1</sup> (ksi)	Normal Condition Allowables		
		F <sub>tb</sub> <sup>2,4</sup> (ksi)	F <sub>vb</sub> <sup>3,4</sup> (ksi)	S.I. <sup>5</sup> (ksi)
100	150.0	100.0	60.0	135.0
200	144.0	96.0	57.6	129.6
300	140.3	93.5	56.1	126.2
400	137.9	91.9	55.2	124.0

Notes:

1. Yield stress values are from Reference [6]
2. Allowable tensile stress, F<sub>tb</sub> = 2/3(S<sub>y</sub>) [1]
3. Allowable shear stress, F<sub>vb</sub> = 0.4S<sub>y</sub> [1]
4. Tension and shear stresses must be combined using the following interaction equation:

$$\frac{\sigma_{tb}^2}{F_{tb}^2} + \frac{\tau_{yb}^2}{F_{yb}^2} \leq 1.0 \quad [1]$$

5. Stress intensity from combined tensile, shear and residual torsion loads, S.I. < 1.35S<sub>m</sub> [1]

**Table 2.12.3-4**  
**Accident Condition Allowable Stresses in Closure Lid Bolts**

Temperature (°F)	Yield Stress <sup>1</sup> (ksi)	Accident Condition Allowables		
		0.6S <sub>y</sub> <sup>3</sup> (ksi)	F <sub>tb</sub> <sup>2,4</sup> (ksi)	F <sub>vb</sub> <sup>3,4</sup> (ksi)
100	150.0	90.0	115.5	69.3
200	144.0	86.4	115.5	69.3
300	140.3	84.2	115.5	69.3
400	137.9	82.7	115.5	69.3

Notes:

1. Yield and tensile stress values are from Reference [6]. Note that S<sub>u</sub> is 165 ksi at all temperatures of interest.
2. Allowable Tensile stress, F<sub>tb</sub> = min (0.7S<sub>u</sub>, S<sub>y</sub>), where 0.7S<sub>u</sub> = 0.7(165) = 115.5 ksi [1].
3. Allowable shear stress, F<sub>vb</sub> = min (0.42S<sub>u</sub>, 0.6S<sub>y</sub>), where 0.42S<sub>u</sub> = 0.42(165) = 69.3 ksi [1].
4. Tension and shear stresses must be combined using the following interaction equation:

$$\frac{\sigma_{tb}^2}{F_{tb}^2} + \frac{\tau_{yb}^2}{F_{yb}^2} \leq 1.0 \quad [1]$$

## **Appendix 2.12.4**

### **Structural Analysis of the Outer Shell**

#### TABLE OF CONTENTS

2.12.4	Structural Analysis of the Outer Shell .....	2.12.4-1
2.12.4.1	Introduction .....	2.12.4-1
2.12.4.2	Description .....	2.12.4-1
2.12.4.3	Materials Input Data .....	2.12.4-1
2.12.4.4	Applied Loads .....	2.12.4-2
2.12.4.5	Partial Groove/Fillet Weld Calculations.....	2.12.4-2
2.12.4.6	Method of Analysis .....	2.12.4-2
2.12.4.7	Analysis Results .....	2.12.4-8
2.12.4.8	References.....	2.12.4-8

LIST OF TABLES

Table 2.12.4-1	Outer Shell Top End Plate Stress Results .....	2.12.4-9
Table 2.12.4-2	Outer Shell Bottom End Plate Stress Results .....	2.12.4-9
Table 2.12.4-3	Outer Shell Cylindrical Plate Stress Results .....	2.12.4-9
Table 2.12.4-4	End Plate Weld Stress Results .....	2.12.4-10
Table 2.12.4-5	Polyester Resin Stress Results .....	2.12.4-10

LIST OF FIGURES

Figure 2.12.4-1	ANSYS® Model for Outer Shell Weldment Evaluation.....	2.12.4-11
Figure 2.12.4-2	Outer Shell Geometry .....	2.12.4-12
Figure 2.12.4-3	NCT Side Drop – Stress Intensity .....	2.12.4-13
Figure 2.12.4-4	NCT Side Drop – Outer Shell Plate Stress Intensity .....	2.12.4-14
Figure 2.12.4-5	NCT Side Drop – Outer Shell Weldment Stress Intensity .....	2.12.4-15
Figure 2.12.4-6	NCT End Drop –Stress Intensity.....	2.12.4-16
Figure 2.12.4-7	NCT End Drop –Outer Shell Plate Stress Intensity .....	2.12.4-17
Figure 2.12.4-8	NCT End Drop –Outer Shell Weldment Stress Intensity .....	2.12.4-18

## 2.12.4 Structural Analysis of the Outer Shell

### 2.12.4.1 Introduction

This section presents the structural analysis of the outer shell of the TN-32B HBU demonstration cask. The outer shell consists of a cylindrical shell section and end plates at each end that connect the shell to the cask body. The outer shell weldment encloses the neutron shield material that surrounds the gamma shield shell forging. The shell is evaluated for normal conditions of transport (NCT) that includes internal pressure and normal handling/tie-down loads. A finite element model (FEM) is created utilizing ANSYS® [1] for the structural analysis of the outer shell and end plates. The model evaluates the shell weldment for the lateral 12g and the axial 26g impact loads. These impact values envelop the worst-case NCT side-drop and end-drop impact loads of 11.3g and 25.5g, respectively, as noted in Appendix 2.12.9. The neutron shield stresses due to vertical and lateral tie-down loads of 4.7g and 5.0g, respectively, are resolved by moment and force components utilizing a cosine pressure distribution with peaking factors. The resulting stresses are compared to the allowable stress limits for non-containment structures in Table 2-4, Chapter 2, to ensure that the design criterion is satisfied.

### 2.12.4.2 Description

The outer shell is constructed from high-strength, low-alloy carbon steel, and is welded to the outer surface of the gamma shield. The outer cylindrical shell plate is 1/2-inch thick, and the end plates are 3/4-inches thick. The outer shell-end plate weld joints are also qualified in the analysis. Pertinent dimensions and welds are shown in Figure 2.12.3-1 and delineated on Drawing 19885-71-2 in Appendix 1.4.1.

### 2.12.4.3 Materials Input Data

The outer cylindrical shell material and end plates are SA-516 Gr 70. Since the maximum temperature of outer shell does not exceed 300 °F, as discussed in Chapter 3, all material properties are extracted at 300 °F. The linear elastic material properties at this temperature for the carbon steel are:

Young's modulus:	$E = 28.1 \times 10^6$ psi
Yield stress:	$S_y = 33.7$ ksi
Ultimate stress:	$S_u = 70.0$ ksi

The allowable stresses for the outer shell weldment analysis are provided in Table 2-4. The Young's modulus for the polyester resin is conservatively assumed to be  $5.0 \times 10^5$  psi at 300 °F, as defined in the MP197HB transport application [3]. The compressive strength of the resin is assumed to be 3,900 psi, as defined in the TN-40 cask transport application [4].

#### Material Density

Due to symmetry, only a 180° segment of the outer shell is modeled and analyzed. The weights are extracted from Table 2-7 to determine the densities of the cask, and the resin for modeling.

#### 2.12.4.4 Applied Loads

The outer shell weldment is analyzed for both side and end drops to identify all the possible maximum stresses resulting from NCT free drop events. For side drop orientation, the acceleration due to gravity is applied on the model in the lateral direction. For the end drop orientation, the gravitational load was applied in the axial direction.

An internal pressure of 25 psig is applied on all the inner walls of the outer shell, and at the interfaces of the partial penetration welds. Figure 2.12.4-1 presents the model for the outer shell weldment evaluation for the side and end drop load configurations, respectively.

#### 2.12.4.5 Partial Groove/Fillet Weld Calculations

All partial penetration welds in the ANSYS® model were represented by couplings as pin joints. Weld stresses are calculated by utilizing nodal forces at the couple nodes that represent the welds. For partial penetration fillet welds, stresses are calculated as follows:

$$F_w = (F_{\text{resultant}})/[(L_{\text{tributary}})(T_{\text{weld}})]$$

where:

$F_{\text{resultant}}$  = maximum resultant nodal force =  $(F_x^2 + F_y^2 + F_z^2)^{1/2}$   
(calculated from the reaction force output listing from ANSYS® model)  
 $L_{\text{tributary}}$  = minimum tributary length associated with the nodes  
 $L_{\text{tributary}} = \pi R/(n-1)$   
 $R = 43.875$  in (for Welds 1 and 4) or  $48.375$  in (for Welds 2 and 3)  
 $n$  = the maximum nodes used at weld interface locations.  
 $T_{\text{weld}}$  = Appropriate weld throat or base metal dimension

#### 2.12.4.6 Method of Analysis

##### ANSYS® Model

An FEM was created for the structural analysis of the outer shell weldment. The cask body, outer shell, and the polyester resin were modeled utilizing elements with eight nodes and three translational degrees of freedom per node.

Contact elements were utilized at the interface of polyester resin and outer shell, and between the resin and the gamma shield interfaces. This gap element potentially introduces nonlinearity in the analysis depending whether it is open or closed. Additionally, weak spring elements (1.0 lb/inch stiffness) were modeled along the interface.

Nonlinear analyses with elastic material properties and large-deflection effects were performed in ANSYS®. NCT analysis on the outer shell was conducted for computing the stresses for both the side and end drops. The maximum NCT g-load (12g for side drop and 26g for end drop), and an internal pressure of 25 psig are utilized in the NCT analysis. The results are compared to NCT allowable stresses. Both the side and end drop conditions satisfied the NCT membrane and bending allowable limits.

The basic geometry of the outer shell and the weld sizes utilized for analysis are illustrated in Figure 2.12.4-2. Weld 1 is a 3/8-inch bevel groove weld plus a 3/16-inch fillet weld cover that corresponds to an overall effective weld size of 0.508 inch. Weld 4 has two 1/4-inch bevel groove welds plus a 3/16-inch fillet weld that corresponds to an effective weld size of 0.633 inch. All weld sizes (Weld 1 through Weld 4) are reduced by 1/8-inch in the weld qualification in the previous section.

Partial penetration welds were simulated utilizing couplings (all degrees of freedom) at the interface of cask to the top and bottom end plates of the outer shell. For the interface of the outer shell longitudinal plate to its top and bottom end plates, the welds were simulated as pin joints.

A single material number and element type is utilized to model the 1/2-inch thick cylindrical plate, and the 3/4-inch thick top and bottom closure end plates in the ANSYS® model. The ANSYS® model for the outer shell evaluation is shown in Figure 2.12.4-2.

#### Boundary Conditions

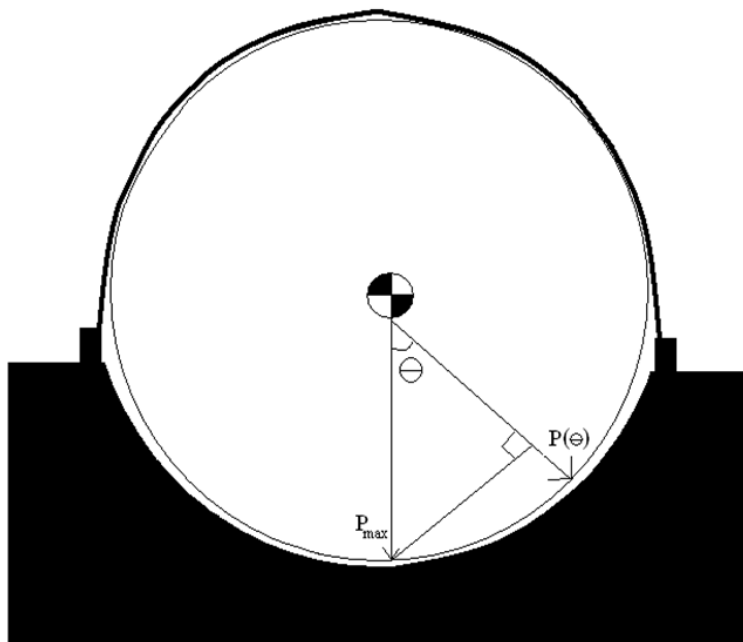
Symmetric boundary conditions are applied at the cut face of the model. For the end drop evaluation, all bottom surface nodes of the cask are constrained in the vertical direction, whereas for the side drop, cask nodes on the outer diameter, above the top end plate and below the bottom end plates, are constrained up to 45° in the hoop direction.

#### Tie-Down Stress Calculation

During transport, the outer shell weldment will react the vertical and lateral loads in the two saddles and straps that form parts of the tie-down configuration. Because there are two saddles/straps, the tie-down system secures the weight of the cask equally. Therefore, each saddle/strap system supports half the cask weight and tie-down.

The pressure distribution of the neutron shield on the strap and saddle is assumed to be a cosine distribution expressed as  $P(\theta) = P_{\max} \cos \theta$ .





By symmetry, the centers of pressure are at the top and bottom of the cask, which correspond to the areas of peak pressure exerted by the 12-inch wide tie-down strap and saddle, respectively. The bearing areas of the outer shell weldment are calculated to be:

$$\text{Saddle Area} = \pi(97.75)(12) \left[ \frac{140}{360} \right] = 1,433.1 \text{ in}^2$$

$$\text{Strap Area} = \pi(97.75)(12) \left[ \frac{180}{360} \right] = 1,842.5 \text{ in}^2$$

$$\text{Half of Cask Weight} = \frac{270,000}{2} = 135,000 \text{ lb}_m$$

#### A. Vertical Loading

Although 10 CFR 71.45(b)(1) [2] specifies a  $\pm 2g$  vertical load, a  $\pm 4.7g$  vertical load is utilized to evaluate the tie-down saddles and straps. For the vertical loading case, the upward load is supported by the strap whereas the downward load is supported by the saddle. Therefore, the average loads on the saddle and strap are:

$$\text{Average Saddle Pressure} = \frac{4.7(135,000)}{1,433.1} = 442.75 \text{ psi}$$

$$\text{Average Strap Pressure} = \frac{4.7(135,000)}{1,842.5} = 344.36 \text{ psi}$$

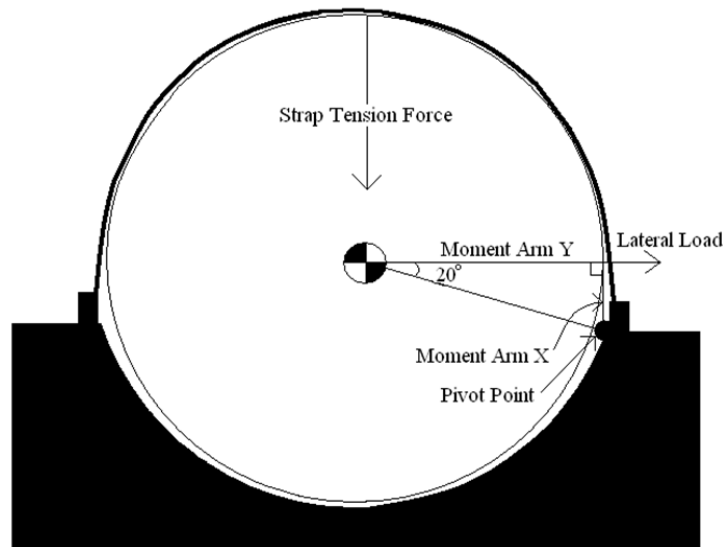
For a  $180^\circ$  cosine or sine distribution, the peak-to-average ratio is found to be  $\pi/2 = 1.571$ . Conservatively assuming the saddle is also a  $180^\circ$  cosine distribution, the peak loads for the saddle and strap are:

$$\text{Peak Saddle Pressure} = 1.571 (442.75) = 695.5 \text{ psi}$$

$$\text{Peak Strap Pressure} = 1.571 (344.36) = 540.9 \text{ psi}$$

## B. Lateral Loading

For the 5g lateral load, the neutron shield is analyzed for the resultant stresses in the outer shell weldment. The lateral load creates an overturning moment tending to rotate the cask out of the saddle, which is restrained by a counter moment created by a vertical force in the strap, as seen in the figure below. Assuming that the maximum saddle pressure (Reaction Force  $F_s$ ) occurs at the pivot point, the reaction corresponds to a point that is  $70^\circ$  from the bottom center of the cask.



The outer radius neutron shield (outer shell),  $R$ , is 48.875 inches. The moment arms  $X$  and  $Y$  are the outer radius of the neutron shield multiplied by the sine and cosine of  $20^\circ$ , respectively.

$$\text{Vertical moment arm } X = R \sin 20^\circ = (48.875) \sin 20^\circ = 16.72 \text{ inch}$$

$$\text{Horizontal moment arm } Y = R \cos 20^\circ = (48.875) \cos 20^\circ = 45.93 \text{ inch}$$

By summing the moments about the pivot point, the reaction force,  $F_T$ , can be determined:

$$\sum M = 0$$

$$F_T Y - F_L X = 0$$

$$\Rightarrow F_T = \frac{F_L(X)}{Y} = \frac{5(135,000)(16.72)}{45.93} = 245,722 \text{ lb}_f$$

Summing the forces in the X and Y directions solves for the strap force  $F_S$ :

$$\sum F_X = 0$$

$$F_L - F_S \sin(70^\circ) = 0$$

$$F_S = \frac{F_L}{\sin(70^\circ)} = \frac{5(135,000)}{\sin(70^\circ)} = 718,320 \text{ lb}_f$$

$$\sum F_Y = 0$$

$$F_S \cos(70^\circ) - F_T$$

$$F_S = \frac{F_T}{\cos(70^\circ)} = \frac{(245,722)}{\cos(70^\circ)} = 718,443 \text{ lb}_f$$

Since the solutions for the strap force are essentially the same in either the X-direction or Y-direction, the force is verified. This results in a strap pressure of:

$$\text{Average Strap Pressure} = \frac{245,722}{1,842.5} = 133.4 \text{ psi}$$

$$\text{Peak Strap Pressure} = 1.571 (133.4) = 209.5 \text{ psi}$$

For the saddle loading conservatively assume that only one-quarter of the saddle area (the final  $35^\circ$  of arc length) supports the saddle load, with a cosine pressure distribution that is maximum at the pivot point. Conservatively assuming a  $\pi/2$  (1.571 versus 1.065 for a  $35^\circ$  distribution) as a peaking factor for the pressure distribution, the resultant saddle loading is:

$$\text{Average Saddle Pressure} = \frac{718,443}{[(1,433.1)/4]} = 2,005 \text{ psi}$$

$$\text{Peak Saddle Pressure} = 1.571(2005.3) = 3,150 \text{ psi}$$

#### C. 5g Lateral and -4.7g Vertical Loading

Utilizing the same methodology described above, the combined loading case of 5g lateral and -4.7g vertical is analyzed. For this loading case, summing the moments about the pivot point solves for the reaction force  $F_T$  for this load condition:

$$\sum M = 0$$

$$F_T Y + F_V Y - F_L X = 0$$

$$\Rightarrow F_T = \frac{F_L(X)}{Y} - F_V = \frac{5(135,000)(16.72)}{45.93} - 4.7(135,000) = -388,778 \text{ lb}_f$$

where,  $F_V$  is the downward (negative) vertical load acting at the center of gravity (CG) of the cask.

The negative force indicates that the lateral induced overturning moment is much less than the counter moment generated by the -4.7g vertical load, which means the strap is not loaded in this case. Instead, the lateral force counteracts the downward vertical force as if the straps were acting on the cask surface. This load case results in the same saddle loading as the 5g lateral load over one-quarter of the saddle area. Therefore, the average and peak saddle loadings are:

$$\text{Average Saddle Pressure} = \frac{718,443}{[(1,433.1)/4]} = 2,005 \text{ psi}$$

$$\text{Peak Saddle Pressure} = 1.571(2005.3) = 3,150 \text{ psi}$$

#### D. 5g Lateral and 4.7g Vertical Loading

Using the same methodology described above, the combined loading case of 5g lateral and +4.7g vertical is analyzed. For this loading case, summing the moments about the pivot point solves for the reaction force  $F_T$  for this load condition:

$$\sum M = 0$$

$$F_T Y - F_V Y - F_L X = 0$$

$$\Rightarrow F_T = \frac{F_L(X)}{Y} + F_V = \frac{5(135,000)(16.72)}{45.93} + 4.7(135,000) = 880,222 \text{ lb}_f$$

This load case represents a conservative worst-case loading on the strap side of the cask by combining the 5g lateral and 4.7g vertical loads. The average and peak bearing pressures on the straps from the outer shell weldment for this bounding case are:

$$\text{Average Strap Pressure} = \frac{880,222}{1,842.5} = 477 \text{ psi}$$

$$\text{Peak Strap Pressure} = 1.571(477.2) = 750 \text{ psi}$$

The worst-case average and peak bearing pressures on the saddles, as noted above, are:

$$\text{Average Saddle Pressure} = \frac{718,443}{[(1,433.1)/4]} = 2,005 \text{ psi}$$

$$\text{Peak Saddle Pressure} = 1.571(2005.3) = 3,150 \text{ psi}$$

The acceptance criterion for the outer shell weldment is conservatively based only on the compressive strength of the polyester resin that supports the 1/2-inch thick outer cylindrical shell. Therefore, the minimum margin of safety (M.S.) for the maximum bearing pressure is:

$$\text{M.S.} = \frac{3,900}{3,150} - 1 = +0.24$$

Since the minimum M.S. is positive, the TN-32B HBU demonstration cask outer shell weldment is qualified to support the vertical and lateral loads of transport for the saddle and strap tie-down configuration.

#### 2.12.4.7 Analysis Results

The outer shell component stress results were post-processed utilizing the ANSYS® commands that linearize the stress distribution through a requested section, resulting in a breakdown of the various stress components. Stress linearization for the outer shell is performed on all possible paths utilizing an ANSYS® post-processing macro. The nodal stress intensities for all loading cases for the outer shell weldment are shown in Figure 2.12.4-3 through Figure 2.12.4-8.

Linearized stress intensity results of the outer shell and comparison to the allowable stress limits are summarized in Table 2.12.4-1 through Table 2.12.4-3. Weld joint stress results are summarized in Table 2.12.4-4. The lateral and vertical load results for the polyester resin are summarized in Table 2.12.4-5. Based on the analyses, it has been demonstrated that the outer shell weldment and the polyester resin are structurally adequate for the cask transportation imposed loads.

#### 2.12.4.8 References

1. ANSYS® Finite Element Computer Code, Version 17.1, ANSYS, Inc. Canonsburg, PA.
2. Title 10, Code of Federal Regulations - Energy, Part 71 (10 CFR 71), "Packaging and Transportation of Radioactive Material," 1-1-2021 Edition, U.S. Nuclear Regulatory Commission, Washington, D.C.
3. NUHOMS® - MP197 Transportation Package Safety Analysis Report, Revision 18 (NRC Docket No. 71-9302), April 2017.
4. Document No. E-31030 (NRC Docket No. 71-9313), "TN-40 Transportation Packaging Safety Analysis Report," Revision 16, June 2011.

**Table 2.12.4-1  
Outer Shell Top End Plate Stress Results**

Component	Load Case	Stress Category	Stress Intensity (ksi)	Allowable Stress (ksi)	Stress Ratio
Outer Shell Top End Plate	Side Drop	$P_m$	2.88	22.50	0.13
		$P_m + P_b$	5.36	33.75	0.16
	End Drop	$P_m$	19.75	22.50	0.88
		$P_m + P_b$	20.94	33.75	0.62
	Maximum	$P_m$	19.75	-	0.88
		$P_m + P_b$	20.94		0.62

**Table 2.12.4-2  
Outer Shell Bottom End Plate Stress Results**

Component	Load Case	Stress Category	Stress Intensity (ksi)	Allowable Stress (ksi)	Stress Ratio
Outer Shell Bottom End Plate	Side Drop	$P_m$	3.16	22.50	0.14
		$P_m + P_b$	5.31	33.75	0.16
	End Drop	$P_m$	20.89	22.50	0.93
		$P_m + P_b$	22.45	33.75	0.67
	Maximum	$P_m$	20.89	...	0.93
		$P_m + P_b$	22.45		0.67

**Table 2.12.4-3  
Outer Shell Cylindrical Plate Stress Results**

Component	Load Case	Stress Category	Stress Intensity (ksi)	Allowable Stress (ksi)	Stress Ratio
Outer Shell Cylindrical Plate	Side Drop	$P_m$	3.25	22.50	0.14
		$P_m + P_b$	3.29	33.75	0.10
	End Drop	$P_m$	9.56	22.50	0.42
		$P_m + P_b$	10.36	33.75	0.31
	Maximum	$P_m$	9.56	...	0.42
		$P_m + P_b$	10.37		0.31

**Table 2.12.4-4  
End Plate Weld Stress Results**

Component	Location	Load Case	Maximum Stress (ksi)	Allowable Stress (ksi)	Stress Ratio
Outer Shell Weld 1	Cask and Outer Shell Top End Plate Interface	Side Drop	2.22	13.48	0.16
		End Drop	3.90		0.29
Outer Shell Weld 2	Outer Shell Longitudinal Shell and Outer Shell Top End Plate Interface	Side Drop	1.94		0.14
		End Drop	2.47		0.18
Outer Shell Weld 3	Outer Shell Longitudinal Shell and Outer Shell Bottom End Plate Interface	Side Drop	1.95		0.14
		End Drop	1.50		0.11
Outer Shell Weld 4	Cask and Outer Shell Bottom End Plate Interface	Side Drop	1.66		0.12
		End Drop	3.52		0.26
Maximum			3.90		0.29

**Table 2.12.4-5  
Polyester Resin Stress Results**

Loading Case	Saddle Area (ksi)		Strap Area (ksi)		Resin S <sub>y</sub> (ksi)	Margin of Safety	
	Avg	Peak	Avg	Peak		Saddle	Strap
± 4.7g Vertical	0.443	0.695	0.344	0.541	3.9	+5.6	+7.2
5g Lateral	2.005	3.150	0.133	0.209		+1.2	+18.6
-4.7g Vertical and 5g Lateral	2.005	3.150	0	0		+1.2	NA
4.7g Vertical and 5g Lateral	2.005	3.150	0.477	0.750		+1.2	+5.2

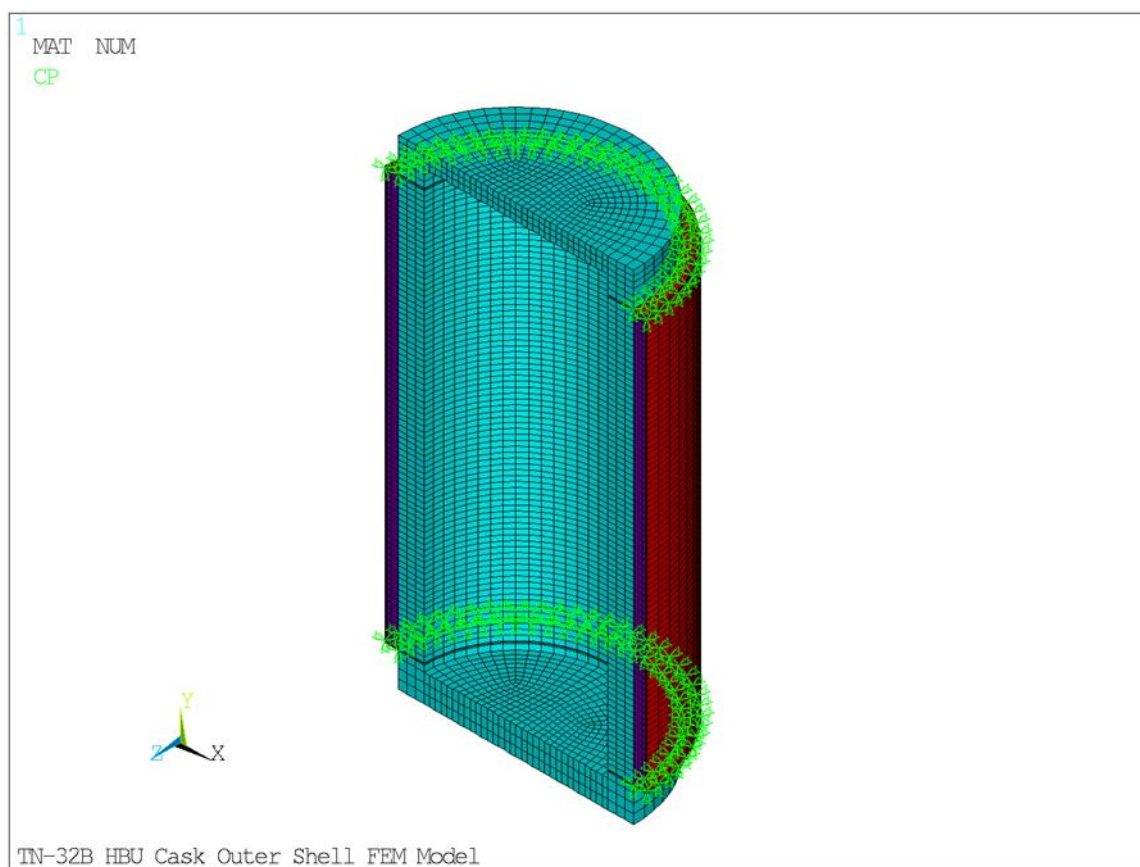


**Figure 2.12.4-1**  
**ANSYS® Model for Outer Shell Weldment Evaluation**





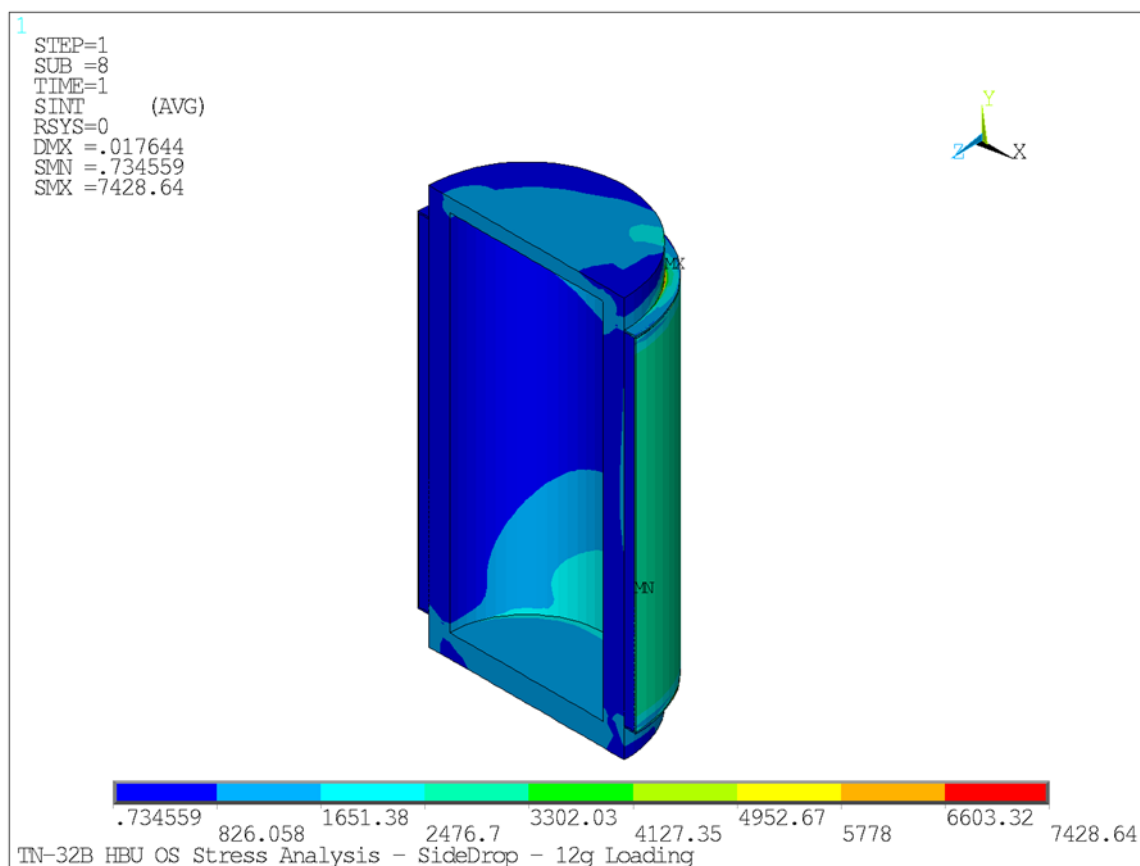


**Figure 2.12.4-3**  
**NCT Side Drop – Stress Intensity**

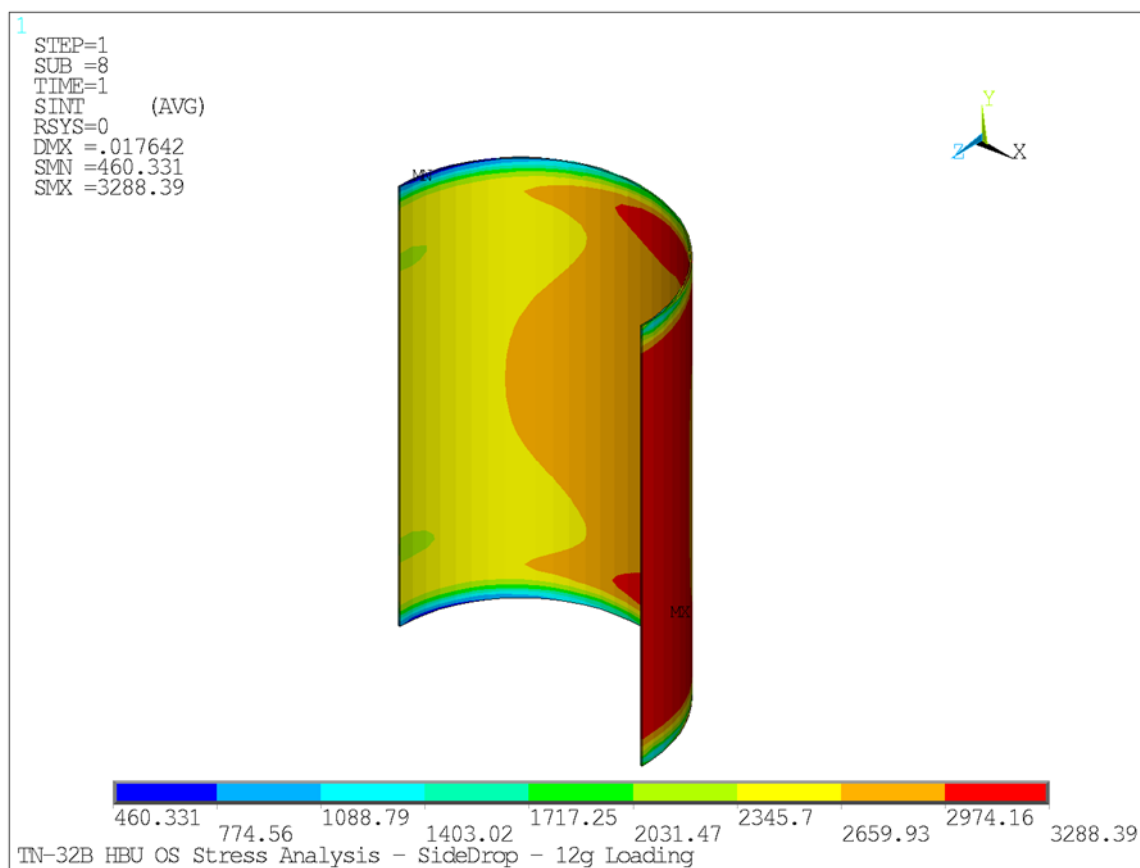


**Figure 2.12.4-4**  
**NCT Side Drop – Outer Shell Plate Stress Intensity**

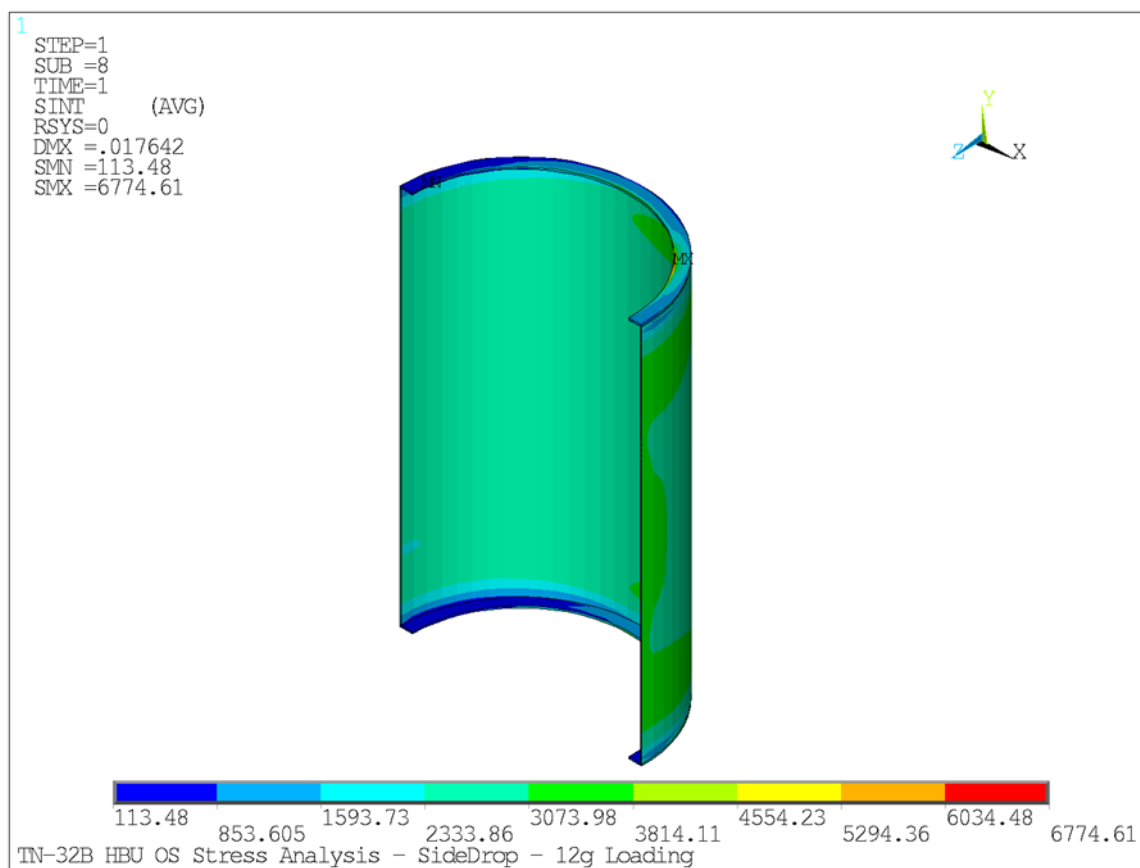


**Figure 2.12.4-5**  
**NCT Side Drop – Outer Shell Weldment Stress Intensity**

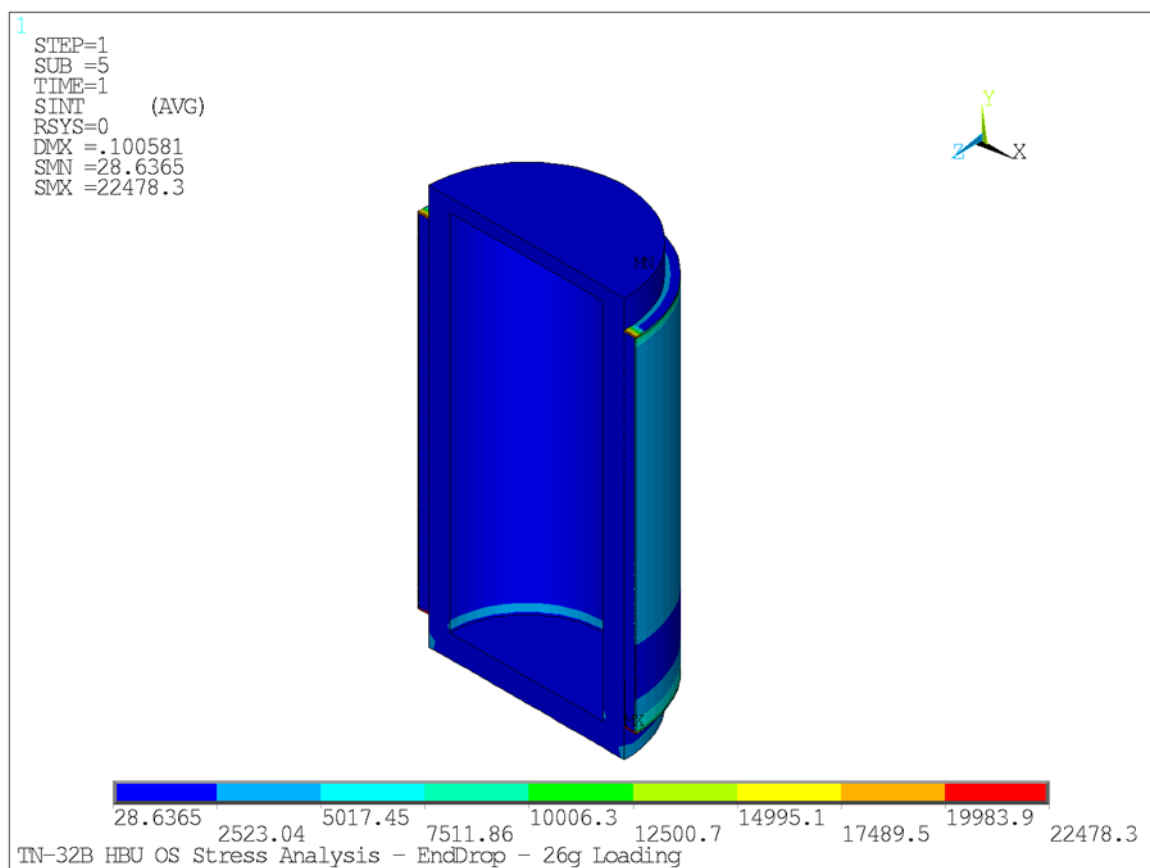


**Figure 2.12.4-6**  
**NCT End Drop –Stress Intensity**

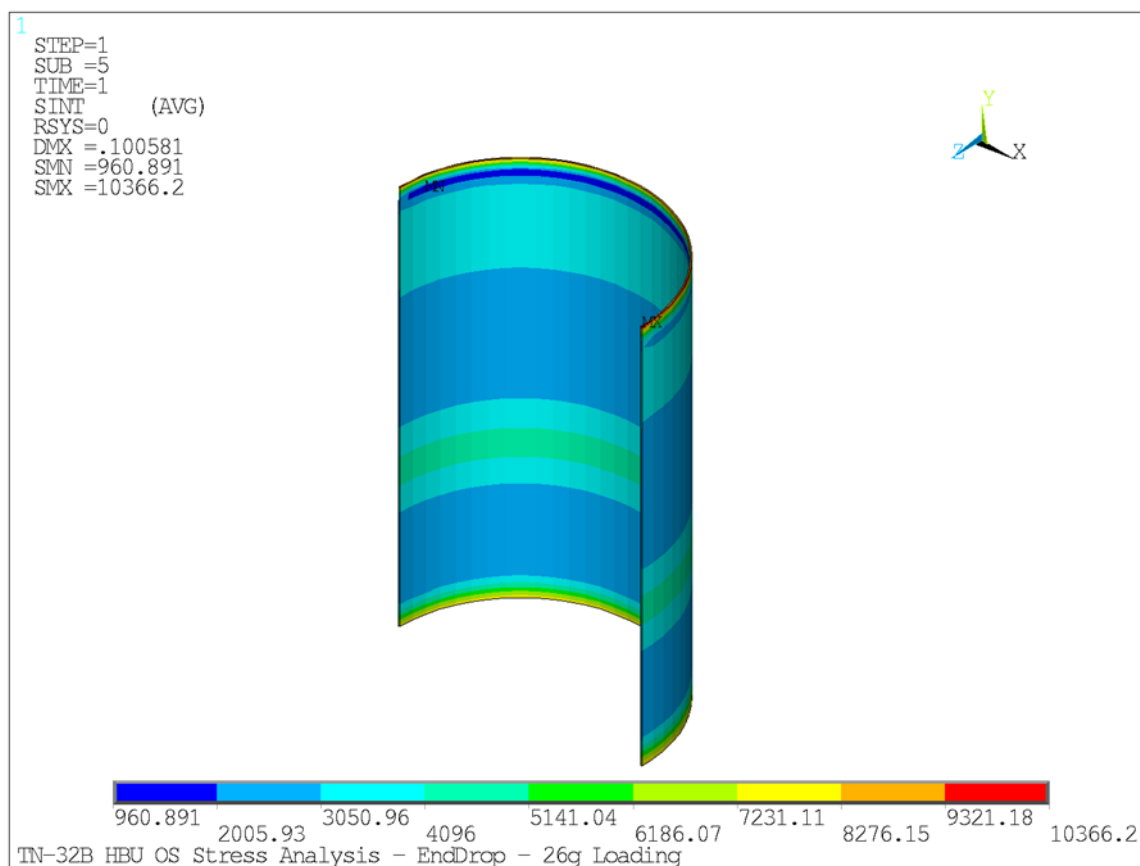


**Figure 2.12.4-7**  
**NCT End Drop –Outer Shell Plate Stress Intensity**

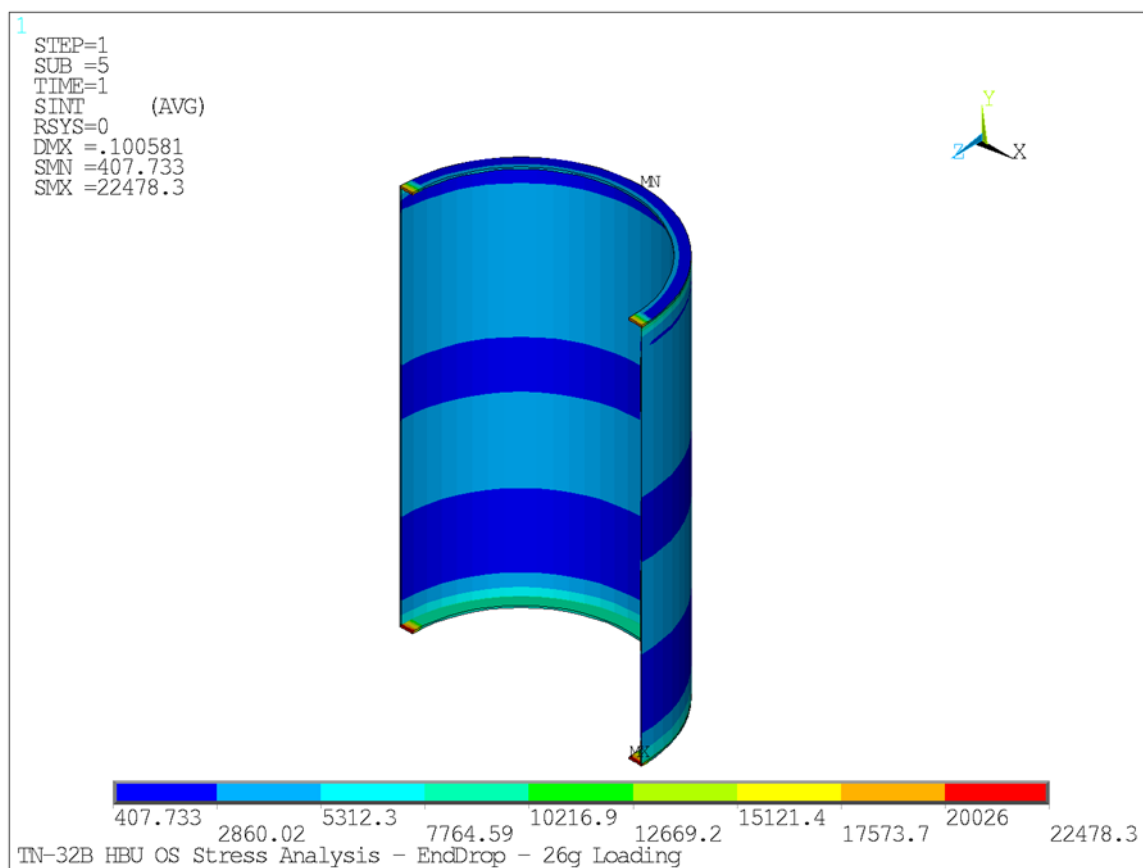


**Figure 2.12.4-8**  
**NCT End Drop –Outer Shell Weldment Stress Intensity**

## **Appendix 2.12.5**

### **Fracture Toughness Evaluation of the TN-32B HBU Cask**

#### TABLE OF CONTENTS

2.12.5	Fracture Toughness Evaluation of the TN-32B HBU Cask.....	2.12.5-1
2.12.5.1	Introduction .....	2.12.5-1
2.12.5.2	Fracture Toughness Requirements of the Cask .....	2.12.5-1
2.12.5.3	Fracture Toughness Evaluation of Cask Components and Welds ....	2.12.5-2
2.12.5.4	Methodology.....	2.12.5-2
2.12.5.5	Locations of Maximum Stresses.....	2.12.5-2
2.12.5.6	Material Fracture Toughness.....	2.12.5-3
2.12.5.7	Fracture Toughness Criteria.....	2.12.5-4
2.12.5.8	Stress Intensity Factor Calculations .....	2.12.5-4
2.12.5.9	Conclusions.....	2.12.5-4
2.12.5.10	NDE Inspection Plan .....	2.12.5-5
2.12.5.11	References.....	2.12.5-6



LIST OF TABLES

Table 2.12.5-1	Summary of Stress Components – NCT Load Combinations .....	2.12.5-7
Table 2.12.5-2	Summary of Stress Components – HAC Load Combinations .....	2.12.5-8
Table 2.12.5-3	Summary of Stress Intensity Factors for NCT Load Combinations .....	2.12.5-9
Table 2.12.5-4	Summary of Stress Intensity Factors for HAC Load Combinations ....	2.12.5-10

LIST OF FIGURES

Figure 2.12.5-1	Critical Locations for Stress and Fracture Evaluation .....	2.12.5-11
Figure 2.12.5-2	Charpy V-Notch Test Results for SA-266 Forging .....	2.12.5-12

## 2.12.5 Fracture Toughness Evaluation of the TN-32B HBU Cask

### 2.12.5.1 Introduction

This appendix documents the fracture toughness evaluation of the TN-32B HBU demonstration cask.

### 2.12.5.2 Fracture Toughness Requirements of the Cask

The TN-32B HBU demonstration cask material is a ferritic steel (penetration covers are stainless steel), and is therefore subject to fracture toughness requirements in order to ensure ductile behavior at the lowest service temperature (LST) of  $-20^{\circ}\text{F}$  ambient.

The inner shell and bottom inner plate are fabricated from SA-203 Gr D plate material, 1.5 inches thick. The shell flange is 4.6 inches thick, fabricated from SA-350 Gr LF3 forging material, and the closure lid plate is 4.5 inches thick, fabricated from SA-203 Gr D material. The 1.5-inch diameter closure lid bolts are fabricated from SA-540 Grade B23, Class1 material.

By interpolating between values provided in NUREG/CR-3826 [1] and NUREG/CR-1815 [2], the nil ductility transition temperatures ( $T_{\text{NDT}}$ ) of the containment boundary materials are:

- Inner shell and bottom inner plates (1.5 in.):  $-80^{\circ}\text{F}$
- Shell flange (4.6 in.):  $-137^{\circ}\text{F}$
- Closure lid plate (4.5 in.):  $-125^{\circ}\text{F}$

The fracture toughness requirements for the closure lid bolt material meet the intent of the American Society of Mechanical Engineers (ASME) Boiler and Pressure Vessel (B&PV) Code, Section III, Subsection NB, NB-2333 [3]. Charpy V-notch testing was performed on several specimens of the material at  $+40^{\circ}\text{F}$ . To satisfy Table NB-2333-1 of this section of the ASME B&PV Code, the material should exhibit a minimum of 25 mils lateral expansion at the “lowest service temperature”. For the TN-32B HBU cask with the 25.84 kW decay heat load, the temperature of the closure lid bolts under  $-20^{\circ}\text{F}$  ambient conditions (i.e., lowest service temperatures) is  $+136^{\circ}\text{F}$ . Therefore, Charpy impact tests of the SA-540 Gr B23 Cl 1 material performed at  $+40^{\circ}\text{F}$  demonstrated that all of the closure lid bolt material satisfies the NB-2300 criteria.

The 1.5-inch thick plate material that formed the inner shell and inner bottom plates were tested and resultant  $T_{\text{NDT}}$  of  $-88^{\circ}\text{F}$ , which satisfies the NUREG fracture arrest criteria.

From the certified material test reports contained in the fabrication data package, the drop weight and Charpy V-notch test results of the shell flange and closure lid plate materials utilized in the TN-32B HBU demonstration cask are tabulated in the following table.

### Recorded Test Data for Shell Flange and Closure Lid Plate Materials

Shell Flange				Closure Lid Plate			
Measured T <sub>NDT</sub> (°F)	Charpy Test Results			Measured T <sub>NDT</sub> (°F)	Charpy Test Results		
	Test Temp. (°F)	Impact Energy (lb <sub>f</sub> -ft)	Lateral Expansion (mils)		Test Temp. (°F)	Impact Energy (lb <sub>f</sub> -ft)	Lateral Expansion (mils)
-139	-80	174	98	-148	-88	230	108
		184	98			227	106
		183	98			224	106

From the recorded test data for the TN-32B HBU demonstration cask containment boundary materials described above, the closure lid plate and the shell flange materials satisfy the NUREG recommended fracture arrest criteria.

#### 2.12.5.3 Fracture Toughness Evaluation of Cask Components and Welds

A fracture toughness evaluation of the TN-32B HBU demonstration cask components and welds based on the lowest service temperature (LST) of -20 °F is performed. The evaluation includes the following:

- Methodology
- Locations of maximum stresses
- Material fracture toughness
- Fracture toughness criteria
- Stress intensity factor calculations
- Conclusions
- Nondestructive examination (NDE) Inspection Plan

#### 2.12.5.4 Methodology

The allowable flaw sizes were determined utilizing linear elastic fracture mechanics (LEFM) methodology from Section XI of ASME B&PV Code [4]. Flaws in the welds, if they occur, are welding defects, rather than initiated cracks. There is no active mechanism for crack initiation and growth at any of the weld locations since all the containment welds are volumetrically examined by radiographic testing (RT) and/or ultrasonic testing (UT) examination to ensure no unacceptable weld defects are present.

#### 2.12.5.5 Locations of Maximum Stresses

Figure 2.12.5-1 illustrates the selected locations on the cask for fracture toughness analysis. Stresses are linearized at these critical locations for maximum tensile membrane and bending stresses. Table 2.12.5-1 and Table 2.12.5-2 list the maximum membrane and bending stresses at these selected locations under normal conditions of transport (NCT) and hypothetical accident condition (HAC), respectively.

#### 2.12.5.6 Material Fracture Toughness

The shell flange is a forged cylinder, nominally 4.6 inches thick by 9 inches long, fabricated from SA-350 Gr LF-3 forging material. The welding of the flange to the containment shell was performed using the sub arc welding (SAW) or flux-cored arc welding (FCAW) processes. The closure lid outer plate is nominally 4.5 inches thick with a 79.50-inch diameter, and fabricated from SA-203 Gr D material.

The electrodes utilized in the shell flange and closure lid plate weldments had a high nickel content. The high alloy content of the electrodes and their typical usage in applications where good toughness is required indicate that the expected fracture toughness values for the weld filler material is as good as or better than that of the base material.

The gamma shield shell is a forged cylinder, nominally 8 inches thick by 168 inches long. The bottom shield plate is nominally 8.78 inches thick and 87.96 inches in diameter. These components were fabricated from SA-266 Cl 2, and SA-516 Gr 70 materials, respectively. Similarly, the 6-inch thick lid shield plate is made from SA-516 Gr 70. The welding at the top flange and bottom plate was performed using the SAW, FCAW, or shielded metal arc welding (SMAW) processes.

The closure lid and shell flange materials have enhanced fracture toughness properties than the SA-266 utilized for the gamma shield shell. Therefore, the low fracture toughness SA-266 forging material can be considered bounding. It is therefore conservative to utilize the fracture toughness properties of the SA-266 forging as the basis for qualifying the TN-32B HBU demonstration cask containment material.

Reference 5 is a very thorough review of correlations between a range of ferritic steel material strength levels and Charpy impact energies. Figure 2.12.5-2 (reproduced from Figure 4-5 of Reference [5]) plots Charpy V-notch impact test results for a normalized SA-266 forging. The actual data points are shown along with a smoothed line that connects the average value at each test temperature. This data demonstrates that a lower bound Charpy impact value of 18 ft-lb<sub>f</sub> is appropriate for an exposure temperature of -20 °F. The various correlations between  $K_{Ic}$  and  $K_{Id}$  given in Table 4-2 of Reference [5] are compared at the 18 ft-lb<sub>f</sub> level. Utilizing the equation for yield strength for 36 to 50 ksi in transition in Table 4-2 of Reference [5], the Charpy impact measurement may be transformed into a fracture toughness value:

$$K_{Id} = [5E(C_v)]^{1/2} = 50,289 \text{ psi} \cdot (\text{in})^{1/2} = 50 \text{ ksi} \cdot (\text{in})^{1/2}$$

where:

$K_{Id}$  = Dynamic Fracture Toughness (based on crack arrest),  $\text{psi} \cdot (\text{in})^{1/2}$   
 $E$  = Modulus of Elasticity,  $28.1 \times 10^6$  psi (conservatively use 300 °F)  
 $C_v$  = Charpy Impact Measurement, 18 ft-lb<sub>f</sub>

For conservatism, the above calculated  $K_{Id}$  was reduced to 47  $\text{ksi} \cdot (\text{in})^{1/2}$  for fracture toughness evaluations of the TN-32B HBU demonstration cask components (containment and non-containment boundary) and welds.

SAW, FCAW and SMAW electrodes used in the gamma shield weldments are alloyed to provide appropriate low temperature properties. Examples are American Welding Society (AWS) Class EN11K, E81T1, and F7P6-EH14 materials. Although Charpy testing is not a requirement for the gamma shield shell material, testing has been conducted by the TN-32B HBU demonstration cask fabricator on the bottom shield plate to demonstrate the toughness of the forged material and the associated welds. The results demonstrate that all regions of the SA-516-70 weldments have fracture toughness values well in excess of the 18 ft-lb<sub>f</sub> specified. Therefore, the use of the fracture properties from the wrought material for locations at or near the weld joints is conservative.

#### 2.12.5.7 Fracture Toughness Criteria

Utilizing the rule of Section XI, IWB-3613 [6], the limiting fracture toughness values are reduced by a factor of  $\sqrt{10}$  for the NCT and  $\sqrt{2}$  for the HAC, to define the limiting allowable  $K_{\text{allowable}}$ . That is,

$$K_{\text{allowable}} \leq K_{\text{ia}} / (\sqrt{10}) = 47 / (\sqrt{10}) = 14.86 \text{ ksi} \cdot (\text{in})^{1/2} \text{ for normal conditions}$$

$$K_{\text{allowable}} \leq K_{\text{ic}} / (\sqrt{2}) = 47 / (\sqrt{2}) = 33.23 \text{ ksi} \cdot (\text{in})^{1/2} \text{ for accident conditions}$$

where:

$K_{\text{ia}}$  = the available fracture toughness based on crack initiation for the corresponding crack tip temperature

$K_{\text{ic}}$  = the available fracture toughness based on crack initiation for the corresponding crack tip temperature

Because of the dynamic loading (1-foot and 30-foot free drops), it is appropriate to utilize the  $K_{\text{id}}$  value (47 ksi-(in)<sup>1/2</sup>) calculated above for  $K_{\text{ia}}$  and  $K_{\text{ic}}$  for the following normal and accident condition fracture toughness evaluations.

#### 2.12.5.8 Stress Intensity Factor Calculations

The total applied stress intensity  $K_I$  (applied) is determined from the membrane and bending stresses. For purpose of analysis, the postulated surface flaws are oriented in both the axial and circumferential directions. The surface crack depth is assumed as 15% of component thickness. However, the maximum crack depth is limited to 1/2 inch. The crack length is assumed to be 10 times the crack depth. The assumed crack sizes are such that they can be readily observed by visual examination. Compared to surface cracks, same size subsurface cracks are less critical. The results of the applied stress intensity  $K_I$  calculations for NCT and HAC are shown in Table 2.12.5-3 and Table 2.12.5-4, respectively.

#### 2.12.5.9 Conclusions

Based on the results of fracture analysis of the TN-32B HBU demonstration cask components and welds with the postulated surface crack sizes, it is concluded that there is no potential of fracture failure due to NCT and HAC transport loadings. The postulated surface flaw sizes are such that they can be readily detected by a visual inspection.

Note that the gamma shield shell is not part of the containment boundary. Cracks postulated in the gamma shield shell will not propagate into the containment boundary due to the geometry of the cask. If the gamma shield shell were to fracture along the length or around the circumference, or around the weld between the gamma shield shell and top flange, there is no credible mechanism that would result in the gamma shielding separating from the containment vessel. The top shield plate is welded to both the closure lid and the seven penetration sleeves, and is captured by the containment vessel. Therefore, if all of the welds were to completely fail, the top shield plate would still remain inside the containment boundary, and would not lose its shielding capability. Therefore, even if a fracture were to occur in the gamma shield shell, or the weld between the gamma shield and top flange, or in the top shield plate, or the welds between top shield plate and closure lid, there would be no safety significance, since containment would be maintained, and shielding would remain in place. The one exception is in the region of the weld of the gamma shield shell to the bottom plate. In this region, if the weld were to completely fail, the bottom plate could become detached and have an impact on the shielding capability of the cask. However, the bottom trunnions are independently welded to the gamma shield shell and the bottom shield plate. These additional attachment points (welds), as well as the lower impact limiter, would resist detachment of the bottom shield plate from the cask.

#### 2.12.5.10 NDE Inspection Plan

The results of the fracture toughness analysis demonstrate that the flaws in the gamma shield shell, and top and bottom shield plates that would result in unstable crack growth or brittle fracture are larger than those generally observed in forged steel and plate components. Therefore, no special examination requirements on the gamma shield shell, top and bottom shield plates are required.

Any flaw sizes in the welds that could result in brittle fracture at -20 °F were detected by NDE methods and repaired during the fabrication of the cask.

The liquid penetrant or magnetic particle method was in accordance with Section V, Article 6 of ASME Code [4].

#### 2.12.5.11 References

1. M. W. Schwartz, "Recommendations for Protecting Against Failure by Brittle Fracture in Ferritic Steel Shipping Containers Greater than Four Inches Thick," NUREG/CR-3826, U.S. Nuclear Regulatory Commission, April 1984.
2. W.R. Holman, R.T. Langland, "Recommendations for Protecting Against Failure by Brittle Fracture in Ferritic Steel Shipping Containers up to Four Inches Thick," NUREG/CR-1815, U.S. Nuclear Regulatory Commission, June 1981.
3. American Society of Mechanical Engineers, ASME Boiler and Pressure Vessel Code, Section III, Subsection NB, 1992.
4. American Society of Mechanical Engineers, ASME Boiler and Pressure Vessel Code, Section V and Section XI, 1992.
5. SIR-98-110, Revision 0, "Allowable Flaw Evaluation of Transnuclear TN-32 Cask," Structural Integrity Associates, Inc. 1998.
6. American Society of Mechanical Engineers, ASME Boiler and Pressure Vessel Code, Section XI, 2013.

**Table 2.12.5-1**  
**Summary of Stress Components – NCT Load Combinations**

Cask Location	Section		Membrane Stress (ksi)			Bending Stress (ksi)		
	Nodes	Max Stress	S <sub>x</sub> (Rad.)	S <sub>y</sub> (Tang.)	S <sub>z</sub> (Axial)	S <sub>x</sub> (Rad.)	S <sub>y</sub> (Tang.)	S <sub>z</sub> (Axial)
Bottom Shield Plate	49734-51679	S <sub>x</sub> (N6)	1.71	-0.24	0.13	2.45	0.27	2.29
	50529-51602	S <sub>y</sub> (N6)	1.73	-0.11	1.16	0.69	0.19	0.80
	50359-49642	S <sub>z</sub> (N6)	-1.11	-0.01	0.51	3.08	0.13	3.14
Gamma Shield Cylinder Mid	14528-13915	S <sub>y</sub> (N11)	3.65	1.23	-0.40	0.99	1.53	0.36
	14527-13916	S <sub>z</sub> (N11)	3.61	1.22	-0.41	1.00	1.53	0.36
Gamma Shield Cylinder	12935-12975	S <sub>y</sub> (N11)	5.21	0.96	-0.15	0.61	0.98	0.21
	11853-11730	S <sub>z</sub> (N11)	-5.31	0.58	-3.17	7.02	3.22	1.00
Shell Flange	151091-151050	S <sub>x</sub> (N11)	0.19	-2.05	-0.84	5.76	4.05	7.37
	150045-150885	S <sub>y</sub> (N11)	-2.76	-0.12	-0.88	1.69	3.24	1.41
	151202-163194	S <sub>z</sub> (N11)	-0.75	0.00	-2.29	1.16	3.45	1.46
Top Shield Plate	74808-76333	S <sub>x</sub> (N11)	-0.67	2.63	-0.04	2.03	3.47	1.23
	74854-76267	S <sub>y</sub> (N11)	-0.25	2.84	-0.41	1.50	3.54	1.70
	63497-74628	S <sub>z</sub> (N11)	-0.98	-0.10	-1.23	3.05	0.76	4.28
Lid	114448-113665	S <sub>x</sub> (N6)	1.68	0.31	1.77	5.83	0.12	5.37
	114447-113631	S <sub>y</sub> (N6)	2.56	1.26	2.73	3.86	0.40	3.90
	113574-139590	S <sub>z</sub> (N6)	1.36	-0.09	2.85	1.98	0.08	5.46
Inner Shell and Bottom Inner Plate	148769-148828	S <sub>x</sub> (N15)	-6.25	-4.24	-3.24	0.04	2.34	0.08
	142411-142413	S <sub>y</sub> (N15)	0.77	-2.13	-2.02	0.32	0.40	0.34
	142411-142413	S <sub>z</sub> (N15)	0.77	-2.13	-2.02	0.32	0.40	0.34
Penetration Sleeves	36984-36893	S <sub>x</sub> (N11)	3.59	5.00	7.80	1.23	7.37	1.26
	36691-36586	S <sub>y</sub> (N11)	7.33	2.85	5.52	0.68	2.49	0.77
	36988-36897	S <sub>z</sub> (N11)	2.16	5.73	6.66	0.85	9.66	2.33
Weld-1	12063-12082	S <sub>y</sub> (N7)	-11.07	5.13	-3.77	1.42	8.26	1.56
	11852-11832	S <sub>z</sub> (N7)	-12.47	5.83	-3.83	1.68	9.43	2.27
Weld-2	75036-73577	S <sub>y</sub> (N11)	-2.89	-2.61	-5.41	0.49	2.03	0.33
	75000-73541	S <sub>z</sub> (N11)	-5.49	-0.01	-6.17	0.41	0.29	0.48
Weld-PS	36499-36361	S <sub>y</sub> (N11)	-3.43	3.95	-2.53	1.28	6.45	1.20
	41862-41704	S <sub>z</sub> (N11)	-6.70	6.19	-10.46	2.53	10.05	0.21
Weld-PL	36691-36586	S <sub>y</sub> (N6)	7.33	2.85	5.52	0.68	2.49	0.77
	26275-26184	S <sub>z</sub> (N6)	4.72	4.36	1.97	1.69	7.26	0.87



**Table 2.12.5-2**  
**Summary of Stress Components – HAC Load Combinations**

Cask Location	Section		Membrane Stress (ksi)			Bending Stress (ksi)		
	Nodes	Max Stress	S <sub>x</sub> (Rad.)	S <sub>y</sub> (Tang.)	S <sub>z</sub> (Axial)	S <sub>x</sub> (Rad.)	S <sub>y</sub> (Tang.)	S <sub>z</sub> (Axial)
Bottom Shield Plate	49959-51839	S <sub>x</sub> (A9)	0.43	-3.32	0.42	1.52	0.28	1.68
	49960-50229	S <sub>y</sub> (A9)	0.76	-2.13	0.76	2.24	1.75	2.24
	49960-50229	S <sub>z</sub> (A9)	0.76	-2.13	0.76	2.24	1.75	2.24
Gamma Shield Cylinder Mid	14521-13922	S <sub>y</sub> (A6)	2.96	-2.36	-0.29	0.38	0.16	0.29
	14526-13917	S <sub>z</sub> (A6)	2.94	-3.08	-0.29	0.33	0.02	0.29
Gamma Shield Cylinder	14518-13925	S <sub>y</sub> (A6)	3.21	-1.93	-0.29	0.40	0.09	0.30
	11853-11730	S <sub>z</sub> (A6)	-5.14	-0.52	-2.87	5.87	4.54	0.65
Shell Flange	151089-151048	S <sub>x</sub> (A5)	-1.13	-3.37	-0.66	6.03	6.58	7.12
	151070-151039	S <sub>y</sub> (A5)	-0.02	-3.58	-0.93	6.34	7.37	6.24
	164171-164198	S <sub>z</sub> (A5)	-3.99	-6.07	-1.83	1.30	4.32	0.30
Top Shield Plate	74808-76333	S <sub>x</sub> (A5)	0.46	-0.95	0.14	1.39	2.16	0.96
	74970-75823	S <sub>y</sub> (A5)	1.02	3.57	0.32	1.69	1.74	0.84
	74946-75911	S <sub>z</sub> (A5)	0.15	1.88	0.37	0.47	0.16	1.27
Lid	114454-113641	S <sub>x</sub> (A6)	1.29	0.08	0.94	5.21	0.58	3.21
	114456-113639	S <sub>y</sub> (A6)	0.02	1.10	-0.04	4.34	0.94	0.63
	113574-139590	S <sub>z</sub> (A6)	-0.66	-0.51	0.14	1.29	0.05	3.36
Inner Shell and Bottom Inner Plate	142428-142431	S <sub>x</sub> (A5)	-0.55	-5.48	0.49	0.58	1.58	0.47
	142179-142173	S <sub>y</sub> (A5)	-0.17	-4.71	0.93	0.11	0.51	0.07
	142411-142413	S <sub>z</sub> (A5)	-0.20	-4.75	0.93	0.09	0.52	0.05
Penetration Sleeves	36686-36581	S <sub>x</sub> (A2)	1.84	3.92	5.88	0.86	6.68	1.23
	36669-36572	S <sub>y</sub> (A2)	2.79	4.95	1.90	1.60	5.97	0.86
	42036-41931	S <sub>z</sub> (A2)	-1.73	5.11	-1.47	2.71	12.16	1.66
Weld-1	12063-12082	S <sub>y</sub> (N1)	-10.21	4.67	-3.99	1.26	7.48	1.29
	11852-11832	S <sub>z</sub> (N1)	-11.24	4.99	-3.35	1.61	7.91	1.68
Weld-2	75036-73577	S <sub>y</sub> (N5)	-2.66	1.76	-5.10	0.05	0.36	0.33
	74999-73540	S <sub>z</sub> (N5)	-4.84	3.43	-4.75	0.13	1.77	0.02
Weld-PS	36500-36360	S <sub>y</sub> (N9)	1.80	0.66	0.67	0.53	1.05	0.27
	41859-41707	S <sub>z</sub> (N9)	3.54	1.98	3.32	1.13	2.94	1.17
Weld-PL	36691-36586	S <sub>y</sub> (N2)	2.21	5.04	2.23	2.28	10.08	1.90
	42036-41931	S <sub>z</sub> (N2)	-1.73	5.11	-1.47	2.71	12.16	1.66

**Table 2.12.5-3**  
**Summary of Stress Intensity Factors for NCT Load Combinations**

Component Location	Thick. t (in.)	Crack depth, a (in.)	Crack length, l (in.)	Max Stress Type	Critical Crack Direction	Stress Intensity Factor (ksi)	Allow. Stress Intensity Factor	Factor of Safety
Bottom Shield Plate	8.75	0.500	5.00	S <sub>x</sub>	Tangential	5.97	14.86	2.49
Gamma Shield Cylinder Mid	8.00	0.500	5.00	S <sub>y</sub>	Axial	3.46	14.86	4.29
Shell Flange	4.60	0.500	5.00	S <sub>z</sub>	Hoop	8.37	14.86	1.78
Top Shield Plate	6.00	0.500	5.00	S <sub>y</sub>	Axial	7.80	14.86	1.91
Lid	4.50	0.500	5.00	S <sub>z</sub>	Hoop	10.09	14.86	1.47
Inner Shell and Bottom Inner Plate	1.50	0.225	2.25	S <sub>y</sub>	Axial	1.73	14.86	8.60
Penetration Sleeves	0.50	0.075	0.75	S <sub>y</sub>	Axial	7.20	14.86	2.07
Weld-1	0.50	0.075	0.75	S <sub>y</sub>	Axial	7.15	14.86	2.08
Weld-2	0.75	0.113	1.125	S <sub>y</sub>	Axial	1.05	14.86	>10
Weld-PS	0.50	0.075	0.75	S <sub>y</sub>	Axial	7.61	14.86	1.95
Weld-PL	0.50	0.075	0.75	S <sub>y</sub>	Axial	5.43	14.86	2.73

S<sub>x</sub> (Radial Stress) – Results in tangential crack

S<sub>y</sub> (Hoop Stress) – Results in axial crack

S<sub>z</sub> (Axial Stress) – Results in hoop crack

Weld-1 – Flange to gamma shield weld

Weld-2 – Lid to gamma shield weld

Weld-PS – Penetration sleeves to top shield plate weld

Weld-PL – Penetration sleeves to closure lid weld

**Table 2.12.5-4**  
**Summary of Stress Intensity Factors for HAC Load Combinations**

Component Location	Thick. t (in)	Crack depth, a (in)	Crack length, l (in)	Max Stress Type	Critical Crack Direction	Stress Intensity Factor (ksi)	Allow. Stress Intensity Factor	Factor of Safety
Bottom Shield Plate	8.750	0.500	5.00	S <sub>z</sub>	Hoop	3.69	33.23	9.01
Gamma Shield Cylinder Mid	8.000	0.500	5.00	S <sub>z</sub>	Hoop	0.35	33.23	>10
Gamma Shield Cylinder	8.000	0.500	5.00	S <sub>y</sub>	Axial	5.42	33.23	6.13
Shell Flange	4.600	0.500	5.00	S <sub>y</sub>	Axial	8.36	33.23	3.97
Top Shield Plate	6.000	0.500	5.00	S <sub>y</sub>	Axial	7.17	33.23	4.64
Lid	4.500	0.500	5.00	S <sub>x</sub>	Tangential	7.63	33.23	4.35
Inner Shell and Bottom Inner Plate	1.500	0.225	2.25	S <sub>z</sub>	Hoop	1.20	33.23	>10
Penetration Sleeves	0.500	0.075	0.75	S <sub>y</sub>	Axial	7.93	33.23	4.19
Weld-1	0.500	0.075	0.75	S <sub>y</sub>	Axial	6.05	33.23	5.49
Weld-2	0.750	0.113	1.125	S <sub>y</sub>	Axial	3.16	33.23	>10
Weld-PS	0.500	0.075	0.75	S <sub>y</sub>	Axial	2.31	33.23	>10
Weld-PL	0.500	0.075	0.75	S <sub>y</sub>	Axial	7.93	33.23	4.19

S<sub>x</sub> (Radial Stress) – Results in tangential crack

S<sub>y</sub> (Hoop Stress) – Results in axial crack

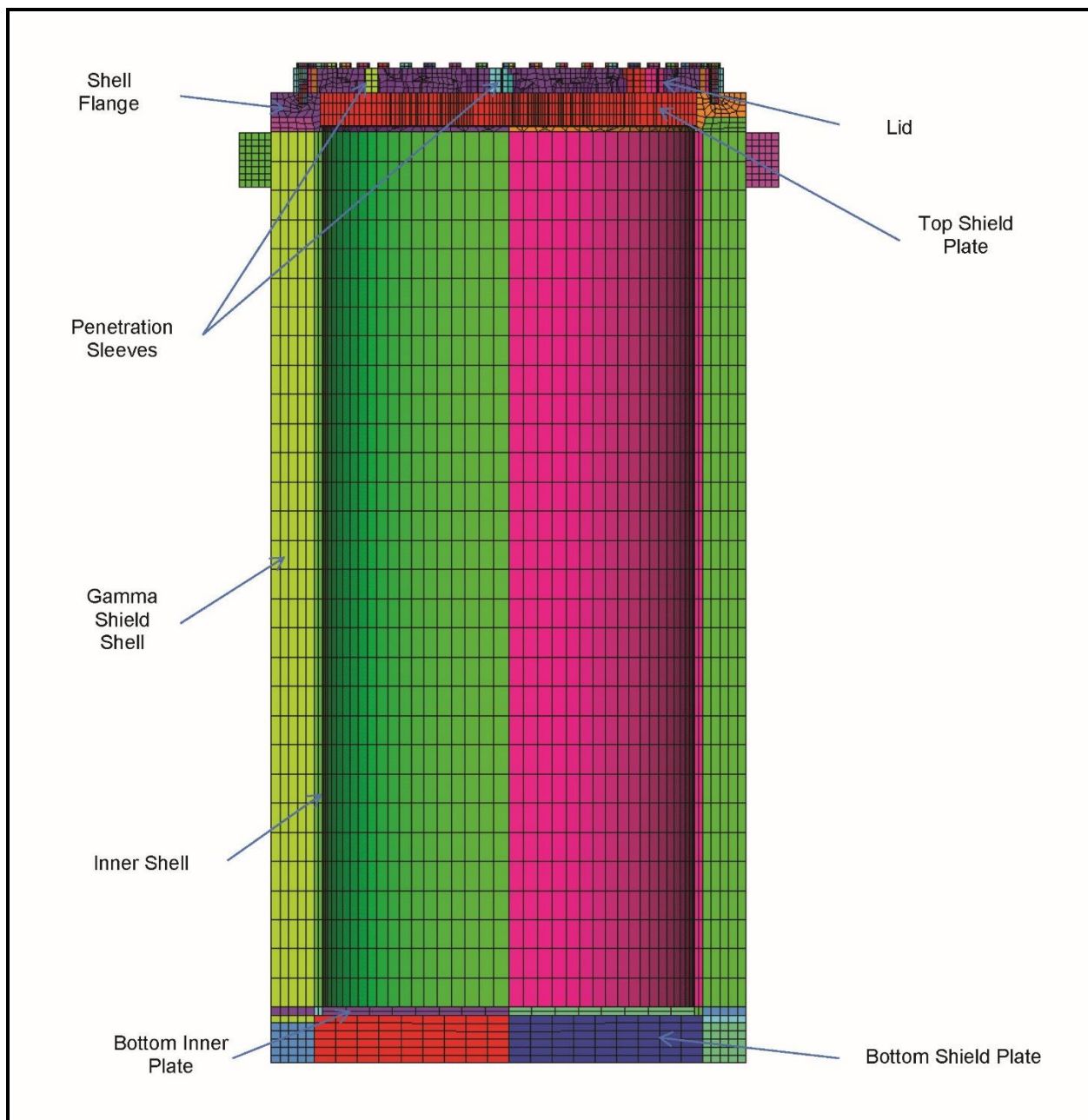
S<sub>z</sub> (Axial Stress) – Results in hoop crack

Weld-1 – Flange to gamma shield weld

Weld-2 – Lid to gamma shield weld

Weld-PS – Penetration sleeves to top shield plate weld

Weld-PL – Penetration sleeves to closure lid weld



Note: Only half of the finite element model is shown above for clarity.

**Figure 2.12.5-1**  
**Critical Locations for Stress and Fracture Evaluation**

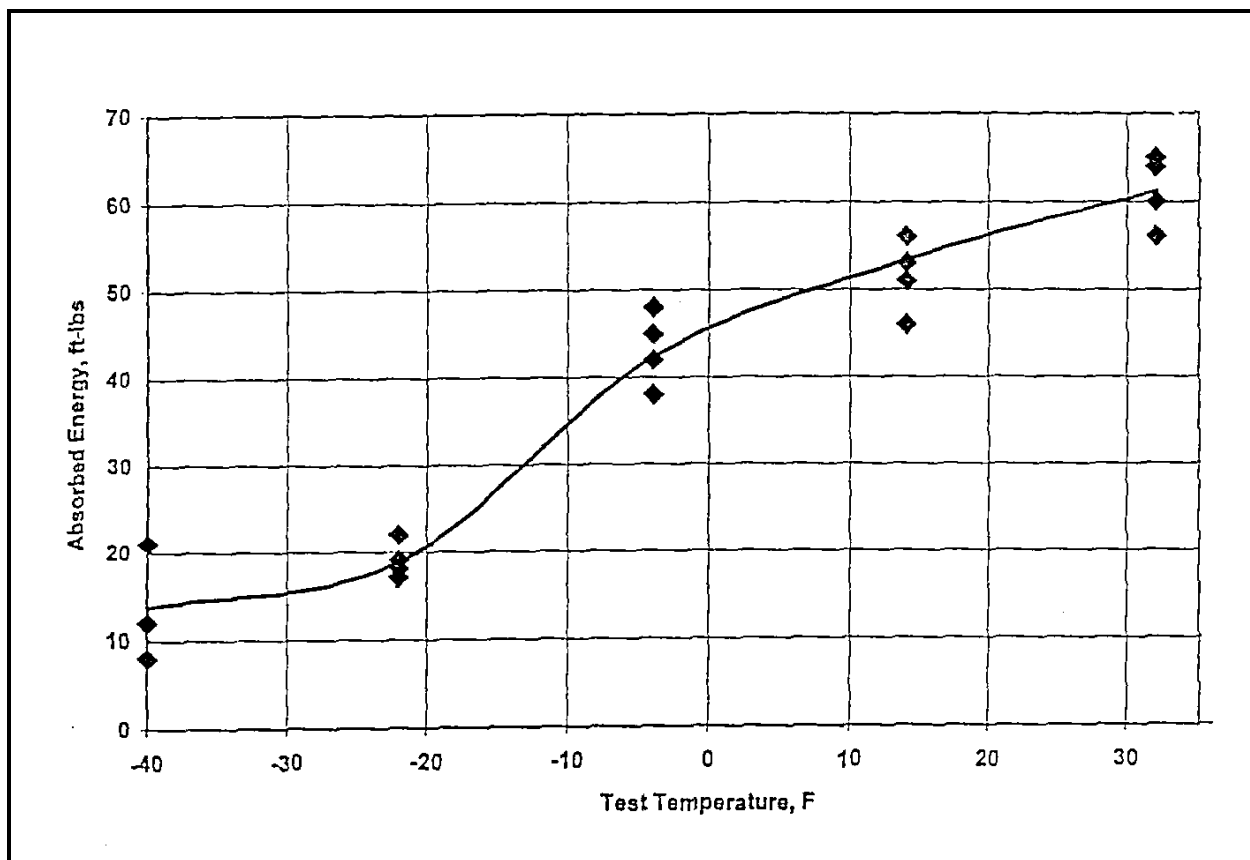


**Figure 2.12.5-2**  
**Charpy V-Notch Test Results for SA-266 Forging**

## **Appendix 2.12.6**

### **Structural Analysis of the TN-32B HBU Cask Basket**

#### TABLE OF CONTENTS

2.12.6	Structural Analysis of the TN-32B HBU Cask Basket.....	2.12.6-1
2.12.6.1	Introduction .....	2.12.6-1
2.12.6.2	Fuel Basket Stress Analysis .....	2.12.6-2
2.12.6.3	Fuel Basket Buckling Analysis.....	2.12.6-9
2.12.6.4	Fusion Welds .....	2.12.6-10
2.12.6.5	Conclusions.....	2.12.6-12
2.12.6.6	References.....	2.12.6-12

#### LIST OF TABLES

Table 2.12.6-1	Material Properties for TN-32B HBU Cask Fuel Basket.....	2.12.6-14
Table 2.12.6-2	Basket Structural Allowable Stresses, NCT .....	2.12.6-15
Table 2.12.6-3	Basket Structural Allowable Stresses, HAC .....	2.12.6-16
Table 2.12.6-4	NCT 0° Side Drop, Basket Stress Analysis Results .....	2.12.6-17
Table 2.12.6-5	NCT 45° Side Drop, Basket Stress Analysis Results .....	2.12.6-18
Table 2.12.6-6	HAC 0° Side Drop, Basket Stress Analysis Results .....	2.12.6-19
Table 2.12.6-7	HAC 30° Side Drop, Basket Stress Analysis Results .....	2.12.6-20
Table 2.12.6-8	HAC 45° Side Drop, Basket Stress Analysis Results .....	2.12.6-21
Table 2.12.6-9	HAC Cask Drop – Maximum Relative Deflection of the Basket at all Cell Compartments .....	2.12.6-22
Table 2.12.6-10	Nonlinear Buckling – Results Summary .....	2.12.6-23

LIST OF FIGURES

Figure 2.12.6-1	HAC Temperature Boundary Condition .....	2.12.6-24
Figure 2.12.6-2	Basket Drop Orientations – HAC Side Drop .....	2.12.6-25
Figure 2.12.6-3	NCT Finite Element Model for Lateral Load Evaluation .....	2.12.6-26
Figure 2.12.6-4	NCT Displacement Constraints – 45° Side Drop.....	2.12.6-27
Figure 2.12.6-5	HAC Finite Element Model for Lateral Load Evaluation .....	2.12.6-28
Figure 2.12.6-6	HAC Finite Element Model for Lateral Load Evaluation – Zoom View near Center.....	2.12.6-29
Figure 2.12.6-7	Material Properties – SA-240 Type 304 – ANSYS® BKIN Model .....	2.12.6-30
Figure 2.12.6-8	Material Properties – SB-209 Type 6061-T651 – ANSYS® BKIN Model.....	2.12.6-31
Figure 2.12.6-9	Loading Boundary Conditions – NCT Side Drop – 0° .....	2.12.6-32
Figure 2.12.6-10	Loading Boundary Conditions – NCT Side Drop – 45° .....	2.12.6-33
Figure 2.12.6-11	Loading Boundary Conditions – HAC Side Drop – 0° .....	2.12.6-34
Figure 2.12.6-12	Loading Boundary Conditions - HAC Side Drop – 30° .....	2.12.6-35
Figure 2.12.6-13	Loading Boundary Conditions – HAC Side Drop – 45° .....	2.12.6-36
Figure 2.12.6-14	NCT 0° Side Drop – Stainless Steel Plates – Membrane plus Bending Stress Intensity at Bottom Face.....	2.12.6-37
Figure 2.12.6-15	NCT 0° Side Drop – Stainless Steel Plates – Primary Membrane plus Bending Stress Ratio Plot – Bottom Face .....	2.12.6-38
Figure 2.12.6-16	NCT 45° Side Drop – Stainless Steel Plates – Primary Membrane plus Bending Stress Ratio Plot – Bottom Face .....	2.12.6-39
Figure 2.12.6-17	HAC 0° Side Drop – Stainless Steel Plates – Membrane plus Bending Stress Intensity at Bottom Face.....	2.12.6-40
Figure 2.12.6-18	HAC 30° Side Drop – Stainless Steel Plates – Membrane plus Bending Stress Intensity at Bottom Face.....	2.12.6-41
Figure 2.12.6-19	HAC 30° Side Drop – Aluminum Plates – Membrane plus Bending Stress Intensity at Bottom Face.....	2.12.6-42
Figure 2.12.6-20	HAC 45° Side Drop – Stainless Steel Plates – Membrane plus Bending Stress Intensity at Top Face .....	2.12.6-43
Figure 2.12.6-21	HAC 45° Side Drop – Aluminum Plates – Membrane plus Bending Stress Intensity at Bottom Face.....	2.12.6-44
Figure 2.12.6-22	HAC 0° Side Drop – Stainless Steel Plates – Primary Membrane plus Bending Stress Ratio Plot – Bottom Face .....	2.12.6-45
Figure 2.12.6-23	HAC 0° Side Drop – Aluminum Plates – Primary Membrane plus Bending Stress Ratio Plot – Bottom Face .....	2.12.6-46
Figure 2.12.6-24	HAC 30° Side Drop – Stainless Steel Plates – Primary Membrane plus Bending Stress Ratio Plot – Bottom Face .....	2.12.6-47

Figure 2.12.6-25	HAC 30° Side Drop – Aluminum Plates – Primary Membrane plus Bending Stress Ratio Plot – Bottom Face .....	2.12.6-48
Figure 2.12.6-26	HAC 45° Side Drop – Stainless Steel Plates – Primary Membrane plus Bending Stress Ratio Plot – Top Face.....	2.12.6-49
Figure 2.12.6-27	HAC 45° Side Drop – Aluminum Plates – Primary Membrane plus Bending Stress Ratio Plot – Top Face .....	2.12.6-50
Figure 2.12.6-28	Thermal Stress Analysis Model with Boundary Conditions .....	2.12.6-51
Figure 2.12.6-29	Thermal Stress Analysis Model – Cut Section View .....	2.12.6-52
Figure 2.12.6-30	Thermal Stress Analysis – Model 1 – Maximum Stainless Steel Stress Intensity.....	2.12.6-53
Figure 2.12.6-31	Thermal Stress Analysis – Model 1 – Maximum Aluminum Stress Intensity.....	2.12.6-54
Figure 2.12.6-32	Thermal Stress Analysis – Model 2 – Maximum Stainless Steel Stress Intensity.....	2.12.6-55
Figure 2.12.6-33	Thermal Stress Analysis – Model 2 – Maximum Aluminum Stress Intensity.....	2.12.6-56
Figure 2.12.6-34	Nonlinear Buckling - Loading Boundary Conditions - Side Drop – 30° .....	2.12.6-57
Figure 2.12.6-35	Nonlinear Buckling – Basket Displacement at Buckling Load – Side Drop – 0° .....	2.12.6-58
Figure 2.12.6-36	Nonlinear Buckling – Basket Displacement at Buckling Load – Side Drop – 30° .....	2.12.6-59
Figure 2.12.6-37	Nonlinear Buckling – Basket Displacement at Buckling Load – Side Drop – 45° .....	2.12.6-60
Figure 2.12.6-38	Nonlinear Buckling – Basket Stress Intensity at Buckling Load – Side Drop – 0° .....	2.12.6-61
Figure 2.12.6-39	Nonlinear Buckling – Basket Stress Intensity at Buckling Load – Side Drop – 30° .....	2.12.6-62
Figure 2.12.6-40	Nonlinear Buckling – Basket Stress Intensity at Buckling Load – Side Drop – 45° .....	2.12.6-63



## 2.12.6 Structural Analysis of the TN-32B HBU Cask Basket

### 2.12.6.1 Introduction

This appendix presents the structural analysis of the TN-32B HBU demonstration cask fuel support basket. The basket is a welded assembly of stainless steel boxes, and is designed to accommodate the (32) HBU PWR fuel assemblies.

#### 2.12.6.1.1 TN-32B HBU Demonstration Cask Fuel Basket Geometry

The details of the TN-32B HBU demonstration cask basket are shown in Appendix 1.4.1. The basket structure consists of an assembly of stainless steel boxes or cells joined by fusion welded stainless steel plugs, and separated by aluminum and neutron poison material (borated aluminum sheets). The aluminum plate and borated aluminum (poison) plates are sandwiched between the stainless steel walls of the adjacent box sections.

The nominal open dimension of each fuel compartment cell or box is  $8.70 \times 8.70$  inches, which provides a minimum of 1/8-inch clearance around the fuel assemblies. The overall basket length (160 inches) is less than the cask cavity.

Structural aluminum rails oriented parallel to the axis of the cask are attached to the inner cavity wall of the cask body to establish and maintain basket orientation.

Under side drop loads, each fuel assembly is assumed to be uniformly supported across the width and along the length of the box wall. The inertia of the basket structure (weight of the basket downward “g” load) is also included in the analysis.

#### 2.12.6.1.2 Weight

The total weight of the TN-32B HBU demonstration cask basket is 13,421 lb<sub>m</sub>. A value of 1,551 lb<sub>m</sub> is assigned for the weight of each fuel assembly, with the total weight of all (32) fuel assemblies 49,632 lb<sub>m</sub>. Under lateral inertial loading each assembly is assumed to be uniformly supported across the width and along the length of the box wall (160 inches).

#### 2.12.6.1.3 Temperature

Thermal analyses are performed to obtain the temperature distributions in the basket for various conditions. These analyses are presented in Chapter 3. The model temperature distributions are shown in Figure 2.12.6-1.

Thermal stresses induced in the fuel basket by the applied temperature distributions are evaluated in Section 2.12.6.2.4.

## 2.12.6.2 Fuel Basket Stress Analysis

### 2.12.6.2.1 Approach

Bounding inertial loads of 13g and 51g are applied for the normal conditions of transport (NCT) and hypothetical accident condition (HAC) transport cask free drop cases, respectively. These inertial loads are extracted from the impact limiter analyses provided in Appendix 2.12.9, and amplified with dynamic load factors (DLFs) provided in Appendix 2.12.7. The 0° and 45° azimuth orientations are analyzed to bound all possible drop orientations. Additionally, a 30° azimuth side drop is analyzed separately for HAC, as shown in Figure 2.12.6-2.

The analytical analysis for the end drop impact is provided in Section 2.12.6.2.3.

The thermal stress analysis of the fuel basket is provided in Section 2.12.6.2.4.

### 2.12.6.2.2 Basket Finite Element Analysis for Side Impact Loads

#### A. Finite Element Model Description

##### NCT Model

A three-dimensional ANSYS® finite element model (FEM) of the fuel basket is constructed utilizing shell elements. Only the stainless steel fuel boxes are included in the model. For conservatism, the strength of the aluminum (1/2-inch thick) and the borated aluminum plates in the basket are neglected by excluding these from the finite element model. However, their weights are accounted for by increasing the stainless steel box material densities. The solid model used in the lateral load evaluation is shown in Figure 2.12.6-3.

To simplify analyses, only an 8-inch long symmetrical section of the basket is modeled. At the two cut faces of the model, symmetrical boundary conditions are applied ( $U_Z = ROT_X = ROT_Y = 0$ ). The displacement constraints for the 45° side drop angle are shown in Figure 2.12.6-4. Similar displacement constraints were applied for the 0° side drop. For clarity, symmetry displacement constraints are not shown.

The stainless steel basket boxes sandwich the aluminum and the borated aluminum plates. The nodes between the steel boxes are coupled together in the out-of-plane direction so that they will bend in unison under surface pressure or other lateral loading. This modeling approach is to simulate the through thickness support provided by the aluminum and borated aluminum plates.

##### HAC Model

A three-dimensional (3-D) ANSYS® FEM of the basket compartments, aluminum plates, and aluminum rails is constructed using ANSYS® SHELL43 (4-node large strain plastic shell) elements.

The plug distance between two adjacent layers in the vertical direction is 8 inches. The sliced portion of the basket is then 8 inches in height. The slice contains the plugs in the middle plane along the vertical direction (Y-direction), such that symmetrical boundary conditions can be applied to the top and bottom cross sections. The compartment box walls and the peripheral support plates are meshed with ANSYS® SHELL43 elements and the plugs are meshed with ANSYS® BEAM188 (3-D linear finite strain beam) elements.

Aluminum rails are bolted to the containment shell. The bolts are not structural members, and their purpose is to secure the rails during fuel loading and fabrication. The bolts are represented by ANSYS® COMBIN14 (longitudinal spring-damper) 3-D springs with stiffness  $k = 1,000 \text{ lb}_f/\text{in}$ . The bolts are not evaluated in this calculation.

The solid model, which includes the fuel compartments, aluminum plates, aluminum rails (Type 1 and Type 2), and fusion welds utilized in the lateral load evaluation, is shown in Figure 2.12.6-5 and Figure 2.12.6-6.

#### B. Material Properties and Design Criteria

For NCT, a linear elastic stress strain model is used to simulate linear behavior at operating temperature. For HAC, the bilinear stress-strain relationship is used to simulate nonlinear behavior at operating temperature. The bilinear stress-strain relationship is applied by using ANSYS® bilinear kinematic hardening method (TB, BKIN). In the elastic-plastic analysis, the material behavior is described by a bilinear stress-strain curve starting at the origin with positive stress and strain values. The initial slope of the curve is selected as the elastic modulus. At the specified yield stress, the curve continues along the second slope defined by the tangent modulus. Rice's hardening rule is used, which takes into account stress relaxation with increasing temperature. It is assumed that the tangent modulus amounts to 5% of elastic modulus for stainless steel, and 1% of elastic modulus for aluminum alloy, as shown in Figure 2.12.6-7 and Figure 2.12.6-8, respectively.

Table 2.12.6-1 lists the material properties utilized in all analyses of the TN-32B HBU demonstration cask fuel basket. Table 2.12.6-2 and Table 2.12.6-3 summarize the stress criteria for the NCT and HAC events, respectively.

#### C. Side Drop/Slapdown Loading Conditions

The basket structure is analyzed for 0° and 45° azimuth side drops. Due to the basket structure symmetry, these orientations of side drops are assumed to envelop all other possible drop orientations. Additionally, a 30° azimuth side drop is analyzed separately for HAC (nonlinear model).

Temperatures at the cross section where the maximum temperatures occur in the basket are used, which are selected from the normal transport condition (100 °F NCT Solar) thermal analysis presented in Chapter 3. The temperature distribution is applied to the NCT and HAC ANSYS® models. Figure 2.12.6-1 illustrates the temperature contour utilized in the HAC analysis.

The load resulting from the fuel assembly weight is applied as pressure on the fuel compartment plates of the basket. For the 0° orientation, the pressure acts only on the horizontal plates. For the 30° and 45-degree orientation, the pressure was divided into components to act on both horizontal and vertical plates of the basket. The pressures for all orientations are calculated below for 13g and 51g accelerations.

#### 0° Orientation

$$\begin{aligned}\text{Pressure for 1g, } p &= (\text{fuel assembly weight})/[(\text{panel span})(\text{panel length})] \\ &= 1,551/[8.805(160)] = 1.10094 \text{ psi}\end{aligned}$$

$$\text{Pressure for 13g} = 13(1.10094) = 14.3122 \text{ psi}$$

$$\text{Pressure for 51g} = 51(1.10094) = 56.1478 \text{ psi}$$

#### 30° Orientation

$$\begin{aligned}\text{Pressure for 1g} \quad p_v &= p \sin 30 = 1.10094(0.50) = 0.5505 \text{ psi} \\ p_h &= p \cos 30 = 1.10094(0.866) = 0.9534 \text{ psi}\end{aligned}$$

$$\begin{aligned}\text{Pressure for 51g} \quad p_v &= p \sin 30 = 51(0.5505) = 28.0739 \text{ psi} \\ p_h &= p \cos 30 = 51(0.9534) = 48.6254 \text{ psi}\end{aligned}$$

#### 45° Orientation

$$\text{Pressure for 1g} \quad p_v = p_h = p \cos 45^\circ = 1.10094(0.7071) = 0.7785$$

$$\text{Pressure for 13g} = 13(0.7785) = 10.1205 \text{ psi}$$

$$\text{Pressure for 51g} = 51(0.7785) = 39.7025 \text{ psi}$$

The load distributions for the 0° and 45° analyses for the NCT drops are shown in Figure 2.12.6-9 and Figure 2.12.6-10, respectively. The load distribution for the 0°, 30°, and 45° HAC drops are shown in Figure 2.12.6-11 through Figure 2.12.6-13.

The accelerations applied in each run are as follows.

Orientation (degrees)	Inertial Load (g)	a <sub>x</sub> (g)	a <sub>y</sub> (g)	a <sub>z</sub> (g)
0	13 (NCT)	0	13	0
	51 (HAC)	51	0	0
30	51 (HAC)	44.167	0	25.5
45	13 (NCT)	-9.192	9.192	0
	51 (HAC)	36.062	0	36.062

## D. Side Drop Analysis and Results

NCT Side Drop Analysis and Results

Linear analyses with elastic material properties and small deflections were performed utilizing ANSYS® for the 0° and 45° drop orientations. Loads corresponding to 13g and 51g were applied in all NCT and HAC side drop analyses, as noted above. A summary of reactions and input load, which reflects the fuel and basket for the 8-inch high basket section, is provided in the following table.

Side Drop Orientation (degrees)	Applied Loads (lbf)	Reaction Forces (lbf)			Resultant Force (lbf)
		F <sub>x</sub>	F <sub>y</sub>	F <sub>z</sub>	
0	13(3,152.63) = 40,984.19	0	40,986.0	0	40,986.0
45	13(3,152.63) = 40,984.19	-28,982.0	28,982.0	0	40,986.7

The nodal membrane-plus-bending stress intensity distribution in the stainless steel boxes at the bottom shell faces, which is the bounding case, is shown in Figure 2.12.6-14.

The allowable stress at each nodal location varies based on the temperature at that node. An ANSYS® macro was developed to calculate the allowable stress at each node for membrane and membrane plus bending stresses using interpolated allowable stress values from Table 2.12.6-2. The primary membrane ( $P_m$ ) and primary membrane plus bending ( $P_m + P_b$ ) allowable for normal condition were calculated utilizing the macro. Stress/allowable stress ratio at each node for membrane, and membrane plus bending stresses at the temperature for that node are calculated. The stress ratio plots for allowable calculated at each node for  $P_m$  and  $P_m + P_b$  stress categories are shown in Figure 2.12.6-15 through Figure 2.12.6-16.

The location where the allowable stress/actual stress ratio is minimum (the location with minimum factor of safety (F.S.)) is determined along with the peak stress regardless of temperature. The results are summarized in Table 2.12.6-4 and Table 2.12.6-5.

The maximum stress ( $P_m + P_b + Q$ ) in the stainless steel plates for normal conditions, 16.30 ksi (=12.21 ksi + maximum thermal stress is 4.09 ksi from Section 2.12.6.2.4), is also lower than the stress limit of 52.5 ksi ( $3S_m$  at 500 °F).

HAC Side Drop Analysis and Results

Nonlinear analyses with bilinear material properties and large deflection were performed in ANSYS® for the 0°, 30°, and 45° drop orientations. Loads corresponding to 51g were applied in all HAC side drop analyses. A summary of reactions and input load, which reflects the fuel, the basket, and rails for the 8-inch high basket section, is provided in the following table.

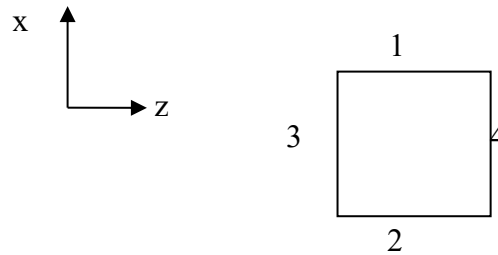
Side Drop Orientation (degrees)	Applied Loads (lbf)	Reaction Forces (lbf)			Resultant Force (lbf)
		$F_x$	$F_y$	$F_z$	
0	$51(3,328.96) = 169,777.0$	169,770	0.08	-1.69	169,770.0
30	$51(3,328.96) = 169,777.0$	147,030	-0.09	84,888	169,775.7
45	$51(3,328.96) = 169,777.0$	120,070	-0.09	120,050	169,790.5

The nodal stress intensity distribution in the stainless steel boxes, aluminum plates, and aluminum rails (Type 1 and Type 2) at the middle, top and bottom shell faces are shown in Figure 2.12.6-17 through Figure 2.12.6-21. The primary membrane ( $P_m$ ) and primary membrane plus bending ( $P_m + P_b$ ) allowable were calculated for the accident condition. The resultant stress ratio for allowable were calculated at each node for  $P_m$  and  $P_m + P_b$  stress categories and are shown in Figure 2.12.6-22 through Figure 2.12.6-27.

The location with the minimum factor of safety, and the peak stress, regardless of temperature, are also calculated. The results are summarized in Table 2.12.6-6 through Table 2.12.6-8.

The stress ratios for aluminum plates for 0° side drop case, exceeds the membrane plus bending allowable at the shell bottom surface (see Figure 2.12.6-23). The maximum stress ratio is 1.0011 (or 0.11% exceedance), which is very close to the allowable. The maximum membrane stress ratio for the aluminum plates for that case is 0.517. The maximum max stress ratio for 0° side drop case for the stainless steel plates is 0.524 (see Figure 2.12.6-22). The aluminum plates primarily function as heat conduction materials and are enclosed by stainless steel plates that have stresses that are well within the limits. Hence, the structural integrity of the baskets is maintained even though the stress ratios of aluminum plates marginally exceed the allowable for that case. Moreover, other conservatisms, such as the use of rounded up acceleration value and worst-case thermal gradients, are built into the analysis. All other cases and basket components have stress ratios less than 1.0.

### Maximum Relative Deflection of the Basket



Absolute maximum relative deflections at all fuel compartments during the 51g side drops of 0°, 30°, and 45° orientations are summarized in Table 2.12.6-9. The relative deflection in the x direction is calculated for every node in Face 2 as x deflection minus the x deflection at corresponding Face 1 node. Similarly, the relative displacement in z direction is the difference in nodal deflections between Face 4 nodes and Face 3 nodes.

The results are calculated for all cell compartments and tabulated in Table 2.12.6-9. The maximum total relative deflection in the critical box is approximately 0.033 inch. It should be noted that the results presented are the total deflection at 51g; permanent deformation will be significantly less.

#### 2.12.6.2.3 Fuel Basket End Drop Analysis

During an end drop, the fuel assemblies and fuel compartments are forced against the bottom of the TN-32B HBU cask. It is important to note that, for any vertical or near vertical loading, the fuel assemblies react directly against the bottom or top end (bottom of closure lid) of the cask, and not through the basket structure as in lateral loading. It is the dead weight of the basket that results in axial compressive stress during an end drop. Axial compressive stresses are conservatively computed by assuming that all impact loads act on the compartment tubes during an end drop. A conservative basket weight of 14.0 kips (actual weight is 13.421 kips) is utilized in the end drop stress calculations.

#### Stainless Steel Basket Components

Assuming that all of the weight is supported by the stainless steel basket:

Area of steel baskets excluding area for drain cutouts:

$$A = 32[(w + 2t)^2 - w^2] = 32[(8.70 - 2.91) + 2(0.105)]^2 - (8.7-2.91)^2] = 79.30 \text{ in}^2$$

$$\text{Stress in steel baskets at 31g loading} = 31(P/A) = 31(14,000/79.3) = 5,473 \text{ psi}$$

$$\text{Stress in steel baskets at 90g loading} = 90(P/A) = 90(14,000/79.3) = 15,889 \text{ psi}$$

The stress generated in the stainless fuel compartments is summarized as shown in the following table.

Condition	Axial Stress (ksi)	Allowable Stress ( $P_m$ ) at 500 °F (ksi)
NCT (31g)	5.47	17.5
HAC (90g)	15.89	42.0

The maximum stress ( $P_m + P_b + Q$ ) for normal conditions, 9.56 ksi (5.47 ksi + maximum thermal stress of 4.09 ksi from Section 2.12.6.2.2), is also less than the criteria of 52.5 ksi ( $3S_m$ ).

#### 2.12.6.2.4 Fuel Basket Thermal Stress Analysis

An elastic ANSYS® finite element analysis (FEA) was conducted on the basket to evaluate the thermal stresses in the stainless steel and aluminum plates. Two different areas in the basket were analyzed, the first configuration (Model 1) included one 1.04-inch thick aluminum plate (2[0.5-inch thick aluminum plates] + 0.04-inch thick borated aluminum plate), and the second configuration (Model 2) included one 0.54-inch thick aluminum plate (0.5-inch thick aluminum plate + 0.04-inch thick borated aluminum plate). The models are similar except for the aluminum plate thickness and the centerline distance between the aluminum middle plate and stainless steel outer plates. The FEMs for both configurations are shown in Figure 2.12.6-28 and Figure 2.12.6-29.

The stainless steel plates are connected by beam elements representing the stainless steel bar and fusion welds. The aluminum plates are connected to the stainless steel bar via gap elements. Although a gap of 0.0 inches was utilized in the model, the actual nominal gap is 0.06 inches.

Elastic material properties that are described in Section 2.12.6.2.2B are utilized, and a uniform temperature of 470 °F is applied.

The maximum stress intensity in the aluminum plates is 2.51 ksi. The maximum stress intensity in the stainless steel plates is 4.09 ksi. The nodal stress intensity distribution in the stainless steel and aluminum plates are shown in Figure 2.12.6-30 through Figure 2.12.6-33 for both configurations.

#### 2.12.6.2.5 Basket Stress Analysis Conclusions

Stresses in the stainless steel plates and plug welds were calculated for the NCT and HAC cask drop cases. The results for the side drop analyses are summarized in Table 2.12.6-4 and Table 2.12.6-5 and Table 2.12.6-6 through Table 2.12.6-8 for the NCT and HAC cases, respectively. The results for the end drop analysis are summarized in Section 2.12.6.2.3. The thermal stresses in the stainless steel plates are provided in Section 2.12.6.2.4. All stresses meet the stress criteria presented in Table 2.12.6-2 and Table 2.12.6-3 for both NCT and HAC evaluations. For the 0° side drop case, the worst-case membrane plus bending stress ratio in the aluminum plates exceeds the allowable stress by 0.11%. This result is justified because the stainless steel plate stresses are well within the allowable limits.



### 2.12.6.3 Fuel Basket Buckling Analysis

#### 2.12.6.3.1 Analysis Approach

The nonlinear buckling analysis is performed utilizing an incremental load approach wherein an FEM (HAC model that is described in Section 2.12.6.2.2) with both material (bilinear kinematic hardening with stress relaxation) and geometric nonlinearities (contact elements, stress stiffening and large deflection effects). The model is then subjected to gradually increasing HAC side drop loads. Nonlinear elastic-plastic FEA is performed to obtain the load level at which buckling failure occurs, so that safety factors may be determined.

To reduce the model runtime and better solution convergence, a lower aluminum tangent modulus ( $E/E_p = 0.001\%$ ) is applied compared to the tangent modulus for stainless steel. This approach is conservative for the prediction of buckling loads.

The three critical azimuth drop orientations analyzed are:

- 0° (load applied in the direction parallel to the basket vertical plates)
- 30° (load applied at 30° relative to the basket vertical plate direction)
- 45° (load applied at 45° relative to the basket vertical plate direction)

#### 2.12.6.3.2 Buckling Analysis Loading Conditions

The basket structure was analyzed for 0°, 30° and 45° side drops. Due to basket structure symmetry, these orientations of side drops are assumed to envelop other possible drop cases of buckling.

Temperatures at the cross section where the maximum temperature occurred for the basket were utilized from the normal transport condition of 100 °F ambient.

Figure 2.12.6-1 illustrates the temperature contour utilized in all buckling analyses.

The load resulting from the fuel assembly weight was applied as pressure on the fuel compartment plates of the basket. At 0° orientation, the pressure acted only on the horizontal plates; while at 30° and 45° orientations, the pressure was divided in components to act on both horizontal and vertical plates of the basket. The pressures for different orientations are calculated below for 120g acceleration:

##### 0° Orientation

$$\begin{aligned}\text{Pressure for 1g, } p &= (\text{fuel assembly weight})/[(\text{panel span})(\text{panel length})] \\ &= (1,551 \text{ lb}_m)/[(8.805 \text{ in})(160 \text{ in})] = 1.10094 \text{ psi}\end{aligned}$$

$$\text{Pressure for 120g} = 120(1.10094) = 132.1124 \text{ psi}$$

##### 30° Orientation

$$\text{Pressure for 1g} \quad p_v = p \sin 30^\circ = 1.10094(0.50) = 0.5505 \text{ psi}$$

$$p_h = p \cos 30^\circ = 1.10094(0.8660) = 0.9534 \text{ psi}$$

$$\text{Pressure for 120g} \quad p_v = p \sin 30^\circ = 120(0.5505) = 66.0562 \text{ psi}$$

$$p_h = p \cos 30^\circ = 120(0.9534) = 114.4127 \text{ psi}$$

#### 45° Orientation

$$\text{Pressure for 1g} \quad p_v = p_h = p \cos 45^\circ = 1.10094(0.7071) = 0.7785 \text{ psi}$$

$$\text{Pressure for 120g} \quad = 120(0.7785) = 93.4176 \text{ psi}$$

The accelerations applied in each run are as follows.

Orientation (degrees)	Inertial Load (g)	a <sub>x</sub> (g)	a <sub>y</sub> (g)	a <sub>z</sub> (g)
0	120	120.0	0	0
30	120	103.923	0	60.0
45	120	84.853	0	84.853

The load distributions for the 30° bounding case are shown in Figure 2.12.6-34.

#### 2.12.6.3.3 Buckling Analysis and Results

A maximum load of 120g is applied to each analysis. For each analysis corresponding to the temperature boundary condition and a side drop orientation angle, the ANSYS® automatic time stepping option 'AUTOTS' is activated. This option allows the program to determine the actual size of the load sub-step for a converged solution. The program stops at the load sub-step that fails to result in a converged solution. The last load step with a converged solution is the buckling load.

The resulting buckling loads and factors of safety against the applied 51g drop load are summarized in Table 2.12.6-10. Displacement and stress intensity plots at the last converged sub-step (buckling load) for these load cases are shown in Figure 2.12.6-35 through Figure 2.12.6-37 and Figure 2.12.6-38 through Figure 2.12.6-40, respectively.

Since the computed buckling loads for the TN-32B HBU basket are greater, with reasonable factors of safety than the maximum applied 51g deceleration, the basket will not fail in buckling during the accident condition side drop event.

#### 2.12.6.4 Fusion Welds

The testing program for the fusion welds ensures that the fusion weld is stronger than the base metal. Section 2.12.6.2.2 calculates stresses in the base metal for normal condition of transport and hypothetical accident conditions and demonstrates that the calculated stresses are below the stress limits. If the stresses in the base metal are below the stress limits and fusion welds are stronger than the base metal, basket integrity is maintained and the welds are qualified.

The testing requirement for the weld nugget is provided in Note 2 of drawing 19885-71-6, Appendix 1.4.1. The testing program for the fusion welds that was implemented during the basket fabrication is provided below:

The fusion spot welds that attach the stainless steel tubes or adjacent structural shapes were performed by the gas tungsten arc welding (GTAW) fusion welding process, and were based on ANSI/AWS D1.3-89. This welding process produces a nugget of weld metal with a minimum 1/2-inch diameter weld shear area at the interface of the tubes and disk.

The GTAW machine welding parameters were preset and automated. For the production phase GTAW fusion spot welds, a 100% percent visual inspection verified the normality of the weld zone. In addition, a mechanical test of one test coupon from each welding machine used verified proper machine settings and operation prior to the start of each working shift. The acceptance criterion was failure of the base metal prior to failure of the weld area, and a visual verification of a 1/2-inch diameter fused weld zone. Any weld repairs were performed in accordance with weld repair procedures (WRP).

The visual acceptance criteria for the fabricated welds were performed as follows:

- Welds located up to 24 inches from the openings of the basket assemblies and directly visible were examined by direct visual inspection utilizing the same acceptance criteria as the workmanship samples.
- All other welds were examined by a remote visual inspection utilizing mirrors and auxiliary lighting. This inspection verified the location, configuration and uniformity of the welds.

Excessive defects will be ground out by mechanical means and re-welded. Lack of penetration was repaired by re-welding over the original weld zone. Re-inspection by visual methods to original standards was required. The automated GTAW fusion joining process was qualified utilizing the guidelines of American Society of Mechanical Engineers (ASME) Boiler and Pressure Vessel (B&PV) Code Section IX and Section VIII Appendix 17.

As part of the weld qualification procedure, nine test specimens were prepared and tested, and documented in a test report. All nine fusion spot welded specimens were prepared and visually inspected for surface soundness, fusion, and external nugget size. Three of the nine specimens were sectioned and microetched.

The acceptance criteria were as follows. The fusion zone shall be sound with complete fusion along the bond line and a 3/32-inch weld penetration into the disk component. There shall be complete freedom from cracks along the bond line and the adjacent heat affected base metal. Small radial cracks at the center of the weld shall be considered non-relevant unless they exceed 1/8-inch in length, as measured from the center of the weld to the end of the crack. The diameter of the weld nugget shall be at least 1/2 inch.

Undercut was considered non-relevant provided thorough fusion exists between the weld and base metal around the circumference of the weld, and the length of the undercut does not exceed 3/16 inch.

Weld reinforcement ranged from 0.10-inch cavity (dish) to 1/16 inch to preclude interference with the test gage.

One of the three sectioned specimens underwent weld zone analysis and testing for delta ferrite in accordance with NF-2433.1 [2]. Delta ferrite testing was performed on weld samples prepared from each combination of sheet and disk heats to be spot welded together. The acceptance criterion was also in accordance with NF-2433.2.

Peel tests were performed on three other specimens, and the acceptance criteria were as follows. The parent metal adjacent to the weld area must fail prior to the weld. The weld nugget at the bond line shall be free of defects, and shall be at least 1/2-inch in diameter. Three test specimens shall mechanically be tested to failure. The base metal must fail prior to the weld zone.

#### 2.12.6.5 Conclusions

Linear elastic analyses with small deflection effects (NCT) and nonlinear analyses with bilinear material properties and large deflections effects (HAC) were performed in ANSYS® for the critical azimuth side drop orientations to determine the membrane and membrane plus bending stresses in all basket components. It was shown that the stresses from the side and end drops are below allowable stress limits for both NCT and HAC free drop impacts. For the NCT analyses, steel tubes, including the intermediate aluminum plates, are connected together in the out-of-plane direction so that they will bend in unison under surface pressure or other lateral loading to simulate the through thickness support provided by the aluminum and borated aluminum plates. For the HAC analyses, the steel tube-aluminum plates, steel tube-rails, and rail-containment interactions are modeled using 3-D node-to-node contact elements that allow only compression in the contact normal directions and with zero friction. The HAC analysis model has both material (bilinear kinematic hardening with stress relaxation) and geometric nonlinearities (contact elements, stress stiffening and large deflection effects).

The nonlinear HAC model was used to determine the critical buckling load for the basket, except large displacement and stress stiffening options were used. The buckling analyses are reported in Section 2.12.6.3. From these analyses, a minimum buckling load of 92.75g was determined.

ANSYS® buckling analyses performed in Sections 2.12.6.3 and 2.12.6.5 for an 8-inch sector assumes temperatures at the hottest section for the 100 °F ambient conditions. The minimum calculated buckling load of 92.75g provides sufficient safety factors for all loading conditions (basket baseline g loads are provided in Section 2.7.1 of Chapter 2).

#### 2.12.6.6 References

1. ANSYS® Finite Element Computer Code, Version 17.1, ANSYS, Inc., Canonsburg, PA.
2. ASME Boiler and Pressure Vessel Code, Section III, Subsection NB, NF, and Appendices; Section VIII, Divisions I and 2, 1992 Edition.
3. "Aluminum Standards and Data," The Aluminum Association, Inc., 1976.

4. ASME Boiler and Pressure Vessel Code, Section II, Materials Specifications, Part D, 2013 Edition.

**Table 2.12.6-1**  
**Material Properties for TN-32B HBU Cask Fuel Basket**

Part	Material	Temperature (°F)	S <sub>y</sub> (ksi)	S <sub>u</sub> (ksi)	E (psi×10 <sup>6</sup> )	α <sub>m</sub> (in/in/°F)	Density (lb <sub>m</sub> /in <sup>3</sup> )
Aluminum Plates	SB-209, Type 6061-T651	70	35.00	42.00	10.0	-	0.098
		200	33.20	36.70	9.6	12.91 × 10 <sup>-6</sup>	
		300	27.40	31.70	9.2	13.22 × 10 <sup>-6</sup>	
		400	13.30	17.70	8.7	13.52 × 10 <sup>-6</sup>	
		500	4.38	7.00	8.1	-	
Stainless Steel Plates	SA-240, Type 304	70	30.00	75.00	28.3	8.5 × 10 <sup>-6</sup>	0.59051 (NCT)
		200	25.00	71.00	27.6	9.4 × 10 <sup>-6</sup>	
		300	22.50	66.00	27.0	9.9 × 10 <sup>-6</sup>	0.290 (HAC)
		400	20.70	64.40	26.5	10.2 × 10 <sup>-6</sup>	
		500	19.40	63.50	25.8	10.5 × 10 <sup>-6</sup>	

## Notes:

- Material properties are obtained from ASME B&PV Code Section III Appendices [2]. Aluminum material properties at elevated temperatures are obtained from aluminum standards and data 2.12.6.6. ANSYS® accepts only a maximum of six property data points to be associated with temperature table.
- Thermal expansion coefficients for stainless steel are extracted from Reference [4].
- For NCT, linear elastic material properties are used. For HAC, 5% of the elastic modulus used as the tangent modulus for stainless steel. For aluminum alloy, 1% of the elastic modulus is used as the tangent modulus.
- The material densities of the individual components are adjusted to capture missing weights / details that were not modeled in ANSYS®. For NCT, the weights of aluminum and borated aluminum plates are included in the weight of the stainless steel plates. For HAC, borated aluminum plate weights are included in the weight of aluminum plates. Moreover, the densities of the stainless steel plates, aluminum plates and aluminum rails are individually adjusted to match the weights of the basket parts.

**Table 2.12.6-2**  
**Basket Structural Allowable Stresses, NCT**

<b>Material</b>	<b>Temperature (°F)</b>	<b>P<sub>m</sub> (S<sub>m</sub> or S) (ksi)</b>	<b>P<sub>m</sub> + P<sub>b</sub> (1.5S<sub>m</sub> or 1.5S) (ksi)</b>
SB-209 Type 6061-T651	70	10.50	15.75
	300	8.40	12.60
	400	4.40	6.60
	500	-	-
SA-240 Type 304	70	20.00	30.00
	300	20.00	30.00
	400	18.70	28.05
	500	17.50	26.25

**Table 2.12.6-3  
Basket Structural Allowable Stresses, HAC**

<b>Material</b>	<b>Temperature (°F)</b>	<b><math>P_m</math> (<math>0.7S_u</math> or <math>S_y+1/3[S_u-S_y]</math>) (ksi)</b>	<b><math>P_m + P_b</math> (<math>0.9 S_u</math>) (ksi)</b>
SB-209 Type 6061-T651	70	37.33	37.80
	300	28.83	28.53
	400	14.77	15.93
	500	5.25	6.30
SA-240 Type 304	70	52.50	67.50
	300	46.20	59.40
	400	45.08	57.96
	500	44.45	57.15

Note:

1. As nonlinear elastic-plastic analysis is used to evaluate accident conditions, the general membrane stress intensity,  $P_m$ , shall not exceed the greater of  $0.7S_u$  and  $S_y+1/3(S_u - S_y)$



**Table 2.12.6-4**  
**NCT 0° Side Drop, Basket Stress Analysis Results**

Component	Stress <sup>(1)</sup> Location	Stress Category	Stress (13g) (ksi)	Temperature (°F)	Allowable Stress (ksi)
Stainless Steel Boxes and Plates	Max Stress	P <sub>m</sub>	4.90	364.3	19.16
		P <sub>m+b</sub>	12.21	409.7	27.88
	Min F.S.	P <sub>m</sub>	4.90	381.0	18.95
		P <sub>m+b</sub>	12.21	412.6	27.82

Note:

1. Since the allowable stress is based on the temperature of the location where the stress is occurring, two locations are reported: Max Stress and Min F.S., where:

Max Stress: Location where maximum stress is occurring regardless of the allowable stress at that location

Min F.S.: Location where the factor of safety is minimum, based on the allowable stress at that location

**Table 2.12.6-5**  
**NCT 45° Side Drop, Basket Stress Analysis Results**

Component	Stress <sup>(1)</sup> Location	Stress Category	Stress (13g) (ksi)	Temperature (°F)	Allowable Stress (ksi)
Stainless Steel Boxes and Plates	Max Stress	P <sub>m</sub>	3.27	393.0	18.79
		P <sub>m+b</sub>	9.88	399.6	28.06
	Min F.S.	P <sub>m</sub>	3.22	424.3	18.41
		P <sub>m+b</sub>	9.87	405.6	27.95

Note:

1. Since the allowable stress is based on the temperature of the location where the stress is occurring, two locations are reported: Max Stress and Min F.S., where:

Max Stress: Location where maximum stress is occurring regardless of the allowable stress at that location

Min F.S.: Location where the factor of safety is minimum based on the allowable stress at that location

**Table 2.12.6-6**  
**HAC 0° Side Drop, Basket Stress Analysis Results**

Component	Stress <sup>(1)</sup> Location	Stress Category	Stress (51g) (ksi)	Temperature (°F)	Allowable Stress (ksi)
Stainless Steel Boxes and Plates	Max Stress	$P_m$	22.92	403.3	45.06
		$P_m + P_b$	30.45	390.2	58.10
	Min F.S.	$P_m$	22.92	403.3	45.06
		$P_m + P_b$	30.45	390.2	58.10
Aluminum Plates	Max Stress	$P_m$	8.46	371.1	18.84
		$P_m + P_b$	18.79	377.3	18.79
	Min F.S.	$P_m$	8.36	390.0	16.17
		$P_m + P_b$	18.71 <sup>(2)</sup>	378.1	18.69 <sup>(2)</sup>
Aluminum Rails Type 1	Max Stress	$P_m$	7.66	338.3	23.45
		$P_m + P_b$	7.96	338.3	23.71
	Min F.S.	$P_m$	7.65	340.9	23.08
		$P_m + P_b$	7.95	340.9	23.38
Aluminum Rails Type 2	Max Stress	$P_m$	9.43	297.8	28.91
		$P_m + P_b$	25.86	300.4	28.48
	Min F.S.	$P_m$	9.43	297.8	28.91
		$P_m + P_b$	25.85	302.9	28.16

## Notes:

- Since the allowable stress is based on the temperature of the location where the stress is occurring, two locations are reported: Max Stress and Min F.S., where:
  - Max Stress: Location where maximum stress is occurring regardless of the allowable stress at that location
  - Min F.S.: Location where the factor of safety is minimum based on the allowable stress at that location
- $P_{m+b}$  stress slightly exceeds the allowable stress.

**Table 2.12.6-7  
HAC 30° Side Drop, Basket Stress Analysis Results**

Component	Stress <sup>(1)</sup> Location	Stress Category	Stress (51g) (ksi)	Temperature (°F)	Allowable Stress (ksi)
Stainless Steel Boxes and Plates	Max Stress	P <sub>m</sub>	20.30	403.3	45.06
		P <sub>m</sub> + P <sub>b</sub>	30.74	390.2	58.10
	Min F.S.	P <sub>m</sub>	20.30	403.3	45.06
		P <sub>m</sub> + P <sub>b</sub>	30.74	390.2	58.10
Aluminum Plates	Max Stress	P <sub>m</sub>	7.72	386.7	16.64
		P <sub>m</sub> + P <sub>b</sub>	18.18	380.7	18.36
	Min F.S.	P <sub>m</sub>	7.71	387.4	16.54
		P <sub>m</sub> + P <sub>b</sub>	17.34	387.7	17.48
Aluminum Rails Type 1	Max Stress	P <sub>m</sub>	6.77	335.3	23.87
		P <sub>m</sub> + P <sub>b</sub>	10.20	315.1	26.63
	Min F.S.	P <sub>m</sub>	6.76	337.9	23.50
		P <sub>m</sub> + P <sub>b</sub>	10.20	315.1	26.63
Aluminum Rails Type 2	Max Stress	P <sub>m</sub>	13.26	289.9	29.21
		P <sub>m</sub> + P <sub>b</sub>	24.83	290.7	28.90
	Min F.S.	P <sub>m</sub>	13.25	292.3	29.12
		P <sub>m</sub> + P <sub>b</sub>	24.81	293.2	28.81

Note:

- Since the allowable stress is based on the temperature of the location where the stress is occurring, two locations are reported: Max Stress and Min F.S., where:

Max Stress: Location where maximum stress is occurring regardless of the allowable stress at that location

Min F.S.: Location where the factor of safety is minimum based on the allowable stress at that location

**Table 2.12.6-8  
HAC 45° Side Drop, Basket Stress Analysis Results**

Component	Stress <sup>(1)</sup> Location	Stress Category	Stress (51g) (ksi)	Temperature (°F)	Allowable Stress (ksi)
Stainless Steel Boxes and Plates	Max Stress	P <sub>m</sub>	19.59	387.5	45.22
		P <sub>m</sub> + P <sub>b</sub>	32.70	379.7	58.25
	Min F.S.	P <sub>m</sub>	19.59	387.5	45.22
		P <sub>m</sub> + P <sub>b</sub>	32.70	379.7	58.25
Aluminum Plates	Max Stress	P <sub>m</sub>	7.70	373.0	18.57
		P <sub>m</sub> + P <sub>b</sub>	18.69	370.3	19.67
	Min F.S.	P <sub>m</sub>	6.63	392.2	15.86
		P <sub>m</sub> + P <sub>b</sub>	17.18	388.1	17.43
Aluminum Rails Type 1	Max Stress	P <sub>m</sub>	8.57	334.4	23.99
		P <sub>m</sub> + P <sub>b</sub>	12.34	315.1	26.63
	Min F.S.	P <sub>m</sub>	8.57	334.4	23.99
		P <sub>m</sub> + P <sub>b</sub>	12.34	315.1	26.63
Aluminum Rails Type 2	Max Stress	P <sub>m</sub>	17.88	289.9	29.21
		P <sub>m</sub> + P <sub>b</sub>	27.43	290.7	28.90
	Min F.S.	P <sub>m</sub>	17.86	292.3	29.12
		P <sub>m</sub> + P <sub>b</sub>	27.35	293.2	28.81

Note:

Since the allowable stress is based on the temperature of the location where the stress is occurring, two locations are reported: Max Stress and Min F.S., where:

Max Stress: Location where maximum stress is occurring regardless of the allowable stress at that location

Min F.S.: Location where the factor of safety is minimum based on the allowable stress at that location

**Table 2.12.6-9**  
**HAC Cask Drop – Maximum Relative Deflection of the Basket at all Cell Compartments**

Cell #	Relative Deflection (inch)					
	0 Degree Drop		30 Degree Drop		45 Degree Drop	
	UX	UZ	UX	UZ	UX	UZ
1	0.010	0.011	0.006	0.017	0.003	0.023
2	0.011	0.010	0.008	0.006	0.005	0.006
3	0.011	0.001	0.011	0.001	0.010	0.002
4	0.012	0.011	0.005	0.006	0.001	0.010
5	0.004	0.006	0.008	0.021	0.007	0.028
6	0.005	0.002	0.005	0.004	0.004	0.005
7	0.002	0.002	0.001	0.002	0.000	0.002
8	0.001	0.011	0.002	0.006	0.002	0.005
9	0.005	0.005	0.005	0.004	0.004	0.006
10	0.004	0.007	0.002	0.005	0.002	0.007
11	0.004	0.002	0.006	0.013	0.006	0.019
12	0.009	0.002	0.008	0.002	0.008	0.002
13	0.009	0.002	0.009	0.002	0.008	0.002
14	0.009	0.004	0.008	0.005	0.006	0.007
15	0.009	0.002	0.007	0.003	0.006	0.004
16	0.004	0.002	0.006	0.004	0.006	0.007
17	0.003	0.003	0.004	0.013	0.003	0.018
18	0.002	0.008	0.002	0.004	0.003	0.003
19	0.006	0.011	0.005	0.006	0.004	0.004
20	0.006	0.001	0.005	0.006	0.004	0.008
21	0.002	0.001	0.002	0.003	0.002	0.004
22	0.004	0.001	0.003	0.008	0.002	0.010
23	0.020	0.007	0.018	0.014	0.017	0.023
24	0.004	0.012	0.002	0.004	0.002	0.003
25	0.004	0.011	0.004	0.005	0.004	0.004
26	0.004	0.001	0.004	0.004	0.004	0.004
27	0.004	0.003	0.005	0.006	0.004	0.009
28	0.020	0.002	0.021	0.011	0.021	0.015
29	0.029	0.002	0.026	0.008	0.021	0.015
30	0.033	0.005	0.029	0.003	0.024	0.003
31	0.033	0.002	0.029	0.002	0.023	0.002
32	0.029	0.005	0.026	0.009	0.021	0.012
<b>Max</b>	<b>0.033</b>	<b>0.012</b>	<b>0.029</b>	<b>0.021</b>	<b>0.024</b>	<b>0.028</b>

**Table 2.12.6-10**  
**Nonlinear Buckling – Results Summary**

Basket Side Drop Orientation	Maximum Load Used in Analyses			Last Converged Load (g)	Actual Maximum Load (g)	Factor of Safety
	Maximum. Acceleration (g)	Vertical Pressure (psi)	Horizontal Pressure (psi)			
0°	120	132.11	0	93.00	51	1.82
30°	120	66.056	114.41	92.75	51	1.82
45°	120	93.418	93.418	97.38	51	1.91

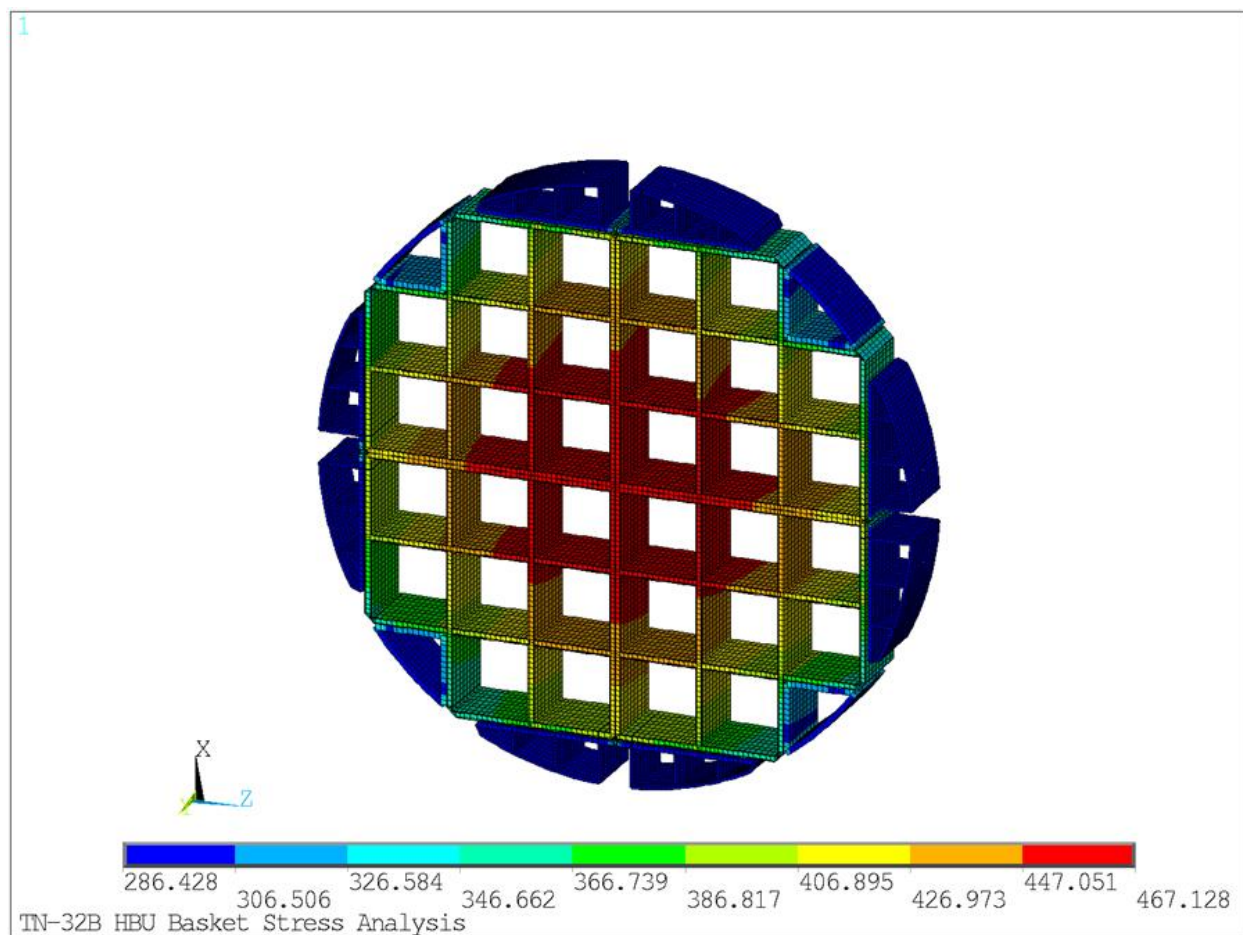


**Figure 2.12.6-1**  
**HAC Temperature Boundary Condition**



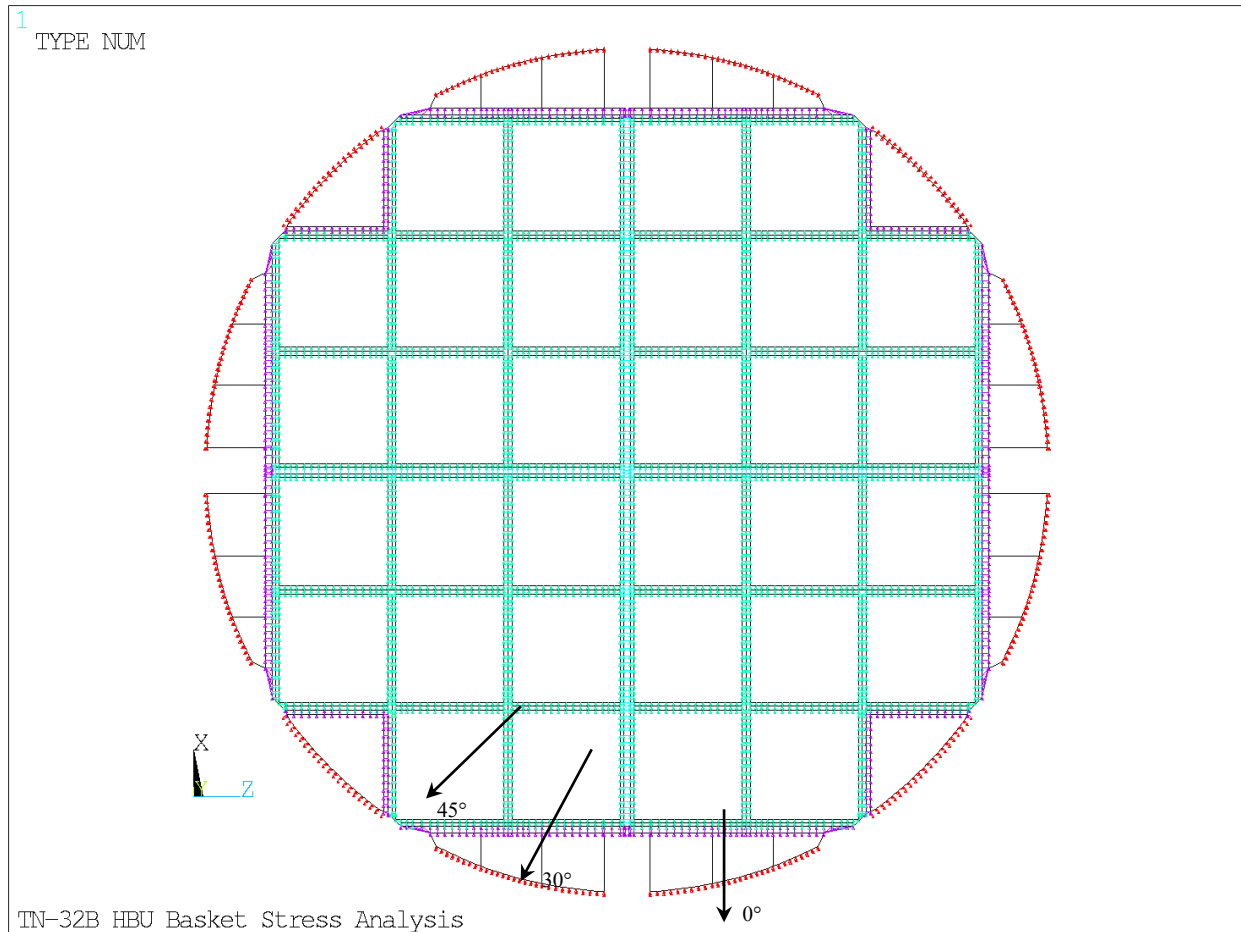


**Figure 2.12.6-2**  
**Basket Drop Orientations – HAC Side Drop**

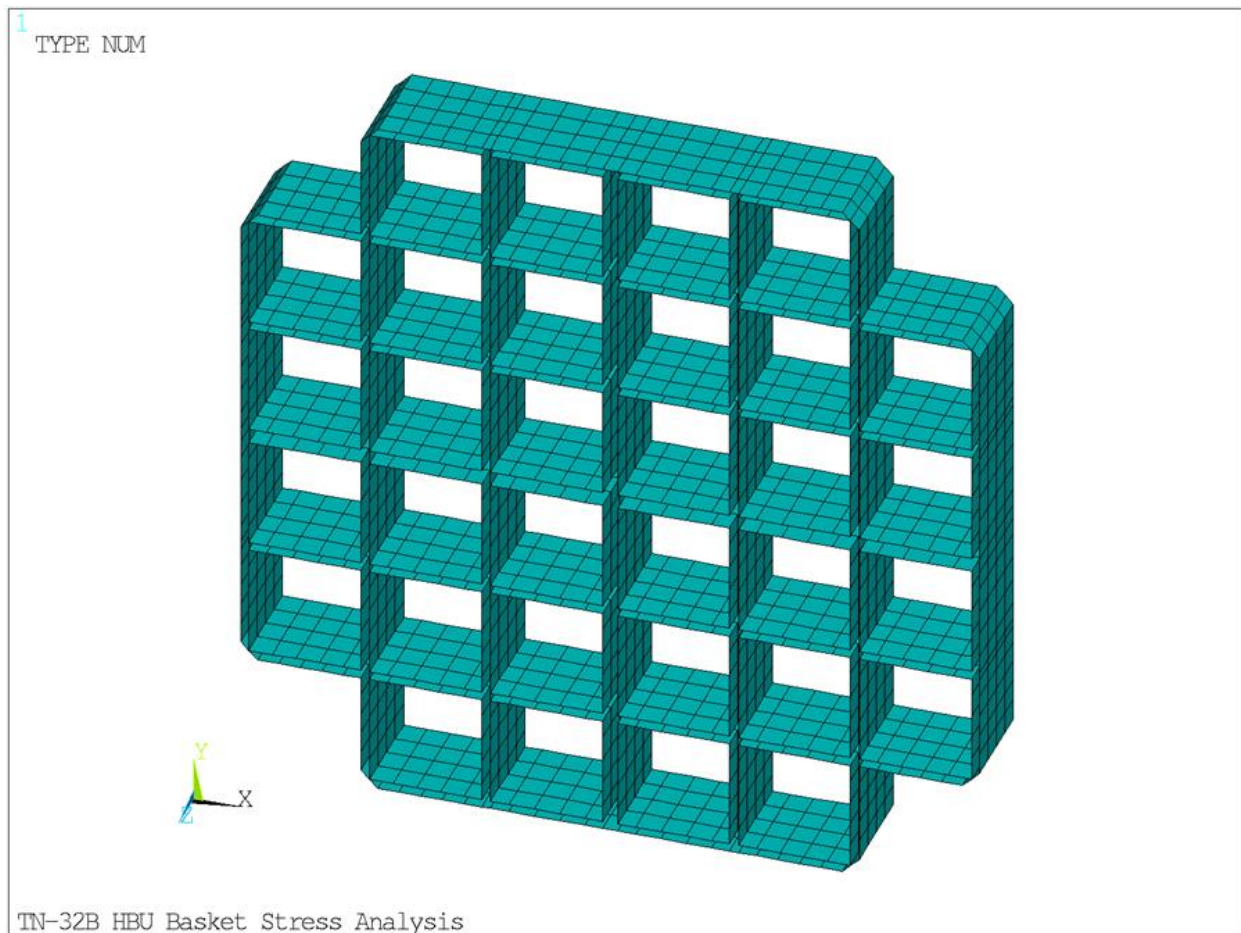


**Figure 2.12.6-3**  
**NCT Finite Element Model for Lateral Load Evaluation**

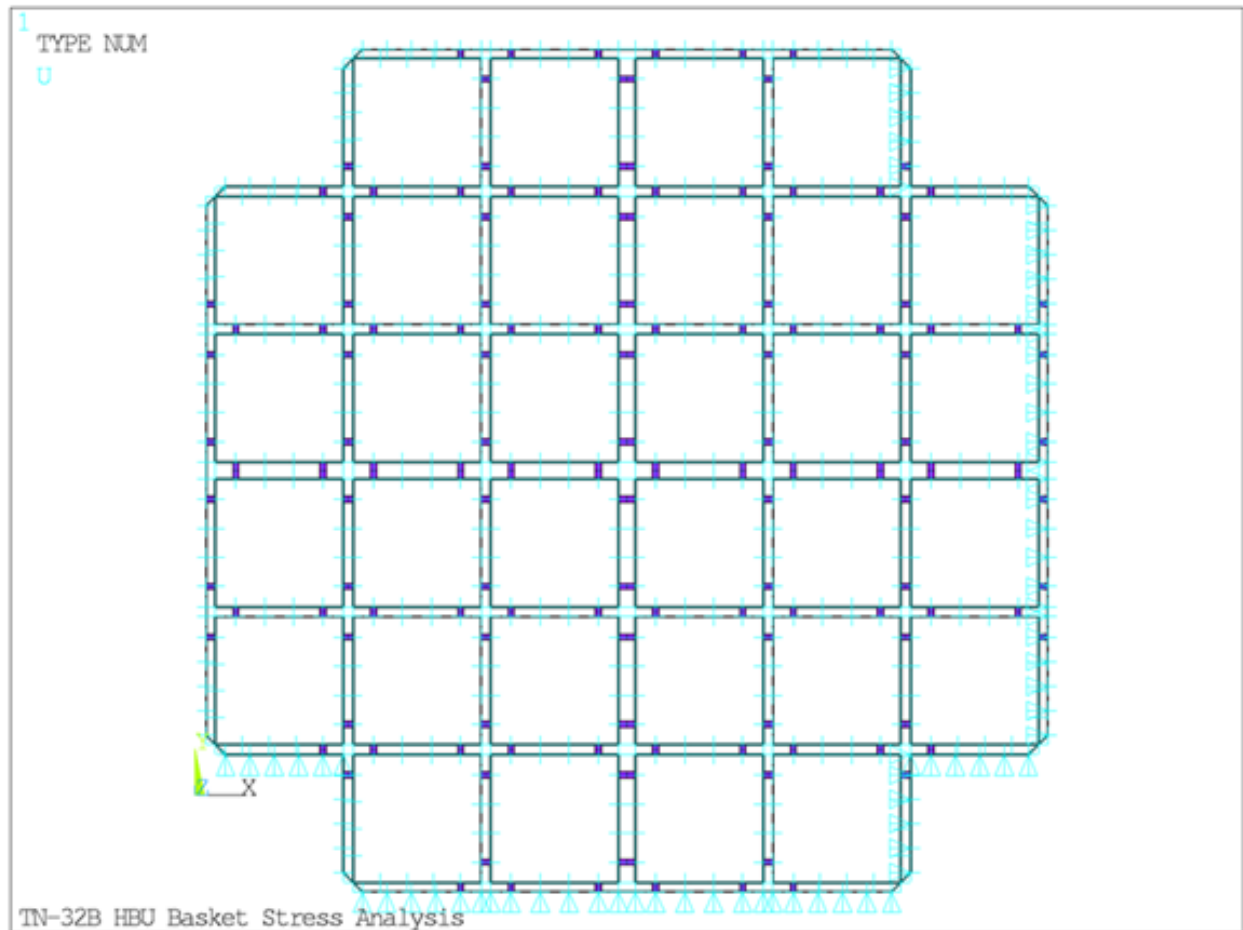
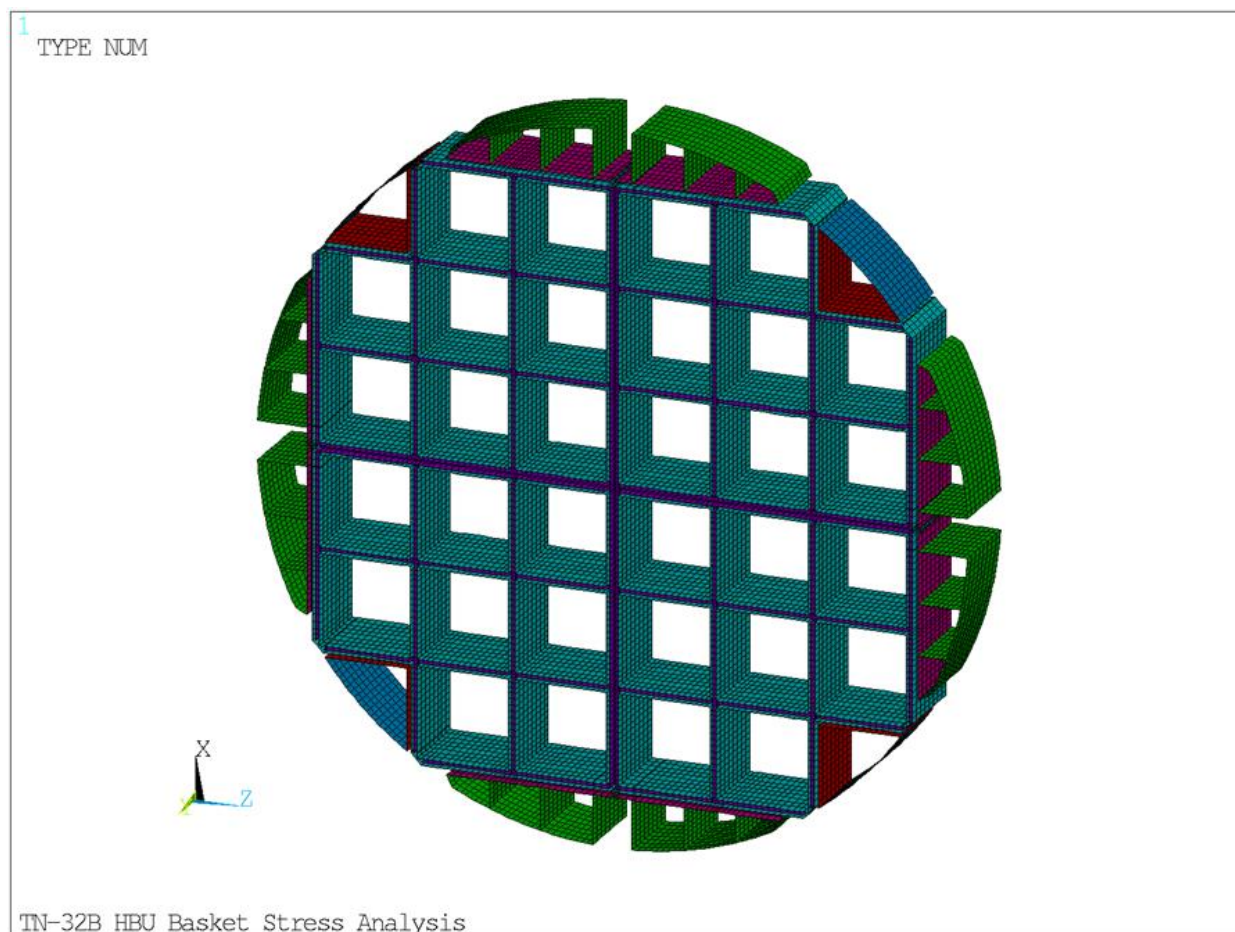


**Figure 2.12.6-4**  
**NCT Displacement Constraints – 45° Side Drop**



Note: Contact, beam and spring elements were unselected (hidden) for simplification in this view.

**Figure 2.12.6-5**  
**HAC Finite Element Model for Lateral Load Evaluation**

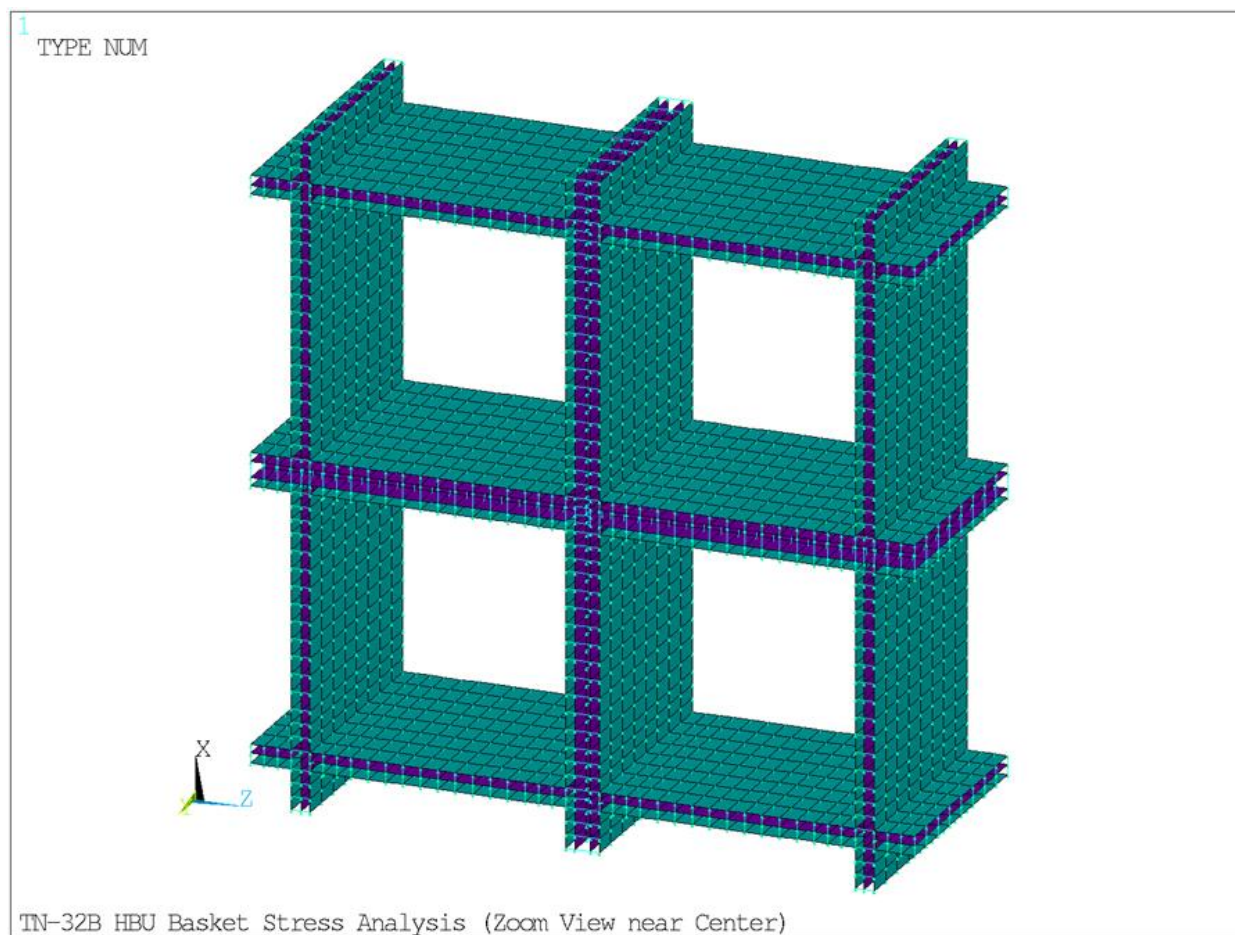


**Figure 2.12.6-6**  
**HAC Finite Element Model for Lateral Load Evaluation – Zoom View near Center**

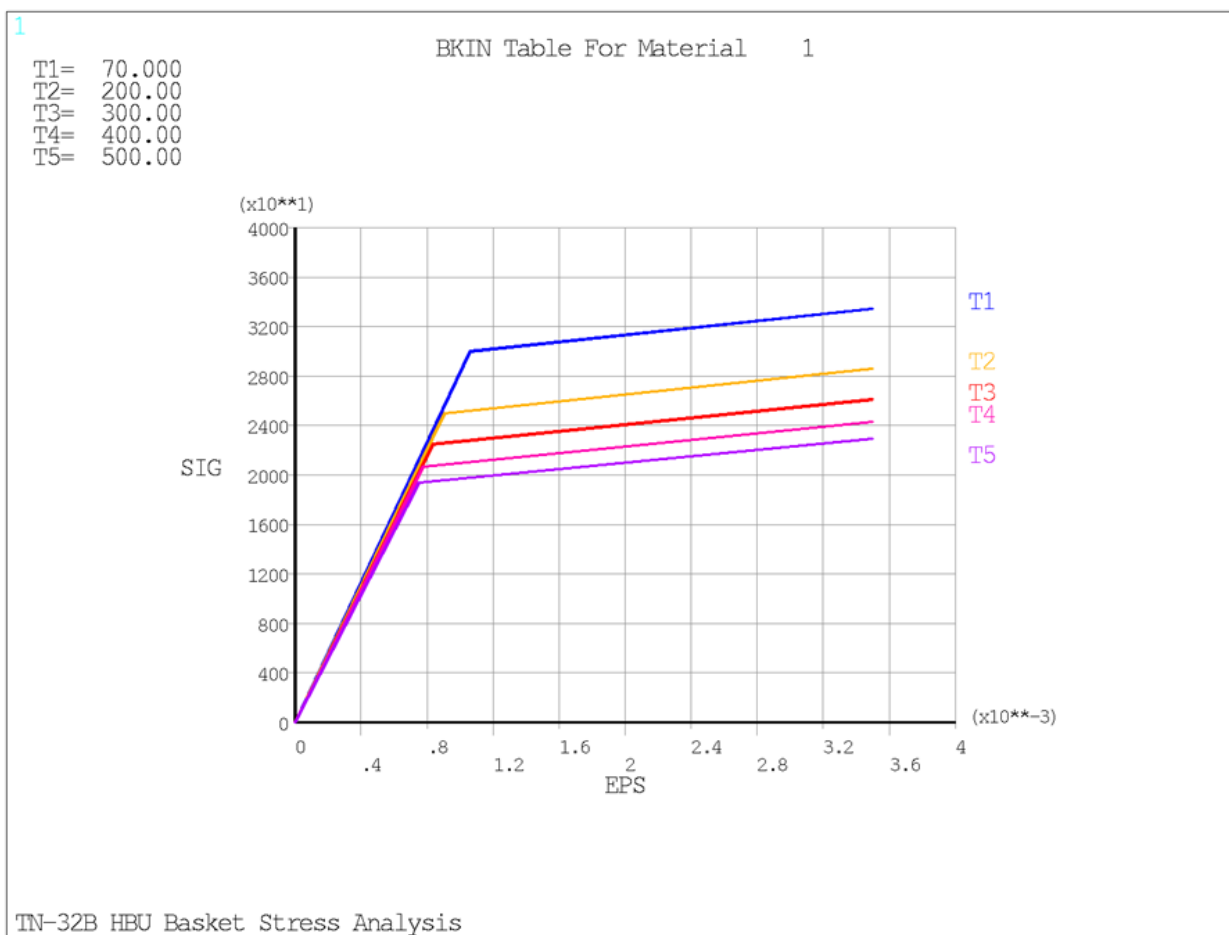


**Figure 2.12.6-7**  
**Material Properties – SA-240 Type 304 – ANSYS® BKIN Model**

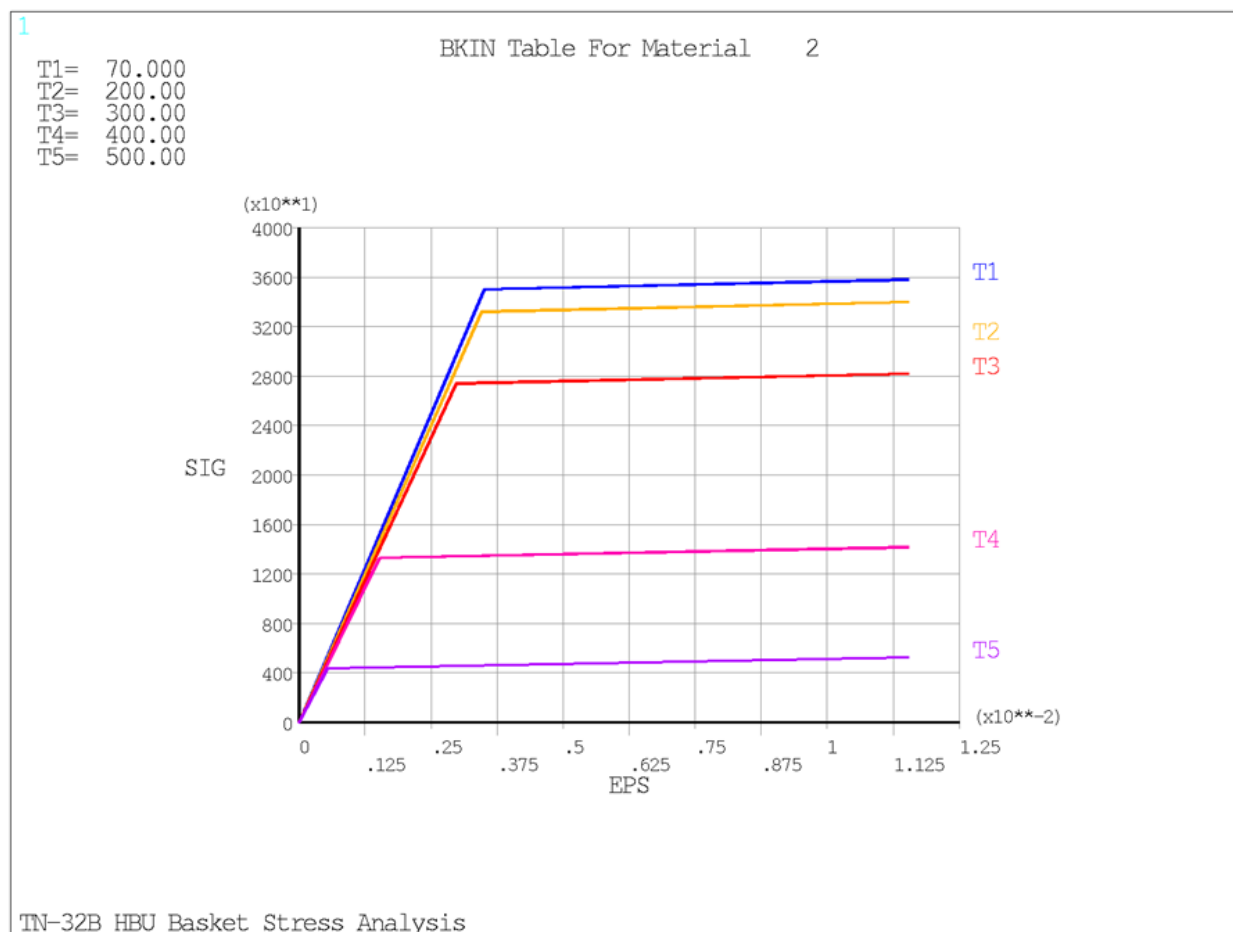


**Figure 2.12.6-8**  
**Material Properties – SB-209 Type 6061-T651 – ANSYS® BKIN Model**

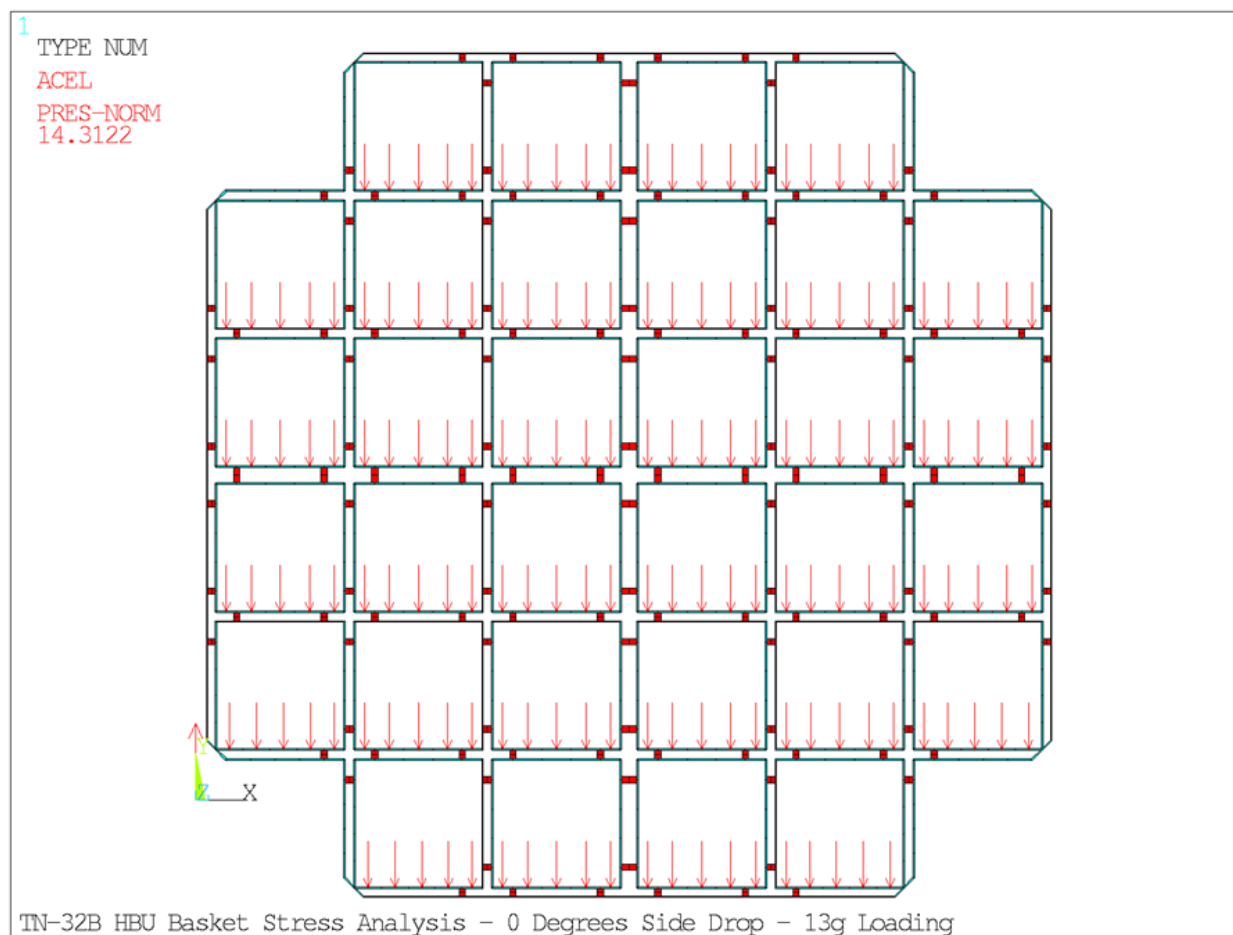


**Figure 2.12.6-9**  
**Loading Boundary Conditions – NCT Side Drop – 0°**



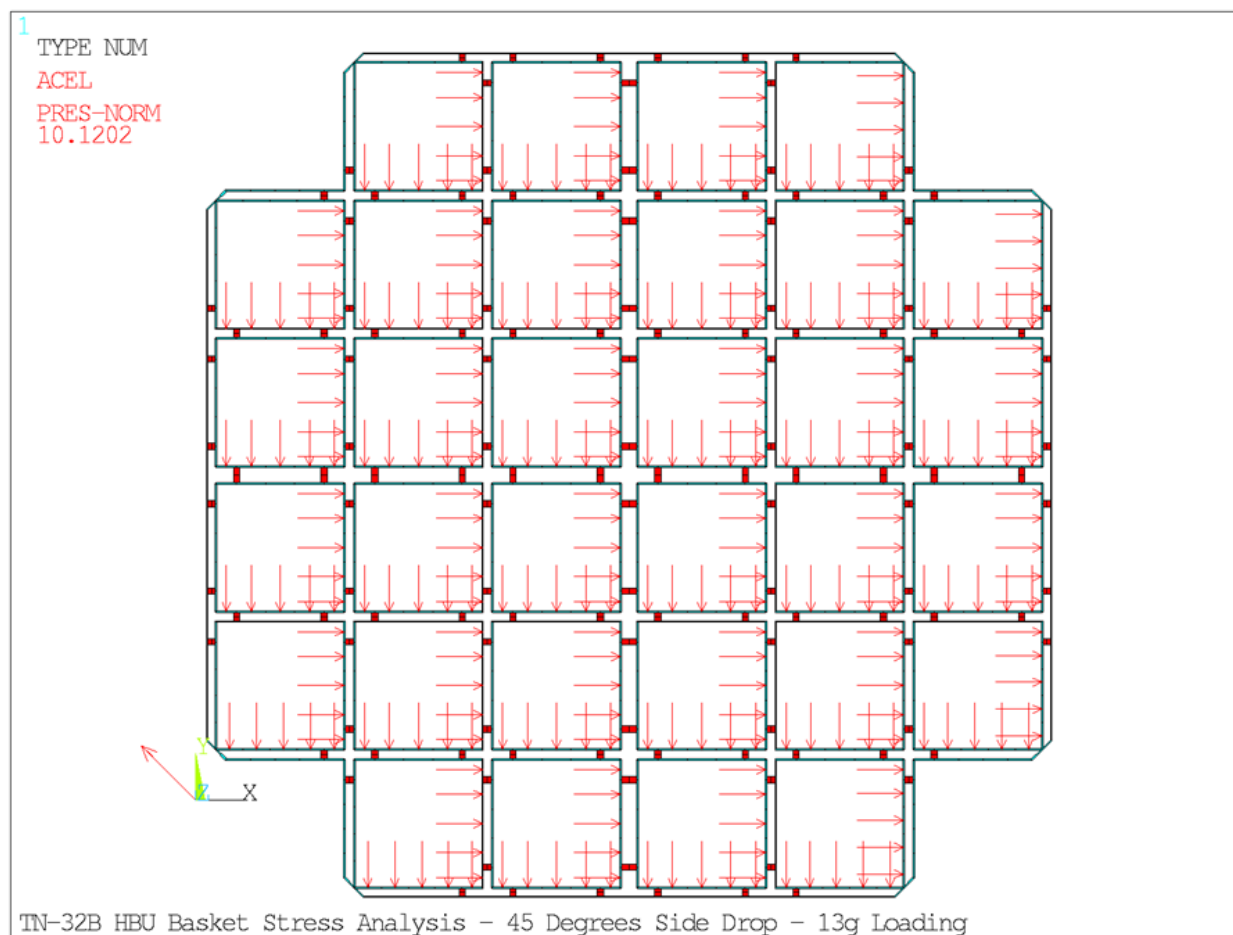


**Figure 2.12.6-10**  
**Loading Boundary Conditions – NCT Side Drop – 45°**

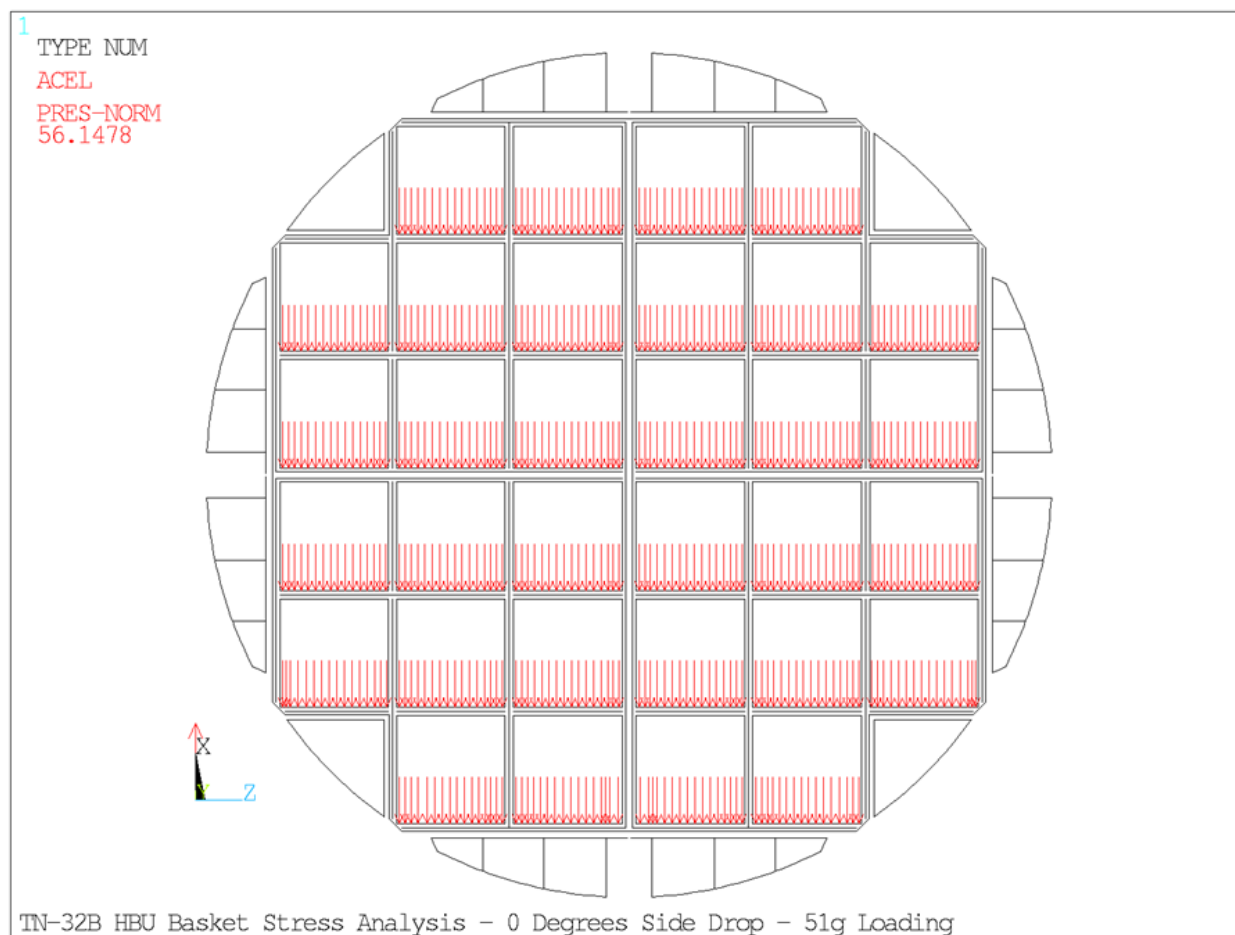


**Figure 2.12.6-11**  
**Loading Boundary Conditions – HAC Side Drop – 0°**

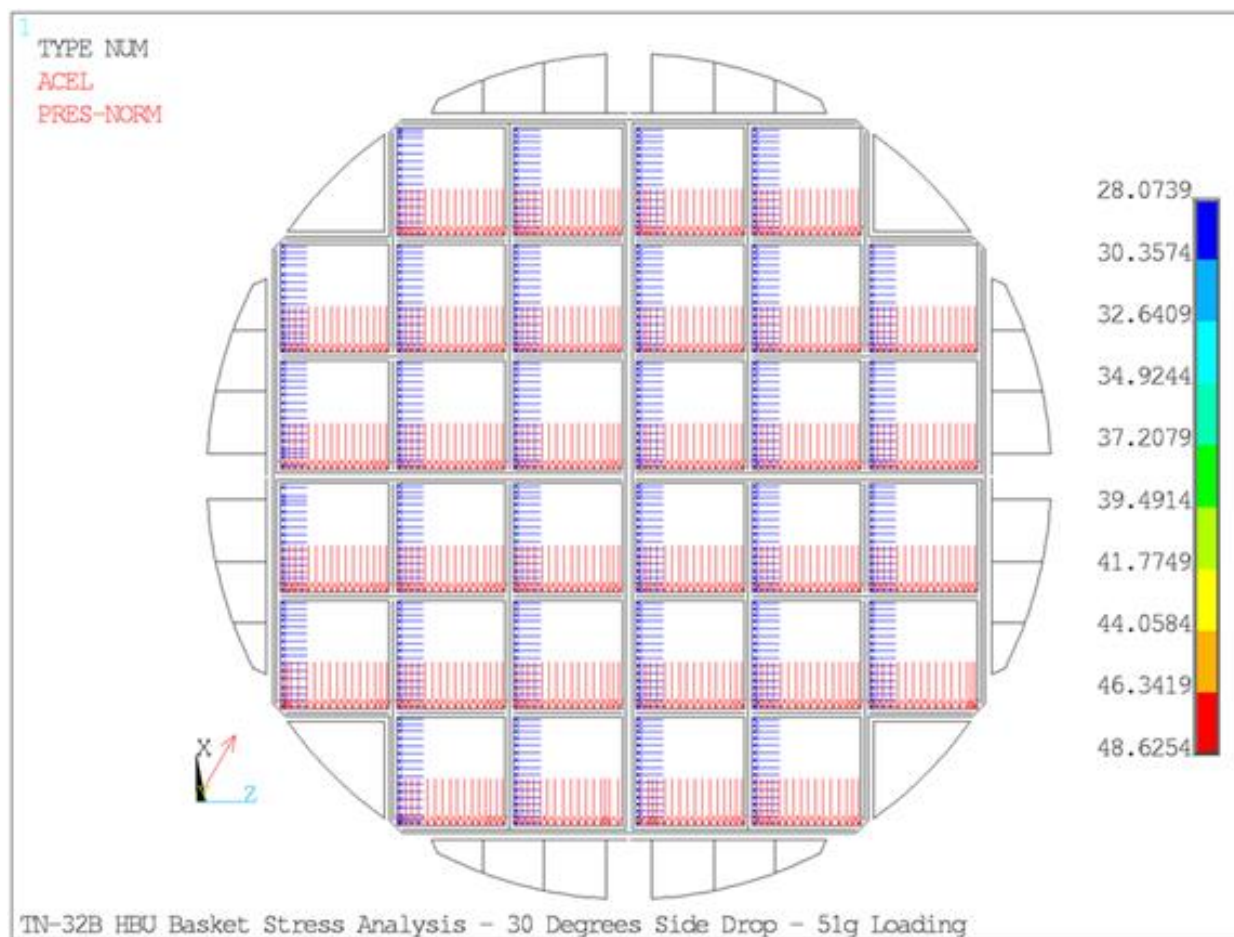


**Figure 2.12.6-12**  
**Loading Boundary Conditions - HAC Side Drop – 30°**

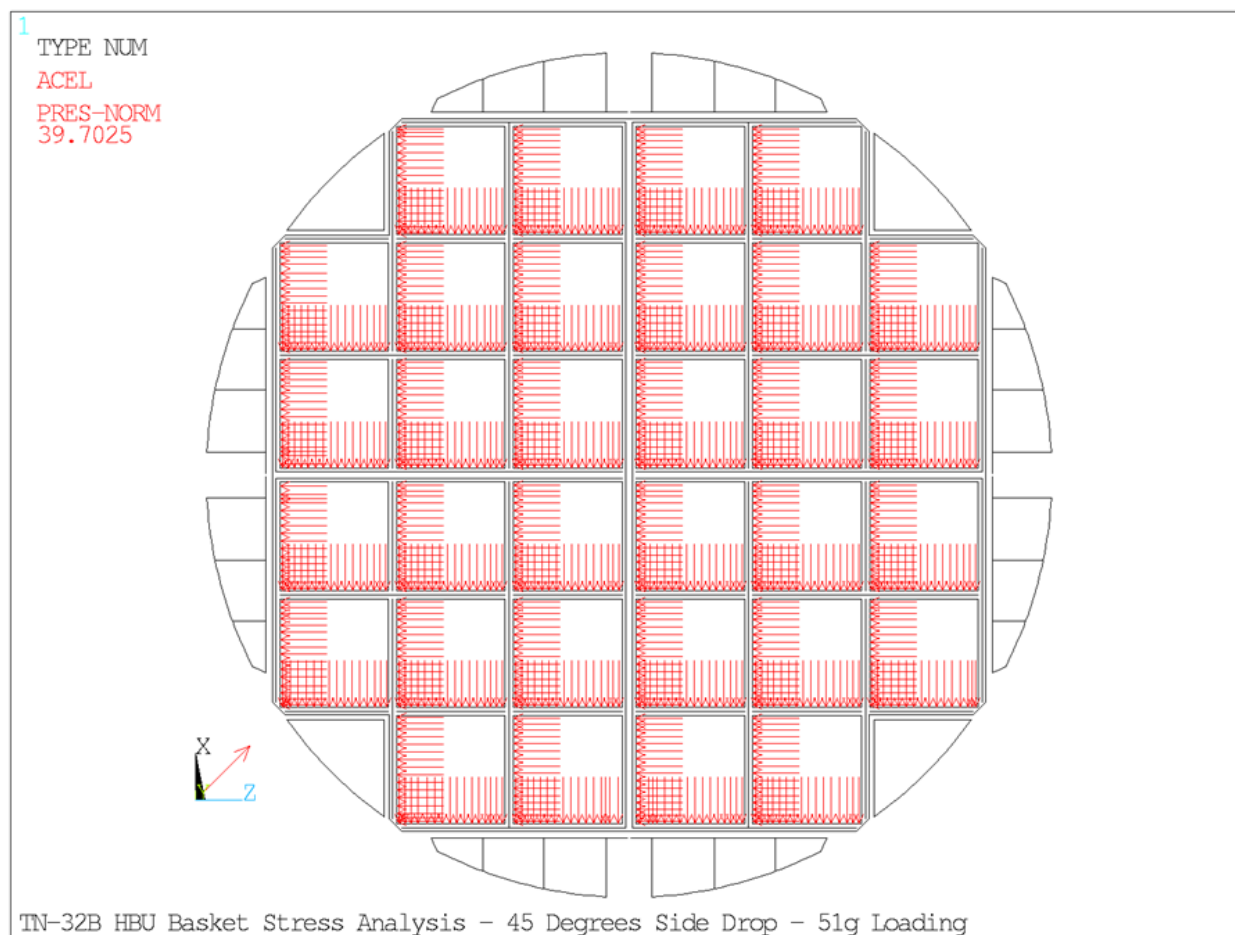


**Figure 2.12.6-13**  
**Loading Boundary Conditions – HAC Side Drop – 45°**

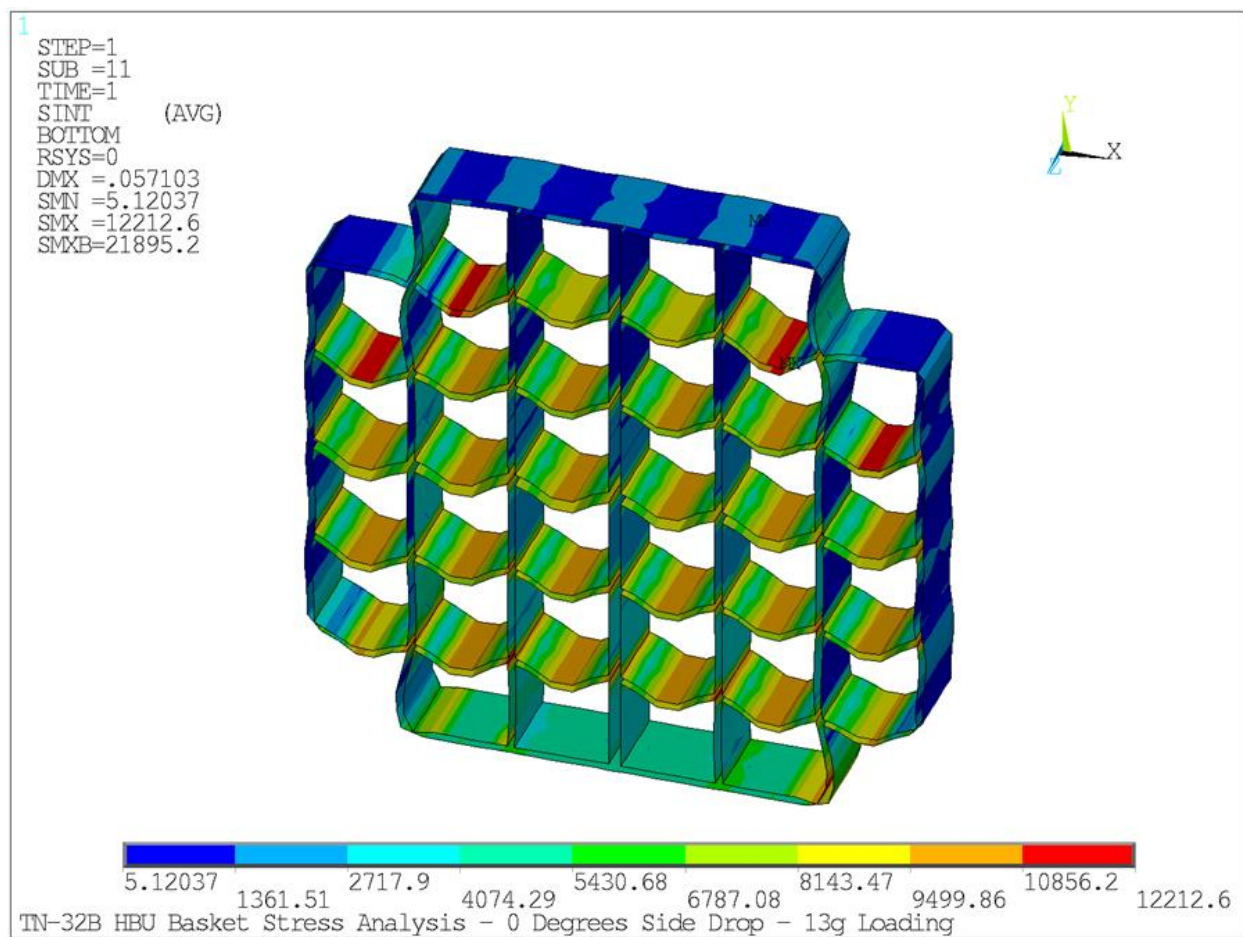


**Figure 2.12.6-14**  
**NCT 0° Side Drop – Stainless Steel Plates – Membrane plus Bending Stress Intensity at Bottom Face**

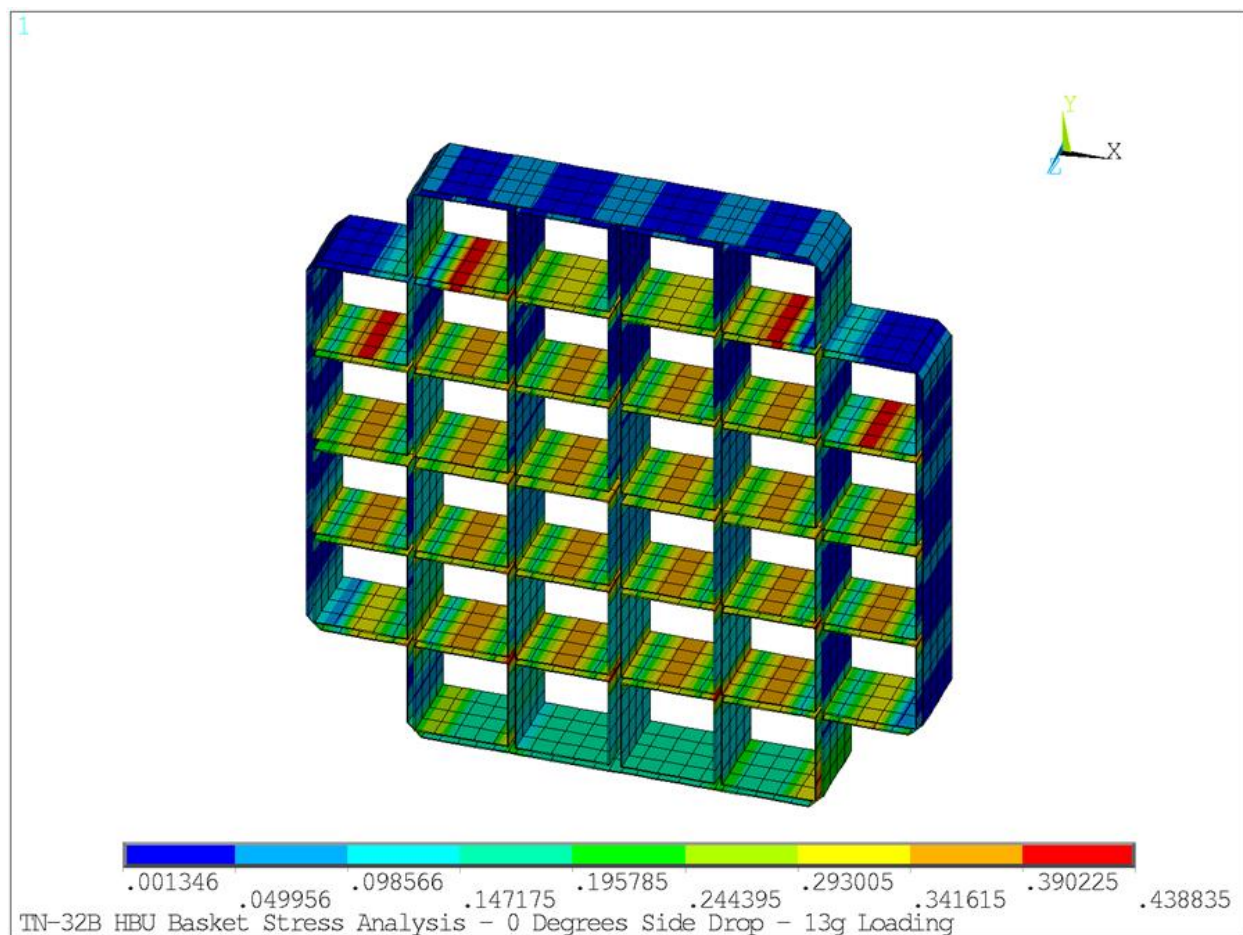


**Figure 2.12.6-15**  
**NCT 0° Side Drop – Stainless Steel Plates – Primary Membrane plus Bending Stress**  
**Ratio Plot – Bottom Face**



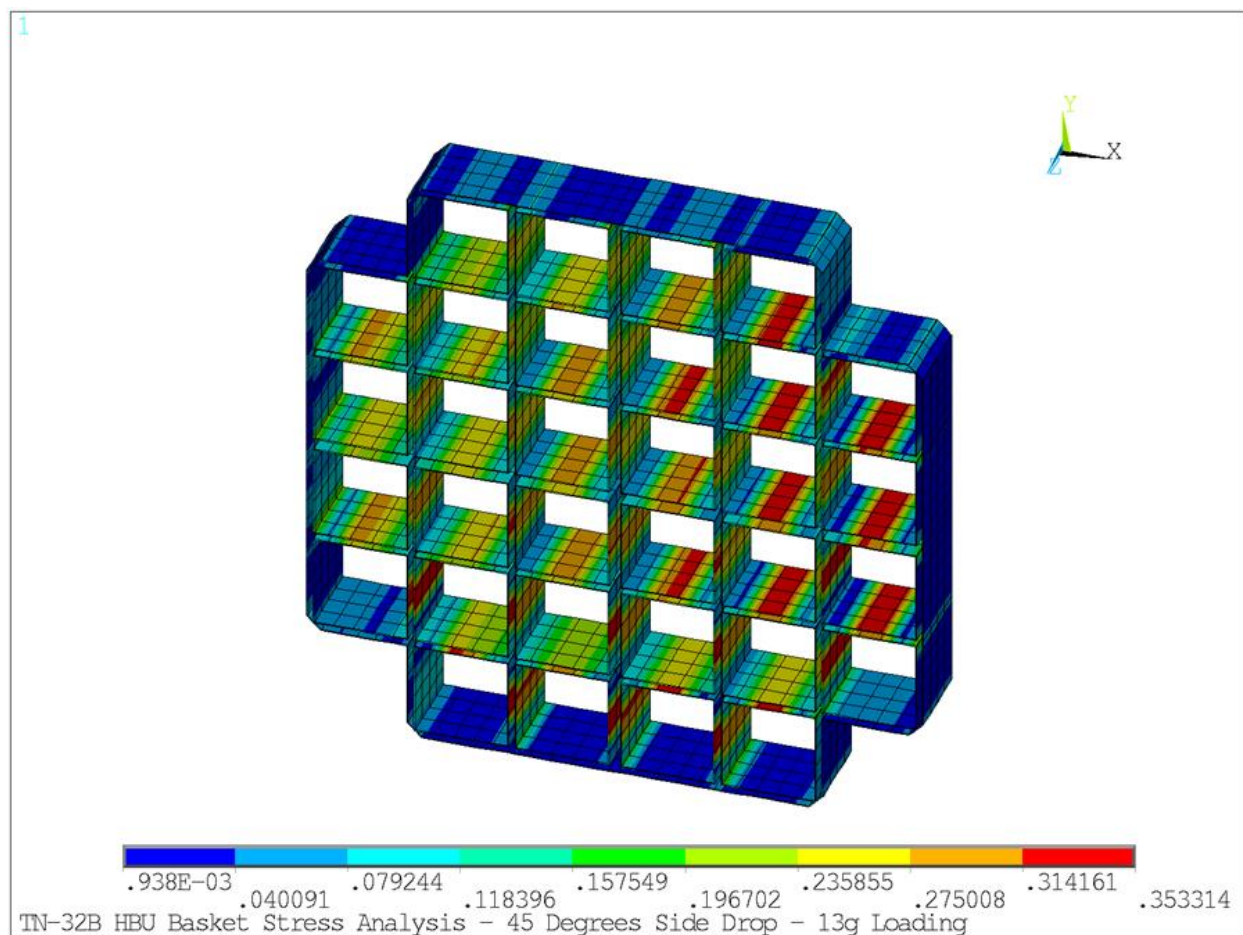


**Figure 2.12.6-16**  
**NCT 45° Side Drop – Stainless Steel Plates – Primary Membrane plus Bending Stress**  
**Ratio Plot – Bottom Face**

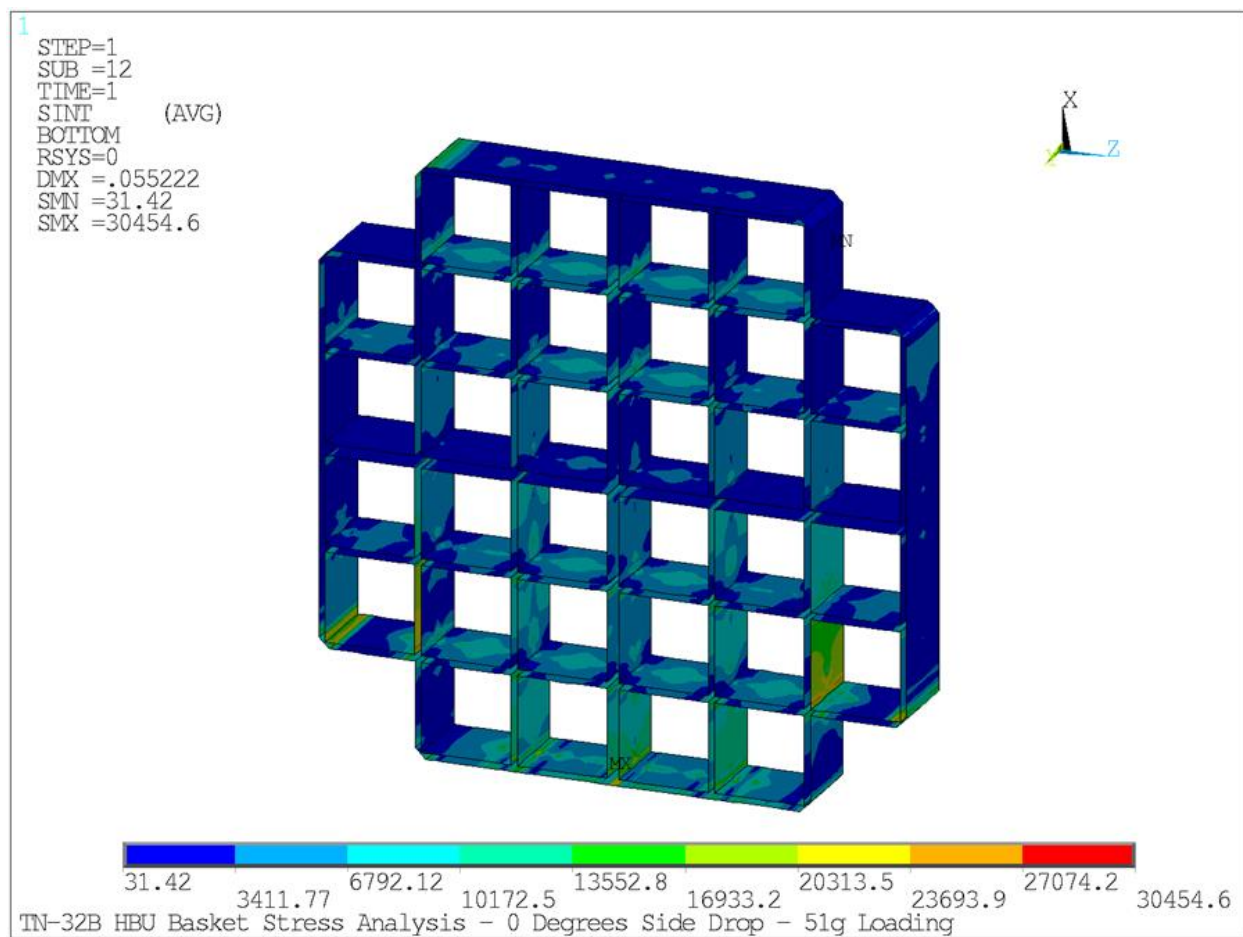


**Figure 2.12.6-17**  
**HAC 0° Side Drop – Stainless Steel Plates – Membrane plus Bending Stress Intensity at Bottom Face**



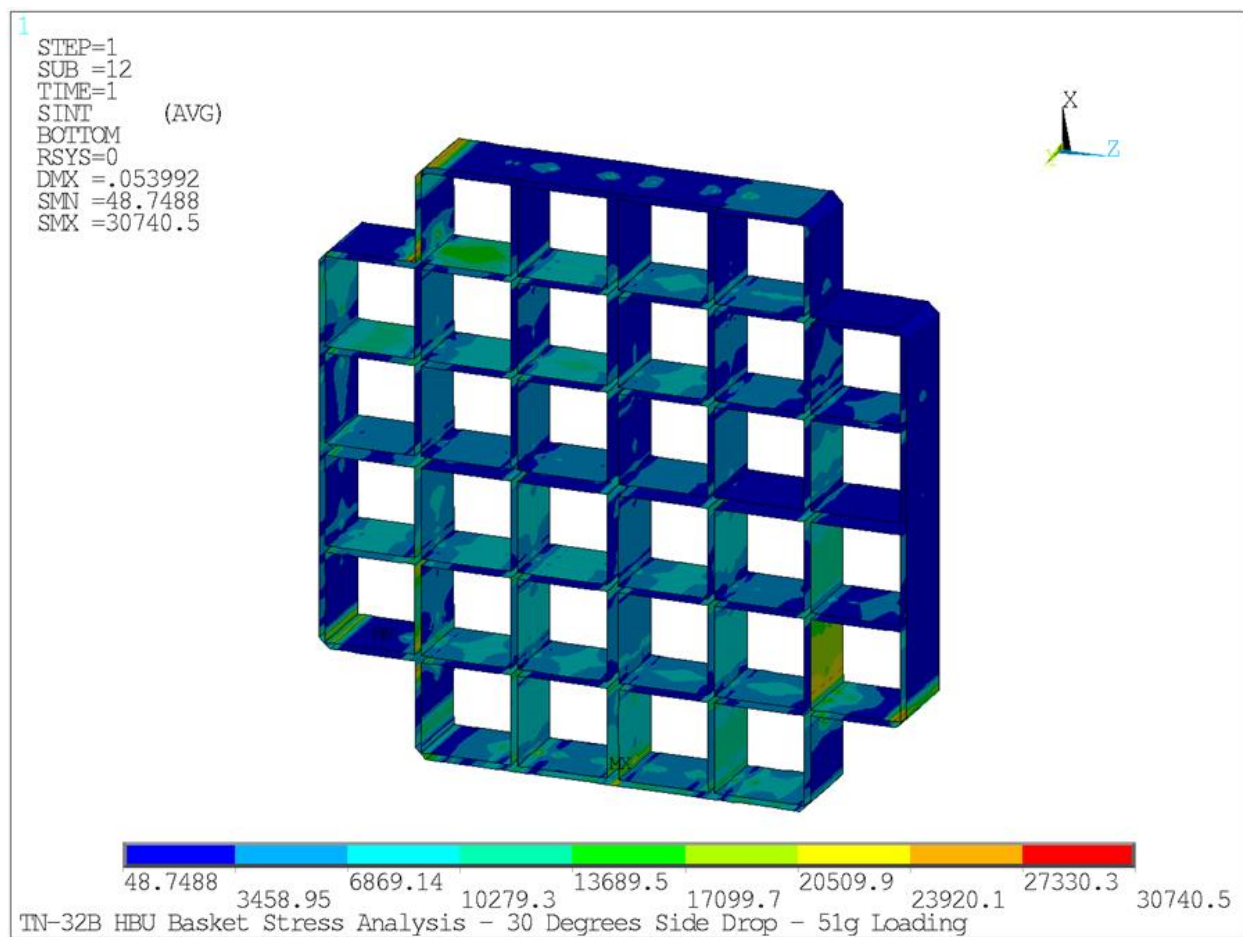


**Figure 2.12.6-18**  
**HAC 30° Side Drop – Stainless Steel Plates – Membrane plus Bending Stress Intensity at Bottom Face**

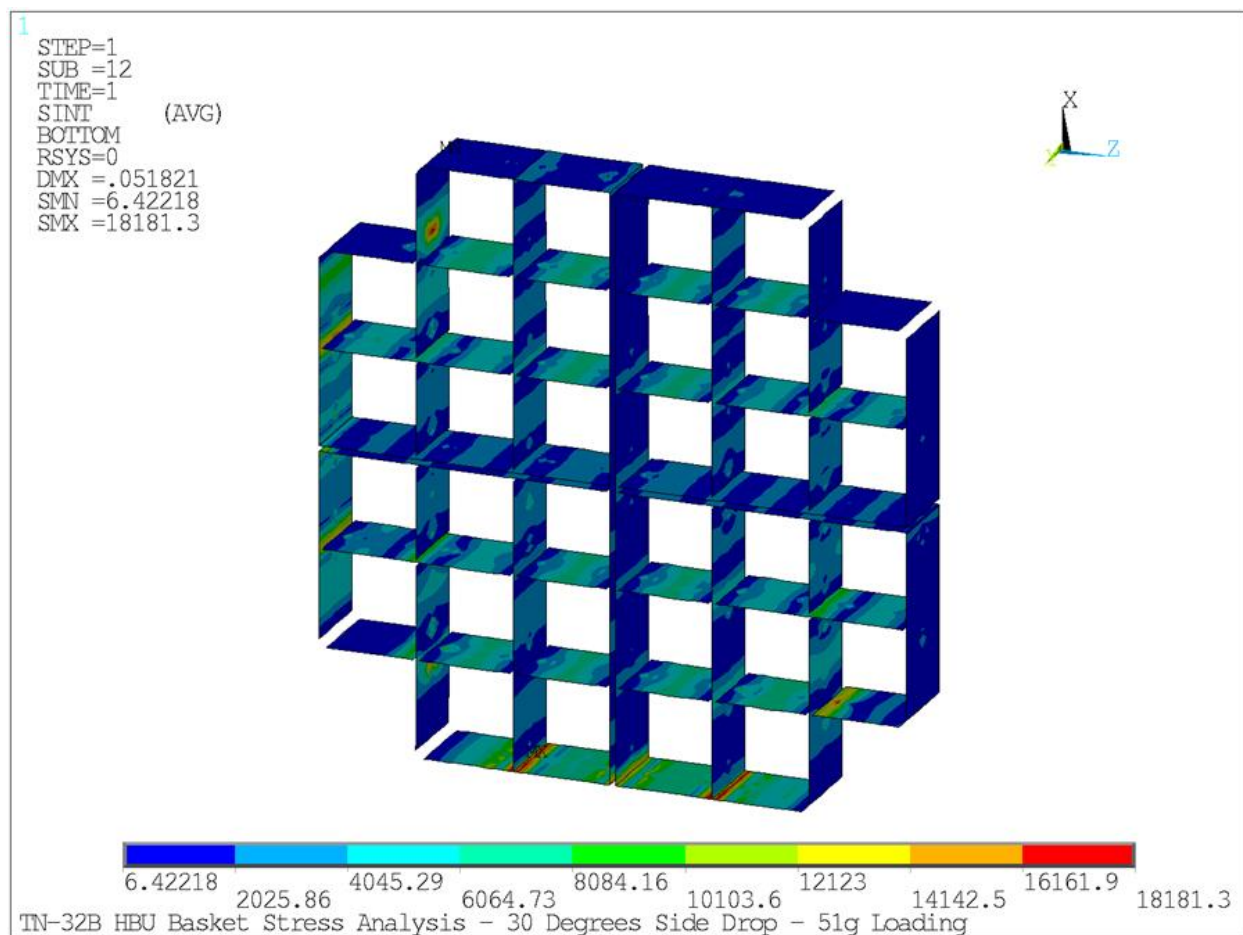


**Figure 2.12.6-19**  
**HAC 30° Side Drop – Aluminum Plates – Membrane plus Bending Stress Intensity at Bottom Face**

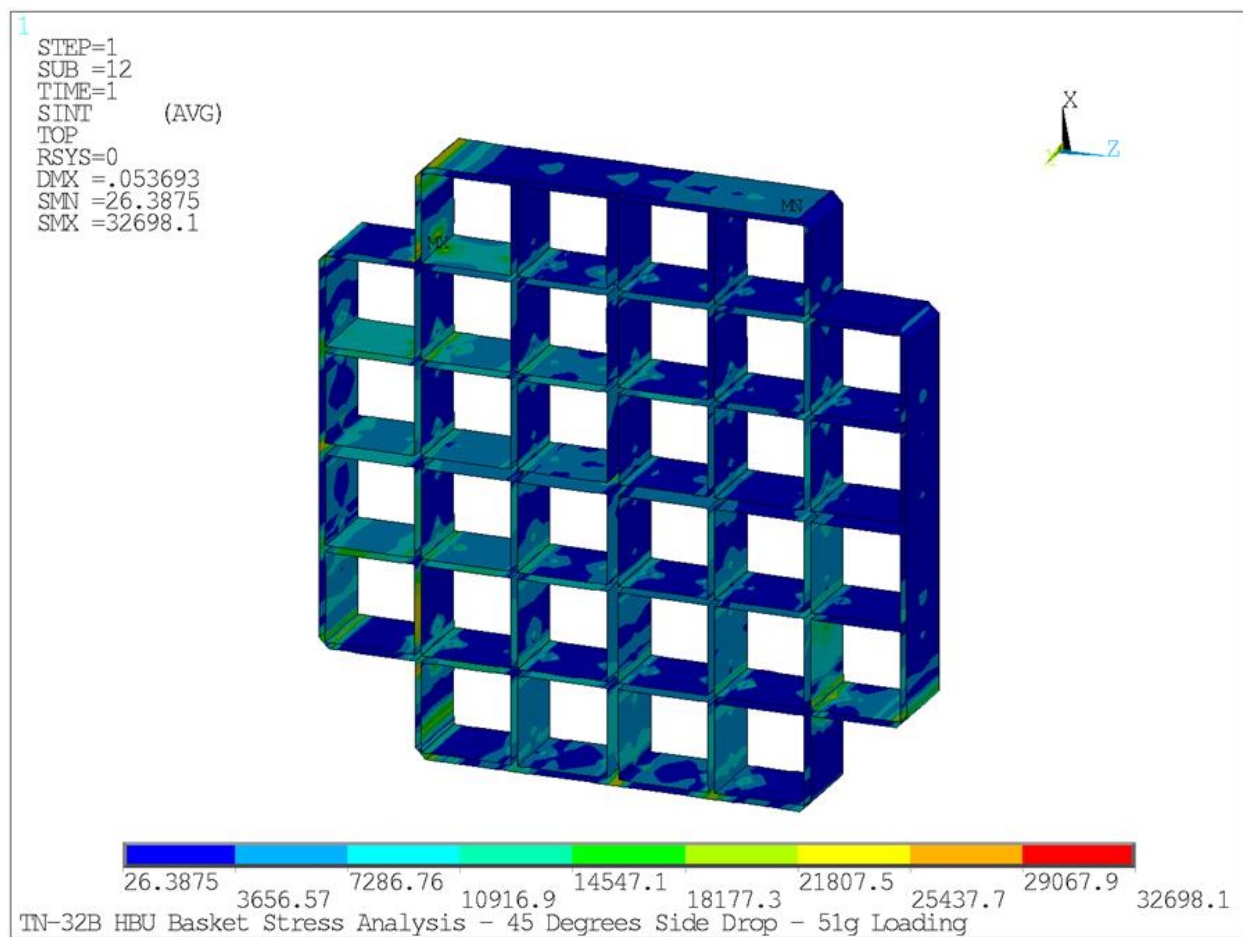


**Figure 2.12.6-20**  
**HAC 45° Side Drop – Stainless Steel Plates – Membrane plus Bending Stress Intensity at Top Face**

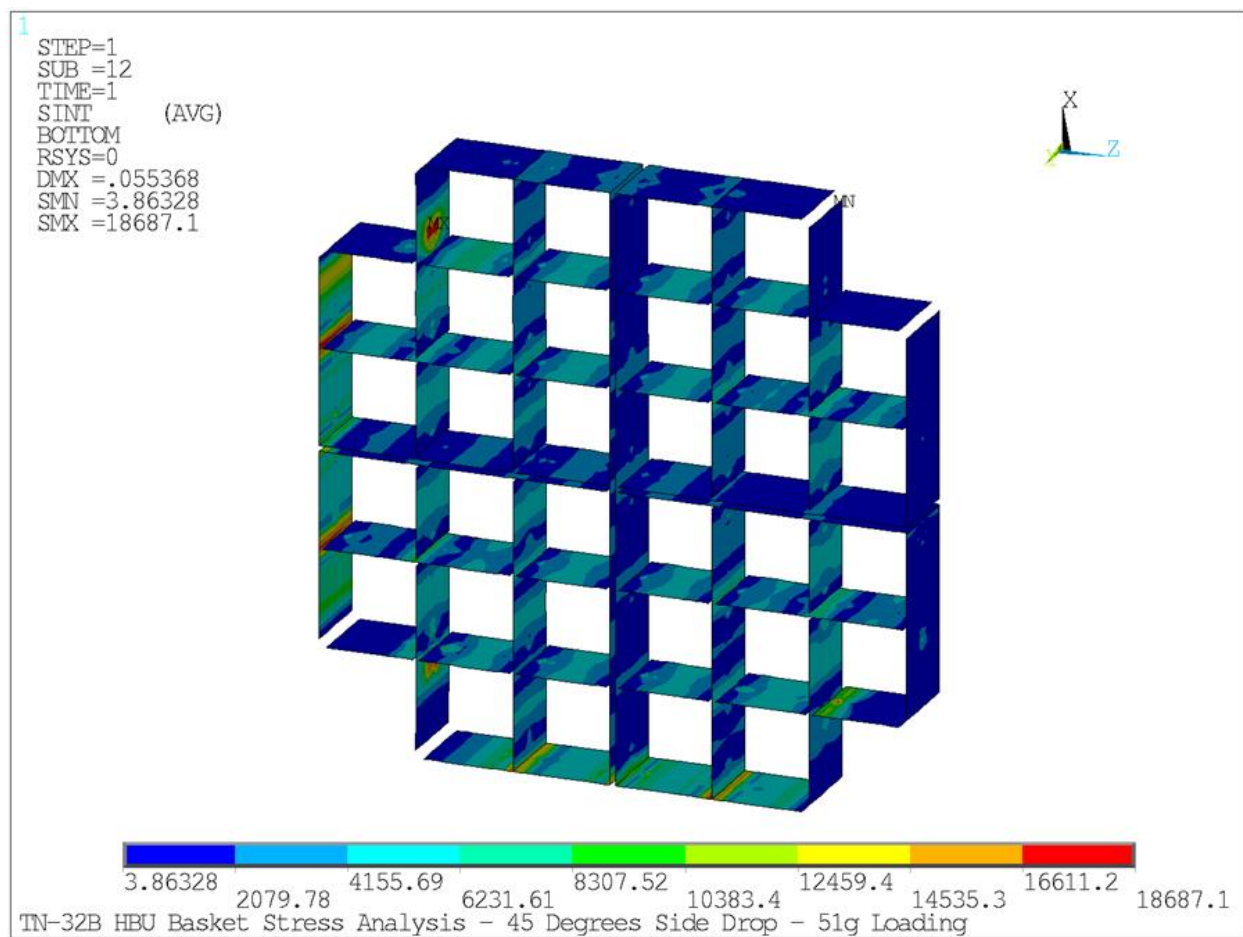


**Figure 2.12.6-21**  
**HAC 45° Side Drop – Aluminum Plates – Membrane plus Bending Stress Intensity at Bottom Face**

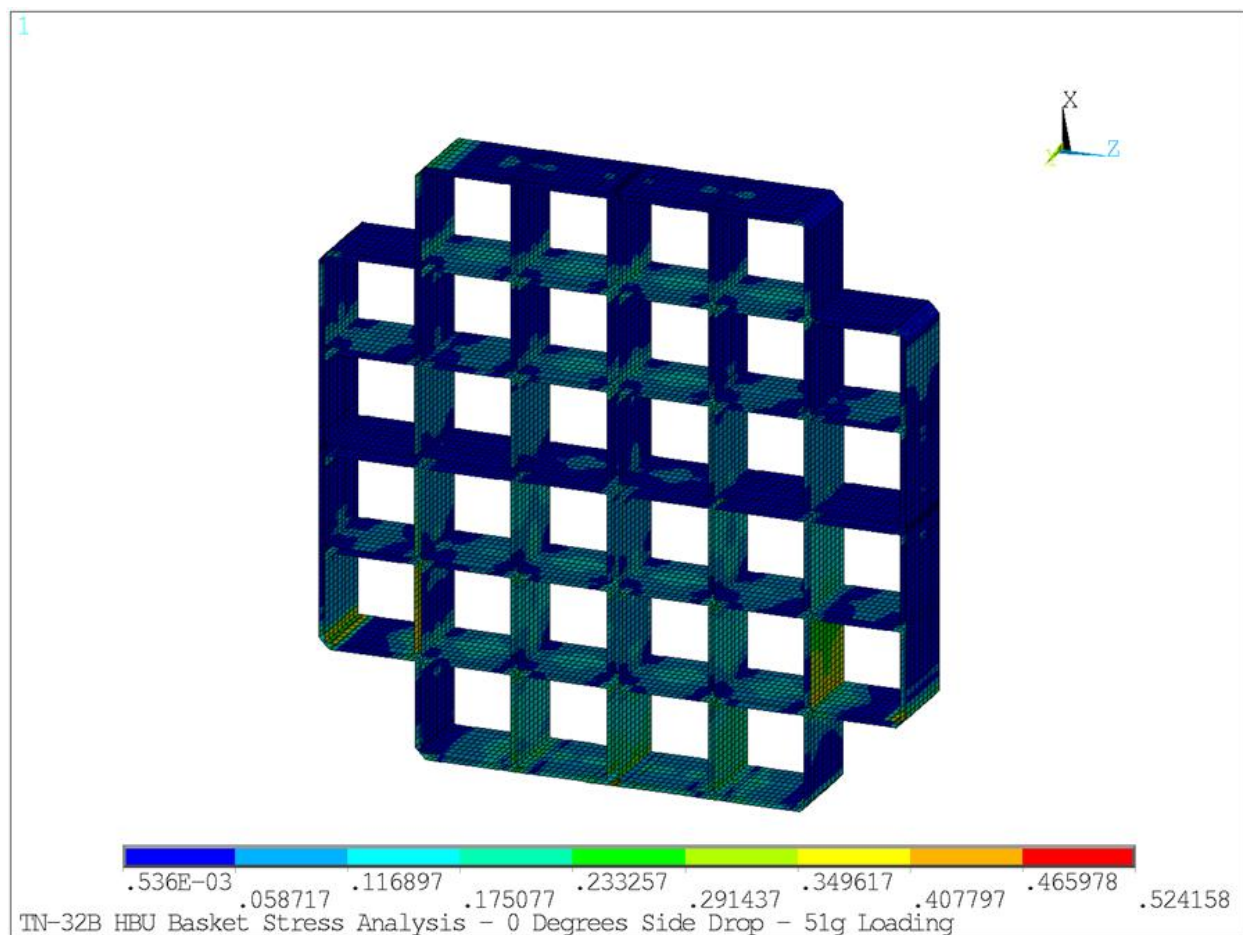


**Figure 2.12.6-22**  
**HAC 0° Side Drop – Stainless Steel Plates – Primary Membrane plus Bending Stress**  
**Ratio Plot – Bottom Face**

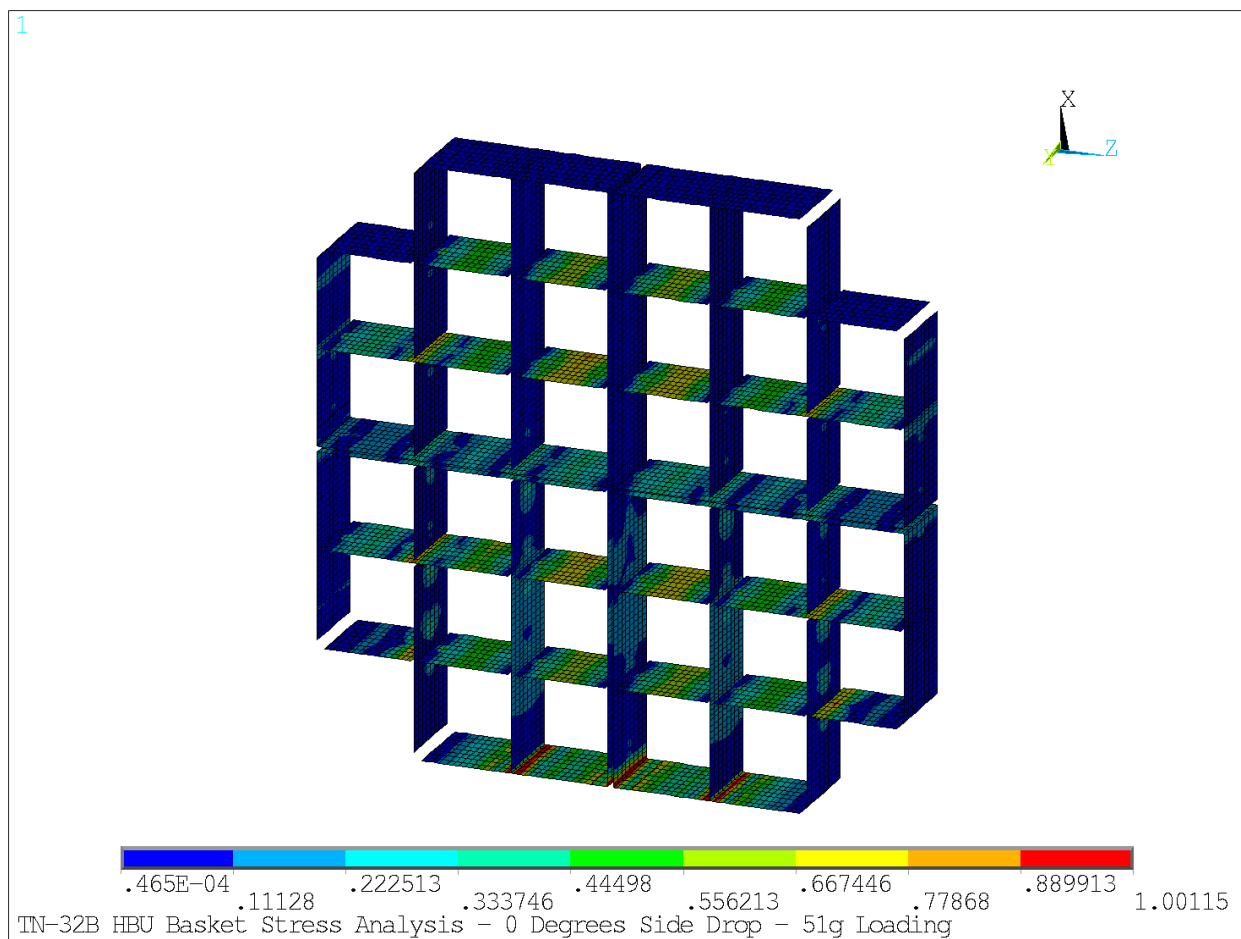


**Figure 2.12.6-23**  
**HAC 0° Side Drop – Aluminum Plates – Primary Membrane plus Bending Stress Ratio**  
**Plot – Bottom Face**



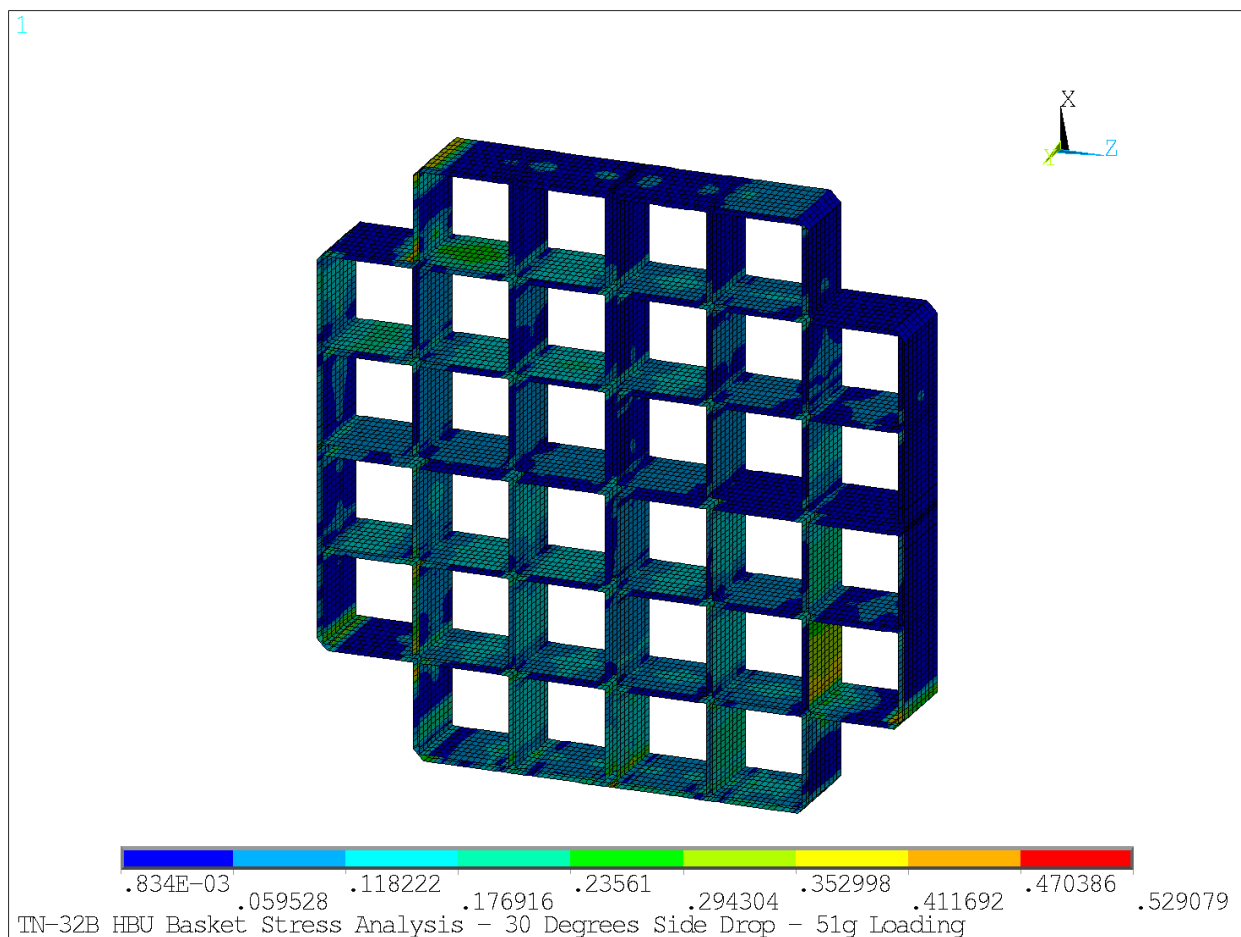


**Figure 2.12.6-24**  
**HAC 30° Side Drop – Stainless Steel Plates – Primary Membrane plus Bending Stress**  
**Ratio Plot – Bottom Face**

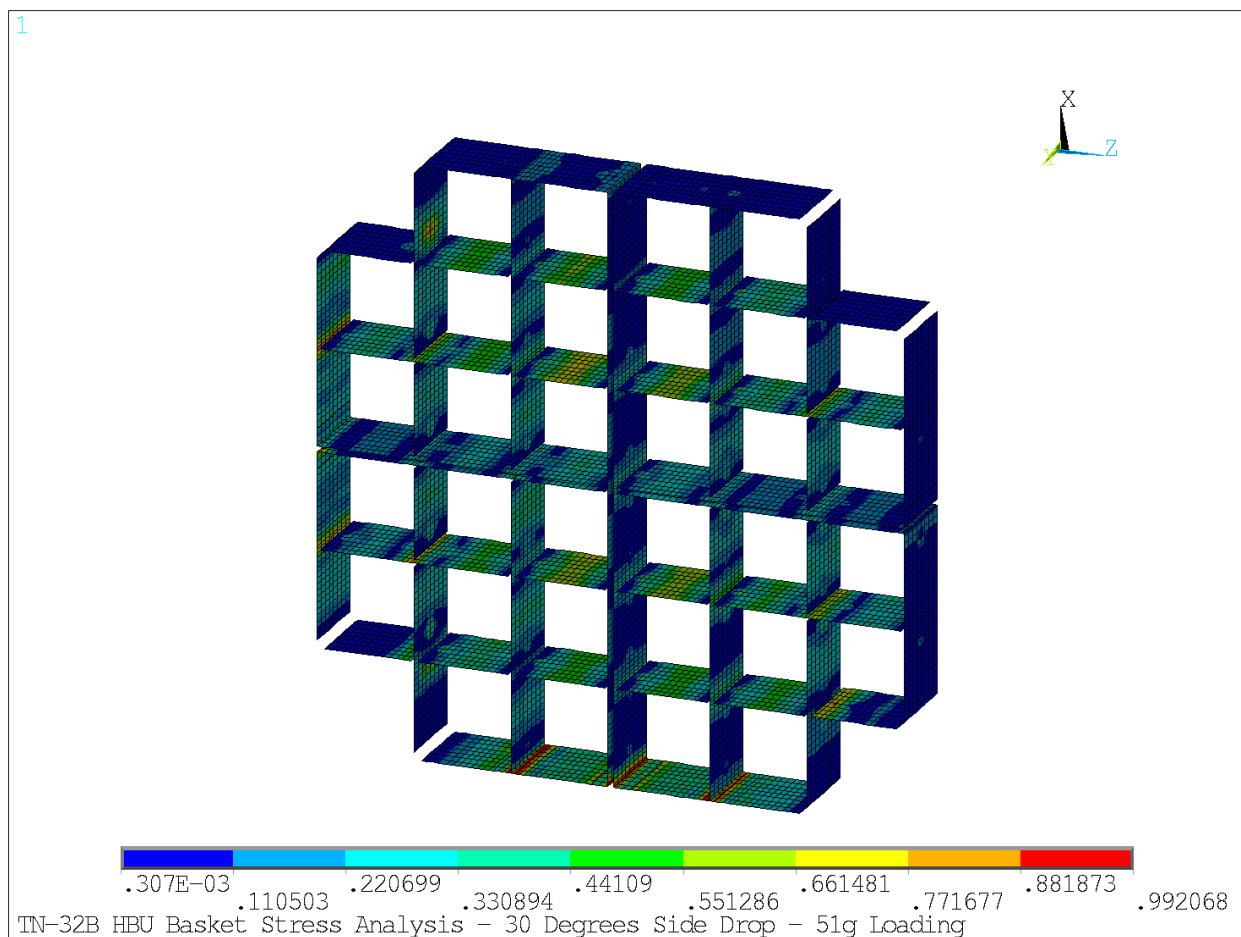


**Figure 2.12.6-25**  
**HAC 30° Side Drop – Aluminum Plates – Primary Membrane plus Bending Stress Ratio**  
**Plot – Bottom Face**



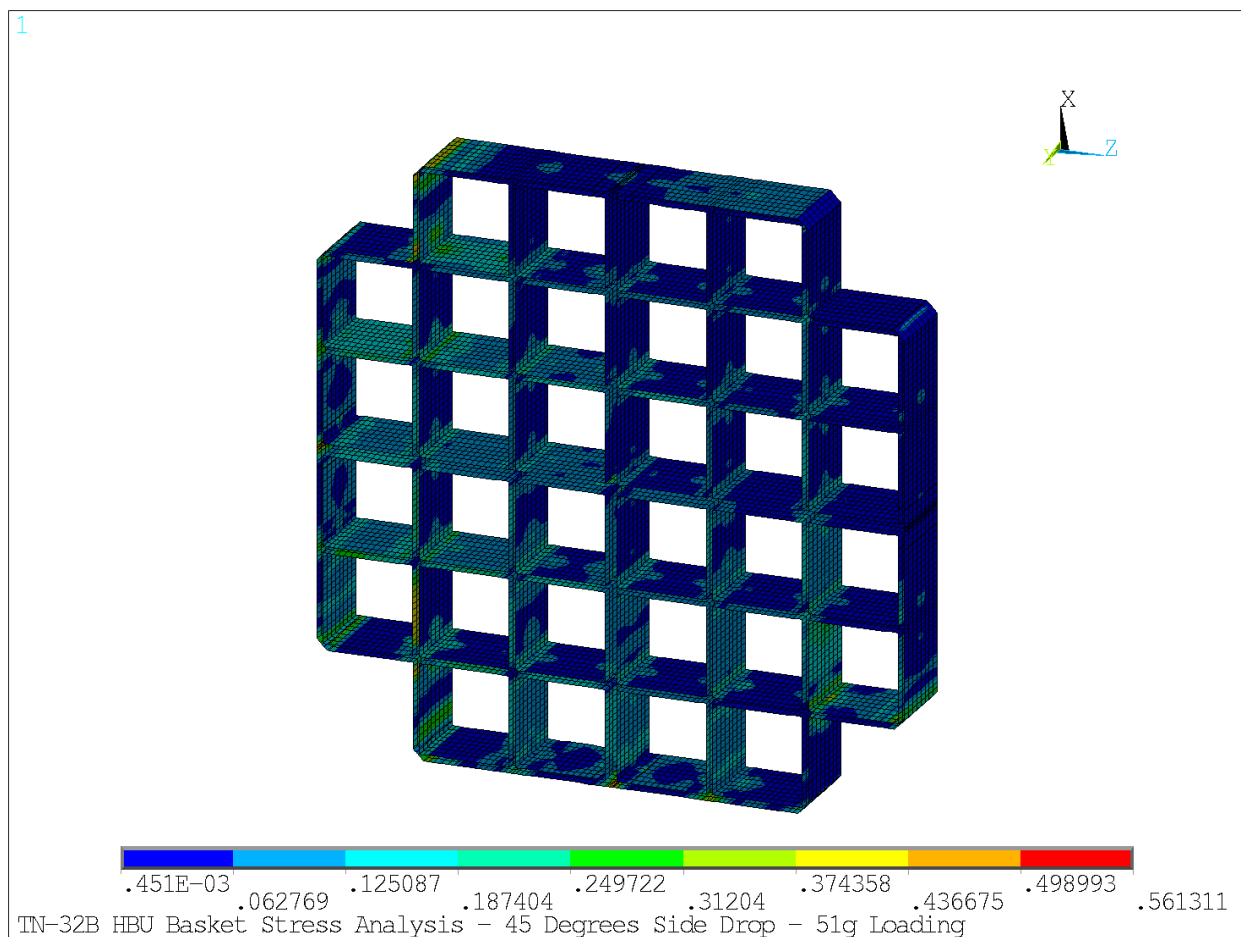


**Figure 2.12.6-26**  
**HAC 45° Side Drop – Stainless Steel Plates – Primary Membrane plus Bending Stress**  
**Ratio Plot – Top Face**

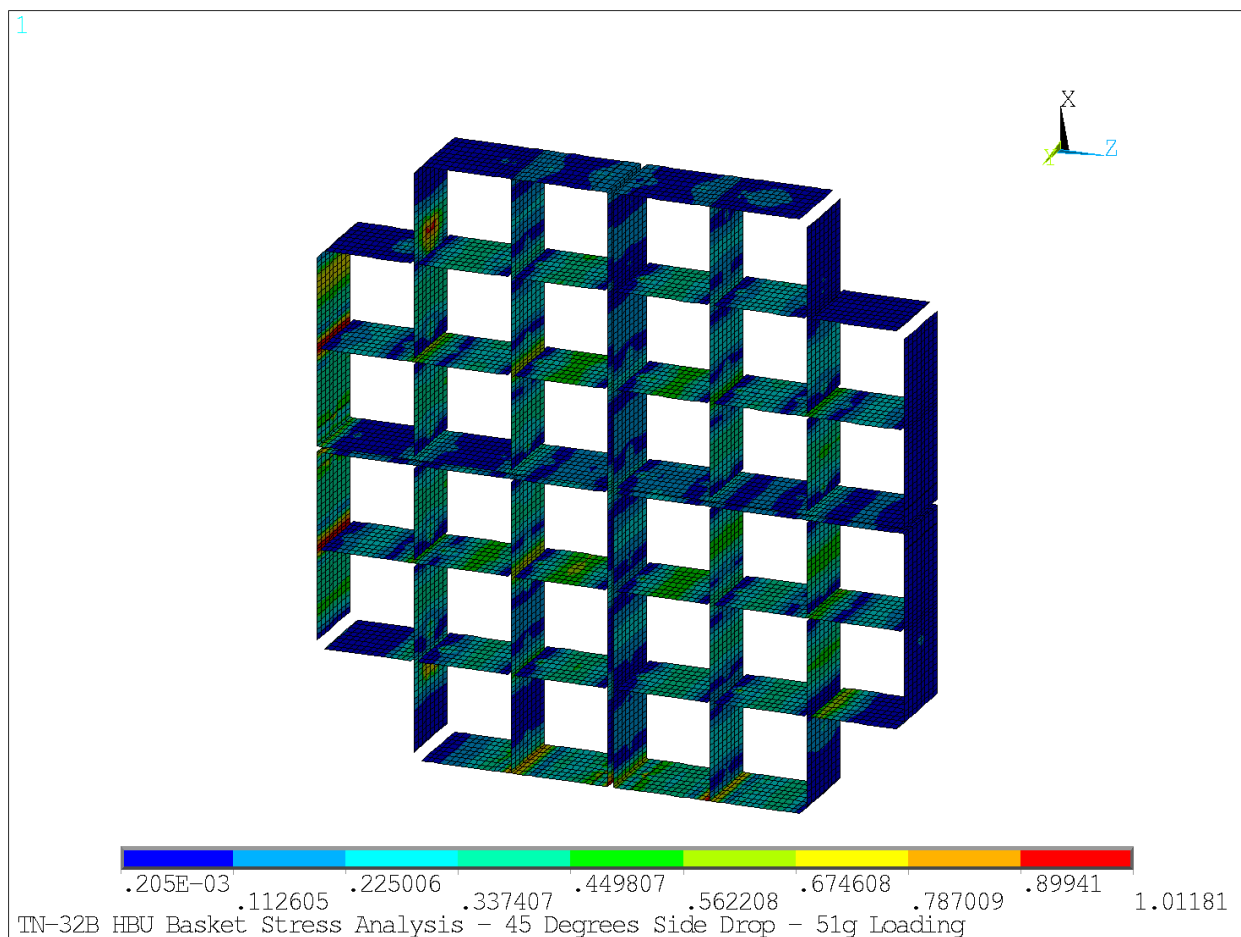


**Figure 2.12.6-27**  
**HAC 45° Side Drop – Aluminum Plates – Primary Membrane plus Bending Stress Ratio**  
**Plot – Top Face**

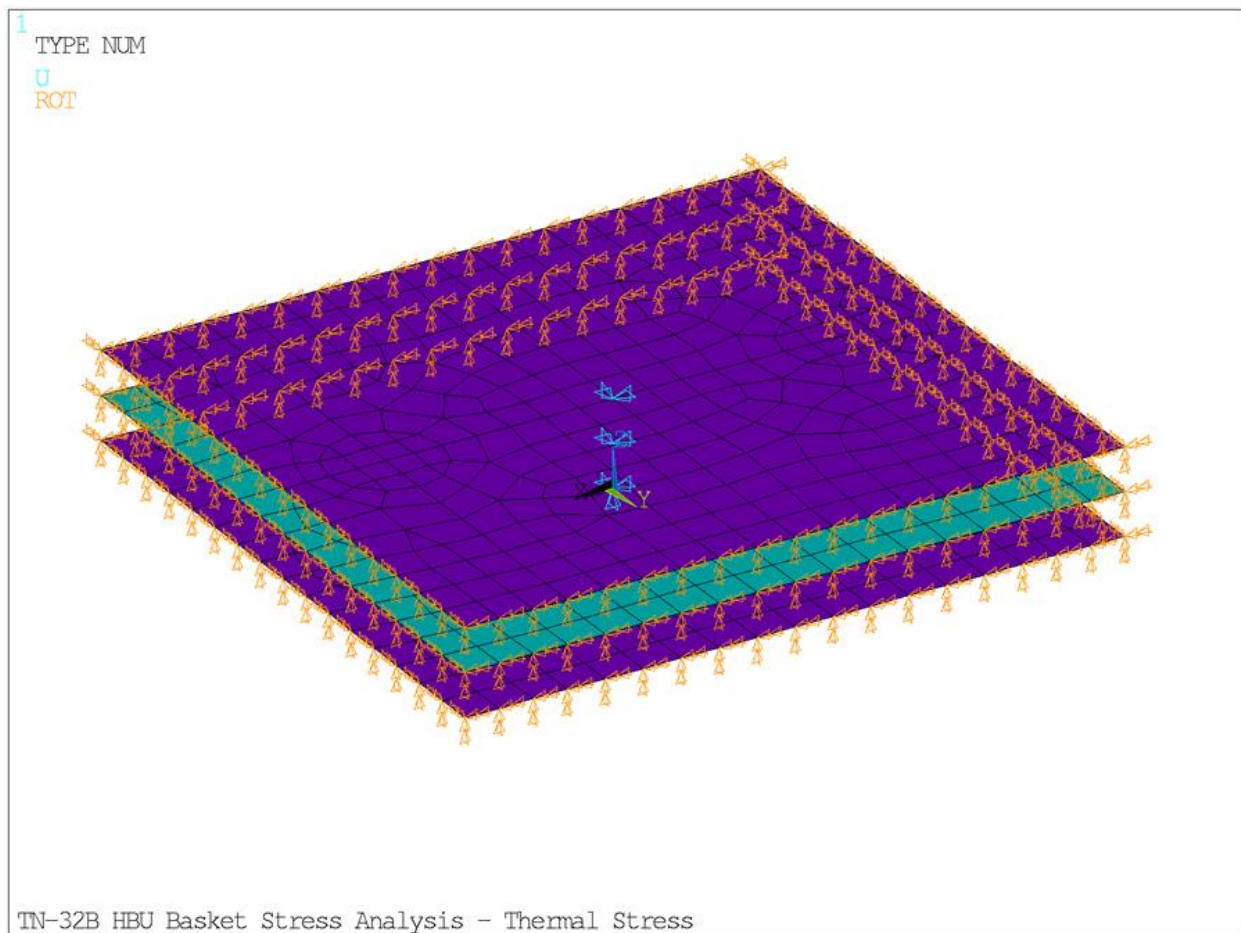
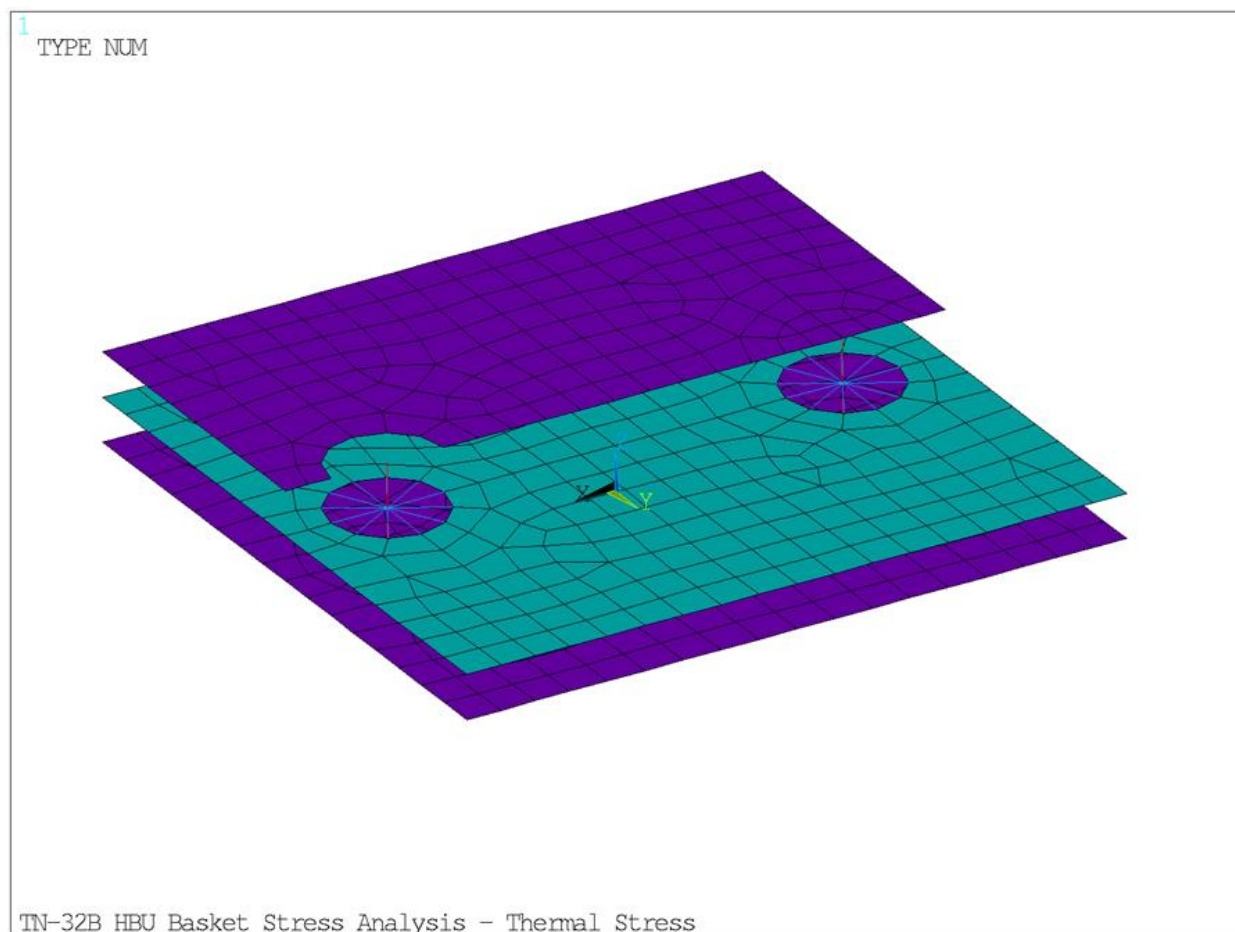


**Figure 2.12.6-28**  
**Thermal Stress Analysis Model with Boundary Conditions**



Note:

1. Some elements were unselected (hidden) to show the BEAM188 and CONTAC52 elements through the thickness of the basket section.
2. Model 1 & Model 2 are essentially same except for the difference in the thickness of aluminum plate and center to center distance between aluminum and stainless steel plates.

**Figure 2.12.6-29**  
**Thermal Stress Analysis Model – Cut Section View**

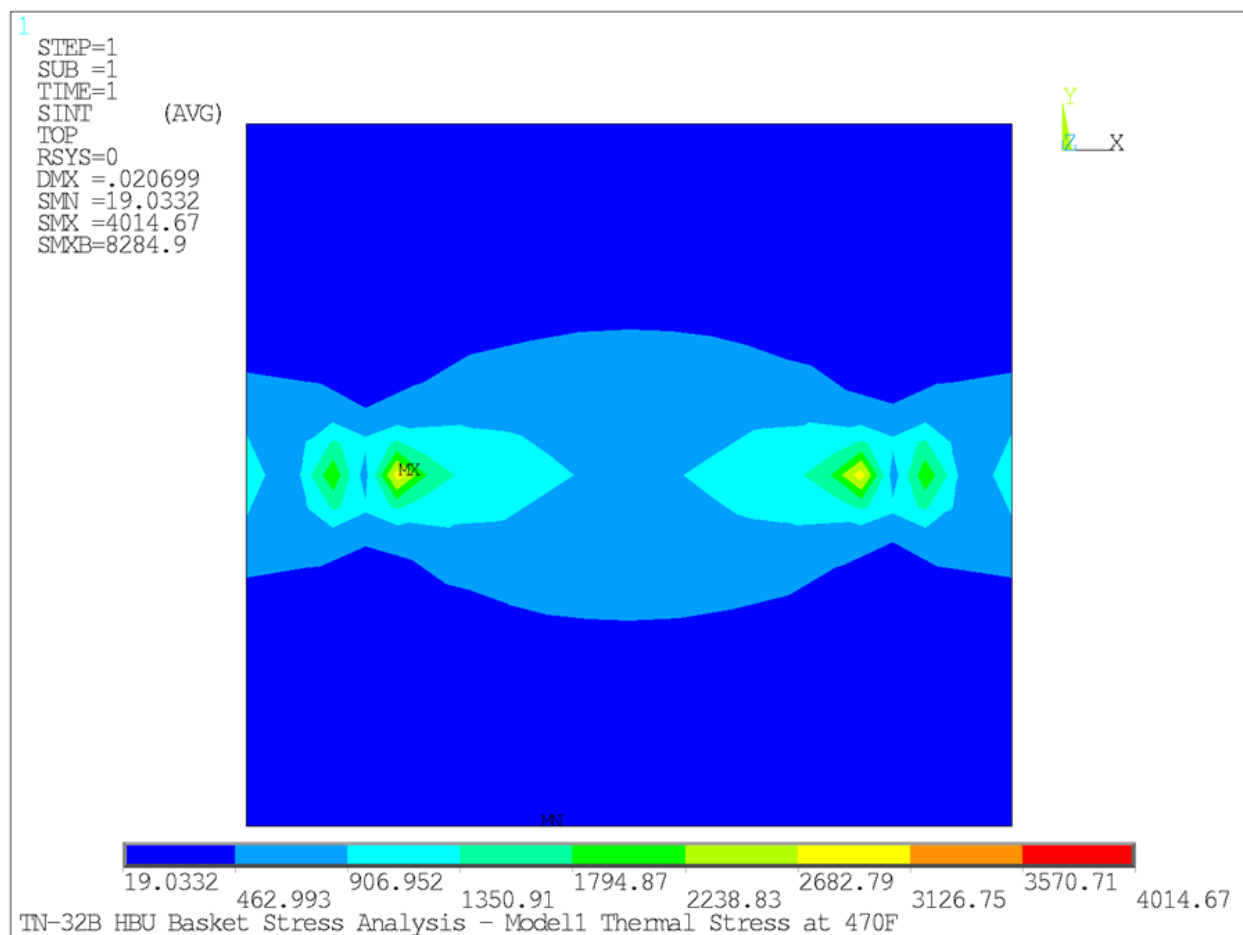


**Figure 2.12.6-30**  
**Thermal Stress Analysis – Model 1 – Maximum Stainless Steel Stress Intensity**

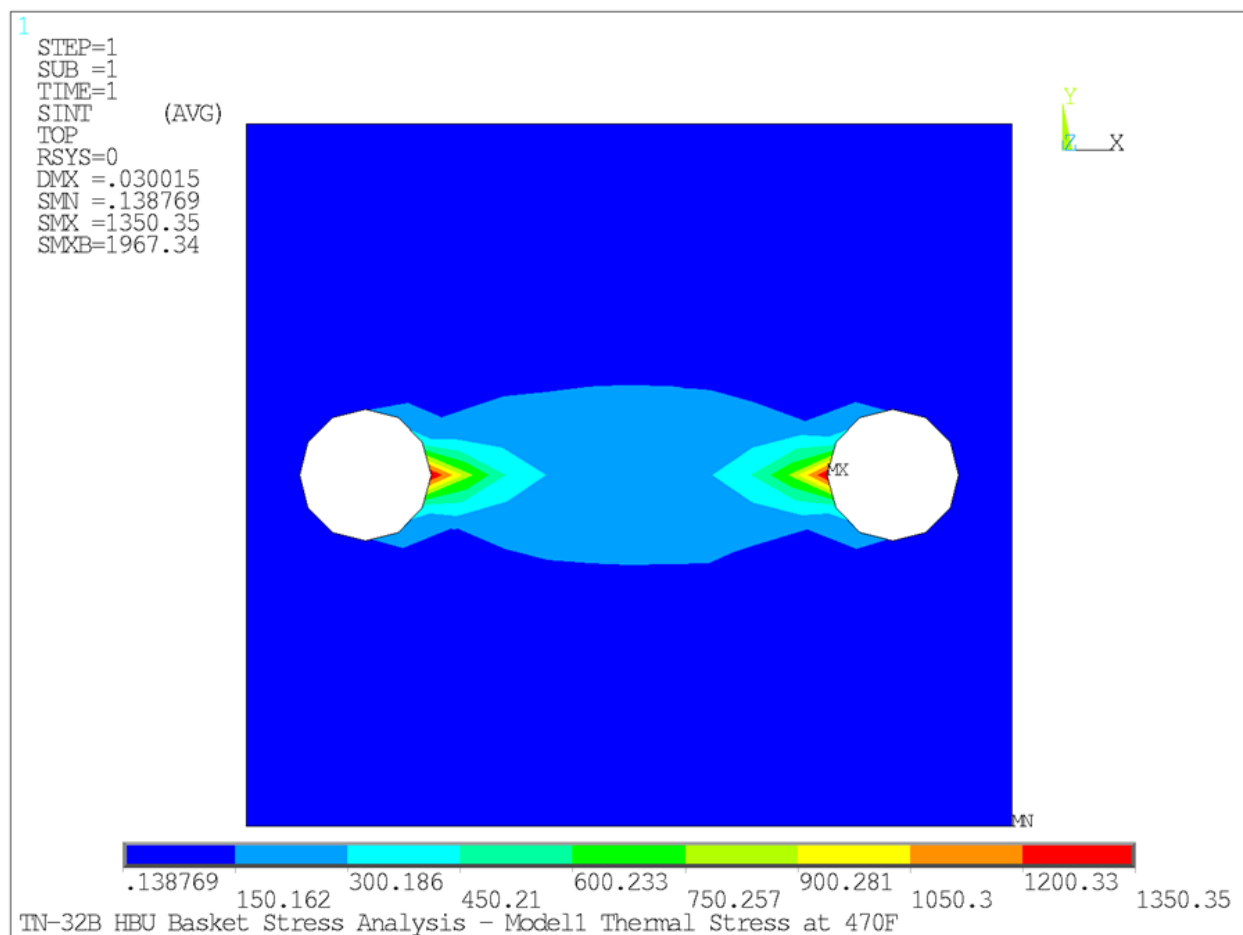


**Figure 2.12.6-31**  
**Thermal Stress Analysis – Model 1 – Maximum Aluminum Stress Intensity**

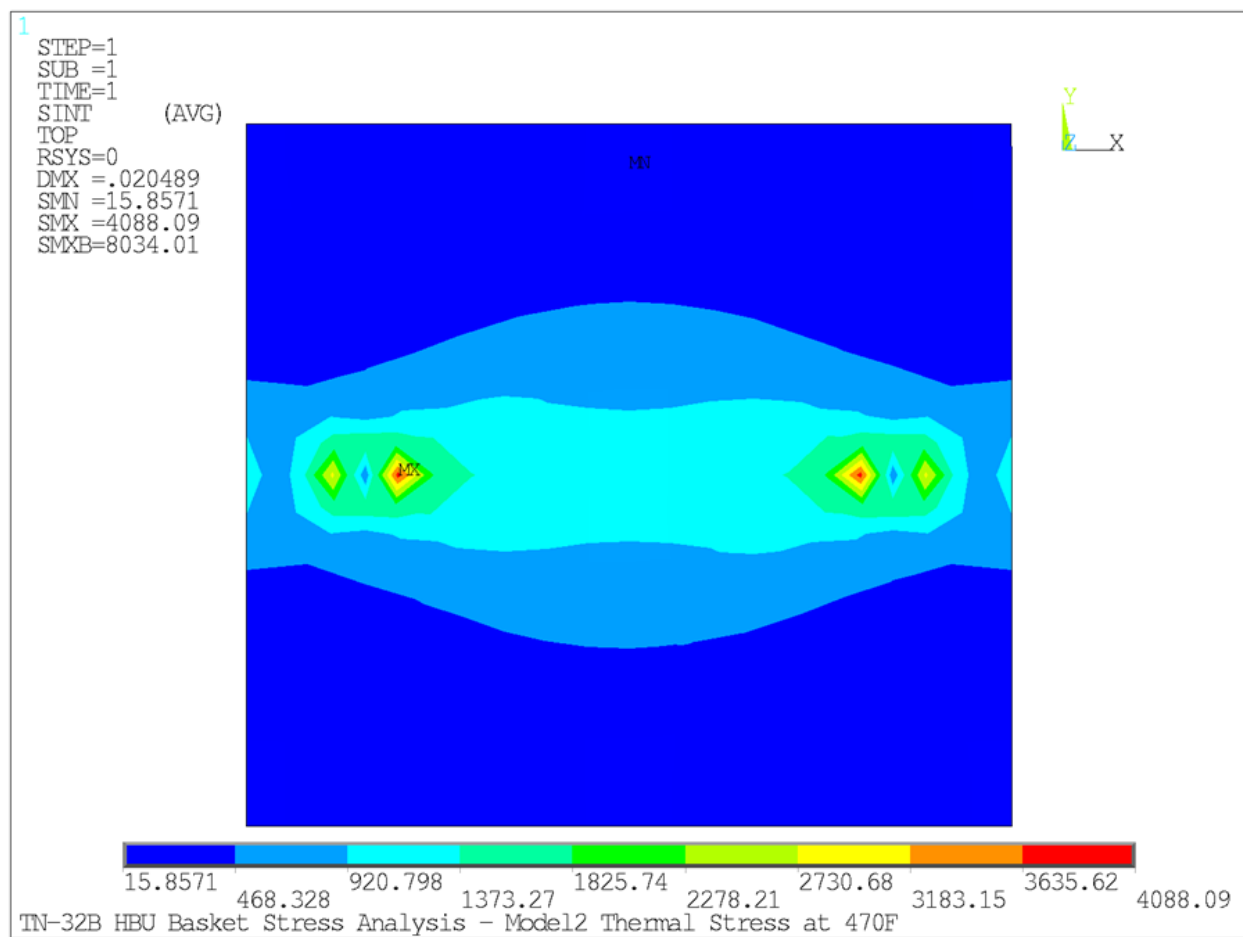


**Figure 2.12.6-32**  
**Thermal Stress Analysis – Model 2 – Maximum Stainless Steel Stress Intensity**

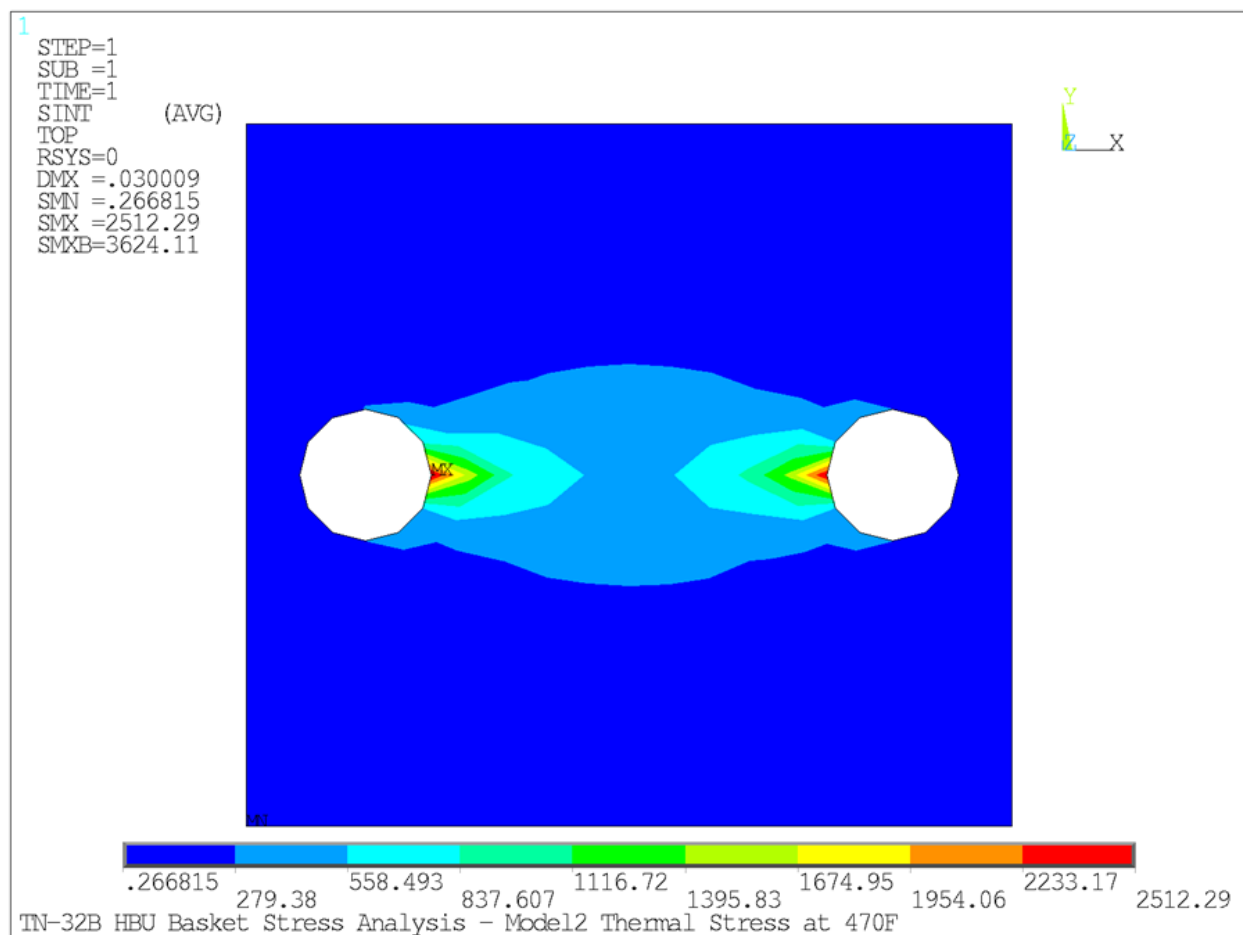


**Figure 2.12.6-33**  
**Thermal Stress Analysis – Model 2 – Maximum Aluminum Stress Intensity**



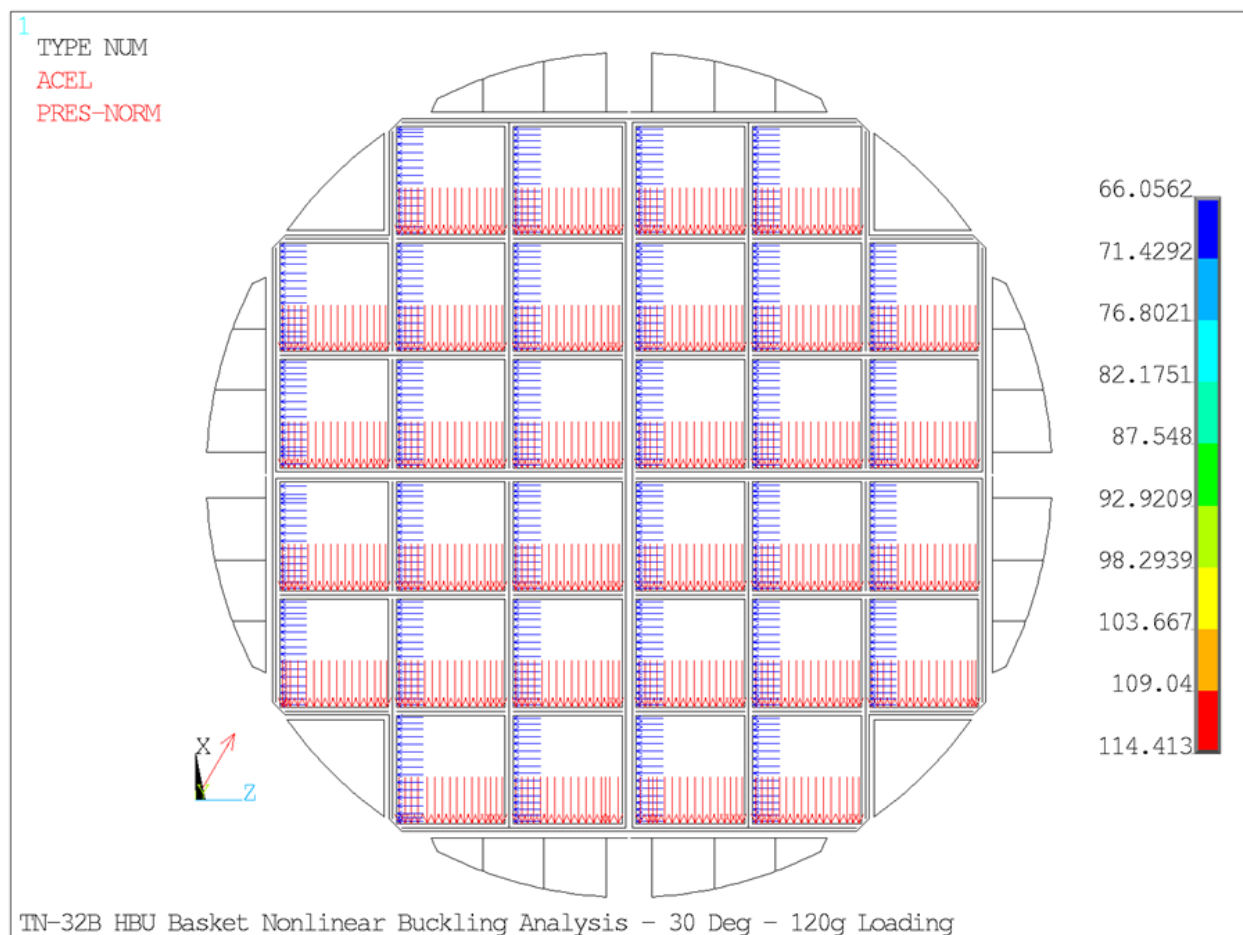


**Figure 2.12.6-34**  
**Nonlinear Buckling - Loading Boundary Conditions - Side Drop - 30°**

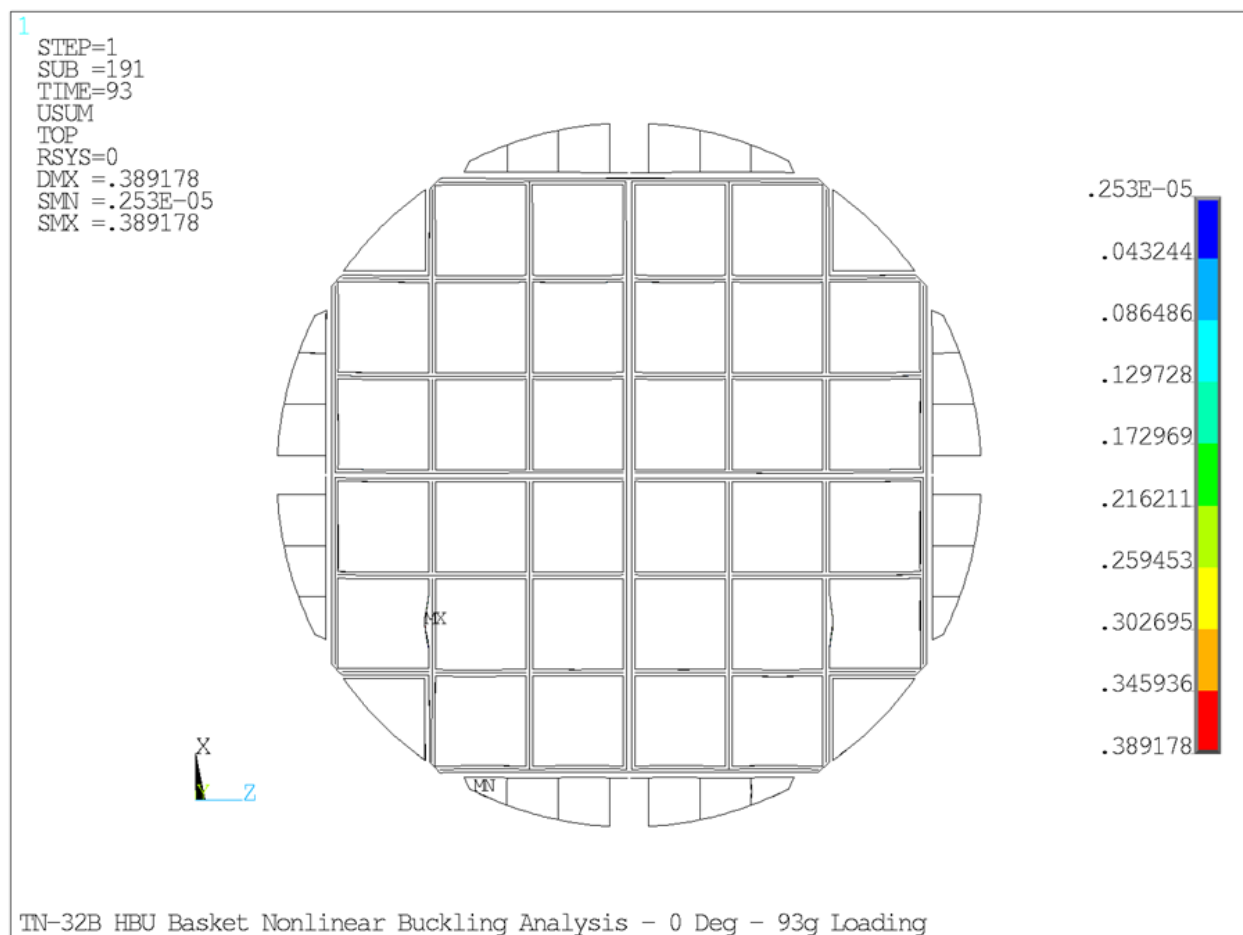


**Figure 2.12.6-35**  
**Nonlinear Buckling – Basket Displacement at Buckling Load – Side Drop – 0°**

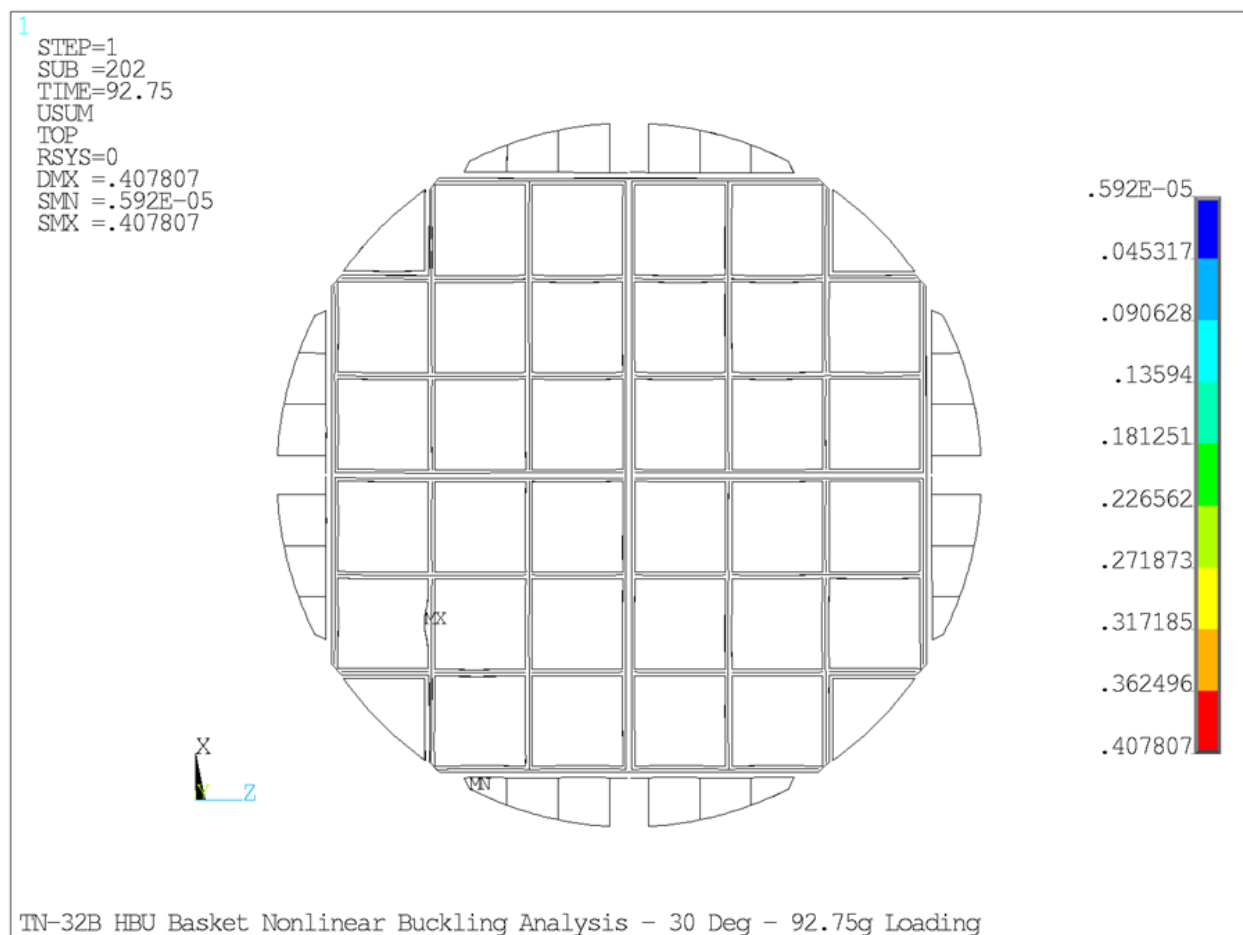


**Figure 2.12.6-36**  
**Nonlinear Buckling – Basket Displacement at Buckling Load – Side Drop – 30°**

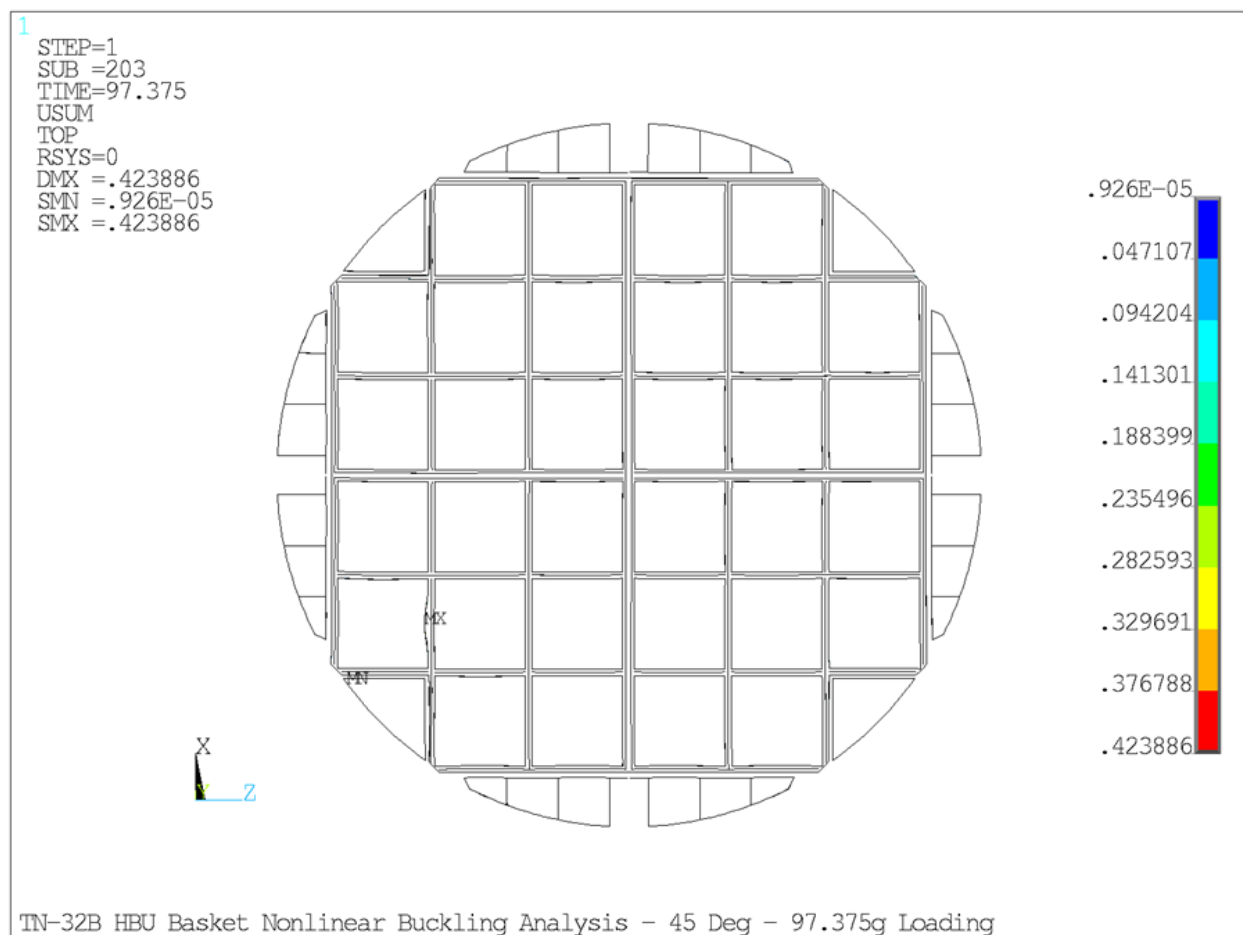


**Figure 2.12.6-37**  
**Nonlinear Buckling – Basket Displacement at Buckling Load – Side Drop – 45°**

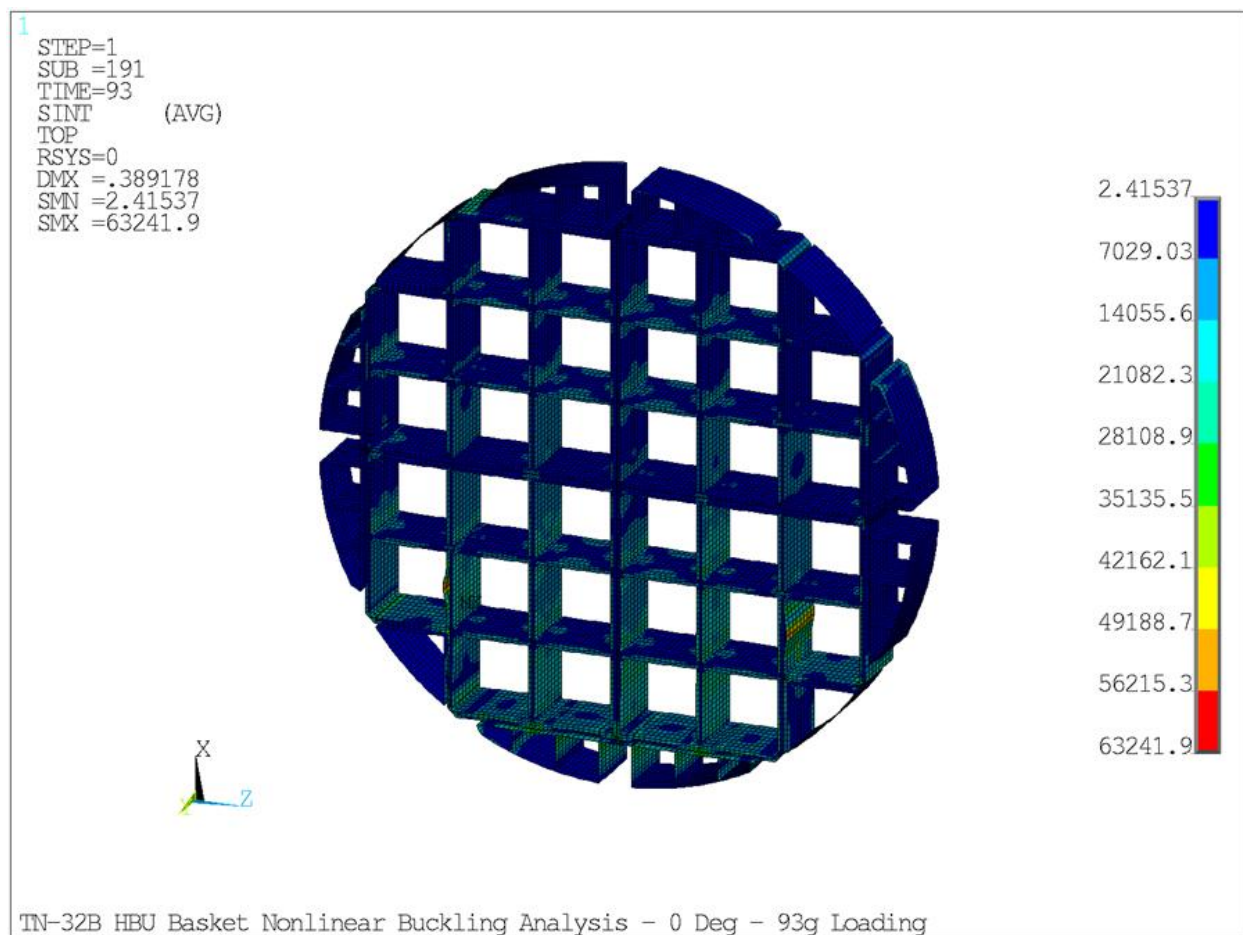


**Figure 2.12.6-38**  
**Nonlinear Buckling – Basket Stress Intensity at Buckling Load – Side Drop – 0°**

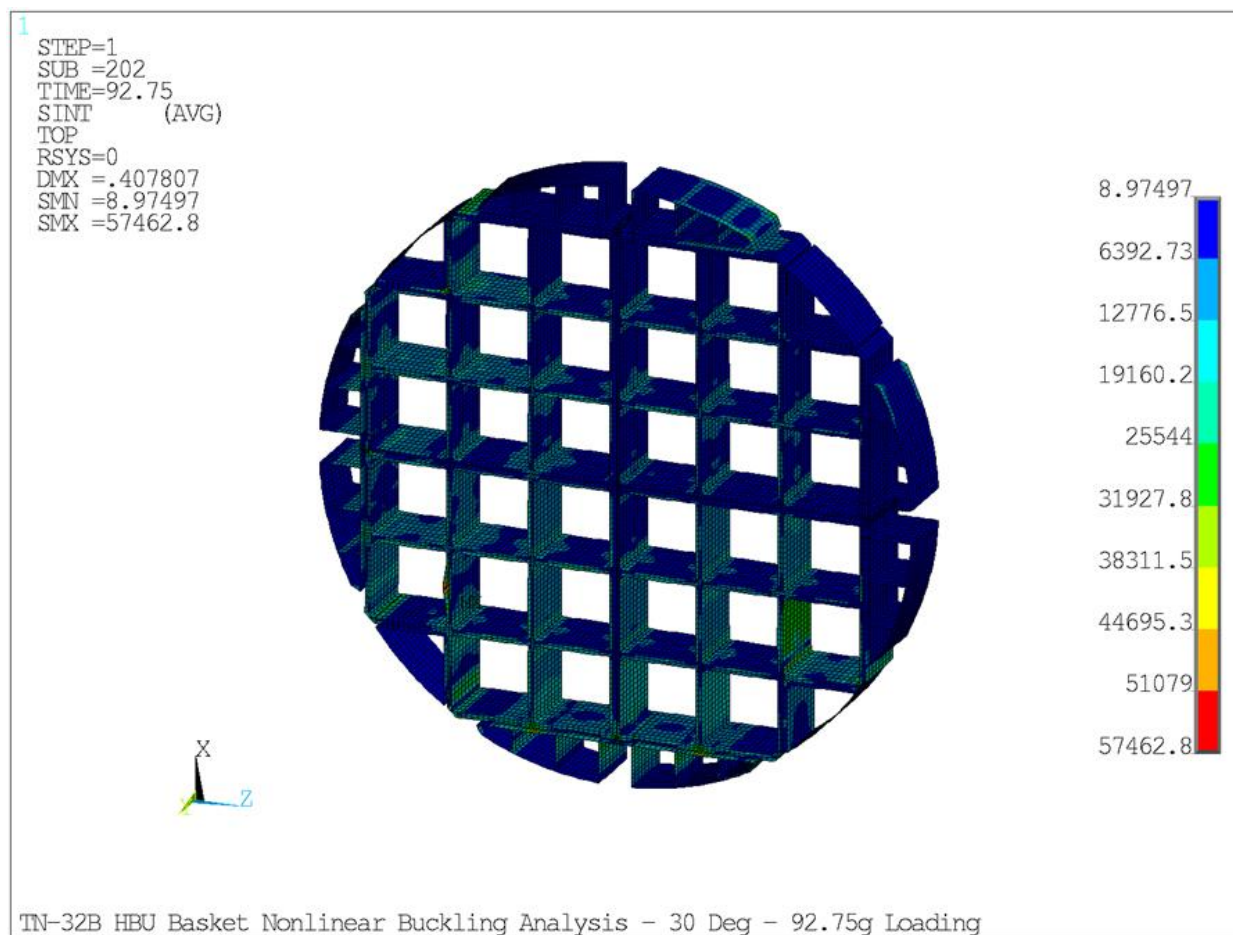


**Figure 2.12.6-39**  
**Nonlinear Buckling – Basket Stress Intensity at Buckling Load – Side Drop – 30°**

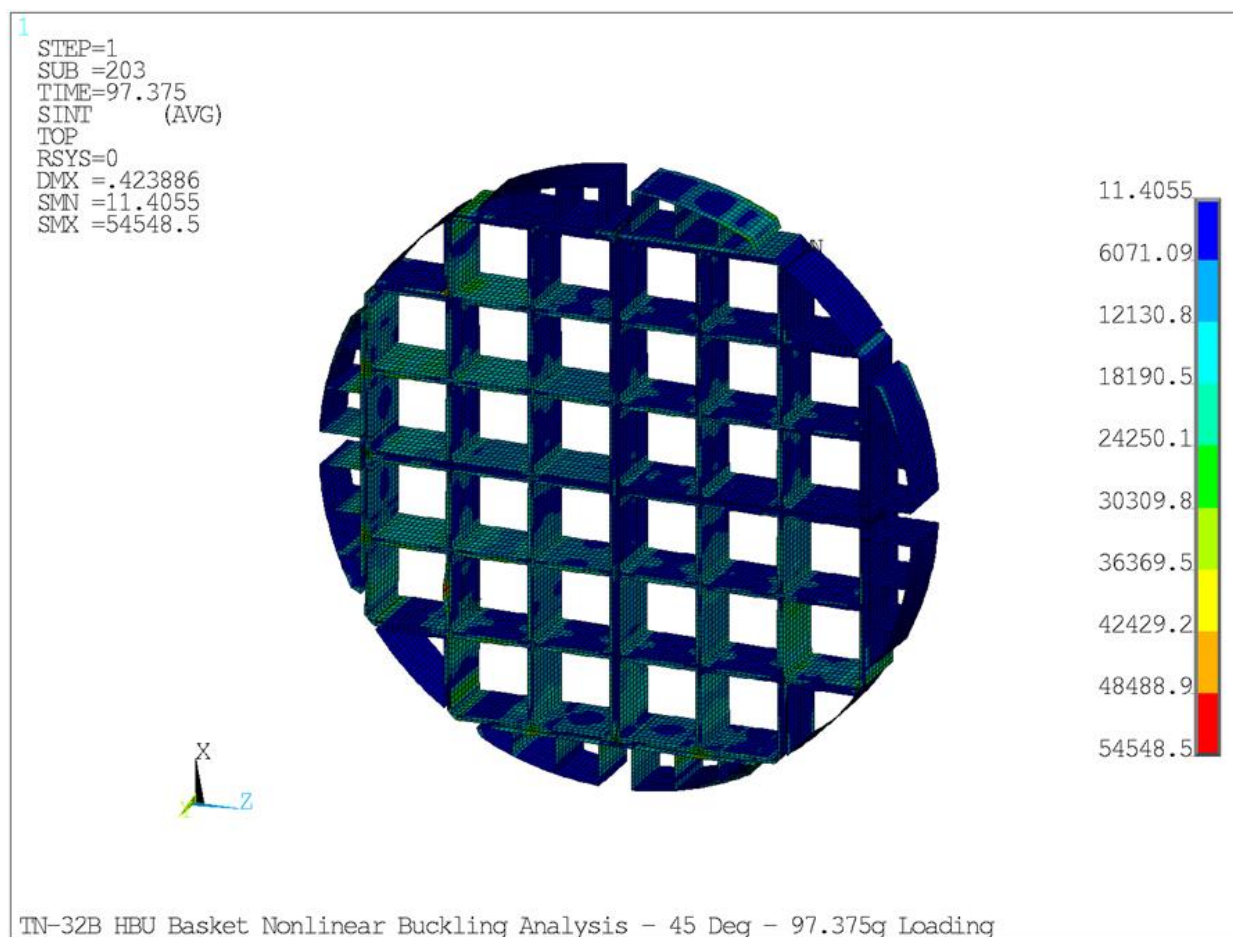


**Figure 2.12.6-40**  
**Nonlinear Buckling – Basket Stress Intensity at Buckling Load – Side Drop – 45°**

## **Appendix 2.12.7**

### **Dynamic Load Factor for Basket Drop Analysis**

#### TABLE OF CONTENTS

2.12.7	Dynamic Load Factor for Basket Drop Analysis .....	2.12.7-1
2.12.7.1	Introduction .....	2.12.7-1
2.12.7.2	Modal Analysis of Basket Side Drop Loading Condition .....	2.12.7-1
2.12.7.3	Dynamic Load Factor Calculations .....	2.12.7-3
2.12.7.4	References.....	2.12.7-4

#### LIST OF FIGURES

Figure 2.12.7-1	TN-32B HBU Basket Finite Element Model .....	2.12.7-5
Figure 2.12.7-2	TN-32B HBU Boundary Conditions of 0° Side Drop.....	2.12.7-6
Figure 2.12.7-3	0° Side Drop - 1st Mode .....	2.12.7-7
Figure 2.12.7-4	45° Side Drop - 1st Mode .....	2.12.7-8
Figure 2.12.7-5	90° Side Drop - 1st Mode .....	2.12.7-9
Figure 2.12.7-6	End Drop - 1st Mode .....	2.12.7-10
Figure 2.12.7-7	DLF Relationship for Cask with an Impact Limiter .....	2.12.7-11



## 2.12.7 Dynamic Load Factor for Basket Drop Analysis

### 2.12.7.1 Introduction

This appendix presents the modal analysis of the TN-32B HBU demonstration cask fuel basket. The TN-32B HBU demonstration cask basket is analyzed for 30 foot end and side drop accidents in Appendix 2.12.6 using equivalent static methods. The equivalent static loads for the drop evaluations of the TN-32B HBU demonstration cask basket are determined by multiplying the baseline rigid body accelerations (as discussed in Section 2.7.1) by the corresponding dynamic load factor (DLF). The purpose of the evaluation in this section is to determine the DLF. The DLF is a function of the rise time of the applied load, the duration of the load, the shape of the load, and the modal frequencies of the structure. This section determines the fundamental frequencies of the basket which have the most significant effect on the response of the basket to the 30 foot drop impact. Utilizing the fundamental frequencies of the basket structure, the DLF is determined from the curve shown in Figure 2.12.7-7, which is extracted from NUREG/CR-3966 [1]. The results provide the DLFs for a half-sine-wave as a function of the ratio of the impulse duration to the natural period of the structure. The half sine wave is used because it provides a reasonable approximation of the actual load experienced by the cask during a drop event.

### 2.12.7.2 Modal Analysis of Basket Side Drop Loading Condition

#### Finite Element Model

Modal analyses were run using an ANSYS® [2] finite element analysis (FEA) model similar to that described in Appendix 2.12.6. The modal analyses were performed for 0, 45, 90-degree side drops, and an end drop condition. Due to the basket structure symmetry, these orientations are assumed to envelop all other orientations. The model utilizes a 16-inch sector of the basket, and is modeled using solid elements and modified such that the fuel weight is included as mass instead of pressure for the modal analysis. The meshed FEA model is shown in Figure 2.12.7-1.

The FEA model is based on nominal dimensions from the basket geometry (Drawing 19885-71-6). There are a few minor differences between the drawing's geometry and the FEA model. These differences include omissions of insignificant details, such as corner fillets and small notches. These are deemed minor and hence the resulting DLF will not measurably change.

The maximum temperature for fuel compartments during normal conditions of transport (NCT) of 100 °F is 463 °F without solar insolation and 468 °F with solar (refer to Table 3-1). For conservatism, the basket was assumed to be at the highest value of 468 °F.

### Boundary Conditions

For the side drop conditions, at the two cut faces, symmetry boundary conditions are applied (e.g.,  $UX = ROTY = ROTZ = 0$ ). The FEA model uses a 16-inch section of the basket, allowing for the symmetry condition to be established on the cut faces in the axial direction. At the outer aluminum plate surfaces (i.e., on the drop side support face), displacement supports constrain translation in the direction parallel and tangential to the drop angle, while the axial direction is free. At the outer aluminum plate surfaces (i.e., perpendicular to the drop side support face), displacement supports constrain translation in the direction perpendicular and tangential to the drop angle, while the axial direction is free. These boundary conditions were chosen to eliminate modes of vibration that are incompatible with the physics of the drop. For instance, side-to-side modes are not important because they are restrained by the cask rails and cask wall and more importantly, because they will have no modal weight in the drop direction and therefore will not be activated by the drop. Boundary conditions for the 0° side drop modal analysis typical to the other side drop orientations are shown in Figure 2.12.7-2.

For the end drop condition, all outer aluminum plate surfaces are frictionless supports constraining translation in the direction perpendicular to the drop angle, while the tangential and axial directions are free. For the ends, the symmetry boundary condition does not apply. Rather, frictionless support is provided on the end drop face only, constraining translation in the direction parallel to the drop angle, while the lateral directions are free.

### Material Properties

For FEA modal analyses, the required material properties are Young's modulus, Poisson's ratio, and density. The stainless steel fuel compartment boxes are constructed of ASTM SA-240, Type 304 stainless steel alloy, while the plugs are ASTM SA-479, Type 304 stainless steel. The aluminum plates and basket periphery plates are constructed of ASTM SB-209, Type 6061-T6 aluminum alloy. The borated aluminum plates are considered ASTM SB-209, Type 6061-T6 aluminum. The following material properties at 468 °F are used [3]:

For SA-240, Type 304 or SA-479, Type 304 at 468 °F:

$$\begin{aligned} E &= 26.024 \times 10^6 \text{ psi} \\ \nu &= 0.29 \\ \rho_{\text{stl}} &= 0.29 \text{ lb}_m/\text{in}^3 \end{aligned}$$

For SB-209, 6061-T6 at 468 °F:

$$\begin{aligned} E &= 8.292 \times 10^6 \text{ psi} \\ \nu &= 0.33 \\ \rho_{\text{AL}} &= 0.098 \text{ lb}_m/\text{in}^3 \end{aligned}$$

The weight of the fuel (1,551 lb<sub>m</sub>) was added to the steel basket density and resolved to 1/10 the 160-inch overall fuel length, matching the FEA model length of 16 inches.

The fuel bounding area is taken over the basket fuel box width of 8.70-inch square fuel basket and the 160-inch maximum fuel box length. The fuel box compartment wall is 0.105 inches thick.

Except for the end drop condition, the steel modified density is increased by projecting the volume over the length of the steel basket lower surface for the 0° and 90° drop and the lower and side surface for the 45° drop, as follows:

$$\rho_{stl.mod} = \rho_{stl} + \frac{1551/10}{(8.7 \times 16 \times 0.105)} = 10.90 \text{ lb}_m$$

$$\rho_{stl.mod.45} = \rho_{stl} + \frac{1551/10}{(8.7 \times 16 \times 0.105 + 8.7 \times 16 \times 0.105)} = 5.596 \text{ lb}_m$$

### Results of the Modal Analysis

The first six modal natural frequencies for each drop angle are summarized in the following table. The deformed mode shape plots for the first mode of each drop are shown in Figure 2.12.7-3, Figure 2.12.7-4, Figure 2.12.7-5, and Figure 2.12.7-6.

**Results Summary - Natural Frequencies**

Mode	Frequency (Hz)			
	0° Drop	45° Drop	90° Drop	End Drop
1	308.9	235.37	328.11	473.08
2	371.59	249.71	384.58	475.4
3	417.08	296.38	411.28	493.9
4	503.25	319.43	503.13	496.49
5	615.58	340.61	543.85	1139.7
6	618.03	373.8	556.71	1241.9

### 2.12.7.3 Dynamic Load Factor Calculations

The DLF is computed for the end and side drops. The impact duration from the LS-DYNA® Model (Appendix 2.12.9) is used to establish the impulse time for the DLF calculation.

From the ratio  $t/T$  in Figure 2.12.7-7, the DLF can be determined. Of note, NUREG/CR-3966 [1] terms the DLF as the dynamic amplification factor (DAF). A shorter duration peak provides a lower ratio, with ratios below three providing the highest possible DLF.

For the side drop, the shortest total peak duration is 15.2 milliseconds (ms) for the NCT cold side drop acceleration (15.9 – 0.7 ms). For the end drop, the shortest total peak duration is 6 ms for the NCT cold end drop acceleration.

The DLF for end and side drops are calculated, using Figure 2.12.7-7 as the equation for the DLF determination. From above, bounding values for the impulse duration are 15.2 ms and 6 ms for the side drop and end drop, respectively. In addition, the lowest natural frequencies are provided in the above table as 235.37 Hz for the side drop and 473.08 Hz for the end drop. The natural period of the basket is the inverse of the lowest natural frequency ( $1/f$ ). In the following table, the resultant DLF is calculated as 1.11 for the end drop and 1.13 for the side drop.

#### Dynamic Load Factor Calculations

Drop Orientation	Natural Frequency, $f$ (Hz)	Natural Time Period, $T$ (Sec.)	Impulse Duration, $t$ (Sec.)	Ratio $t/T$	DLF (from Figure 2.12.7-7)
End Drop	473.08	0.00211	0.006	2.84	1.11
Side Drop	235.37	0.00425	0.0152	3.58	1.13

#### 2.12.7.4 References

1. T. A. Nelson, R. C. Chun, "Methods for Impact Analysis of Shipping Containers," U.S. Nuclear Regulatory Commission, NUREG/CR-3966, November 1987.
2. ANSYS® MAPDL and Workbench, Version 17.1, ANSYS Inc., Canonsburg, PA.
3. ASME Boiler and Pressure Vessel Code, Section II-D "Section II Materials, Part D - Properties – Includes 1992 Edition, July 1, 1992 with 1992 Addenda," December 31, 1992.

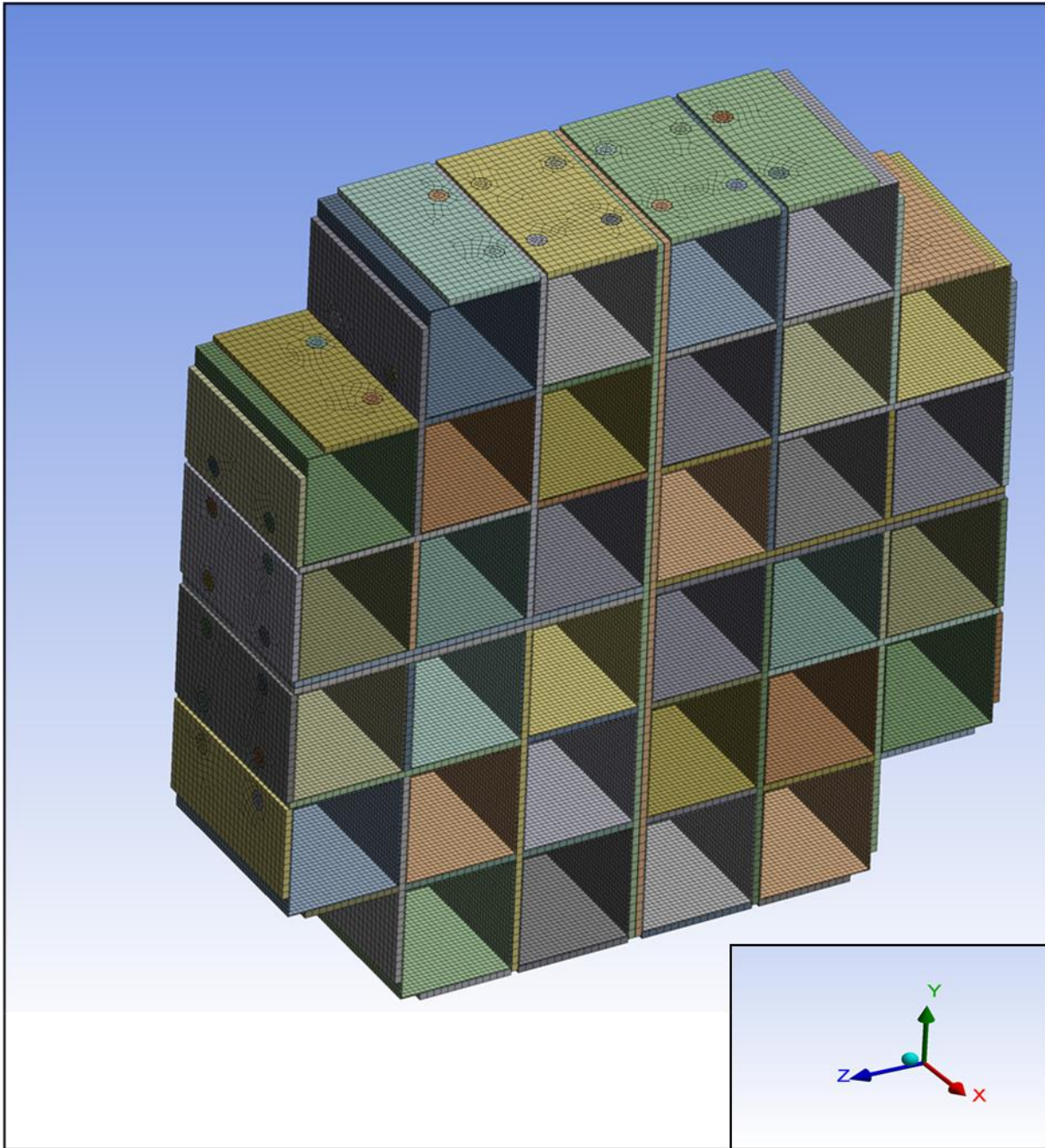


**Figure 2.12.7-1**  
**TN-32B HBU Basket Finite Element Model**

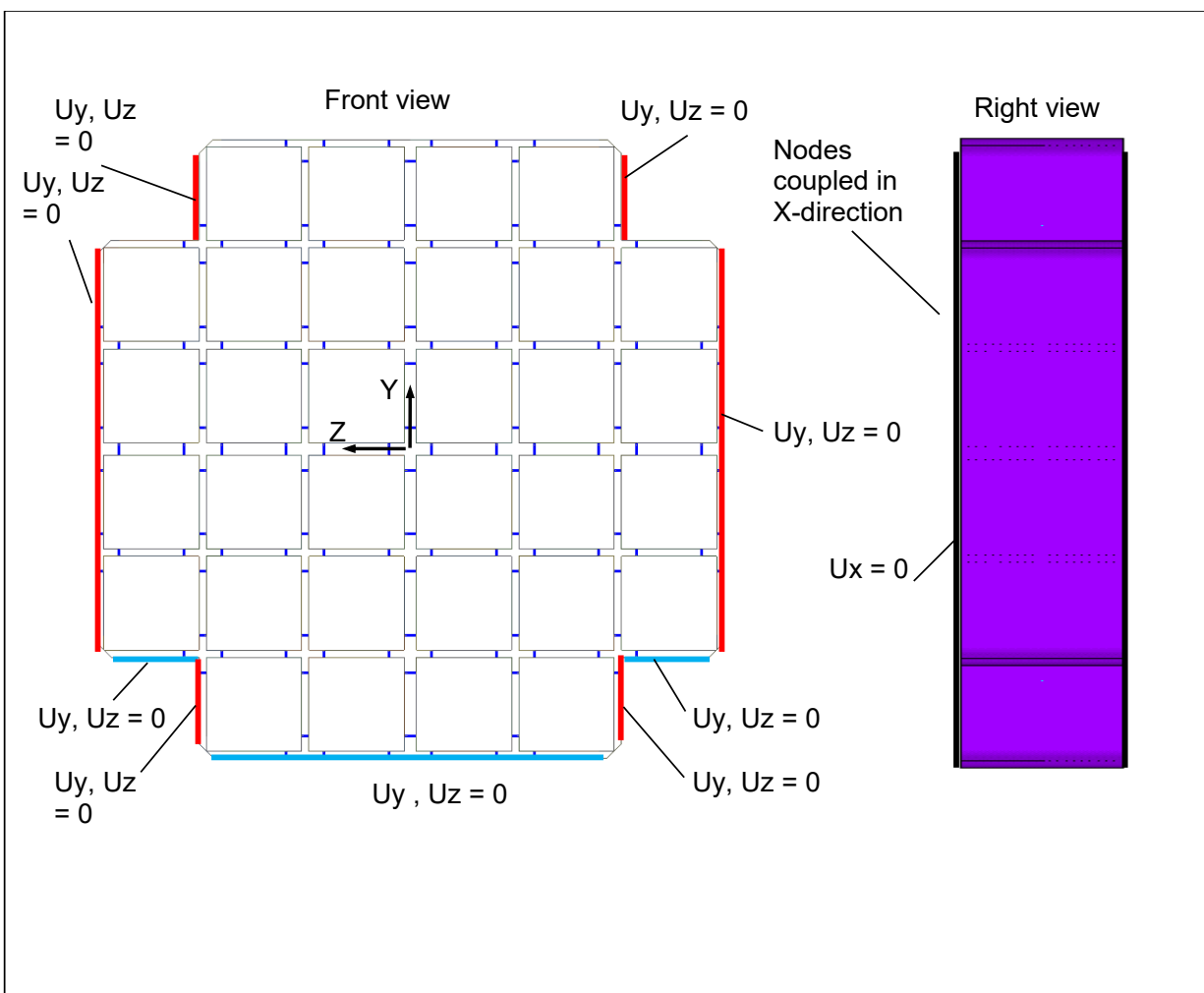


**Figure 2.12.7-2**  
**TN-32B HBU Boundary Conditions of 0° Side Drop**

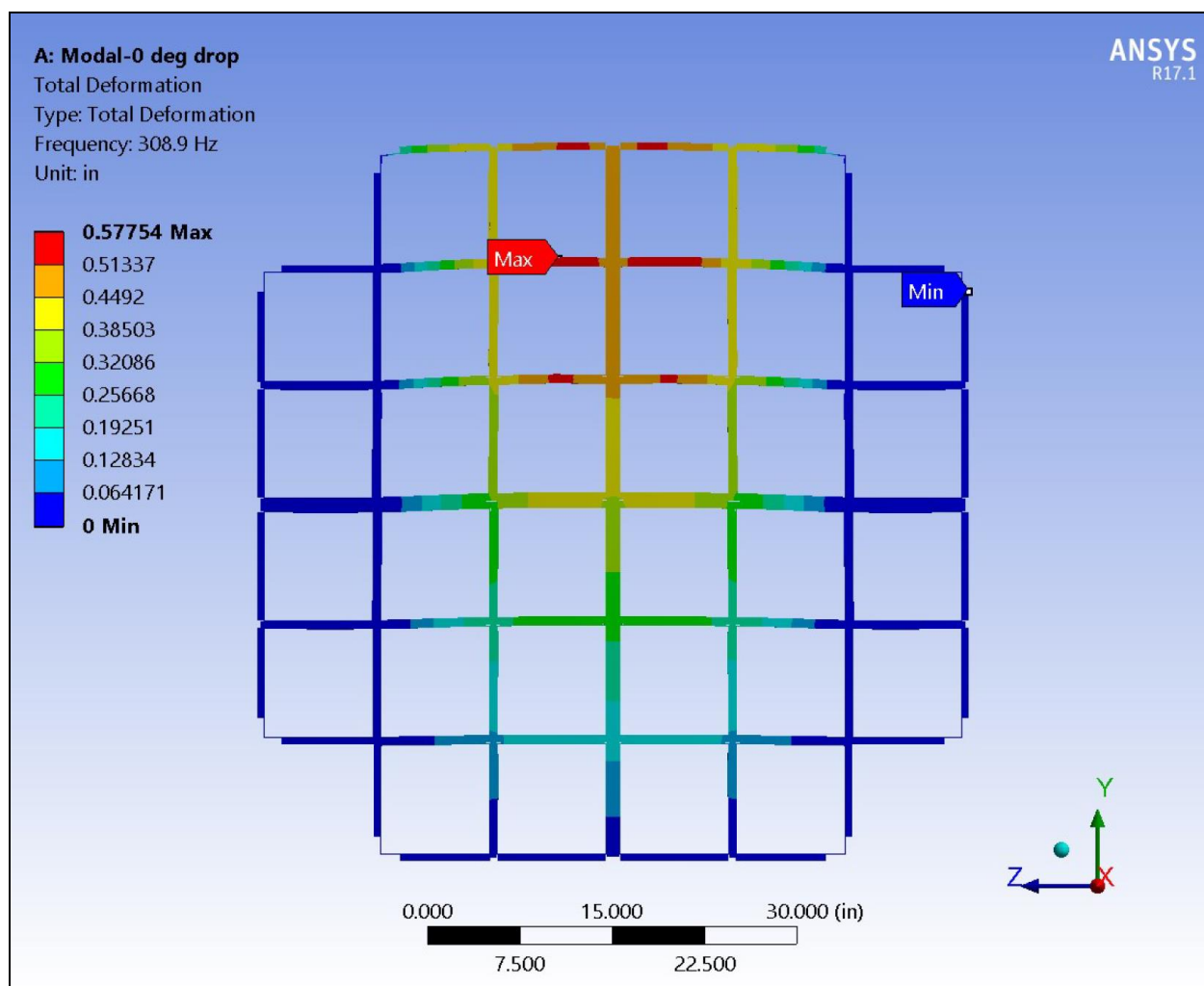


**Figure 2.12.7-3**  
**0° Side Drop - 1st Mode**

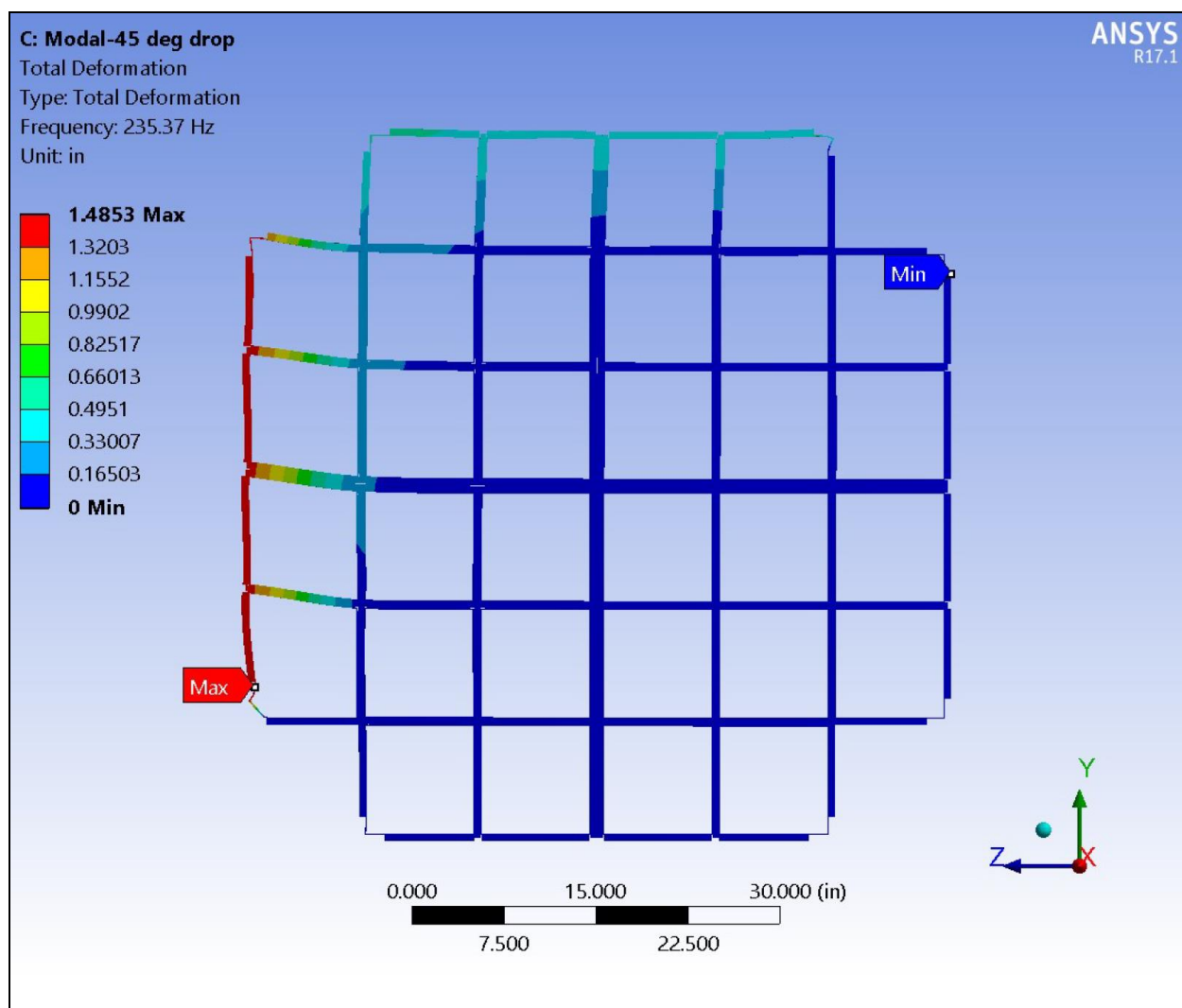


**Figure 2.12.7-4**  
**45° Side Drop - 1st Mode**



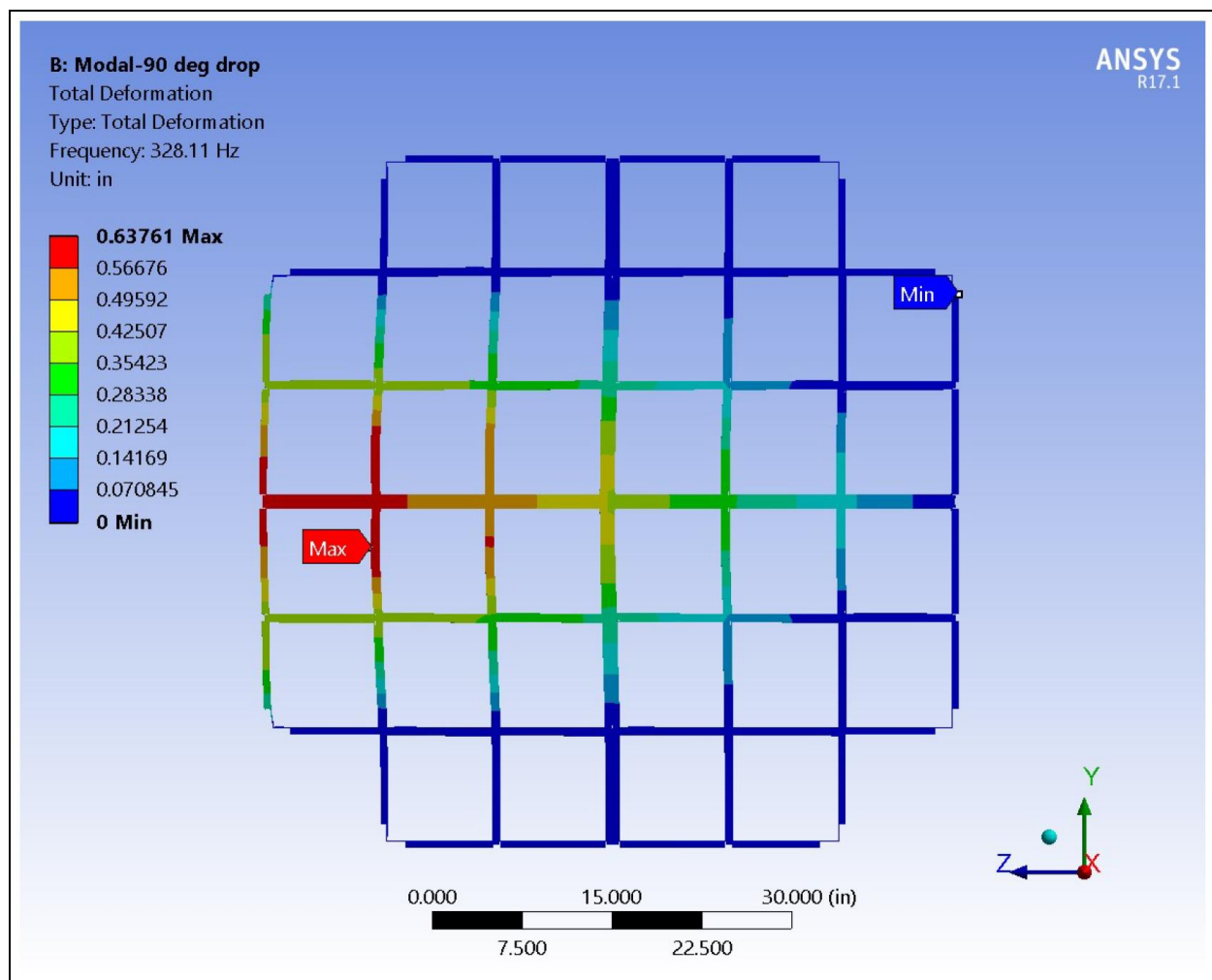


**Figure 2.12.7-5**  
**90° Side Drop - 1st Mode**

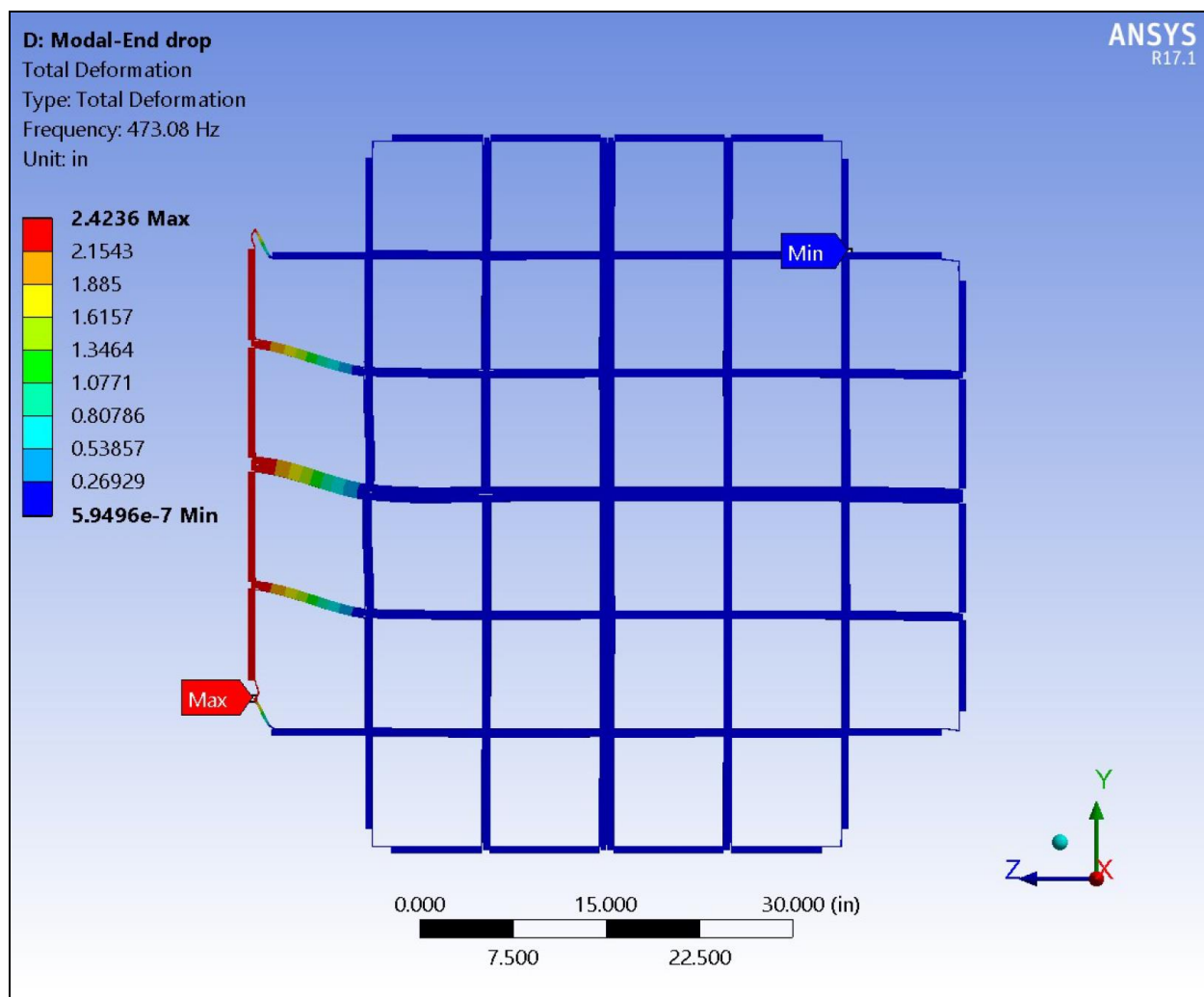


Figure 2.12.7-6  
End Drop - 1st Mode

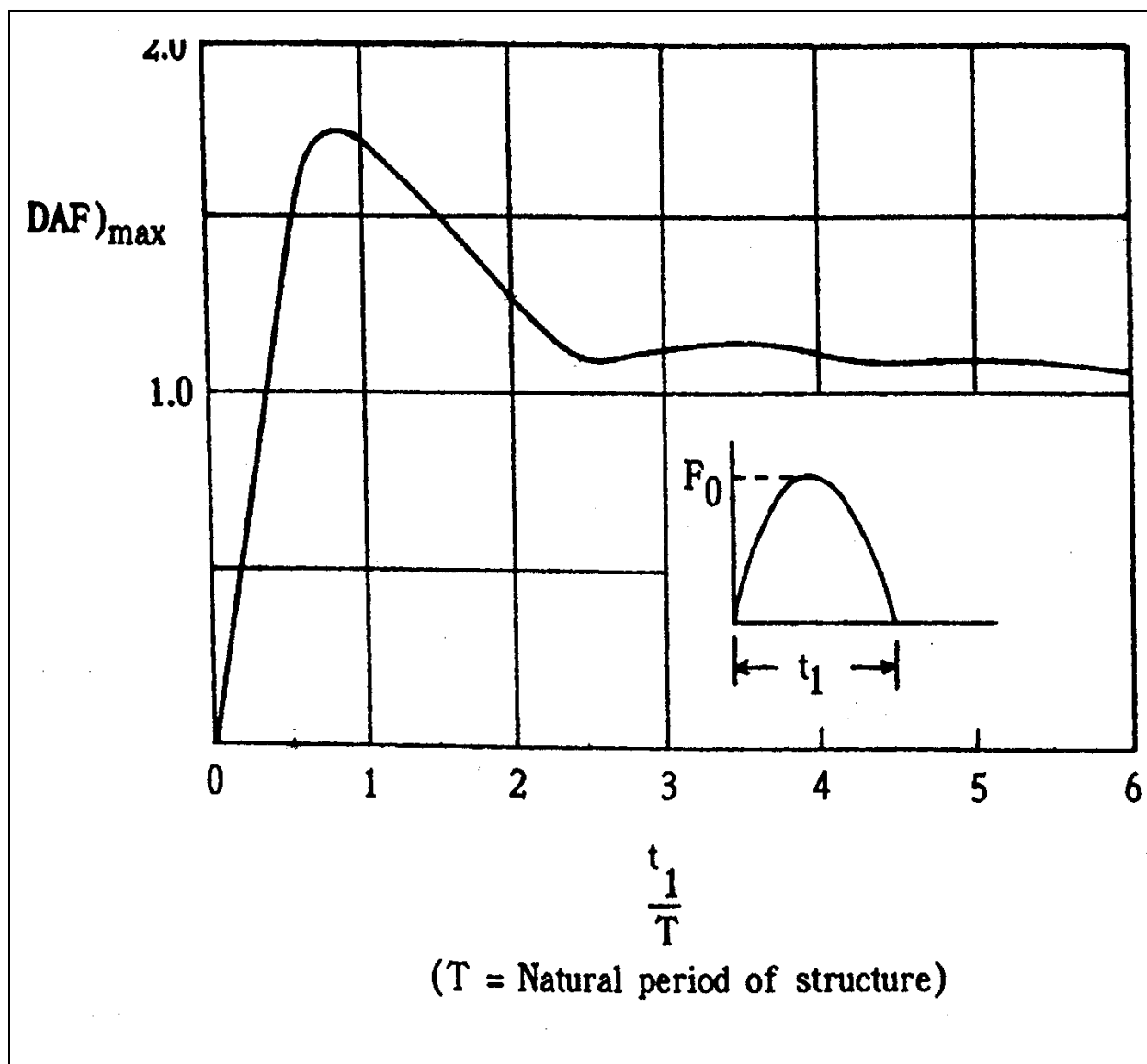


Figure 2.12.7-7  
DLF Relationship for Cask with an Impact Limiter  
(Reproduced from Figure 2.15 of Reference [1])

Proprietary Information on Pages 2.12.8-i through 2.12.8-iii  
and Pages 2.12.8-1 through 2.12.8-44  
Withheld Pursuant to 10 CFR 2.390

## **Appendix 2.12.9**

### **Structural Evaluation of the Impact Limiters**

#### TABLE OF CONTENTS

2.12.9	Structural Evaluation of the Impact Limiters .....	2.12.9-1
2.12.9.1	Introduction .....	2.12.9-1
2.12.9.2	Methodology.....	2.12.9-1
2.12.9.3	Assumptions.....	2.12.9-13
2.12.9.4	Computation.....	2.12.9-13
2.12.9.5	Normal Conditions of Transport Results .....	2.12.9-15
2.12.9.6	Hypothetical Accident Conditions Results .....	2.12.9-16
2.12.9.7	Conclusions.....	2.12.9-24
2.12.9.8	References.....	2.12.9-25

LIST OF TABLES

Table 2.12.9-1	Package Characteristics/Dimensions .....	2.12.9-26
Table 2.12.9-2	IL Shell Properties .....	2.12.9-26
Table 2.12.9-3	Mechanical Properties of Wood .....	2.12.9-27
Table 2.12.9-4	Typical Wood Material Properties .....	2.12.9-27
Table 2.12.9-5	Warm Redwood Load Curves.....	2.12.9-27
Table 2.12.9-6	Cold Redwood Load Curves.....	2.12.9-28
Table 2.12.9-7	Warm Balsa Load Curves.....	2.12.9-28
Table 2.12.9-8	Cold Balsa Load Curves.....	2.12.9-28
Table 2.12.9-9	TN-32B HBU Cask Model Parts, Lower IL .....	2.12.9-29
Table 2.12.9-10	TN-32B HBU Cask Model Parts, Upper IL .....	2.12.9-30
Table 2.12.9-11	TN-32B HBU Cask Model Parts, Misc. Components .....	2.12.9-31
Table 2.12.9-12	Section Properties .....	2.12.9-31
Table 2.12.9-13	Material Models .....	2.12.9-32
Table 2.12.9-14	Hourglass Definitions.....	2.12.9-32
Table 2.12.9-15	FEA Model/Scale Test Unit Weight Comparison.....	2.12.9-32
Table 2.12.9-16	FEA Model/ TN-32B HBU Cask Weight Comparison .....	2.12.9-33
Table 2.12.9-17	Inertia g-Load versus Initial Angle of Impact for 30 Foot Drop .....	2.12.9-33
Table 2.12.9-18	Maximum IL Deformation versus Initial Angle of Impact for 30 Foot Drop .....	2.12.9-34
Table 2.12.9-19	Maximum Inertial g-Load during 1 Foot Drop.....	2.12.9-34
Table 2.12.9-20	Maximum IL Deformation versus Initial Angle of Impact for 1 Foot Drop .....	2.12.9-34
Table 2.12.9-21	Tie-Rod Loads for 30 Foot Cold Side Drop.....	2.12.9-35
Table 2.12.9-22	Tie-Rod Loads for 30 Foot Warm Side Drop.....	2.12.9-35
Table 2.12.9-23	Tie-Rod Loads for 30 Foot Cold Slapdown .....	2.12.9-36
Table 2.12.9-24	Tie-Rod Loads for 30 Foot Warm Slapdown.....	2.12.9-36
Table 2.12.9-25	Tie-Rod Loads for 30 Foot Cold Corner Drop .....	2.12.9-37
Table 2.12.9-26	Tie-Rod Loads for 30 Foot Warm Corner Drop.....	2.12.9-37
Table 2.12.9-27	Tie-Rod Loads for 30 Foot Cold End Drop.....	2.12.9-38
Table 2.12.9-28	Tie-Rod Loads for 30 Foot Warm End Drop .....	2.12.9-38
Table 2.12.9-29	IL Attachment Bolt Loads for 30 Foot Cold Side Drop.....	2.12.9-39
Table 2.12.9-30	IL Attachment Bolt Loads for 30 Foot Warm Side Drop .....	2.12.9-39
Table 2.12.9-31	IL Attachment Bolt Loads for 30 Foot Cold Slapdown.....	2.12.9-40
Table 2.12.9-32	IL Attachment Bolt Loads for 30 Foot Warm Slapdown.....	2.12.9-40

Table 2.12.9-33	IL Attachment Bolt Loads for 30 Foot Cold Corner Drop .....	2.12.9-40
Table 2.12.9-34	IL Attachment Bolt Loads for 30 Foot Warm Corner Drop .....	2.12.9-41
Table 2.12.9-35	IL Attachment Bolt Loads for 30 Foot Cold End Drop .....	2.12.9-41
Table 2.12.9-36	IL Attachment Bolt Loads for 30 Foot Warm End Drop .....	2.12.9-41

### LIST OF FIGURES

Figure 2.12.9-1	Package with ILs .....	2.12.9-42
Figure 2.12.9-2	NCT Cold Side Drop Acceleration .....	2.12.9-43
Figure 2.12.9-3	NCT Cold Side Drop Deflection .....	2.12.9-43
Figure 2.12.9-4	NCT Cold Side Drop Deformation .....	2.12.9-44
Figure 2.12.9-5	NCT Warm Side Drop Acceleration .....	2.12.9-45
Figure 2.12.9-6	NCT Warm Side Drop Deflection .....	2.12.9-45
Figure 2.12.9-7	NCT Warm Side Drop Deformation .....	2.12.9-46
Figure 2.12.9-8	NCT Cold End Drop Acceleration .....	2.12.9-47
Figure 2.12.9-9	NCT Cold End Drop Deflection .....	2.12.9-47
Figure 2.12.9-10	NCT Cold End Drop Deformation .....	2.12.9-48
Figure 2.12.9-11	NCT Warm End Drop Acceleration .....	2.12.9-49
Figure 2.12.9-12	NCT Warm End Drop Deflection .....	2.12.9-49
Figure 2.12.9-13	NCT Warm End Drop Deformation .....	2.12.9-50
Figure 2.12.9-14	HAC Cold Side Drop Acceleration .....	2.12.9-51
Figure 2.12.9-15	HAC Cold Side Drop Deflection .....	2.12.9-51
Figure 2.12.9-16	HAC Cold Side Drop Deformation .....	2.12.9-52
Figure 2.12.9-17	HAC Warm Side Drop Acceleration .....	2.12.9-53
Figure 2.12.9-18	HAC Warm Side Drop Deflection .....	2.12.9-53
Figure 2.12.9-19	HAC Warm Side Drop Deformation .....	2.12.9-54
Figure 2.12.9-20	HAC Cold Secondary Slapdown Acceleration .....	2.12.9-55
Figure 2.12.9-21	HAC Cold Slapdown Deflection .....	2.12.9-55
Figure 2.12.9-22	HAC Cold Slapdown Deformation .....	2.12.9-56
Figure 2.12.9-23	HAC Warm Secondary Slapdown Acceleration .....	2.12.9-57
Figure 2.12.9-24	HAC Warm Slapdown Deflection .....	2.12.9-57
Figure 2.12.9-25	HAC Warm Slapdown Deformation .....	2.12.9-58
Figure 2.12.9-26	HAC Cold Corner Drop Acceleration .....	2.12.9-59
Figure 2.12.9-27	HAC Cold Corner Drop Deflection .....	2.12.9-59
Figure 2.12.9-28	HAC Cold Corner Drop Deformation .....	2.12.9-60

Figure 2.12.9-29	HAC Warm Corner Drop Acceleration .....	2.12.9-61
Figure 2.12.9-30	HAC Warm Corner Drop Deflection .....	2.12.9-61
Figure 2.12.9-31	HAC Warm Corner Drop Deformation .....	2.12.9-62
Figure 2.12.9-32	HAC Cold End Drop Acceleration .....	2.12.9-63
Figure 2.12.9-33	HAC Cold End Drop Deflection.....	2.12.9-63
Figure 2.12.9-34	HAC Cold End Drop Deformation .....	2.12.9-64
Figure 2.12.9-35	HAC Warm End Drop Acceleration.....	2.12.9-65
Figure 2.12.9-36	HAC Warm End Drop Deflection .....	2.12.9-65
Figure 2.12.9-37	HAC Warm End Drop Deformation .....	2.12.9-66
Figure 2.12.9-38	IL Lifting Lug Geometry .....	2.12.9-66



## 2.12.9 Structural Evaluation of the Impact Limiters

### 2.12.9.1 Introduction

This appendix is used to predict the accelerations and deformation of the impact limiters (ILs) for multiple orientations of normal conditions of transport (NCT) and hypothetical accident condition (HAC) free drops per 10 CFR Part 71 [1]. The performance of the TN-32B HBU cask ILs is modeled utilizing a representation of the 1/3-scale TN-40 IL test unit described in Appendix 2.12.10. The analysis utilizes LS-DYNA® [2] to predict the acceleration (g-loads) of the TN-32B HBU demonstration cask in various situations and orientations.

#### 2.12.9.1.1 Impact Limiter Design Comparison

The design of the TN-32 HBU demonstration cask ILs is nearly identical to the TN-40 IL design. The characteristics described herein for the TN-40 cask are found in the TN-40 SAR [3]. The characteristics for the TN-32B HBU demonstration cask ILs are found in Section 1.4.1 and Section 2.1.3.

The weights of the two packages are nearly identical with the gross weight of the TN-40 package at 271.5 kips, and the maximum gross weight of the TN-32B HBU demonstration cask at 269.0 kips. Key dimensions of the packages and the ILs are provided in Table 2.12.9-1.

#### 2.12.9.2 Methodology

The simulations seek to bound the response of the TN-40 1/3-scale test unit (Appendix 2.12.10), and, therefore, bound the response of the TN-32B HBU cask, which is of similar design, size, and weight as the TN-40 cask. The ILs are modeled in full symmetry to capture the out-of-symmetry plane response of the internal IL gussets. The cask body, lid, and payload are not explicitly modeled, but are represented by a rigid solid cylinder that approximates that of the 1/3 scale test unit (Assumption 1). The inertial properties are calculated by hand and are assigned directly to the model based on the dimensions of the test unit.

The package model simulation represents a drop on a completely rigid drop pad to analyze the energy absorbing capabilities of the ILs when subjected to the testing requirements of 10 CFR Part 71. The package is initially positioned with its lowest point against the drop pad with an appropriate initial velocity representing an initial drop height of either 1 foot for the NCT free drop (10 CFR 71.71) or 30 feet for the HAC free drops (10 CFR 71.73). The package free drops are simulated at various impact orientations for both warm and cold ambient temperature conditions. Refer to Figure 2.12.9-1 for a view of the finite element analysis (FEA) model. The set of simulations includes the following:

1. NCT cold 0° side drop, with adjustments to stiffen the wood core material, to determine the highest transverse acceleration on the package during normal conditions of transportation,
2. NCT warm 0° side drop, with adjustments to soften the wood core material, to determine the highest transverse deformation on the package during normal conditions of transportation,

3. NCT cold 90° end drop, with adjustments to stiffen the wood core material to provide input accelerations for dependent structural calculations,
4. NCT warm 90° end drop, with adjustments to soften the wood core material, to determine the highest axial deformation on the package during normal conditions of transportation,
5. HAC cold 0° side drop, with adjustments to stiffen the wood core material, to determine the highest transverse acceleration on the package,
6. HAC warm 0° side drop, with moisture content adjustments to soften the wood core material, to demonstrate that the trunnions will not strike the surface of the drop pad,
7. HAC cold 20°, slapdown, with adjustments to stiffen the wood core material, to determine the highest combined axial and transverse acceleration on the package,
8. HAC warm 20°, slapdown, with adjustments to soften the wood core material, to determine the highest combined axial and transverse acceleration on the package,
9. HAC cold 64° center of gravity (CG) drop, with adjustments to stiffen the wood core material, to demonstrate that the ILs provide the package adequate edge protection in the stiffer case,
10. HAC warm 64° CG drop, with adjustments to soften the wood core material, to demonstrate that the ILs provide the package adequate edge protection in the softer case,
11. HAC cold 90° end drop, with adjustments to stiffen the wood core material, to obtain the highest axial acceleration, and
12. HAC warm 90° end drop, with adjustments to soften the wood core material, to compare against drop test results.

The material properties for these simulations are based on properties from the Wood Handbook [5] and cases documented in Appendix 2.10.8 of the TN-40 SAR [3].

Other than remaining attached to the cask, there are no specific acceptance criteria for the IL performance characteristics evaluated in this document. The IL provides no protection from the HAC fire event. The IL design is driven by the cask's ability to remain leaktight and maintain adequate biological shielding, both of which are demonstrated by analysis in separate calculations.

#### 2.12.9.2.1 Material Properties

Both the TN-32B HBU and the 1/3-scale test unit ILs are fabricated primarily from Type 304 stainless steel with a wood core consisting of redwood and balsa wood (see Section 1.4.1 and Appendix 2.12.10). The ILs are secured to the cask body with ASTM A540, Grade B21, (Class 1 on the test unit and Class 2 on the TN-32B HBU cask) hex bolts, and are connected to each other with tie-rods fabricated from ASTM A193, Grade B7 steel. The cask body and puncture plate are not explicitly modeled, but are included as a rigid body (Assumption 1). These materials are assigned a typical elastic modulus for steel.

### 2.12.9.2.2 Impact Limiter Shell Material

The cask IL shell, gussets, and bolt bosses are modeled with ASTM A240/ASME SA-240 Type 304 stainless steel using a plastic kinematic material for all simulations (LS-DYNA® Material Model 3). The temperature of the steel ranges from -20 °F (cold ambient temperature) to 23 °F for the cold case, and 100 °F to 145 °F for warm drop case (Section 3.1.3).

The following properties are from Reference [4], and are converted to true stress-strain as shown below. The elastic modulus of Type 304 (18Cr-8Ni) stainless steel is for Material Group G found in Table TM-1, while the yield stress is found in Table Y-1. The ultimate strength is found in Table U. The ultimate strain is considered as the elongation from Table 2 from the material specification for SA-240 in Part A of the American Society of Mechanical Engineers (ASME) Boiler and Pressure Vessel (B&PV) Code. These values are presented in Table 2.12.9-2, along with the calculated values for true stress, strain, and the tangent modulus, which are calculated below for the cold ambient temperature range of -20 °F to 100 °F. Calculation of the warm data (100 °F ambient with a peak shell temperature of 145 °F) is not explicitly shown. A value of 0.31 is used for Poisson's ratio in the model (Table PRD of Reference [4]).

- True Yield Stress:  $S_{yt} = S_y \left( 1 + \left( \frac{S_y}{E} + 0.002 \right) \right) = 30.1 \text{ ksi}$
- True Ultimate Stress:  $S_{ut} = S_u (1 + e_u) = 105.0 \text{ ksi}$
- True Yield Strain:  $\epsilon_{yt} = \ln \left( 1 + \left( \frac{S_y}{E} + 0.002 \right) \right) = 0.00306$
- True Ultimate Strain:  $\epsilon_{ut} = \ln(1 + e_u) = 0.336$
- True Tangent Modulus:  $T_{tant} = \frac{S_{ut} - S_{yt}}{\epsilon_{ut} - \epsilon_{yt}} = 225.0 \text{ ksi}$

These values are utilized for the cold (-20 °F ambient) simulations, which is reasonable for the desired simulation data. The impact accelerations and crush deformations will not be significantly affected by the change in strength of the stainless steel IL shell going outside the range of -20 °F to 23 °F. The high temperature region is highly localized to the steel surrounding the cask body, which is also backed by the relatively rigid structure of the cask. In addition, the simulation results are predominantly driven by the crush strength of the redwood components of the core.

The 1/4-inch thick shell is thin compared to the 144-inch IL outer diameter and would contribute much less to the energy absorption capacity of the IL. The change to the crush strength of the IL steel shell due to the temperature variation is assumed to be negligible.

### 2.12.9.2.3 Impact Limiter Bolting Material

The IL attachment bolt material in the 1/3-scale model is ASTM A540, Grade B21, Class 1 steel. The IL bolt washer is also steel. The IL bolts and washers utilize the plastic kinematic material model 3 for LS-DYNA®.

The modulus of elasticity is  $29.0 \times 10^6$  psi (for 1Cr-1/2Mo-V, the material group is C in Table TM-1 of Reference [4]) and Poisson's ratio is input as 0.30 in Table PRD of Reference [4]. The elastic-plastic curve is represented by a bilinear curve with a yield strength of 150 ksi and an ultimate strength of 165 ksi at 10% elongation [4]. The tangent modulus for the slope of the plastic curve is determined below along with the true stress-strain properties.

Alloy ASTM A540, Grade B21, Class 1 at 70 °F

- Elastic Modulus (200 °F):  $E = 29,000$  ksi
- Yield Stress:  $S_y = 150.0$  ksi
- Ultimate Stress:  $S_u = 165.0$  ksi
- Elongation:  $\epsilon_u = 0.10$
- Density:  $\rho = 0.280$  lb<sub>m</sub>/in<sup>3</sup>
- True Yield Stress:  $S_{yt} = S_y \left( 1 + \left( \frac{S_y}{E} + 0.002 \right) \right) = 151.1$  ksi
- True Ultimate Stress:  $S_{ut} = S_u (1 + \epsilon_u) = 181.5$  ksi
- True Yield Strain:  $\epsilon_{yt} = \ln \left( 1 + \left( \frac{S_y}{E} + 0.002 \right) \right) = 0.0071$
- True Ultimate Strain:  $\epsilon_{ut} = \ln(1 + \epsilon_u) = 0.095$
- True Tangent Modulus:  $T_{tant} = \frac{S_{ut} - S_{yt}}{\epsilon_{ut} - \epsilon_{yt}} = 345.8$  ksi

#### 2.12.9.2.4 Impact Limiter Tie-Rod Material

The IL tie-rod material in the 1/3-scale model is ASTM A193, Grade B7 steel. The IL tie-rods use the plastic kinematic material model 3 for LS-DYNA®.

The modulus of elasticity is  $29.0 \times 10^6$  psi (for 1Cr-1/5Mo, the material group is C in Table TM-1 of Reference [4]) and Poisson's ratio is input as 0.30 in Table PRD of Reference [4]. The elastic-plastic curve is represented by a bilinear curve with a yield strength of 105 ksi and an ultimate strength of 125 ksi at 16% elongation [4]. The tangent modulus for the slope of the plastic curve is determined below, along with the true stress-strain properties.

Alloy ASTM A193, Grade B7 at 70 °F

- Elastic Modulus (200 °F):  $E = 29,000$  ksi
- Yield Stress:  $S_y = 105.0$  ksi
- Ultimate Stress:  $S_u = 125.0$  ksi
- Elongation:  $\epsilon_u = 0.16$
- Density:  $\rho = 0.280$  lb<sub>m</sub>/in<sup>3</sup>
- True Yield Stress:  $S_{yt} = S_y \left( 1 + \left( \frac{S_y}{E} + 0.002 \right) \right) = 105.6$  ksi

- True Ultimate Stress:  $S_{ut} = S_u(1 + e_u) = 145.0 \text{ ksi}$
- True Yield Strain:  $\epsilon_{yt} = \ln\left(1 + \left(\frac{S_y}{E} + 0.002\right)\right) = 0.0056$
- True Ultimate Strain:  $\epsilon_{ut} = \ln(1 + e_u) = 0.148$
- True Tangent Modulus:  $T_{tant} = \frac{S_{ut} - S_{yt}}{\epsilon_{ut} - \epsilon_{yt}} = 276.7 \text{ ksi}$

#### 2.12.9.2.5 Essentially Unyielding (Rigid Body) Material

The cask, payload, and drop pad are modeled with the rigid material model 20 for LS-DYNA®. This material does not absorb energy and no stresses or strains are calculated for it. The density of each component is controlled to model the appropriate weight of the item. The elastic modulus and Poisson's ratio of steel are used, but only relevant to the contact algorithms. The cask, payload, and drop pad are constrained through their respective rigid material definition. The base of the drop pad is constrained in all directions and all rotations, which makes it a completely immovable target surface.

#### 2.12.9.2.6 Impact Limiter Wood Material

LS-DYNA® Material Type 126, \*MAT\_MODIFIED\_HONEYCOMB, is utilized to represent both balsa wood and redwood. This material type has three yield surfaces available, of which only the first yield surface was chosen due to the uncoupled nature of its load curves. This material model works with solid element formulations 0, 1, 2, and 9. Solid element formulation is defined in the section card as Type 1; therefore, the local stress-strain curves (e.g., Eaa, Ebb, and Ecc) are uncoupled until the material reaches its fully compacted point. This point occurs at 60% strain for redwood and 80% strain for balsa wood (Section 2.10.8.4.2 of the TN-40 SAR [3]). Note that with this material type it is essential to maintain the stress values of the stress-strain curve greater than zero.

This material type requires hourglass control type 2, Flanagan-Belytschko viscous form, which is defined within the core material section card.

#### Material Coordinate System

The coordinate system for the core material properties is aligned with the axis of the cask. The a-axis of the system is aligned with the axis of the cask. The b-axis extends along the global z-axis. The c-axis is orthogonal to the other two axes and points downward when the cask is oriented for a side drop. The defining vectors for this coordinate system are defined for coordinate with AOPT=2.0, as shown in Figure 2-3 of the LS-DYNA® Keyword User's Manual, Volume II [6].

## Redwood Material Properties

The redwood may be aligned either with its grain perpendicular or parallel to the axis of the cask. When aligned perpendicular to the package centerline, the longitudinal properties will be oriented with the b-axis, the radial will be oriented with the a-axis, and the tangential will be oriented with the c-axis. When aligned parallel to the package centerline, the longitudinal properties will be oriented with the a-axis, the radial will be oriented with the c-axis, and the tangential will be oriented with the b-axis.

The IL wood has an average value of 109 °F in the upper IL and 111 °F in the lower IL (Section 3.1.3) when exposed to the hottest environmental loads (i.e., the 100 °F ambient NCT with insolation thermal case). A value of 120 °F is used for the warm drop cases for both ILs. The average wood temperature of the upper and lower ILs drops to -17 °F in the -20 °F ambient NCT case. A temperature of -20 °F is used for both ILs in the cold drop cases.

A value of 12% moisture content will be used for the warm cases and a value of 6% will be utilized for the cold cases to properly bound the deformation and acceleration in the warm and cold cases, respectively.

Per the IL drawings (Section 1.4.1), the allowable density for redwood in the design is from 18.7 to 27.5 lb<sub>m</sub>/ft<sup>3</sup> with a nominal value of 23.1 lb<sub>m</sub>/ft<sup>3</sup> (3.4596 × 10<sup>-5</sup> lb<sub>r</sub>-s<sup>2</sup>/in<sup>4</sup>). The value is adjusted to increase the weight of the ILs to the approximate weight listed in the weight calculation. A value of 4.240 × 10<sup>-5</sup> lb<sub>r</sub>-s<sup>2</sup>/in<sup>4</sup> is used in the model.

## Elastic Moduli

In general, the elastic moduli of wood decrease as the moisture content of the wood increases. The moisture content for both balsa and redwood in the IL is limited to a range of 6 to 12% (Section 1.4.1). In this evaluation, the warm material properties are calculated based on elastic moduli at 12% moisture content while cold material properties are calculated based on elastic moduli at 6% moisture content.

### Warm Properties

The longitudinal modulus of elasticity from the Wood Handbook for old-growth at 12% moisture content is 1.34 × 10<sup>6</sup> psi (Table 5-3b of Reference [5]).

$$\text{Longitudinal Modulus of Elasticity:} \quad E_{12} = 1.34 \times 10^6 \text{ psi}$$

The change in the elastic modulus due to the 120 °F temperature is extrapolated from the values found in Table 5-15 of Reference [5]. The percent change at 12% moisture content is:

$$p_{EW} = \frac{120^\circ\text{F} - (68^\circ\text{F})}{122^\circ\text{F} - (68^\circ\text{F})} (-7\% - 0\%) + 0\% = -6.7\%$$

The longitudinal elastic modulus decreased to:

$$\text{Longitudinal Modulus of Elasticity:} \quad E_{bb} = E_{12}(1 + p_{EW}) = 1.25 \times 10^6 \text{ psi}$$

The radial and tangential direction modulus of elasticity are  $0.087\epsilon_{bb}$  and  $0.089\epsilon_{bb}$ , respectively (based on the ratios from Table 5-1 of the Reference [5]). The three moduli of rigidity, from the wood handbook, are  $G_{ab} = 0.066\epsilon_{bb}$ ,  $G_{bc} = 0.077\epsilon_{bb}$ , and  $G_{ca} = 0.011\epsilon_{bb}$ . The values, with the wood grain aligned perpendicular to the axis of the cask, are calculated below.

$$\text{Radial Modulus of Elasticity: } E_{aa} = 0.087E_{bb} = 1.09 \times 10^5 \text{ psi}$$

$$\text{Tangential Modulus of Elasticity: } E_{cc} = 0.089E_{bb} = 1.11 \times 10^5 \text{ psi}$$

$$\text{Radial/Longitudinal Shear Modulus: } G_{ab} = 0.066E_{bb} = 8.25 \times 10^4 \text{ psi}$$

$$\text{Longitudinal/Radial Shear Modulus: } G_{bc} = 0.077E_{bb} = 9.63 \times 10^4 \text{ psi}$$

$$\text{Tangential/Radial Shear Modulus: } G_{ca} = 0.011E_{bb} = 1.38 \times 10^4 \text{ psi}$$

The elastic moduli for the warm case are listed in Table 2.12.9-3.

### Cold Properties

To obtain the values at 6% moisture content, Equation 5-3 in Chapter 5 of Reference [5] is utilized with moisture content constant ( $M_p$ ) equal to 21 from Table 5-13 for redwood. From Table 5-3b of Reference [5], the elastic modulus for green old-growth redwood is  $1.18 \times 10^6$  psi. The modulus of elasticity for 6% moisture,  $E_{06}$ , is:

$$E_{06} = E_{12} \left[ \frac{E_{12}}{E_g} \right]^{\frac{12-x}{M_p-12}} = E_{12} \left[ \frac{E_{12}}{E_g} \right]^{\frac{12-6}{21-12}} = 1.46 \times 10^6 \text{ psi}$$

The change in the elastic modulus due to the -20 °F ambient temperature is doubly interpolated between 68 °F and -58 °F and moisture content of 0 to 12%, from the values found in Table 5-15 of Reference [5]. The percent change is:

$$p_{Ec} = \frac{-20^\circ\text{F} - (-58^\circ\text{F})}{68^\circ\text{F} - (-58^\circ\text{F})} \left( 0\% - \frac{+17\% + (+11\%)}{2} \right) + \frac{+17\% + (+11\%)}{2} = 9.78\%$$

The longitudinal elastic modulus is increased to:

$$\text{Longitudinal Modulus of Elasticity: } E'_{bb} = E_{06}(1 + p_{Ec}) = 1.60 \times 10^6 \text{ psi}$$

The values for the cold drop cases, with the wood grain aligned perpendicular to the axis of the cask, are calculated below.

$$\text{Radial Modulus of Elasticity: } E'_{aa} = 0.087E'_{bb} = 1.39 \times 10^5 \text{ psi}$$

$$\text{Tangential Modulus of Elasticity: } E'_{cc} = 0.089E'_{bb} = 1.42 \times 10^5 \text{ psi}$$

$$\text{Radial/Longitudinal Shear Modulus: } G'_{ab} = 0.066E'_{bb} = 1.06 \times 10^5 \text{ psi}$$

$$\text{Longitudinal/Radial Shear Modulus: } G'_{bc} = 0.077E'_{bb} = 1.23 \times 10^5 \text{ psi}$$

$$\text{Tangential/Radial Shear Modulus: } G'_{ca} = 0.011E'_{bb} = 1.76 \times 10^4 \text{ psi}$$

The elastic moduli for the cold case are listed in Table 2.12.9-3.

### Stress-Strain Curves

As noted in Section 8.1.5.1.3, the acceptable range of the average compressive stress (ACS) for redwood is 5,100 to 6,630 psi. These values will be confirmed at ambient temperature and are independent of the moisture content of the wood. In order to provide bounding deformation in the drop cases, the lower end value of 5,100 psi will be used for the warm cases.

### Warm Properties

The change in the compressive strength parallel to the grain at 120 °F with a moisture content of 12% is extrapolated from the values found in Table 5-15 of Reference [5]. The percent change is:

$$p_{sw} = \frac{120^\circ\text{F} - (68^\circ\text{F})}{122^\circ\text{F} - (68^\circ\text{F})} (-25\% - 0\%) + 0\% = -24.1\%$$

The longitudinal compressive strength,  $\sigma_{bb}$ , is:

$$\sigma_{bb} = (1 + p_{sw})5,100 = 3,871 \text{ psi}$$

The longitudinal yield strain,  $\epsilon_{bb}$ , is calculated as:

$$\epsilon_{bb} = \frac{\sigma_{bb}}{E_{bb}} = \frac{3,871}{1.25 \times 10^6} = 0.0031 \text{ in/in}$$

Based on the relationship between the compressive lateral and longitudinal yield stresses in Table 5-3b of Reference [5], the lateral compressive stress is estimated to be approximately 11% of the longitudinal ACS, which is 426 psi. The lateral yield strain,  $\epsilon_{aa}$ , is calculated as:

$$\epsilon_{aa} = \epsilon_{cc} = \frac{\sigma_{cc}}{E_{cc}} = \frac{426}{1.11 \times 10^5} = 0.0038 \text{ in/in}$$

Due to the similarities between radial and tangential elastic moduli, the same load curve will be used for both directions.

Based on the relationship between the compressive lateral and shear stresses in Table 5-3b of Reference [5], the shear stress is estimated to be approximately 15% of the longitudinal ACS, which is 581 psi. The shear yield strain,  $\epsilon_{bc}$ , is calculated as:

$$\epsilon_{bc} = \epsilon_{ca} = \epsilon_{ab} = \frac{\tau_{bc}}{G_{bc}} = \frac{581}{9.63 \times 10^4} = 0.0060 \text{ in/in}$$

The lock-up stress for redwood is assumed to occur at 60% strain (Assumption 4).

At lock-up, the modulus for all redwood curves rises steeply. This rise proceeds until the material reaches a maximum volumetric strain that is somewhat less than 100%. However, the material curve extends to 100% compressive strain to help ensure stability of the model. The lockup modulus is assumed to be 10 times the maximum crush stress for the warm stress curves. The stress at 100% crush calculated as:



$$\sigma_{bb,L} = E_L \Delta\epsilon + \sigma_{bb} = 10\sigma_{bb} \Delta\epsilon + \sigma_{bb} = 10(3,871)(1.00 - 0.60) + \sigma_{bb} = 19,355 \text{ psi}$$

$$\sigma_{cc,L} = E_{cc,L} \Delta\epsilon + \sigma_{cc} = 10\sigma_{cc} \Delta\epsilon + \sigma_{cc} = 10(426) \times (1.00 - 0.60) + \sigma_{cc} = 2,130 \text{ psi}$$

$$\tau_L = G_{bc,L} \Delta\epsilon + \tau_{bc} = 10\tau_{bc} \Delta\epsilon + \tau_{bc} = 10(581) \times (1.00 - 0.60) + \tau_{bc} = 2,905 \text{ psi}$$

The stress-strain warm curves are shown in the first two columns of Table 2.12.9-5.

### Cold Properties

The upper end of 6,630 psi will be used with the cold cases to bound the resultant accelerations. The change in the compressive strength parallel to the grain at -20 °F with a moisture content of 6% is interpolated from the values found in Table 5-15 of Reference [5]. The percent change is:

$$p_{Sc} = \frac{-20^\circ\text{F} - (-58^\circ\text{F})}{68^\circ\text{F} - (-58^\circ\text{F})} \left( 0\% - \frac{20\% + 50\%}{2} \right) + \frac{20\% + 50\%}{2} = 24.4\%$$

The longitudinal compressive strength is:

$$\sigma'_{bb} = (1 + p_{Sc})6,630 = 8,248 \text{ psi}$$

The longitudinal yield strain is calculated as:

$$\epsilon'_{bb} = \frac{\sigma'_{bb}}{E'_{bb}} = \frac{8,248}{1.60 \times 10^6} = 0.0052 \text{ in/in}$$

Again, based on the relationship between the compressive lateral and longitudinal yield stresses in Table 5-3b of Reference [5], the lateral compressive stress is estimated to be approximately 11% of the longitudinal ACS, which is 907 psi. The lateral yield strain is calculated as:

$$\epsilon'_{aa} = \epsilon'_{cc} = \frac{\sigma'_{cc}}{E'_{cc}} = \frac{907 \text{ psi}}{1.42 \times 10^5 \text{ psi}} = 0.0064 \text{ in/in}$$

Based on the relationship between the compressive longitudinal and shear stresses in Table 5-3b of the Wood Handbook, the shear stress is estimated to be approximately 15% of the longitudinal ACS, which is 1,237 psi. The shear yield strain is calculated as:

$$\epsilon'_{bc} = \epsilon'_{ca} = \epsilon'_{ab} = \frac{\tau'_{bc}}{G'_{bc}} = \frac{1,237}{1.23 \times 10^5} = 0.0101 \text{ in/in}$$

The lockup modulus is assumed to be 10 times the maximum crush stress for the cold stress curves. The stress at 100% crush is calculated as:

$$\sigma'_{bb,L} = E'_{bb,L} \Delta\epsilon + \sigma'_{bb} = 10\sigma'_{bb} \Delta\epsilon + \sigma'_{bb} = 10(8,248)(1.00 - 0.60) + \sigma'_{bb} = 41,240 \text{ psi}$$

$$\sigma'_{cc,L} = E'_{cc,L} \Delta\epsilon + \sigma'_{cc} = 10\sigma'_{cc} \Delta\epsilon + \sigma'_{cc} = 10(907 \text{ psi})(1.00 - 0.60) + \sigma'_{cc} = 4,535 \text{ psi}$$

$$\tau'_L = G'_{bc,L} \Delta\epsilon + \tau'_{bc} = 10\tau'_{bc} \Delta\epsilon + \tau'_{bc} = 10(1,237)(1.00 - 0.60) + \tau'_{bc} = 6,185 \text{ psi}$$

The stress-strain cold curves are shown in Table 2.12.9-6.

### Balsa Wood Material Properties

The balsa wood is aligned perpendicular to the package centerline, the longitudinal properties are oriented with the b-axis, the radial are oriented with the a-axis, and the tangential are oriented with the c-axis.

Per the IL drawings (Section 1.4.1), the allowable density for balsa wood is from 7 to 12 lb<sub>m</sub>/ft<sup>3</sup>. The nominal value of 9.5 lb<sub>m</sub>/ft<sup>3</sup> ( $1.4228 \times 10^5$  lb<sub>r</sub>-s<sup>2</sup>/in<sup>4</sup>) is used in the model.

### **Elastic Moduli**

#### Warm Properties

The longitudinal modulus of elasticity from the Wood Handbook for balsa at 12% moisture content is  $0.49 \times 10^6$  psi (Table 5-5b of Reference [5]).

$$\text{Longitudinal Modulus of Elasticity: } E_{12} = 4.9 \times 10^5 \text{ psi}$$

The change in the elastic modulus above due to the 120 °F temperature is the same as the -6.7% extrapolated for warm redwood property above. The longitudinal compressive strength decreases to:

$$\text{Longitudinal Modulus of Elasticity: } E_{bb} = E_{12}(1 - p_{EW}) = 4.57 \times 10^5 \text{ psi}$$

The radial and tangential direction modulus of elasticity are  $0.046E_{bb}$  and  $0.015E_{bb}$  respectively (based on the ratios from Table 5-1 of Reference [5]). The three moduli of rigidity, from the wood handbook, are  $G_{ab}=0.054E_{bb}$ ,  $G_{bc}=0.037E_{bb}$ , and  $G_{ca} 0.005E_{bb}$ . The values, with the wood grain aligned perpendicular to the axis of the cask, are calculated below.

$$\text{Radial Modulus of Elasticity: } E_{aa} = 0.046E_{bb} = 2.10 \times 10^4 \text{ psi}$$

$$\text{Tangential Modulus of Elasticity: } E_{cc} = 0.015E_{bb} = 6.86 \times 10^3 \text{ psi}$$

$$\text{Radial/Longitudinal Shear Modulus: } G_{ab} = 0.054E_{bb} = 2.50 \times 10^4 \text{ psi}$$

$$\text{Longitudinal/Radial Shear Modulus: } G_{bc} = 0.037E_{bb} = 1.69 \times 10^4 \text{ psi}$$

$$\text{Tangential/Radial Shear Modulus: } G_{ca} = 0.005E_{bb} = 2.29 \times 10^3 \text{ psi}$$

The elastic moduli for the warm case are listed in Table 2.12.9-3.

#### Cold Properties

Equation 5-3 of Chapter 5 of Reference [5] cannot be utilized to determine the elastic modulus at 6% moisture content without assuming values for moisture content and the modulus of elasticity for green wood. However, given the relative toughness of balsa wood to redwood, it is unlikely that the unaccounted moisture content change will be significant in the analysis. Therefore, the change in strength due to the moisture content change from 12% to 6% is not included in this analysis.

Longitudinal Modulus of Elasticity:  $E_{06} = E_{12} = 4.90 \times 10^5 \text{ psi}$

The change in the elastic modulus above due to the -20 °F ambient temperature is the same as the 9.78% interpolated for redwood above. The longitudinal modulus of elasticity increases to:

Longitudinal Modulus of Elasticity:  $E'_{bb} = E_{06}(1 + p_{Ec}) = 5.38 \times 10^5 \text{ psi}$

The values for the cold drop cases, with the c-vector, and the wood grain, aligned perpendicular to the axis of the cask are calculated below.

Radial Modulus of Elasticity:  $E'_{aa} = 0.046E'_{bb} = 2.47 \times 10^4 \text{ psi}$

Tangential Modulus of Elasticity:  $E'_{cc} = 0.015E'_{bb} = 8.07 \times 10^3 \text{ psi}$

Radial/Longitudinal Shear Modulus:  $G'_{ab} = 0.054E'_{bb} = 2.91 \times 10^4 \text{ psi}$

Longitudinal/Radial Shear Modulus:  $G'_{bc} = 0.037E'_{bb} = 1.99 \times 10^4 \text{ psi}$

Tangential/Radial Shear Modulus:  $G'_{ca} = 0.005E'_{bb} = 2.69 \times 10^3 \text{ psi}$

The elastic moduli for the cold case are listed in Table 2.12.9-3.

### Stress-Strain Curves

As noted in Section 8.1.5.1.3, the acceptable range of the ACS for balsa wood is 1,500 to 1,930 psi. These values will be confirmed at ambient temperature and are independent of the moisture content of the wood. In order to provide bounding deformation in the drop cases, the lower end value of 1,500 psi will be used for the warm cases.

### Warm Curves

The change in the stresses above due to the 120 °F temperature is the same as the -24.1% extrapolated for redwood above. The longitudinal compressive strength,  $\sigma_{bb}$ , is:

$$\sigma_{bb} = (1 + p_{sw})1,500 \text{ psi} = 1,139 \text{ psi}$$

The longitudinal yield strain,  $\epsilon_{bb}$ , is calculated as:

$$\epsilon_{bb} = \frac{\sigma_{bb}}{E_{bb}} = \frac{1,139}{4.57 \times 10^5} = 0.0025 \text{ in/in}$$

Based on the relationship observed in the redwood between the compressive lateral and longitudinal yield strains calculated above, the lateral compressive strain of the balsa wood is expected to be similar in magnitude, but greater than, the longitudinal strain. Conservatively, the lateral yield strain is assumed to be the same as the longitudinal strain. This value is utilized to calculate the lateral shear stress.

$$\sigma_{aa} = \sigma_{cc} = E_{aa}(\epsilon_{aa}) = (2.10 \times 10^4)(0.0025) = 52.5 \text{ psi}$$

For software stability reasons, this value will be increased to 200 psi.

Based on the relationship between the compressive longitudinal and shear stresses in Table 5-5b of the Wood Handbook, the shear stress is estimated to be approximately 14% of the longitudinal ACS, which is 159 psi. The shear yield strain is calculated as:

$$\epsilon_{ab} = \epsilon_{bc} = \epsilon_{ca} = \frac{\tau_{ab}}{G_{ab}} = \frac{159 \text{ psi}}{2.50 \times 10^4 \text{ psi}} = 0.0064 \text{ in/in}$$

The lockup modulus is assumed to be 10 times the maximum crush stress for the warm stress curves (Assumption 5). The stress at 100% crush calculated as:

$$\sigma_{bb,L} = E_L \Delta\epsilon + \sigma_{bb} = 10\sigma_{bb} \Delta\epsilon + \sigma_{bb} = 10(1,139 \text{ psi})(1.00 - 0.80) + \sigma_{bb} = 3,417 \text{ psi}$$

For software stability reasons, the 100% crush stress will be used in the warm balsa materials. The stress-strain warm curves are shown in Table 2.12.9-7.

### Cold Curves

The upper end of 1,930 psi will be used with the cold cases to bound the resultant accelerations. The change in the stresses above due to the -20 °F ambient temperature is the same as the 24.4% interpolated for the cold redwood above. The longitudinal compressive strength is:

$$\sigma'_{bb} = (1 + p_{sc})1,930 = 2,401 \text{ psi}$$

The longitudinal yield strain is calculated as:

$$\epsilon'_{bb} = \frac{\sigma'_{bb}}{E'_{bb}} = \frac{2,401}{5.38 \times 10^5} = 0.0045 \text{ in/in}$$

Again, the lateral yield strain is assumed to be the same as the longitudinal strain. This value is used to calculate the lateral shear stress.

$$\sigma'_{aa} = \sigma'_{cc} = E'_{aa}(\epsilon'_{aa}) = (2.47 \times 10^4)(0.0045) = 111 \text{ psi}$$

For software stability, this value will be increased to 200 psi.

Based on the relationship between the compressive longitudinal and shear stresses in Table 5-5b of Reference [5], the shear stress is estimated to be approximately 14% of the longitudinal ACS, which is 336 psi. The shear yield strain is calculated as:

$$\epsilon'_{ab} = \epsilon'_{bc} = \epsilon'_{ca} = \frac{\tau'_{ab}}{G'_{ab}} = \frac{336}{2.91 \times 10^4} = 0.012 \text{ in/in}$$

The lockup modulus is assumed to be 10 times the maximum crush stress for the cold stress curves (Assumption 5). The stress at 100% crush calculated as:

$$\sigma'_{bb,L} = E'_L \Delta\epsilon + \sigma'_{bb} = 10\sigma'_{bb} \Delta\epsilon + \sigma'_{bb} = 10(2,401)(1.00 - 0.80) + \sigma'_{bb} = 7,203 \text{ psi}$$

For software stability reasons, the 100% crush stress will be used in the warm balsa wood materials. The stress-strain cold curves are shown in Table 2.12.9-8.

### 2.12.9.3 Assumptions

The following assumptions are utilized:

1. The cask and payload are assumed to be completely rigid for the impact simulations. The structural integrity of the cask is evaluated in a separate calculation and the cask is significantly robust compared to the ILs. The payload does not affect the IL performance, except for the gross package weight and is, therefore, included with the cask as rigid.
2. The CG-over-corner drop is inclined at an angle of 64° from the horizontal plane, which assumes that the payload and dunnage weight are evenly distributed over the payload cavity.
3. The preload is determined by using  $T = KF_d$ , where the nominal bolt torque  $T$  is 9 lb<sub>r</sub>-ft in 1/3-scale,  $K$  is an assumed torque (nut) factor of 0.15, and  $d$  is the bolt thread diameter of 1.5 in. The bolts are to be lubricated with a nickel-based nuclear grade lubricant, which is the reason the torque factor is assumed to be 0.15. No preload is specified for the tie-rods.
4. For redwood crush strength curves, the wood is assumed to lock up at 60% of volume reduction. For balsa wood crush strength curves, the lockup is at 80%. This assumption is based upon previous analyses for this style of IL (TN-40 SAR [3], Section 2.10.8.4.2, Assumption 4 utilizing Figure 2.10.8-2 and Figure 2.10.8-3 as examples).
5. The lockup modulus for both the redwood and balsa wood are assumed to be 10 times the maximum crush stress. Refer to Appendix 2.10.8 of the TN-40 Transportation SAR [3]).

### 2.12.9.4 Computation

A general description of the computational model is followed by case-by-case details.

#### 2.12.9.4.1 Model Description

A basic FEA model was created to represent the 1/3-scale TN-40 test unit and the full-scale TN-32B HBU demonstration cask. The model was created fully symmetric to capture the effects of the impact limiter (IL) gussets buckling along the symmetry plane of the model.

The geometry, parts, materials, loads, and constraints for the model are explicitly defined within a series of LS-DYNA® input files. The model consists of 77 parts, 175,034 elements, and 219,816 nodes. Each part is listed in Table 2.12.9-9 through Table 2.12.9-11 with its material of construction; and its section, material, hourglass and hourglass card definitions. Key properties of the section card definitions are listed in Table 2.12.9-12. Material models and hourglass card definitions are listed in Table 2.12.9-13 and Table 2.12.9-14, respectively.

Tied contacts are used to connect the tie-rod attachment brackets (towers in the model) to the IL surfaces. Automatic contacts are utilized between the model components.

The models are initially positioned a fraction of an inch above the drop pad with an initial velocity due to the regulatory drop height. The NCT model is given an initial velocity of 96.3 inch/sec to represent a one-foot drop height. The HAC models are given an initial velocity of 527.45 inch/sec to represent a thirty-foot drop height. A body force with an acceleration of 386.4 inch/sec<sup>2</sup> is applied to the model to represent the force of gravity.

The TN-32B HBU demonstration cask calculated maximum weight is 269,000 lb<sub>m</sub> (Section 2.1.3). However, a maximum weight of 273,000 lb<sub>m</sub> is utilized in the evaluation of the ILs. Based on the mass of the cask and the test unit, the scaling factor for the mass-based accelerations is:

$$SF = \left[ \frac{273,000}{10,047} \right]^{1/3} = 3.0$$

The model weights and the equivalent test unit component weights are compared in Table 2.12.9-15. The model weights and the TN-32B HBU weights are compared in Table 2.12.9-16. The comparisons demonstrate that there is very little difference between the weight of the test unit and the model using the nominal weight of the package. The variation between the model and the TN-32B HBU cask, considering a scaling factor, is approximately 1%. Therefore, using an LS-DYNA® model of the scaled test unit will provide comparable results to the full-scale TN-32B HBU demonstration cask.

#### 2.12.9.4.2 Filtering

In all cases, the time history acceleration data obtained from the numerical simulations contains high frequency structural vibration and numerically induced noises that are filtered out to provide an accurate assessment of the loadings on the package. In post-processing these simulations, the time history acceleration data is processed with a low-pass Butterworth filter. The cutoff frequencies for the filter are based on the mass of the test article and the experience based relationship found in Section 701.9 of IAEA Specific Safety Guide No. SSG-26 [7].

The high-pass cutoff frequency of the package is:

$$f_c = \{100 \text{ to } 200 \text{ Hz}\} \left( \frac{100}{m} \right)^{\frac{1}{3}} = 271 \text{ to } 542 \text{ Hz}$$

where m is the mass of the scale test unit in tons. A cutoff frequency of 600 Hz is utilized as a bounding cutoff frequency.

## 2.12.9.5 Normal Conditions of Transport Results

### 2.12.9.5.1 NCT Cold Side Drop (-20 °F Ambient)

The acceleration and maximum deflection of the NCT cold side drop model are shown in Figure 2.12.9-2, Figure 2.12.9-3, and Figure 2.12.9-4. The peak acceleration is calculated to be 33.9g, which corresponds to 11.3g in the full-scale cask. The maximum deflection (or crush) of the ILs is estimated based on the rigid body deflection of the cask. The maximum deflection is 0.52 inch, which equates to 1.6 inches in the full-scale package, as shown in Figure 2.12.9-3. The maximum package deformation occurs approximately at 11.6 milliseconds and is shown in Figure 2.12.9-4.

Beam forces are plotted for the tie-rods and the IL attachment bolts. The maximum tensile force in the tie-rods is 2,973 lb<sub>f</sub>, which is 26,757 lb<sub>f</sub> in the full-scale package. The maximum bolt force is 1,541 lb<sub>f</sub>, which is 13,869 lb<sub>f</sub> in the full-scale package.

### 2.12.9.5.2 NCT Warm Side Drop (100 °F Ambient)

The acceleration and maximum deflection of the NCT warm side drop model are shown in Figure 2.12.9-5, Figure 2.12.9-6, and Figure 2.12.9-7. The peak acceleration is calculated to be approximately 27.9g, which corresponds to 9.3g in the full-scale cask. The maximum crush of the ILs is estimated based on the rigid body deflection of the cask. The maximum deflection is 0.57 inch, which equates to 1.7 inches in the full-scale package, as shown in Figure 2.12.9-6. The maximum package deformation occurs approximately at 13.1 milliseconds and is shown in Figure 2.12.9-7.

Beam forces are plotted for the tie-rods and the IL attachment bolts. The maximum tensile force in the tie-rods is 2,790 lb<sub>f</sub>, which is 25,110 lb<sub>f</sub> in the full scale package. The maximum bolt force is 1,450 lb<sub>f</sub>, which is 13,050 lb<sub>f</sub> in the full-scale package.

### 2.12.9.5.3 NCT Cold End Drop (-20 °F Ambient)

The acceleration and maximum deflection of the NCT cold end drop model are shown in Figure 2.12.9-8, Figure 2.12.9-9, and Figure 2.12.9-10. The peak acceleration is calculated to be 76.4g, which corresponds to 25.5g in the full-scale cask. The maximum deflection (or crush) of the ILs is estimated based on the rigid body deflection of the cask. The maximum deflection is 0.23 inches, which equates to 0.69 inches in the full-scale package, as shown in Figure 2.12.9-9. The maximum package deformation occurs approximately at 4.2 milliseconds and is shown in Figure 2.12.9-10.

Beam tensile forces are plotted for the tie-rods and the IL attachment bolts. The maximum tensile force in the tie-rods is 2,042 lb<sub>f</sub>, which is 18,378 lb<sub>f</sub> in the full-scale package. The maximum bolt force is 1,987 lb<sub>f</sub>, which is 17,883 lb<sub>f</sub> in the full-scale package.

#### 2.12.9.5.4 NCT Warm End Drop (100 °F) Ambient

The acceleration and maximum deflection of the NCT warm end drop model are shown in Figure 2.12.9-11, Figure 2.12.9-12, and Figure 2.12.9-13. The peak acceleration is calculated to be 74.5g, which corresponds to 24.8g in the full-scale cask. The maximum deflection (or crush) of the ILs is estimated based on the rigid body deflection of the cask. The maximum deflection is 0.24 inches, which equates to 0.72 inches in the full-scale package, as shown in Figure 2.12.9-12. The maximum package deformation occurs approximately at 4.4 milliseconds and is shown in Figure 2.12.9-13.

Beam tensile forces are plotted for the tie-rods and the IL attachment bolts. The maximum tensile force in the tie-rods is 1,928 lb<sub>f</sub>, which is 17,352 lb<sub>f</sub> in the full-scale package. The maximum bolt force is 1,923 lb<sub>f</sub>, which is 17,307 lb<sub>f</sub> in the full-scale package.

#### 2.12.9.6 Hypothetical Accident Conditions Results

##### 2.12.9.6.1 HAC Cold Side Drop (-20 °F Ambient)

The acceleration and maximum deflection of the cold side drop model are shown in Figure 2.12.9-14, Figure 2.12.9-15, and Figure 2.12.9-16. The peak acceleration is calculated to be approximately 133.8g, which corresponds to 44.6g in the full-scale cask. The maximum crush deformation of the IL is 4.94 inches, occurs at 15.8 milliseconds, and equates to 14.8 inches in the full-scale package.

The maximum tensile force in the tie-rods is 8,552 lb<sub>f</sub>, which is 76,968 lb<sub>f</sub> in the full-scale package. The maximum bolt force is 5,610 lb<sub>f</sub>, which is 50,490 lb<sub>f</sub> in the full-scale package.

##### 2.12.9.6.2 HAC Warm Side Drop (100 °F Ambient)

The acceleration and maximum deflection of the warm side drop model are shown in Figure 2.12.9-17, Figure 2.12.9-18, and Figure 2.12.9-19. The peak acceleration is calculated to be approximately 112.9g, which corresponds to 37.6g in the full-scale cask. The maximum crush deformation of the IL is 5.96 inches, occurs at 18.8 milliseconds, and equates to 17.9 inches in the full-scale package.

Beam forces are plotted for the tie-rods and the IL bolts. The maximum tensile force in the tie-rods is 8,605 lb<sub>f</sub>, which is 77,445 lb<sub>f</sub> in the full-scale package. The maximum bolt force is 6,377 lb<sub>f</sub>, which is 57,393 lb<sub>f</sub> in the full-scale package.

##### 2.12.9.6.3 HAC Cold 20° Slapdown (-20 °F Ambient)

The secondary impact acceleration and maximum deflection of the associated IL are shown in Figure 2.12.9-20, Figure 2.12.9-21, and Figure 2.12.9-22. Secondary impact acceleration is measured from the average acceleration of nodes. These nodes are located near the attachment points of the 1/3-scale drop test accelerometers.



The peak secondary impact acceleration is calculated to be approximately 103.1g, which corresponds to 34.4g in the full-scale cask. The maximum crush deflection of the IL is determined from the deformation of the exterior IL gusset, as shown in Figure 2.12.9-21. Maximum crush is predicted to occur at 56.9 milliseconds and is:

$$\Delta = 8.57 - \frac{6.15 + 6.56}{2} = 2.22 \text{ in}$$

where 8.57 inches is the width of the model of the gusset at the cask recess before deformation, and 6.15 inches and 6.56 inches are the width of the gusset at the two locations indicated in the figure. The full-scale crush deformation in the secondary IL will be 6.66 inches.

Beam forces are plotted for the tie-rods and the IL bolts. The maximum tensile force in the tie-rods is 15,400 lb<sub>f</sub>, which is 138,600 lb<sub>f</sub> in the full-scale package. The maximum bolt force is 18,122 lb<sub>f</sub>, which is 163,098 lb<sub>f</sub> in the full-scale package.

#### 2.12.9.6.4 HAC Warm 20° Slapdown (100 °F Ambient)

The secondary impact acceleration and maximum deflection of the associated IL are shown in Figure 2.12.9-23, Figure 2.12.9-24, and Figure 2.12.9-25. Secondary impact acceleration is measured from the average acceleration of nodes 423302 (-Z position), 425924 (-Y position), 428637 (+Y position), and 431259 (+Z position). These nodes are located near the attachment points of the 1/3 scale drop test accelerometers.

The peak secondary impact acceleration is calculated to be approximately 84.1g, which corresponds to 28.0g in the full-scale cask. The maximum crush deflection of the IL is determined from the deformation of the exterior IL gusset as shown in Figure 2.12.9-24. Maximum crush is predicted to occur at 58.6 milliseconds and is:

$$\Delta = 8.57 - \frac{5.25 + 5.54}{2} = 3.18 \text{ in}$$

where 8.57 inches is the width of the model of the gusset at the cask recess before deformation, and 5.25 inches and 5.54 inches are the widths of the gusset at the two locations indicated in the figure. The full-scale crush deformation in the secondary IL will be 9.5 inches.

Beam forces are plotted for the tie-rods and the IL bolts. The maximum tensile force in the tie-rods is 12,844 lb<sub>f</sub>, which is 115,596 lb<sub>f</sub> in the full-scale package. The maximum bolt force is 12,418 lb<sub>f</sub>, which is 111,762 lb<sub>f</sub> in the full-scale package.

#### 2.12.9.6.5 HAC Cold Corner Drop (-20°F Ambient)

The acceleration and maximum deflection of the cold corner drop, at 64° from the horizontal, are shown in Figure 2.12.9-26, Figure 2.12.9-27, and Figure 2.12.9-28. The peak acceleration is calculated to be approximately 87.9g, which corresponds to 29.3g in the full-scale cask. The maximum crush deformation of the IL is 8.49 inches, occurs at 25.0 milliseconds, and equates to 25.5 inches in the full-scale package.

Beam forces are plotted for the tie-rods and the IL bolts. The maximum tensile force in the tie-rods is 16,620 lb<sub>f</sub>, which is 149,580 lb<sub>f</sub> in the full-scale package. The maximum bolt force is 7,983 lb<sub>f</sub>, which is 71,847 lb<sub>f</sub> in the full-scale package.

#### 2.12.9.6.6 HAC Warm Corner Drop (100 °F Ambient)

The acceleration and maximum deflection of the warm corner drop, at 64° from the horizontal, are shown in Figure 2.12.9-29, Figure 2.12.9-30, and Figure 2.12.9-31. The peak acceleration is calculated to be approximately 67.7 g, which corresponds to 22.6 g in the full-scale cask. The maximum crush deformation of the IL is 9.90 inches, occurs at 30.0 milliseconds, and equates to 29.7 inches in the full-scale package.

Beam forces are plotted for the tie-rods and the IL bolts. The maximum tensile force in the tie-rods is 15,533 lb<sub>f</sub>, which is 139,797 lb<sub>f</sub> in the full-scale package. The maximum bolt force is 7,045 lb<sub>f</sub>, which is 63,405 lb<sub>f</sub> in the full-scale package.

#### 2.12.9.6.7 HAC Cold End Drop (-20°F Ambient)

The acceleration and maximum deflection of the end drop model are shown in Figure 2.12.9-32, Figure 2.12.9-33, and Figure 2.12.9-34. The peak acceleration is calculated to be approximately 222.7g, which corresponds to 74.2g in the full-scale cask. The maximum crush deformation of the IL is 2.23 inches, occurs at 7.4 milliseconds, and equates to 6.7 inches in the full-scale package.

Beam forces are plotted for the tie-rods and the IL bolts. The maximum tensile force in the tie-rods is 5,557 lb<sub>f</sub>, which is 50,013 lb<sub>f</sub> in the full-scale package. The maximum bolt force is 2,541 lb<sub>f</sub>, which is 22,869 lb<sub>f</sub> in the full-scale package.

#### 2.12.9.6.8 HAC Warm End Drop (100 °F Ambient)

The acceleration and maximum deflection of the end drop model are shown in Figure 2.12.9-35, Figure 2.12.9-36, and Figure 2.12.9-37. The peak acceleration is calculated to be approximately 142.7g, which corresponds to 47.6g in the full-scale cask. The maximum crush deformation of the IL is 3.12 inches, occurs at 11.9 milliseconds, and equates to 9.4 inches in the full-scale package.

Beam forces are plotted for the tie-rods and the IL bolts. The maximum tensile force in the tie-rods is 5,804 lb<sub>f</sub>, which is 52,236 lb<sub>f</sub> in the full-scale package. The maximum bolt force is 2,093 lb<sub>f</sub>, which is 18,837 lb<sub>f</sub> in the full-scale package.

#### 2.12.9.6.9 Trunnion Clearance Check

The clearance between the drop pad and the trunnion is calculated based on the difference between the trunnion extension beyond the cask outer surface and the remaining thickness of the crushed IL.

During impact, the exterior surface of the cask will come into contact with the interior cylindrical surface of the IL shell. The trunnion extends beyond the outer surface of the cask body (i.e., gamma shield surface) by:

$$L_T = \frac{1}{2}(102.25 - 87.96) = 7.15 \text{ inches}$$

where 102.25 inches is the maximum dimension between the outer faces of the trunnions and 87.96 inches is the maximum diameter of the cask body at the locations of the trunnions (Section 1.4.1, Drawing 19885-71-2, Section A-A). The thickness of the IL in the region of crush is reduced to:

$$T_{IL} = \frac{1}{2}(144 - 89) - 17.9 = 9.60 \text{ inches}$$

where 144 inches and 89 inches are the nominal inner and outer diameter of the ILs, respectively, in the region of the cask recess (Section 1.4.1, Drawings 19885-71-9 and 19885-71-10, Section A-A), and 17.9 inches is the maximum radial crush predicted by the analysis in Section 2.12.9.6.2. Note that this crush is about 65% strain in the wood from the original 27.5 inches of thickness in this region of the ILs. Based on these dimensions, a clearance of 2.45 inches remains between the trunnions and the impact surface.

The typical gap between the steel IL shell and the wood of the IL core is modeled as approximately 1/8 inch radially and 1/16 inch axially. Therefore, the 2.45-inch clearance is a slightly conservative prediction for the side impact clearance than if the wood completely filled the IL cavities.

#### 2.12.9.6.10 Tie-Rod Stress Analysis

For the tie-rod evaluation, the forces in the tie-rods developed during the free drops analyzed by the LS-DYNA® model will be utilized to demonstrate the acceptability of the IL attachments.

The IL attachments are designed to keep the ILs attached to the cask body during all NCT and HAC events. The ILs are attached to each other using 13 tie-rods, and to the cask body by bolt attachment brackets welded to the outer shell in eight locations (four bolting locations per IL). The HAC tensile loads in the tie-rods are listed in Table 2.12.9-21 through Table 2.12.9-28. The four cases with the highest tensile loads are analyzed below.

#### 2.12.9.6.11 Tie-Rods

The maximum IL surface temperature at the bracket attachment to tie-rod is approximately 120 °F (Chapter 3, Figure 3-10), conservatively 200 °F is utilized for the material properties. The tie-rod material is A193 Grade B7, which has an ultimate strength,  $S_u$ , of 125 ksi [4] at 200 °F and a yield strength of  $S_y = 98$  ksi [4] at 200 °F. The maximum allowable stress is the lesser of  $0.7S_u$  or  $S_y$  (Level D, Bolted Joint, F1335.1, [8]). Therefore, the allowable is the smaller of  $0.7(125 \text{ ksi}) = 87.5 \text{ ksi}$  or  $S_y = 98 \text{ ksi}$ , which is then 87.5 ksi.

The tensile area for the 1½ - 8UNC-2A threaded ends of the tie-rods is 1.490 in<sup>2</sup> per Reference [9].

### Case 1, Cold Corner Drop

For the cold corner drop case, the maximum tie-rod tensile load is 149,580 lbf (See Table 2.12.9-25). The tensile stress is:

$$\sigma_{tr} = \frac{149,580}{1.490} = 100.4 \text{ ksi}$$

The stress in the tie-rod is greater than the allowable stress of 87.5 ksi. In total, the load is exceeded in the two tie-rods connecting the two ILs opposing the impact location (See Figure 2.12.9-28). However, loss of attachment is also contingent on failure of the attachment bolts. See Case 1 in Section 2.12.9.6.12 below.

### Case 2, Warm Corner Drop

For the warm corner drop case, the maximum tie-rod tensile load is 139,797 lbf (See Table 2.12.9-26). The tensile stress is:

$$\sigma_{tr} = \frac{139,797}{1.490} = 93.8 \text{ ksi}$$

The stress in the tie-rod is greater than the allowable stress of 87.5 ksi. In total, the load is exceeded in the top five tie-rods connecting the two ILs opposing the impact location (See Figure 2.12.9-31). However, loss of attachment is also contingent on failure of the attachment bolts. See Case 2 in Section 2.12.9.6.12 below.

### Case 3, Cold Slap Down

For the cold slapdown case, the maximum tie-rod tensile load is 138,600 lbf (See Table 2.12.9-23). The tensile stress is:

$$\sigma_{tr} = \frac{138,600 \text{ lbf}}{1.490 \text{ in}^2} = 93.0 \text{ ksi}$$

The stress in the tie-rod is greater than the allowable stress of 87.5 ksi. In total, the load is exceeded in the top five tie-rods connecting the two ILs opposing the impact location (See Figure 2.12.9-22). However, loss of attachment is also contingent on failure of the attachment bolts. See Case 3 in Section 2.12.9.6.12 below.

### Case 4, Warm Slap Down

For the warm slapdown case, the maximum tie-rod tensile load is 115,596 lbf (See Table 2.12.9-24). The tensile stress is:

$$\sigma_{tr} = \frac{115,596}{1.490} = 77.6 \text{ ksi}$$

The stress in the tie-rod is less than the allowable stress of 87.5 ksi. Therefore, the ILs remain attached during the warm corner drop. Note that this load bounds the remainder of the tie-rod tensile loads in Table 2.12.9-21. Therefore, no further tie-rods are evaluated.

#### 2.12.9.6.12 Attachment Bolts

The maximum IL surface temperature at the bracket attachment to bolt is approximately 120 °F (Chapter 3, Figure 3-10), conservatively 200 °F is used for the material allowables. The bolting material is A540 Grade B21, Class 2, which has an ultimate strength,  $S_u$ , of 155 ksi [4] at 200 °F and a yield strength of  $S_y = 145.1$  ksi [4] at 200 °F. The maximum allowable stress is the lesser of  $0.7S_u$  or  $S_y$  (Level D, Bolted Joint, F1335.1, [8]). Therefore, the allowable is smaller of  $0.7(155 \text{ ksi}) = 108.5$  ksi or  $S_y = 145.1$  ksi, which is then 108.5 ksi.

The minimum tensile area of the 1½ - 8UNC-2A attachment bolt is the same as for the tie-rods, i.e., 1.490 in<sup>2</sup>.

The tensile loads in the attachment bolts are listed in Table 2.12.9-29 through Table 2.12.9-36 for HAC.

##### Case 1, Cold Corner Drop

For the cold corner drop case, the maximum tensile load in the attachment bolts is 71,847 lb<sub>f</sub>. The tensile stress is:

$$\sigma_{tr} = \frac{71,847}{1.490} = 48.2 \text{ ksi}$$

The tensile stress in the attachment bolt is less than the allowable stress. Therefore, the ILs remain attached during the cold corner drop.

##### Case 2, Warm Corner Drop

For the warm corner drop case, the maximum tensile load in the attachment bolts is 63,405 lb<sub>f</sub>. The tensile stress is:

$$\sigma_{tr} = \frac{63,405}{1.490} = 42.6 \text{ ksi}$$

The tensile stress in the attachment bolt is less than the allowable stress. Therefore, the ILs remain attached during the warm corner drop.

##### Case 3, Cold Slapdown

For the cold corner slapdown, the maximum tensile load in the attachment bolts is 163,098 lb<sub>f</sub>. The tensile stress is:

$$\sigma_{tr} = \frac{163,098}{1.490} = 109.5 \text{ ksi}$$

The tensile stress in the attachment bolt is slightly greater than the allowable stress. Therefore, the bolt may be damaged. Similar damage is expected on the rear symmetrical attachment bolt. However, based on the damage assessment of Appendix 2.12.10, the ILs will remain attached to the cask.

Case 4, Warm Slapdown

For the warm corner slapdown, the maximum tensile load in the attachment bolts is 111,762 lb<sub>f</sub>. The tensile stress is:

$$\sigma_{tr} = \frac{111,762 \text{ lb}_f}{1.490 \text{ in}^2} = 75.0 \text{ ksi}$$

The tensile stress in the attachment bolt is less than the allowable stress. Therefore, the ILs remain attached during the cold corner drop.

## 2.12.9.6.13 Tie-Rod Brackets

The material used for the tie-rod brackets and IL gussets is A-240 Type 304 stainless steel. The allowable stress for the brackets and IL gussets is  $S_U$  or 71 ksi at 200 °F. The load used for this analysis is 115,596 lb<sub>f</sub> from the warm slapdown tie-rod analysis case above.

For the 1/4 inch fillet welds that attach the brackets to the IL, the throat width is  $1/4\sin(45^\circ) = 0.1768 \text{ in}$ . For the single bracket attachment, the stress in the weld is:

$$\text{Area of weld} = (0.1768 \text{ in})[2(13 \text{ in} + 6 \text{ in})] = 6.718 \text{ in}^2$$

$$\sigma_{\text{weld}} = \frac{115,596}{6.718} = 17.2 \text{ ksi} < 71 \text{ ksi}$$

For the double bracket attachment, the stress in the weld is:

$$\text{Area of weld} = (0.1768)[2(11 + 21.62)] = 11.534 \text{ in}^2$$

$$\sigma_{\text{weld}} = \frac{2(115,596)}{11.534} = 20.0 \text{ ksi} < 71 \text{ ksi}$$

## 2.12.9.6.14 Impact Limiter Gussets

Since the gussets are fillet welded on both sides to the top plate of the IL, the cross-sectional area of the gusset is the critical tensile area. Assume the tensile force from the tie-rods acts over the length of the 3/16-inch thick gusset plate. The load utilized for this analysis is 115,596 lb<sub>f</sub> from the warm slapdown tie-rod analysis case above.

Single Bracket

$$\text{Active tensile area of gusset} = (0.19)(20.0) = 3.80 \text{ in}^2$$

$$\sigma_{\text{gusset}} = \frac{115,596}{3.80} = 30.4 \text{ ksi}$$

The tensile stress in the single bracket is less than the allowable stress of 71 ksi.

Double Bracket

$$\text{Active tensile area of gusset} = (0.19)(20.0) = 3.80 \text{ in}^2$$

$$\sigma_{\text{gusset}} = \frac{2(115,596)}{3.80} = 60.8 \text{ ksi}$$

The tensile stress in the double bracket is less than the allowable stress of 71 ksi.

#### 2.12.9.6.15 Lifting Lug Analysis

The weight of the top and bottom ILs is 16,600 lb<sub>m</sub> each. For the following analysis conservatively use a weight of 16,750 lb<sub>m</sub> per impact limiter. Each IL is supported by two lifting lugs. The material used for the lifting lugs is also ASTM A-240 Type 304 stainless steel. The maximum temperature at outer surface of IL is 144 °F (Table 3-1 of Chapter 3). From Table 2.12.9-2, the yield strength,  $S_y$ , at this temperature is 27.8 ksi. The allowable shear stress is  $0.5S_y = 13.9$  ksi, and the allowable primary-plus-bending stress is  $S_y = 27.8$  ksi [4].

A 60° angle between the slings and horizontal is assumed. This assumption allows the slings to clear the IL. The applied load is assumed to be three times the weight of the IL. The lifting lugs are located on the IL CG. Figure 2.12.9-38 illustrates the geometry of the IL lifting lugs.

The tension,  $T$ , in the lifting sling is,

$$T = \frac{3(16,750)}{2} \frac{1}{\sin(60^\circ)} = 29,011 \text{ lb}_f$$

The normal stress  $\sigma_n$  in the lifting lug is conservatively computed in the following way:

$$\text{Normal Force } F_n = 29,011 \sin(30^\circ) = 14,506 \text{ lb}_f$$

$$\text{Normal Area, } A = (1)(5-1.5) = 3.5 \text{ in}^2$$

$$\text{Normal Stress } \sigma_n = 14,506/3.5 = 4,145 \text{ psi}$$

The bending stress  $\sigma_b$  in the lifting lug is computed in the following way.

$$\text{Moment of Inertia, } I = (1/12)(1)(5^3) = 10.42 \text{ in}^4$$

$$F_b = 29,011 (\cos(30^\circ)) = 25,124 \text{ lb}_f$$

$$\sigma_b = \frac{2.5(2.5)(25,124)}{10.42} = 15,070 \text{ psi}$$

The shear stress  $\tau$  in the lug is conservatively computed as follows.

$$\text{Shear area} = 2(2.5 - 0.75)(1) = 3.50 \text{ in}^2$$

$$\tau = 29,011/3.50 = 8,289 \text{ psi.}$$

The total stress intensity, S.I., is,

$$\text{S.I.} = \sqrt{(4,145 + 15,070)^2 + 4(8,289)^2} = 25,378 \text{ psi} < 27,800 \text{ psi}$$

The stresses in the lifting lug weld are computed as follows.

$$\text{Stress Area, } A_{\text{lug}} = (0.375)\sin(45^\circ)((5)2+1(2)) = 3.18 \text{ in}^2$$

$$\text{Normal Stress } \sigma_n = 14,506/3.18 = 4,562 \text{ psi}$$

$$\text{Moment of Inertia, } I_{\text{weld}} = (2/12)(0.375)\sin(45^\circ)(5^3) + (2/12)(1)[0.375 \sin(45^\circ)]^3 + 2[0.375 \sin(45^\circ)](1)(2.5^2) = 8.84 \text{ in}^4.$$

$$\sigma_b = \frac{2.5(2.5)(25,124)}{8.84} = 17,763 \text{ psi}$$

$$\tau = (25,124)/(3.18) = 7,901 \text{ psi}$$

The total stress intensity, S.I., is,

$$\text{S.I.} = \sqrt{(4,562+17,763)^2 + 4(7,901)^2} = 27,352 \text{ psi} < 27,800 \text{ psi}$$

#### 2.12.9.7 Conclusions

This analysis uses the explicit analysis functions of the finite element code LS-DYNA<sup>®</sup> to predict the g-loads on the TN-32B HBU package. The values of the 1/3-scale test unit accelerations, as reported in Sections 2.12.9.5 and 2.12.9.6, are summarized in Table 2.12.9-17 below. Comparisons are made between the adjusted full size package accelerations and the LS-DYNA<sup>®</sup> results. Based on the analysis, the bounding values for the full-scale packages are 74.2g axially and 44.6g in the transverse direction.

The values of the 1/3-scale test unit deformations, as reported in Sections 2.12.9.5 and 2.12.9.6, are summarized in Table 2.12.9-18 below. Comparisons are made between the test unit deformations and the LS-DYNA<sup>®</sup> results. Based on the analysis, the bounding value for full-size IL deformation in the radial direction is 17.9 inches. The bounding value for full-size IL deformation in the axial direction is 9.4 inches.

The NCT drop and acceleration and deformation are also shown in Table 2.12.9-19 and Table 2.12.9-20, respectively. The maximum side drop acceleration is predicted to be 11.3 g in the cold case. The maximum radial deformation is predicted to be 1.7 inches in the warm case. The maximum NCT end drop acceleration and deformation are 25.5g in the cold case and 0.72 inch in the warm case, respectively.

As demonstrated in the TN-40 IL tests, a few of the tie-rods and/or attachment bolts are predicted to fail in 30-foot cold slapdown drop orientation, as noted in Table 2.12.9-23 and Table 2.12.9-31. However, the ILs will remain secured to the cask body by the undamaged tie-rods and attachments bolts.



#### 2.12.9.8 References

1. Title 10, Code of Federal Regulations - Energy, Part 71 (10 CFR Part 71), "Packaging and Transportation of Radioactive Material," 1-1-2021 Edition, U.S. Nuclear Regulatory Commission, Washington, D.C.
2. Livermore Software Technology Corp. (LSTC), "LS-DYNA® Keyword User's Manual Volume I," Version R7.0, February 2013, Livermore, CA.
3. Document No. E-31030 (NRC Docket No. 71-9313), "TN-40 Transportation Packaging Safety Analysis Report," Revision 16, June 2011.
4. American Society of Mechanical Engineers, ASME Boiler and Pressure Vessel Code, Section II, "Materials Properties (Customary)," Part D, 2013 Edition.
5. General Technical Report FPL-GTR-190, "Wood Handbook, Wood as an Engineering Material," U.S. Department of Agriculture, Forest Service, Forest Products Laboratory, 2010.
6. LSTC, "LS-DYNA® Keyword User's Manual, Volume II, Material Models," Version R7.0, February 2013, Livermore, CA.
7. SSG-26, "Advisory Material for the IAEA Regulations for the Safe Transport of Radioactive Material (2012 Edition)," IAEA Safety Standards, International Atomic Energy Agency.
8. American Society of Mechanical Engineers, ASME Boiler and Pressure Vessel Code, Section III, "Appendices," 2013 Edition.
9. American Society of Mechanical Engineers, Unified Inch Screw Threads, UN and UNR thread Form, ASME B1.1-2003.
10. NTS Report No. TR63014-07N, "Dynamic Qualification Report for the Transnuclear TN-40 1/3-Scale Model IL," National Technical Systems.

**Table 2.12.9-1**  
**Package Characteristics/Dimensions**

Characteristic	TN-40	TN-32B HBU	Difference
Envelope length, in	260.9	263.19	+0.88%
Envelope diameter, in	144.0	144.0	0%
Cask length, in	184.7 <sup>(1)</sup>	187.19 <sup>(2)</sup>	+1.3%
Cask neutron shield diameter, in	101.00	97.75	-3.2%
Cask diameter at IL, in	91.00	87.75	-3.6%
Cask trunnion extension, in	104.50	102.21	-2.2%
Upper IL, lb <sub>m</sub>	17,500 <sup>(3)</sup>	16,600	-5.1%
Lower IL, lb <sub>m</sub>	17,500 <sup>(3)</sup>	16,600	-5.1%
Loaded cask w/o ILs, lb <sub>m</sub>	236,500 <sup>(4)</sup>	235,700 <sup>(5)</sup>	-0.34%
Maximum Weight, lb <sub>m</sub>	271,500 <sup>(4)</sup>	273,000 <sup>(5)</sup>	+0.55%
<b>Impact Limiters</b>			
Overall Length, in	50.00	50.00	0%
Outer Diameter, in	144.00	144.00	0%
Cask Recess Depth, in	12.00	12.00	0%
Cask Recess Diameter, in	92.00	89.00	-3.3%
Trunnion pocket extension, in	106.00	103.5	-2.4%

Notes:

1. Length of cask with IL Spacer.
2. Length of cask with the puncture resistant plate installed.
3. Combined weight of TN-40 ILs divided by two from Table 1-1 of the TN-40 SAR [3].
4. Total loaded weight of TN-40 from Table 1-1 of the TN-40 SAR [3].
5. For TN-32B HBU cask weights, refer to Section 2.1.3, Table 2-7.

**Table 2.12.9-2**  
**IL Shell Properties**

Property	Symbol	Temperature (°F)		
		-20 to 100	145	200
Elastic Modulus, $\times 10^3$ ksi	E	28.3	28.0	27.6
Yield Stress, ksi	S <sub>y</sub>	30.0	27.8	25.0
Ultimate Stress, ksi	S <sub>u</sub>	75.0	73.2	71.0
Elongation <sup>1</sup>	e <sub>u</sub>	0.40		
Density, lb <sub>m</sub> /in <sup>3</sup>	ρ	0.290		
True Yield Stress, ksi	S <sub>yt</sub>	30.1	27.9	
True Ultimate Stress, ksi	S <sub>ut</sub>	105.0	102.5	
True Yield Strain, in/in	ε <sub>yt</sub>	0.00306	0.00299	
True Ultimate Strain, in/in	ε <sub>ut</sub>	0.336		
True Tangent Modulus, ksi	T <sub>tant</sub>	225.0	224.0	

Note:

1. Elongation from Part A, Table 2, ASME B&PV Code for ASME SA-240 Type 304 stainless steel.

**Table 2.12.9-3  
Mechanical Properties of Wood**

Property	Redwood		Balsa Wood	
	Warm (120 °F)	Cold (-20 °F)	Warm (120 °F)	Cold (-20 °F)
Longitudinal Elastic Modulus (psi)	$1.25 \times 10^6$	$1.60 \times 10^6$	$4.57 \times 10^5$	$5.38 \times 10^5$
Radial Elastic Modulus (psi)	$1.09 \times 10^5$	$1.39 \times 10^5$	$2.10 \times 10^4$	$2.47 \times 10^4$
Tangential Elastic Modulus (psi)	$1.11 \times 10^5$	$1.42 \times 10^5$	$6.86 \times 10^3$	$8.07 \times 10^3$
Radial/Longitudinal Shear Modulus (psi)	$8.25 \times 10^4$	$1.06 \times 10^5$	$2.50 \times 10^4$	$2.91 \times 10^4$
Longitudinal/Radial Shear Modulus (psi)	$9.63 \times 10^4$	$1.23 \times 10^5$	$1.69 \times 10^4$	$1.99 \times 10^4$
Tangential/Radial Shear Modulus (psi)	$1.38 \times 10^4$	$1.76 \times 10^4$	$2.29 \times 10^3$	$2.69 \times 10^3$

**Table 2.12.9-4  
Typical Wood Material Properties**

Property	Redwood	Balsa Wood
Density	18.7 – 27.5 lb <sub>m</sub> /ft <sup>3</sup>	7 – 12 lb <sub>m</sub> /ft <sup>3</sup>
<b>Parallel to Grain</b>		
Crush Stress	3,871 – 8,248 psi	1,139 – 2,401 psi
Locking Strain	0.6	0.8
Locking Modulus	10 × (max. crush stress)	10 × (max. crush stress)
<b>Perpendicular to Pour Direction</b>		
Crush Stress	426 – 907 psi	200 psi
Locking Strain	0.6	0.8
Locking Modulus	10 × (max. crush stress)	10 × (max. crush stress)
Shear Stress	581 – 1,237 psi	159 – 336 psi

**Table 2.12.9-5  
Warm Redwood Load Curves**

Parallel to Grain		Perpendicular-to-Grain		Shear Stress	
Strain (in/in)	Stress (psi)	Strain (in/in)	Stress (psi)	Strain (in/in)	Stress (psi)
0	0	0	0	0	0
0.0031	3,871	0.0038	426	0.0060	581
0.6	3,871	0.6	426	0.6	581
1	19,355	1	2,130	1	2,905

**Table 2.12.9-6  
Cold Redwood Load Curves**

Parallel-to-Grain		Perpendicular-to-Grain		Shear Stress	
Strain (in/in)	Stress (psi)	Strain (in/in)	Stress (psi)	Strain (in/in)	Stress (psi)
0	0	0	0	0	0
0.0052	8,248	0.0064	907	0.0101	1,237
0.6	8,248	0.6	907	0.6	1,237
1	41,240	1	4,535	1	6,185

**Table 2.12.9-7  
Warm Balsa Load Curves**

Parallel-to-Grain		Perpendicular-to-Grain		Shear Stress	
Strain (in/in)	Stress (psi)	Strain (in/in)	Stress (psi)	Strain (in/in)	Stress (psi)
0	0	0	0	0	0
0.0025	1,139	0.0025	200	0.0064	159
0.8	1,139	0.8	200	0.8	159
1	3,417	1	3,417	1	3,417

**Table 2.12.9-8  
Cold Balsa Load Curves**

Parallel-to-Grain		Perpendicular-to-Grain		Shear Stress	
Strain (in/in)	Stress (psi)	Strain (in/in)	Stress (psi)	Strain (in/in)	Stress (psi)
0	0	0	0	0	0
0.0045	2,401	0.0045	200	0.012	336
0.8	2,401	0.8	200	0.8	336
1	7,203	1	7,203	1	7,203

**Table 2.12.9-9**  
**TN-32B HBU Cask Model Parts, Lower IL**

Item	Heading	Material	SECID	MID	HGID	THK
1	Outer Shell	Type 304	1	1	1	0.094
2	Middle Shell	Type 304	1	1	1	0.094
3	Center Shell	Type 304	1	1	1	0.094
4	Recess Shell	Type 304	1	1	1	0.094
5	Inner Gusset	Type 304	5	1	1	0.063
6	Outer Gusset	Type 304	5	1	1	0.063
7	Bolt Gusset	Type 304	7	1	1	0.094
8	End Plate	Type 304	1	1	1	0.094
9	Recess Plate	Type 304	1	1	1	0.094
10	Inner Plate	Type 304	1	1	1	0.094
12	End Balsa	Balsa Wood	12	12	12	--
13	End Balsa	Balsa Wood	12	12	12	--
14	End Balsa	Balsa Wood	12	12	12	--
15	Redwood	Redwood	15	15	12	--
16	Redwood	Redwood	15	15	12	--
17	Redwood	Redwood	15	17	12	--
18	Redwood	Redwood	15	17	12	--
19	Redwood	Redwood	15	17	12	--
20	Redwood	Redwood	15	15	12	--
21	Redwood	Redwood	15	15	12	--
22	Inner Balsa	Balsa Wood	12	12	12	--
23	Large Tower Base Plates	Type 304	23	1	23	--
24	Large Tower Bolt Plates	Type 304	23	1	23	--
25	Large Tower Gussets	Type 304	25	1	1	0.172
26	Small Tower Base Plates	Type 304	23	1	23	--
27	Small Tower Bolt Plates	Type 304	23	1	23	--
28	Small Tower Gussets	Type 304	25	1	1	0.172
29	Lower IL Bolt 1	A540, Grade B21, Cl 1 Steel	29	29	--	0.5
30	Lower IL Bolt 2	A540, Grade B21, Cl 1 Steel	29	29	--	0.5
31	Lower IL Bolt 3	A540, Grade B21, Cl 1 Steel	29	29	--	0.5
32	Lower IL Bolt 4	A540, Grade B21, Cl 1 Steel	29	29	--	0.5

**Table 2.12.9-10**  
**TN-32B HBU Cask Model Parts, Upper IL**

Item	Heading	Material	SECID	MID	HGID	THK
101	Outer Shell	Type 304	1	1	1	0.094
102	Middle Shell	Type 304	1	1	1	0.094
103	Center Shell	Type 304	1	1	1	0.094
104	Recess Shell	Type 304	1	1	1	0.094
105	Inner Gusset	Type 304	5	1	1	0.063
106	Outer Gusset	Type 304	5	1	1	0.063
107	Bolt Gusset	Type 304	7	1	1	0.094
108	End Plate	Type 304	1	1	1	0.094
109	Recess Plate	Type 304	1	1	1	0.094
110	Inner Plate	Type 304	1	1	1	0.094
112	End Balsa	Balsa Wood	12	12	12	--
113	End Balsa	Balsa Wood	12	12	12	--
114	End Balsa	Balsa Wood	12	12	12	--
115	Redwood	Redwood	15	15	12	--
116	Redwood	Redwood	15	15	12	--
117	Redwood	Redwood	15	17	12	--
118	Redwood	Redwood	15	17	12	--
119	Redwood	Redwood	15	17	12	--
120	Redwood	Redwood	15	15	12	--
121	Redwood	Redwood	15	15	12	--
122	Inner Balsa	Balsa Wood	12	12	12	--
123	Large Tower Base Plates	Type 304	23	1	23	--
124	Large Tower Bolt Plates	Type 304	23	1	23	--
125	Large Tower Gussets	Type 304	25	1	1	0.172
126	Small Tower Base Plates	Type 304	23	1	23	--
127	Small Tower Bolt Plates	Type 304	23	1	23	--
128	Small Tower Gussets	Type 304	25	1	1	0.172
129	Lower IL Bolt 1	A540, Grade B21, Cl 1 Steel	29	29	--	0.5
130	Lower IL Bolt 2	A540, Grade B21, Cl 1 Steel	29	29	--	0.5
131	Lower IL Bolt 3	A540, Grade B21, Cl 1 Steel	29	29	--	0.5
132	Lower IL Bolt 4	A540, Grade B21, Cl 1 Steel	29	29	--	0.5

**Table 2.12.9-11**  
**TN-32B HBU Cask Model Parts, Misc. Components**

Item	Heading	Material	SECID	MID	HGID	THK
51	Tie-Rod 1	A193, Gr B7	51	51	--	0.5
52	Tie-Rod 2	A193, Gr B7	51	51	--	0.5
53	Tie-Rod 3	A193, Gr B7	51	51	--	0.5
54	Tie-Rod 4	A193, Gr B7	51	51	--	0.5
55	Tie-Rod 5	A193, Gr B7	51	51	--	0.5
56	Tie-Rod 6	A193, Gr B7	51	51	--	0.5
57	Tie-Rod 7	A193, Gr B7	51	51	--	0.5
58	Tie-Rod 8	A193, Gr B7	51	51	--	0.5
59	Tie-Rod 9	A193, Gr B7	51	51	--	0.5
60	Tie-Rod 10	A193, Gr B7	51	51	--	0.5
61	Tie-Rod 11	A193, Gr B7	51	51	--	0.5
62	Tie-Rod 12	A193, Gr B7	51	51	--	0.5
63	Tie-Rod 13	A193, Gr B7	51	51	--	0.5
151	Cask Body	RIGID MATERIAL	151	151	--	--
901	Pad	RIGID MATERIAL	901	901	--	--

**Table 2.12.9-12**  
**Section Properties**

SecID	Element Type	Form	Thickness/Diameter (in)
1	Shell	16 (Fully Integrated)	0.094
5	Shell	16 (Fully Integrated)	0.063
7	Shell	16 (Fully Integrated)	0.094
12	Solid	0 (1 point corotational)	--
15	Solid	0 (1 point corotational)	--
23	Solid	2 (Fully integrated S/R solid)	--
25	Shell	16 (Fully Integrated)	0.172
29	Beam	1 (Hughes-Liu with cross section integration)	0.5
51	Beam	1 (Hughes-Liu with cross section integration)	0.5
151	Solid	1 (Constant stress solid element)	--
901	Solid	1 (Constant stress solid element)	--

**Table 2.12.9-13**  
**Material Models**

Material ID	Model Description	Material Description
1	Plastic-Kinematic	Type 304 @ -20 °F to 100 °F
12	Modified Honeycomb	Balsa, grain perpendicular-to-axis
15	Modified Honeycomb	Redwood, grain perpendicular-to-axis
17	Modified Honeycomb	Redwood, grain parallel-to-axis
29	Plastic-Kinematic	Alloy steel, A540, Gr B21, Cl 1
51	Plastic-Kinematic	Alloy steel, A193, Gr B7
151	Rigid Material	Carbon Steel
901	Rigid Material	Carbon Steel

**Table 2.12.9-14**  
**Hourglass Definitions**

HGID	Hourglass Control Type (IHQ)	Hourglass Coefficient (QM)
1	full projection warping stiffness (8)	0.1
12	Flanagan-Belytschko viscous form (2)	--
23	Belytschko-Bindeman [1993] assumed strain co-rotational stiffness form (6)	--

**Table 2.12.9-15**  
**FEA Model/Scale Test Unit Weight Comparison**

Component	Model Part ID <sup>(1)</sup>	Weight (lb <sub>m</sub> )		Percent Difference
		Scale Test Unit <sup>(2)</sup>	Finite Element Model	
Lower IL	1-28	606	672.54	+11%
Upper IL	101-128	608	672.26	+11%
Loaded Cask Body and hardware	29-32, 51-63, 129-132, and 151	8,833	8,806	-0.31%
Total Package <sup>(3)</sup>	all parts except 901 (drop pad)	10,047	10,182	+1.34%

Notes:

1. See Table 2.12.9-9, Table 2.12.9-10, and Table 2.12.9-11 for Part ID descriptions.
2. Section 4.1 of the TN-40 IL Test Report [10].
3. Weight is average of the two test articles assembled [10].



**Table 2.12.9-16**  
**FEA Model/ TN-32B HBU Cask Weight Comparison**

Component	Model Part ID <sup>(1)</sup>	Weight (lb <sub>m</sub> )		Percent Difference
		TN-32B HBU <sup>(2)</sup>	Finite Element Model	
Lower IL, nominal weight	1-28	16,600	$672.54 \times (3.0)^3$ = 18,159	+9.4%
Upper IL, nominal weight	101-128	16,600	$672.26 \times (3.0)^3$ = 18,151	+9.4%
Loaded Cask Body and hardware <sup>(3)</sup>	29-32, 51-63, 129-132, and 151	235,700	$8806 \times (3.0)^3$ = 237,762	+0.87%
Total Package, nominal weight	all parts except 901 (drop pad)	269,000	$10,182 \times (3.0)^3$ = 274,914	+2.2%
Total Package, maximum weight	all parts except 901 (drop pad)	273,000	$10,182 \times (3.0)^3$ = 274,914	+0.70%

Notes:

1. See Table 2.12.9-9, Table 2.12.9-10, and Table 2.12.9-11 for Part ID descriptions.
2. Refer to Section 2.1.3 for maximum weight.
3. Loaded cask body and hardware minus ILs.

**Table 2.12.9-17**  
**Inertia g-Load versus Initial Angle of Impact for 30 Foot Drop**

Drop Case	Drop Angle	Scale Model	Full Size	Test <sup>(1)</sup>	Difference (Full/Test)
Cold Side	0°	133.8	44.6	57	-22%
Warm Side	0°	112.9	37.6		-34%
Cold Slapdown (Secondary Impact)	20°	103.1	34.4	61	-44%
Warm Slapdown (Secondary Impact)	20°	84.1	28.0		-54%
Cold Corner	64°	87.9	29.3	34	-14%
Warm Corner	64°	67.7	22.6		-34%
Cold End	90°	222.7	74.2	57	30%
Warm End	90°	142.7	47.6		-17%

**Table 2.12.9-18**  
**Maximum IL Deformation versus Initial Angle of Impact for 30 Foot Drop**

Drop Case	Drop Angle	Scale Model	Full Size	Test <sup>(1)</sup>	Difference (Scale/Test)
Cold Side	0°	4.94	14.8	2.72	+82%
Warm Side	0°	5.96	17.9		+119%
Cold Slapdown (Secondary Impact)	20°	2.22	6.7	4.69	-53%
Warm Slapdown (Secondary Impact)	20°	3.18	9.5		-32%
Cold Corner	64°	8.49	25.5	8.5	0%
Warm Corner	64°	9.90	29.7		+16%
Cold End	90°	2.23	6.7	3	-26%
Warm End	90°	3.12	9.4		+4%

**Table 2.12.9-19**  
**Maximum Inertial g-Load during 1 Foot Drop**

Drop Case	Drop Angle	Scale Model	Full Size
Cold Side	0°	33.9 g	11.3 g
Warm Side	0°	27.9 g	9.3 g
Cold End	90°	76.4 g	25.5 g
Warm End	90°	74.5 g	24.8 g

**Table 2.12.9-20**  
**Maximum IL Deformation versus Initial Angle of Impact for 1 Foot Drop**

Drop Case	Drop Angle	Scale Model	Full Size
Cold Side	0°	0.52	1.6
Warm Side	0°	0.57	1.7
Cold End	90°	0.23	0.69
Warm End	90°	0.24	0.72

**Table 2.12.9-21**  
**Tie-Rod Loads for 30 Foot Cold Side Drop**

Tie-Rod No.	Position (Degrees)	Scale Model Tensile Force (lbf)	Full Scale		Margin of Safety
			Force (lbf)	Stress (ksi)	
1	184	5,861	52,749	35.39	1.47
2	176	5,369	48,321	32.42	1.70
3	150	3,230	29,070	19.51	3.49
4	120	4,255	38,295	25.69	2.41
5	90	5,110	45,990	30.85	1.84
6	60	4,326	38,934	26.12	2.35
7	30	3,304	29,736	19.95	3.39
8	4	5,504	49,536	33.23	1.63
9	356	5,937	53,433	35.85	1.44
10	315	4,033	36,297	24.35	2.59
11	266	8,552	76,968	51.63	0.70
12	274	8,388	75,492	50.64	0.73
13	240	4,626	41,634	27.93	2.13

**Table 2.12.9-22**  
**Tie-Rod Loads for 30 Foot Warm Side Drop**

Tie-Rod No.	Position (Degrees)	Scale Model Tensile Force (lbf)	Full Scale		Margin of Safety
			Force (lbf)	Stress (ksi)	
1	184	5,294	47,646	31.96	1.74
2	176	4,907	44,163	29.63	1.95
3	150	2,685	24,165	16.21	4.40
4	120	2,136	19,224	12.90	5.78
5	90	2,799	25,191	16.90	4.18
6	60	2,078	18,702	12.54	5.98
7	30	2,540	22,860	15.34	4.71
8	4	4,834	43,506	29.19	2.00
9	356	5,106	45,954	30.82	1.84
10	315	3,954	35,586	23.88	2.67
11	266	7,884	70,956	47.60	0.84
12	274	8,605	77,445	51.96	0.68
13	240	4,161	37,449	25.12	2.48

**Table 2.12.9-23**  
**Tie-Rod Loads for 30 Foot Cold Slapdown**

Tie-Rod No.	Position (Degrees)	Scale Model Tensile Force (lbf)	Full Scale		Margin of Safety
			Force (lbf)	Stress (ksi)	
1	184	11,941	107,469	72.09	0.21
2	176	11,516	103,644	69.52	0.26
3	150	15,284	137,556	92.27	-0.05
4	120	14,692	132,228	88.70	-0.01
5	90	15,059	135,531	90.92	-0.04
6	60	14,752	132,768	89.07	-0.02
7	30	15,400	138,600	92.98	-0.06
8	4	11,732	105,588	70.84	0.24
9	356	12,081	108,729	72.94	0.20
10	315	8,431	75,879	50.90	0.72
11	266	2,175	19,575	13.13	5.67
12	274	1,504	13,536	9.08	8.64
13	240	6,863	61,767	41.43	1.11

**Table 2.12.9-24**  
**Tie-Rod Loads for 30 Foot Warm Slapdown**

Tie-Rod No.	Position (Degrees)	Scale Model Tensile Force (lbf)	Full Scale		Margin of Safety
			Force (lbf)	Stress (ksi)	
1	184	10,206	91,854	61.62	0.42
2	176	9,676	87,084	58.42	0.50
3	150	12,648	113,832	76.36	0.15
4	120	11,959	107,631	72.20	0.21
5	90	12,069	108,621	72.87	0.20
6	60	12,022	108,198	72.58	0.21
7	30	12,844	115,596	77.55	0.13
8	4	9,822	88,398	59.30	0.48
9	356	10,349	93,141	62.49	0.40
10	315	4,121	37,089	24.88	2.52
11	266	2,929	26,361	17.69	3.95
12	274	3,512	31,608	21.20	3.13
13	240	5,753	51,777	34.73	1.52

**Table 2.12.9-25**  
**Tie-Rod Loads for 30 Foot Cold Corner Drop**

Tie-Rod No.	Position (Degrees)	Scale Model Tensile Force (lbf)	Full Scale		Margin of Safety
			Force (lbf)	Stress (ksi)	
1	184	2,377	21,393	14.35	5.10
2	176	2,893	26,037	17.47	4.01
3	150	3,096	27,864	18.69	3.68
4	120	2,985	26,865	18.02	3.86
5	90	3,818	34,362	23.05	2.80
6	60	2,437	21,933	14.72	4.95
7	30	2,664	23,976	16.09	4.44
8	4	2,530	22,770	15.28	4.73
9	356	2,372	21,348	14.32	5.11
10	315	16,620	149,580	100.35	-0.13
11	266	12,701	114,309	76.68	0.14
12	274	12,719	114,471	76.79	0.14
13	240	16,585	149,265	100.13	-0.13

**Table 2.12.9-26**  
**Tie-Rod Loads for 30 Foot Warm Corner Drop**

Tie-Rod No.	Position (Degrees)	Scale Model Tensile Force (lbf)	Full Scale		Margin of Safety
			Force (lbf)	Stress (ksi)	
1	184	2,493	22,437	15.05	4.81
2	176	2,954	26,586	17.84	3.91
3	150	3,213	28,917	19.39	3.51
4	120	2,964	26,676	17.89	3.89
5	90	3,209	28,881	19.37	3.52
6	60	2,212	19,908	13.35	5.55
7	30	2,982	26,838	18.00	3.86
8	4	2,573	23,157	15.54	4.63
9	356	2,327	20,943	14.05	5.23
10	315	15,533	139,797	93.78	-0.07
11	266	11,974	107,766	72.30	0.21
12	274	11,920	107,280	71.97	0.22
13	240	15,504	139,536	93.61	-0.07

**Table 2.12.9-27**  
**Tie-Rod Loads for 30 Foot Cold End Drop**

Tie-Rod No.	Position (Degrees)	Scale Model Tensile Force (lbf)	Full Scale		Margin of Safety
			Force (lbf)	Stress (ksi)	
1	184	2,289	20,601	13.82	5.33
2	176	2,544	22,896	15.36	4.70
3	150	5,295	47,655	31.97	1.74
4	120	5,088	45,792	30.72	1.85
5	90	3,001	27,009	18.12	3.83
6	60	5,343	48,087	32.26	1.71
7	30	5,557	50,013	33.55	1.61
8	4	2,388	21,492	14.42	5.07
9	356	1,919	17,271	11.59	6.55
10	315	4,167	37,503	25.16	2.48
11	266	2,348	21,132	14.17	5.17
12	274	2,753	24,777	16.62	4.26
13	240	5,019	45,171	30.30	1.89

**Table 2.12.9-28**  
**Tie-Rod Loads for 30 Foot Warm End Drop**

Tie-Rod No.	Position (Degrees)	Scale Model Tensile Force (lbf)	Full Scale		Margin of Safety
			Force (lbf)	Stress (ksi)	
1	184	2,034	18,306	12.28	6.13
2	176	2,926	26,334	17.67	3.95
3	150	5,228	47,052	31.56	1.77
4	120	5,108	45,972	30.84	1.84
5	90	3,750	33,750	22.64	2.87
6	60	5,804	52,236	35.04	1.50
7	30	5,179	46,611	31.27	1.80
8	4	1,838	16,542	11.09	6.89
9	356	1,850	16,650	11.17	6.83
10	315	4,970	44,730	30.00	1.92
11	266	1,708	15,372	10.31	7.48
12	274	1,832	16,488	11.06	6.91
13	240	5,341	48,069	32.25	1.71

**Table 2.12.9-29**  
**IL Attachment Bolt Loads for 30 Foot Cold Side Drop**

Bolt No.	Position (Degrees)	Scale Model Tensile Force (lbf)	Full Scale		Margin of Safety
			Force (lbf)	Stress (ksi)	
1	135	1,731	15,579	10.45	9.38
2	225	5,052	45,468	30.50	2.56
3	315	5,610	50,490	33.87	2.20
4	45	1,712	15,408	10.33	9.50
5	45	1,721	15,489	10.39	9.44
6	315	1,441	12,969	8.70	11.48
7	225	1,441	12,969	8.70	11.48
8	135	1,658	14,922	10.01	9.84

**Table 2.12.9-30**  
**IL Attachment Bolt Loads for 30 Foot Warm Side Drop**

Bolt No.	Position (Degrees)	Scale Model Tensile Force (lbf)	Full Scale		Margin of Safety
			Force (lbf)	Stress (ksi)	
1	135	1,546	13,914	9.34	10.62
2	225	6,377	57,393	38.50	1.82
3	315	6,088	54,792	36.76	1.95
4	45	1,564	14,076	9.45	10.49
5	45	1,536	13,824	9.28	10.70
6	315	1,687	15,183	10.19	9.65
7	225	1,710	15,390	10.32	9.51
8	135	1,569	14,121	9.48	10.45

**Table 2.12.9-31**  
**IL Attachment Bolt Loads for 30 Foot Cold Slapdown**

Bolt No.	Position (Degrees)	Scale Model Tensile Force (lbf)	Full Scale		Margin of Safety
			Force (lbf)	Stress (ksi)	
1	135	1,543	13,887	9.32	10.65
2	225	18,122	163,098	109.41	-0.01
3	315	17,965	161,685	108.46	0.00
4	45	1,543	13,887	9.32	10.65
5	45	14,113	127,017	85.21	0.27
6	315	3,517	31,653	21.23	4.11
7	225	3,379	30,411	20.40	4.32
8	135	14,345	129,105	86.61	0.25

**Table 2.12.9-32**  
**IL Attachment Bolt Loads for 30 Foot Warm Slapdown**

Bolt No.	Position (Degrees)	Scale Model Tensile Force (lbf)	Full Scale		Margin of Safety
			Force (lbf)	Stress (ksi)	
1	135	1,504	13,536	9.08	10.95
2	225	12,114	109,026	73.14	0.48
3	315	12,418	111,762	74.97	0.45
4	45	1,520	13,680	9.18	10.82
5	45	9,470	85,230	57.18	0.90
6	315	4,138	37,242	24.98	3.34
7	225	3,169	28,521	19.13	4.67
8	135	9,551	85,959	57.66	0.88

**Table 2.12.9-33**  
**IL Attachment Bolt Loads for 30 Foot Cold Corner Drop**

Bolt No.	Position (Degrees)	Scale Model Tensile Force (lbf)	Full Scale		Margin of Safety
			Force (lbf)	Stress (ksi)	
1	135	2,333	20,997	14.08	6.70
2	225	1,528	13,752	9.23	10.76
3	315	1,475	13,275	8.90	11.19
4	45	2,306	20,754	13.93	6.79
5	45	1,558	14,022	9.41	10.54
6	315	7,983	71,847	48.20	1.25
7	225	7,950	71,550	48.00	1.26
8	135	1,547	13,923	9.34	10.62



**Table 2.12.9-34**  
**IL Attachment Bolt Loads for 30 Foot Warm Corner Drop**

Bolt No.	Position (Degrees)	Scale Model Tensile Force (lbf)	Full Scale		Margin of Safety
			Force (lbf)	Stress (ksi)	
1	135	2,227	20,043	13.44	7.07
2	225	1,489	13,401	8.99	11.07
3	315	1,532	13,788	9.25	10.73
4	45	2,181	19,629	13.17	7.24
5	45	1,519	13,671	9.17	10.83
6	315	6,813	61,317	41.14	1.64
7	225	7,045	63,405	42.53	1.55
8	135	1,528	13,752	9.23	10.76

**Table 2.12.9-35**  
**IL Attachment Bolt Loads for 30 Foot Cold End Drop**

Bolt No.	Position (Degrees)	Scale Model Tensile Force (lbf)	Full Scale		Margin of Safety
			Force (lbf)	Stress (ksi)	
1	135	2,117	19,053	12.78	7.49
2	225	2,098	18,882	12.66	7.57
3	315	2,093	18,837	12.63	7.59
4	45	2,084	18,756	12.58	7.62
5	45	2,346	21,114	14.16	6.66
6	315	2,541	22,869	15.34	6.07
7	225	2,406	21,654	14.53	6.47
8	135	2,405	21,645	14.52	6.47

**Table 2.12.9-36**  
**IL Attachment Bolt Loads for 30 Foot Warm End Drop**

Bolt No.	Position (Degrees)	Scale Model Tensile Force (lbf)	Full Scale		Margin of Safety
			Force (lbf)	Stress (ksi)	
1	135	2,093	18,837	12.63	7.59
2	225	1,753	15,777	10.58	9.26
3	315	1,736	15,624	10.48	9.35
4	45	2,085	18,765	12.58	7.62
5	45	1,441	12,969	8.70	11.48
6	315	1,441	12,969	8.70	11.48
7	225	1,441	12,969	8.70	11.48
8	135	1,440	12,960	8.70	11.48

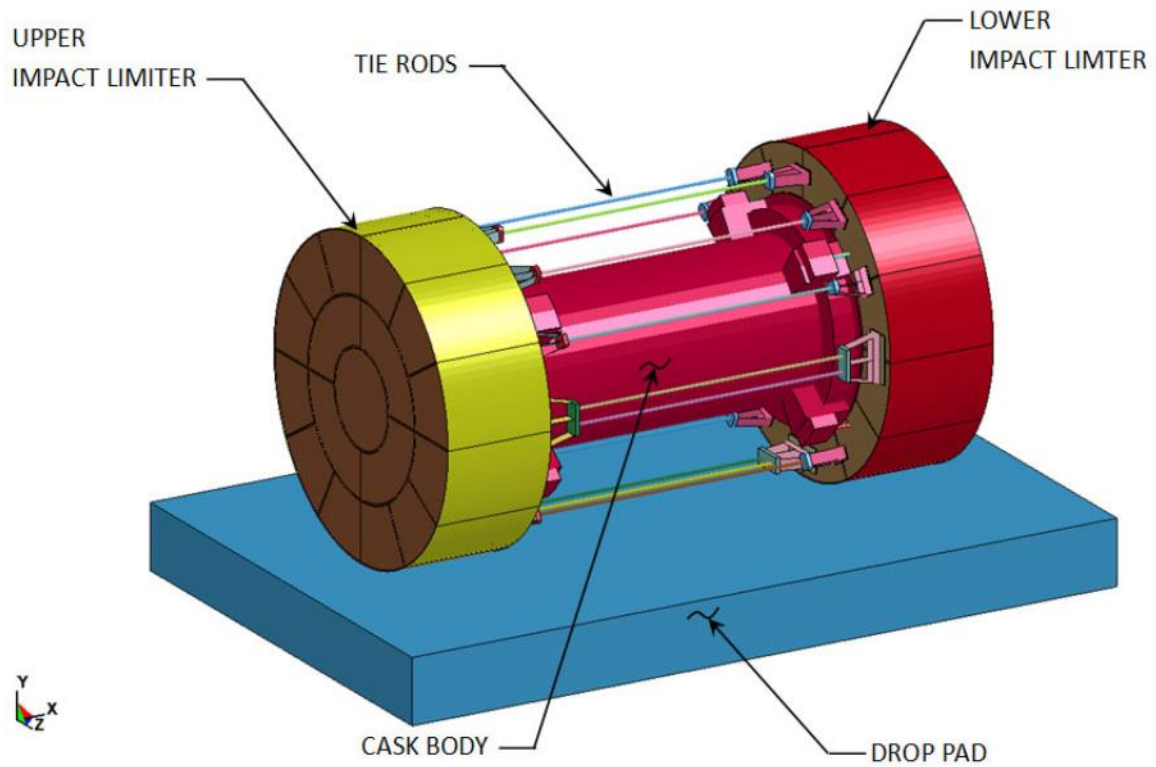


**Figure 2.12.9-1**  
**Package with ILs**

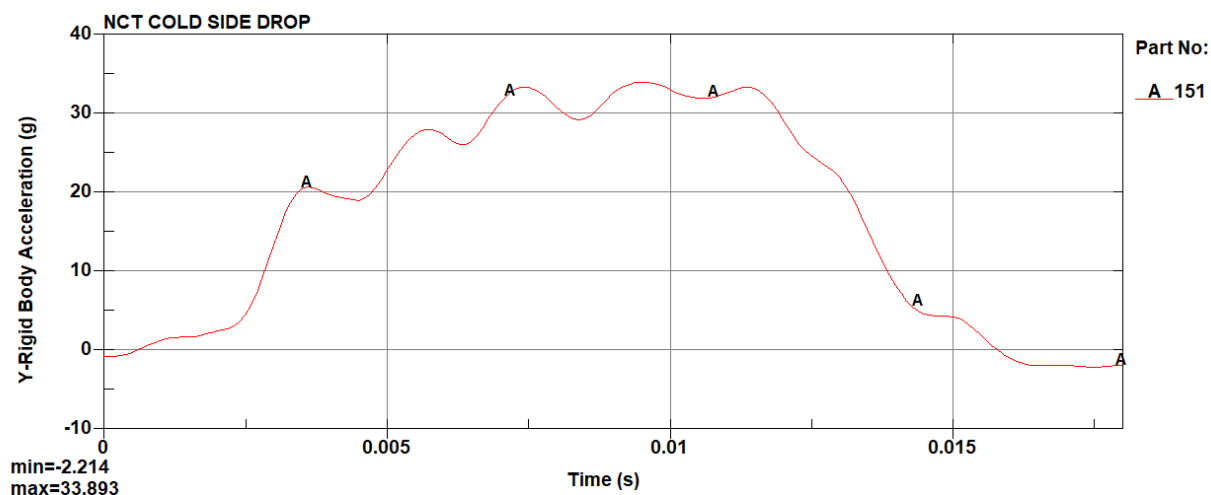


**Figure 2.12.9-2**  
**NCT Cold Side Drop Acceleration**

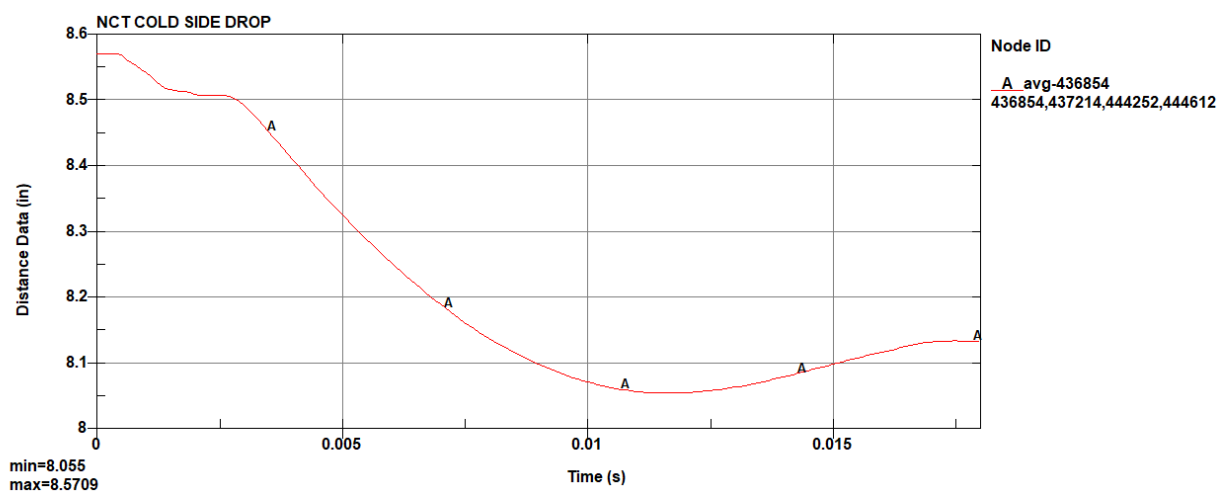


**Figure 2.12.9-3**  
**NCT Cold Side Drop Deflection**

NCT COLD SIDE DROP  
Time = 0.011599

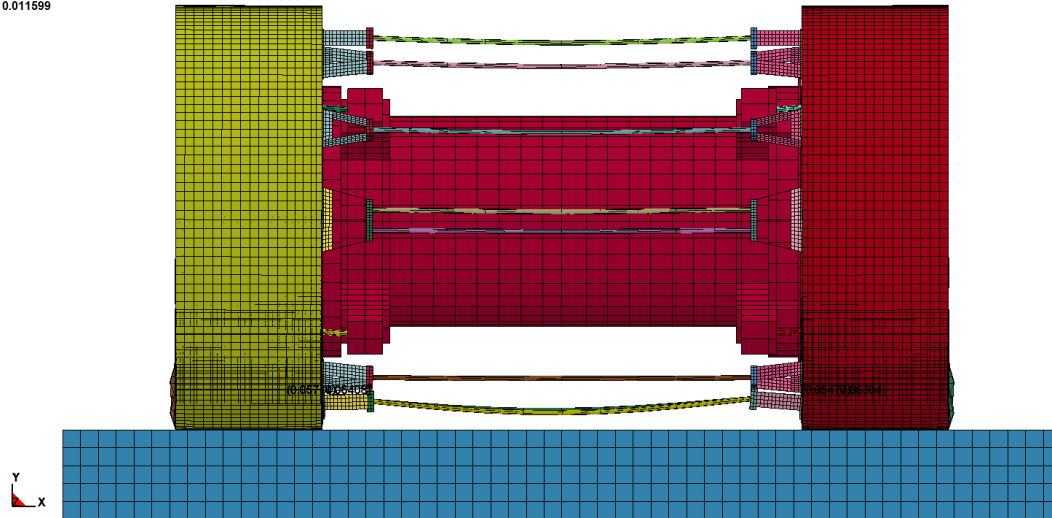


**Figure 2.12.9-4**  
**NCT Cold Side Drop Deformation**

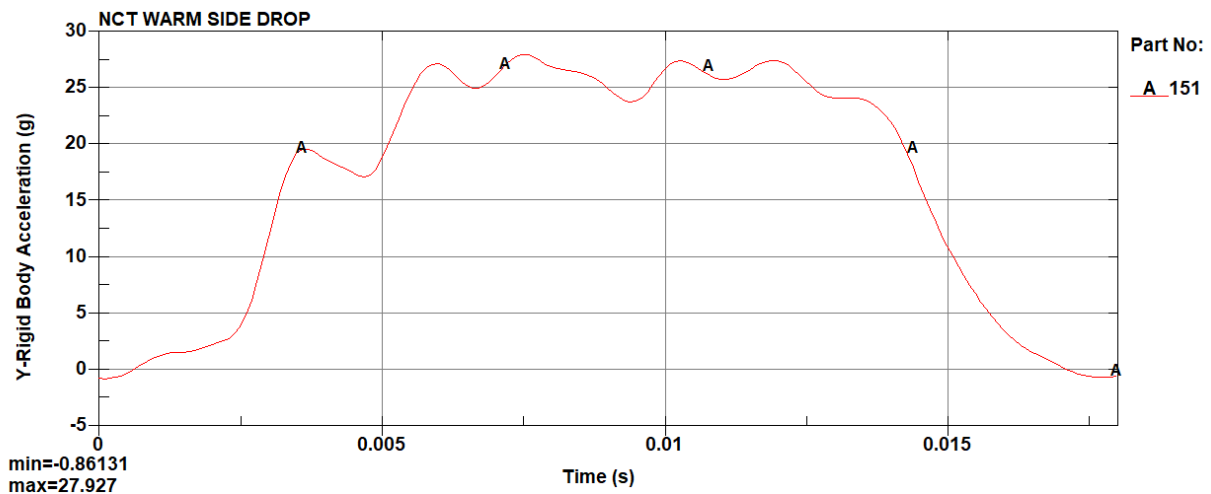


**Figure 2.12.9-5**  
**NCT Warm Side Drop Acceleration**

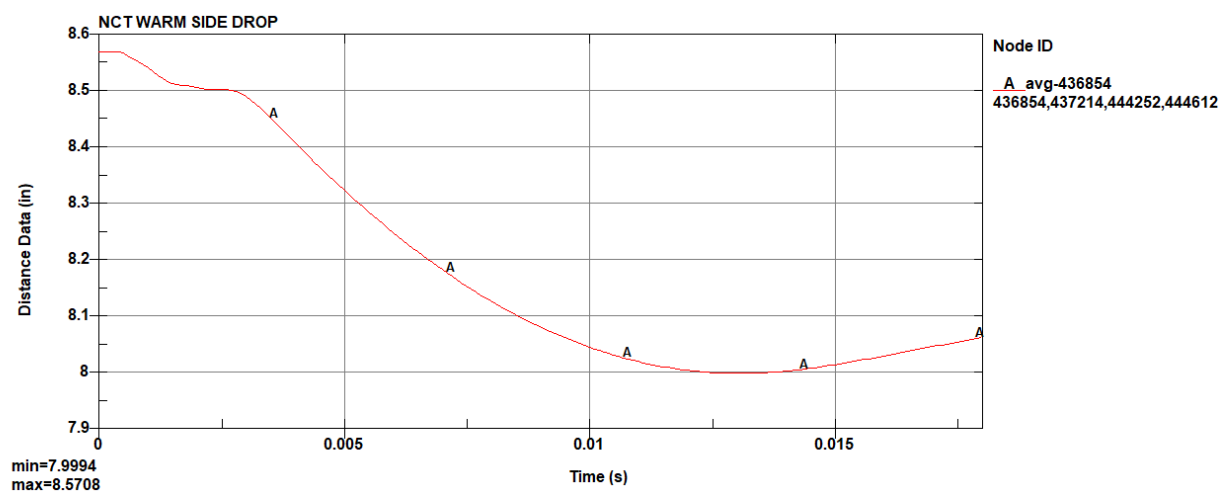


**Figure 2.12.9-6**  
**NCT Warm Side Drop Deflection**

NCT WARM SIDE DROP  
Time = 0.013099

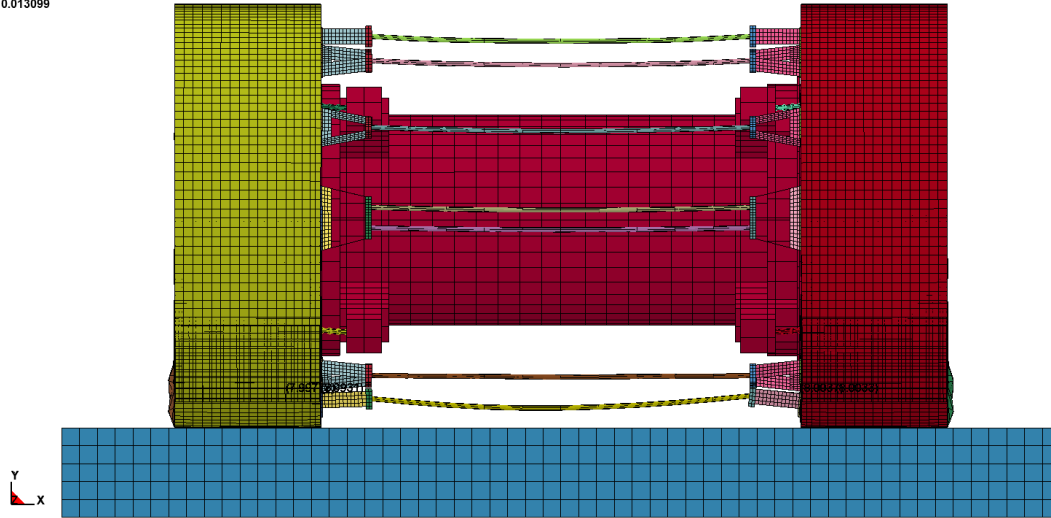


**Figure 2.12.9-7**  
**NCT Warm Side Drop Deformation**

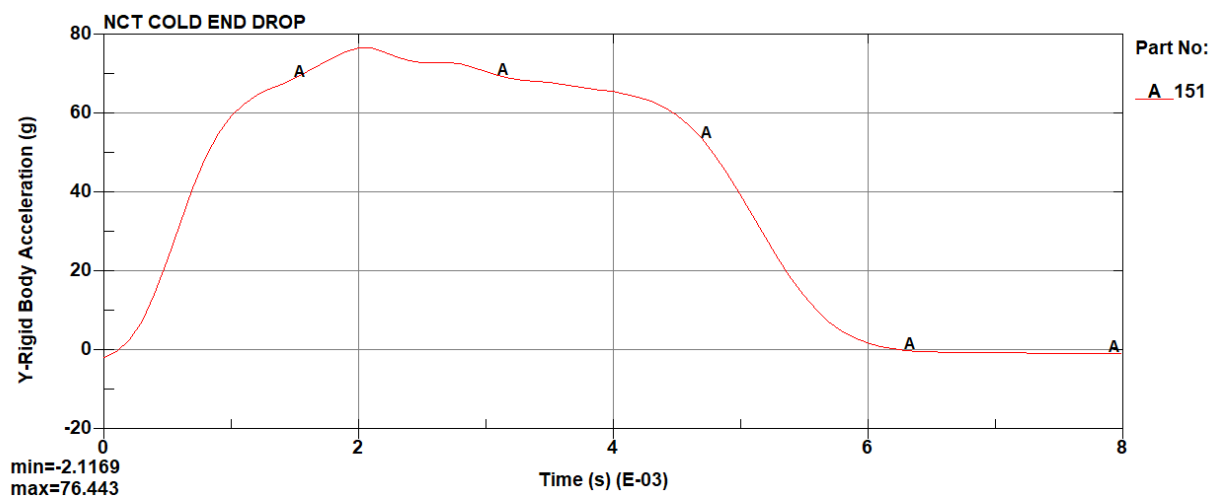


**Figure 2.12.9-8**  
**NCT Cold End Drop Acceleration**

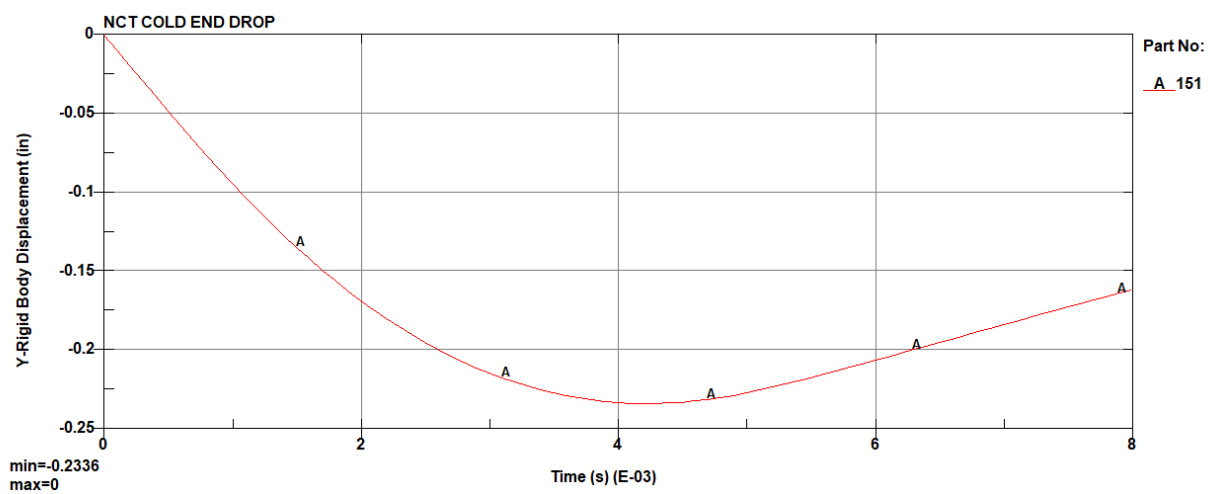


**Figure 2.12.9-9**  
**NCT Cold End Drop Deflection**

NCT COLD END DROP  
Time = 0.0042

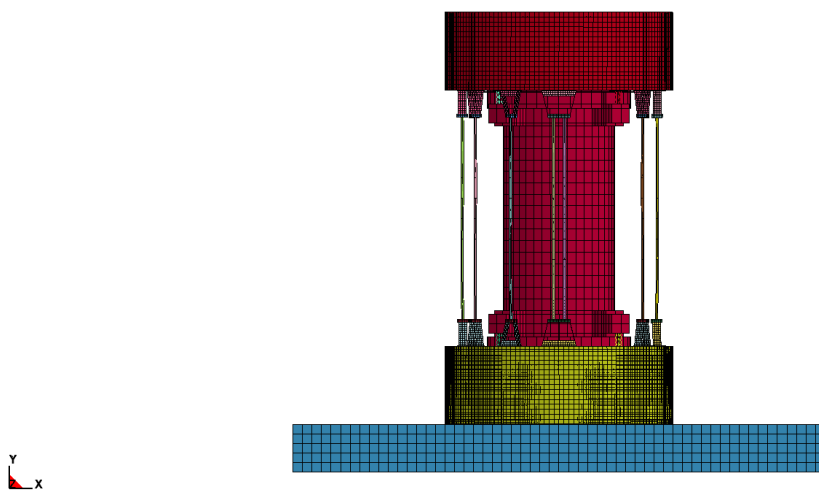


**Figure 2.12.9-10**  
**NCT Cold End Drop Deformation**



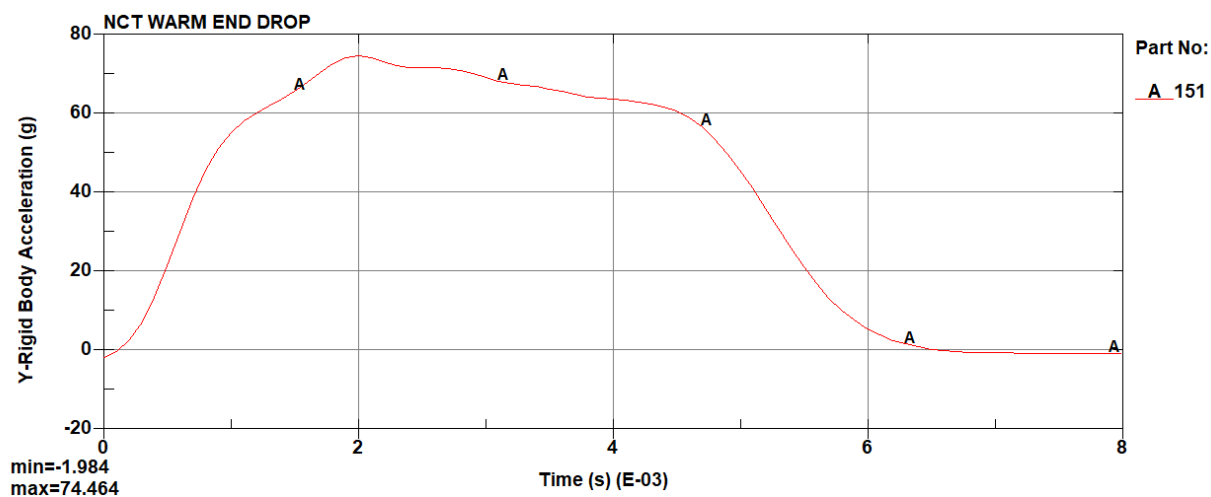


**Figure 2.12.9-11**  
**NCT Warm End Drop Acceleration**

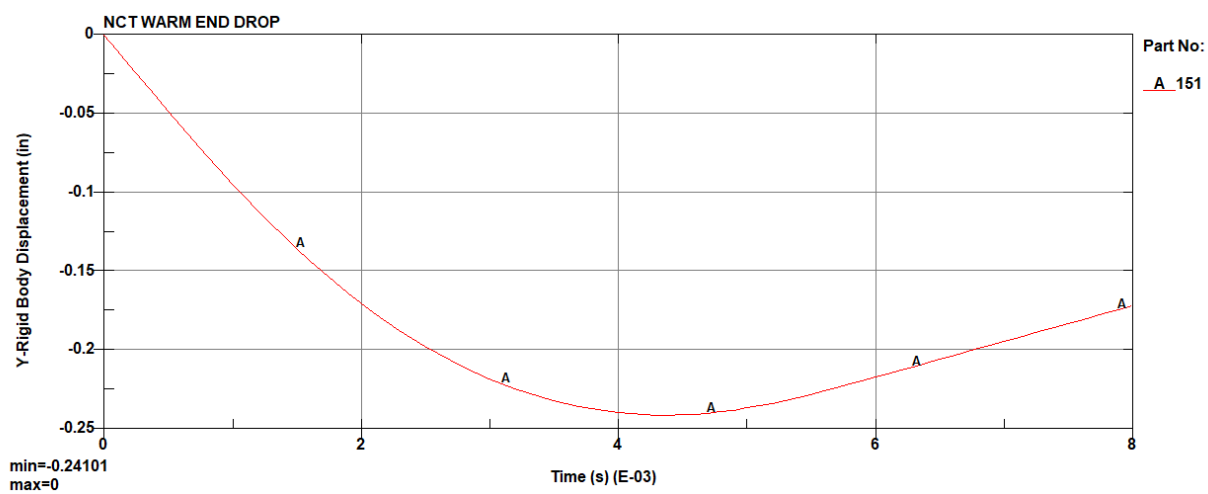


**Figure 2.12.9-12**  
**NCT Warm End Drop Deflection**

NCT WARM END DROP  
Time = 0.0043992

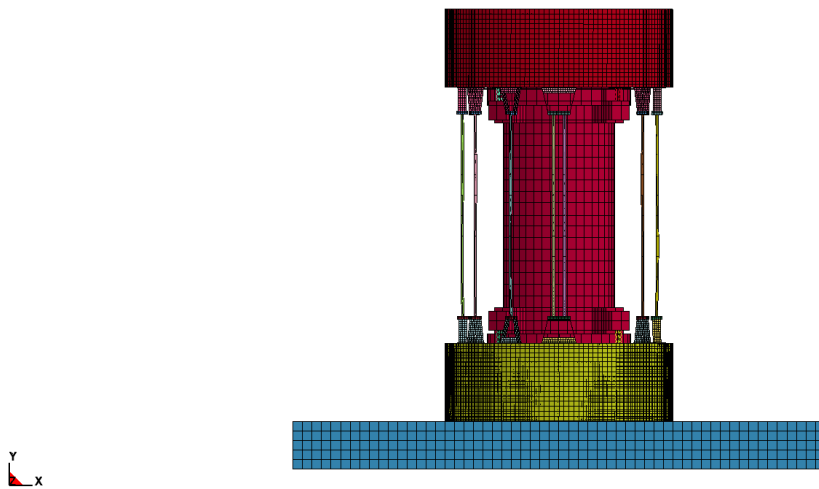


**Figure 2.12.9-13**  
**NCT Warm End Drop Deformation**

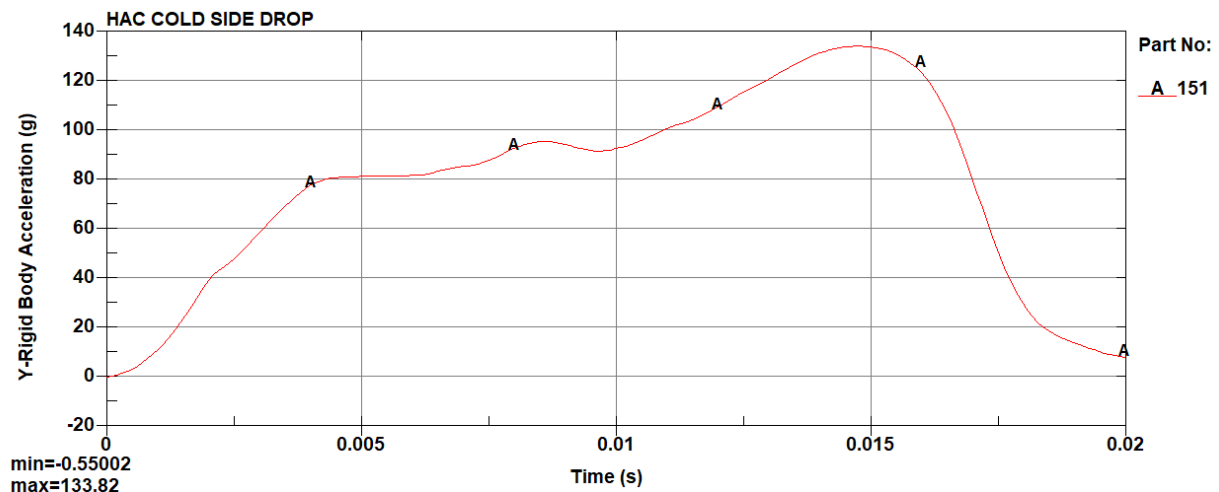


Figure 2.12.9-14  
HAC Cold Side Drop Acceleration

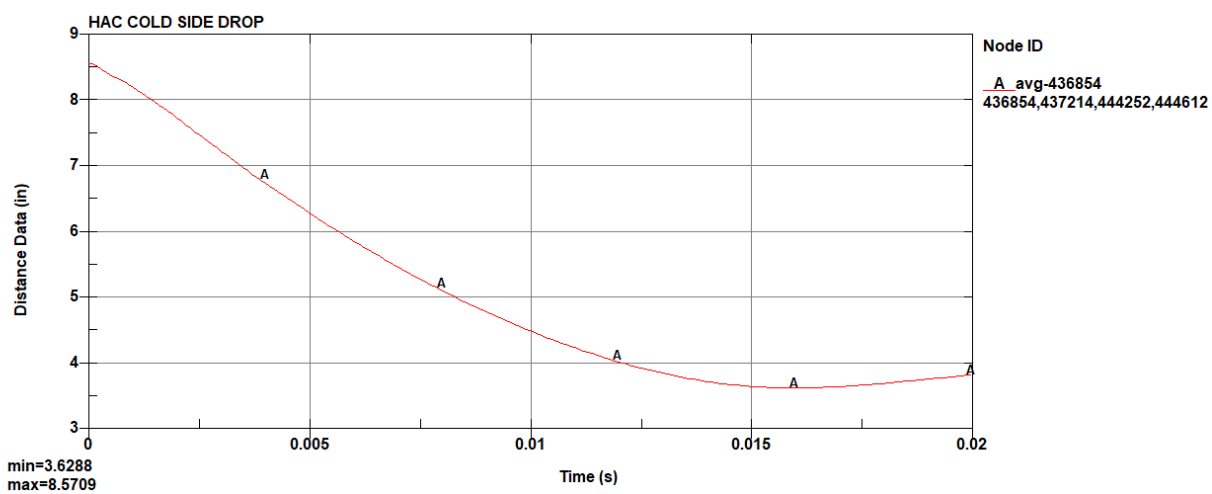
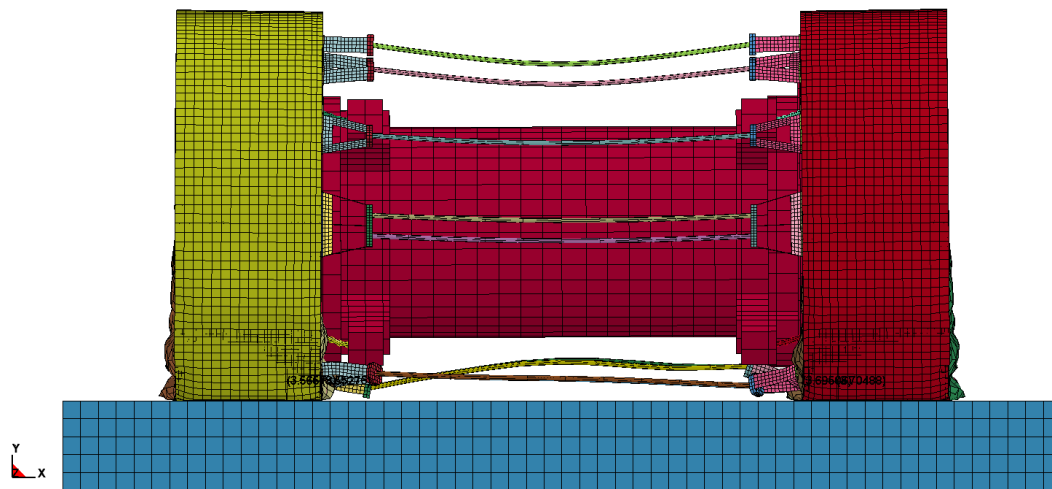


Figure 2.12.9-15  
HAC Cold Side Drop Deflection

HAC COLD SIDE DROP  
Time = 0.015799



**Figure 2.12.9-16**  
**HAC Cold Side Drop Deformation**

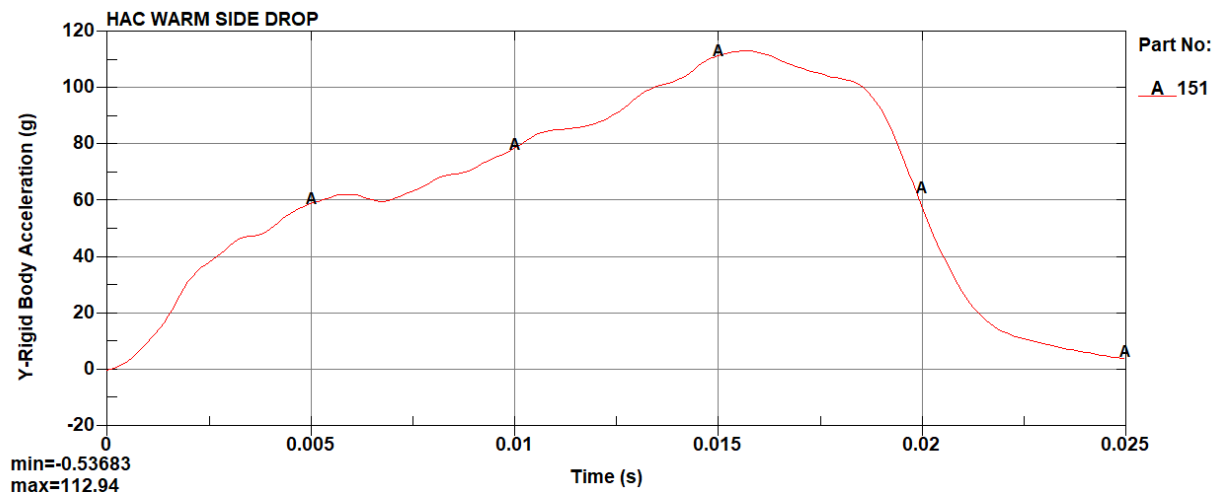


Figure 2.12.9-17  
HAC Warm Side Drop Acceleration

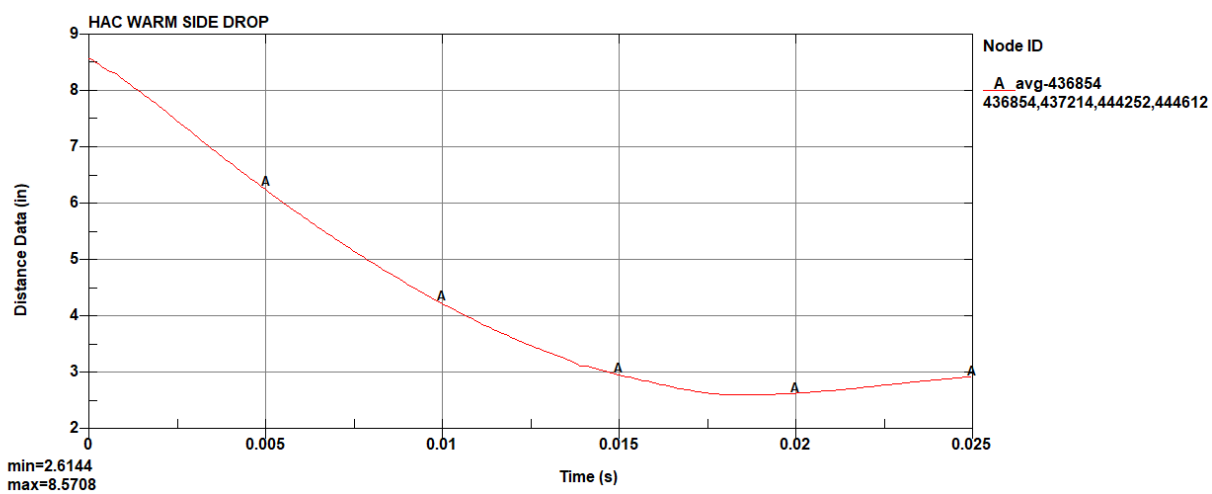
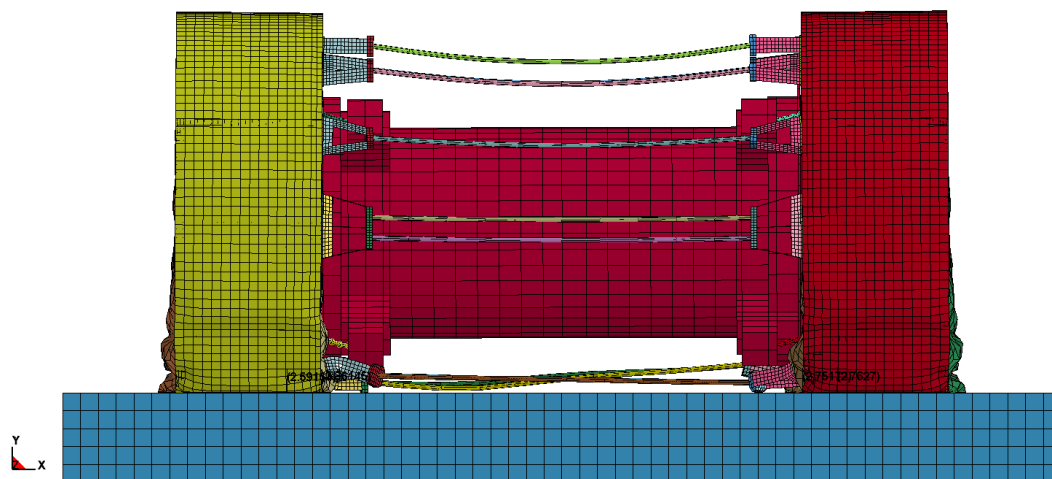


Figure 2.12.9-18  
HAC Warm Side Drop Deflection

HAC WARM SIDE DROP  
Time = 0.018799



**Figure 2.12.9-19**  
**HAC Warm Side Drop Deformation**

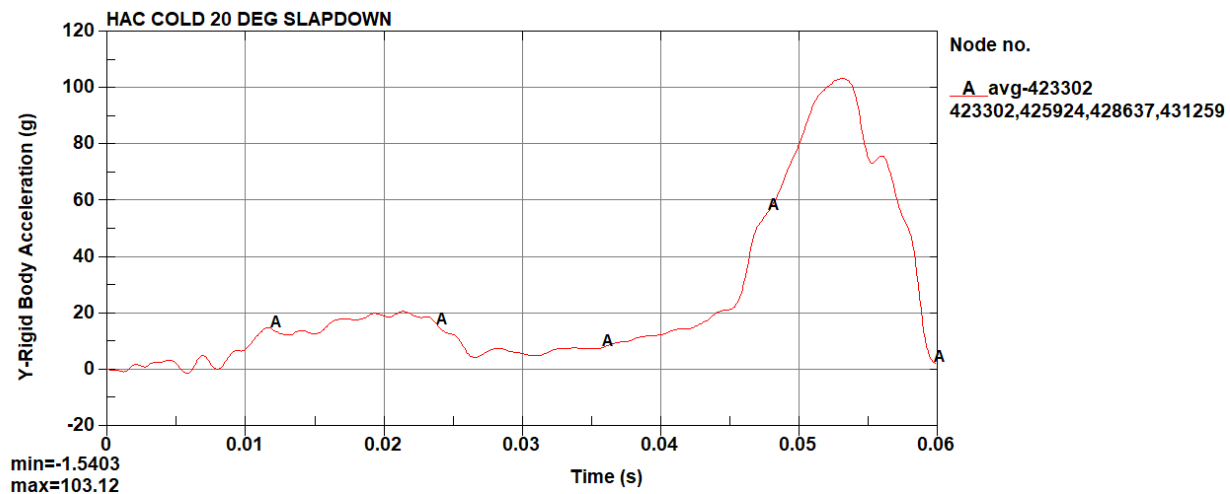


Figure 2.12.9-20  
HAC Cold Secondary Slapdown Acceleration

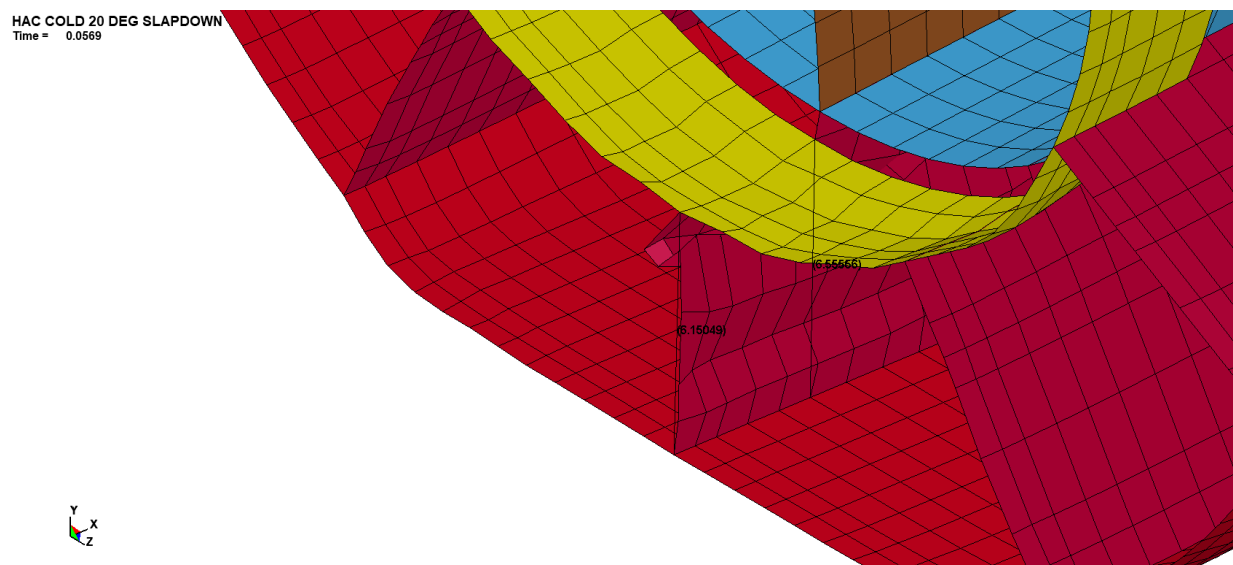
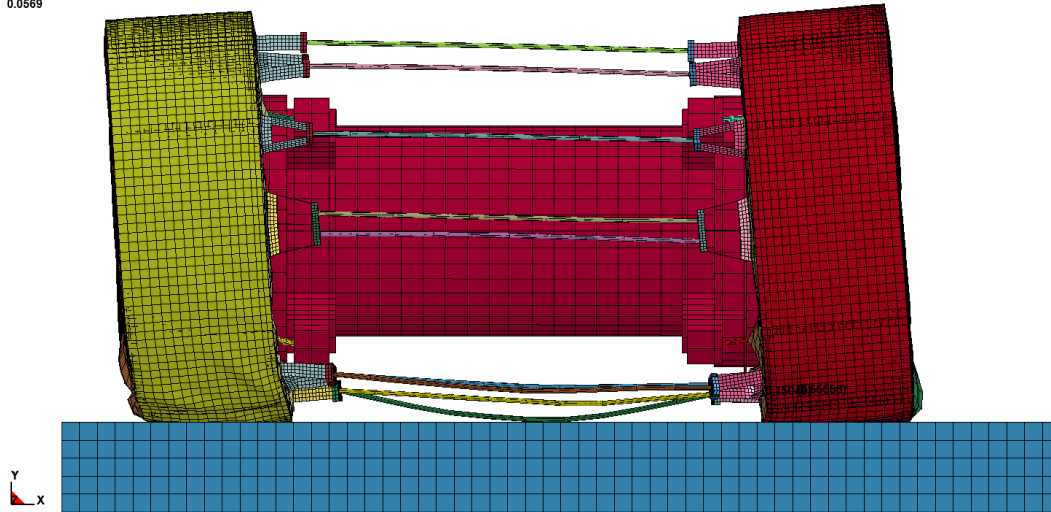


Figure 2.12.9-21  
HAC Cold Slapdown Deflection

HAC COLD 20 DEG SLAPDOWN  
Time = 0.0569



**Figure 2.12.9-22**  
**HAC Cold Slapdown Deformation**



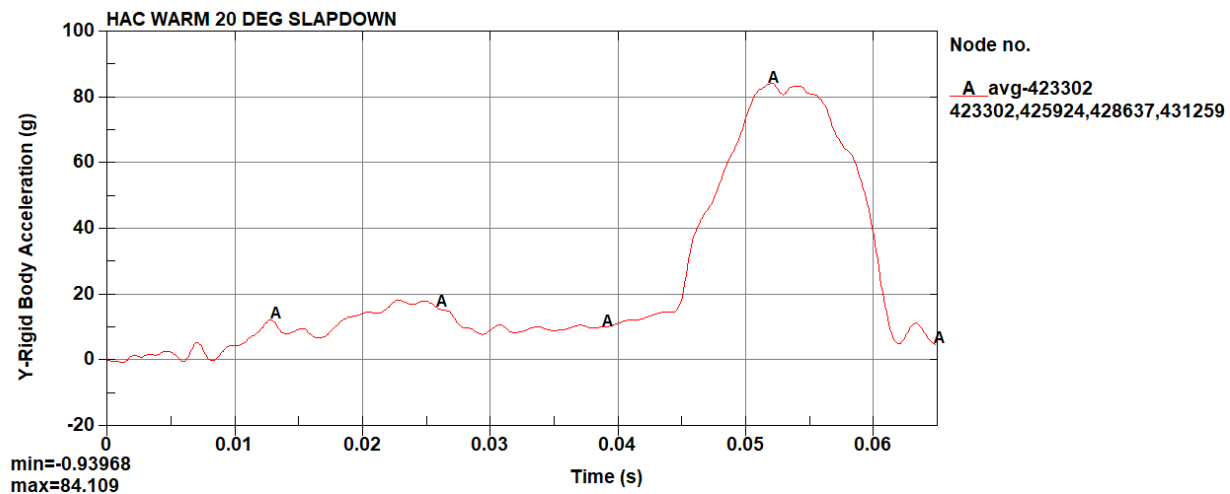


**Figure 2.12.9-23**  
**HAC Warm Secondary Slapdown Acceleration**

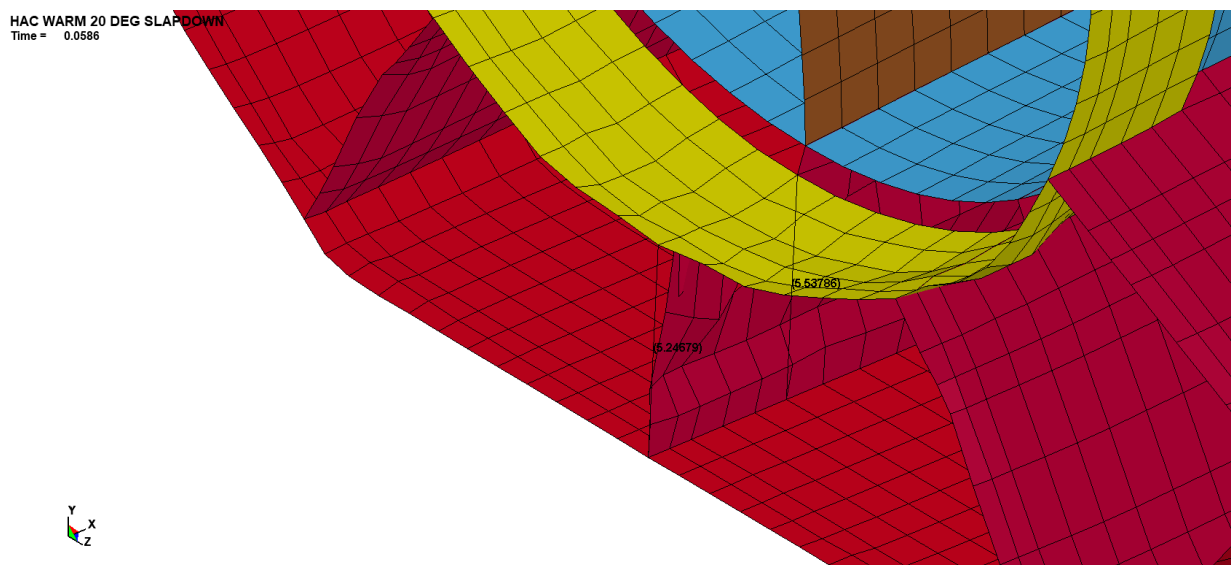


**Figure 2.12.9-24**  
**HAC Warm Slapdown Deflection**

HAC WARM 20 DEG SLAPDOWN  
Time = 0.0586

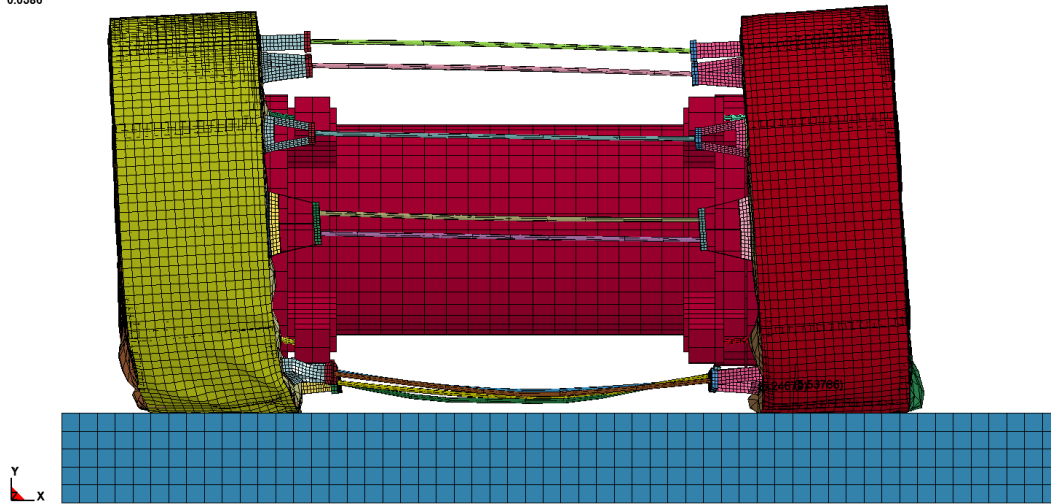


**Figure 2.12.9-25**  
**HAC Warm Slapdown Deformation**

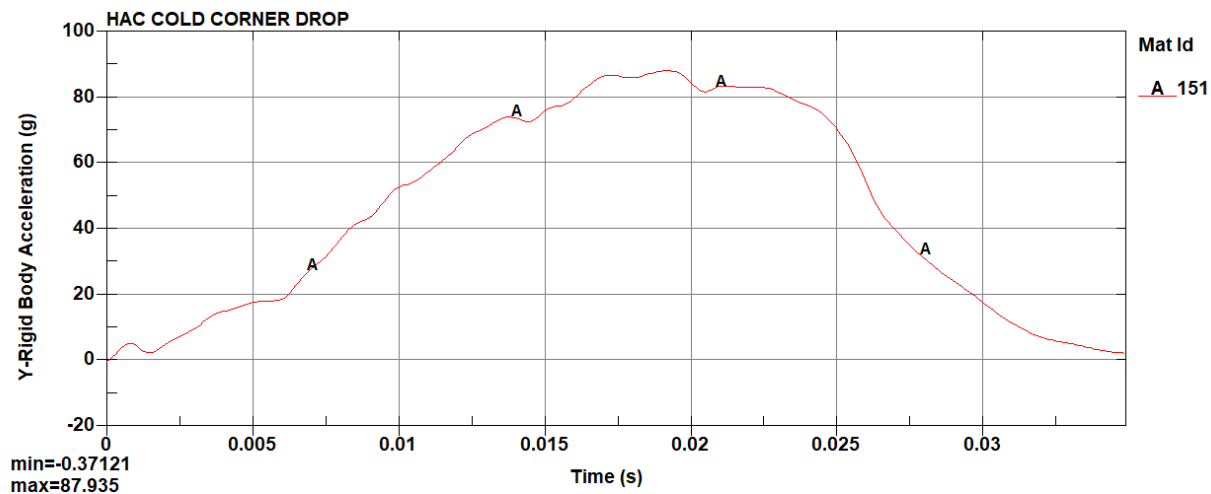


Figure 2.12.9-26  
HAC Cold Corner Drop Acceleration

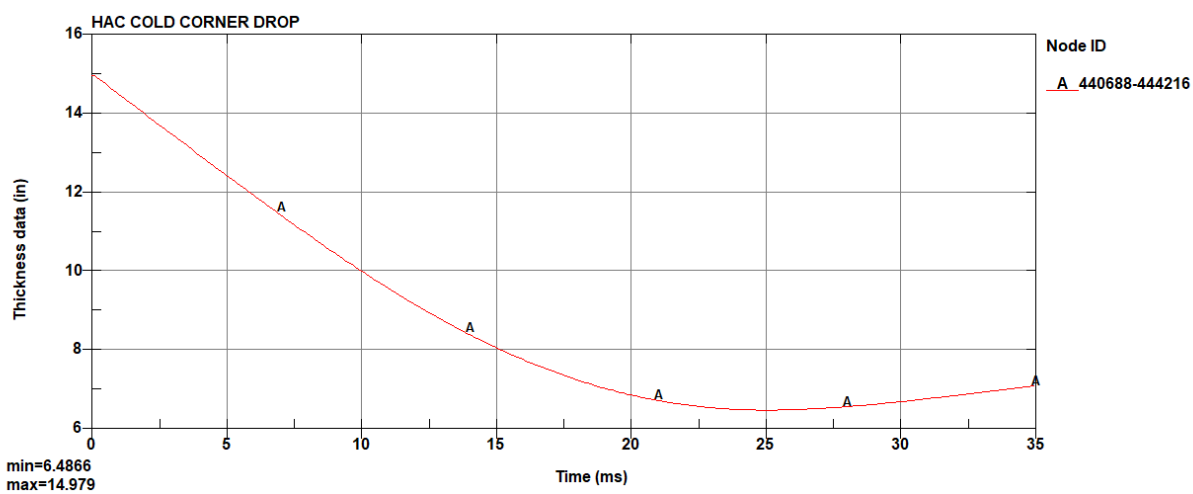
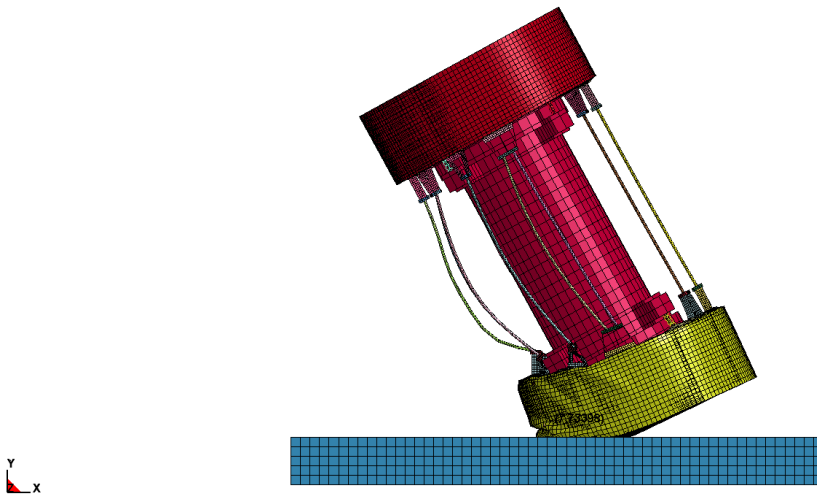


Figure 2.12.9-27  
HAC Cold Corner Drop Deflection

HAC COLD CORNER DROP  
Time = 0.024999



**Figure 2.12.9-28**  
**HAC Cold Corner Drop Deformation**

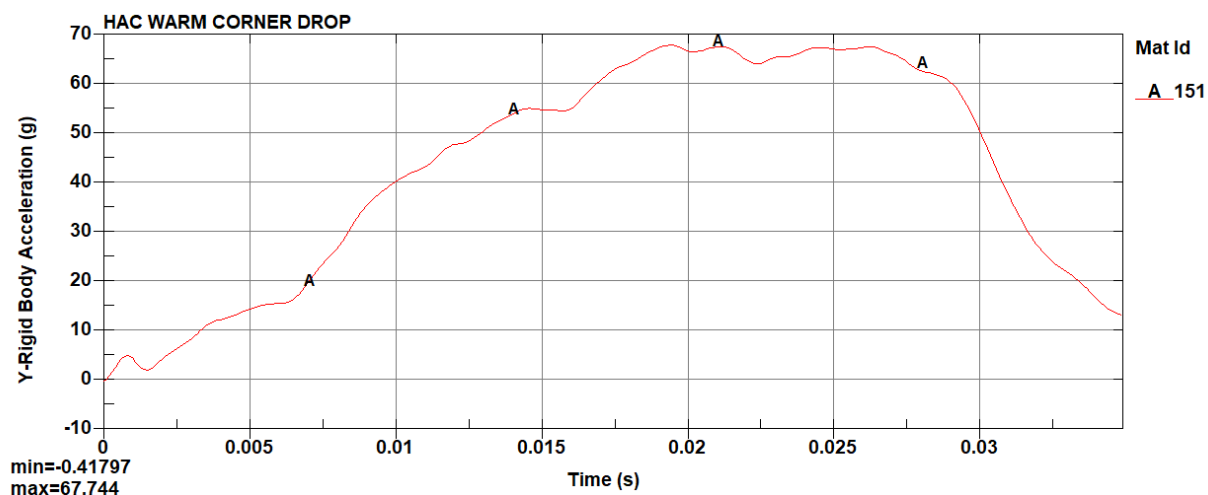


Figure 2.12.9-29  
HAC Warm Corner Drop Acceleration

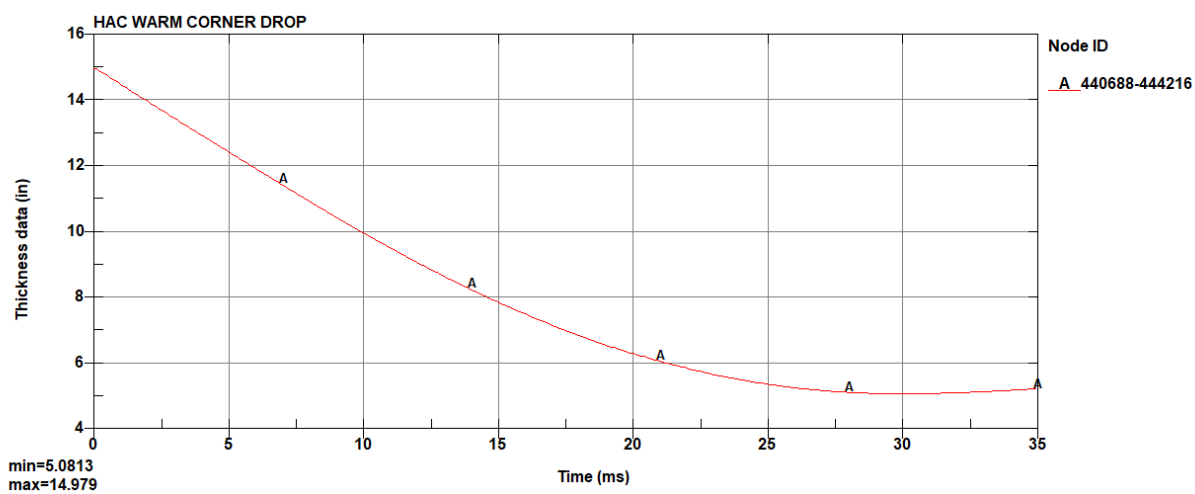
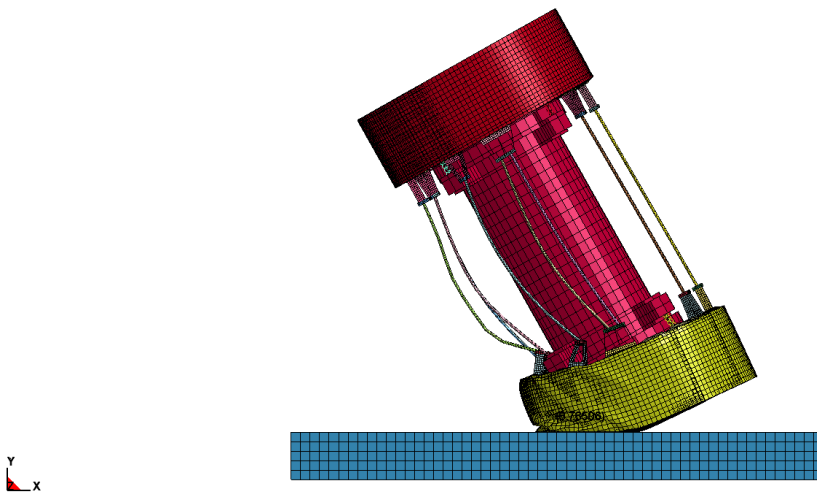


Figure 2.12.9-30  
HAC Warm Corner Drop Deflection

HAC WARM CORNER DROP  
Time = 0.029999



**Figure 2.12.9-31**  
**HAC Warm Corner Drop Deformation**

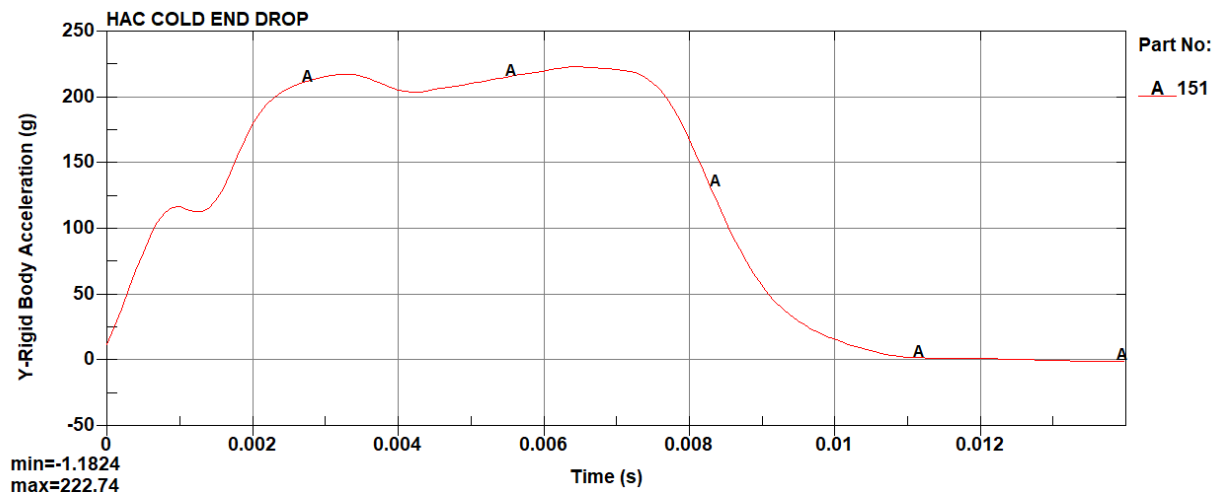


Figure 2.12.9-32  
HAC Cold End Drop Acceleration

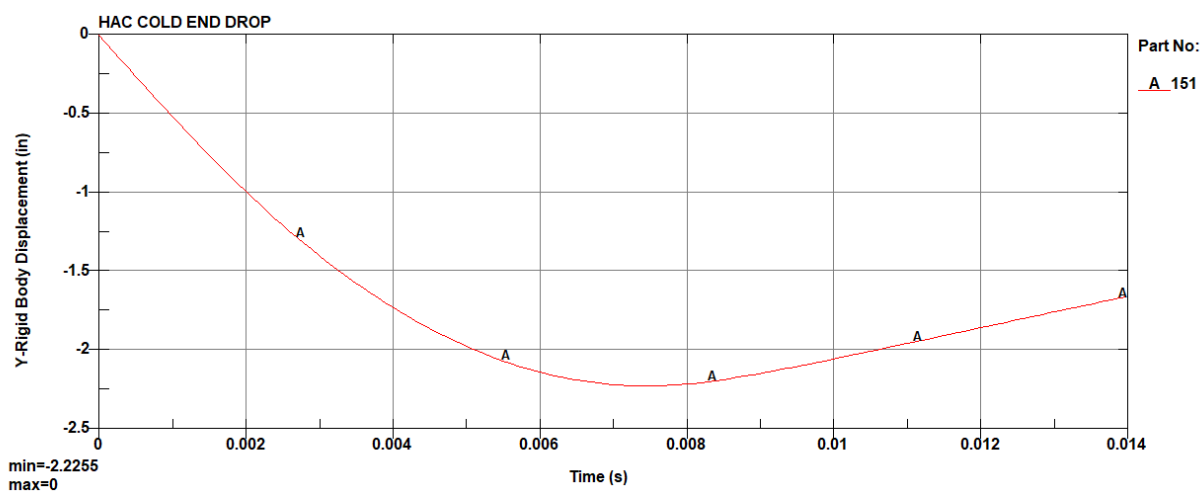
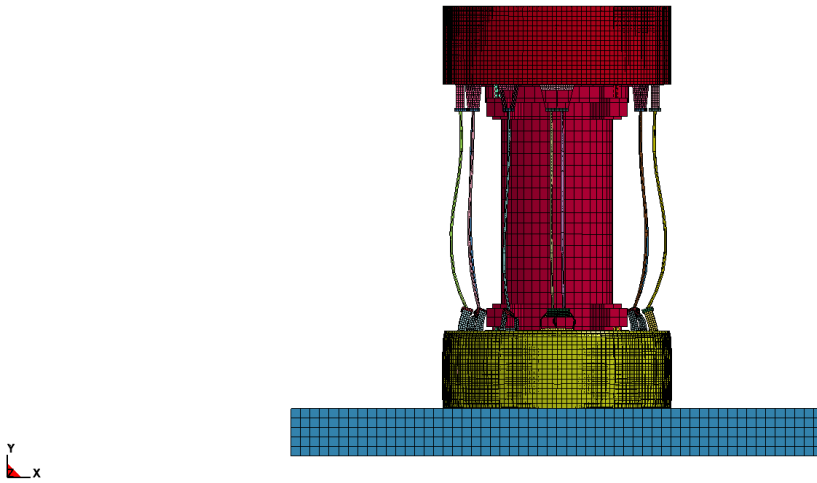


Figure 2.12.9-33  
HAC Cold End Drop Deflection

HAC COLD END DROP  
Time = 0.0073992



**Figure 2.12.9-34**  
**HAC Cold End Drop Deformation**



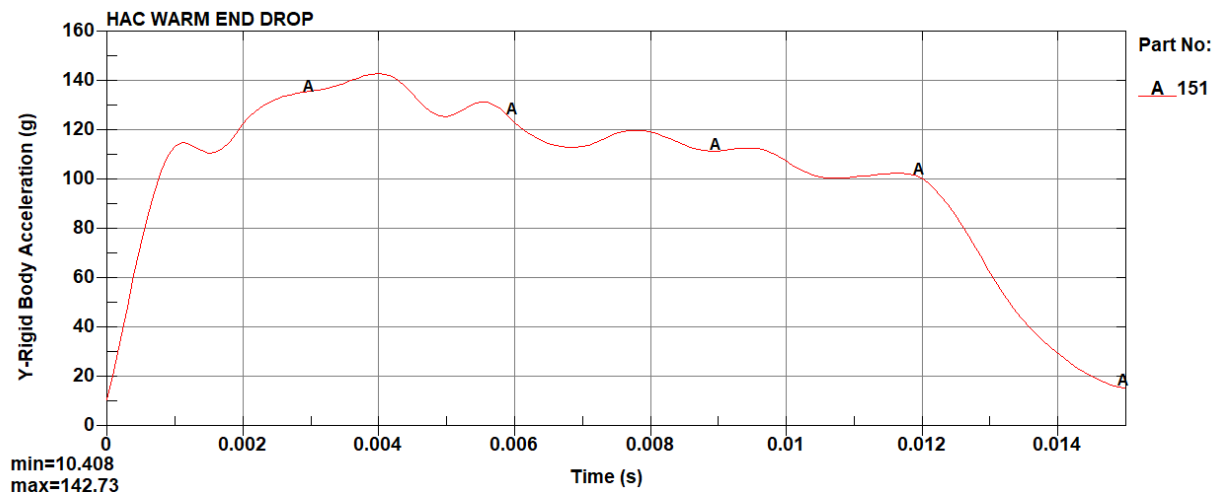


Figure 2.12.9-35  
HAC Warm End Drop Acceleration

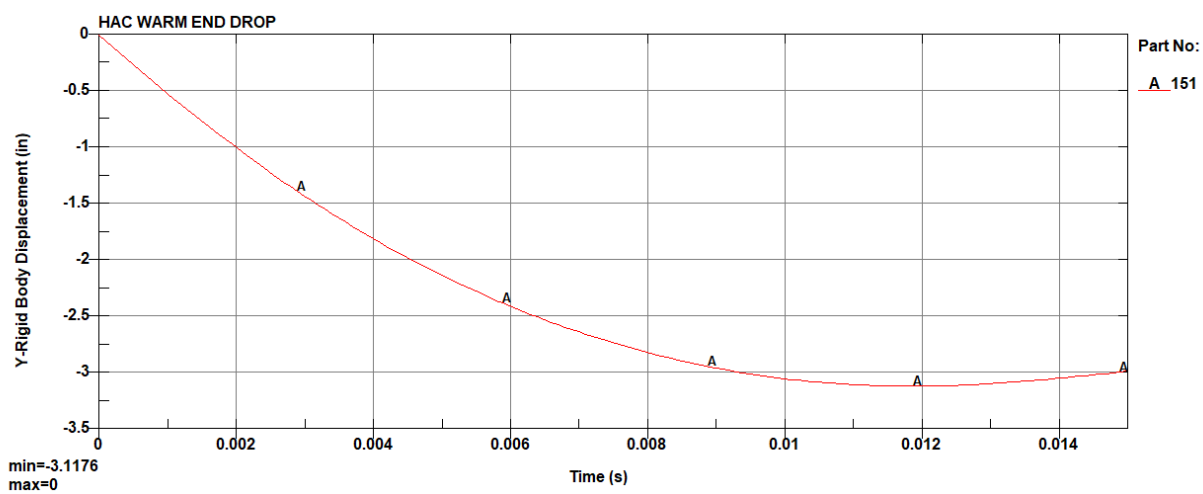
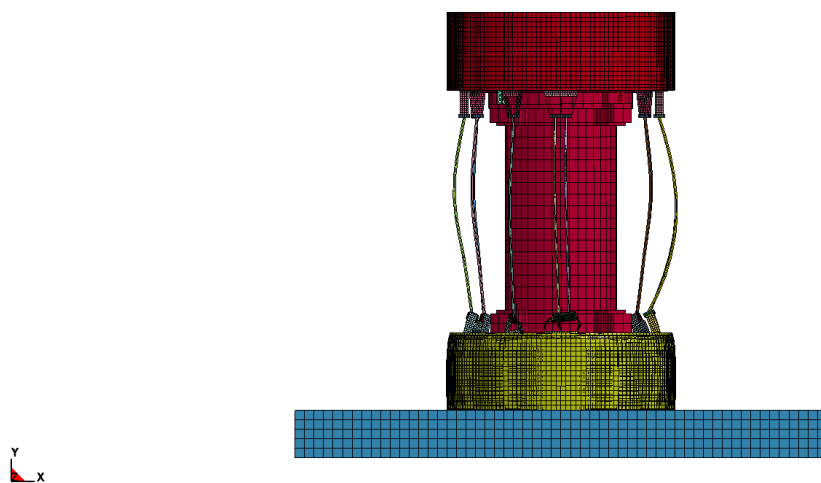
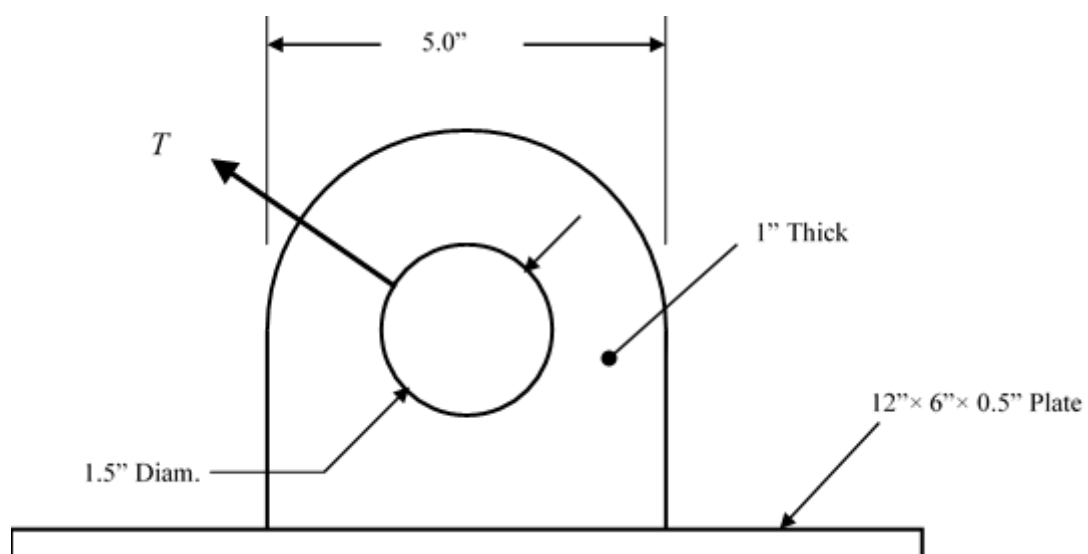


Figure 2.12.9-36  
HAC Warm End Drop Deflection

HAC WARM END DROP  
Time = 0.011899



**Figure 2.12.9-37**  
**HAC Warm End Drop Deformation**



**Figure 2.12.9-38**  
**IL Lifting Lug Geometry**

**Appendix 2.12.10**  
**TN-40 Package Impact Limiter Testing**

TABLE OF CONTENTS

2.12.10	TN-40 Package Impact Limiter Testing .....	2.12.10-1
2.12.10.1	Introduction .....	2.12.10-1
2.12.10.2	Scaling Relationships .....	2.12.10-1
2.12.10.3	Test Article Description .....	2.12.10-2
2.12.10.4	Test Description .....	2.12.10-2
2.12.10.5	Data Measurement.....	2.12.10-7
2.12.10.6	Test Data and Results.....	2.12.10-8
2.12.10.7	Conclusions.....	2.12.10-15
2.12.10.8	References.....	2.12.10-17

LIST OF TABLES

Table 2.12.10-1	Summary of the Test Results .....	2.12.10-18
-----------------	-----------------------------------	------------

LIST OF FIGURES

Figure 2.12.10-1	TN-40 One-Third Scale Test Article .....	2.12.10-19
Figure 2.12.10-2	TN-40 Accelerometer Locations .....	2.12.10-20
Figure 2.12.10-3	0° TN-40 Side Drop Test Setup .....	2.12.10-21
Figure 2.12.10-4	TN-40 CG-Over-Corner Drop Test Setup .....	2.12.10-22
Figure 2.12.10-5	TN-40 20° Slap Down Test Setup .....	2.12.10-23
Figure 2.12.10-6	TN-40 90° End Drop Test Setup .....	2.12.10-24
Figure 2.12.10-7	TN-40 Puncture Drop Test Setup .....	2.12.10-25
Figure 2.12.10-8	TN-40 Test Article and Accelerometer Locations .....	2.12.10-26
Figure 2.12.10-9	TN-40 0° Side Drop Test Rigging .....	2.12.10-27
Figure 2.12.10-10	TN-40 Acceleration Time History, 0° Side Drop .....	2.12.10-28
Figure 2.12.10-11	TN-40 Test Article After 0° Side Drop .....	2.12.10-29
Figure 2.12.10-12	TN-40 Test Article After 0° Side Drop, Upper End Details .....	2.12.10-30
Figure 2.12.10-13	TN-40 Test Article After 0° Side Drop, Lower End Details .....	2.12.10-31
Figure 2.12.10-14	TN-40 Impact Limiter Shell Damage After 0° Side Drop .....	2.12.10-32
Figure 2.12.10-15	TN-40 CG-Over-Corner Drop Test Rigging .....	2.12.10-33
Figure 2.12.10-16	TN-40 CG-Over-Corner Drop Acceleration Time History .....	2.12.10-34
Figure 2.12.10-17	TN-40 CG-Over-Corner Drop Impacted Surface Damage .....	2.12.10-35
Figure 2.12.10-18	TN-40 CG-Over-Corner Drop Impact Limiter Deformation .....	2.12.10-36
Figure 2.12.10-19	TN-40 20° Slap Down Test Rigging .....	2.12.10-37
Figure 2.12.10-20	TN-40 20° Slap Down Drop Acceleration Time History .....	2.12.10-38
Figure 2.12.10-21	TN-40 Test Article After 20° Slap Down Drop .....	2.12.10-39
Figure 2.12.10-22	TN-40 Impact Limiter (Slap Down End) After 20° Slap Down Drop .....	2.12.10-40
Figure 2.12.10-23	TN-40 90° End Drop Test Rigging .....	2.12.10-41
Figure 2.12.10-24	TN-40 Acceleration Time History, 90° End Drop .....	2.12.10-42
Figure 2.12.10-25	TN-40 Test Dummy and Chilled Impact Limiter After Initial 90° End Drop .....	2.12.10-43
Figure 2.12.10-26	TN-40 Test Dummy and Chilled Impact Limiter Post-Drop Detail .....	2.12.10-44
Figure 2.12.10-27	TN-40 Puncture Drop Test Rigging .....	2.12.10-45
Figure 2.12.10-28	TN-40 Test Article After Puncture Drop .....	2.12.10-46
Figure 2.12.10-29	TN-40 Puncture Pin Damage to Impact Limiter .....	2.12.10-47

## 2.12.10 TN-40 Package Impact Limiter Testing

This appendix was extracted from the TN-40 Transportation Packaging Safety Analysis Report (SAR) [1]. The impact limiter scale testing of the TN-40 cask is utilized for benchmarking the response of the similar TN-32B HBU demonstration cask, as described in Appendix 2.12.9.

### 2.12.10.1 Introduction

A series of dynamic tests have been performed on one-third scale models of the TN-40 transport package impact limiters. The tests were performed to evaluate the effects of the 30 foot free drop hypothetical accident defined in 10 CFR 71.73(c)(1) [2]. The test results are used to verify the analyses performed for the TN-40 transport package. The objectives of the TN-40 impact limiter test program are:

- Demonstrate that the inertia  $g$  values and forces calculated in Appendix 2.10.8, and are utilized in the analyses presented in Appendices 2.10.1 through 2.10.7 of Reference [1] are adequate,
- Demonstrate that the extent of crush depths is acceptable, i.e., limiters do not bottom out and the neutron shield or trunnions do not impact the target,
- Demonstrate the adequacy of the impact limiter enclosure,
- Demonstrate adequacy of the impact limiter attachment design,
- Evaluate the effects of low temperature (-20 °F) on the crush strength and dynamic performance of the impact limiters, and,
- Evaluate the effects (puncture depth and shell damage) of a 40-inch drop onto a scaled 6- inch diameter puncture bar on a previously crushed impact limiter, as per 10 CFR 71.73(c)(3).

### 2.12.10.2 Scaling Relationships

The scale models of the TN-40 cask and impact limiter are constructed with a geometric scale factor of  $1/\lambda = 1/3$ . As shown in Appendix B of Reference [3], the following scale factors apply.

Length:	$L_p = \lambda L_m$
Surface area:	$A_p = \lambda^2 A_m$
Moment of inertia:	$I_p = \lambda^4 I_m$
Section modulus:	$S_p = \lambda^3 S_m$
Weight:	$W_p = \lambda^3 W_m$
Energy absorbed during drop: (from same height $h$ )	$E_p = W_p h = \lambda^3 W_m h = \lambda^3 E_m$
Velocity at beginning of impact:	$V_p = (2gh)^{1/2} = V_m$

where:  $\lambda$  is the scale factor, the subscript  $p$  refers to the full size, and the subscript  $m$  refers to the model.

During impact, the impact limiter materials will deform or crush. Since the model and full size impact limiters are made of the same materials, they deform under the same stress,

$$S_p = S_m$$

Therefore we have the following relationships:

$$\begin{aligned} \text{Force during impact: } F_p &= S_p A_p = S_m \lambda^2 A_m = \lambda^2 F_m \\ \text{Deformation: } D_p &= E_p / F_p = \lambda^3 E_m / \lambda^2 F_m = \lambda D_m \\ \text{Impact duration: } T_p &= D_p / V_p = \lambda D_m / V_m = \lambda T_m \\ \text{Impact deceleration: } a_p &= V_p / T_p = V_m / \lambda T_m = 1/\lambda a_m \end{aligned}$$

### 2.12.10.3 Test Article Description

The test article for the dynamic tests consists of a solid carbon steel test body with an impact limiter on each end. The test article, shown in Figure 2.12.10-1, is constructed to be as close as possible to one-third of the full-size packaging.

The impact limiters are attached to each other by thirteen 0.5-inch diameter tie rods, tightened snug tight. Each limiter is also fastened to the test dummy with four 0.5-inch bolts.

The test article weighs approximately 10,100 lb<sub>m</sub> (the total weight of the full-size package is 271,460 lb<sub>m</sub>), and has maximum dimensions of approximately 87.0 inches long by 48.0 inches in diameter (the full size dimensions for the TN-40 cask are 260.87 inches long and 144.0 inches in diameter).

The test body and each impact limiter are equipped with lifting lugs to facilitate lifting during handling and testing.

### 2.12.10.4 Test Description

#### 2.12.10.4.1 Equipment and Instrumentation

The drop testing was performed at the National Technical Systems (NTS) facility located at Acton, Massachusetts. The drop testing was performed in accordance with approved written procedures.

Lifting and dropping the test article was accomplished using a mobile crane. A quick-release mechanism was used to initiate the drop. It consists of a hydraulic piston that loaded a bolt to failure releasing a shackle supporting the test article via a rigging system. The rigging system consists of nylon straps and padded shackles to minimize damage to the accelerometers installed on the test dummy.

An inclinometer was used to measure the initial angle ( $\pm 1^\circ$ ) of the test body longitudinal axis with respect to the drop pad (i.e., impact surface). A measured line, 30 feet long (+3.0, -0.0 inches), was attached to the lowest point on the test package to assure the proper drop height.

The impact surface was a 2-inch thick steel plate attached to a concrete block weighing approximately 250,000 lb<sub>m</sub> resting on bedrock. This configuration can be considered as an essentially unyielding surface.

A puncture bar made of cold-rolled steel was welded to the impact surface for the 40-inch (1-meter) puncture drop. The bar was scaled to match the test article resulting in a 2-inch diameter bar with the upper end edges rounded to a radius of approximately 0.083 inch.

Accelerometers were used to measure the impact *g* load for all drops performed. Twelve PicoCoulomb (PCB) Piezotronics 353B18 accelerometers were attached to aluminum blocks, which were bolted to the test body at 0°, 90°, 180°, and 270° orientations at three elevations: the approximate center of gravity location and adjacent to each impact limiter. The 12 accelerometer locations are shown in Figure 2.12.10-2.

PCB Model 353B18 quartz shear accelerometers were used to measure the test dummy response. These transducers have a measurement range of  $\pm 500g$ , with a nominal frequency range of 1 – 10,000 Hz ( $\pm 5\%$ ). The accelerometers were connected to a Spectral Dynamics, Inc. Puma System signal analyzer. The accelerometer responses were recorded digitally and processed after completion of the test.

The output signals were filtered using a 600 Hz low pass filter to remove the higher frequencies present in the data. The high frequencies represent vibrations of the test dummy due to small displacements (low stresses), which excite the accelerometers and tend to mask the low frequency rigid body acceleration. This low frequency acceleration is masked, because both low frequency rigid body and high frequency natural vibration accelerations are superimposed and the net acceleration is recorded. Filtering the data is necessary to remove these high frequency accelerations.

#### 2.12.10.4.2 Drop Test Orientations

##### A. Pre-Test Orientations

The four, 1/3-scale impact limiters that were utilized for the test are identified as 1, 2, 3, and 4. The drop test orientations were performed in the following sequence.

**Drop Test Original Sequence**

Test Number	Drop Orientation	Drop Height	Impact Limiter Number	Impact Sequence	Comments
1	0° Side Drop	30 feet	1	-	Limiters 1 and 2 were installed
			2	-	
2	64° CG-Over-Corner Drop	30 feet	1	1 <sup>st</sup>	The test article was rotated 180° so the undamaged portion of the impact limiters contacts the impact surface.
			2	2 <sup>nd</sup>	
3	20° Slap Down	30 feet	3	1 <sup>st</sup>	Limiters 1 and 2 were removed and replaced with limiters 3 and 4 before the drop.
			4	2 <sup>nd</sup>	
4	90° End Drop	30 feet	3	1 <sup>st</sup>	Limiter 3 was removed and chilled at -20 °F for 24 hours before reinstallation on the test dummy.
			4	None	
5	90° End Drop (Puncture Test)	40 inches	3	1 <sup>st</sup>	Drop onto 2 inch diameter puncture bar.
			4	None	

The 0° side drop was performed to obtain the highest transverse acceleration and to demonstrate that no portion of the test dummy (including trunnions) impacted the surface of the pad.

The 64° CG-over-corner drop was performed to predict the maximum crush distance from the corner of the impact limiter and to demonstrate the corners of the test dummy were protected by the impact limiter.

The 20° slap down drop was performed to demonstrate that the impact limiters stay attached to the test dummy because the second impact (slap down) puts the highest load on the impact limiter attachments, and impact limiter stainless steel shell.

The 90° end drop orientation was performed to obtain the highest axial deceleration. For the 90° end drop, the bottom impact limiter (3) was chilled at -20 °F for at least 24 hours in order to acquire the most conservative estimate of the axial *g* load.

A 40-inch puncture drop onto a 1/3-scale 6-inch diameter bar (i.e., 2-inch) was performed in accordance with 10 CFR 71.73(c)(3) in order to evaluate the effects of this drop on the TN-40 transport package. The test article was dropped in the 90° end drop orientation onto the puncture bar subsequent to the 30 foot end drop. The test article was positioned so that it impacted the puncture bar close to its axial centerline and thus near the center of gravity. This orientation was chosen because it assures that the puncture impact absorbs nearly 100% of the drop energy. Also, the center of the impact limiter outer plate, where the puncture impact occurs, is the weakest portion of the impact limiter since there are no gussets in this location.



## B. Modified Drop Tests

After the initial drop test (0° side drop), the accelerometer data was determined to be unusable because of an auto-scaling feature of the data acquisition system that did not perform as expected. After NTS reset the system for manual scaling, the second planned drop was conducted. This was the 64° CG-over-corner drop using the same pair of impact limiters. After the CG-over-corner drop test a second 0° side drop test was performed. The same pair of impact limiters was used. The test package was rotated 90° so that the undamaged portion of the impact limiter would contact the impact surface, thus providing undamaged crush material. The accelerometers were left in their original locations, but since they were equally spaced at four locations around the test body, the desired impact accelerations could still be obtained after reorienting the accelerometers to be perpendicular with the impact surface.

After the 90° end drop examination of the test data revealed results that were inexplicable. Several data channels showed accelerations that were opposite sign from the expected values and had significant differences in magnitude. In order to salvage useful data from the existing test hardware, a second end drop was performed at a later date using the least damaged test limiter for the impacted end drop limiter. The limiter was not chilled; however, since the environmental control of the wood had been compromised due to previous test damage.

The original sequence of the tests shown in Section A, above, was modified to list all the drop tests that were performed:

**Modified Drop Test Sequence**

Test Number	Drop Orientation	Drop Height	Impact Limiter Number	Impact Sequence	Comments
1	0° Side Drop	30 feet	1	-	Limiters 1 and 2 installed.
			2	-	
2	64° CG-Over-Corner drop	30 feet	1	1st	The 1 and 2 impact limiters were rotated 180° so that the undamaged portion of the impact limiters face the pad.
			2	2nd	
3	0° Side Drop (2nd test)	30 feet	1	-	The test body and limiters were rotated 90° so that an undamaged portion of the impact limiters faced the pad.
			2	-	
4	20° Slap Down	30 feet	3	1st	Limiters 1 and 2 were removed and replaced with limiters 3 and 4.
			4	2nd	
5	90° End Drop	30 feet	3	1st	Limiter 3 was removed and chilled at -20 °F for 48 hours before being re-installed on the test body.
			4	-	
6	90° End Drop (Puncture Test)	40 inches	3	1st	Drop onto 2-inch diameter puncture bar.
			4	-	
7	90° End Drop (2nd test)	30 feet	2	1st	Limiters 2 and 4 were used. The center portion of limiter 2 was relatively undamaged by previous drops and thus provided a useable crush volume.
			4	-	

The test setup for the 0° side drop is shown in Figure 2.12.10-3. For the side drop test, the accelerometers were oriented to measure accelerations in the drop direction (perpendicular to the drop pad surface).

The test setup for the 64° CG-over-corner drop is shown in Figure 2.12.10-4. The accelerometers located along the center of gravity and near the top and bottom impact limiter (first impact) were oriented to measure accelerations 64° from the axis of the test model (perpendicular to the drop pad surface when the test model is oriented at a 64° angle). The other accelerometers were oriented to measure accelerations parallel to the test model axis.

The same pair of impact limiters was rotated 90° so the undamaged portion of the limiter would be face down for the second side drop (test number 3). The accelerometers were re-oriented to measure accelerations in the drop direction (perpendicular to the impact surface). The test setup is the same as shown in Figure 2.12.10-3 except for the 90° rotation of the test article.

The test setup for the 20° slap down drop is shown in Figure 2.12.10-5. The accelerometers located along the side of the test dummy were oriented to measure accelerations 70° from the axis of the test model (perpendicular to the drop pad surface when the test model is oriented at a 20° angle). The accelerometers along the top and bottom of the test dummy were oriented to measure accelerations perpendicular to the test model axis (perpendicular to the drop pad surface during slap down when the test modal axis is parallel to the impact surface).

The test setup for the 90° end drop is shown in Figure 2.12.10-6. The package was oriented with the test dummy bottom facing down so that the impact occurred on the bottom end of the package. For the end drop test, the accelerometers were oriented to measure accelerations in the drop (axial) direction. The bottom impact limiter (3) was kept in a temperature chamber held at a temperature of -20 °F for more than 24 hours immediately prior to the test. The time between removal of the impact limiter from the conditioning chamber and the drop was approximately 2 hours.

Examination of the test data from the first 90° end drop revealed results that were inexplicable. Several data channels showed accelerations that were opposite sign from the expected values and had significant differences in magnitude. In order to extract useful data from the existing test hardware, a second 90° end drop test (test Number 7) was performed at a later date using the least-damaged test impact limiter for the impacted end drop. The limiter was not chilled -20 °F; however, since the environmental control of the wood had been compromised due to previous test damage.

Impact limiters 2 and 4 were reused for the second 90° end drop test (test number 7). The location and orientations of the accelerometers were same as for the first 90° end drop test. The purpose of this test was to predict the g load at the room temperature. The test setup was the same as for the first end drop and is shown in Figure 2.12.10-6.

The test setup for the 90° puncture drop is shown in Figure 2.12.10-7. During the puncture drop the package was oriented so that the puncture bar impacted on the bottom end of the package. A 2-inch diameter solid cylindrical puncture bar, 18 inches long was utilized. The puncture bar was constructed from mild steel and was welded to the drop pad with its long axis oriented in the vertical direction. Accelerometer data was not taken during the puncture drop test.

A photograph of the accelerometer locations for each channel is shown in Figure 2.12.10-8. Accelerometers 1 through 4 are on the front (left end of test dummy), 5 through 8 are in the middle, and 9 through 12 are on the right end of the test dummy. Note that accelerometers 4, 8 and 12 are not visible in Figure 2.12.10-8.

#### 2.12.10.5 Data Measurement

The following data was measured and recorded before, during, and after each drop test.

1. Prior to each drop test
  - a) Torque of the impact limiter bolts.
  - b) Impact limiter dimensions.

- c) Height from test article to drop pad.
  - d) Angular orientation of the test article to the impact surface.
  - e) Atmospheric condition data, i.e., ambient temperature, wind speed, immediately and prior to the release of the test article.
- 2. During each drop test
  - a) Test article behavior on videotape.
  - b) Date and time of test.
  - c) Observations of damage or unexpected behavior of the test article
  - d) Impact acceleration time histories (excluding the puncture drop test).
- 3. Following each drop test
  - a) Observations of the damage to the test article on features other than the limiters, i.e., attachment bolts.
  - b) Measurements of deformation to each impact limiter to fully describe the extent of the damage. These measurements include:
    - i. Depth of internal and external crush of the impact limiter.
    - ii. Overall thickness of each impact limiter after each test.
    - iii. Dimensions of impact footprint.

#### 2.12.10.6 Test Data and Results

For purposes of reviewing test results, it should be noted that the energy to be absorbed by the scale model is approximately 1/27 of the full-scale TN-40 package energy. The acceleration of the model is approximately three times that of the full-size cask, and the crush deformation of the model limiter is approximately one-third that of the full-size limiter. The impact force applied to the model is determined by multiplying the mass by the rigid body acceleration ( $F = ma$ ). The model force is 1/9 of the full-scale force.

##### 2.12.10.6.1 0° Side Drop Test

The first drop test performed was the 0° side drop. Impact limiters 1 and 2 were installed on the test dummy. Two lifting straps were used to connect the test article to a padded shackle that attached the test article to the release mechanism. Figure 2.12.10-9 is a photograph of the test configuration prior to the 0° drop.

#### Accelerometer Data

As described in the previous section, the acceleration time history data for the first 0° side drop test was lost due to a problem with the self-scaling routine of the data acquisition software. After resolving the scaling problems, a second 0° side drop was performed. The acceleration time histories from channels 2, 6, and 10 were selected as providing the highest accelerations along the length of the test dummy. The plots generally show a single rounded peak roughly 0.02 seconds long, with a high frequency low amplitude signal superimposed on top of it.

The following table shows the maximum transverse accelerations measured by the accelerometers during the second 0° side drop (converted to full scale), as well as the maximum acceleration predicted by ADOC as described in Appendix 2.10.8 of Reference [1].

Accelerometer Location	Measured Transverse Acceleration (gs) (converted to full scale)	Average Measured Transverse Acceleration (gs)	Predicted Maximum Transverse Acceleration (gs)
Top (2)	68	57	51
Center of Gravity (6)	50		
Bottom (10)	55		

The accelerations measured during the side drop are higher than predicted by the ADOC computer program. The acceleration results presented in the above table are taken from the measured acceleration data filtered with a 600 Hz low pass filter. Figure 2.12.10-10 shows the filtered acceleration time history from accelerometer 6, which is characteristic of the acceleration plots in general. Note that the acceleration plotted in Figure 2.12.10-10 is for the 1/3-scale package, and thus is equivalent to three times the full-scale accelerations.

#### Crush Depth Measurements

After the first 0° side drop test, crush depths of the impact limiters were measured. Even though acceleration data from the first test was not useable, the crush values are valid. There was evidence of both inside and outside crushing. The following table summarizes the measured and predicted crush depths for the bottom impact limiter. A spring back of 0.50 inch is assumed (based on previous crush tests). See Appendix 2.10.4 of Reference [3].

	Impact Limiter Number 1	Impact Limiter Number 2
Maximum Inside Crush Depth (in.)	1.44	1.50
Maximum Outside Crush Depth (in.)	0.75	0.75
Spring Back (in.)	0.50	0.50
Total Crush Depth (in.)	2.69	2.75
Predicted Crush Depth × 1/3 (in.) (From ADOC)	4.52	

From the above table it can be seen that the measured crush depths are slightly less than those predicted by the ADOC computer program. Note that the actual scale test measurements are used for all deflection evaluations, with the ADOC results scaled to the 1/3 scale test.

It should also be noted that neither the neutron shield nor the trunnions would contact the impact surface during the impact. The distance between the outer diameter of the neutron shield and the outside diameter of the impact limiter is 7.16 in. Therefore, a clearance of  $7.16 - 2.75 = 4.41$  inches would remain between the impact surface and the neutron shield, based on the measured crush depth. Similarly, a distance of 3.84 inches would remain between a trunnion and the impact surface.

### Damage Assessment

Both impact limiters remained attached to the test dummy during and after the side drop impact. All of the tie rods and tie rod brackets remained intact, thus preventing separation of the impact limiters from the test dummy. In addition, the impact limiter attachment bolts remained in place, in spite of damage to two of the eight bolting brackets.

Only a single small opening in the stainless steel shell of each of the impact limiters was evident. Both openings consisted of a tear along the weld between two of the outer flat plates of the impact limiter. The tears were roughly 4 inches long. Despite these tears, all impact limiter wood remained completely confined within the shell.

Figure 2.12.10-11 through Figure 2.12.10-14 are photographs of the test article after the 0° side drop.

#### 2.12.10.6.2 64° CG-over-Corner Test

The second drop test performed was the 64° CG-over-corner test. Impact limiters 1 and 2 were again used. The test article was rotated about its longitudinal axis 180° so that an undamaged portion of the limiter was exposed to the impact surface. The rigging for this test is shown in Figure 2.12.10-15.

### Accelerometer Data

Accelerometer results from accelerometers 9, 10, 11, and 12 at the upper end of the test dummy were used to evaluate this drop orientation. These represented the four highest accelerations. The output from accelerometer 10 is shown in Figure 2.12.10-16. Accelerometers 9 and 11 were oriented parallel with the test dummy axis while accelerometers 10 and 12 were adjusted so that their axes were parallel with the drop (i.e., perpendicular to the test pad surface). The average acceleration of the four accelerometers in the direction of the test dummy axis is 34gs. This includes correcting the values of accelerometers 10 and 12 to account for their orientation. The predicted acceleration is taken from ADOC results given in Appendix 2.10.8 [1]. Note that the predicted acceleration value is slightly less than the measured value.

#### Measured Versus Predicted Accelerations

Accelerometer Location (see Figure 2.12.10-2)		Measured Acceleration (gs) (converted to full scale)	Average Measured Acceleration (gs)	Predicted Maximum Acceleration (gs)
Axial Acceleration (1 <sup>st</sup> Impact)	9	28	34	32
	10	37		
	11	39		
	12	33		

### Crush Depth Measurements

The crush depths of the impact limiters were measured after the CG-over-corner drop. The following table summarizes the measured and predicted crush depths for the bottom impact limiter. A spring back of 0.50 inch is assumed (based on previous crush tests). See Appendix 2.10.4 of Reference [3].

	Impact Limiter Number 1
Maximum Inside Crush Depth (in.)	0.0
Maximum Outside Crush Depth (in.)	8.0
Spring Back	0.5
Total Crush Depth (in.)	8.5
Predicted Crush Depth $\times 1/3$ (in.) (from ADOC)	10.3

The above table shows that the measured crush depths are slightly less than those predicted by the ADOC computer program.

### Damage Assessment

The primary purpose of the CG-over-corner drop test is to demonstrate that the impact limiter has sufficient material to protect the corner of the test dummy in this orientation and to demonstrate the adequacy of the impact limiter attachment design.

Both impact limiters remained attached to the test dummy during and after the CG-over-corner drop impact. All of the tie-rods, and all but one of the tie-rod brackets remained intact, thus preventing separation of the impact limiters from the test dummy. In addition, the impact limiter attachment bolts and brackets, although damaged, prevented the test dummy from separating from either impact limiter.

Several tears along welds on the impacted surface were noted. However, all of the shell plates remained in place and therefore would prevent significant loss of wood during a post-drop fire accident. The tears varied between 2 and 8 inches long. Despite these tears, all impact limiter wood remained completely confined within the shell.

Figure 2.12.10-17 and Figure 2.12.10-18 are photographs of the test article after the CG-over-corner drop.

#### 2.12.10.6.3 20° Slap Down Test

The 20° slap down drop test was performed using newly installed impact limiters 3 and 4. The test article was oriented as shown in Figure 2.12.10-5. A two-point strap rigging system was used to lift the test model by two lifting lugs. The two legs of the rigging system join at a single point that was shackled to the quick-release mechanism. Figure 2.12.10-19 is a photograph of the test package rigging just prior to the 20° slap down drop.

### Accelerometer Data

The slap down event consists of two distinct impacts. The initial impact is the smaller of the two as it only stops the leading end of the test article and converts much of its kinetic energy from linear to rotational. The second impact is more severe because the velocity of the second impact limiter is greater than that resulting from a 30 foot drop due to the added rotational velocity. The impact limiter attachment design is also exposed to unique loads due to the centrifugal forces caused by the test dummy rotation after the first impact.

The following table shows the maximum acceleration as measured by accelerometer 9 during the 20° slap down (converted to full scale), as well as the acceleration predicted by ADOC.

#### **Measured Versus Predicted Accelerations during Second Impact**

<b>Accelerometer Location (see Figure 2.12.10-2)</b>		<b>Measured Acceleration (gs)</b>	<b>Predicted Maximum Acceleration (gs)</b>
Top (2 <sup>nd</sup> Impact)	9	61 (Transverse + Rotational)	78 (Transverse + Rotational)

The accelerations measured during the slap down drop test are low relative to the maximum predicted by the ADOC computer program. The acceleration results presented in the above table are taken from the measured acceleration data filtered with a 600 Hz. low pass filter. Figure 2.12.10-20 shows the filtered acceleration time history from accelerometer 9, which experienced the highest acceleration of all locations. The plot of the accelerometer 9 located near impact limiter 4 (second impact, highest acceleration) shows a single peak roughly 0.009 second long with a magnitude of approximately 182 g. The initial impact causes a much smaller peak approximately 0.035 second prior to the second impact. Note that the acceleration shown in Figure 2.12.10-20 is for the 1/3-scale package, which is equivalent to three times the full scale acceleration.

### Crush Depth Measurements

After the slap down test, the impact limiter crush depths were measured. There was evidence of both inside and outside crushing. The following table summarizes the measured and predicted crush depths for the top and bottom impact limiters. A spring back of 0.50 inches is assumed (based on previous crush tests). See Appendix 2.10.4 of Reference [3].

	<b>Impact Limiter 3 (Bottom)</b>
<b>Maximum Inside Crush Depth (in.)</b>	3.06
<b>Maximum Outside Crush Depth (in.)</b>	1.13
<b>Spring Back (in.)</b>	0.50
<b>Total Crush Depth (in.)</b>	4.69
<b>Predicted Crush Depth × 1/3 (in.)</b>	5.17

The above table shows that the measured crush depth is less than that predicted by the ADOC computer program.



It should also be noted that neither the neutron shield nor the trunnions would contact the target during the impact. Since the crush pattern on the top and bottom impact limiters occur at a 20° angle, and only at the outer edge, there is no possibility of the neutron shield impacting the target during the slap down impact.

#### Damage Assessment

Both impact limiters remained attached to the test dummy during and after the slap down impact.

Considerable crushing from the inside occurred, resulting in significant failure of welds between the impact limiter inner cylinder to the inner base plate. However, since the test dummy remained attached to the limiters, no exposure of the wood to the post-drop fire accident would occur.

Small tears in the impact limiter external shell welds were evident in the impacted area. However, these openings were small and impact limiter wood remained completely confined within the shell.

Figure 2.12.10-21 and Figure 2.12.10-22 are photographs of the test dummy and impact limiters after the 20° slap down drop.

#### 2.12.10.6.4 90° End Drop Test

The fourth orientation tested was the 90° end drop. Impact limiters 3 and 4 were reused for this test, with impact limiter 3 used for impacting the impact surface. The test article orientation is shown in Figure 2.12.10-6. Two straps were attached to the test article's top two lifting lugs and to the quick-release mechanism with padded shackles. Figure 2.12.10-23 is a photograph of the test package set up just before the 90° end drop test. To provide an extreme condition drop test, impact limiter 3 was chilled to -20 °F prior to the drop.

#### Accelerometer Data

The first end drop test results were deemed unacceptable after examination of the accelerometer results. Several of the accelerometer traces showed a sign reversal that could not reflect any physical response of the test dummy. Consequently, the test was redone at a later date using impact limiters 2 and 4 that had been dropped previously. Impact limiter 2 was used for the impacting limiter because the wood in the end drop crush area was relatively undamaged due to the orientation of the prior drops. However, the second end drop was not done at a chilled temperature. The acceleration time history plots for the second 90° end drop test appeared qualitatively reasonable. The plots generally show a single rounded peak duration of 0.0165 second, with a high frequency low amplitude signal superimposed on top of it. The measured 1/3-scale impact duration of 0.0165 second corresponds to 0.0495 second for the full-size package.

The following table shows the axial acceleration measured by the accelerometers shown, during the 90° end drop, as well as the maximum axial acceleration predicted by ADOC.

<b>Accelerometer Location (see Figure 2.12.10-2)</b>	<b>Measured Axial Acceleration (gs)</b>	<b>Average Axial Acceleration (gs)</b>	<b>ADOC Maximum Predicted Axial Acceleration (gs)</b>
Upper Elevation Avg.	52	57	49
CG Elevation Avg.	58		
Bottom Elevation Avg.	60		

The acceleration results presented in the above table are taken from the measured acceleration data filtered with a 600 Hz low pass filter. Figure 2.12.10-24 shows the filtered acceleration time history from accelerometer 7. Note that the acceleration plotted in Figure 2.12.10-24 is for the 1/3-scale package, which is equivalent to three times the full scale acceleration.

#### Crush Depth Measurements

After the initial end drop test, the crush depths of the bottom impact limiter were measured. There was evidence of both inside and outside crushing. The following table summarizes the measured and predicted crush depths for the bottom impact limiter (impact limiter 3). Note that these results are for the chilled limiter used in the initial end drop. A springback of 0.50 inch is assumed based on Appendix 2.10.4 of Reference [4].

	<b>Impact Limiter 3</b>
<b>Maximum Inside Crush Depth (in.)</b>	2.0
<b>Maximum Outside Crush Depth (in.)</b>	0.50
<b>Spring Back (in.)</b>	0.50
<b>Total Maximum Crush Depth (in.)</b>	3.00
<b>Predicted Total Max Crush Depth <math>\times</math> 1/3 (in.)</b>	3.41

The relatively low crush depth measured after the initial 90° end drop, compared with predicted values can be attributed to the fact that the bottom impact limiter was chilled to -20 °F prior to the drop test.

#### Damage Assessment

Both impact limiters remained attached to the test dummy during and after the first end drop impact, and all impact limiter attachment bolts remained intact.

No openings in the stainless steel impact limiter external shell were evident, and no welds in the external shell failed. Due to the considerable inside deformation, however, the inner disk that contacts the end of the test dummy completely separated from the inner cylindrical shell that encloses the end of the test dummy cylinder. The impact limiter wood remained completely confined within the shell.

Figure 2.12.10-25 and 2.12.10-26 are photographs of the test dummy and impact limiter 3 after the first 90° end drop.

#### 2.12.10.6.5 Puncture Drop Test

The final drop test performed was the puncture drop. In order to simulate the proper sequence of accident events specified in 10 CFR 71.73, the impact limiters used for the first end drop test remained on the test dummy without adjustment or tightening of the attachment bolts. Two straps, attached to the top two lifting lugs, were used to support the test model in the same 90° vertical orientation as for the prior end drop. The puncture bar impacted impact limiter 3, which was previously crushed during the 90° end drop. No accelerometer data is provided, since the purpose of the puncture drop is to obtain impact limiter damage data only. Figure 2.12.10-7 depicts the test setup up for the 90° puncture drop test and Figure 2.12.10-27 is a photograph of the test article rigging just prior to the drop.

##### Test Results

The puncture bar impacted the test package near the center of the outer flat surface of the impact limiter shell. The puncture bar cleanly punched through the outer shell of the impact limiter and was imbedded in the impact limiter wood. The test package came to rest in the vertical position, balanced on top of the puncture bar and then tilted to one side, bending the bar.

The puncture bar sheared a circular section, roughly 2 inches in diameter, of the outer shell of the impact limiter. No other sections of the impact limiter were damaged, and no welds on the impact limiter shell were broken. The impact limiter wood remained completely contained by the impact limiter shell, and no impact limiter wood could be seen at the puncture point.

The puncture bar penetration was stopped by a thin wedge of impact limiter wood that was compacted between the top of the puncture bar and the inner shell of the impact limiter. The puncture bar did not penetrate the inner stainless steel shell of the impact limiter.

Both impact limiters remained attached to the test dummy during the puncture drop event, and no additional impact limiter attachment bolts were damaged.

Figure 2.12.10-28 and Figure 2.12.10-29 are photographs of the test article after the puncture drop.

#### 2.12.10.7 Conclusions

Table 2.12.10-1 summarizes the inertial loads measured during the dynamic testing program. Section 2.7.1 of Chapter 2 [1] goes through detail descriptions to establish the baseline g-loads to be utilized for the cask body, basket, and fuel rod structural evaluations.

The results of the dynamic tests show that:

- The crush depths do not result in lockup of the wood in the limiters.
- The crush depths for all the drop cases demonstrate that the neutron shield or trunnions would not impact the target.

- The impact limiter enclosure is structurally adequate in that it successfully confines the wood inside the steel shell.
- The impact limiter attachment design is structurally adequate in that the impact limiters remain on the ends of the test dummy during and after all drop orientations.
- A 40-inch drop onto a scaled 6-inch diameter puncture bar, per 10 CFR 71.73(c)(3), does not significantly damage the impact limiter nor are there any indications of damage to the test dummy. The impact limiters remained firmly secured to the test dummy, and the impact limiter wood was confined.

#### 2.12.10.8 References

1. Transnuclear, Inc., TN-40 Transportation Packaging, Safety Analysis Report, Revision 16 (CoC 9313, Docket No. 71-9313), June 2011.
2. Title 10, Code of Federal Regulations - Energy, Part 71 (10 CFR 71), "Packaging and Transportation of Radioactive Material," 1-1-2021 Edition, U.S. Nuclear Regulatory Commission, Washington, D.C.
3. Mok, Gerald C., et al., "Guidelines for Conducting Impact Tests on Shipping Packages for Radioactive Material," UCRL-ID-121673, September, 1995.
4. Transnuclear, Inc., TN-BRP Spent Fuel Package Safety Analysis Report for Transport, Revision 10, October, 2001, U.S. NRC Docket 71-9202.

**Table 2.12.10-1  
Summary of the Test Results**

<b>30 Foot Drop Orientation</b>	<b>g Load Measured by Testing</b>
90° End Drop	54 g Axial <sup>(1)</sup>
0° Side Drop	51 g Transverse <sup>(1)</sup>
CG-Over-Corner Drop	34 g Axial
20° Slapdown (Second Impact)	58 g <sup>(1)(2)</sup> , 62 g <sup>(1)(3)</sup>

Notes:

1. The g-loads reported in the tables contained in Section 2.12.10.6 are based on the peak value of the raw data recorded from the test results. For design purposes, the region around the peak response has been smoothed to remove the scatter of the test data and provide a representative maximum acceleration. The resulting maximum acceleration values are reported in this table.
2. The g load measured at this location represents the maximum combined transverse and rotational g-load for the basket structural analysis due to the slap down drop case.
3. The maximum combined g-load at the top end of the cask body (at the outer surface of the cask lid).
4. In order to bound the impact values presented here, the maximum density and minimum moisture content of the full-size impact limiter redwood will be bounded by the values measured for the test articles. The test article average redwood density and moisture content were 23.0 lb<sub>m</sub>/ft<sup>3</sup> and 9.8%, respectively. The specified ranges specified on SAR Drawing 10421-71-41 [1] were changed to 18.7 – 23.0 lb<sub>m</sub>/ft<sup>3</sup> and 9.8 – 15% for the redwood density and moisture content, respectively. Balsa values remained unchanged because the balsa wood has little effect on the impact levels.

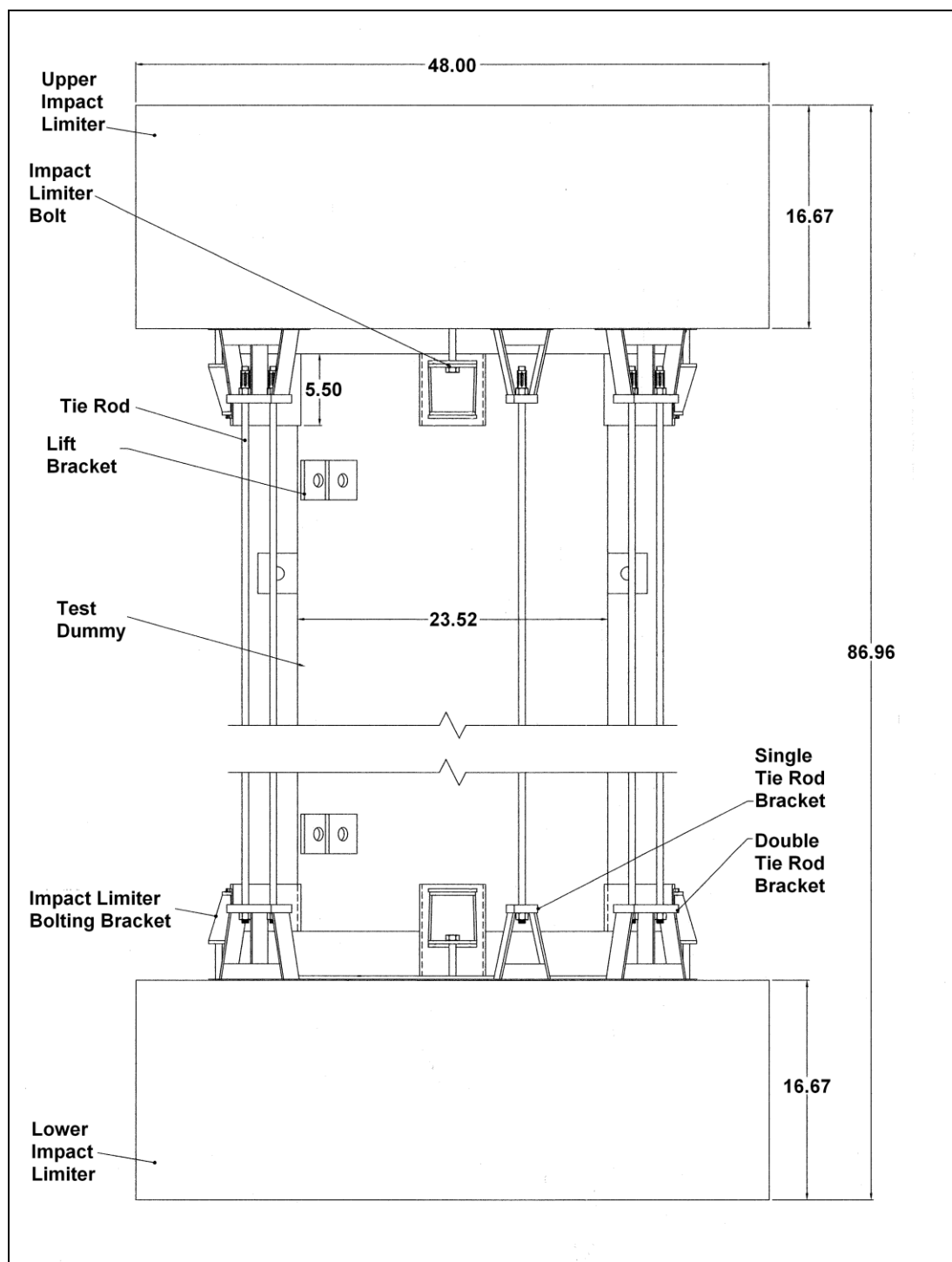


**Figure 2.12.10-1**  
**TN-40 One-Third Scale Test Article**

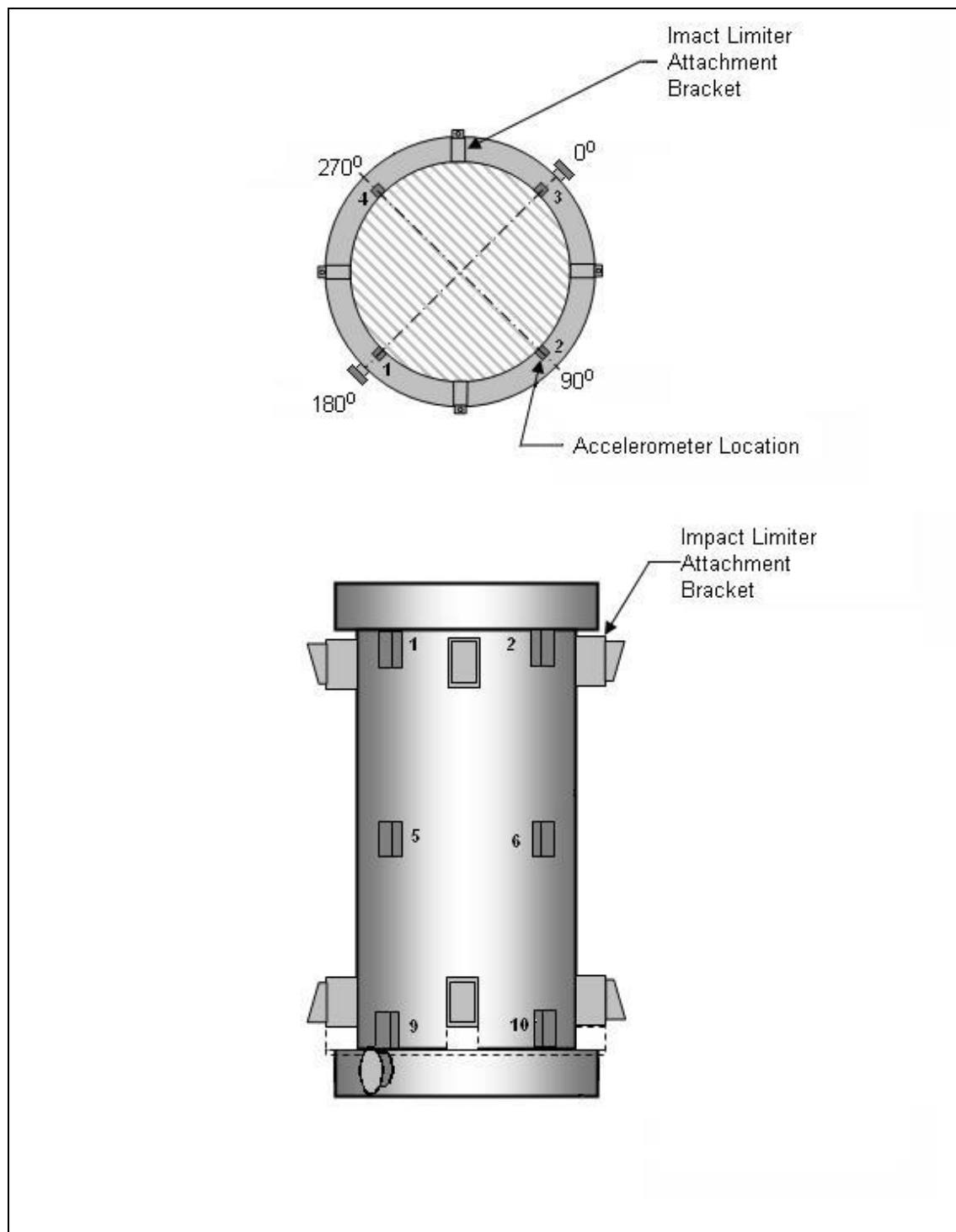


**Figure 2.12.10-2**  
**TN-40 Accelerometer Locations**



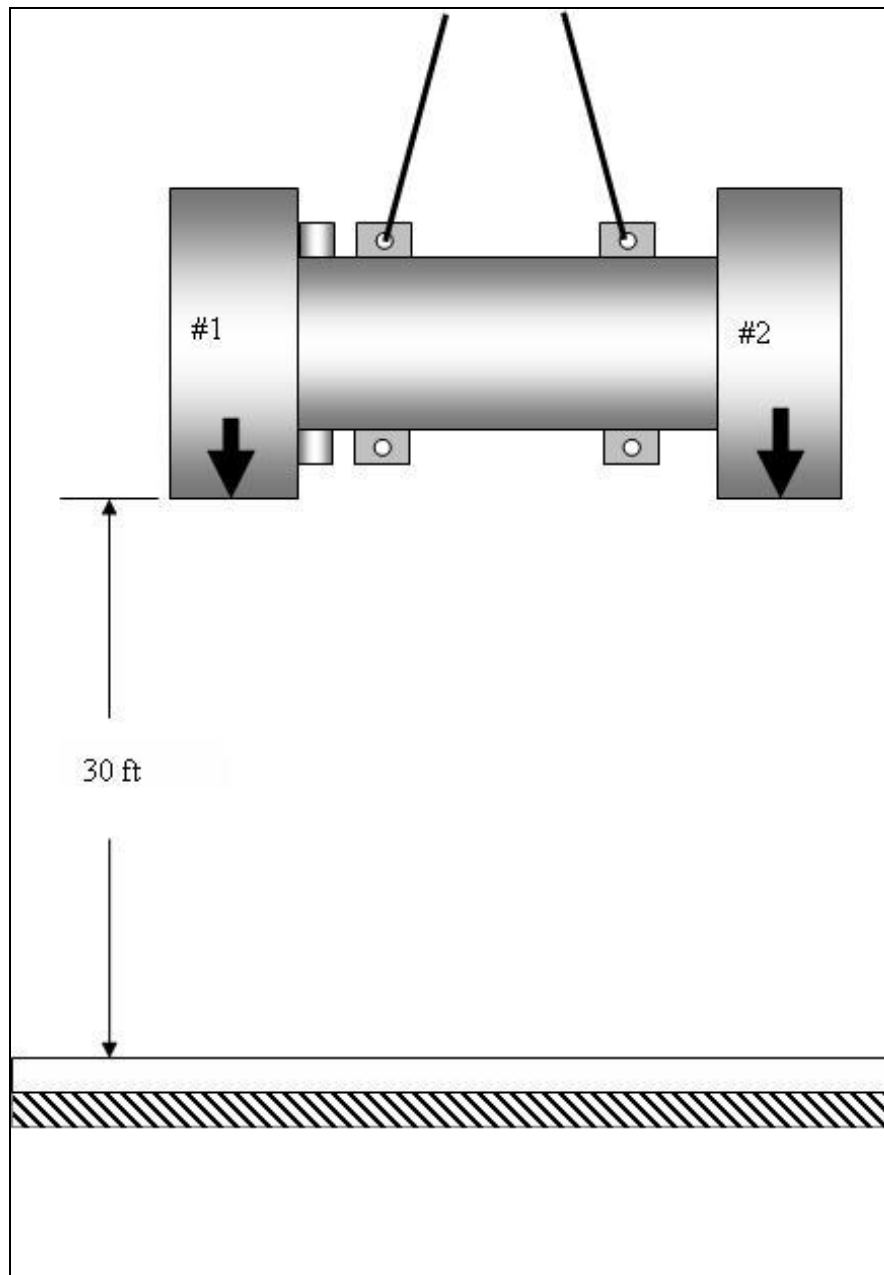


**Figure 2.12.10-3**  
**0° TN-40 Side Drop Test Setup**

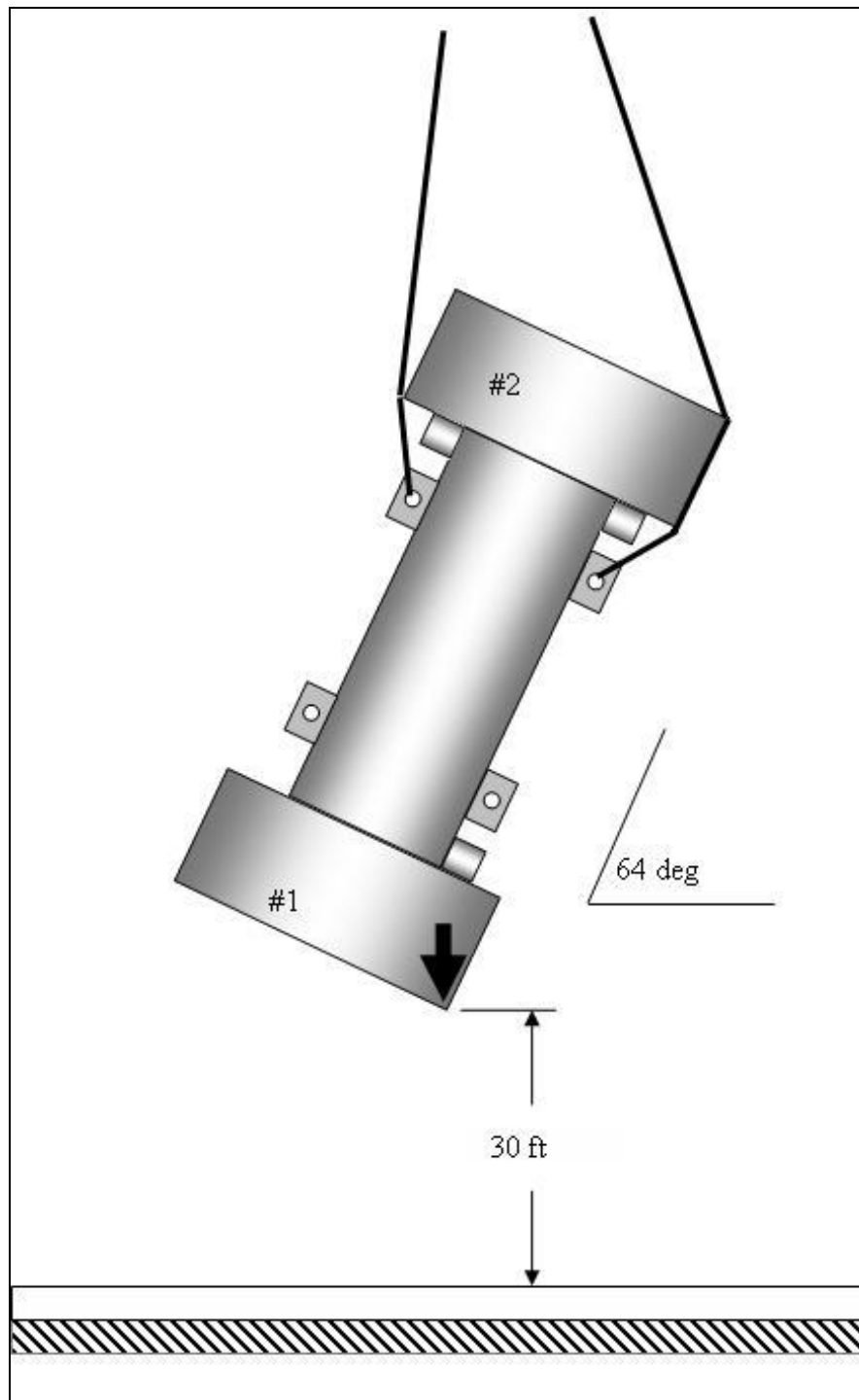


**Figure 2.12.10-4**  
**TN-40 CG-Over-Corner Drop Test Setup**

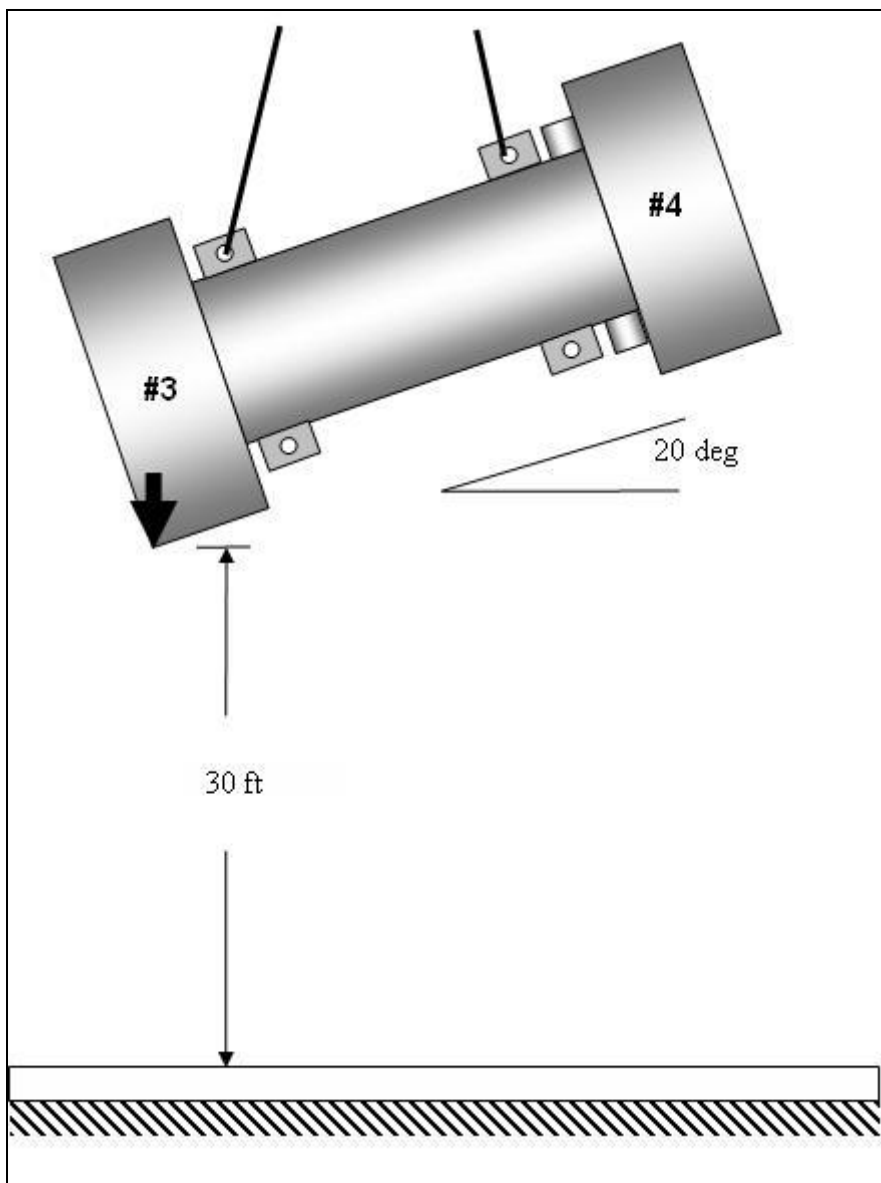


**Figure 2.12.10-5**  
**TN-40 20° Slap Down Test Setup**

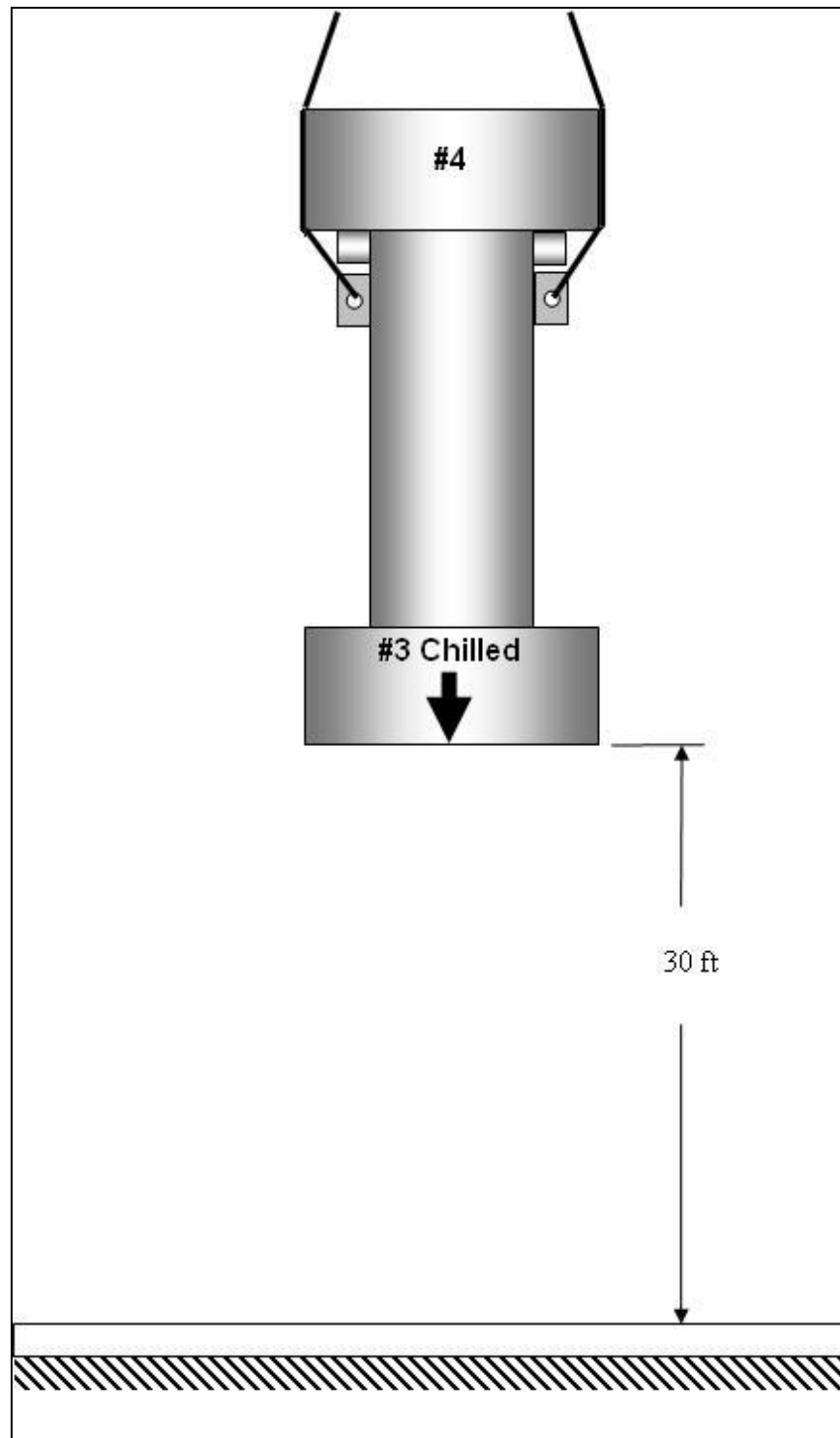


**Figure 2.12.10-6**  
**TN-40 90° End Drop Test Setup**

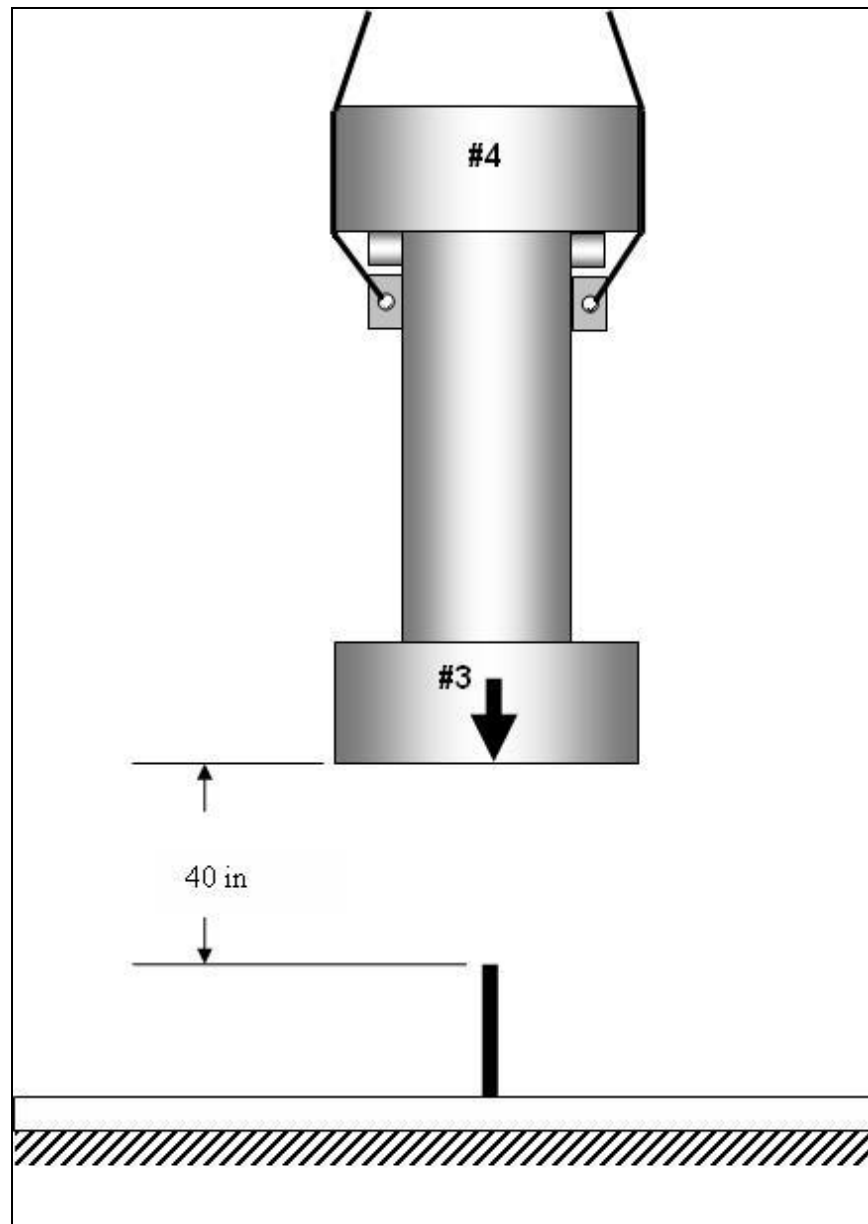


**Figure 2.12.10-7**  
**TN-40 Puncture Drop Test Setup**

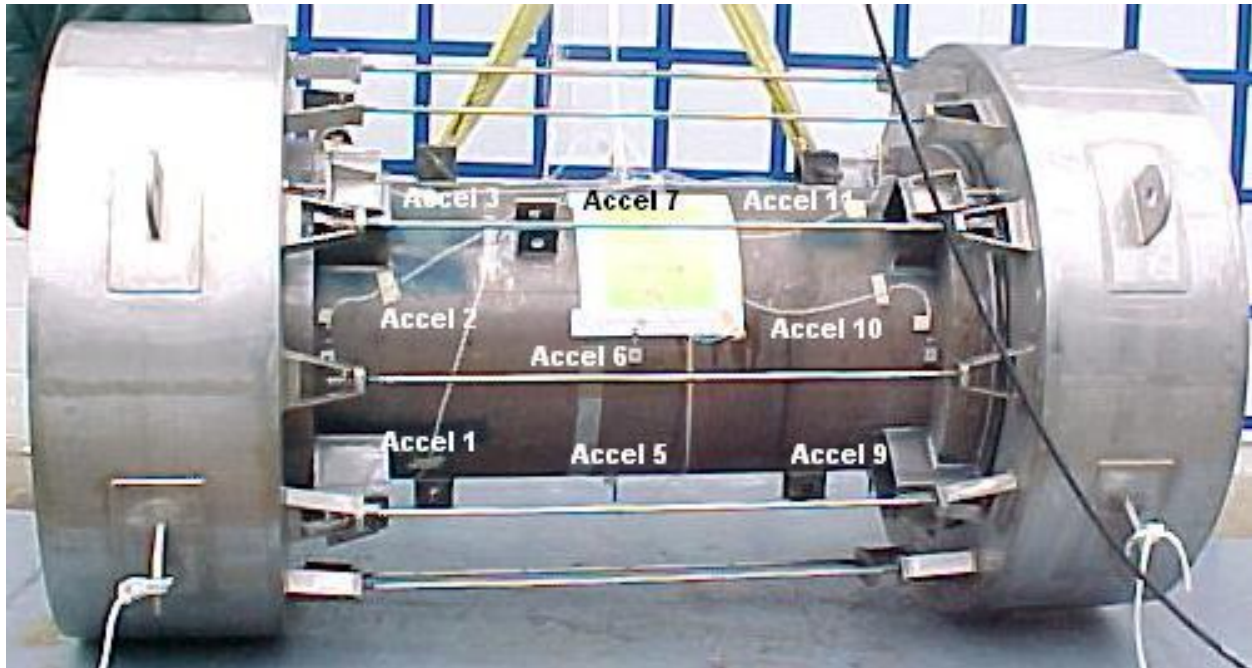


**Figure 2.12.10-8**  
**TN-40 Test Article and Accelerometer Locations**



**Figure 2.12.10-9**  
**TN-40 0° Side Drop Test Rigging**

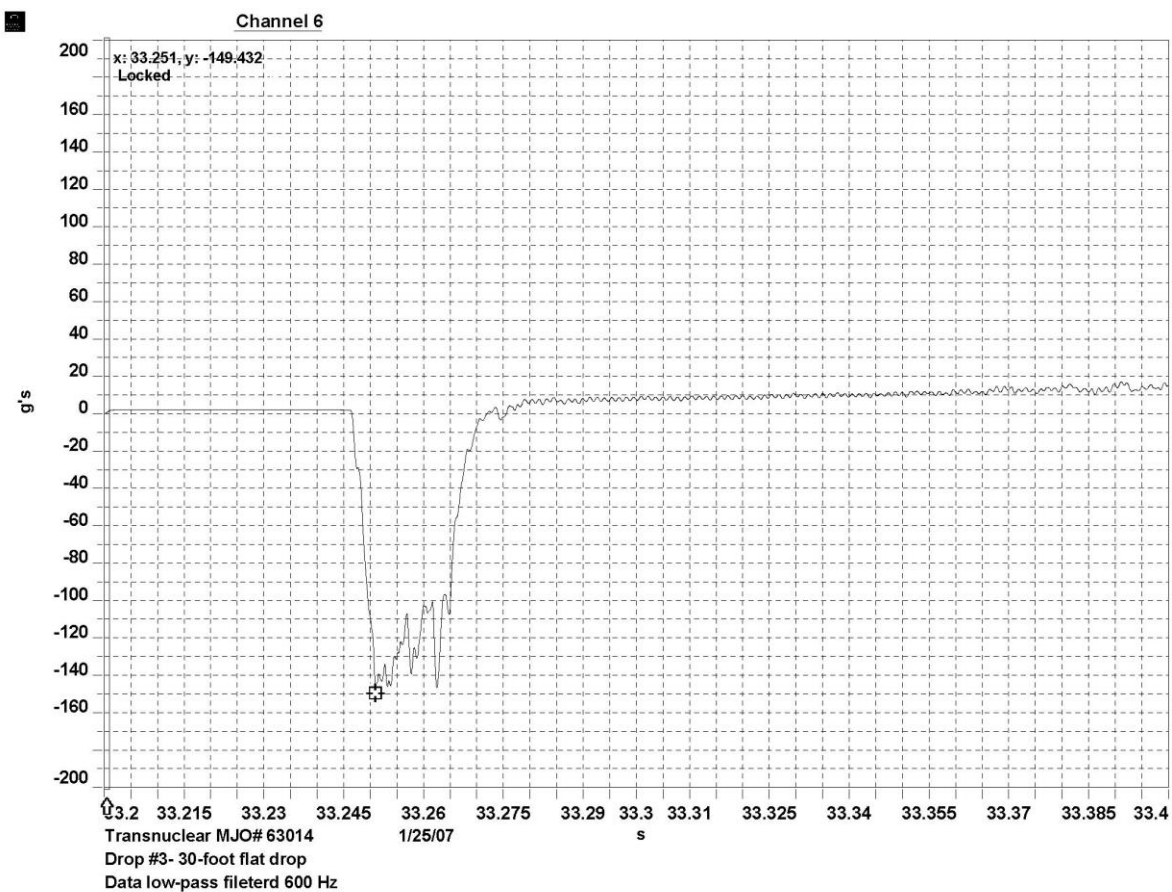


**Figure 2.12.10-10**  
**TN-40 Acceleration Time History, 0° Side Drop**





**Figure 2.12.10-11**  
**TN-40 Test Article After 0° Side Drop**

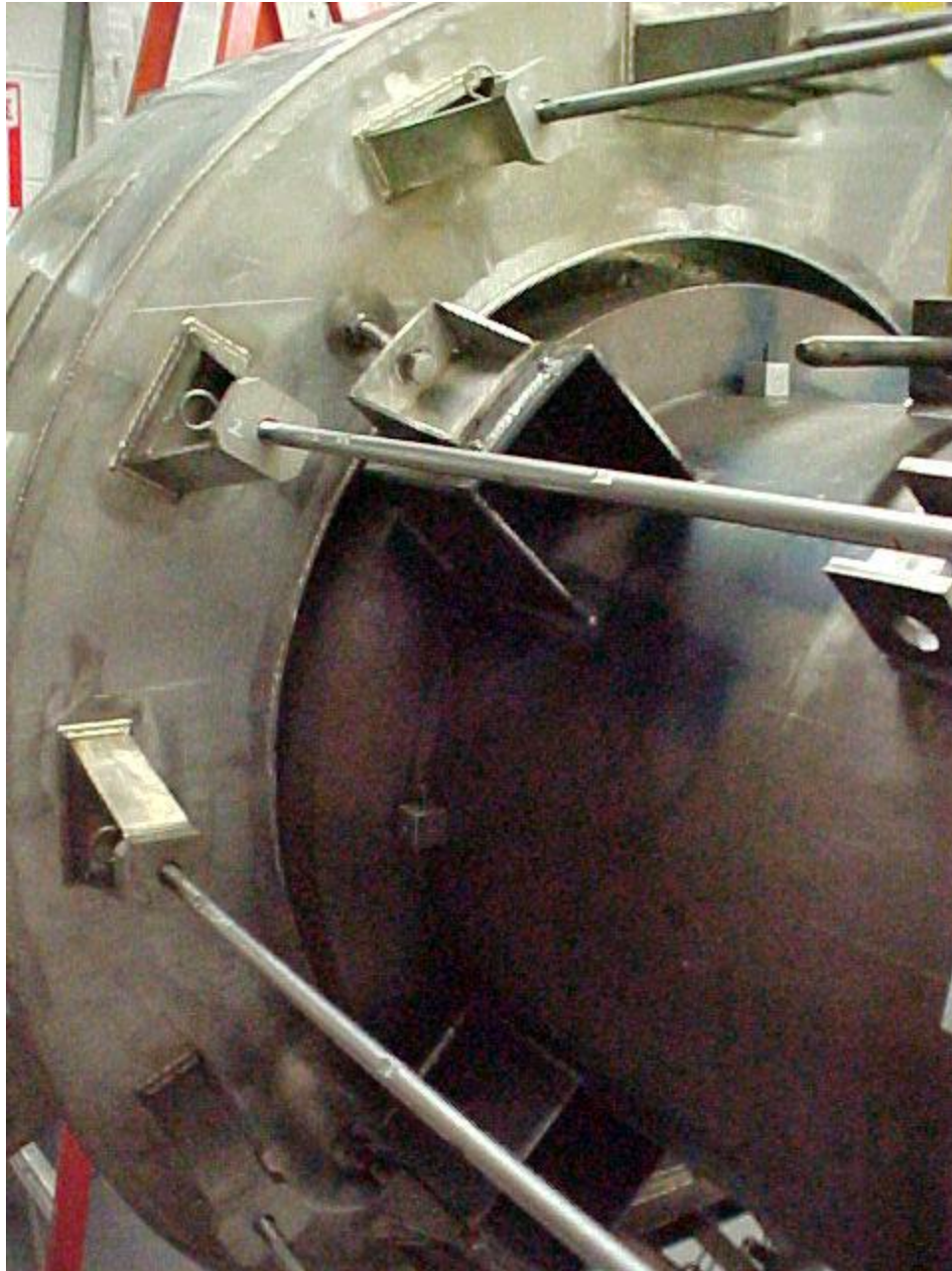


**Figure 2.12.10-12**  
**TN-40 Test Article After 0° Side Drop, Upper End Details**





**Figure 2.12.10-13**  
**TN-40 Test Article After 0° Side Drop, Lower End Details**

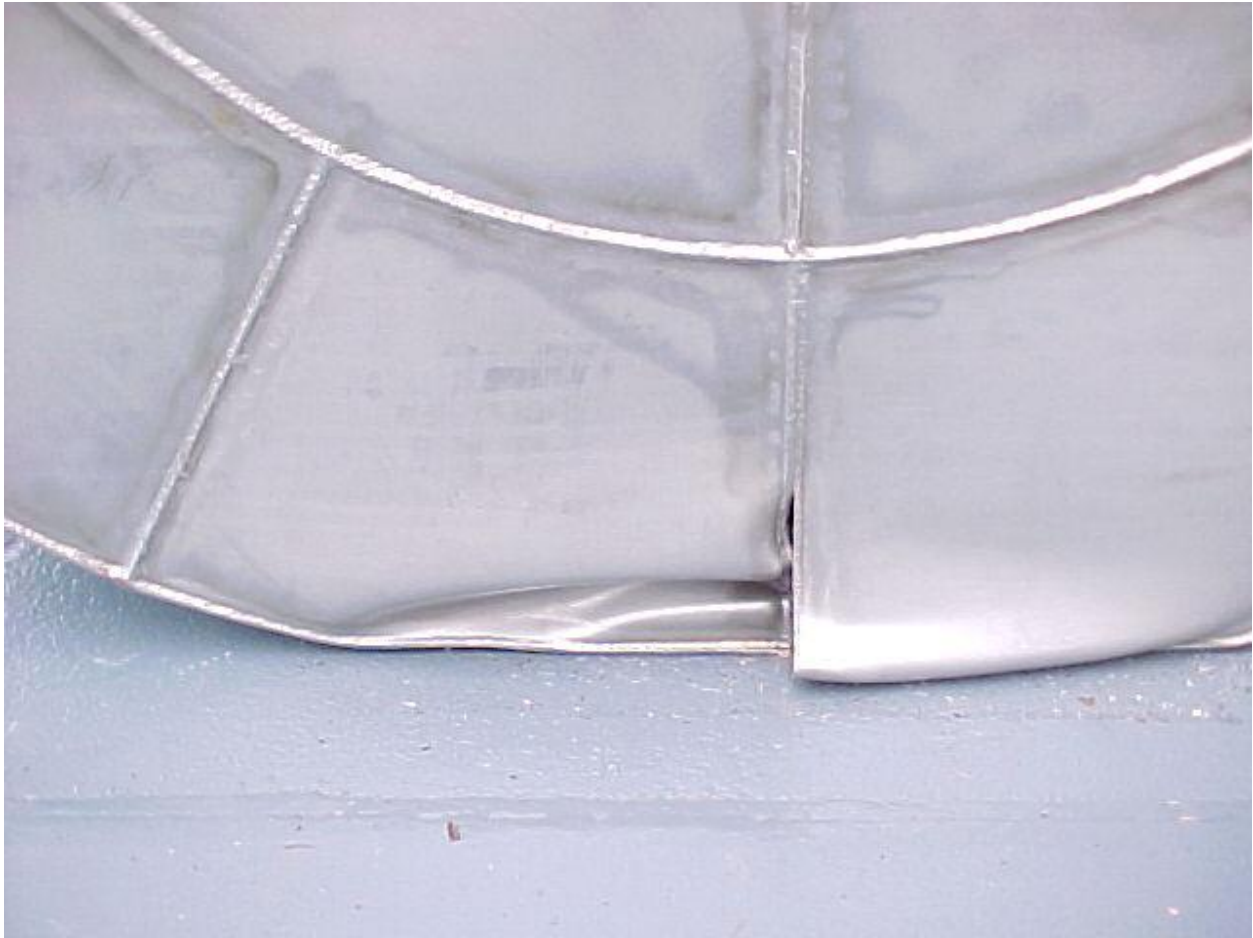


**Figure 2.12.10-14**  
**TN-40 Impact Limiter Shell Damage After 0° Side Drop**



**Figure 2.12.10-15**  
**TN-40 CG-Over-Corner Drop Test Rigging**

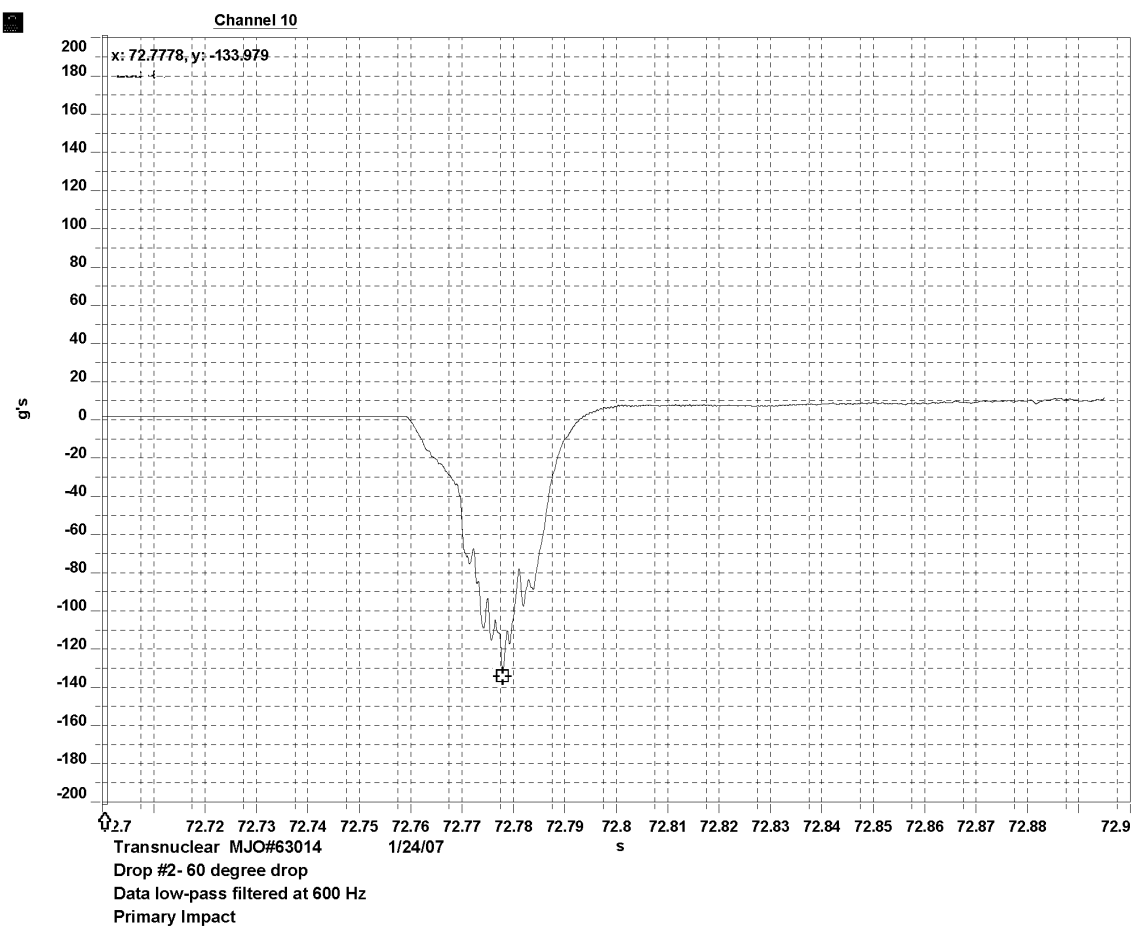


**Figure 2.12.10-16**  
**TN-40 CG-Over-Corner Drop Acceleration Time History**





**Figure 2.12.10-17**  
**TN-40 CG-Over-Corner Drop Impacted Surface Damage**



**Figure 2.12.10-18**  
**TN-40 CG-Over-Corner Drop Impact Limiter Deformation**





**Figure 2.12.10-19**  
**TN-40 20° Slap Down Test Rigging**

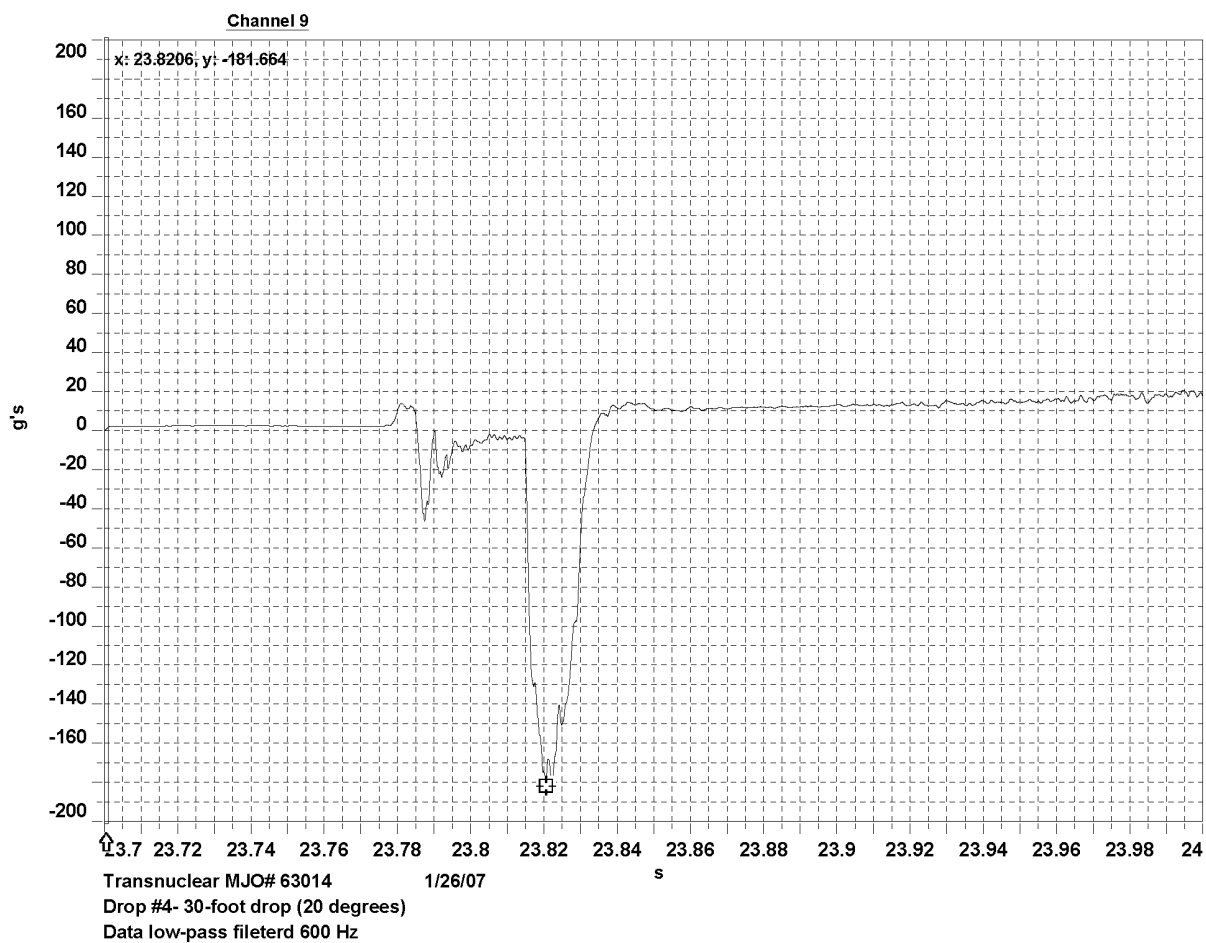


**Figure 2.12.10-20**  
**TN-40 20° Slap Down Drop Acceleration Time History**



**Figure 2.12.10-21**  
**TN-40 Test Article After 20° Slap Down Drop**



**Figure 2.12.10-22**  
**TN-40 Impact Limiter (Slap Down End) After 20° Slap Down Drop**



**Figure 2.12.10-23**  
**TN-40 90° End Drop Test Rigging**

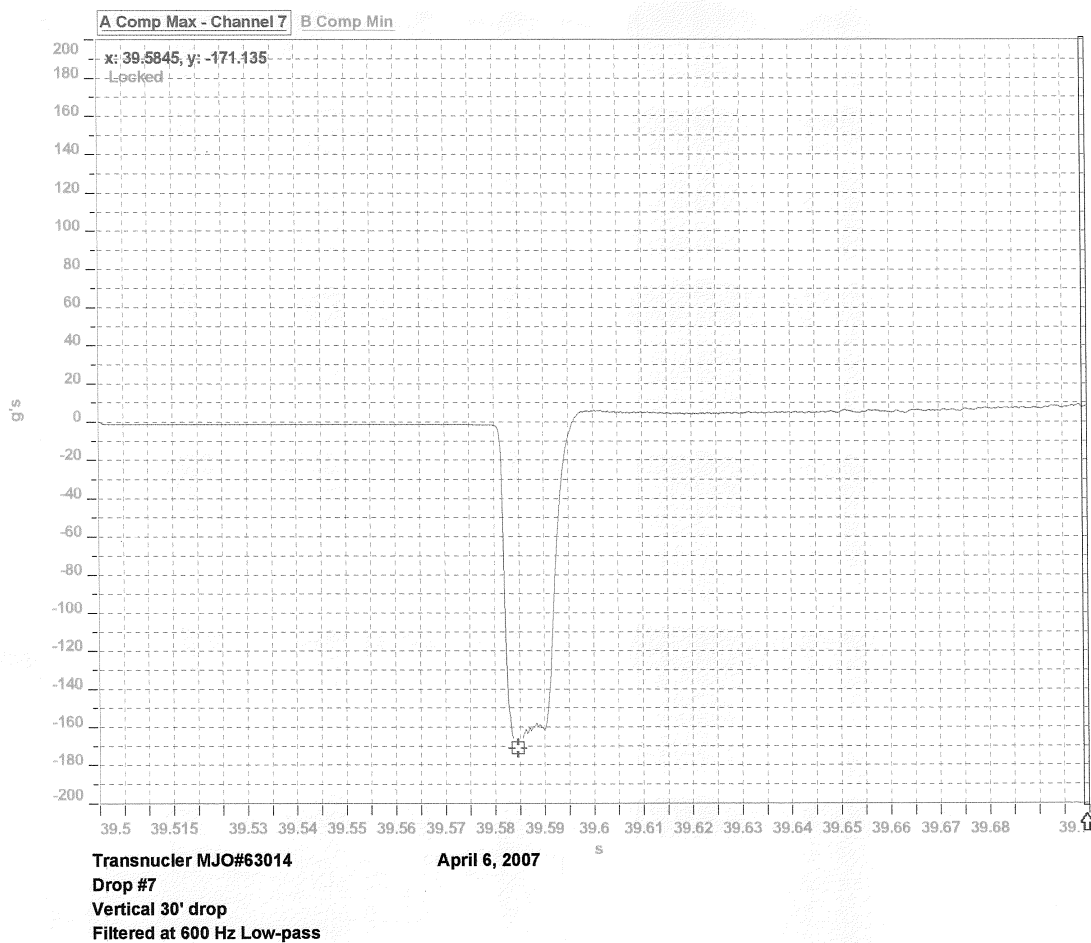


**Figure 2.12.10-24**  
**TN-40 Acceleration Time History, 90° End Drop**





**Figure 2.12.10-25**  
**TN-40 Test Dummy and Chilled Impact Limiter After Initial 90° End Drop**



**Figure 2.12.10-26**  
**TN-40 Test Dummy and Chilled Impact Limiter Post-Drop Detail**



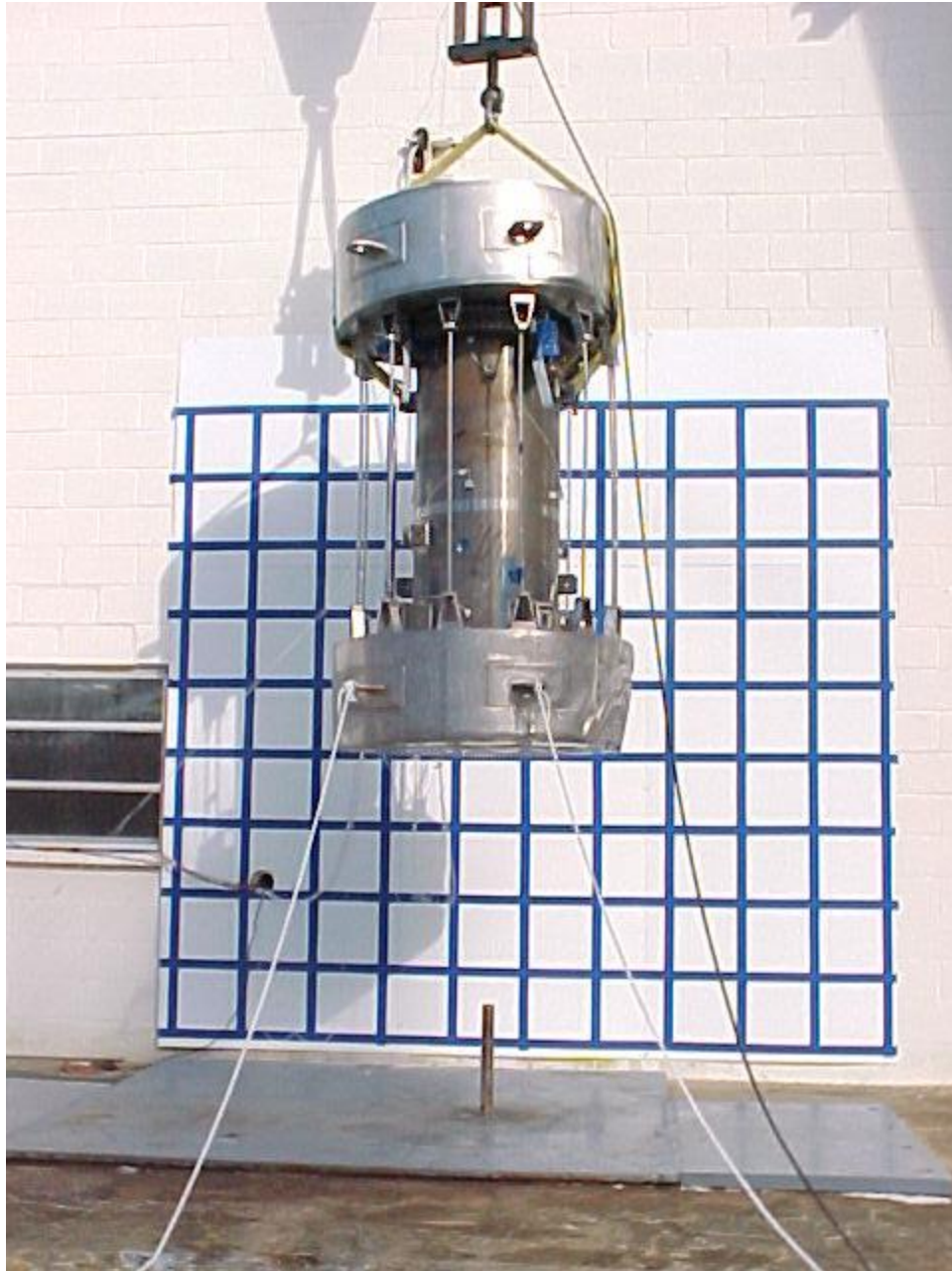


**Figure 2.12.10-27**  
**TN-40 Puncture Drop Test Rigging**



**Figure 2.12.10-28**  
**TN-40 Test Article After Puncture Drop**



**Figure 2.12.10-29**  
**TN-40 Puncture Pin Damage to Impact Limiter**

## **Appendix 2.12.11 Deep Water Immersion**

### **TABLE OF CONTENTS**

2.12.11	Deep Water Immersion.....	2.12.11-1
2.12.11.1	Hoop and Axial Compressive Stresses.....	2.12.11-1
2.12.11.2	Axial Compressive Stress and Buckling Stresses.....	2.12.11-4
2.12.11.3	Amplified Axial Stress.....	2.12.11-5
2.12.11.4	Interaction Equations for Local Buckling.....	2.12.11-6
2.12.11.5	References.....	2.12.11-7

### 2.12.11 Deep Water Immersion

The cask containment shell must be demonstrated to withstand the combined external pressure due to fabrication (or shrink fit), and the 290 psi external pressure due to the deep water immersion accident specified in 10 CFR 71.61 [1]. The following evaluation follows the American Society of Mechanical Engineers (ASME) Boiler and Pressure Vessel (B & PV) Code Case N-284-4 [2] to demonstrate that collapsing or buckling will not occur due to the applied fabrication and immersion pressures. The 8-inch thick gamma shell is conservatively ignored apart from imparting the fabrication stress pressure.

#### 2.12.11.1 Hoop and Axial Compressive Stresses

Cask dimensions utilized in this evaluation are extracted from Appendix 1.4.1. For cylinders of same modulus of elasticity and radial interference “ $\delta$ ”, the interface pressure “ $p$ ” is provided by Reference [3]:

$$p = \frac{E\delta(b^2 - a^2)(c^2 - b^2)}{2b^3(c^2 - a^2)}$$

where:

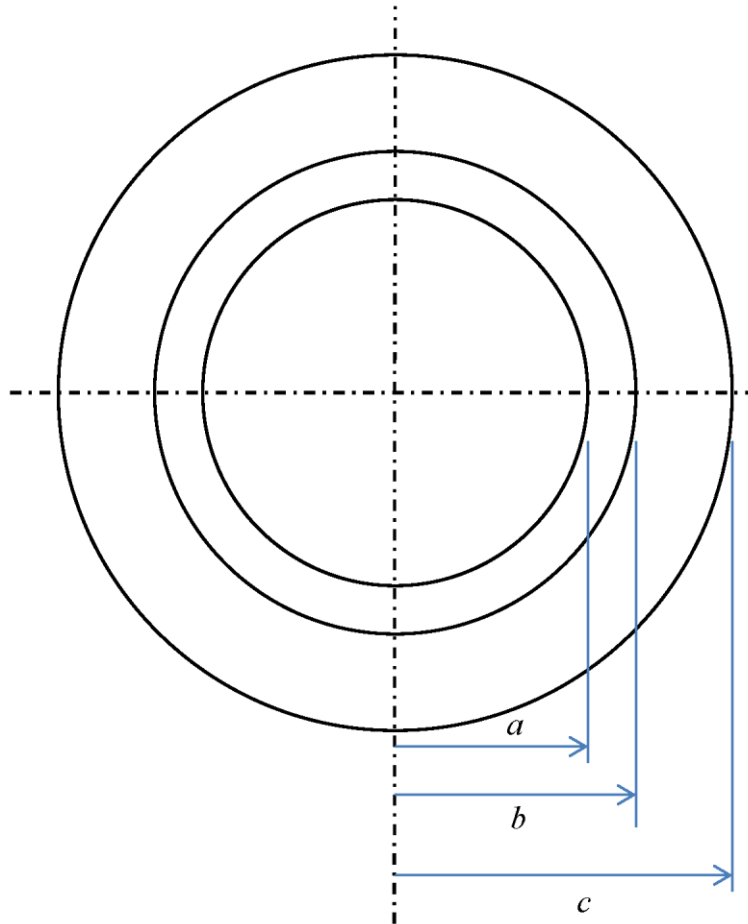
$a$  = 34.375 inches (containment cylinder inner radius)

$b$  = 35.875 inches (containment cylinder outer radius)

$c$  = 43.875 inches (gamma cylinder outer radius)

$\delta$  = 0.02 inch





For a conservative interface pressure “p”, a higher Young’s modulus ( $E = 29.3 \times 10^6$  at 70 °F [4]), is assumed for both cylinders.

$$p = \frac{(29.3 \times 10^6)(0.02)(35.875^2 - 34.375^2)(43.875^2 - 35.875^2)}{2(35.875^3)(43.875^2 - 34.375^2)} = 573.91 \text{ psi}$$

The maximum compressive (hoop) stress due to the shrink-fit pressure occurs in the inner cylinder [3], and is:

$$\sigma_{H_1} = \frac{2pb^2}{(b^2 - a^2)} = \frac{2(573.91)(35.875^2)}{(35.875^2 - 34.375^2)} = 14,019 \text{ psi}$$

Assuming no structural support from the 8-inch thick gamma shield, the deep immersion pressure of 290 psi will also produce a compressive hoop stress in the inner containment shell, which is:

$$\sigma_{H_3} = \frac{pR}{t} = \frac{290(35.875)}{1.5} = 6,936 \text{ psi}$$

Combining the hoop stresses for the two pressures results in the total compressive hoop stress,  $\sigma_\theta$ , in the inner containment shell:

$$\sigma_\theta = \sigma_{H_1} + \sigma_{H_3} = 14,019 + 6,936 = 20,955 \text{ psi}$$

The axial compressive stress,  $\sigma_\phi$ , due to 290 psig external pressure is:

$$\sigma_\phi = \frac{pR}{2t} = \frac{290(35.125)}{2(1.5)} = 3,395 \text{ psi}$$

The theoretical buckling stress per paragraph -1712.1 of Reference [2] of the inner cylinder depends on whether the cylinder is experiencing hydrostatic (end pressure included) or radial pressure. The shrink fit pressure can be considered a radial pressure while the immersion pressure is a hydrostatic pressure. Input parameters for the analysis are:

$$R = \text{average shell radius} = \frac{(a + b)}{2} = \frac{(34.375 + 35.875)}{2} = 35.125 \text{ inch}$$

where:

$t$  = shell thickness = 1.5 inches

$E$  = Young's modulus =  $27.8 \times 10^6$  psi

$L = l_\phi$  = overall length of shell =  $(163.25 + 6) = 169.25$  inches

$l_\theta$  = circumferential length =  $2\pi(R) = 2\pi(35.125) = 220.697$  inches

For this configuration, the hydrostatic case bounds the radial pressure (i.e., has a lower theoretical buckling stress), and is evaluated per paragraph -1511 [2]:

$$\frac{R}{t} = \frac{35.125}{1.5} = 23.417$$

$$1.65 \frac{R}{t} = \frac{1.65(35.125)}{1.5} = 38.64$$

$$M_\phi = \frac{l_\phi}{\sqrt{Rt}} = \frac{169.25}{\sqrt{35.125(1.5)}} = 23.317$$

$$M_\theta = \frac{l_\theta}{\sqrt{Rt}} = \frac{220.697}{\sqrt{35.125(1.5)}} = 30.405$$

$$M = \text{minimum } (M_\phi, M_\theta) = 23.317$$

For  $3.5 \leq M_\phi < 1.65(R/t)$ , and elastic buckling coefficient,  $C_{\theta h}$ , in hoop direction for cylinders with end pressure included ( $K = 0.5$ ), is:

$$C_{\theta h} = \frac{0.92}{M_\phi - 0.636} = \frac{0.92}{23.317 - 0.636} = 0.04056$$

The theoretical buckling stress,  $\sigma_{\theta eL}$ , is:

$$\sigma_{\theta eL} = \sigma_{\theta eL} = C_{\theta r} E \frac{t}{R} = 0.04056 (27.8 \times 10^6) \left[ \frac{1.5}{35.125} \right] = 48,152 \text{ psi}$$

For  $3.0 \leq M_\phi < 1.65(R/t)$ , the elastic buckling coefficient,  $C_{\theta r}$ , with no end pressure ( $K = 0$ ), is:

$$C_{\theta r} = \frac{0.92}{M_\phi - 1.17} = \frac{0.92}{23.317 - 1.17} = 0.04154$$

The theoretical buckling stress,  $\sigma_{reL}$ , is:

$$\sigma_{\theta eL} = \sigma_{reL} = C_{\theta r} \frac{Et}{R} = (0.04154) \left[ \frac{27.8 \times 10^6 (1.5)}{35.125} \right] = 49,316 \text{ psi}$$

The plasticity reduction factor,  $\eta_\theta$ , for buckling in hoop compression per paragraph -1611 of Reference [2] is calculated as follows:

$$\Delta = \frac{\alpha_{\theta L} \sigma_{\theta eL}}{\sigma_y} = \frac{0.8(48,152)}{37,000} = 1.0411, \text{ therefore, } 0.67 < \Delta < 4.2$$

$$\eta_\theta = \frac{2.53}{1 + 2.29\Delta} = \frac{2.53}{1 + 2.29(1.0411)} = 0.7476$$

The combine hoop stress in the containment cylinder is summarized in the following table, and is evaluated below.

#### Combined Hoop Stress

	Accident Condition
Calculated Hoop Compressive Stress, $\sigma_\theta$	20,955
Factor of Safety (FS) (Sec. -1400 of [2]) for HAC (Level D Service Limits)	1.34
Capacity Reduction, $\alpha_{\theta L}$ (Reference [2], Sec. -1511)	0.8
Hoop Elastic Amplified Stress, $\sigma_{\theta s} = \frac{\sigma_\theta (FS)}{\alpha_{\theta L}}$	35,100
Plastic Reduction Factor, $\eta_\theta$ (Reference [2], Sec. -1611)	0.7476
Theoretical Buckling Stress, $\sigma_{\theta eL}$	48,152

#### 2.12.11.2 Axial Compressive Stress and Buckling Stresses

The axial compressive stress due to the 290 psig external pressure is:

$$\sigma_\phi = \frac{pR}{2t} = \frac{290(35.125)}{2(1.5)} = 3,395 \text{ psi}$$



For SA-203, Gr D containment material,  $\sigma_y = 37,000$  psi, and  $E = 27.8 \times 10^6$  psi [4], the theoretical buckling stress is determined as follows:

$$\sigma_{\phi_{eL}} = C_{\phi} \frac{Et}{R}$$

Since  $M_{\phi} \geq 1.73$ ,  $C_{\phi} = 0.605$ , the theoretical buckling stress is, therefore:

$$\sigma_{\phi_{eL}} = C_{\phi} \frac{Et}{R} = 0.605 \left[ \frac{27.8 \times 10^6 (1.5)}{35.125} \right] = 718,249 \text{ psi}$$

This high theoretical axial buckling stress demonstrates that there is no potential for axial collapse or buckling of the cylindrical shell.

### 2.12.11.3 Amplified Axial Stress

The axial compressive stress due to the 290 psig external pressure is:

$$\sigma_{\phi} = 3,395 \text{ psi}$$

The capacity reduction factor per paragraph -1511 of Reference [2] is determined as follows:

#### (1) Effect of R/t

$$\alpha_{\phi_L} = \text{minimum} \left\{ \frac{1.52 - 0.473 \log_{10}(R/t)}{\frac{300\sigma_y}{E} - 0.033} \right\} = \text{minimum} \left\{ \frac{1.52 - 0.473 \log_{10} \left[ \frac{35.125}{1.5} \right]}{\frac{300(37,000)}{27.8 \times 10^6} - 0.033} \right\}$$

$$\alpha_{\phi_L} = \text{minimum} \left\{ \frac{0.872}{0.3663} \right\} = 0.3663$$

#### (2) Effect of Length

$$\alpha_{\phi_L} = 0.207 \text{ since } M_{\phi} \geq 10$$

Utilizing the larger value for  $\alpha_{\phi_L}$  from (1) and (2) [ $\alpha_{\phi_L} = 0.3663$ ], the elastic amplified stress is:

$$\text{Elastic Amplified Stress} = \frac{\sigma_{\phi} FS}{\alpha_{\phi_L}} = \frac{3,395 (1.34)}{0.3663} = 12,420 \text{ psi}$$

The plasticity reduction factor,  $\eta_\phi$ , for buckling in axial compression per -1611 of Reference [2] is calculated as follows:

$$\Delta = \frac{\alpha_{\phi_L} \sigma_{\phi eL}}{\sigma_y} = \frac{0.3663(718,249)}{37,000} = 7.1107, \text{ therefore } \Delta \geq 1.7 \text{ and,}$$

$$\eta_\phi = \frac{1}{\Delta} = \frac{1}{7.1107} = 0.1406 \text{ as } \Delta \geq 6.25$$

#### 2.12.11.4 Interaction Equations for Local Buckling

##### 2.12.11.4.1 Elastic Interaction Equations

With FS = 1.34, the allowable stresses for axial compression plus hoop compression are given by the following expressions per paragraph -1713.1.1 of Reference [2]:

$$\sigma_{xa} = \frac{\alpha_{\phi_L} \sigma_{\phi eL}}{FS} = \frac{0.3663(718,249)}{1.34} = 196,339 \text{ psi}$$

$$\sigma_{ha} = \frac{\alpha_{\theta_L} \sigma_{heL}}{FS} = \frac{0.8(48,152)}{1.34} = 28,747 \text{ psi}$$

$$\sigma_{ra} = \frac{\alpha_{\theta_L} \sigma_{reL}}{FS} = \frac{0.8(49,316)}{1.34} = 29,442 \text{ psi}$$

The ratio of the axial membrane force per unit length to the hoop compressive membrane force per unit length, K, is (with  $t_\phi = t_\theta$ );

$$K = \frac{\sigma_\phi t_\phi}{\sigma_\theta t_\theta} = \frac{3,395}{20,955} \times 1 = 0.1620 \therefore K < 0.5$$

With  $K < 0.5$ , no interaction check is required for axial compression plus hoop compression if  $\sigma_\theta < \sigma_{ha}$ :

$$\sigma_\theta = 20,955 \text{ psi} < \sigma_{ha} = 28,747 \text{ psi}$$

Since this stress condition is satisfied, the no interaction check is performed, and the elastic interaction equation for local buckling is satisfied.

##### 2.12.11.4.2 Inelastic Interaction Equations

Per paragraph -1713.2.1 of Reference [2], inelastic buckling relationships are satisfied as  $\eta_i < 1.0$ . The allowable stresses for inelastic buckling are:

$$\sigma_{xc} = \eta_\phi \sigma_{xa} = 0.1406(196,339) = 27,605 \text{ psi}$$

$$\sigma_{rc} = \eta_\theta \sigma_{ra} = 0.7476(29,442) = 22,011 \text{ psi}$$

As noted in -1713.2, no interaction equations are provided for meridional (axial) compression plus hoop compression because it is conservative to ignore interaction of the two stress components when buckling is inelastic. For axial compression or hoop compression, the interaction equations for the fabrication stress ( $\sigma_\phi$ ) and the 290 psig immersion pressure ( $\sigma_\theta$ ) are:

$$\frac{\sigma_\phi}{\sigma_{xc}} \leq 1.0, \quad \frac{\sigma_\theta}{\sigma_{rc}} \leq 1.0,$$

$$\frac{3,395}{27,605} \leq 1.0, \quad \frac{20,955}{22,011} \leq 1.0$$

$$0.1223 \leq 1.0, \quad 0.952 \leq 1.0$$

Since both stress ratios are less than 1.0, the inner containment cylindrical shell has been demonstrated to withstand the combined external pressure due to fabrication stress and the 290 psi deep immersion pressure without collapsing or buckling.

#### 2.12.11.5 References

1. Title 10, Code of Federal Regulations - Energy, Part 71 (10 CFR 71), "Packaging and Transportation of Radioactive Material," 1-1-2021 Edition, U.S. Nuclear Regulatory Commission, Washington, D.C.
2. American Society of Mechanical Engineers, ASME Boiler and Pressure Vessel Code, Code Case N-284-4, "Metal Containment Shell Buckling Design Methods," Section III, Division 1, Class MC, October 2012.
3. John Harvey, "Theory and Design of Modern Pressure Vessel," Second Edition.
4. American Society of Mechanical Engineers, ASME Boiler and Pressure Vessel Code, Section III, Division 1, Appendices, 1992 Edition.

**Appendix 2.12.12**  
**Structural Analysis of Thermocouple Lance Assembly**

TABLE OF CONTENTS

2.12.12	Structural Analysis of Thermocouple Lance Assembly .....	2.12.12-1
2.12.12.1	Introduction .....	2.12.12-1
2.12.12.2	Lance Closure Calculations .....	2.12.12-2
2.12.12.3	Thermocouple Lance Oversheath .....	2.12.12-11
2.12.12.4	Lance Seal Lateral Displacement Test .....	2.12.12-14
2.12.12.5	Conclusions.....	2.12.12-16
2.12.12.6	References.....	2.12.12-17

LIST OF TABLES

Table 2.12.12-1	Design Parameters for Lance Jacking Screw Analysis .....	2.12.12-18
Table 2.12.12-2	Jacking Screw Data.....	2.12.12-19
Table 2.12.12-3	Lance Assembly Material Properties at 300 °F .....	2.12.12-20
Table 2.12.12-4	Normal Condition Allowable Stresses in Jacking Screws.....	2.12.12-21
Table 2.12.12-5	Accident Condition Allowable Stresses in Lance Jacking Screws .....	2.12.12-22
Table 2.12.12-6	Normal Condition Allowable Stresses in Jacking & Compression Plates .....	2.12.12-23
Table 2.12.12-7	Accident Condition Allowable Stresses in Jacking Plate Internal Screw Threads .....	2.12.12-24

LIST OF FIGURES

Figure 2.12.12-1	Thermocouple Lance Assembly Components .....	2.12.12-25
Figure 2.12.12-2	Lance Jacking Plate Cross-Section .....	2.12.12-26
Figure 2.12.12-3	Lance Compression Plate Cross-Section .....	2.12.12-27
Figure 2.12.12-4	Thermocouple Lance Body.....	2.12.12-28
Figure 2.12.12-5	ANSYS® Thermocouple Lance Model.....	2.12.12-29
Figure 2.12.12-6	Overall Stress Intensity, ANSYS® Thermocouple Lance Model .	2.12.12-30
Figure 2.12.12-7	Magnified Stress Intensity, ANSYS® Thermocouple Lance Model .....	2.12.12-31
Figure 2.12.12-8	Modified Penetration Sleeve on Test Stand.....	2.12.12-32
Figure 2.12.12-9	Lance Seal Lateral Displacement Test Setup .....	2.12.12-33
Figure 2.12.12-10	Close-up of Test Setup with Lance Positioned Towards Top .....	2.12.12-34
Figure 2.12.12-11	Load–Displacement Curve for Lateral Seal Displacement Test .	2.12.12-35
Figure 2.12.12-12	Damage to Lance Body Edge/O-ring Seal (Lower Right Quadrant).....	2.12.12-36
Figure 2.12.12-13	Close-up of Damage to Outer O-ring Seal .....	2.12.12-37
Figure 2.12.12-14	Damage to Penetration Sleeve Sealing Surface .....	2.12.12-38
Figure 2.12.12-15	Measurements of Penetration Sleeve Sealing Surface Damage .....	2.12.12-39

## 2.12.12 Structural Analysis of Thermocouple Lance Assembly

### 2.12.12.1 Introduction

This appendix evaluates the ability of the thermocouple lance assemblies (TLAs) to maintain the containment boundary and a leaktight seal under events defined by normal conditions transport (NCT) and the hypothetical accident conditions (HAC). The analysis of the jacking screws is performed in accordance with NUREG/CR-6007 [1], as applicable.

The TLA in the TN-32B HBU demonstration cask closure lid is shown in Figure 2.12.12-1. The lance assembly is designed to be inserted into a designated fuel assembly, and seat a Helicoflex® HND-229 seal in the closure lid with the Type 304/304L stainless steel lance body. The 161-inch long lance that contains the nine thermocouples is enclosed within a welded Inconel Alloy 600 (UNS N06600) sheath. An additional welded Inconel oversheath that extends 6.75 inches from the lance body provides additional reinforcement of the lance sheath.

For securing the assemblies in the closure lid, two plates that are fabricated from SA-387, Grade 91, Class 2 material are installed over the lance body to apply the clamping axial force. The jacking plate has eight 5/8-18UNF socket head set (jacking) screws, fabricated from SA-193 Grade B7 material, that are threaded into it. The jacking screw compressive force is then transferred to the compression plate, which bears against the lance body. These two plates are secured inside the recess of the penetration sleeve, which is fabricated from SA-350 Grade LF3, and welded into the closure lid and shield plate, by reacting the axial jacking force against a stainless steel (Grade 316) retaining ring. The total weight of a lance assembly is 30 lb<sub>m</sub>. The weight of the stainless steel lance body alone is 11 lb<sub>m</sub>. However, a conservative TLA weight of 40 lb<sub>m</sub> will be utilized for analysis.

Since the TLAs are retained in the closure lid by the retaining ring, the jacking screws, and the jacking and compression plates, maintaining the containment boundary primarily requires demonstrating that the lance closure is maintained for all NCT and HAC tests. Therefore, the following evaluations of the thermocouple lance assembly are presented in this appendix:

- Jacking screw compressive load
- Seal seating load
- Pressure loads (internal and external)
- Temperature load
- Free NCT and HAC drop loads
- Load combinations for NCT and HAC
- Bearing stress
- Retaining ring stress
- Lance oversheath stresses and allowable stresses

The design parameters of the thermocouple lance assembly closure, extracted from Drawing 19885-71-7 in Appendix 1.4.1 and Reference [2], are summarized in Table 2.12.12-1. The jacking screw data and material allowable stresses are presented in Table 2.12.12-2 through Table 2.12.12-4. Based on results of thermal analyses presented in Chapter 3, a maximum temperature of 300 °F is utilized in the thermocouple lance region for both NCT and HAC evaluations. The following load cases are considered in the analysis.

1. Preload + Temperature Load (NCT)
2. Pressure Load + 1 Foot End Drop (NCT)
3. Pressure Load + 30 Foot End Drop (HAC)
4. 30 Foot Side Drop (HAC)

## 2.12.12.2 Lance Closure Calculations

### 2.12.12.2.1 Jacking Screw Compressive Load

To develop the compressive force on the compression plate, a tightening torque range of 60 to 70 lb<sub>f</sub>-ft is specified for the jacking screws. For the minimum tightening torque of 60 lb<sub>f</sub>-ft, the axial force per screw,  $F_{a-min}$ , is:

$$F_{a-min} = (Q_{min})/KD_b = (720)/(0.127(0.625)) = 9,071 \text{ lb}_f$$

where:

$$\begin{aligned} Q_{min} &= \text{applied tightening torque} = 60(12) = 720 \text{ lb}_f\text{-in} \\ K &= \text{nut factor} = 0.127 \text{ (determined experimentally for TN-32 casks)} \\ D_b &= \text{screw diameter} = 0.625 \text{ inch} \end{aligned}$$

For the maximum tightening torque,  $Q_{max}$ , of 70 lb<sub>f</sub>-ft, the axial force per screw,  $F_{a-max}$ , is:

$$F_{a-max} = (Q_{max})/KD_b = (70 \times 12)/(0.127(0.625)) = 10,583 \text{ lb}_f$$

The residual torsional moment,  $M_{tr}$ , is:

$$M_{tr-max} = 0.5(Q_{max}) = 0.5(70 \times 12) = 420 \text{ lb}_f\text{-in}$$

$$M_{tr-min} = 0.5(Q_{min}) = 0.5(60 \times 12) = 360 \text{ lb}_f\text{-in}$$

The maximum axial force,  $F_a$ , per jacking screw for the maximum tightening torque will be:

$$F_a = F_{a-max} = 10,583 \text{ lb}_f$$

## 2.12.12.2.2 Seal Seating Load

Seal characteristics for the Helicoflex® HND-229 seals with a silver jacket, and a 0.161 seal cross section are extracted from Reference [3]. The diameter of the inner seal,  $D_{is}$ , is 4.72 in, and the diameter of the outer seal,  $D_{os}$ , is 5.85 in. The force to seat the seals is approximately 1,827 lb<sub>f</sub>/in for a silver jacket [3]. Therefore, the total force required to seat the seals is:

$$\text{Inner Seal Seat Load: } \pi(4.72)(1,827) = 27,091 \text{ lb}_f$$

$$\text{Outer Seal Seat Load: } \pi(5.85)(1,827) = 33,577 \text{ lb}_f$$

$$\text{Total load to seat the seals, } F_a, = 27,091 + 33,577 = 60,668 \text{ lb}_f$$

Therefore, the required seal seating load per jacking screw is:

$$(F_a)/8 = 60,668/8 = 7,584 \text{ lb}_f/\text{screw}$$

Since the minimum axial compressive force developed in each screw is 9,071 lb<sub>f</sub>, the specified preload exceeds the required force to seat the seals.

## 2.12.12.2.3 Jacking Screw Load Due to Internal Pressure

The axial force per jacking screw due to a 100 psig internal design pressure ( $F_{a-p}$ ) with an assumed 0 psig external pressure is:

$$F_{a-p} = \frac{\pi D_{ig}^2 (P_{li} - P_{lo})}{4 N_b}$$

Utilizing the outer seal diameter for  $D_{ig}$  (conservative) = 5.85 in., then,

$$F_{a-p} = \frac{\pi(5.85^2)(100-0)}{4(8)} = 336 \text{ lb}_f/\text{screw}$$

Since this force is positive (outward acting), the force acts as an additional compressive load on the jacking screws. Therefore, the maximum compressive load ( $F_{a-max}$ ) on each jacking screw under normal conditions is:

$$F_{a-max} = F_a + F_{a-p} = 10,583 + 336 = 10,919 \text{ lb}_f$$

For analytical purposes, a conservative load of 14,000 lb<sub>f</sub> will be utilized for the maximum compressive axial load on the jacking screws for both normal and accident conditions.



## 2.12.12.2.4 Jacking Screw Load Due to Temperature

The jacking screw material is SA-193 Gr B7 (1Cr – 1/5Mo). This material is Group 1 in the thermal coefficients of expansion tables in Reference [4]. The closure lid is SA-203 Gr D (3½Ni), and the penetration sleeve is SA-350 Gr. LF3 (3½Ni), which are also in Group 1. Consequently, the jacking screws, closure lid, and penetration sleeve have the same coefficient of thermal expansion ( $7.3 \times 10^{-6}$  in/in-°F at 300 °F). Therefore, heating of the assembly to the maximum isothermal temperature will not generate any additional stress in the jacking screws or the closure.

## 2.12.12.2.5 Jacking Screw Load Due to Free Drop Impacts

Since the thermocouple lance assemblies are installed axially in the closure lid, the 90-degree impact on the end of the cask will generate the largest impact force on the lance closure that could affect the jacking screws, jacking plate, compression plate, and the retaining ring.

NCT Impact Loads

For the 1-foot normal condition end free drop on the closure lid end, a bounding impact of 30g will be applied to the thermocouple lance assembly mass, including the jacking and compression plates and the jacking screws. This impact is conservative since the maximum impact for the cold end drop presented in Appendix 2.12.9 is 25.5g. Therefore, the additional compressive axial load on a jacking screw for this impact is:

$$F_{a-NCT-end} = \frac{30g (LA_{mass})}{N_b} = \frac{(30g)(40)}{(8)} = 150 \text{ lb}_f/\text{screw}$$

where:

$$\begin{aligned} LA_{mass} &= \text{total mass of lance assembly} = 40 \text{ lb}_m \\ N_b &= \text{number of jacking screws} = 8 \end{aligned}$$

HAC Impact Loads

For the 30-foot HAC end free drop on the closure lid end, a bounding impact of 80g will be applied to the thermocouple lance assembly mass, including the jacking and compression plates and the jacking screws. This impact is conservative since the maximum impact for the cold end drop presented in Appendix 2.12.9 is 74.2g. Therefore, the additional compressive axial load on a jacking screw for this impact is:

$$F_{a-NCT-end} = \frac{80g (LA_{mass})}{N_b} = \frac{(80g)(40)}{(8)} = 400 \text{ lb}_f/\text{screw}$$

where:

$$\begin{aligned} LA_{mass} &= \text{total mass of lance assembly} = 40 \text{ lb}_m \\ N_b &= \text{number of jacking screws} = 8 \end{aligned}$$

For the 30-foot HAC side free drop, a bounding impact of 50g will be applied to the thermocouple lance assembly mass, including the jacking and compression plates and the jacking screws. This impact is conservative since the maximum impact for the cold side drop presented in Appendix 2.12.9 is 44.6g. Therefore, the side impact will result in a lateral force,  $F_{\text{I-HAC-side}}$ , on the TLA of:

$$F_{\text{I-HAC-side}} = 50g(LA_{\text{mass}}) = (50g)(40) = 2,000\text{lb}_f$$

where:

$$LA_{\text{mass}} = \text{total mass of lance assembly} = 40\text{ lb}_m$$

Since the jacking screws are only in compression, there is no additional force applied to the screws for this impact side orientation. Additionally, the jacking and compression plates will also not be adversely affected by this impact because the plates are in compression perpendicular to the drop orientation. The primary reaction of the TLA to the side impact is the potential to slide between the compression plate and the penetration sleeve. Because this sliding action is directly related to the sliding frictional force developed by the axial compression of the jacking screws on the compression plate/lance body/sealing surface interface, the effect of this impact was experimentally determined on a heated prototypic assembly, as discussed in Section 2.12.12.4. From that test, the maximum lateral force to initiate sliding of the TLA was determined to be approximately [ ] Conservatively assuming a worst-case dynamic load factor of 2.0, the margin of safety (M.S.) against sliding of a TLA in the penetration sleeve from a HAC side drop is:

$$\text{M.S.} = \frac{11,300}{(2)(2,000)} - 1 = \frac{11,300}{4,000} - 1 = +1.83$$

Note that the assume weight being inertial loaded is the total mass of a complete TLA, not just the 11-pound stainless steel lance body. Since the M.S. is positive, the TLA will not lateral slide from a worst-case side impact, and will remain in its leaktight, as-loaded condition during transport.

#### 2.12.12.2.6 External Pressure Load of 290 psig

The axial force due to the deep immersion pressure of 290 psig ( $F_{\text{a-p}}$ ) per 10 CFR 71.61 will result in an inward force on the lance body, which reduces the compressive load on the jacking screws. For this external pressure with an assumed 0 psig internal pressure, the negative axial force per jacking screw is:

$$F_{\text{a-p}} = \frac{\pi D_{\text{lg}}^2 (P_{\text{li}} - P_{\text{lo}})}{4 N_{\text{b}}}$$

Utilizing the outer seal diameter for  $D_{\text{lg}}$  (conservative) = 5.85 in., then,

$$F_{\text{a-p}} = \frac{\pi(5.85^2)(0 - 290)}{4(8)} = -974\text{lb/screw}$$

This reduction in the jacking screw force does not exceed the compressive screw force that is developed by the tightening torque. Additionally, the immersion pressure will apply additional downward force on the metallic containment seal.

#### 2.12.12.2.7 Summary of Analysis Results

The loads calculated in the previous sections are summarized in the following table.

**Lance Jacking Screw Individual Load Summary**

Load Case	Applied Load		Compressive Axial Force, $F_a$ (lb <sub>f</sub> )	Torsional Moment, $M_t$ (in-lb <sub>f</sub> )
Compression	Residual	Maximum Torque	10,583	420
		Minimum Torque	9,071	360
Seal	Seating Load		7,584	0
Pressure	100 psig Internal		336	0
Impact	1 Foot Normal Condition Free Drop		150	0
	30 foot Accident Condition Free End Drop		400	0
External Pressure	290 psig External		-974	0

#### 2.12.12.2.8 Lance Jacking Screw Load Combinations

A summary of normal and accident condition load combinations is presented in the following table. The method used for the following combination is extracted from Table 4.9 of Reference [1].

**Lance Jacking Screw Normal and Accident Load Combinations**

Load Case	Combination Description		Axial Compressive Force, $F_a$ (lb <sub>f</sub> )	Torsional Moment, $M_t$ (in-lb <sub>f</sub> )
1	Preload + Temperature (Normal Condition)	Maximum Torque	10,583	420
		Minimum Torque	9,071	360
2	Pressure + Normal Impact (Normal Condition)		486	0
3	Pressure + Accident Impact (Accident Condition)		736	0
4	Internal & External Pressure		-638	0

As noted previously, a maximum axial compressive load of 14,000 lb<sub>f</sub> bounds all load combinations for both NCT and HAC, and will be utilized in the analyses of the lance jacking screws.

## 2.12.12.2.9 Jacking Screw Stress Analysis

Since the NCT allowable stresses are more conservative than the HAC allowable stresses, only the evaluation for NCT load combinations is performed.

For the maximum applied compressive load, the average compressive stress ( $\sigma$ ) in a jacking screw is:

$$\sigma = \frac{F_{a-\max}}{A_{js}} = \frac{-14,000}{0.256} = -54.7 \text{ ksi}$$

where:

$$\begin{aligned} F_{a-\max} &= \text{maximum compressive load} = 14,000 \text{ lb}_f \\ A_{js} &= \text{tensile stress area of jacking screws} = 0.256 \text{ in}^2 \\ &\quad (\text{Table 2.12.12-2}) \end{aligned}$$

The M.S. on the compressive stress ( $\sigma_{cs}$ ) for the allowable stress ( $S_m$ ) for the SA-193 Grade B7 material is:

$$\text{M.S.} = \frac{S_m}{\sigma_{cs}} = \frac{62.7}{54.7} - 1 = +.15$$

where:

$$S_m = \text{allowable stress at } 300^\circ\text{F} = 62.7 \text{ ksi (Table 2.12.12-3)}$$

The shear stress due to the residual torque ( $\tau$ ) in the jacking screw is conservatively assumed to be equal to 50% of the maximum installation tightening torque. Per Table 5.1 of Reference [1], the shear stress is:

$$\tau = 5.093 \frac{M_t}{(D_{ba})^3} = 5.093 \frac{(420)}{(0.571)^3} = 11.5 \text{ ksi}$$

The combined average stress intensity ( $SI_{ave}$ ) for the jacking screw is:

$$SI_{ave} = \sqrt{(\sigma_{cs})^2 + 4(\tau)^2} = \sqrt{(-54.7)^2 + 4(11.5)^2} = 59.3 \text{ ksi}$$

The M.S. for the jacking screws in the normal condition with the average stress intensity is:

$$\text{M.S.} = \frac{1.35S_m}{SI_{ave}} = \frac{1.35(62.7)}{59.3} - 1 = +.43$$

## 2.12.12.2.10 Jacking Plate Internal Thread Analysis

Since the material strength of the jacking screws ( $S_y = 94.1$  ksi) is greater than the material strength of the jacking plate ( $S_y = 54.8$  ksi), the evaluation of the threads for the maximum axial load is demonstrated for the internal threads in the jacking plate. The net length of thread engagement for a jacking screw ( $L_e$ ) is determined as follows:

$$L_e = L_{JS} - [D_{PS} - (T_{J-plt} + T_{C-plt} + T_{L-A})] = 1.88 - [4.33 - (1.00 + 1.00 + 1.26)] = 0.81 \text{ inch}$$

where:

$L_{JS}$	= length of jacking screw = 1.88 inches
$D_{PS}$	= depth of penetration sleeve below retaining ring groove = 4.33 inches
$T_{J-plt}$	= thickness of jacking plate = 1.00 inch
$T_{C-plt}$	= thickness of compression plate = 1.00 inch
$T_{L-A}$	= thickness of lance body = 1.26 inches

From Table 2.12.12-2, the shear area per unit length for a 5/8-18UNF-2B internal thread is 1.367 in<sup>2</sup>/inch. The total shear area ( $A_{int-\tau}$ ) for the jacking screw engagement is:

$$A_{int-\tau} = (1.367)(0.81) = 1.107 \text{ in}^2$$

The shear stress ( $\tau_{int}$ ) in the internal threads for the 14,000 lb<sub>f</sub> maximum axial compressive load is:

$$\tau_{int} = \frac{14,000}{(1.107)} = 12.6 \text{ ksi}$$

The shear allowable stress for the SA-387 Grade 91, Class 2 plate is  $0.6S_m$ . From Table 2.12.12-3, the allowable stress ( $S_m$ ) at 300 °F is 28.3 ksi. Therefore, the M.S. for the internal threads is:

$$M.S. = \frac{0.6S_m}{\tau_{int}} = \frac{0.6(28.3)}{12.6} - 1 = +.35$$

## 2.12.12.2.11 Bearing Loads

The compression plate in the thermocouple lance assembly will have two bearing interfaces that will result in bearing stresses. The first interface will be the jacking screws bearing on the compression plate, and then the plate bearing on the stainless steel thermocouple lance body.

Jacking Screw – Compression Plate Interface

For the screw interface, the jacking screws have a 5/8 inch diameter foot that contacts the compression plate. The bearing stress ( $\sigma_1$ ) underneath a jacking screw due to the 12,000 lbf maximum axial load is:

$$\sigma_1 = \frac{14,000}{\pi/4 (0.625)^2} = 45.6 \text{ ksi}$$

Per Table 2.12.12-6, the bearing stress limit is the yield strength ( $S_y$ ) of the material. At 300 °F, the minimum yield stress for the compression plate is 54.8 ksi per Table 2.12.12-3. Therefore, the M.S. for the bearing stress in the compression plate is:

$$\text{M.S.} = \frac{S_y}{\sigma_1} = \frac{54.8}{45.6} - 1 = +.20$$

Compression Plate – Lance Body Interface

The bearing stress between the thermocouple lance body and the compression plate ( $\sigma_2$ ), when the instrument is centered, is:

where:

$F_{a\text{-max}}$  = maximum compressive force = 14,000 lbf

$D_{lo}$  = Lance body net outer diameter = [ ] inches

Compression plate net inner diameter = 3.13 inches

$N_b$  = Number of jacking screws = 8

At 300 °F, the minimum yield stress ( $S_y$ ) for the thermocouple lance body is 22.4 ksi per Table 2.12.12-3. Therefore, the M.S. for bearing on this lance body bearing interface is:

$$\text{M.S.} = \frac{S_y}{\sigma_2} = \frac{22.4}{4.9} - 1 = +3.57$$

## 2.12.12.2.12 Vibration/Shock

Because the TN-32B HBU demonstration cask will be shipped by rail car, the shock and vibration loadings for rail configurations will only be considered.

Rail Car Shock:

Since the TN-32B HBU demonstration cask will only be transported once with the HBU spent fuel payload, the rail car shock will assume an average of a 3,000 mile one-way trip. Reference [4] reports that there are roughly nine shock cycles per 100 miles of rail car transport. Therefore, the total number of cycles is: 3,000 miles  $\times$  1 one-way trip  $\times$  1 shipment  $\times$  0.09 shocks per mile = 270 cycles. This very low number of cycles due to rail transport will have no fatigue effect on the jacking screws or a thermocouple lance assembly.

Reference [4] also specifies a peak shock loading of 4.7g in the longitudinal direction for rail car transport. Consequently, the jacking screw force due to rail car shock is:

$$(40 \text{ lb}_m)(4.7g)/[(8 \text{ bolts})(0.256 \text{ in}^2 \text{ per bolt})] = 91.8 \text{ psi}$$

The conservative applied axial load of 14,000 lb<sub>f</sub> for a jacking screw bounds any rail car shock, which has negligible effect on the clamping force for the lance closure.

Vibration:

According to Reference [4], the peak vibration load on the deck of a rail car in the longitudinal direction is 0.19g. This vibration results in a stress of less than 4 psi, which is negligible for the high strength jacking screw.

## 2.12.12.2.13 Retaining Ring

The retaining ring is installed in the penetration sleeve, and reacts the compressive force from the jacking plate to retain the lance closure. As specified on Drawing 19885-71-2 in Appendix 1.4.1 the retaining ring is fabricated from ASTM A313 Type 316 stainless steel [5]. The specified minimum tensile ( $S_u$ ) and shear strengths ( $S_\tau$ ) for this spring steel material are 175 ksi and 99 ksi, respectively [5]. The shear limit load ( $P_r$ ) for the retaining ring will then be:

$$P_r = \frac{\pi DT(S_\tau)}{SF} = \frac{\pi(7.0)(0.165)(99,000)}{3} = 119,742 \text{ lb}_f$$

where:

D	= inside diameter of the penetration sleeve = 7.0 inches
T	= the total spring thickness = 0.165 inches
$S_\tau$	= 99,000 psi
SF	= safety factor = 3 (recommended by manufacturer)

The load applied to the ring, utilizing the maximum jacking screw compressive load, is:

$$F_{a\text{-ring}} = N_b(14,000) = 8(14,000) = 112,000 \text{ lb}_f$$

where:

$F_{a-ring}$  = bounding conservative axial load = 14,000 lb<sub>f</sub>  
 $N_b$  = number of jacking screws = 8

The M.S. for the retaining ring shear load limit is:

$$M.S. = \frac{P_r}{F_{a-ring}} = \frac{119,742}{112,000} - 1 = +.07$$

The groove in the penetration sleeve that the retaining ring sets into must not yield to ensure the lance assembly retains the containment seal. Per Reference [5], the groove allowable shear (thrust) load ( $P_g$ ) limit for the SA-350 Grade LF3 material is:

$$P_g = \frac{\pi D d (S_y)}{SF} = \frac{\pi (7.0)(0.1575)(33,200)}{1} = 114,992 \text{ lb}_f$$

where:

$D$  = penetration sleeve diameter = 7.0 inches  
 $d$  = ring groove depth =  $(7.315 - 7.000)/2 = 0.1575$  inch  
 $S_y$  = yield strength at 300 °F = 33.2 ksi (Table 2.12.12-3)  
 $SF$  = safety factor = 1.0 for normal condition bearing stress

The M.S. against yielding the retaining ring groove under normal conditions is:

$$M.S. = \frac{P_g}{F_{a-ring}} = \frac{114,992}{112,000} - 1 = +.03$$

### 2.12.12.3 Thermocouple Lance Oversheath

Because the oversheath forms a boundary between the payload cavity and the environment, the Inconel oversheath is considered part of the containment boundary of the TN-32B HBU demonstration cask.

#### 2.12.12.3.1 Lateral Displacement of Fuel/Basket

Since the thermocouple lance is secured in the closure lid, there is a possibility of relative lateral movement between a fuel assembly and the basket with the fixed lance assembly. This condition may occur when the cask is subjected to a 30-foot HAC side drop.



To analyze this condition, an ANSYS® model of the thermocouple lance assembly, including the overshield, was created, as shown in Figure 2.12.12-5. The following material properties for the [ ] at 400 °F [2] were utilized in the model. The higher temperature is to conservatively account for a higher temperature in the top nozzle of the fuel assembly than in the lance body/closure lid area.

Young's Modulus [ ]  
 Poisson's Ratio  $\mu = 0.31$   
 Density  $\rho =$  [ ]  
 Class 1 Allowable Stress [ ]  
 Minimum Ultimate Strength [ ]  
 Minimum Yield Strength [ ]

A lateral displacement of [ ] of the overshield was applied at a free distance of [ ] from the lance body surface to the top nozzle of the fuel assembly (FA) where the lance reinforcing overshield contacts the fuel assembly. As specified on the drawings in Appendix 1.4.1 and for a maximum fuel assembly length of [ ] the free distance from the fixed joint on the lance body is determined as follows:

Lower surface of closure lid = 5.00 inches  
 Minimum gap between closure lid and top of FA = [ ]  
 Distance from FA top nozzle to FA top nozzle corner post = [ ]  
 Distance from top of FA spring elevation to top nozzle corner post = [ ]  
 Distance between lance body and first lateral FA supporting plate = [ ]

The [ ] lateral displacement is the resultant maximum deflection of the top of a basket cell with a fuel assembly from a 55g side drop of the cask. This impact is conservative since the maximum impacts for the cold side and slap down drops presented in Appendix 2.12.9 is 44.6g. For this case, the maximum stress intensity in the reinforcing overshield from ANSYS® model is [ ] as illustrated in Figure 2.12.12-6 and Figure 2.12.12-7. The ASME B&PV Class 1 (membrane + bending) allowable stress for accident conditions is equal to the minimum ultimate strength  $S_u$ . The resultant M.S. for the lance reinforcing overshield is:

## 2.12.12.3.2 Deep Immersion

For the thermocouple lance assembly, the containment boundaries that would be exposed to the 290 psig external pressure, as required by 10 CFR 71.61, are the lower closure plug and the thermocouple lance oversheath. Assuming both the lower closure plug and lance oversheath are exposed to this external pressure conservatively ignores the upper closure plug that seals the body and the lance cavity above these components.

Assuming the inner cavity was pressurized to the 290 psig pressure, the hoop stress ( $\sigma_\theta$ ) and the longitudinal stress ( $\sigma_2$ ) for the oversheath treated as a thin-walled cylinder will be:

where:

$p$  = immersion pressure = 290 psig  
 $D$  = oversheath outer diameter = [                      ]  
 $D_m$  = oversheath mean diameter =  $D - t =$  [                      ]  
 $T$  = wall thickness = [                      ]

The stress intensity (S.I.) for these internal pressure stresses is:

From Table 2.12.12-3, the allowable stress intensity ( $S_m$ ) for the Inconel at 500 °F is 23.3 ksi. The M.S. against failure is:

[ ] With a lance oversheath outer diameter (D) and thickness (t) of [ ] respectively, and again treating the oversheath as a thin-walled cylinder, the weld area ( $A_{tip}$ ) is:

The tensile stress ( $\sigma_w$ ) in the tip weld due to the 290 psig internal pressure is:

For the SB-166 Inconel (UNS N06600) material at 500 °F, the HAC allowable tensile stress is the lessor of  $2.4S_m$  or  $0.7S_u$ . Since  $2.4S_m = 55.9$  ksi is less than  $0.7S_u = 56$  ksi, the allowable stress is  $0.7S_u = 55.9$  ksi. Therefore, the resultant M.S. for the tip circumferential weld joint is then:

Since all M.S. are positive, the thermocouple lance assembly satisfies the requirements of 10 CFR 71.61.

#### 2.12.12.4 Lance Seal Lateral Displacement Test

The lance assembly seal lateral displacement test [6] was conducted in order to demonstrate that the containment seal maintained its leak tightness when subject to a 30-foot side drop impact. The two objectives of this test were:

1. To determine the maximum lateral force to initiate sliding of the lance body/metallic O-ring seal, and
2. To determine the leak tightness of the metallic O-ring seal should sliding of the lance body occur.

The setup consisted of a prototypic thermocouple lance assembly with a metallic O-ring seal, and a prototypic lance closure (e.g., jacking screws, compression plate, bearing plate retaining ring) that were installed in a modified prototypic penetration sleeve. The modification to the penetration sleeve, which is shown in Figure 2.12.12-8, was to provide access for the lance closure contact plate to apply the lateral force to the lance body. The test setup, including a helium mass spectrometer leak detector (MSLD), is shown in Figure 2.12.12-9.

To replicate the installed condition of the TLAs in the cask, the test setup was heated to 230 °F, which bounds the NCT closure lid hot temperature, and installed the TLA towards the top of the penetration sleeve to replicate the maximum possible lateral displacement, as shown in Figure 2.12.12-10. Prior to initiating the displacement test, a leakage rate test of the TLA containment boundary was performed utilizing an evacuated envelope in accordance with American National Standards Institute (ANSI) N14.5 [7]. The measured leakage rate was  $<1 \times 10^{-7}$  ref cm<sup>3</sup>/sec, which confirmed that the assembly was leaktight per ANSI N14.5.

As the lateral force was applied to the lance body, gaps between all of the components in the test setup were closed, which occurred between 0 and 0.04 inches of displacement. At this displacement, the recorded force was approximately [ ] a linear displacement [ ] was recorded. Beyond [ ] the displacement steadily increased as additional force was applied. The test continued up to a maximum displacement of 0.65 inch, which resulted in a maximum applied force of [ ] The applied load versus displacement data is graphically presented in Figure 2.12.12-11.

Following the end of the test, a post-test helium leakage rate test of the containment boundary was attempted. However, the MSLD could not establish a vacuum, which indicated that a leak path was present. As part of the troubleshooting, the tightness of the jacking screws was then checked, and found that the upper three screws [ ] were loosened slightly. The remaining five jacking screws were found to be tight. After re-tightening the three jacking screws, second attempt to perform a post-test leakage rate test of the TLA was made. However, the MSLD could still not establish a vacuum, so that effort was abandoned.

After the TLA was disassembled, it was evident that damage had occurred to the lower edge of the stainless steel lance body, the outer O-ring (non-containment) seal, and the stainless steel sealing surface in the penetration sleeve. The damage to these components is shown in Figure 2.12.12-12, Figure 2.12.12-13, and Figure 2.12.12-14. The lack of damage to the inner containment O-ring, which was [ ] from the outer O-ring, indicates a lack of contact with the damaged sealing surface. Subsequent measurement of the sealing surface damage revealed that the damage occurred over a radial segment of approximately 30° with a maximum width of approximately [ ] as shown in Figure 2.12.12-15, which was approximately [ ] of the total circumferential contact area.

From the observed sealing surface and seal damage, and the slight loss of compression in the upper three jacking screws, it was apparent that the lance body had tilted towards the bottom edge when sufficient force was applied to the lance body to laterally slide. The most likely reason for this test result was that the penetration sleeve sealing surface was not absolutely parallel with the vertical axis of the test machine, which would result in an applied force perpendicular to the sealing surface.

#### 2.12.12.5 Conclusions

- A lance assembly jacking screw tightening torque range of 60 to 70 lb<sub>r</sub>-ft is utilized to achieve the desired preload.
- For the minimum preload, a positive (compressive) load is maintained on the TLA and containment O-ring seal during all NCT and HAC load combinations.
- The TLA will not slide in the penetration sleeve under the worst-case, postulated 30-foot side drop orientation. Therefore, the sealing surface and the metallic containment seal will remain in its leaktight, as-loaded condition.
- The M.S. for all containment boundary welds of the lance assembly remain positive for all worst-case load conditions.

#### 2.12.12.6 References

1. G. Mok C., L. Fischer E., S. Hsu T., "Stress Analysis of Closure Bolts for Shipping Casks," NUREG/CR-6007, UCRL-ID-110637, U.S. Nuclear Regulatory Commission, January 1993.
2. American Society of Mechanical Engineers, ASME Boiler and Pressure Vessel Code, Section II Part D, and Appendix, 2013.
3. HELICOFLEX® Spring Energized Seal Catalog, Technetics Group, EnPro Industries Companies.
4. C. F. Magnuson, L.T. Wilson, "Shock and Vibration Environments for Large Shipping Containers on Rail Cars and Trucks," NUREG766510, U.S. Nuclear Regulatory Commission, June 1977.
5. Smalley Steel Spring Company, Medium Heavy Duty, 3-Turn Spirolox Retaining Ring, Part Number WHT-700-S16, [www.smalley.com](http://www.smalley.com).
6. Framatome Inc., "HBU Closure Seal Performance Test Results," Document No. 51-9318617-000, October 2020.
7. ANSI N14.5-2014, "Leakage Tests on Packages for Shipment of Radioactive Materials," American National Standards Institute (ANSI), Inc.
8. American Society of Mechanical Engineers, Unified Inch Screw Threads, UN and UNR thread Form, ASME B1.1-2003.

**Table 2.12.12-1**  
**Design Parameters for Lance Jacking Screw Analysis**

- $D_b$  Nominal diameter of jacking screw, 0.625 inch
  - $K$  Nut factor for empirical relation between the applied torque and achieved preload is 0.127 for N-5000
  - $Q$  Applied tightening torque for the preload (lb<sub>r</sub>-in)
  - $D_{lb}$  Jacking plate at screw circle, 5.29 inches
- 
- $N_b$  Total number of jacking screws per lance assembly, 8
  - $P_{li}$  Internal pressure inside the cask cavity, 100 psig
  - $P_{lo}$  Pressure outside the lance assembly, assume 0 psig

**Table 2.12.12-2**  
**Jacking Screw Data**

Parameters necessary to utilize formulas of Reference [1], Table 5.1.

- Screw: 5/8 – 18UNF – 2A
- N: No. of threads per inch = 18
- p: Pitch = 1/18 in = .056 inch
- D<sub>b</sub>: Nominal diameter = 0.625 inch
- D<sub>ba</sub>: Screw thread diameter for stress calculations =  $D_b - 0.9743p = 0.571$  in
- A<sub>js</sub>: Screw thread tensile stress area =  $(\pi/4)(D_{ba})^2 = 0.256$  in<sup>2</sup>
- Internal thread shear stress area for a 5/8-18UNF thread = 1.367 in<sup>2</sup>/inch [8]



**Table 2.12.12-3**  
**Lance Assembly Material Properties at 300 °F**

<b>Component</b>	<b>Material</b>	<b>Ultimate Strength <math>S_u</math> (ksi)</b>	<b>Yield Strength <math>S_y</math> (ksi)</b>	<b>Allowable Strength <math>S/S_m</math> (ksi)</b>	<b>Young's Modulus <math>E</math> (psi)</b>	<b>Thermal Expansion (in/in/°F)<sup>(2)</sup></b>
Jacking Screws	SA-193, Grade B7	125.0	94.1	25.0/62.7 <sup>(3)</sup>	$28.5 \times 10^6$	$7.3 \times 10^{-6}$
Jacking and Compression Plates	SA-387, Grade 91, Class 2	85.0	54.8	24.3/28.3	$29.7 \times 10^6$	$6.5 \times 10^{-6}$
Lance Body & Upper Closure Plug	SA-479 Type 304/304L	66.2	22.4	15.0/20.0	$27.0 \times 10^6$	$9.9 \times 10^{-6}$
Penetration Sleeve	SA-350, Grade LF3	70.0	33.2	20.0/22.1	$26.7 \times 10^6$	$7.3 \times 10^{-6}$
Thermocouple Lance Sheath						
Thermocouple Lance Lower Closure & Tip Plugs						

Notes:

1. All material properties are provided from Reference [2], unless otherwise specified.
2. Instantaneous coefficients (conservative).
3. Defined as  $2/3S_y$  per Reference [1].
4. Material properties for the SB-163 and SB-166 annealed materials are provided for 500 °F to account for the higher temperature environment in a spent fuel assembly that surrounds the thermocouple lance sheath.

**Table 2.12.12-4**  
**Normal Condition Allowable Stresses in Jacking Screws**

Temperature (°F)	Yield Stress <sup>(1)</sup> (ksi)	Normal Condition Allowables		
		$F_{tb}$ <sup>(2)</sup> (ksi)	$F_{vb}$ <sup>(3)</sup> (ksi)	S.I. <sup>(4)</sup> (ksi)
100	105.0	70.0	42.0	94.5
200	98.0	65.3	39.2	88.2
300	94.1	62.7	37.6	84.6
400	91.5	61.0	36.6	92.4

## Notes:

1. Yield ( $S_y$ ) stress values are from Reference [2].
2. Allowable tensile stress,  $F_{tb} = S_m = 2/3(S_y)$  from Reference [1].
3. Allowable average shear stress,  $F_{vb} = 0.6S_m$  from Reference [1].
4. Stress intensity from combined tensile, shear and residual torsion loads,  
 $S.I. < 1.35S_m$  [1].

**Table 2.12.12-5**  
**Accident Condition Allowable Stresses in Lance Jacking Screws**

Temperature (°F)	Yield Stress <sup>(1)</sup> (ksi)	Accident Condition Allowables		
		0.6S <sub>y</sub> <sup>(3)</sup> (ksi)	F <sub>tb</sub> <sup>(2,4)</sup> (ksi)	F <sub>vb</sub> <sup>(3,4)</sup> (ksi)
100	105.0	63.0	97.5	52.5
200	98.0	58.8	97.5	52.5
300	94.1	56.5	94.1	52.5
400	91.5	54.9	91.5	52.5

Notes:

1. Yield (S<sub>y</sub>) and ultimate (S<sub>u</sub>) stress values are from Reference [2]. Note that S<sub>u</sub> is 125 ksi at all temperatures of interest.
2. Allowable tensile stress, F<sub>tb</sub> = min (0.7S<sub>u</sub>, S<sub>y</sub>), where 0.7S<sub>u</sub> = 0.7(125) = 87.5 ksi from Reference [1].
3. Allowable average shear stress, F<sub>vb</sub> = min (0.42S<sub>u</sub>, 0.6S<sub>y</sub>), where 0.42S<sub>u</sub> = 0.42(125) = 52.5 ksi from Reference [1].
4. Tension and shear stresses must be combined using the following interaction equation:

$$\frac{\sigma_{tb}^2}{F_{tb}^2} + \frac{\tau_{yb}^2}{F_{yb}^2} \leq 1.0 \quad [1]$$

**Table 2.12.12-6**  
**Normal Condition Allowable Stresses in Jacking & Compression Plates**

Temperature (°F)	Yield Stress <sup>(1,2)</sup> (ksi)	Allowable Stress $S_m$ (ksi)	Normal Condition Allowables		
			$F_{tb}$ <sup>(3)</sup> (ksi)	$F_{vb}$ <sup>(4)</sup> (ksi)	S.I. <sup>(5)</sup> (ksi)
100	60.0	35.4	35.4	21.2	53.1
200	55.9	35.4	35.4	21.2	53.1
300	54.8	35.4	35.4	21.2	53.1
400	54.7	35.4	35.4	21.2	53.1

Notes:

1. Yield ( $S_y$ ) stress values are from Reference [2]. Note that  $S_u$  is 85 ksi at all temperatures of interest.
2. Allowable bearing stress,  $F_{br} = S_y$  [2]
3. Allowable tensile stress,  $F_{tb} = S_m$  [2]
4. Allowable shear stress,  $F_{vb} = 0.6S_m$  [2]
5. Allowable stress intensity S.I. =  $1.5S_m$  [2]

**Table 2.12.12-7**  
**Accident Condition Allowable Stresses in Jacking Plate Internal Screw Threads**

Temperature (°F)	Yield Stress <sup>(1)</sup> (ksi)	Accident Condition Allowables		
		0.6S <sub>y</sub> <sup>(3)</sup> (ksi)	F <sub>tb</sub> <sup>(2)</sup> (ksi)	F <sub>vb</sub> <sup>(3)</sup> (ksi)
100	60.0	36.0	59.5	35.7
200	55.9	33.5	55.9	33.5
300	54.8	32.9	54.8	32.9
400	54.7	32.8	54.7	32.8

Notes:

1. Yield (S<sub>y</sub>) and ultimate (S<sub>u</sub>) stress values are from Reference [2]. Note that S<sub>u</sub> is 85 ksi at all temperatures of interest.
2. Allowable average tensile stress, F<sub>tb</sub> = min (0.7S<sub>u</sub>, S<sub>y</sub>) , where 0.7S<sub>u</sub> = 0.7(85) = 59.5 ksi per Reference [1].
3. Allowable average shear stress, F<sub>vb</sub> = min (0.42S<sub>u</sub>, 0.6S<sub>y</sub>), where 0.42S<sub>u</sub> = 0.42(85) = 35.7 ksi from Reference [1].
4. Tension and shear stresses must be combined using the following interaction equation:

$$\frac{\sigma_{tb}^2}{F_{tb}^2} + \frac{\tau_{yb}^2}{F_{yb}^2} \leq 1.0 \quad [1]$$

Proprietary Information on This Page  
Withheld Pursuant to 10 CFR 2.390

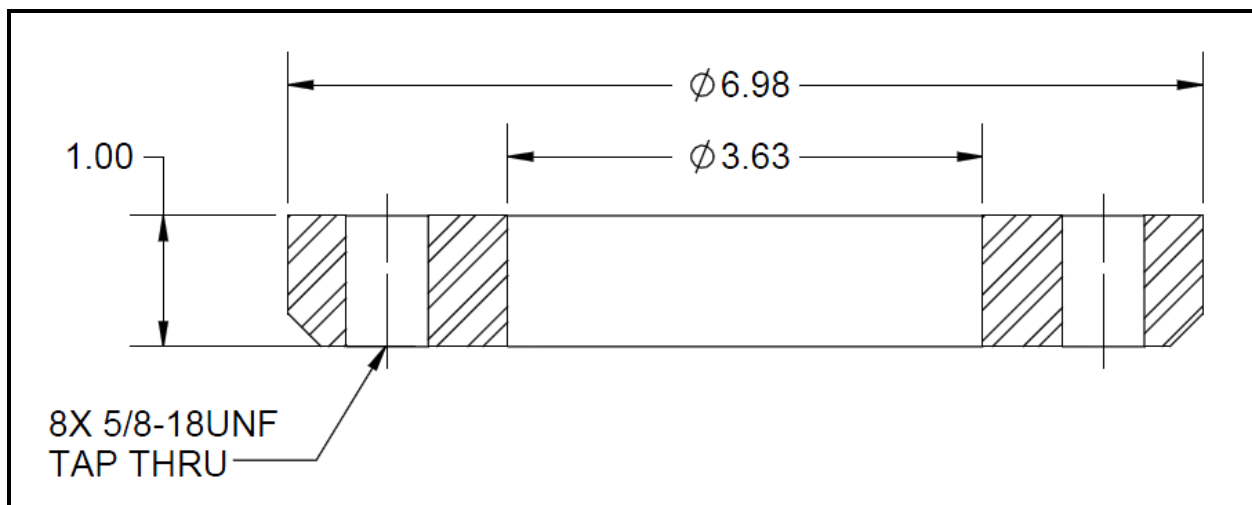


**Figure 2.12.12-2**  
**Lance Jacking Plate Cross-Section**

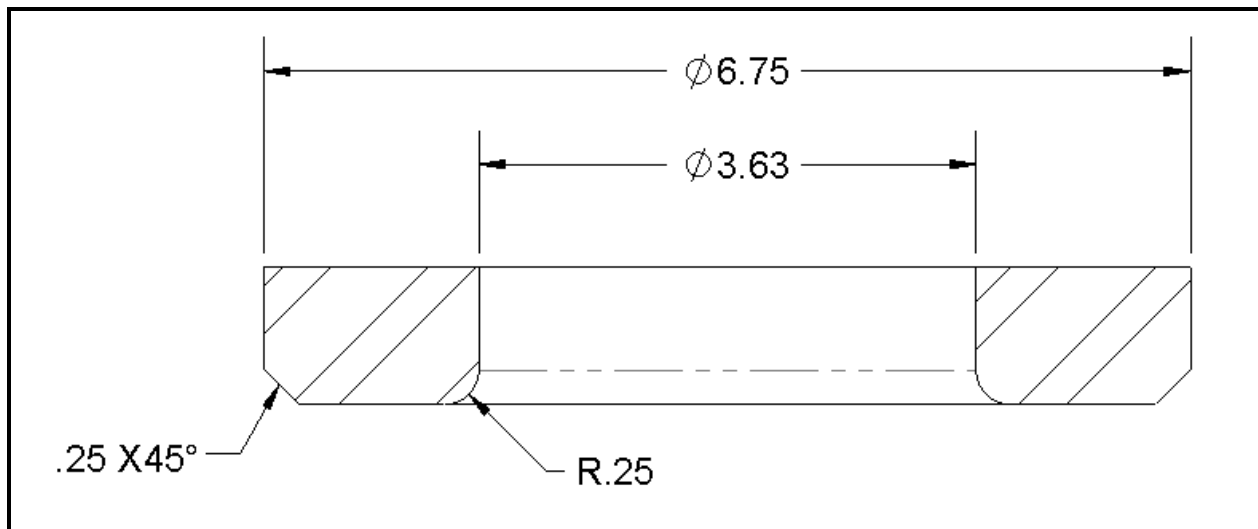


**Figure 2.12.12-3**  
**Lance Compression Plate Cross-Section**



Proprietary Information on Pages 2.12.12-28 through 2.12.12-31  
Withheld Pursuant to 10 CFR 2.390

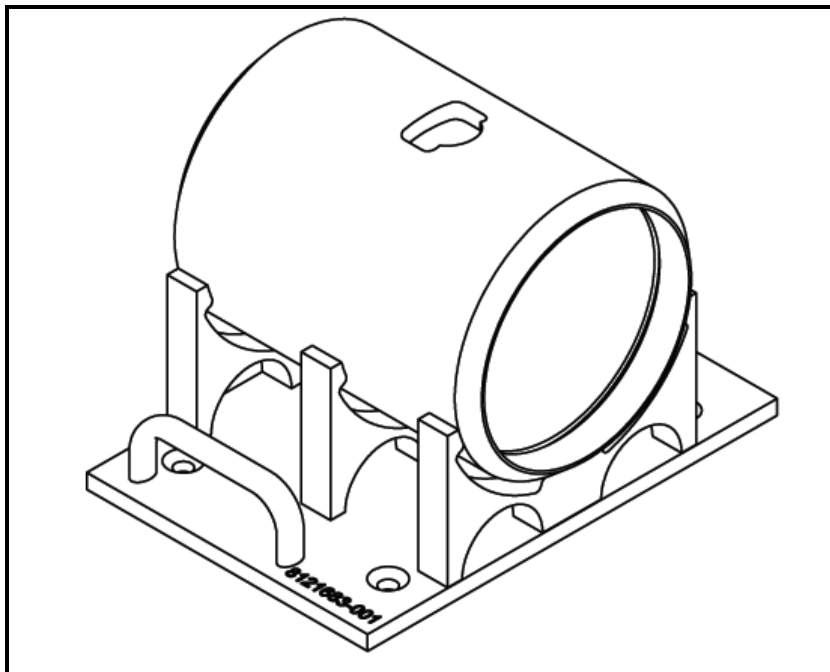


**Figure 2.12.12-8**  
**Modified Penetration Sleeve on Test Stand**

Proprietary Information on Pages 2.12.12-33 through 2.12.12-37  
Withheld Pursuant to 10 CFR 2.390

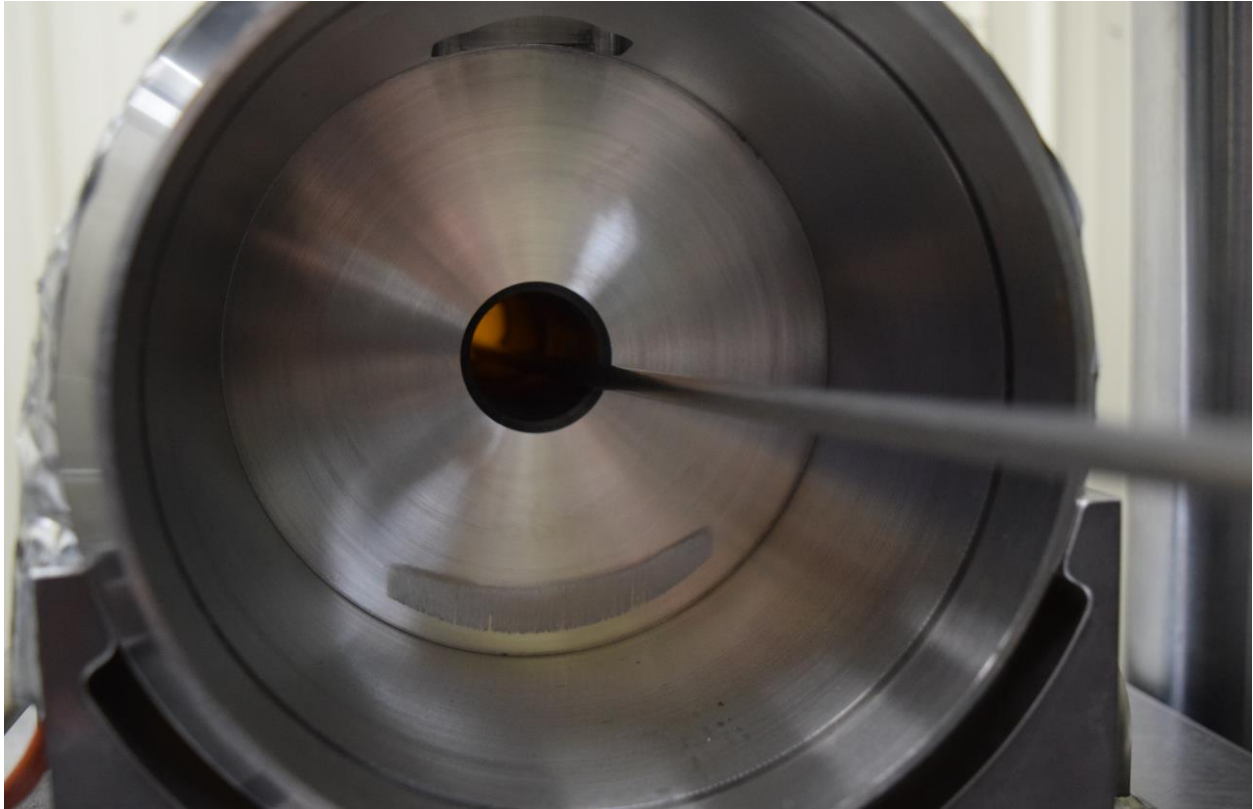


**Figure 2.12.12-14**  
**Damage to Penetration Sleeve Sealing Surface**

Proprietary Information on This Page  
Withheld Pursuant to 10 CFR 2.390

### Appendix 2.12.13 ASME B&PV Code Alternatives

Both the cask containment boundary and basket are designed, fabricated, and inspected in accordance with the ASME B&PV Code, Subsection NB, to the maximum practical extent. The gamma shielding, which is primarily for shielding, but also provides structural support to the containment boundary during NCT and HAC events, was designed in accordance with Subsection NF of the code. Inspections of the gamma shielding are performed in accordance with ASME B&PV Code, Subsection NF. Other cask components, such as the outer shell and the neutron shielding, are not governed by the ASME B&PV Code.

Component	Reference ASME Code/Section	Code Requirement	Alternatives, Justification & Compensatory Measures
TN-32B HBU Cask	NB-1100/Subsection NCA, NB-2000	Stamping and preparation of reports by the Certificate Holder, Surveillances, Use of ASME Certificate Holders	The TN-32B HBU demonstration cask is not N/TP stamped, nor is there a code design specification or stress report generated. A design criteria document is generated in accordance with TN's QA Program and the design and analysis is performed under TN's QA Program and presented in the SAR. The cask may also be fabricated by other than N-stamp holders and materials may be supplied by other than ASME Certificate holders. Surveillances are performed by TN and utility personnel rather than by an Authorized Nuclear Inspector (ANI).
TN-32B HBU Cask	NCA-3800	QA Requirements	The quality assurance requirements of NQA-1 or 10 CFR 71 are imposed in lieu of NCA-3800 requirements.
Pressure Test of the Containment Boundary	NB-6200	Hydrostatic Testing	The containment vessel is hydrostatically tested in accordance with the requirements of the ASME B&PV Code, Section III, Article NB-6200 with the exception that some of the containment vessel is installed in the gamma shield shell during testing. The containment vessel is supported by the gamma shield during all design and accident events.
Weld of bottom inner containment plate to the containment shell	NB-5231	Full penetration corner welded joints require the fusion zone and the parent metal beneath the attachment surface to be UT after welding.	The required UT inspection was performed on a best efforts basis. The joint was examined by both RT and MT methods in accordance with ASME Subsection NB requirements.

Component	Reference ASME Code/Section	Code Requirement	Alternatives, Justification & Compensatory Measures
Containment Shell Rolling Qualification	NB-4213	The rolling process used to form the inner vessel should be qualified to determine that the required impact properties of NB-2300 are met after straining by taking test specimens from three different heats.	The two plates that were utilized for the containment shell were of the same heat, which were tested to verify the impact properties.
Containment Vessel Material	NB-2120	Materials to be ASME Class 1 material	Standard Review Plan, NUREG-1536 has accepted the use of either Subsection NB (Class 1) or NC (Class 2 or 3) of the Code for the containment. SA-203 Grade D is similar to SA-203 Grade E, which is a Class 1 material. The chemical content of the two grades are identical, except that Grade E restricts the carbon to 0.20 max., while Grade D further restricts the carbon content to 0.17 max. Grade D is acceptable as a Class 2 material up to 500 °F. Grade D was selected because of its ductility, since the higher strength is not required. SA-203 Grade D has better elongation than Grade E and due to its lower strength, is more likely to have the good fracture toughness at low temperatures. In selecting materials for storage and transport casks, one of the major selection criteria is fracture toughness at low temperatures. Grade D was selected on this basis. There is no similar requirement for pressure vessels, as they are used at much higher temperatures.
Weld of Shield Plate to Closure Lid Plate	NB-4335	Impact testing of weld and heat affected zone of lid to shield plate	If two different materials are joined, the fracture toughness requirements of either may be used for the weld metal. There are no fracture toughness requirements on the shield plate, and therefore, none are performed on the base metal or the heat affected zones. This weld is not subject to low temperatures, as it is inside the cask cavity. An evaluation of this weld at low temperatures is presented in Appendix 2.12.5.

Component	Reference ASME Code/Section	Code Requirement	Alternatives, Justification & Compensatory Measures
Containment Vessel and Lid Penetration Cover Materials	NB-2000	Requires materials to be supplied by ASME approved material supplier; Quality assurance to meet NCA requirements.	Material supplied by TN-approved suppliers with Certified Material Test reports (CMTR) in accordance with NB-2000 requirements. The cask is not code stamped. The quality assurance requirements of NQA-1 or 10 CFR 71 are imposed in lieu of the requirements of NCA-3800.
Gamma Shielding	NB-1132.2	Non-pressure retaining structural attachments shall conform to Subsection NF.	The primary function of the gamma shield is shielding, although credit is taken for the gamma shielding in the structural analysis. The welds are examined in accordance with NF acceptance criteria. A fracture toughness evaluation is presented in Appendix 2.12.5.
Gamma Shielding	NB-2190	Material in the component support load path and not performing a pressure retaining function welded to pressure retaining material shall meet the requirements of NF-2000.	The gamma shielding materials were procured to ASTM or ASME material specifications. Material testing is performed in accordance with the applicable specification. Impact testing is not performed on the gamma shielding materials (including welding materials). An evaluation of the gamma shielding due to impact at low temperatures is provided in Appendix 2.12.5.
Closure Lid & Flange	NB-4121.3	Repetition of surface examination after machining.	Recommended fracture arrest criteria for the closure lid and flange is demonstrated in Appendix 2.12.5. Additionally, the containment flange and the lid were procured with both a UT and MT examination.
Basket	NB-4000 NF-5000	Fabrication/Welding/ NDE inspection	Basket fabrication and welding procedures are qualified in accordance with ASME Section IX. Due to the unique nature of these basket and welds, special inspections and tests were developed for these welds.
Basket neutron poison material	NB-2000	Use of ASME Materials	The basket neutron poison material is not used for structural analysis, but to provide criticality control and heat transfer. They are not code materials.



Component	Reference ASME Code/Section	Code Requirement	Alternatives, Justification & Compensatory Measures
Aluminum used for basket rails, aluminum plates between the compartments, and aluminum plates at the basket periphery	NB-2000	Use of ASME Materials	The aluminum plate is not a Class 1 material. It was selected for its properties. Aluminum has excellent thermal conductivity and a high strength to weight ratio. NUREG-3854 and NUREG-1617 allow materials other than ASME Code materials to be used in the cask and basket fabrication. ASME Code does provide the material properties for the aluminum and also allows the material to be used for Section III applications (Class 2 and 3). Note: $S_m$ and $S$ values for aluminum are taken from ASME Code Section VIII, Division 2 [23]. $S$ is extracted from Section III or the lower of $S_{II}/4$ or $2/3 S_y$ . Aluminum material properties at elevated temperatures are taken from "Aluminum Standards and Data" [12].
Basket buckling analysis	ASME Section III, Appendix F-1341.4	Applied load shall not exceed $0.7 P_L$	Factors of safety are used to account for geometrical imperfections, residual stresses, load eccentricity, and modeling assumptions. The buckling analyses reported in Section 2.12.6.3 have a minimum safety factor of 1.82 (93/51). The analyses modeled a full 360-degree sector of the basket with elastic-plastic material and large deflection effects. Additionally, the analyses also utilized a conservative value for the fuel weight. The results demonstrated a safety factor of 1.82 with respect to the design load of 51g. These analyses demonstrate the basket to be structurally adequate.
Penetration sleeve to closure lid weld	Subsection NB	Category C weld joints in vessels and similar weld joints in other components shall be a full penetration joint. These welds shall be examined by UT or radiographic testing (RT) and either PT or magnetic particle testing (MT)	As an alternative to the Category C full penetration weld per the 1992 edition of the ASME III Code, these welds were multi-layer partial penetration welds as allowed by more recent editions of the Code, e.g., 2013 edition. NDE was a PT examination for each weld layer in accordance with NUREG-1536 Revision 1. The multi-level PT examination provides reasonable assurance that flaws of interest were identified. The PT examination was performed by qualified personnel, in accordance with Section V and the acceptance standards of Section III, Subsection NB-5000. The penetration sleeve-to-lid welds were designed to meet the guidance provided in Section 8.4.7.3 of NUREG-1536 Revision 1, for stress reduction factor.

Component	Reference ASME Code/Section	Code Requirement	Alternatives, Justification & Compensatory Measures
<p>Thermocouple Lance Assembly</p> <ul style="list-style-type: none"><li>• Lance body to lower closure plug weld</li><li>• Reinforcing overshield to lower closure plug weld</li><li>• Reinforcing overshield to overshield</li><li>• Overshield to tip plug</li></ul>	<p>NB-3000 NB-5000</p>	<p>Category D weld joints in vessels shall be a full or partial penetration joint. These welds shall be examined by either liquid particle testing (PT) or magnetic particle testing (MT)</p>	<p>All containment boundary welds were inspected utilizing the PT NDE method. The acceptance criteria for these welds exceeded the acceptance standards of Subsection NB-5352.</p>

### **Chapter 3**

### **Thermal Evaluation**

#### TABLE OF CONTENTS

3.1	Description of Thermal Design .....	3-2
3.1.1	Design Features .....	3-2
3.1.2	Content's Decay Heat .....	3-2
3.1.3	Summary Tables of Temperatures .....	3-4
3.1.4	Summary Tables of Maximum Pressures .....	3-4
3.2	Material Properties and Component Specifications .....	3-5
3.2.1	Material Properties .....	3-5
3.2.2	Component Specifications .....	3-6
3.3	Thermal Evaluation under Normal Conditions of Transport .....	3-18
3.3.1	Heat and Cold .....	3-18
3.3.2	Maximum Normal Operating Pressure .....	3-30
3.4	Thermal Evaluation under Hypothetical Accident Conditions .....	3-31
3.4.1	Initial Conditions .....	3-31
3.4.2	Fire Test Conditions .....	3-31
3.4.3	Maximum Temperatures and Pressure .....	3-32
3.4.4	Maximum Thermal Stresses .....	3-33
3.4.5	Accident Conditions for Fissile Material Packages for Air Transport .....	3-33
3.5	References .....	3-34
3.6	Appendix .....	3-61

#### LIST OF TABLES

Table 3-1	NCT Component Temperatures in the TN-32B HBU Cask .....	3-36
Table 3-2	HAC Temperatures for TN-32B HBU Cask .....	3-37

LIST OF FIGURES

Figure 3-1	NCT Hot (100 °F Ambient) Temperatures Distribution for TN-32B HBU Cask .....	3-38
Figure 3-2	NCT Hot (100 °F Ambient) Peak Cask Temperature Cross-Section.....	3-39
Figure 3-3	NCT Hot (100 °F Ambient) Neutron Shield Resin Temperature Profile.....	3-40
Figure 3-4	NCT Hot (100 °F Ambient) Wood Temperature Profile.....	3-41
Figure 3-5	NCT Hot (100 °F Ambient) Aluminum Cask Rails Temperature Profile .....	3-42
Figure 3-6	TN-32B HBU Model Mesh – Side View .....	3-43
Figure 3-7	TN-32B HBU Cask Mesh – End View .....	3-44
Figure 3-8	TN-32B HBU Impact Limiter Mesh – End View .....	3-45
Figure 3-9	TN-32B HBU Cask Homogenized Basket Cross Section .....	3-46
Figure 3-10	TN-32B HBU Surfaces with Solar – Rotated View.....	3-47
Figure 3-11	NCT Hot (100 °F Ambient) Peak Basket Temperature at Max Cross Section.....	3-48
Figure 3-12	NCT Hot (100 °F Ambient) Neutron Shield Boxes Temperature Profile.....	3-49
Figure 3-13	NCT Cold (-20 °F Ambient) Package Temperature Profile .....	3-50
Figure 3-14	Side View – TN-32B HBU Cask Model with Impact Limiter Damage .....	3-51
Figure 3-15	End View – TN-32B HBU Cask Model with Impact Limiter Damage.....	3-52
Figure 3-16	Wood Areas Exposed to Char Immediately after 30-minute Fire .....	3-53
Figure 3-17	TN-32B HBU Cask HAC Temperature Distribution at End of 30 Minute Fire .....	3-54
Figure 3-18	TN-32B HBU Cask HAC Temperature Distribution at End of 30 Minute Post-Fire Smolder .....	3-55
Figure 3-19	TN-32B HBU Cask HAC Temperature Distribution at End of 40 Hour Cool Down (Follows 30-minute fire and 30-minute smolder) .....	3-56
Figure 3-20	TN-32B HBU Cask HAC Maximum Fuel Temperature History .....	3-57
Figure 3-21	TN-32B HBU Cask HAC Maximum Cask Component Temperature History .....	3-58
Figure 3-22	TN-32B HBU Cask HAC Maximum Seals Temperature History .....	3-59
Figure 3-23	TN-32B HBU Cask HAC Inner Shell Temperature History .....	3-60

### **Chapter 3**

## **Thermal Evaluation**

This chapter identifies and describes the principle thermal design aspects of the TN-32B high burnup (HBU) demonstration cask. Further, this chapter presents the evaluations that demonstrate the thermal safety of the TN-32B HBU demonstration cask, and compliance with the thermal requirements of 10 CFR 71 [1] when transporting the HBU spent fuel assembly payload with a maximum of 25.84 kW of decay heat. Specifically, all cask components are demonstrated to remain within their respective temperature limits under the design basis normal conditions of transport (NCT), and the hypothetical accident conditions (HAC) of transport.

The cask is demonstrated to structurally withstand the damage arising from the HAC free drop scenarios and retain sufficient thermal protection to maintain all cask component temperatures within their short-term limits during the regulatory fire event and the post-fire test cool down period.

Objectives of the thermal analyses performed for this evaluation include:

- Determination of maximum and minimum temperatures with respect to cask materials limits to ensure components perform their intended safety functions
- Determination of temperature distributions to support the calculation of thermal stresses
- Determination of the cask cavity gas temperature to support containment pressure calculations
- Determination of the maximum fuel cladding temperature

Chapter 2 presents the principal design bases for the TN-32B HBU demonstration cask.

### 3.1 Description of Thermal Design

The TN-32B HBU demonstration cask, as illustrated in Figure 1-1 in Chapter 1, is designed to passively reject decay heat under NCT and HAC while maintaining packaging temperatures and pressures within specified limits.

#### 3.1.1 Design Features

The design features of the TN-32B HBU basket are described in Section 1.2.1.5. The basket is a welded assembly of stainless steel fuel compartment boxes separated by aluminum and borated aluminum (poison) plates that form a sandwich panel. The center panels consist of two 0.50-inch thick aluminum plates that sandwich a 0.040-inch thick poison plate. In general, the remaining panels consist of stainless steel that sandwich a 0.50-inch thick aluminum plate. The aluminum provides heat conduction paths from the fuel assemblies to the basket peripheral plates. The poison plate provides the necessary criticality control. This method of construction forms a very strong honeycomb-like structure of cell liners that provide compartments for the 32 HBU fuel assemblies. The aluminum basket rails are bolted to the inner shell and provide a conduction path from the basket to the inner shell. These thermal design features of the basket allow the heat generated by the fuel assemblies to be conducted efficiently from the basket to the shell.

A thermal design feature of the cask is the conduction path created by the aluminum boxes that contain the radial neutron shielding material as described in Section 1.2. The neutron shielding material is provided by a resin compound cast into long slender aluminum boxes placed around the gamma shield shell and enclosed within a 1/2-inch thick steel outer shell. The aluminum boxes are designed to fit tightly against the steel shell surfaces, thus improving the heat transfer across the neutron shield.

The design of the steel-encased wood impact limiters is described in Section 1.2. These components are included in the thermal analysis because of their contribution as a thermal insulator. The impact limiters provide protection to the closure lid and bottom regions from the external heat load applied during the HAC thermal event.

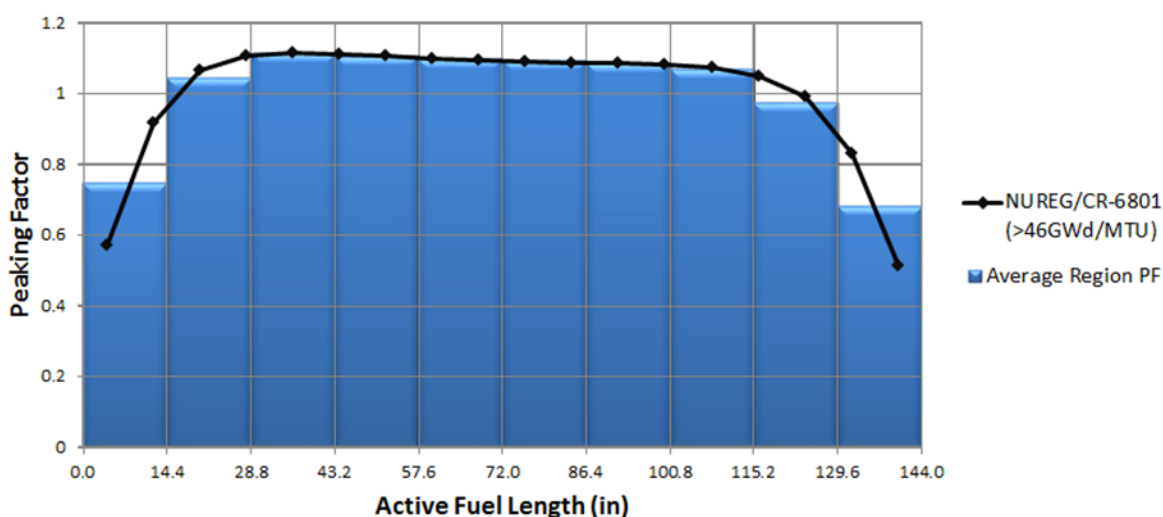
A personnel barrier prevents access to the outer surfaces of the cask body during transport. The barrier, which consists of stainless steel expanded metal attached to a stainless steel frame, will enclose the cask body between the impact limiters, and has an open area of approximately 75%.

#### 3.1.2 Content's Decay Heat

As discussed in Section 1.2.2, the total decay heat load is 25.84 kW from the (32) HBU assemblies (maximum 0.878 kW/assy). The TN-32B HBU demonstration cask geometry is half symmetric about a vertical plane through the centerline of the cask. However, the decay heat load of the fuel loading pattern in the basket is not symmetric about this plane. The maximum element wattage for each corresponding basket location across the symmetry plane is evaluated.

The heat load for each fuel element is deposited over the active fuel length as a volumetric heat generation. Since all the fuel elements in this package have a burn-up greater than 50 GWd/MTU, the axial peaking factors from Table 2 of NUREG/CR-6801 [2] are utilized in this evaluation. This use of the peaking factors is appropriate since the table is applicable for fuel with burn-ups greater than 46 GWd/MTU.

The axial peaking factors are listed with respect to 18 axial data points over a total height of 144 inches (converted from % to inches). A sixth-order polynomial fit is applied to the NUREG/CR-6801 values for interpolation, as illustrated in the figure below as the black data points with interpolated fit. The area under the curve is approximated as the average between adjacent peaking factors over 10 increments of 14.4 inches. The value for the first and last peaking factors (representing 0% and 100% axial height) are not explicitly listed in NUREG/CR-6801, so an approximation based on 90% of the highest and lowest values given in NUREG/CR-6801 are manually iterated until the closest value of the actual power value was achieved. Finally, the average peaking factor is calculated by dividing the area under the curve by the increment length of 14.4 inches.



Axial Height (inches)	>46 GWd/MTU (Polynomial fit)	Area under Power Curve	Average Peaking Factor
0	0.516	10.73	0.745
14.4	0.975	15.03	1.044
28.8	1.113	16.007	1.112
43.2	1.110	15.915	1.105
57.6	1.100	15.814	1.098
72	1.096	15.736	1.093
86.4	1.089	15.619	1.085
100.8	1.080	15.368	1.067
115.2	1.054	14.046	0.975
129.6	0.897	9.773	0.679
144	0.461	-	-

### 3.1.3 Summary Tables of Temperatures

Steady-state thermal analyses were performed utilizing the maximum decay heat load of 25.84 kW, an ambient temperature of 100 °F (38 °C) in still air, and maximum insolation. The temperature distribution within the cask body and basket is shown in Figure 3-1. The temperature distributions as calculated in the fuel assemblies and the neutron shield are shown in Figure 3-2 and Figure 3-3, respectively. The temperature distributions within the impact limiter wood and basket rails are shown in Figure 3-4 and Figure 3-5, respectively. A summary of the calculated cask component temperatures for NCT and HAC are provided in Table 3-1 and Table 3-2, respectively.

### 3.1.4 Summary Tables of Maximum Pressures

The maximum normal operating pressure (MNOP) for the TN-32B HBU cask is 30.5 psig, as calculated in Section 3.3.2 for the bounding NCT condition. For the HAC condition, the maximum cavity pressure is 93.1 psig, as calculated in Section 3.4.3.2. Therefore, the internal pressure of the TN-32B HBU cask will remain below the design pressure of 100 psig when loaded with the HBU fuel assemblies.



## 3.2 Material Properties and Component Specifications

### 3.2.1 Material Properties

The TN-32B HBU demonstration cask is fabricated using nickel alloy steels (predominately SA-350 Gr. LF3 and SA-203 Gr. D) for containment boundary components, carbon steels for gamma shielding components (SA-266 Gr. 2 and SA-516 Gr. 70), and carbon steel for the cask trunnions (SA-105). Neutron shielding is provided by a borated polyester resin compound cast into long, slender aluminum boxes (ASTM B221, 6063-T5) placed around the cask gamma shield shell. It should be noted that the closure lid is modeled as a continuous plate neglecting the detail of the thermocouple penetrations, closure lid bolts (SA-540 Gr. B23, Cl 1), and the vent/drain penetrations. This modeling approach is conservative since the thermal conductivity of the plate material is higher than the helium or bolting material it replaces, and, therefore, maximizes the temperature around the metallic containment O-ring seals and closure lid bolts.

The impact limiter shell is fabricated from stainless steel (ASTM A-240, Type 304). The thermal properties for this material are also cited from the ASME B&PV Code.

The aluminum basket rails (ASTM B221, 6061-T6) secured to the cavity wall provide a conduction path from the basket periphery to the cavity wall. The design of the basket allows the heat from the fuel assemblies to be conducted along the aluminum plates to the basket rails, and to be dissipated to the cavity wall. The basket is constructed as a laminated type structure with homogenized thermal properties. The thermal properties for these materials are cited from the ASME B&PV Code. The thermal properties for temperatures above 400 °F are linearly extrapolated from those at lower temperatures (70 °F to 400 °F). This extrapolation is justified because the thermal data in Figure 3.6.2.0 of Reference [3] illustrates a positive trend for both thermal conductivity and heat capacity for the 6061-T6 aluminum material at higher temperatures.

The aluminum material utilized to create the radial neutron shield boxes is ASTM B-221, 6063-T5 aluminum. These boxes provide a heat conduction path through the outer neutron shield. The thermal properties for these materials are cited from the ASME B&PV Code. The thermal properties for temperatures above 400 °F are linearly extrapolated from those values at lower temperatures (i.e., 70 °F to 400 °F). This extrapolation is appropriate since Figure 3 of Reference [4] illustrates that the thermal conductivity of 6063-T5 aluminum material remains relatively constant up to approximately 1,076 °F (580 °C).

The HBU payload is supported by a fuel basket inside the cask. The basket consists of an assembly of 32 stainless steel (SA-240 Type 304) fuel compartments with aluminum and borated aluminum (poison) plates sandwiched between them. The compartments are plug-welded together to form the basket. The thermal properties of the layered basket plates are homogenized to simplify the analytical model, as shown in Figure 3-9.

The spent fuel assembly thermal properties are also homogenized across the full cross section of each individual basket compartment when filled with helium for ease of computation.

Redwood and balsa wood blocks encased in the stainless steel impact limiters are modeled as a homogenized region containing bounding material properties. The minimum bounding conductivity value for moisture content of 0% and specific gravity of 0.08 is  $k_{\min}=0.0019$  BTU/hr-in-°F [5]. A low thermal conductivity value is selected to conservatively reduce heat transfer out of the impact limiter during NCT evaluations.

Wood thermal conductivity varies as a function of HAC time and event. The range of wood thermal conductivities considered is 0.0657 to 0.1768 Btu/hr-in-°F [5] during pre-fire NCT and cool-down period to reduce heat transfer out of the cask. The maximum wood thermal conductivity of 0.0379 Btu/hr-in-°F [5] is used during the 30-minute fire and wood char period immediately after the fire to maximize heat transfer into the cask. The elevated temperature of the charred wood maximizes heat flow into the cask by considering the maximum wood thermal conductivity and treating the air gaps within the impact limiter as metal during the smoldering event.

Solid neutron absorbing polyester resin is considered to decompose completely during the 30-minute fire. The resin is included in the model during the fire and the properties are changed to air for the remaining analyses. Elements representing the resin are given air thermal conductivity during the 30-minute wood char and cool-down time periods.

The thermal properties for air and helium are derived from curve fits provided in Reference [6]. Because the thermal conductivity of air varies significantly with temperature, the computer model calculates the thermal conductivity between the package and the ambient as a function of the mean film temperature. Thermal radiation at the external surfaces of the cask is also considered. With the exception of the trunnions, all the exterior surfaces of the cask and impact limiters are painted white. Reference [7] provides an emissivity between 0.92 to 0.96 and a solar absorptivity between 0.06 to 0.23 for white paints. To account for dust and dirt, and to bound the problem, the thermal analysis utilizes a solar absorptivity of 0.3 and an emissivity of 0.9 for the white painted exterior surfaces. After the fire, the cask surface will be partially covered in soot (absorptivity = 0.95, Reference [7]). The HAC thermal analysis conservatively assumes an absorptivity of 1.0 and an emissivity of 0.9 for the cool-down period.

The emissivity of oxidized steel has been measured as 0.79 to 0.94 in Table 129 of Reference [8]. The solar absorptivity of mild steel has been measured to be between 0.41 and 0.74 in Table 403 of Reference [8]. The emissivity and absorptivity of the exterior surfaces of the cask trunnions are assumed to be 0.94 and 0.74, respectively. This assumption is justified because the majority of the trunnion surfaces are exposed carbon steel surfaces that are subject to wear during cask down-ending and lifting operations.

### 3.2.2 Component Specifications

The thermally sensitive materials used in the TN-32B HBU demonstration cask are the metallic containment seals, puncture resistant plate O-rings seals, neutron shield polyester resin, thermocouple lance assemblies, and the irradiated fuel payload. The other materials either have temperature limits above the maximum expected temperatures or are not considered essential to the function of the package.

The metallic seals utilized in the packaging are Helicoflex® HND 229 double metallic and HN-200 single metallic O-ring seals with silver jacketing, and the Viton® O-ring seals in the puncture resistant plate. Maximum allowable temperature is based on the cross-section of the seal. Three seals in the closure lid assembly with associated maximum allowable temperature are as follows:

- Primary lid containment seal with a cross section of 0.260 inch: 842 °F (450 °C),
- Vent port/drain port/lance assembly O-ring seals with a cross section of 0.161 inch: 669 °F (354 °C), and
- Overpressure port seal with a cross section of 0.16 inch: 663 °F (351 °C).

Thermal limits for some additional components are:

- Puncture resistant plate Viton® O-ring seal with a cross-sectional diameter of Ø0.375 inch: 400 °F (205 °C) [9],
- Thermocouple lance overshield is a high nickel material tube of Ø0.312 inch: 800 °F (427 °C).

To maintain thermal stability for the neutron shield polyester resin, a maximum allowable NCT temperature of 300 °F (149 °C) was established for this material.

In accordance with 10 CFR §71.43 (g), the maximum temperature of accessible package surfaces in the shade is limited to 185 °F (85 °C) for an exclusive use shipment.

The thermal limit of the fuel cladding temperature is 400 °C (752 °F) for NCT. This limit is established for fuel assemblies with an inert cover gas, as stated in NUREG-1536 [10].

The allowable temperature of the alloy steel components (i.e., SA-203 Gr. D, SA-350 Gr LF3, and SA-540 Gr. 23 Cl 1 bolts), the SA-240 Type 304/304L, and the SB-163 and SB-166 UNS N06600 materials that form the containment boundary are limited to 650 °F for compliance with the ASME B&PV Code [11] for all conditions of transport. The upper limit for all other steel components that do not serve a structural purpose (e.g., the gamma shell) is limited to 2,600 °F (1,427 °C) (i.e., the melting temperature of low carbon steel [11]) in normal conditions.

Although Type 304 stainless steel has a melting point above 2,500 °F (1,371 °C), the ASME B&PV Code limits the maximum allowable temperature to 800 °F (427 °C) if the component serves a structural purpose (e.g., the material's structural properties are relied upon for loads postulated to occur in the respective operating mode or accidental free drop condition). As such, the appropriate upper temperature limit under normal conditions is 800 °F for stainless steel components that are used in the fuel basket. The upper limit for all other stainless steel components is 2,500 °F for NCT.

The maximum allowable temperature of all aluminum components that serve a structural function is limited to 400 °F (204 °C) for NCT in compliance with the ASME B&PV Code.

The maximum allowable temperature limit for the impact limiter wood is 230 °F (110 °C) to prevent excessive reduction in structural properties at elevated temperatures [12].

With the exception of the Viton® O-ring seals on the puncture resistant plate, the minimum allowable service temperature for all the TN-32B HBU demonstration cask components is equal to or below -40 °F (-40 °C). The Viton® seals have a minimum service temperature rating of -15 °F (-26 °C) [9]. Since the minimum temperature in the seal area is not less than 120 °F for the -40 °F NCT ambient condition, the Viton® O-ring seals are acceptable.

For HAC conditions, the metallic containment O-ring seals, the containment boundary, and the fuel cladding perform their safety function within their allowable temperature limit, as shown in Table 3-2. Since the Viton® O-ring seals are not required to function during or following the HAC fire event, there is no temperature limit for these seals.

#### 1. PWR Fuel Assembly

The effective density, thermal conductivity, and specific heat are calculated utilizing the physical properties of the representative homogenized 17 x 17 PWR HBU fuel assemblies that are loaded in this cask. The fuel conductivity analysis, including the specific heat and density, are provided in Appendix 3.6.1.

Temperature (°F)	$k_{axial}$ (Btu/hr-in-°F)	Temperature (°F)	$k_{trans}$ (Btu/hr-in-°F)	Temperature (°F)	$C_{p, eff}$ (Btu/lb <sub>m</sub> -°F)
100	0.0601	151	0.0206	80	0.0584
200	0.0636	244	0.0239	260	0.0650
300	0.0670	338	0.0276	692	0.0721
400	0.0703	433	0.0321	1,500	0.0782
500	0.0735	528	0.0373	$\rho_{eff} = 0.0130 \text{ lb}_m/\text{in}^3$	
600	0.0765	624	0.0430		
700	0.0796	721	0.0494		
800	0.0827	819	0.0564		
900	0.0858	916	0.0642		
1,000	0.0890	1,014	0.0725		
1,100	0.0923	1,113	0.0807		

## 2. Aluminum (used for basket rails and radial neutron shield boxes) [11]

Material	Temperature (°F)	Thermal Conductivity (Btu/hr-in-°F)	Specific Heat (Btu/lb <sub>m</sub> -°F) <sup>1</sup>	Density (lb <sub>m</sub> /in <sup>3</sup> )
ASTM B-209, Type 6061-T6/T651 ASTM B-221, Type 6061-T6	70	8.008	0.213	0.098 <sup>3</sup>
	100	8.075	0.215	
	150	8.167	0.218	
	200	8.250	0.221	
	250	8.317	0.223	
	300	8.383	0.226	
	350	8.442	0.228	
	400	8.492	0.230	
	450 <sup>2</sup>	8.610	0.233	
	500 <sup>2</sup>	8.685	0.235	
	550 <sup>2</sup>	8.760	0.238	
	600 <sup>2</sup>	8.835	0.240	
ASTM B-221, Type 6063-T5	70	10.067	0.214	0.097 <sup>3</sup>
	100	10.025	0.215	
	150	9.975	0.219	
	200	9.925	0.221	
	250	9.858	0.223	
	300	9.858	0.226	
	350	9.825	0.229	
	400	9.800	0.231	
	450 <sup>2</sup>	9.740	0.233	
	500 <sup>2</sup>	9.700	0.235	
	550 <sup>2</sup>	9.660	0.238	
	600 <sup>2</sup>	9.620	0.240	

## Notes:

1. The values of specific heat ( $c_p$ ) are derived from thermal conductivity ( $k$ ), thermal diffusivity ( $\alpha$ ), and density ( $\rho$ ) values cited from ASME B&PV Code [11] in accordance with the following equation:

$$c_p = k/(\rho \times \alpha)$$

2. Thermal conductivity and specific heat values for values larger than 400 °F are linearly extrapolated from those at lower temperatures.
3. Density is cited from Table PRD in the 2013 version of Section II, Part D of Reference [13].

## 3. Poison Plates

As a conservative measure, this analysis assumes that the borated aluminum poison plates have virtually no thermal conductance and are, therefore, neglected to calculate effective conductivity for homogenized fuel basket plates in the ANSYS 6. thermal model.

## 4. Stainless Steel SA-240, Type 304 (fuel compartments &amp; impact limiter shells) [11]

Temperature (°F)	Thermal Conductivity, k (Btu/hr-in-°F)	Specific heat, $C_p$ <sup>2</sup> (Btu/lb <sub>m</sub> -°F)
-40 <sup>1</sup>	0.680	0.109
-20 <sup>1</sup>	0.688	0.110
70	0.717	0.114
100	0.725	0.114
150	0.750	0.117
200	0.775	0.119
250	0.800	0.121
300	0.817	0.122
350	0.842	0.122
400	0.867	0.126
450	0.883	0.127
500	0.908	0.128
550	0.925	0.129
600	0.942	0.130
650	0.967	0.131
700	0.983	0.132
750	1.000	0.132
800	1.017	0.132
850	1.042	0.134
900	1.058	0.134
950	1.075	0.135
1,000	1.100	0.136
1,050	1.117	0.136
1,100	1.133	0.137
1,150	1.150	0.137
1,200	1.167	0.138
1,250	1.192	0.139
1,300	1.208	0.139
1,350	1.225	0.140
1,400	1.242	0.140
1,450	1.258	0.141
1,500	1.275	0.141
$\rho = 0.290 \text{ lb}_m/\text{in}^3$ <sup>3</sup>		

## Notes:

1. Thermal conductivity and specific heat values for -20 °F and -40 °F are linearly and quadratically extrapolated from those at higher temperatures, respectively.
2. The values of specific heat ( $C_p$ ) are derived from thermal conductivity ( $k$ ), thermal diffusivity ( $\alpha$ ), and density ( $\rho$ ) values cited from ASME B&PV Code [11] in accordance with the following equation:

$$C_p = k/(\rho \times \alpha)$$

3. Density is cited from Table PRD in the 2013 version of Section II, Part D of Reference [13].

## 5. Low Nickel Alloy Steel SA-203, Gr D and SA-350, Gr LF3 (containment shell) [13]

Temperature (°F)	Thermal Conductivity, k (Btu/hr-in-°F)	Specific heat, $C_p$ <sup>1</sup> (Btu/lb <sub>m</sub> -°F)
70	1.908	0.109
100	1.933	0.111
150	1.967	0.114
200	1.983	0.118
250	2.000	0.121
300	2.008	0.124
350	2.000	0.126
400	1.992	0.129
450	1.975	0.131
500	1.950	0.133
550	1.933	0.137
600	1.908	0.139
650	1.883	0.143
700	1.858	0.146
750	1.825	0.148
800	1.800	0.151
850	1.767	0.154
900	1.742	0.159
950	1.708	0.163
1,000	1.675	0.169
1,050	1.642	0.175
1,100	1.600	0.183
1,150	1.558	0.192
1,200	1.517	0.206
1,250	1.467	0.222
1,300	1.408	0.248
1,350	1.317	0.238
1,400	1.292	0.184
1,450	1.283	0.164
1,500	1.275	0.152
$\rho = 0.280 \text{ lb}_m/\text{in}^3$ <sup>2</sup>		

## Notes:

- The values of specific heat ( $C_p$ ) are derived from thermal conductivity (k), thermal diffusivity ( $\alpha$ ), and density ( $\rho$ ) values cited from ASME B&PV Code [11] in accordance with the following equation:

$$C_p = k/(\rho \times \alpha)$$

- Density is cited from Table PRD in the 2013 version of Section II, Part D of Reference [13].

## 6. Helium (utilized for gaps within the cask cavity) [14]

Temperature (°F)	Density <sup>1</sup> (lb <sub>m</sub> /in <sup>3</sup> )	Specific Heat (Btu/lb <sub>m</sub> -°F)	Dynamic Viscosity (lb <sub>m</sub> /ft-hr)	Thermal Conductivity (Btu/hr-ft-°F)	Prandtl Number <sup>2</sup>	Coef. of Thermal Exp. <sup>3</sup> (R <sup>-1</sup> )
100	Use Ideal Gas Law w/ molecular wt = 4.0026 g/mole	1.240	0.04944	0.0886	Computed as Pr = c <sub>p</sub> μ/k	Computed as β = 1/(°F + 459.67)
200			0.05520	0.0981		
300			0.06088	0.1075		
400			0.06643	0.1177		
500			0.07153	0.1291		
600			0.07640	0.1403		
700			0.08116	0.1508		
800			0.08580	0.1607		
900			0.09033	0.1702		
1,000			0.09475	0.1793		
1,100			0.09906	0.1883		
1,300			0.10738	0.2058		
1,500			0.11531	0.2231		

## Notes:

1. Density computed from ideal gas law as  $\rho = PM/RT$ , where  $R = 1545.35 \text{ ft-lb/lb}_m\text{-mole-R}$ ,  $T$  = temperature in °R,  $P$  = pressure in lb<sub>f</sub>/ft<sup>2</sup>, and  $M$  = molecular weight of helium.
2. Prandtl number computed as  $Pr = c_p(\mu)/k$ , where  $c_p$  = specific heat,  $\mu$  = dynamic viscosity, and  $k$  = thermal conductivity.
3. Coefficient of thermal expansion is computed as the inverse of the absolute temperature.



7. SA-266 Gr. 2 and SA-516 Gr. 70 Carbon Steel (gamma shield shell, outer shell, and closure lid) [11]

Material	Temperature (°F)	Thermal Conductivity (Btu/hr-in-°F)	Specific Heat (Btu/lb <sub>m</sub> -°F) <sup>1</sup>	Density (lb <sub>m</sub> /in <sup>3</sup> )
SA-266 Gr 2 SA-516 Gr 70	70	1.967	0.107	0.280 <sup>2</sup>
	100	1.992	0.112	
	150	2.017	0.116	
	200	2.033	0.120	
	250	2.033	0.122	
	300	2.033	0.124	
	350	2.025	0.127	
	400	2.017	0.130	
	450	1.992	0.132	
	500	1.975	0.135	
	550	1.950	0.136	
	600	1.925	0.138	
	650	1.892	0.141	
	700	1.867	0.145	
	750	1.833	0.148	
	800	1.808	0.151	
	850	1.767	0.153	
	900	1.742	0.158	
	950	1.708	0.162	
	1,000	1.667	0.167	
	1,050	1.633	0.171	
	1,100	1.600	0.174	
	1,150	1.558	0.181	
	1,200	1.517	0.191	
	1,250	1.458	0.202	
	1,300	1.392	0.223	
	1,350	1.317	0.274	
	1,400	1.275	0.411	
	1,450	1.258	0.203	
	1,500	1.258	0.185	

Notes:

- The values of specific heat ( $c_p$ ) are derived from thermal conductivity ( $k$ ), thermal diffusivity ( $\alpha$ ), and density ( $\rho$ ) values cited from ASME B&PV Code [11] in accordance with the following equation:

$$c_p = k/(\rho \times \alpha)$$

- Density is cited from Table PRD in the 2013 version of Section II, Part D of Reference [13].

## 8. SA-105 Carbon Steel (Trunnions) [11]

Material	Temperature (°F)	Thermal Conductivity (Btu/hr-in-°F)	Specific Heat (Btu/lb <sub>m</sub> -°F) <sup>1</sup>	Density (lb <sub>m</sub> /in <sup>3</sup> )
SA-105	70	2.500	0.107	0.2802 <sup>2</sup>
	100	2.492	0.109	
	150	2.467	0.112	
	200	2.433	0.116	
	250	2.408	0.119	
	300	2.367	0.122	
	350	2.333	0.125	
	400	2.300	0.128	
	450	2.258	0.130	
	500	2.217	0.133	
	550	2.175	0.136	
	600	2.133	0.137	
	650	2.092	0.140	
	700	2.050	0.143	
	750	2.000	0.147	
	800	1.958	0.150	
	850	1.917	0.154	
	900	1.875	0.157	
	950	1.825	0.161	
	1,000	1.783	0.166	
	1,050	1.733	0.171	
	1,100	1.683	0.177	
	1,150	1.633	0.183	
	1,200	1.583	0.191	
	1,250	1.525	0.200	
	1,300	1.467	0.211	
	1,350	1.400	0.230	
	1,400	1.350	0.408	
	1,450	1.308	0.237	
	1,500	1.300	0.179	

## Notes:

- The values of specific heat ( $c_p$ ) are derived from thermal conductivity ( $k$ ), thermal diffusivity ( $\alpha$ ), and density ( $\rho$ ) values cited from ASME B&PV Code [11] in accordance with the following equation:

$$c_p = k/(\rho \times \alpha)$$

- Density is cited from Table PRD in the 2013 version of Section II, Part D of Reference [13].

9. Fuel Basket with Homogenized Thermal Properties

## 10. Air [14]

Temperature (°F)	Density <sup>1</sup> (lb <sub>m</sub> /in <sup>3</sup> )	Specific Heat (Btu/lb <sub>m</sub> -°F)	Dynamic Viscosity (lb <sub>m</sub> /ft-hr)	Thermal Conductivity (Btu/hr-ft-°F)	Prandtl Number <sup>2</sup>	Coef. of Thermal Exp. <sup>3</sup> (R <sup>-1</sup> )
-40	Use Ideal Gas Law w/ molecular wt = 28.966	0.240	0.03673	0.0121	Computed as Pr = c <sub>p</sub> μ/k	Computed as β = 1/(°F +459.67)
-20		0.240	0.03815	0.0126		
0		0.240	0.03953	0.0131		
50		0.240	0.04288	0.0143		
100		0.241	0.04607	0.0155		
200		0.242	0.05207	0.0178		
300		0.243	0.05764	0.0199		
400		0.245	0.06286	0.0220		
500		0.248	0.06778	0.0240		
600		0.251	0.07242	0.0259		
700		0.253	0.07680	0.0278		
800		0.256	0.08098	0.0297		
900		0.259	0.08500	0.0315		
1,000		0.262	0.08887	0.0333		
1,200		0.269	0.09620	0.0366		
1,400		0.274	0.10306	0.0397		
1,500		0.277	0.10633	0.0412		

## Notes:

- Density computed from ideal gas law as  $\rho = PM/RT$ , where  $R = 1545.35 \text{ ft-lb/lb}_m\text{-mole-R}$ ,  $T =$  temperature in R,  $P =$  pressure in lb<sub>f</sub>/ft<sup>2</sup>, and  $M =$  molecular weight of air. For example: At 100 °F and atmospheric pressure of 14.69 lb<sub>f</sub>/in<sup>2</sup>,  $\rho = (14.69 \times 144 \text{ in}^2/\text{ft}^2 \times 28.966 \text{ lb}_m/\text{lb-mole}) / (1545.35 \times (100 + 459.67)) = 0.071 \text{ lb}_m/\text{ft}^3$ .
- Prandtl number computed as  $Pr = c_p \mu / k$ , where  $c_p =$  specific heat,  $\mu =$  dynamic viscosity, and  $k =$  thermal conductivity. For example: At 100 °F,  $Pr = 0.241 \times 0.04607 / 0.0155 = 0.72$ .
- Coefficient of thermal expansion is computed as the inverse of the absolute temperature. For example: At 100 °F,  $\beta = 1 / (100 + 459.67) = 0.00179$ .

## 11. Wood

The thermal properties utilized to model the wood core of the impact limiters for NCT and HAC are listed in the table below. Bounding values for the thermal conductivity are based on the limits found in Figure 5 of Reference [5]. The figure presents conductivity for woods with oven-dry specific gravities ranging from 0.08 to 0.80, and moisture content from 0 to 30%. The figure presents that the conductivity of wood across the grain ranges from 0.275 BTU-in/hr-ft<sup>2</sup>-°F to 1.95 BTU-in/hr-ft<sup>2</sup>-°F. Also, as noted in Reference [5], the conductivity parallel to the grain is normally 2.0 to 2.8 times the conductivity across the grain. Note that the conductivity is relatively insensitive to species or temperature.

Conservatively, the lower bounding conductivity value is utilized for NCT while the upper bounding value, multiplied by a factor of 2.8, is utilized for HAC.

$$k_{\text{NCT}} = 0.275 \frac{\text{Btu-in}}{\text{hr-ft}^2\text{-}^\circ\text{F}} = 0.0019 \frac{\text{Btu}}{\text{hr-in-}^\circ\text{F}}$$

$$k_{\text{HAC}} = 2.8 \left( 1.95 \frac{\text{Btu-in}}{\text{hr-ft}^2\text{-}^\circ\text{F}} \right) = 0.0379 \frac{\text{Btu}}{\text{hr-in-}^\circ\text{F}}$$

The specific heat is calculated using a moisture content of 0% from Equation 4-17 of Reference [15].

$$c_{p,x} = \frac{c_{p0} + c_{pw} \frac{x}{100}}{1 + \frac{x}{100}} + A_c$$

where:

$x$  = moisture content in percentage from 6 to 12%

$c_{pw}$  = heat capacity of water = 1 BTU/(lb<sub>m</sub>-°F)

$c_{p0}$  = dry heat capacity of the wood calculated using the equation

$c_{p0} = 0.2605 + 0.0005132(T)$

$A_c$  is calculated using Equation 4-18 of Reference [15]:

$$A_c = x(b_1 + b_2T + b_3x)$$

With the constants  $b_1 = -0.000423$ ,  $b_2 = 0.0000312$ , and  $b_3 = -0.0000317$ . The density of the wood is based on the nominal values, as specified on drawings 19885-71-9 and 19885-71-10 in Appendix 1.4.1.

Temperature (°F)	NCT Conductivity (BTU/hr-in-°F)	HAC Conductivity (BTU/hr-in-°F)	Specific Heat (BTU/lb <sub>m</sub> -°F)	Density (lb <sub>m</sub> /in <sup>3</sup> )
100	0.0019	0.0379	0.312	0.013
200			0.363	
300			0.414	
400			0.466	
500			0.517	
600			0.568	

## 12. Neutron Shielding (Polyester Resin) [16]

Thermal Conductivity (Btu/hr-in-°F)	Specific Heat (Btu/lb <sub>m</sub> -°F)	Density (lb <sub>m</sub> /in <sup>3</sup> )
0.0083	0.311	0.057

### 3.3 Thermal Evaluation under Normal Conditions of Transport

#### 3.3.1 Heat and Cold

##### 3.3.1.1 Thermal Models

The thermal model for the TN-32B HBU demonstration cask was developed with ANSYS® Version 17.1 [17], which is a comprehensive thermal, structural, and fluid flow analysis package providing a full-height, 180-degree representation of the cask utilizing approximately 1,159,282 thermal nodes, 1,110,014 solid thermal elements, and 142,910 planar elements. The NCT thermal performance is determined using a single 3-D thermal model of the TN-32B HBU demonstration cask with its single HBU payload. The finite element analysis code is capable of solving steady-state and transient thermal analysis problems in one, two or three dimensions. Heat transfer via a combination of conduction, radiation and convection can be modeled by ANSYS®. All cask components including the gaps are modeled by SOLID70 conducting elements. Exterior surfaces of the cask are overlaid with SURF152 shell elements with applied free convection boundary conditions.

To determine temperatures of components within the cask body and basket during NCT, a finite element model of the basket and cask is developed. The cask model includes the wood filled impact limiters, trunnions, neutron shield, cask shell, cask bottom plate, cask closure lid, basket, and fuel assemblies (see Figure 3-6 through Figure 3-9). The model simulates the effective thermal properties of the fuel with a homogenized material occupying the volume within the basket where the 144 inch active length of the fuel is stored. The inner shell and gamma shield shell are assembled with an interference fit. This assembly ensures thermal contact at the shell interface. [

]

The radial neutron shielding consists of 60 long resin filled aluminum boxes placed between the gamma shield shell and outer shield shell. The aluminum resin boxes are confined between these shells, and butt against the adjacent shells. [

]

For HAC, the principal modifications consist of the deformed impact limiters to reflect the post HAC drop events, capturing the thermal charring of the wood under HAC conditions, changing the cask surface emissivities to reflect the assumed presence of soot and/or surface oxidation, assuming zero air gap contact associated with the cask and impact limiters to maximize heat flow into the package, and assuming maximum thermal conductivity of wood to maximize heat transfer into the cask during the fire and wood char events. During the fire event, all air gaps with the cask and impact limiters representing contact resistances are removed and conservatively replaced with the thermal conductivity of the adjacent material to maximize the heat flow into the cask. The air gaps are then restored for the post-fire 30-minute charred wood event, and the subsequent 20-hour cool-down period to maximize thermal resistance.

#### 1. Basket Model

The basket model is an integrated part of the finite element model which reflects the structure of the basket. The basket structure is composed of 32 stainless steel fuel compartments (8.70 inch square) sandwiching three regions of aluminum and borated aluminum (poison) plates. The fuel compartments are joined by welded stainless steel plugs that pass through the aluminum and poison plates. The fuel compartments are plug-welded together to form the basket.

## 2. Impact Limiter Model

Similar to the basket model, the impact limiters are an integrated part of the finite element model which determines the maximum accessible surface temperature during NCT.

The redwood and balsa wood within the impact limiters are modeled as a homogenized region containing bounding material properties.

All heat transfer across the gaps is by gaseous conduction. Other modes of heat transfer are neglected. The finite element end view plot of the impact limiter model is shown in Figure 3-8.



### 3.3.1.2 Heat Dissipation

The TN-32B HBU demonstration cask thermal model utilizes several subroutines created in ANSYS® APDL to calculate convection heat transfer coefficients for natural (free) convection on the exterior package surfaces under the regulatory NCT conditions. During the NCT evaluations, the convection coefficient values calculated for the free convection on the exterior package range from 0.57 Btu/hr-ft<sup>2</sup>-°F to 1.65 Btu/hr-ft<sup>2</sup>-°F.

The free convection subroutines use the semi-empirical relationships published in Section 3.3 of Reference [19] to iteratively calculate the convection heat transfer coefficients at the mean film temperature. The correlations utilized are further described below.

The convective heat transfer coefficient,  $h_c$ , has a form of:

$$h_c = Nu \frac{k}{L}$$

where  $k$  is the thermal conductivity of the gas at the mean film temperature, and  $L$  is the characteristic length of the vertical or horizontal surface. The convection coefficient is correlated via semi-empirical relationships against the local Rayleigh number and the characteristic length. The Rayleigh number,  $Ra_L$ , is defined as:

$$Ra_L = \frac{\rho^2 g_c \beta L^3 \Delta T}{\mu^2} (Pr)$$

where:

$g_c$  = gravitational acceleration, 386.4 in/s<sup>2</sup>

$\beta$  = coefficient of thermal expansion, °R<sup>-1</sup>

$\Delta T$  = temperature difference, °F

$\rho$  = density of air at the film temperature, lb<sub>m</sub>/in<sup>3</sup>

$\mu$  = dynamic viscosity, lb<sub>m</sub>/in-s

$Pr$  = Prandtl number =  $(c_p \mu)/k$

$L$  = characteristic length, ft

$k$  = thermal conductivity at film temp., Btu/in-hr-°F

$c_p$  = specific heat, Btu/lb<sub>m</sub> -°F

$Ra_L$  = Rayleigh number, based on length 'L'

Note that  $k$ ,  $c_p$ , and  $\mu$  are each a function of air temperature. Values for  $\rho$  are computed using the ideal gas law,  $\beta$  for an ideal gas is simply the inverse of the absolute temperature of the gas, and  $Pr$  is computed using the values for  $k$ ,  $c_p$ , and  $\mu$ . Unit conversion factors are used as required to reconcile the units for the various properties used.

The natural convection from a discrete vertical surface is computed using Equations, 4.13, 4.24, 4.31, and 4.33 of Reference [6], which are applicable over the range  $1 < \text{Rayleigh number } (Ra) < 10^{12}$ :

$$Nu^T = \overline{C}_L Ra^{1/4} \quad (4.33a)$$

$$\overline{C}_L = \frac{0.671}{\left(1 + \left(\frac{0.492}{Pr}\right)^{9/16}\right)^{4/9}} \quad (4.13)$$

$$Nu_L = \frac{2.0}{\ln\left(1 + \frac{2.0}{Nu_T}\right)} \quad (4.33b)$$

$$Nu_t = \frac{C_t^V(f)Ra^{\frac{1}{3}}}{1 + 1.4 \times 10^9 \frac{Pr}{Ra}} \quad (4.33c)$$

$$f = 1.0 + 0.078 \left( \frac{T_{surf}}{T_{\infty}} - 1 \right) \quad (4.31)$$

$$C_t^V = \frac{0.13Pr^{0.22}}{(1 + 0.61Pr^{0.81})^{0.42}} \quad (4.24)$$

$$Nu = \frac{h_c L}{k} = [(Nu_L)^6 + (Nu_t)^6]^{1/6} \quad (4.33d)$$

The natural convection from a horizontal cylindrical surface is computed by applying a correction factor to the laminar Nusselt number ( $Nu_L$ ) determined utilizing the same methodology, and  $Nu_t$  for a vertical plate (see above).

Calculation of the convection coefficient from a long, isothermal horizontal cylindrical surface in an isothermal environment is computed using Equations 4-13 and 4-45, where the characteristic length,  $D$ , is the outer diameter of the cylinder. This equation has a root mean square (RMS) deviation from the equation of less than 5%, and is applicable for  $10^{-10} < Ra < 10^7$ , as follows:

$$\overline{C}_L = \frac{0.671}{\left(1 + \left(\frac{0.492}{Pr}\right)^{9/16}\right)^{4/9}} \quad (4.13)$$

$$Nu^T = 0.772 \times \overline{C}_L \times Ra^{1/4} \quad (4.45a)$$

$$Nu_l = \frac{2f}{\ln(1 + 2f/Nu^T)} \quad (4.45b)$$

$$f = 1 - \frac{0.13}{(Nu^T)^{0.16}} \quad (4.45b)$$

$$Nu_t = \overline{C}_t \times Ra^{1/3} \quad (4.45c)$$

$$Nu = \frac{hL_c}{k} = [(Nu_l)^m + (Nu_t)^m]^{1/m}, m \approx 10 \quad (4.45d)$$

$\overline{C}_t$  values may be found in Table 4-2 of Reference [6]. Note  $\overline{C}_t$  for air ( $Pr=0.71$ ) is 0.103.

Heat transfer from the surface of the package by radiation to the ambient environment is defined by the following equation, as described in Equation 1.36 of [6]:

$$h_r = \frac{1}{R_{th}A} = \frac{\sigma \varepsilon (T_w^4 - T_a^4)}{T_w - T_a}$$

where:

$\varepsilon$  = surface emissivity

$\sigma$  = Stefan–Boltzmann constant,  $0.1714 \times 10^{-8}$  Btu/hr-ft<sup>2</sup>- R<sup>4</sup>

$T_w$  = wall temperature, R

$T_a$  = ambient temperature, R

The total heat transfer coefficient  $H_t = h_r + h_c$ , is applied as a boundary condition on the outer surfaces of the finite element model.

### 3.3.1.3 Solar Heat Load

The total insolation for a 12-hour period in a day is 1,475 Btu/ft<sup>2</sup> (400 g-cal/cm<sup>2</sup>) for curved surfaces and 737 Btu/ft<sup>2</sup> (200 g-cal/cm<sup>2</sup>) for flat surfaces not transported horizontally per 10 CFR §71.71(c)(1). This insolation is averaged over a 24-hr period (daily averaged value) and applied as a constant steady state value to the external surfaces of the thermal models.

All outer surfaces of the TN-32 HBU demonstration cask are painted white. An emissivity between 0.92 and 0.96, and a solar absorptivity between 0.06 and 0.23 are provided for white paints by Reference [7]. To account for dust and dirt, and to bound the problem, the thermal analysis utilizes an emissivity of 0.9 and a solar absorptivity of 0.3 for white painted surfaces, as discussed in Section 4.2 of Reference [7]. Daily averaging of the solar heat load is justified based on the large thermal inertia of the TN-32 HBU demonstration cask. The solar heating is limited to the unshaded portions of the package, which is 75% of the total exposed surface area. The model includes the exposed surfaces of the impact limiters and the cask body to 45 degrees below the horizontal centerline, as shown in Figure 3-10. The inner vertical surfaces of the impact limiters and the cask body receive the full solar heating input (no reduction due to the personnel barrier).

The total solar input is determined by applying the solar factors listed above to the total exposed areas. The area of the cylindrical cask body and the impact limiters is:

$$A_{Cyl} = A_{Cyl-IL} + A_{Cyl-Cask}$$

$$A_{Cyl} = \pi \left[ 2 \left[ \frac{(144 \text{ in})(50 \text{ in})}{144} \right] + \left[ \frac{(97.75 \text{ in})(263.2 \text{ in} - 2(50 \text{ in}))}{144} \right] \right] [0.75] = 497 \text{ ft}^2$$

The area of the inner and outer flat ends of the impact limiters is:

$$A_{vPL} = 2(A_{outside} + A_{inside}) = \frac{\pi}{4} \left( 4 \left( \frac{144 \text{ in}}{12} \right)^2 - 2 \left( \frac{97.75 \text{ in}}{12} \right)^2 \right) = 348 \text{ ft}^2$$

The total insolation heat input,  $Q_{\text{solar}}$ , is:

$$Q_{\text{solar}} = (497 \text{ ft}^2) \left( 1475 \frac{\text{Btu}}{\text{ft}^2} \right) + (348 \text{ ft}^2) 737 \frac{\text{Btu}}{\text{ft}^2} = 989,551 \text{ Btu}$$

The corresponding solar input for the entire cask will be:

$$\frac{989,551 \text{ Btu}}{24 \text{ hr}} = 41,231 \text{ Btu/hr}$$

Since the model is a half-symmetrical model, the corresponding solar thermal input applied to the model is:

$$(0.5)(41,231 \text{ Btu/hr}) = 20,616 \text{ Btu/hr}$$

The absorptivity for the white paint is 0.3, and the corresponding solar thermal input is:

$$(0.3)(20,616 \text{ Btu/hr}) = 6,185 \text{ Btu/hr}$$

The solar flux for the cask from the model is 6,453 Btu/hr. The required heat flux from the fuel assemblies for the half-symmetry model is  $25.84 \text{ kW}/2 = 12.92 \text{ kW}$  (44,085 Btu/hr). The corresponding model input is 44,562 Btu/hr. Additionally, the fuel assemblies included in the model constitute more than half of the total heat load. Therefore, the thermal inputs are conservatively applied.

#### 3.3.1.4 Maximum Temperatures

Table 3-1 presents the predicted TN-32B HBU demonstration cask temperatures under the evaluated NCT Hot scenario. Given the mass of the package, the maximum package component temperatures are computed using the regulatory insolation loading averaged over 24 hours. The results demonstrate that thermal margins exist for all packaging components with the minimum thermal margin of 2 °F (i.e., 300 °F - 298 °F) occurring in a small area of the radial neutron resin near the bottom end of the cask. This area of the resin is less than 0.10% of the total neutron resin volume. The maximum temperature of any containment structural component is less than 368 °F (187 °C). The maximum containment seal temperature 232 °F (111 °C) during NCT is well below the 663 °F (351 °C) long-term limit specified for continued seal function. The maximum neutron shield resin temperature is below 300 °F (149 °C), and no degradation of the neutron shielding is expected. The predicted maximum fuel cladding temperature (510 °F [266 °C]) is well within the allowable fuel temperature limit of 752 °F (400 °C).

The temperature distribution within the package is shown in Figure 3-1. Figure 3-2 presents a cross-section of the cask at the axial location of the peak fuel temperature. The differing fuel decay heats of the various elements can be clearly seen in the resulting temperature distribution. Figure 3-11 presents a cross-section of the basket at the axial location for the peak fuel temperature occurs. The neutron resin shield thermal profile is shown in Figure 3-3. The aluminum cask rails and aluminum neutron resin boxes are shown in Figure 3-5 and Figure 3-12, respectively. The thermal profile of the impact limiter wood is illustrated in Figure 3-4. As shown, the peak wood temperature of 120 °F occurs locally next to the cask body in the lower impact limiter. The bulk average wood temperature in the top and bottom limiters is only 109 °F and 111 °F, respectively.

In addition, thermal performance tests conducted on the TN-32B cask design documented in Reference [20] demonstrates that the thermal model considers adequately the insulating effect of the neutron shield and the gaps between multiple shells of the cask and bounds properly the uncertainties and imperfections expected in the fabrication of this type of cask.

#### 3.3.1.5 Maximum Accessible Surface Temperature in the Shade

The analysis demonstrates that without the personnel barrier, the maximum accessible cask surface temperature with 100 °F (38 °C) ambient in the shade is 290 °F (143 °C), which exceeds the exclusive use shipment limit of 185 °F (85 °C) per 10 CFR §71.43(g). Therefore, a personnel barrier is required during transport of the TN-32B HBU demonstration cask.

The accessible surfaces of the TN-32B HBU demonstration cask consist of the personnel barrier and outermost vertical and radial surfaces of the impact limiters. The personnel barrier, which utilizes expanded metal, surrounds the cask body between impact limiters and has an open area of approximately 75%.

The presence of the barrier has negligible effect on heat transfer between the cask surface and the environment. Convection is not affected because the distance between the barrier and the cask and the 75% open area of the barrier ensures that the airflow around the cask is not restricted. Radiant heat transfer to or from the cask surface is not significantly affected because the open area of the barrier allows the cask to “see” the ambient environment, and the distance between the cask and the barrier ensures the screen is very close to ambient temperature. Thus, the 25% of the barrier surface area that the cask sees is also very close to the ambient temperature.

With the installation of the personnel barrier, the accessible surfaces of the cask are limited to the impact limiter and the personnel barrier outer surfaces. The NCT model without insolation at 100 °F (38 °C) ambient temperature demonstrates that the accessible surface temperature of the impact limiters does not exceed 101 °F (38 °C). The maximum accessible surface temperature of the impact limiters and the maximum cask outer shell temperature at this ambient temperature in the shade are 116 °F (47 °C) and 290 °F (143 °C), respectively. The accessible surface temperature of the packaging in the shade is calculated as follows.

The personnel barrier is exposed to thermal radiation from cask outer shell and dissipates heat via thermal radiation and natural convection to ambient. This part of the personnel barrier is sufficiently separated from the cask outer shell and is not exposed to the hot air streams from the cask.

Conservatively, omitting the convection heat dissipation from the barrier and assuming the maximum cask outer shell temperature for the entire outer shell surface gives the heat balance for the personnel barrier as follows.

$$\begin{aligned}
 q_{in\_rad} &= q_{out\_rad} \\
 q_{in\_rad} &= \frac{\sigma (T_{shell}^4 - T_{PB}^4)}{\frac{1 - \epsilon_{shell}}{\epsilon_{shell} A_{shell}} + \frac{1}{F_{PB-shell} A_{PB}} + \frac{1 - \epsilon_{PB}}{\epsilon_{PB} A_{PB}}} \\
 q_{out\_rad} &= \frac{\sigma (T_{PB}^4 - T_{\infty}^4)}{\frac{1 - \epsilon_{PB}}{\epsilon_{PB} A_{PB}} + \frac{1}{F_{PB-\infty} A_{PB}}} \\
 q_{out\_rad} &= \frac{\sigma (T_{PB}^4 - T_{\infty}^4)}{\frac{1 - \epsilon_{PB}}{\epsilon_{PB} A_{PB}} + \frac{1}{(1) A_{PB}} \left( \frac{\epsilon_{PB}}{\epsilon_{PB}} \right)} \\
 q_{out\_rad} &= \frac{\sigma (T_{PB}^4 - T_{\infty}^4)}{\frac{1 - \epsilon_{PB}}{\epsilon_{PB} A_{PB}} + \frac{\epsilon_{PB}}{\epsilon_{PB} A_{PB}}} \\
 q_{out\_rad} &= \frac{\sigma (T_{PB}^4 - T_{\infty}^4)}{\frac{1 - \epsilon_{PB} + \epsilon_{PB}}{\epsilon_{PB} A_{PB}}} \\
 q_{out\_rad} &= \epsilon_{PB} A_{PB} \sigma (T_{PB}^4 - T_{\infty}^4)
 \end{aligned}$$

$$q_{in\_rad} = \frac{\sigma (T_{shell}^4 - T_{PB}^4)}{\frac{1 - \epsilon_{shell}}{\epsilon_{shell} A_{shell}} + \frac{1}{F_{PB-shell} A_{PB}} + \frac{1 - \epsilon_{PB}}{\epsilon_{PB} A_{PB}}}$$

$$\frac{\sigma (T_{shell}^4 - T_{PB}^4)}{\frac{1 - \epsilon_{shell}}{\epsilon_{shell} A_{shell}} + \frac{1}{F_{PB-shell} A_{PB}} + \frac{1 - \epsilon_{PB}}{\epsilon_{PB} A_{PB}}} = \epsilon_{PB} A_{PB} \sigma (T_{PB}^4 - T_{\infty}^4)$$

where:

- $\sigma$  = Stefan-Boltzmann constant =  $0.119 \times 10^{-10}$  (Btu/hr-in<sup>2</sup>-°R<sup>4</sup>)
- $T_{shell}$  = maximum cask outer shell temperature = 290 °F = 750 °R
- $T_{PB}$  = maximum personnel barrier temperature (°R)
- $T_{\infty}$  = ambient temperature = 100 °F = 560 °R
- $\epsilon_{shell}$  = emissivity of painted outer shell = 0.9 (see Section 3.2 for discussion)
- $\epsilon_{PB}$  = emissivity of personnel barrier = 0.3
- $F_{PB-shell}$  = view factor from personnel barrier to cask outer shell
- $F_{PB-\infty}$  = view factor from personnel barrier to ambient = 1.0
- $A_{PB}$  = surface area of personnel barrier upper part (in<sup>2</sup>)
- $A_{shell}$  = surface area of cask outer shell upper part (in<sup>2</sup>)

The diameters of the cask outer shell ( $D_{shell}$ ) and personnel barrier ( $D_{PB}$ ) are 98.10 - 98.17 inch (nominally 98.14 inch) and 144 inch, respectively, as shown in drawing 19885-71-1, Appendix 1.4.1.

$$\frac{A_{shell}}{A_{PB}} = \frac{D_{shell}}{D_{PB}} = \frac{98.14}{144}$$

Since the personnel barrier surrounds the upper part of cask outer shell completely and has an open area of approximately 75%, a view factor of 0.25 can be considered for the cask outer shell to the barrier ( $F_{shell-PB}$ ). The view factor of the barrier to the cask outer surface ( $F_{PB-shell}$ ) can be calculated as follows.

$$(F_{PB-shell})(A_{PB}) = (F_{shell-PB})(A_{shell})$$

$$F_{PB-shell} = F_{shell-PB} \left[ \frac{A_{shell}}{A_{PB}} \right] = F_{shell-PB} \left[ \frac{D_{shell}}{D_{PB}} \right] = 0.25 \frac{98.14}{144} = 0.17$$

The surface temperature for the personnel barrier can be determined by substituting the above values in the heat balance equation as follows:

$$\frac{\sigma (T_{shell}^4 - T_{PB}^4)}{\frac{1 - \epsilon_{shell}}{\epsilon_{shell} A_{shell}} + \frac{1}{F_{PB-shell} A_{PB}} + \frac{1 - \epsilon_{PB}}{\epsilon_{PB} A_{PB}}} = \epsilon_{PB} A_{PB} \sigma (T_{PB}^4 - T_{\infty}^4)$$

$$\frac{(750^4 - T_{PB}^4)}{\frac{1 - 0.9}{0.9(\pi)98.14L} + \frac{1}{0.17(\pi)144L} + \frac{1 - 0.3}{0.3(\pi)144L}} = 0.3\pi(144)(T_{PB}^4 - 560^4)$$

$$\frac{(750^4 - T_{PB}^4)}{0.3\pi \frac{144^2}{4} L \left( \frac{1-0.9}{0.9(\pi)98.14L} + \frac{1}{0.17(\pi)144L} + \frac{1-0.3}{0.3(\pi)144L} \right)} = (T_{PB}^4 - 560^4)$$

$$\frac{(750^4 - T_{PB}^4)}{2.3279} = (T_{PB}^4 - 560^4)$$

$$\frac{(750^4 - T_{PB}^4)}{2.3279} + 560^4 = (T_{PB}^4)$$

$$(750^4) + 2.3279(560)^4 = 2.3279(T_{PB}^4) + T_{PB}^4$$

$$(750^4) + 2.3279(560)^4 = 3.3279(T_{PB}^4)$$

$$\frac{(750^4) + 2.3224(560)^4}{3.3279} = (T_{PB}^4)$$

$$T_{PB} = \left( \frac{(750^4) + 2.3224(560)^4}{3.3279} \right)^{1/4} = 636 \text{ } ^\circ\text{R} = 176 \text{ } ^\circ\text{F}$$

With the maximum outer surface temperature of the impact limiters at 101 °F (38 °C) and the maximum personnel barrier surface temperature conservatively calculated to be 176 °F (80 °C) for 100 °F (38 °C) ambient in the shade, the accessible surfaces of the packaging remain below the 10 CFR §71.43(g) regulatory limit of 185 °F (85 °C) for an exclusive use shipment.

#### 3.3.1.6 Minimum Temperatures

Under the minimum temperature condition of -40 °F (-40 °C) ambient, the resulting packaging component temperatures will approach -40 °F if no credit is assumed for the decay heat load. Since the package materials, including containment structures and the seals, continue to function at this temperature, the minimum temperature condition has no adverse effect on the performance of the TN-32B HBU demonstration cask. However, decay heat loads are included in the thermal analysis.

Temperature distributions at ambient temperatures of -20 °F and -40 °F with maximum decay heat and no insulation are determined. Table 3-1 lists the results of the analyses, with the temperature distributions shown in Figure 3-13. The minimum allowable service temperature for all the TN-32B HBU cask components is equal to or below -40 °F (-40 °C) ambient with the exception of the Viton® O-rings seals on the puncture resistant plate, which has a minimum service temperature rating of -26 °C (-15 °F) [9]. The minimum predicted temperature in the seal area is not less than 119 °F (48 °C) for the conservative -40 °F (-40 °C) ambient NCT case (refer to Table 3-1); therefore, the use of the Viton® seals is acceptable.

#### 3.3.1.7 Evaluation of Cask Performance for Normal Conditions of Transport

The thermal analysis of NCT demonstrates that the TN-32B HBU demonstration cask design meets all applicable requirements, as documented in Table 3-1. The maximum temperatures calculated using conservative assumptions are well below specified limits.



The maximum temperature of any containment structural component is 368 °F (187 °C).

The maximum seal temperature is 232 °F (111 °C) during NCT, which is well below the lowest maximum temperature limit specified for all of the metallic seals of 663 °F (351 °C) for the overpressure port (OP) seal. The temperature limits for the remaining seals are even higher, (669 °F [354 °C]) for the vent/drain ports and thermocouple lance assemblies (TLAs), and (842 °F [450 °C]) for the closure lid seal, and hence, have greater temperature margins.

The maximum neutron shield temperature of 298 °F (143 °C) is below the conservative 300 °F (149 °C) allowable temperature. However, the model and analysis are conservative in that the personnel barrier is not included in the model. The personnel barrier would reduce the solar load on the cask exterior. Additionally, the decay heat input is slightly higher than half of the 25.84 kW decay heat (the fuel assemblies included in the half model produce more than half of the total decay heat). Factoring these conservatisms into the actual transport condition, the maximum temperature of the resin will be lower. Additionally, resin sensitivity and grid convergence were evaluated and documented in Reference [22] to demonstrate that the thermal analysis models the resin accurately. Therefore, no degradation of the neutron shield is expected.

The predicted maximum fuel cladding temperature of 510 °F (266 °C) is well below the allowable fuel temperature limit of 752 °F (400 °C).

Thermal performance tests conducted on two standard TN-32 casks documented in Reference [20] demonstrates that the thermal model adequately considers the insulating effect of the neutron shield and the gaps between multiple shells of the cask, and properly bounds the uncertainties and imperfections expected in the as-fabricated condition of this cask.

Based on the thermal evaluation of the TN-32B HBU cask, the thermal margins of the fuel cladding and seal (main containment critical components) temperatures when compared to the maximum allowable temperature limits are:

Fuel cladding margin:  $752 - 510 = 242$  °F

Containment O-ring seal margin:  $663 - 232 = 431$  °F

Note that 663 °F corresponds to the lowest temperature rating for the O-ring seals.

The gaps between various cask components assumed in the analysis are conservative; therefore, where the gaps assumed in the analysis are not equivalent to the gaps present in the as-fabricated cask, the measured temperatures are expected to be lower than the analytical values.

### 3.3.2 Maximum Normal Operating Pressure

The cask cavity is filled with helium following the draining process. In accordance with Section 4.2.1 of Reference [21] for the leaktight containment of the TN-32B HBU demonstration cask, release calculations for postulated failure of the HBU payload are not required. However, this conservative condition will be utilized, and additional pressure due to fission gases from the fuel rods will be included.

In accordance with the storage license Technical Specifications, the cask void volume was specified to be filled with  $2,230 \pm 100$  mbar of helium. During the loading operation, an initial backfill pressure of 2,180 mbar (31.6 psia) was recorded following a 3-day thermal soaking of the cask. To maximize the mass of the helium gas, the initial fill temperature is assumed to be the average measured external cask surface temperature at the time of the fill (179 °F), which is conservative.

From Reference [22], the net cavity volume,  $V_{cav}$ , is 308,645 in<sup>3</sup> (5.058 m<sup>3</sup>). The fuel rod fill and irradiation gasses will result in a total of 123 and 391 moles [22], respectively. Assuming a 3% release of these gasses per Reference [21] and the net cavity volume, the total pressure in the cavity,  $P_{cav}$ , is determined as follows:

$$P_{cav} = 31.6 \text{ psia} \frac{(417 \text{ °F} + 460 \text{ °F})}{(179 \text{ °F} + 460 \text{ °F})} + \frac{(.03)(514 \text{ mol})[8.314 \frac{\text{J}}{\text{mol-K}}](417 \text{ °F} + 460 \text{ °F})(.556 \text{ K/°R})}{(5.058 \text{ m}^3)(6,894.8 \text{ Pa/psi})}$$

$$P_{cav} = 45.2 \text{ psia} = 30.5 \text{ psig}$$

The MNOP in the TN-32B HBU demonstration cask is 30.5 psig for the bounding NCT condition. Therefore, the internal pressure of the TN-32B HBU cask will remain below the maximum design pressure of 100 psig with the HBU payload.

### 3.4 Thermal Evaluation under Hypothetical Accident Conditions

The TN-32B HBU demonstration cask is evaluated under the HAC sequence of 10 CFR §71.73 [1]. The top impact limiter protects the TN-32B HBU demonstration cask closure lid, containing the drain/vent port seals, and thermocouple lances from the thermal accident environment. Analytical models are developed to demonstrate that seal temperatures are below their material temperature limits during and following the HAC thermal event.

#### 3.4.1 Initial Conditions

The initial conditions for the cask prior to the HAC event are described below in terms of modifications made to the NCT thermal model to simulate the assumed cask conditions prior to and during the HAC event. The modifications are as follows:

- Simulated the worst-case damage arising from the postulated HAC free and puncture drops. Refer to Figure 3-14 and Figure 3-15.
- The pre-fire nodal temperatures are retrieved from the result file of a solar insolation normal conditions (NCT) model without deformed impact limiters at 100 °F ambient. Nodal temperatures are transferred to the HAC model as the initial condition utilizing the "IC" command in ANSYS® prior to the 30-minute fire.

#### 3.4.2 Fire Test Conditions

The fire test conditions analyzed to address 10 CFR §71.73(c) requirements are as follows:

- The initial ambient conditions are 100 °F ambient with insolation and deformed impact limiters from the HAC (side and end) drops and the puncture,
- At time = 0, a fully engulfed fire environment of 1,475 °F (800 °C) ambient with an effective fire emissivity of 0.9 and surface emissivity of 0.8 are utilized to simulate the average flame temperature of the hydrocarbon fuel/air fire event.
- The convection heat transfer coefficient between the cask and ambient during the 30-minute fire event considers a bounding value of 4.5 Btu/hr-ft<sup>2</sup>-°F, based on data from Reference [23]. The convection and radiation heat transfer coefficients from the 30-minute fire event to TN-32 HBU demonstration cask outer surfaces are combined together in form of total heat transfer coefficient.
- All air gaps associated with the cask and impact limiters representing contact resistances are removed, and conservatively replaced with the thermal conductivity of the material adjacent to the gap with the higher thermal conductivity during the fire and 30-minute charred wood events to maximize heat input from the fire into the cask. The gaps associated with the cask are restored to air during the post-fire 30-minute charred wood event, and subsequent 20-hour cool-down period to maximize the thermal resistance, and thus, maximize peak component temperatures. The gaps associated with the impact limiter conservatively remain metal during the 30-minute charred wood period since the outer faces of the charred wood interfacing with the impact limiter exterior shell are set at an elevated charred wood temperature, as shown in Figure 3-16. Thermal conductivity of the air gaps associated with the impact limiter is restored to air after the 30-minute charred wood event for the cool-down period.

- It is assumed all exposed surfaces of the cask are covered with soot after the fire. The solar absorptivity of soot is 0.95 per Reference [23]. To bound the post-fire condition, the analysis utilized a solar absorptivity of 1.0 and an emissivity of 0.9 for all cask surfaces exposed to the environment during the cool-down period.
- For the post fire cool-down period, the convection and radiation to ambient are combined in the form of a total heat transfer coefficient.
- Solar radiation is considered as a constant heat flux applied to ANSYS® SURF152 shell elements overlaid on the outer surfaces of the cask. The amount of solar heat flux over a 12-hour solar day is averaged over a 24-hour period to calculate the solar heat flux. The averaged solar heat flux is considered as the maximum amount of solar radiation that is available for absorption on any surface. This value is multiplied by the absorptivity factor of the cask outer surfaces to calculate the amount of solar heat flux that each surface absorbs.

### 3.4.3 Maximum Temperatures and Pressure

#### 3.4.3.1 Maximum Temperatures

Table 3-2 lists the predicted peak temperature of the TN-32B HBU demonstration cask under HAC conditions. As seen from the table, significant thermal margins exist for all components. The closure lid, the vent/drain ports, and the TLA seals remain below their maximum allowable temperatures.

Figure 3-17 illustrates the temperature profile within the TN-32B HBU demonstration cask at the end of the 30-minute hypothetical fire. The illustrated profile demonstrates the thermal protection afforded to the cask by the neutron shield, gamma shield, and wood-filled impact limiters by the fact that the high temperatures are limited to narrow regions on the exterior of the cask and impact limiter exterior shell. This thermal protection occurs despite the conservative level of damage assumed for the impact limiters.

Figure 3-18 illustrates the temperature profile within the cask at the end of a 30-minute post-fire smolder, and Figure 3-19 illustrates the temperature profile of a 40-hour cool-down following the 30-minute fire and the 30-minute post-fire smolder. The maximum temperature response profiles for the fuel assemblies and selected components are illustrated in Figure 3-20 through Figure 3-23. The relatively low temperature rise observed for the fuel assemblies and the cask components over the HAC event demonstrates the adequacy of the thermal protection of the cask design.

The thermal analysis of the hypothetical accident conditions concludes that the TN-32B HBU demonstration cask design meets all applicable requirements. The predicted maximum fuel cladding temperature is well below the HAC allowable fuel temperature limit of 1,058 °F (570 °C) by  $1,058\text{ °F} - 554\text{ °F} = 504\text{ °F}$ .

The maximum temperatures calculated utilizing conservative assumptions are low. The following seal temperatures are below the associated maximum seal temperature:

- Closure lid-to-flange containment seal:  $842\text{ °F} - 279\text{ °F} = 563\text{ °F}$

- Drain/vent port and lance containment seals: 669 °F - 279 °F = 390 °F
- Overpressure port seal: 663 °F - 279 °F = 384 °F

### 3.4.3.2 Maximum Pressure

The peak cask cavity pressure under HAC conditions is conservatively estimated in a similar manner as the NCT conditions (i.e., the bulk average cavity gas temperature is assumed to be equal to the mean of the average inner shell temperature and the average fuel basket temperature and the release of payload gasses).

Under the HAC condition, the peak bulk average helium temperature achieved under the HAC transient is 457 °F, as listed in Table 3-2. As discussed in Section 3.3.2, the cask void volume was filled with 2,180 mbar (31.6 psia) of helium. The initial gas fill temperature is assumed to be the average measured external cask temperature at the time of the fill (179 °F), where the temperatures and pressures are as reported data.

The 100% release of fuel rod fill and irradiation gasses results in 123 and 391 moles, respectively, of additional gasses. Therefore, the maximum cavity pressure,  $P_{cav}$ , for HAC is then:

$$P_{cav} = 31.6 \text{ psia} \frac{(457 \text{ °F} + 460 \text{ °F})}{(179 \text{ °F} + 460 \text{ °F})} + \frac{(514 \text{ mol})[8.314 \frac{\text{J}}{\text{mol-K}}](457 \text{ °F} + 460 \text{ °F})(.556 \text{ K/°R})}{(5.058 \text{ m}^3)(6,894.8 \text{ Pa/psi})}$$

$$P_{cav} = 107.8 \text{ psia} = 93.1 \text{ psig}$$

The maximum pressure in the TN-32B HBU cask is 93.1 psig for the bounding HAC condition. Therefore, the internal pressure of the TN-32B HBU demonstration cask will remain below the maximum design pressure of 100 psig with the HBU fuel assembly payload.

### 3.4.4 Maximum Thermal Stresses

The maximum thermal stresses for HAC conditions are presented in Subsection 2.7.4.2 of Chapter 2.

### 3.4.5 Accident Conditions for Fissile Material Packages for Air Transport

The TN-32B HBU demonstration cask is not transported by air transport. Therefore, this section does not apply.

### 3.5 References

1. Title 10, Code of Federal Regulations - Energy, Part 71 (10 CFR 71), "Packaging and Transportation of Radioactive Material," 1-1-2021 Edition, U.S. Nuclear Regulatory Commission, Washington, D.C.
2. U.S. Nuclear Regulatory Commission, "Recommendations for Addressing Axial Burnup in PWR Burnup Credit Analyses," NUREG/CR-6801, March 2003.
3. U.S. Department of Defense Handbook, MIL\_HNBK\_5J, "Metallic Materials and Elements for Aerospace Vehicle Structures," 2003.
4. Viggiani, P, Urthaler, Y, Payares, C, Rojas-Solórzano, L, "Study of the Transient Temperature Profiles Induced by Changes of the Welding Parameters during Aluminum Two-Plate Arc Butt-Welding," American Society of Mechanical Engineers, Pressure Vessels and Piping Division (Publication) PVP Vol. 417, pp. 3-10, 2000.
5. U.S Department of Agriculture, Wood Handbook, pp. 46-47, "Agriculture Handbook No. 72," 1955.
6. Rohsenow, M. W., Cho, Y. I., and Hartnett, J. P., Handbook of Heat Transfer, 3<sup>rd</sup> Edition, 1998.
7. Siegel, Howell, "Thermal Radiation Heat Transfer," 4th Edition, 2002.
8. Gubareff, G., Janssen, J., and Torborg, R., "Thermal Radiation Properties Survey", 2<sup>nd</sup> Edition, Honeywell Research Center, 1960.
9. Parker Viton O-Rings, [www.sealingdevices.com/viton-o-rings](http://www.sealingdevices.com/viton-o-rings).
10. U.S. Nuclear Regulatory Commission, "Standard Review Plan for Spent Fuel Dry Storage Systems at a General License Facility," NUREG-1536 Rev.1, July 2010.
11. American Society of Mechanical Engineers, ASME Boiler and Pressure Vessel Code, Section III, Division 1, and Appendices, 1992 Edition with 1992 Addenda.
12. U.S. Nuclear Regulatory Commission, Effects of Temperature on the Energy Absorbing Characteristics of Redwood, NUREG/CR-0322, August 1978.
13. American Society of Mechanical Engineers, ASME Boiler and Pressure Vessel Code, Section II, Part D, 2013 Edition.
14. W. M. Rohsenow, J. P. Hartnett, "Handbook of Heat Transfer Fundamentals," 2<sup>nd</sup> Edition, 1985.
15. U.S Department of Agriculture, Wood Handbook, Wood as an Engineering Material, Forest Service, 2010.
16. Transnuclear, Inc., TN-24 Dry Storage Cask Topical Report, Revision 2A, Hawthorne, NY, 1989.

17. ANSYS® Engineering Analysis System, User's Manual for ANSYS® Release 8.0, and 8.1 ANSYS, Inc., Canonsburg, PA.
18. Transnuclear, Inc., "TN-32 Updated Final Safety Report," Rev. 6", Certificate of Compliance 1021.
19. Guyer, "Handbook of Applied Thermal Design," McGraw-Hill Inc., 1989.
20. Transnuclear, Inc., Letter to USNRC, "TN-32 Cask Thermal Testing," Docket No. 72-1021, December 1, 2000, Transnuclear Document No. E-18578, Project 1066.
21. U.S. Nuclear Regulatory Commission, Dry Storage and Transportation of High Burnup Spent Nuclear Fuel, NUREG-2224, November 2020.
22. Transnuclear, Inc., "TN-32B HBU Demonstration Cask Design/Licensing Basis Document (DLBD)," Document No. E-42038, Revision 9, November 15, 2019.
23. Gregory, et al., "Thermal Measurements in a Series of Large Pool Fires," SAND85-0196, TTC-0659, Sandia National Laboratories, 1987.

**Table 3-1**  
**NCT Component Temperatures in the TN-32B HBU Cask**

Component	Temperature (°F)				
	NCT Hot (No Solar)	NCT Hot <sup>1</sup>	NCT Cold (-20 °F)	NCT Cold (-40 °F)	Allowable (°F) <sup>2</sup>
Fuel Cladding	505	510	434	421	752
Thermocouple Lance <sup>3</sup>					800
Basket	463	468	386	372	800
Basket Rails	314	320	231	216	400
Cask Body Containment (Inner Shell, Cask Bottom Inner Plate, and Flange)	363	368 <sup>4</sup>	282	267	650
Gamma Shield Shell and Lid Shield Plate	341	347	259	244	2,600
Closure Lid	225	232	138	122	650
Closure Lid Bolts	224	230	136	121	
Main Containment Seal	224	230	136	121	842
OP Port Seal	225	232	138	122	663
Vent/Drain Ports and TLA Seals	225	232	138	122	669
Puncture Resistant Plate	222	229	134	119	2,600
Puncture Resistant Plate Viton <sup>®</sup> Seals	222	228	134	119	400
Radial Neutron Shield Aluminum Boxes	284	290	201	186	400
Radial Neutron Shield Resin	292	298	209	194	300
Outer Shield Shell	290	295	207	192	2,600
Top Impact Limiter Wood	Max	115	122	-2	230
	Avg	103	110	-16	
Bottom Impact Limiter Wood	Max	155	162	-43	230
	Avg	108	115	-11	
Impact Limiter Shell	Max	161	168	50	2,500
	Acc	101	113	-18	
Personnel Barrier <sup>5</sup>	176	-	-	-	185
Average Cavity Gas	412	417	336	323	-
Max. Accessible Surface	176	-	-	-	185

## Notes:

1. Based on steady-state evaluation with 24-hour average of regulatory insolation loading.
2. See Section 3.2.2 for basis of listed temperature criterion.
3. Thermocouple lance assemblies not explicitly modeled. Fuel assembly temperature is bounding.
4. Maximum payload cavity containment temperature.
5. Personnel barrier not explicitly modeled; temperature from Section 3.3.1.5.



**Table 3-2**  
**HAC Temperatures for TN-32B HBU Cask**

<b>Component</b>	<b>Maximum Transient Temperature (°F)</b>	<b>Time (hr)</b>	<b>Allowable (°F)</b>
Fuel Cladding	554	15.6	1,058
Basket	516	14.3	- <sup>1</sup>
Basket Rails	396	2.9	- <sup>1</sup>
Cask Body Containment (Inner Shell, Cask Bottom Inner Plate, and Flange)	411	16.6	- <sup>1</sup>
Gamma Shield Shell	684	0.5	- <sup>1</sup>
Closure Lid	279	29.0	650-
Closure Lid Bolts	279	27.5	
Main Containment Seal	279	27.9	842
Drain/Vent, and TLA Seals	279	29.2	663
Puncture Resistant Plate	277	32.5	- <sup>1</sup>
Radial Neutron Shield Aluminum Boxes	1,202	0.5	- <sup>1</sup>
Impact Limiter Surface	1,476	0.5	- <sup>1</sup>
Average Cavity Gas	457	17.4	N/A

## Notes:

1. The components perform their intended function within the allowable temperature limit.

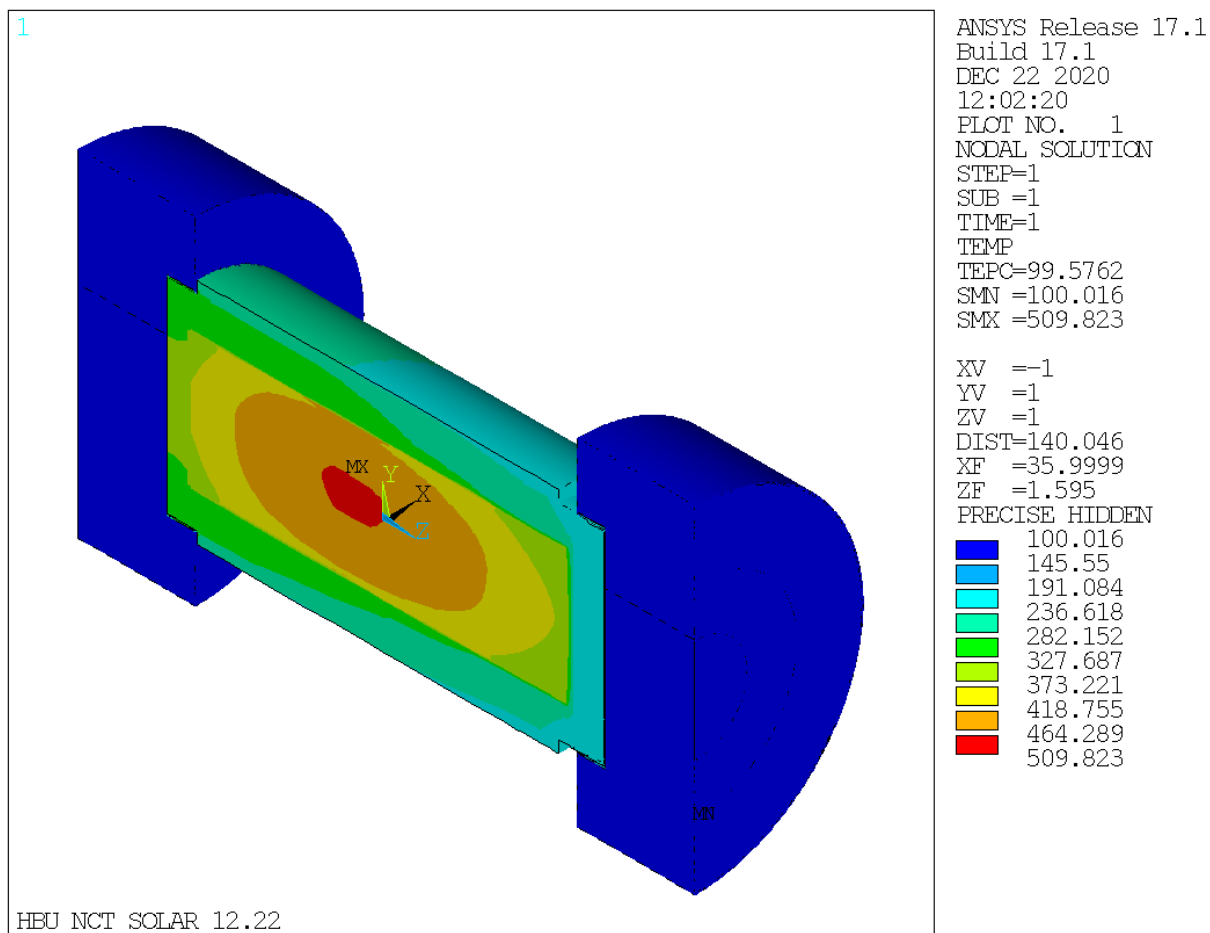


**Figure 3-1**  
**NCT Hot (100 °F Ambient) Temperatures Distribution for TN-32B HBU Cask**

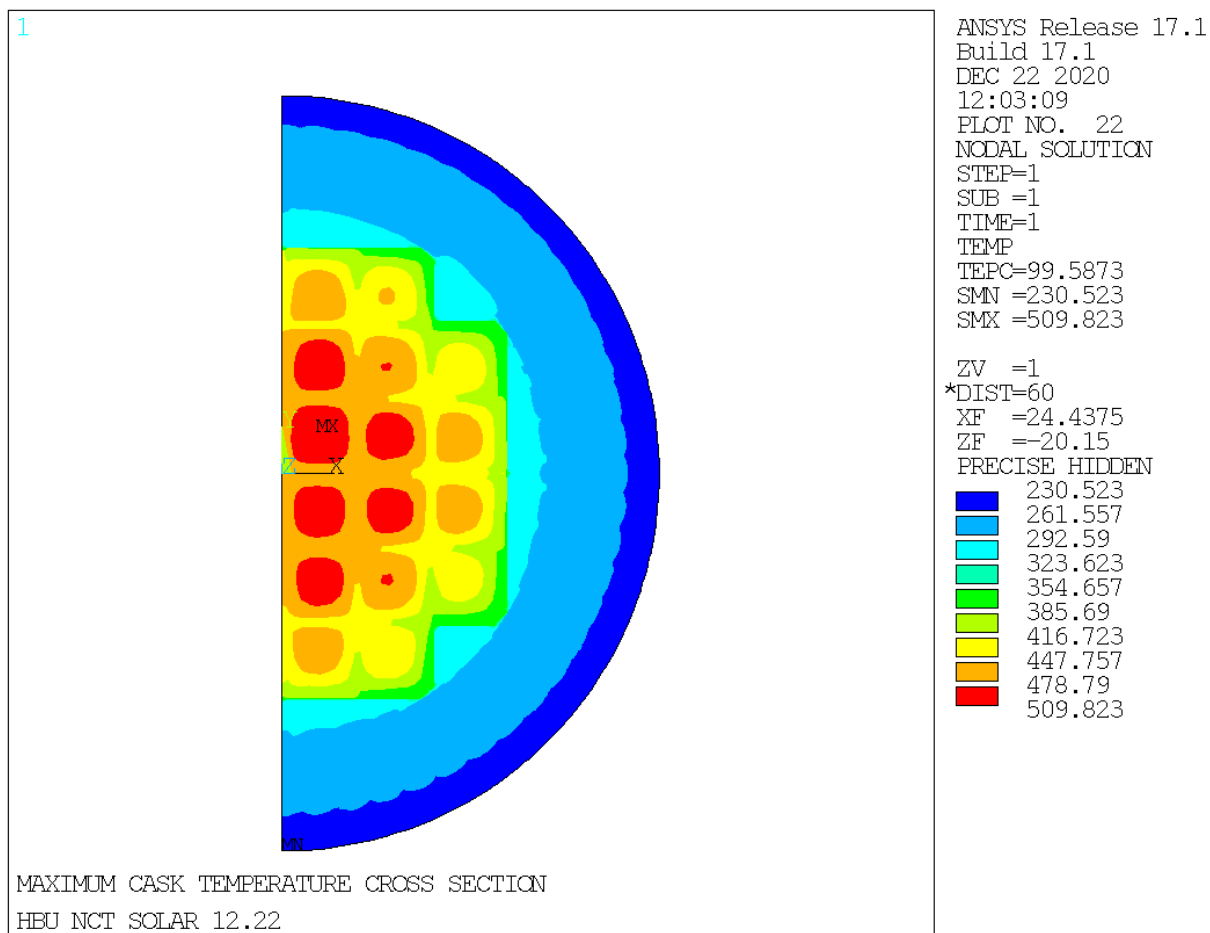


**Figure 3-2**  
**NCT Hot (100 °F Ambient) Peak Cask Temperature Cross-Section**

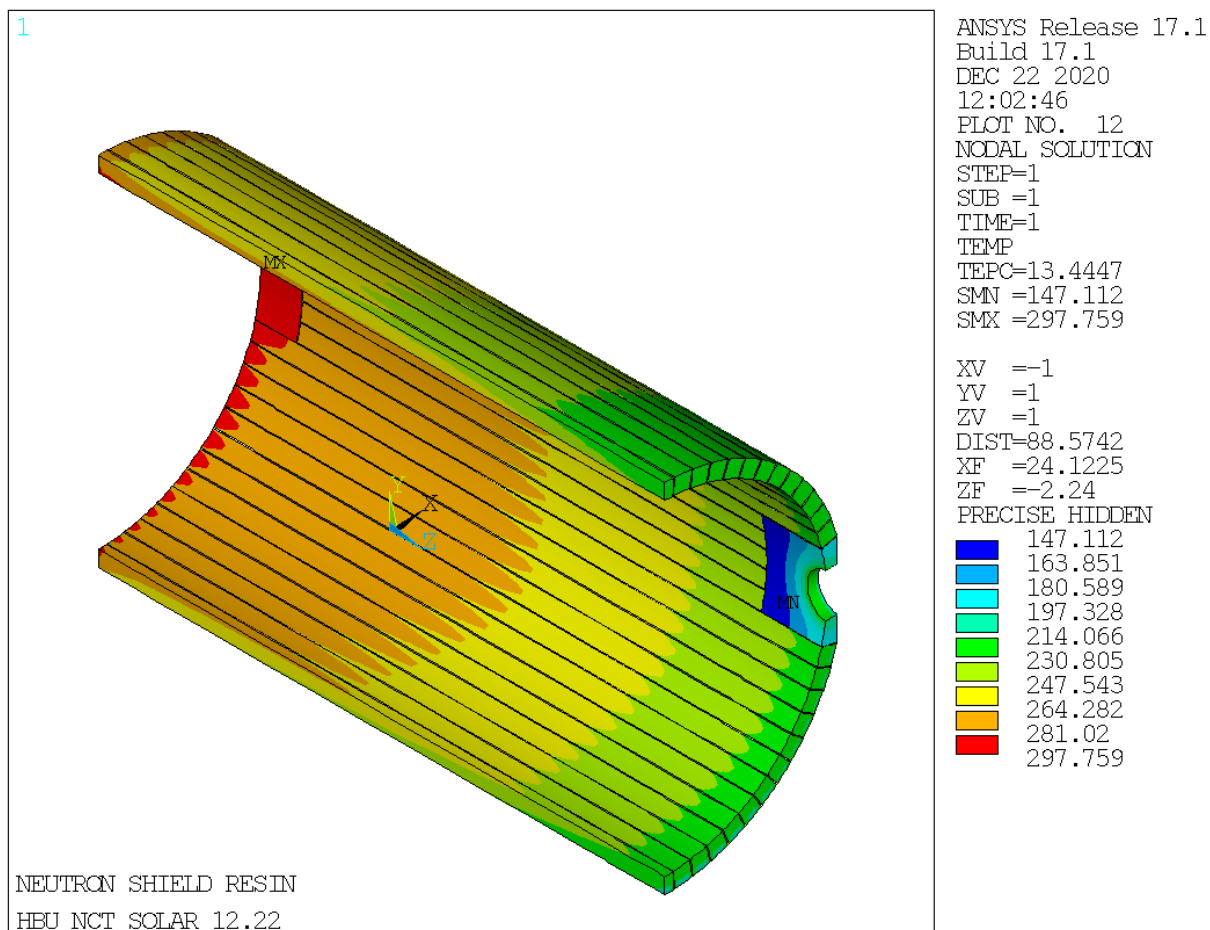


**Figure 3-3**  
**NCT Hot (100 °F Ambient) Neutron Shield Resin Temperature Profile**

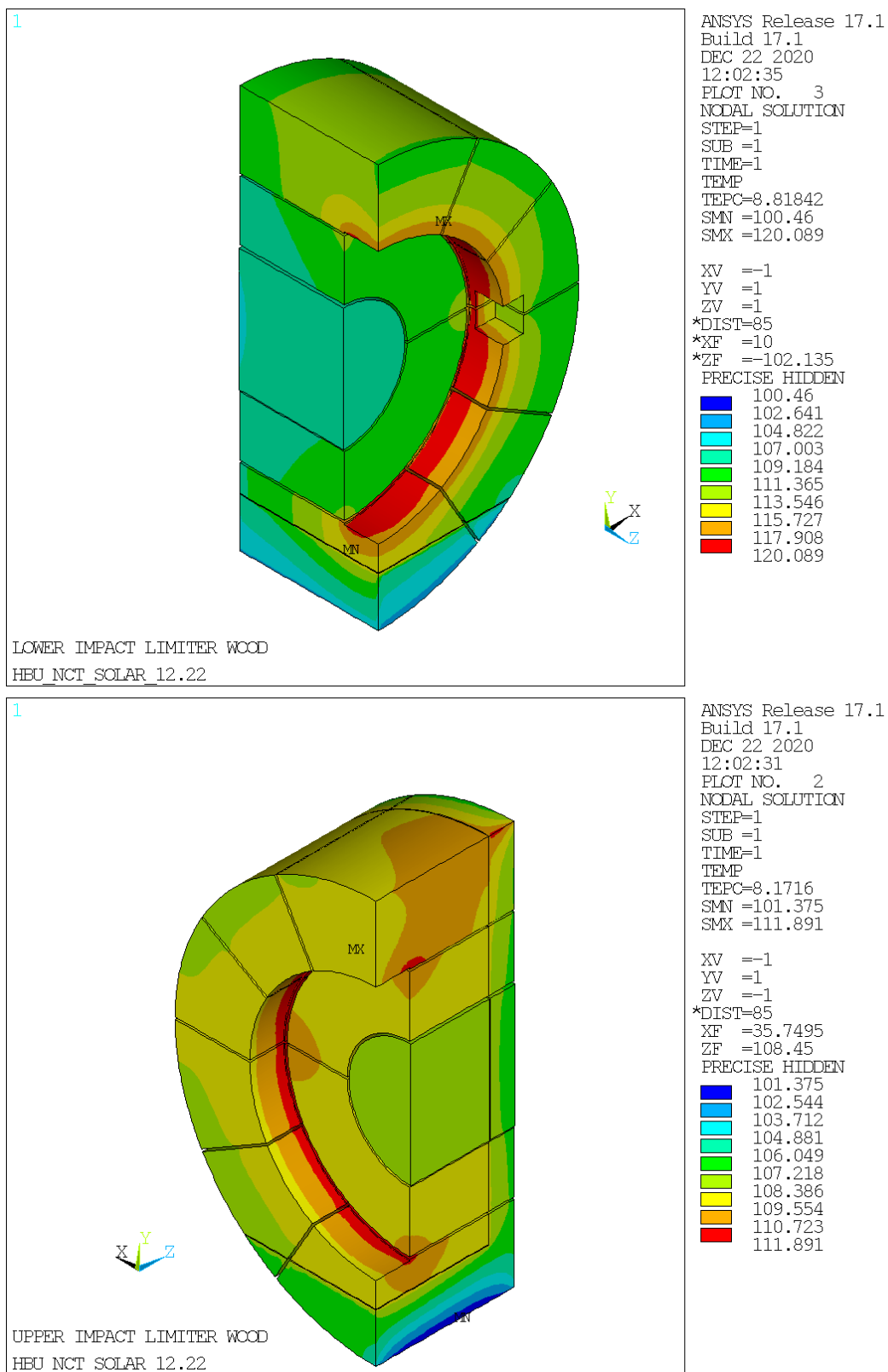


**Figure 3-4**  
**NCT Hot (100 °F Ambient) Wood Temperature Profile**

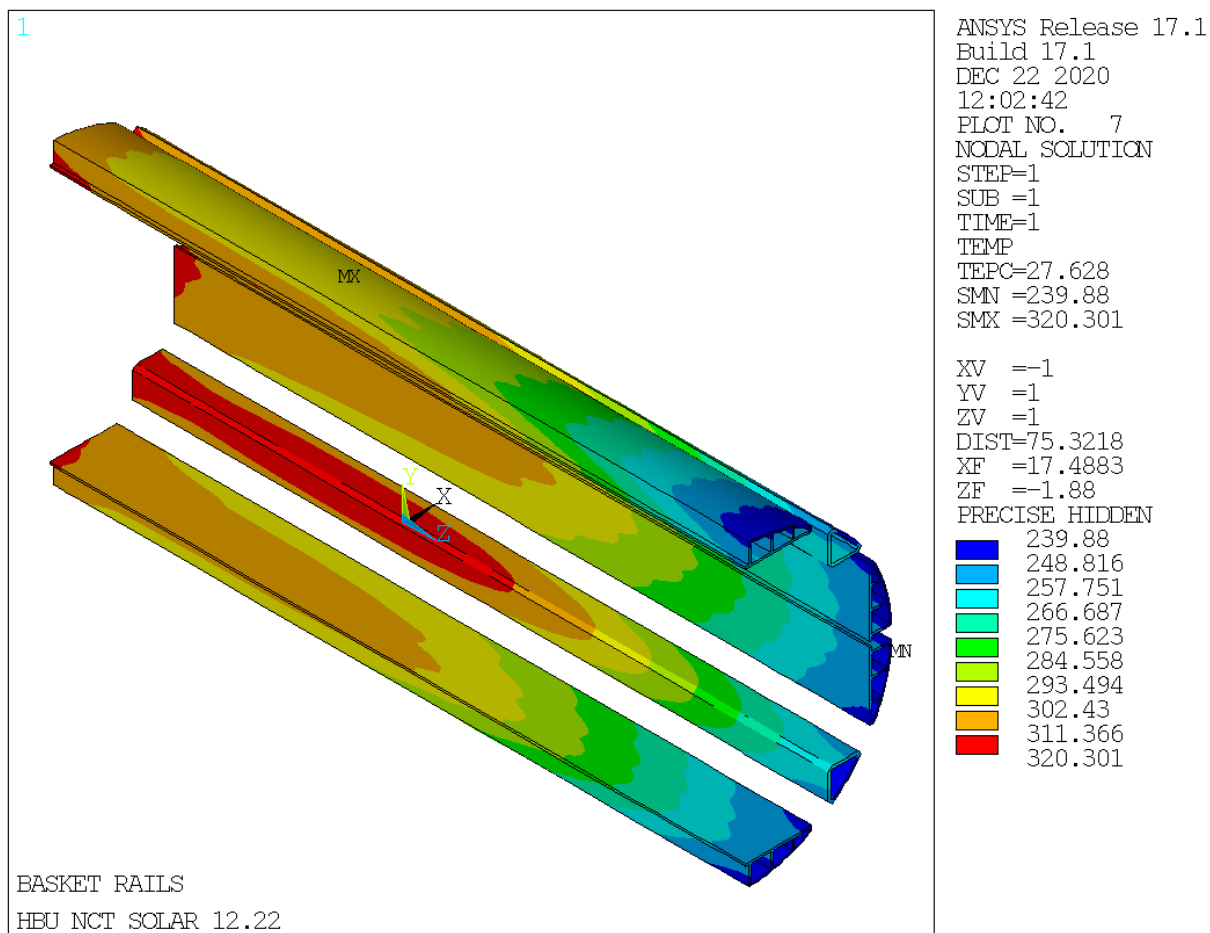


**Figure 3-5**  
**NCT Hot (100 °F Ambient) Aluminum Cask Rails Temperature Profile**

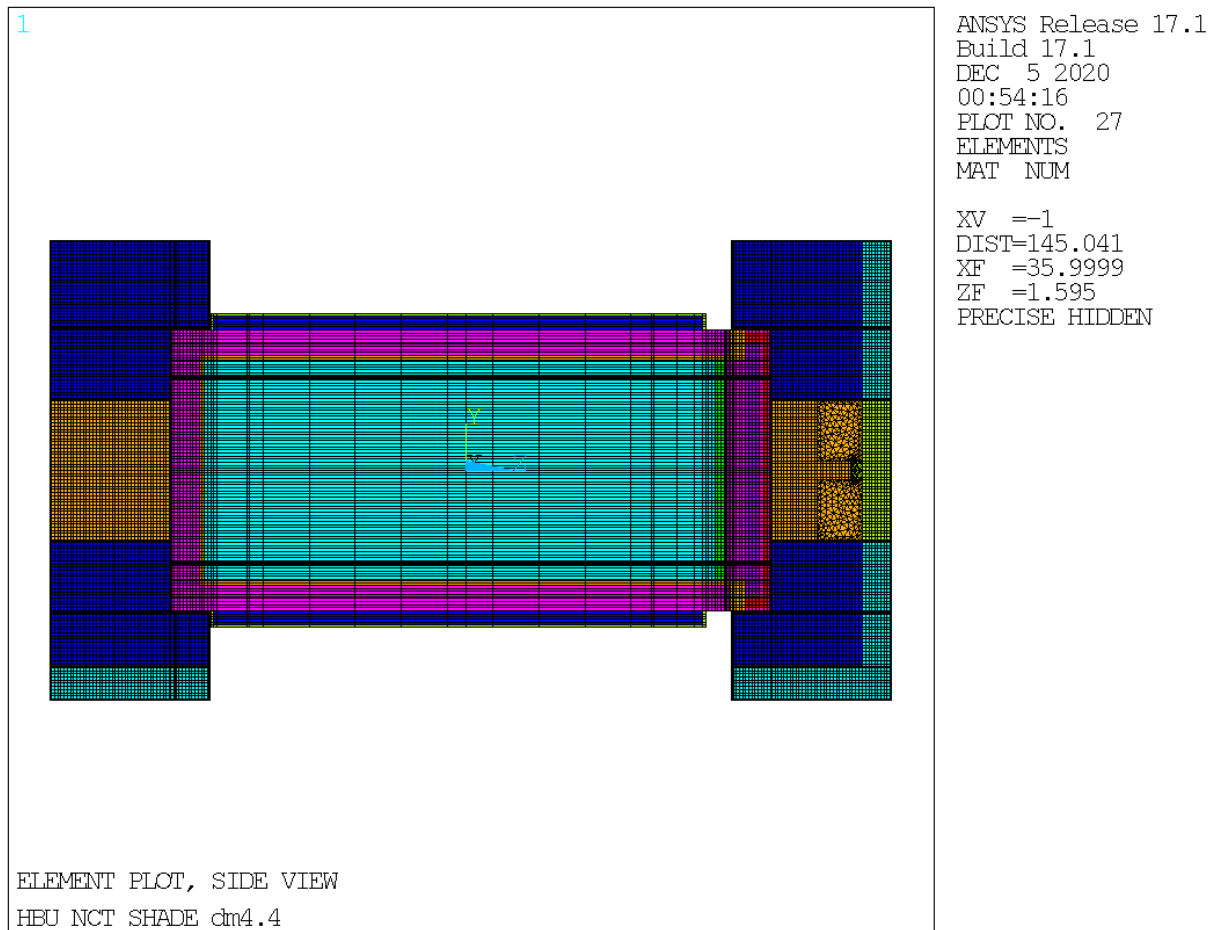


**Figure 3-6**  
**TN-32B HBU Model Mesh – Side View**

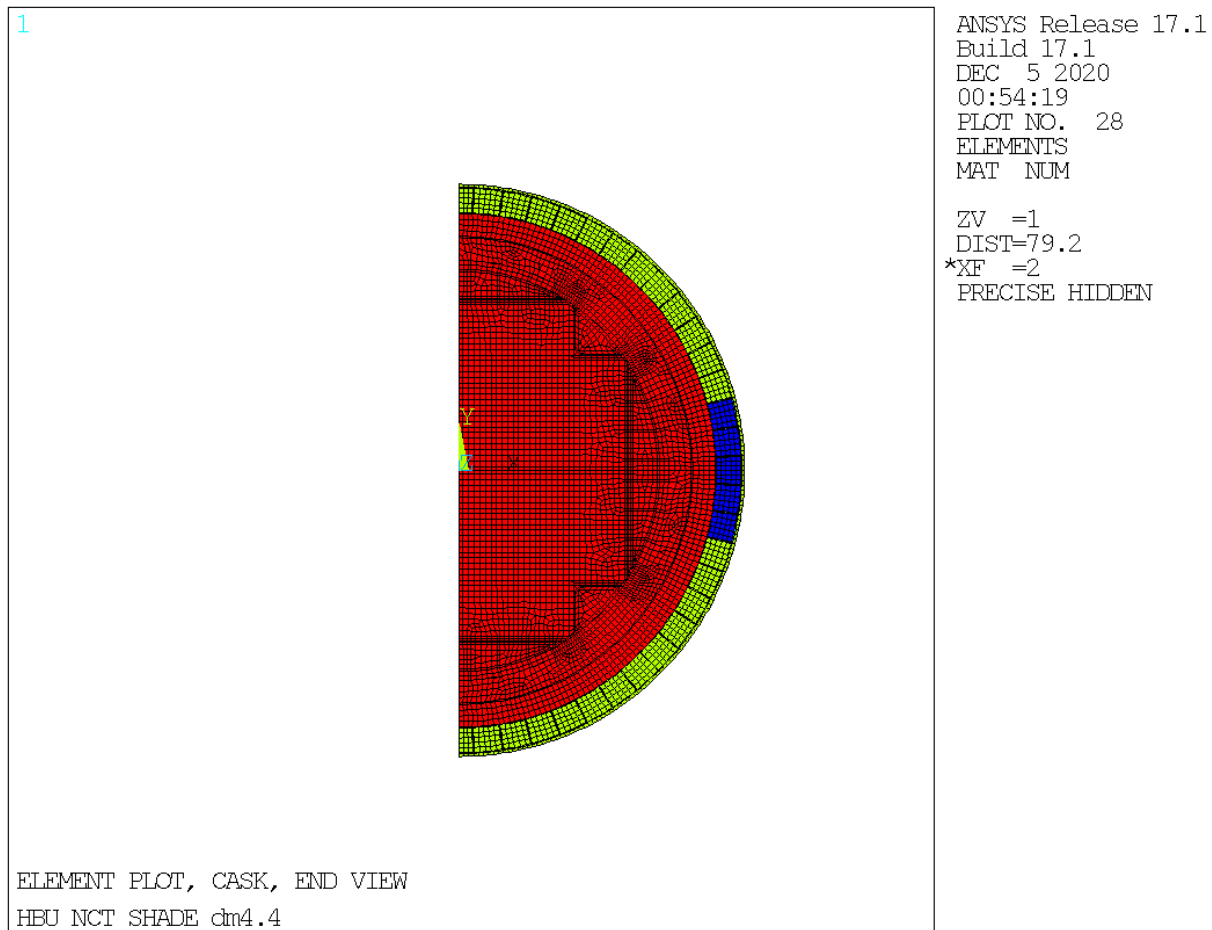


**Figure 3-7**  
**TN-32B HBU Cask Mesh – End View**



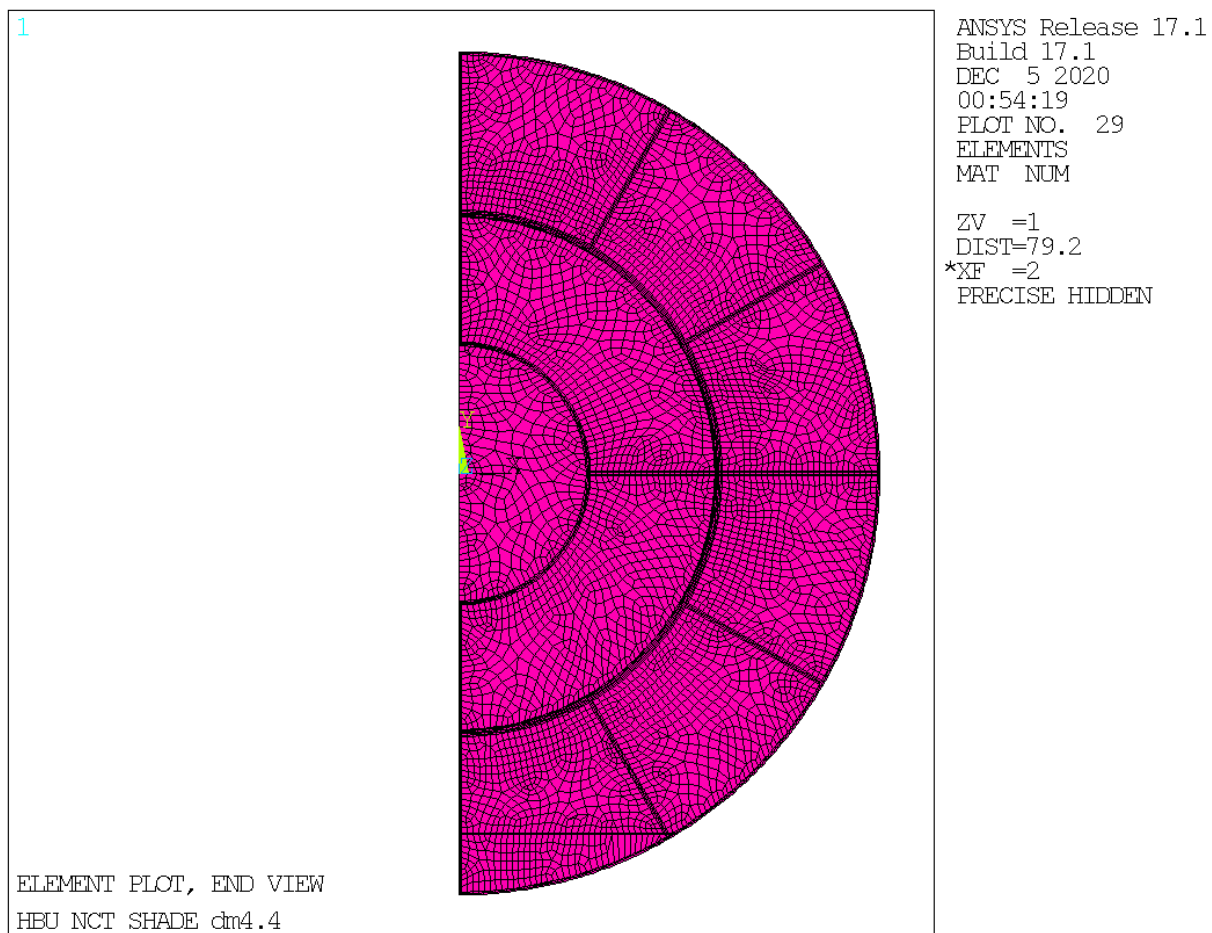


**Figure 3-8**  
**TN-32B HBU Impact Limiter Mesh – End View**

Proprietary Information on This Page  
Withheld Pursuant to 10 CFR 2.390

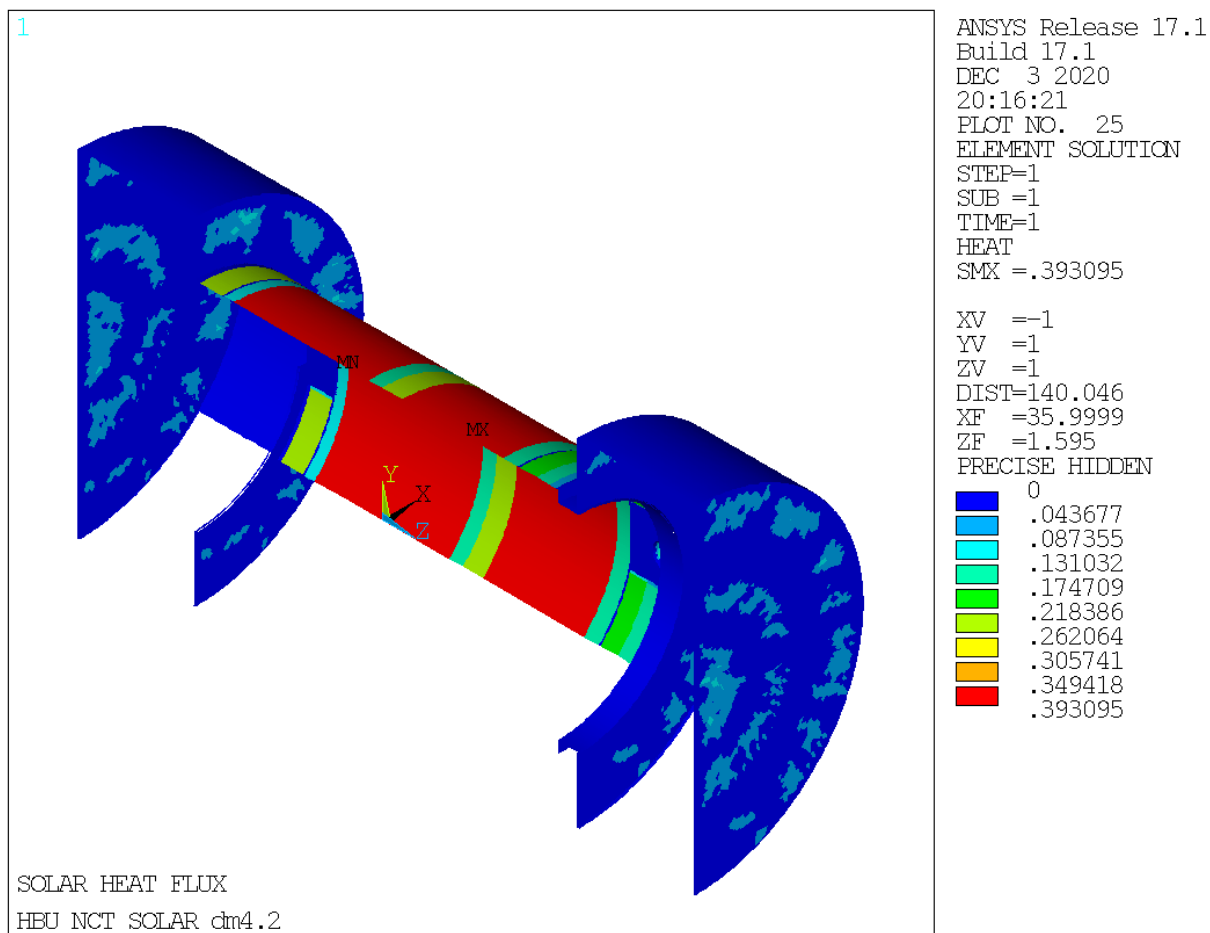
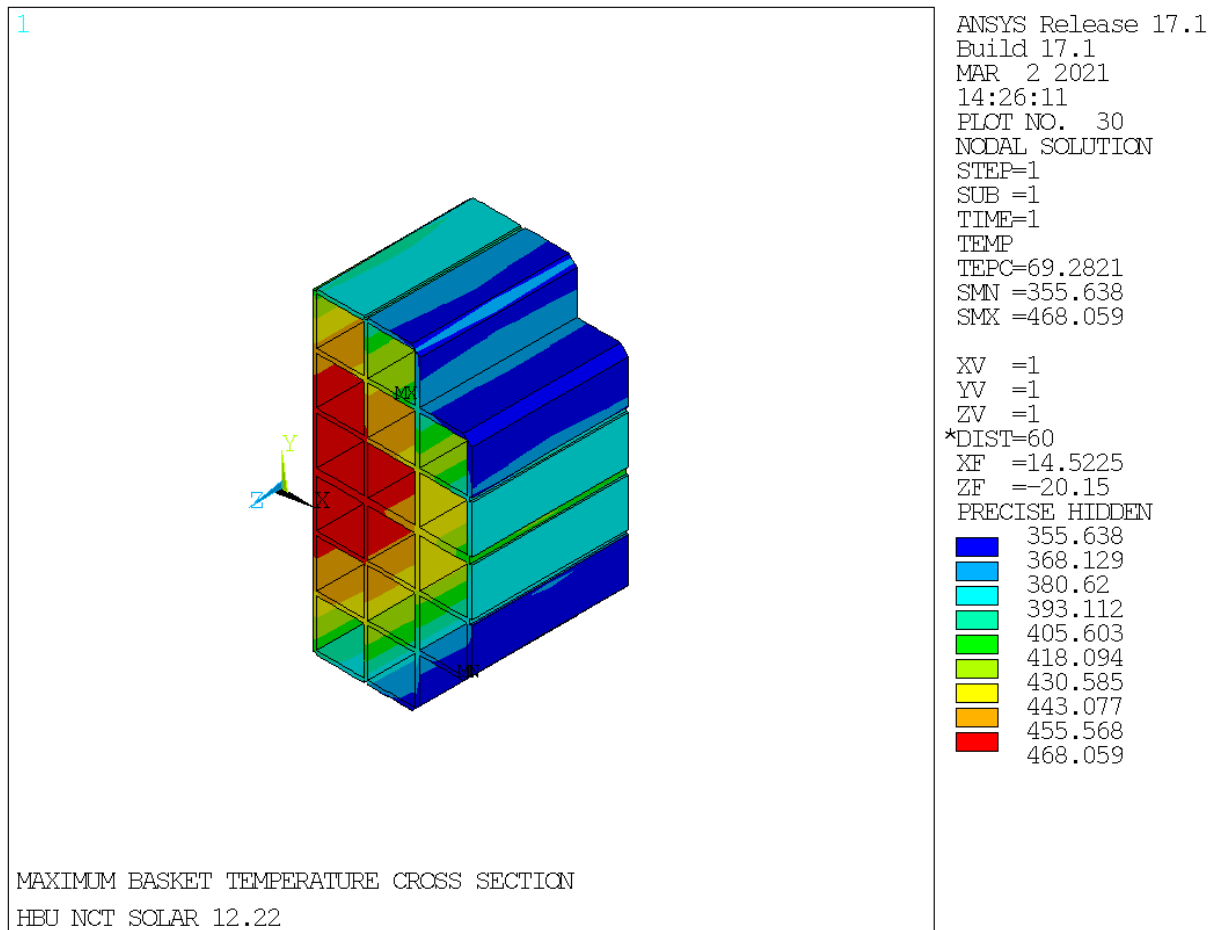
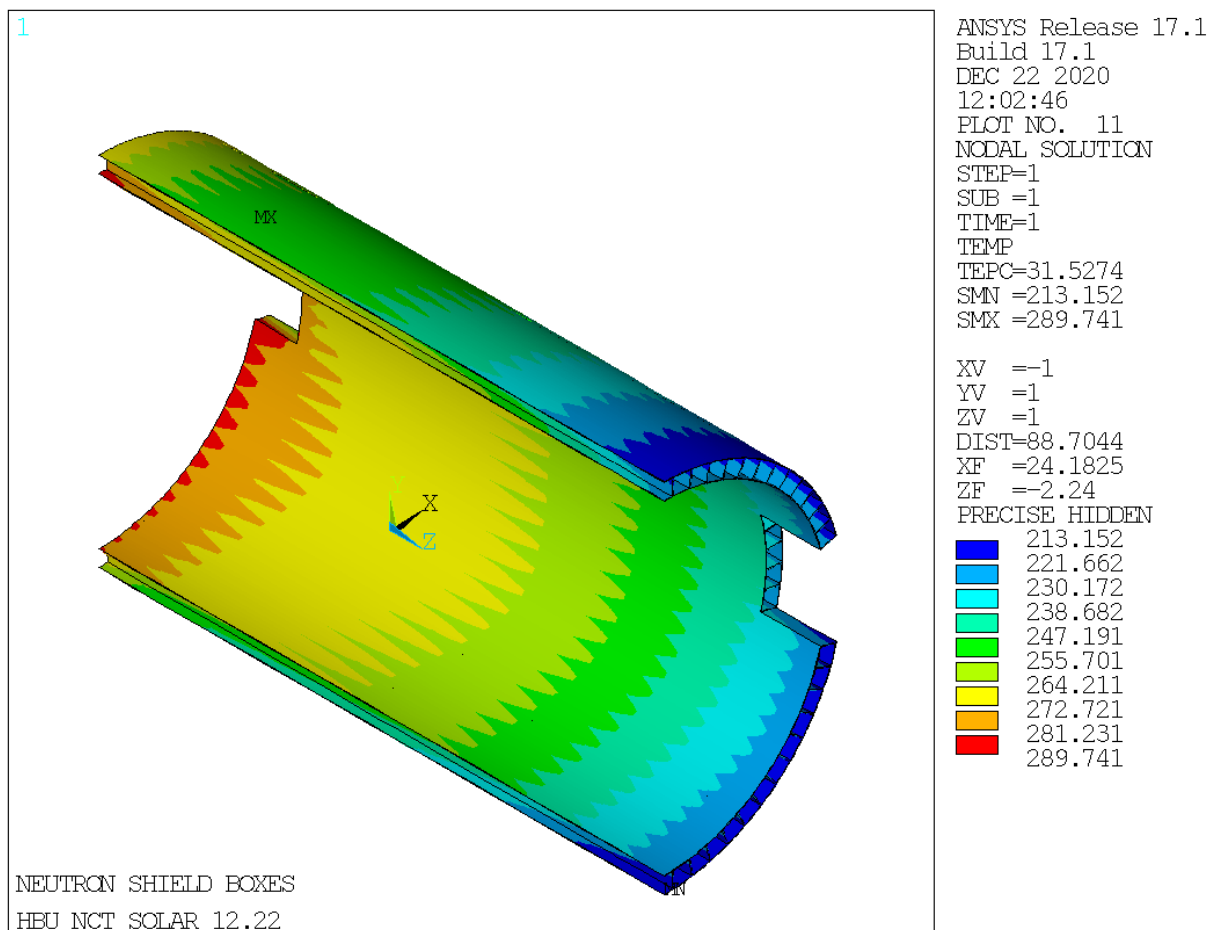


Figure 3-10  
TN-32B HBU Surfaces with Solar – Rotated View



**Figure 3-11**  
**NCT Hot (100 °F Ambient) Peak Basket Temperature at Max Cross Section**



**Figure 3-12**  
**NCT Hot (100 °F Ambient) Neutron Shield Boxes Temperature Profile**

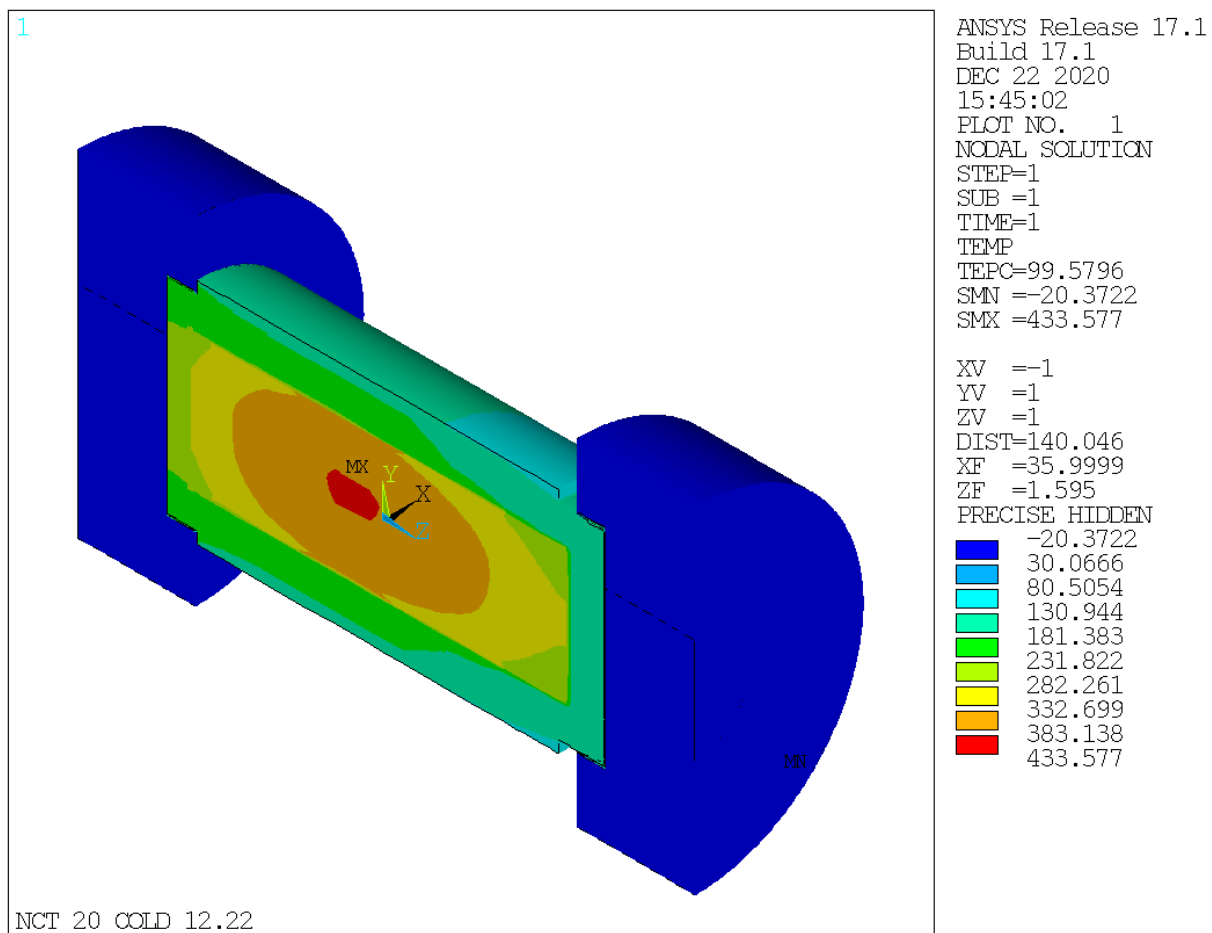


**Figure 3-13**  
**NCT Cold (-20 °F Ambient) Package Temperature Profile**

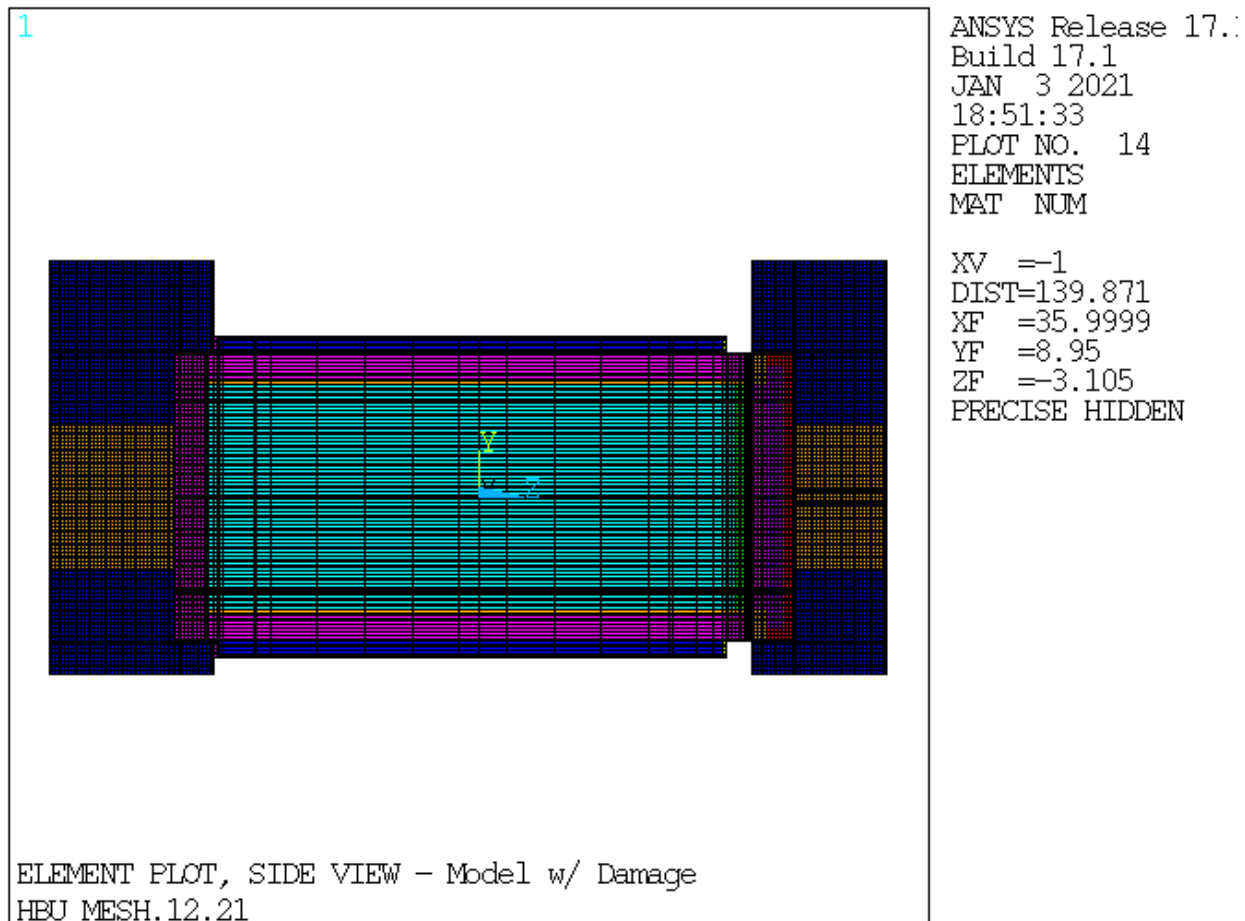


**Figure 3-14**  
**Side View – TN-32B HBU Cask Model with Impact Limiter Damage**

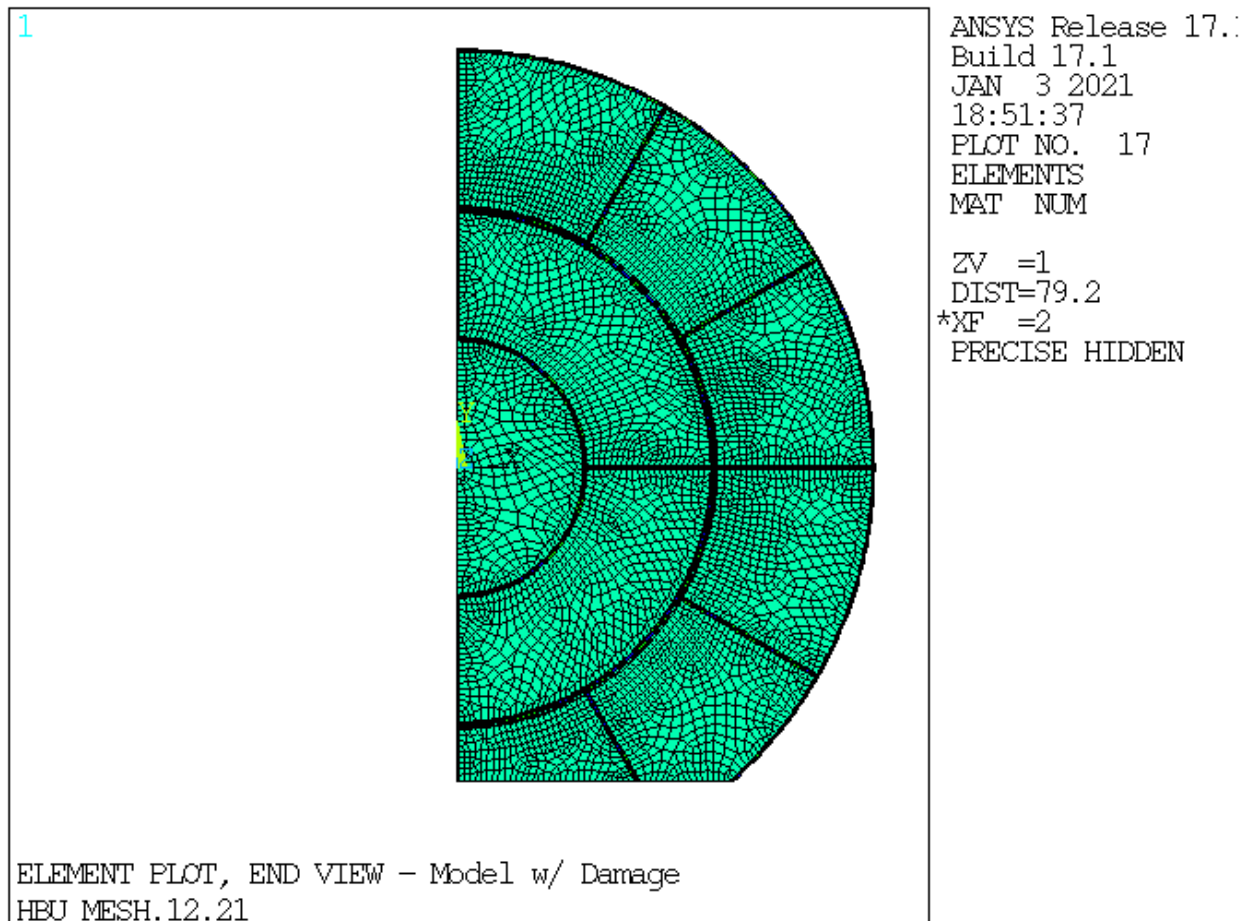


**Figure 3-15**  
**End View – TN-32B HBU Cask Model with Impact Limiter Damage**



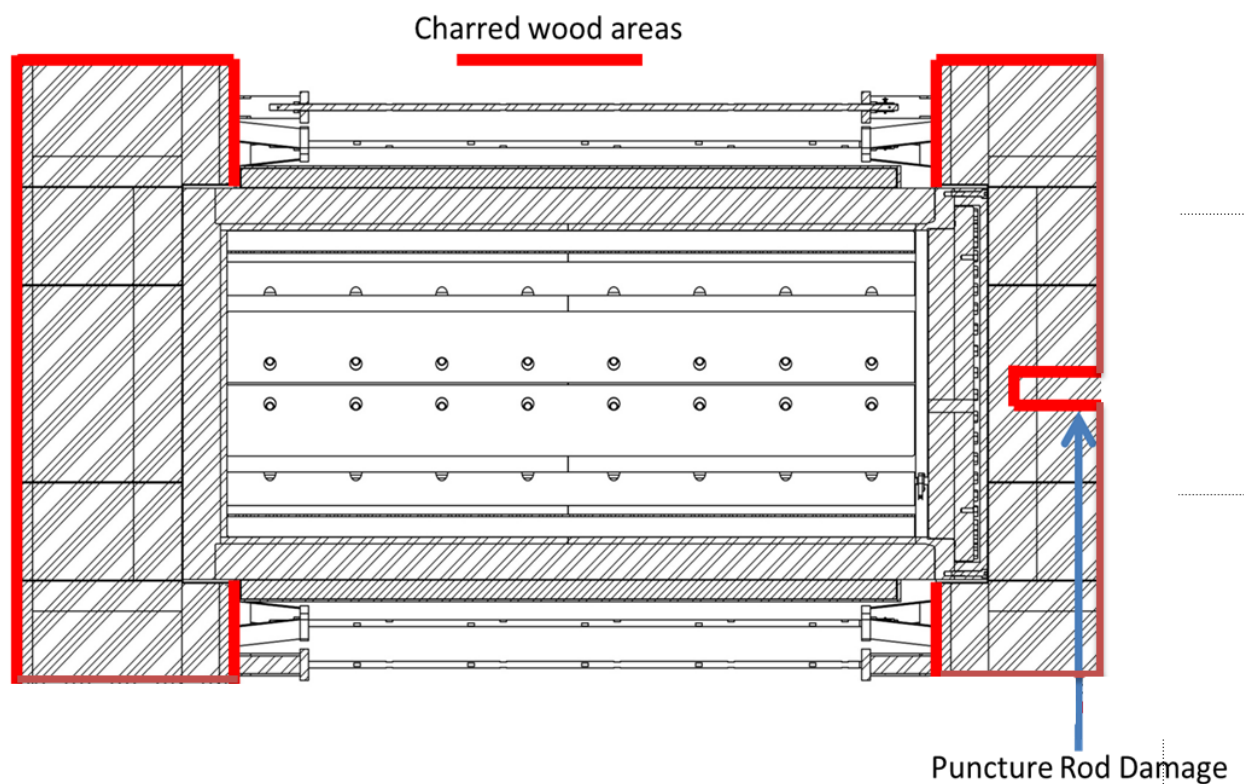


**Figure 3-16**  
**Wood Areas Exposed to Char Immediately after 30-minute Fire**

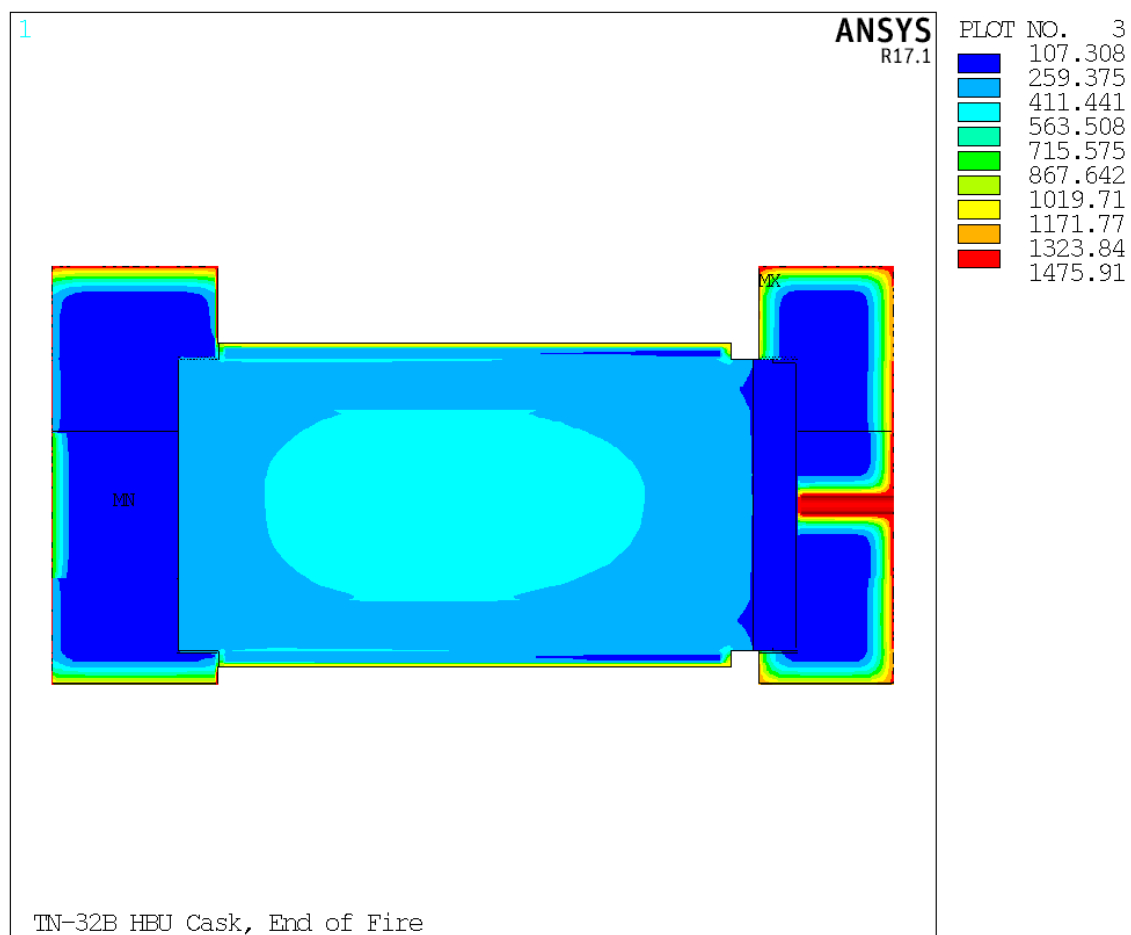
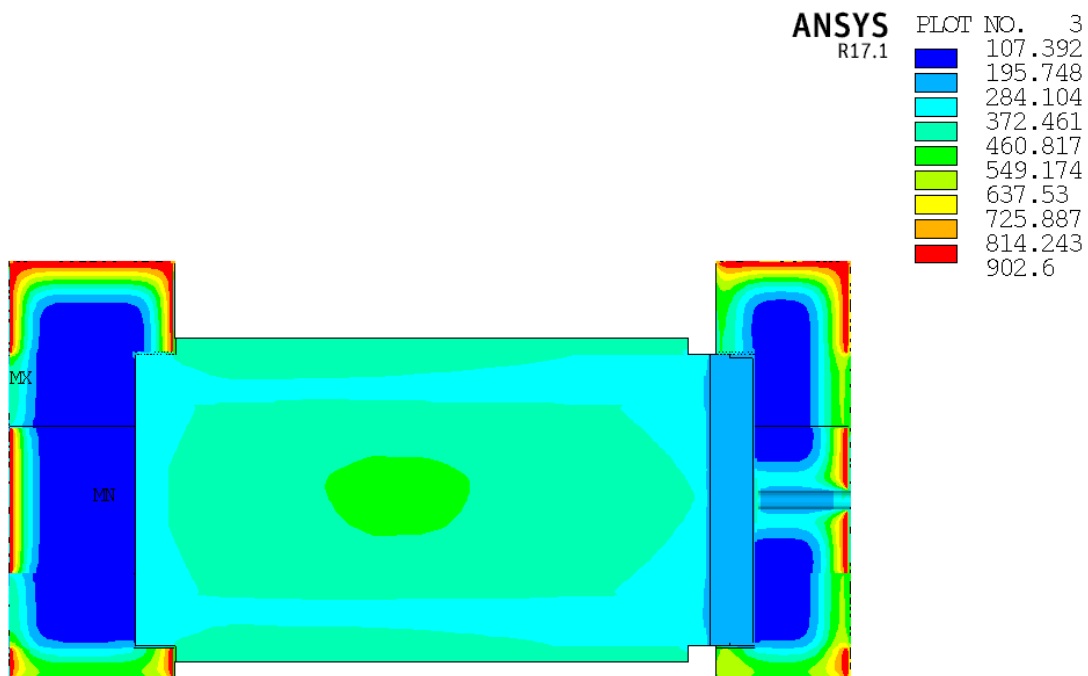
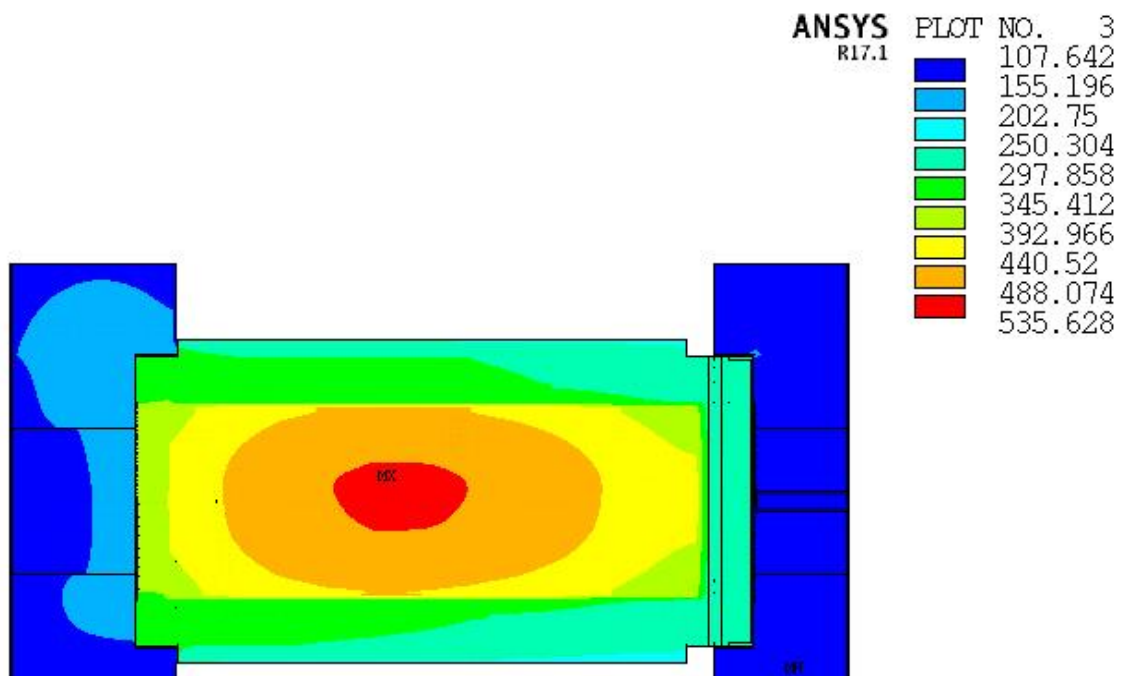


**Figure 3-17**  
**TN-32B HBU Cask HAC Temperature Distribution at End of 30 Minute Fire**



TN-32B HBU Cask, End of Smoldering

**Figure 3-18**  
**TN-32B HBU Cask HAC Temperature Distribution at End of 30 Minute Post-Fire Smolder**



TN-32B HBU Cask, End of Cool-down

**Figure 3-19**  
**TN-32B HBU Cask HAC Temperature Distribution at End of 40 Hour Cool Down (Follows 30-minute fire and 30-minute smolder)**

## FUEL Temperature History

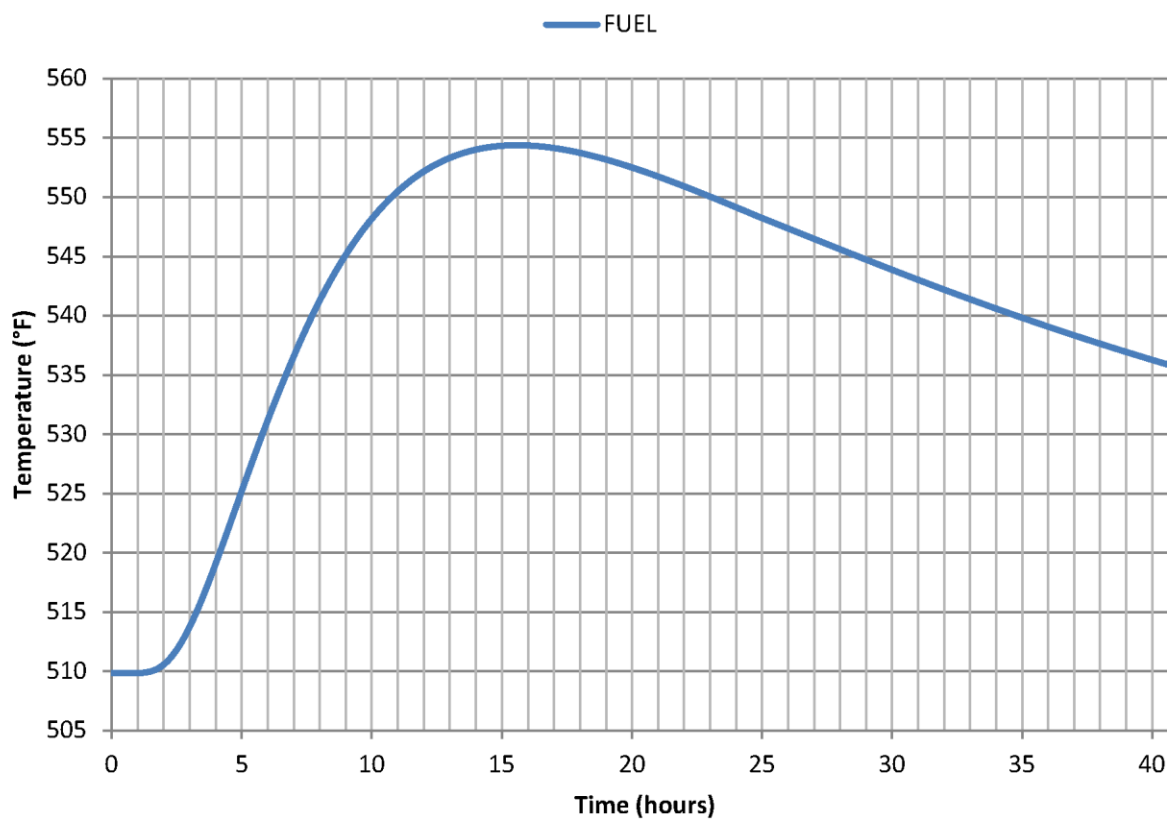


**Figure 3-20**  
**TN-32B HBU Cask HAC Maximum Fuel Temperature History**

## Cask Component Temperature History

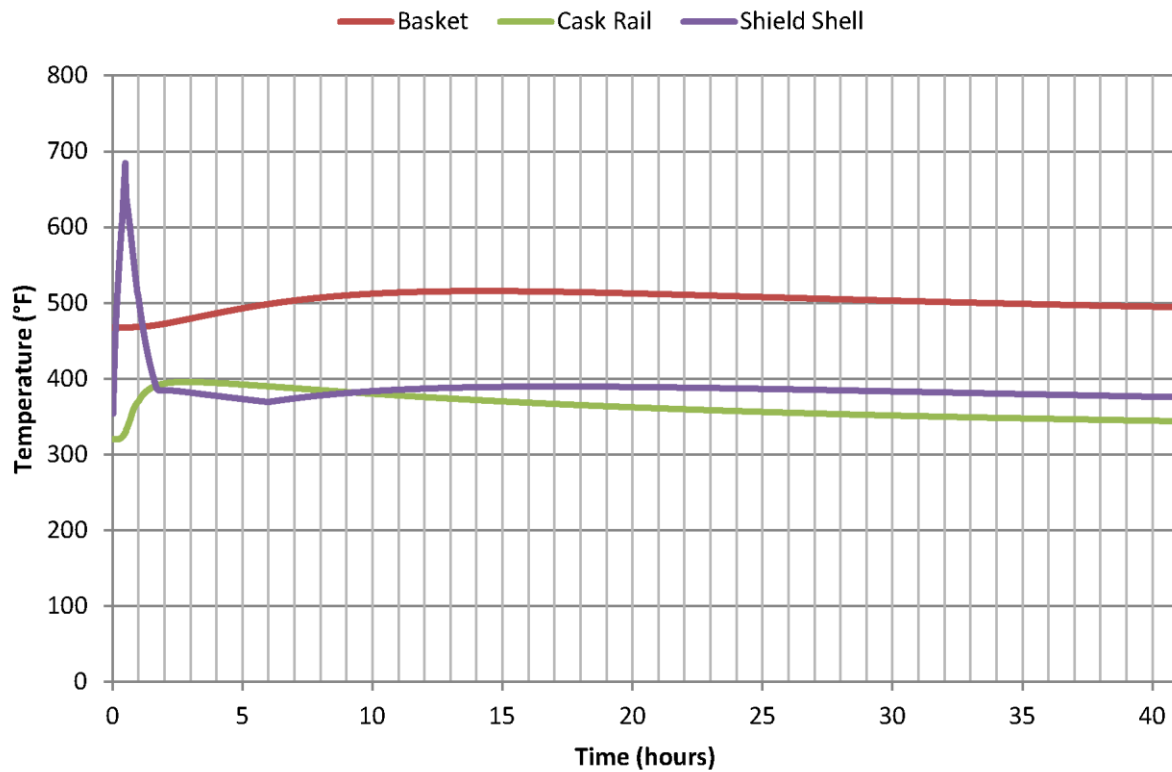


**Figure 3-21**  
**TN-32B HBU Cask HAC Maximum Cask Component Temperature History**

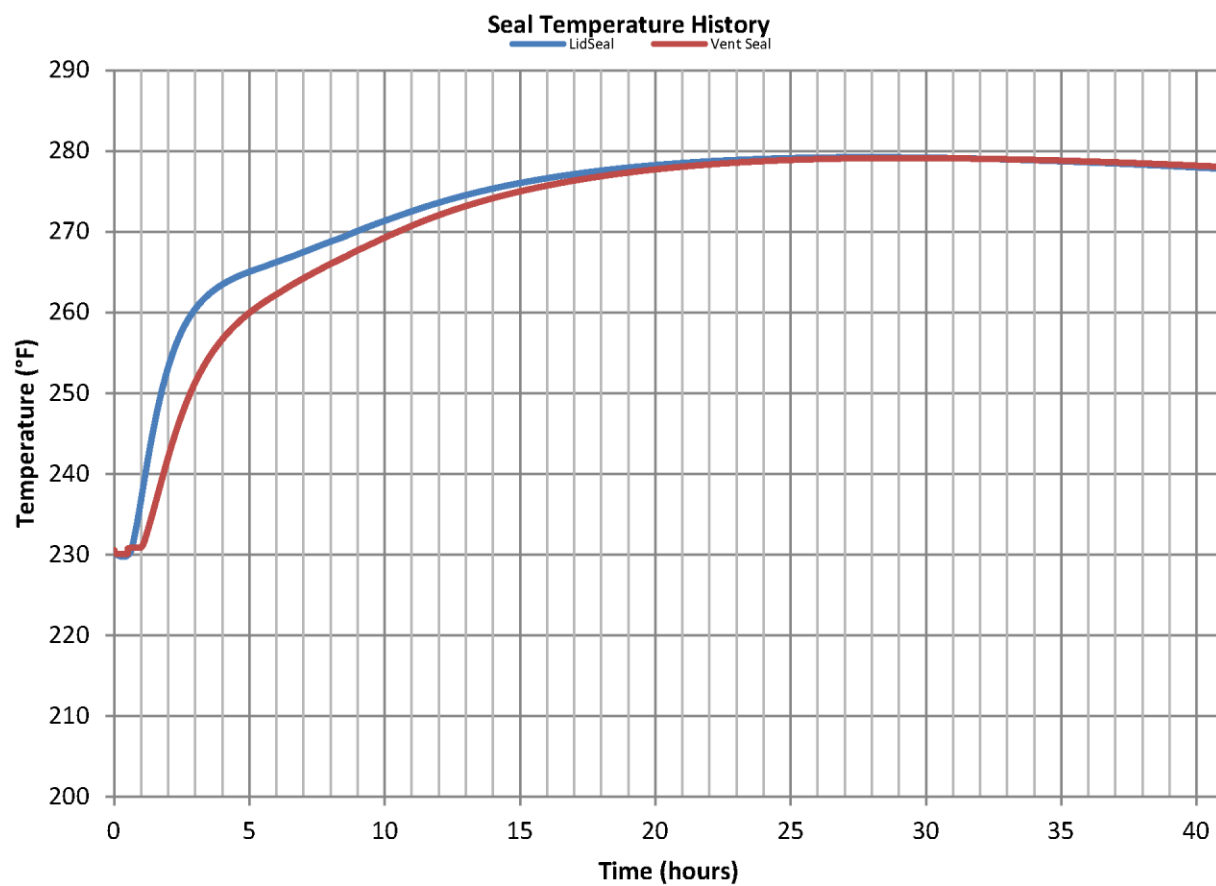


**Figure 3-22**  
**TN-32B HBU Cask HAC Maximum Seals Temperature History**

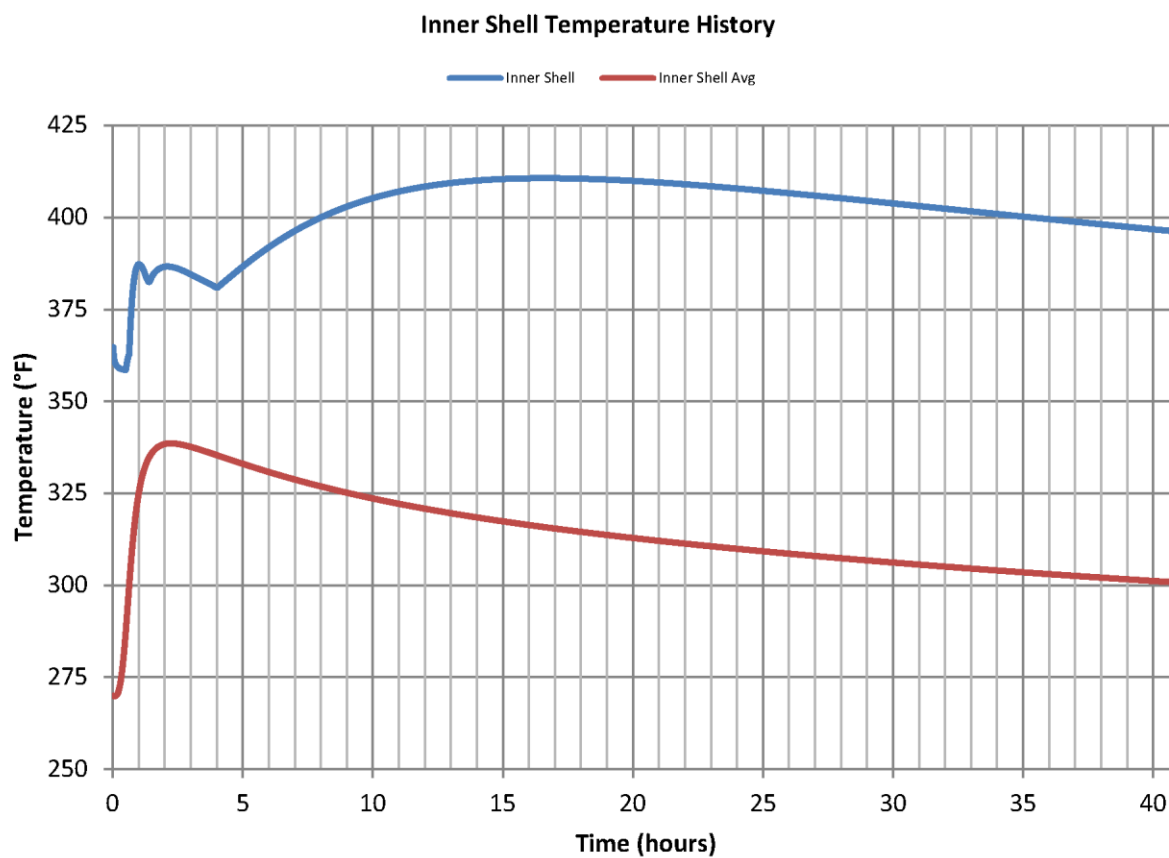


**Figure 3-23**  
**TN-32B HBU Cask HAC Inner Shell Temperature History**



### **3.6 Appendix**

The detailed thermal properties of the TN-32B HBU demonstration cask are included in the following appendix:

Appendix 3.6.1 Effective Thermal Properties for the Fuel Assembly

### **Appendix 3.6.1**

#### **Effective Thermal Properties for the Fuel Assembly**

##### TABLE OF CONTENTS

3.6.1	Effective Thermal Properties for the Fuel Assembly .....	3.6.1-1
3.6.1.1	Discussion.....	3.6.1-1
3.6.1.2	Conservatism .....	3.6.1-1
3.6.1.3	Assumptions.....	3.6.1-1
3.6.1.4	Design Input.....	3.6.1-1
3.6.1.5	Methodology.....	3.6.1-2
3.6.1.6	Conclusion .....	3.6.1-7
3.6.1.7	References.....	3.6.1-8

##### LIST OF TABLES

Table 3.6.1-1	Physical Properties of Helium .....	3.6.1-9
Table 3.6.1-2	Physical Properties of the Fuel Pellet (UO <sub>2</sub> ) .....	3.6.1-10
Table 3.6.1-3	Physical Properties of Zircaloy .....	3.6.1-11
Table 3.6.1-4	Temperature Results from Thermal Analysis of WE 17 × 17 SFA .....	3.6.1-12
Table 3.6.1-5	Effective Physical Properties of WE 17 × 17 SFA.....	3.6.1-13

##### LIST OF FIGURES

Figure 3.6.1-1	Finite Element Model of WE 17 × 17 SFA .....	3.6.1-14
Figure 3.6.1-2	Typical Temperature Distribution within the WE 17 × 17 SFA. ....	3.6.1-15
Figure 3.6.1-3	Effective Thermal Conductivity of the WE 17 × 17 SFA.....	3.6.1-16
Figure 3.6.1-4	Effective Specific Heat Capacity of the WE 17 × 17 SFA .....	3.6.1-17

### 3.6.1 Effective Thermal Properties for the Fuel Assembly

#### 3.6.1.1 Discussion

This appendix is to evaluate the effective density, thermal conductivity, and specific heat capacity of the spent fuel assemblies (SFA), Westinghouse 17 × 17, which are loaded into the TN-32B HBU demonstration cask. It is customary, when modeling a nuclear fuel storage/transportation package, for thermal analysis to represent each SFA inside the package as a homogeneous region with equivalent macroscopic physical properties. These effective properties are determined from a separate, detailed model that includes all or most of the small-scale components, and a series of calculations are performed to determine these properties as a function of some macroscopic parameter. For these thermal properties, the parameter is the average temperature of the SFA.

#### 3.6.1.2 Conservatism

1. Heat transfer by convection in the SFA is conservatively ignored.
2. Heat transfer by radiation across the narrow, cylindrical gap between the fuel pellet and the cladding is neglected.
3. The calculation of the effective thermal conductivity in the axial direction considers only the heat transfer along the zircaloy cladding and tubes as required by Reference [1]. The contributions of the fuel pellets and the helium gas have been neglected.
4. The calculation of the effective specific heat ignores the heat capacity of the helium gas, which is assumed to be negligible relative to the other components.

#### 3.6.1.3 Assumptions

1. The narrow, cylindrical gap between the fuel pellet and the cladding is assumed to be filled with helium that has the same thermal conductivity as the helium located outside the cladding. The effect of the presence of any fission products on the conductivity is ignored.
2. The SFA is assumed to be located at the center of the fuel compartment to conservatively minimize the heat transfer by conduction to the compartment walls.
3. The residual heat load of the SFA is assumed to be 1.20 kW. However, the residual heat load has a negligible effect on the effective thermal conductivity.

#### 3.6.1.4 Design Input

The inputs for a thermal calculation include the geometry of the components to be modeled, the physical properties of the materials (including surface emissivities of components that can transfer heat via radiation), and the heat load per SFA.

#### 3.6.1.4.1 Geometry

The SFA that is modeled is a Westinghouse 17 × 17 with dimensions that are identified as follows:

Pellet diameter, inch	0.3225	Pin OD, inch	0.374
Cladding thickness, inch	0.0225	Pin pitch	0.496
Guide tube OD, inch	0.474	Active fuel length, inch	144
Guide tube thickness, inch	0.016	No. of fuel pins	264
Instrument tube OD, inch	0.474	No. of guide tubes	24
Instrument tube thickness, inch	0.016	No. of instrument tubes	1

In the transverse direction, this basket compartment is square with a width of 8.70 inches, as delineated on Drawing 19885-71-6 in Appendix 1.4.1.

#### 3.6.1.4.2 Material Properties

##### Helium

This gas is utilized only by the finite-element model to calculate the transverse heat transfer through the SFA. Since this is a steady-state calculation, only the thermal conductivity of helium is needed. The thermal conductivity values of helium are presented in Table 3.6.1-1, and were calculated from formulas in Reference [2].

##### Uranium Oxide Fuel

The fuel pellets are assumed to be irradiated with a burnup of 62 GWd/MTU, which is bounding for the HBU fuel assemblies selected for this cask, and results in a conservatively low thermal conductivity. The density of  $\text{UO}_2$  is taken from SCALE's Standard Composition Library [3], where it is assumed that the pellet has 95% of the density given in the reference. The thermal conductivity is calculated from Equation (2.3-9) and the specific heat is calculated from Equation (2.2-1) of Reference [4]. The physical properties are presented in Table 3.6.1-2.

##### Zircaloy Cladding

The density of the cladding is taken from SCALE's Standard Composition Library [3]. The thermal conductivity is calculated from Equation (3.2-1) and the specific heat capacities at four temperatures are taken from Table 3.6.1-1 of Reference [4]. These properties are presented in Table 3.6.1-3. The cladding is assumed to have an oxide coating. Its surface emissivity is assumed to be 0.8, based on Figure 3.4-1 of Reference [4].

##### Stainless Steel

As specified on Drawing 19885-71-6 in Appendix 1.4.1, the inner surface of the compartment holding the SFA is stainless steel. In the finite-element model, this surface forms the outer boundary of the model, and is assumed to have an emissivity of 0.3, which is consistent with unpolished stainless steel [5].

### 3.6.1.5 Methodology

Three effective properties are calculated for the SFA: the density, the thermal conductivity, and the specific heat. The methodology used to calculate each effective property is described below.

#### 3.6.1.5.1 Effective Density

The density is calculated by dividing the total mass of the components of the SFA by the volume of the homogeneous region that represents the SFA. Since the geometry is uniform in the axial direction, the density can be calculated by considering only the transverse cross-section of the individual components. Therefore, the effective density is

$$\rho_{\text{eff}} = \frac{N_f(m'_{\text{UO}_2} + m'_{\text{clad}}) + N_g m'_g + N_i m'_i}{A}$$

where:

$N_f$  = number of fuel pins  
 $m'_{\text{UO}_2}$  = mass per unit length of the  $\text{UO}_2$  fuel  
 $m'_{\text{clad}}$  = mass per unit length of the zircaloy cladding  
 $N_g$  = number of guide tubes  
 $m'_g$  = mass per unit length of the guide tubes  
 $N_i$  = number of instrument tubes  
 $m'_i$  = mass per unit length of the instrument tubes  
 $A$  = the cross-sectional area of the compartment

The mass per unit length of the components are calculated from their cross-sectional areas:

$$m'_{\text{UO}_2} = \rho_{\text{UO}_2} A_{\text{UO}_2}, \quad m'_{\text{clad}} = \rho_{\text{zirc}} A_{\text{clad}}, \quad m'_g = \rho_{\text{zirc}} A_g, \quad m'_i = \rho_{\text{zirc}} A_i$$

where:

$\rho_{\text{UO}_2}$  = density of the fuel pellet ( $\text{UO}_2$ ),  
 $\rho_{\text{zirc}}$  = density of zircaloy,  
 $A_{\text{UO}_2}$  = cross-sectional area of the fuel,  
 $A_{\text{clad}}$  = cross-sectional area of the fuel cladding,  
 $A_g$  = cross-sectional area of the guide tubes,  
 $A_i$  = cross-sectional area of the instrument tube.

The cross-sectional areas are calculated from the geometry of the components. The area of each stack of fuel pellets is

$$A_{\text{UO}_2} = \frac{\pi}{4} d_{\text{pel}}^2$$

Where:

$d_{\text{pel}}$  = diameter of fuel pellets

The areas of the cladding and tubes all have the same form:

$$A_{\text{clad}} = \pi \left( d_{\text{pin}} - \frac{t_{\text{clad}}}{2} \right) t_{\text{clad}}, \quad A_g = \pi \left( d_g - \frac{t_g}{2} \right) t_g, \quad A_i = \pi \left( d_i - \frac{t_i}{2} \right) t_i$$

Where:

$d_{\text{pin}}$  = OD of the fuel pins  
 $t_{\text{clad}}$  = fuel cladding thickness  
 $d_g$  = OD of the guide tubes  
 $t_g$  = guide tube thickness  
 $d_i$  = OD of the instrument tube  
 $t_i$  = instrument tube thickness

The area of the compartment, A, is:

$$A = s^2$$

Where:

s = width of the fuel compartment.

### 3.6.1.5.2 Effective Thermal Conductivity

Because of the geometry of the SFA, heat transfer within the SFA is anisotropic. Therefore, two effective thermal conductivities are determined. The first is for the transverse direction, where the heat transfer occurs by conduction in solids, in the helium between the pins and tubes and by radiation heat transfer between the cladding, the tube surfaces, and the compartment wall. The other is for the axial direction, where heat transfer primarily occurs through conduction in the metallic components.

#### Transverse Direction

A detailed, two-dimensional (2-D) finite-element model of the SFA is used to determine the effective thermal conductivity by calculating the heat transfer within the SFA in the transverse direction. The solution is the temperature field across the 2-D domain. This model is shown in Figure 3.6.1-1 and includes all of the fuel pellets, the cladding, the guide tubes, the central instrument tube, the compartment walls, and the helium. Only one quarter of the SFA is explicitly modeled. Symmetric boundary conditions (zero heat flux) are used on the right and top sides of the model to represent the rest of the SFA. A uniform temperature is prescribed on the other two sides of the model, which represent the compartment walls. Heat transfer by radiation among the surfaces of the pins and tubes and the outer edge of the model is accomplished by ANSYS®'s [6] radiation matrix method. Heat transfer by radiation across the gap between the fuel pellet and the pin cladding is not included in the model.

The calculation approach outlined in Section II.5.4 of Reference [7] is utilized to determine the equivalent transverse thermal conductivity of the fuel region. It is assumed that the SFA is centered within the compartment, and that the decay heat of 1.2 kW (4,098 Btu/hr) is uniformly distributed over the entire active fuel length. Therefore, the volumetric heat load within each pin is

$$Q_{\text{pin}} = \frac{Q_a/L}{N_f A_{\text{UO}_2}} = 1.32 \frac{\text{Btu}}{\text{hr-in}^3}$$

Where:

$Q_a$  = heat load per SFA  
 $L$  = active fuel length

This value is adjusted to 1.34 Btu/hr-in<sup>3</sup> to compensate for differences between the SFA geometry and the discretized geometry utilized by the finite-element model, so as to accurately match the total SFA heat load.

Finite-element calculations are performed with a volumetric heat source in the fuel pellets that is representative of the decay heat generated by the SFA and a prescribed, uniform temperature at the outer boundary of the model. The finite-element solution is compared with the temperature field that results from a homogeneous region with the same uniform boundary condition and the same total volumetric heat source distributed uniformly throughout the region, the analytical form of which is known. The thermal conductivity of the homogeneous region that results in the same peak temperature as that of the finite-element solution is taken to be the effective thermal conductivity of the SFA.

With this volumetric heat source, a set of steady-state load steps were performed for a series of uniform boundary temperature values (representing the temperature of the compartment walls), beginning at 100 °F, and increasing by 100 °F for each successive load step until 1,100 °F. The maximum temperature within the SFA was determined for each load step and is compared to the maximum temperature that would occur in a homogeneous region of the same size with a constant, uniform rate of heat generation and identical boundary conditions. Heat transfer through the homogeneous region to the sides is accomplished via conduction with an effective thermal conductivity. An analytical solution for this two-dimensional heat transfer problem is known, and an approximation for the maximum temperature  $T_c$  of the region is given in Reference [4]:

$$T_c = T_o + 0.29468 \frac{Qa^2}{k_{\text{eff}}}$$

Where:

$T_o$  = uniform temperature on the boundary of the fuel region  
 $Q$  = constant, uniform volumetric rate of heat generation  
 $a$  =  $s/2$ , one-half the width of the square fuel region  
 $k_{\text{eff}}$  = effective thermal conductivity of the SFA

Since the finite element model represents only a quarter of the SFA, the effective thermal conductivity can be calculated from:

$$k_{\text{eff}} = 0.29468 \frac{Qa^2}{T_c - T_0}$$

Because the SFA is approximated in the model by discretizing the geometry into small three- and four- sided elements, the total area of the elements representing the  $\text{UO}_2$  pellets differs slightly from the cross-sectional area that is used to calculate the volumetric heat load  $Q_{\text{pin}}$ , and so, the total heat load in the finite-element model is slightly different than  $Q_a/4L$ . Therefore, the total heat load,  $Qa^2$ , is taken from the calculation results  $Q_{\text{react}}$  by using the total rate of heat flow across the outer boundary of the model:

$$k_{\text{eff}} = 0.29468 \frac{Q_{\text{react}}}{T_c - T_0}$$

Each calculation in the series provides a value of  $k_{\text{eff}}$ , which is taken to be the effective transverse thermal conductivity of the homogenized region at the average temperature,  $T = (T_0 + T_c)/2$ .

#### Axial Direction

Since the transverse geometry is uniform throughout the axial extent of the active fuel region, a detailed model is not necessary. Instead, it is assumed that conduction in the metallic fuel cladding and tubes dominates the heat transfer in the axial direction, and the contributions of the other components are ignored. That is, heat transfer in the helium gas is negligible, and the gaps between individual fuel pellets in a stack of pellets substantially limit the axial heat transfer rate along the stack.

The amount of heat that is carried in the axial direction by the zircalloy cladding and tubing, which is proportional to their physical conductivity and cross-sectional area, must be equal to the amount of heat carried in the axial direction by the homogeneous region, whose cross-sectional area encompasses the entire fuel compartment. The effective axial thermal conductivity used for this region is calculated to satisfy this requirement.

If only the conduction in the metallic cladding and tubing is considered, then the heat flow per unit time in the axial direction is

$$Q_z = -k_{\text{zirc}} A_{\text{zirc}} \frac{\partial T}{\partial z}$$

Where:

$k_{\text{zirc}}$  = thermal conductivity of zircalloy  
 $T$  = temperature field  
 $z$  = axial direction

and the cross-sectional area of the zirconium is the sum of the cross-sectional areas of the three components,



$$A_{\text{zirc}} = N_f A_{\text{clad}} + N_g A_g + N_i A_i$$

The heat flow in a homogeneous region with an effective axial conductivity  $[k_{\text{eff}}]_z$  is

$$Q_z = -[k_{\text{eff}}]_z A \frac{\partial T}{\partial z}$$

Where:

$A = s^2$ , cross-sectional area of the homogeneous region (fuel compartment)

Therefore, to achieve the same rate of heat flow, the effective axial conductivity of the SFA is:

$$[k_{\text{eff}}]_z = \frac{N_f A_{\text{clad}} + N_g A_g + N_i A_i}{A} k_{\text{zirc}}$$

This methodology is consistent with Reference [1], which requires that the effective axial conductivity is limited to cladding conductivity weighted by its fractional area.

#### Effective Specific Heat

This property is determined by assuming that each component of the SFA contributes independently to the total heat capacity of the SFA. Thus, the effective specific heat capacity is the mass-weighted average of the specific heat capacities of the component materials:

$$[c_p]_{\text{eff}} = \frac{N_f m'_{\text{UO}_2} [c_p]_{\text{UO}_2} + (N_f m'_{\text{clad}} + N_g m'_g + N_i m'_i) [c_p]_{\text{zirc}}}{N_f m'_{\text{UO}_2} + N_f m'_{\text{clad}} + N_g m'_g + N_i m'_i}$$

Where:

$[c_p]_{\text{UO}_2}$  = specific heat capacity of a fuel pellet ( $\text{UO}_2$ )

$[c_p]_{\text{zirc}}$  = specific heat capacity of zircaloy

#### 3.6.1.6 Conclusion

Eleven steady-state load steps are performed for eleven compartment wall temperatures, which vary from 100 °F to 1,100 °F. Figure 3.6.1-2 illustrates a typical temperature field that is calculated by ANSYS®. The key temperatures from these results – the boundary temperature, maximum temperature, and average temperature – are presented in Table 3.6.1-4.

The effective physical properties of a homogeneous region that is utilized to model a basket compartment containing a SFA are listed in Table 3.6.1-5. The effective thermal conductivities of the WE 17 × 17 SFA are shown in Figure 3.6.1-3. The effective specific heat capacity is shown in Figure 3.6.1-4.

### 3.6.1.7 References

1. U.S. Nuclear Regulatory Commission, "Standard Review Plan for Spent Fuel Dry Storage Systems at a General License Facility," NUREG-1536 Rev.1, July 2010.
2. Rohsenow, M. W., Cho, Y. I., and Harnett, J. P., Handbook of Heat Transfer, 3<sup>rd</sup> Edition, 1998.
3. Oak Ridge National Lab, "Scale: A Comprehensive Modeling and Simulation Suite for Nuclear Safety Analysis and Design, Version 6.1," ORNL/TM-2005/39, 2011.
4. U.S. Nuclear Regulatory Commission, Luscher and Geelhood, "Material Property Correlations: Comparisons between FRAPCON-3.4, FRAPTRAN 1.4, and MATPRO," NUREG/CR-7024 (PNNL-19417).
5. Paloposki and Liedquist, "Steel Emissivity at High Temperatures," NT Technical Report 570, Nordic Innovation Centre, Oslo, Norway, 2006.
6. ANSYS® Mechanical APDL, Release 14.0, ANSYS, Inc., Canonsburg, PA.
7. Sandia National Labs, "A Method for Determining the Spent-Fuel Contribution to Transport Cask Containment Requirements," Technical Report SAND90-2406, TTC-1019, UC-820, 1992.

**Table 3.6.1-1**  
**Physical Properties of Helium**

<b>Temperature (°F)</b>	<b>Conductivity [2] (10<sup>-3</sup> Btu/hr-in-°F)</b>
0	6.53
100	7.38
200	8.17
300	8.96
400	9.81
500	10.8
600	11.7
700	12.6
800	13.4
900	14.2
1,000	14.9*

\* Conservatively used for temperatures above 1,000 °F

**Table 3.6.1-2**  
**Physical Properties of the Fuel Pellet (UO<sub>2</sub>)**

Temperature (°F)	Conductivity [4] (Btu/hr-in-°F)	Temperature (°F)	Specific heat [4] (10 <sup>-3</sup> Btu/lb <sub>m</sub> -°F)
100	0.138	80	5.65
200	0.133	260	6.35
300	0.128	692	7.06
400	0.123	1500	7.58
500	0.119	Density [3]: 0.376 lb <sub>m</sub> /in <sup>3</sup>	
600	0.116		
700	0.112		
800	0.109		
900	0.107		
1,000	0.105		
1,100	0.104		
1,200	0.103		
1,300	0.102		

**Table 3.6.1-3**  
**Physical Properties of Zircaloy**

Temperature (°F)	Conductivity [4] (Btu/hr-in-°F)	Temperature (°F)	Specific heat [4] (10 <sup>-2</sup> Btu/lb <sub>m</sub> -°F)
100	0.618	80	6.71
200	0.655	260	7.21
300	0.690	692	7.91
400	0.723	1500	8.96
500	0.756	Density [3]: 0.237 lb <sub>m</sub> /in <sup>3</sup>	
600	0.787		
700	0.819		
800	0.851		
900	0.883		
1,000	0.916		
1,100	0.950		
1,200	0.985		
1,300	1.02		

**Table 3.6.1-4**  
**Temperature Results from Thermal Analysis of WE 17 × 17 SFA**

Temperature (°F)		
Wall $T_0$	Maximum $T_c$	Average $\bar{T}$
100	202	151
200	288	244
300	376	338
400	465	433
500	556	528
600	649	624
700	742	721
800	837	819
900	933	916
1,000	1,029	1,014
1,100	1,126	1,113

**Table 3.6.1-5**  
**Effective Physical Properties of WE 17 × 17 SFA**

Temperature (°F)	Transverse Conductivity (10 <sup>-2</sup> Btu/hr-in-°F)	Temperature (°F)	Axial Conductivity (10 <sup>-2</sup> Btu/hr-in-°F)	Temperature (°F)	Specific Heat (10 <sup>-2</sup> Btu/lb <sub>m</sub> -°F)
151	2.06	100	6.01	80	5.84
244	2.39	200	6.36	260	6.50
338	2.76	300	6.70	692	7.21
433	3.21	400	7.03	1,500	7.82
528	3.73	500	7.35	Density: 0.130 lb <sub>m</sub> /in <sup>3</sup>	
624	4.30	600	7.65		
721	4.94	700	7.96		
819	5.64	800	8.27		
916	6.42	900	8.58		
1,014	7.25	1,000	8.90		
1,113	8.07	1,100	9.23		

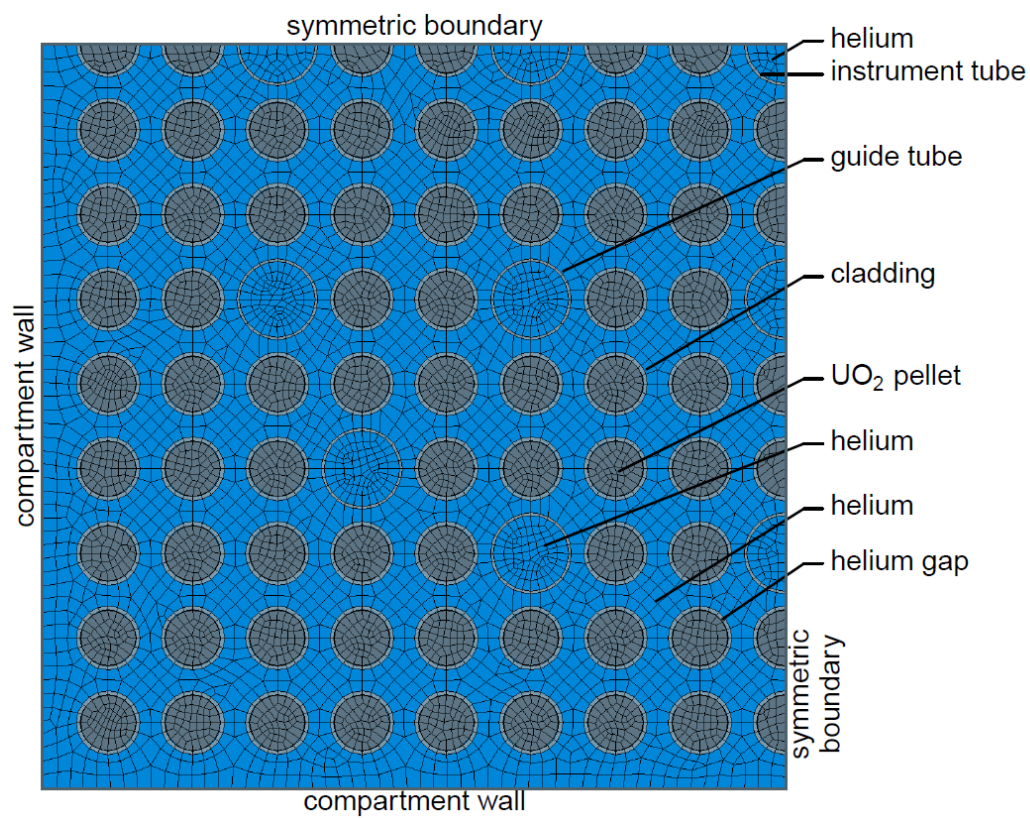
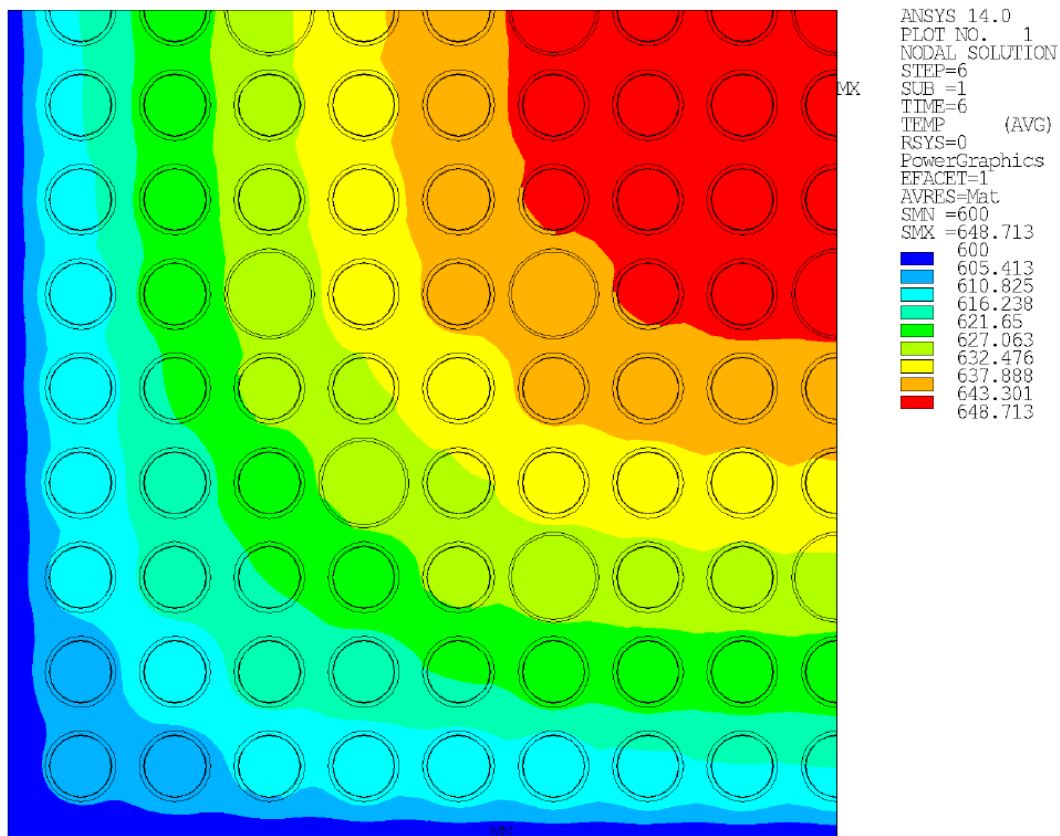


**Figure 3.6.1-1**  
**Finite Element Model of WE 17 x 17 SFA**





Note: Contour values are in degrees Fahrenheit

**Figure 3.6.1-2**  
**Typical Temperature Distribution within the WE 17 × 17 SFA.**

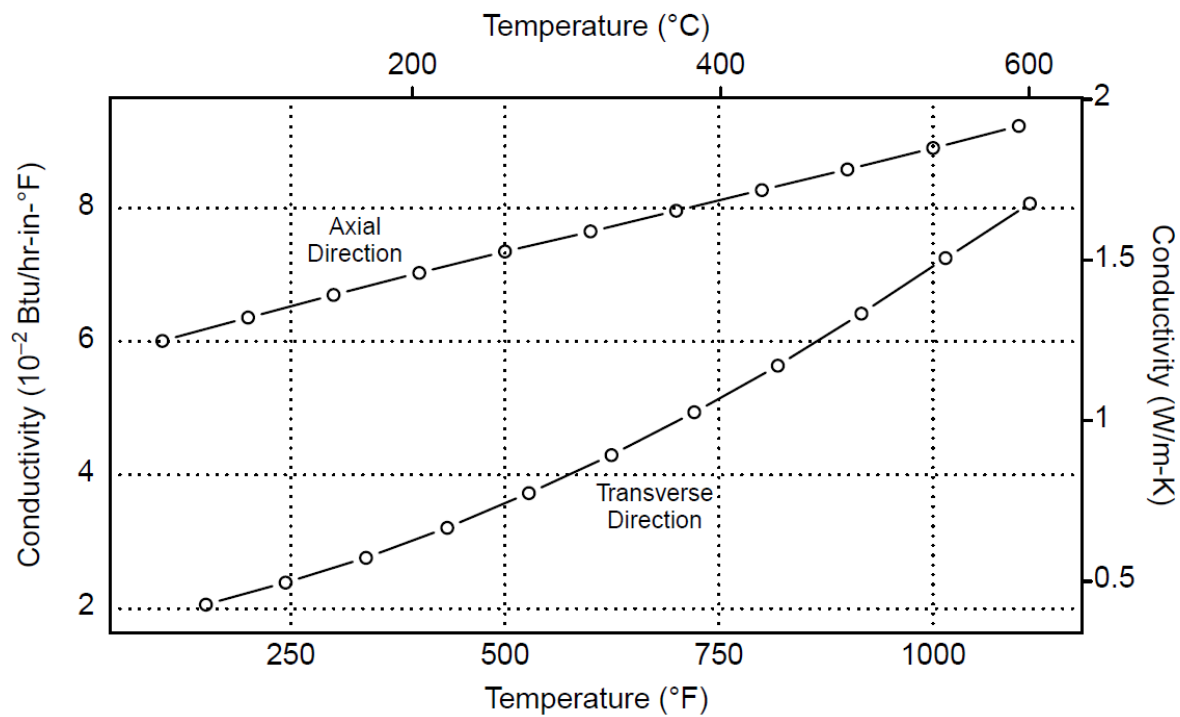


**Figure 3.6.1-3**  
**Effective Thermal Conductivity of the WE 17 × 17 SFA**

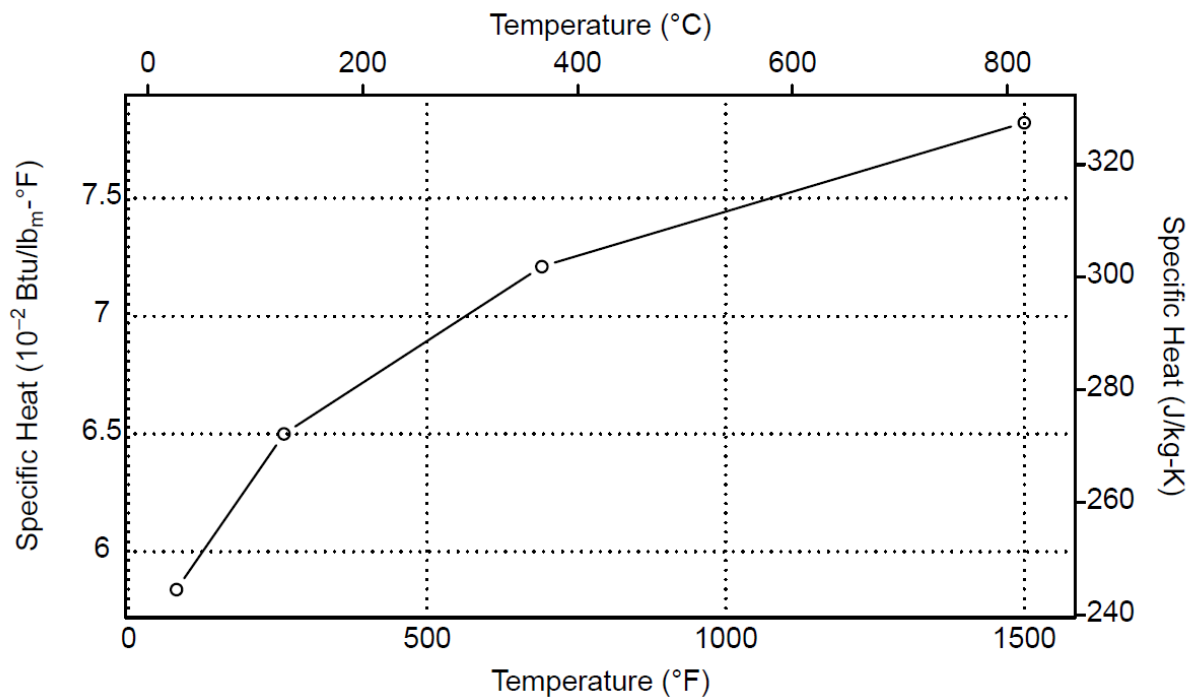


**Figure 3.6.1-4**  
**Effective Specific Heat Capacity of the WE 17 × 17 SFA**

## Chapter 4 Containment

### TABLE OF CONTENTS

4.1	Description of the Containment System.....	4-1
4.1.1	Containment Vessel.....	4-1
4.1.2	Containment Penetrations.....	4-2
4.1.3	Seals and Welds.....	4-2
4.1.4	Closure .....	4-4
4.2	Containment under Normal Conditions of Transport.....	4-4
4.2.1	Containment of Radioactive Material.....	4-5
4.2.2	Pressurization of Containment Vessel.....	4-5
4.2.3	Containment Criterion .....	4-5
4.3	Containment under Hypothetical Accident Conditions .....	4-5
4.3.1	Fission Gas Products.....	4-5
4.3.2	Containment of Radioactive Material.....	4-5
4.3.3	Containment Criterion .....	4-6
4.4	Leakage Rate Tests for Type B Packages.....	4-6
4.5	References.....	4-7

### LIST OF FIGURES

Figure 4-1	TN-32B HBU Demonstration Cask Containment Boundary Components .....	4-8
Figure 4-2	Closure Lid, Vent And Drain Port, and TLA Metallic Seals .....	4-9
Figure 4-3	As-Machined Penetration Sleeve Sealing Surface .....	4-10

## **Chapter 4 Containment**

### **4.1 Description of the Containment System**

The containment boundary components consist of the inner shell and bottom inner plate, shell flange, closure lid outer plate, vent/drain port covers, and thermocouple lance assemblies. Also included in the containment components are the associated seals and bolts. The containment boundary is illustrated in Figure 4-1. The construction of the containment boundary is presented on Drawings 19885-71-2, 19885-71-3, and 19885-71-7 provided in Appendix 1.4.1. The containment vessel prevents potential leakage of radioactive material from the cask cavity. It also maintains an inert atmosphere (helium) in the cask cavity. Helium gas assists in heat removal and provides a non-reactive environment to protect fuel assemblies against fuel cladding degradation that might otherwise lead to gross rupture.

#### **4.1.1 Containment Vessel**

The containment vessel of the TN-32B high burnup (HBU) demonstration cask consists of an inner shell, which is a welded carbon steel cylinder, and is welded to a carbon steel bottom inner plate and a shell flange forging. The vessel closure is a carbon steel lid with bolts, vent cover with bolts, drain cover with bolts, and thermocouple lance assemblies (TLAs) with jacking screws. The closure lid outer plate thickness is 4.5 inches. The overall containment vessel length is 171.02 inches with a nominal wall thickness of 1.5 inch. The cylindrical cask cavity has an inner diameter of 68.80 inches and a length of 163.38 inches.

The containment shell, bottom inner plate, and the closure lid outer plate material is SA-203 Grade D, and the inner shell flange and the thermocouple penetration sleeve forging material is SA-350 Grade LF3. The structural materials for the TLAs are dual-certified, SA-479 Type 304/304L austenitic stainless steel and annealed Inconel.

The cask design, fabrication, and testing were performed under TN Americas' Quality Assurance Program, which conforms to the criteria in Subpart H of 10 CFR Part 71 [1]. The thermocouple lance assemblies' design, fabrication, and testing were performed under Framatome Inc.'s (formerly AREVA, Inc.) Quality Assurance Program, which conforms to the criteria in Subpart B of 10 CFR Part 50 [2].

Except as noted in the ASME code alternatives in Appendix 2.12.13, the materials of construction meet the requirements of Section III, Subsection NB-2000 [3] and Section II, Material Specifications [4] [5] or the corresponding ASTM Specifications. The containment vessel was designed to the American Society of Mechanical Engineers (ASME) Boiler & Pressure Vessel (B&PV) Code, Section III, Subsection NB, Article NB-3200 to the maximum practicable extent. The containment vessel was fabricated and examined in accordance with Subsections NB-2500, NB-4000, and NB-5000. Also, weld filler materials conform to NB-2400 and the material specification requirements of Section II, Part C of the ASME B&PV Code. Excluding the TLAs, the assembled containment vessel was hydrostatically pressure tested in accordance with the requirements of the ASME B&PV Code, Section III, Subsection NB, Article NB-6200, when it was originally fabricated in 2000. The TLAs were hydrostatically pressure tested to 3,125 psig during the fabrication of the assemblies in 2017.

Alternatives to the ASME B&PV Code requirements are specified in Section 2.13.

#### 4.1.2 Containment Penetrations

There are nine penetrations through the containment vessel, all located in the closure lid. Two of the penetrations are the drain port and the vent port. The other seven penetrations are the thermocouple lances that extend into their respective spend fuel assemblies in the cavity. A double O-ring metallic seal and a mechanical closure are provided for each penetration. The vent and drain penetrations incorporate a bolted cover, while the thermocouple lance assemblies (TLAs) are secured via jacking and compression plates, and a retaining ring.

#### 4.1.3 Seals and Welds

##### 4.1.3.1 Seals

Double metallic seals (O-rings) are utilized on the closure lid and the nine lid penetrations, which are Helicoflex® HND [6] seals. The O-ring seals are shown in Figure 4-2. The Helicoflex® metallic face O-ring seals on the closure lid and closure lid penetrations possess long-term stability as well as high corrosion resistance. These high performance metallic seals consist of an inner spring, a lining, and a silver jacket. The spring is Inconel® X-750 material, while the lining and jacket are stainless steel and silver, respectively. Additionally, all metallic seal seating surfaces are a stainless steel overlay for improved surface control. Note that the fabrication process ensured an adequate sealing surface for the TLAs initially. As illustrated in Figure 4-3, the capability of the sealing surfaces was demonstrated by meeting the leaktight acceptance criteria per ANSI N14.5 [7], both during the fabrication acceptance leakage rate testing as well as the pre-shipment leakage rate testing during loading of the HBU payload.

The internal spring and lining maintain the necessary rigidity and sealing force, and provide some elastic recovery capability. The outer silver jacket provides a ductile material that ensures leak tightness. The jacket also provides a connecting sheet between the inner and outer seals. Holes in this sheet allow for attachment of machine screws, and for communication between the overpressure (OP) port and the space between the seals. This sheet, which is approximately 0.020 inch. thick, has insufficient strength to transmit radial forces significant to overcome the axial compressive forces on the seals. The O-ring seal for the OP port is a single metallic seal of a similar design (Helicoflex® HN200).

The closure lid and penetration seals described above are contained in a groove in the closure lid or the port covers/lance body assemblies. A high level of sealing over the transport period is ensured by utilizing seals in a deformation-controlled design. The deformation of the seals is constant since bolt and jacking screw loads ensure that the mating surfaces remain in metal-to-metal contact. The seal deformation is set by the original O-ring cross section and the depth of the groove. The specified preload has the required force to seat the seals, as demonstrated in Appendix 2.12.3.2.2 for the closure lid seal, and Appendix 2.12.12.2.2 for the TLA seals.

The Inconel® X-750 spring material has equivalent or better corrosion properties, service temperature, and modulus of rigidity and elasticity that ensures the seal will not be affected by relaxation. Thus, the seal can be maintained at the specified temperatures for extended periods.

Helicoflex® metallic seals are all capable of limiting leak rates to less than  $1 \times 10^{-7}$  ref cm<sup>3</sup>/s. After loading for storage in November 2017, all closure lid and cover/lance seals were leakage rate tested in accordance with ANSI N14.5 [7]. All of the seals were demonstrated to be leaktight, i.e.,  $\leq 1 \times 10^{-7}$  ref cm<sup>3</sup>/s, per ANSI N14.5.

During the storage period, all containment boundary O-ring seals were monitored by the OP system to ensure the containment boundary was maintained.

#### 4.1.3.2 Welds

Except for the TLA penetration sleeve welds, the containment boundary welds consist of the circumferential, full-penetration welds attaching the bottom inner plate and the shell flange to the inner shell. Also, the longitudinal weld(s) on the rolled plate, closing the cylindrical inner shell, and the circumferential weld(s) attaching the rolled shells together are full-penetration containment welds.

The penetration sleeves for receiving the TLAs are welded to the closure lid and the shield plate with partial penetration groove welds, which make them integral to the lid. Since the upper groove weld attaches the forging to the closure lid, that weld joint is part of the containment boundary. To verify the integrity of upper groove weld (which is classified as a Category C weld under Section NB of the ASME B&PV Code), the weld was visually and nondestructively examined (NDE) by multi-level liquid penetrant (PT) examination in the root, and on each pass in accordance with Section V and the acceptance standards of Section III, Subsection NB-5000 of the ASME B&PV Code.

The TLAs extend the containment boundary into the fuel assemblies that are monitored. A TLA consists of a welded Inconel oversheath that contains nine K-type thermocouples, a reinforcing Inconel oversheath, and a Type 304/304L stainless steel insert that is welded to a Type 304/304L stainless steel body. Except for the square weld that joins the sheath tip plug to the oversheath, the lance containment boundary welds are fillet and partial penetration welds. For these assemblies, the welds are classified as a Category D, which permits fillet and partial penetration welds, under Section III, Subsection NB-3352.4 of the ASME B&PV Code. All welds were performed utilizing the gas tungsten arc welding (GTAW) process, and examined by liquid penetrant (PT) process using acceptance standards that exceeded the acceptance standards of Section III, Subsection NB-5352. Additionally, the TLAs were hydrostatically pressure tested to an external pressure of 3,125 psig.

#### 4.1.4 Closure

The containment vessel contains an integrally-welded bottom closure, and a bolted and flanged top closure lid, and the TLA closures that are secured to the welded penetration sleeves. The outer lid plate is attached to the shell flange with 48 bolts and hardened washers. The bolt tightening torque required to seal the metallic seals located in the closure lid and maintain containment under normal and accident conditions are provided in Drawings 19885-71-2 and 19885-71-3 in Appendix 1.4.1. The closure lid bolt analysis is presented in Appendix 2.12.3.

As previously mentioned, the closure lid contains two penetrations that are sealed by flanged cover plates secured to the lid by eight bolts each, and seven thermocouple lance assemblies that are each secured by eight socket head jacking screws via a jacking plate and compression plate. The tightening torque required to seat the metallic seals in the penetration covers and thermocouple lance assemblies, and maintain containment under normal and accident conditions is specified in Drawings 19885-71-2 and 19885-71-3, which are provided in Appendix 1.4.1.

## 4.2 Containment under Normal Conditions of Transport

In accordance with 10 CFR 71.51, a Type B package must be designed, constructed, and prepared for shipment so that “no loss or dispersal of radioactive contents, as demonstrated to a sensitivity of  $10^{-6}$  A<sub>2</sub> per hour” will occur under the tests specified in 10 CFR 71.71 for normal conditions of transport.



#### 4.2.1 Containment of Radioactive Material

The results of the NCT structural and thermal evaluations presented in Sections 2.6 and 3.3 demonstrate that there is no release of radioactive materials from the TN-32B HBU demonstration cask per the “leaktight” definition of ANSI N14.5 [7] under any of the NCT tests described in 10 CFR §71.71. All of the cask containment seals have been demonstrated to be leaktight at the time of loading of the HBU payload. In addition, the metallic containment boundary of the cask body was tested during the closure lid modification to verify leak tightness to the maximum extent possible (refer to Section 8.1.4). To ensure the containment seals maintained their leaktight condition during the storage period, all of the seals were continuously monitored by the overpressure (OP) system. Under these leaktight conditions, release calculations are not required to demonstrate compliance with the regulatory release limits of 10 CFR §71.51 per NUREG-2224 [8].

#### 4.2.2 Pressurization of Containment Vessel

The maximum normal operating pressure (MNOP) of the TN-32B HBU demonstration cask is 30.5 psig per Section 3.3.2. The design pressure of the containment boundary is 100 psig. Based on the structural evaluations performed in Chapter 2, pressure increases to 100 psig will not reduce the effectiveness of the TN-32B HBU demonstration cask to maintain containment integrity per Section 4.2.1.

#### 4.2.3 Containment Criterion

As noted in Section 4.2.1, the TN-32B HBU demonstration cask has been shown to be leaktight for the normal conditions of transport. Therefore, there will be no release, loss, or dispersal of the HBU payload from the TN-32B HBU demonstration cask.

### 4.3 Containment under Hypothetical Accident Conditions

#### 4.3.1 Fission Gas Products

There is no need to explicitly determine a source term available for release. As noted earlier, the TN-32B HBU demonstration cask has been tested to a leakage rate of  $1 \times 10^{-7}$  ref cm<sup>3</sup>/s, defined as leaktight per ANSI N14.5 [7]. Additionally, the structural and thermal evaluations presented in Chapter 2 and Chapter 3 verify that the containment boundary remains elastic, and does not exceed material temperature limits.

#### 4.3.2 Containment of Radioactive Material

The TN-32B HBU demonstration cask was tested to demonstrate that the containment boundary is maintained, and is leaktight for transporting the HBU payload. The results of the structural and thermal evaluations presented in Chapter 2 and Chapter 3 will satisfy the leakage rate criteria of 10 CFR 71.51 for the hypothetical accident conditions.

#### 4.3.3 Containment Criterion

The results of the hypothetical accident condition (HAC) structural and thermal evaluations presented in Sections 2.7 and 3.4 demonstrate that there is no release of radioactive materials from the TN-32B HBU demonstration cask per the “leaktight” definition of ANSI N14.5 under any of the HAC tests described in 10 CFR 71.73. Since the cask has been determined to be leaktight, release calculations are not required to demonstrate compliance with the regulatory release limits of 10 CFR 71.51 per NUREG-2224 [8].

### 4.4 Leakage Rate Tests for Type B Packages

Leakage tests performed on the TN-32B HBU demonstration cask are based on those listed in Chapter 7 of ANSI N14.5 [7]. A description of these tests is provided below.

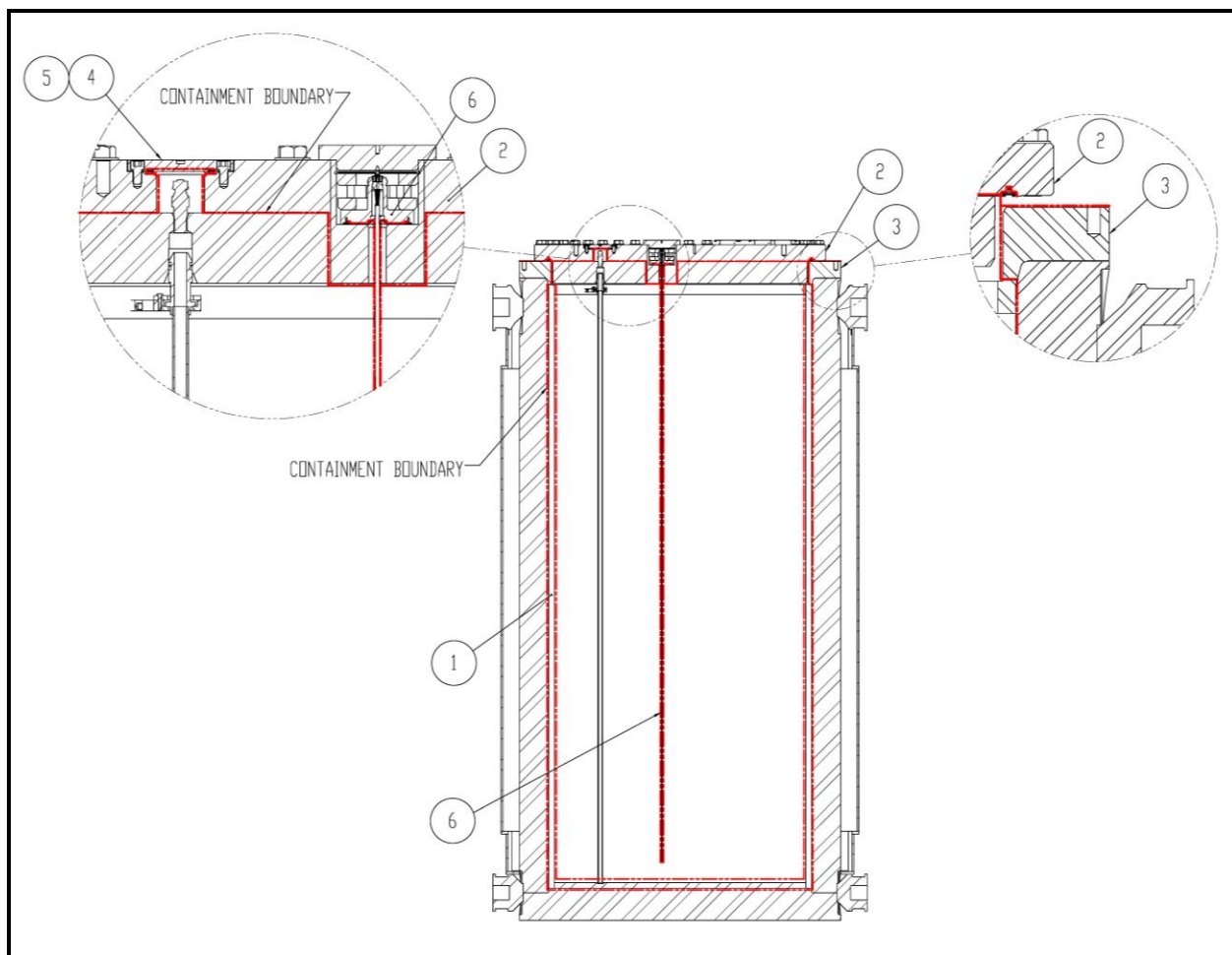
Design Leakage Rate Test: The containment boundary has been designed with appropriate materials and dimensions to provide containment for normal and accident conditions of transport. Analyses described within this document demonstrate the containment boundary design is acceptable for both normal and accident conditions of transport.

Fabrication Leakage Rate Test: As described in Section 8.1.4, fabrication leakage rate tests were performed on all of the containment O-ring seals with an acceptance criteria of  $1 \times 10^{-5}$  ref cm<sup>3</sup>/s, during the original fabrication of the cask. During the closure lid modification, all containment O-ring seals and the containment boundary forgings and welds for the thermocouple lance assemblies were performed with an acceptance criteria of  $1 \times 10^{-7}$  ref cm<sup>3</sup>/s. Additionally, a “best-effort” helium leakage rate test was performed on the metallic containment boundary as part of the closure lid modification. That leakage rate test recorded a helium leakage rate of less than  $1 \times 10^{-8}$  atm cm<sup>3</sup>/s after 2 hours on three separate tests. That leakage rate is convincing objective evidence that the metallic containment boundary is leaktight. This conclusion is further supported by considering the fact that the cask cavity maintained a pressurized helium atmosphere for over 13 years during the cask storage.

Pre-shipment Leakage Rate Test: Prior to shipment of the packaging, a leakage rate test of the replacement of the vent port seal will be performed, as described in Section 7.1.3. Typically, a helium mass spectrometer test is performed with an acceptance criterion of  $1 \times 10^{-4}$  ref cm<sup>3</sup>/s and a sensitivity of  $5 \times 10^{-5}$  ref cm<sup>3</sup>/s or less for an assembly verification leakage rate test. Since all of the metallic seals are not utilized for more than one transport, the pre-shipment testing also fulfills the requirements for the maintenance and periodic leakage rate tests.

## 4.5 References

1. Title 10, Code of Federal Regulations - Energy, Part 71 (10 CFR 71), "Packaging and Transportation of Radioactive Material," 1-1-2021 Edition, U.S. Nuclear Regulatory Commission, Washington, D.C.
2. Title 10, Code of Federal Regulations – Energy, Part 50 (10 CFR Part 50), "Domestic Licensing of Production and Utilization Facilities," 10-1-2020 Edition, U.S. Nuclear Regulatory Commission, Washington, D.C.
3. American Society of Mechanical Engineers Boiler and Pressure Vessel Code, Section III, "Rules for Construction of Nuclear Facility Components," 1992 Edition.
4. American Society of Mechanical Engineers Boiler and Pressure Vessel Code, Section II, Part D, 1992 Edition with 1992 Addenda.
5. American Society of Mechanical Engineers Boiler and Pressure Vessel Code, Section II, Part D, 2013 Edition.
6. Metal Seals Technical Catalogue, Technetics Group, Columbia, SC.
7. ANSI N14.5–2014, "Leakage Tests on Packages for Shipment of Radioactive Materials," American National Standards Institute, Inc.
8. "Dry Storage and Transportation of High Burnup Spent Nuclear Fuel," NUREG-2224, U.S. Nuclear Regulatory Commission, November 2020.



Notes:

1. Figure not to scale. Features exaggerated for clarity.
2. Phantom lines ( — . . . . . ) indicate containment boundary.
3. Containment boundary components are listed below:
  - 1 Inner shell.
  - 2 Closure lid outer plate, closure bolts and inner O-ring seals.
  - 3 Shell flange.
  - 4 Vent port cover plate, bolts and O-ring seal.
  - 5 Drain port cover plate, bolts and O-ring seal (not shown).
  - 6 Thermocouple lance assembly and inner O-ring seal (one of seven shown for clarity)

**Figure 4-1**  
**TN-32B HBU Demonstration Cask Containment Boundary Components**

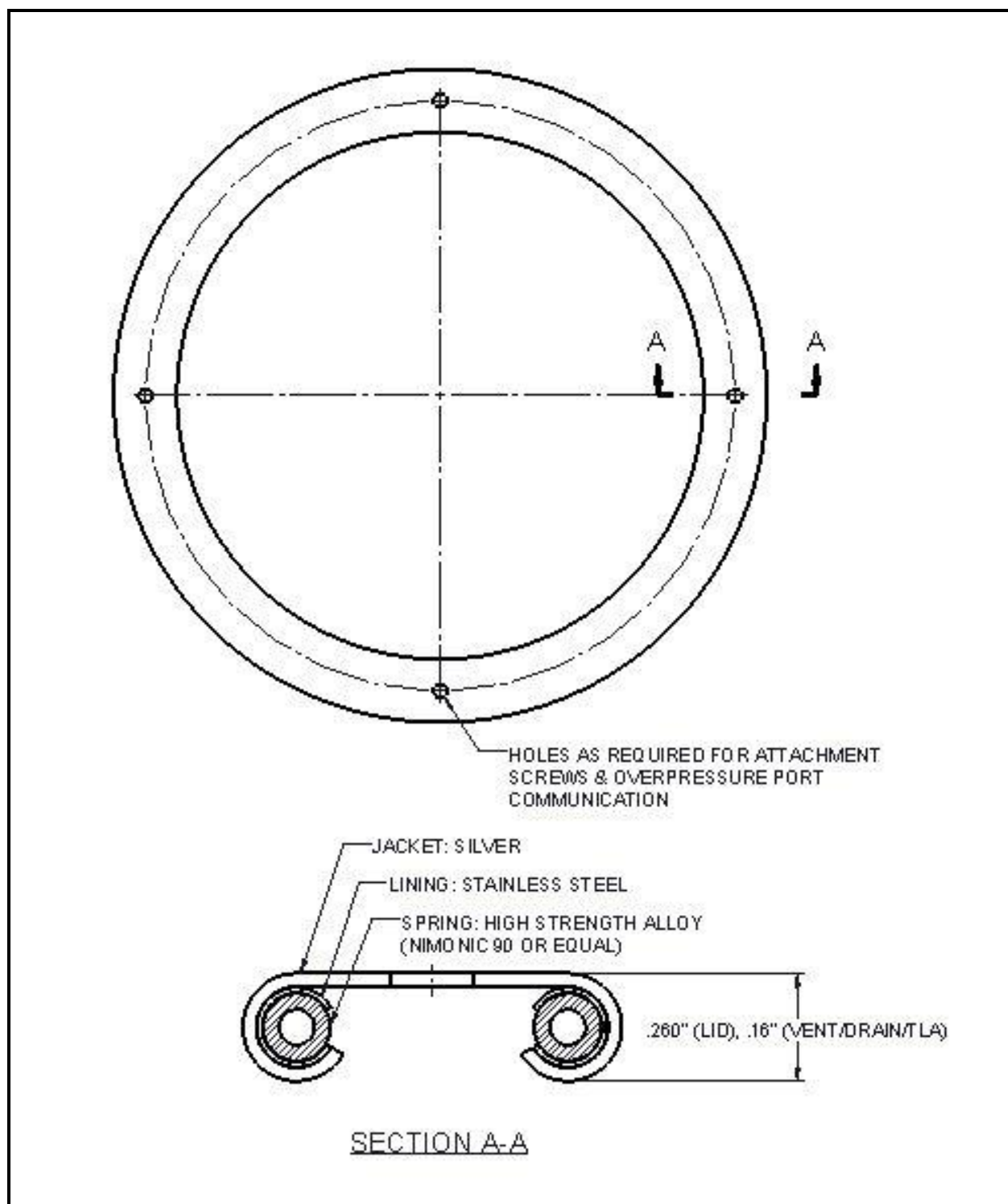


**Figure 4-2**  
**Closure Lid, Vent And Drain Port, and TLA Metallic Seals**

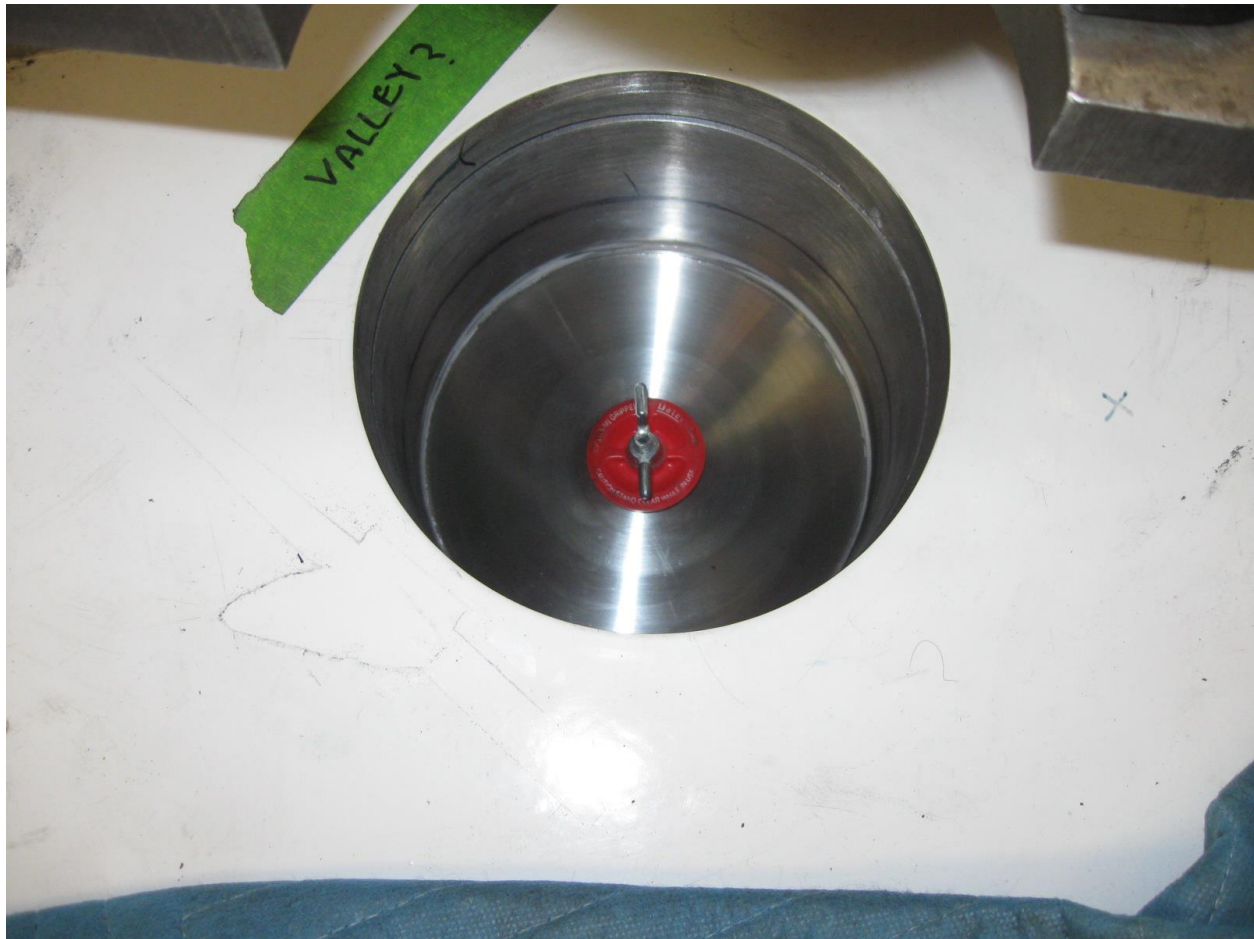


**Figure 4-3**  
**As-Machined Penetration Sleeve Sealing Surface**

## Chapter 5 Shielding Evaluation

### TABLE OF CONTENTS

5.1	Description of Shielding Design .....	5-1
5.1.1	Design Features .....	5-1
5.1.2	Summary of Maximum Radiation Levels .....	5-2
5.2	Source Specification .....	5-2
5.2.1	Gamma Source .....	5-4
5.2.2	Neutron Source .....	5-4
5.3	Shielding Model .....	5-5
5.3.1	Configuration of Source and Shielding .....	5-5
5.3.2	Material Properties .....	5-7
5.4	Shielding Evaluation .....	5-7
5.4.1	Methods .....	5-7
5.4.2	Input and Output Data .....	5-8
5.4.3	Flux-to-Dose-Rate Conversion .....	5-9
5.4.4	External Radiation Levels .....	5-9
5.5	References .....	5-13
5.6	Input File Listing .....	5-14
5.6.1	ORIGEN-ARP Input File .....	5-14
5.6.2	NCT Primary Gamma MCNP Model Input File .....	5-16
5.6.3	NCT Side Neutron MCNP Model Input File .....	5-49

LIST OF TABLES

Table 5-1	TN-32B HBU Demonstration Cask Key Dimensions .....	5-82
Table 5-2	Summary of TN-32B HBU Demonstration Cask Dose Rates .....	5-83
Table 5-3	Fuel Assembly Hardware Characteristics.....	5-84
Table 5-4	Material Compositions for Fuel Assembly Hardware Materials.....	5-85
Table 5-5	MTU and Initial Enrichment per Assembly.....	5-86
Table 5-6	Fuel Cycle Data per Assembly .....	5-87
Table 5-7	ORIGEN Scaling Factors .....	5-89
Table 5-8	Axial Peaking Factors .....	5-90
Table 5-9	F40 Gamma Source.....	5-91
Table 5-10	0A4 Gamma Source .....	5-92
Table 5-11	5D5 Gamma Source .....	5-93
Table 5-12	5D9 Gamma Source .....	5-94
Table 5-13	3F6 Gamma Source.....	5-95
Table 5-14	4F1 Gamma Source.....	5-96
Table 5-15	6F2 Gamma Source.....	5-97
Table 5-16	3T2 Gamma Source.....	5-98
Table 5-17	3T6 Gamma Source.....	5-99
Table 5-18	5T9 Gamma Source.....	5-100
Table 5-19	6T0 Gamma Source.....	5-101
Table 5-20	3U4 Gamma Source .....	5-102
Table 5-21	3U6 Gamma Source .....	5-103
Table 5-22	3U9 Gamma Source .....	5-104
Table 5-23	4V4 Gamma Source .....	5-105
Table 5-24	3K4 Gamma Source .....	5-106
Table 5-25	3K7 Gamma Source .....	5-107
Table 5-26	5K1 Gamma Source .....	5-108
Table 5-27	5K6 Gamma Source .....	5-109
Table 5-28	5K7 Gamma Source .....	5-110
Table 5-29	6K4 Gamma Source .....	5-111
Table 5-30	6V0 Gamma Source .....	5-112
Table 5-31	30A Gamma Source .....	5-113
Table 5-32	57A Gamma Source .....	5-114
Table 5-33	15B Gamma Source .....	5-115
Table 5-34	20B Gamma Source .....	5-116



Table 5-35	22B Gamma Source .....	5-117
Table 5-36	28B Gamma Source .....	5-118
Table 5-37	30B Gamma Source .....	5-119
Table 5-38	50B Gamma Source .....	5-120
Table 5-39	54B Gamma Source .....	5-121
Table 5-40	56B Gamma Source .....	5-122
Table 5-41	F40 Neutron Source.....	5-123
Table 5-42	0A4 Neutron Source .....	5-124
Table 5-43	5D5 Neutron Source .....	5-125
Table 5-44	5D9 Neutron Source .....	5-126
Table 5-45	3F6 Neutron Source.....	5-127
Table 5-46	4F1 Neutron Source.....	5-128
Table 5-47	6F2 Neutron Source.....	5-129
Table 5-48	3T2 Neutron Source.....	5-130
Table 5-49	3T6 Neutron Source.....	5-131
Table 5-50	5T9 Neutron Source.....	5-132
Table 5-51	6T0 Neutron Source.....	5-133
Table 5-52	3U4 Neutron Source .....	5-134
Table 5-53	3U6 Neutron Source .....	5-135
Table 5-54	3U9 Neutron Source .....	5-136
Table 5-55	4V4 Neutron Source .....	5-137
Table 5-56	3K4 Neutron Source .....	5-138
Table 5-57	3K7 Neutron Source .....	5-139
Table 5-58	5K1 Neutron Source .....	5-140
Table 5-59	5K6 Neutron Source .....	5-141
Table 5-60	5K7 Neutron Source .....	5-142
Table 5-61	6K4 Neutron Source .....	5-143
Table 5-62	6V0 Neutron Source .....	5-144
Table 5-63	30A Neutron Source .....	5-145
Table 5-64	57A Neutron Source .....	5-146
Table 5-65	15B Neutron Source .....	5-147
Table 5-66	20B Neutron Source .....	5-148
Table 5-67	22B Neutron Source .....	5-149
Table 5-68	28B Neutron Source .....	5-150
Table 5-69	30B Neutron Source .....	5-151

Table 5-70	50B Neutron Source .....	5-152
Table 5-71	54B Neutron Source .....	5-153
Table 5-72	56B Neutron Source .....	5-154
Table 5-73	Fuel Atom Densities (atom/b-cm).....	5-155
Table 5-74	Fuel Total Mass Densities (g/cm <sup>3</sup> ).....	5-156
Table 5-75	Advanced Mk-BW 17×17 Assembly Axial Region Lengths.....	5-156
Table 5-76	Thermocouple Locations of Lid Holes .....	5-156
Table 5-77	Carbon Steel.....	5-156
Table 5-78	Stainless Steel .....	5-157
Table 5-79	Neutron Polyester Resin .....	5-157
Table 5-80	Redwood .....	5-157
Table 5-81	Balsa Wood .....	5-157
Table 5-82	Flux-to-Dose-Rate Conversion Factors .....	5-158
Table 5-83	Maximum NCT Dose Rates with Relative Error.....	5-159
Table 5-84	Maximum HAC Dose Rates with Relative Error .....	5-160
Table 5-85	Occupied Location Dose Rates with Relative Error .....	5-160

LIST OF FIGURES

Figure 5-1	TN-32B HBU Demonstration Cask Transportation Configuration .....	5-161
Figure 5-2	TN-32B HBU Demonstration Cask MCNP NCT Model – Y-Z Plane .....	5-162
Figure 5-3	TN-32B HBU Demonstration Cask MCNP NCT Model – X-Y Plane Plot at Z=180 .....	5-163
Figure 5-4	MCNP Model for Lid Holes Locations – X-Y Plane .....	5-164
Figure 5-5	MCNP Model of a Thermocouple Penetration – YZ Plane .....	5-165
Figure 5-6	Isometric Sketch of TN-32B HBU Demonstration Cask on Railcar .....	5-166
Figure 5-7	Side View Sketch of TN-32B Demonstration Cask on Railcar .....	5-167
Figure 5-8	End View Sketch of TN-32B Demonstration Cask on Railcar .....	5-168
Figure 5-9	NCT Dose Rates (mrem/hr) at Enclosed Package Surface .....	5-169
Figure 5-10	NCT Dose Rates (mrem/hr) at Vehicle Side .....	5-170
Figure 5-11	NCT Dose Rates (mrem/hr) at Vehicle Rear .....	5-171
Figure 5-12	NCT Dose Rates (mrem/hr) at Vehicle Front .....	5-172
Figure 5-13	NCT Dose Rates (mrem/hr) at 2 meters from Vehicle Side .....	5-173
Figure 5-14	NCT Dose Rates (mrem/hr) at 2 meters from Vehicle Rear .....	5-174
Figure 5-15	NCT Dose Rates (mrem/hr) at 2 meters from Vehicle Front .....	5-175
Figure 5-16	HAC Dose Rates (mrem/hr) at 1 meter from Side .....	5-176
Figure 5-17	HAC Dose Rates (mrem/hr) at 1 meter from Rear .....	5-177
Figure 5-18	HAC Dose Rates (mrem/hr) at 1 meter from Front .....	5-178

## Chapter 5 Shielding Evaluation

### 5.1 Description of Shielding Design

#### 5.1.1 Design Features

Shielding for the TN-32B HBU demonstration cask is provided mainly by the steel cask body. The cask body is made up of the containment vessel and the closure lid, both of which provide gamma shielding. A borated polyester resin compound contained in aluminum boxes radially surrounds the containment vessel to provide additional neutron shielding. Additional shielding is provided by the steel outer shell surrounding the resin layer, the aluminum rails inside the cavity, and by the steel and aluminum structure of the fuel basket. The basket is steel and borated aluminum.

The fuel assemblies acceptable for transport in the TN-32B HBU demonstration cask are listed in Section 1.2.2.

The radial neutron shield of borated polyester resin contained in aluminum boxes is 4.50 inches thick. The boron isotopes contained in the resin is based on natural abundances (19.9 at.% B-10 and 80.1 at.% B-11). A 1/2-inch thick steel shell surrounds the exterior of the resin boxes, which is the enclosed package surface.

For gamma shielding, the sides have 9.50-inch thick steel walls under the resin boxes. The thickness of steel in the closure lid is 10.50 inches with an additional 1.75-inch thick puncture resistant plate installed over the closure lid and the thermocouple penetrations. Prior to attaching the puncture resistant plate, each individual thermocouple penetration is covered by a 2.13-inch thick steel lance cover plate, creating a 1.26-inch gap between the top of the closure lid and the bottom of the puncture resistant plate. The steel thickness in the bottom end of the cask is 10.25 inches.

An aluminum basket maintains the contents in a fixed position within the package. The basket structure is a grid of aluminum and steel panels, which have a total thickness of 3/4 inches. The periphery of the basket has additional steel structures.

The impact limiters are wood surrounded by a 0.25-inch thick steel shell with interior steel gussets. The wood is primarily redwood except in two areas, where the wood is balsa.

The primary method of conveyance for the TN-32B HBU demonstration cask is via a railcar. Buffer cars may precede and follow the railcar transporting the cask. Dimensions for a typical standard railcar are assumed.

Figure 5-1 shows the configuration of the package shielding. Table 5-1 lists key dimensions relevant to shielding. Note that the discrepancies between nominal and modeled dimensions are due to the shielding model being created prior to finalizing the drawings in Appendix 1.4.1. The minor differences between nominal and modeled dimensions have a negligible impact on the calculated dose rates.

### 5.1.2 Summary of Maximum Radiation Levels

Because the cask contains spent nuclear fuel and only one cask will be transported per vehicle (railcar), exclusive use dose rate limits are applied.

Maximum normal conditions of transport (NCT) and hypothetical accident conditions (HAC) dose rates when transporting the TN-32B HBU demonstration cask irradiated payload are reported in Table 5-2. Occupied Location dose rates for NCT for a typical railcar length of 40 feet are also reported. These maximum radiation levels are applicable to the fuel specifications (e.g., burnup, enrichment, cooling time, position in the cask) of the payload evaluated.

The cask is transported in a horizontal orientation in an open vehicle. Because the transport vehicle type is open with an enclosure, the NCT dose rate limits per 10 CFR 71.47 are 1000 mrem/hr for the enclosed package surface, 200 mrem/hr for the vehicle surface, 10 mrem/hr at 2 meters from the vehicle surface, and 2 mrem/hr for occupied locations. The HAC dose rate limit per 10 CFR 71.51(a)(2) is 1000 mrem/hr at 1 meter from the cask surface.

The railcar is assumed to be 10 feet-8 inches wide (128 inches or 325.12 cm) and 40 feet long (1219.2 cm). The fuel inside the cask is assumed to have the bottom fuel assembly fitting in contact with the bottom of the cavity inside the cask, as in the storage configuration. The package surface is the enclosed surface of the cask, and the undersides of the impact limiters underneath the personnel barrier. The bottom end of the cask is oriented to face forward toward the locomotive. Because the sides of the impact limiters will overhang the sides of a standard railcar (144 inches compared to 128 inches), and there is a personnel barrier spanning the space between the upper and lower impact limiters, the vehicle surface is taken to be the cylindrical side of the personnel barrier loaded onto the railcar, with a diameter of 128 inches. The front and back vehicle surfaces are the lower and upper impact limiters, respectively. The 2-meter dose rate is computed 2 meters from the vehicle surfaces, while the occupied location (i.e., the operator and engineer inside the cab of the locomotive) is computed  $\pm 20$  feet at approximately the axial center of the fuel in the cask.

All dose rates are below applicable limits. Under NCT, the maximum enclosed package surface dose rate is 211.8 mrem/hr, the maximum vehicle surface dose rate is 35.2 mrem/hr, the maximum dose rate 2 meters from the vehicle surface dose rate is 7.6 mrem/hr, and the dose rate in the occupied location for a 40 foot railcar is 0.7 mrem/hr. Under HAC, the maximum dose rate at 1 m from the cask is 505 mrem/hr.

## 5.2 Source Specification

The source term is calculated using the ORIGEN-ARP module of the SCALE 6.1 code system and the ENDF/B-VII nuclear data cross-section library. The payload is 32 unique, intact high burnup spent fuel assemblies from the North Anna Power Station (NAPS).

Three different manufacturers of Westinghouse-type 17×17 fuel assemblies are present in the TN-32B HBU demonstration cask: AMBW (Advanced Mk-BW), North Anna Improved Fuel (NAIF), and Low Parasitic (LOPAR). The range of initial uranium fuel loading of the fuel assemblies is between 0.460 MTU and 0.466 MTU. The range of initial enrichments spans from a minimum of 3.59 wt% to a maximum of 4.55 wt% U-235; however, the source calculation adjusts the enrichment by -0.05 wt% to account for uncertainties in the batch enrichment. [

] The final burnup of the spent fuel assemblies ranges from a minimum of 50.047 GWd/MTU to a maximum of 55.496 GWd/MTU; [

] The earliest shipment date is October 1, 2023. Therefore, the cooling times at time of shipment will range from 11.56 years to 36.45 years.

ORIGEN-ARP was used to generate four gamma source terms (bottom end fitting, in-core region, plenum, and top end fitting) and one in-core neutron source term for each of the 32 fuel assemblies. The following information is used when building the ORIGEN-ARP code inputs: Table 5-3 provides the fuel assembly hardware materials and masses on a per component basis. Table 5-4 provides the material composition of fuel assembly hardware materials and is extracted from Reference [2]. Table 5-5 lists the MTU loading and initial enrichment in each assembly, and Table 5-6 lists the fuel cycle data for each assembly.

The ORIGEN-ARP code can be used to predict the activity of the hardware irradiated in each fuel assembly based on the reactor power history; however, the fueled, in-core region of the fuel assembly is the only region where ORIGEN-ARP results are directly applicable. Table 5-7 provides the scaling factors from Reference [4], which are applied to the mass inputs that account for changes in the neutron flux and the energy spectrum when estimating source components outside the fueled region. The material compositions of the fuel assembly hardware are included in the ORIGEN-ARP model on a per assembly basis. A representative ORIGEN-ARP code input is in Section 5.6.1.

The axial burnup distributions applied when modeling the neutron and gamma sources in MCNP are provided in Table 5-8 and come from the data for >46 GWd/MTU fuel provided in Reference [3]. The gamma source is directly proportional to the burnup. However, the neutron source is not a linear function of the flux; the neutron source has been shown to be a function of the fourth power of the burnup.

These factors correspond to discrete points equally distributed along the axial height of the in-core source term definition, which are linearly interpolated by MCNP to make the axial peaking profile. For the gamma distribution, the average value is 1.0. The average value of the axial neutron distribution may be interpreted as the ratio of the true total neutron source in an assembly to the neutron source calculated by ORIGEN-ARP for an average assembly burnup. Therefore, to properly correct the magnitude of the total neutron source calculated, the neutron source is multiplied by the average value of the neutron source distribution, which is 1.152.

Each of the axial fuel regions are modeled as homogenized material.

### 5.2.1 Gamma Source

The gamma source terms as a function of energy for the fueled, in-core region and activated hardware regions for each fuel assembly are provided in Table 5-9 through Table 5-40. The source terms are specified per region per fuel assembly, and take into account the unique design MTU loading and irradiation history of each fuel assembly. The total gamma source term for all 32 fuel assemblies including hardware is  $1.0439\text{E}+17$  y/sec.

The gamma source spectra are presented in the 18-group structure consistent with the SCALE 27n-18 $\gamma$  cross-section library. The gamma source for the fuel assembly hardware is primarily from the activation of cobalt. This activation contributes primarily to SCALE Energy Groups 9 and 10.

For gamma contributions from the end hardware, the ORIGEN-ARP code generates the source for the fuel and hardware combined, and then selects only the isotopes in the hardware materials. Scaling factors from Reference [4] and shown in Table 5-7 are applied during calculation of the inputs from which the ORIGEN-ARP code will estimate the plenum, top nozzle, and bottom nozzle gamma contributions. Mixing tables are created to calculate the ORIGEN-ARP input materials for the end hardware.

Non-fuel hardware that has been irradiated in a core, such as control assemblies or shrouds, will not be transported in the TN-32B HBU demonstration cask.

An axial burnup profile has been developed as discussed in Section 5.2. Table 5-8 provides design axial gamma peaking factors that are utilized in the primary gamma MCNP shielding model.

Additionally, neutron interactions with shielding material result in the production of energetic gammas near the package surface. This secondary gamma contribution is calculated by the secondary gamma MCNP models included in the shielding analysis.

### 5.2.2 Neutron Source

Table 5-41 through Table 5-72 provide the neutron source term as a function of energy for each fuel assembly. The entirety of the neutron source terms are calculated from all contributing nuclides, and includes all reactions (e.g., both spontaneous fission and ( $\alpha$ ,n) reactions; as delayed neutron contributions are determined to be non-contributing). The most significant nuclide contributor to the spontaneous fission activity of the neutron source is Cm-244. The total neutron source term for all 32 fuel assemblies calculated by ORIGEN-ARP is  $1.1778\text{E}+10$  n/sec.

The neutron subcritical multiplication due to the fissile material in the HBU payload is accounted for by a separate criticality calculation. Note that since the NONU card was used, the neutron weight card and secondary gamma weight card includes a  $1/(1-k_{\text{eff}})$  term, where  $k_{\text{eff}}$  is the neutron multiplication factor when the cask is in the dry condition. From Section 6.3.4.13, the  $k_{\text{eff}}$  is 0.38563. The  $k_{\text{eff}}$  of the payload is incorporated by multiplying the neutron source by  $1/(1-k_{\text{eff}})$ , or  $1/0.61437 = 1.6277$ .

The neutron source is not linearly dependent with burnup, and therefore calculations were performed to determine the axial neutron source distribution. Table 5-8 provides axial neutron peaking factors that are utilized in the neutron and secondary gamma MCNP shielding models.

After applying the neutron subcritical multiplication factor and the average axial neutron peaking factor to the ORIGEN-ARP total neutron source term, the MCNP total neutron source term is as follows:

$$1.1778\text{E}10 \left( \frac{\text{neutrons}}{\text{second}} \right) \times 1.152 \times 1.6277 = 2.2085\text{E}10 \frac{\text{neutrons}}{\text{second}}$$

## 5.3 Shielding Model

The Monte Carlo computer code MCNP5v1.60 [5] is used for calculating the gamma and neutron dose rates in this analysis.

### 5.3.1 Configuration of Source and Shielding

Base models were constructed for NCT and HAC. For each base model, three contribution models are built. The first model calculates the neutron contribution, the second calculates the secondary gamma contribution resulting from neutron interactions, and the third is the primary gamma contribution. Variance reduction for all particles was accomplished by means of importance splitting. Note that the models calculating the neutron contributions were split into multiple models to have special variance reduction in regions of interest in order to decrease the time to converge.

Fuel is modeled as four axial zones: bottom end fitting, in-core, plenum, and top end fitting. The sources are uniformly homogenized over the cross section of the fuel in the basket and the appropriate zone length, with appropriate axial peaking factors applied in the in-core fuel region as discussed in Section 5.2. Each base model is executed in three separate computer runs to calculate the contributions from the following sources:

- Primary gamma radiation from the active fuel and from activated hardware within the top end fitting, plenum region and bottom end fitting (axial and radial directions).
- Neutron radiation from the active fuel region.
- Secondary gamma radiation from neutron interactions.

The sources in the active fuel region (gamma and neutron) are modeled as uniform radially but vary axially due to application of the axial peaking factors. The sources in the structural hardware regions (plenum, top end fitting, and bottom end fitting) are modeled as uniform both radially and axially. The results from the individual runs are summed to provide the total gamma, neutron and total dose rates for the package.



MCNP model geometry is derived from the drawings in Appendix 1.4.1. A comparison between the drawing dimensions and the MCNP model dimensions is shown in Table 5-1. The MCNP model origin (0, 0, 0) is on the cask centerline and the approximate axial center of the active fuel region. The bottom of the fuel assembly is modeled to sit on the cavity bottom as if in the upright position. The model surface types are mainly planes (denoted as px, py, or pz), and right circular cylinders (denoted as cz). The basket is modeled discretely with stainless steel boxes surrounded with aluminum plates. The rails and neutron shield resin boxes are also modeled discretely.

The borated neutron poison plates integrated in the basket are modeled as plain aluminum which conservatively neglects the neutron absorption qualities of boron. Also, trunnion locations are modeled as void; no shielding credit is taken for the steel of the trunnions.

The NCT transportation MCNP models are modified to create the HAC transportation MCNP models. Changes include removing the radial borated polyester resin, the steel outer shell surrounding the resin layer, and the impact limiters.

Atom densities and mass densities of homogenized contents of the four axial zones are calculated and relevant results are in Table 5-73 and Table 5-74. Though there are three types of  $17 \times 17$  fuel assemblies, modeling simplifications are made so that the fuel region lengths are the same for all types of fuel assemblies. The lengths of these axial zones are derived from the reference dimensions in Reference [8] and are shown in Table 5-75. A sketch of the NCT cask model with impact limiters oriented in the storage configuration (top lid pointing up) is in Figure 5-2. A view of the cross section of the cask model is in Figure 5-3.

Voids are neglected within the fuel assemblies. The voids within the cask cavity are modeled.

#### 5.3.1.1 Thermocouple Penetrations

One important geometry feature is the presence of holes in the original lid for the thermocouples. During transport, a [ ] steel lance cover plate is placed over each penetration, and then the 1.75-inch thick puncture resistant steel plate is installed over the closure lid. The holes for the thermocouples in the closure lid were added at the locations outlined in Table 5-76, where (0,0) corresponds to the center of the closure lid. Figure 5-4 shows the MCNP model of the lid with these holes in the X-Y plane, and Figure 5-5 shows the MCNP model of the steel insert, and the puncture-resistant steel plate with one of the holes in the Y-Z plane.

[

]

### 5.3.2 Material Properties

The material densities have been calculated for an Advanced Mk-BW 17 × 17 fuel design general fuel assembly with an enrichment of 4 wt% U-235 in the in-core region. The fuel assembly atom densities are shown in Table 5-73 and the fuel assembly mass densities are shown in Table 5-74.

Carbon steel, Type 304 stainless steel, redwood, balsa wood, and aluminum material cards contents are extracted from the SCALE Standard Composition Library [1]. Carbon steel, stainless steel, redwood, and balsa wood material compositions are provided in Table 5-77, Table 5-78, Table 5-80, and Table 5-81, respectively. The density of pure aluminum is assumed to be 2.702 g/cm<sup>3</sup>. The natural abundance of B-10 and B-11 is assumed to be 19.9 at.% and 80.1 at.%, respectively. The material card for the neutron polyester resin is shown in Table 5-79.

The thermal stability of the neutron polyester resin is evaluated. For the temperatures the package will experience during NCT, no substantial hydrogen loss is predicted, as discussed in Section 1.2.1.2. For potential temperatures the package could experience during HAC, the neutron polyester resin is completely absent, and hence, is not considered for shielding purposes.

## 5.4 Shielding Evaluation

The package is evaluated to demonstrate that it satisfies the shielding requirements of 10 CFR Part 71 [7].

### 5.4.1 Methods

MCNP is a general-purpose Monte Carlo N-Particle code that can be used for neutron, photon, or coupled neutron/photon transport. The code treats an arbitrary three-dimensional (3-D) configuration of materials in geometric cells bounded by first- and second-degree surfaces and some special fourth-degree surfaces. Continuous energy cross-section data are used. For neutrons, all reactions given in a particular cross-section evaluation are accounted for in the cross-section set. For photons, the code takes into account incoherent and coherent scattering, the possibility of fluorescent emission after photoelectric absorption, absorption in pair production with local emission of annihilation radiation, and bremsstrahlung. Mesh tally capabilities (F4 type tallies) were utilized in calculating dose rates distributed over and around the surface of the TN-32B HBU demonstration cask. The MCNP code is selected for its ability to handle thick, multi-layered shields, like the TN-32B HBU demonstration cask body, using 3-D geometry.

The NCT models calculate primary gamma, secondary gamma, and neutron dose rates, which are summed to determine the maximum dose rate for each specified tally location. Package dose rates are calculated by mesh tallies over the external surface of the radial neutron resin shield and along the undersides of the impact limiters (surfaces enclosed by the personnel barrier), and over the exposed surfaces of the impact limiters. Vehicle dose rates are calculated by mesh tallies over the personnel barrier and over the exposed surfaces of the impact limiters. As the mesh tallies over the exposed surfaces of the impact limiters are defined to be the same for both package and vehicle surfaces, some of the mesh tallies are redundant. Mesh tallies calculate dose rates 2 meters from the personnel barrier and top and bottom vehicle surfaces. Also, mesh tallies calculate dose rates at potential occupied locations. The closest occupied space would be the locomotive cab that houses the engineer and the operator; however, because the length of the railcar or locomotive to be used is unknown, occupied dose tallies are set up at regular intervals from the top and bottom of the package.

The HAC models calculate primary gamma, secondary gamma, and neutron dose rates, which are summed to determine the maximum dose rate. The HAC models have mesh tallies calculate dose rates at 1 meter from the cask cylindrical surface with the neutron shield and impact limiters absent.

The cross-section data used in the primary gamma shielding models is the continuous energy ENDF/B-VI Release 8 library provided with the MCNP5 code. For the neutron and secondary gamma shielding models, the cross-section data used is the continuous energy ENDF/B-VII.0 library, unless the cross-section data is not available in that library, then an alternative library is used. For the source terms, ORIGEN relies on decay data in ENDF/B-VII that is distributed with SCALE 6.1. The cross-section data allow a coupled neutron/gamma dose rate evaluation to be made to account for secondary gamma radiation. Dose rates from secondary gammas are calculated by using gamma (photon) tallies in MODE N P in the MCNP neutron source model. Since all 32 HBU fuel assemblies are intact, reconfiguration of the fuel is not modeled.

#### 5.4.2 Input and Output Data

The vehicle surfaces are taken to be a horizontal cylinder the diameter of the personnel barrier (128 inches or 325.12 cm) increasing to the diameter of the impact limiters (144 inches or 365.76 cm) with vertical surfaces along the top and bottom surfaces of the impact limiters. As the width of a railcar is 10 feet- 8 inches (128 inches) and the diameter of the impact limiters is 144 inches, the impact limiters will overhang the sides of the railcar. Since a personnel barrier is installed between the impact limiters that will restrict access to the side surface of the cask, the transport vehicle type is considered Open with Enclosure, per Reference [7]. Because of this classification, the package surface of the cask (enclosed by a personnel barrier) is limited to a dose rate of 1000 mrem/hr. The 200 mrem/hr limit in Reference [7] is applicable to the vehicle surface bounded axially by the external surfaces of the impact limiters and radially by the vertical planes extending from a 10 feet- 8 inches wide rail car and the top of the personnel barrier. The model calculates dose rates along the curved surfaces, which produces more conservative dose rates in comparison to the dose rates at the vertical planes projected from the edges of the rail car. Sketches of the mesh tally configurations are in Figures 5-6, 5-7, and 5-8.

Dose rates were calculated both axially and radially outside the cask. All tallies are mesh (F4) tallies and are converted into dose rates using energy-dependent dose conversion factors listed in Table 5-82. The tally locations were chosen to completely cover the exterior of the cask and all possible radiation streaming paths. The tally mesh sizes are selected to be small enough to capture any streaming path and allow analysis of any spatial peaking.

For the NCT package side surface, mesh tallies calculate the maximum dose rates in approximately 25 cm × 25 cm square tallies along the cylindrical side, the gap between the top impact limiter and the top of the neutron resin shield, and the undersides of the impact limiters.

For the NCT vehicle surface, mesh tallies calculate the maximum dose rates in approximately 30 cm × 30 cm square tallies along the cylindrical side, and similarly sized mesh tallies by area on the front and back of the vehicle.

For the NCT 2 meters from the vehicle surface, mesh tallies calculate the maximum dose rates in approximately 100 cm × 100 cm square tallies along the cylindrical side, and similarly sized mesh tallies by area 2 meters from the front and back of the vehicle.

As the actual occupied location would vary depending on the design of the freight locomotive, a bounding railcar length of 40 feet is analyzed. The occupied location tallies are set up ±20 feet from the model center of the cask. A cylindrical mesh tally 144 inches (365.76 cm) in diameter and 10 cm thick is set to simulate the amount of space a person would fill.

For HAC conditions, mesh tallies calculate maximum dose rates in approximately 60 cm × 60 cm square tallies 1 meter from the cylindrical side. Mesh tallies calculate maximum dose rates in similarly sized mesh tallies by area 1 meter from the top and bottom ends of the cask body.

The Monte Carlo uncertainty associated with the limiting dose rate locations are less than 2%. All tallies converge to be less than 10%. The MCNP runs are carried out for a sufficient time to ensure convergence and acceptable statistical uncertainties.

#### 5.4.3 Flux-to-Dose-Rate Conversion

Conversion of the flux to dose rate is based on ANSI/ANS 6.1.1-1977 [6], and is shown in Table 5-82. The conversion factors have been multiplied by a factor of 1000 to generate dose rates in units of mrem/hr rather than rem/hr.

#### 5.4.4 External Radiation Levels

The NCT maximum dose rate results are summarized in Table 5-83 and Table 5-85 for the TN-32B HBU demonstration cask, separated by contributor. In all cases, the dose rates are well below the limits. Figure 5-9 through Figure 5-18 graphically present the dose rates calculated on the surfaces and planes of interest.

The HAC maximum dose rates at 1 m are computed using mesh tallies. HAC results are provided in Table 5-84. Dose rates are well below the limit of 1000 mrem/hr.

The MCNP models for each of the three radiation contributors (i.e., primary gamma, neutron, and secondary gamma) are executed separately. This allows the tally nomenclature to be the same in each MCNP model. In other words, each tally number covers the same surface of the cask model with the same sized meshes for each radiation contributor. Post processing scripts are used to “match up” the meshes from each contributor and calculate the total dose rates for each mesh.

In general, the results indicate peaking near the top and bottom of the cask side surface and streaming around the radial neutron shield. These results are expected due to the reduced shielding in these areas. Higher dose rates are calculated originating from the bottom surface of the cask relative to the top (closure lid end) surface of the cask. The bottom end of the cask will face forward toward the locomotive/transport vehicle during transport. The thermocouple holes have no noticeable effect on the dose rates calculated for the top end surface of the cask with exception to the streaming illustrated in Figure 5-10.

On average, the dose rates are dominated by the neutron source term, but the neutron contribution decreases as distance from the spent fuel source increases or the shielding effects of the wood in the impact limiters is considered. The results indicate that typically the NCT total dose rates from the side are comprised of 32% to 52% primary gamma, up to 16% secondary gamma and 44% to 60% neutron. However, the primary gamma source produces the majority of the dose rate at the ends of the package; the average contribution from primary gamma is in the range of 57% to 64%, 34% to 39% secondary gamma and <4% neutron. This decrease in neutron contribution and increase in secondary gamma contribution is a direct result of the shielding from the wood in the impact limiters. As expected, the HAC total dose rates along the side are produced mostly from the neutron source (95%) due to the loss of the neutron shielding material.

Note that the neutron shield extends from -188 cm to +205 cm axial range in the MCNP calculational model. Figure 5-9 illustrates that there is a dose rate increase from +190 cm to +224 cm axial coordinate range, and at approximately -188 cm when considering dose rates at radial distances not exceeding the radius of impact limiters. The dose rates at those locations are larger than at the middle of the cask because of less steel shielding due to the “flat area” near the locations of the trunnions (trunnions are conservatively modeled as void) and the absence of neutron shielding.

#### 5.4.4.1 NCT Results

##### 5.4.4.1.1 Enclosed Package Surface

Figure 5-9 presents the calculated dose rates under NCT conditions on the cask (enclosed package) surface. The y-axis is approximately axially centered about the active fuel length of the spent fuel payload. The negative y direction is toward the bottom of the cask, and the positive y direction is toward the upper end of the cask. Note that the cask is transported horizontally with the lower end facing forward. The black horizontal lines indicate the bottom of the upper impact limiter and the top of the lower impact limiter (i.e., the undersides of the impact limiters). This figure illustrates the streaming near the top of the cask due to the significant gap between the radial neutron shield and the bottom of the upper end impact limiter. The streaming near the bottom of the cask is due to a much smaller (approximately 1/2-inch) gap between the radial neutron shield and the top of the lower impact limiter. The maximum dose rate is 211.8 mrem/hr. Tallies placed between the top of the neutron radial shield and the bottom of the impact limiter are considered when determining the maximum side surface dose rates reported in Table 5-2 and Table 5-83. The maximum dose rate complies with the 1000 mrem/hr 10 CFR 71.47 limit for enclosed surfaces in NCT configuration.

##### 5.4.4.1.2 Vehicle Surface

Figures 5-10, 5-11, and 5-12 present the calculated dose rates for NCT vehicle surface side, back (upper impact limiter), and front (lower impact limiter) surfaces, respectively. Figure 5-10 is also approximately axially centered about the active fuel of the spent fuel payload. The black horizontal lines indicate the axial locations of the upper and lower impact limiters in relation to the calculated dose rates, with the personnel barrier spanning the open space between the impact limiters. There is still a pronounced streaming path around the top of the radial neutron resin shield, and a noticeable but not significant streaming path around the bottom of the radial neutron shield. The maximum dose rate is determined to be the streaming path around the top of the radial neutron shield. There is a second peak below the approximately axial center of the model and slightly below the axial center of the active fuel length. Since the TN-32B HBU demonstration cask payload is high burnup fuel assemblies, this dose profile is expected. The maximum dose rate in Figure 5-10 is 35.2 mrem/hr, which is comprised of 15.7 mrem/hr neutron, 1.4 mrem/hr secondary gamma, and 18.1 mrem/hr primary gamma. Therefore, the dose rates on the sides are approximately 45% neutron.

Figure 5-11 and Figure 5-12 present the calculated dose rates on the ends of the vehicle in NCT configuration. The maximum dose rate from the back (upper) impact limiter surface is 2.7 mrem/hr, which is comprised of 0.1 mrem/hr neutron, 1.0 mrem/hr secondary gamma, and 1.6 mrem/hr primary gamma. The maximum dose rate from the front (lower) impact limiter surface is 8.1 mrem/hr, which is comprised of 0.3 mrem/hr neutron, 3.2 mrem/hr secondary gamma, and 4.6 mrem/hr primary gamma. The total neutron contribution is <3% of the total dose rate on the top impact limiter, and <4% of the total dose rate on the lower impact limiter. Note that any indication of the streaming paths through the thermocouple holes has become not noticeable when calculating dose rates on the upper impact limiter. These maximum dose rates comply with the 200 mrem/hr, 10 CFR 71.47 limit for package and vehicle surfaces in NCT configuration.

#### 5.4.4.1.3 2 Meters from Vehicle Surface

Figure 5-13 through Figure 5-15 present the calculated NCT dose rates at 2 meters from vehicle surface side, back (upper) impact limiter, and front (lower) impact limiter surfaces, respectively. Figure 5-13 also coordinates the 0 cm dimension with the approximate axial center of the model. The horizontal lines indicate the axial locations of the upper and lower impact limiters. At 2 meters, there is no longer a noticeable streaming path around the top of the radial neutron resin shield. The maximum dose rate in Figure 5-13 is 7.5 mrem/hr, which is comprised of 4.0 mrem/hr neutron, 1.2 mrem/hr secondary gamma, and 2.4 mrem/hr primary gamma. Therefore, the dose rates 2 meters from the vehicle side are approximately 53% neutron.

Figure 5-14 and Figure 5-15 present the calculated dose 2 meters from the back and front of the vehicle, respectively. The maximum dose rate 2 meters from the back of the vehicle is 0.5 mrem/hr, which is comprised of <0.1 mrem/hr neutron, 0.2 mrem/hr secondary gamma, and 0.3 mrem/hr primary gamma. The maximum dose rate 2 meters from the front of the vehicle is 1.3 mrem/hr, which is comprised of 0.1 mrem/hr neutron, 0.5 mrem/hr secondary gamma, and 0.8 mrem/hr primary gamma. The total neutron contribution is <2% of the total dose rate 2 meters from the back of the vehicle and <3% of the total dose rate 2 meters from the front of the vehicle. These maximum dose rates comply with the 10 CFR 71.47 limit of 10 mrem/hr at 2 meters from the vehicle surfaces in the NCT configuration.

#### 5.4.4.2 HAC Results

##### 5.4.4.2.1 1 Meter from Cask Surface

Figure 5-16 through Figure 5-18 present the calculated HAC dose rates at 1 meter from the cask side, back (top of cask), and front (bottom of cask) surfaces, respectively, without the radial neutron resin shield or impact limiters. Figure 5-16 is approximately axially centered about the active fuel of the spent fuel payload. For HAC at 1 meter from the cask surface, there are no noticeable streaming paths. The maximum dose rate in Figure 5-16 is 504.6 mrem/hr, which is comprised of 477.7 mrem/hr neutron, 1.4 mrem/hr secondary gamma, and 25.5 mrem/hr primary gamma. Therefore, the dose rates 1 meter from the cask side for HAC are approximately 95% neutron.

Figure 5-17 and Figure 5-18 present the calculated dose rates for HAC 1 meter from the ends of the cask without the impact limiters. The maximum dose rate 1 meter from the top of the cask surface is 37.9 mrem/hr, which is comprised of 27.6 mrem/hr neutron, 0.2 mrem/hr secondary gamma, and 10.1 mrem/hr primary gamma. The maximum dose rate 1 meter from the bottom cask surface is 140.1 mrem/hr, which is comprised of 107.7 mrem/hr neutron, 0.5 mrem/hr secondary gamma, and 31.9 mrem/hr primary gamma. The total neutron contribution is approximately 73% of the total dose rate 1 meter from the top of the cask, and approximately 77% of the total dose rate 1 meter from the bottom surface of the cask. These maximum dose rates comply with the 10 CFR 71.51(a)(2) limit of 1000 mrem/hr at 1 meter from the cask surfaces in the HAC configuration.

## 5.5 References

1. SCALE 6.1, "Scale: A Comprehensive Modeling and Simulation Suite for Nuclear Safety Analysis and Design," CCC-785, Oak Ridge National Laboratory, June 2011.
2. Ludwig, S.B., and Renier, J. P., "Standard- and Extended-Burnup PWR and BWR Reactor Models for the ORIGEN2 Computer Code," ORNL/TM-11018, Oak Ridge National Laboratory, December 1989.
3. Parks, C. V., DeHart, M. D., and Wagner, J. C., "Recommendations for Addressing Axial Burnup in PWR Burnup Credit Analyses," NUREG/CR-6801, March 2003.
4. Luksic, A., "Spent Fuel Assembly Hardware: Characterization and 10 CFR 61 Classification for Waste Disposal," PNL-6906, Vol. 1, June 1989.
5. MCNP5v1.60, "MCNP – A General Monte Carlo N-Particle Transport Code, Version 5, Volume I: Overview and Theory," CCC-701, Los Alamos National Laboratory, February 2008.
6. "American National Standard Neutron and Gamma-Ray Flux-to-Dose-Rate Factors," ANSI/ANS-6.1.1-1977, La Grange Park, IL, 1977.
7. Title 10, Code of Federal Regulations - Energy, Part 71 (10 CFR 71), "Packaging and Transportation of Radioactive Material", 1-1-2021 Edition, U.S. Nuclear Regulatory Commission, Washington, D.C.



Proprietary Information on Pages 5-14 through 5-82  
Withheld Pursuant to 10 CFR 2.390

**Table 5-2**  
**Summary of TN-32B HBU Demonstration Cask Dose Rates**  
 (Exclusive Use)

Normal Conditions of Transport		Package Surface mSv/hr (mrem/hr) <sup>(1)</sup>		Vehicle Surface <sup>(2)</sup> mSv/hr (mrem/hr)		2 meters from Vehicle Surface mSv/hr (mrem/hr)	
Radiation	Side	Top	Side	Bottom	Top	Side	Bottom
Gamma	0.841 (84.1)	0.026 (2.6)	0.195 (19.5)	0.078 (7.8)	0.005 (0.5)	0.036 (3.6)	0.013 (1.3)
Neutron	1.277 (127.7)	0.001 (0.1)	0.157 (15.7)	0.003 (0.3)	<0.001 (<0.1)	0.040 (4.0)	<0.001 (<0.1)
Total	2.118 (211.8)	0.027 (2.7)	0.352 (35.2)	0.081 (8.1)	0.005 (0.5)	0.076 (7.6)	0.013 (1.3)
10 CFR §71.47 Limit	10 (1000)	2 (200)	2 (200)	2 (200)	0.1 (10)	0.1 (10)	0.1 (10)

- (1) Includes tallies set between the top of the radial neutron shield and the undersides of the impact limiters. Package surface is enclosed by the personnel barrier, which allows the surface radiation limit to be 10 mSv/hr (1000 mrem/hr) per 10 CFR 71.47(b)(1).
- (2) Vehicle surface is bounded axially by the external surfaces of the impact limiters/personnel barrier and radially by the vertical planes extending from a 10-foot 8-inch wide vehicle. The bounding radial dose rates are shown for all surfaces.

Hypothetical Accident Conditions	1 meter from Package Surface mSv/hour (mrem/hour) <sup>(1)</sup>		
Radiation	Top	Side	Bottom
Gamma	0.102 (10.2)	0.269 (26.9)	0.324 (32.4)
Neutron	0.276 (27.6)	4.777(477.7)	1.077 (107.7)
Total	0.378 (37.8)	5.046 (504.6)	1.401 (140.1)
10 CFR §71.51(a)(2) Limit	10 (1000)	10 (1000)	10 (1000)

- (1) The neutron shield and the impact limiters are assumed not to be present.

Rail Car Length (feet)	Occupied Location Dose Rates As A Function of Railcar Length mSv/hour (mrem/hour)								10 CFR §71.47 Limit
	Primary Gamma		Secondary Gamma		Neutron		Total		
	Top	Bottom	Top	Bottom	Top	Bottom	Top	Bottom	
40	0.001 (0.1)	0.004 (0.4)	0.001 (0.1)	0.003 (0.3)	<0.001 (<0.1)	<0.001 (<0.1)	0.003 (0.3)	0.007 (0.7)	0.02 (2)

General Note: The total dose rate is the sum of unrounded values.

**Table 5-3  
Fuel Assembly Hardware Characteristics**

FA Region	Fuel Assembly Part	Material	FA Weight	
			kg	lb <sub>m</sub>
Top Nozzle	Upper Tie Plate	SS 304	7.0	15.4
	Hold Down Springs	Inconel 718	1.1	2.4
Plenum	Plenum Spring	SS 302	4.7	10.4
	Cladding & Guide Tubes	M5™ <sup>(1)</sup>	6.3	13.9
	Grid	Inconel 718	0.7	1.5
In core Region	Cladding & Guide Tubes	M5™ <sup>(1)</sup>	109.9	242.3
	Grids - Zr-4	Zircaloy-4	8.2	18.1
	Grids - Inconel 718	Inconel 718	0.8	1.8
	Miscellaneous (Ferrules)	M5™ <sup>(1)</sup>	0.1	0.2
Bottom Nozzle	Bottom Tie Plate	SS 304	4.3	9.5

(1) M5™ is assumed to have the same composition as Zircaloy-4.

**Table 5-4**  
**Material Compositions for Fuel Assembly Hardware Materials**

Element	Atomic Number	Grams per kg of metal							Parts per thousand heavy metal
		Zircaloy-4	Zircaloy-2	Inconel-718	Inconel-X-750	Stainless Steel 304	Stainless Steel 302	Nicrobraz 50	UO2 Fuel
H	1	1.30E-02	1.30E-02						
Li	3								1.00E-03
B	5	3.30E-04	3.30E-04					5.00E-02	1.00E-03
C	6	1.20E-01	1.20E-01	4.00E-01	3.99E-01	8.00E-01	1.50E+00	1.00E-01	8.94E-02
N	7	8.00E-02	8.00E-02	1.30E+00	1.30E+00	1.30E+00	1.30E+00	6.60E-02	2.50E-02
O	8	9.50E-01	9.50E-01					4.30E-02	1.34E+02
F	9								1.07E-02
Na	11								1.50E-02
Mg	12								2.00E-03
Al	13	2.40E-02	2.40E-02	5.99E+00	7.98E+00			1.00E-01	1.67E-02
Si	14			2.00E+00	2.99E+00	1.00E+01	1.00E+01	5.11E-01	1.21E-02
P	15					4.50E-01	4.50E-01	1.03E+02	3.50E-02
S	16	3.50E-02	3.50E-02	7.00E-02	7.00E-02	3.00E-01	3.00E-01	1.00E-01	
Cl	17								5.30E-03
Ca	20								2.00E-03
Ti	22	2.00E-02	2.00E-02	7.99E+00	2.49E+01			1.00E-01	1.00E-03
V	23	2.00E-02	2.00E-02						3.00E-03
Cr	24	1.25E+00	1.00E+00	1.90E+02	1.50E+02	1.90E+02	1.80E+02	1.50E+02	4.00E-03
Mn	25	2.00E-02	2.00E-02	2.00E+00	6.98E+00	2.00E+01	2.00E+01	1.00E-01	1.70E-03
Fe	26	2.25E+00	1.50E+00	1.80E+02	6.78E+01	6.88E+02	6.97E+02	4.71E-01	1.80E-02
Co	27	1.00E-02	1.00E-02	4.69E+00	6.49E+00	8.00E-01	8.00E-01	3.81E-01	1.00E-03
Ni	28	2.00E-02	5.00E-01	5.20E+02	7.22E+02	8.92E+01	8.92E+01	7.44E+02	2.40E-02
Cu	29	2.00E-02	2.00E-02	9.99E-01	4.99E-01				1.00E-03
Zn	30								4.03E-02
Zr	40	9.79E+02	9.79E+02					1.00E-01	
Nb	41			5.55E+01	8.98E+00				
Mo	42			3.00E+01					1.00E-02
Ag	47								1.00E-04
Cd	48	2.50E-04	2.50E-04						2.50E-02
In	49								2.00E-03
Sn	50	1.60E+01	1.60E+01						4.00E-03
Gd	64								2.50E-03
Hf	72	7.80E-02	7.80E-02						
W	74	2.00E-02	2.00E-02					1.00E-01	2.00E-03
Pb	82								1.00E-03
Bi	83								4.00E-04
U	92	2.00E-04	2.00E-04						1.00E+03

Proprietary Information on Pages 5-86 through 5-88  
Withheld Pursuant to 10 CFR 2.390

**Table 5-7**  
**ORIGEN Scaling Factors**

<b>Region</b>	<b>Westinghouse Assembly Scaling Factors</b>
Top End Fitting	0.1
Gas Plenum	0.2
Fueled Region	1.0
Bottom End Fitting	0.2

**Table 5-8**  
**Axial Peaking Factors**

<b>Axial Height (%)</b>	<b>Gamma</b>	<b>Neutron</b>
2.78	0.573	0.108
8.33	0.917	0.707
13.89	1.066	1.291
19.44	1.106	1.496
25.00	1.114	1.540
30.56	1.111	1.524
36.11	1.106	1.496
41.69	1.101	1.469
47.22	1.097	1.448
<b>52.80<sup>(1)</sup></b>	1.093	1.427
58.33	1.089	1.406
63.89	1.086	1.391
69.44	1.081	1.366
75.00	1.073	1.326
80.56	1.051	1.220
86.11	0.993	0.972
91.67	0.832	0.479
97.22	0.512	0.069
<b>Average</b>	1.000	1.152

- (1) Reference [3] appears to have a typo for this value. It lists a value of 57.8, which is a different interval from the other sections, and page 30/121 of Reference [3] has a statement that the burnup profile is represented by equally-spaced axial regions.

Proprietary Information on Pages 5-91 through 5-154  
Withheld Pursuant to 10 CFR 2.390



**Table 5-73**  
**Fuel Atom Densities (atom/b-cm)**

<b>Element</b>	<b>Bottom Region</b>	<b>In-Core Region</b>	<b>Plenum Region</b>	<b>Top Region</b>
Li	0.0000E+00	2.4650E-07	0.0000E+00	0.0000E+00
B-10	0.0000E+00	3.4075E-08	2.1719E-09	0.0000E+00
B-11	0.0000E+00	1.3716E-07	8.7422E-09	0.0000E+00
C	4.6619E-05	1.7076E-05	3.8209E-05	4.8928E-05
N	6.4960E-05	5.7474E-06	3.0487E-05	7.3144E-05
F	0.0000E+00	9.6362E-07	0.0000E+00	0.0000E+00
Na	0.0000E+00	1.1163E-06	0.0000E+00	0.0000E+00
Mg	0.0000E+00	1.4079E-07	0.0000E+00	0.0000E+00
P	1.0168E-05	1.9334E-06	3.8754E-06	9.8947E-06
S	6.5483E-06	4.7003E-07	2.9727E-06	6.6056E-06
Cl	0.0000E+00	2.5578E-07	0.0000E+00	0.0000E+00
Ca	0.0000E+00	8.5382E-08	0.0000E+00	0.0000E+00
Ti	0.0000E+00	6.9326E-07	6.7809E-06	1.7864E-05
V	0.0000E+00	2.6757E-07	1.4038E-07	0.0000E+00
Co	9.5010E-06	3.2997E-07	6.8433E-06	1.7762E-05
Cu	0.0000E+00	2.0585E-07	7.3710E-07	1.6825E-06
Zn	0.0000E+00	1.0542E-06	0.0000E+00	0.0000E+00
Nb	0.0000E+00	1.7178E-06	2.3733E-05	6.3933E-05
Ag	0.0000E+00	1.5862E-09	0.0000E+00	0.0000E+00
Cd	0.0000E+00	3.8146E-07	7.9519E-10	0.0000E+00
In	0.0000E+00	2.9803E-08	0.0000E+00	0.0000E+00
Sn	0.0000E+00	5.7322E-05	4.8192E-05	0.0000E+00
Gd	0.0000E+00	2.7201E-08	0.0000E+00	0.0000E+00
Hf	0.0000E+00	1.8567E-07	1.5625E-07	0.0000E+00
W	0.0000E+00	6.4835E-08	3.8898E-08	0.0000E+00
Pb	0.0000E+00	8.2576E-09	0.0000E+00	0.0000E+00
H	0.0000E+00	5.4797E-06	4.6116E-06	0.0000E+00
O	0.0000E+00	1.4371E-02	2.1231E-05	0.0000E+00
Al	0.0000E+00	2.0753E-06	9.1379E-06	2.3760E-05
Si	2.4920E-04	9.4189E-07	9.7804E-05	2.5011E-04
Cr	2.5575E-03	2.0853E-05	1.0772E-03	2.8797E-03
Fe	8.6689E-03	2.7082E-05	3.4903E-03	8.7823E-03
Ni	1.0634E-03	2.6313E-05	7.5728E-04	1.9827E-03
Mn	2.5480E-04	3.1230E-07	9.8685E-05	2.5183E-04
Zr	0.0000E+00	4.5598E-03	3.8374E-03	0.0000E+00
Mo	0.0000E+00	1.0775E-06	1.2423E-05	3.3466E-05
Bi	0.0000E+00	7.1335E-09	0.0000E+00	0.0000E+00
U-235	0.0000E+00	2.9123E-04	2.1910E-12	0.0000E+00
U-238	0.0000E+00	6.9014E-03	2.9830E-10	0.0000E+00
<b>Total</b>	<b>1.2932E-02</b>	<b>2.6298E-02</b>	<b>9.5683E-03</b>	<b>1.4444E-02</b>

**Table 5-74**  
**Fuel Total Mass Densities (g/cm<sup>3</sup>)**

Element	Bottom Region	In-Core Region	Plenum Region	Top Region
Total	1.1632E+00	3.9336E+00	1.1029E+00	1.3098E+00

**Table 5-75**  
**Advanced Mk-BW 17×17 Assembly Axial Region Lengths**

Region	Length (inches)
Bottom	3.18
In-core	144
Plenum	9.12
Top	5.32
Total	161.62

**Table 5-76**  
**Thermocouple Locations of Lid Holes**

x (inches)	y (inches)
-12.937	14.425
-4.975	-3.487
-14.425	-15.913
-4.975	25.363
6.463	4.975
4.975	-25.363
23.875	-15.913

**Table 5-77**  
**Carbon Steel**

Model ZAIID	Element	Wt. %
6000	C	1.0
26000	Fe	99.0
Density	7.8212	g/cm <sup>3</sup>

**Table 5-78  
Stainless Steel**

Model ZAID	Element	Wt. %
6000	C	0.08
14000	Si	1
15031	P	0.045
24000	Cr	19
25055	Mn	2
26000	Fe	68.375
28000	Ni	9.5
Density	7.94	g/cm <sup>3</sup>

**Table 5-79  
Neutron Polyester Resin**

Model ZAID	Element	Wt. %
1001	H	5.05
5010	B-10	0.194
5011	B-11	0.856
6000	C	35.13
8016	O	41.73
13027	Al	14.93
30000	Zn	2.11
Density	1.58	g/cm <sup>3</sup>

**Table 5-80  
Redwood**

Model ZAID	Element	Atoms per Molecule
6000	C	6
1001	H	10
8016	O	5
Density	0.387	g/cm <sup>3</sup>

**Table 5-81  
Balsa Wood**

Model ZAID	Element	Atoms per Molecule
6000	C	6
1001	H	10
8016	O	5
Density	0.125	g/cm <sup>3</sup>

**Table 5-82**  
**Flux-to-Dose-Rate Conversion Factors**

Neutron		Gamma	
E (MeV)	(mrem/hr)/(n/cm <sup>2</sup> -s)	E (MeV)	(mrem/hr)/(γ/cm <sup>2</sup> -s)
2.50E-08	3.67E-03	0.01	3.96E-03
1.00E-07	3.67E-03	0.03	5.82E-04
1.00E-06	4.46E-03	0.05	2.90E-04
1.00E-05	4.54E-03	0.07	2.58E-04
1.00E-04	4.18E-03	0.10	2.83E-04
0.001	3.76E-03	0.15	3.79E-04
0.01	3.56E-03	0.20	5.01E-04
0.1	2.17E-02	0.25	6.31E-04
0.5	9.26E-02	0.30	7.59E-04
1	1.32E-01	0.35	8.78E-04
2.5	1.25E-01	0.40	9.85E-04
5	1.56E-01	0.45	1.08E-03
7	1.47E-01	0.50	1.17E-03
10	1.47E-01	0.55	1.27E-03
14	2.08E-01	0.60	1.36E-03
20	2.27E-01	0.65	1.44E-03
		0.70	1.52E-03
		0.80	1.68E-03
		1.00	1.98E-03
		1.40	2.51E-03
		1.80	2.99E-03
		2.20	3.42E-03
		2.60	3.82E-03
		2.80	4.01E-03
		3.25	4.41E-03
		3.75	4.83E-03
		4.25	5.23E-03
		4.75	5.60E-03
		5.00	5.80E-03
		5.25	6.01E-03
		5.75	6.37E-03
		6.25	6.74E-03
		6.75	7.11E-03
		7.50	7.66E-03
		9.00	8.77E-03
		11.00	1.03E-02
		13.00	1.18E-02
		15.00	1.33E-02

**Table 5-83**  
**Maximum NCT Dose Rates with Relative Error**

Normal Conditions of Transport	Package Surface (mrem/hour) <sup>(1)</sup>		Vehicle Surface (mrem/hour) <sup>(2)</sup>						2 meters from Vehicle Surface (mrem/hour)					
	Side		Top		Side		Bottom		Top		Side		Bottom	
	Result	Error	Result	Error	Result	Error	Result	Error	Result	Error	Result	Error	Result	Error
Primary Gamma	81.8	2.71%	1.6	5.62%	18.1	1.11%	4.6	0.96%	0.3	3.47%	2.4	0.69%	0.8	0.82%
Secondary Gamma	2.3	2.83%	1.0	3.48%	1.4	0.98%	3.2	1.86%	0.2	2.17%	1.2	0.19%	0.5	1.22%
Neutron	127.7	1.62%	0.1	0.89%	15.7	1.15%	0.3	2.19%	<0.1	0.60%	4.0	0.72%	<0.1	1.91%
Total	211.8	1.43%	2.7	3.61%	35.2	0.77%	8.1	0.92%	0.5	2.33%	7.6	0.44%	1.3	0.67%
10 CFR §71.47 Limit	1000		200		200		200		10		10		10	

(1) Includes tallies set between the top of the radial neutron shield and the undersides of the impact limiters. Package surface is enclosed by the personnel barrier, which allows the surface radiation limit to be 10 mSv/hr (1000 mrem/hr) per 10 CFR 71.47(b)(1).

(2) Vehicle surface is bounded axially by the external surfaces of the impact limiters/personnel barrier and radially by the vertical planes extending from a 10-foot 8-inch wide vehicle. The bounding radial dose rates are shown for all surfaces.

General Note: The total dose rate is the sum of rounded values.

**Table 5-84**  
**Maximum HAC Dose Rates with Relative Error**

Hypothetical Accident Conditions	1 meter from Package Surface (mrem/hour) <sup>(1)</sup>					
Radiation	Top		Side		Bottom	
	Result	Error	Result	Error	Result	Error
Primary Gamma	10.1	1.57%	25.5	0.38%	31.9	0.75%
Secondary Gamma	0.2	8.46%	1.4	1.10%	0.5	4.70%
Neutron	27.6	1.94%	477.7	0.20%	107.7	1.03%
Total	37.9	1.48%	504.6	0.19%	140.1	0.81%
10 CFR §71.51(a)(2) Limit	1000		1000		1000	

(1) The neutron shield and impact limiter are assumed not to be present.

General Note: The total dose rate is the sum of rounded values.

**Table 5-85**  
**Occupied Location Dose Rates with Relative Error**

Radiation	Occupied Location Dose Rates (mrem/hr)			
	40 feet from Top		40 feet from Bottom	
	Result	Error	Result	Error
Primary Gamma	0.1	0.88%	0.4	0.32%
Secondary Gamma	0.1	0.23%	0.3	0.14%
Neutron	<0.1	2.51%	<0.1	2.32%
Total	0.3	0.53%	0.7	0.20%
10 CFR §71.47 Limit	2		2	

General Note: The total dose rate is the sum of rounded values.

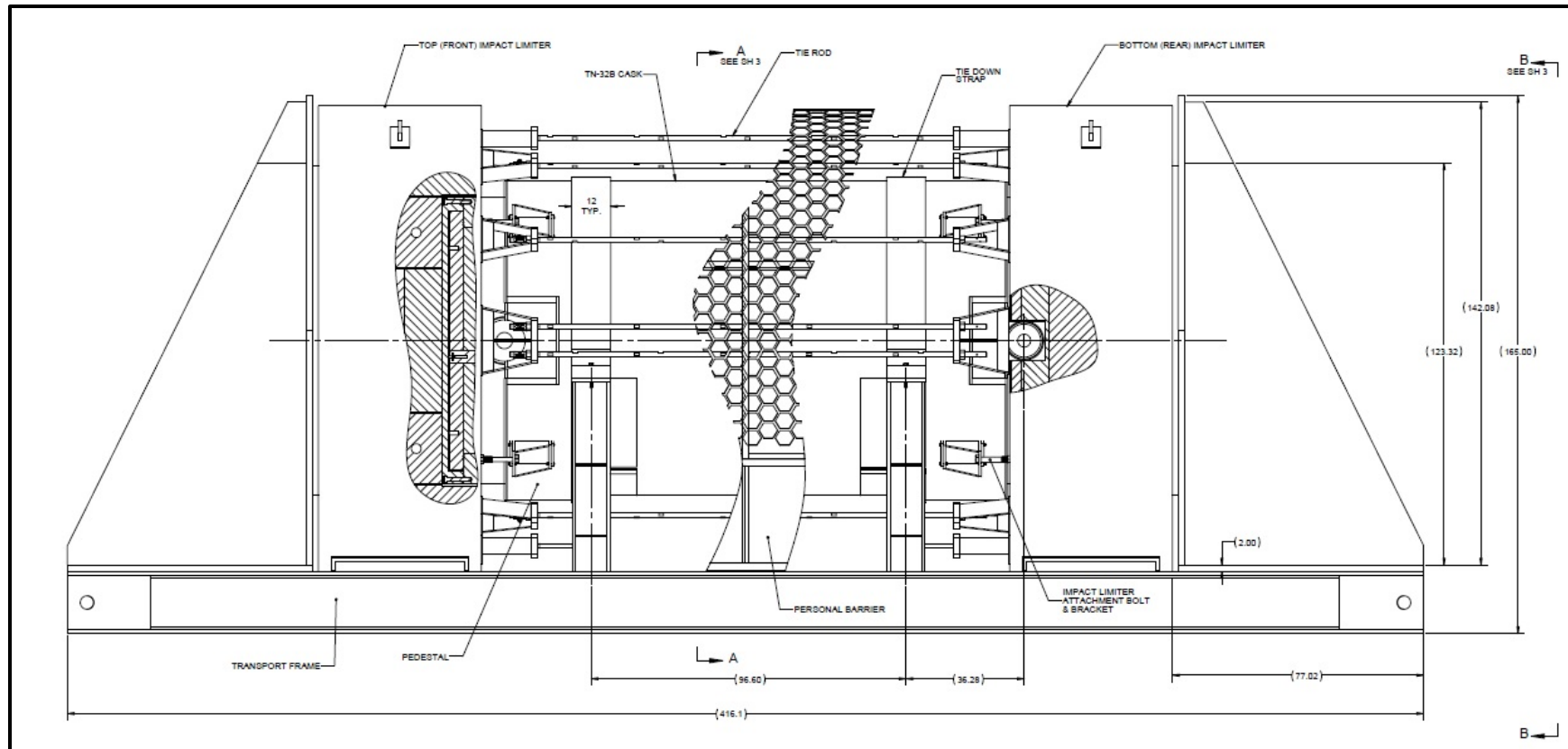


**Figure 5-1**  
**TN-32B HBU Demonstration Cask Transportation Configuration**

Proprietary Information on Pages 5-162 and 5-163  
Withheld Pursuant to 10 CFR 2.390



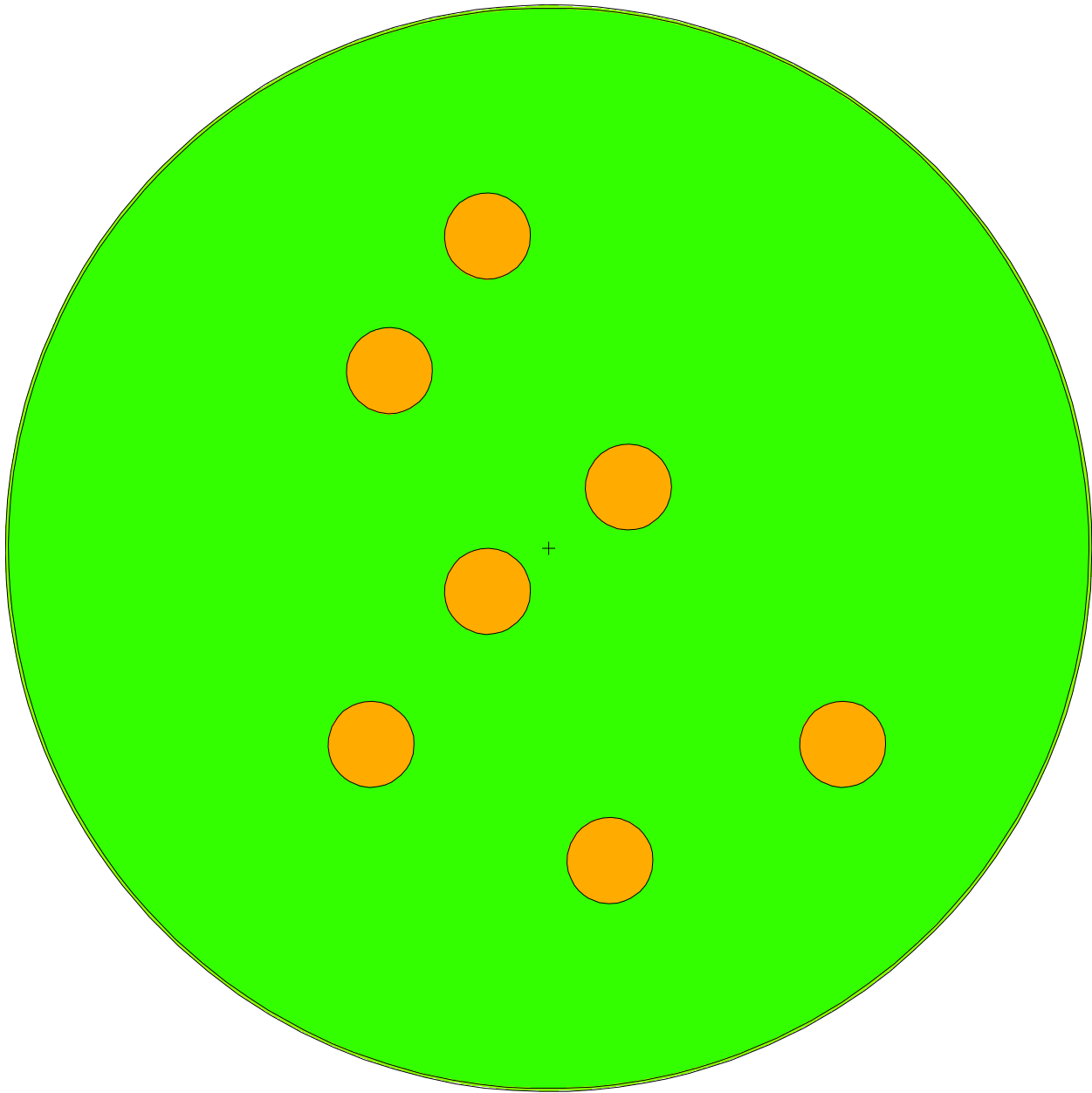


**Figure 5-4**  
**MCNP Model for Lid Holes Locations – X-Y Plane**

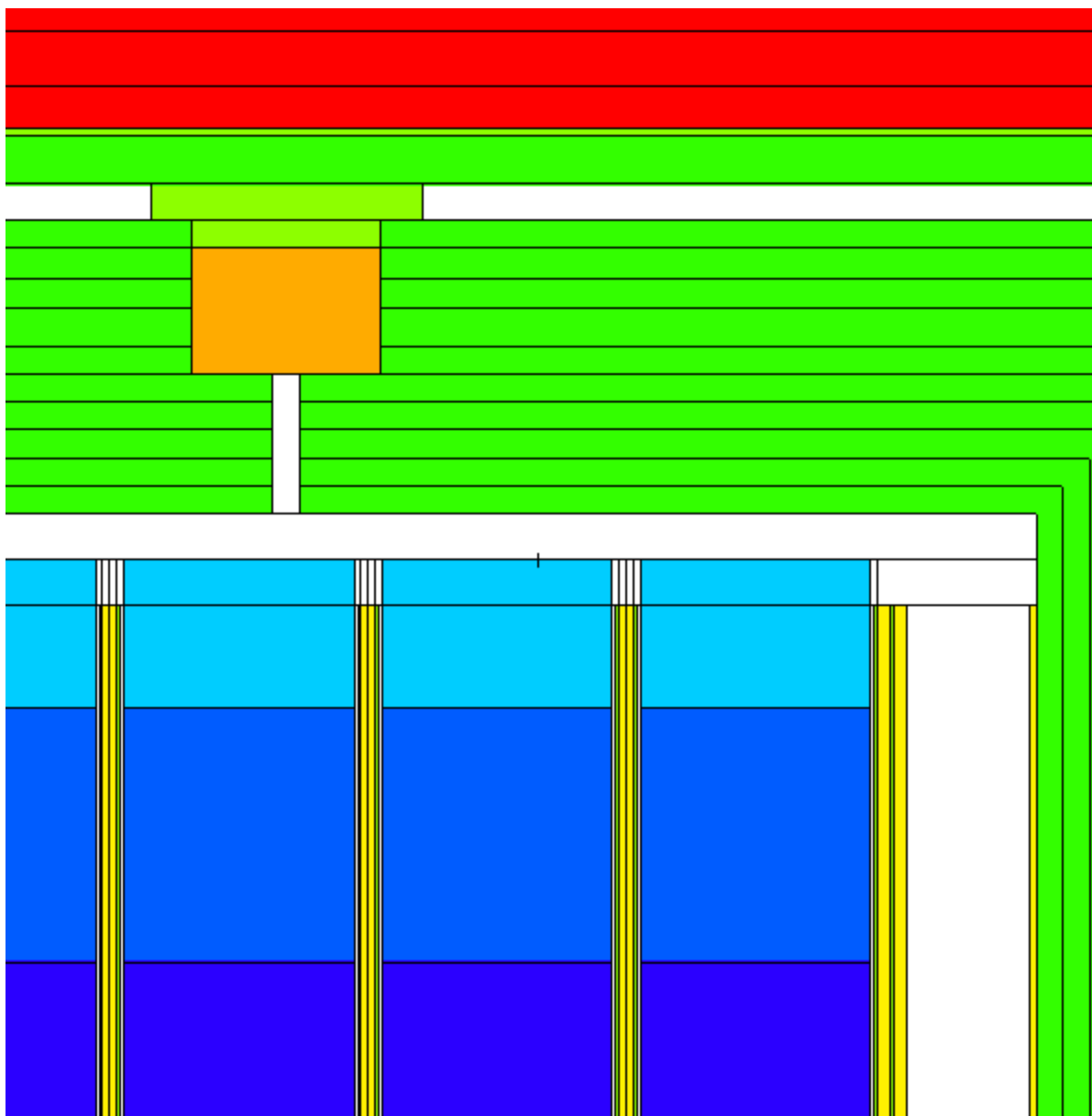


**Figure 5-5**  
**MCNP Model of a Thermocouple Penetration – YZ Plane**

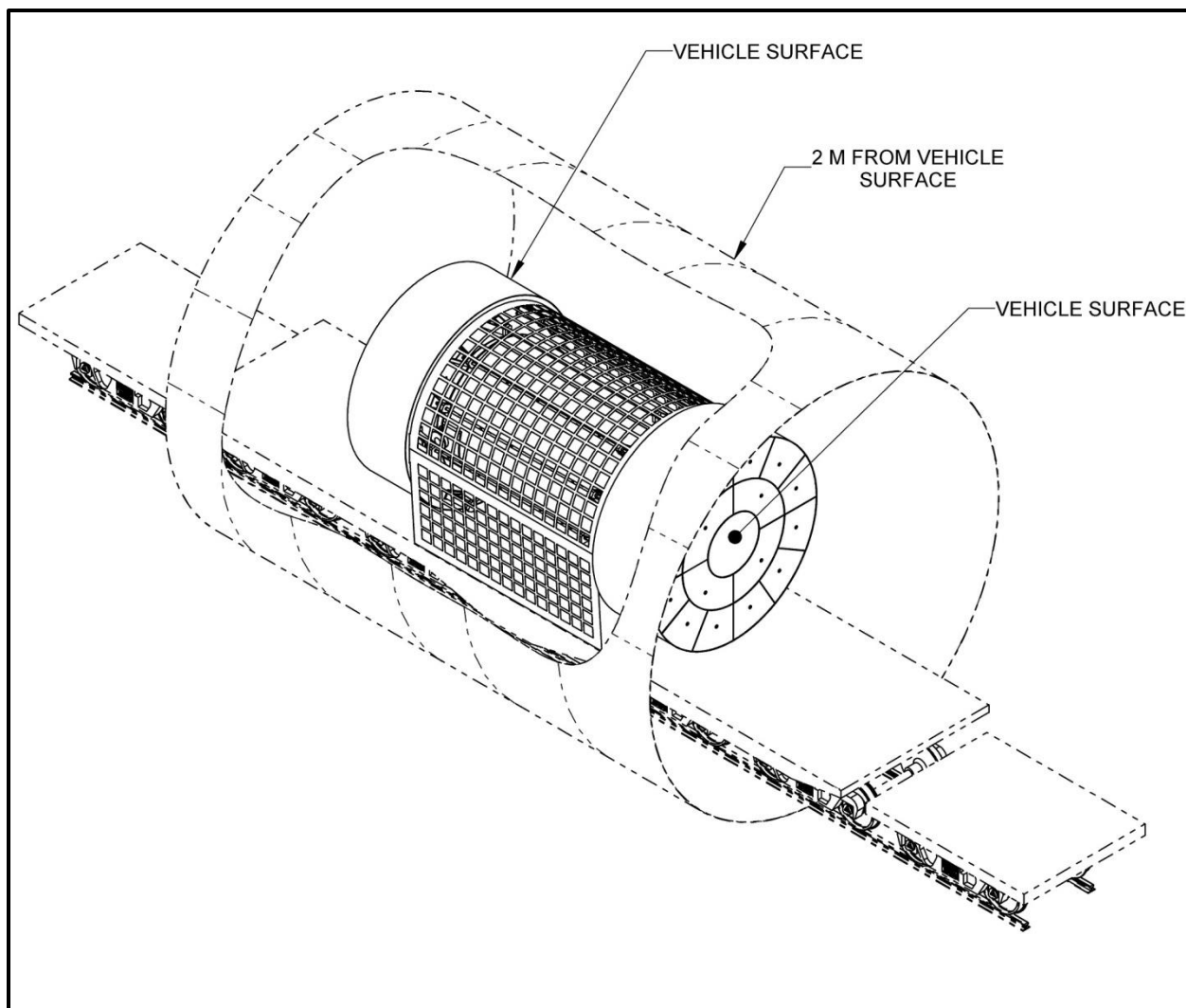


**Figure 5-6**  
**Isometric Sketch of TN-32B HBU Demonstration Cask on Railcar**

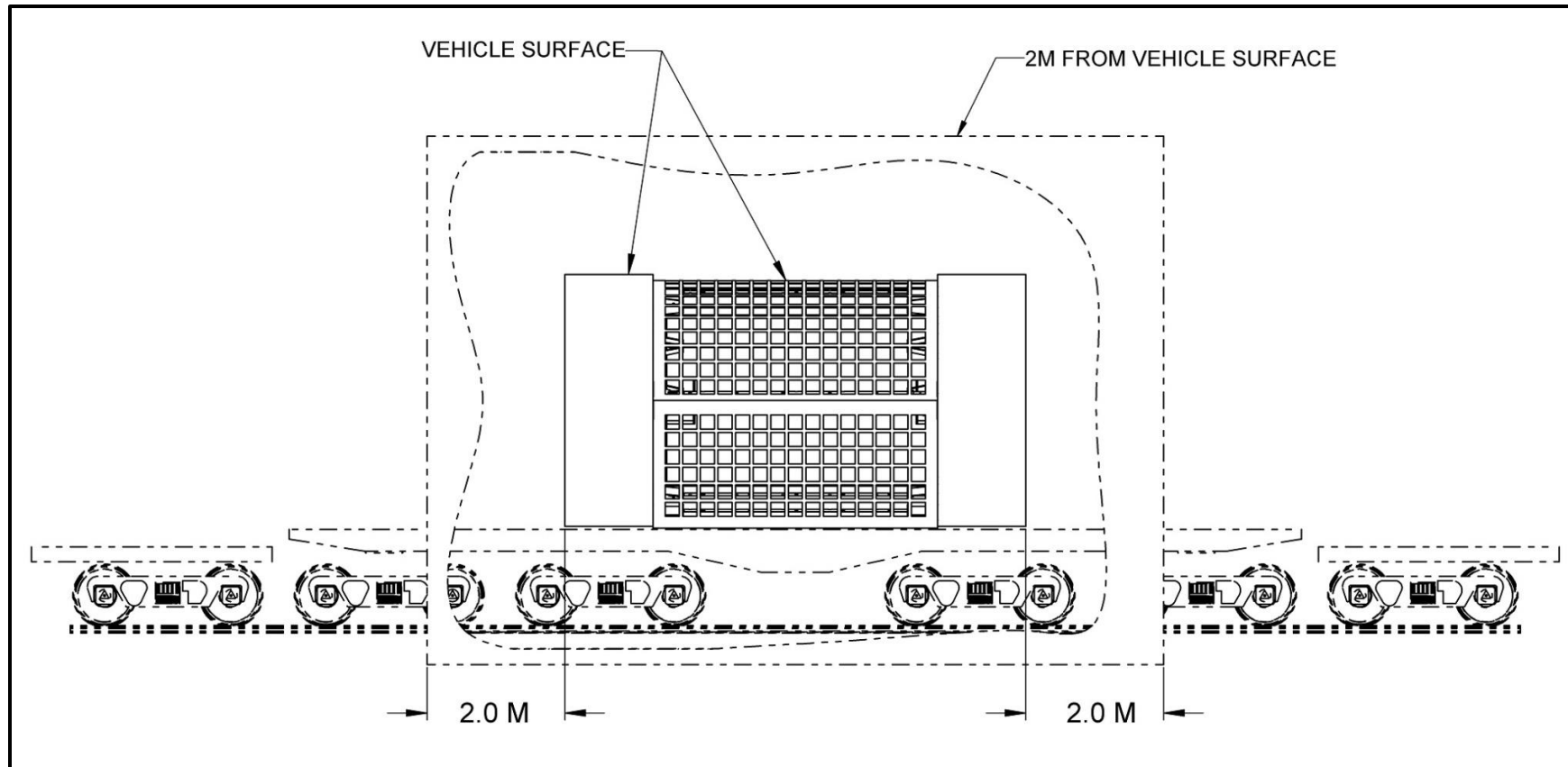


**Figure 5-7**  
**Side View Sketch of TN-32B Demonstration Cask on Railcar**

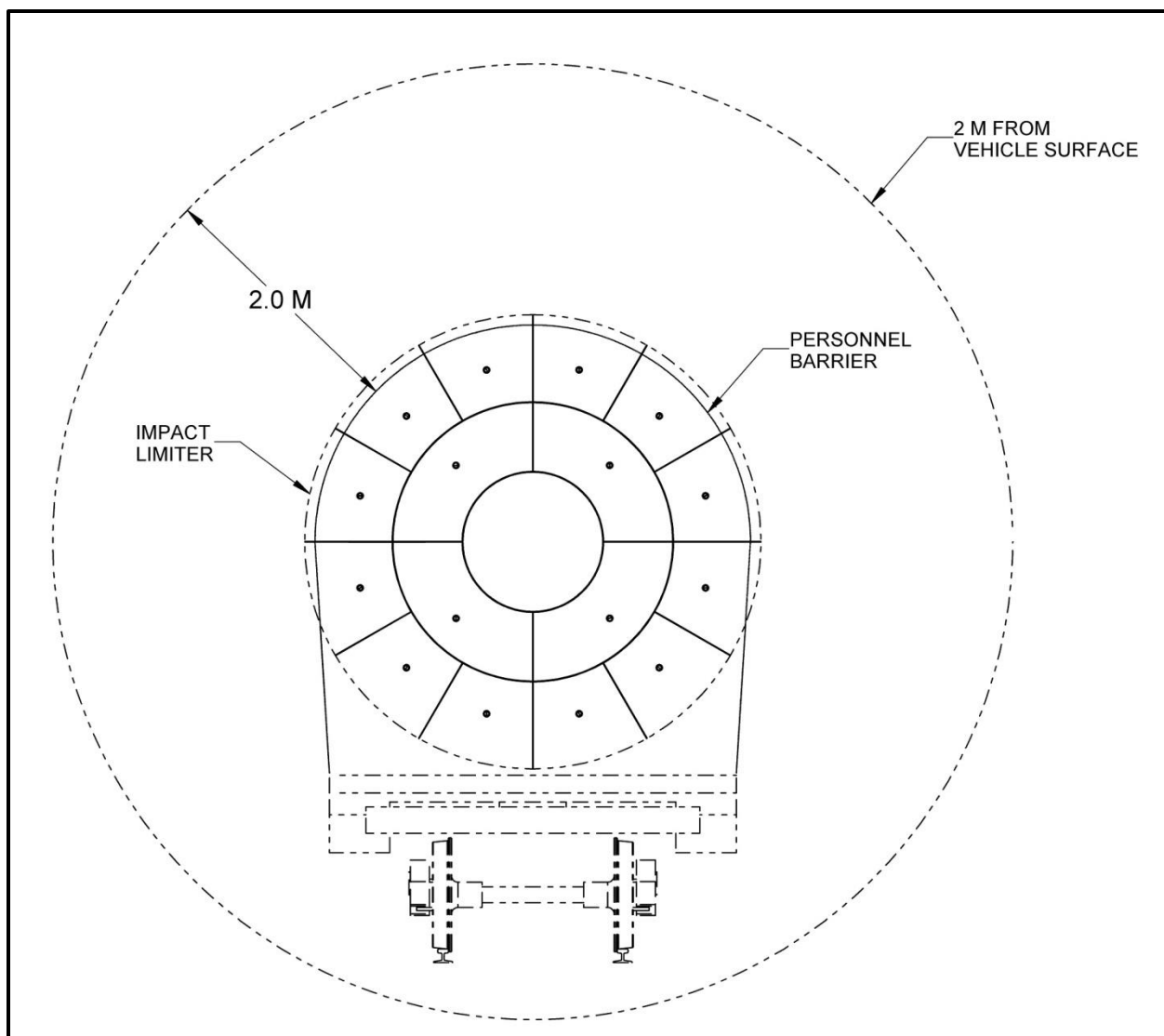


**Figure 5-8**  
**End View Sketch of TN-32B Demonstration Cask on Railcar**

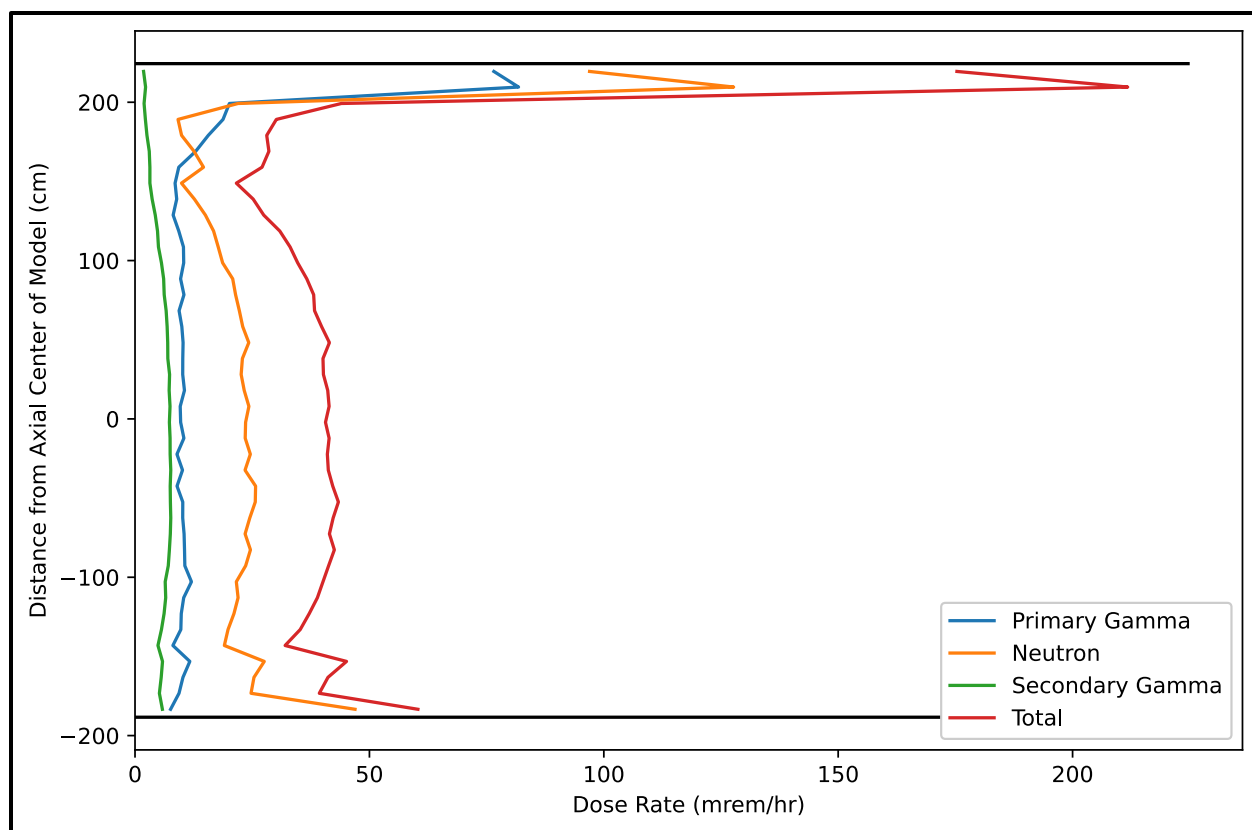


**Figure 5-9**  
**NCT Dose Rates (mrem/hr) at Enclosed Package Surface**

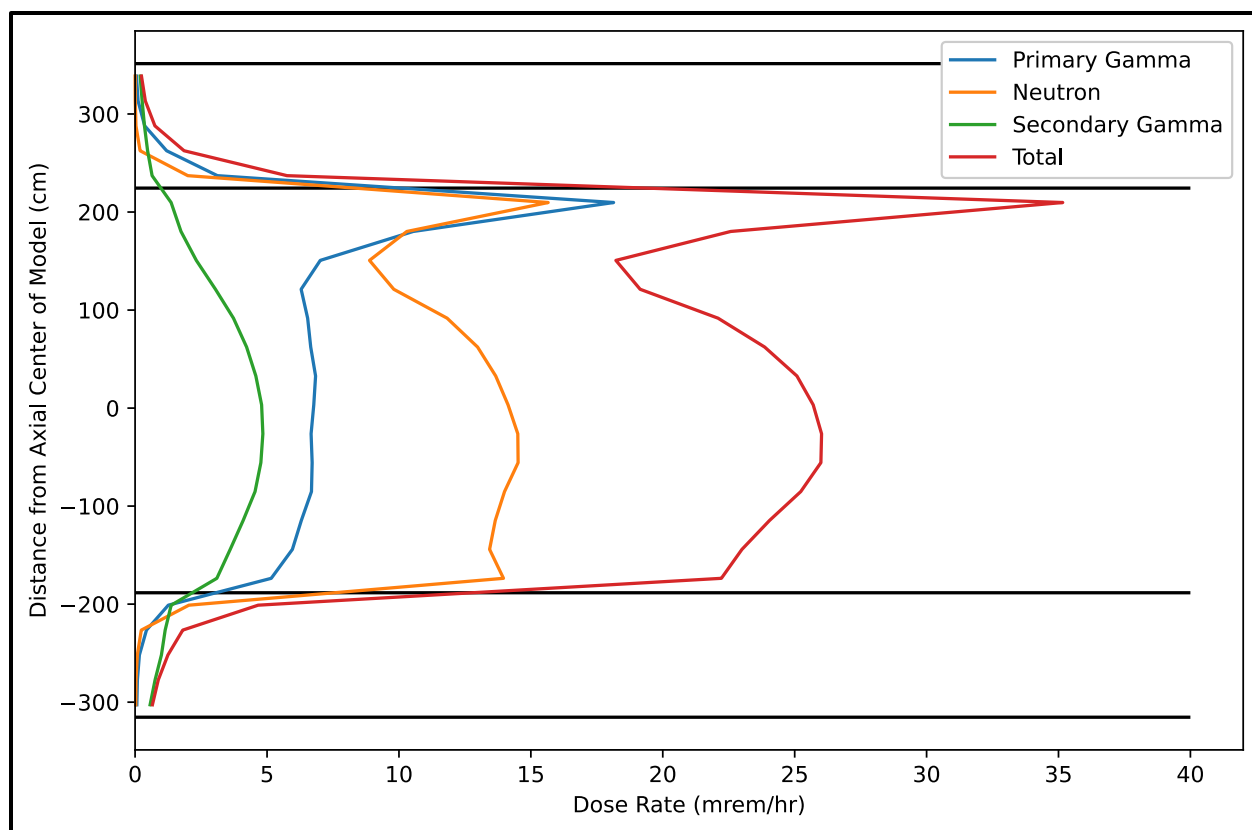


**Figure 5-10**  
**NCT Dose Rates (mrem/hr) at Vehicle Side**

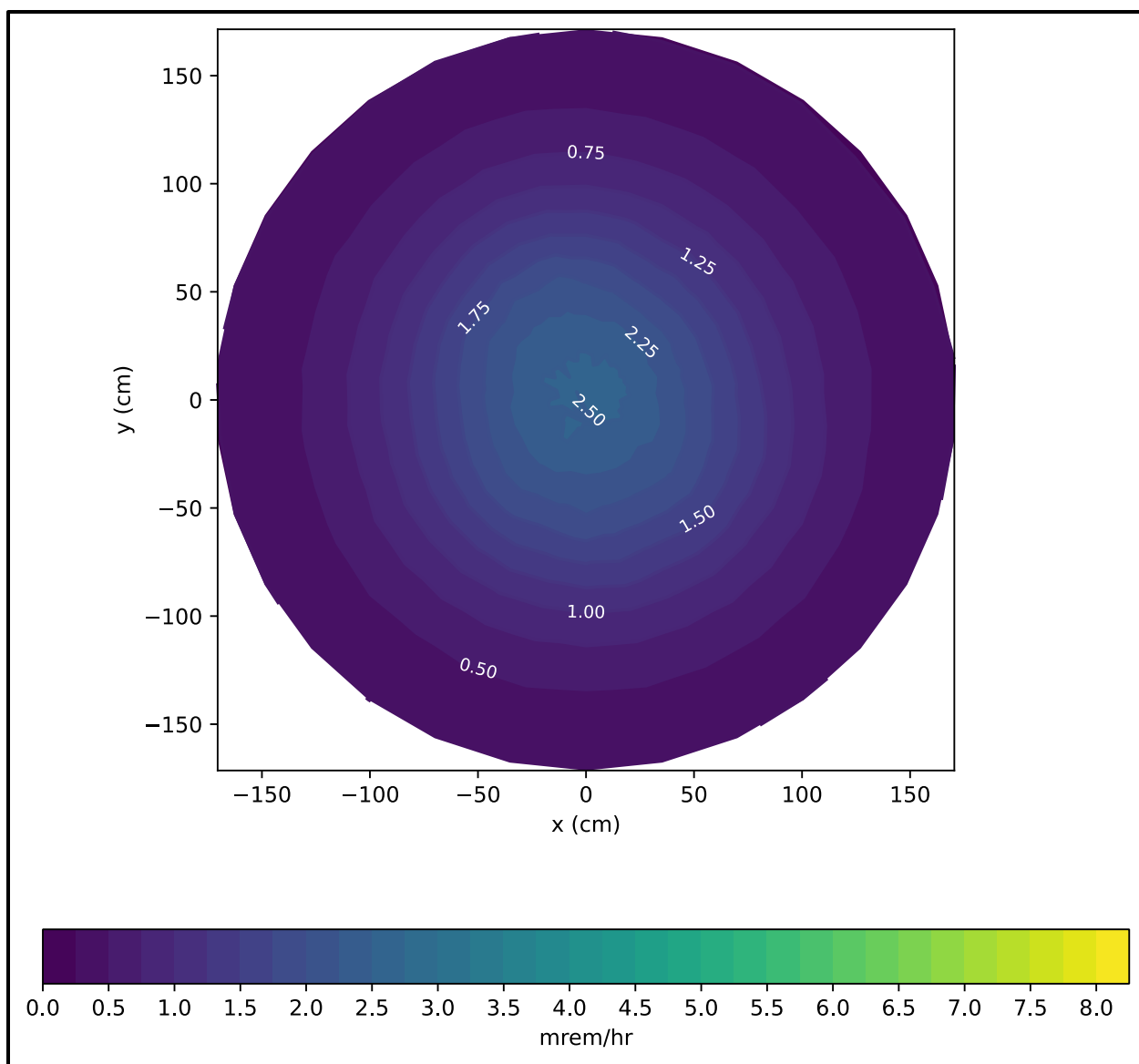


**Figure 5-11**  
**NCT Dose Rates (mrem/hr) at Vehicle Rear**



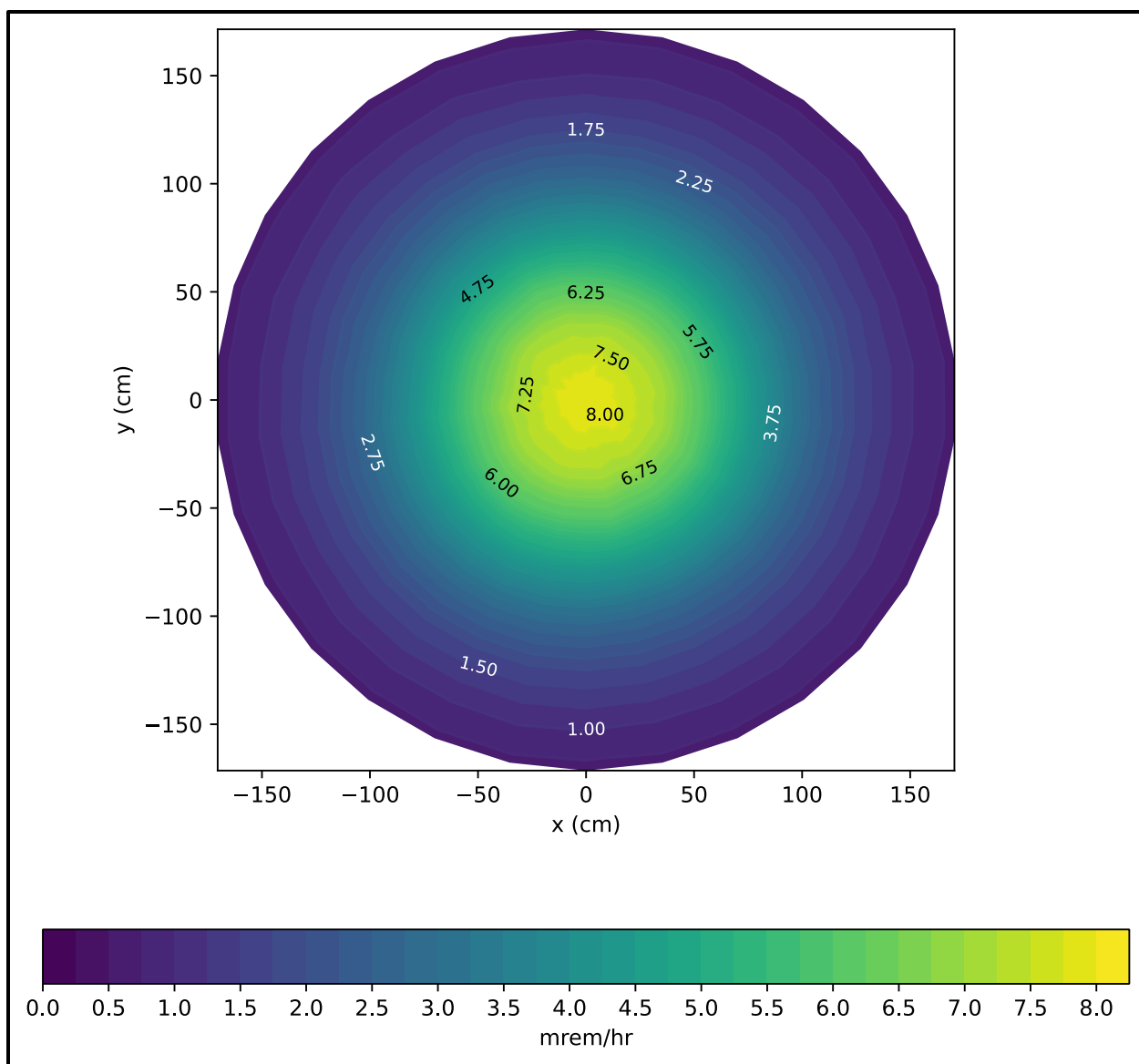


**Figure 5-12**  
**NCT Dose Rates (mrem/hr) at Vehicle Front**

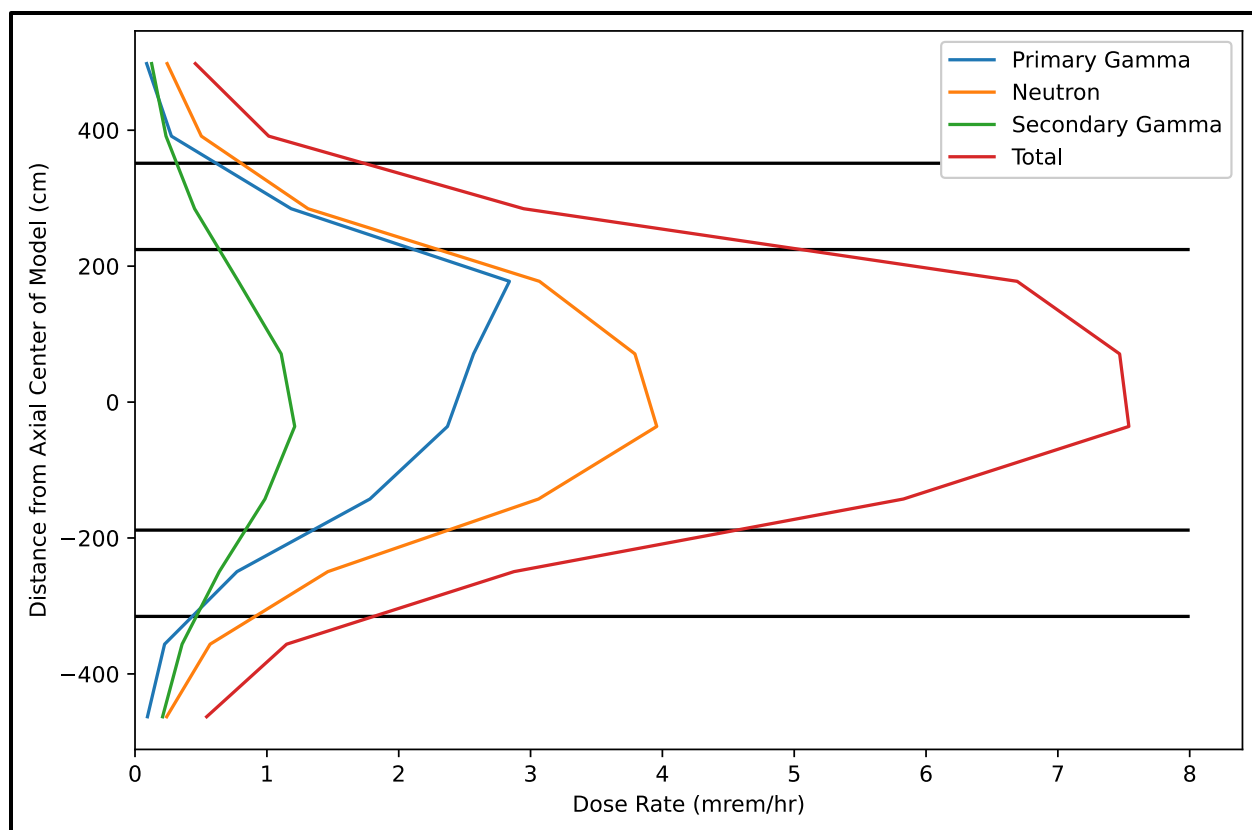


**Figure 5-13**  
**NCT Dose Rates (mrem/hr) at 2 meters from Vehicle Side**

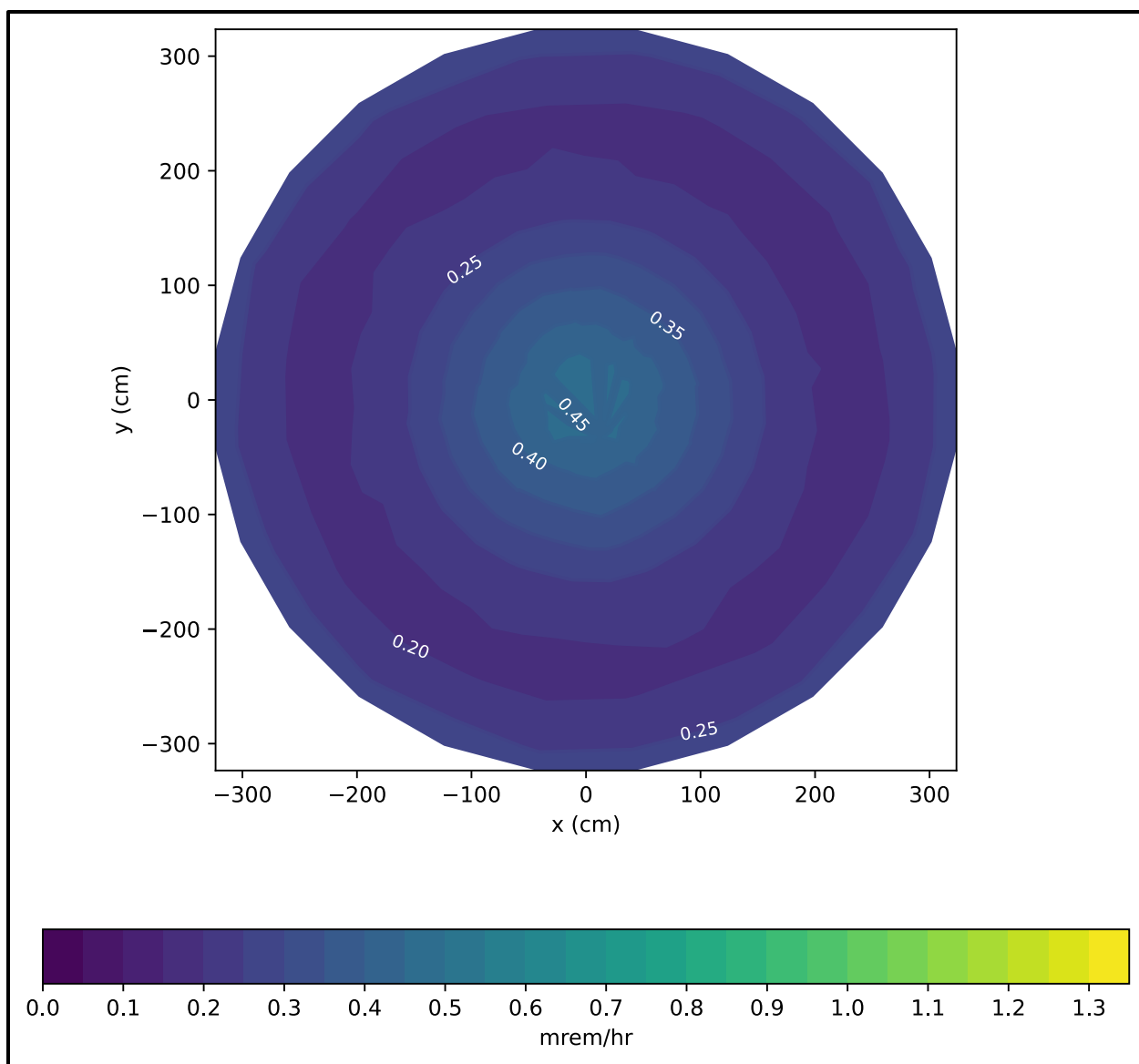


**Figure 5-14**  
**NCT Dose Rates (mrem/hr) at 2 meters from Vehicle Rear**

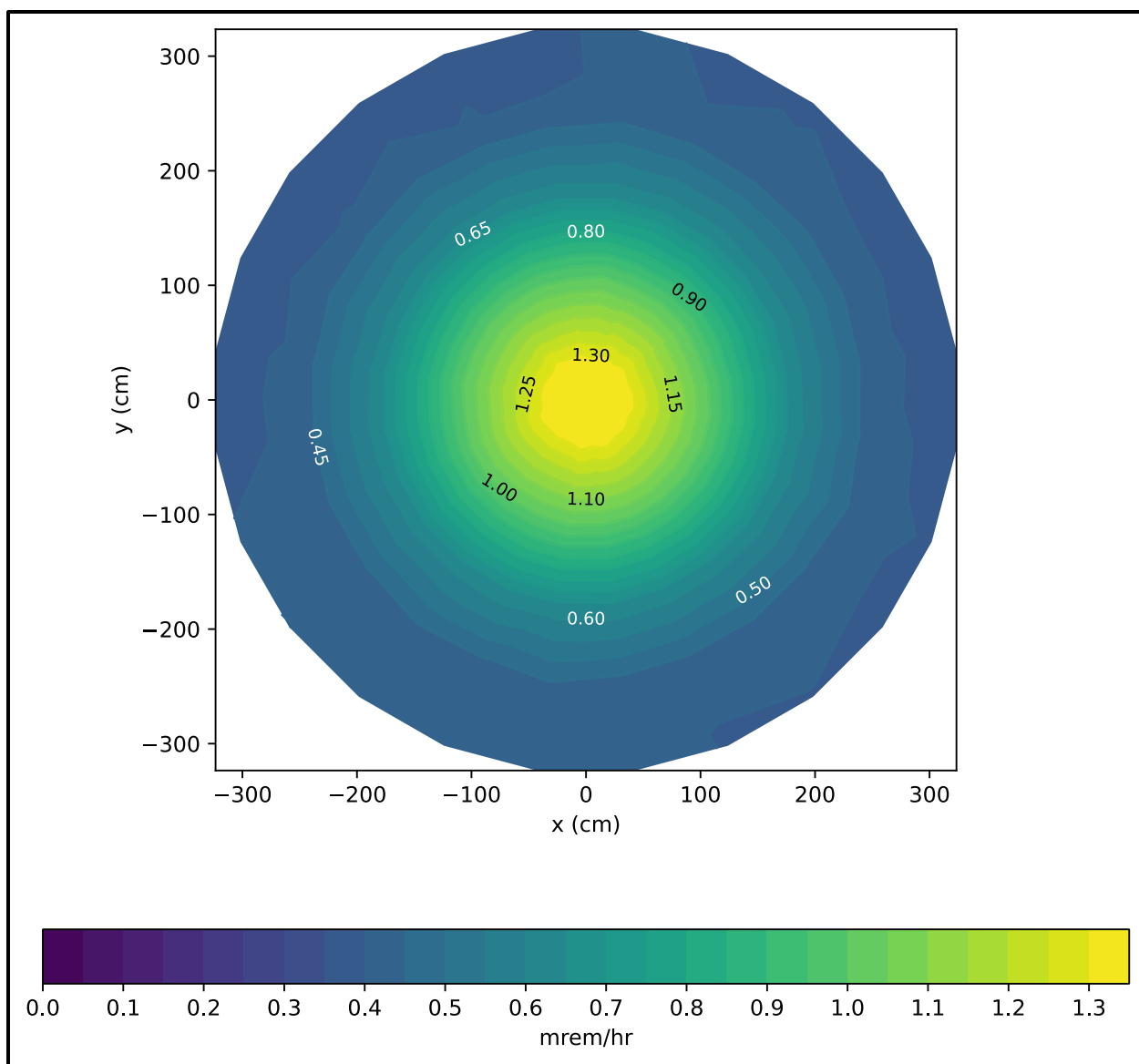


**Figure 5-15**  
**NCT Dose Rates (mrem/hr) at 2 meters from Vehicle Front**

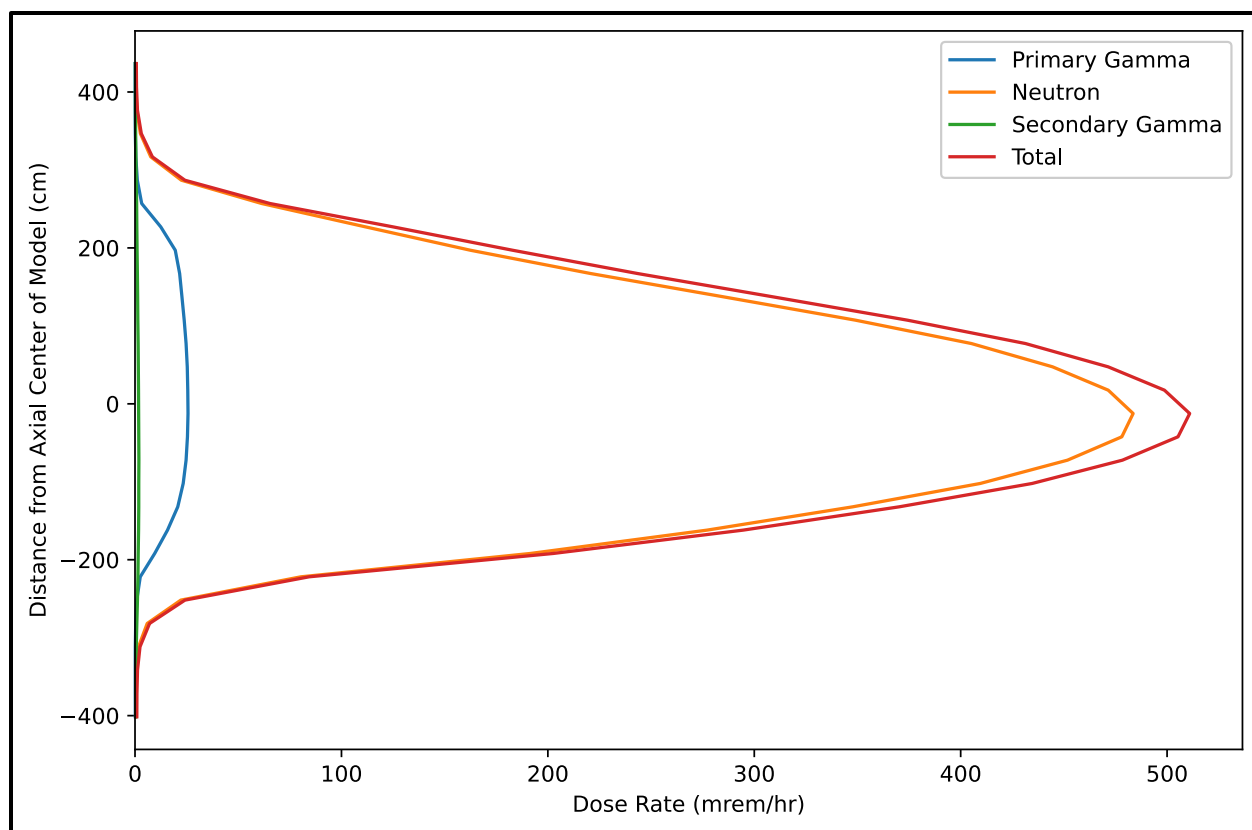


**Figure 5-16**  
**HAC Dose Rates (mrem/hr) at 1 meter from Side**

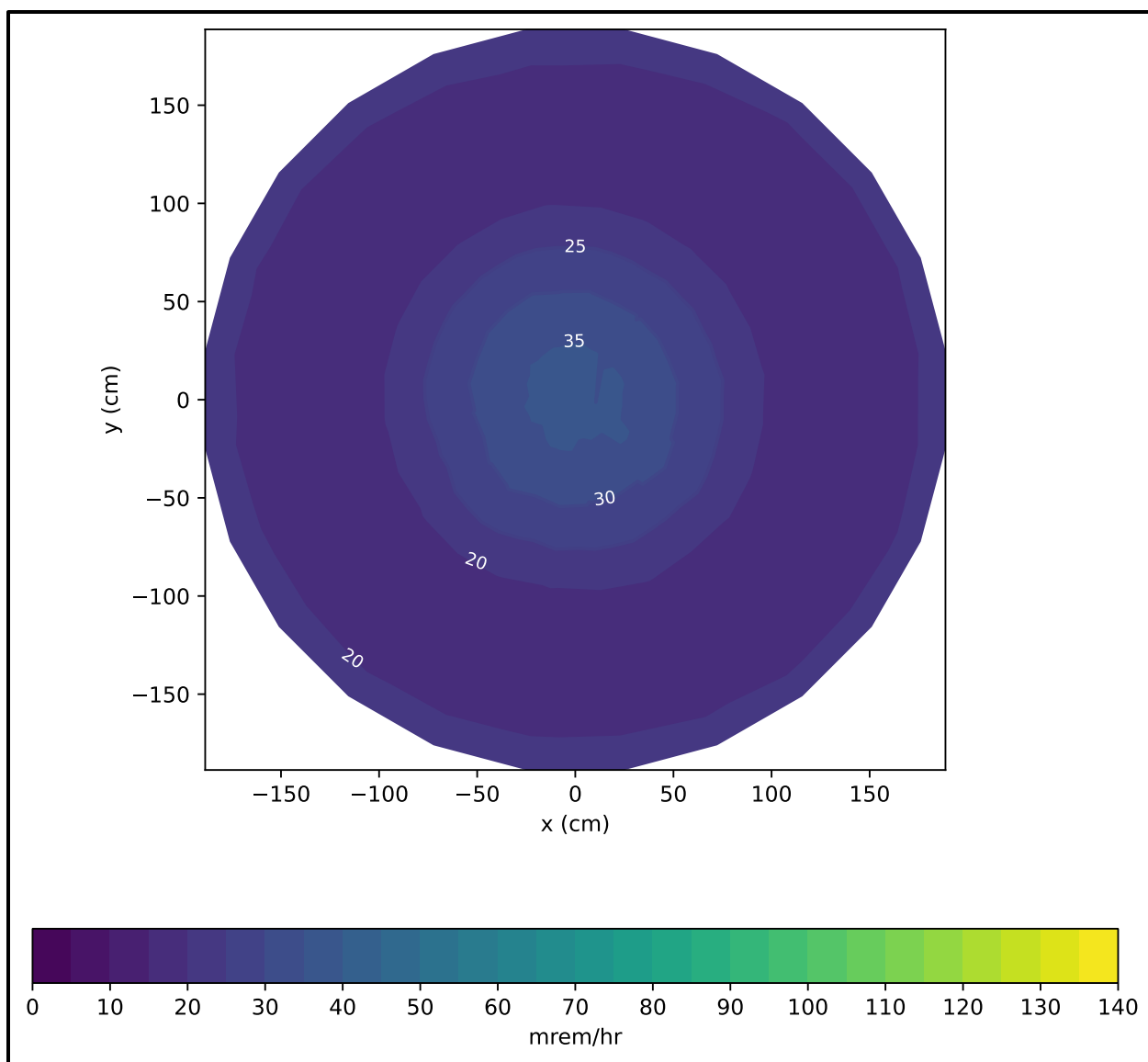


**Figure 5-17**  
**HAC Dose Rates (mrem/hr) at 1 meter from Rear**

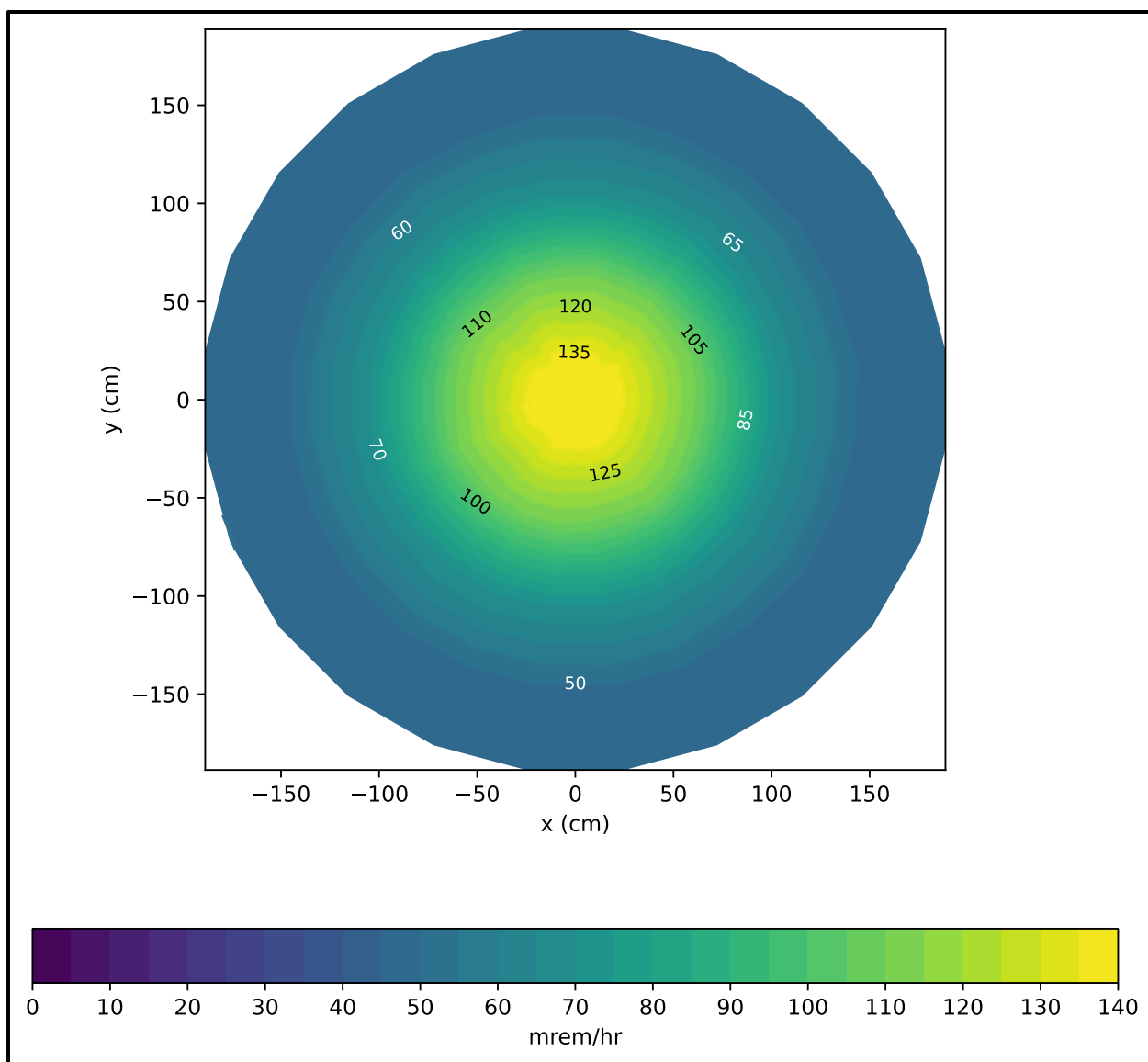


**Figure 5-18**  
**HAC Dose Rates (mrem/hr) at 1 meter from Front**

## Chapter 6 Criticality Evaluation

### TABLE OF CONTENTS

6.1	Description of Criticality Design .....	6-1
6.1.1	Design Features .....	6-1
6.1.2	Summary Table of Criticality Evaluations .....	6-2
6.1.3	Criticality Safety Index .....	6-3
6.2	Fissile Material Contents .....	6-3
6.2.1	Burnup Credit Methodology .....	6-4
6.3	General Considerations .....	6-5
6.3.1	Model Configuration .....	6-5
6.3.2	Material Properties .....	6-16
6.3.3	Analysis Methods and Nuclear Data .....	6-17
6.3.4	Demonstration of Maximum Reactivity .....	6-22
6.4	Single Package Evaluation .....	6-26
6.4.1	Configuration .....	6-26
6.4.2	Results .....	6-26
6.5	Evaluation of Package Arrays under Normal Conditions of Transport .....	6-26
6.5.1	Configuration .....	6-26
6.5.2	Results .....	6-26
6.6	Package Arrays under Hypothetical Accident Conditions .....	6-27
6.6.1	Configuration .....	6-27
6.6.2	Results .....	6-27
6.7	Fissile Material Packages for Air Transport .....	6-27
6.8	Benchmark Evaluations .....	6-27
6.8.1	Applicability of Benchmark Experiments .....	6-28
6.8.2	Bias Determination .....	6-32
6.9	Burnup Credit .....	6-38
6.9.1	Limits for the Licensing Basis .....	6-38
6.9.2	Code Validation .....	6-39
6.9.3	Licensing Basis Model Assumptions .....	6-44
6.9.4	Loading Curve and Burnup Verification .....	6-45
6.9.5	Assigned Burnup Loading Value .....	6-46
6.9.6	Estimate of Additional Reactivity Margin .....	6-46



6.10	Appendix .....	6-48
6.10.1	References .....	6-48
6.10.2	Sample Input Files .....	6-50

LIST OF TABLES

Table 6-1	TN-32B HBU Cask Geometry in KENO Models .....	6-199
Table 6-2	Non-Fuel Design Parameters in KENO .....	6-200
Table 6-3	Summary Table of Criticality Results.....	6-201
Table 6-4	Summary of Fuel Inventory and BECT in the TN-32B HBU Cask.....	6-202
Table 6-5	Design Input for the 17×17 Fuel Assembly (TRITON and KENO) .....	6-203
Table 6-6	Summary of Parameters Selected for Depletion Calculations .....	6-204
Table 6-7	Axial Burnup Profile for Burnup >46 GWd/MTU .....	6-205
Table 6-8	Isotopes Important for Burnup Credit .....	6-206
Table 6-9	Material Property Data in TRITON Models .....	6-207
Table 6-10	Material Property Data in KENO Models .....	6-208
Table 6-11	Sensitivity Evaluation of Depletion Environment Parameters on Reactivity ( $\Delta k$ ).....	6-209
Table 6-12	Design Parameters of Burnable Poison Rods in TRITON Models .....	6-209
Table 6-13	Sensitivity Evaluation of Exposure to Burnable Poisons on Reactivity ( $\Delta k$ ).....	6-210
Table 6-14	Sensitivity Evaluation of Variations in Specific Power on Reactivity ( $\Delta k$ ).....	6-210
Table 6-15	Baseline for Determining Most Reactive Configuration .....	6-211
Table 6-16	Axial Off-Set Analysis .....	6-212
Table 6-17	Fuel Compartment Tolerance.....	6-213
Table 6-18	Neutron Poison Plate Thickness .....	6-214
Table 6-19	Fuel Cladding Gap .....	6-215
Table 6-20	[     ] Clad Thinning – Expanding Gap .....	6-216
Table 6-21	[     ] Clad Thinning – Contracting Exterior.....	6-217
Table 6-22	Most Reactive [     ] Orientation.....	6-218
Table 6-23	Missing Fuel Rods .....	6-218
Table 6-24	Uniform Pitch Expansion.....	6-219
Table 6-25	Nonuniform Pitch Expansion .....	6-220
Table 6-26	Most Reactive Configuration .....	6-221
Table 6-27	Variable Moderator Density.....	6-222
Table 6-28	Experimental Parameters of Critical Experiments from KENO V.a Outputs .....	6-223
Table 6-29	Experimental Parameters of Critical Experiments from KENO V.a Inputs ....	6-227
Table 6-30	Correlation Coefficient Determined from Critical Experiments .....	6-233
Table 6-31	Area of Applicability .....	6-233
Table 6-32	USL Determined Using Computational Method for Critical Experiments .....	6-234

Table 6-33	Qualitative Comparison of Fuel Characteristics.....	6-235
Table 6-34	Qualitative Comparison of Basket and Cask Characteristics .....	6-236
Table 6-35	Comparison of Global Parameters – Criticality .....	6-236
Table 6-36	Comparison of Global Parameters – Energy of Average Lethargy Causing Fission (EALF) .....	6-236
Table 6-37	Comparison of Global Parameters – Average Energy Fission Group .....	6-236
Table 6-38	Comparison of Global Parameters – Moderator-to-Fuel Volume Ratio .....	6-237
Table 6-39	Comparison of Global Parameters – H/X Ratio .....	6-237
Table 6-40	Similarity Analysis – $c_k$ Parameter Results .....	6-237
Table 6-41	Minor Actinides and Fission Product Worth.....	6-237

LIST OF FIGURES

Figure 6-1	TN-32B HBU Cask Model Thermocouple (TC) and Poison Rod Assembly (PRA) Locations .....	6-238
Figure 6-2	TN-32B HBU Demonstration Cask Model of 17×17 Quadrant-Symmetric Fuel Assembly without BPRAs .....	6-239
Figure 6-3	TN-32B HBU Demonstration Cask Model of 17×17 Quadrant-Symmetric Fuel Assembly with BPRAs.....	6-240
Figure 6-4	Full Cask Cross Section of the TN-32B HBU Cask Basket.....	6-241
Figure 6-5	Close-Up Cross Section Center of the TN-32B HBU Cask Basket .....	6-242
Figure 6-6	Cross Section of the Fuel Axially Centered .....	6-243
Figure 6-7	Axial Cross Section of the Borated Aluminum Plates .....	6-244
Figure 6-8	Axial View with Fuel Shifted [            ].....	6-245
Figure 6-9	Axial View with Fuel Shifted [            ].....	6-246
Figure 6-10	Minimum Fuel Compartment Dimension Quarter Core.....	6-247
Figure 6-11	Maximum Fuel Compartment Dimension Quarter Core.....	6-248
Figure 6-12	Fuel Cladding Gap with Water .....	6-249
Figure 6-13	Fuel Cladding Gap with Void.....	6-250
Figure 6-14	[        ] Clad Thinning – Expanding Gap .....	6-251
Figure 6-15	[        ] Clad Thinning – Contracting Exterior.....	6-252
Figure 6-16	Fuel Assembly 30A Oriented 90° .....	6-253
Figure 6-17	Fuel Assembly [        ] Oriented 180° .....	6-254
Figure 6-18	Uniform Pitch Expansion.....	6-255
Figure 6-19	Nonuniform Pitch Expansion .....	6-256
Figure 6-20	Most Reactive Fuel Configuration with Cooling Time Groups.....	6-257
Figure 6-21	Axial View of Most Reactive Fuel Configuration with Cooling Time Groups.....	6-258
Figure 6-22	Pitch Contraction with Cooling Time Groups .....	6-259
Figure 6-23	TN-32B HBU Demonstration Cask Basket Cross Section for Subcritical Multiplication .....	6-260
Figure 6-24	Enrichment versus $k_{eff}$ for Critical Experiments.....	6-261
Figure 6-25	Fuel Pitch versus $k_{eff}$ for Critical Experiments.....	6-262
Figure 6-26	EALF versus $k_{eff}$ for Critical Experiments.....	6-263
Figure 6-27	AEG versus $k_{eff}$ for Critical Experiments .....	6-264
Figure 6-28	Fuel Rod Radius versus $k_{eff}$ for Critical Experiments .....	6-265
Figure 6-29	Moderator to Fuel Ratio versus $k_{eff}$ for Critical Experiments .....	6-266
Figure 6-30	Moderator to Fissile Density Ratio versus $k_{eff}$ for Critical Experiments .....	6-267

Figure 6-31	Pu/Pu+U versus $k_{eff}$ for Critical Experiments .....	6-268
-------------	---	-------

## Chapter 6

### Criticality Evaluation

The TN-32B HBU demonstration cask, as transported, will provide criticality control to meet the criticality performance requirements specified in 10 CFR 71.55 and 71.59 [1]. The criticality control design ensures that the effective multiplication factor ( $k_{\text{eff}}$ ) of the contained fuel is no greater than an upper subcritical limit (USL) for the most reactive configuration. The USL includes a confidence band with an administrative safety margin of 0.05. The design has a criticality safety index (CSI, given in 10 CFR 71.59(b) as  $\text{CSI} = 50/\text{"N"}$ ) of 0 because "N" is infinity ( $\infty$ ). The number "N" is based on all of the following conditions being satisfied, assuming packages are stacked together in any arrangement and with close full reflection on all sides of the stack by water:

1. Five times "N" undamaged packages for normal conditions of transport (NCT) with nothing between the packages are subcritical;
2. Two times "N" damaged packages, if each package is subjected to the tests specified in 10 CFR 71.73 for hypothetical accident conditions (HAC) is subcritical with optimum interspersed hydrogenous moderation; and
3. The value of "N" cannot be less than 0.5.

#### 6.1 Description of Criticality Design

A comprehensive description of the TN-32B HBU demonstration cask is provided in Section 1.2 and in the drawings in Appendix 1.4.1. This section summarizes those design features important for criticality.

##### 6.1.1 Design Features

The TN-32B HBU demonstration cask basket utilizes fixed borated aluminum neutron poison plates (referred to as poison plates) for criticality control. The internal stainless steel basket consists of 32 stainless steel fuel compartments with the space between adjacent compartments containing aluminum sandwiching neutron poison plates. The aluminum and poison plates form an "egg crate" structure. The poison plates are made of borated aluminum alloy of minimum areal density 10 mg/cm<sup>2</sup> B-10; however, only credit for 90% of the B-10 content is taken, for a reduced areal density of 9 mg/cm<sup>2</sup> B-10. The aluminum plates and the poison plates together provide a heat conduction path from the fuel assemblies to the canister shell. Each fuel tube is welded together at certain axial locations with stainless steel insert strips, which separate the aluminum and poison plates. Nominal dimensions of the TN-32B HBU demonstration cask are in Table 6-1.

For additional criticality control, six unirradiated poison rod assemblies (PRAs) with pellets made of boron carbide neutron poison were inserted into specific fuel compartment locations in the TN-32B HBU demonstration cask fuel assembly payload. Only 50% credit is assumed for the PRA inserts. Seven thermocouple lance assemblies (TLAs) are also included with the fuel assemblies in the high burnup (HBU) payload. The TLAs are fabricated from stainless steel and aluminum. The nominal dimensions for the borated aluminum poison plate in the basket, TLA, and PRA dimensions are in Table 6-2. The TLAs are installed in assembly numbers (KENO unit numbers) 57A (1), 3U6 (14), 5T9 (15), 30A (21), 3K7 (23), 3U9 (25), and 3U4 (29). The PRAs were installed in assembly numbers (KENO unit numbers) 30B (2), 20B (4), 0A4 (9), F40 (17), 50B (26), and 56B (28). The TC and PRA locations are shown in Figure 6-1.

The TN-32B HBU demonstration cask is radially surrounded by neutron poison resin, which is encased in a welded steel shell.

### 6.1.2 Summary Table of Criticality Evaluations

The upper subcritical limit (USL) for ensuring that the TN-32B HBU demonstration cask is acceptably subcritical, as determined in Section 6.8:

$$USL = 0.95$$

The package is considered to be acceptably subcritical if the  $k_{eff}$ , which is defined as  $k_{KENO}$  plus twice the statistical uncertainty ( $\sigma_{KENO}$ ) plus all applicable biases, is less than or equal to the USL, or:

$$k_{eff} = k_{KENO} + 2 \times \sigma_{KENO} + (\beta_i + \Delta k_i) + (\beta + \Delta k_\beta) + \Delta k_x \leq USL$$

The USL only incorporates an administrative margin of 0.05. The benchmark analysis in Section 6.8 calculates a USL value that incorporates the effects of code computational bias and bias uncertainty due to major actinides ( $\beta + \Delta k_\beta$ ) in addition to an administrative margin. However, to more easily statistically combine the bias uncertainties, all biases and bias uncertainties are accounted for in the calculation of  $k_{eff}$ . The  $k_{eff}$  incorporates the combined effects of the computer calculated  $k_{eff}$  ( $k_{KENO} + 2 \sigma_{KENO}$ ), depletion bias and bias uncertainty ( $\beta_i + \Delta k_i$ ), code computational bias and bias uncertainty due to major actinides ( $\beta + \Delta k_\beta$ ), and code computational bias due to minor actinides and fission products ( $\Delta k_x$ ). The  $\beta_i$ ,  $\beta$ , and  $\Delta k_x$  bias values are added directly to the computer calculated  $k_{eff}$ , while the bias uncertainties ( $\Delta k_i$  and  $\Delta k_\beta$ ) are statistically combined, like so:

$$\sigma_{bias} = \sqrt{\Delta k_i^2 + \Delta k_\beta^2}$$

The criterion for subcriticality is then:

$$k_{eff} = k_{KENO} + 2 \times \sigma_{KENO} + \beta_i + \beta + \Delta k_x + \sqrt{\Delta k_i^2 + \Delta k_\beta^2} \leq USL$$

A summary of the criticality analysis results for the TN-32B HBU demonstration cask payload is presented in Table 6-3. Moderation by water in the most reactive credible configuration is utilized in both the NCT and HAC analyses. In the single package and array NCT models, full-density water fills all cavities, while in the single package and array HAC models variable-density water fills all cavities. In all single package models, 30 cm (12 in) of water reflection is utilized, surrounded by vacuum boundary conditions. Analysis results for single package NCT and HAC are in Section 6.4. In all array models, reflective boundary conditions simulate an infinite array of closely-packed casks. Analysis results for NCT arrays are in Section 6.5, and results for HAC arrays are in Section 6.6.

The results of the criticality analysis indicate that there is a margin to the USL of approximately 0.00782 in  $\Delta k_{\text{eff}}$ , which verifies the TN-32B HBU demonstration cask to be subcritical at the time of shipment. The criticality analysis results demonstrate compliance with the requirements of 10 CFR 71.55(b), (d), and (e), 10 CFR 71.59(a)(1), and 10 CFR §71.59(a)(2).

### 6.1.3 Criticality Safety Index

The designated payload of the TN-32B HBU demonstration cask is shown to be subcritical for an infinite array of flooded undamaged casks and for an infinite array of damaged casks after being subjected to HAC events. The design has a CSI of 0 as “N” is equal to infinity ( $\infty$ ). A CSI of 0 (less than 50) ensures that, per 10 CFR 71.59(c)(1), the package may be shipped by a carrier in a nonexclusive conveyance, from a criticality requirements point of view.

## 6.2 Fissile Material Contents

The TN-32B HBU demonstration cask contains 32 pre-selected, undamaged Westinghouse-type 17×17 pressurized water reactor (PWR) fuel assemblies irradiated to high burnup at the North Anna Power Station (NAPS). The fuel assemblies in the TN-32B HBU demonstration cask are HBU fuel assemblies, i.e., > 45 GWd/MTU, as discussed in Chapter 1, and are only those listed in Table 6-4. This table also lists the burnup, enrichment, and cooling time (BECT) fuel parameters for the selected PWR fuel assemblies. In summary, the minimum and maximum assembly burnups of the HBU payload are 50.047 GWd/MTU and 55.496 GWd/MTU, respectively, and the minimum and maximum initial enrichments are 3.59 wt% and 4.55 wt%, respectively. Cooling times on the earliest shipment date (October 1, 2023) range from a minimum of 11.56 years to a maximum of 36.45 years. The initial enrichment is uniform for all fuel rods in each assembly; axial blankets are not considered. Gadolinium is not considered.



The types of fuel assemblies present in the TN-32B HBU demonstration cask are the Westinghouse 17×17 LOPAR, NAIF, and AREVA 17×17 AMBW. For simplification, only the dimensions of the Advanced Mk-BW (AMBW) fuel assembly design are evaluated for this application since the AMBW fuel bounds the other fuel assembly types from a criticality point of view. Nominal dimensions and characteristics of the fuel assembly, including active fuel length, are in Table 6-5. The initial, pre-irradiation mass of heavy metal for each individual assembly can be found in Table 5-5, Chapter 5. Calculations to determine a bounding quantity of fissile nuclides present based on cooling time and the isotopic concentrations at the time of transport are described in Section 6.3.4.

Fuel rods have been removed from two assemblies in the HBU payload, and replaced with stainless steel rods that displace an equal amount of water. The reactivity effect of missing rods is evaluated in Section 6.3.4.6.

Six unirradiated PRAs are inserted into fuel assemblies in the HBU payload for criticality control. Nominal dimensions and characteristics of the PRAs are in Table 6-2. No irradiated non-fuel hardware is included with the spent nuclear fuel (SNF) contents.

#### 6.2.1 Burnup Credit Methodology

The burnup credit methodology employed to ensure the subcriticality of the TN-32B HBU demonstration cask is based on a “burned fuel” representation of the spent fuel assemblies. Credit for the negative reactivity of the fuel assemblies as a result of irradiation, or “burnup credit” is employed in this application. The maximum burnup “credited” in this analysis does not exceed 60 GWd/MTU. [

]

Utilizing burnup credit requires a different analytical approach for criticality analysis than is used in traditional analyses with a fresh fuel assumption. For fresh fuel, the key parameters to be taken into account in the analyses are the initial enrichment and the most reactive fuel configuration. [

] The reactor operating parameters during assembly irradiation is discussed in Section 6.3.1.1. The range of reactor operating parameters analyzed is summarized in Table 6-6.

## 6.3 General Considerations

Criticality calculations for the TN-32B HBU demonstration cask are performed using several modules of SCALE 6.1 [2]. Descriptions of the TRITON fuel assembly depletion models and simplified and full STARBUCS/CSAS5/KENO cask criticality models are given in Section 6.3.1. The material properties for all materials used in the models are provided in Section 6.3.2. The computer code and cross section libraries used as well as the bases and assumptions made for the models are provided in Section 6.3.3. Finally, the most reactive configuration is determined in Section 6.3.4.

### 6.3.1 Model Configuration

This analysis can be separated into two parts: depletion and criticality. The depletion calculations consist of a set of general fuel assembly depletion models that encompass the operating histories and depletion parameters of interest experienced by the actual fuel assemblies selected for transport in the TN-32B HBU demonstration cask. The depletion calculations determine the isotopic composition of the burned fuel at the time of discharge from the reactor. The TRITON control module of SCALE 6.1 [2] and the ENDF/B-VII cross section libraries are used when performing the depletion calculations. The TRITON models are described in Section 6.3.1.1. Problem-specific ORIGEN-ARP libraries are created by TRITON based on the range of reactor depletion parameters experienced by the 32 pre-selected spent fuel assemblies in Table 6-3. As a result, the ORIGEN-ARP libraries created take into account the effects of the 17×17 Westinghouse-type fuel assembly design and the specific NAPS reactor operating conditions on the resulting isotopic composition of the fuel. After creation of the ORIGEN-ARP libraries, the bounding depletion parameters are determined by sensitivity study using a simplified STARBUCS/KENO criticality cask model, the results of which are discussed in Sections 6.3.1.1.1 through 6.3.1.1.4. The most bounding ORIGEN-ARP library created with the most bounding depletion parameters is then used in the subsequent full criticality analyses.

For the criticality analyses, the STARBUCS control module of SCALE 6.1 [2] is used to calculate the isotopic inventories present for a given BECT. STARBUCS then calls the CSAS5 module to perform a criticality calculation that considers the geometry of the TN-32B HBU demonstration cask. The STARBUCS/CSAS5 inputs include the KENO V.a 3-D geometry model of the cask and HBU payload. The KENO V.a model of the cask system utilized to demonstrate compliance with 10 CFR 71.55(b) is described in Section 6.3.1.2.

In Section 6.3.4, a set of STARBUCS runs using the option to perform single criticality safety calculations with burnup credit is used to determine the most reactive fuel configuration, i.e., the most reactive physical orientation of the fuel assemblies within the basket in the cask. For each fuel configuration considered, a set of calculations is performed that spans the ranges of burnup, initial enrichment, and cooling times for the fuel assemblies in the TN-32B HBU demonstration cask. Then, STARBUCS is used to calculate the isotopic inventory for each axial node for each of the six cooling time groups that the fuel is sorted into. Six different fuel types are modeled in the CSAS5 inputs for the criticality safety calculations. [

]

The treatment of the modeling parameters relevant to this burnup credit criticality analysis is based on the guidance and examples provided in Reference [6]. The TRITON and KENO V.a models consider a heterogeneous model of each fuel rod in each fuel assembly. The TRITON models use reflective boundary conditions to simulate an infinite fuel assembly array, which is conservative. The KENO V.a models have 32 discrete fuel assemblies within the cask; a partially loaded cask is not considered in the KENO V.a model, since the TN-32B HBU demonstration cask payload is fixed and was loaded into the cask in November 2017. No damaged fuel assemblies will be transported in this cask. Other modeling bases and assumptions are listed in Section 6.3.3.

The design basis KENO V.a model described in Section 6.3.1.2 is an NCT array model. All cask and fuel dimensions for NCT and HAC KENO V.a models are the same; only the boundary conditions and/or water densities of the flooded areas differ between the configurations. For NCT and HAC single package models, 30 cm (12 in.) of water reflection outside the cask is utilized, surrounded by vacuum boundary conditions. NCT single package and array models consider full density unborated water in the interior and exterior of the cask, including flooding in the fuel cladding gap and in between the steel fuel compartments next to the borated aluminum plates. HAC single package and array models consider the reactivity effects of variable density unborated water of the internal and external volumes of the cask. In the NCT and HAC infinite array models, an infinite array of the same TN-32B HBU demonstration cask with the same 32 fuel assemblies is modeled by using reflective radial boundary conditions and specular axial boundary conditions. For all KENO V.a models, the neutron shield and the outermost steel skin of the cask are removed.

Credit is taken for the fixed geometry of the basket, as the analytical results reported in Chapter 2, demonstrate that the cask containment boundary and basket structure do not experience any significant distortion under hypothetical accident conditions. The analytical results reported in Appendix 2.12.8 demonstrate that the fuel assemblies do not undergo any permanent plastic deformation.

#### 6.3.1.1 Description of the TRITON T-DEPL Models

The TRITON module utilizes data describing a fuel assembly as it is initially loaded into a reactor. [

]

Proprietary Information on This Page  
Withheld Pursuant to 10 CFR 2.390

The remainder of this section describes in detail the effects of the various modeling parameters utilized in the TRITON model and their effects on the subsequent burnup credit criticality analyses.

#### B. Fuel Temperature

The effect of fuel temperature is discussed in Reference [6]. Table 3 of that reference recommends selecting the maximum pellet-average temperature for the bounding fuel temperature. [

]

#### C. Moderator Temperature and Density

The effect of moderator temperature and density is discussed in Reference [6]. [

Table 3 of Reference [6] recommends selecting the maximum core outlet temperature for the bounding moderator temperature. [

]

#### D. Soluble Boron Concentration

The effect of soluble boron concentration is discussed in Reference [6]. [

]

#### E. Burnable Poison Rod Assemblies

A parametric study of the effect of burnable poison rods for PWR burnup credit was performed in Reference [7]. Burnable poison competes with the U-235 for neutrons thereby reducing the neutron reaction rate in the U-235 and flattening the neutron distribution in the core. However, the presence of burnable absorbers, particularly the burnable poison rods, results in spectral hardening and consequently an increase in the residual reactivity of the fuel assembly following discharge. The results documented in Reference [7] recommend the use of burnable poison rods in all the guide tubes of the fuel assembly for the maximum duration of the depletion when calculating maximum residual reactivity.

[

]

The effects of BPRAs on reactivity depend on the duration of exposure, assembly burnup, BPRA design, and initial fuel-assembly enrichment. To quantify this effect, the  $k_{\text{eff}}$  of cases with and without BPRAs are compared. ORIGEN-ARP libraries are prepared with TRITON for fuel assembly models with and without BPRAs for the enrichment range 3.0 – 5.0 wt. % U-235 and up to the maximum burnup (approximately 80 GWd/MTU) with the bounding fuel temperature, moderator temperature and density, and soluble boron concentration discussed in subsections B, C, and D. Then, STARBUCS generates the isotopic concentrations for the three enrichments (3.0, 4.0, and 5.0 wt. % U-235) and two burnup values (50 and 60 GWd/MTU), with a cooling time of five years. STARBUCS incorporates the TN-32B HBU demonstration cask details via KENO V.a. A summary of the modeling parameters utilized in the TRITON calculations for the treatment of BPRAs is shown in Table 6-12. The results of the sensitivity evaluations are in Table 6-13.

F. Control Rods

[

]

G. Axial Blankets

[

]

H. Specific Power and Down Time

The behavior of reactivity with respect to specific power is studied in detail in Reference [7]. It is noted in the reference that reactivity decreases with increasing specific power when fission products are included in the fuel composition. The difference is also more notable at higher burnups where the rate of production of fission products is higher. While lower specific powers increase reactivity, the design basis specific power is selected such that it is representative of the actual payload of the cask.



Per Section 4.2.4 of Reference [9], specific power and operating history effects are driven by the balance of the various equilibrium states of the nuclides present, as a function of power. Rather than attempt to determine a real operating history that would bound all other operating histories, histograms were developed to represent the key aspects of operating histories in this reference. Each variation results in a different equilibrium concentration for nuclides. It was found that when fission product worth was considered as well as actinide worth, low-power operation toward end of life yields the most conservative estimate of reactivity. The net effect is rather small, up to 0.2%  $\Delta k/k$ . In Reference [8], the neutron multiplication factor was observed to increase when adding some downtime between cycles for moderately to highly burned fuel. The maximum change for the downtime cases studied in Reference [8], when fission products are considered in the criticality calculation, was 0.06%  $\Delta k/k$ . References [8] and [9] both conclude that the optimum approach is to assume a simple continuous-power operating history, and add in margin to account for operating-history-induced effects (0.2% uncertainty in  $k_{\text{eff}}$ ). [

]

To study the impact of specific power on the spent fuel assembly (SFA) reactivity, the specific power used in the depletion was changed from a bounding value of 60 MW/MTU (which also forms the base case for the depletion parameters study) to 40 and 50 MW/MTU. Bounding values for the fuel temperature, moderator temperature and density, and soluble boron concentration are used while changing only the specific power. The  $k_{\text{eff}}$  values obtained from STARBUCS using isotopic compositions generated from the different specific power depletion scenarios are obtained for the three enrichments (3.0, 4.0, and 5.0 wt. % U-235) and two burnup values (50 and 60 GWd/MTU). A cooling time of five years is assumed. The results of the sensitivity evaluations are provided in Table 6-14.

#### I. Horizontal Burnup Distribution

In Reference [6], the effect of a horizontal burnup bias was studied for a Generic Burnup [

]

## J. Summary of TRITON Modeling Parameters

The depletion parameters important to burnup credit are fuel temperature, moderator temperature and density, cycle average soluble boron concentration, and presence of poison inserts (BPRAs, control rods, etc.). Down time between cycles and specific power have relatively minor effects on the subsequent criticality analyses as shown in Reference [9]. This analysis utilizes bounding parameters for the fuel depletion so that the resulting fuel assembly reactivity at the time of transportation is maximized. Even though none of the assemblies present in the TN-32B HBU demonstration cask are depleted at these bounding parameters, it is conservative to perform calculations with these parameters.

The results presented in these depletion calculations support the selection of design basis depletion parameters to employ the burnup credit methodology for the HBU payload.

### 6.3.1.1.1 Depletion Environment Parameters

In the case of depletion environment parameters, the base criticality case against which all others are compared is the  $k_{\text{eff}}$  obtained using isotopic concentrations from the bounding depletion parameters. The sensitivity effect is quantified by comparing this  $k_{\text{eff}}$  to an identical case obtained after changing a parameter value to nominal. Table 6-11 presents the differences in reactivity between isotopic compositions obtained using bounding and nominal parameters and their associated uncertainty.

#### 6.3.1.1.2 Burnable Poison Rods

#### 6.3.1.1.3 Specific Power

The behavior of reactivity with respect to specific power is studied in detail in Reference [8]. It is noted in the reference that reactivity decreases with increasing specific power when fission products are included in the fuel composition. The difference is also more notable at higher burnups where the rate of production of fission products is higher. [

]

In this study of specific power, the base case against which all other specific powers are compared is the  $k_{\text{eff}}$  obtained using isotopic concentrations from the bounding depletion environment parameters with 60 MW/MTU. The sensitivity effect is quantified by comparing this  $k_{\text{eff}}$  to identical cases obtained with specific powers of 40 and 50 MW/MTU. The reactivity effect of variation in specific power is provided in Table 6-14.

Also, note that References [8] and [9] support the assumption for a simple operating history (constant specific power with no downtime between cycles), and suggest adding in a margin to account for operating-history-induced effects. Reference [8] states that it is not obvious how to conservatively treat specific power variations when the effects of fission products are included in criticality calculations, like for burnup credit uncertainty in  $k_{\text{eff}}$  (200 pcm) to conservatively account for the potential uncertainty on reactivity resulting from modeling a simplified operating history (i.e., no downtime between cycles). However, even including this recommended margin with the margin from the demonstrated variation due to specific power (i.e., 286 pcm plus 200 pcm), demonstrates that the potential reactivity effects from variations in specific power and downtime combined are overwhelmed by the difference in  $k_{\text{eff}}$  observed for variations in other parameters.

#### 6.3.1.1.4 Assessment of Reactivity Margin

The desired quantity that enables comparison of the effect of the depletion parameters on reactivity is the effective neutron multiplication factor ( $k_{\text{eff}}$ ). This is output from the criticality sensitivity analysis performed using the STARBUCS/KENO modules of the SCALE 6.1 [2] code. Two  $k_{\text{eff}}$  values are compared: a  $k_{\text{eff}}$  corresponding to the case using the baseline parameters, and another  $k_{\text{eff}}$  corresponding to a case with a nominal parameter replacing one baseline parameter. The difference in  $k_{\text{eff}}$  is calculated by the following equation along with the associated uncertainties, which are summed in quadrature as follows:

$$\Delta k = k_1 - k_2$$

$$\sigma = \sqrt{\sigma_1^2 + \sigma_2^2}$$

As it applies to the depletion environment parameters,  $k_1$  pertains to the multiplication factor obtained using bounding parameters while  $k_2$  applies to the case in which the parameter under consideration is changed to nominal. As it applies to BPRAs,  $k_1$  pertains to the multiplication factor obtained without control components and using bounding depletion parameters while  $k_2$  applies to the case with control components and bounding depletion parameters. For the specific power variation,  $k_1$  pertains to the multiplication factor obtained using a specific power of 60 MW/MTU, while  $k_2$  applies to the case with a specific power of 40 or 50 MW/MTU.

### 6.3.1.2 Description of the TN-32B HBU Demonstration Cask KENO Model

For transportation, the TN-32B HBU demonstration cask system's criticality safety is ensured by fixed neutron absorbers in the basket, PRAs, and favorable basket geometry. [

]

Per Section 8.1.6.2 the borated aluminum poison plates in the basket have been tested and documented to contain an effective boron-10 areal density of  $\geq 10 \text{ mg/cm}^2$ . For added conservatism, only 90% of this value ( $0.009 \text{ mg/cm}^2$ ) is credited in the criticality analysis. [

]

Dimensions of the TN-32B HBU demonstration cask KENO V.a geometrical model are specified in Table 6-1, and are extracted from Appendix 1.4.1. Figure 6-4 illustrates a cross section of the cask model. Figure 6-5 illustrates a close up of the cross section of the middle of the cask. Figure 6-6 illustrates an axial cross section of the cask model, with the 18 axial zones differentiated. Figure 6-7 illustrates an axial cross section of the cask model, with the welded plugs in the borated aluminum plates visible. Material properties used in the KENO V.a geometry models are in Table 6-10.

The fuel assemblies are all shifted in their basket compartments towards the cask centerline, which is typically the most reactive assembly configuration. This shift is noticeable in Figure 6-5. The cask and basket material are all modeled for the nominal dimensions, except the fuel compartment is modeled at its minimum size of 8.64 inches.

The peripheral aluminum rails are modeled as a homogeneous mixture of aluminum and fresh water. The volume fractions of the aluminum and water were determined to be 0.303 and 0.697, respectively. The radial neutron shield is not modeled in either NCT or HAC models.

The cask body is surrounded by 30 cm of water for the NCT and HAC single package evaluations. For NCT and HAC array evaluations, reflective boundary conditions are implemented along the sides of the cask, with water boundary conditions at the top and bottom of the cask. These boundary conditions create an infinite array.

### 6.3.2 Material Properties

The physical and nuclear data required for the depletion and criticality analyses include the fuel assembly and burnable poison design parameters and material compositions, basket material and composition and dimensions and cross-section data. The depletion and criticality analysis uses the 238-group ENDF/B-VII cross-section library. The material definition for fuel, cladding and cask structural material are available in the SCALE 6.1 standard composition library. Details of materials and dimensions of fuel and component design are included in Table 6-2, Table 6-5, Table 6-9, Table 6-10, and Table 6-12.

For STARBUCS runs using KENO V.a, the initial uranium isotopic composition is calculated using Table 3.12 from Reference [11], shown below.

$$^{234}\text{U} = ^{235}\text{U} \times 0.0089$$

$$^{236}\text{U} = ^{235}\text{U} \times 0.0046$$

$$^{238}\text{U} = 100 - ^{234}\text{U} - ^{235}\text{U} - ^{236}\text{U}$$

The STARBUCS module of SCALE 6.1 [1] is used to calculate the fissile nuclides present and their concentrations in each of the 18 burnup-dependent axial regions of an assembly using the axial burnup profile in Table 6-7. The STARBUCS module then calls CSAS5, which implements the KENO V.a geometry model.

For the simplified STARBUCS model supporting the depletion analysis, STARBUCS calculates the spent fuel nuclide concentrations for each region using assembly irradiation history and an assumed cooling time of five years. STARBUCS calculates  $k_{\text{eff}}$  for 3.0, 4.0, and 5.0 wt. % U-235 enrichments, burnups of 50 and 60 GWd/MTU.

For the full STARBUCS model used to determine the most reactive configuration, the initial uranium enrichments modeled are 3.5 wt. % and 4.6 wt. % U-235, which bounds all selected fuel assemblies' enrichments in Table 6-4.

For the CSAS5 models used to determine compliance with the licensing limits, six STARBUCS models are used to calculate the isotopic inventory for six different cooling time groups. All  $\text{UO}_2$  fuel types modeled in the STARBUCS single criticality safety calculations with burnup credit have an initial enrichment of 4.6 wt. % U-235 and a burnup of 50 GWd/MTU, since these values bound all initial enrichments and burnups of the fuel assemblies present in the TN-32B HBU demonstration cask.

[

    ] Fuel assemblies are sorted into cooling time groups where they have the same cooling time modeled or slightly more (longer cooling time, thereby conservative). These groups are shown in Table 6-4.

### 6.3.3 Analysis Methods and Nuclear Data

The CSAS5 input file for the most limiting licensing configuration analyzed (HAC Array) can be found in Section 6.10.2.3.

#### 6.3.3.1 Computer Codes and Cross-Section Libraries

The criticality sensitivity calculations and isotopic inventory calculations are performed with the STARBUCS module in SCALE 6.1 [2], and the NCT and HAC array and single package criticality calculations are performed with the CSAS5 module in SCALE 6.1. The total number of histories traced for each STARBUCS calculation was approximately 5,000,000, and histories traced for each CSAS5 calculation was approximately 50,000,000. This number of histories was sufficient to converge the source and produce standard deviations of less than 0.0005 in  $\Delta k_{\text{eff}}$ .

All evaluations in this calculation are performed using the SCALE 6.1 code system. The TRITON two-dimensional (2-D) depletion sequence was used to perform depletion calculations and generate ORIGEN-ARP cross-section libraries that are subsequently accessed by STARBUCS to generate isotopic concentrations corresponding to the various depletion environment parameters and operational histories. These isotopic concentrations are then manually input into the SCALE 6.1 CSAS5 control sequence or automatically called by STARBUCS. The 238 group ENDF/B-VII cross-section library is used for all calculations.

The TRITON 2-D depletion sequence has the capability to simulate multiple mixtures in a fuel assembly model, which allows a detailed representation of the local flux distribution for a specific fuel rod in the assembly. The flux normalization in a TRITON calculation can be performed using as a basis the power in a specified mixture, the total power corresponding to multiple mixtures, or the assembly power. In this calculation, the flux is normalized to mixture 1 ( $\text{UO}_2$ ).

The ORIGEN-ARP methodology offers a faster alternative to the TRITON depletion sequence, provided that cross-section libraries are pre-generated. Using the TRITON-generated libraries, ORIGEN-S performs the depletion calculations to generate compositions for all unique fuel regions. During STARBUCS and CSAS5 execution, the ORIGEN-S-generated isotopic compositions are input in the three dimensional KENO V.a Monte Carlo criticality TN-32B HBU demonstration cask model to compute the effective neutron multiplication factor ( $k_{\text{eff}}$ ) of the complete system.

#### 6.3.3.2 Physical and Nuclear Data

The physical and nuclear data required for the depletion and criticality analyses include the fuel assembly and burnable poison design parameters and material compositions, basket material and composition and dimensions and cross-section data. The depletion and criticality analysis uses the 238 group ENDF/B-VII cross-section library. The material definition for fuel, cladding and cask structural material are available in the SCALE 6.1 standard composition library and are in Table 6-9. Isotopic number densities are calculated internally by STARBUCS.

#### 6.3.3.3 Bases and Assumptions

The analytical results reported in Chapter 2 demonstrate that the cask containment boundary and basket structure do not experience any significant distortion under HACs. The analytical results reported in Appendix 2.12.8 demonstrate that the fuel assemblies do not undergo any permanent plastic deformation. Therefore, for both normal and HACs, the cask geometry is identical as both conditions remove the neutron shield and outer steel shell. The neutron shield and steel shell are conservatively modeled as water. The most reactive configurations from this calculation are used as the basis for this evaluation.

To demonstrate compliance with the requirements specified in 10 CFR 71.55(b), the fuel assemblies are modeled in the appropriate conditions (moderation and configurations), as detailed in Sections 6.4, 6.5, and 6.6.

The following assumptions are incorporated into the TRITON depletion calculations:

3. The boundary condition in the depletion model is reflective. This means that the fuel assemblies are depleted at locations away from the periphery and surrounded by identical fuel assemblies in an infinite array.

8. The depletion analysis calculations for each axial zone are performed for all nuclides. ORIGEN-S data libraries contain cross-section and decay data for more than 1000 unique actinides, fission products, and structural activation products. The specific nuclides to be considered in the criticality  $k_{\text{eff}}$  analysis are those isotopes of interest in Table 6-8.



9. [ ] The justification for this assumption is taken from Table 13 of Reference [6], where the effect of horizontal bias was studied for a generic high-capacity burnup credit-style cask (designated GBC-32, Generic Burnup Credit cask), and was found to be negligible. [ ]

]

10. No fuel grids are modeled. Neglecting grids was found to produce a conservative result when calculating key nuclides.
11. A cooling time of five years is assumed. Assuming a cooling time of five years is sufficient to capture maximum reactivity, as the cooling times of the fuel assemblies prior to potential shipment are longer than five years.

The cask is modeled with KENO V.a using the available geometry input. This option allows a model to be constructed that uses regular geometric shapes to define the material boundaries.

The following assumptions are incorporated into the CSAS5/STARBUCS/KENO V.a criticality calculations:

1. Water in the TN-32B HBU demonstration cask cavity contains no soluble boron, and is assumed to be at 100% water density, including water inside the pellet-cladding gap. Full moderator density represents the most reactive condition because the assemblies are designed to be slightly under-moderated. Fresh, unborated water is placed in the annulus of all fuel rods, except where noted.
2. Temperature is 293 K (20 °C) for all mixtures used in the criticality model.
3. All zirconium-based materials (including M5™) in the fuel are modeled as Zircaloy-4. The small differences in the composition of the various cladding/guide tube materials have negligible effect on the results of the calculations. M5™ and Zircaloy-4 are shown to have similar properties in Reference [12]; therefore, this assumption is justified.
4. A zero horizontal bias is assumed.
5. In the cask rail region, the aluminum rails and unborated water are homogenized. The volume fraction of the aluminum rails is 0.303 per the sample input file in Reference [10]. Thus, the volume fraction of unborated water is 0.697.

6. The material composition of the fuel top nozzle region is modeled as a rectangular column of 3 inches high fresh water and the fuel bottom nozzle region is modeled as a rectangular column of 4 inches high fresh water. Note that there is a total of 12 inches of fresh water above the active fuel. Only the active fuel length of each assembly is explicitly modeled. The criticality analysis models have water boundary conditions on the ends and reflective boundary conditions on the sides, essentially becoming an "infinite cask array" configuration. Calculations were performed with the infinite cask array configuration to obtain a CSI of 0. The subcritical multiplication model is an exception, which has all water replaced by void and vacuum boundary conditions on all sides.
  7. The cask basket has holes in the poison plates at the location of the stainless steel plugs to which the fuel compartments are welded. The part of the plug which is through the borated aluminum plate is modeled as stainless steel. However, the part of the plug which is through the aluminum is not modeled as stainless steel and remains aluminum. This modeling simplification has a negligible effect on criticality results.
  8. The gaps on either side of the poison plates within the basket are modeled as filled with fresh water, with exception to the gaps in the internal variable water density evaluations and the subcritical multiplication model.
  9. The material composition of the thermocouples inserted in the fuel assembly is modeled as aluminum. The thermocouples are modeled as inserted into the same guide tube in each of the seven assemblies that carries a thermocouple. Because it is predominately aluminum, this simplification will not affect criticality results.
  10. [ ]
  11. It is assumed that for all cases the neutron shield and outer steel shell of the cask are stripped away, and the infinite array of casks are moved close together with moderator in the interstitial spaces.
  12. All fuel assemblies are displaced inwards into the corners nearest to the center of the TN-32B HBU demonstration cask basket to maximize reactivity.
  13. The bounding configuration for an infinite reflective model is assumed to be the same as a single package.
  14. The cask geometry and basket geometry are assumed undamaged under both NCTs and HAC. This assumption is consistent with the structural analysis in Chapter 2.
  15. The loaded fuel assemblies were well characterized and placed within the cask in specific locations during development of the storage license. Because the fuel will not be removed and replaced prior to transportation, certain analyses that are common to standard fleet transportation license applications are eliminated (i.e., criticality analyses for reconfigured (damaged) and misloaded fuel assemblies).
- [ ]

#### 6.3.4 Demonstration of Maximum Reactivity

The most credible reactive configuration for the identified fuel assemblies is assessed in this evaluation, and is compared to the USL to verify subcriticality of the HBU payload. Credit is utilized for the fixed geometry, neutron poison in the basket, and boron carbide in the PRAs in their installed position in the basket. In addition, burnup credit of the spent fuel is utilized. The fuel reconfigurations analyzed in the NCT array configuration are: axial off-set, fuel compartment tolerance, neutron poison plate thickness, moderated fuel cladding gap, clad thinning, and uniform and nonuniform pitch expansion. Sister rods that were removed from two assemblies in the HBU payload were replaced by stainless steel rods. The impact on reactivity for these removed rods is evaluated in Section 6.3.4.6. The most reactive model is determined from the NCT evaluations. For HAC, two situations due to free drop are considered: fuel pins slide within the grid spacers, and collapse of fuel pin spacer grids. The most reactive normal model is used to model the pin contraction employed when evaluating the HAC fuel pin spacer grid collapse. In addition, variable water density is also evaluated for HAC.

Features of the baseline model include modeling the active fuel region as axially centered with the borated aluminum poison plates in the basket (see Figure 6-6), the minimum fuel compartment tolerance (see Figure 6-10), nominal dimensions of the neutron poison plate thickness (see Figure 6-7), 100% fresh water in the fuel cladding gap (see Figure 6-12), full fuel clad thickness (see also Figure 6-12), and no fuel rods missing (see Figure 6-4 and Figure 6-5).

The baseline reactivity results for the range of the BECTs of interest to which subsequent criticality sensitivity evaluations are compared are summarized in Table 6-15. For the NCT and HAC licensing evaluations, the most reactive configuration is then updated to model six different types of burned fuel assemblies. The six types of fuel assemblies are all bounded by the BECT modeled in the sensitivity calculations; therefore, the most reactive fuel configuration determined from the criticality sensitivity evaluation is the same configuration for the criticality safety calculations.

##### 6.3.4.1 Axial Off-Set Analysis

The axial position of the active fuel region is shifted [ ] about the axial center to become offset from the borated aluminum poison plates, which are the same axial length as the active fuel. The results are shown in Table 6-16. The results indicate that modeling the fuel shifted up [ ] increases reactivity and is more conservative. Figure 6-8 and Figure 6-9 show the overall change axially due to shifting the active fuel region.

#### 6.3.4.2 Fuel Compartment Tolerance

For the fuel compartment tolerance, a tolerance of [ ] is assumed for the inside dimension of the compartment. However, neither the nominal nor upper tolerance dimension can be modeled without infringing on the nominal inner cask diameter. The baseline case models the minimum tolerance [ ] so the additional case models the compartments at their maximum possible size with the basket still fitting within the cask cavity. The results are shown in Table 6-17, and indicate that modeling a larger fuel compartment inside dimension is not conservative, and modeling the minimum fuel compartment tolerance as in the baseline is more conservative. Figure 6-10 illustrates the minimum fuel compartment tolerance, and Figure 6-11 illustrates the maximum fuel compartment tolerance in relation to the inside of the cask cavity.

#### 6.3.4.3 Neutron Poison Plate Thickness

Although the widths of all neutron poison plates are reduced by [ ] the results indicate that reducing the thickness of the neutron poison plates does not have much of an effect. However, the largest  $\Delta k_{\text{eff}}$  calculated is positive. Modeling a reduced neutron poison plate thickness is taken to be slightly more conservative. The results are presented in Table 6-18.

#### 6.3.4.4 Fuel Cladding Gap

The baseline configuration places fresh, unborated water in the annulus of all fuel rods. An additional case was run with the annulus filled with void. The results are shown in Table 6-19. The results indicate that modeling water in the fuel pellet gap is conservative. Figure 6-13 illustrates the fuel cladding gap filled with void.

#### 6.3.4.5 Cladding Thinning

For the cladding thinning configuration, the fuel cladding thickness is reduced by [ ]. However, deterioration of the clad can occur from the inside out (expanding gap) or the outside in (contracting exterior). The results of an expanding gap are presented in Table 6-20, and the results of a contracting exterior are presented in Table 6-21. The results indicate that modeling [ ] clad thinning with a contracting exterior is conservative. Figure 6-14 illustrates the reduction of cladding thickness through an expanding gap and Figure 6-15 illustrates reduction of cladding thickness through a contracting exterior.

#### 6.3.4.6 Missing Fuel Rods

[ ] Missing fuel rods were replaced with stainless steel rods. The orientation of [ ] in relation to the other fuel assemblies in the basket was determined to be 90°. Since the orientation of [ ] is unknown, it is rotated and evaluated at 0°, 90°, 180°, and 270°. The results are presented in Table 6-22, and indicate that the most reactive configuration of [ ] is rotated 180°. The direct criticality runs spanning all BECT were performed, and is shown in Table 6-23. The results indicate that not modeling the missing rods as stainless steel rods is slightly more conservative. Figure 6-16 illustrates [ ] with fuel rods missing and replaced by stainless steel pins, and oriented 90°. Figure 6-17 illustrates [ ] with fuel rods missing, and replaced by stainless steel pins and oriented 180°.

#### 6.3.4.7 Uniform Pitch Expansion

For the uniform pitch expansion configuration, the fuel pin pitch is expanded until the outer fuel pins of the assemblies contact the insides of the fuel compartments. The results are presented in Table 6-24. The results indicate that modeling the fuel pin pitch at the maximum pitch possible is conservative compared to the baseline configuration. Figure 6-18 illustrates the uniform pitch expansion.

#### 6.3.4.8 Nonuniform Pitch Expansion

For the nonuniform pitch expansion configuration, “birdcaging” is modeled by expanding pitches in one region and contracting pitches in another region. The outer fuel pins in nonuniform pitch expansion contact the insides of the fuel compartments. The results are presented in Table 6-25. The results indicate that modeling the nonuniform pitch expansion is more conservative than modeling a more simple uniform pitch expansion configuration. Figure 6-19 illustrates the nonuniform pitch expansion.

#### 6.3.4.9 Most Reactive Fuel

The worst-case normal model is modeled with the fuel shifted [ ] in relation to the axial center, minimum fuel compartment dimensions, minimum neutron poison plate thickness, water in the fuel cladding gap, [ ] clad thinning with a contracting exterior, not modeling the missing rods as stainless steel, and nonuniform pitch expansion. The results are shown in Table 6-26. The worst-case normal model determined is utilized to evaluate the fuel pin spacer grid collapse accident evaluation.

After the most reactive fuel configuration is determined, the burned fuel isotopic inventory is refined to take into account the cooling times of the fuel at the time of shipment. This approach is done by dividing the fuel assemblies into six cooling time groups that more accurately model the amount of decay individual assemblies have experienced. The cooling time groups are associated with the relevant fuel assemblies, and are presented in Table 6-4. These additional STARBUCS models accounting for cooling times are run with initial enrichment of 4.6 wt. % U-235 and 50 GWd/MTU, which are the most conservative attributes of any fuel assembly present in the TN-32B HBU demonstration cask. Cooling time groups are: 11.56 years, 13.05 years, 14.56 years, 15.04 years, 23.55 years, and 36.45 years. Figure 6-20 and Figure 6-21 present the most reactive configuration with cooling time groups illustrated.

All criticality safety calculations are run with the refined cooling time groups (i.e., NCT single package and array, HAC single package and array). The calculations described in the remainder of in this section utilize the cooling time groups.

#### 6.3.4.10 Variable Moderator Density

For accident conditions, the next set of calculations performed determines the effect of variable internal and external moderator density using the most reactive fuel configuration with cooling time groups. Varying the internal moderator consists of the moderation in the fuel cladding gap, between fuel rods within the fuel compartments, above and below the basket, and the water in the homogenized aluminum rail and unborated water. The moderator density is varied from 0% to 100% density. It was found that modeling 100% internal moderator density is the most conservative. Then, the external moderator density is varied while keeping the internal moderator density at 100%. The results demonstrate that the configuration with 100% internal cask moderator density and 30% external cask moderator density is the most reactive. The results of these calculations are presented in Table 6-27.

#### 6.3.4.11 Fuel Pin Spacer Grid Collapse – Pitch Contraction

For the fuel pin spacer grid collapse, the fuel rods move closer together and reduced fuel pin pitch is evaluated. The fuel is modeled with pin pitch uniformly reduced using the most reactive fuel model with cooling time groups, not the baseline model. The external moderator density is varied from 0% to 100% to ensure maximum reactivity is captured. The results are presented in Table 6-27. The results indicate that modeling the pins closer together decreases reactivity in comparison to the most reactive configuration. Figure 6-22 illustrates a cross section of the basket with the fuel pitch reduced.

#### 6.3.4.12 Axial Repositioning

For the axial repositioning, the fuel pins slide within the fuel compartment to above or below the neutron absorber poison plates, becoming misaligned with the borated neutron poison plates. As this is the same configuration analyzed for NCT, no additional criticality runs for HAC are performed.

#### 6.3.4.13 Subcritical Multiplication Factor

A subcritical multiplication factor is calculated for use in the shielding analysis. All water is removed from the most reactive normal fuel configuration with cooling time groups, and the boundary conditions are changed to be a vacuum on all sides. The resulting best estimate system reactivity  $k_{KENO} + 2\sigma_{KENO}$  is 0.33899. Taking into account all biases and bias uncertainties, the subcritical multiplication factor is a  $k_{eff}$  of 0.38563. The result is presented in Table 6-27. Figure 6-23 illustrates the full cross section of the basket without any water present.

### 6.4 Single Package Evaluation

For both NCT and HAC, the basket and cask geometry is identical. The neutron shield and outer steel shell are conservatively modeled as water, as done for the infinite arrays. Once the most reactive array configurations are determined, the boundary conditions are changed to vacuum to model a single package.

#### 6.4.1 Configuration

The NCT single package configuration is calculated from the most reactive fuel model evaluated in Section 6.3.4, except the infinite reflective array is replaced by 30 cm of full density water and vacuum boundary conditions. The HAC single package configuration is the exact same as the NCT Single Package, except the exterior is 30 cm of 30% density water.

#### 6.4.2 Results

The NCT and HAC single package results are shown with the array results and USL in Table 6-3. The maximum  $k_{eff}$  for the NCT single package is 0.94184.

### 6.5 Evaluation of Package Arrays under Normal Conditions of Transport

#### 6.5.1 Configuration

For NCT array, the basket and cask geometry is unchanged. The neutron shield and outer steel shell are conservatively modeled as water allowing the casks to be more closely packed together than physically possible. Reflective boundary conditions simulate an infinite array.

#### 6.5.2 Results

The NCT array results are tabulated in Table 6-3. The maximum  $k_{eff}$  for the NCT array is 0.94048.

## **6.6 Package Arrays under Hypothetical Accident Conditions**

### **6.6.1 Configuration**

For HAC array, the basket and cask geometry is unchanged. The neutron shield and outer steel shell are conservatively modeled as water allowing the casks to be more closely packed together than physically possible. Reflective boundary conditions simulate an infinite array. The internal and external moderator densities were varied independently to determine the most reactive configuration.

Pitch contraction simultaneously with variable water density was also considered. Results are presented in Table 6-27.

### **6.6.2 Results**

The HAC array results are tabulated in Table 6-3. The maximum  $k_{\text{eff}}$  for the HAC array is 0.94218.

## **6.7 Fissile Material Packages for Air Transport**

The TN-32B HBU demonstration cask is not transported by air. Therefore, this section does not apply.

## **6.8 Benchmark Evaluations**

The computational method validation of SCALE 6.1 [1] is performed utilizing critical experiments. The critical experiments for burnup credit analysis are suggested in References [14] and [15], and are obtained from the IHECSBE (Reference [16]) and the HTC program (Reference [15]). The HTC experiment data are published in a series of four reports by the French Institut de Radioprotection et de Sûreté Nucléaire (IRSN). The critical experiments for this analysis are selected such that the experiments have similar material composition, geometrical characteristics and support structure (e.g., support plates) to the TN-32B HBU demonstration cask, and are listed in Table 6-28.

All the KENO V.a simulations are performed with the number of generations (GEN), number of particles per generation (NPG), and number of skipped generations (NSK) selected for each CSAS experiment model recommended for use by Reference [14]. In the KENO V.a simulations, the ENDF/B-VII (v7-238 group) library is used. A sufficiently large number of neutron histories are run so that the standard deviation is less than or equal to 0.0005 for all calculations.



The primary objective of computational method validation is to establish the relationship between reality and calculated results. Computational method validation includes determination of bias and bias uncertainty based on statistical analysis of critical experiment simulation results. The bias and bias uncertainty sometimes vary significantly as a function of one or more characteristics. Per References [16] and [17], the statistical analysis should include evaluation of the critical experiment results for trends occurring as functions of relevant parameters that may affect bias and bias uncertainty. The parameters of interest considered for trending analysis are: U-235 wt. % enrichment, fuel pitch, EALF, AEG, fuel rod radius, moderator to fuel ratio, hydrogen to fissile ratio, and plutonium content. A trending analysis is performed for each parameter of interest using SCALE 6.1 simulations of critical experiments to determine the correlation coefficient ( $r$ ) between the  $k_{\text{eff}}$  and the experimental parameters.

A computational method in NUREG/CR-6698 (Reference [19]) is utilized to determine the USL value.

#### 6.8.1 Applicability of Benchmark Experiments

Proprietary Information on Pages 6-29 through 6-31  
Withheld Pursuant to 10 CFR 2.390

## 6.8.2 Bias Determination

## 6.8.2.1 USL Trending Parameters

The values of the parameters of interest are collected either from experimental descriptions (References [15] and [16]) or from KENO V.a simulation outputs of the selected critical experiments. Using the values of parameters, trending analysis is performed for parameters against  $k_{\text{eff}}$  obtained for each experiment. The parameter values are described below:

A.  $^{235}\text{U}$  wt. %

B. Fuel Pitch (cm)

C. EALF (eV)

D. AEG

E. Fuel Rod Radius (cm)

The values of the fuel rod radius are taken from the experimental description provided in References [15] and [16]. [

]

F. Moderator to Fuel Ratio

The moderator to fuel ratio is obtained by taking the ratio of water to that region of fuel covered by water. This is obtained by calculating the area covered by moderator as well as the fuel as shown in the examples below. The dimensions used to calculate moderator to fuel ratio in the following examples are from MIX-COMP-THERM-002-001s (for square pitch) and MIX-COMP-THERM-005-001 (for triangular pitch). Note that P represents pitch and D represents diameter in the following equations.

The area of the moderator is calculated using Equation 1,

$$(\text{Moderator Area}) = A_1 - A_2 \quad \text{Equation 1}$$

where:

$$A_1 = \text{Total Area} = \begin{cases} P^2, & \text{for square – pitched arrays; where } P = 1.778 \text{ cm} \\ \left( \frac{1}{2}(P) \frac{\sqrt{3}}{2} P \right), & \text{for triangular – pitched arrays; where } P = 2.159 \text{ cm} \end{cases}$$

$A_2 = \text{Area enclosed by the clad} =$

$$\begin{cases} \frac{\pi(D_2)^2}{4}, & \text{for square – pitched arrays; where } D_2 = 1.435 \text{ cm} \\ \frac{1}{2} \left[ \frac{\pi(D_2)^2}{4} \right], & \text{for triangular – pitched arrays; where } D_2 = 1.434 \text{ cm} \end{cases}$$

The moderator area for square-pitched arrays is calculated as:

$$= (1.778^2) - [\pi(1.435^2/4)] = 1.544 \text{ cm}^2$$

The moderator area for triangular-pitched arrays is calculated as:

$$= [(1/2)(\sqrt{3}/2)(2.159^2)] - [1/2(\pi)(1.434^2/4)] = 1.211 \text{ cm}^2$$

The moderator to fuel ratio is calculated using Equation 2,

$$\text{Moderator to Fuel Ratio} = \frac{\text{Moderator Area}}{\text{Fuel Area}} \quad \text{Equation 2}$$

where:

Fuel Area =

$$\begin{cases} \frac{\pi(D_1)^2}{4}, & \text{for square – pitched arrays, where } D_1 = 1.283 \text{ cm} \\ \frac{1}{2} \left[ \frac{\pi(D_1)^2}{4} \right], & \text{for triangular – pitched arrays, where } D_1 = 1.264 \text{ cm} \end{cases}$$

The fuel area for square-pitched arrays is calculated as,

$$= \pi(1.283^2/4) = 1.292 \text{ cm}^2$$

The fuel area for triangular-pitched arrays is calculated as,

$$= 1/2(\pi)(1.264^2/4) = 0.627 \text{ cm}^2$$

Therefore, the moderator to fuel ratio for square-pitched arrays is:

$$1.544 \text{ cm}^2 / 1.292 \text{ cm}^2 = 1.945,$$

and the moderator to fuel ratio for triangular-pitched arrays is:

$$1.211 \text{ cm}^2 / 0.627 \text{ cm}^2 = 1.931$$

The range of the moderator to fuel volume ratio in the selected experiments for burnup credit analysis is 1.1112 to 11.5875.

#### G. Hydrogen to Fissile Density Ratio

The hydrogen to fissile density ratio is calculated by taking the ratio of number of atoms of hydrogen in the moderator to the number of atoms of fissile nuclides ( $^{235}\text{U}$ ,  $^{239}\text{Pu}$ , and  $^{241}\text{Pu}$ ) in the fuel. The atom densities of H,  $^{235}\text{U}$ ,  $^{239}\text{Pu}$ , and  $^{241}\text{Pu}$  for each experiment are collected from the material description provided in References [15] and [16]. The hydrogen to fissile density ratio is calculated by taking the ratio of atom density of hydrogen to the sum of atom densities of  $^{235}\text{U}$ ,  $^{239}\text{Pu}$ , and  $^{241}\text{Pu}$ . This value is multiplied with moderator to fuel ratio. As shown in Equation 3.

$$\frac{H}{X} = \frac{\text{Atom density of H}}{\text{Atom density of (U-235+Pu-239+Pu-241)}} * \frac{\text{moderator volume}}{\text{fuel volume}} \quad \text{Equation 3}$$

The range of values of hydrogen to fissile density ratio in the selected experiments for burnup credit analysis is from 146.15 to 1149.55.

#### H. Plutonium Content (Pu/U+Pu)

The Pu weight fraction values are taken from Table A.1 of Reference [14]. The range of plutonium content in the selected critical experiments for burnup credit analysis is from 0.01104 and 0.03990.

### 6.8.2.2 Determination of Correlation Coefficient

The parameters of interest and the  $k_{\text{eff}}$  values are taken from References [14] and [16] and KENO V.a output. Trending analysis is performed by plotting the graph of  $k_{\text{eff}}$  values as a function of experimental parameters of interest. The linear correlation coefficient is then obtained by determining  $r^2$  value by utilizing trend line option in the graph, and also a correlation function, as shown in Table 6-30.

The critical experiment data for each parameter is also evaluated to determine the model coefficients for the weighted linear fit. The individual equations are included in the graphs of Figure 6-24 through Figure 6-31.

### 6.8.2.3 Determination of USL Value

The  $k_{\text{calc}}$  and  $\sigma_{\text{calc}}$  values are taken from the KENO V.a output. Per Reference [19], the validation of the computational method involves determining a weighted mean that incorporates the uncertainty from both the measurement ( $\sigma_{\text{exp}}$ ) and the calculation method ( $\sigma_{\text{calc}}$ ). In the critical experiments, an overall uncertainty in the measured critical parameters has been determined and presented. A combined error can then be determined, since one is derived from actual measurement errors and the other is a calculational error of the method, by applying Equation 3 of Reference [19]:

$$\sigma_t = \sqrt{\sigma_{\text{calc}}^2 + \sigma_{\text{exp}}^2} \quad \text{Equation 4}$$

An adjustment is made to the calculated  $k_{eff}$  ( $k_{calc}$ ) since the critical experiments being modeled were slightly super critical or subcritical, and not exactly critical. This adjustment is done by normalizing the  $k_{calc}$  value to the  $k_{exp}$  value. To normalize  $k_{eff}$ , Equation 9 of Reference [19] is applied:

$$k_{eff} = k_{norm} = \frac{k_{calc}}{k_{exp}} \quad \text{Equation 5}$$

A weighted mean  $k_{eff}$  ( $\overline{k_{eff}}$ ) is calculated by using the weighting factor  $1/\sigma_i^2$ . The use of this factor reduces the “weight” of data with high uncertainty. Within a set of data, the “i<sup>th</sup>” member of that set is shown with a subscript “i”. Henceforth, the uncertainty for an “i<sup>th</sup>”  $k_{eff}$  is shown as  $\sigma_i$  and is taken to mean the combined calculational and experimental uncertainty, shown in Equation 4 as  $\sigma_i$ .

The weighted mean  $k_{eff}$  value is determined by the following equation:

$$\overline{k_{eff}} = \frac{\sum \frac{1}{\sigma_i^2} k_{eff\ i}}{\sum \frac{1}{\sigma_i^2}} \quad \text{Equation 6}$$

The variance about the mean is determined by the following equation:

$$s^2 = \frac{\left(\frac{1}{n-1}\right) \sum \frac{1}{\sigma_i^2} (k_{eff\ i} - \overline{k_{eff}})^2}{\frac{1}{n} \sum \frac{1}{\sigma_i^2}} \quad \text{Equation 7}$$

The average total uncertainty is determined by the following equation:

$$\overline{\sigma}^2 = \frac{n}{\sum \frac{1}{\sigma_i^2}} \quad \text{Equation 8}$$

The square root of the pooled variance,  $S_p$ , is determined by the following equation:

$$S_p = \sqrt{s^2 + \overline{\sigma}^2} \quad \text{Equation 9}$$

where:

$s^2$  = variance about the mean

$\overline{\sigma}$  = average total uncertainty

$n$  = number of critical experiments used in the validation

For a desired population fraction of 95% and a rank order of 1 (the smallest data sample, conservative for a sample size of 157), the percent confidence that a fraction of the population is above the lowest observed value is:

$$\beta = 1 - 0.95^n \quad \text{Equation 10}$$

where:

$\beta$  = degree of confidence for 95% of the population

For non-parametric data analysis,  $K_L$  is determined using Equation 20 of Reference [18], shown in the following equation:

$$K_L = [\text{Smallest } k_{\text{eff}} \text{ value}] - [\text{Uncertainty for Smallest } k_{\text{eff}}] - \text{NPM} \quad \text{Equation 11}$$

where:

$K_L$  = weighted single-sided lower tolerance limit

NPM = non-parametric margin

Smallest  $k_{\text{eff}}$  value = the lowest calculated value in the data sample.

The non-parametric margin is added to account for small sample size and is obtained from Table 2.2 of Reference [19]. Since  $\beta$  is >90%, the NPM is 0.0.

The USL is determined using Equation 35 of Reference [18], shown in the following equation:

$$USL = K_L - \Delta_{SM} - \Delta_{AOA} \quad \text{Equation 12}$$

where:

$\Delta_{SM} = 0.05$ , administrative margin to ensure subcriticality

$\Delta_{AOA} = 0$ , because extensions are not made to the area of applicability

The most reactive configuration with the most reactive BECT is confirmed to be contained within the area of applicability determined by the critical experiments in this calculation. The area of applicability is shown in Table 6-31.

The USL value is calculated utilizing a computational method from Reference [19] and the results are in Table 6-32. The USL determined for burnup credit analysis critical experiments using this method is 0.9279, and the bias and bias uncertainty due to major actinides is 0.02209. Using Equation 12 above:

$$USL = 0.9779 - 0.00 - 0.05 = 0.9279$$

The  $\beta_i$ ,  $\beta$ , and  $\Delta k_x$  bias values are added directly to the calculated system  $k_{\text{eff}}$  ( $k_{\text{KENO}} + 2 \times \sigma_{\text{KENO}}$ ), while bias uncertainties  $\Delta k_i$  and  $\Delta k_\beta$  can be statistically combined, per Reference [3]:

$$\sigma_{\text{bias}} = \sqrt{\Delta k_i^2 + \Delta k_\beta^2}$$

The term  $(\beta + \Delta k_\beta)$  was determined during the calculation of the USL value 0.9279.  $K_L$  was the combination of bias and bias uncertainty.  $K_L$  is a lower limit above which a defined fraction of the true population of benchmarking  $k_{\text{eff}}$  is expected to lie, with a prescribed confidence and within the area of applicability. In other words, there is 95% confidence that 95% of the data lies above  $K_L$ . Because the benchmarking data were determined to be not normally distributed, the data was analyzed by non-parametric techniques. [

]



Proprietary Information on Pages 6-38 through 6-43  
Withheld Pursuant to 10 CFR 2.390

### 6.9.3 Licensing Basis Model Assumptions

#### 6.9.3.1 Reactor Operating History and Parameter Values

The fuel assemblies in the TN-32B HBU demonstration cask are PWR 17×17 assemblies. The baseline geometry and design input parameters of the fuel assemblies used in this calculation are shown in Table 6-5. [

]

This criticality analysis is not intended to cover an entire population of casks, but only the 32 discrete fuel assemblies present in one TN-32B HBU demonstration cask. It is not necessary to create a loading curve for one cask, as criticality safety is able to be demonstrated with CSAS5.

#### 6.9.4.2 Misload Evaluation

The misload analysis addresses the [ ] of fuel assemblies into a storage or transportation system that do not meet the proposed loading curve. However, the loaded fuel assemblies in this cask were well characterized and placed within the cask in specific locations during development of the TN-32B HBU demonstration cask storage license. Because the specific HBU fuel will not be removed and replaced prior to transportation, certain analyses that are common to standard fleet transportation license applications are not required (i.e., criticality analyses for reconfigured (damaged) and misloaded fuel assemblies). NAPS operating procedures included a double verification that ensured that the cask was loaded with the correct thirty-two HBU fuel assemblies, the fuel assemblies were undamaged, and the fuel assemblies were loaded in the correct cask cell locations in the basket.

#### 6.9.6 Estimate of Additional Reactivity Margin

Overall, the criticality calculations are performed utilizing bounding parameters and conservative assumptions. Consequently, these evaluations result in significant additional margin to the calculated  $k_{eff}$ .

In conclusion, the results of the criticality calculations and the sensitivity calculations demonstrate that the maximum  $k_{\text{eff}}$ , including statistical uncertainty, is less than the USL determined from a statistical analysis of benchmark criticality experiments and includes an allowance for burned fuel. The main results of the criticality calculations are shown in Table 6-3. The statistical analysis procedure includes a 95% confidence band with an administrative safety margin of 0.05.

## 6.10 Appendix

### 6.10.1 References

1. Title 10, Code of Federal Regulations - Energy, Part 71 (10 CFR 71), "Packaging and Transportation of Radioactive Material," 1-1-2021 Edition, U.S. Nuclear Regulatory Commission, Washington, D.C.
2. Oak Ridge National Laboratory, RSICC Computer Code Collection, "SCALE: A Comprehensive Modeling and Simulation Suite for Nuclear Safety Analysis and Design," June 2011.
3. U.S. Nuclear Regulatory Commission, Spent Fuel Project Office Interim Staff Guidance (ISG)-8, "Burnup Credit in the Criticality Safety Analyses of PWR Spent Fuel in Transportation and Storage Casks," Revision 3.
4. U.S. Nuclear Regulatory Commission, "An Approach for Validating Actinide and Fission Product Burnup Credit Criticality Safety Analyses – Isotopic Composition Predictions," NUREG/CR-7108, April 2012.
5. U.S. Nuclear Regulatory Commission, "Recommendations for Addressing Axial Burnup in PWR Burnup Credit Analyses," NUREG/CR-6801, March 2003.
6. U.S. Nuclear Regulatory Commission, "Assessment of Reactivity Margins and Loading Curves for PWR Burnup-Credit Cask Designs," NUREG/CR-6800, March 2003.
7. U.S. Nuclear Regulatory Commission, "Parametric Study of the Effect of Burnable Poison Rods for PWR Burnup Credit," NUREG/CR-6761, March 2002.
8. Oak Ridge National Laboratory, "Sensitivity and Parametric Evaluations of Significant Aspects of Burnup Credit for PWR Spent Fuel Packages, ORNL/TM-12973, May 1996.
9. C. V. Parks, M. D. DeHart, and J. C. Wagner, "Review and Prioritization of Technical Issues Related to Burnup Credit for LWR Fuel," NUREG/CR-6665, February 2000.
10. TN Americas, LLC, TN-32 Updated Final Safety Analysis Report, Revision 6 (CoC 1021, Docket No. 72-1021), April 2014.
11. U.S. Nuclear Regulatory Commission, "Technical Support for a Proposed Decay Heat Guide Using SAS2H/ORIGEN-S Data," NUREG/CR-5625, July 1994.
12. European Commission, Joint Research Centre, "Development of M5 Cladding Material Correlations in the TRANSURANUS Code," Revision 1, 2016.
13. Pacific Northwest National Laboratory, "High Burnup Spent Fuel Data Project, Sister Rod Test Plan Overview", FCRD-UFD-2016-000063/PNNL-25374, April 29, 2016.

14. U.S. Nuclear Regulatory Commission, "An Approach for Validating Actinide and Fission Product Burnup Credit Criticality Safety Analyses – Criticality ( $k_{\text{eff}}$ ) Predictions," NUREG/CR-7109, April 2012.
15. U.S. Nuclear Regulatory Commission, "Evaluation of the French Haut Taux de Combustion (HTC) Critical Experiment Data," NUREG/CR-6979, September 2008.
16. NEA Nuclear Science Committee, "International Handbook of Evaluated Criticality Safety Benchmark Experiments," NEA/NSC/DOE(95)03, July 2019.
17. American Nuclear Society, "American National Standard, Nuclear Criticality Safety in Operations with Fissionable Materials Outside Reactors," ANSI/ANS-8.1-2014.
18. U.S. Nuclear Regulatory Commission, "Standard Review Plan for Fuel Cycle Facilities License Applications," NUREG-1520, Revision 2, June 2015.
19. U.S. Nuclear Regulatory Commission, "Guide for Validation of Nuclear Criticality Safety Calculational Methodology," NUREG/CR-6698, January 2001.
20. U.S. Nuclear Regulatory Commission, "Standard Review Plan for Transportation Packages for Spent Fuel and Radioactive Materials," NUREG-2216, August 2020.
21. U.S. Nuclear Regulatory Commission, "Computational Benchmark for Estimation of reactivity Margin from Fission Products and Minor Actinides in PWR Burnup Credit," NUREG/CR-6747, October 2001.

Proprietary Information on Pages 6-50 through 6-198  
Withheld Pursuant to 10 CFR 2.390



**Table 6-1**  
**TN-32B HBU Cask Geometry in KENO Models**

Parameter	KENO Model		Cask Design Nominal Value (in)
	(in)	(cm)	
Cask Length <sup>(1)</sup>	184	467.36	186.06
Cask Shell Outer Diameter	87.75	222.89	87.75
Cask Top Shell Thickness	10.50	26.67	10.50
Cask Bottom Shell Thickness	10.25	26.04	10.25
Cask Wall Thickness	9.50	24.13	9.50
Cask Cavity Length	163.25	414.66	163.25
Cask Cavity Diameter	68.75	174.63	68.75
Basket Length	160	406.40	160
Basket Diameter	68.75	174.63	68.75
Fuel Compartment Length	160	406.40	160
Fuel Compartment Wall Thickness	0.105	0.27	0.105
Fuel Compartment Inner Dimension <sup>(2)</sup>	8.64	21.95	8.70
Fuel Top Nozzle	3	7.62	3
Active Fuel	144	365.76	144
Fuel Bottom Nozzle	4	10.16	4
Water Boundary Condition	11.81	30.00	11.81

Notes:

1. Overall cask length modeled does not include the puncture resistant plate over the lid. The TN-32B HBU demonstration cask design nominal length is puncture resistant plate inclusive. Presence of puncture resistant plate has negligible effect on criticality results.
2. Nominal value of compartment is 8.7" × 8.7". However, a dimensional tolerance of 0.06" is applied. Compartments modeled closer together are conservative.

**Table 6-2**  
**Non-Fuel Design Parameters in KENO**

Parameter	KENO Model	KENO Model	TN-32B HBU Cask Nominal Value
	(in)	(cm)	
Poison Plates in Basket			
Enriched Boron in Poison Plate	-	9 mg/cm <sup>c</sup>	10 mg/cm <sup>2</sup>
B-10 Fraction in Enriched Boron	0.8377		
Poison Material in Poison Plate	Borated Aluminum		Borated Aluminum
Borated Aluminum Density <sup>(1)</sup>	-	2.693 g/cm <sup>3</sup>	2.693 g/cm <sup>3</sup>
Borated Aluminum Plate Length	144	365.76	144 in
Borated Aluminum Plate Width	8.25	20.955	8.25 in
Borated Aluminum Plate Thickness	0.04	0.1016	0.04 in
Poison Rod Assembly			
Number of PRAs	6		6
Number of Poison Rods per PRA	24		24
Poison Pellet Diameter	0.295	0.7493	0.295 in
Poison Pellet Material	B <sub>4</sub> C		B <sub>4</sub> C
Credit taken per PRA	50%		50%
Poison Cladding Material	Zircaloy-4		M5®
Poison Rod Diameter	0.374	0.94996	0.374 in
Poison Rod Clad Thickness	0.0225	0.05715	0.0225 in
Bottom Gap <sup>(2)</sup>	1.951	4.95554	1.951 in
Thermocouple Insert			
Number of FAs with TLA	7		7
Thermocouple Insert Material	Aluminum		Aluminum
Thermocouple Insert Diameter	[       ]	[       ]	[       ]

Notes:

1. Per Reference [10]
2. The offset is modeled by replacing the bottom 1.951 inches of B<sub>4</sub>C material as Zircaloy-4.

Proprietary Information on Pages 6-201 and 6-202  
Withheld Pursuant to 10 CFR 2.390

**Table 6-5**  
**Design Input for the 17×17 Fuel Assembly (TRITON and KENO)**

Parameter	TRITON Model		KENO Model (in)	Fuel Assembly Nominal Parameters
	(in)	(cm)		
Assembly Pitch <sup>(1)</sup>	8.466	21.50	8.224	21.50 cm
Number of Fuel Rods	264		264	264
Guide Tubes per Assembly	24		24	24
Instrument Tubes per Assembly	1		1	1
Fuel Cell Pitch	0.4960	1.26	0.4960	1.26 cm
Pellet OD	0.3225	0.8192	0.3225	0.8192 cm
Fuel Rod Clad ID	0.329	0.836	0.3290	0.836 cm
Fuel Rod Clad OD	0.374	0.950	0.3740	0.95 cm
Fuel Rod Clad Material	Zircaloy-4		Zircaloy-4	Zirconium based
Active Fuel Length	144	365.76	144	365.76 cm
Guide Tube ID	0.45	1.144 <sup>(2)</sup>	0.45	0.45079 in
Guide Tube OD <sup>(3)</sup>	0.482	1.224	0.482	0.49016 in
Guide Tube Material	Zircaloy-4		Zircaloy-4	Zircaloy-4
Instrument Tube ID	0.45	1.144 <sup>(2)</sup>	0.45	0.442-0.450 in, depending on fuel design
Instrument Tube OD <sup>(3)</sup>	0.482	1.224	0.482	0.49016 in
Instrument Tube Material	Zircaloy-4		Zircaloy-4	Zircaloy-4

## Notes:

1. The assembly pitch in the KENO models is smaller than nominal values so as to model the assemblies shifted towards the center of the cask, which is conservative.
2. Guide Tube ID and Instrument Tube ID converts from 0.45 in to 1.143 cm; however, 1.144 cm is modeled.
3. Though the models' Guide Tube OD and Instrument Tube OD are smaller than the customer data, modeling a thinner tube wall will have a negligible effect on reactivity results.

**Table 6-6**  
**Summary of Parameters Selected for Depletion Calculations**

Parameters	NAPS Values		NUREG Values <sup>(8)</sup>
	Lower Nominal	Upper Nominal	
Fuel Temperature (K) <sup>(5)</sup>			1100
Moderator Temperature (K) <sup>(4)</sup>			610
Moderator Density (g/cm <sup>3</sup> ) <sup>(5)</sup>			0.630
Cycle Average Boron Concentration (ppm)			1000
Specific Power (MW/MTU)			60 <sup>(2)</sup>
Downtime (days)	various	various	0 <sup>(7)</sup>

## Notes:

1. NAPS fuel data
2. Higher but credible specific power values are more bounding, per Table 13 Reference [6].
3. Referred to as core average depletion power in NAPS fuel data. Note that SFP TRITON inputs have up to 58.2 MW/MTU specific power.
4. NAPS fuel data, though SFP TRITON inputs use up to 610 K for moderator temperature.
5. Fuel temperature and moderator density nominal range deduced from SFP TRITON inputs.
6. 815 ppm is selected as the "lower nominal" value because it bounds the lower end of the average boron in NAPS fuel data.
7. From Section 3.4.2.2 of Reference [8].
8. All values in this column are from Reference [4] unless otherwise noted.
9. Although the moderator density is higher, the lower density of 0.61661 g/cm<sup>3</sup> was bounding.

Proprietary Information on Pages 6-205 and 6-206  
Withheld Pursuant to 10 CFR 2.390

**Table 6-9**  
**Material Property Data in TRITON Models**

Material Number	Material	Density	Composition (wt.%)	
1	uo2	95.5% theoretical	Uranium-235	3.0-5.0
			Uranium-238	95.0-97.0
2, 4, 7	zirc4	standard	100	
3	h2o	variable	100	
	wtptbor	variable	Natural Boron	1100 ppm
5, 6	wtptair	0.0012 g/cm <sup>3</sup> <sup>(1)</sup>	Carbon	0.0126
			Nitrogen	76.5081
			Oxygen	23.4793
8 <sup>(2)</sup>	Al <sub>2</sub> O <sub>3</sub> -B <sub>4</sub> C 3.000 wt. % B <sub>4</sub> C (wtptbpr)	3.1 g/cm <sup>3</sup> <sup>(3)</sup>	Boron-10	0.42262
			Boron-11	1.92525
			Carbon	0.65213
			Oxygen	45.66268
			Aluminum	51.33732

Notes:

1. Composition and density from Reference [2].
2. Composition from Table 6 of Reference [7].
3. Density from SFP TRITON inputs.

**Table 6-10**  
**Material Property Data in KENO Models**

Material Number	Material	Density (g/cm <sup>3</sup> )	Composition (wt. %)	
1	uo2	95.5% theoretical	Uranium-235	3.5-4.6
2	zirc4	standard	100	
3, 5, 7, 17	h2o	standard	100	
4	ss304	standard	100	
6	PRA (b4c)	50% theoretical	100	
8, 15	Al (includes TC)	standard	100	
9	Enriched Borated Aluminum Poison Plate 9 mg/cm <sup>2</sup>	2.693 g/cm <sup>3</sup>	Boron-10 (86.4 wt. %)	0.032927
			Boron-11 (13.6 wt. %)	0.005183
			Aluminum	0.96189
10	Homogenized Aluminum Rail and Unborated Water	standard	Aluminum	0.303
		standard	H <sub>2</sub> O	0.697
16	cask shell (carbon steel)	standard	100	



**Table 6-11**  
**Sensitivity Evaluation of Depletion Environment Parameters on Reactivity ( $\Delta k$ )**

Parameter	Burnup (GWd/MTU)	Enrichment (wt. % U-235)					
		3.0		4.0		5.0	
		$\Delta k$	$\sigma$	$\Delta k$	$\sigma$	$\Delta k$	$\sigma$
Fuel Temperature $\Delta k = k_{(1100K)} - k_{(994K)}$	50.0	0.00322	0.00069	0.00238	0.00069	0.00039	0.00069
	60.0	0.00259	0.00069	0.00200	0.00069	0.00228	0.00069
Moderator Temperature $\Delta k = k_{(610K)} - k_{(562K)}$	50.0	0.01306	0.00069	0.00971	0.00069	0.00649	0.00068
	60.0	0.01490	0.00069	0.01193	0.00069	0.00878	0.00069
Boron Concentration $\Delta k = k_{(1100ppm)} - k_{(815ppm)}$	50.0	0.00440	0.00069	0.00398	0.00069	0.00218	0.00069
	60.0	0.00596	0.00069	0.00340	0.00069	0.00343	0.00069

Bounding Values: Moderator temperature = 610 K, fuel temperature = 1100 K, boron concentration = 1100 ppm

Nominal Values: Moderator temperature = 562 K, fuel temperature = 994 K, boron concentration = 815 ppm

**Table 6-12**  
**Design Parameters of Burnable Poison Rods in TRITON Models**

Parameter	TRITON Model (cm)
Absorber Material	$Al_2O_3-B_4C$
BPRA Design	24 fingers 3.0 wt. % $B_4C$
Density ( $g/cm^3$ )	3.1
BPR Pellet OD	0.802 <sup>(1)</sup>
BPR Cladding Material	Zircaloy-4
BPR Cladding ID	0.828
BPR Cladding OD	0.968

[

]

Proprietary Information on This Page  
Withheld Pursuant to 10 CFR 2.390

**Table 6-15**  
**Baseline for Determining Most Reactive Configuration**

	Cooling Time (years)	Enrichment (wt. % U-235)	Burnup (GWd/MTU)	$k_{KENO}$	$\sigma_{KENO}$	$k_{KENO} + 2\sigma_{KENO}$
tn32b_crit_ct10_e35_bu50_baseline	10	3.5	50			0.79364
tn32b_crit_ct20_e35_bu50_baseline	20	3.5	50			0.77029
tn32b_crit_ct30_e35_bu50_baseline	30	3.5	50			0.75628
tn32b_crit_ct40_e35_bu50_baseline	40	3.5	50			0.74949
tn32b_crit_ct10_e46_bu50_baseline	10	4.6	50			0.85637
tn32b_crit_ct20_e46_bu50_baseline	20	4.6	50			0.83802
tn32b_crit_ct30_e46_bu50_baseline	30	4.6	50			0.82623
tn32b_crit_ct40_e46_bu50_baseline	40	4.6	50			0.81985
tn32b_crit_ct10_e35_bu56_baseline	10	3.5	56			0.77444
tn32b_crit_ct20_e35_bu56_baseline	20	3.5	56			0.74914
tn32b_crit_ct30_e35_bu56_baseline	30	3.5	56			0.73396
tn32b_crit_ct40_e35_bu56_baseline	40	3.5	56			0.72551
tn32b_crit_ct10_e46_bu56_baseline	10	4.6	56			0.83663
tn32b_crit_ct20_e46_bu56_baseline	20	4.6	56			0.81348
tn32b_crit_ct30_e46_bu56_baseline	30	4.6	56			0.80183
tn32b_crit_ct40_e46_bu56_baseline	40	4.6	56			0.79596

**Table 6-16**  
**Axial Off-Set Analysis**

	$k_{KENO}$	$\sigma_{KENO}$	$k_{KENO} + 2\sigma_{KENO}$	$\Delta k_{eff}$
<b>Fuel Shifted Up [ ]</b>				
tn32b_crit_ct10_e35_bu50_AxialOffSet			0.79931	0.00567
tn32b_crit_ct20_e35_bu50_AxialOffSet			0.77688	0.00659
tn32b_crit_ct30_e35_bu50_AxialOffSet			0.76531	0.00903
tn32b_crit_ct40_e35_bu50_AxialOffSet			0.75631	0.00682
tn32b_crit_ct10_e46_bu50_AxialOffSet			0.86368	0.00731
tn32b_crit_ct20_e46_bu50_AxialOffSet			0.84574	0.00772
tn32b_crit_ct30_e46_bu50_AxialOffSet			0.83422	0.00799
tn32b_crit_ct40_e46_bu50_AxialOffSet			0.82940	0.00955
tn32b_crit_ct10_e35_bu56_AxialOffSet			0.78043	0.00599
tn32b_crit_ct20_e35_bu56_AxialOffSet			0.75679	0.00765
tn32b_crit_ct30_e35_bu56_AxialOffSet			0.74296	0.00900
tn32b_crit_ct40_e35_bu56_AxialOffSet			0.73511	0.00960
tn32b_crit_ct10_e46_bu56_AxialOffSet			0.84388	0.00725
tn32b_crit_ct20_e46_bu56_AxialOffSet			0.82225	0.00877
tn32b_crit_ct30_e46_bu56_AxialOffSet			0.81113	0.00930
tn32b_crit_ct40_e46_bu56_AxialOffSet			0.80532	0.00936
<b>Fuel Shifted Down [ ]</b>				
tn32b_crit_ct10_e35_bu50_AxialOffSetAlt			0.79408	0.00044
tn32b_crit_ct20_e35_bu50_AxialOffSetAlt			0.77044	0.00015
tn32b_crit_ct30_e35_bu50_AxialOffSetAlt			0.75674	0.00046
tn32b_crit_ct40_e35_bu50_AxialOffSetAlt			0.74723	-0.00226
tn32b_crit_ct10_e46_bu50_AxialOffSetAlt			0.85738	0.00101
tn32b_crit_ct20_e46_bu50_AxialOffSetAlt			0.83868	0.00066
tn32b_crit_ct30_e46_bu50_AxialOffSetAlt			0.82779	0.00156
tn32b_crit_ct40_e46_bu50_AxialOffSetAlt			0.82063	0.00078
tn32b_crit_ct10_e35_bu56_AxialOffSetAlt			0.77427	-0.00017
tn32b_crit_ct20_e35_bu56_AxialOffSetAlt			0.74885	-0.00029
tn32b_crit_ct30_e35_bu56_AxialOffSetAlt			0.73385	-0.00011
tn32b_crit_ct40_e35_bu56_AxialOffSetAlt			0.72625	0.00074
tn32b_crit_ct10_e46_bu56_AxialOffSetAlt			0.83654	-0.00009
tn32b_crit_ct20_e46_bu56_AxialOffSetAlt			0.81235	-0.00113
tn32b_crit_ct30_e46_bu56_AxialOffSetAlt			0.80279	0.00096
tn32b_crit_ct40_e46_bu56_AxialOffSetAlt			0.79649	0.00053

**Table 6-17**  
**Fuel Compartment Tolerance**

	$k_{KENO}$	$\sigma_{KENO}$	$k_{KENO} + 2\sigma_{KENO}$	$\Delta k_{eff}$
tn32b_crit_ct10_e35_bu50_FuelCompTol			0.79245	-0.00119
tn32b_crit_ct20_e35_bu50_FuelCompTol			0.76873	-0.00156
tn32b_crit_ct30_e35_bu50_FuelCompTol			0.75433	-0.00195
tn32b_crit_ct40_e35_bu50_FuelCompTol			0.74815	-0.00134
tn32b_crit_ct10_e46_bu50_FuelCompTol			0.85580	-0.00057
tn32b_crit_ct20_e46_bu50_FuelCompTol			0.83563	-0.00239
tn32b_crit_ct30_e46_bu50_FuelCompTol			0.82605	-0.00018
tn32b_crit_ct40_e46_bu50_FuelCompTol			0.81973	-0.00012
tn32b_crit_ct10_e35_bu56_FuelCompTol			0.77376	-0.00068
tn32b_crit_ct20_e35_bu56_FuelCompTol			0.74874	-0.00040
tn32b_crit_ct30_e35_bu56_FuelCompTol			0.73325	-0.00071
tn32b_crit_ct40_e35_bu56_FuelCompTol			0.72495	-0.00056
tn32b_crit_ct10_e46_bu56_FuelCompTol			0.83501	-0.00162
tn32b_crit_ct20_e46_bu56_FuelCompTol			0.81323	-0.00025
tn32b_crit_ct30_e46_bu56_FuelCompTol			0.79916	-0.00267
tn32b_crit_ct40_e46_bu56_FuelCompTol			0.79431	-0.00165

**Table 6-18**  
**Neutron Poison Plate Thickness**

	$k_{KENO}$	$\sigma_{KENO}$	$k_{KENO} + 2\sigma_{KENO}$	$\Delta k_{eff}$
tn32b_crit_ct10_e35_bu50_NeutronPoisonThick			0.79310	-0.00054
tn32b_crit_ct20_e35_bu50_NeutronPoisonThick			0.76974	-0.00055
tn32b_crit_ct30_e35_bu50_NeutronPoisonThick			0.75626	-0.00002
tn32b_crit_ct40_e35_bu50_NeutronPoisonThick			0.74975	0.00026
tn32b_crit_ct10_e46_bu50_NeutronPoisonThick			0.85728	0.00091
tn32b_crit_ct20_e46_bu50_NeutronPoisonThick			0.83726	-0.00076
tn32b_crit_ct30_e46_bu50_NeutronPoisonThick			0.82584	-0.00039
tn32b_crit_ct40_e46_bu50_NeutronPoisonThick			0.82012	0.00027
tn32b_crit_ct10_e35_bu56_NeutronPoisonThick			0.77463	0.00019
tn32b_crit_ct20_e35_bu56_NeutronPoisonThick			0.74871	-0.00043
tn32b_crit_ct30_e35_bu56_NeutronPoisonThick			0.73525	0.00129
tn32b_crit_ct40_e35_bu56_NeutronPoisonThick			0.72629	0.00078
tn32b_crit_ct10_e46_bu56_NeutronPoisonThick			0.83509	-0.00154
tn32b_crit_ct20_e46_bu56_NeutronPoisonThick			0.81506	0.00158
tn32b_crit_ct30_e46_bu56_NeutronPoisonThick			0.80257	0.00074
tn32b_crit_ct40_e46_bu56_NeutronPoisonThick			0.79556	-0.00040

**Table 6-19**  
**Fuel Cladding Gap**

	$k_{KENO}$	$\sigma_{KENO}$	$k_{KENO} + 2\sigma_{KENO}$	$\Delta k_{eff}$
tn32b_crit_ct10_e35_bu50_FuelCladGap			0.78880	-0.00484
tn32b_crit_ct20_e35_bu50_FuelCladGap			0.76485	-0.00544
tn32b_crit_ct30_e35_bu50_FuelCladGap			0.75232	-0.00396
tn32b_crit_ct40_e35_bu50_FuelCladGap			0.74502	-0.00447
tn32b_crit_ct10_e46_bu50_FuelCladGap			0.85237	-0.00400
tn32b_crit_ct20_e46_bu50_FuelCladGap			0.83246	-0.00556
tn32b_crit_ct30_e46_bu50_FuelCladGap			0.82109	-0.00514
tn32b_crit_ct40_e46_bu50_FuelCladGap			0.81628	-0.00357
tn32b_crit_ct10_e35_bu56_FuelCladGap			0.77004	-0.00440
tn32b_crit_ct20_e35_bu56_FuelCladGap			0.74420	-0.00494
tn32b_crit_ct30_e35_bu56_FuelCladGap			0.72992	-0.00404
tn32b_crit_ct40_e35_bu56_FuelCladGap			0.72122	-0.00429
tn32b_crit_ct10_e46_bu56_FuelCladGap			0.83150	-0.00513
tn32b_crit_ct20_e46_bu56_FuelCladGap			0.80956	-0.00392
tn32b_crit_ct30_e46_bu56_FuelCladGap			0.79713	-0.00470
tn32b_crit_ct40_e46_bu56_FuelCladGap			0.79092	-0.00504

**Table 6-20**  
**[       ] Clad Thinning – Expanding Gap**

	$k_{KENO}$	$\sigma_{KENO}$	$k_{KENO} + 2\sigma_{KENO}$	$\Delta k_{eff}$
tn32b_crit_ct10_e35_bu50_CladThin25			0.80205	0.00841
tn32b_crit_ct20_e35_bu50_CladThin25			0.77764	0.00735
tn32b_crit_ct30_e35_bu50_CladThin25			0.76399	0.00771
tn32b_crit_ct40_e35_bu50_CladThin25			0.75665	0.00716
tn32b_crit_ct10_e46_bu50_CladThin25			0.86474	0.00837
tn32b_crit_ct20_e46_bu50_CladThin25			0.84508	0.00706
tn32b_crit_ct30_e46_bu50_CladThin25			0.83521	0.00898
tn32b_crit_ct40_e46_bu50_CladThin25			0.82882	0.00897
tn32b_crit_ct10_e35_bu56_CladThin25			0.78172	0.00728
tn32b_crit_ct20_e35_bu56_CladThin25			0.75530	0.00616
tn32b_crit_ct30_e35_bu56_CladThin25			0.74020	0.00624
tn32b_crit_ct40_e35_bu56_CladThin25			0.73246	0.00695
tn32b_crit_ct10_e46_bu56_CladThin25			0.84219	0.00556
tn32b_crit_ct20_e46_bu56_CladThin25			0.82135	0.00787
tn32b_crit_ct30_e46_bu56_CladThin25			0.80970	0.00787
tn32b_crit_ct40_e46_bu56_CladThin25			0.80293	0.00697



**Table 6-21**  
**[        ] Clad Thinning – Contracting Exterior**

	$k_{KENO}$	$\sigma_{KENO}$	$k_{KENO} + 2\sigma_{KENO}$	$\Delta k_{eff}$
tn32b_crit_ct10_e35_bu50_CladThin25Alt			0.80172	0.00808
tn32b_crit_ct20_e35_bu50_CladThin25Alt			0.77892	0.00863
tn32b_crit_ct30_e35_bu50_CladThin25Alt			0.76508	0.00880
tn32b_crit_ct40_e35_bu50_CladThin25Alt			0.75668	0.00719
tn32b_crit_ct10_e46_bu50_CladThin25Alt			0.86647	0.01010
tn32b_crit_ct20_e46_bu50_CladThin25Alt			0.84617	0.00815
tn32b_crit_ct30_e46_bu50_CladThin25Alt			0.83566	0.00943
tn32b_crit_ct40_e46_bu50_CladThin25Alt			0.83044	0.01059
tn32b_crit_ct10_e35_bu56_CladThin25Alt			0.78416	0.00972
tn32b_crit_ct20_e35_bu56_CladThin25Alt			0.75595	0.00681
tn32b_crit_ct30_e35_bu56_CladThin25Alt			0.74323	0.00927
tn32b_crit_ct40_e35_bu56_CladThin25Alt			0.73436	0.00885
tn32b_crit_ct10_e46_bu56_CladThin25Alt			0.84444	0.00781
tn32b_crit_ct20_e46_bu56_CladThin25Alt			0.82285	0.00937
tn32b_crit_ct30_e46_bu56_CladThin25Alt			0.81060	0.00877
tn32b_crit_ct40_e46_bu56_CladThin25Alt			0.80380	0.00784

**Table 6-22**  
**Most Reactive [      ] Orientation**

	$k_{KENO}$	$\sigma_{KENO}$	$k_{KENO} + 2\sigma_{KENO}$	$\Delta k_{eff}$
tn32b_crit_ct10_e46_bu50_MissingRods0			0.85606	-0.00031
tn32b_crit_ct10_e46_bu50_MissingRods90			0.85626	-0.00011
tn32b_crit_ct10_e46_bu50_MissingRods180			0.85679	0.00042
tn32b_crit_ct10_e46_bu50_MissingRods270			0.85621	-0.00016

**Table 6-23**  
**Missing Fuel Rods**

	$k_{KENO}$	$\sigma_{KENO}$	$k_{KENO} + 2\sigma_{KENO}$	$\Delta k_{eff}$
tn32b_crit_ct10_e35_bu50_MissingRods			0.79283	-0.00081
tn32b_crit_ct20_e35_bu50_MissingRods			0.76960	-0.00069
tn32b_crit_ct30_e35_bu50_MissingRods			0.75688	0.00060
tn32b_crit_ct40_e35_bu50_MissingRods			0.74833	-0.00116
tn32b_crit_ct10_e46_bu50_MissingRods			0.85679	0.00042
tn32b_crit_ct20_e46_bu50_MissingRods			0.83575	-0.00227
tn32b_crit_ct30_e46_bu50_MissingRods			0.82510	-0.00113
tn32b_crit_ct40_e46_bu50_MissingRods			0.81946	-0.00039
tn32b_crit_ct10_e35_bu56_MissingRods			0.77387	-0.00057
tn32b_crit_ct20_e35_bu56_MissingRods			0.74744	-0.00170
tn32b_crit_ct30_e35_bu56_MissingRods			0.73349	-0.00047
tn32b_crit_ct40_e35_bu56_MissingRods			0.72512	-0.00039
tn32b_crit_ct10_e46_bu56_MissingRods			0.83504	-0.00159
tn32b_crit_ct20_e46_bu56_MissingRods			0.81283	-0.00065
tn32b_crit_ct30_e46_bu56_MissingRods			0.80252	0.00069
tn32b_crit_ct40_e46_bu56_MissingRods			0.79449	-0.00147

**Table 6-24**  
**Uniform Pitch Expansion**

	$k_{KENO}$	$\sigma_{KENO}$	$k_{KENO} + 2\sigma_{KENO}$	$\Delta k_{eff}$
tn32b_crit_ct10_e35_bu50_UniformExp			0.81478	0.02114
tn32b_crit_ct20_e35_bu50_UniformExp			0.78871	0.01842
tn32b_crit_ct30_e35_bu50_UniformExp			0.77508	0.01880
tn32b_crit_ct40_e35_bu50_UniformExp			0.76784	0.01835
tn32b_crit_ct10_e46_bu50_UniformExp			0.88147	0.02510
tn32b_crit_ct20_e46_bu50_UniformExp			0.86093	0.02291
tn32b_crit_ct30_e46_bu50_UniformExp			0.84945	0.02322
tn32b_crit_ct40_e46_bu50_UniformExp			0.84244	0.02259
tn32b_crit_ct10_e35_bu56_UniformExp			0.79487	0.02043
tn32b_crit_ct20_e35_bu56_UniformExp			0.76882	0.01968
tn32b_crit_ct30_e35_bu56_UniformExp			0.75327	0.01931
tn32b_crit_ct40_e35_bu56_UniformExp			0.74394	0.01843
tn32b_crit_ct10_e46_bu56_UniformExp			0.85944	0.02281
tn32b_crit_ct20_e46_bu56_UniformExp			0.83730	0.02382
tn32b_crit_ct30_e46_bu56_UniformExp			0.82413	0.02230
tn32b_crit_ct40_e46_bu56_UniformExp			0.81775	0.02179

**Table 6-25**  
**Nonuniform Pitch Expansion**

	$k_{KENO}$	$\sigma_{KENO}$	$k_{KENO} + 2\sigma_{KENO}$	$\Delta k_{eff}$
tn32b_crit_ct10_e35_bu50_NonuniformExp			0.82373	0.03009
tn32b_crit_ct20_e35_bu50_NonuniformExp			0.79815	0.02786
tn32b_crit_ct30_e35_bu50_NonuniformExp			0.78453	0.02825
tn32b_crit_ct40_e35_bu50_NonuniformExp			0.77656	0.02707
tn32b_crit_ct10_e46_bu50_NonuniformExp			0.89208	0.03571
tn32b_crit_ct20_e46_bu50_NonuniformExp			0.87013	0.03211
tn32b_crit_ct30_e46_bu50_NonuniformExp			0.85821	0.03198
tn32b_crit_ct40_e46_bu50_NonuniformExp			0.85258	0.03273
tn32b_crit_ct10_e35_bu56_NonuniformExp			0.80361	0.02917
tn32b_crit_ct20_e35_bu56_NonuniformExp			0.77600	0.02686
tn32b_crit_ct30_e35_bu56_NonuniformExp			0.76149	0.02753
tn32b_crit_ct40_e35_bu56_NonuniformExp			0.75326	0.02775
tn32b_crit_ct10_e46_bu56_NonuniformExp			0.86910	0.03247
tn32b_crit_ct20_e46_bu56_NonuniformExp			0.84587	0.03239
tn32b_crit_ct30_e46_bu56_NonuniformExp			0.83522	0.03339
tn32b_crit_ct40_e46_bu56_NonuniformExp			0.82759	0.03163

**Table 6-26**  
**Most Reactive Configuration**

	$k_{KENO}$	$\sigma_{KENO}$	$k_{KENO} + 2\sigma_{KENO}$	$\Delta k_{eff}$
tn32b_crit_ct10_e35_bu50_MostReactive			0.83416	0.04052
tn32b_crit_ct20_e35_bu50_MostReactive			0.81187	0.04158
tn32b_crit_ct30_e35_bu50_MostReactive			0.79870	0.04242
tn32b_crit_ct40_e35_bu50_MostReactive			0.79083	0.04134
tn32b_crit_ct10_e46_bu50_MostReactive			0.90375	0.04738
tn32b_crit_ct20_e46_bu50_MostReactive			0.88551	0.04749
tn32b_crit_ct30_e46_bu50_MostReactive			0.87354	0.04731
tn32b_crit_ct40_e46_bu50_MostReactive			0.86636	0.04651
tn32b_crit_ct10_e35_bu56_MostReactive			0.81493	0.04049
tn32b_crit_ct20_e35_bu56_MostReactive			0.78998	0.04084
tn32b_crit_ct30_e35_bu56_MostReactive			0.77474	0.04078
tn32b_crit_ct40_e35_bu56_MostReactive			0.76710	0.04159
tn32b_crit_ct10_e46_bu56_MostReactive			0.88186	0.04523
tn32b_crit_ct20_e46_bu56_MostReactive			0.85912	0.04564
tn32b_crit_ct30_e46_bu56_MostReactive			0.84980	0.04797
tn32b_crit_ct40_e46_bu56_MostReactive			0.84332	0.04736

**Table 6-27**  
**Variable Moderator Density**

	$k_{KENO}$	$\sigma_{KENO}$	$k_{KENO} + 2\sigma_{KENO}$	$\Delta k_{eff}$
<b>Internal Moderator Density, in % of Water, with Nonuniform Pitch Expansion</b>				
NCTarray_ctxxxx_e46_bu50			0.89384	-
HACarray_ctxxxx_e46_bu50_imd090			0.87006	-0.02378
HACarray_ctxxxx_e46_bu50_imd060			0.76562	-0.13813
HACarray_ctxxxx_e46_bu50_imd030			0.60725	-0.29650
HACarray_ctxxxx_e46_bu50_imd010			0.45793	-0.44582
HACarray_ctxxxx_e46_bu50_imd000			0.34129	-0.56246
<b>External Moderator Density, in % of Water, with Nonuniform Pitch Expansion</b>				
NCTarray_ctxxxx_e46_bu50			0.89384	-
HACarray_ctxxxx_e46_bu50_emd090			0.89327	-0.00057
HACarray_ctxxxx_e46_bu50_emd060			0.89521	0.00137
HACarray_ctxxxx_e46_bu50_emd030			<b>0.89554</b>	0.00170
HACarray_ctxxxx_e46_bu50_emd010			0.89518	0.00134
HACarray_ctxxxx_e46_bu50_emd000			0.89548	0.00164
<b>Internal and External Moderator Density, 0% Water, with Nonuniform Pitch Expansion</b>				
SubcriticalMult_ctxxxx_e46_bu50			0.33899	-0.55485
<b>External Moderator Density, in % of Water, and Pitch Contraction</b>				
HACarray_ctxxxx_e46_bu50_emd100_MinPitch			0.84155	-
HACarray_ctxxxx_e46_bu50_emd090_MinPitch			0.84281	0.00126
HACarray_ctxxxx_e46_bu50_emd060_MinPitch			0.84200	0.00045
HACarray_ctxxxx_e46_bu50_emd030_MinPitch			0.84275	0.00120
HACarray_ctxxxx_e46_bu50_emd010_MinPitch			0.84218	0.00063
HACarray_ctxxxx_e46_bu50_emd000_MinPitch			0.84251	0.00096

**Table 6-28**  
**Experimental Parameters of Critical Experiments from KENO V.a Outputs**  
 (4 Pages)

Critical Experiment	EALF (eV)	AEG	k <sub>eff</sub>	σ <sub>t</sub>
MIX-COMP-THERM-002-001s				0.00600
MIX-COMP-THERM-002-002s				0.00470
MIX-COMP-THERM-002-003s				0.00310
MIX-COMP-THERM-002-004s				0.00240
MIX-COMP-THERM-002-005s				0.00250
MIX-COMP-THERM-002-006s				0.00270
MIX-COMP-THERM-004-001				0.00460
MIX-COMP-THERM-004-002				0.00460
MIX-COMP-THERM-004-003				0.00460
MIX-COMP-THERM-004-004				0.00390
MIX-COMP-THERM-004-005				0.00390
MIX-COMP-THERM-004-006				0.00390
MIX-COMP-THERM-004-007				0.00400
MIX-COMP-THERM-004-008				0.00400
MIX-COMP-THERM-004-009				0.00400
MIX-COMP-THERM-004-010				0.00510
MIX-COMP-THERM-004-011				0.00510
mct005-01				0.00220
mct005-02				0.00260
mct005-03				0.00290
mct005-04				0.00280
mct005-05				0.00360
mct005-06				0.00420
mct005-07				0.00420
mct006-01				0.00510
mct006-02				0.00360
mct006-03				0.00360
mct006-04				0.00440
mct006-05				0.00540
mct006-06				0.00510
mct006-07				0.00450
mct006-08				0.00440
mct006-09				0.00440
mct006-10				0.00440
mct006-11				0.00440
mct006-12				0.00440
mct006-13				0.00440
mct006-14				0.00440
mct006-15				0.00440
mct006-16				0.00450

**Table 6-28**  
**Experimental Parameters of Critical Experiments from KENO V.a Outputs**  
 (4 Pages)

Critical Experiment	EALF (eV)	AEG	k <sub>eff</sub>	σ <sub>t</sub>
mct006-29				0.00870
mct006-30				0.00870
mct006-31				0.00870
mct006-32				0.00870
mct006-33				0.00870
mct006-34				0.00870
mct006-35				0.00870
mct006-36				0.00870
mct006-37				0.00870
mct006-38				0.00870
mct007-01				0.00350
mct007-02				0.00390
mct007-03				0.00460
mct007-04				0.00570
mct007-05				0.00610
MIX-COMP-THERM-008-001				0.00320
MIX-COMP-THERM-008-002				0.00300
MIX-COMP-THERM-008-003				0.00380
MIX-COMP-THERM-008-004				0.00470
MIX-COMP-THERM-008-005				0.00560
MIX-COMP-THERM-008-006				0.00650
MIX-COMP-THERM-008-007				0.00390
MIX-COMP-THERM-008-008				0.00390
MIX-COMP-THERM-008-009				0.00390
MIX-COMP-THERM-008-010				0.00390
MIX-COMP-THERM-008-011				0.00390
MIX-COMP-THERM-008-012				0.00390
MIX-COMP-THERM-008-013				0.00390
MIX-COMP-THERM-008-014				0.00390
MIX-COMP-THERM-008-015				0.00390
MIX-COMP-THERM-008-016				0.00390
MIX-COMP-THERM-009-001				0.00540
MIX-COMP-THERM-009-002				0.00490
MIX-COMP-THERM-009-003				0.00500
MIX-COMP-THERM-009-004				0.00620
MIX-COMP-THERM-009-005				0.00740
MIX-COMP-THERM-009-006				0.00800
htc-001-v7-c01				0.00188
htc-001-v7-c02				0.00187
htc-001-v7-c03				0.00188



**Table 6-28**  
**Experimental Parameters of Critical Experiments from KENO V.a Outputs**  
 (4 Pages)

Critical Experiment	EALF (eV)	AEG	k <sub>eff</sub>	σ <sub>t</sub>
htc-001-v7-c04				0.00188
htc-001-v7-c05				0.00188
htc-001-v7-c06				0.00188
htc-001-v7-c07				0.00188
htc-001-v7-c08				0.00188
htc-001-v7-c09				0.00188
htc-001-v7-c10				0.00188
htc-001-v7-c11				0.00188
htc-001-v7-c12				0.00188
htc-001-v7-c13				0.00188
htc-001-v7-c14				0.00188
htc-001-v7-c15				0.00188
htc-001-v7-c16				0.00188
htc-001-v7-c17				0.00188
htc-001-v7-c18				0.00188
htc-003-v7-c01				0.00326
htc-003-v7-c02				0.00326
htc-003-v7-c03				0.00326
htc-003-v7-c04				0.00326
htc-003-v7-c05				0.00326
htc-003-v7-c06				0.00326
htc-003-v7-c12				0.00258
htc-003-v7-c13				0.00258
htc-003-v7-c14				0.00259
htc-003-v7-c15				0.00259
htc-003-v7-c16				0.00259
htc-003-v7-c17				0.00259
htc-003-v7-c18				0.00259
htc-003-v7-c19				0.00258
htc-003-v7-c20				0.00259
htc-003-v7-c21				0.00258
htc-003-v7-c22				0.00259
htc-003-v7-c23				0.00259
htc-003-v7-c24				0.00259
htc-003-v7-c25				0.00259
htc-003-v7-c26				0.00259
htc-004pb-v7-c01				0.00852
htc-004pb-v7-c02				0.00852
htc-004pb-v7-c03				0.00852
htc-004pb-v7-c04				0.00852

**Table 6-28**  
**Experimental Parameters of Critical Experiments from KENO V.a Outputs**  
 (4 Pages)

Critical Experiment	EALF (eV)	AEG	k <sub>eff</sub>	σ <sub>t</sub>
htc-004pb-v7-c05				0.00560
htc-004pb-v7-c06				0.00560
htc-004pb-v7-c07				0.00474
htc-004pb-v7-c08				0.00560
htc-004pb-v7-c09				0.00560
htc-004pb-v7-c10				0.00560
htc-004pb-v7-c11				0.00560
htc-004pb-v7-c12				0.00879
htc-004pb-v7-c13				0.00879
htc-004pb-v7-c14				0.00879
htc-004pb-v7-c15				0.00355
htc-004pb-v7-c16				0.00355
htc-004ss-v7-c01				0.00781
htc-004ss-v7-c02				0.00782
htc-004ss-v7-c03				0.00782
htc-004ss-v7-c04				0.00781
htc-004ss-v7-c05				0.00592
htc-004ss-v7-c06				0.00592
htc-004ss-v7-c07				0.00592
htc-004ss-v7-c08				0.00592
htc-004ss-v7-c09				0.00592
htc-004ss-v7-c10				0.00592
htc-004ss-v7-c11				0.00449
htc-004ss-v7-c12				0.00656
htc-004ss-v7-c13				0.00656
htc-004ss-v7-c22				0.00493
htc-004ss-v7-c23				0.00493
htc-004ss-v7-c24				0.00687
htc-004ss-v7-c25				0.00687
htc-004ss-v7-c26				0.00686
htc-004ss-v7-c27				0.00687
htc-004ss-v7-c28				0.00687
htc-004ss-v7-c29				0.00687
htc-004ss-v7-c30				0.00192
htc-004ss-v7-c31				0.00192
htc-004ss-v7-c32				0.00192
htc-004ss-v7-c33				0.00192

**Table 6-29**  
**Experimental Parameters of Critical Experiments from KENO V.a Inputs**  
 (6 Pages)

Critical Experiment	Fuel Rod Radius (cm)	Fuel Pitch (cm)	Enrichment (wt. % <sup>235</sup> U)	H/X * Mod/Fuel Ratio	Mod/Fuel Ratio	Pu/(U+Pu)
MIX-COMP-THERM-002-001s	0.7176	1.7780	0.71	146.20	1.1946	0.0204
MIX-COMP-THERM-002-002s	0.7176	1.7780	0.71	146.15	1.1946	0.0204
MIX-COMP-THERM-002-003s	0.7176	2.2091	0.71	308.99	2.5249	0.0204
MIX-COMP-THERM-002-004s	0.7176	2.2091	0.71	308.83	2.5249	0.0204
MIX-COMP-THERM-002-005s	0.7176	2.5145	0.71	445.57	3.6410	0.0204
MIX-COMP-THERM-002-006s	0.7176	2.5145	0.71	445.41	3.6410	0.0204
MIX-COMP-THERM-004-001	0.6115	1.8250	0.71	407.06	2.4201	0.0300
MIX-COMP-THERM-004-002	0.6115	1.8250	0.71	408.32	2.4201	0.0299
MIX-COMP-THERM-004-003	0.6115	1.8250	0.71	409.62	2.4201	0.0298
MIX-COMP-THERM-004-004	0.6115	1.9560	0.71	500.49	2.9761	0.0300
MIX-COMP-THERM-004-005	0.6115	1.9560	0.71	502.17	2.9761	0.0299
MIX-COMP-THERM-004-006	0.6115	1.9560	0.71	505.29	2.9761	0.0298
MIX-COMP-THERM-004-007	0.6115	2.2250	0.71	712.57	4.2387	0.0300
MIX-COMP-THERM-004-008	0.6115	2.2250	0.71	715.24	4.2387	0.0299
MIX-COMP-THERM-004-009	0.6115	2.2250	0.71	717.56	4.2387	0.0298
MIX-COMP-THERM-004-010	0.6115	2.4740	0.71	933.51	5.5521	0.0300
MIX-COMP-THERM-004-011	0.6115	2.4740	0.71	936.95	5.5521	0.0299
mct005-01	0.7169	2.1590	0.71	157.55	1.9313	0.0399
mct005-02	0.7169	2.3622	0.71	209.30	2.5656	0.0399
mct005-03	0.7169	2.6670	0.71	295.65	3.6242	0.0399
mct005-04	0.7169	2.9032	0.71	369.77	4.5327	0.0399
mct005-05	0.7169	3.5204	0.71	593.11	7.2706	0.0399
mct005-06	0.7169	4.0640	0.71	825.34	10.1173	0.0399
mct005-07	0.7169	4.3180	0.71	945.27	11.5875	0.0399
mct006-01	0.7176	2.0320	0.71	185.10	1.5154	0.0204
mct006-02	0.7176	2.3622	0.71	303.87	2.4878	0.0204
mct006-03	0.7176	2.6670	0.71	429.36	3.5152	0.0204

**Table 6-29**  
**Experimental Parameters of Critical Experiments from KENO V.a Inputs**  
 (6 Pages)

Critical Experiment	Fuel Rod Radius (cm)	Fuel Pitch (cm)	Enrichment (wt. % <sup>235</sup> U)	H/X * Mod/Fuel Ratio	Mod/Fuel Ratio	Pu/(U+Pu)
mct006-04	0.7176	2.9032	0.71	537.06	4.3970	0.0204
mct006-05	0.7176	3.3528	0.71	767.30	6.2819	0.0204
mct006-06	0.7176	3.5204	0.71	861.62	7.0541	0.0204
mct006-07	0.7176	2.6670	0.71	429.36	3.5152	0.0204
mct006-08	0.7176	2.6670	0.71	429.36	3.5152	0.0204
mct006-09	0.7176	2.6670	0.71	429.36	3.5152	0.0204
mct006-10	0.7176	2.6670	0.71	429.36	3.5152	0.0204
mct006-11	0.7176	2.6670	0.71	429.36	3.5152	0.0204
mct006-12	0.7176	2.6670	0.71	429.36	3.5152	0.0204
mct006-13	0.7176	2.6670	0.71	429.36	3.5152	0.0204
mct006-14	0.7176	2.6670	0.71	429.36	3.5152	0.0204
mct006-15	0.7176	2.6670	0.71	429.36	3.5152	0.0204
mct006-16	0.7176	2.6670	0.71	429.36	3.5152	0.0204
mct006-29	0.7176	3.3528	0.71	767.30	6.2819	0.0204
mct006-30	0.7176	3.3528	0.71	767.30	6.2819	0.0204
mct006-31	0.7176	3.3528	0.71	767.30	6.2819	0.0204
mct006-32	0.7176	3.3528	0.71	767.30	6.2819	0.0204
mct006-33	0.7176	3.3528	0.71	767.30	6.2819	0.0204
mct006-34	0.7176	3.3528	0.71	767.30	6.2819	0.0204
mct006-35	0.7176	3.3528	0.71	767.30	6.2819	0.0204
mct006-36	0.7176	3.3528	0.71	767.30	6.2819	0.0204
mct006-37	0.7176	3.3528	0.71	767.30	6.2819	0.0204
mct006-38	0.7176	3.3528	0.71	767.30	6.2819	0.0204
mct007-01	0.7176	2.3622	0.71	331.88	2.4878	0.0199
mct007-02	0.7176	2.6670	0.71	468.80	3.5152	0.0199
mct007-03	0.7176	2.9032	0.71	586.82	4.3970	0.0199
mct007-04	0.7176	3.3528	0.71	837.39	6.2819	0.0199

**Table 6-29**  
**Experimental Parameters of Critical Experiments from KENO V.a Inputs**  
 (6 Pages)

Critical Experiment	Fuel Rod Radius (cm)	Fuel Pitch (cm)	Enrichment (wt. % <sup>235</sup> U)	H/X * Mod/Fuel Ratio	Mod/Fuel Ratio	Pu/(U+Pu)
mct007-05	0.7176	3.5204	0.71	940.14	7.0541	0.0199
MIX-COMP-THERM-008-001	0.7176	2.0320	0.71	214.99	1.5154	0.0200
MIX-COMP-THERM-008-002	0.7176	2.3622	0.71	352.84	2.4878	0.0200
MIX-COMP-THERM-008-003	0.7176	2.6670	0.71	498.82	3.5152	0.0200
MIX-COMP-THERM-008-004	0.7176	2.9032	0.71	644.61	4.3970	0.0200
MIX-COMP-THERM-008-005	0.7176	3.3528	0.71	891.82	6.2819	0.0200
MIX-COMP-THERM-008-006	0.7176	3.5204	0.71	1000.44	7.0541	0.0200
MIX-COMP-THERM-008-007	0.7176	2.6670	0.71	498.82	3.5152	0.0200
MIX-COMP-THERM-008-008	0.7176	2.6670	0.71	498.82	3.5152	0.0200
MIX-COMP-THERM-008-009	0.7176	2.6670	0.71	498.82	3.5152	0.0200
MIX-COMP-THERM-008-010	0.7176	2.6670	0.71	498.82	3.5152	0.0200
MIX-COMP-THERM-008-011	0.7176	2.6670	0.71	498.82	3.5152	0.0200
MIX-COMP-THERM-008-012	0.7176	2.6670	0.71	498.82	3.5152	0.0200
MIX-COMP-THERM-008-013	0.7176	2.6670	0.71	498.82	3.5152	0.0200
MIX-COMP-THERM-008-014	0.7176	2.6670	0.71	498.82	3.5152	0.0200
MIX-COMP-THERM-008-015	0.7176	2.6670	0.71	498.82	3.5152	0.0200
MIX-COMP-THERM-008-016	0.7176	2.6670	0.71	498.82	3.5152	0.0200
MIX-COMP-THERM-009-001	0.5385	1.3970	0.16	226.05	1.1112	0.0150
MIX-COMP-THERM-009-002	0.5385	1.5240	0.16	319.23	1.5694	0.0150
MIX-COMP-THERM-009-003	0.5385	1.8034	0.16	552.76	2.7176	0.0150
MIX-COMP-THERM-009-004	0.5385	2.0320	0.16	773.01	3.8005	0.0150
MIX-COMP-THERM-009-005	0.5385	2.2860	0.16	1048.53	5.1551	0.0150
MIX-COMP-THERM-009-006	0.5385	2.3622	0.16	1137.57	5.5925	0.0150
htc-001-v7-c01	0.4750	2.300	1.57	1149.27	9.2522	0.0110
htc-001-v7-c02	0.4750	2.300	1.57	1149.55	9.2522	0.0110
htc-001-v7-c03	0.4750	2.300	1.57	1149.55	9.2522	0.0110
htc-001-v7-c04	0.4750	1.900	1.57	727.99	5.8593	0.0110

**Table 6-29**  
**Experimental Parameters of Critical Experiments from KENO V.a Inputs**  
 (6 Pages)

Critical Experiment	Fuel Rod Radius (cm)	Fuel Pitch (cm)	Enrichment (wt. % <sup>235</sup> U)	H/X * Mod/Fuel Ratio	Mod/Fuel Ratio	Pu/(U+Pu)
htc-001-v7-c05	0.4750	1.900	1.57	727.99	5.8593	0.0110
htc-001-v7-c06	0.4750	1.900	1.57	727.99	5.8593	0.0110
htc-001-v7-c07	0.4750	1.700	1.57	547.32	4.4051	0.0110
htc-001-v7-c08	0.4750	1.700	1.57	547.32	4.4051	0.0110
htc-001-v7-c09	0.4750	1.700	1.57	547.32	4.4051	0.0110
htc-001-v7-c10	0.4750	1.500	1.57	386.76	3.1126	0.0110
htc-001-v7-c11	0.4750	1.500	1.57	386.76	3.1126	0.0110
htc-001-v7-c12	0.4750	1.500	1.57	386.76	3.1126	0.0110
htc-001-v7-c13	0.4750	1.300	1.57	246.23	1.9816	0.0110
htc-001-v7-c14	0.4750	1.300	1.57	246.23	1.9816	0.0110
htc-001-v7-c15	0.4750	1.300	1.57	246.23	1.9816	0.0110
htc-001-v7-c16	0.4750	1.700	1.57	547.43	4.4051	0.0110
htc-001-v7-c17	0.4750	1.700	1.57	547.43	4.4051	0.0110
htc-001-v7-c18	0.4750	1.700	1.57	547.43	4.4051	0.0110
htc-003-v7-c01	0.4750	1.600	1.57	466.21	3.7387	0.0110
htc-003-v7-c02	0.4750	1.600	1.57	466.21	3.7387	0.0110
htc-003-v7-c03	0.4750	1.600	1.57	466.21	3.7387	0.0110
htc-003-v7-c04	0.4750	1.600	1.57	466.21	3.7387	0.0110
htc-003-v7-c05	0.4750	1.600	1.57	466.21	3.7387	0.0110
htc-003-v7-c06	0.4750	1.600	1.57	466.16	3.7387	0.0110
htc-003-v7-c12	0.4750	1.600	1.57	466.15	3.7387	0.0110
htc-003-v7-c13	0.4750	1.600	1.57	466.27	3.7387	0.0110
htc-003-v7-c14	0.4750	1.600	1.57	466.27	3.7387	0.0110
htc-003-v7-c15	0.4750	1.600	1.57	466.27	3.7387	0.0110
htc-003-v7-c16	0.4750	1.600	1.57	466.27	3.7387	0.0110
htc-003-v7-c17	0.4750	1.600	1.57	466.27	3.7387	0.0110
htc-003-v7-c18	0.4750	1.600	1.57	466.27	3.7387	0.0110

**Table 6-29**  
**Experimental Parameters of Critical Experiments from KENO V.a Inputs**  
 (6 Pages)

Critical Experiment	Fuel Rod Radius (cm)	Fuel Pitch (cm)	Enrichment (wt. % <sup>235</sup> U)	H/X * Mod/Fuel Ratio	Mod/Fuel Ratio	Pu/(U+Pu)
htc-003-v7-c19	0.4750	1.600	1.57	466.27	3.7387	0.0110
htc-003-v7-c20	0.4750	1.600	1.57	466.27	3.7387	0.0110
htc-003-v7-c21	0.4750	1.600	1.57	466.27	3.7387	0.0110
htc-003-v7-c22	0.4750	1.600	1.57	466.27	3.7387	0.0110
htc-003-v7-c23	0.4750	1.600	1.57	466.27	3.7387	0.0110
htc-003-v7-c24	0.4750	1.600	1.57	466.32	3.7387	0.0110
htc-003-v7-c25	0.4750	1.600	1.57	466.32	3.7387	0.0110
htc-003-v7-c26	0.4750	1.600	1.57	466.32	3.7387	0.0110
htc-004pb-v7-c01	0.4750	1.600	1.57	466.05	3.7387	0.0110
htc-004pb-v7-c02	0.4750	1.600	1.57	466.05	3.7387	0.0110
htc-004pb-v7-c03	0.4750	1.600	1.57	466.05	3.7387	0.0110
htc-004pb-v7-c04	0.4750	1.600	1.57	466.05	3.7387	0.0110
htc-004pb-v7-c05	0.4750	1.600	1.57	466.05	3.7387	0.0110
htc-004pb-v7-c06	0.4750	1.600	1.57	466.05	3.7387	0.0110
htc-004pb-v7-c07	0.4750	1.600	1.57	465.98	3.7387	0.0110
htc-004pb-v7-c08	0.4750	1.600	1.57	465.98	3.7387	0.0110
htc-004pb-v7-c09	0.4750	1.600	1.57	466.05	3.7387	0.0110
htc-004pb-v7-c10	0.4750	1.600	1.57	466.05	3.7387	0.0110
htc-004pb-v7-c11	0.4750	1.600	1.57	466.05	3.7387	0.0110
htc-004pb-v7-c12	0.4750	1.600	1.57	466.27	3.7387	0.0110
htc-004pb-v7-c13	0.4750	1.600	1.57	466.27	3.7387	0.0110
htc-004pb-v7-c14	0.4750	1.600	1.57	466.27	3.7387	0.0110
htc-004pb-v7-c15	0.4750	1.600	1.57	466.47	3.7387	0.0110
htc-004pb-v7-c16	0.4750	1.600	1.57	466.47	3.7387	0.0110
htc-004ss-v7-c01	0.4750	1.600	1.57	466.14	3.7387	0.0110
htc-004ss-v7-c02	0.4750	1.600	1.57	466.21	3.7387	0.0110
htc-004ss-v7-c03	0.4750	1.600	1.57	466.21	3.7387	0.0110

**Table 6-29**  
**Experimental Parameters of Critical Experiments from KENO V.a Inputs**  
 (6 Pages)

Critical Experiment	Fuel Rod Radius (cm)	Fuel Pitch (cm)	Enrichment (wt. % <sup>235</sup> U)	H/X * Mod/Fuel Ratio	Mod/Fuel Ratio	Pu/(U+Pu)
htc-004ss-v7-c04	0.4750	1.600	1.57	466.56	3.7387	0.0110
htc-004ss-v7-c05	0.4750	1.600	1.57	466.56	3.7387	0.0110
htc-004ss-v7-c06	0.4750	1.600	1.57	466.56	3.7387	0.0110
htc-004ss-v7-c07	0.4750	1.600	1.57	466.59	3.7387	0.0110
htc-004ss-v7-c08	0.4750	1.600	1.57	466.59	3.7387	0.0110
htc-004ss-v7-c09	0.4750	1.600	1.57	466.59	3.7387	0.0110
htc-004ss-v7-c10	0.4750	1.600	1.57	466.59	3.7387	0.0110
htc-004ss-v7-c11	0.4750	1.600	1.57	466.59	3.7387	0.0110
htc-004ss-v7-c12	0.4750	1.600	1.57	466.27	3.7387	0.0110
htc-004ss-v7-c13	0.4750	1.600	1.57	466.35	3.7387	0.0110
htc-004ss-v7-c22	0.4750	1.600	1.57	466.27	3.7387	0.0110
htc-004ss-v7-c23	0.4750	1.600	1.57	466.11	3.7387	0.0110
htc-004ss-v7-c24	0.4750	1.600	1.57	466.11	3.7387	0.0110
htc-004ss-v7-c25	0.4750	1.600	1.57	466.11	3.7387	0.0110
htc-004ss-v7-c26	0.4750	1.600	1.57	466.11	3.7387	0.0110
htc-004ss-v7-c27	0.4750	1.600	1.57	466.11	3.7387	0.0110
htc-004ss-v7-c28	0.4750	1.600	1.57	466.11	3.7387	0.0110
htc-004ss-v7-c29	0.4750	1.600	1.57	466.11	3.7387	0.0110
htc-004ss-v7-c30	0.4750	1.600	1.57	466.11	3.7387	0.0110
htc-004ss-v7-c31	0.4750	1.600	1.57	466.11	3.7387	0.0110
htc-004ss-v7-c32	0.4750	1.600	1.57	466.11	3.7387	0.0110
htc-004ss-v7-c33	0.4750	1.600	1.57	466.11	3.7387	0.0110



**Table 6-30**  
**Correlation Coefficient Determined from Critical Experiments**

Parameters	r
<sup>235</sup> U wt.% Enrichment	<b>0.4867</b>
Fuel Pitch	-0.3624
EALF	[       ]
AEG	[       ]
Fuel Rod Radius	-0.4210
Moderator to Fuel Ratio	[       ]
Hydrogen to Fissile Density Ratio	-0.1487
Plutonium Content	-0.0978

**Table 6-31**  
**Area of Applicability**

Parameters	Range		Application	AOA Covers Application?
	Min	Max		
<sup>235</sup> U wt. % Enrichment	0.16	1.57	1.34	Yes
Fuel Pitch	1.3	4.318	1.3958	Yes
EALF	[       ]	[       ]	0.32198	Yes
AEG	[       ]	[       ]	195.64	Yes
Fuel Rod Radius	0.475	0.7176	0.461	No <sup>(1)</sup>
Moderator to Fuel Ratio	1.1112	11.588	2.430	Yes
Hydrogen to Fissile Density Ratio	146.15	1149.6	304.42	Yes
Plutonium Content	0.0110	0.0399	0.0153	Yes

- Note that the fuel rod radius is reduced by [       ] for the most reactive application configuration. However, the full thickness of the fuel rod of the baseline case is a radius of [       ] Additionally, the application's fuel pellet radius is covered by the range represented in the critical experiments.

**Table 6-32**  
**USL Determined Using Computational Method for Critical Experiments**

USL-Computational Method	
n	157
$\Delta_{SM}$	0.05
$\overline{\sigma}^2$	1.0852E-05
$\overline{k_{eff}}$	0.99834
$s^2$	7.1973E-06
$S_p$	4.2485E-03
$\beta$	0.9997
NPM	0.0
Smallest $k_{eff}$	0.98591
Uncertainty for Smallest $k_{eff}$	0.00800
$K_L$	0.9779
$\Delta_{AOA}$	0.00
USL	0.9279

**Table 6-33**  
**Qualitative Comparison of Fuel Characteristics**

Parameter	Westinghouse 17×17 OFA		AMBW	
	Dimensions (inches)	Dimensions (cm)	Dimensions (inches)	Dimensions (cm)
Fuel Pellet Diameter	0.3088	0.7844	0.3225	0.8192
Fuel Pellet Material	UO <sub>2</sub>		UO <sub>2</sub>	
Cladding Inside Diameter	0.3150	0.8001	0.329	0.8357
Cladding Outside Diameter	0.3600	0.9144	0.374	0.9500
Cladding Radial Thickness	0.0225	0.0572	0.0225	0.0572
Fuel Cladding Material	Zircaloy-4		Zircaloy-4	
Fuel Rod Pitch	0.4960	1.2598	0.496	1.2598
Moderator Material	H <sub>2</sub> O		H <sub>2</sub> O	
Guide/Instrument Tube ID	0.4420	1.1227	0.450	1.1430
Guide/Instrument Tube OD	0.4740	1.2040	0.482	1.2243
Guide/Instrument Tube Thickness	0.0160	0.0406	0.016	0.0406
Active Fuel Length	144	365.76	144	365.76
Number of Fuel Rods	264		264	
Number of Guide Tubes	24		24	
Number of Instrument Tubes	1		1	

**Table 6-34**  
**Qualitative Comparison of Basket and Cask Characteristics**

Components/Parameters	GBC-32	TN-32B HBU Demonstration Cask
Poison Plate Material	Boral®	Borated Aluminum
B-10 Areal Density	22.5 mg B-10/cm <sup>2</sup>	9.0 mg B-10/cm <sup>2</sup>
Poison Plate Thickness	0.25654 cm	0.1016 cm
Cask Outer Shell Thickness	20 cm	24.13 cm
Cask Outer Shell Material	Steel	Steel
Fuel Compartment Cell Pitch <sup>(1)</sup>	23.7565 cm	22.2123 cm
Fuel Assembly	Westinghouse 17×17 OFA	AMBW

1. Fuel compartment cell pitch is the fuel compartment inner width plus the fuel compartment thickness

**Table 6-35**  
**Comparison of Global Parameters – Criticality**

Burnup (GWd/MTU)	GBC-32			TN-32B HBU Demonstration Cask		
	k <sub>keno</sub>	σ	k <sub>eff</sub>	k <sub>keno</sub>	σ	k <sub>eff</sub>
50	0.92131	0.00048	0.92227	0.89843	0.00049	0.89941
57	0.89687	0.00049	0.89785	0.87529	0.00047	0.87623

**Table 6-36**  
**Comparison of Global Parameters – Energy of Average Lethargy Causing Fission (EALF)**

Burnup (GWd/MTU)	GBC-32		TN-32B HBU Demonstration Cask	
	EALF	σ	EALF	σ
50	0.320834	0.000446	0.415425	0.000775
57	0.327918	0.000520	0.425442	0.000918

**Table 6-37**  
**Comparison of Global Parameters – Average Energy Fission Group**

Burnup (GWd/MTU)	GBC-32		TN-32B HBU Demonstration Cask	
	AEG	σ	AEG	σ
50	195.698	0.015369	192.545	0.020398
57	195.531	0.017518	192.379	0.023452

**Table 6-38**  
**Comparison of Global Parameters – Moderator-to-Fuel Volume Ratio**

Parameter	Westinghouse 17×17 OFA	AMBW
Pitch (cm)	1.2598	1.2598
Clad Diameter (cm)	0.9144	0.9500
Fuel Diameter (cm)	0.7844	0.8192
Pitch Area (cm <sup>2</sup> )	1.5871	1.5871
Fuel Rod Area (cm <sup>2</sup> )	0.6567	0.7088
Fuel Pellet Area (cm <sup>2</sup> )	0.4832	0.5271
$V_m/V_f$	1.9253	1.6663

**Table 6-39**  
**Comparison of Global Parameters – H/X Ratio**

Burnup (GWd/MTU)	GBC-32	TN-32B HBU Demonstration Cask
	H/X Ratio	H/X Ratio
50	236.050	204.295
57	260.925	225.824

**Table 6-40**  
**Similarity Analysis –  $c_k$  Parameter Results**

Burnup (GWd/MTU)	Correlation Coefficient	
	$c_k$	$\sigma$
50	0.9967	0.0006
57	0.9965	0.0005

**Table 6-41**  
**Minor Actinides and Fission Product Worth**

	$k_{KENO}$	$\sigma_{KENO}$	$k_{KENO} + 2\sigma_{KENO}$	$\Delta k_{eff}$
HACarray_ctxxxx_e46_bu50_emd030	[REDACTED]	[REDACTED]	0.89554	0.09508
HACarray_ctxxxx_e46_bu50_emd030_noMinAFP			0.99062	

Proprietary Information on This Page  
Withheld Pursuant to 10 CFR 2.390

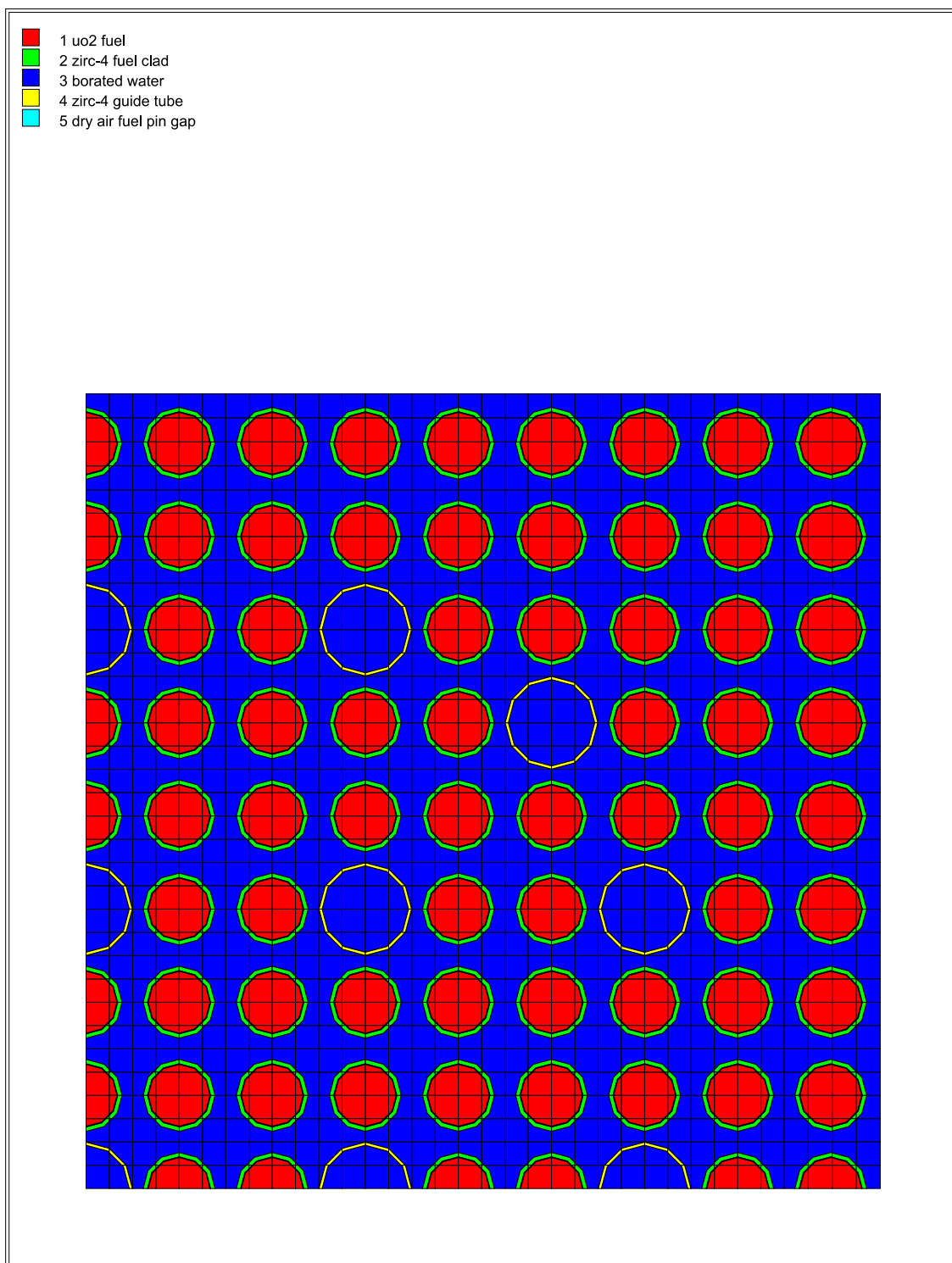


**Figure 6-2**  
**TN-32B HBU Demonstration Cask Model of 17×17 Quadrant-Symmetric Fuel Assembly**  
**without BPRAs**

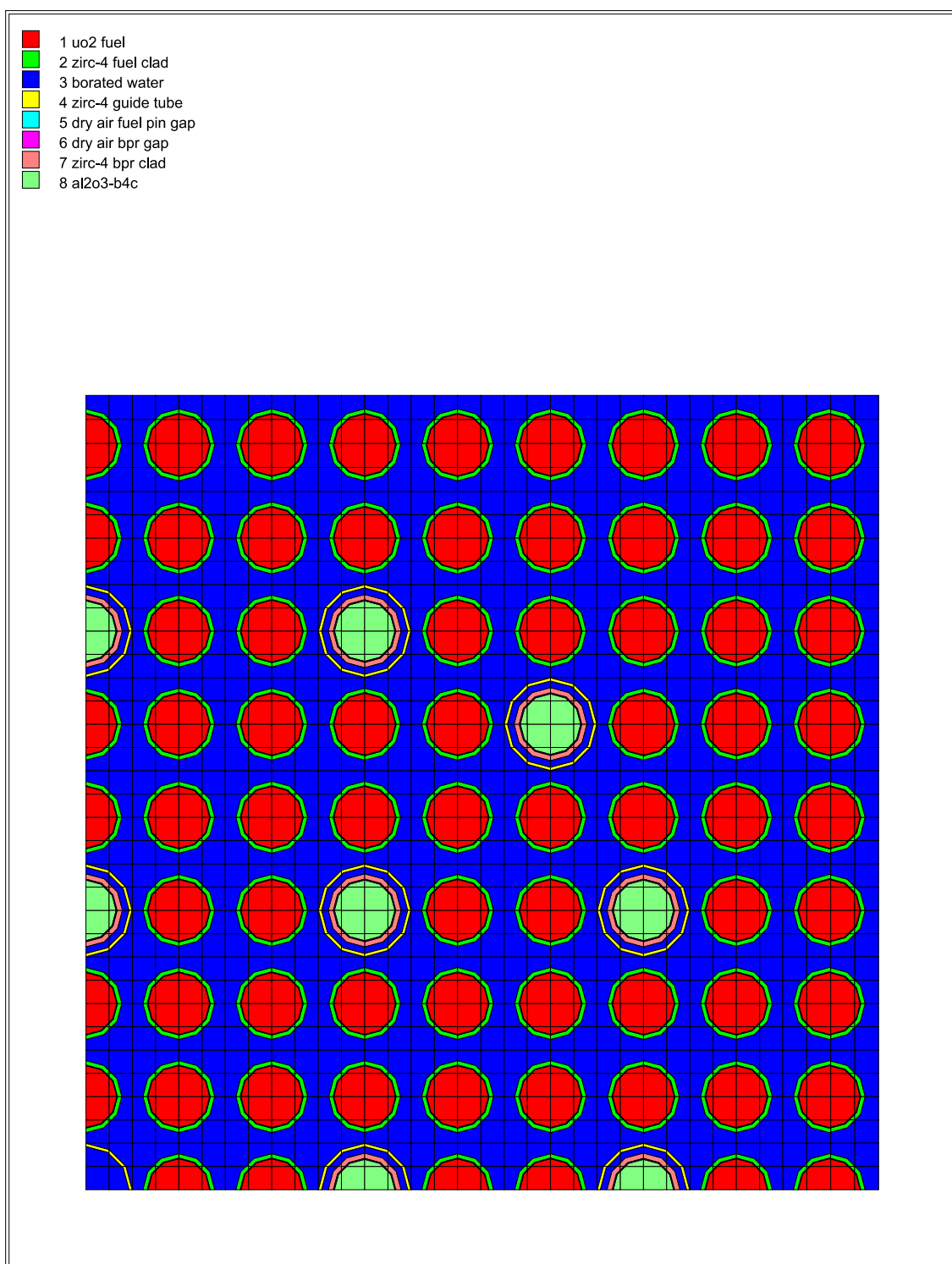


**Figure 6-3**  
**TN-32B HBU Demonstration Cask Model of 17×17 Quadrant-Symmetric Fuel Assembly with BPRAs**



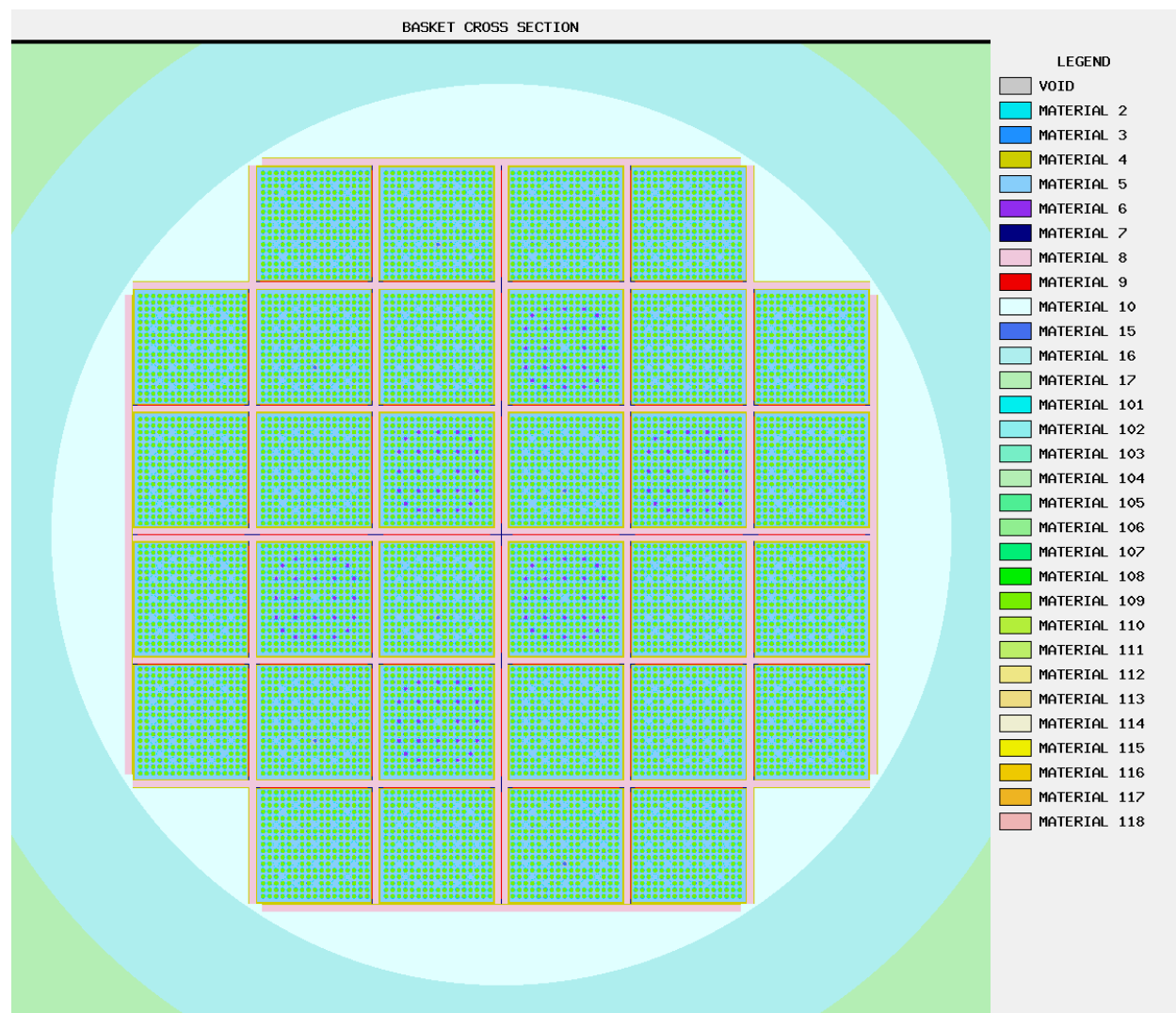


**Figure 6-4**  
**Full Cask Cross Section of the TN-32B HBU Cask Basket**

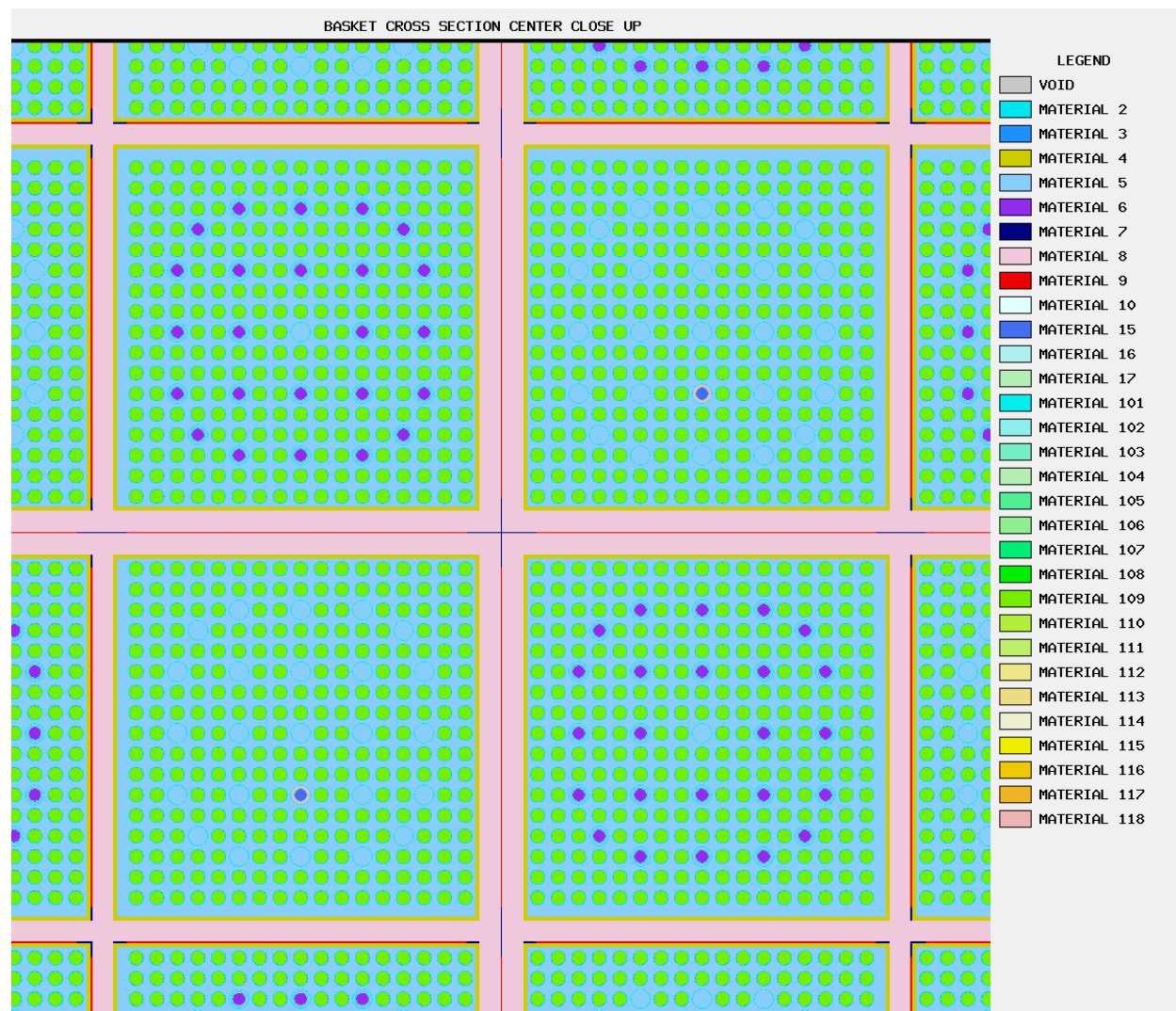


**Figure 6-5**  
**Close-Up Cross Section Center of the TN-32B HBU Cask Basket**

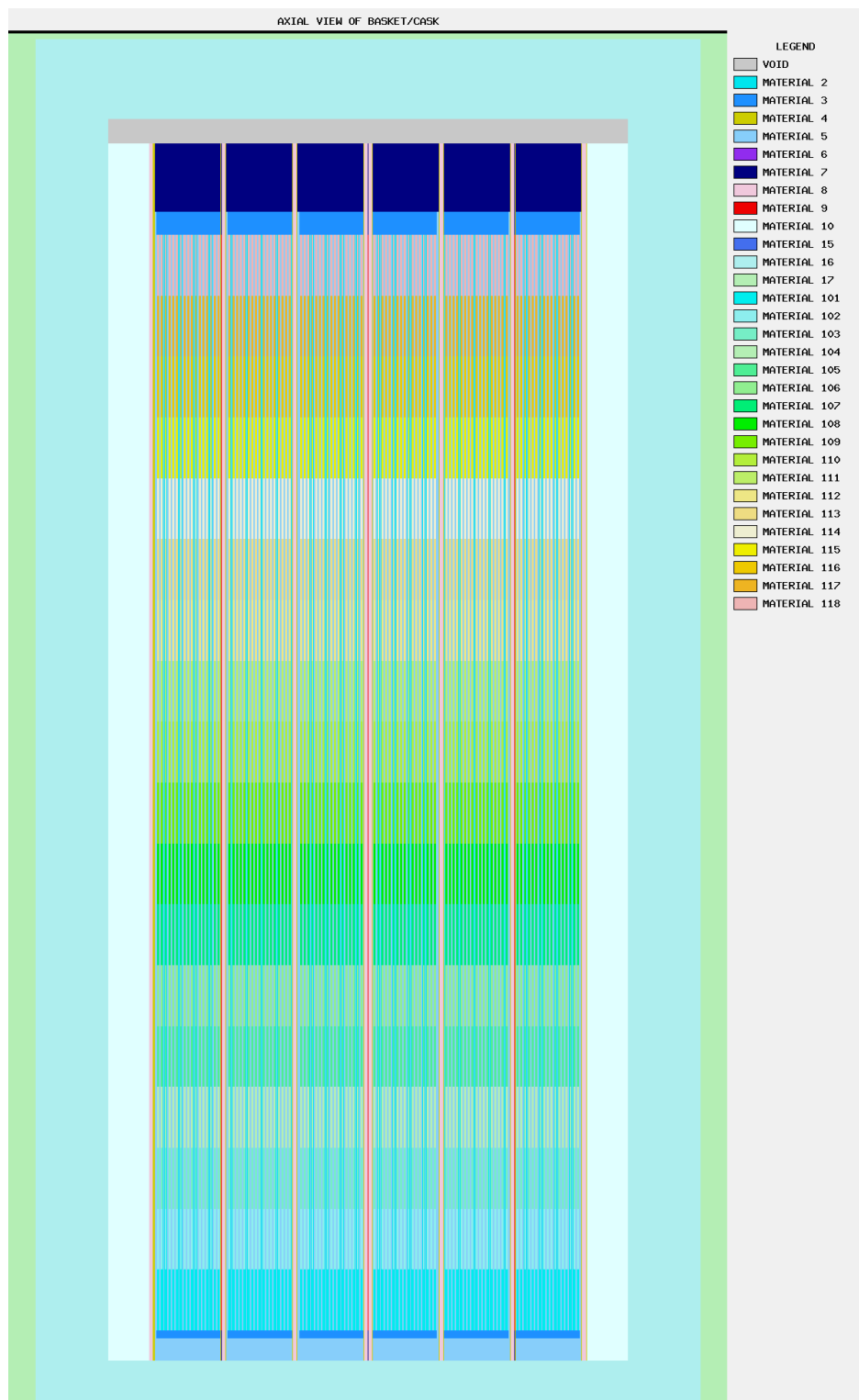


**Figure 6-6**  
**Cross Section of the Fuel Axially Centered**

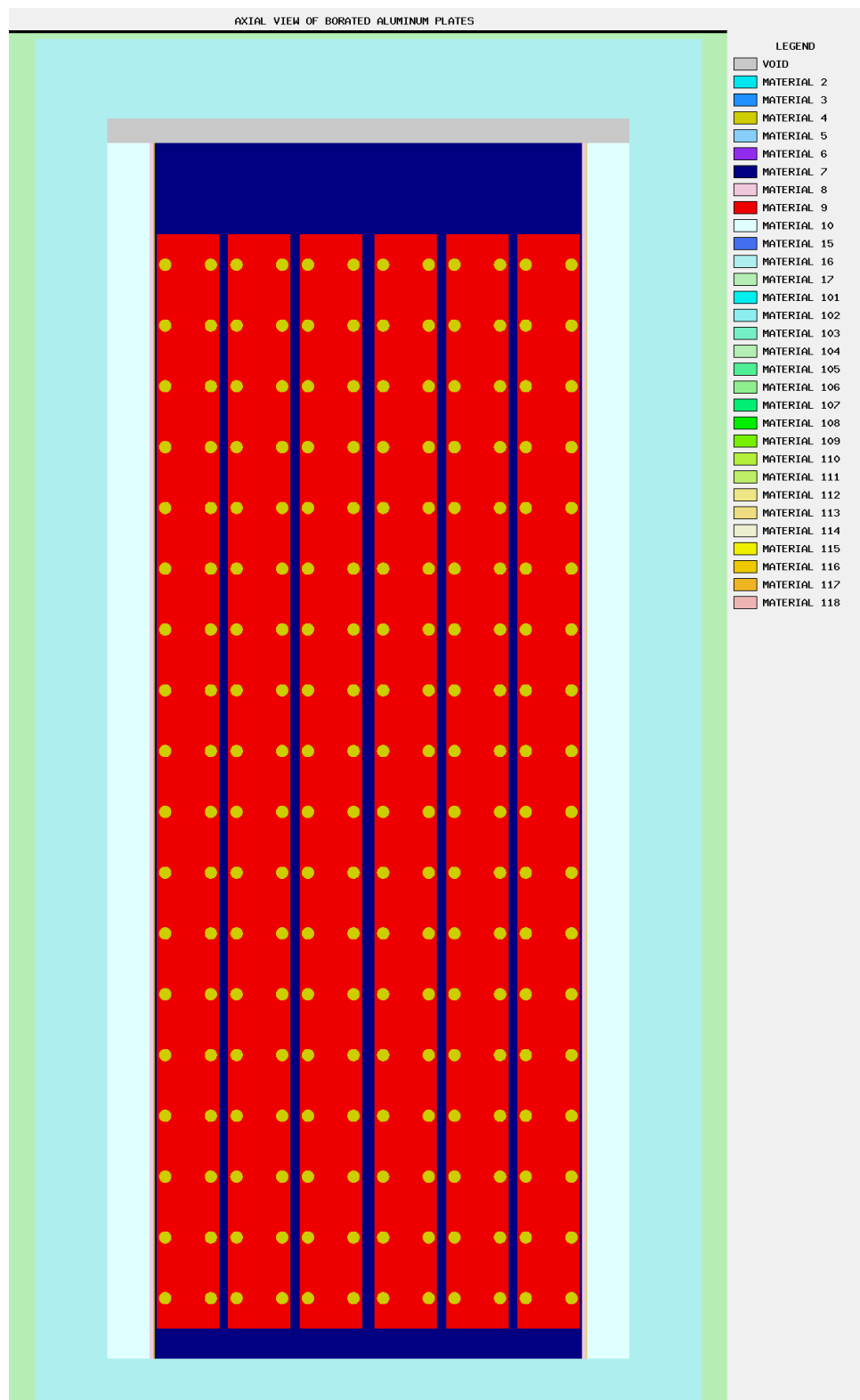


**Figure 6-7**  
**Axial Cross Section of the Borated Aluminum Plates**

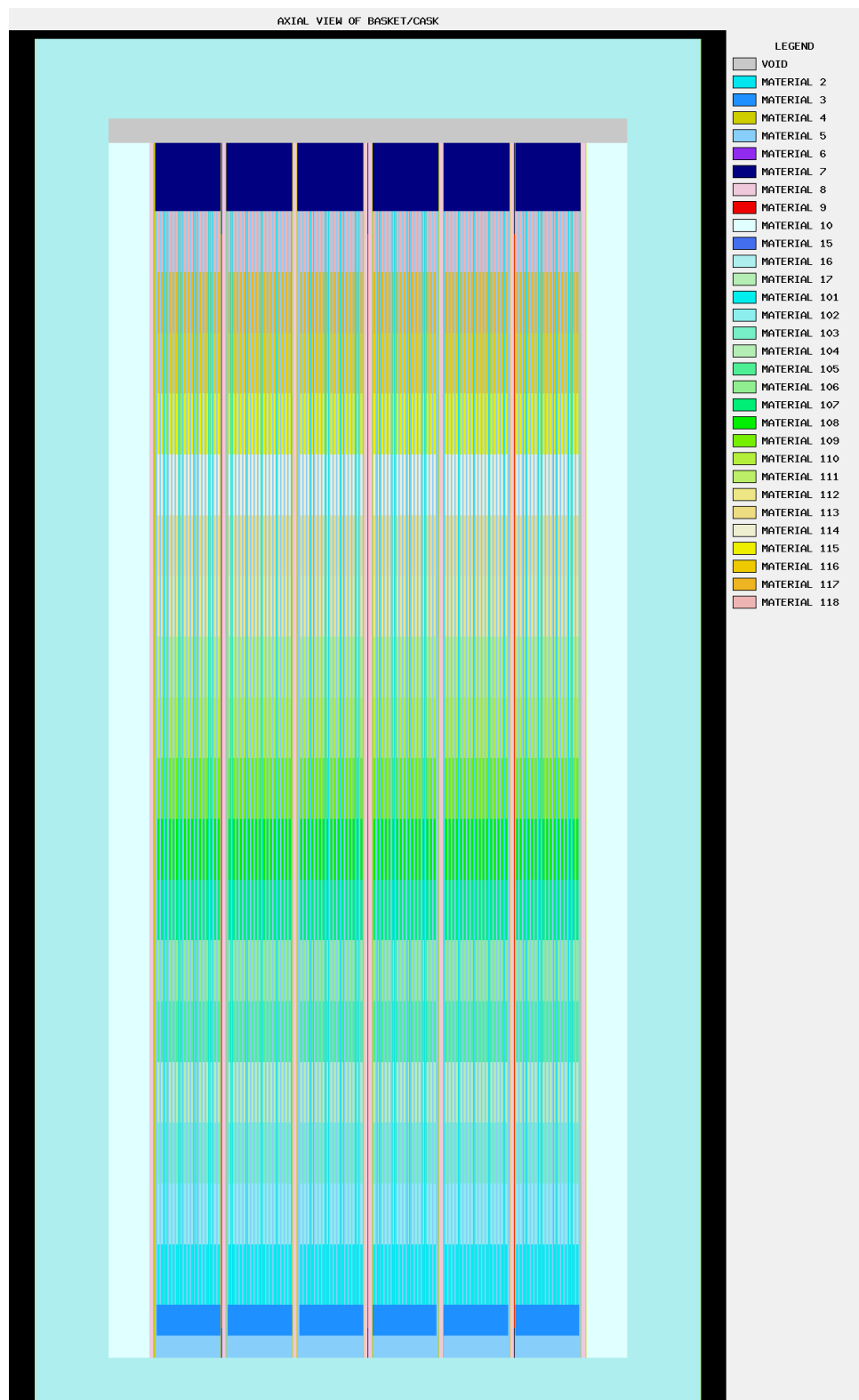


Figure 6-8  
Axial View with Fuel Shifted [ ]

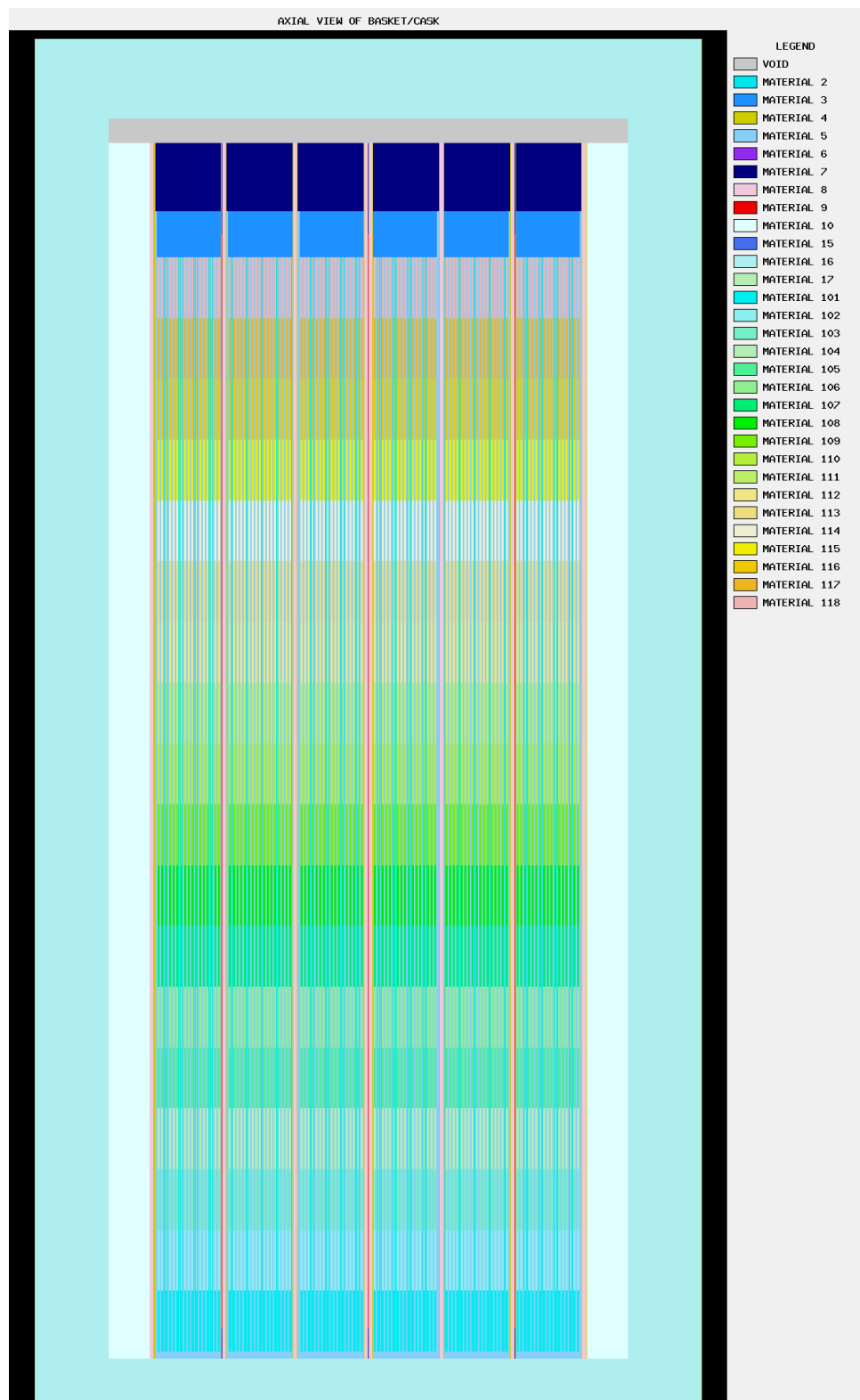
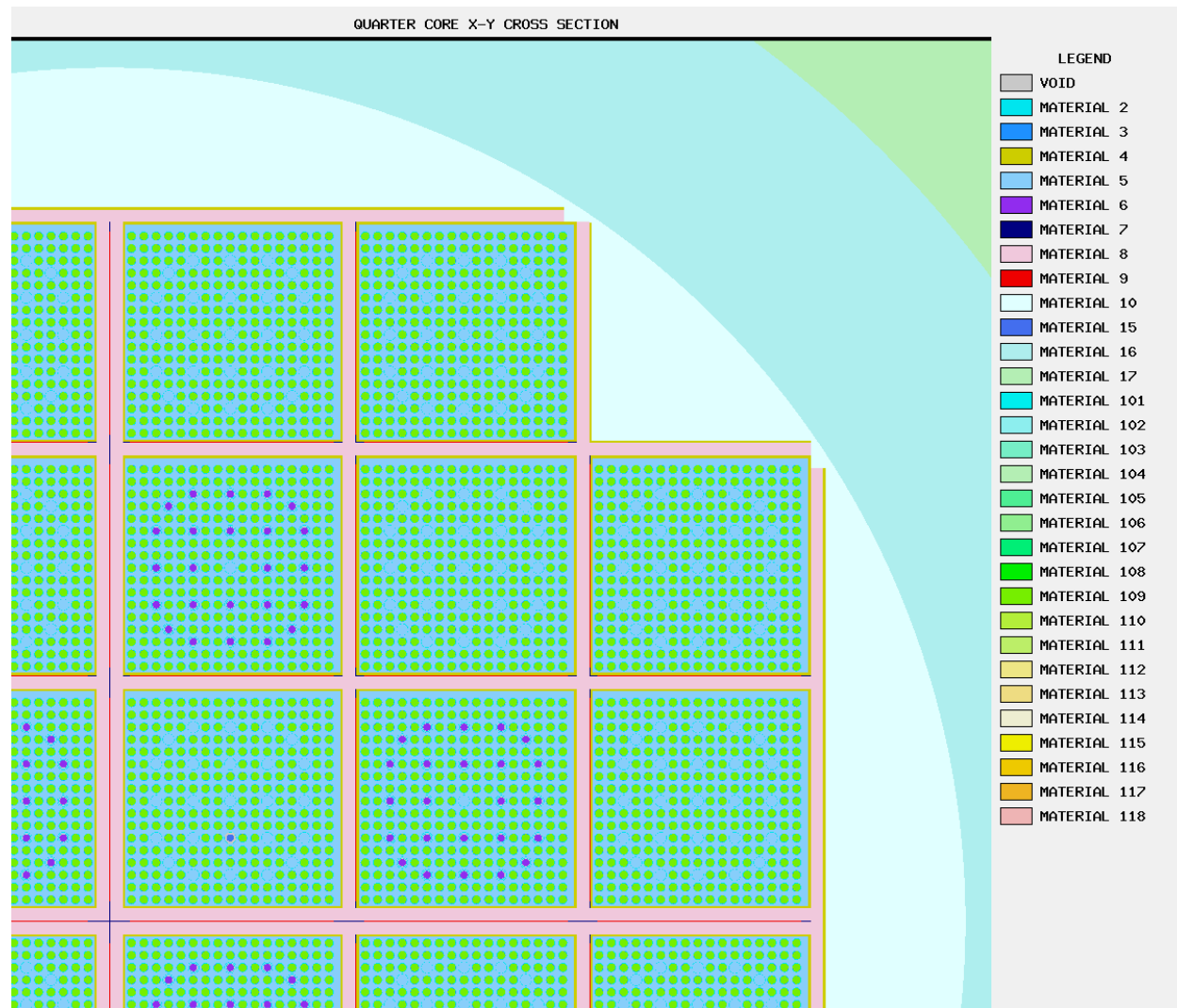


Figure 6-9  
Axial View with Fuel Shifted [ ]



**Figure 6-10**  
**Minimum Fuel Compartment Dimension Quarter Core**

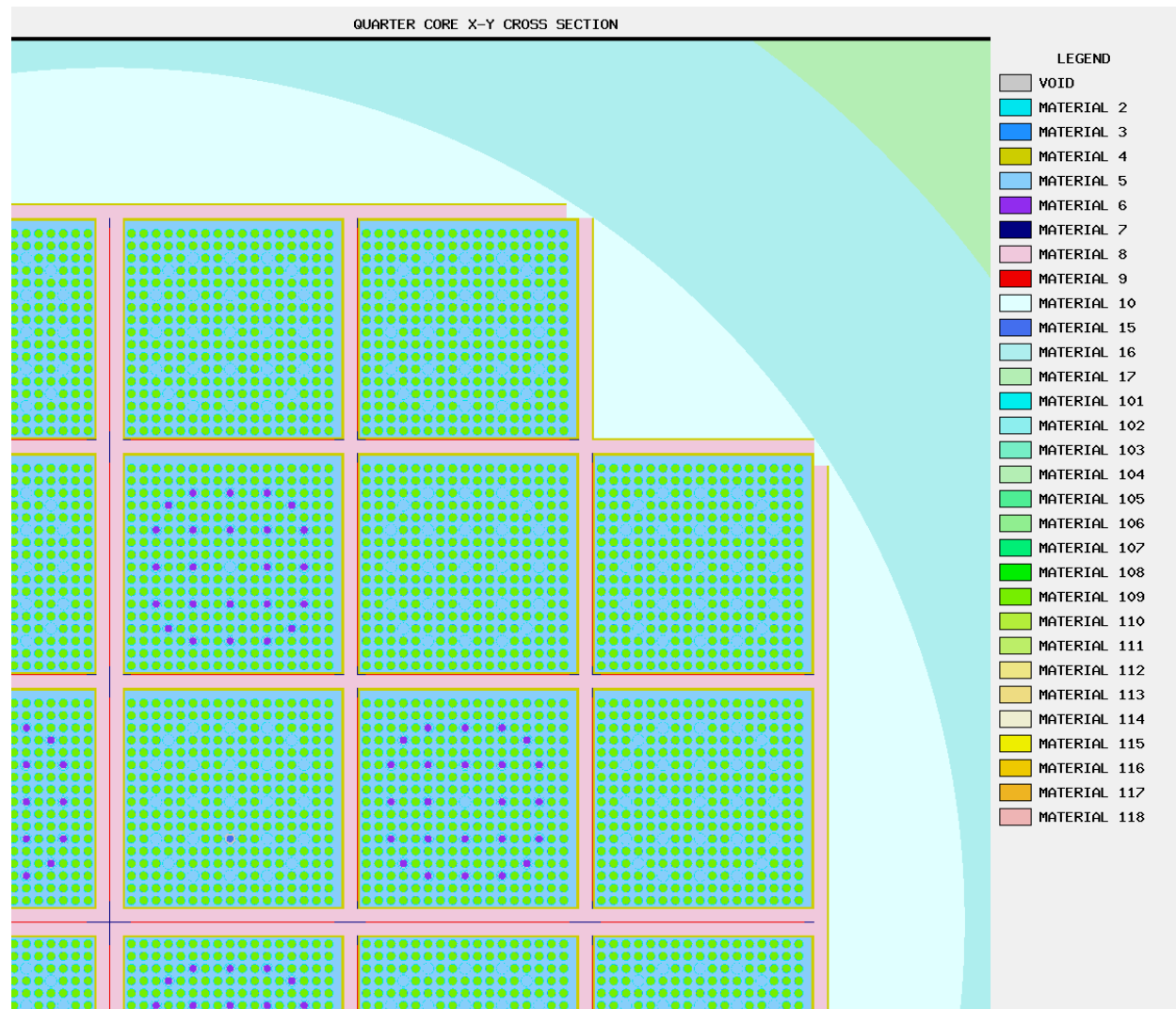
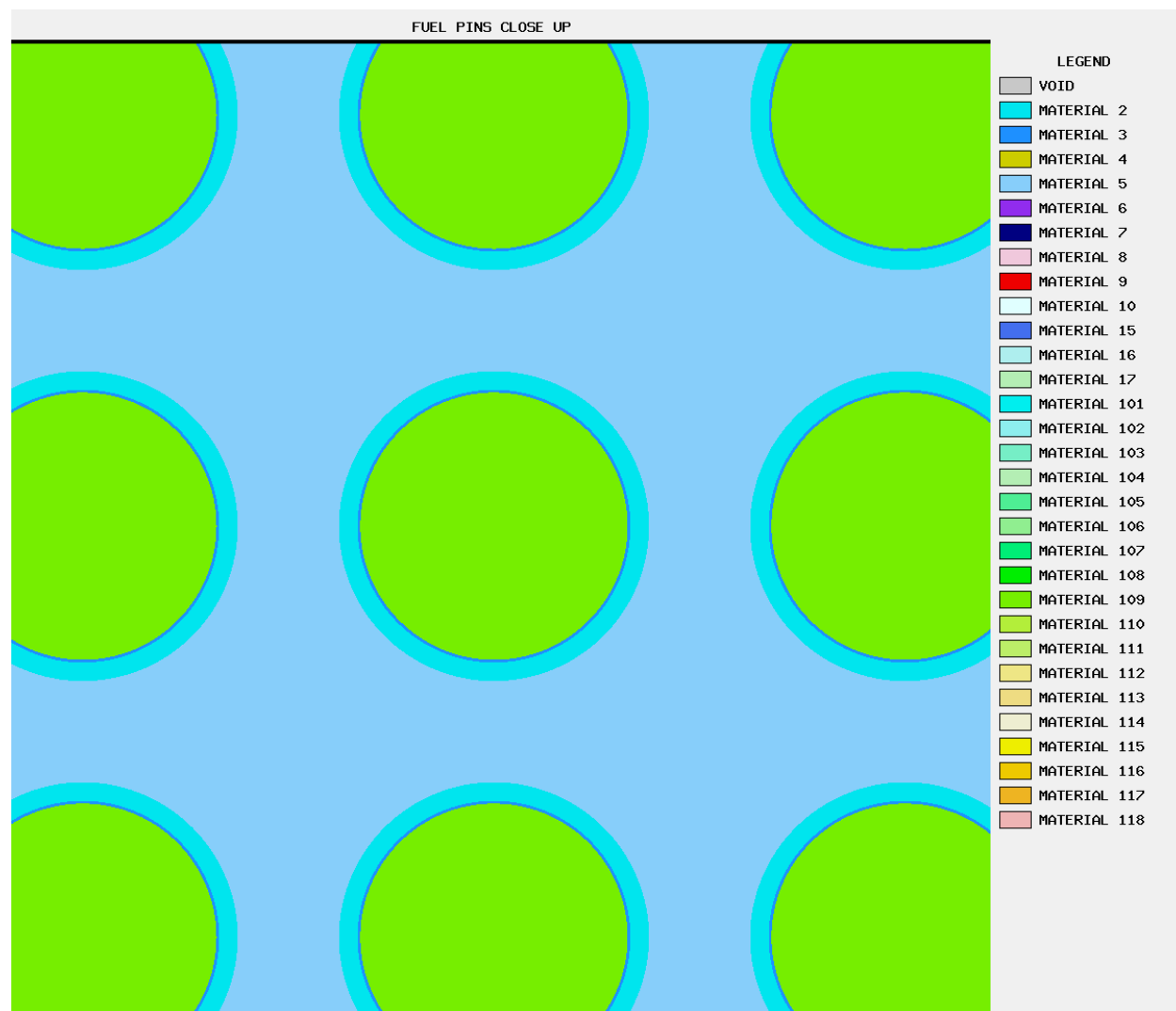
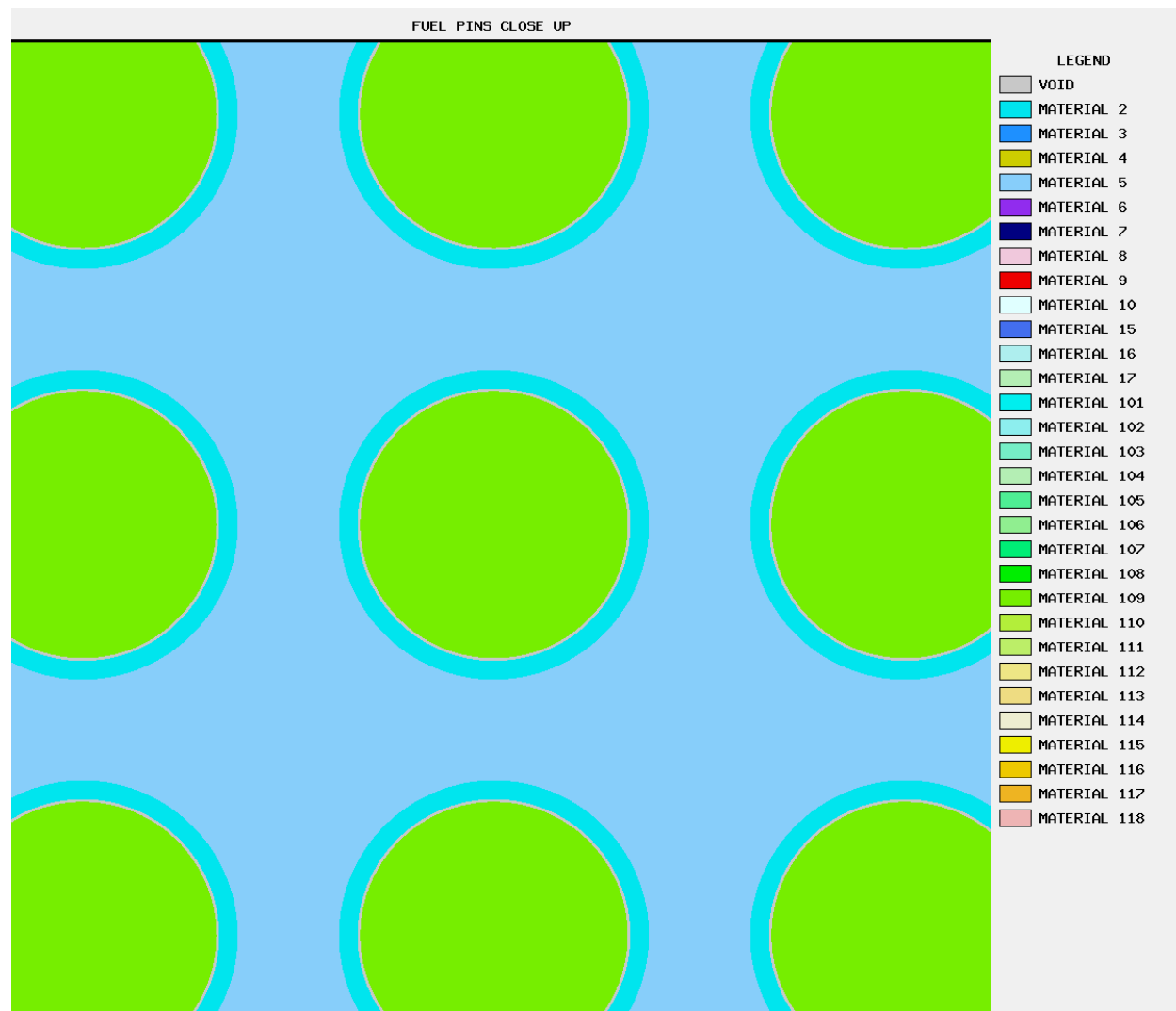


Figure 6-11  
Maximum Fuel Compartment Dimension Quarter Core





**Figure 6-12**  
**Fuel Cladding Gap with Water**



**Figure 6-13**  
**Fuel Cladding Gap with Void**

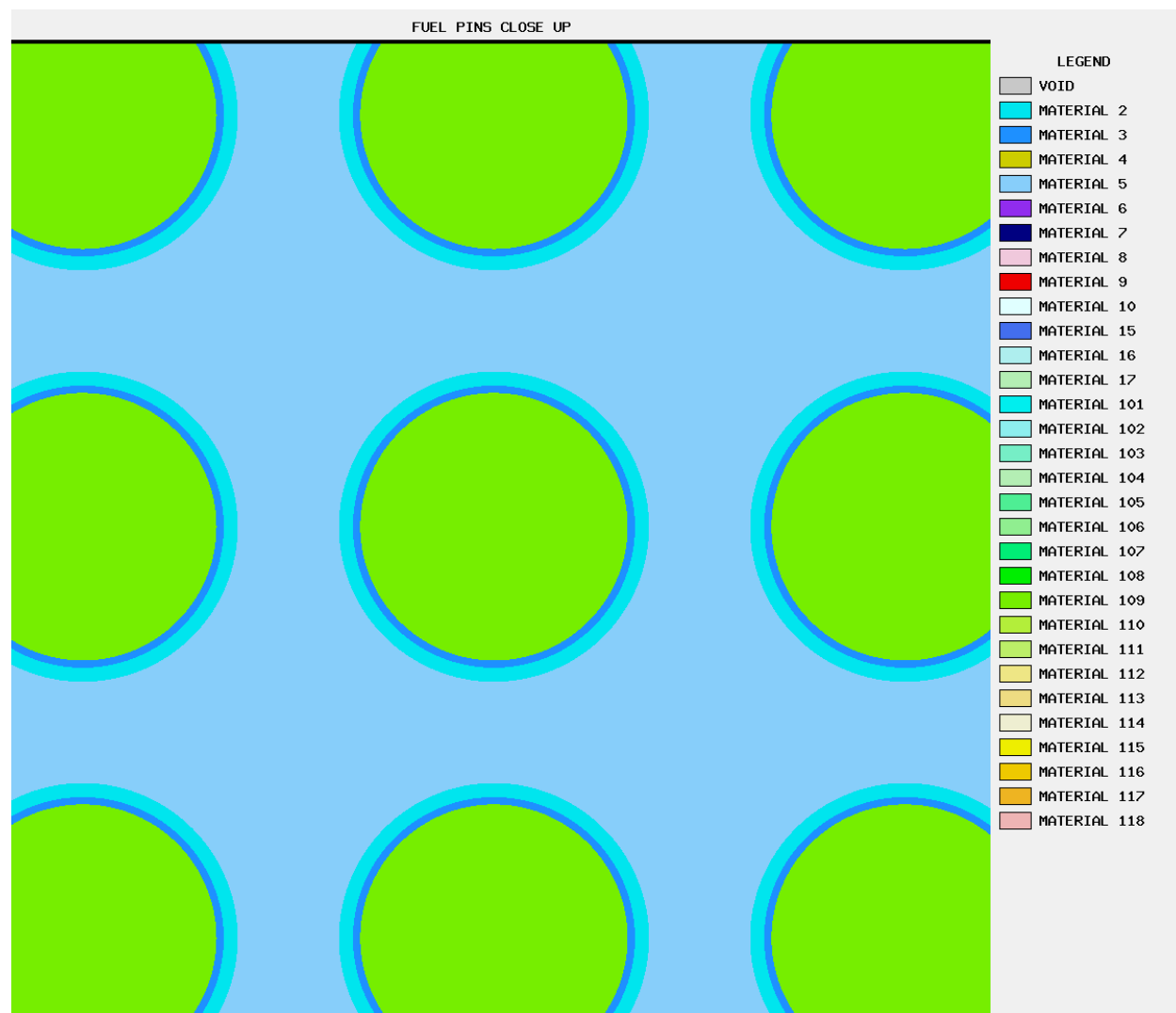


Figure 6-14  
[ ] Clad Thinning – Expanding Gap

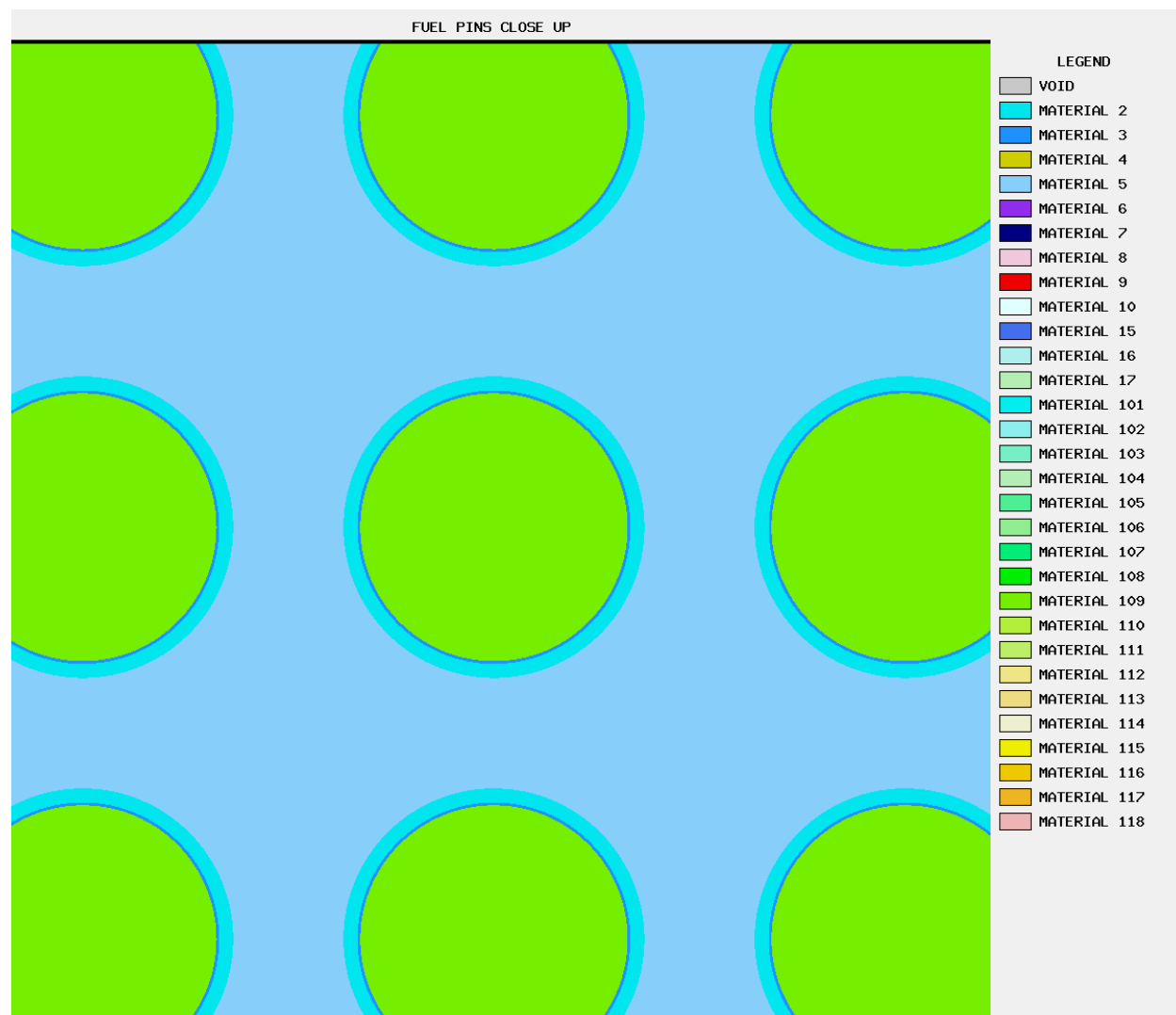


Figure 6-15  
[ ] Clad Thinning – Contracting Exterior



Note: The dark blue circle with the yellow outline to the right of center is a thermocouple.

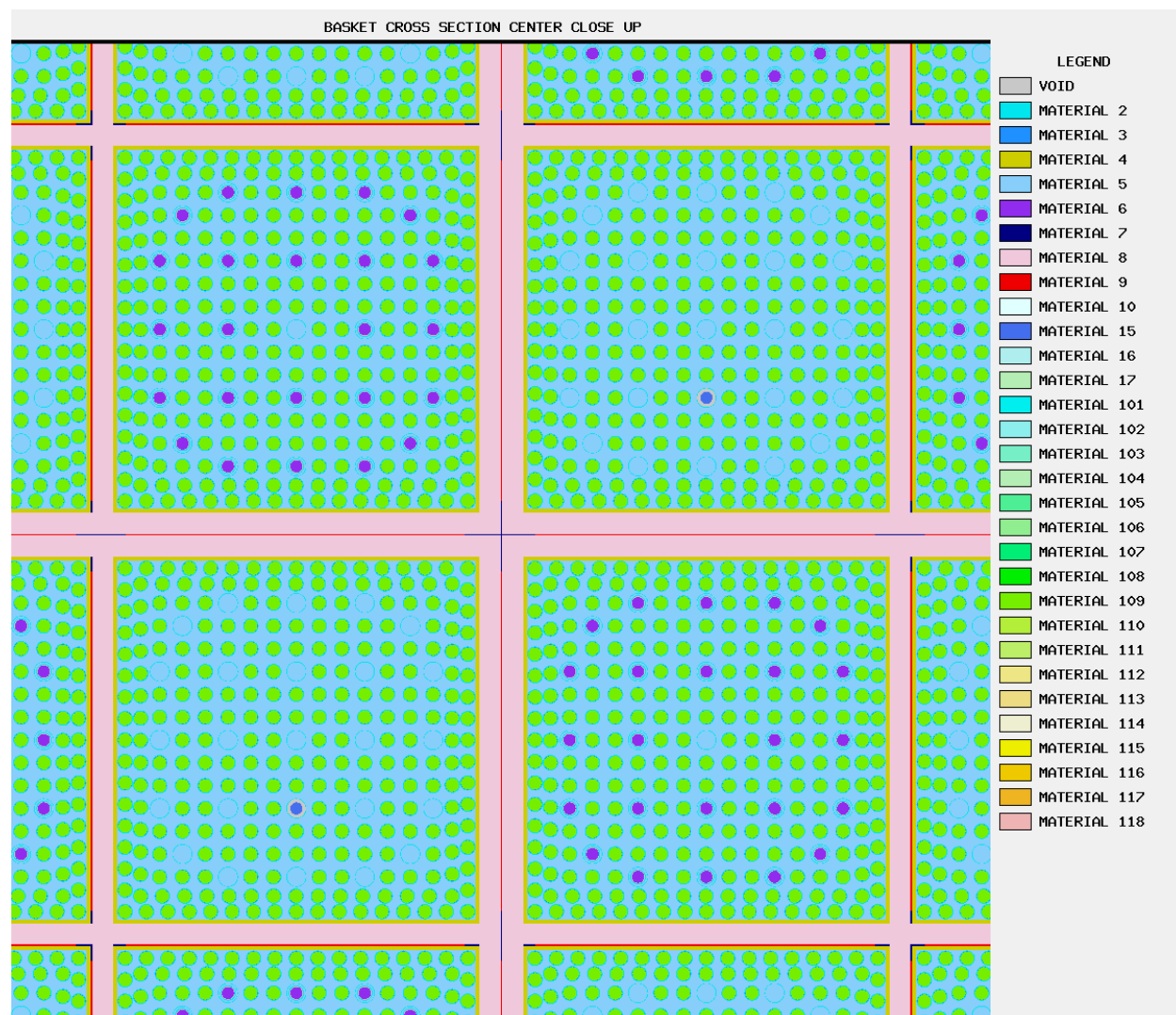
**Figure 6-16**  
**Fuel Assembly 30A Oriented 90°**



Figure 6-17  
Fuel Assembly [ ] Oriented 180°



**Figure 6-18**  
**Uniform Pitch Expansion**



**Figure 6-19**  
**Nonuniform Pitch Expansion**



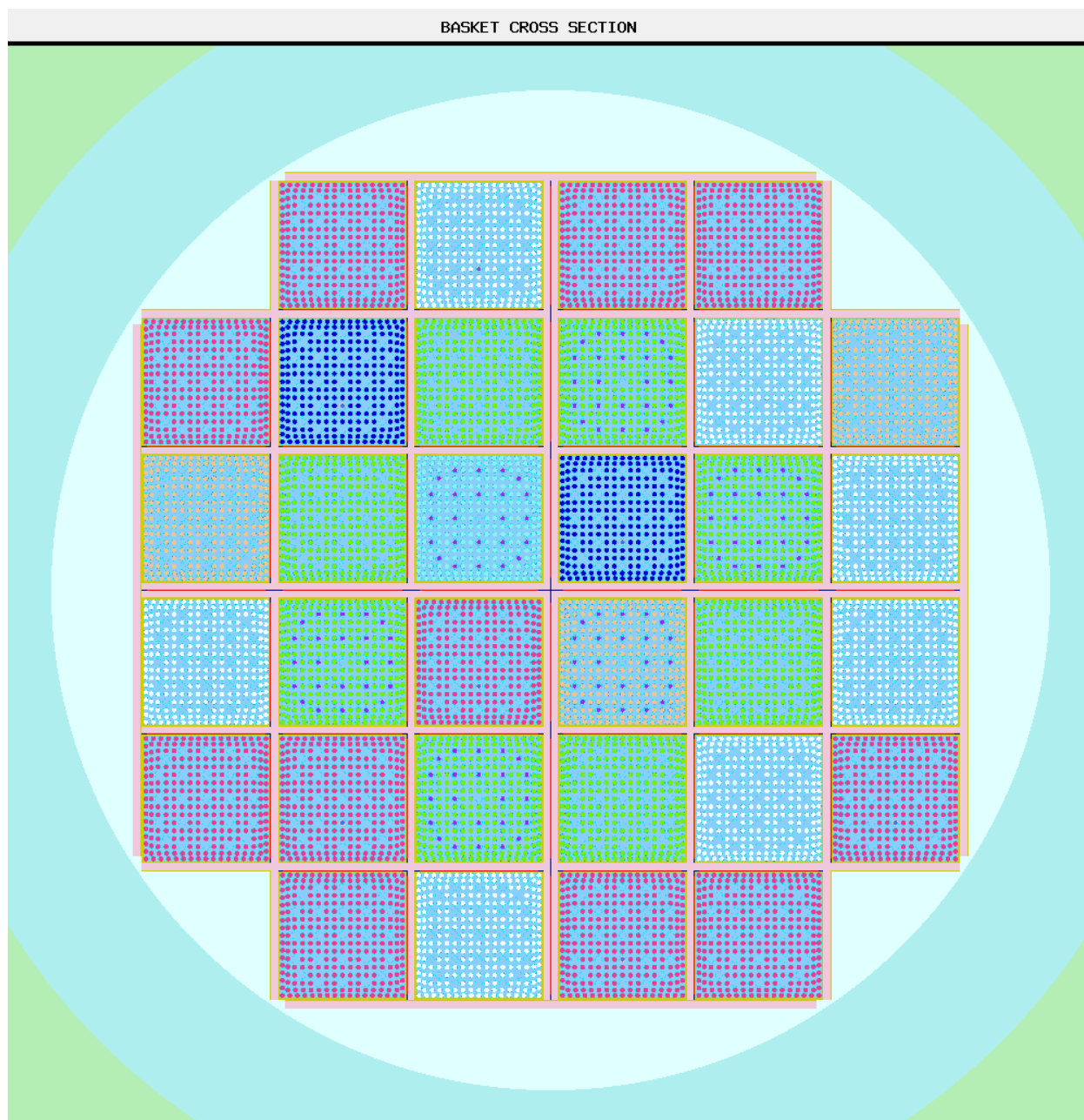


**Figure 6-20**  
**Most Reactive Fuel Configuration with Cooling Time Groups**

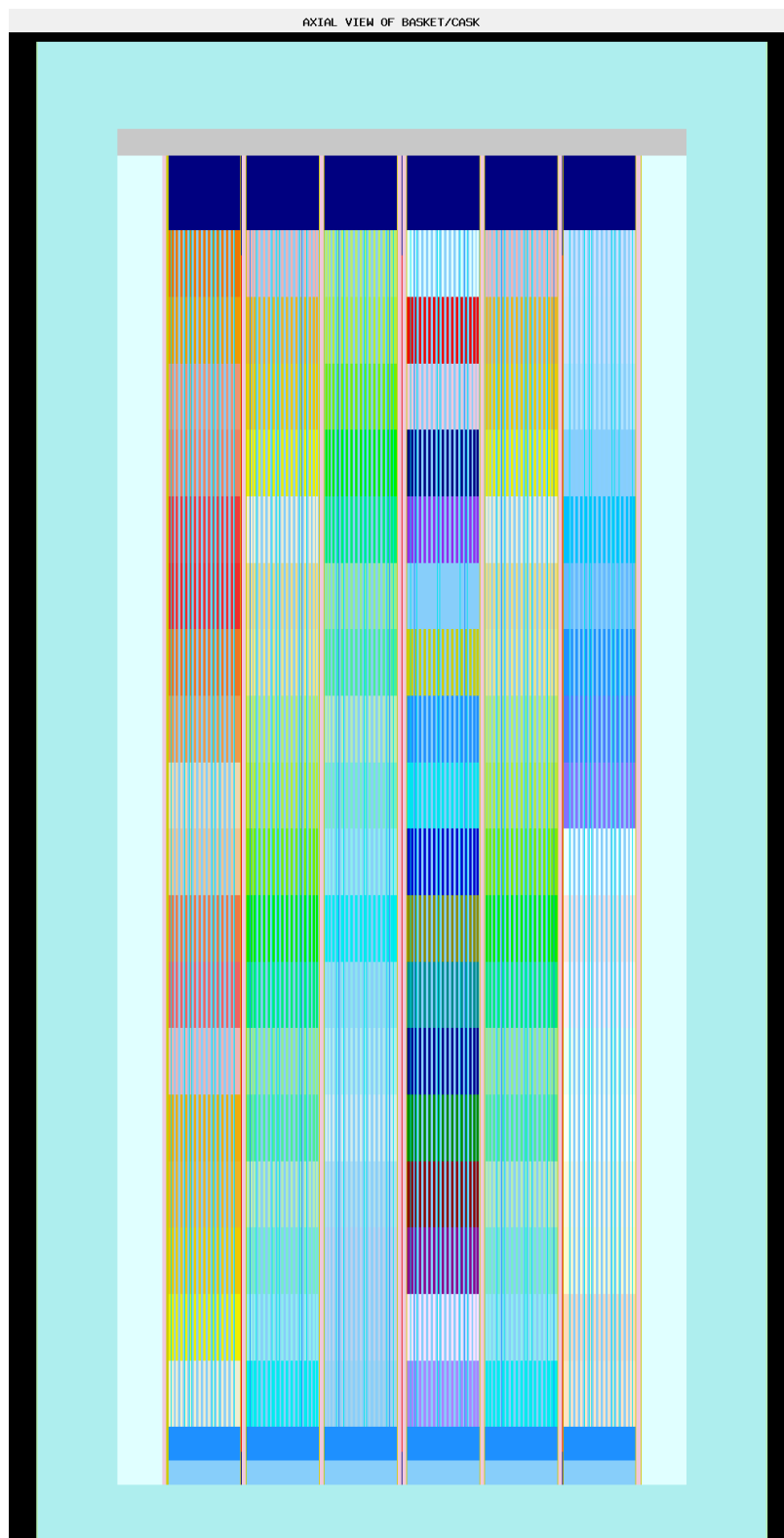


**Figure 6-21**  
**Axial View of Most Reactive Fuel Configuration with Cooling Time Groups**

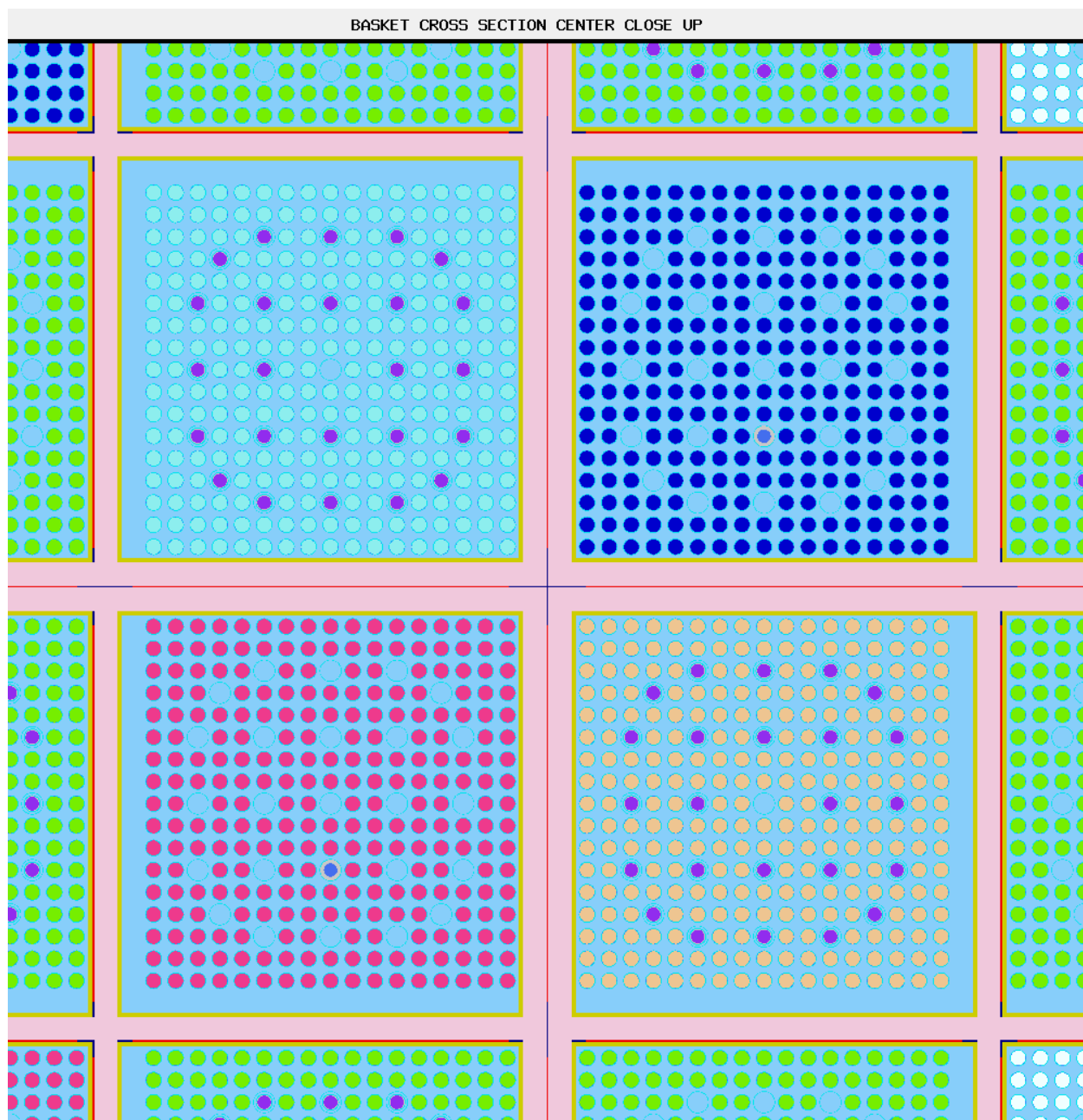


**Figure 6-22**  
**Pitch Contraction with Cooling Time Groups**

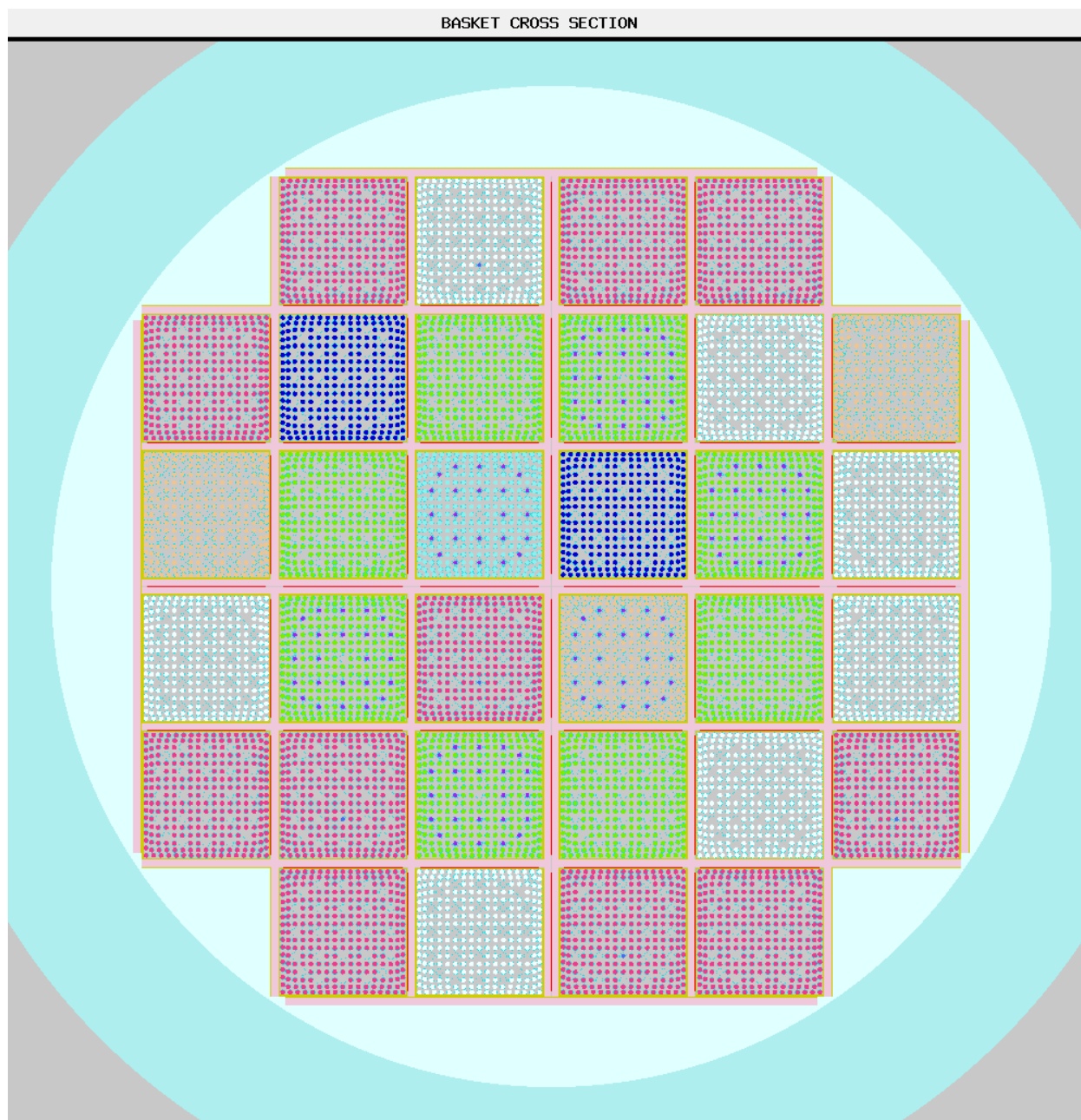


**Figure 6-23**  
**TN-32B HBU Demonstration Cask Basket Cross Section for Subcritical Multiplication**

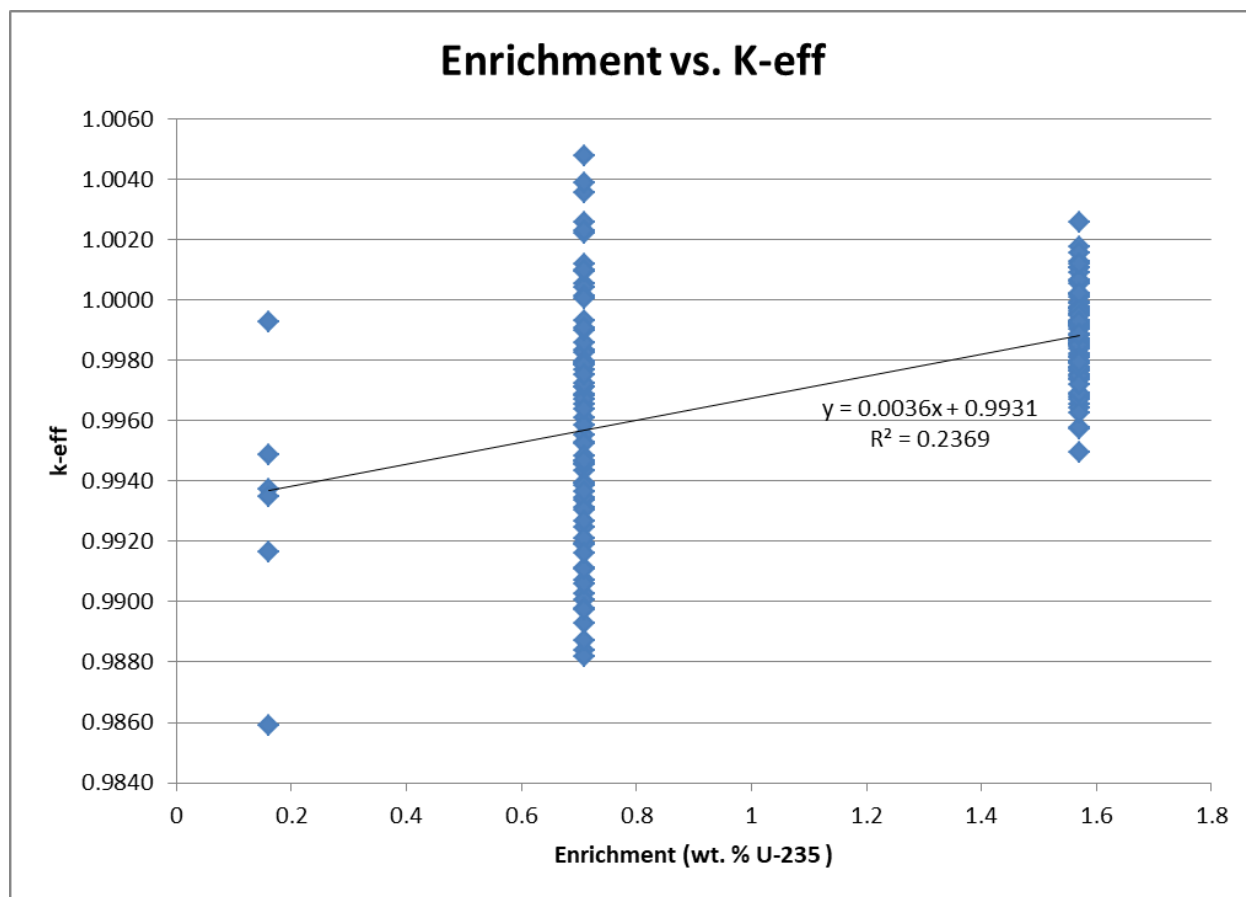


**Figure 6-24**  
**Enrichment versus  $k_{\text{eff}}$  for Critical Experiments**

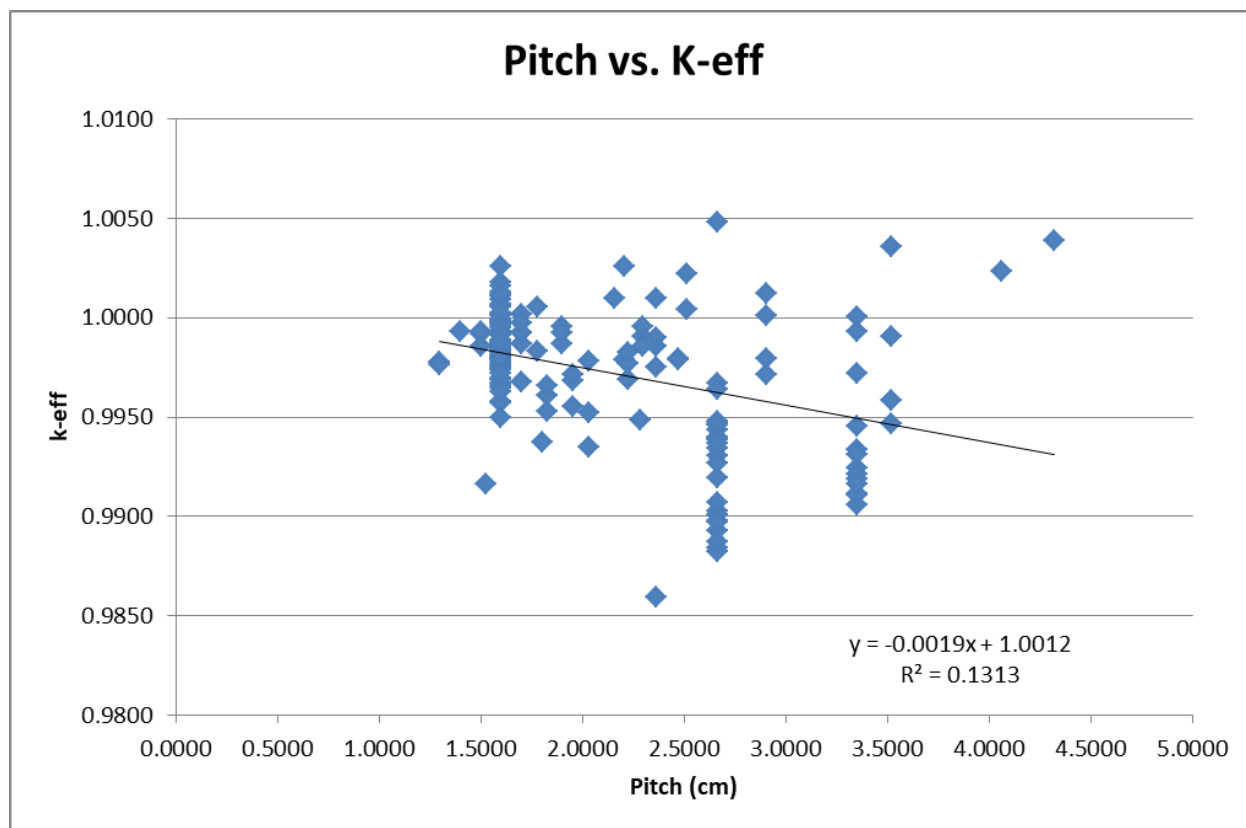


**Figure 6-25**  
**Fuel Pitch versus  $k_{eff}$  for Critical Experiments**

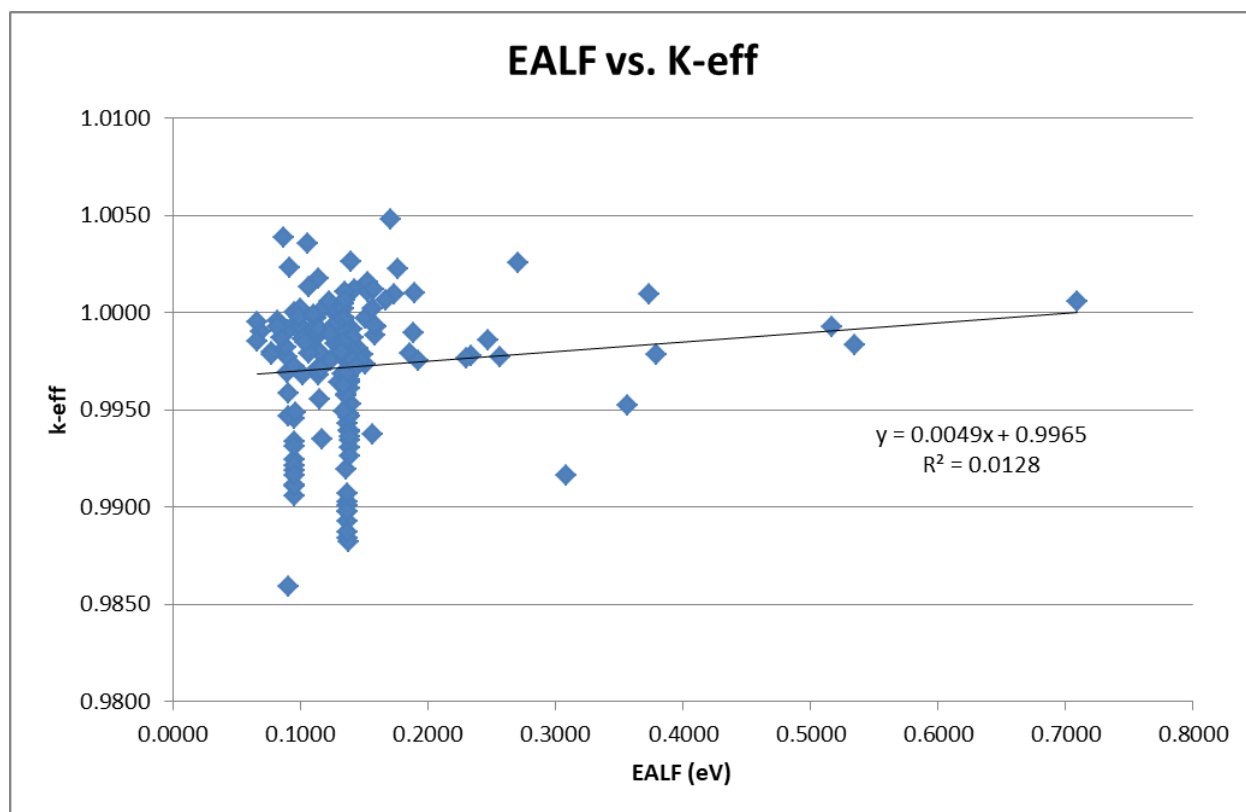


**Figure 6-26**  
**EALF versus  $k_{\text{eff}}$  for Critical Experiments**

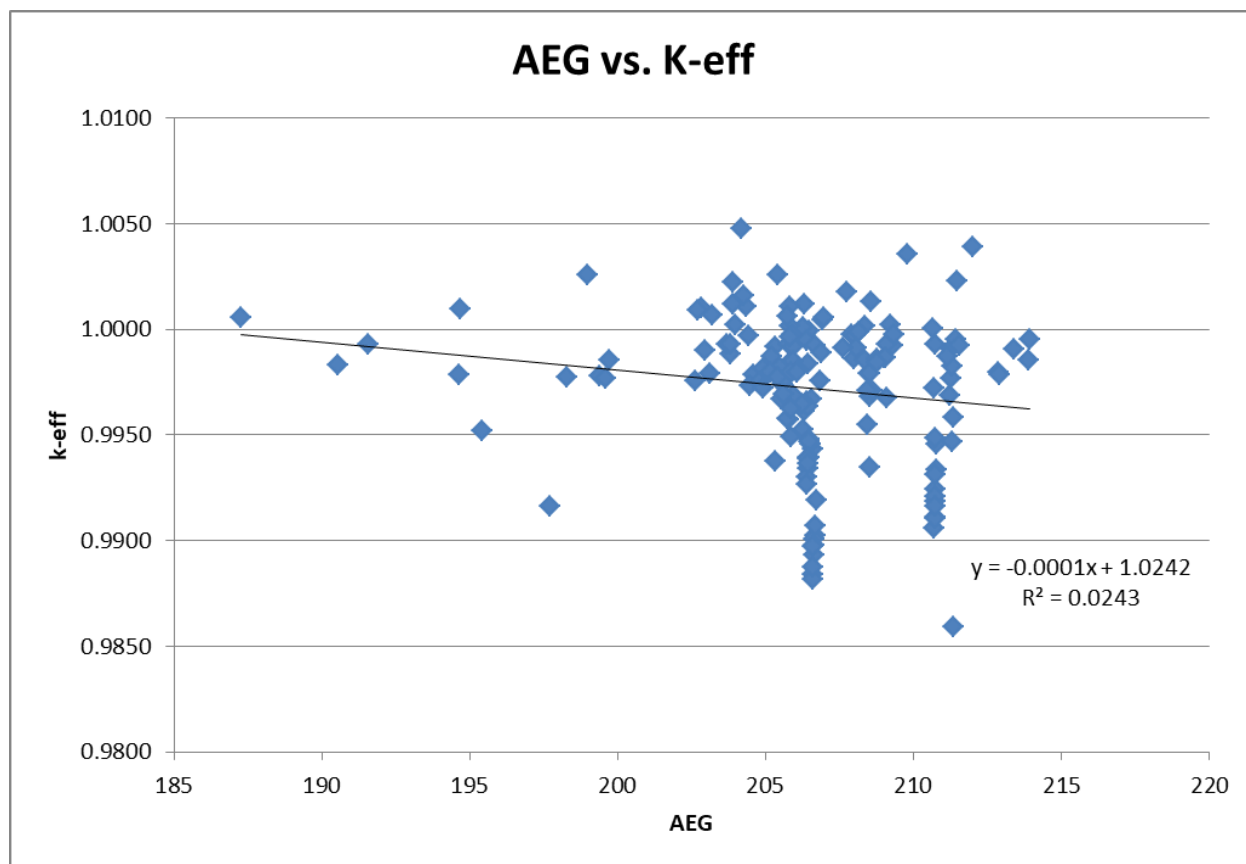


**Figure 6-27**  
**AEG versus  $k_{\text{eff}}$  for Critical Experiments**



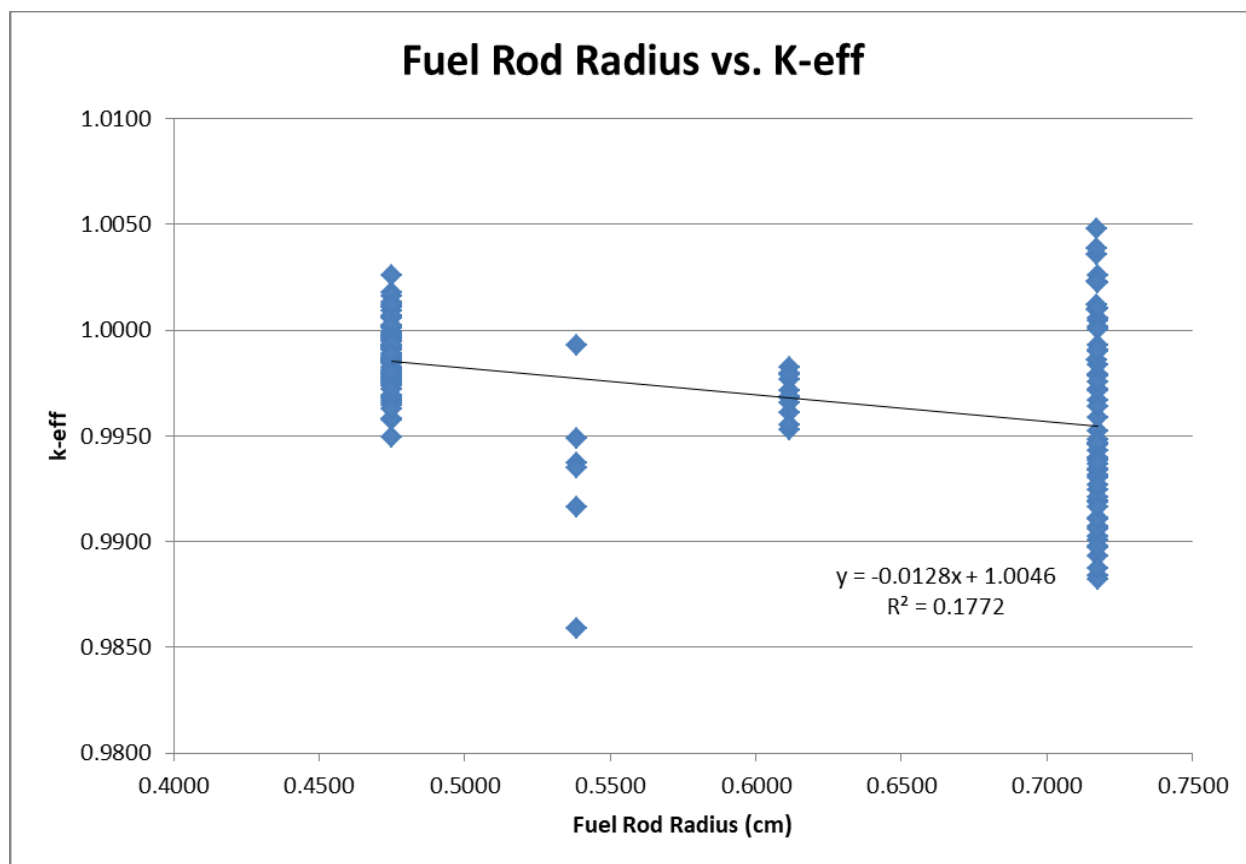


**Figure 6-28**  
**Fuel Rod Radius versus  $k_{eff}$  for Critical Experiments**

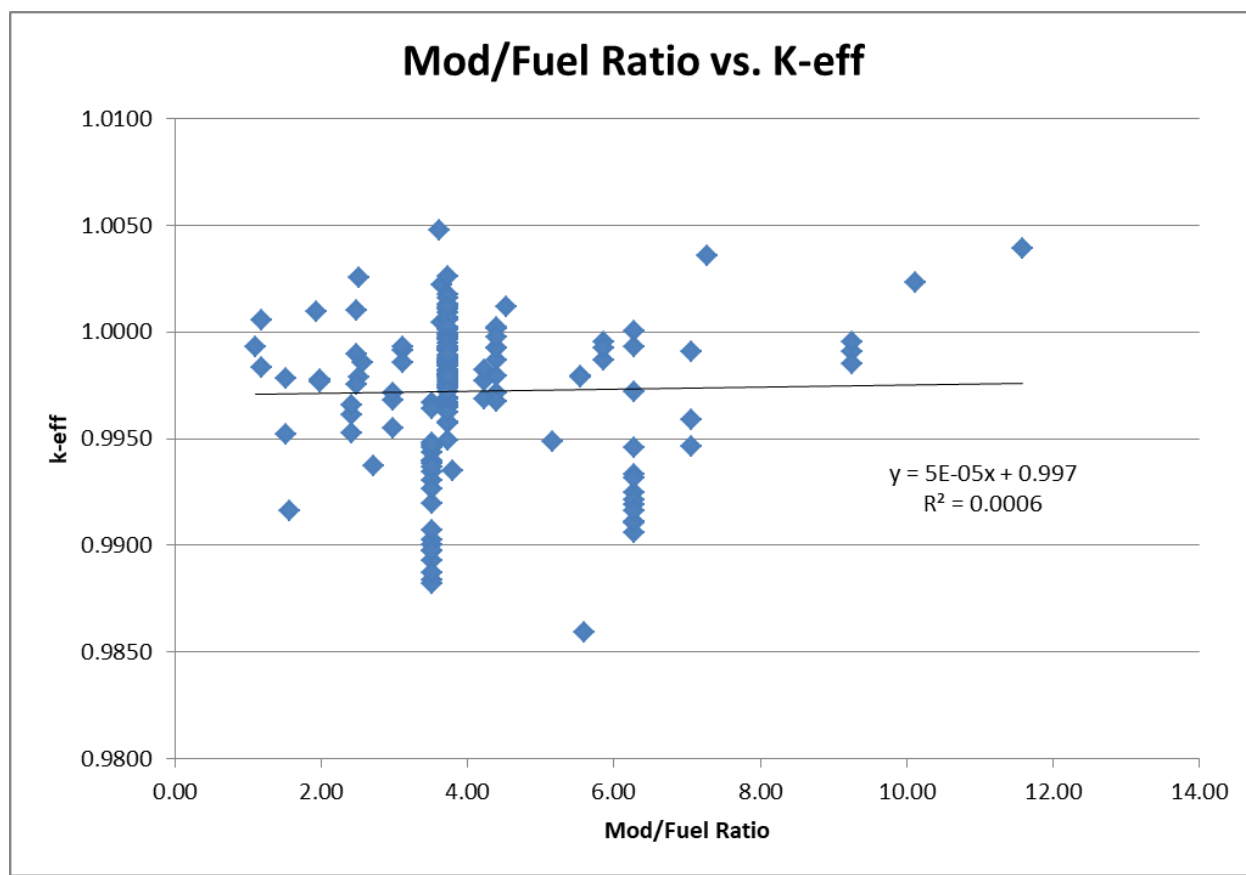


**Figure 6-29**  
**Moderator to Fuel Ratio versus  $k_{eff}$  for Critical Experiments**

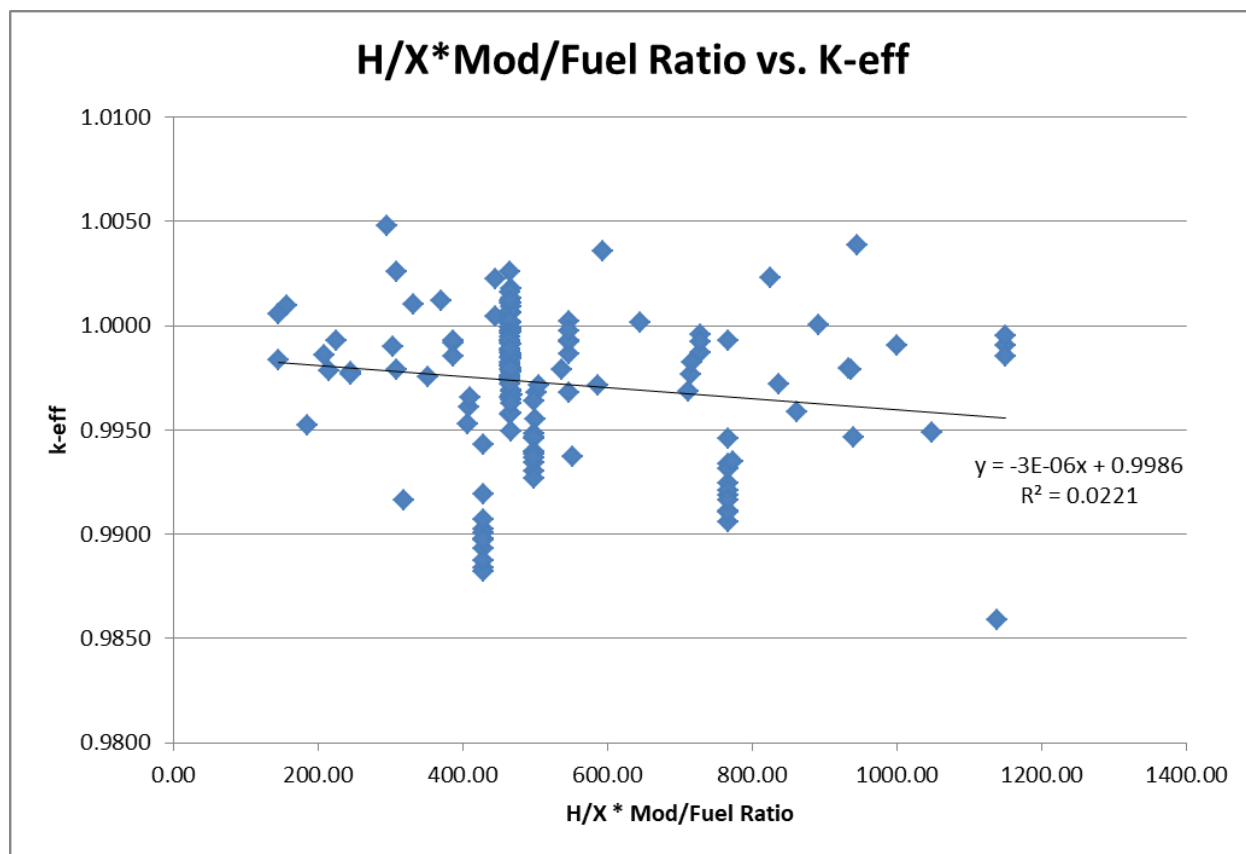


**Figure 6-30**  
**Moderator to Fissile Density Ratio versus  $k_{eff}$  for Critical Experiments**

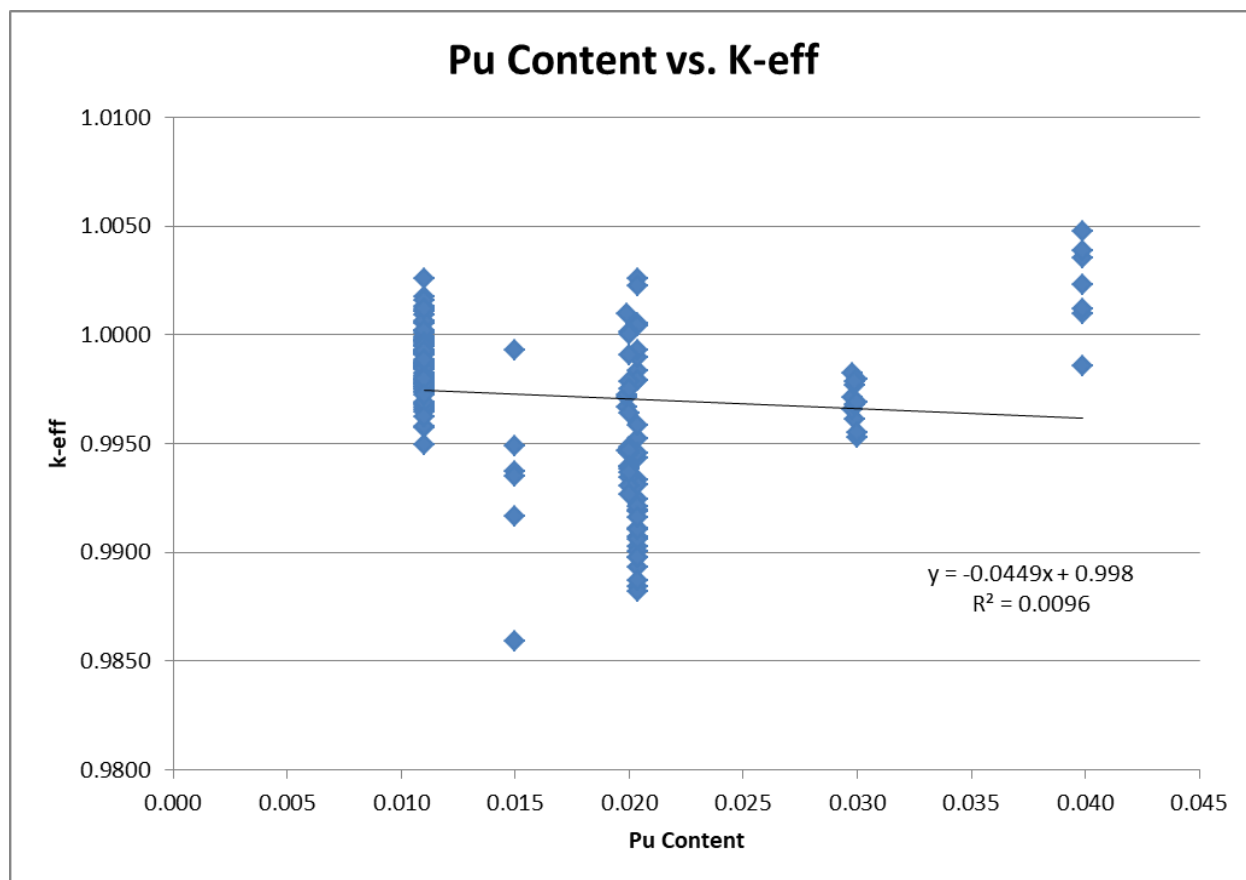


**Figure 6-31**  
**Pu/Pu+U versus  $k_{\text{eff}}$  for Critical Experiments**

## **Chapter 7**

### **Operating Procedures**

#### TABLE OF CONTENTS

7.1	Package Loading.....	7-1
7.1.1	Preparation for Loading.....	7-1
7.1.2	Loading of Contents.....	7-1
7.1.3	Preparation for Transport.....	7-1
7.2	Package Unloading .....	7-4
7.2.1	Receipt of Package from Carrier .....	7-4
7.2.2	Removal of Contents .....	7-5
7.3	Preparation of Empty Package for Transport.....	7-6
7.4	Other Operations .....	7-7
7.5	References .....	7-7

#### LIST OF FIGURES

Figure 7-1	Fastener Tightening Patterns .....	7-9
------------	------------------------------------	-----

## **Chapter 7 Operating Procedures**

This chapter contains TN-32B HBU demonstration cask loading and unloading procedures that are intended to demonstrate the general approach to cask operational activities. A separate Operations and Maintenance (O&M) Manual will be prepared for the TN-32B HBU demonstration cask to describe the operational steps in greater detail. The O&M manual, along with the information in this chapter, will be utilized to prepare the site-specific procedures that will address the particular operational considerations for the unique TN-32B HBU demonstration cask. The operations required to convert the TN-32B HBU demonstration cask from its storage configuration to its transport configuration are also described here.

### **7.1 Package Loading**

The TN-32B HBU demonstration cask was loaded with 32 high burnup (HBU) spent fuel assemblies from the North Anna Power Station (NAPS) in November 2017. The loaded cask was then placed on the NAPS Independent Spent Fuel Storage Installation (ISFSI) for storage under 10 CFR 72 [1] requirements in accordance with the NAPS site-specific license (NRC Docket 72-16), and the amended NAPS Special Nuclear Materials (SNM) License No. 2507 for this special storage cask.

#### **7.1.1 Preparation for Loading**

The TN-32B HBU demonstration cask was previously prepared for loading the HBU spent fuel payload in November 2017. Therefore, no additional loading preparations of the cask are required.

#### **7.1.2 Loading of Contents**

The TN-32B HBU demonstration cask was previously loaded with the HBU spent fuel payload in November 2017. Therefore, no additional loading operations for the cask are required.

#### **7.1.3 Preparation for Transport**

The TN-32B HBU demonstration cask was designed for storage as well as transport. The following steps are required to convert the TN-32B HBU demonstration cask from its storage configuration to its transport configuration.

The accessible surfaces of the cask shall be visually inspected for evidence of cracks in the carbon steel shell.

Review the maintenance records of the cask for situations where air may have leaked into the cask while it was in its storage configuration, i.e., while on the storage pad. If air has leaked into the cask while it was in its storage configuration, perform an evaluation prior to transportation of the HBU fuel cladding for potential rod splitting due to exposure to an oxidizing atmosphere utilizing the methodology provided in ISG-22 [2].

1. Disconnect and remove the thermocouple (TC) lance data logger system (cart, conduit, electrical connectors, mounting bracket, and securement straps) from the cask.
2. Position the cask transporter over the cask.
3. Engage the lifting arms and lift the cask to the designated lift height.
4. Move the cask to the north bay of the NAPS Decontamination Building.
5. Lower the cask down onto the floor, disconnect and remove the cask transporter.
6. Depressurize or evacuate the overpressure (OP) system to atmospheric pressure.
7. Remove the access cover bolts and disconnect the OP system from the access cover.
8. Disconnect the TC leads from the junction box that is mounted on the protective cover.
9. Remove the 12 hex bolts that secure the protective cover and then remove the cover. Store the cover in a secure location for future use.
10. Remove the vent port access plug in the top neutron shield cover.
11. Remove the 8 socket head cap screws (SHCSs) that secure the vent port cover, and then remove the cover.
12. Collect a cavity gas sample through the vent port quick-disconnect coupling. If desired, additional samples may also be collected for supplemental analysis of the cavity gas.
13. Analyze the gas sample for radioactive material and add necessary precautions based on the cavity gas sample results.

**Note:** If degraded fuel is suspected, additional measures, appropriate for the specific conditions, are to be planned, reviewed, and approved by appropriate site personnel, as well as implemented to minimize worker exposure and radiological releases to the environment. These additional measures may include provision of filters, as well as respiratory protection and other methods to control releases and exposure to ALARA.

14. Install a new metallic O-ring seal, and re-install the vent port cover. Tighten the vent port cover SHCS to  $85 \pm 15$  lbf-ft, following the tightening sequence illustrated in Figure 7-1.
15. Perform a leakage rate test of the vent port O-ring seal in accordance with Section 8.2.2, Leakage Rate Tests.
16. Disconnect the OP system metal hose from the thermocouple lance valve manifold. The connection is at the end of the manifold.
17. Disconnect the thermocouple lance OP tubing for each lance from the manifold. The connection is upstream of the shutoff valve.
18. Remove the OP tank assembly, including the thermocouple lance OP manifold, the OP port bolts and cover, and the top neutron shield.

19. Install a plug into each of the OP tubing connected to the thermocouple lances per the details delineated in the drawings in Appendix 1.4.1.
20. Install the transport OP port cover. Tighten the bolts to  $25 \pm 5$  lbf-ft torque following the tightening sequence illustrated in Figure 7-1.
21. Verify and retighten (as necessary) all of the closure lid, vent and drain port cover bolts, and the thermocouple lance jacking screws to the following specified tightening torque and pattern per Figure 7-1:
  - Closure lid bolts:  $1,085 \pm 145$  lbf-ft
  - Vent and drain port bolts:  $85 \pm 15$  lbf-ft
  - Thermocouple lance socket head jacking screws:  $65 \pm 5$  lbf-ft
22. Install a lance cover plate over each thermocouple lance penetration in the closure lid per the details delineated in Appendix 1.4.1, General Arrangement Drawings.
23. Wrap each thermocouple cable and OP tubing around its lance cover plate. When fully wrapped around the lance cover, secure the cable/OP tubing to one of the sheet metal extensions using a metallic cable tie-wrap.
24. Perform a neutron and gamma dose rate survey over the entire surface of the cask to demonstrate the adequacy of the shielding design and to check if the surface dose rates are within the regulatory limits. Check surface contamination levels to verify that levels satisfy the requirements of 49 CFR 173.443 [3].
25. Install the puncture resistant plate over the closure lid, and then remove the plate lifting eye bolts.
26. Install the puncture resistant plate SHCSs, and tighten to  $80 \pm 10$  lbf-ft torque.
27. Remove the test port cap and plug from the puncture resistant plate test port. Connect a vacuum pump to the test port. Perform a pre-shipment a high-vacuum test of the inner and outer elastomer O-ring seals. The acceptable vacuum level is less than 200 mTorr (0.266 mbar).
28. Disconnect the vacuum pump from the test port, and re-install the test port plug and test port cap. Tighten the plug and cap to 8 to 10 lbf-ft torque.
29. Position the cask lift yoke over the cask.
30. Engage the lifting arms and lift the cask to the designated lift height.
31. Move the cask to the upending/downending frame, and place the rear trunnions on the rear trunnion supports.
32. Rotate the cask from the vertical to the horizontal position.
33. Using a spreader bar and lifting straps, lift the cask from the upending/downending frame and lower it onto the transport frame, with the closure lid end oriented on the rear of the frame.
34. Install the tie-down straps to the transport frame.



35. Prior to installing the impact limiters, inspect them visually for damage. If any wood has been exposed, the impact limiters may not be utilized without repair. Damage due to handling other than small dings and scratches must be evaluated for their effect on the performance during the hypothetical free and puncture drop accidents.
36. Install the 8 impact limiter brackets to the welded bars on the cask outer shell on each end. Secure the brackets to the cask body by tightening the bracket bolts and nuts to  $9 \pm 1$  lbf-ft torque.
37. Install the front (top) and the rear (bottom) impact limiters onto the cask.
38. Lubricate the impact limiter attachment bolts with Loctite N-5000 or an equivalent, and tighten to  $70 \pm 10$  lbf-ft torque on the final pass.
39. Install 13 impact limiter attachment tie-rods between the front and rear impact limiters. Secure the tie-rods to the impact limiters with the hex nuts by tightening the nuts to a snug tight condition. Install a lock sleeve on the end of each tie-rod.
40. Render the impact limiter lifting lugs inoperable by covering the lifting holes or installing a bolt inside the holes to prevent their inadvertent use.
41. Install the security seal on one tie-rod and lock sleeve.
42. Install the personnel barrier. Verify that the surface temperature on all accessible surfaces is less than 185 °F (85 °C).
43. Perform a final radiation survey of the cask radiation levels to ensure compliance with 49 CFR 173.441.
44. Verify that surface contamination levels of the cask comply with the limits of 49 CFR 173.443.
45. Apply appropriate NRC and DOT labels and placards in accordance with 10 CFR 71.85(c) [1] and 49 CFR 172 [4], respectively.
46. Prepare the final shipping documentation.
47. Release the loaded cask for shipment.

## **7.2 Package Unloading**

### **7.2.1 Receipt of Package from Carrier**

1. Upon arrival of the loaded cask, perform a receipt inspection of the cask to check for any damage or irregularities. Verify that the security seal is intact, and perform a radiation survey.
2. Verify that the records for the packaging are complete and accurate.
3. Remove the personnel barrier, the security seal, tie-rods, and the associated hardware. Remove the impact limiter attachment bolts.
4. Render the impact limiter lifting lugs operable by removing the covering on the lifting holes, or the bolt inside the lifting holes, that prevented their inadvertent use.
5. Remove the front and rear impact limiters, using a suitable crane and a two-legged sling or equivalent.

6. Remove the tie down straps.
7. Place an upending/downending frame near the transport vehicle.
8. Using a spreader bar and lift slings, lift the cask from the transport vehicle and place it on the upending/downending frame.
9. Attach the lift beam to the cask handling crane hook, and then engage the lift beam to the two upper (top) trunnions.
10. Rotate the cask slowly from the horizontal to the vertical position.
11. Lift the cask from the upending/downending frame, and place it in the designated work area.
12. Disengage the lift beam from the cask, and move the crane as well as the lift beam from the area.
13. Remove the SHCSs and the puncture resistant plate from the top of the cask.
14. Clean the external surfaces of the cask, if necessary, to remove any accumulated road/rail debris.
15. To demonstrate that the seals did not degrade during transport, perform a leakage rate test of the cask O-ring seals. Leakage rate test the closure lid, vent and drain port cover seals, and the thermocouple lance assembly seals by utilizing the sniffer technique per Section A.5.8, Trace gas-sniffer technique (hood technique), of ANSI N14.5 [5]. The maximum acceptable cask seal leakage rate is  $1 \times 10^{-4}$  ref-cm<sup>3</sup>/sec. The use of a helium mass spectrometer leak detector (MSLD) is the preferred method for this test. After the leakage rate test, replace the storage overpressure port cover with the transport overpressure port cover.

#### 7.2.2 Removal of Contents

Since the objective of the TN-32B HBU demonstration cask is to obtain spent fuel properties after a minimum 5.87-year storage period, the contents should only be unloaded in a hot cell to avoid quenching the fuel rods, and potentially altering the mechanical properties.

1. Remove the vent port bolts and cover.
2. Collect a cavity gas sample through the vent port quick-disconnect coupling.
3. Analyze the gas sample for any radioactive material, and add necessary precautions based on the cavity gas sample results. If desired, additional samples may also be collected for supplemental analysis of the cavity gas.

**Note:** If degraded fuel is suspected, additional measures, appropriate for the specific conditions, are to be planned, reviewed, and approved by the appropriate site personnel, as well as implemented to minimize worker exposures and radiological releases to the environment. These additional measures may include provision of filters, as well as respiratory protection and other methods to control releases and exposures to as low as reasonably achievable (ALARA).

4. In accordance with the site requirements, vent the cavity helium gas through the vent port until atmospheric pressure is reached.

5. Re-install the vent port cover and bolts.
6. Loosen the closure lid bolts and remove all but six bolts, approximately equally spaced. Install the alignment pins through the closure lid.
7. Attach the lifting equipment to the closure lid, and connect the crane to the lifting hardware.
8. Raise the cask to the required height, and move the cask to the transfer skid for the hot cell.
9. Lower the cask to the hot cell transfer skid, and disconnect the crane.
10. Move the TN-32B HBU demonstration cask into the hot cell in accordance with the site procedures.
11. Connect the hot cell crane to the lifting equipment on the closure lid, remove the six remaining closure lid bolts, and lift the closure lid until it clears the cask body.

**Note:** The thermocouple lance assemblies extend 155.33 in. (~13 ft) below the closure lid. In order to clear the thermocouple lance assemblies from the cask body, the hot cell crane must have a minimum of 13 ft of height clearance to remove the closure lid/thermocouple lances.

12. Optional: Remove the funnel guides from the seven spent fuel assemblies.
13. Optional: Remove the six poison rod assemblies (PRAs) from the spent fuel assemblies.
14. Unload the spent fuel assemblies in accordance with the site procedures.
15. Using the hot cell crane and lifting equipment, lower the closure lid, placing it on the cask shell flange over the three alignment pins.
16. Re-install six closure lid bolts equally spaced around the lid, and tighten to a snug tight condition. Disconnect the hot cell crane from the lifting equipment.
17. Move the TN-32B HBU demonstration cask out of the hot cell in accordance with site procedures.
18. Re-install the remaining closure lid bolts and tighten to  $400 \pm 20$  lbf-ft torque, following the tightening sequence illustrated in Figure 7-1.

### 7.3 Preparation of Empty Package for Transport

1. Verify that the cask is empty and decontaminate the cask until acceptable inner and outer surface contamination levels are obtained in accordance with Department of Transportation (DOT) regulations for empty packages as directed in 49 CFR 173.428 [3].
2. If not previously installed, lubricate and install the closure lid bolts and washers. Tighten to  $400 \pm 20$  lbf-ft torque, following the tightening sequence illustrated in Figure 7-1. A circular pattern of tightening may be used afterwards to eliminate further bolt movement.
3. Remove the plug from the neutron shield vent, and reinstall the pressure relief valve, ensuring that it is operable and set.
4. Install the vent and drain port covers.

5. Re-engage the lift beam to the upper (top) trunnions of the cask.
6. Move the transport vehicle with transport frame installed into the loading position and place the upending/downending frame near the transport vehicle.
7. Lift the cask off the decontamination pad, and place the rear trunnions on the rear trunnion supports of the upending/downending frame.
8. Rotate the cask from the vertical to the horizontal position.
9. Using a spreader bar and lift slings, lift the cask from the upending/downending frame and place it on the transport frame.
10. Install the tie-down straps.

**Note:** If the impact limiters are to be shipped separately, skip the next four steps.

11. Install the SHCSs and the puncture resistant plate over the closure lid, and then remove the plate lifting eye bolts. Tighten the SHSCs to  $80 \pm 10$  lbf-ft torque.
12. Install the front (top) and the rear (bottom) impact limiters onto the cask.
13. Lubricate the impact limiter attachment bolts with Loctite N-5000 or an equivalent, and tighten to  $70 \pm 10$  lbf-ft torque on the final pass.
14. Install 13 impact limiter attachment tie-rods between the front and the rear impact limiters. Secure the tie-rods to the impact limiters with the hex nuts by tightening the nuts to a snug tight condition. Install a lock sleeve on the end of each tie-rod.
15. Render the impact limiter lifting lugs inoperable, by covering the lifting holes or installing a bolt inside the holes to prevent their inadvertent use.
16. Perform a final radiation and contamination survey to ensure compliance with 49 CFR 173.428 [3].
17. Remove or cover previous DOT labels and placards and attach an "Empty" label to the package in accordance with 49 CFR 172.450 [4], and prepare the final shipping documentation.
18. Release the empty cask for shipment.

## 7.4 Other Operations

There are no other operations required to operate the TN-32B HBU demonstration cask.

## 7.5 References

1. Title 10, Code of Federal Regulations - Energy, Part 72 (10 CFR 72), "Licensing requirements for the Independent Storage of Spent Nuclear Fuel, High-Level Radioactive Waste, and Reactor-Related Greater Than Class C Waste," 1-1-2021 Edition, U.S. Nuclear Regulatory Commission, Washington, D.C.
2. U.S. Nuclear Regulatory Commission, Interim Staff Guidance-22 (ISG-22), "Potential Rod Splitting Due to Exposure to an Oxidizing Atmosphere During Short-Term Cask Loading Operations in LWR or Other Uranium Oxide Based Fuel," May 2006.
3. Title 49, Code of Federal Regulations - Transportation, Part 173 (49 CFR Part 173), "Shippers – General Requirements for Shipments and Packagings," 10-1-2020 Edition, U.S. Department of Transportation, Washington, D.C.
4. Title 49, Code of Federal Regulations - Transportation, Part 172 (49 CFR Part 172), "Hazardous Materials Tables and Hazardous Communications Regulations," 10-1-2020 Edition, U.S. Department of Transportation, Washington, D.C.
5. ANSI N14.5–2014, "Leakage Tests on Packages for Shipment of Radioactive Materials," American National Standards Institute (ANSI), Inc.

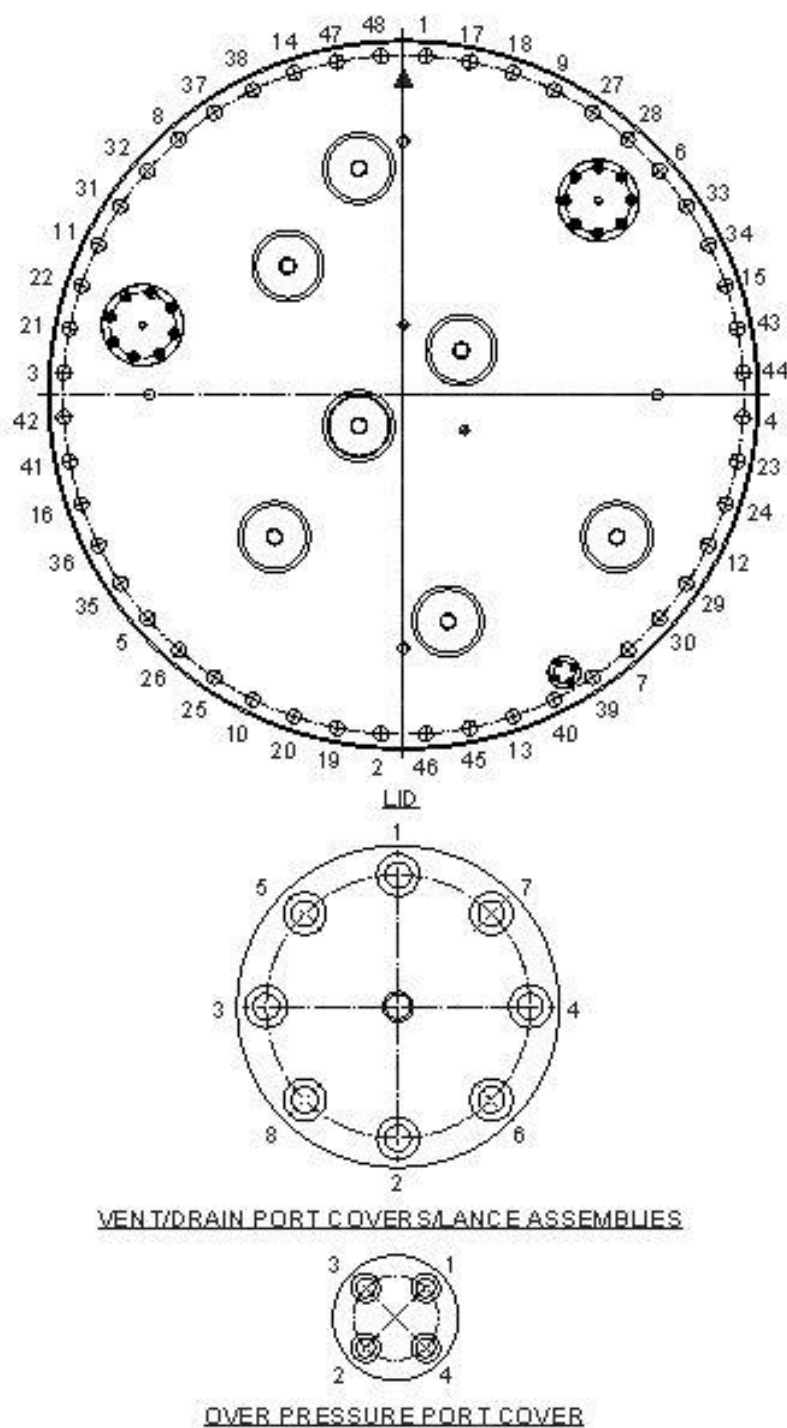


**Figure 7-1**  
**Fastener Tightening Patterns**

## **Chapter 8**

### **Acceptance Tests and Maintenance Program**

#### TABLE OF CONTENTS

8.1	Acceptance Tests .....	8-1
8.1.1	Visual Inspections and Measurements .....	8-1
8.1.2	Weld Examinations .....	8-2
8.1.3	Structural and Pressure Tests .....	8-2
8.1.4	Leakage Tests .....	8-3
8.1.5	Component and Material Tests .....	8-6
8.1.6	Shielding Tests .....	8-8
8.1.7	Thermal Tests .....	8-10
8.1.8	Miscellaneous Tests .....	8-11
8.2	Maintenance Program .....	8-12
8.2.1	Structural and Pressure Tests .....	8-12
8.2.2	Leakage Rate Tests .....	8-12
8.2.3	Component and Material Tests .....	8-12
8.2.4	Thermal .....	8-13
8.2.5	Miscellaneous Tests .....	8-13
8.3	References .....	8-14

## **Chapter 8**

### **Acceptance Tests and Maintenance Program**

#### **8.1 Acceptance Tests**

The following reviews, inspections, and tests shall be performed on the TN-32B HBU demonstration cask prior to initial transport. Many of these tests were previously performed at the fabricator's facility prior to delivery of the cask to the North Anna Power Station (NAPS). Tests were performed in accordance with written procedures approved by TN Americas LLC. For the TN-32B HBU demonstration cask that was fabricated, loaded, and utilized for storage under the NAPS site-specific 10 CFR Part 72 requirements, the acceptance tests performed during its fabrication are acceptable.

##### **8.1.1 Visual Inspections and Measurements**

Visual inspections were performed at the fabricator's facility prior to initial use for storage to ensure that the packaging conforms to the drawings and specifications. The visual inspections included:

- Cleanliness inspections,
- Visual weld inspections as required by American Society of Mechanical Engineers (ASME) Boiler and Pressure Vessel (B&PV) Code [1],
- Inspection of sealing surface finish, and
- Dimensional inspections for conformance with the drawings included in Appendix 1.4.1 and referenced in the Certificate of Compliance.

The visual inspection included verifying that all specified coatings are applied and the packaging is clean and free of cracks, pinholes, uncontrolled voids, or other defects that could significantly reduce its effectiveness. To the maximum extent practical, weld inspection was performed in accordance with the applicable sections of the ASME B&PV Code [1]. Dimensions and tolerances shown on the drawings provided in Appendix 1.4.1 were confirmed by measurements. The sealing surfaces on the flange, closure lid, covers, and thermocouple lances were inspected to ensure that there are no gouges, cracks, or scratches that could result in an unacceptable leakage rate.

Prior to shipping and payload loading following the closure lid modification, the packaging was inspected to ensure that it is in good physical condition. This inspection included verification that all accessible cask surfaces are free of grease, oil, or other contaminants, and that all cask components are in an acceptable condition for use.



### 8.1.2 Weld Examinations

The containment welds are designed, fabricated, tested and inspected in accordance with ASME B&PV Code, Section III, Subsection NB. Alternatives to the code regarding the containment vessel are described in Appendix 2.12.13 of Chapter 2. The fuel basket was designed, fabricated, and inspected in accordance with the ASME B&PV Code Subsections NB/NF. Fusion weld tests, as required, are delineated on Drawing 19885-71-6. Alternatives regarding the basket are also described in Appendix 2.12.13 of Chapter 2. Noncontainment structural welds were inspected per the Nondestructive Examination (NDE) acceptance criteria of ASME B&PV Code, Section III, Subsection NF.

The impact limiter attachment bolt material, ASTM A540 Gr B21 Cl 2, is tested to demonstrate the Charpy fracture toughness is at least 20 ft-lbf at -20 °F. The tie-rod material, ASTM A193 Gr B7, is tested to demonstrate the Charpy impact test energy is at least 35 ft-lbf at -20 °F.

The structural analyses performed on the packaging are presented in Chapter 2. To ensure that the packaging can perform its design function, the structural materials are chemically and physically tested to confirm that the required properties were met. To the maximum extent practical, welding was performed using qualified processes and qualified personnel, according to the ASME B&PV Code [1]. Base materials and welds were also examined in accordance with the ASME B&PV Code requirements. NDE requirements for welds are specified on the drawings provided in Appendix 1.4.1. All NDE is performed in accordance with written and approved procedures. The inspection personnel are qualified in accordance with SNT-TC-1A [2].

### 8.1.3 Structural and Pressure Tests

#### 8.1.3.1 Pressure Tests

Prior to the initial use of the cask for storage, a hydrostatic pressure test was performed on the cask assembly at a pressure of 45 psig. This pressure is nearly equal to the 1.5 times the maximum normal operating pressure (MNOP) of 30.5 psig, which is conservative. The test pressure was held for a minimum of 10 minutes, and performed in accordance with ASME B&PV Code, Section III, Subsection NB, Article NB-6200. All accessible weld joints of the containment boundary were then examined utilizing the magnetic particle (MT) examination for possible defects.

In addition, a bubble leakage rate test was performed at a pressure of 4.4 psig on the neutron shield enclosure (outer shell, outer shell top and bottom rings). The purpose of this test was to identify any potential leak passages in the enclosure welds. The bubble leakage rate test pressure is greater than the relief valve set pressure of 3 psig.

The containment boundary of the thermocouple lance assemblies were hydrostatically pressure tested to an external pressure of 3,125 psig, and then helium leakage rate tested. The lance assemblies successfully passed both tests.

#### 8.1.3.2 Structural Tests

The lifting trunnions were designed to exceed 10 CFR 71.45(a) lifting requirements. A load test of 383 kips (three times the design lift load) was applied to each of the lifting (upper) trunnions for a minimum period of 10 minutes, to ensure that the trunnions perform satisfactorily. At the conclusion of the test, the lifting trunnions (including the attachment welds) were:

- a) Visually examined for defects and permanent deformations.
- b) Examined by the magnetic particle method for defects. Acceptance standards were in accordance with ASME B&PV Code, Section III, Subsection NF-5340.

Following these examinations, the lifting trunnions were determined to be acceptable.

A force equal to a minimum of 1.5 times the impact limiter weight will be applied to the lifting lugs of each limiter for a minimum period of ten minutes. At the conclusion of the test, the impact limiter lifting lugs (including welds) will be:

- a) Visually examined for defects and permanent deformations.
- b) Examined by the liquid penetrant method for defects. Acceptance standards will be in accordance with ASME B&PV Code, Section III, Subsection NF-5350.

#### 8.1.4 Leakage Tests

Leakage tests were performed on the containment boundary at both the original fabricator's facility and the closure lid modification fabricator's facility, as described below. These tests were performed utilizing a mass spectrometer leak detector (MSLD) with helium tracer gas. The leakage tests were performed in accordance with American National Standards Institute (ANSI) N14.5 [3], and a maximum acceptance criterion of  $1 \times 10^{-4}$  ref cm<sup>3</sup>/s. The personnel performing the leakage tests were qualified in accordance with SNT-TC-1A.

As part of the initial cask fabrication in 2003, the TN-32B HBU demonstration cask was assembled with the containment boundary metallic O-ring seals on the closure lid, the vent, and the drain were leakage rate tested. These leakage rate tests were in accordance with Section 7.3, *Fabrication leakage rate test*, of ANSI N14.5 [3], with an acceptance criterion for the sum of all seal leakage rates not exceeding  $1 \times 10^{-5}$  atm cm<sup>3</sup>/s, He, in accordance with the storage license requirements. The resultant helium leakage rate sum for the three containment seals was  $3.0 \times 10^{-7}$  atm cm<sup>3</sup>/s, He. Note that the ANSI N14.5 standard does not require summing the leakage rates of individual leak paths to determine the leak tightness of the containment boundary. For a single containment O-ring seal, the maximum measured leakage rate was  $1.8 \times 10^{-7}$  atm cm<sup>3</sup>/s, He.

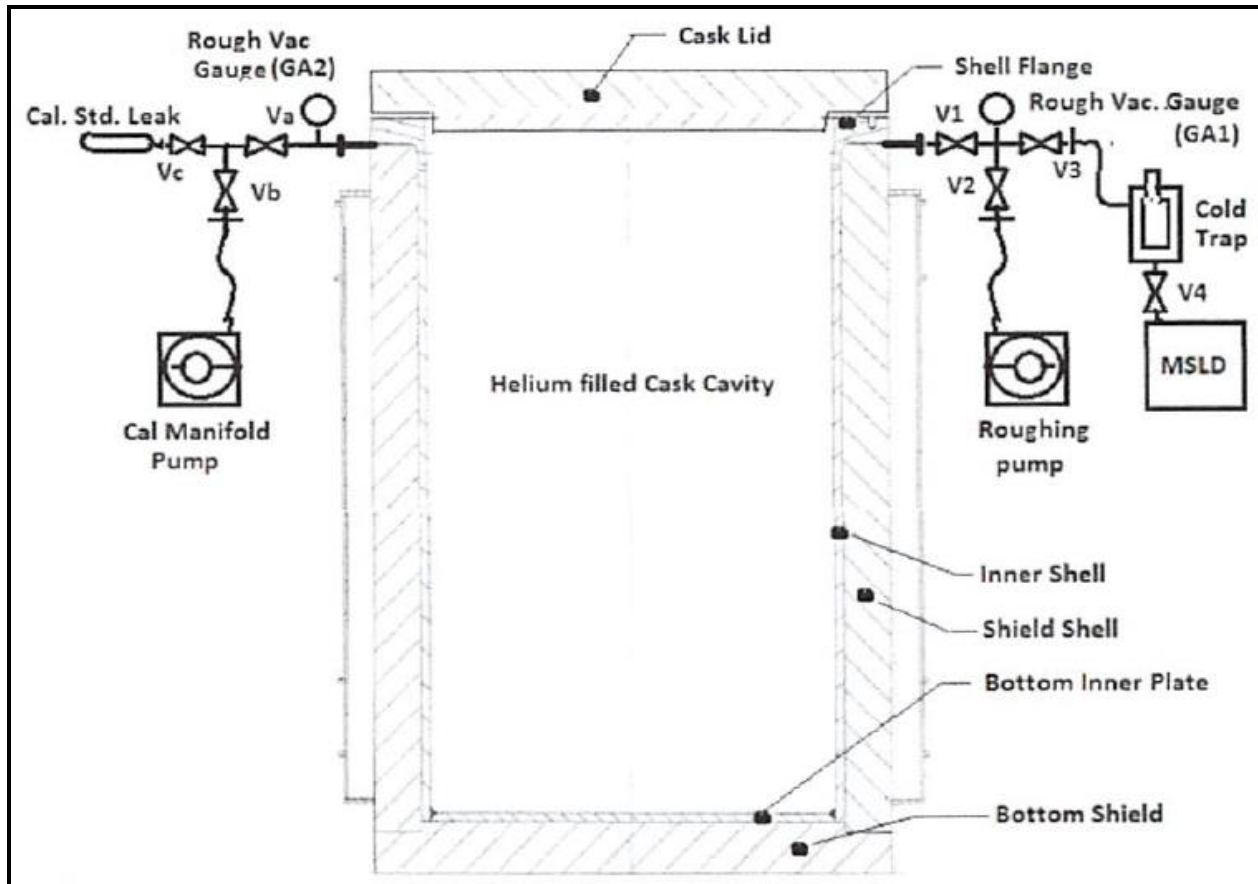
At the completion of the original fabrication of the TN-32B HBU demonstration cask, the cask was assembled so the cavity could be evacuated and backfilled with helium gas. This configuration was to provide an inert atmosphere in the cavity for the long-term storage and future use of the cask for spent fuel storage.

Prior to opening the cask in July 2015 for the closure lid modification, the helium gas concentration and pressure in the cavity were measured, and determined to be 80.5% and 25 psig, respectively. The fact that the TN-32B HBU demonstration cask maintained the pressurized helium gas atmosphere for 13 years provides objective evidence that the containment boundary is leaktight. However, additional leakage rate testing of the metallic containment boundary was undertaken prior to storage of the HBU spent fuel payload.

After the thermocouple lance forgings were welded to the closure lid, a leakage rate test of the forgings and the weld joints was performed to demonstrate leak tightness of the modified containment boundary. These leakage rate tests satisfied the requirements of Section 7.3, *Fabrication leakage rate test* of ANSI 14.5 [4] for the lid modification. The leakage rate test was performed utilizing a helium mass spectrometer leak detector (MSLD) following the guidelines of Section A.5.3, *Gas Filled Envelope – Gas Detector* of ANSI N14.5. The measured leakage rate for all weld joints and the forgings were demonstrated to be leaktight, i.e.,  $1 \times 10^{-7}$  ref cm<sup>3</sup>/s.

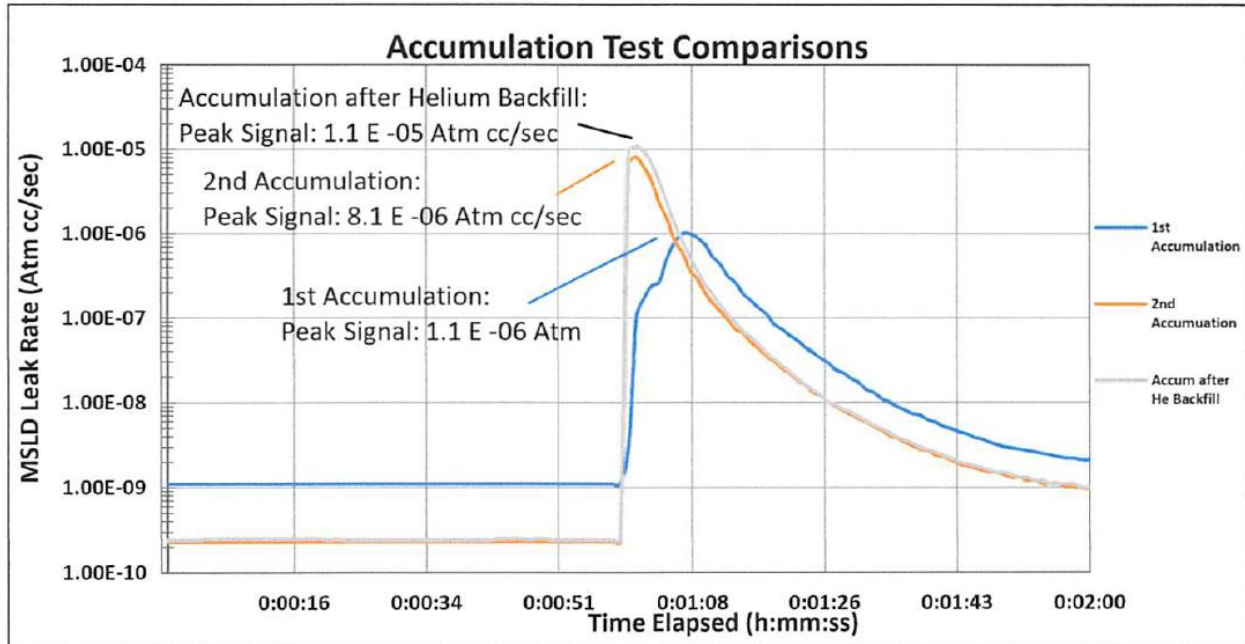
At the completion of the lid modification of the TN-32B HBU demonstration cask for the HBU storage project, a “best effort” leakage test of the entire metallic containment boundary was performed in August 2017 at the fabrication facility for the closure lid modification. Since the metallic containment boundary of the cask body, which is an interference fit with the gamma shell, was not previously tested during the original cask fabrication, only a “best effort” leakage rate test of this boundary could be performed due to the restricted access of the outer surface of the inner containment shell.

For this “best effort” leakage rate test, two holes were drilled through the 1/2-inch groove weld joint in the body flange/gamma shield to access the annulus between the 1½-inch thick containment boundary shell and the 8-inch thick gamma shield. The two access holes were circumferentially located 180 degrees apart. A helium mass spectrometer leak detector (MSLD) and a roughing vacuum pump were connected to one access hole, and a calibrated standard leak and another roughing vacuum pump connected to the other access hole. The leakage rate test configuration is shown in the following figure.



Two accumulation tests of the cask annulus were performed with the cask cavity under vacuum. During these two tests, the annulus pressure decreased to 3.4 mTorr within 30 minutes. The MSLD measured peak helium leakage rates for each accumulation test of  $1.0 \times 10^{-6}$  atm cm<sup>3</sup>/s and  $8.1 \times 10^{-6}$  atm cm<sup>3</sup>/s, respectively, at approximately one hour into the test. These background helium leakage rates were attributed to lack of cleanliness between the shield and inner shell surfaces of the annulus, and not an indication of a leak in the containment boundary.

A third accumulation test was then performed with helium gas introduced into the cavity with a pressure differential of 740 Torr (14.3 psid) between the cavity and the annulus. For this test, a peak helium leakage rate of  $1.1 \times 10^{-5}$  atm cm<sup>3</sup>/s was measured at approximately one hour into the test. In all three accumulation tests, the helium leakage rate decreased to less than  $1.0 \times 10^{-8}$  atm cm<sup>3</sup>/s after 2 hours, indicating that there was no leak path in those areas of the annulus that had conductance to the sensing port at the top of the cask. Following the "best effort" leakage rate test, an alloy steel circular plug was inserted into each access hole, and welded in place. The accumulation test results are compared in the following figure.



At the completion of the closure lid modification, the cask was fully assembled utilizing new metallic O-ring seals, and a helium leakage rate test of all of 10 seals (closure lid, vent, drain, and thermocouple lance assemblies), and the overpressure (OP) system was performed in September 2017 to satisfy the fabrication leakage rate test for the lid modifications, as specified in Section 7.3, *Fabrication leakage rate test*, of ANSI N14.5. The system was demonstrated to be leaktight, i.e.,  $1 \times 10^{-7}$  ref cm<sup>3</sup>/s.

After loading of the (32) PWR spent fuel assemblies in November 2017, new metallic O-ring seals, and a helium leakage rate test of all of 10 seals (closure lid, vent, drain, and thermocouple lance assemblies) was performed to satisfy the requirements of Section 7.4, *Maintenance leakage rate test*, of ANSI N14.5. The seals were demonstrated to be leaktight, i.e.,  $1 \times 10^{-7}$  ref cm<sup>3</sup>/s.

#### 8.1.5 Component and Material Tests

##### 8.1.5.1 Impact Limiter Wood

This section establishes the requirements and acceptance criteria for testing of the redwood and balsa wood utilized within the impact limiters for the TN-32B HBU demonstration cask.

##### 8.1.5.1.1 Moisture

The moisture content of each redwood and balsa wood lot shall be determined in accordance with ASTM D4442 [5] or ASTM D4444 [6]. Alternately, ASTM D7438 [7] may also be utilized to determine the moisture content. At least five test samples shall be taken from each wood lot. The moisture content for redwood and balsa wood shall be within the range of 6% - 12%.

#### 8.1.5.1.2 Density

The density of each redwood and balsa wood lot shall be determined in accordance with ASTM D2395 [8]. At least five test samples shall be taken from each wood lot. The density for redwood and balsa wood shall be within the range of 18.7 lb<sub>m</sub>/ft<sup>3</sup> - 27.5 lb<sub>m</sub>/ft<sup>3</sup> and 7 lb<sub>m</sub>/ft<sup>3</sup> - 12 lb<sub>m</sub>/ft<sup>3</sup>, respectively.

#### 8.1.5.1.3 Compressive Strength

The compressive strength of each redwood and balsa wood lot shall follow the guidelines of ASTM D143 [9]. At least five test samples shall be taken from each wood lot. The lockup strains and average compressive strengths for redwood and balsa wood samples shall be in accordance with the following table.

Material – Grain Direction	Lockup Strain (%)	Ave Crush Strength Range (psi)
Redwood – Parallel-to-Grain	57 – 63	5,100 – 6,630
Balsa – Parallel-to-Grain	76 – 84	1,500 – 1,930

#### 8.1.5.2 Valves, Rupture Discs, and Fluid Transport Devices

There are no valves in the packaging performing a safety related function. The TN-32B HBU demonstration cask design incorporates quick-disconnect couplings for ease of draining and venting. However, these couplings do not form part of the containment boundary. The couplings are covered by bolted closures with metallic O-ring seals. There is no required acceptance test for these components.

#### 8.1.5.3 Seals

The closure lid and all other containment penetrations are sealed utilizing double metallic O-ring seals, with the inner seal forming part of the containment boundary. Metallic seals are not temperature sensitive, and are therefore, tested at room temperature. Metallic seals of the same type as those to be used for transport were installed for the fabrication leak test, described in Section 8.1.3. The tested seals were replaced before loading the packaging for storage. Any O-ring metallic seals that are replaced during the storage period are leakage rate tested, as described in Chapter 7.

#### 8.1.5.4 Impact Limiter Leakage Test

The following test will be performed prior to initial use, after all the seal welds are completed on the impact limiter, to verify that the impact limiter wood will be protected from any moisture exchange with the environment.

Pressurize each impact limiter container to a pressure between 2 and 3 psig utilizing helium or dry air. Test all the weld seams for leakage utilizing a soap bubble test.

#### 8.1.5.5 Functional Tests

The following functional tests were performed prior to first use of the cask for storage, and were performed at the fabrication facility.

- a) Installation and removal of the closure lid, penetration covers, and other fittings were observed. Each component was checked for difficulties in installation and removal. After removal, each component was visually examined for indications of deformation, galling, improper functioning, etc. No defects were noted prior to acceptance of the cask.
- b) After installation of the basket, each basket compartment was checked utilizing a fuel assembly gage to demonstrate that the HBU spent fuel assemblies would fit in each basket cell. This functional test was repeated during the closure lid modification fabrication at the fabricator's facility.

### 8.1.6 Shielding Tests

The analyses performed to ensure the shielding integrity are presented in Chapter 5. The two shielding components, the radial neutron shield and the borated aluminum neutron absorber, are discussed in the following sections.

#### 8.1.6.1 Radial Neutron Shield

The radial neutron shield is protected from damage or loss by the aluminum and steel enclosure. The neutron shield material is a proprietary, borated, reinforced polymer.

The primary function of the resin is to provide neutron shielding, which is performed primarily by the hydrogen content of the resin. The resin also provides some gamma shielding, which is a function of the overall resin density, and is not sensitive to composition.

The shielding performance of the resin was verified to be adequate by chemical analysis and verification of density. Uniformity was assured by installation process control.

The following are the acceptance values for density and chemical composition for the resin. The values used in the shielding calculations of Chapter 5 are included for comparison.

Chapter 5 Values		Acceptance Testing Values		
Element	Nominal wt %	Element	wt %	Range (%)
H	5.05	H	5.05	-10 / +20
B	1.05	B	1.05	± 20
C	35.13	C	35.13	± 20
Al	14.93	Al	14.93	± 20

The minimum resin density in acceptance testing is 1.547 g/cm<sup>3</sup>.

Density testing was performed on every mixed batch of resin. Chemical analysis was made on the first batch mixed with a given set of components, and thereafter, whenever a new lot of one of the major components was introduced. Major components are aluminum oxide, zinc borate and the polyester resin, which combined make up 92% of the resin by weight.

Qualification tests of the personnel and procedure utilized for mixing and pouring the polyester resin used for radial neutron shielding were performed. Qualification testing includes verification that the chemical composition and density were achieved, and the process was performed in such a manner as to prevent voids.

The TN-32B HBU demonstration cask was fabricated and loaded under a site-specific Part 72 license. Cask surface dose rate measurements (both neutron and gamma dose rates) after loading of the cask were performed, as required by Part 72 Technical Specifications. Results of these measurements demonstrate the adequacy of the as-fabricated gamma and neutron shielding, and may be utilized as test data. The shielding is not expected to lose its effectiveness under long term storage conditions based on prior experience with loaded storage casks. In addition, during the 10-year storage period of the spent fuel, the cask will not experience dynamic loads that could result in damage or failure of the shielding. Thus, a periodic test during the storage period is not performed.

In addition, prior to transport of the package, gamma and neutron dose rate measurements will be performed over the cask surface to demonstrate the continued performance of the shielding. These measurements document both the shielding design and durability of the shielding materials, as well as demonstrate the loaded cask satisfies DOT shipping requirements.

Periodic testing of the shielding is not required for transportation since the TN-32B HBU demonstration cask is a single use cask.

#### 8.1.6.2 Neutron Absorber Tests

The neutron absorber consists of borated aluminum containing 4.5 wt% boron that is isotopically enriched to 95 wt% B-10. Because of the negligibly low solubility of boron in solid aluminum, the boron appears entirely as discrete second phase particles of  $\text{AlB}_2$  in the aluminum matrix. The matrix is limited to any 1000 series aluminum, aluminum alloy 6063, or aluminum alloy 6351 so that no boron-containing phases other than  $\text{AlB}_2$  are formed. Titanium may also be added to form  $\text{TiB}_2$  particles, which are finer.

The 4.5 wt% converts to a nominal areal density of B-10 as follows:

$$(2.69 \text{ g/cm}^3 \text{ BAl})(4.5 \text{ wt\% B})(95 \text{ wt\% B10})(0.040 \text{ inch})(2.54 \text{ cm/inch}) = 0.012 \text{ g/cm}^2 \text{ B10}$$

This result is slightly above the design minimum value of 10 mg/cm<sup>2</sup> B-10.



Effective B-10 content was verified by neutron transmission testing of material coupons extracted from the borated aluminum sheets that were utilized in the basket fabrication. The transmission through the coupons was compared with transmission through calibrated standards composed of a homogenous boron compound without other significant neutron absorbers, for example zirconium diboride or titanium diboride. These standards were paired with aluminum shims sized to match the scattering by aluminum in the neutron absorber sheets. The transmission measurement was performed about 1/4 to 1/3 of the distance from the end of the coupon. Thus, random placement of the coupons in the test fixture resulted in testing at two locations across the sheet width. The effective B-10 content of each coupon, minus  $3\sigma$  based on the neutron counting statistics for the coupon, was shown to be  $\geq 10 \text{ mg/cm}^2 \text{ B-10}$ .

Due to the verification of B-10 areal density via comprehensive testing, the calculations in Chapter 6 consider 90% of the B10 content in the borated aluminum sheets in the TN-32B HBU demonstration cask basket.

Based on this discussion, no additional neutron absorber testing of the TN-32B HBU demonstration cask is required.

#### 8.1.6.3 Gamma Shield

The gamma shield is 8 inches thick that surrounds the cask body, 8.75 inches thick on the cask bottom, and 6 inches thick on the closure lid. During the original cask fabrication, these materials were examined by NDE methods to verify no defects existing prior to being installed in the assembly. Additionally, dose rates for both gamma and neutron have been measured and recorded following loading the HBU payload into the cask cavity, and prior to placing the cask on the NAPS ISFSI pad under the Part 72 storage license. These measurements demonstrate the adequacy of the as-fabricated gamma and neutron shielding, and can be utilized as test data. The gamma shielding is not expected to lose its effectiveness during the storage period. In addition, the cask does not experience dynamic loads during the storage period that could result in failure of the shielding. Thus, a periodic shield test during the storage period is not performed.

Prior to transport of the cask, gamma and neutron dose rate measurements will be taken over the cask surface to demonstrate the continued performance of the shielding. This survey documents both the shielding design and the durability of the shielding materials. These measurements also demonstrate that the loaded cask satisfies the radiation levels per 49 CFR 173.441 prior to transport.

#### 8.1.7 Thermal Tests

The thermal evaluation presented in Chapter 3 is based on design configurations and thermal properties taken from industry recognized standards for the specified materials. To demonstrate the adequacy of the cask thermal performance, thermal testing of two TN-32 casks during fabrication was performed and documented as part of the NRC storage license [10]. Utilizing a 32.7 kW heatload, the thermal testing concluded that the design features dissipate the interior heatload as intended. Therefore, no additional thermal testing of the TN-32B HBU demonstration cask is required.

#### 8.1.8 Miscellaneous Tests

There are no additional acceptance tests required to prepare the TN-32B HBU demonstration cask for transport.

## 8.2 Maintenance Program

### 8.2.1 Structural and Pressure Tests

The TN-32B HBU demonstration cask was utilized as a storage cask prior to use as a transport cask. When the cask is removed from storage and prepared for transport, no additional structural or pressure testing beyond the initial fabrication tests is required prior to shipment.

### 8.2.2 Leakage Rate Tests

After a vent/drain port cover removal, the affected metallic containment seals shall be replaced. The containment boundary of the replaced seal shall be tested prior to spent fuel transport to demonstrate a leakage rate less than  $1 \times 10^{-4}$  ref cm<sup>3</sup>/sec utilizing the sniffer technique per Section A.5.8, *Trace gas-sniffer technique (hood technique)*, of ANSI N14.5 [4]. These tests are usually performed using the helium mass spectrometer method. Alternative methods are acceptable, provided that the required sensitivity is achieved. Because the seals are utilized only once, the pre-shipment leakage rate tests may be used to fulfill the ANSI N14.5 requirements for maintenance and periodic testing.

### 8.2.3 Component and Material Tests

#### 8.2.3.1 Fasteners

The vent, drain, and OP transport cover bolts shall be inspected for deformed or stripped threads whenever they are removed. Damaged fasteners shall be evaluated for continued use and replaced as required.

#### 8.2.3.2 Impact Limiters

A visual examination of the impact limiters prior to shipment will be performed to ensure that the impact limiters have not been degraded while in storage. If there is no evidence of weld cracking or other damage that could result in water in-leakage, the wood will not be degraded. If there is visual damage, the impact limiter will be removed from service, repaired, if possible, and inspected for degradation of the wood. Impact limiters will be leak tested once every five years to ensure that water has not entered the impact limiters. If the leakage rate test indicates that the impact limiters have a leak, a humidity test will be performed to verify that there is no free water in the impact limiters. An impact limiter that has a leak will be removed from service and repaired.

#### 8.2.3.3 Valves, Rupture Discs, and Gaskets on Containment Vessel

During the storage period, gas samples from the cavity may be obtained as part of the HBU demonstration project. If a gas sample is removed from the cavity through the vent port, a new metallic O-ring seal will be required, and the vent port cover re-installed in accordance with Section 7.1.3.

Although not part of the containment boundary, the OP system test port cover is replaced by the transport OP port cover. This cover requires a single metallic O-ring seal to be installed to seal the port in accordance with Section 7.1.3.

There are no valves or rupture discs on the TN-32B HBU demonstration cask.

#### 8.2.4 Thermal

Since the primary heat transfer mode is conduction through the metallic cask body, there are no periodic tests or inspections required for the TN-32B HBU demonstration cask heat transfer components.

#### 8.2.5 Miscellaneous Tests

There are no additional tests required to maintain the TN-32B HBU demonstration cask.

##### 8.2.5.1 Valves and Rupture Discs

There are no valves or rupture discs on the TN-32B HBU demonstration cask containment boundary.

##### 8.2.5.2 Gaskets

The containment boundary seals for the TN-32B HBU demonstration cask utilize metallic O-ring seals. These O-ring seals are on the closure lid, the vent and drain port covers, and the thermocouple lance assemblies. Since these metallic O-ring seals are a single use seal, no periodic maintenance or inspection is required. However, if a port cover is removed, the O-ring seal will be replaced. When the TN-32B HBU demonstration cask is converted from storage to transport use, the HBU spent fuel remains in the cask. Therefore, the closure lid will not be removed. In this condition, the closure lid O-ring seal and O-ring seals of penetrations that have not been opened or removed will not be replaced.

The seal leak test port (the OP port in the storage configuration) is closed by the OP transport cover with a single metallic O-ring seal. This flange and seal are not part of the containment boundary. The quick connect couplings in the vent and drain ports are also not part of the containment boundary.

##### 8.2.5.3 Shielding

There are no periodic shielding tests or inspections required for the TN-32B HBU demonstration cask. Radiation surveys will be performed of the package exterior to ensure that the limits specified in 10 CFR 71.47 are met prior to shipment.

### 8.3 References

1. American Society of Mechanical Engineers (ASME) Boiler and Pressure Vessel Code, Section III, "Rules for Construction of Nuclear Facility Components," 1992 Edition.
2. SNT-TC-1A, "Personnel Qualification and Certification in Nondestructive Testing," American Society for Nondestructive Testing, 2016 Edition.
3. ANSI N14.5–1997, "Leakage Tests on Packages for Shipment of Radioactive Materials," American National Standards Institute, Inc.
4. ANSI N14.5–2014, "Leakage Tests on Packages for Shipment of Radioactive Materials," American National Standards Institute, Inc.
5. ASTM-D4442-16, "Standard Test Methods for Direct Moisture Content Measurements of Wood and Wood-Based Materials," American Society for Testing and Materials.
6. ASTM-D4444-13(2018), "Standard Test Methods for Laboratory Standardization and Calibration of Hand-Held Moisture Meters," American Society for Testing and Materials.
7. ASTM-D7438-13, "Standard Practice for Field Calibration and Application of Hand-Held Moisture Meters," American Society for Testing and Materials.
8. ASTM-D2395-17, "Standard Test Methods for Density and Specific Gravity (Relative Density) of Wood and Wood-Based Materials," American Society for Testing and Materials.
9. ASTM-D143-14, "Standard Test Methods for Small Clear Specimens of Timber," American Society for Testing and Materials.
10. Transnuclear, Inc., Letter to U.S. NRC, "TN-32 Cask Thermal Testing," Docket No. 72-1021, December 1, 2000, Transnuclear Document No. E-18578, Project 1066.

## Listing of Computer Files Contained in Enclosure 5

Disk ID No. (size)	Discipline	System/Component	File Series (topics)	Number of Files
Enclosure 5  One Computer Hard Drive  Total (140.57 GB)	<b>Structural (49.8 GB)</b>	<b>TN-32B HBU Cask Base G-Loads LS-DYNA drop analyses</b>	<p><b>Appendix 2.12.9</b></p> <p><b>Folder: \Structural\TN32BHBU-0221-000\</b></p> <p>Input and output files for the LS-DYNA drop cases. Bounding cases are NCT cold end drop (90°) [subfolder: nct_90_cold] and HAC cold end drop (90°) [subfolder: hac_90_cold] analyses. Governing accelerations are in Table 2.12.9-19 and Table 2.12.9-20.</p>	286
		<b>TN-32B HBU Cask Stress Analysis</b>	<p><b>Chapter 2.0 and Appendix 2.12.2</b></p> <p><b>Folder: \Structural\TN32BHBU-0222-000\</b></p> <p>Input and output files for the Cask bounding NCT and HAC analyses (ANSYS Evaluation)</p> <p>Subfolder: nl_buckling Immersion analysis and nonlinear buckling analysis FEM files. Results presented in Section 2.7.7, Figure 2-2 and Figure 2-3.</p> <p>Subfolder: Excel_files Stress Intensity Results for all major components. Stress Intensity results are presented in Table 2-14 through Table 2-18 (NCT), Tables 2-22 through 2-29 (HAC) and Table 2.12.2-2.</p> <p>Subfolders: run_nct and run_hac ANSYS analysis input files for selected individual cases. All individual loads, load combination result input and output files for NCT and HAC.</p> <p>Subfolders: post_nct, post_hac and post_welds ANSYS results post-processing input and output files. Selected maximum stress result files are presented.</p>	306
		<b>TN-32B HBU Outer Shell Stress Analysis</b>	<p><b>Appendix 2.12.4</b></p> <p><b>Folder: \Structural\TN32BHBU-0224-000\</b></p> <p>Input and output files for the Cask outer shell bounding analyses (ANSYS Evaluation). Bounding case is end drop analysis.</p>	38

## Listing of Computer Files Contained in Enclosure 5

Disk ID No. (size)	Discipline	System/Component	File Series (topics)	Number of Files
		<b>TN-32B HBU Cask Fracture Toughness Evaluation</b>	<b>Appendix 2.12.5</b>  <b>Folder: \Structural\TN32BHBU-0231-000\ (TN-32B HBU Fracture Toughness Evaluation for Critical Load Cases)</b>  Input and Output files for fracture toughness evaluation (ANSYS)	27
		<b>TN-32B HBU DLF for Basket</b>	<b>Appendix 2.12.7</b>  <b>Folder: \Structural\TN32BHBU-0234-000 (TN-32B HBU Cask DLF for Basket Drops)</b>  Input and output files for the calculation of natural frequencies and DLFs. (ANSYS Evaluation)	75
		<b>TN-32B HBU Basket NCT drop analysis</b>	<b>Appendix 2.12.6</b>  <b>Folder: \Structural\TN32BHBU-0235-000 (TN-32B HBU Basket Stress NCT)</b>  Input and output files for Basket NCT Stress Analysis. Bounding case, 0° drop input and output files. (ANSYS Evaluation)	36
		<b>TN-32B HBU Basket HAC drop analysis</b>	<b>Appendix 2.12.6</b>  <b>Folder: \Structural\TN32BHBU-0236-000 (TN-32B HBU Basket Stress HAC)</b>  Input and output files for Basket HAC Stress Analysis (ANSYS Evaluation).  Subfolder: basket_run_hac All input and output files for bounding case 0° drop angle.  Subfolder: nlbuckle_inc Nonlinear Buckling analysis of the basket. ANSYS model, 30° drop case (bounding) and post-processing files.	95

## Listing of Computer Files Contained in Enclosure 5

Disk ID No. (size)	Discipline	System/Component	File Series (topics)	Number of Files
		<b>TN-32B HBU Fuel cladding side drop analysis</b>	<p><b>Appendix 2.12.8</b></p> <p><b>Folder: \Structural\TN32BHBU-0237-000 (TN-32B HBU Fuel Cladding Side Drop)</b></p> <p>All Input and output files (ANSYS Evaluation)</p> <p>Subfolder: modal_analysis All input and output files for modal analysis.</p> <p>Subfolder: side_drop_analysis All input and output files for side drop analysis (ANSYS).</p>	33
		<b>TN-32B HBU Fuel cladding side drop analysis</b>	<p><b>Appendix 2.12.8</b></p> <p><b>Folder: \Structural\TN32BHBU-0238-000 (TN-32B HBU Fuel Cladding End Drop)</b></p> <p>Bounding LS-DYNA drop cases input and output files.</p> <p>Subfolder: nhac004np NAIF 30ft drop with 0.04 inch gap and no IP.</p> <p>Subfolder: nhac004wp NAIF 30ft drop with 0.04 inch gap and 1400 psi IP</p> <p>Subfolder: nnct004np NAIF 1ft drop with 0.04 inch gap and no IP</p> <p>Subfolder: nnct004wp NAIF 1ft drop with 0.04 inch gap and 1400 psi IP</p>	677



## Listing of Computer Files Contained in Enclosure 5

Disk ID No. (size)	Discipline	System/Component	File Series (topics)	Number of Files
Enclosure 5  One Computer Hard Drive  Total (140.57 GB)	<b>Thermal (90 GB)</b>	<b>TN-32B HBU Cask ANSYS NCT Thermal Analyses (TN32-HBU in Normal Condition of Transport)</b>	<p><b>Chapter 3.0</b></p> <p><b>Folder: \Thermal\TN32BHBU-0412-001\</b></p> <p>Input and output files for the bounding thermal analysis for NCT (ANSYS Evaluation). Bounding case is NCT Hot or “solar”. Governing temperatures are in Table 3-1.</p> <p>All input and output files are in zipped format (7-zip).</p> <p>Zip file: solar.07.26.zip ANSYS Analysis files (input and output) for bounding case (NCT Hot or Solar).</p> <p>Zip file: solar_post.07.26.zip ANSYS post-processing files (input and output) for bounding case.</p> <p>Zip file: spreadsheets.07.28 Results presented in MS Excel format.</p>	3 zip files

## Listing of Computer Files Contained in Enclosure 5

Disk ID No. (size)	Discipline	System/Component	File Series (topics)	Number of Files
		<b>TN-32B HBU Cask ANSYS HAC Thermal Analyses (TN32-HBU in Hypothetical Accident Conditions)</b>	<p><b>Chapter 3.0</b></p> <p><b>Folder: \Thermal\TN32BHBU-0413-001\</b></p> <p>Input and output files for all thermal analysis for HAC (ANSYS Evaluation).</p> <p>All input and output files are in zipped format (7-zip).</p> <p>Zip file: fire_07.29.zip ANSYS Run to compute TN-32B HBU Cask 30 minute fire event for 10 CFR 71.</p> <p>Zip file: smld_07.29.zip ANSYS Run to compute TN-32B HBU Cask 30 minute charred wood event for 10 CFR 71.</p> <p>Zip files: cldn_08.02.zip, cldn_08.02.z01, cldn_08.02.z02 and cldn_08.02.z03. ANSYS Run to compute TN-32B HBU Cask cool-down post 30 minute fire and 30 minute charred wood events for 10 CFR 71.</p> <p>Zip file: cldnpost.08.02.zip ANSYS Run to generate additional post processing output.</p> <p>Zip file: excel_files.zip MS Excel post-processing files.</p>	8
Enclosure 5  One Computer Hard Drive  Total (140.57 GB)	<b>Shielding (6.8 MB)</b>	<b>TN-32 HBU_HAC (TN32-HBU in Hypothetical Accident Conditions)</b>	<p><b>Table 5-84 "Maximum HAC Dose Rates with Relative Error"</b></p> <p><b>Folder: \HAC\Gamma</b> MCNP input/output files for gamma dose rates calculation under HAC (input, output and mesh tally output)</p> <p><b>Folder: \HAC\Neutron</b> MCNP input/output files for neutron and secondary gamma dose rates calculation under HAC (input, output and mesh tally output)</p>	6

## Listing of Computer Files Contained in Enclosure 5

Disk ID No. (size)	Discipline	System/Component	File Series (topics)	Number of Files
		TN-32 HBU_NCT (TN32-HBU in Normal Condition of Transport)	<p><b>Table 5-83 “Maximum NCT Dose rates with Relative Error”</b></p> <p><b>Folder: \NCT\Gamma</b> MCNP input/output files for gamma dose rates calculation under NCT (input, output and mesh tally output)</p> <p><b>Folder: \NCT\Neutron\NCT Neutron Bottom</b> MCNP input/output files for neutron dose rates calculation under NCT for cask bottom (input, output and mesh tally output)</p> <p><b>Folder: \NCT\Neutron\NCT Neutron Side</b> MCNP input/output files for neutron dose rates calculation under NCT for cask side (input, output and mesh tally output)</p> <p><b>Folder: \NCT\Neutron\NCT Neutron Top</b> MCNP input/output files for neutron dose rates calculation under NCT for cask top (input, output and mesh tally output)</p> <p><b>Folder: \NCT\Neutron\NCT Secondary Gamma</b> MCNP input/output files for secondary gamma dose rates calculation under NCT (input, output and mesh tally output)</p>	15

## Listing of Computer Files Contained in Enclosure 5

Disk ID No. (size)	Discipline	System/Component	File Series (topics)	Number of Files
Enclosure 5  One Computer Hard Drive  Total (140.57 GB)	<b>Criticality (765 MB)</b>	<b>TN-32 HBU_HAC</b>	<b>Folder: \HAC\HAC_single_package</b> SCALE6.1 CSAS5 input/output files for HAC single package (input, output)  <b>Folder: \HAC\HAC_Array</b> SCALE6.1 CSAS5 input/output files for HAC array of packages (input, output)	12
		<b>TN-32 HBU_NCT</b>	<b>Folder: \NCT\NCT_single_package</b> SCALE6.1 CSAS5 input/output files for NCT single package (input, output)  <b>Folder: \NCT\NCT_Array</b> SCALE6.1 CSAS5 input/output files for NCT array of packages (input, output)	4
		<b>TN-32 HBU_TRITON_bpra (TRITON)</b>	<b>Folder: \TRITON_bpra</b> Folders for TRITON files for WE17x17 fuel type with BPRA insertion during depletion (input and output files)	10